IREFCON 2026
16TH INDIA INTERNATIONAL REFRACTORIES CONGRESS

ORGANISED BY

IRMA
PARTNERING HEATING SOLUTIONS
INDIAN REFRACTORY MAKERS ASSOCIATION

16th Indian International Refractories Congress
November 2 - 4, 2026 | Kochi, India

TECHNICAL PROCEEDINGS

THEME

Innovative Solutions for a Sustainable Tomorrow

www.irefcon.com

Presented at:

16th INDIA INTERNATIONAL REFRACTORIES CONGRESS
2nd – 4th November 2026, Grand Hyatt Convention Centre, Kochi, India

C/o Indian Refractory Makers Association
41, Shakespeare Sarani, Duckback House
Unit - 2B, 2nd Floor
Kolkata – 700017

Phone: +91 33 4003 2748
E-mail: support@irmaindia.org
Website: www.irmaindia.org

Printed & Published by:

Indian Refractory Makers Association
41, Shakespeare Sarani, Duckback House
Unit-2B, 2nd Floor
Kolkata – 700017

Phone: +91 33 4003 2748
E-mail: support@irmaindia.org
Website: www.irmaindia.org

The views expressed in the articles are solely of the respective authors.
Indian Refractory Makers Association is in no way responsible for the same.

Copyright: Indian Refractory Makers Association

All rights reserved, 2026

No part of the content of the proceedings can be reproduced in any format without the written consent of Indian Refractory Makers Association.

SPONSORS

TITLE SPONSOR

Calderys India Refractories Ltd

CULTURAL NIGHTS SPONSOR

Hindalco Industries Ltd

BAR SPONSOR

Maithan Ceramic Ltd

WELCOME DINNER SPONSOR

TRL Krosaki Refractories Ltd

DIAMOND PARTNERS

Almatis Alumina Pvt Ltd

Vesuvius India Ltd

Carborundum Universal Ltd

PLATINUM PARTNERS

IFGL Refractories Ltd

RHI Magnesita India Ltd

Aarya Metallurgicals (India) Pvt Ltd

GOLD SPONSORS

Mahakoshal Refractories Pvt Ltd

Orind Special Refractories Pvt Ltd

Totale Global Pvt Ltd

Shinagawa Refra Co Ltd

IMERYS

SILVER SPONSORS

F G K Thermal Pvt Ltd

Refratechnik (India) Pvt Ltd

ABS Refractories Pvt Ltd

Refractory Shapes Ltd

Ironbuild Systems Pvt Ltd

SMM Refractories Pvt Ltd

Vishva Vishal Refractory Ltd

INDEX

1	KEYNOTE SPEECHES			
SR. NO.	TOPIC	AUTHOR	ORGANIZATION	PAGE NUMBER
1.1	REFRACTORIES AND THEIR IMPACT ON STEEL QUALITY AND PRODUCTIVITY	MARK RUNGE	REFRATECHNIK STEEL, GMBH	1
1.2	REFRACTORY RAW MATERIALS - NEW DEVELOPMENTS AND FUTURE PERSPECTIVES	CHRIS PARR	IMERYS	3
1.3	AI-DRIVEN REFRACTORY R&D: TURNING DATA INTO FASTER, SMARTER MATERIAL DEVELOPMENT	ANNELOUISE VAN DIJKE	RHI MAGNESITA LEOBEN	13

2	THEME LECTURES			
SR. NO.	TOPIC	AUTHOR	ORGANIZATION	PAGE NUMBER
2.1	STEEL MEETS REFRACTORY PLATFORM – CONCEPT AND EXPERIENCES	ANDUS BUHR	ALMATIS GMBH	21
2.2	INDUSTRIAL EXPERIENCE AND EMERGING CHALLENGES	FELIX FIRSBACH	BADISCHE STAHLWERKE ENGINEERING (BSW) GMBH	29

3	CASE STUDIES				
SR. NO.	TOPIC	AUTHOR	ORGANIZATION	PARTNER ORGANIZATION	PAGE NUMBER
3.1	PROGRESS IN APPLICATION OF SOL-GEL METHOD IN REFRACTORIES	ZHANG ZIYING	SINOSTEEL LUOYANG INSTITUTE OF REFRACTORY RESEARCH CO., LTD.	JIAOZUO JINXIN HENGTUO NEW MATERIALS CO., LTD.	39
3.2	IMPROVED SLAG CORROSION RESISTANCE OF	QILONG CHEN	PUYANG REFRACTORIES GROUP CO.,LTD.	ZHENGZHOU HAIMAI HIGH	50

	MGO-C REFRACTORIES FOR LADLE SLAG LINE USING CARBON-ENHANCED COMPOSITE AGGREGATES		(PRCO)	TEMPERATURE MATERIALS CO., LTD.	
3.3	PRIME-X: HIGH DURABILITY SEN FOR ENHANCED TUNDISH CAMPAIGN LIFE	GAURAV PANDEY	TRL KROSAKI REFRACTORIES LTD.	TATA STEEL LTD. (INDIA)	61
3.4	SUCCESSFUL IMPLEMENTATION OF TRM IN RH DEGASSER UNIT - A UNIQUE AND COLLABORATIVE APPROACH TOWARDS PERFORMANCE IMPROVEMENT, HIGHER RELIABILITY & PRODUCTIVITY, OPTIMIZED INVENTORY CONTROL	RAJESH GHOSH	TRL KROSAKI REFRACTORIES LTD.	JINDAL STEEL LIMITED, RAIGARH	74
3.5	INTEGRATED REFRACTORY SOLUTION FOR A 140-TON ALUMINUM REVERBERATORY FURNACE (NOVELIS ULSAN): FROM GLOBAL DESIGN COLLABORATION TO PARTNER-DRIVEN INSTALLATION AND COMMISSIONING	WOONG KIM	CALDERYS KOREA	HANSUNG CO., LTD.	83
3.6	NEXT-GENERATION RAPID HEATING THROUGH CASTABLES: ENHANCING PERFORMANCE AND SUSTAINABILITY THROUGH SUPERIOR	ARUP KUMAR SAMANTA	TRL KROSAKI REFRACTORIES LTD.	IMERYS S.A., FRANCE	90

	CORROSION RESISTANCE AND REDUCED CARBON EMISSIONS				
3.7	THE BEHAVIOUR OF DIFFERENT ALUMINOSILICATE REFRACTORIES EXPOSED TO HYDROGEN AND CARBON MONOXIDE	GOUTAM BHATTACHARYA	IMERYS SA, PARIS, FRANCE	GOUDA REFRACTORIES BV, GOUDA, THE NETHERLANDS	104
3.8	DEVELOPMENT OF A HIGH STRENGTH NO-CEMENT CASTABLE WITH ENHANCED INTERMEDIATE TEMPERATURE PROPERTIES	SACHI DULAL MAJUMDAR	IFGL REFRACTORIES LTD.	ELKEM SOUTH ASIA PRIVATE. LTD.	112
3.9	MATRIX DEVELOPMENT OF LOW CEMENT SELF-FLOW CASTABLES FOR BF BLOWPIPE APPLICATION	SACHI DULAL MAJUMDAR	IFGL REFRACTORIES LTD.	ALMATIS ALUMINA PVT. LTD.	122
3.10	INFLUENCE OF CALCINED ALUMINA CHARACTERISTICS ON THE ABRASION RESISTANCE OF CASTABLE	ANKITA DAS	CALDERYS INDIA REFRACTORIES LIMITED, NAGPUR	ALMATIS ALUMINA PVT. LTD.	129
3.11	MICROSTRUCTURAL ENGINEERING OF ZIRCONIA–MULLITE REFRACTORY USING A SPECIAL REACTIVE ALUMINA FOR ENHANCED HIGH TEMPERATURE PERFORMANCE	ANKITA DAS	CALDERYS INDIA REFRACTORIES LIMITED, NAGPUR	ALMATIS ALUMINA PVT. LTD.	135
3.12	RESEARCH ON SLAG ADHESION TREATMENT TECHNOLOGY IN THE MELTING AND CASTING INDUSTRY	CHUNXIA CHEN	CALDERYS CHINA	HUANGSHIDONGBEI CASTING CO., LTD.	143

3.13	FROM VARIABILITY TO CONSISTENCY: THE IMPACT OF ENGINEERED MICROSILICA ON CASTABLE PERFORMANCE	SUMIT SAMANTA	CALDERYS INDIA REFRACTORIES LIMITED	ELKEM SOUTH ASIA PRIVATE. LTD.	150
3.14	ADVANCED REFRACTORY SOLUTIONS FOR COKE DRY QUENCHING: A FOCUS ON HIGH-PERFORMANCE ANDALUSITE BRICKS	GOUTAM BHATTACHARYA	IMERYS VIZAG PVT. LTD.	MAHAKOSHAL REFRACTORIES PVT. LTD., KATNI	161
3.15	DEVELOPMENT OF INDIGENOUS GUNNING MASS FOR EOF (ENERGY OPTIMISED FURNACE) AND ESTABLISHING ITS PERFORMANCE FOR THE HOT MAINTENANCE	PRAVASH GOURAV	CALDERYS INDIA REFRACTORIES LTD.	JAI RAJ STEEL	170
3.16	ENHANCING REHEATING FURNACE (ROLLING MILL) CAMPAIGN LIFE: THE IMPACT OF ENGINEERED REACTIVE ALUMINA ON PRECAST BLOCK PERFORMANCE	SHANKHA CHATTERJEE	ALMATIS ALUMINA PVT LTD.	MAHAKOSHAL REFRACTORIES PVT. LTD., KATNI	181
3.17	PERFORMANCE ENHANCEMENT OF SEN THROUGH GEOMETRIC MODIFICATION OF THE SLAG ZONE	SACHI DULAL MAJUMDAR	IFGL REFRACTORIES LTD.	TATA STEEL LTD.	190
3.18	A CASE STUDY ON LANCE PERFORMANCE IMPROVEMENT ON TATA STEEL KALINGA NAGAR VIA VOC	SAMIK SARKAR	CALDERYS INDIA REFRACTORIES LTD.	TATA STEEL KPO, KALINGANAGAR	201
3.19	STUDY ON THE	AJAY	AARYA	JSW DOLVI	207

	INFLUENCE OF PROCESS PARAMETER ON STEEL TEEMING LADLE REFRACTORY PERFORMANCE IN SECONDARY STEEL MAKING PROCESS USING ANALYTICAL TOOLS.	NARAYANAN	METALLURGICALS INDIA PRIVATE LTD.		
3.20	DEVELOPMENT OF MINI-AUTOMATIC FLUX FEEDER FOR SMALL & MEDIUM STEEL PLANT	DHANANJOY GHOSH	CALDERYS STEELCASTING INDIA PVT. LTD.	KIRLOSKAR FERROUS INDUSTRIES LIMITED (KFIL)	214
3.21	ZONE-SPECIFIC AL_2O_3–SIC–C REFRACTORY SYSTEMS FOR TORPEDO LADLES:WEAR MECHANISMS, FIELD INVESTIGATION AND REFRACTORY OPTIMISATION	ALOK PATRO	CALDERYS INDIA REFRACTORIES LTD., NAGPUR	JSW STEEL	220
3.22	OPTIMISATION OF ALUMINA-SPINEL CASTABLE FOR USE IN PRECAST BOTTOM FOR LARGE CAPACITY STEEL LADLE	NATHAN LEICHT	SHINAGAWA REFRACTORIES AUSTRALASIA	ALMATIS GMBH, FRANKFURT	228
3.23	MEETING THE 2200 °C+ CHALLENGE IN CARBON BLACK REACTORS WITH DEVELOPMENT OF ADVANCED ZIRCONIA REFRACTORY	PM SIVARAM	CARBORUNDUM UNIVERSAL LTD.	IMERYS SA, FRANCE	235

4	TECHNICAL PAPERS			
SR. NO.	**TOPIC**	**AUTHOR**	**ORGANIZATION**	**PAGE NUMBER**
4.1	ENERGY SAVING SOLUTIONS – THE	SHARMILA BOSE	TECHNIP ENERGIES LTD.	243

	REFRACTORIES DESIGN, PROCUREMENT AND INSTALLATION FOR AN ETHYLENE CRACKING FURNACE			
4.2	MODULAR REHEATING FURNACE INSULATION WITH REDUCED DOWNTIME, FUEL CONSUMPTION AND CARBON FOOTPRINT	JULIE HARDY	MONOCON INTERNATIONAL REFRACTORIES LTD.	255
4.3	FIBERSTONE™ - A PRE-CAST CERAMIC METAL COMPOSITE	JEREMY PEAT	FIBERSTONE LTD.	260
4.4	RIP IT OUT AND START AGAIN: NO LONGER A SIDESHOW, RECYCLING REFRACTORIES IS OUT OF THE SHADOWS	MIKE O'DRISCOLL	IMFORMED	267
4.5	WAKE UP AND SMELL THE COFFEE: PREVENTING ODOUR EMISSIONS FROM REFRACTORIES AT TATA STEEL IJMUIDEN	WARBOUT TESSELAAR	TATA STEEL IJMUIDEN	272
4.6	NEXT GENERATION TUNDISH GATE SLIDE PLATE WITH MULTIFUNCTIONAL ADDITIVES FOR OXYGEN RICH CALCIA TREATED STEEL CASTING	SOVAN KHAN	TRL KROSAKI REFRACTORIES LTD.	282
4.7	DRIVING EFFICIENCY: A NOVEL APPROACH TO BULLNOSE REFRACTORY PERFORMANCE AND RELIABILITY IN WALKING BEAM FURNACES	KSHITISH KUMAR JENA	TATA STEEL, JAMSHEDPUR	291
4.8	DEVELOPMENT OF CHROME BEARING HIGH ALUMINA BRICK FOR SETTLING CHAMBER OF EAF BY USING GREEN RAW MATERIALS – A SUSTAINABLE APPROACH TOWARDS MANUFACTURING OF COST-EFFECTIVE HIGH-END REFRACTORIES	AAKASH DALUI	TRL KROSAKI REFRACTORIES LTD.	298
4.9	DEVELOPMENT OF A HIGHER-SERVICE - LIFE	SUBHADEEP CHOWDHURY	TRL KROSAKI REFRACTORIES LTD.	305

	COLLECTOR NOZZLE			
4.10	EFFECT OF SILICON CARBIDE ON THE PROPERTIES OF HIGH-DENSITY SILICA BRICKS FOR COKE-OVEN APPLICATIONS	DEEPTAYAN BANERJEE	TRL KROSAKI REFRACTORIES LTD.	313
4.11	DEVELOPMENT OF HYDRATION RESISTANT MAGNESIA BASED BRICKS FOR STEEL AND CEMENT INDUSTRIES	AVISHEK MITRA	CALDERYS INDIA REFRACTORIES LTD.	325
4.12	DEVELOPMENT OF AN ADVANCED ALKALI–SULFUR CORROSION RESISTANT MAGNESIA SPINEL REFRACTORIES IN HIGH AFR CEMENT KILNS	AVISHEK MITRA	CALDERYS INDIA REFRACTORIES LTD.	332
4.13	WATER-FREE, QUICK-DRYING AND HIGH STRENGTH SOL-BONDED GUNNING MASS FOR ENERGY-EFFICIENT LIME KILN APPLICATIONS	ARUP KUMAR SAMANTA	TRL KROSAKI REFRACTORIES LTD.	341
4.14	GUNNING ROBOTS FOR THE HOT REPAIR	CHRISTIAN WOLF	VELCO GMBH	355
4.15	ENERGY EFFICIENT MAGNESIA CARBON BRICKS SOLUTION FOR STEEL LADLE	AVISHEK MITRA	CALDERYS INDIA REFRACTORIES LTD.	363
4.16	TAILORING 80% ALUMINA CEMENTS FOR HIGH-PERFORMANCE REFRACTORY CASTABLES	GOUTAM BHATTACHARYA	IMERYS VIZAG PVT. LTD.	371
4.17	ENERGY SAVING IN STEEL LADLES WITH INNOVATIVE LINING CONCEPTS	ANDREAS BUHR	ALMATIS GMBH	379
4.18	ENHANCED CORROSION RESISTANCE OF LOW-CARBON MGO–C BRICKS FOR SECONDARY REFINING FURNACES BY FERROCHROME ADDITION	HAYATE KAWANO	KROSAKI HARIMA CORPORATION	386
4.19	ADVANCING CEMENT KILN RELIABILITY WITH	HONG PENG	ELKEM SILICON PRODUCTS	395

	DUAL-STAGE BONDED NO-CEMENT CASTABLES: ENHANCED THERMAL-SHOCK AND ALKALINE RESISTANCE		DEVELOPMENT	
4.20	COMPARATIVE EVALUATION OF HYDRATION BEHAVIOR IN MAGNESIA BASED REFRACTORIES	SIRSHENDU DAS	TRL KROSAKI REFRACTORIES LTD.	405
4.21	ROLE OF ANTIOXIDANTS ON THE THERMOMECHANICAL PROPERTIES OF MAGNESIA CARBON REFRACTORIES	SIRSHENDU DAS	TRL KROSAKI REFRACTORIES LTD	411
4.22	INNOVATIVE COLD START REFRACTORY TECHNOLOGIES FOR CONTINUOUS CASTING WITHOUT FUEL GAS PREHEATING, REPRESENTING AN APPROACH TOWARD ENHANCED ENVIRONMENTAL SUSTAINABILITY	SUDIPTA PALIT	TRL KROSAKI REFRACTORIES LTD.	418
4.23	HIGH TEMPERATURE HYDROGEN RESISTANCE OF SYNTHETIC ALUMINA BASED CASTABLES	SHANKHA CHATTERJEE	ALMATIS ALUMINA PVT. LTD.	426
4.24	MULTIFUNCTIONAL ADDITIVE SOLUTIONS FOR OPTIMIZING SILICA FUME-BASED CASTABLE SYSTEMS	SOUROJIT PAL	ALMATIS ALUMINA PVT. LTD.	435
4.25	EXPERIENCE OF COMPENSATOR DESIGN AND PERFORMANCE FOR BLAST FURNACE STOVE AT TATA STEEL	GOUTAM GHOSH	TATA STEEL	443
4.26	ZIRCONIA: MAINTAINING THE STABILITY OF AN ESSENTIAL MINERAL IN REFRACTORY FORMULATIONS	GOUTAM BHATTACHARYA	IMERYS VIZAG PVT. LTD.	451
4.27	SYSTEMATIC EVALUATION OF RECLAIMED MATERIALS FROM INDUSTRIAL SOURCES FOR	GAURAV SINHA	CALDERYS INDIA REFRACTORIES LTD.	460

	LOW-CEMENT CASTABLES			
4.28	TAILORING LOW-CEMENT CASTABLE RHEOLOGY VIA MICROSILICA PROPERTIES	GAURAV SINHA	CALDERYS INDIA REFRACTORIES LTD.	469
4.29	LANCE: DELIVERING CUSTOMISED SOLUTIONS FOR DIVERSE CUSTOMER NEEDS	GAURAV SINHA	CALDERYS INDIA REFRACTORIES LTD.	475
4.30	OPTIMIZATION OF SEN SLEEVE FOR RECORD BREAKING SEQUENCE CASTING AT JSW BPSL THIN SLAB CASTER	LEELA NAGARJUNA VANGARA	VESUVIUS INDIA LTD.	481
4.31	PHOSPHATE FREE RAMMING MASS FOR MONOBLOCK TUNDISH NOZZLE PLATE (MTNP) APPLICATION	SATYANANDA BEHERA	VESUVIUS INDIA LTD.	488
4.32	HIGH PERFORMANCE HIGH FLEXIBILITY (HPHF) DURAFLEX LADLE SHROUD FOR LONG LIFE MULTIPLE COLD REUSE APPLICATION	SUDIP BANERJEE	VESUVIUS INDIA LTD.	496
4.33	ACHIEVING BOTH THERMAL INSULATION AND DURABILITY WITH FIBER-ADDED CASTABLE REFRACTORIES	MAKOTO OKINO	SHINAGAWA REFRA CO., LTD.	501
4.34	DRY GUNNING MATERIAL “SIG (SHINAGAWA IMPROVED GUNNING)” WITH HIGH DURABILITY AND QUICK DRYING PROPERTIES	MAKOTO OKINO	SHINAGAWA REFRA CO., LTD.	509
4.35	ENERGY CONSERVATION IN STEELMAKING VESSELS THROUGH HYBRID REFRACTORY LINING SYSTEMS	TOSHIKAZU SETOGUCHI	ISOLITE CERAMIC FIBERS SDN. BHD. (ICF)	516
4.36	APPLICATION OF SHOTLESS CERAMIC FIBER AND LINING TECHNOLOGY IN COLD-ROLLING FACILITIES	TOSHIKAZU SETOGUCHI	ISOLITE CERAMIC FIBERS SDN. BHD. (ICF)	524
4.37	APPLICATIONS OF CERAMIC FIBER IN REHEATING	TOSHIKAZU SETOGUCHI	ISOLITE CERAMIC FIBERS SDN. BHD.	529

	FURNACES AND ITS CONTRIBUTION TO CARBON NEUTRALITY		(ICF)	
4.38	BAUXITE–ZIRCON CASTABLE FOR ALUMINUM APPLICATIONS: NUMERICAL ANALYSIS OF RAPID DRYING	HIROTAKA GOTO	CALDERYS JAPAN	535
4.39	DEVELOPMENT OF A PLASTIC GUNNING MIX: A UNIQUE SYSTEM FOR MECHANIZED APPLICATION	SANTOSH UPADHYAY	CALDERYS INDIA REFRACTORIES LTD.	544
4.40	TUNDISH PERFORMANCE BENCHMARK WITH SHROUD EXCHANGE MECHANISM 3085	ARIJIT BHATTACHARYYA	VESUVIUS INDIA LTD.	551
4.41	ADVANCING TROUGH REFRACTORIES WITH A NO-CEMENT BINDER SYSTEM	ANKITA MISHRA	ELKEM SOUTH ASIA PRIVATE LTD.	558
4.42	DEVELOPMENT OF A READY-TO-USE REFRACTORY MORTAR WITH EXTENDED SHELF LIFE FOR STEELMAKING APPLICATIONS	SACHI DULAL MAJUMDAR	IFGL REFRACTORIES LTD.	569
4.43	ADVANCED MOULD FLUX DESIGN FOR IMPROVED SURFACE QUALITY IN HIGH- AND LOW-SPEED CASTERS	MD. SHAMIM AHMED	CALDERYS STEEL CASTING INDIA PVT LTD.	580
4.44	UTILIZATION OF ALUMINIUM SALT SLAG FOR THE PRODUCTION OF CORDIERITE	JAN URBÃ¡NEK	UCT PRAGUE	586
4.45	DEVELOPMENT AND PERFORMANCE EVALUATION OF CALCIUM ALUMINATE CEMENT (CAC 50) BASED REFRACTORY SHOTCRETE WITH HIGH THERMAL AND ACID RESISTANCE	BUKET POLAT	ÇİMSA CEMENT	590
4.46	SUSTAINABLE USE OF RECYCLED SILICON CARBIDE IN MONOLITHICS: A VIABLE REPLACEMENT FOR VIRGIN SIC	SUMIT SAMANTA	CALDERYS INDIA REFRACTORIES LTD.	594

4.47	FUNDAMENTAL DESIGN APPROACH FOR SYNTHETIC SLAG TO CONTROL INCLUSION	SAURABH TATYASAHEB TAMBE	CALDERYS STEELCASTING INDIA PRIVATE LTD.	603
4.48	RESILIENT REFRACTORY PERFORMANCE SOLUTION: HIGH-PERFORMANCE MGO-C BRICKS REIMAGINED	DEBASISH CHANDRA	REFRATECHNIK	611
4.49	ADVANCING EAF ROOF DELTA REFRACTORIES: BENEFITS OF NON-CEMENT HYBRID BONDED CASTABLE	DEBASISH CHANDRA	REFRATECHNIK	622
4.50	PARTIAL REPLACEMENT OF MICROSILICA BY REACTIVE ALUMINA IN CASTABLE APPLICATION	RAVI J MOHARE	HINDALCO INDUSTRIES LTD.	635
4.51	TAILORED ALUMINA PARTICLE SIZE DISTRIBUTION IN ENHANCING PACKING DENSITY AND REFRACTORY CASTABLE PROPERTIES	INDU	HIC ALUMINA, HINDALCO INDUSTRIES LTD.	644
4.52	REDUCING FIRING FUEL COSTS AND IMPROVING QUALITY OF CONTINUOUS CASTING NOZZLES BY UTILIZING RESIN REACTIONS	AKANE KITAMURA	TYK CERAMICS INDIA PRIVATE LTD.	652
4.53	DEVELOPMENT OF ECO FRIENDLY TAP HOLE CLAY FOR BLAST FURNACE	TUHIN KANTI PATRANABISH	CALDERYS INDIA REFRACTORIES LTD.	657
4.54	IMPACT OF MINOR MATRIX CONSTITUENTS ON THE LONG-TERM STABILITY OF SILICA BRICKS IN GLASS TANK FURNACE	RAGHUNATH SHARMA	SAINT-GOBAIN INNOVATION HUB INDIA	663
4.55	GREEN TAP HOLE CLAY: SUSTAINABLE STEPS TOWARDS CLEANER SOLUTIONS & CHALLENGES	PALADUGU SRINIVASA RAO	VESUVIUS REFRACTORY INDIA PVT LTD.	669
4.56	A NEXT-GENERATION SPINEL AGGREGATE FOR SUPERIOR REFRACTORY PERFORMANCE	RAMKRISHNA HALDER	INDIANO CHROME PVT LTD.	676
4.57	SHINAGAWA & SAINT	ROJALINA	SAINT GOBAIN	685

	GOBAIN PARTNERSHIP FOR ADVANCED TROUGH AND RUNNER REFRACTORY SOLUTIONS FOR THE INDIAN STEEL INDUSTRY	NANDA	PERFORMANCE CERAMICS AND REFRACTORIES	
4.58	IMPROVEMENT OF TAP HOLE CLAY DRILLING BEHAVIOUR FOR HIGH-SEVERITY BLAST FURNACE OPERATION	SOUVIK PALUI	CALDERYS INDIA REFRACTORIES LTD.	691
4.59	SEVERITY BLAST FURNACE OPERATION	RISHI MUKHERJEE	CALDERYS INDIA REFRACTORIES LTD.	702
4.60	ADVANTAGE OF SINGLE COMPONENT PLASTIC REFRACTORY IN SKID & POST OF WALKING BEAM FURNACE	RISHI MUKHERJEE	CALDERYS INDIA REFRACTORIES LTD.	707
4.61	EFFECT OF TAPING TIME ON TAP HOLE CLAY PROPERTIES AND BLAST FURNACE OPERATION	ROJALINA NANDA	SAINT GOBAIN PERFORMANCE CERAMICS AND REFRACTORIES	711
4.62	NON-WETTING CASTABLES FOR ALUMINIUM FURNACES: CORROSION RESISTANCE AND CRYOLITE STABILITY	SATHIYAKUMAR MURUGESAN	TOTALE GLOBAL PRIVATE LTD.	719
4.63	HYBRID BOND CASTABLES FOR LADLE LININGS: ENHANCED SLAG RESISTANCE AND SERVICE LIFE	SATHIYAKUMAR MURUGESAN	TOTALE GLOBAL PRIVATE LTD.	726
4.64	DEVELOPMENT OF A NOVEL TROWELABLE REFRACTORY FOR ABRASION RESISTANT DUCT LININGS IN PELLETIZING PLANTS	SATHIYAKUMAR MURUGESAN	TOTALE GLOBAL PRIVATE LIMITED	732
4.65	ENHANCING OXIDATION RESISTANCE OF Si_3N_4–BONDED SIC REFRACTORIES FOR COPPER SHAFT FURNACE PERFORMANCE	RANJAN DEY	CARBORUNDUM UNIVERSAL LTD.	738
4.66	NEW GENERATION SPECIAL CASTABLE FOR FOUNDRY INDUSTRY	SUDIP KUMAR PAUL	RHI MAGNESITA INDIA LTD.	746

4.67	ANALYSIS OF REFRACTORY WEAR IN MIDDLE ZONE OF DRI KILNS DUE TO PELLET AND IMPORTED COAL USAGE	DHWANI GUPTA PASSARY	PASSARY REFRACTORIES	756
4.68	REAL KILN FEED TEST: A PRACTICAL EVALUATION FOR DRI KILNS	DHWANI GUPTA PASSARY	PASSARY REFRACTORIES	763
4.69	REDUCING THERMAL EXPANSION OF MAGNESIA–CARBON REFRACTORIES USED IN CONTINUOUS CASTING OF STEEL MAKING	SHEKHAR KUMAR SHRIVASTAVA	CALDERYS INDIA REFRACTORIES LTD.	770
4.70	DEVELOPMENT OF INDIGENOUS BASIC HEARTH MASS FOR THE COLD AND HOT REPAIR OF ELECTRIC ARC FURNACE AND CONARC FURNACE	PRAVASH GOURAV	CALDERYS REFRACTORY INDIA LTD.	779
4.71	DRIVING PRODUCTIVITY EXCELLENCE IN IF GRADE STEEL: A NOBLE INITIATIVE AT TATA STEEL KALINGANAGAR	NABID ANJUM KHAN	CALDERYS REFRACTORY INDIA LTD.	786
4.72	DESIGN, DISCIPLINE, AND SUSTAINABILITY: A TUNDISH REFRACTORY SUCCESS AT TATA NINL	AAYUSH SHUKLA	TATA STEEL NEELACHAL	791
4.73	ENHANCING REHEATING FURNACE CAMPAIGN LIFE THROUGH OPTIMIZED REFRACTORY ANCHOR DESIGN AND STANDARDIZATION	BISWAJIT PAL	TATA STEEL LTD.	797
4.74	GREEN RECYCLED REFRACTORIES -MGO C MAGNESIA CARBON	ISHAN AGARWAL	JBTC-JAI BALAJEE TRADING COMPANY	803
4.75	THE OPERATIONAL STATUS OF THE FIRST COMMERCIAL REX-ROBO LSG AND THE FUTURE DEVELOPMENTS OF REX-ROBO SERIES	MAMORU YOSHIMURA	KROSAKI HARIMA CORPORATION	812
4.76	ENHANCEMENT OF CORROSION RESISTANCE IN MGO-C FOR CONVERTER	DAISUKE TOMITA	KROSAKI HARIMA CORPORATION	822

4.77	USE OF RECYCLE REFRACTORIES AND ITS IMPACT ON REFRACTORY PRODUCTS	JAYANT KUMAR SAHU	VISHVA VISHAL REFRACTORY INDUSTRIES	830
4.78	DEVELOPMENT OF OPEN-FIRED LADLE SHROUD FOR REUSE APPLICATION	ABHISHEK KING	RHI MAGNESITA INDIA LTD.	838
4.79	BASIC SLIDE GATE PLATE FOR LADLE FOR HIGH CA STEEL	SHIBAYAN CHATTERJEE	RHI MAGNESITA INDIA	845
4.80	COMPARATIVE STUDY ON SINTERED, FUSED, AND TABULAR ALUMINA AGGREGATES FOR CASTABLES	DAIMU MUTO	ITOCHU CERATECH CORPORATION	854
4.81	EFFECT OF CA F_2 - CONTAINING FLUX ON PHASE STABILITY AND MICROSTRUCTURAL EVOLUTION OF STABILIZED ZIRCONIA GRAINS	CINTOALAPPAT	CUMI-EMD	869

REFRACTORIES AND THEIR IMPACT ON STEEL QUALITY AND PRODUCTIVITY

Mr Mark Runge

Refratechnik Steel GmbH

Abstract

India's finished-steel consumption reached about 164 Mt in FY 2025–26, growing roughly 7–8% YoY, while crude-steel production reached about 168.4 Mt with while finished-steel production increased about 6.4%.This is significant because it indicates that demand is growing faster than domestic finished-steel production, creating pressure on producers to improve both capacity utilization and product availability;implies a substantial requirement for additional capacity, productivity improvement and higher-value steel grades.Construction and infrastructure account for roughly two-thirds of steel demand in India. The steel quality mainly demands higher strength, cleaner steel, précised chemistry and better surface quality. Productivity is becoming as important as capacity especially for Indian steel producers; rather installing new capacity,higher productivity with lower energy, lower refractory consumption, lower quality rejections to get cost effective outcome would be the preferred target.

Quality and productivity are directly connected; a useful way to present this relationship isRaw-material quality → Process stability → Productivity → Steel quality → Customer acceptance → Profitability. For example, poor DRI quality can lead to high gangue → higher slag → higher energy consumption → longer melting time → increased refractory attack → lower productivity → higher cost.Similarly, poor refractory performance causes premature lining failure→ unplanned stoppage → reduced availability and output → higher refractory cost → higher conversion cost.

For refractory industry, this market trend creates a very clear opportunity.The Indian steel industry will increasingly demand refractories that deliver longer campaign life, lower consumption, higher productivity, fewer stoppages yield out consistent steel quality.Instead of selling only on ₹/ton of refractory, the value proposition should move toward ₹/ton of liquid steel, campaign life, productivity gain and quality improvement. For example, a MgC brick that costs slightly more but provides higher campaign life, lower MgO dissolution, lower slag penetration, better thermal-shock resistance, reduced relining frequency and fewer production interruptions can generate substantially greater value for the steel plant.The bottom line is The Indian steel market is entering a phase where "quality+ productivity + cost + sustainability" will determine competitiveness. Globally sourced refractory raw materials traditionally supplied through China-dominated value chains, experiencing significant supply fluctuations over recent years. These disruptions have created uncertainty in pricing, availability, and inventory management risking excessive dependence on a single source geography. Refractory producers are therefore in process of establishing alternative sourcing strategies. Geopolitical developments increasingly influence energy availability and cost structures. Refractory systems must therefore contribute to lower energy consumption through improved insulation, minimized heat loss, better thermal efficiency, and optimized furnace operation.The transition toward lower-carbon steelmaking introduces new operating conditions. Alternate fuels produce different combustion characteristics, chemical environments, and thermal profiles. Simultaneously, increased DRI usage introduces new slag chemistries and process dynamics. Such inputs often generate aggressive slag conditions, increased wear mechanisms, and higher thermal fluctuations. Refractory solutions are getting ready to withstand harsher operating conditions while maintaining productivity and safety.Modern technologies enable unprecedented monitoring and control capabilities through sophisticated machinery and systems. Such approaches transform refractory management from reactive

maintenance into predictive asset optimization.

Future refractory success depends not only on material performance but also on supply-chain resilience.

India's steel demand is expanding strongly, but the next competitive advantage will not simply be who produces more steel. It will increasingly be who produces higher-quality steel, faster, with lower energy, lower refractory consumption, lower emissions and fewer quality failures. We are looking forward to strong partnerships on designing technical solutions between steel producers and refractory suppliers to achieve a win-win situation, as modern challenges cannot be addressed through product development alone.

Keywords

RM Logistics, China Supply Chain, Geo-Political Issues, Emissions, Alternative Fuels, DRI Usage, Quantity-Quality Optimization, Lifecycle Cost, Sustainability, Future Technical Solutions.

REFRACTORY RAW MATERIALS - NEW DEVELOPMENTS AND FUTURE PERSPECTIVES

Christopher Parr[1], Jean-Michel Auvray, Valérie Germain, Scot Gradick, Frédéric Lacoue, Liu Chunfeng, Ratana Soth, Christoph Wöhrmeyer, Alexandre Sevagen

1. VP, Science and Technology, Refractories, Abrasives and Construction Solutions, Imerys, Paris, France

Corresponding author's e-mail: chris.parr@imerys.com

Abstract

Raw materials for Refractories have continuously evolved —aggregates, binders, and fillers—to enhance technical performance and cost-efficiency. This progress is driven by a strategic balance of "market pull" and "technology push," often catalyzed by academic-industry partnerships that bridge fundamental science with industrial applications. While durability remains vital, sustainability has emerged as a primary driving force. This shift prioritizes Intrinsically Sustainable Products, such as andalusite, which requires no high-temperature pre-processing. Additionally, Low-Carbon Enablers, including novel aggregates and advanced binder systems, reduce the carbon footprint of final products while improving dry-out safety and insulation. This paper reviews breakthroughs in alumina silicate, calcium aluminate, and zirconia raw materials applied across the refractory spectrum. It provides a roadmap for future developments, emphasizing how the synergy of expertise continues to modernize refractory technology for high-temperature industrial applications.

Keywords: Sustainability, Binders, Aggregates, Energy

1. Introduction

The refractory industry has seen a continuous evolution of raw materials—including aggregates, binders, and fillers—focused on enhancing both technical performance and cost-efficiency for bricks and monolithics[1]. This long-term development has been fundamental to the global success of refractories, driven by a strategic balance of "market pull" (specific industrial needs) and "technology push" (scientific breakthroughs). These advancements are frequently supported by academic-industry partnerships that bridge the gap between fundamental science and real-world industrial applications[2] and can be an essential catalyst. While the pursuit of improved durability and performance remains constant with cost/performance being primordial, the current landscape has shifted to include sustainability as a primary driving force. The key benefits are values shared throughout the value chain and the usage values can be expressed in terms of:

1. Lower greenhouse gas emissions and lower environmental footprints,
2. Lower material consumption/recycling, efficient energy. Though it has to be said this is something that the refractory industry is well versed in having embedded the principle of seeking higher performance and refractories which last longer in application which by definition reduces material consumption[1].
3. More effective use of energy. This raises the question of which technologies reduce greenhouse gas emissions most cost-effectively. To answer this, McKinsey developed the Marginal Abatement Cost Curve (MACC), which ranks emission-reduction strategies from lowest to highest cost[3]. The MACC illustrates that certain "low-hanging fruit," such as energy conservation through insulation, actually save more money over time than they cost to implement. In other words, saving energy can be more efficient than alternative forms of energy generation.

4. Reliable and safe refractories.
• Intrinsically Sustainable Products: Raw materials like andalusite, which require no high temperature pre-processing, contributing to lower greenhouse gas emissions.
• Low-Carbon Enablers with new aggregates and advanced binder systems which reduce the carbon footprint of final refractory products while simultaneously addressing performance limitations, such as enhancing safety through faster dry-out schedules or boosting insulation properties to conserve energy[4].

This paper reviews recent breakthroughs in alumina-silicate, calcium aluminate, and zirconia refractory compositions. We demonstrate how collaborative innovation modernizes high-temperature technology to support the energy transition, including two case studies on energy conservation and efficiency.

2. Enhancing Technical Performance

2.1 Intrinsically Sustainable

The most obvious example is Andalusite which has a remarkably low CO_2eq footprint of around 312 kg/CO_2eq[5] depending upon source and grade. This unique mineral provides a clear route to low-CO2eq refractory products due to its unique stature as a refractory raw material that does not require calcination before use. It has a wide range of usage values in targeted applications, and its intrinsic properties are difficult to copy through alternative formulation approaches with different aggregates. The key advantages lie in being able to deliver tunable properties through the specific mullitization reactions leading to designed microstructures for different applications coupled with a low CO2eq footprint.

In order to progress and reduce environmental footprints of other raw materials, progress around process innovation needs to be made. An example of this is the transition of combustion from carbon heavy fossil fuels to biomass, considered as carbon neutral, for the Mulcoa® alumino-silicate aggregates products. By late 2024, the switch successfully eliminated 50% of the emissions for Mulcoa® low-alumina (LG) products and 18% for Mulcoa high-alumina (HG) products. And total carbon footprints for these products have shifted significantly below the standard emission factors published by the World Refractory Association for calcined aluminosilicates. Imerys intends to continue this progression with Mulcoa® to achieve an 80% total avoidance of GHG emissions by 2030 compared to 2018 levels, aligning the plant with COP21 2°C climate trajectory commitments. A second example of process innovation to reduce intrinsic footprints through process innovation is the PRECIZE[6] project, a strategic initiative led by Imerys to decarbonize calcium aluminate cement (CAC) production by replacing fossil fuels with Hydrogen and opening the way to future carbon capture. Funded by France 2030, the initiative centers on the development of a new pilot-scale furnace technology utilizing oxy-hydrogen combustion. In 2025, a successful 12-days industrial trial demonstrated the switch to hydrogen-based combustion is technically viable with the product metrics showing equivalence to existing products and a post-mortem analysis revealed no refractory degradation. This project represents a world-first demonstration establishing foundational scaling laws for transitioning to full-scale industrial low-carbon manufacturing with the future option of carbon capture.

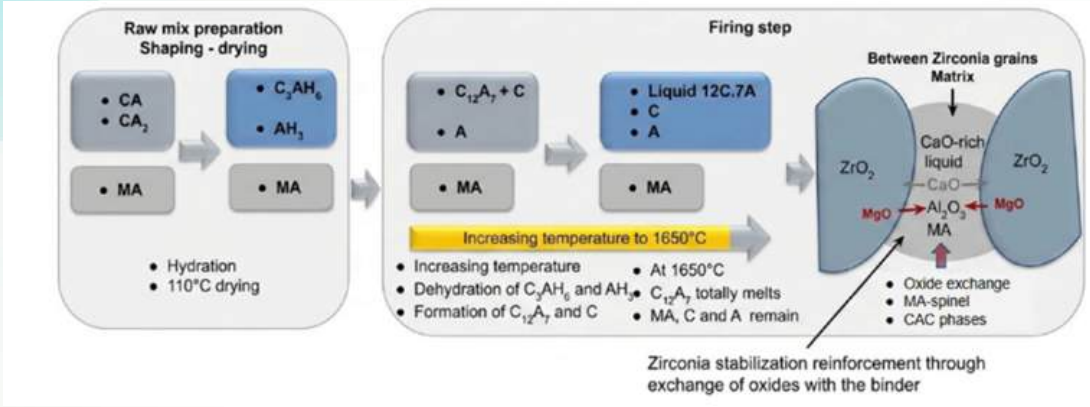
2.2 Low-Carbon Enablers

Raw materials serving as low-carbon enablers serve as a multifaceted solution to modern sustainability constraints, reducing raw material consumption with a lower environmental footprint through the usage chain, providing greater lifetimes, facilitating energy conservation through better insulation and enhancing reliability and safe use.

2.2.2 Multi-Mineral and Multi-Material

Developments have been at the core of newly launched products over many years. These are often as the result of upstream research programs. A recent example is in the field of Zirconia Refractories for flow control applications. A structured program anchored by a partnership between the Technical University of Freiberg and Imerys opens the way and marks a significant leap forward in optimizing refractory performance through advanced in-situ microstructural engineering. By exploring the powerful synergies between innovative binding systems and tailored zirconia aggregates, Imerys is developing a suite of high-performance solutions designed to extend component life and minimize catastrophic operational failures. Traditional monoclinic zirconia naturally suffers from disruptive phase changes during standard heating and cooling cycles, leading to volumetric fluctuations, micro-cracking, and premature component degradation. This development program addresses this operational bottleneck by delivering pre-stabilized solutions engineered to minimize destabilization. For flow control applications requiring minimal structural shifts under rigorous conditions, this innovation introduces high-calcia monoclinic formulations. This advanced grade yields an exceptional cubic phase content of up to 98.4% that remains uniquely stable after re-sintering and severe thermal cycling, delivering virtually hysteresis free expansion characteristics[7]. A novel finding of the project is the discovery of an active oxide-exchange mechanism between specialized binders (such as calcium aluminate spinel CMA 72) and fine zirconia grains within the matrix. During high-temperature operation at 1650°C, a migratory exchange occurs, providing localized, additional in-situ stabilization along grain boundaries and fine matrices. For customers, this means a boost in Thermal Shock Resistance (TSR). Systems configured with double-stabilized aggregates or high-calcia binders retain a superior residual flexural strength even after five brutal thermal shock cycles (950°C to room temperature), guaranteeing structural dependability when thermal gradients are steepest (Figure 1). In addition to resilience to thermal shocks, these compositions deliver exceptional resistance to highly aggressive continuous casting slags. The controlled interactions within the matrix prompt the controlled dissolution of zirconia grains followed by a protective precipitation of calcium zirconate ($CaZrO_3$) directly around the aggregates. This in-situ formed boundary layer acts as a physical shield, slowing down slag progression and preventing premature wear, allowing plants to maximize sequence times, maintain cleaner steel flow, and optimize total cost in use.

Figure 1: Mechanism between binder (CMA72) and Zirconia to enhance thermal shock resistance



2.2.3 Advanced Binder Systems

Refractory binders have evolved over the last 50 years along two axes of enabling new formulation logics to reduce CaO content in castables as well as alternative chemistries that mitigate the presence of CaO[8]. A new binder system for no cement castables (NCC) has been developed[9] which aims to reconcile the trade-offs that previously had to be made between installation simplicity, robustness, installed properties, whilst offering enhanced thermo-mechanical and corrosion resistance. The novel powder-based binder system for NCC represents a significant advancement in refractory technology, effectively addressing the limitations inherent in traditional colloidal silica-based binders. By replacing liquid chemical binders with a versatile powder solution, this technology enhances both operational efficiency and material performance. The system offers simplified logistics and ease of use, requiring only the addition of water on-site. This simplifies job-site logistics, eliminates sensitivity to freezing, and extends shelf life to 12–24 months. Furthermore, the system is efficient, requiring only a 5% dosage, which is significantly lower than the 9–10% typically required for sol-gel systems. One of the most problematic aspects of prior NCC formulations was the difficulty in controlling setting times under varying ambient temperatures.

Figure. 2: Hardening kinetics measured by ultrasonic velocity at 5°C

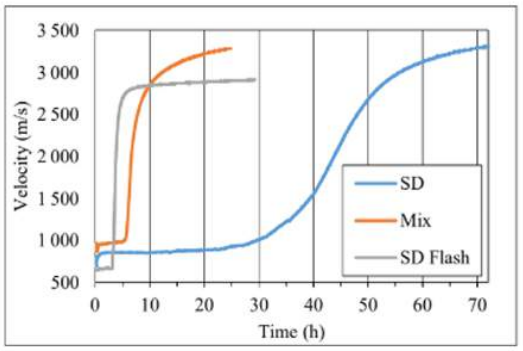
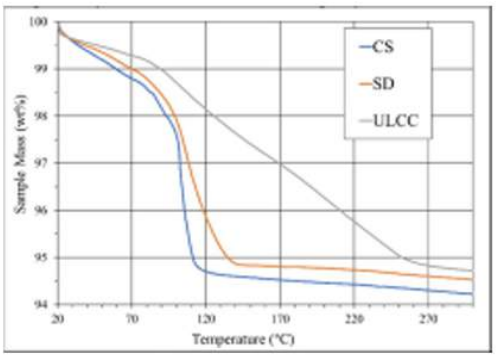


Figure 3: Thermogravimetric curves for 10x10x10 cm cubes at 50°C/h



This new system provides formulators with unprecedented flexibility with customizable fluidity and setting kinetics. The range includes a standard "SD" version tailored for normal to warm ambient temperatures, and a highly reactive "SD Flash" version engineered for fast setting in colder conditions. The binder hardens via an amorphous gel-formation process that effectively bridges solid particles together. Formulators can precisely blend the SD and SD Flash versions to adapt working and hardening kinetics for

specific application requirements or varying temperatures. For example, the SD binder alone provides an extended working time over 3 hours at 20°C, while a 50/50 mix drastically reduces hardening time. The system effectively mitigates low-temperature delays. Under 5°C conditions, the SD Flash binder achieves a rapid setting time of 6–8 hours, and a 50/50 mix allows for safe demolding in less than 24 hours (Figure 2). Dehydration of the gel-like bonding structure yields high air permeability in the critical 100–200°C temperature zone. This lets most of the free water escape safely below 200°C (Figure 3). By reducing internal pressure buildup, the system protects against explosive spalling and enables fast drying. Safety during drying is critical for refractory materials. This binder system achieves rapid drying capabilities and minimizes the risk of explosive spalling. Furthermore, unlike other types of 'gel' bonding castables that suffer from heavy micro-cracking and early shrinkage, this powder system retains a stable microstructure with minimal crack formation.

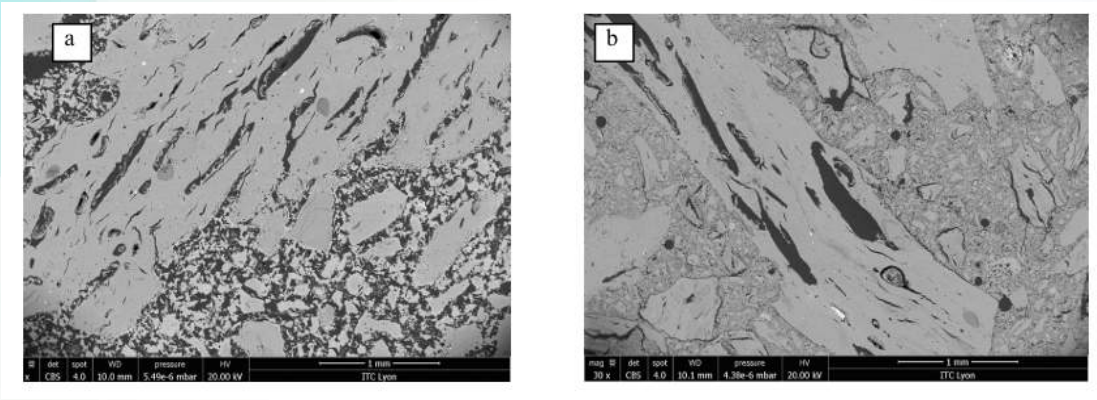
3. Energy Conservation and Efficiency

Two examples of improved energy conservation and efficiency relying on material developments are demonstrated.

3.1 Lightweight materials

Emerging new raw materials can deliver better mechanical performance at lower density and lower thermal conductivity and contribute to better energy conservation in thermal processes. One such example is a new, lightweight (LW) mullite-rich aggregate (43% Al_2O_3, 31% porosity) developed by Imerys and designed for high application temperatures. The primary goal is to optimize energy efficiency in high-temperature industrial furnaces by reducing thermal conductivity and density, a common challenge given the typically lower mechanical strength of lightweight materials[10]. As expected, due to higher aggregate porosity, lightweight castable formulations require significantly more water for casting compared to dense versions (60% aggregates). However, this can be mitigated using medium cement castable (MCC) formulation logic compared to regular conventional castable (RCC). An MCC LW composition achieves higher Cold Crushing Strength (CCS) than the RCC composition, despite similar density levels. This suggests that the dense matrix in the MCC formulation provides superior bonding and structural integrity. A high thermal stability is obtained for the lightweight aggregates, with deformation points (T0.5) exceeding 1250°C for the regular LW castable and increasing to 1370°C for the LW MCC. An SEM analysis shown in Figure 4 reveals that lightweight aggregates contain significant intragranular porosity. In MCC LW samples, this porosity is concentrated within the aggregates, while the surrounding matrix remains dense, contributing to the observed strength improvements. The research validates that Imerys's engineered lightweight mullite-rich aggregates are a robust, versatile solution for refractory applications. They effectively reduce both weight and thermal conductivity without sacrificing necessary structural stability. Thermal conductivity shows a 40% reduction with the incorporation of this aggregate. This adaptability allows for tailored lining solutions—ranging from back-lining insulation to semi insulating monolithics—that contribute directly to improved energy efficiency in high-temperature industrial processes.

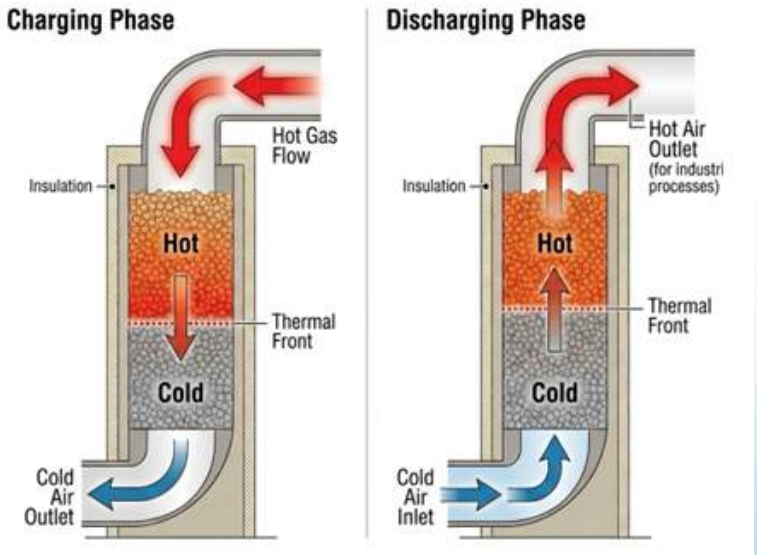
Fig. 4: Microstructure of RCC LW (a), MCC LW (b) after firing at 1300°C at a 30x magnification



3.2 Thermal Energy Storage systems (TES)

Industrial decarbonization is heavily constrained by the limitations of traditional alternative fuels; biofuels face availability limits, green hydrogen remains economically weak, and carbon capture operates effectively only at massive scales and significant cost. Consequently, the electrification of high-temperature processes stands as the core pillar of long-term sustainability strategy[11]. In parallel, the rapid growth of intermittent renewable energy sources, such as solar and wind power, has driven significant volatility in electricity pricing (can be below standard prices and event negative) and highlighted an urgent need for large-scale energy storage solutions. While chemical batteries (e.g., lithium-ion) excel at short-term grid stabilization, their capital expenditure and reliance on scarce materials limit their viability for massive, high-temperature industrial thermal applications. Capital expenditure for a material-based thermal storage system is estimated significantly lower than an electrical battery system (approx. 200 k€/MWh vs. 250–400 k€/MWh). High-temperature (TES) systems operating under a Power to-Heat framework are emerging to offer a cost-effective, sustainable alternative with perspectives of up to 200Wh/kg material capacities. By using engineered refractory solutions, industrial facilities can store low-cost off-peak electricity as heat and release it for processes like drying and calcination. The system operates through three distinct structural phases as shown in Figure 5.

Figure 5: Visualization of the Thermocline TES process (Charging and Discharging phases)



1. **Charging:** During periods when excess energy is available (such as off-peak electricity, solar collectors, or industrial waste heat), a transfer fluid (preferentially a gas like air in high temperature systems) passes through the storage medium to heat it and increase its temperature.

2. **Storage:** The heated material is kept within an insulated container to preserve its temperature and minimize external thermal losses for as long as possible.

3. **Discharging:** When energy is required by an application (e.g., an industrial drying or calcination process), the heat is extracted back out of the storage medium, subsequently lowering its temperature.

Multiple technologies and combinations are emerging with operating temperatures ranging from 600°C to more than 1200°C with a recent estimate from 2024 of $950M USD invested to date across start-ups[12] with a wide range of storage media considered. An order of magnitude estimate reveals that for 50MWh capacity 500t of minerals would be needed for a 200m3 volume. To guarantee system efficiency and operational longevity, selected storage media must meet rigid physical and thermodynamic criteria:

● Volumetric Energy Density: The primary criterion requires a high product of density multiplied by heat capacity to maximize energy storage within a minimal physical footprint.
● Cyclic Durability: Materials must withstand more than 10,000 thermal cycles without structural degradation or turning to dust, operating consistently across wide temperature bands (typically 600°C to 1200°C).
● Thermal Shock Resistance: The system experiences severe thermal gradients during rapid charging and discharging phases, necessitating exceptional resistance to cracking.
● Optimum Sizing: Precise geometries needed to minimize system pressure drops and manage mechanical stability under heavy thermal expansion loads.

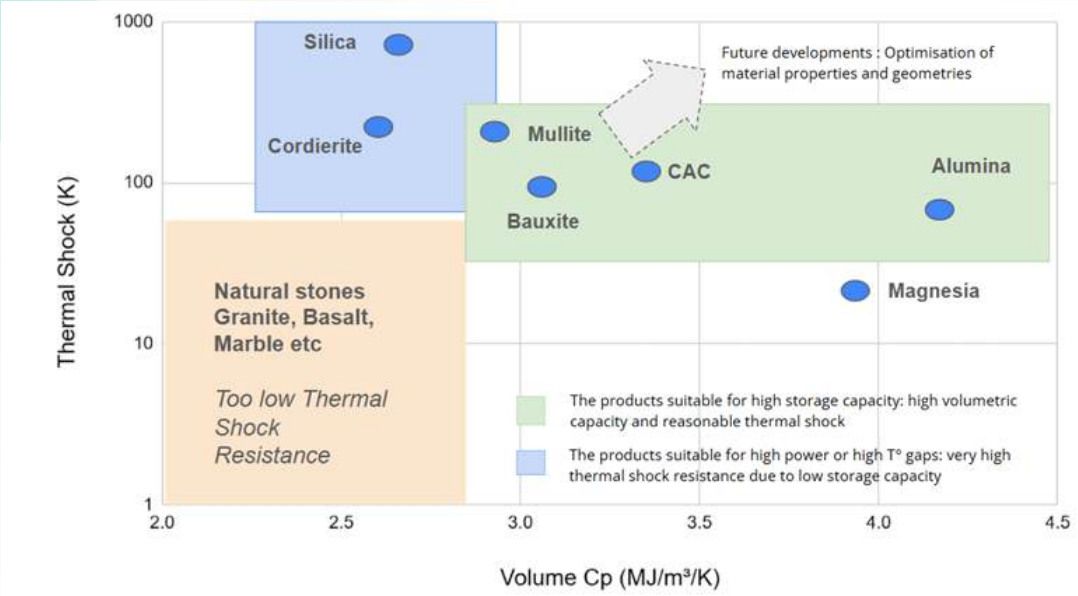
Imerys is pioneering the development using its wide minerals and materials portfolio coupled with advanced binder systems and would include reprocessed raw materials further reducing environmental impact. This approach yields specific advantages with controlled geometry and is intrinsically sustainable with a potential for high loading ratios of recycled materials, minimizing raw material carbon footprints while optimizing matrix density. To translate these fundamental material properties into true plant-level performance measuring system effectiveness, comprehensive thermodynamic modeling is required. A successful system must operate as a true thermocline (piston effect), where a sharp "heat wave" propagates through a storage column. Forced convection is the dominant heat transfer mechanism during active cycles, ensuring distinct separation between hot and cold zones, which is critical for maintaining system energy efficiency. During charging, a hot gas stream (typically air at 600°C) is forced down from the top. This creates a sharp thermal piston effect where the hot and cold boundaries remain distinct, maintaining a regular delivery temperature when discharging and an overall system energy efficiency over 90% (provided the storage volume is optimized relative to the wavelength of thermal exchange). Multi-scale simulations are used to evaluate both thermal and mechanical performance across the different operating phases. The simulations confirm that forced convection is the dominant heat transfer mechanism during active cycles, whereas solid-to-solid conduction and radiation drive the thermal dissipation shape only during standby phases. To maintain system yield, the storage must be operated avoiding uncompleted charge or discharge. Supported by these multi-scale numerical simulations, development of new materials and structures can progress rapidly.

Table 1: Generic Material Properties

Storage Medium	Operating temp. °C	Volumetric storage Capacity: kWh/m^3	Advantage	Challenges
Water / Hot Water	20–80°C	70	Ideal for low-temperature heating applications.	Limited in temperature capacity; requires massive volumes t
Storage Oil	150–300°C	90	Good for low-to-moderate industrial drying/process heat.	Utilization is in decline globally; limited temperature ceilings.
Molten Salts	300–565°C	150 - 200	Standard solution for concentrated solar power plants.	Severe corrosion of equipment, high safety risks,
Standard Minerals (Stone, sand, gravel)	20–600°C	100 - 150	Low cost; utilizes locally available materials or mining wastes.	Risk of "plugging" from dust/fines over time; limited performance
Engineered Refractory Minerals (Pellets or bricks)	20–1250°C	150 - 225	Excellent storage density. High durability (>10,000 cycles) and thermal shock resistance.	High processing & manufacturing costs; structural stability. Creep A challenge > 900°C.
Advanced Structured Materials (3D printed, Phase Change Materials)	> 1250°C	300–450	Storage density equivalent to chemical batteries. Employs custom geometries	High manufacturing cost; currently at lower Creep and dilatation risks.

Imerys leverages a wide mineral portfolio to match these demanding requirements, focusing on a balance of thermal performance, refractoriness, and cost-effectiveness. Several generic applications can be identified with candidate materials as shown in table 1. If higher temperature domains are considered, candidate refractory raw materials can be positioned by their thermal shock resistance and volumetric heat capacity as shown in Figure 6. Rather than relying on un-engineered raw materials like natural sand or basalt gravel—which have poor thermal utilization performance, the belief is that industry will pivot in the future to engineered refractory systems.

Figure 6: Material characteristics and suitability for TES



4. Future Trends and Conclusions

It is expected that multi-mineral/material developments will continue as application environments evolve. New materials and systems will be needed. This will in turn generate a focus on novel compositions as well as processing to yield refractory raw material grains with unique properties but also composites (e.g. gradients such as density through grains). Process innovations remain a key for reducing the carbon footprint of existing as well as future materials and future developments will integrate sustainability from the idea conception to value delivery. Academic partnerships can provide a catalyst to structured development programs injecting calibrated ideas for product development as the result of multi partner collaborative research programs. Development cycles will inevitably decrease, and fail-fast approaches can accelerate the process through rapid prototyping and customer evaluation in parallel with enhanced numerical simulation. The challenges of scaling can also be enhanced through simulation.

Looking forward, the continued modernization of refractory technology will depend on the robust synergy of academic-industry partnerships and the integration of digital material informatics. By leveraging enhanced numerical simulations and accelerated, fail-fast development cycles, the industry is well-positioned to deliver the next generation of high-performance, sustainable industrial solutions required for the global energy transition.

References

1. Historical Overview of Refractory Technology in the Steel Industry, K. Sugita, Nippon Steel Technical Report, 98 July 2008

2. Effective collaboration for the transfer of refractory basic science to real-life refractory applications, C. Parr, C. Wöhrmeyer, V. Pandolfelli, In-Ho Jung, D. Chudíková, Unitecr, Cancun, Mexico, 2025

3. Automating MACC generation, McKinsey.com

4 A. Gurtler, The insulation contribution to decarbonize industry, https://www.eiif.org/sites/default/files/2022 04/EiiF_Study_2021.pdf

5. Data-based carbon footprint of Imerys specialty minerals for refractories, S. Ranaivoharilala, N. Bunt, C. Wöhrmeyer UNITECR Chicago, USA, 2023

6. PRECIZE: A Novel Approach to Decarbonizing Specialty binders through Hydrogen Combustion, Bela Kumar, CAC conference, Lausanne, Switzerland, 2026

7. R. Soth, C. Wöhrmeyer, C. Parr, E. Frier, M. Lievin, R.M. Mineau, Optimization of Thermal Shock Resistance of Zirconia Refractories through Synergies between Zirconia and Refractory Binders, CIMTEC proceedings Italy 2026

8.Refractory raw materials for non-ferrous applications - Binders, C. Parr, C. Wöhrmeyer, S. Gradick, F. Lacoue, JM Auvray, Refractory Ceramics Division, St. Louis, 2026

9. Development of a novel powder-based binder system for the formulation of rapid-drying No-Cement Castables (NCC), F. Lacoue, E. Chabas, JM. Auvray, C. Wöhrmeyer, C. Parr, ICR 2026, Aachen, Germany 2026

10. Performance characteristics of refractory castables formulated with engineered lightweight mullite-rich aggregates, V. Germain, S. Graddick, C. Wöhrmeyer, ICR 2026, Aachen, Germany 2026

11. Electrification of Industry: Potential, Challenges and Outlook. M. Wei, C. McMillan, De la Rue du Can, S.Curr Sustainable Renewable Energy Rep 6, 140–148 (2019). https://doi.org/10.1007/s40518-019-00136-1

12. Innovation trends on high-temperature thermal energy storage to defossilize energy systems, AM Pantaleo, S.Trevisan, F. Matteucci, L.Cabez, Journal of Energy Storage, Volume 103, Part A, 1 December 2024, 114261

AI-DRIVEN REFRACTORY R&D: TURNING DATA INTO FASTER, SMARTER MATERIAL DEVELOPMENT

Annelouise van Dijke

RHI Magnesita GmbH, Digital Research & AI, Vienna, Austria

Corresponding author's e-mail: Annelouise.vandijke@rhimagnesita.com

Abstract

Refractory research and development (R&D) involves complex material systems and development cycles that can require extensive testing and validation. At the same time, R&D generates a growing amount of experimental, production and application data. This data is a valuable asset, but it is often spread across different systems and formats and can therefore be difficult to reuse. Artificial intelligence (AI) offers practical opportunities to improve access to existing knowledge, reduce repeated work and support faster, more informed material development. This paper presents an industrial perspective on two main applications: AI-enabled knowledge management and machine-learning-based property prediction. Knowledge tools can help researchers find and summarize relevant prior work, while predictive models can screen formulation options and focus experimental trials on the most promising candidates. Combined with expert knowledge and experimental validation, these approaches can shorten search time, reduce unnecessary trials and support better decisions across performance, cost, sustainability and raw-material availability.

Keywords: Artificial intelligence; Refractory R&D; Knowledge management; Property prediction.

Introduction

Refractory materials support high-temperature processes in steel, non-ferrous metals, cement, glass and lime production. Their development depends on composition, raw materials, processing conditions and the service environment. Because these factors interact, researchers often need to compare several formulation and testing options before selecting a suitable solution. A formulation that performs well in one application may behave differently when raw-material origin, production route, thermal history, atmosphere, slag chemistry or mechanical loading changes. As a result, material development involves many interacting variables, making it challenging to identify the most promising formulations efficiently.

At the same time, refractory R&D generates valuable data from laboratory tests, production, trials, application reports, post-mortem examinations and previous projects. However, this information is often distributed across regions, functions, languages and generations of information systems. A significant amount of this knowledge remains embedded in unstructured documents or in the experience of individual researchers. Improving access to this information can reduce repeated work, preserve expert knowledge and give researchers a stronger starting point for new developments.

AI offers practical opportunities to make better use of this knowledge and data. It can help researchers find relevant information more quickly, learn from previous work and identify promising directions for new developments. AI can also support property prediction and the screening of formulation options.[1,2] Used together with scientific expertise and experimental validation, these tools can support faster and more informed decisions, while researchers remain responsible for interpreting the evidence and defining the next steps.

This paper presents an industrial perspective

on how AI can support refractory R&D through two main applications: AI-enabled knowledge management and AI-driven material property prediction. It focuses on practical opportunities, implementation needs and limitations rather than reporting a single experimental study. The expected benefits are therefore discussed qualitatively, including improved knowledge reuse, shorter search time and more focused experimental work.

2. Challenges and opportunities for AI in refractory R&D

2.1 Challenges for applying AI in refractory R&D

AI has significant potential to support refractory R&D, but its successful application depends on understanding the characteristics of refractory materials and the available data.

First, refractory performance depends on more than chemical composition. Raw-material origin, impurities, particle-size distribution, processing conditions and the final application all influence the material's properties. As a result, formulations with similar compositions may perform differently in service, making it difficult to predict behaviour using composition alone.

Second, the available data varies in format, quality and level of detail. Some properties are measured routinely under standardized laboratory conditions, while others are only available for selected projects. Test methods and reporting practices may also differ between locations or change over time. In addition, unsuccessful or inconclusive trials are often poorly documented, even though they contain valuable information for future developments.

Third, industrial performance data is limited and often only becomes available after long service periods. Furthermore, performance cannot always be measured using a single objective parameter. For some customers, a refractory is considered successful if it reaches the required number of campaigns or service life, meaning that the outcome may only be recorded as sufficient or insufficient. In other cases, performance can only be evaluated relative to other products used under comparable operating conditions. Installation quality, operating conditions and maintenance practices also influence the result. These factors make it difficult to directly link laboratory measurements and material characteristics to in-service performance.

Finally, refractory development relies on experimental work that can require significant time, resources and coordination, particularly for pilot scale and industrial trials. AI therefore creates the greatest value when it helps researchers make better use of existing knowledge, identify the most promising formulations and select the most informative experiments.

2.2 Where AI creates value in R&D

The value of AI in refractory R&D should be measured by how well it supports researchers in their daily work rather than by the complexity of the underlying algorithms.

For knowledge management, AI can reduce the time needed to find relevant information, connect related work across projects and regions, and make previous experience easier to reuse. This helps preserve expert knowledge, reduces duplicated work and provides researchers with a stronger starting point for new developments.

For material innovation, AI can analyse historical data to identify relationships between formulation, processing and material properties. Predictive models can narrow the range of promising formulations, identify influential variables and focus experimental work on the candidates with the highest potential. Rather than replacing

experiments, AI helps ensure that available resources are used more efficiently.

The greatest benefit is achieved when knowledge management and property prediction are combined. Information retrieved from historical reports provides context for interpreting experimental data, while predictive models identify where additional data or experiments are needed. Together, these capabilities create a continuous learning process in which existing knowledge supports new developments and new results continuously improve the available knowledge base (Figure 1). At present, many of these benefits are assessed qualitatively. As the tools become more integrated into R&D workflows, their value can be measured through indicators such as time from a question to relevant evidence, reuse of previous work, duplicated trials identified before execution and the efficiency of experimental programmes.

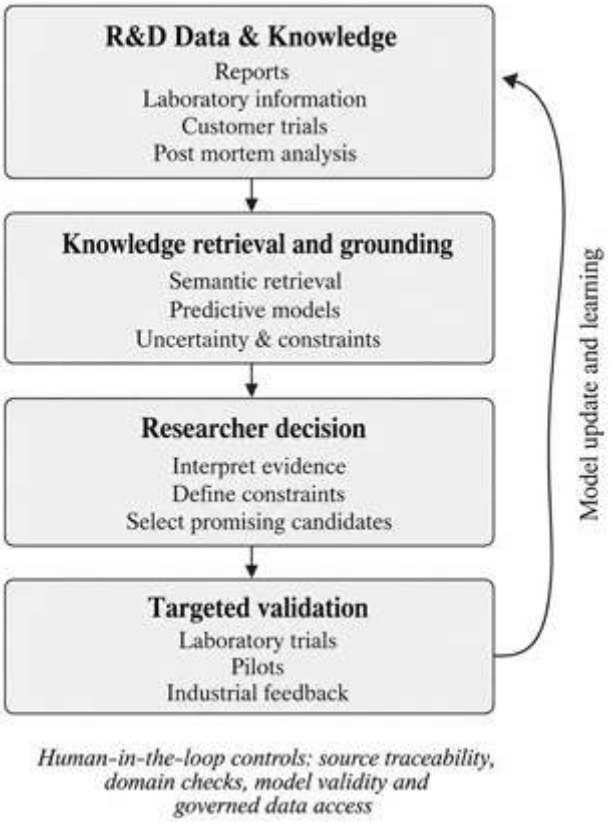


Figure 1 AI-supported refractory R&D loop linking knowledge reuse, prediction and targeted validation

3. AI-enabled knowledge management

3.1 From documents to actionable knowledge

One of the most immediate applications of AI in refractory R&D is improving access to existing knowledge. Conventional keyword searches are often limited because terminology differs between regions, languages, product generations and historical naming conventions. Semantic retrieval allows researchers to search using technical questions rather than exact keywords, making it easier to find relevant information across project reports, technical documents, patents, test summaries and other sources.

The retrieved information can be summarized and linked directly to the original documents, allowing IREFCON 2026 - Annelouise van Dijke 2 researchers to understand previous work while maintaining traceability to the source. This reduces search time, improves knowledge reuse and provides a stronger

starting point for technical investigations. From a technical perspective, documents are converted into machine-readable text and tagged with metadata such as material family, application, test method, project and date. AI then retrieves the most relevant passages and generates summaries or comparisons while preserving links to the original documents. Related work in materials science has shown how natural-language processing can turn unstructured literature into reusable datasets.[3]

For refractory R&D, the greatest value is practical rather than technical. The system makes relevant evidence easier to find, while researchers assess its relevance, limitations and technical implications. Better access to historical knowledge can support more consistent decisions, preserve valuable experience and reduce unnecessary repetition.

3.2 Knowledge reuse in R&D

The real value of AI is not simply finding documents, but helping researchers use existing knowledge more effectively. A researcher may start with a technical problem, a required property range, a raw-material restriction or the need for a lower cost alternative. AI can quickly retrieve similar projects, summarize previous approaches and highlight where they were successful or unsuccessful. Researchers can then review the original documents, combine this information with their own expertise and define the next steps.

This approach reduces dependence on personal networks while maintaining the contribution of experienced researchers. It also supports knowledge continuity when employees change roles or retire. Rather than presenting one definitive answer, AI can compare evidence from previous projects and help researchers understand why similar formulations performed differently under different conditions.

Beyond solving immediate technical questions, AI can support future innovation. By analysing historical knowledge across material families, applications and sustainability topics, it can identify trends, recurring challenges and underexplored areas for further investigation. These patterns provide prompts for scientific review and can help guide future R&D activities.

3.3 Building trust and adoption

For AI to become part of everyday R&D, researchers must be able to trust the information it provides. AI-generated answers should always remain linked to the original documents so that the underlying evidence can be reviewed. Where information is incomplete or uncertain, this should be clearly indicated. AI should support technical decisions, not replace scientific judgement.

It is equally important that existing access rights and confidentiality are maintained. Researchers should only be able to retrieve information they are authorized to access, while document versions, ownership and metadata should remain properly managed. Applying the FAIR principles - making information findable, accessible under appropriate conditions, interoperable and reusable - helps create a reliable and sustainable knowledge base for AI applications.[4]

Successful implementation also depends on how well AI fits into existing R&D workflows. Early applications should focus on well-defined use cases that provide clear value to researchers. User feedback can then be used to improve search quality, document organization and AI responses, creating a continuous learning process that increases both system performance and user confidence over time.

4. AI-driven property prediction and material innovation

4.1 Property prediction

The second main application of AI in refractory R&D is the prediction of material properties from formulation and processing data. Depending on the information available, models can use chemical composition, raw materials, particle-size distribution, binder content, processing conditions and test results to estimate a material property or the likelihood that a formulation will meet a defined requirement.

The main value of these models is their ability to support decisions on new formulations. To determine whether a model will be useful in practice, it should be tested on cases that were not used during its development, such as new products, different raw materials or previously unseen formulation families. This gives researchers a more realistic indication of how reliably the model can make predictions beyond the data on which it was trained.

The type of model should be selected according to the amount, quality and structure of the available data. For limited or heterogeneous industrial datasets, relatively simple and explainable approaches may be more suitable than highly complex models. Algorithms such as Random Forest, Gradient Boosting and XGBoost often provide a favourable balance between predictive accuracy, computational efficiency and the ability to explain which input variables influence the results. More complex deep-learning approaches may become advantageous when sufficiently large, consistent and high-quality datasets are available.

In addition to providing accurate predictions, the model should help researchers understand which formulation or processing factors have the greatest influence on the result. This can increase confidence in the prediction and support scientific interpretation, while expert judgement remains essential. The model should also indicate the level of confidence or uncertainty associated with each prediction. A result that clearly indicates uncertainty is more useful for decision-making than a precise-looking value that is not sufficiently supported by the available data.[5]

The practical benefit is virtual screening. Researchers can evaluate many candidate formulations computationally, eliminate those that are unlikely to meet the required criteria and focus experimental work on the most promising options. Rather than replacing laboratory work, AI helps make experimentation more targeted and efficient.

4.2 AI-supported formulation design

Property prediction models can also be used to work backwards from a desired performance target. Instead of asking "What properties will this formulation have?", researchers can ask "Which formulations are most likely to achieve the required properties?"

In practice, there is rarely a single optimum solution. A useful AI system should therefore propose a range of feasible candidates while making the trade-offs between different objectives visible. These objectives may include performance, cost, raw-material availability, recyclability, carbon footprint and manufacturing capability. For example, one formulation may provide the highest predicted corrosion resistance but depend on a scarce raw material, while another may offer slightly lower performance with better supply security and increased recycled content.

Any proposed formulation must remain technically realistic. AI-generated candidates should comply with formulation constraints, processing limitations and known material behaviour. Scientific and manufacturing knowledge is therefore needed to assess whether the proposed solutions are practical and suitable for further development.

4.3 Prioritizing experiments

One of the greatest opportunities for AI is helping researchers decide which experiment should be performed next. AI can identify candidates that are either most likely to meet the target or most likely to provide new information. This approach, often referred to as active learning, is particularly relevant when experiments require significant time and resources.[7]

AI can propose a prioritized list of experiments rather than an automatic decision. Researchers can then consider raw-material availability, laboratory capacity, project priorities and the value of reference formulations before selecting the final experimental plan.

The results of these experiments can be fed back into the model, allowing it to improve over time. Including both successful and unsuccessful trials helps expand the available knowledge and gradually improves prediction quality. The true value of this approach is not measured by model accuracy alone, but by its ability to reduce unnecessary trials, improve learning and support better R&D decisions.

4.4 Future opportunities

Recent advances in generative AI have demonstrated the ability to propose inorganic material candidates based on desired properties. MatterGen, for example, generates crystal structures under property constraints and illustrates the potential of generative approaches for inverse materials design.[7]

While these developments are highly relevant for materials science, they cannot yet be directly transferred to refractory development. Refractory materials are complex, multiphase systems whose performance depends not only on composition, but also on raw materials, processing conditions, microstructure and the service environment. In addition, industrial refractory datasets are generally smaller and more diverse than the datasets used to develop many advanced AI models.

For the foreseeable future, the greatest opportunity lies in hybrid approaches that combine AI with scientific expertise and experimental validation. AI can expand the range of candidates considered and structure the search process, while human judgement remains important for problem framing, interpretation, validation and final decision-making.

5. Integrating AI into the R&D workflow

5.1 Keeping the researcher at the centre

AI is most effective when it supports researchers. Researchers remain responsible for defining the problem, interpreting results and making the final technical decisions. AI provides access to knowledge, predicts material behaviour and helps prioritize experiments, but scientific expertise and experimental validation remain essential.

For AI to be trusted, the reasoning behind its recommendations should be transparent. IREFCON 2026 - Annelouise van Dijke 4 Knowledge-based answers should remain linked to the original documents, while prediction models should indicate how reliable their results are. Understanding why AI suggests a particular solution is often as important as the suggestion itself.

5.2 Building a strong data foundation

Reliable AI depends on reliable data. Experimental results, production data and application experience should be captured consistently and linked to the corresponding formulations, processing conditions and test methods. Well-structured and well documented data not only improve prediction quality but also make knowledge easier to retrieve and reuse.

Continuous feedback is equally important. Laboratory results, production trials and application experience should be used to improve both the knowledge base and prediction models. Although industrial performance data is often delayed, intermediate information such as production observations, installation feedback and post mortem examinations can already provide valuable insights.

Successful implementation is best achieved step by step. Many organizations start by improving access to historical knowledge, followed by property prediction and, finally, the integration of AI into broader R&D decision-making. This gradual approach allows researchers to build confidence while continuously improving both the available data and the AI models.

5.3 Adoption and measuring value

Successful AI adoption depends on trust, usability and close integration with existing R&D workflows. Researchers should be involved throughout the development process to ensure that AI tools address real technical challenges and fit naturally into the way R&D is carried out. Training should focus not only on how to use AI, but also on how to critically evaluate its recommendations.

The value of AI should be measured by its contribution to everyday R&D activities. Useful indicators include reduced search time, improved knowledge reuse, fewer duplicated experiments, more targeted experimental programmes and faster identification of promising formulations. As AI becomes more integrated into R&D, these improvements can also be measured through increased development efficiency and better informed technical decisions.

6. Outlook: Towards AI-supported R&D decision-making

As AI-enabled knowledge management and property prediction continue to evolve, they may become an integrated part of refractory R&D. Future systems could combine historical evidence, experimental data and predictive models to support decisions throughout the development process, rather than addressing each task in isolation. Looking ahead, AI could support researchers in balancing multiple objectives such as performance, cost, sustainability and raw-material availability. It could also help identify promising formulation opportunities, recommend the most valuable experiments and highlight where additional knowledge or data are needed. By bringing together information from different sources, AI can provide a broader view of complex R&D challenges and support more consistent decision-making.

Beyond individual development projects, AI also offers opportunities for more strategic R&D planning. Historical knowledge and newly generated data can be used to identify emerging trends, recurring opportunities for sustainability material challenges and technical substitution or improvements. This can help organizations connect short-term customer needs with longer-term innovation priorities and make better use of the knowledge already available. Ultimately, the success of AI in refractory R&D will depend less on the algorithms themselves and more on how well they are integrated into everyday R&D activities. Combined with high-quality data, scientific expertise and continuous experimental validation, AI has the potential to become a core capability that supports faster, smarter and more resilient material development.

7. Conclusions

Artificial intelligence offers practical opportunities to strengthen refractory R&D by making better use of existing knowledge and supporting more efficient material development. AI-enabled knowledge management helps researchers find and reuse previous work more effectively, while property prediction supports the identification of promising formulations and more targeted experimental programmes. Together, these approaches can reduce search time, avoid unnecessary trials and support faster, better-informed decision-making.

The successful application of AI in refractory R&D depends on more than the technology itself. Data quality, traceable sources, appropriate validation and scientific expertise all influence whether an AI output is useful. Researchers are also more likely to trust and adopt AI systems when they can understand the basis of a recommendation or prediction. Showing which formulation or processing factors have the greatest influence on a result can support scientific interpretation and increase confidence in the model. However, such explanations should complement, rather than replace, expert judgement and technical approval.

Looking ahead, AI has the potential to become an integral part of refractory R&D. By combining knowledge management, property prediction and continuous learning, it can help teams balance performance, cost, sustainability and raw-material availability while making experimental work more focused. Used in this way, AI can develop from a stand-alone digital tool into a practical R&D capability for faster, smarter and more resilient material development.

References

1. R. Batra, L. Song and R. Ramprasad: Nature Reviews Materials, Vol. 6, 2021, pp. 655-678.

2. K.T. Butler, D.W. Davies, H. Cartwright, O. Isayev and A. Walsh: Nature, Vol. 559, 2018, pp. 547-555.

3. E. Kim, K. Huang, A. Saunders, A. McCallum, G. Ceder and E. Olivetti: Chemistry of Materials, Vol. 29, 2017, pp. 9436-9444.

4. M.D. Wilkinson et al.: Scientific Data, Vol. 3, 2016, Article 160018.

5. N. Artrith, K.T. Butler, F.-X. Coudert, S. Han, O. Isayev, A. Jain and A. Walsh: Nature Chemistry, Vol. 13, 2021, pp. 505-508.

6. T. Lookman, P.V. Balachandran, D. Xue and R. Yuan: npj Computational Materials, Vol. 5, 2019, Article 21.

7. C. Zeni, R. Pinsler, D. Zügner et al.: Nature, Vol. 639, 2025, pp. 624-632.

STEEL MEETS REFRACTORY PLATFORM – CONCEPT AND EXPERIENCES

Andreas Buhr[1], Annika Mertke[2]

1. Almatis GmbH Frankfurt, Germany, 2. Salzgitter Flachstahl GmbH, Germany

andus.buhr@almatis.com

Abstract

The dialogue and networking between experts from the refractories and the steel industries is essential for successful development of new refractory concepts, products, and solutions. It becomes even more relevant with the upcoming challenges when transforming the carbon-intensive steel making process to carbon neutrality. New technologies in steel making require adjustments of refractories, and refractories have an influence on the process performance in multiple ways, both technically and economically. This paper discusses the long tradition of technical cooperation between the steel and refractories industries in Germany and how the new platform "Steel Meets Refractory" (SMR) continues this important technical exchange between experts of both industries.

1. Historical development

Refractories are fundamental for the steel making process as linings for furnaces and treatment and transport vessels. In many cases, they also fulfill a functional role by facilitating fundamental metallurgical operations, such as the use of bottom purging plugs in steel ladles. When looking back a couple of decades it becomes clear that the strategic role of refractories for steel making companies has undergone changes because of significant developments in the steel making technology such as the transfer from open heart furnaces to oxygen blowing converters, the continuous casting of steel, and the introduction of secondary metallurgy in the steel ladle.

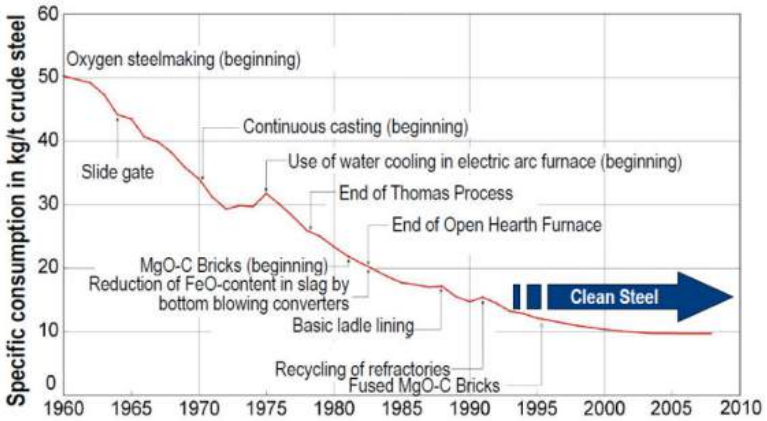


Figure 1 Specific refractory consumption in steel making and technology changes[1]

As a consequence, two major trends have become evident in the field of refractories. Firstly, significant progress has been achieved in reducing specific refractory consumption in steelmaking, from about 50 to less than 10 kg per tonne of steel (fig. 1), while simultaneously improving refractory performance and quality. Secondly, refractory materials have increasingly evolved from purely protective linings to functional components that facilitate metallurgical processes, such as gas purging through bottom plugs in steel ladles. In the 1960 and 1970s many steel companies had own refractory manufacturing plants or companies in order to secure supply and

consequently they also had dedicated refractory departments. The German Steel Association VDEh had a refractory committee, where refractory experts from the steel companies regularly met and discussed trends, technical challenges or experiences with testing refractories. The following topics were discussed and published just to give a few examples: Experiences with different brick materials for BOF lining[2]; Development of refractories testing to provide information on the suitability of refractories for industrial applications[3]; Wear characteristics of blast furnace runner mixes[4]; Trend of refractories in the European steel industry[5]; Refractory lining for steel ladles[6] .

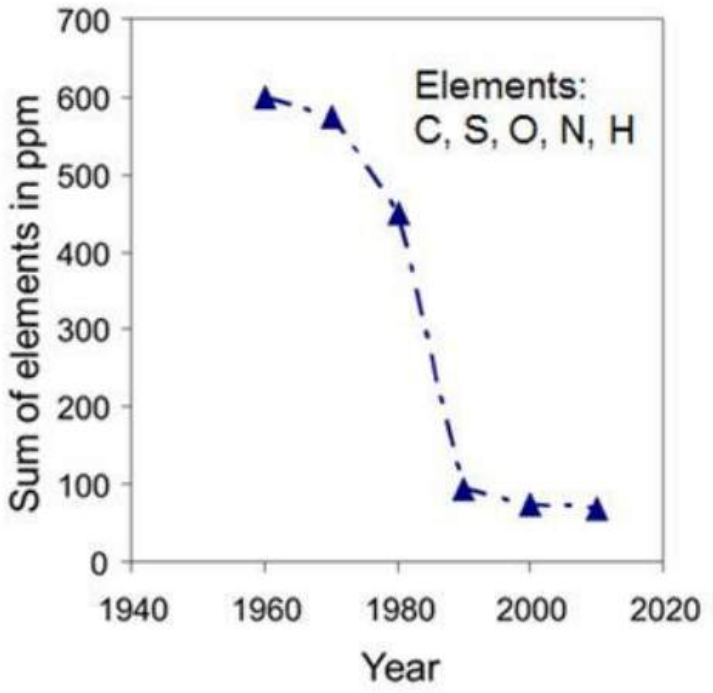


Figure 2 Achievable contents after secondary metallurgical treatment between 1960 and 2010[7]

Starting in the 1970s and then very intensively in the 1980s the above mentioned steel technology changes (fig. 2) led to the introduction and development of new refractories and a refocus of many steel companies on their core business and away from own refractory production. The significantly higher performance requirements for refractory products and the increasing complexity of refractory manufacturing technologies required companies focusing on that business. As a consequence, resources in the refractories departments in many steel works were reduced and some laboratories closed. This led to a situation, that a low participation and contribution of new results and developments was jeopardizing the future of the refractory committee of the German steel association. Therefore, it was decided in 1993 to include refractory suppliers as committee members. In the following years this proved a very successful approach to sustain and further develop this platform for technical exchange and networking between experts from both sides, suppliers and users of refractories for steel making. Examples for published output are papers on requirements on refractories for ladle metallurgy[8], refractories and raw materials situation for steel production in Europe[9], trends in clean steel technology and refractories engineering[10], and the committee´s perspective on various refractory products and requirements in steel applications[11] .

In 2017, VDEh decided to stop all technical committee work of the association including the refractories committee.

2. New platform “Steel meets Refractory”

The value of such technical exchange platform was very obvious to stake holders from the refractories and the steel industries. Although refractories are essential for the steel making process, they are often not very much in focus in the management of the entire steel making process. Refractories represent less than 2% of cost in the steel making process. And only very few engineers in the steel industry do have strictly refractories dedicated roles in their organizations.

Therefore it is important for those engineers being in charge of refractories having a network of technical experts also outside their organization. They can exchange experiences, get input and develop new ideas and approaches to address and solve technical challenges in the use of refractories in various applications. This can never be a “lonefighter-show” as the young Andus Buhr was told by his supervisor Manfred Koltermann right away when starting his career in the Dortmund steelworks in 1990.

Also for the engineers in the refractory industry it is very important having technically competent partners at their steel customers in order to develop a thorough understanding of specific requirements for improving existing and developing new refractory products and solutions. Refractories do influence the process costs in steel making beyond the cost for material and installation, e.g. through impact on the steel quality, yield in production, and energy saving or losses during the process.

These indirectly related refractory costs are higher than the direct ones and it can be both, economic gains or losses for the entire process (fig.3). This integrated approach to refractories is discussed in detail by Siebring et al.[12] and named “Value in Use” at Tata Steel IJmuiden.

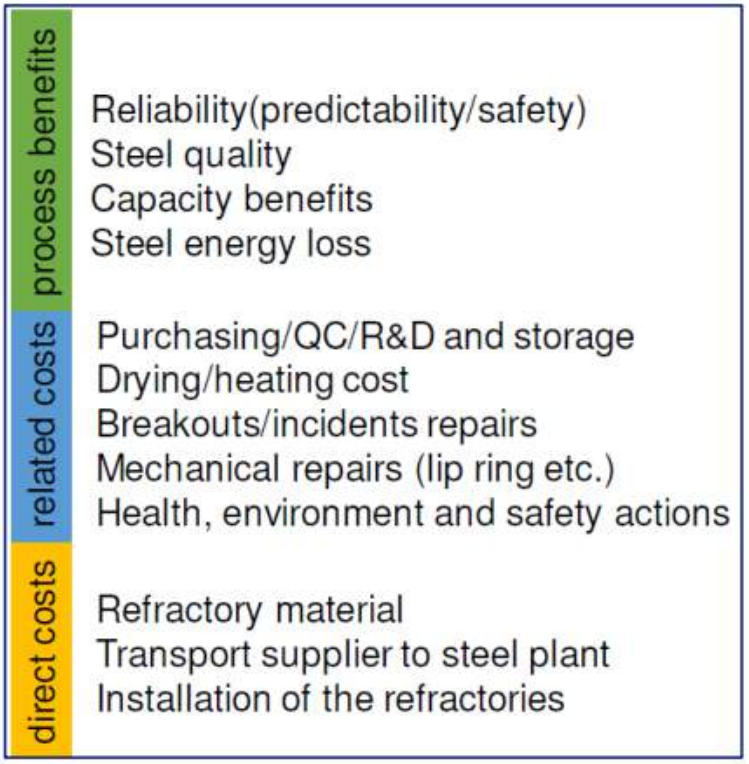


Figure 3 Direct refractory cost (~30%), refractory related cost (~30%) and the process benefits influencing the Value in Use (~40%) [12]

In 2018, activities were started by key stake holders from the refractories and steel industries in Germany for establishing a new platform for regular technical exchange. A considerable share of German refractory manufacturing is located in Rhineland-Palatinate. And the European Centre for Refractories (ECREF) in Höhr-Grenzhausen supports the interests of the German and European refractory manufacturers to sustainably strengthen the global position of the refractories industry with coordinated and networked measures and programs in education/training, research, and innovation.

Through an initiative of the network of refractories experts within the ECREF, the German Refractory Association (GRA) in cooperation with the Ministry of Economics of the Federal State RhinelandPalatinate have established in 2019 the "Steel Meets Refractory" meetings as industry dialogue format. At the first meeting, state secretary Daniela Schmitt highlighted the importance of dialogue and networking of experts in the value chain as an important factor for successful innovation and consequently investments, employment, and competitiveness. Therefore the Ministry is supporting the technical-scientific exchange between the steel and the refractories industries.

Under the patronage of the Ministry, the meetings take place twice a year in spring and autumn with invitations send from the GRA to selected technical experts from their member companies and the steel industry in Germany, Austria, and the Netherlands. Compliance is assured through a representative from the Ministry and a lawyer being present through the entire event and highlighting the guidelines at the start.

The following general thematic areas are covered in the meetings: 1) environmental, health, and safety (e.g. classification of refractory products), 2) specific actual technical problems and challenges (e.g. recycling of refractory products), 3) innovation (e.g. digitalisation in refractories management).

3. Experiences

3.1 Meeting format

So far, twelve meetings took place. The first one in August 2019 and prior to the Corona pandemic with physical presence in Koblenz and including a plant visit to GRA member Steuler-KCH GmbH at their plant in Höhr-Grenzhausen on the second day of meeting. The following three meetings were online events. Since 2022, the meeting takes place physically twice a year. The first meeting in spring time including a plant visit to a refractories producer or a steelworks (fig. 4), and the second one in autumn in Aachen on the day prior to the International Conference on Refractories. That helps to attract steel people joining the refractories conference after the SMR meeting.

Participation is around 50 technical experts at each event with about 40% coming from the steel industry. We have typically two to three topics for the meeting and for one of them we do a teamwork session to foster exchange and learning amongst the participants. For that, the group is split up in smaller teams so that everybody is getting actively involved. Such teamwork sessions were also successfully used to prepare the panel discussions at UNITECR 2023. Three months prior to SMR, the chairmen have separate preparation online calls with the steel and the refractory participants to organize the agenda and presentations for the meeting. In the following some examples of topics from SMR will be briefly discussed.



Figure 4 SMR meeting at Salzgitter Flachstahl GmbH Germany

3.2 Green Deal and CO_2 reduction

Global climate protection and reduction of CO_2- emissions is a key challenge for energy intensive industries such as steel and refractories. The European Green Deal as decided by the European Commission means a CO_2-reduction by 55% in 2030 (when compared to 1990) and climate neutrality by 2050. An overview of steel production in Germany and Europe in relation to the climate targets and a review of coking coal production in Germany with regard to globalisation and decarbonization were given in the first meeting.

The roadmaps of seven steel companies towards carbon neutrality were briefly presented in the third meeting. Iron ore reduction with coal is inherently the major contributor of CO_2 emission in steel making. Replacing carbon by green hydrogen produced with renewable energy is therefore key element in all concepts towards carbon neutrality (fig. 5). With a share of about 60% of iron ore based steel manufacturing in EU 28 (incl. UK), the magnitude of transformation required in Europe is obvious.

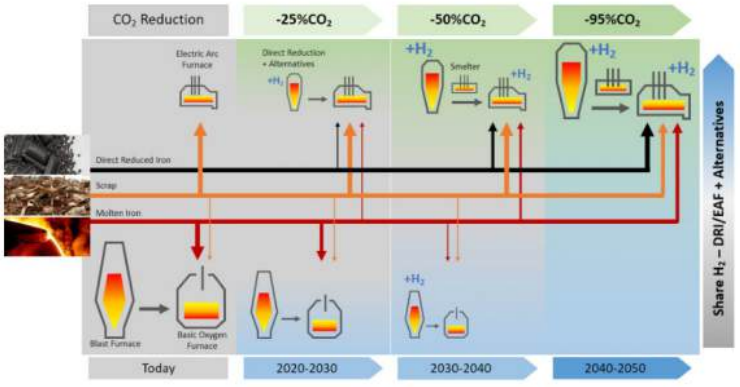


Figure 5 Transformation from carbon to hydrogen based steel production[13]

Although the concepts of steel companies show some differences in the technical approaches, they have one thing in common: these technology changes will have an influence on processing conditions and consequently on the refractory linings. Direct reduction processes of iron ore are applied already since decades but their share in

overall steel production was rather small so far. This will change dramatically in the future. Research is needed e.g. on the stability of refractories in hydrogen containing atmosphere and extended investigations were started[14,15]. Replacement of blast furnace by DRI converter and EAF will also require changes in secondary metallurgy and potential changes in steel ladle lining[16] .

Refractories have an influence on the energy efficiency of steel making processes. Refractory materials with higher carbon content (including graphite) as refractory linings in the steel ladle side wall result in 10-20K higher temperature losses of the steel when compared to carbon-free linings. The cost for such temperature losses are in the range of the refractory lining cost of the steel ladle[10] .

Another example was presented by Johan Richaud from Vesuvius regarding refractory applications in continuous casting, concluding that it is important to consider this process impact of refractories when performing life cycle analyses and not just the carbon footprint of a specific refractory product.

3.3 Sustainability and recycling

Sustainability, circular economy and recycling of materials in order to secure and protect natural resources is another important element of the Green Deal. While steel can be considered a benchmark with regard to recycling, refractories recycling is so far only applied to some extent and not comparable with the level achieved in steel. One example are used BOF or EAF bricks being reworked into steel ladle bricks. It was presented and discussed in two meetings, that regional value chains are essential for an economically successful approach to recycling. Besides close cooperation and trust between the business partners, also short supply chains are mandatory because long distance or intercontinental transport would erase all ecological gains and economic competitiveness from recycling.

This aspect was also discussed by Helge Jansen during his keynote lecture “Sustainable refractory concepts made in Germany” at the ICR in Aachen 2021. If refractory recycling shall be extended in the steel industry, sustainability must become an additional factor when designing refractory linings.

Antioxidants (AOX) in carbon-bonded bricks are a challenge for recycling because hydraulic phases such as aluminium carbide are formed during use at high temperature. Recently a literature research study on pros and cons of AOX was initiated by the German refractories research association FGF, which was triggered through discussion at SMR. It is sponsored by partners from the steel and the refractory industries.

3.4 Refractories classification and digitalisation

The classification and labelling of refractory products and what is legally required versus the expectations for product information from the end users was intensively discussed during the autumn 2020 meeting. It became clear, that a mutual approach between suppliers and users of refractories might provide a better solution than only relying on legislation here, which in cases creates an enormous administrative effort without providing real value to the customer concerned. This was also discussed by Liefhebber et al.[17] .

The World Refractories Association WRA has a task force for developing a refractory exchange data standard[18]. The main goal is to define and standardise data sets to exchange relevant data with customers and also to approach a higher level of automation in exchange. The intend is not the exchange of sensitive or confidential data of refractory suppliers, their customers and/or collaborating OEMs. During the discussion in SMR, the steel participants confirmed the relevance of this project because in the current situation too much administrative work is required by transferring relevant

information (regarding the material itself but also logistics etc.) manually into ERP systems of the steel works. Steel engineers confirmed their openness to collaboration for developing this standard and provided qualified feedback along the process. A first digital version shall be tested soon.

4. Conclusion / outlook

The "Steel Meets Refractory" platform has proven its value in the past eight years. The brief example of topics addressed in this paper shows the complexity of refractory business in the steel making process and which challenges the industry is facing already in the near future. The know how transfer in industrial practice and on the shop floor of the plants is the focus of our next meeting. The raw material situation and a refocus on regional supply chains is another area which will be addressed in future. Successful solutions will require a close cooperation between suppliers and customers of refractories and a mutual effort of the entire industry. The dialogue and networking between experts in the industry plays an essential role in this long term journey.

Acknowledgement

In the name of all participants, the authors express their gratefulness to the Ministry of Economics in the state of Rhineland-Palatinate for supporting "Steel Meets Refractory" and Thomas Kaczmarek with the German Refractory Association for organising the events.

References

1. Statistisches Jahrbuch der Stahlindustrie, www.stahl-online.de.

2. M. Hater, R. Klages, M. Koltermann, R. Schrott: Erfahrungen mit verschiedenen Steinmaterialien bei der Ausmauerung von „LD-AC" Konvertern, stahl und eisen 90 (1970), no. 26, 1510-1515.

3. H. Schäfer, M. Koltermann: Stand, Entwicklungsrichtungen und betriebliche Aussagefähigkeit der Prüftechnik feuerfester Stoffe, stahl und eisen 94 (1974), no. 15, 657-664.

4. K.R. Hüsig, M. Koltermann: Ergebnisse von Untersuchungen des Verschleißverhaltens von Hochofenrinnenmassen mit einer halbtechnischen Versuchsanlage, stahl und eisen 97 (1977), no. 1, 23-28.

5. M. Koltermann: Refractories from the European viewpoint – development and trend of refractories in the steel industry, Proceedings of the 1st International Conference on Refractories, Nov. 15-18, 1983, Tokyo, Japan, 63-83.

6. G. Klages, H.-D. Köhlau, M. Koltermann, H. Sperl: State of the art of refractory linings for steel ladles in Germany, Proc. UNITECR´89, Anaheim CA, Nov. 1- 4, 1989, 576-585.

7. R. Fandrich, B. Kleimt, H. Liebig, T. Pieper, F. Treppschuh, W. Urban: Stand der Pfannenmetallurgie und aktuelle Trends (Status of secondary metallurgy and present trends), stahl und eisen 131 (2011) no. 6/7, 75-89.

8. N. Bannenberg, A. Buhr: Anforderungen an das Feuerfestmaterial in der Pfannenmetallurgie, stahl und eisen 118 (1998), no. 10, 83-87.

9. J. Pischke, A. Baaske, D. Dübers, R. Fandrich, P. Quirmbach, L. Schöttler: Current situation of refractories and their raw materials for steel production in Europe, ICR Aachen 19-20 Sep. 2012, presentation at the dedicated raw materials session.

10. A. Buhr, R. Bruckhaus, R. Fandrich: The steel industry in Germany – Trends in clean steel technology and refractory engineering, UNITECR´15 keynote lecture published in Refractories Worldforum 8 (2016), no. 1, 57-63.

11. A. Baaske, R. Fandrich, J. Pischke, P. Quirmbach, J. Rzepczyk, L. Schöttler: Refractory Products – the TC Refractories Perspective, Refractories Worldforum 9, no. 2 (2017), 15-23.

12. R. Siebring, S. Sinnema, W. Tesselaar, "Bridging the gap between refractory supplier and the refractory user in the steel plant - Real Value in Use, Refractories Worldforum 9 (2017), no. 3, 71-75.

13. L. Rebouillat, CESAREF project proposal, Nov. 2021.

14. A. Razavi, I. Henn, A. Sax, P. Quirmbach: XRT evaluation of microstructure weakening by hydrogen attack on Al2O3-SiO2 refractories, Int. J. Ceramic Eng. Sci. 2024, https://doi.org/10.1002/ces2.10211

15. S. Kuiper, S. Klaus, D. Schmidtmeier, A. Buhr, I. Henn, J. Dutton: Hydrogen resistance of refractories based on synthetic alumina raw materials, UNITECR 2025, Cancun, Mexico, pp. 602-605.

16. M. Peekel, A.G. Gil: Brown field change to green steelmaking, IREFCON 2024, Goa, India, pp. 12-17.

17. J. Liefhebber, R. Siebring, H. Hoek, N. Mustacevic, "Impact of health and safety regulations on refractories buying and selection at Tata Steel IJmuiden", ICR Aachen Sep 29-30, 2021, 31-34.

18. A. Platzer, B. Barros, WRA: A new standard from WRA for digital exchange of refractories data, UNITECR 2023, Frankfurt, Germany, pp. 654-657.

INDUSTRIAL EXPERIENCE AND EMERGING CHALLENGES IN EAF MELTING OF GAS-BASED, COAL-BASED AND HYDROGEN-BASED DRI

Felix Firsbach, Jens Apfel, Andrea Pezza, Per Lückhoff and Keno Sparrenborg

Badische Stahl-Engineering GmbH, Kehl, Germany

Corresponding author's e-mail: felix.firsbach@bse-kehl.de

Abstract

Gas-based and coal-based direct reduced iron (DRI) provide extensive industrial experience for electric arc furnace (EAF) operation, while hydrogen-based DRI is intended for future low-carbon steelmaking. The three products are not interchangeable. Their carbon, metallization, gangue, temperature, fines, and handling properties define different energy, slag, and refractory regimes. Published results are compared with anonymized Badische EAF benchmark data and an illustrative slag mass balance. Gas-based DRI is the mature reference for high-DRI flat-bath operation. Coal-based DRI accounts for roughly one-third of global DRI and is concentrated in India. H_2-DRI may provide high metallization but essentially no intrinsic carbon. Its use therefore requires revised carbon-oxygen control, advanced slag design and control, and verification of refractory exposure.

Keywords: direct reduced iron, electric arc furnace, hydrogen, refractory

1. Introduction

The transition from blast-furnace ironmaking to direct reduction and electric steelmaking is often described as the substitution of one iron unit by another: BF-grade pellets, sinter and lump ore by DRI and scrap. For EAF operations, this view is incomplete because there is no generally valid "DRI". Direct reduction does not remove a liquid slag; residual oxide, pellet gangue and additives enter the EAF together with metallic iron. The reduction route also changes product carbon, porosity, fines generation, temperature and handling. These variables determine the electrical and chemical energy balance, slag mass and composition, metal yield, feeding limit and refractory exposure [16].

Natural-gas shaft-furnace and coal-based rotary-kiln DRI provide the present industrial experience. According to Midrex [15], global DRI production reached 140.8 Mt in 2024, of which 65.7% was natural-gas-based and 34.3% coal-based. India produced 54.7 Mt, comprising 45.5 Mt coal-based and 9.4 Mt gas-based DRI; consequently, about 94% of global coal-based DRI originated in India (Figure 1). This scale makes Indian operating experience central to any assessment of DRI melting. Hydrogen reduction is intended to remove fossil carbon from ironmaking, but H_2-DRI is not simply gas-based DRI with a lower upstream emission factor. This paper separates industrially demonstrated behavior, engineering consequences expected for H_2-DRI, and unresolved research topics.

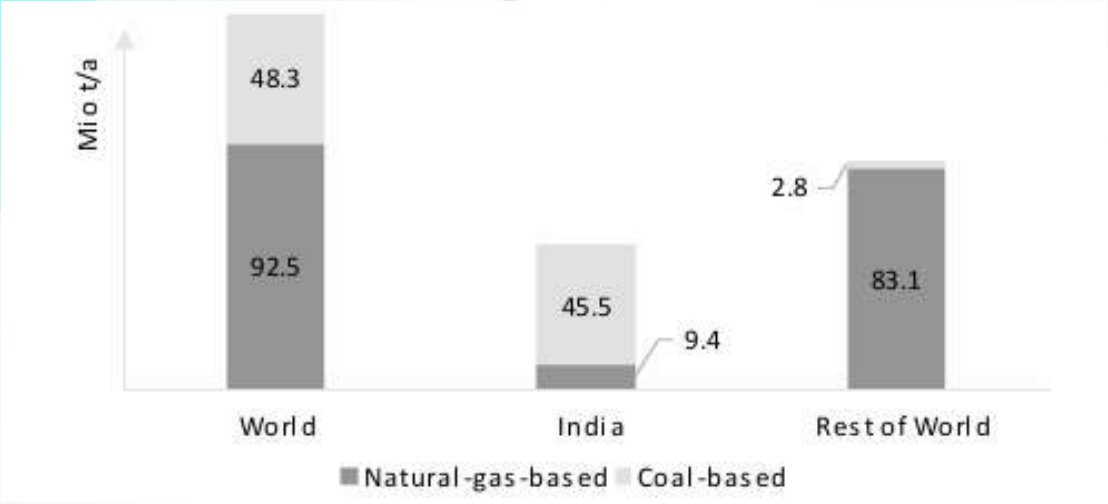


Figure 1 Global and Indian DRI production by reductant in 2024. Values in Mio tonnes per year and calculated from Midrex World Direct Reduction Statistics 2024 [15]

2. Present industrial experience

The useful descriptors for an DRI in EAF operation are metallization, total iron, carbon, acidic and basic gangue, phosphorus, sulphur, particle-size distribution, apparent density and charging temperature. The route label is only a first classification. Publications about gas-based DRI already show substantial variation, and coal based products can vary even more because ore, coal, ash separation and kiln operation interact [1,2,14]. The EAF process, furnace design, and refractory concept must therefore be designed around a DRI quality envelope rather than a nominal DRI percentage.

Product carbon can reduce residual FeO, transfer carbon to the bath, generate CO for slag foaming, and contribute chemical energy after oxidation. Metallization determines the amount of residual iron oxide that must be reduced or lost to slag. Gangue remains decisive even at high metallization because SiO_2 and Al_2O_3 require flux, increase the mass to be heated, and alter MgO saturation and slag viscosity. Physical quality links the direct reduction plant and meltshop: intact pellets can penetrate slag and reach the bath, whereas fines may oxidize, remain in the slag or leave during slag-off [2,3,10,13].

2.1. Gas-based DRI as the reference case

High-DRI EAF operation is normally based on continuous charging through the roof into a liquid heel. The furnace remains in flat-bath operation for a large share of the heat; active power, feed rate, bath superheat, oxygen and carbon additions must remain balanced. The Badische global benchmark (Figure 2 and Figure 3) shows that electrical energy cannot be described by DRI percentage alone: selected industrial cases between about 35% and 98% DRI/HBI span roughly 300-570 kWh/t liquid steel, including a spread of more than 100 kWh/t at similar DRI shares [11]. Feed temperature, product carbon, metallization, gangue, transformer loading, hot heel, and process design explain much of this scatter. Published ranges remain useful as external context but should not be interpreted as universal DRI penalties [2,16].

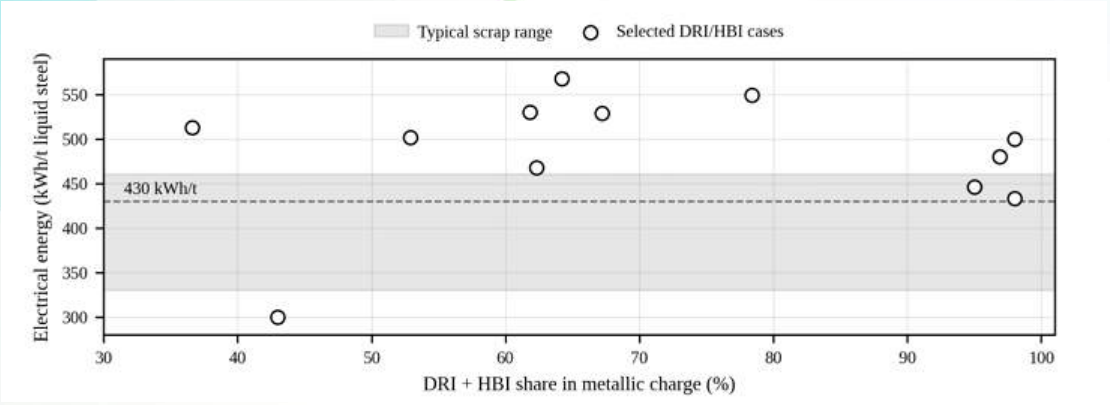


Figure 2 Electrical energy versus DRI/HBI share in selected industrial EAF data. Source: Badische Global EAF Benchmark "Best Practice", anonymized internal data [11]

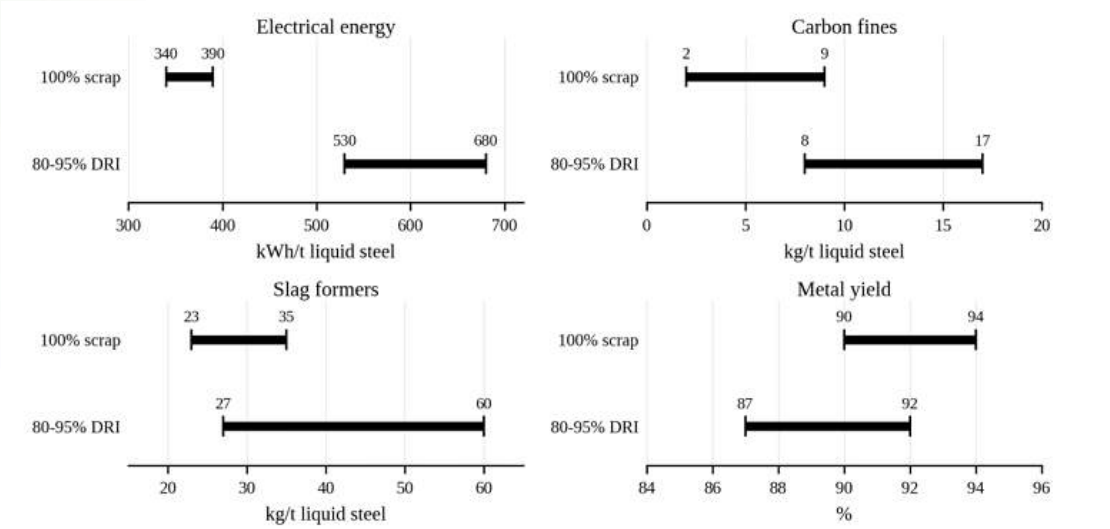


Figure 3 EAF consumption comparison of scrap-based furnaces versus 80-95% DRI share furnaces in selected industrial EAF data. Source: Badische Global EAF Benchmark "Best Practice", anonymized internal data [11]

2.2. Coal-based DRI as current industrial experience

Coal-based DRI is an established alternative iron source. Conventional rotary-kiln products commonly require cooling and magnetic separation from residual coal, char, ash, and desulphurizing additions. Dutta and Sah [1] identify low product carbon, lower productivity, higher reduction-plant energy consumption and the absence of hot feeding to EAF or hot briquetting as characteristic disadvantages. Gordon [14] describes the same route as strongly dependent on ore, coal and kiln practice.

For the EAF, coal-based DRI has the tendency to combine low product carbon with wider variability in metallization, gangue, fines and residual char or ash. Lower metallization increases the FeO load of DRI; additional gangue requires more flux and slag heating; fines can remain in foamy slag and leave during slag-off. Industrial DRI experience has addressed these losses through upstream screening, briquetting or controlled pre melting of fines [13]. Coal-based operation therefore provides a useful warning for H_2-DRI, but not a direct analogue: well-beneficiated H_2-DRI may have high metallization and low sulphur even though it contains no carbon.

3. Process implications for DRI utilization in EAF

3.1. Energy demand is the main KPI for EAF productivity control

The energy input changes depending on the DRI property. Figure 4 compiles source-specific sensitivity estimates: higher acid gangue increases energy demand, whereas higher metallization, carbon, and charging temperature reduce it. These estimates are useful engineering orders of magnitude, but their transferability to H_2-DRI and the sign-normalized representation require industrial confirmation. Without DRI carbon, electrical power and feed temperature gain importance, and oxygen use must be coupled to an external, controllable carbon source or to an alternative slag practice.

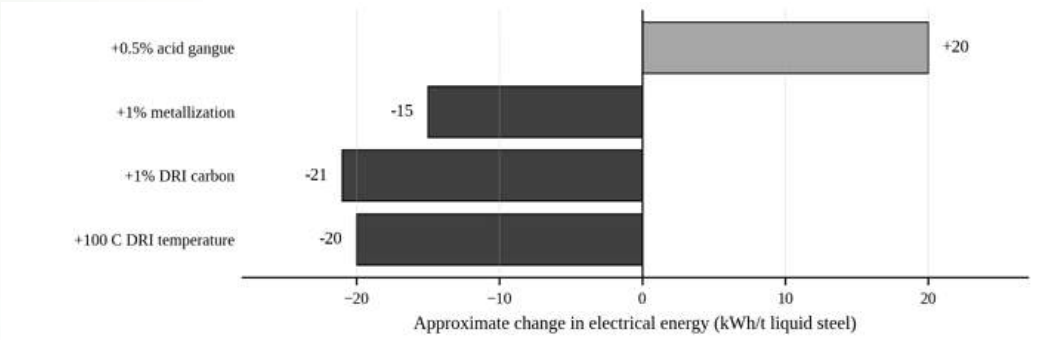


Figure 4 Source-specific estimates of DRI-quality effects on EAF electrical energy; signs normalized to show the effect of increasing each listed parameter.

3.2. DRI quality and influence on refractory and slag design

Carbon is not only a raw material but also a control lever for the EAF operation. DRI carbon can reduce residual FeO, transfer carbon to the bath, generate CO for slag foaming, and contribute chemical energy after oxidation [4-6]. However, the refractory-relevant consequence of DRI quality is often the oxide burden. Poor DRI quality creates a coupled compromise: high gangue and low metallization increase oxide input; maintaining B_2 = 2.0 2.2 requires more quicklime and dolime; the resulting slag can approach 400 kg/t; lowering B_2 to 1.6-1.8 reduces flux and slag mass; and the large liquid slag volume can already provide physical arc coverage reducing the demand for injection carbon. Nevertheless, lower basicity and reduced carbon injection can leave a high FeO, MgO-undersaturated slag that is more corrosive to MgO-C refractories. The relevant control variable is therefore not merely slag height, but the time-dependent combination of basicity, FeO, dissolved MgO, temperature and flow. Figure 5 demonstrates why high SiO_2 input can drive slag quantities toward 400 kg/t at different binary basicities [2,16-19].

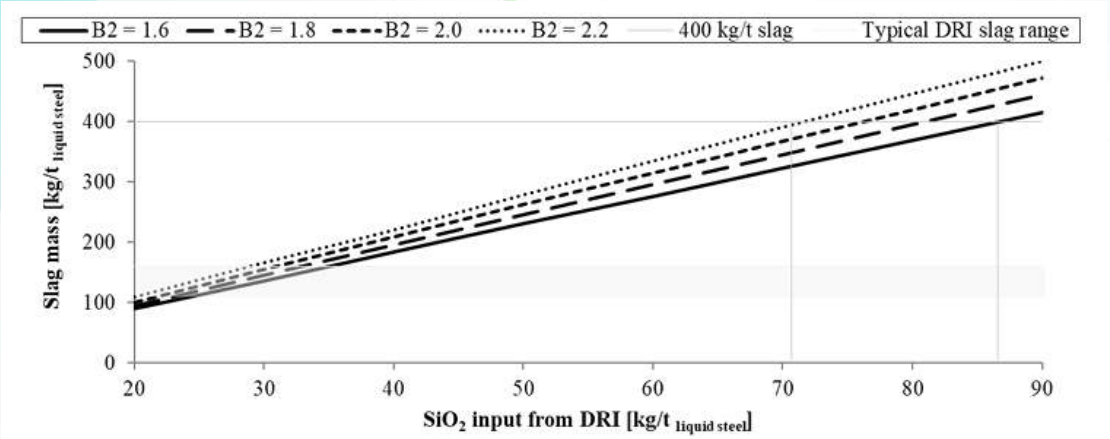


Figure 5 Illustrative influence of SiO_2 input and target binary basicity on slag mass. Assumptions: Al_2O_3 = 25% of SiO_2 input, final slag = 30% FeO and 8% MgO. Calculation by the authors, based on the mass-balance approach discussed in Firsbach et al. [16]

The amount of MgO charged is also insufficient as a design criterion. Dissolution studies on dolomite-, limestone- and dolime-based additions show that calcination condition and material properties determine whether CaO and MgO become available within the short EAF process time [18,19]. For high-DRI operation, early MgO availability is critical because the most aggressive refractory exposure may occur during continuous feeding, before the final slag sample is taken. Refractory zoning should therefore distinguish hearth and banks exposed to local cooling and accretions, the slag line exposed to FeO and undersaturation, the slag door and breast exposed to sustained overflow, and sidewalls exposed to altered slag height and arc coverage.

3.3. Refractory operating window for low-quality DRI

Three operating strategies can be distinguished when poor DRI quality generates a very high oxide burden. Maintaining conventional basicity protects the chemical slag concept but maximizes flux and slag mass. Reducing basicity lowers slag volume but increases the need for rapid MgO dissolution provided by flux and strict FeO control. Reducing injection carbon solely because the slag already covers the arcs is unsafe: at 30% FeO, an additional 280 kg/t slag contains 84 kg FeO/t, equivalent to approximately 65 kg Fe/t or 6.5 percentage points of metallic yield potential. The carbon strategy must therefore be separated into its functions of FeO reduction, bath carburization, chemical energy and physical foaming [16-19].

Table 1 summarizes the resulting refractory trade-off. The numerical ranges are an engineering scenario for review, not a universal plant specification. They should be replaced or confirmed with the final Badische mass balance and benchmark dataset [11] before submission.

Table 1 Engineering scenarios for the slag-volume/basicity/refractory trade-off with low-quality DRI. Ranges for author review; framework based on Firsbach et al. and MgO-source dissolution studies [16-19]

Scenario	Slag rate	B2	FeO tendency	Carbon approach	Primary refractory concern
Good-quality DRI	120-160 kg/t	2.0-2.2	Controlled	Normal FeO control and foaming	Conventional slag-line exposure
Poor DRI, full basicity	350-400 kg/t	2.0-2.2	High unless carbon is sufficient	Limit physical foaming, retain FeO-reduction function	Slag height, overflow, erosion and long exposure
Poor DRI reduced basicity	250-320 kg/t	1.6-1.8	Must be tightly controlled	Reduced, not eliminated	Low basicity, MgO undersaturation and FeO attack

4. Future H2-DRI

4.1. Planned H2-DRI future and current research topics

Hydrogen reduction removes the principal mechanism by which carbon is incorporated during natural-gas direct reduction. H2-DRI should therefore be treated as a carbon-free feedstock at the point of EAF charging unless a defined post-reduction carburization step is included - like natural gas quenching. The direct benefit is low carbon and sulphur input. The EAF consequence is the loss of intrinsic reducing capacity, carbon boil, and chemical energy supplied by carburized DRI [7-9].

High metallization is beneficial, but it does not eliminate slag formation. Vickerfalt et al. [7] melted hydrogen reduced self-fluxing pellets with reduction degrees of 91.0-99.3%. The FeO content of the resulting slag was reduced to 22 wt%. A reduction degree of 98.1% corresponded to a slag mass of about 8% of the metal mass, whereas 94.2% corresponded to about 17%. Figure 6 presents this laboratory result.

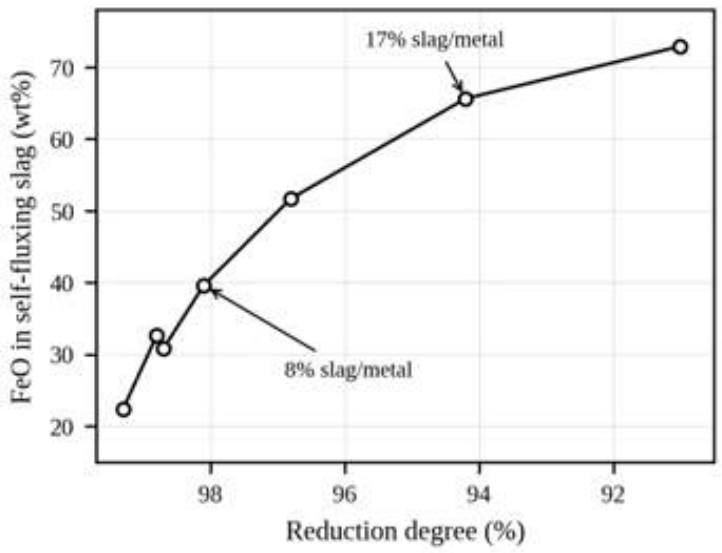


Figure 6 FeO in self-fluxing slag after melting H_2-reduced pellets, redrawn from Vickerfalt et al. [7]; Note from authors: reduction degree is associable with metallization degree

The laboratory results prove that H_2-DRI forms an oxide-rich autogenous slag, but they do not define a full scale continuous EAF practice. The open questions are dynamic FeO at the feed zone, dissolution of pellet gangue, interaction with quicklime and dolime, residence of fines, local bath cooling, accretion formation, and the time available for phosphorus transfer. Final-slag samples are insufficient because the critical exposure can occur during feeding rather than at tapping.

4.2. Priorities for first industrial H2-DRI campaigns

The first industrial campaigns should be designed as controlled comparisons rather than as isolated demonstration heats. The minimum trial matrix should vary DRI reduction degree, carbon strategy and charging temperature while holding steel grade, tap weight, hot heel, transformer program and target tap temperature as constant as practical. Material sampling must cover intact pellets, fines and any reoxidized fraction. A matching natural-gas DRI reference is especially valuable because it separates the effect of missing product carbon from the effects of gangue, metallization, and physical quality. Published laboratory work provides the expected direction of FeO and slag changes, but only plant trials can establish the various process topics (Table 2) like the feed-rate and process limits under arc heating, oxygen injection and continuous slag overflow [2,7,12].

Table 2 Evidence status for major H_2-DRI/EAF questions

Topic	Industrially demonstrated	Engineering expectation	Research need
Feeding	Continuous cold/hot DRI feeding and flat-bath control [2,15].	Feed rate must follow active power and bath superheat.	Local cooling, fines residence and accretion limit for hot H_2-DRI.
Energy and carbon	DRI carbon can reduce FeO, carburize metal and support foaming	Zero-carbon DRI shifts load to electricity, hot charging and external	Optimum carbon source, location, timing and oxygen

	[4-6].	carbon.	balance.
Slag and P	Industrial DRI slag control and MgO saturation practice are available [2].	Autogenous slag composition follows reduction degree and pellet gangue.	Transient FeO, dephosphorization and slag mixing during continuous feed.
Refractories	Wear control by basicity, FeO, MgO saturation and foaming is established [2].	Low slag mass can still be aggressive when FeO is high or MgO is undersaturated.	Campaign-scale wear maps for H_2 DRI, feed-zone attack and thermal cycling.

The measurement package should synchronize feed mass and temperature, active electrical power, oxygen and carbon flow, off-gas CO/CO_2, bath temperature, metal analysis, and repeated slag samples during feeding. Refractory evaluation should combine shell-temperature trends, visual or laser mapping, gunning consumption, and post-campaign lining inspection with the time-resolved slag data. Fines captured in dust and slag should be included in the iron-yield balance. Trial stop or correction criteria should be defined in advance for excessive FeO, loss of slag cover, abnormal shell temperature, feed-zone accretion and falling bath superheat. This approach converts H_2-DRI from a route-level assumption into a quantified operating envelope and provides the evidence needed for equipment, productivity and refractory guarantees [2,7,13].

5. Conclusions

Gas-based, coal-based and hydrogen-based DRI are not interchangeable EAF feedstocks, as shown in Table 3. Gas-based DRI is the mature reference for high-DRI flat-bath operation and benefits from product carbon and hot charging. Coal-based DRI represents approximately one-third of global DRI production and is concentrated in India; its operational relevance is therefore much greater than is implied by many European transformation studies. H_2-DRI may combine high metallization with essentially zero carbon, increasing dependence on electricity, hot charging and controlled external carbon [15].

Table 3 Comparison of present industrial DRI routes and the planned H_2-DRI operating regime

Route	Typical carbon	Metallization and gangue	Primary EAF consequences	Maturity
Gas-based	Often 1.5-4.3 wt% in published industrial examples [2]	Usually high, but plant data show a broad envelope; pellet gangue remains in DRI [2]	Established flat-bath feeding; DRI carbon supports FeO reduction, CO generation and chemical energy; hot charging is proven [2-5]	Industrial
Coal-based	Usually below 1	Sensitive to ore,	External carbon	Industrial

	wt%; residual char is not equivalent to controlled DRI carbon [1,19]	coal, ash separation and fines; hot charging is normally unavailable in conventional rotary-kiln practice [1,19]	and flux demand may increase; broad size distribution and residual ash or char complicate yield and slag control.	
H_2-based	Essentially zero before defined post-reduction carburization [7-9]	Potentially high metallization; pellet gangue and residual FeO form autogenous slag [7,8]	Electrical power, hot charging and controlled external carbon become more important; transient FeO, foaming and refractory exposure require validation.	Emerging

For refractory design, poor DRI quality creates a choice between very high slag volumes at conventional basicity and lower slag volumes at reduced basicity. Neither option is safe without dynamic FeO control and timely MgO saturation. Future EAF trials should therefore combine time-resolved slag sampling, mass and energy balances, feed-zone observations, shell-temperature monitoring and refractory mapping. Equipment and performance guarantees must be based on the actual DRI quality and temperature envelope, not the nominal reduction route or DRI percentage alone.

References

1. S.K. Dutta and R. Sah: "Direct Reduced Iron: Production" in Encyclopedia of Iron, Steel, and Their Alloys, Taylor & Francis, New York, 2016, pp. 1082-1108, doi: 10.1081/E-EISA-120050996.

2. M. Kirschen, T. Hay and T. Echterhof: "Process Improvements for Direct Reduced Iron Melting in the Electric Arc Furnace with Emphasis on Slag Operation" in Processes, vol. 9, 2021, 402, doi: 10.3390/pr9020402.

3. J.A.T. Jones: "Use of DRI in EAF Steelmaking," AIST Direct Reduced Iron and Pellet Workshop, 2021.

4. G. Kim, Y. Kacar and P.C. Pistorius: "Effect of Carbon Bonding State and Concentration on Melting of Direct Reduced Iron" in Proc., AISTech 2019, Pittsburgh, USA, 2019, pp. 661-668, doi: 10.33313/377/069.

5. Y. He and P.C. Pistorius: "Carbon Transfer During Melting of Direct Reduced Iron" in Iron & Steel Technology, vol. 14, no. 1, 2017, pp. 68-71.

6. E. Sharifi and M. Barati: "The Reaction Behavior of Direct Reduced Iron (DRI) in Steelmaking Slags: Effect of DRI Carbon and Preheating Temperature" in Metallurgical and Materials Transactions B, vol. 41, 2010, pp. 1018-1024.

7. A. Vickerfalt, J. Martinsson and D. Sichen: "Effect of Reduction Degree on Characteristics of Slag Formed by Melting Hydrogen-Reduced DRI and Partitions of P and V between Slag and Metal" in Steel Research International, vol. 92, no. 3, 2021, 2000432, doi: 10.1002/srin.202000432.

8. H. Pousette: Investigation into Melting Characteristics of Hydrogen-Reduced Iron

Ore Pellets, Master's thesis, KTH Royal Institute of Technology, Stockholm, 2019.

9. S.A. Hornby: "Hydrogen-Based DRI EAF Steelmaking - Fact or Fiction?" in Iron & Steel Technology, vol. 19, no. 1, 2022, pp. 60-70.

10. R.J. O'Malley: The Heating and Melting of Metallic DRI Particles in Steelmaking Slags, PhD thesis, Massachusetts Institute of Technology, Cambridge, USA, 1983.

11. Badische Stahl-Engineering GmbH: Best Practice Benchmark Database, internal unpublished data, Kehl, Germany, 2026. an Electric

12. A. Hassan, G. Kotelnikov and H. Abdelwahed: "Melting Characteristics of Alternative Charging Materials in Arc Furnace Steelmaking" in Ironmaking & Steelmaking, 2021, doi: 10.1080/03019233.2021.1945876.

13. R.L. Gonzalez, F.L. Acosta, M. Lowry, D. Kundrat, A. Wyatt and H. Fuchs: "Management of DRI Fines to Maximize Iron Yield in the EAF" in Proc., AISTech 2016, Pittsburgh, USA, 2016.

14. R. Gordon: "DR Technology (Non-Gas Based)," AIST Direct Reduced Iron and Pellet Workshop, 2021.

15. Midrex Technologies, Inc.: World Direct Reduction Statistics 2024, Midrex Technologies, Charlotte, USA, 2025.

16. F. Firsbach, P. Lückhoff, R. Schweikle, A. Pezza, P. Hansert, P. van der Velden and M. Krause: "Defossilization of Integrated Plants - Benefits and Challenges of Different EAF Designs" in Proc., AISTech 2024, Columbus, USA, 2024, doi: 10.33313/388/199.

17. E. Perrin, F. Firsbach, M. Nispel, J. Beatty and W. Johnson: "Value Creation Investigation of Dolime Compared to MgO Alternatives for EAF Application" in Proc., AISTech 2021, Nashville, USA, 2021, doi: 10.33313/382/159.

18. S. Lesiak, E. Cheremisina, J. Rieger, J. Schenk, F. Firsbach, W. Johnson, T. Chopin and M. Nispel: "Calcination Condition of Dolomite-Based Materials Influencing Static Dissolution in Synthetic Electric Arc Furnace Slag" in Steel Research International, vol. 93, no. 5, 2022, 2100675, doi: 10.1002/srin.202100675.

19. E. Cheremisina, S. Lesiak, J. Rieger, J. Schenk, F. Firsbach, W. Johnson, T. Chopin and M. Nispel: "Assessment of the Dissolution Rate and Behaviour of Raw Dolomite and Limestone with Different Calcination Degrees in Primary Steelmaking Slags" in Ironmaking & Steelmaking, vol. 50, no. 4, 2023, pp. 379-391, doi: 10.1080/03019233.2022.2119064.

20. M. Powell, A. Pezza, H. Lachmund and F. Firsbach: "Challenges of the Secondary Metallurgy in the Transformation from Converter to Electric Steel Making" in Proc., AISTech 2025, Nashville, USA, 2025, doi: 10.33313/389/228.

PROGRESS IN APPLICATION OF SOL-GEL METHOD IN REFRACTORIES

Zhang Ziying[1], Gao Qiaogang[2], Zhang Xiaohui[1] and Qiu Haifeng[1]

1.Engineer:Sinosteel Luoyang Institute of Refractory Research Co., Ltd., Luoyang 471039, Henan, China;

2.Engineer:Jiaozuo Jinxin Hengtuo New Materials Co., Ltd., Jiaozuo 454450, Henan, China;

3.Engineer:Sinosteel Luoyang Institute of Refractory Research Co., Ltd., Luoyang 471039, Henan, China;

4.Engineer:Sinosteel Luoyang Institute of Refractory Research Co., Ltd., Luoyang 471039, Henan, China;

Corresponding author's e-mail:290261067@qq.com

Abstract

This paper introduces the basic principle, technological process and unique advantages of the sol-gel method. It deeply discusses the specific application of this method in the preparation of refractory materials such as powders, aerogels and coatings. Furthermore, the existing problems and future development trends of the sol-gel method in the application of refractories are analyzed and prospected, aiming to provide a comprehensive reference for the research, development and production of refractory materials.

Keywords: Sol-gel method; Refractories; Powder; Aerogel; Coating

1. Introduction

Refractories play a vital role in high-temperature industries such as iron and steel, non-ferrous metals, glass, ceramics, aerospace and other fields. Their properties directly determine the efficiency, quality and cost of relevant industrial production processes. Conventional preparation methods for refractories can hardly satisfy the modern high-temperature industry's demands for high-performance, multi-functional and refined refractories to a certain extent. As an advanced material-preparation technology, the sol-gel method possesses many unique advantages and has found expanding applications in the field of refractories, offering new approaches for the innovative development of refractories[1]. This paper screens sol-gel-related papers published in the journal《Refractories》, reviews the application status of the sol-gel method in refractories, and points out its development trends in refractory applications.

2. Overview of sol-gel method

2.1 Basic principles

The sol-gel method is a wet-chemical synthesis technique. Generally, metal alkoxides or inorganic salts are adopted as precursors, which undergo hydrolysis and polycondensation reactions in organic or aqueous solutions to form sols. The sols are then subjected to aging, drying and other treatments to convert into gels, and the target materials can be obtained after high-temperature heat treatment[2]. The hydrolytic sol-gel method is the most widely used one, whose reactions mainly involve hydrolysis of precursors and polycondensation of hydrolyzed products. Taking metal alkoxid $M(OR)_n$ (M denotes a metal element and R represents an alkyl group) as an example, the hydrolysis reaction is expressed as:

$M(OR)_n+nH_2O \rightarrow M(OH)_n+nROH$.

Polycondensation consists of dehydration polycondensation and dealcoholization polycondensation. The dehydration polycondensation:

-M-OH+HO-M-⟶-M-O-M-+H_2O; the

dealcoholization polycondensation:-M-OR+HO-M-⟶-M-O-M-+ROH. The structure and properties of sols and gels can be regulated by controlling the reaction rate and conditions of hydrolysis and polycondensation. Nevertheless, raw materials such as metal alkoxides are usually expensive and impose strict requirements on the purity of organic solvents during reactions. Accordingly, the non-hydrolytic sol-gel method has been developed. It is applicable for fabricating water-sensitive materials (e.g. Ti and Zr based materials), where sols and gels are generated via reactions between metal halides and organometallic compounds or other organic reagents (such as ethers and ketones).

2.2 Technological process

The general technological process for material preparation via the sol-gel method includes wet-gel preparation, aging, drying and high-temperature treatment[3]. Firstly, precursors are selected and dissolved: appropriate metal alkoxides or inorganic salts are chosen according to target materials and dissolved in suitable solvents. Secondly, hydrolysis and polycondensation reactions proceed. Under stirring, heating or catalyst addition, precursors react to produce sols. Thirdly, sol aging is carried out to further promote particle growth and agglomeration and improve sol stability. Afterwards, the sol is dried to remove solvents and obtain gels. Finally, gels are treated by high-temperature heat treatment to decompose organic components and crystallize inorganic phases, yielding refractories with specific crystal structures and properties.

2.3 Unique advantages

Compared with conventional refractory preparation technologies, the sol-gel method possesses prominent strengths[4]: 1) Materials with high purity and good homogeneity can be synthesized at relatively low temperatures. Since reactions proceed in liquid-phase solutions, all components are fully mixed and homogeneously dispersed at the molecular level. It avoids composition segregation caused by insufficient raw-material mixing in traditional solid-state reactions, which facilitates the synthesis of high-performance refractories. 2) The chemical composition and microstructure of materials can be precisely controlled. By adjusting precursor types, concentrations as well as hydrolysis-polycondensation conditions, materials with designated crystal structures, pore-size distributions and phase compositions can be prepared, so as to realize accurate performance regulation of refractories. 3) Materials with special morphologies (e.g. nanoparticles, fibers and thin films) can be fabricated. Such materials deliver distinctive properties: nanoparticles

feature high specific surface area to enhance material activity and reactivity; fibrous materials can improve material toughness, which enables the development of novel refractories.

2.4 Research status

Based on the Citexs comprehensive literature database, bibliometric analysis was performed on published English papers in materials science indexed with the keyword “sol-gel” from January 1, 2015 to December 31, 2024 by means of the Citexs SciThink data-analysis platform[5]. A total of 53 355 sol-gel-related papers were retrieved, with an annual average publication output of 5 336 papers, as shown in Fig. 1. Among the top 100 countries/regions in global sol-gel research publications, China ranks first with 14 108 papers (26.44 %), followed by India (8 411 papers, 15.76 %) and the United States (3 495 papers, 6.55 %). Fig. 2 shows the top 20 global research institutions in terms of sol-gel-related publications. The French National Centre for Scientific Research and the Chinese Academy of Sciences occupy the top two positions, with 1 133 and 947 publications respectively, and King Saud University ranks third with 508 publications. It indicates that China’s annual proportion of sol-gel-related papers remained above 23 % over the decade, taking a leading position worldwide. Papers published by Chinese researchers and institutions cover multiple new materials synthesized by the sol-gel route including nanopowders, fibers, functional coatings and aerogels, with applications spanning optics, electronics, sensors, catalysis, energy storage, pharmaceutics, refractories and many other fields.

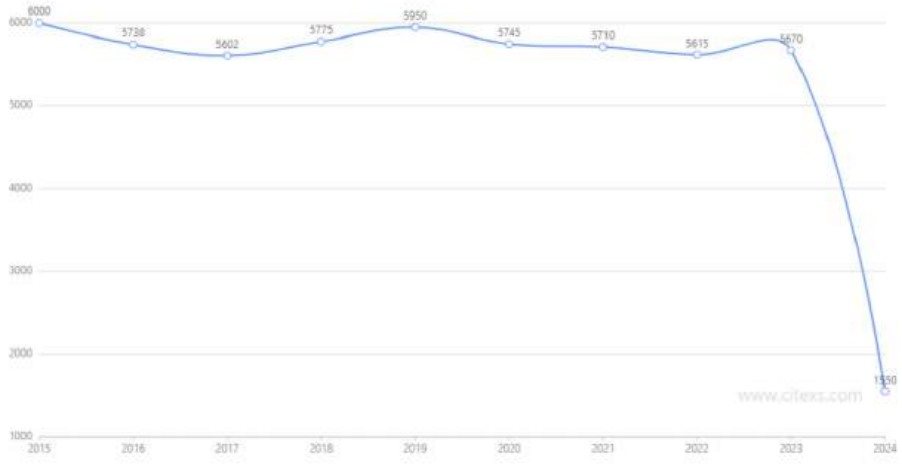


Figure 1 Annual publication trend of sol-gel-related papers from 2015-01-01 to 2024-12-31

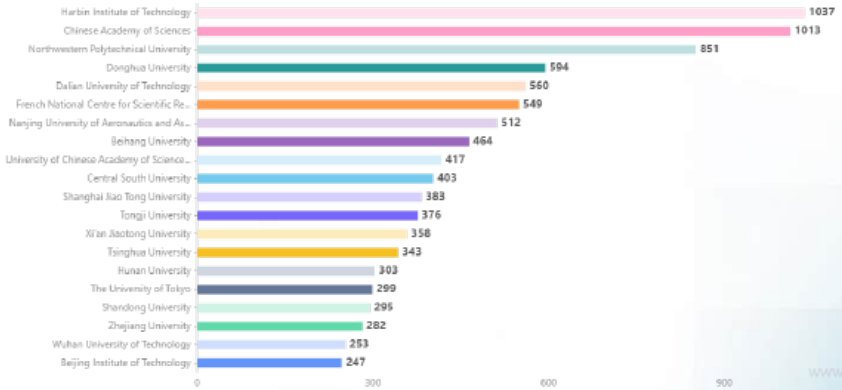


Figure 2 Analysis of research institutions for sol-gel publications from 2015-01-01 to 2024-12-31

3. Applications of sol-gel method in refractories

3.1 Preparation of powder materials by the sol-gel method

Ma Junhua et al.[6] synthesized $KAlSi_2O_6$ (KAS4) particles via the sol-gel method, obtaining core-shell structured particles with an aluminosilicate core and a thin KAS4 shell. It was found that the sol-gel method reduced the formation temperature of pure-phase KAS4 from 1 300 °C (solid-state reaction) to 1 200 °C. Accordingly, compared with the solid-state reaction method, the sol-gel route enables fabrication of core-shell particles with continuous thin shells at lower temperatures. Moreover, the $KAlSi_2O_6$ material exhibits superior corrosion resistance against $Li(Ni_xCo_yMn_z)O_2$, showing promise as a main kiln furniture material for sintering ternary lithium-ion battery cathodes.

Liu Deqi[7] adopted black liquor from papermaking and sodium silicate as raw materials to synthesize lignin-SiO_2 gel by the sol-gel method. Using the gel as a SiC precursor, SiC nanopowder was obtained after carbonization and high-temperature carbothermal reduction. Qin Xing et al.[8] employed citric acid monohydrate as the complexing agent and tetra-n-butyl titanate as the titanium source to prepare citrate complex precursors via sol-gel processing. After heat-treating the precursors at 1 200 °C under nitrogen atmosphere, equiaxed TiN powder with an average particle size of approximately 60 nm was produced. Cao Yingnan et al.[9] synthesized ZrB_2 hollow-sphere powder by the sol-gel method using carbon microspheres as templates, zirconium oxychloride and boric acid as raw materials.

Wang Jianwu et al.[10] took silicon carbide, yttrium nitrate hexahydrate, aluminum nitrate nonahydrate and hexamethylenetetramine as main raw materials. The sintering-aid Y_2O_3-Al_2O_3 gel was introduced through the sol-gel method to uniformly coat SiC particles. The xerogel was completely transformed into $Y_3Al_5O_{12}$ (YAG) phase at around 920 °C, and SiC-YAG composite powder with fine particles homogeneously dispersed on SiC surfaces was finally acquired. Li Jing et al.[11] slowly dropped four aluminum sulfate solutions of different concentrations into ammonia-ammonium chloride buffer containing polyethylene glycol under mechanical stirring to obtain $Al(OH)_3$ sol. Spherical nano-sized α-Al_2O_3 powder was yielded after calcination at 1 150 °C for 1 h. Zhao Zhilong et al.[12] used zirconium oxychloride octahydrate ($ZrOCl_2 \cdot 8H_2O$) as raw material, ammonia water ($NH_3 \cdot H_2O$) and sodium hydroxide (NaOH) solutions as precipitants, and prepared ZrO_2 powder with fine grain size and tetragonal-phase content up to 45.8 wt% via the sol-gel method.

Tang Tao et al.[13] synthesized high-purity mullite ultrafine powder with narrow particle-size distribution and an average particle size of 0.54 μm using aluminum nitrate and tetraethyl orthosilicate as main raw materials by the sol-gel method. Ma Qing et al.[14] adopted aluminum nitrate nonahydrate ($Al(NO_3)_3 \cdot 9H_2O$) and tetraethyl orthosilicate (TEOS) as raw materials. Mullite ultrafine powder of 50 nm was obtained by combining sol-gel technology with spray-drying. Gao Hongsheng et al.[15] prepared mullite gel from pseudo-boehmite and amorphous SiO_2 micropowder via the sol-gel process. After drying and calcination, flaky crystalline mullite powder was produced and applied to aluminum titanate ceramics and sintered corundum bricks. The flaky mullite promoted sintering and lowered the firing temperature, and remarkably improved the strength of aluminum titanate-mullite multiphase ceramics and corundum bricks. Zhao Huizhong et al.[16] synthesized Al_2O_3-SiO_2 nanocomposite powder by the sol-gel method combined with supercritical fluid drying, using tetraethyl orthosilicate and aluminum isopropoxide as main starting materials. Hao Yinlei et al.[17] fabricated green bodies of reaction-bonded SiC ceramics by combining organic-inorganic hybrid materials synthesized via sol-gel processing with mixed SiC-C powder.

Zhao Junhong et al.[18] synthesized magnesia-alumina spinel nanopowder by the non-hydrolytic sol-gel method with anhydrous aluminum trichloride and anhydrous magnesium chloride as main raw materials. Wei Yingna et al.[19] prepared Al_2O_3 gel with nanoporous structure and high specific surface area from anhydrous aluminum chloride and isopropyl ether via the non-hydrolytic sol-gel route. Taking this gel as the aluminum source and carbon black as the

carbon source, AlN ultrafine powder with a particle size of about 400 nm and good dispersion was synthesized at low temperature after carbothermal reduction-nitridation at 1 450 °C for 2 h. Lü Dongfeng et al.[20] prepared sol by adding anhydrous ferric chloride ($FeCl_3$) catalyst to analytically pure silicon tetrachloride ($SiCl_4$) and tetraethyl orthosilicate (TEOS). The sol was transferred into an autoclave to obtain high-activity SiO_2 xerogel, which was further processed by carbothermal reduction to produce β-SiC powder with fine and uniform grain size. Dong Zhanliang et al.[21] synthesized active aluminosilicate gel by the non-hydrolytic sol-gel method using tetraethyl orthosilicate, anhydrous aluminum chloride and dichloromethane, and then obtained β-SiAlON powder through carbothermal reduction-nitridation. Liu Huixing et al.[22] adopted titanium tetrachloride and isopropyl ether as main raw materials and dichloromethane as solvent. TiO_2 gel prepared by the non-hydrolytic sol-gel method served as titanium source for synthesizing TiN powder via carbothermal reduction-nitridation. Zhang Hui et al.[23] used magnesium chloride hexahydrate ($MgCl_2·6H_2O$), aluminum chloride hexahydrate ($AlCl_3·6H_2O$) and tetraethyl orthosilicate ($(C_2H_5O)_4Si$) as raw materials according to the stoichiometric ratio of cordierite. Cordierite precursor powder was prepared by the sol-gel method after calcination at 600 ℃. Cordierite with high α-phase content and 90% of theoretical density was obtained at 1 250 ℃ without any sintering additives.

The sol-gel method can be used to prepare oxide powders, and is more favorable for fabricating non-oxide powders as well as composite powders. Its prominent merits include: solution-phase reaction enabling molecular- or atomic-level homogeneity for multi-component systems; highly accurate stoichiometric control and easy doping modification; and relatively low sintering temperature. Therefore, the as-prepared powders feature uniform chemical composition, fine particle size and high reaction activity. In short, the sol-gel method possesses unique advantages in synthesizing nano-powders with uniform particle size, specific morphology and controllable composition. Nevertheless, it suffers from drawbacks such as long processing cycles and relatively high costs.

3.2 Preparation of aerogels via the sol-gel method

Aerogel is a porous solid material with a three-dimensional nano-network structure, in which gas accounts for more than 95 % of its volume as the dispersed phase. It possesses outstanding properties including ultra-low density, ultra-high specific surface area, ultra-low thermal conductivity and superior adsorption capacity, showing great application prospects in industrial thermal insulation, building energy conservation, aerospace, environmental treatment, chemical metallurgy and other fields[4]. The thermal conductivity of SiO_2 aerogel is lower than 0.02 $W·m^{-1}·K^{-1}$ at room temperature, which can effectively suppress heat transfer. Nevertheless, it suffers from low mechanical strength and poor dimensional stability above 600 °C. Al_2O_3 aerogel features low density and better heat resistance, yet its excellent properties degrade due to phase transformation at high temperatures, which restricts its practical applications. By combining SiO_2 and Al_2O_3 to produce synergistic effects, SiO_2-Al_2O_3 aerogel achieves remarkably optimized performances, and is expected to be applied in more high-end fields such as aircraft engines, thermal protection for flight vehicles and thermal insulation of high-temperature equipment[2]. Fig. 3 shows the schematic diagram for the preparation procedure of SiO_2-Al_2O_3 composite aerogel. Sols are separately prepared from aluminium and silicon sources by the sol-gel method, then mixed and converted into wet gels with network structures under the action of catalysts. During wet-gel preparation by the sol-gel route, major influencing factors include precursor selection, preparation parameters and solution pH.

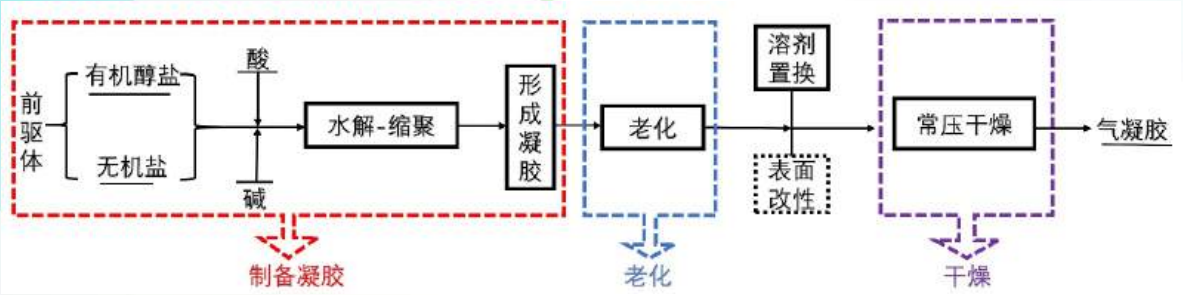


Figure 3 Schematic diagram of preparation procedure for SiO_2-Al_2O_3 composite aerogel[2]

Wang Dongdong et al.[24-25] adopted industrial silica sol as silicon source with formamide and dimethylformamide added respectively for sol-gel processing: (1) SiO_2 aerogel with nano-porous structure, specific surface area of 220-235 $m^2 \cdot g^{-1}$ and density of 180-198 $kg \cdot m^{-1}$ was fabricated via supercritical CO_2 drying[24]; (2) SiO_2 aerogel with bulk density of 0.140-0.400 $g \cdot cm^{-3}$, specific surface area of 150-250 $m^2 \cdot g^{-1}$ and average pore size of 7-12 nm was obtained by ambient-pressure drying[25], whose SEM image is presented in Fig. 4. Cheng Juan et al.[26] prepared monolithic SiO_2 wet gel from tetraethyl orthosilicate (TEOS) via the sol-gel method. Subsequent hydrophobic modification with trimethylchlorosilane and hydrophilic modification with 3-aminopropyltrihydroxysilane were performed, followed by supercritical CO_2 drying to obtain SiO_2 aerogel with internal hydrophobicity and surface hydrophilicity. Ren He et al.[27] used aluminium isopropoxide as precursor, ethanol as solvent and glacial acetic acid as catalyst to synthesize Al_2O_3 aerogel by sol-gel processing combined with supercritical drying (see Fig. 5 for its SEM image). Its average pore size was smaller than the mean free path of air molecules (69 nm) without obvious macropores. It delivered a room-temperature specific surface area of 458 $m^2 \cdot g^{-1}$, which still remained 102 $m^2 \cdot g^{-1}$ after heat treatment at 1 000 °C. Cong Peiyuan et al.[28] synthesized Al_2O_3-SiO_2 aerogel by the sol-gel method combined with vacuum freeze-drying, using $AlCl_3 \cdot 6H_2O$ and TEOS as main raw materials and NH_4OH and $(NH_4)_2CO_3$ as precipitants respectively.

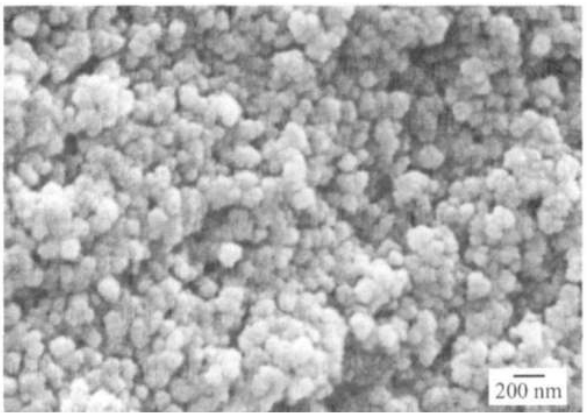


Figure 4 SEM image of SiO_2 aerogel[25]

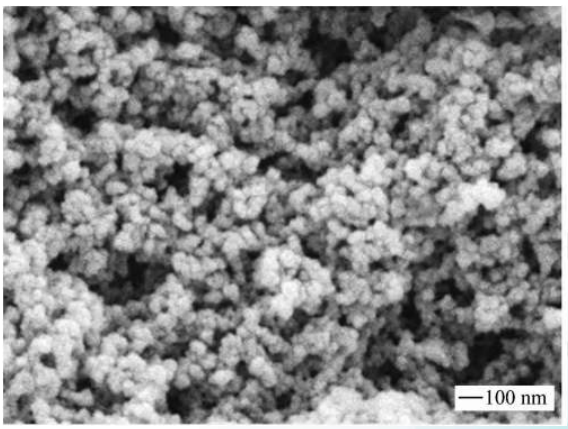


Figure 5 SEM image of Al_2O_3 aerogel[27]

At present, aerogel preparation still faces drawbacks including difficulty in fabricating intact large-size monoliths, complicated processes and high costs. Improving the high-temperature thermal-insulation performance of aerogels remains an important research direction.

(1) Cost: Certain aerogel preparations require expensive special chemical raw materials such as organosilicon sources, which keep material costs high. For silicon-based aerogels, material costs account for approximately 48 % of total costs. Preparation processes such as supercritical drying demand high-cost professional equipment including autoclaves. Large-scale mass production has not yet been realized, making it hard to cut unit-product costs effectively.

(2) Process technology: Wet-gel synthesis via the sol-gel method requires precise control over ratios and reaction conditions of precursors, catalysts and solvents, leading to cumbersome workflows. Drying also calls for specialized techniques and equipment; both supercritical drying and ambient-pressure drying have respective technical challenges and operating requirements. Consequently, long production cycles and difficult quality control are encountered.

(3) Performance: Owing to ultra-high porosity and uniform nano-scale skeletal microstructure, aerogels exhibit poor mechanical properties with high brittleness and fragility. Common SiO_2 aerogel contains abundant hydrophilic hydroxyl groups on its surface and is prone to water absorption. Water intake will impair its microstructure and properties and may even trigger structural collapse, deteriorating its thermal-insulation performance.

3.3 Preparation of fiber precursors via the sol-gel method

Ji Wenling et al.[29] synthesized mullite precursor gel by the non-hydrolytic sol-gel method. Spinning solution was prepared with polyvinylpyrrolidone (PVP) as spinning-aid agent, absolute ethanol and N,N-dimethylformamide (DMF) as solvents. Mullite precursor gel-PVP fibers were obtained by electrospinning and converted into mullite fibers after calcination at 1 000 °C. Zhao Yueming et al.[30] synthesized shear-thinning mullite-fiber-precursor sol with optimal spinnability by the sol-gel method using aluminium powder, crystalline aluminium chloride and silica sol as raw materials. Wang Longqing et al.[31] adopted α-Al_2O_3 micropowder as aluminium source, fused quartz and industrial silica sol as silicon sources, industrial $AlF_3{\cdot}3H_2O$ as additive and PAA as foaming agent. Mullite whiskers with maximum length of 360 μm, diameter of 3-9 μm and aspect ratio of 40-120 were prepared via foaming-sol-gel forming process. Xu Peipei et al.[32] synthesized spinnable and stable zirconia sol by the sol-gel method with zirconium oxychloride as raw material, hydrogen peroxide as hydrolysis accelerator and acetic acid as complexing-stabilizing agent, from which high-performance zirconia fibers were fabricated. Li Qiuxia et al.[33] prepared zirconia-fiber-precursor sol using zirconium oxychloride as main raw material, yttrium nitrate as phase stabilizer, acetic acid and citric acid as organic additives, and further synthesized polycrystalline zirconia fibers. Fu Shunde et al.[34] fabricated 80-type polycrystalline alumina fibers with an average diameter of 3.8 μm and average monofilament tensile strength above 1 000 MPa via the sol-gel method from crystalline aluminium chloride, aluminium powder and silica sol. Xu Jianfeng et al.[35] prepared colloid by the sol-gel method with aluminium powder, crystalline aluminium chloride and silica sol as starting materials, and produced 95-type polycrystalline alumina fibers by centrifugal spinning. Qiao Jian et al.[36] synthesized polycrystalline Al_2O_3-$Y_3Al_5O_{12}$ (YAG) multiphase fibers with smooth surface and uniform diameter (9-10 μm) through sol-gel processing combined with centrifugal spinning, using anhydrous aluminium chloride, aluminium powder, yttrium nitrate, yttrium acetate and acetic acid as raw materials. Zhang Chunye et al.[37] successfully fabricated dense ultrafine magnesium oxide ceramic fibers (diameter below 1 μm) with uniform diameter and smooth surface by the sol-gel method from basic magnesium carbonate and citric acid. Li Xinwei et al.[38] synthesized silicon carbide whiskers (β-SiCw) with high yield, smooth surface, diameter of 60-100 nm, high straight-crystal ratio and uniform aspect ratio by the sol-gel method. TEOS and sucrose served as raw materials, absolute ethanol as solvent, and HCl (pH 1-2) as catalyst. Ji Wenling et al.[39] also prepared spinning

solution by the sol-gel method with anhydrous lanthanum trichloride and zirconium oxychloride octahydrate as raw materials and PVP as spinning-aid agent. Precursor fibers were obtained by electrospinning and calcined at 800 °C, 1 000 °C and 1 200 °C for 8 h respectively to yield $La_2Zr_2O_7$ ultrafine fibers.

The sol-gel method enables fabrication of continuous, uniform and fine-diameter fibers at relatively low temperatures. The resulting fibers possess good densification, homogeneity, high purity and stable properties. Featuring simple workflows and high design flexibility, it is a promising fiber-preparation route. Besides, its firing temperature for fiber production is 400-500 °C lower than that of conventional processes, leading to reduced energy consumption.

3.4 Fabrication of coatings by the sol-gel method

Modification can be realized by forming uniform protective coatings on the surface of refractory products or raw materials to improve service performance with favorable application effects. The sol-gel method is one of the available coating-preparation techniques. According to the material and performance requirements of refractories or raw materials, sol materials shall be selected so as to achieve uniform adhesion on substrates. The thermal-expansion coefficient of heat-treated gel products should match that of substrates, and low oxygen-diffusion rate is preferred[40]. Tang Xunhai et al.[41] took industrial $ZrOCl_2 \cdot 8H_2O$ as precursor, urea $CO(NH_2)_2$ as hydrolysis gelling agent and CaO as stabilizer. Sol was formed by heating and aging, and vacuum-impregnated onto green bodies of unfired ZrO_2 sizing nozzles. After room-temperature drying for 24 h, intact gel films were obtained. Subsequent firing at 1 800 °C for 3 h yielded surface-coating-modified sizing nozzles. The optimal impregnation cycle was 4-5 times. The post-firing apparent porosity decreased from initial 20 % to 11 %, and surface densification was significantly enhanced. It helps extend continuous casting time of sizing nozzles, improve cast-billet quality and increase caster operating rate. Liu Shuxian et al.[42] immersed stainless-steel substrates (after polishing, derusting and degreasing) into as-prepared SiO_2-ZrO_2-Al_2O_3-Cr_2O_3 sol for a certain period, and uniform sol coatings were obtained via dip-coating. After vacuum drying for 48 h and heat treatment at 700 °C for 1 h, SiO_2-ZrO_2-Al_2O_3-Cr_2O_3 composite ceramic coatings were acquired. The coatings were dense without cracking or peeling. Coated samples exhibited good corrosion resistance, oxidation resistance and wear resistance, which can prolong service life of stainless-steel protective tubes for thermocouples in cement kilns.

3.5 Preparation of porous materials by the sol-gel method

The principle for fabricating porous ceramics via the sol-gel method lies in the extension and bridging among sol particles. Colloidal particles build network structures during gelation, and volatile solution fills the gaps within networks. Pore structures are formed after solvent evaporation under appropriate thermal treatment. The sol-gel method can produce porous ceramics with micro-nano-scale pores, porosity below 95 % and pore size ranging from 2 nm to 10 nm. Wang Gang et al.[43] prepared porous ceramics via gel-casting using silica sol and ammonium chloride as raw materials. The products mainly consisted of pure-phase α-Al_2O_3 with minor mullite. Alumina-mullite multiphase porous ceramics synthesized by sol-gel processing show low sintering shrinkage and are suitable for large-size specimen preparation.

4 Conclusions and outlook

Despite multiple merits of the sol-gel method in refractory applications, practical challenges still remain. First of all, raw-material costs are high. Precursors such

as metal alkoxides are relatively expensive, and massive organic solvents are consumed during preparation, pushing up production costs and limiting its large-scale industrial application to some extent. Secondly, the process is complex and hard to control. The sol-gel route involves multiple chemical and physical processes including hydrolysis, polycondensation, aging and drying. Precise condition control is required for every step; otherwise problems such as unstable sols and cracked gels may occur, imposing high requirements for production equipment and operators. Thirdly, large volume shrinkage takes place during drying and sintering. Volume shrinkage arises from solvent evaporation and chemical reactions upon sol-to-gel transition and gel heat treatment, readily inducing cracks and defects, degrading material performances and product yield. Special measures such as pore-former addition and heating-rate control should be adopted to mitigate volume shrinkage.

With continuous technological advances, the sol-gel method will follow the developmental trends below for refractory applications:

1. Localized production and cost reduction of raw materials will constitute an important research direction. Developing low-cost and stable precursors and seeking green alternatives for organic solvents will cut production costs and promote wide industrial adoption of the sol-gel method in refractory manufacturing.
2. Process simplification and automation. In-depth understanding of sol-gel mechanisms, development of novel reaction equipment and process-control technologies will realize workflow simplification and automatic control, improving production efficiency and product-quality stability. For instance, microwave-assisted or ultrasonic-field-assisted sol-gel techniques can accelerate reactions, shorten processing time and enhance material homogeneity.
3. Development of multi-functional composite refractories will become a research hotspot. Taking advantages of the sol-gel method, further exploration on composites of different oxides, non-oxides and functional materials (e.g. smart materials, biomaterials) will enable fabrication of refractories with special functions such as self-healing and biocompatibility, to satisfy unique demands of emerging high-temperature industries including new energy and biomedical engineering.
4. Combined application of the sol-gel method with other manufacturing techniques will gain increasing attention. For example, combining it with conventional solid-state sintering, hot pressing and other methods can complement respective strengths, produce refractories with superior performances and expand performance boundaries and application scope of refractory materials.

References

[1] Cao Y N, Du S, Zhang H J, et al. Research status on preparation of non-oxide ultrafine powders by sol-gel process[J]. *Refractories*, 2014, 48(4): 302-306.

[2] Wang Z Z, Guo Y X, Yang X D, et al. Research progress on atmospheric-pressure drying preparation technology of SiO_2-Al_2O_3 composite aerogel[J]. *Refractories*, 2024, 58(2): 179-184.

[3] Zhou Q, Zhang M, Guo M. Research progress on preparation technology of Al_2O_3-SiO_2 composite aerogel[J]. *Refractories*, 2017, 51(4): 305-309.

[4] Tong T B, Ren H, Wang H Z, et al. Research progress on high-temperature resistant Al_2O_3 aerogel thermal-insulating materials[J]. *Refractories*, 2022, 56(3): 272-276.

[5] Citexs SciThink Platform. Bibliometric analysis on research trends of sol-gel[EB/OL]. (Fill in your retrieval date).

https://www.citexs.com/Summary?sId=25953&xueKe=C192562407&KeyWord=sol-gel&Source=noPhrase-C192562407&Species=human&eDate=2024-12-31&sDate=2015-01-01.

[6] Ma J H, Luo Z T, Li Y, et al. Corrosion study of Li($Ni_xCo_YMn_z$)O_2 cathode material against $KAlSi_2O_6$ prepared by sol-gel method[J]. *Refractories*, 2023, 57(4): 305-309.

[7] Liu D Q. Study on synthesis of nano-SiC from lignin-SiO_2 gel precursor[J]. *Refractories*, 2001(4): 187-189.

[8] Qin X, Zhang J H, Wang J R, et al. Preparation of TiN powder by citrate complex precursor method[J]. *Refractories*, 2021, 55(3): 198-202.

[9] Cao Y N, Wang J K, Zhang H J, et al. Synthesis of ZrB_2 hollow-sphere powder by sol-gel method combined with boro-carbothermal reduction[J]. *Refractories*, 2016, 50(1): 20-24.

[10] Wang J W, Yang H, Guo X Z, et al. Preparation of SiC-$Y_3Al_5O_{12}$ multiphase ceramics by introducing sintering aids via sol-gel method[J]. *Refractories*, 2005(3): 192-195.

[11] Li J, Jiang M X. Preparation and characterization of spherical nano-sized α-Al_2O_3 powder[J]. *Refractories*, 2007(1): 30-32,40.

[12] Zhao Z L, Xue Q H, Ding D H, et al. Study on preparation process of ZrO_2 powder by sol-gel method[J]. *Refractories*, 2017, 51(6): 422-425.

[13] Tang T, Zhang X T, Zhang Q T. Preparation of mullite ultrafine powder[J]. *Refractories*, 2004(3): 193-195.

[14] Ma Q, Ge S, Zhao H Z, et al. Preparation of ultrafine Al_2O_3-SiO_2 binary powder material by sol-gel-spray-drying method[J]. *Refractories*, 2005(5): 347-350.

[15] Gao H S, Chen H. Preparation of flaky mullite powder by gel method and its application[J]. *Refractories*, 1994(4): 212-215.

[16] Zhao H Z, Ji D J, Lei Z X, et al. Supercritical preparation and properties of Al_2O_3-SiO_2 nanocomposite powder[J]. *Refractories*, 2003(2): 69-74.

[17] Hao Y L, Zhao W X. Preparation and sintering mechanism of reaction-bonded SiC ceramics[J]. *Refractories*, 2000(6): 313-315.

[18] Zhao J H, Wei H Y, Wei Y N, et al. Synthesis of $MgAl_2O_4$ nanopowder by non-hydrolytic sol-gel method[J]. *Refractories*, 2012, 46(6): 421-423.

[19] Wei Y N, Bu J L, Wei H Y, et al. Synthesis of AlN ultrafine powder via carbothermal reduction-nitridation of Al_2O_3 derived from non-hydrolytic sol-gel route[J]. *Refractories*, 2013, 47(2): 97-100.

[20] Lü D F, Kang J, Wei H Y, et al. Preparation of β-SiC powder by non-hydrolytic sol-gel method combined with carbothermal reduction[J]. *Refractories*, 2017, 51(6): 438-441.

[21] Dong Z L, Wang R S, Wei H Y, et al. Preparation of β-SiAlON powder by non-hydrolytic sol-gel coupled with carbothermal reduction-nitridation[J]. *Refractories*, 2015, 49(4): 251-254.

[22] Liu H X, Bu J L, Wei H Y, et al. Formation process of TiN powder synthesized by non-hydrolytic sol-gel carbothermal reduction-nitridation[J]. *Refractories*, 2015, 49(5): 321-325.

[23] Zhang H, Xue Q H, Ma L J. Effect of firing temperature on properties of cordierite ceramics prepared by sol-gel method[J]. *Refractories*, 2017, 51(1): 1-4.

[24] Wang D D, Wang G, Wang J D, et al. Effects of formamide and dimethylformamide additions on properties of SiO_2 aerogel[J]. *Refractories*, 2012, 46(3): 182-185.

[25] Wang D D, Ding S Q, Wang Z Q, et al. Preparation of SiO_2 aerogel powder by ambient-pressure drying method[J]. *Refractories*, 2011, 45(2): 96-99.

[26] Cheng J, He F, Wu J Y, et al. Preparation and characterization of inner-hydrophobic outer-hydrophilic SiO_2 aerogel[J]. *Refractories*, 2014, 48(5): 338-342.

[27] Ren H, Tong T B, Liu M, et al. Study on temperature resistance of alumina aerogel[J]. *Refractories*, 2024, 58(4): 297-301.

[28] Cong P Y, Zhao H Z. Effect of precipitants on Al_2O_3-SiO_2 aerogel[J]. *Refractories*, 2007, 41(3): 194-196,212.

[29] Ji W L, Hu S L, Cui Y, et al. Effects of spinning-solution parameters on mullite nanofibers fabricated by electrospinning[J]. *Refractories*, 2018, 52(2): 93-98.

[30] Zhao Y M, Wang C X, Guo C S, et al. Study on spinnability of mullite-fiber-precursor sol[J]. *Refractories*, 2014, 48(3): 205-207.

[31] Wang L Q, Feng T, Wang G, et al. Preparation of mullite whiskers by foaming-sol-gel forming process[J]. *Refractories*, 2018, 52(5): 326-329,333.

[32] Xu P P, Wang X F, Fu S D. Preparation of spinnable zirconia sol[J]. *Refractories*, 2011, 45(4): 282-284.

[33] Li Q X, Wang X F. Effects of organic additives and aging temperature on stability of zirconia-fiber-precursor sol[J]. *Refractories*, 2010, 44(6): 430-432.

[34] Fu S D, Xu J F, Liu L B, et al. Influences of colloid viscosity and fiber-forming process parameters on properties of 80-type polycrystalline alumina fibers[J]. *Refractories*, 2010, 44(2): 116-118,122.

[35] Xu J F, Fu S D, Liu L B. Effects of heating rate and firing temperature on properties of 95-type polycrystalline alumina fibers[J]. *Refractories*, 2011, 45(2): 81-84.

[36] Qiao J, Liu H Y, Zhu Y L, et al. Preparation of Al_2O_3-$Y_3Al_5O_{12}$(YAG) multiphase fibers by sol-gel method[J]. *Refractories*, 2015, 49(1): 48-51.

[37] Zhang C Y, Shen X Q, Wang T P, et al. Preparation of ultrafine magnesia ceramic fibers by sol-gel method[J]. *Refractories*, 2004(6): 389-392.

[38] Li X W, Qu D L, Wu F, et al. Effect of sol-gel behavior of TEOS on synthesis of silicon carbide whiskers[J]. *Refractories*, 2016, 50(6): 420-423.

[39] Ji W L, Wei H Y, Cui Y, et al. Preparation of lanthanum zirconate ultrafine fibers by electrospinning[J]. *Refractories*, 2016, 50(6): 424-427.

[40] Zhang Y L, Wang H M, Wang G, et al. Research progress of novel coating modification methods for refractories[J]. *Refractories*, 2018, 52(4): 310-314.

[41] Tang X H, Gu H Z, Yang L, et al. Study on surface densification of ZrO_2 sizing nozzle[J]. *Refractories*, 2006(04): 273-275.

[42] Liu S X, Yang L R, Huang Z H. Properties of SiO_2-ZrO_2-Al_2O_3-Cr_2O_3 ceramic coatings on stainless-steel surface[J]. *Refractories*, 2007(2): 118-121.

[43] Wang G, Yuan B, Han J S, et al. Preparation of novel Al_2O_3-based porous ceramic thermal-insulating materials[J]. *Refractories*, 2014, 48(4): 241-244.

IMPROVED SLAG CORROSION RESISTANCE OF MgO-C REFRACTORIES FOR LADLE SLAG LINE USING CARBON-ENHANCED COMPOSITE AGGREGATES

Qilong Chen, Tianqing Li, Cheng Liu, Jie Gao, Baikuan Liu, Qixiu Zuo, Qian Zhang, Hailing Yuan, Xu Zhao

Puyang Refractories Group Co., Ltd., Puyang, China

Corresponding author's email: 18772646448@163.com

Abstract

Superior slag resistance is strictly required for MgO-C ladle slag lines. The present work reports a significant enhancement in slag resistance of MgO-C refractories achieved by utilizing carbon-enhanced sintered magnesia (CSM) aggregates. The results revealed that the incorporation of CSM aggregates reduced the slag corrosion index of MgO-C specimens from 11.0% to 9.1%, representing a 17.3% decrease relative to the conventional specimen. Meanwhile, as the CSM aggregates content increased from 0 to 60wt%, the slag penetration depth was decreased from 2549μm to 889μm (>65% reduction). On one hand, the abundant carbon-enhanced phases in CSM aggregates fill the pores and defects in the structure, reducing the accessibility of slag penetration channels. On the other hand, the continuous homogeneous carbon barriers originating from CSM aggregates interrupt the continuity of the glass phase and inhibit further slag infiltration and corrosion.

Keywords: MgO-C refractories; slag corrosion resistance; slag line; carbon composite aggregates

1. Introduction

With the increasing demand for high-quality steel, secondary refining and alloying technologies have advanced rapidly, including LF, VD, VOD, RH processes. In fact, the ladle plays a critical role in molten steel refining because all the mentioned processes are performed in the ladle[1-4]. MgO-C refractories have gained widespread acceptance in slag line of refining ladles, primarily because of their satisfactory slag corrosion resistance and reliable thermal shock resistance[5-7]. However, the service environment of ladle slag lines has become increasingly severe in recent years, which can be attributed to various factors, such as fluctuations in slag basicity, the increased proportion of scrap steel and the higher refining ratio[8,9]. Therefore, improving the slag resistance of MgO-C slag lines is critical to the safe and stable operation of refining ladles.

Typically, magnesia aggregates account for 60~75wt% of the composition in MgO-C refractories, which significantly determines the slag corrosion resistance[10]. It is acknowledged that the corrosion behavior of magnesia aggregates by molten slag is governed by the infiltration–reaction-degradation mechanism. Aggressive molten slag preferentially infiltrates periclase grains through accessible pores and grain boundaries, reacting with impurities (such as CaO, SiO_2 and Fe_2O_3) along the periclase boundaries to form complex multicomponent low-melting-point systems dominated by MgO-CaO-SiO_2-Al_2O_3-Fe_2O_3. Such phases exist as liquid glassy phases under service temperatures, and consequently accelerate the periclase disintegration. Benavidez et al.[11] systematically investigated the interfacial corrosion behavior between ladle slag and MgO-C refractories containing diverse magnesia aggregates. Compared with sintered magnesia, fused magnesia with low open pores and large periclase crystal size could remarkably limit grain-boundary slag infiltration, which benefited the overall slag resistance of refractories. Nonetheless, fused magnesia exhibits remarkably greater carbon emission levels (3.937–4.804 kg

CO_2-eq/kg) in comparison with sintered magnesia (2.151–3.064 kg CO_2-eq/kg) because of its ultra-high temperature electric melting process[12]. Evidently, sintered magnesia struggles to compete with fused magnesia when exposed to aggressive slag even though it is considered a greener raw material with low carbon emissions and favorable economics. Currently, MgO-C refractories prepared from traditional sintered magnesia aggregates can hardly meet the long-service-life requirements of refining ladle slag lines due to their relatively poor slag resistance.

In this study, the novel carbon-enhanced composite sintered magnesia (CSM) aggregates via carbon impregnation technology were employed to prepare magnesia-carbon refractories. The role of CSM aggregate addition on the slag resistance of magnesia-carbon refractories was thoroughly explored. Furthermore, the interfacial microstructures after static cup test were observed with the aim to ascertain their degradation mechanism.

2. Experimental

2.1 Starting materials and preparation processes

The starting materials included sintered magnesia aggregates (SM, 5-0mm, PRCO, Qinghai, China), carbon-enhanced sintered magnesia aggregates (CSM, 5-0mm, PRCO, Puyang, China), fused magnesia (FM, 5-0mm, ≤0.088mm, MgO≥96.5wt%, Liaoning, China), Graphite (≤0.15mm, C≥94wt%, Qingdao, China), Al powder (≤0.088mm, Al≥99wt%, Luxi, China) and Si powder (≤0.088mm, Si≥98wt%, Shandong, China). The organic binder with 47wt% carbon yield was provided by Shengquan company.

The designed batch formulations are shown in Table 1. In this work, conventional SM aggregates were gradually replaced with CSM aggregates, and the batches were named as CR0, CR30 and CR60 according to the percentage of CSM added.

All the materials and the binder were mixed in Eirich intensive mixer for 40 minutes. Subsequently, the standard slag line bricks (200mm×165/135mm×100mm) were compacted using hydraulic press (2500T) and then the green bricks were tempered at 200℃ for 10h to solidify the resin binder. After that, the MgO-C samples with required sizes and shape were obtained for various tests. For instance, rectangular specimens (150mm×25mm×25mm) and crucible specimens (100mm×100mm×100mm) with a hole (φ45mm×55mm) were used for different property evaluations. Subsequently, the obtained specimens were subjected to carbonization treatment, reaching 1600 ℃ at a heating rate of 5 ℃/min with a 3 h soaking duration.

Table 1 Batch formulations of MgO-C samples (wt%)

	CR0	CR30	CR60
SM aggregate	60	30	0
CSM aggregate	0	30	60
FM aggregate	15	15	15
FM powder	11	11	11
Graphite	13	13	13
Antioxidant (Al+Si)	1	1	1
Liquid resin	+3	+3	+3

2.2 Characterization and test

Static crucible test was performed to evaluate the slag resistance of magnesia carbon refractories. Refining ladle slag was loaded into the prepared crucibles and treated at 1600℃ for three hours under an air atmosphere. The typical chemical compositions of refining ladle slag are provided in Table 2. MgO-C specimens were cut along the central axis to acquire cross-sectional surfaces after cup test. Thereafter, the slag corrosion index of individual MgO-C samples was determined following the national standard[13]. Also, the corroded microstructures of the tested MgO-C samples were also investigated using SEM.

Table 2 Chemical components of ladle slag(wt%)

Al_2O_3	CaO	SiO_2	MgO	Fe_2O_3	TiO_2	K_2O	MnO
41.77	23.42	21.60	6.87	1.84	0.67	0.04	3.79

The microstructure of magnesia aggregates and magnesia carbon specimen was performed by using scanning electron microscope (SEM, FEI-Nova-Nano230, JOEL, Japan) equipped with energy dispersive X-ray spectroscope (INCA).

The apparent porosity (AP) and bulk density (BD) of both magnesia aggregates and MgO-C samples were determined using Archimedes principle, employing kerosene as the immersion medium. The cold modulus of rupture (CMOR) was evaluated via three-point bending tests on bar-shaped samples (GB/T301-2007). The cold crushing strength (CCS) of such specimens were carried out following the specification of GB/T 5072-2008.

3. Results and discussion

3.1 Characterization of carbon-enhanced composite aggregates

The novel carbon-enhanced composite aggregates (namely CSM, supplied by Puyang Refractories Co., Ltd., PRCO) were prepared from conventional sintered magnesia via a carbon impregnation technique. Figure 1 shows the macrophotographs of 5-3mm SM and CSM aggregates. It can be observed that the SM aggregates (yellowish-white) and

CSM aggregates (grayish-black) exhibit distinct differences in surface color.

The fundamental physicochemical properties of various aggregates are illustrated in Table 3-4. There are no obvious differences in impurities content (such as CaO, SiO_2, Fe_2O_3 and Al_2O_3) between SM and CSM aggregates. Notably, CSM aggregates contain 1.18wt% carbon, which distinguishes them from conventional SM aggregates. Compared with SM aggregates, CSM aggregates have lower apparent porosity (3.0%) and higher bulk density (3.28g/cm3).

Figure 2 shows the microstructure of the SM (a-b) and CSM (c-d) aggregates. There are micron-sized pores and a small amount of impurities (indicated by arrows) uniformly distributed in SM aggregates. Unlike SM aggregates, carbon-enhanced phase was found within the pores and the periclase grain boundary regions in CSM aggregates. Therefore. CSM aggregates exhibited better physical properties than SM aggregates.

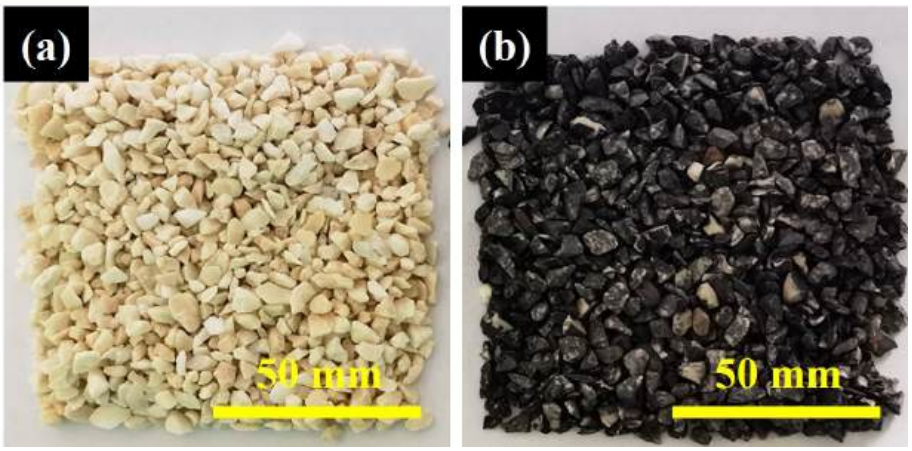


Figure 1 Macrophotographs of the SM (a) and CSM (b) aggregates (5-3mm)

Table 3 Chemical compositions of various magnesia aggregates (wt%)

	MgO	CaO	SiO_2	Fe_2O_3	Al_2O_3	C
SM	96.50	2.86	0.35	0.15	0.14	/
CSM	95.57	2.70	0.30	0.13	0.12	1.18

Table 4 Batch formulations of MgO-C samples (wt%)

	Apparent porosity (%)	Bulk density(g/cm^3)
SM	5.8	3.25
CSM	3.0	3.28

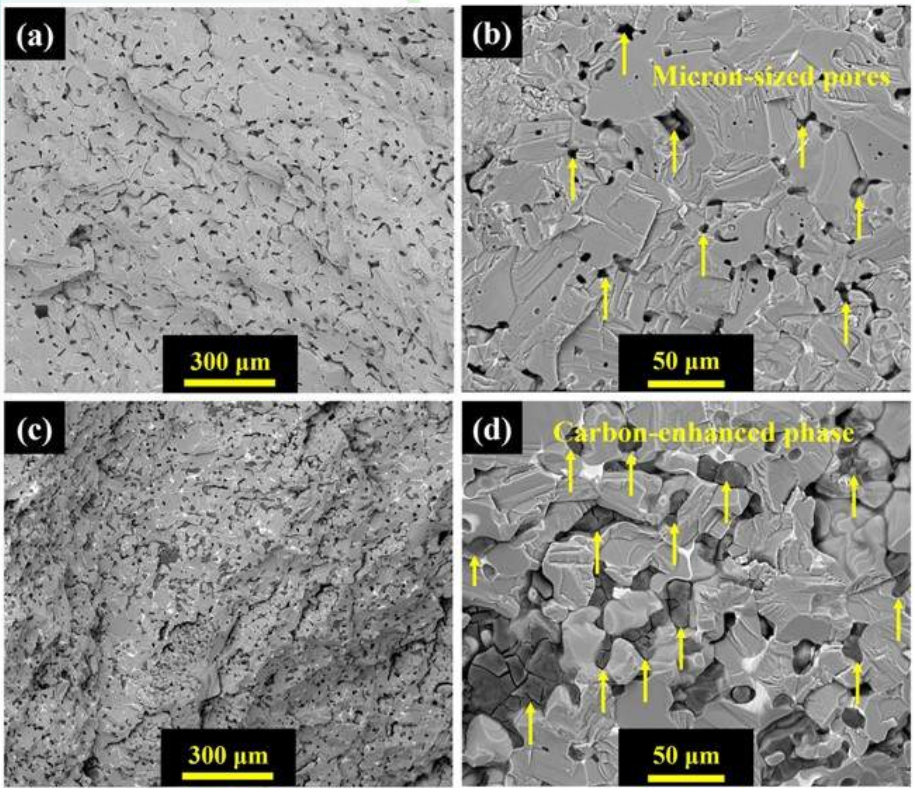


Figure 2 Microstructure of the SM (a-b) and CSM (c-d) aggregates

3.2 Slag resistance

Static cup test was performed to clarify the impact of CSM aggregate incorporation on the slag resistance of magnesia carbon samples. Figure 3 presents the relevant cross-sectional images of such specimens (CR0, CR30 and CR60) after high-temperature corrosion. Compared with the specimen without CSM aggregates, the specimen containing 60wt% CSM aggregates exhibited straighter and clearer interface, demonstrating improved slag resistance. The original crucible area (blue marked) and corroded area (red marked) were quantified via image processing software to acquire the slag corrosion index of MgO-C samples. As presented in Figure 4, the slag corrosion indexes of specimen CR0, CR30 and CR60 were 11.0%, 9.6% and 9.1%, respectively. It was indicated that the MgO-C specimen with partial replacement of traditional SM aggregates by CSM aggregates exhibited better slag corrosion resistance.

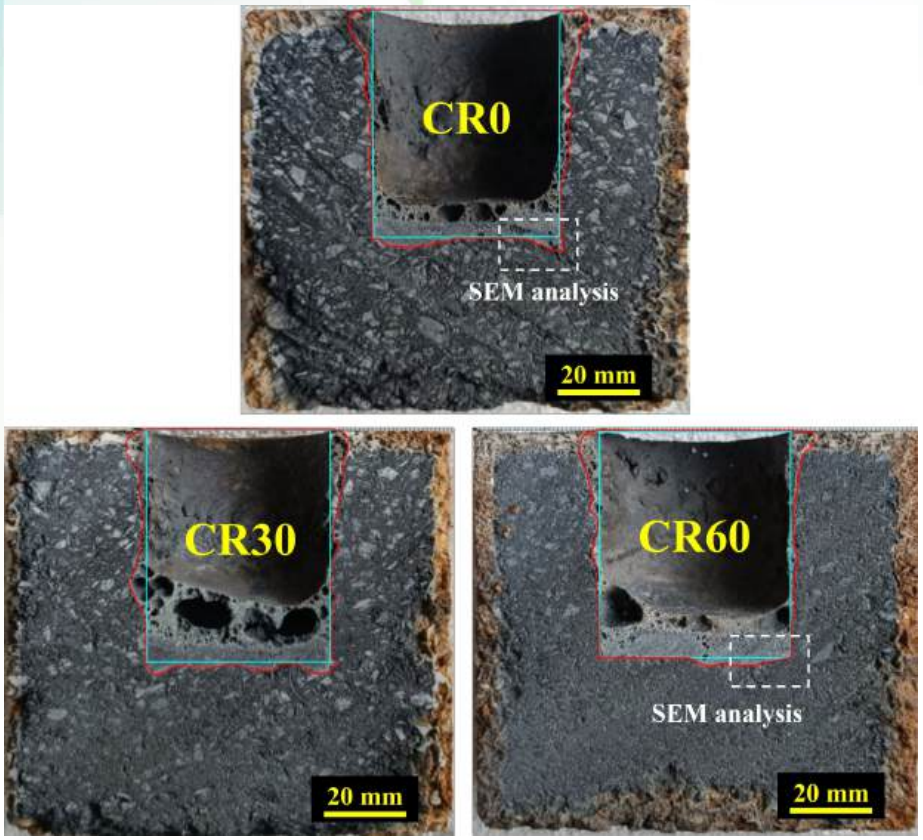


Figure 3 Cross-sectional photographs of MgO-C specimen after cup test

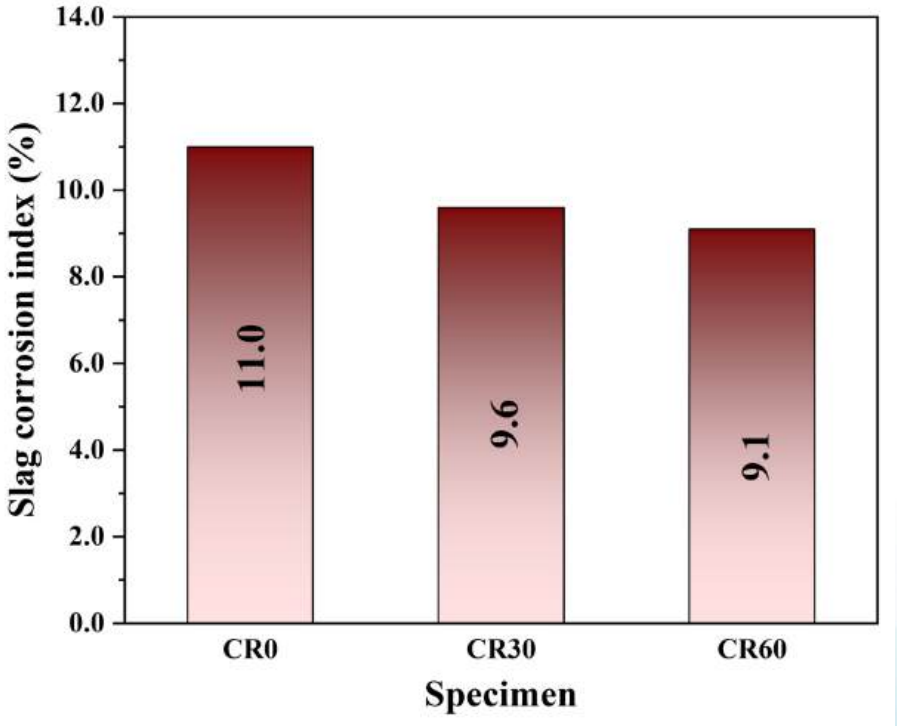


Figure 4 Overall slag corrosion index of MgO-C specimens

3.3 Discussion

In general, the damage of slag to magnesia carbon samples arises from physical infiltration and chemical corrosion. Accordingly, it is essential to investigate the physical properties and microstructure of original specimens, as these factors greatly govern slag infiltration difficulty. Figure 5 presents the physical properties and mechanical properties of MgO-C specimens tempered at 200℃ and coked at 1600℃. It was obvious that the physical properties of MgO-C specimen improved with addition of CSM aggregates, which was attributed to the differences between SM and CSM aggregates. Specifically, the apparent porosity of specimen containing 60wt% CSM aggregates tempered at 200℃ decreased from 4.2% to 3.2% and bulk density increased from 2.94 g/cm3 to 2.97g/cm3. Moreover, the strength (CCS) of MgO-C specimen treated at 200℃ and 1600℃ were both enhanced after adding CSM aggregates, which was consistent with improved physical properties.

Figure 6 depicts the microstructure of polished original MgO-C specimens (CR0 and CR60) tempered at 200℃. As for CR0 (Figure 6(a-b)) specimen, the SM aggregates, fused magnesia aggregates and graphite were uniformly distributed within the structure, with neither obvious pores nor cracks in the matrix. Also, the SM aggregates were well bonded with the matrix, exhibiting good contact interface. Particularly, some open pores were found within the structure of SM aggregates, with pore diameters ranging from 8~42μm.

In specimen CR60, CSM aggregates also showed favorable interfacial bonding with the matrix, and were uniformly coated by graphite, as illustrated in Figure 6(c). Notably, there were numerous carbon-enhanced phase filled in the open pores and distributed along the periclase grain boundaries (Figure 6(d)). It was the presence of the carbon-enhanced phase that repaired most of the structural defects, which contributed to a denser and more compact structure of specimens containing CSM aggregates.

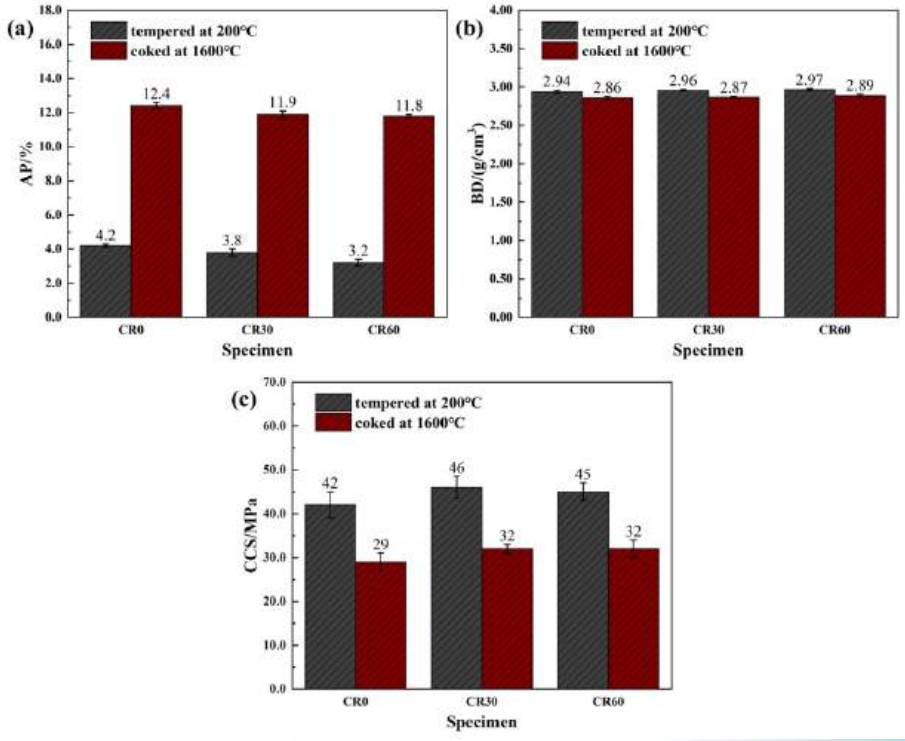


Figure 5 Apparent porosity, bulk density and strength of MgO-C specimens treated at different temperature

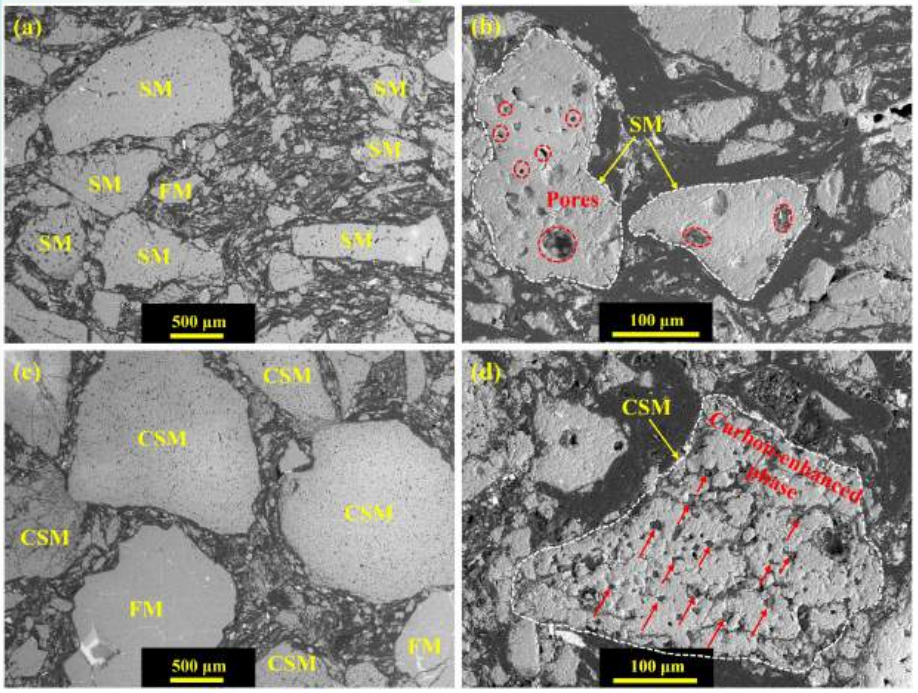


Figure 6 SEM graphs of original specimens treated at 200℃: (a-b)CR0; (c-d)CR60

The interfacial microstructures of corroded specimens at the slag-refractory contact zone were examined by SEM coupled with EDS. The overall and detailed morphological characteristics of corroded CR0 and CR60 specimens are provided in Figures 7-8, while Table 5 shows the matched EDS analysis results. For specimen CR0, slag layer (SL), penetration layer (PL) and origin layer (OL) could be observed because of the infiltration of slag. Notably, the penetration layer depth of CR0 specimen reached as high as 2549μm (Figure 7(a)), indicating their poor resistance to slag penetration. Further magnified BEI observations of the interfacial region and matched elemental mapping scanning results, are exhibited in Fig. 7(b–c). Obviously, numerous $MgAl_2O_4$ spinel particles were formed at the interface between the slag and the SM aggregates (Figure 7(b)) owing to the in-situ reaction between alumina-rich components in slag and magnesia. Periclase grains near the slag layer were surrounded by low-melting-point phases comprised of CaO, SiO_2 and Al_2O_3 and gradually disintegrated into smaller periclase grains, which was confirmed by other reports[14-16]. Although SM aggregates still retained a relatively intact structure, significant slag penetration was observed at structural defects, including open pores, cracks, and grain boundaries. The distribution of Al, Ca and Si elements from Al_2O_3-CaO-SiO_2 slag was detected by EDS mapping results, reflecting the penetration of slag to the SM aggregates. Furthermore, MgO-SiO_2-CaO-Al_2O_3 oxide mixtures were identified (Point 1, 2 and 3), which might be ascribed to the interaction between Al_2O_3 and CaO components in the penetrated slag and impurities at the grain boundaries of SM aggregates.

Similar stratification phenomena were also observed in corroded CR60 specimen (Figure 8). Compared with the conventional MgO-C specimen (CR0), the thickness of slag penetration layer was significantly decreased from 2549μm to 889μm (>65% reduction) with addition of CSM aggregates. In the slag layer, $MgAl_2O4$ spinel particles were distributed among the low-melting-point phases composed of Al_2O_3-CaO-SiO_2. Particularly, a distinct and clear interface was found for both CSM aggregates and large-crystal fused magnesia aggregates when exposed to slag attack, demonstrating their comparable acceptable slag resistance (Figure 8(b)). CSM aggregates maintain a relatively stable structure and severe slag infiltration hardly occurs along grain boundaries, which restricted the spalling of periclase grains. As illustrated in Figure 8(c), merely slight slag infiltration occurs at grain

boundaries of CSM aggregates, and most of the aggressive slag was inhibited according to the elemental mapping.

Schematic corrosion mechanism diagrams of various magnesia aggregates were presented to clarify the positive role of CSM aggregates in improving the slag resistance of magnesia carbon refractories. As shown in Figure 9, fewer open pores and a denser structure were obtained in CSM aggregates than conventional SM aggregates owing to the filling effect of carbon-enhanced phase on their structural defects. So, the effective infiltration channels of the slag were decreased, contributing to improved slag penetration resistance of CSM aggregates. The interfacial reactions between the infiltration layer and molten slag promoted the in-situ generation of $MgAl_2O_4$ spinel grains. Meanwhile, significant disintegration of periclase grains was induced by the attack of glass phase along the grain boundaries. Particularly, interconnected slag infiltration pathways composed of glass phase were formed within the SM aggregates, which accelerated the grain disintegration and promoted further slag infiltration. Different from SM aggregates, CSM aggregates exhibited unique corrosion behavior against the slag. Obviously, only limited and relatively isolated glass phase infiltrated into the interior of CSM aggregates, thereby effectively mitigating the disintegration of periclase grains. Also, the carbon barrier made of carbon-enhanced phase interrupted the continuity of the glass phase owing to their poor wettability toward slag. Furthermore, the continuous generation of CO gas from the oxidation of the carbon-enhanced phases could form a micro-positive pressure zone, which might have a marginal contribution to the improved slag penetration resistance of the refractories.

Based on the above analysis, CSM aggregates may serve as promising alternatives to conventional magnesia aggregates. The resulting MgO-C refractories with satisfactory slag resistance are expected to achieve favorable performance in ladle slag line service.

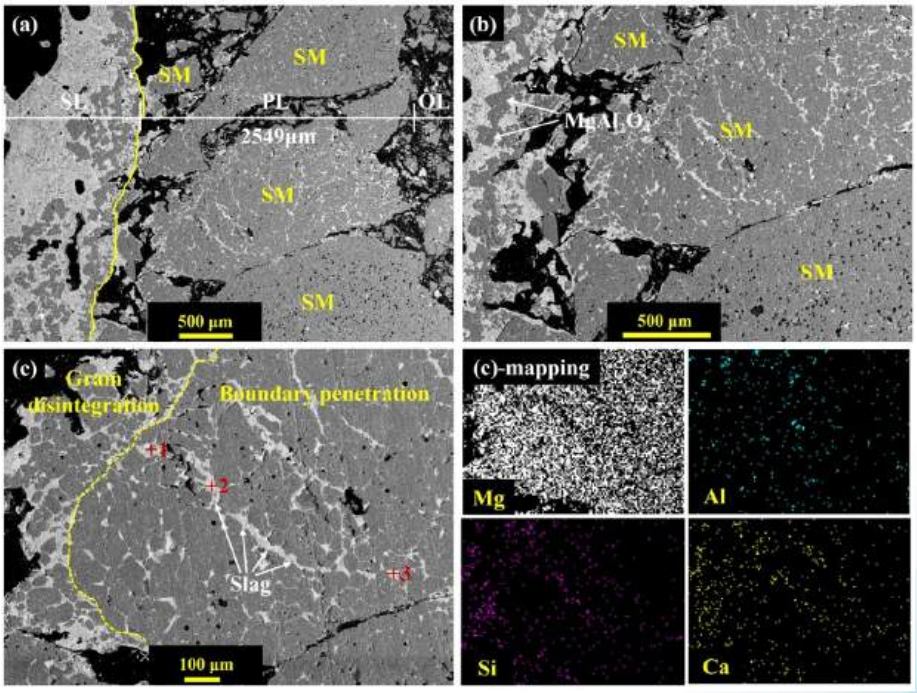


Figure 7 SEM micrographs of corroded CR0 specimen after cup test: SL-slag layer, PL-penetration layer, OL-origin layer

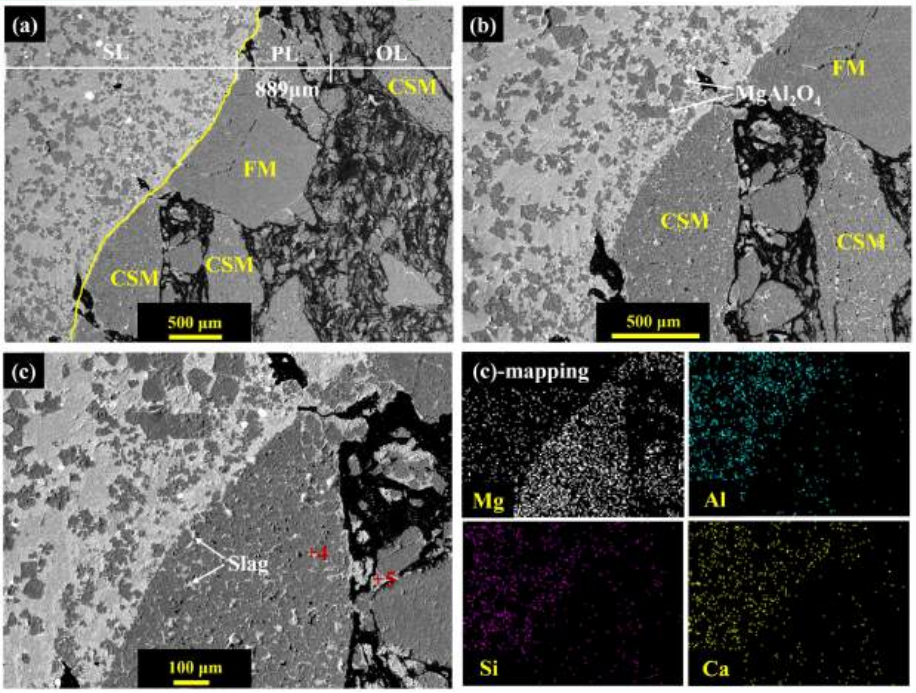


Figure 8 SEM micrographs of corroded CR60 specimen after cup test

Table 5 EDS point results in Figure 7-8 (Atomic%)

Point	Mg	Al	Ca	Si	O
1	9.89	6.24	10.08	14.82	58.97
2	8.33	6.67	12.06	14.18	58.76
3	15.49	/	11.46	15.37	57.68
4	8.99	/	15.49	17.02	58.50
5	15.97	/	7.56	17.65	58.82

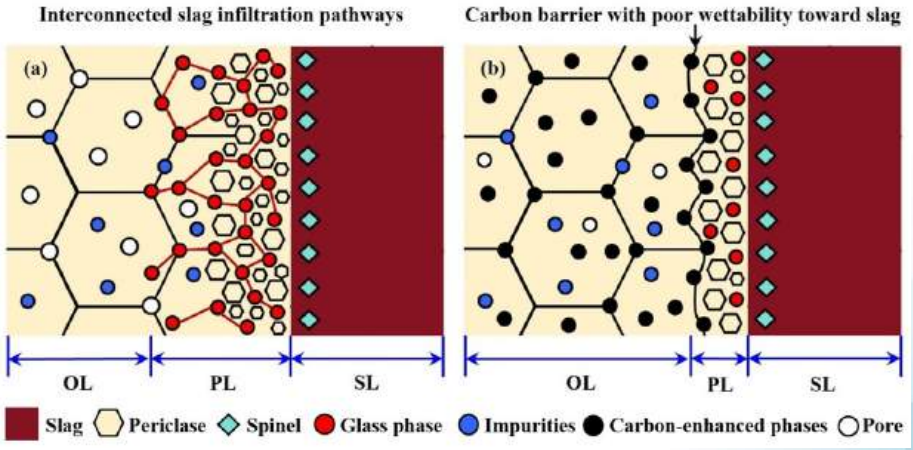


Figure 9 Schematic diagram of corrosion mechanism of SM aggregates (a) and CSM aggregates (b) : SL-slag layer, PL-penetration layer, OL-origin layer.

4. Conclusions

In the present work, novel carbon-enhanced sintered magnesia (CSM) aggregates prepared via vacuum impregnation were introduced into magnesia-carbon refractories, with the aim of clarifying the role of CSM aggregate addition in the slag resistance of such refractories. The conclusions are summarized as follows:

(1) Partial substitution of conventional SM aggregates with CSM aggregates greatly improves the slag resistance of MgO-C refractories, particularly slag penetration resistance. The slag penetration depth of specimen containing 60wt% CSM aggregates is sharply decreased from 2549μm to 889μm (with a reduction of over 65%) compared with CSM-free specimen.

(2) Carbon-enhanced phases distributed within the CSM aggregates repair internal structural defects by filling effect, which effectively reduce the accessibility of slag penetration channels and impede the slag infiltration. Meanwhile, the continuous and homogeneous carbon barriers interrupt the continuity of the infiltrated glass phases and restrain the periclase disintegration.

References

[1] T. Q. Li: International Journal of Applied Ceramic Technology, Vol. 14, 2017, p. 731.
[2] T. F. Wang: Materials Processing Fundamentals Congress, TMS 2025, p. 51.
[3] D. Kavić: Metallurgical and Materials Transactions B, Vol. 56, 2025, p. 5682.
[4] Z. C. Xin: Journal of Iron and Steel Research International, Vol. 31, 2024, p. 289.
[5] W. J. Huang, Y. J. Liu and M. Chen: International Journal of Applied Ceramic Technology, Vol. 17, 2020, p. 1052.
[6] X. Qi, X. D. Luo and H. Z. Gu: International Journal of Applied Ceramic Technology, Vol. 21, 2024, p. 4380.
[7] T. B. Zhu, Y. H. Zhang and Y. W. Li: Journal of the European Ceramic Society, Vol. 45, 2025, p. 117349.
[8]. T. D. Xiao, M. Y. Li and Y. J. Kong: Refractories, Vol. 56, 2022, p. 527.
[9] J. H. Wang, Q. Fang and W. J. Zhu: Ironmaking & Steelmaking, Vol. 52, 2025, p. 525.
[10] Z. Y. Liu, K. X. Cheng and W. Qiu: Journal of Industrial and Engineering Chemistry, Vol. 145, 2025, p. 123.
[11] E. Benavidez, E. Brandaleze and L. Musante: International Congress of science and technology of Metallurgy and Materials, SAM-CONAMET, 2015, p.228.
[12] L. Zhao, J S Feng and H. Dong: Journal of Cleaner Production, Vol. 334, 2022, p. 130194.
[13] B. Y. Ma, X. M. Ren and Z. Gao: International Journal of Applied Ceramic Technology, Vol. 19, 2022, p. 1265.
[14] W. X. Zhang, A. Huang and Y. S. Zou: Journal of the American Ceramic Society, Vol. 103, 2020, p. 2128.
[15] Y. S. Zou, H. Z. Gu and A. Huang: Materials & Design, Vol. 233, 2023, p.112245.
[16] Y. B. Xu, J. Y. Ren and K. Q. Ding: Construction and Building Materials, Vol. 497, 2025, p. 143916.

HIGH-PERFORMANCE SEN FOR ENHANCED TUNDISH CAMPAIGN LIFE

Sahin Ali[1], Amit Banik[1], Saikat Mandal[1], Sunanda Sengupta[1], P K Naik[1], Sadano Takashi[2], Nakamura Hitoshi[2], Hiroshi Nagata[2], Takahashi Tomofumi[2], Navneet Sinha[3], Alok Kumar[3] and Gaurav Pandey

Tundish Management - Technical Support and Services
TRL Krosaki Refractories Limited, Jamshedpur, India

(1. TRL Krosaki Refractories Limited, 2. Krosaki Harima Corporation, 3. Tata Steel Limited, Jamshedpur)

Corresponding author's e-mail: gaurav.pandey@trlkrosaki.com

Abstract

Integrated steel plants convert iron ore into steel through blast furnace smelting, steelmaking, continuous casting, and rolling to produce finished products. Continuous casting plays a critical role by continuously pouring molten steel into a mold to form semi-finished products such as slabs, blooms, or billets. In thin slab casting, the tundish positioned above the mold delivers molten steel through the Submerged Entry Nozzle (SEN). Tundish refractories—including the ladle shroud, tundish working lining, monoblock stopper (MBS), and SEN—are essential for preventing re oxidation, ensuring controlled metal flow, and maintaining safe and stable casting operations. SEN performance, particularly at the slag line, strongly influences casting stability, tundish campaign life, and overall plant productivity. To meet increasing demands for higher output and reduced carbon footprint, a new high-performance SEN has been developed. It significantly reduces slag line erosion, resulting in improved casting stability, extended tundish life, lower energy consumption, and reduced waste generation. Its enhanced durability minimizes ramping practices, improves steel quality, and delivers more consistent process performance. In addition, optimized interaction with mold powder enables increased Ramping duration without compromising SEN behaviour. This paper presents the implementation of high-performance SEN and its impact on tundish performance. Phased industrial trials conducted under real casting conditions demonstrated substantial improvements in SEN service life and tundish campaign duration, establishing a new performance benchmark for thin slab continuous casting operations.

Keywords: High Zirconia SEN, Continuous Casting, Tundish Performance, Slag-Line Erosion.

1. Introduction

Steel is one of the most widely used engineering materials and plays a vital role in modern infrastructure, transportation, construction, and manufacturing industries. In integrated steel plants, steel is produced through a series of ironmaking and steelmaking processes. Ironmaking involves producing liquid iron in a blast furnace using iron ore, coke, fluxes, sinter, and pellets, along with a hot blast of air and pulverized coal injection.

The liquid iron produced is then transferred to the Steel Melting Shop (SMS), where it is converted into liquid steel through the primary steelmaking process, typically using the Basic Oxygen Furnace (BOF) route. The liquid steel is subsequently treated in secondary steelmaking facilities to achieve the desired chemical composition, cleanliness, and temperature required for specific steel grades. Secondary steelmaking operations generally include the Ladle Refining Furnace (LRF), On-Line Purging (OLP), RH Degasser, and CAS-OB processes. These units enable precise control of alloy additions, impurity removal, and steel refinement. After secondary metallurgical treatment, the steel attains the required

quality for continuous casting and further downstream processing. Fig.1 illustrates the typical ironmaking and steelmaking route followed in integrated steel plants



Fig 1 General process route of Integrated Steel Plant

The liquid steel is transported between these processes in a refractory-lined ladle. Once the desired chemistry and temperature are attained, the ladle is transferred to the Continuous Casting Machine (CCM), where liquid steel is converted into semi-finished products. The major components of a CCM are the ladle, tundish, mold, and segments. The tundish, positioned between the ladle and mold, acts as a reservoir that ensures a continuous supply of steel, particularly during ladle changeovers. Fig.2 shows the general arrangement at CCM and various sizes of semi-finished products produced.

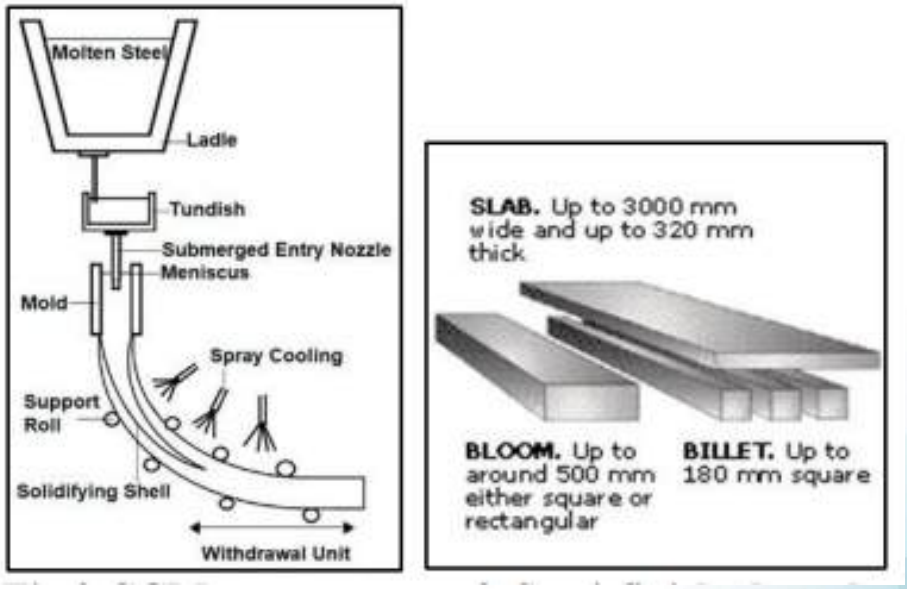


Fig 2 CCM arrangement & Semi-finished product

The water-cooled copper mold solidifies the liquid steel into semi-finished products such as billets, blooms, slabs, and thin slabs. Accordingly, continuous casting machines

are classified as Billet & Bloom Casters, Slab Casters, or Thin Slab Casters based on the product they produce. The tundish refractory system contains several specialized refractories, among which the Submerged Entry Nozzle (SEN), made of alumina-graphite, plays a critical role. The SEN controls and directs the flow of liquid steel from the tundish into the mold. Its performance significantly influences tundish sequence length, casting productivity, and steel quality. The following sections discuss the importance of the SEN, its impact on sequence length, and the trials conducted to improve its operational life.

Role Tundish & Its Refractories

Tundish not only serves as reservoir between Ladle and Mold, promotes inclusion removal, minimizes slag carryover, and helps maintain steel cleanliness and quality during continuous casting. The major refractories used in Tundish for Thin Slab Caster are depicted in Fig.3

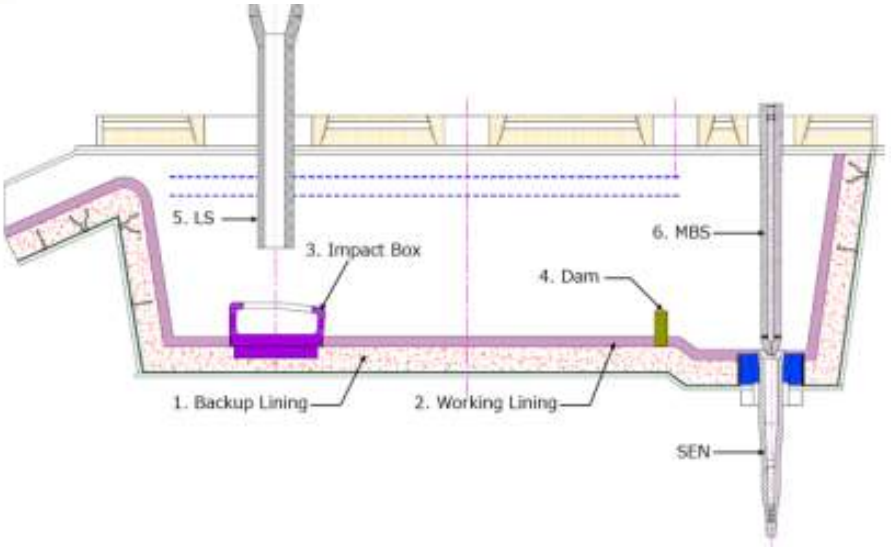


Fig 3 Thin Slab Caster Tundish

1. **Backup Lining** – It provides thermal insulation and structural support to the working lining, reducing heat loss and protecting the steel shell from high temperatures.
2. **Working Lining** – Dry Vibro MassTM is used as the innermost refractory layer of the tundish that comes in direct contact with molten steel, providing thermal insulation and protecting the permanent lining from wear and erosion.
3. **Impact Box^{TM}:** is a refractory flow-control device installed at the tundish inlet beneath the ladle shroud to reduce the impact of the incoming steel stream, dissipate turbulence, promote inclusion flotation, and ensure smooth distribution of molten steel within the tundish.
4. **Dam:** A refractory flow-control device installed in the tundish to direct molten steel flow, increase residence time, and enhance inclusion flotation for improved steel cleanliness.
5. **Ladle Shroud (LS):** It is a Alumina Graphite refractory tube connecting the ladle to the tundish, designed to protect molten steel from reoxidation and nitrogen pickup by preventing contact with atmospheric air during transfer.
6. **Monoblock Stopper (MBS) :** It is a Alumina Graphite refractory used to control the flow or stop the flow of molten steel from the tundish to the mold by controlling the opening of the nozzle.
7. **Submerged Entry Nozzle (SEN) :** It is a Alumina Graphite Refractory positioned between the tundish and mold that transfers molten steel

below the mold powder surface, preventing reoxidation and ensuring controlled, uniform steel flow during continuous casting.

The Submerged Entry Nozzle (SEN) is a critical refractory component in thin slab caster tundishes. Its complex design, operating conditions, and the high casting speeds involved make maintaining stable performance a significant challenge, particularly during long casting sequences. As continuous casting is the final stage of steel production, where the refined liquid steel is converted into semi-finished products, the reliable operation of the SEN is essential. Any SEN failure can result in an unplanned casting interruption, leading to loss of molten steel in the tundish and ladle, reduced productivity, increased operational costs, and prolonged caster downtime. Consequently, enhancing SEN performance and service life is crucial for improving casting efficiency and overall plant productivity.

Sequence Life of SEN

The SEN consists of two refractory materials: Alumina-Graphite (Al_2O_3-C) and Zirconia-Graphite (ZrO_2-C). The slag-line region of the SEN, which is exposed to mold powder within the mold consists of Zirconia-Graphite owing to its superior resistance to slag attack and erosion caused by Mold Powder. The remaining portion of the SEN is composed of Alumina-Graphite, providing the required thermal shock resistance, mechanical strength, and operational stability during continuous casting. When the SEN is positioned for casting, the mold powder interacts with the Zirconia-Graphite (ZG) band and causes localized erosion at the slag-line region. To prevent excessive wear at a single location and maximize SEN service life, the SEN along with the tundish is periodically moved either upward or downward during casting. This practice shifts the eroded region away from the mold powder interface and exposes a fresh, uneroded section of the ZG band to the slag environment. The time interval between two successive position adjustments is referred to as the ramping duration, while the vertical displacement of the SEN during each adjustment is known as the ramping distance. The ramping duration is estimated by trial-and-error method. It should be optimum such that maximum available ZG thickness can be consumed with good remaining thickness. The localized eroded zone generated during each casting stage is termed the ramping band. Consequently, the overall service life of an SEN is determined by the number of ramping bands that can be utilized and the corresponding ramping duration achieved at each band. This relationship can be expressed as: Refer Figure no 4 for understanding Ramping Band & Ramping Duration SEN Life= No of Ramping Bands × Ramping Duration.

Since, Thin Slab Caster Tundish has fixed type of SEN, so the SEN sequence life is equal to the sequence life of Tundish.

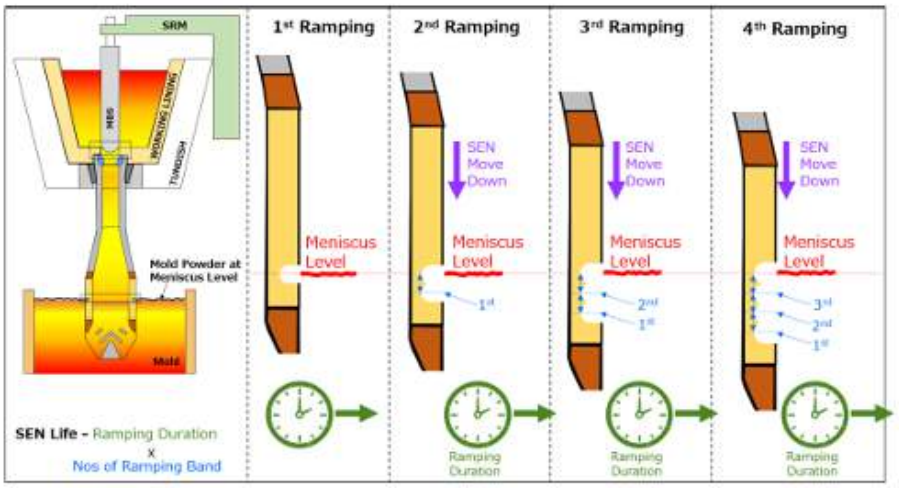


Fig 4 SEN Ramping Duration & Value

Limiting Factors for SEN Erosion

As mentioned earlier, The sequence life of SEN = No of Ramping Bands × Ramping Duration. To achieve the aim to increase the sequence life of SEN, either the number of Ramping Bands or Ramping Duration need to be increased. Number of Ramping bands that can be taken is defined by

1. Maximum Tundish Lowered position: - Casting of SEN in maximum immersed position is defined by the maximum lowered position Tundish be taken during casting.

2. Minimum Immersion depth Level: - Immersion depth is defined as the gap between SEN Port top to the meniscus level. Practically minimum 100mm

immersion (distance from meniscus level to top of SEN Port) gap should be maintained to ensure smooth casting operation. Thus, maximum upward lifting of the Tundish is constrained by minimum immersion depth required.

Thus, to increase the number of Ramping band, either of the two can be evaluated and selection can be done for which side there is a space for increasing Ramping Band.

Or,

The Ramping duration per band can be increased to increase the casting duration.

For customer A, TRL Krosaki supplies Thin Slab SEN, and aimed to increase the casting duration of the SEN. Study was done to check feasibility of
either increasing the number of Ramping Band or Ramping Duration. It was evaluated that number of Ramping Band in use was already saturated. Thus,
further evaluation and experiments were conducted to increase Ramping Duration.

Ramping duration per band was to be increased, thus the improvement was required which could reduce the rate of erosion caused by the Mold Powder. First,
we need to understand the mechanism of erosion.

Erosion Mechanism by Mold Powder

During continuous casting, mold powder melts and forms a liquid slag layer with a glassy structure. This layer performs several important functions, including thermal insulation of the molten steel surface, prevention of re-oxidation, lubrication between the mold wall and the solidifying steel shell, and absorption of non-metallic inclusions. These functions are essential for maintaining stable casting conditions and ensuring smooth and efficient continuous casting operations. The melted mold powder

is harmful for the SEN, as it is highly corrosive in nature. The liquid mold powder floats over the liquid steel.

1. Liquid Mold powder has low wettability against carbon on refractory, so metal stays in contact with refractory, then the carbon is dissolute in the metal,

2. ZrO2 rich surface is exposed.

3. The liquid mold powder has good wettability against ZrO2; thus, it penetrates in the refractory surface. Powder film is generated on the refractory surface, and the ZrO2 is then dissolute in the powder film.

4. After dissolution, again the carbon rich surface is exposed, being lower wettability of liquid mold powder with carbon, it moves away & metal come in contact with refractory surface.

5. The same process repeats from point no 1, and the cycle continues.

Figure 5 depicts the rising up period of boundary between slag and metal. Figure 6 depicts the dropping down period of boundary between slag and metal.

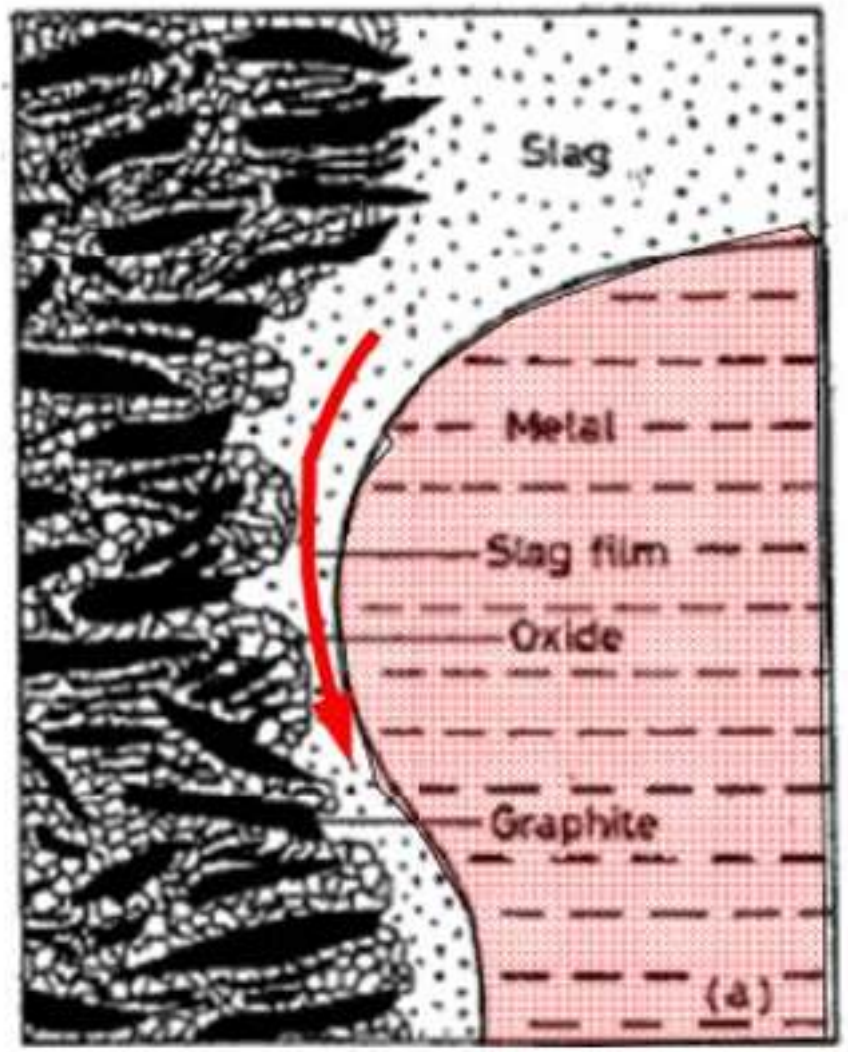


Fig 5 Rising up period of boundary between slag and metal

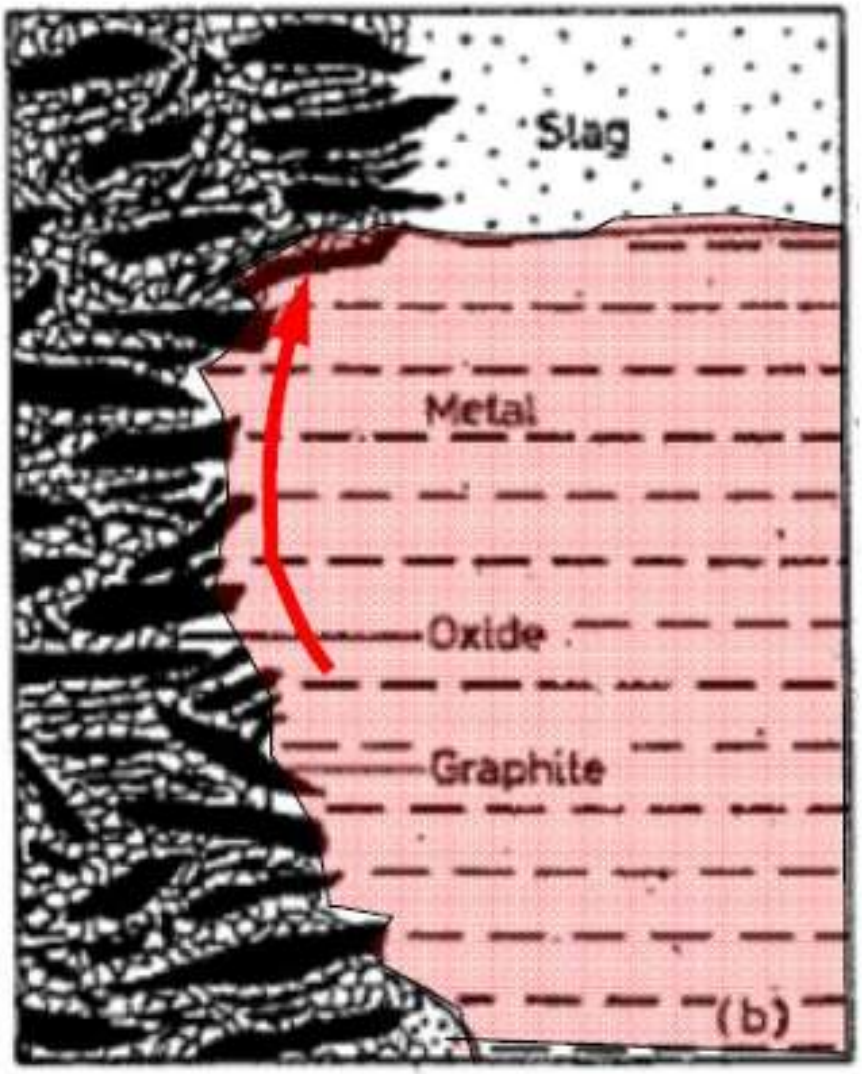


Fig 6 Dropping down period of boundary between slag and metal

Methodology for Improvement

The erosion is caused at the phase when the Molten powder penetrates the ZrO2 rich refractory surface, and a powder film is formed. Then the ZrO2 is dissolved in the powder film. To reduce the erosion, it was important to reduce the molten powder penetration in the refractory surface. To reduce the penetration, the porosity was aimed to be reduced. Thus, a new material development was required which could resist the erosion to a better extent. The following concept was followed for new material.

1. Higher Density & Lowered Porosity
The aim to increase the erosion resistant to ZG material adds up other challenges of losing thermal spalling properties. Figure 7

2. Optimize Particle size composition
depicts the matrix of Corrosion Resistance and Thermal Spalling with different combination of material.

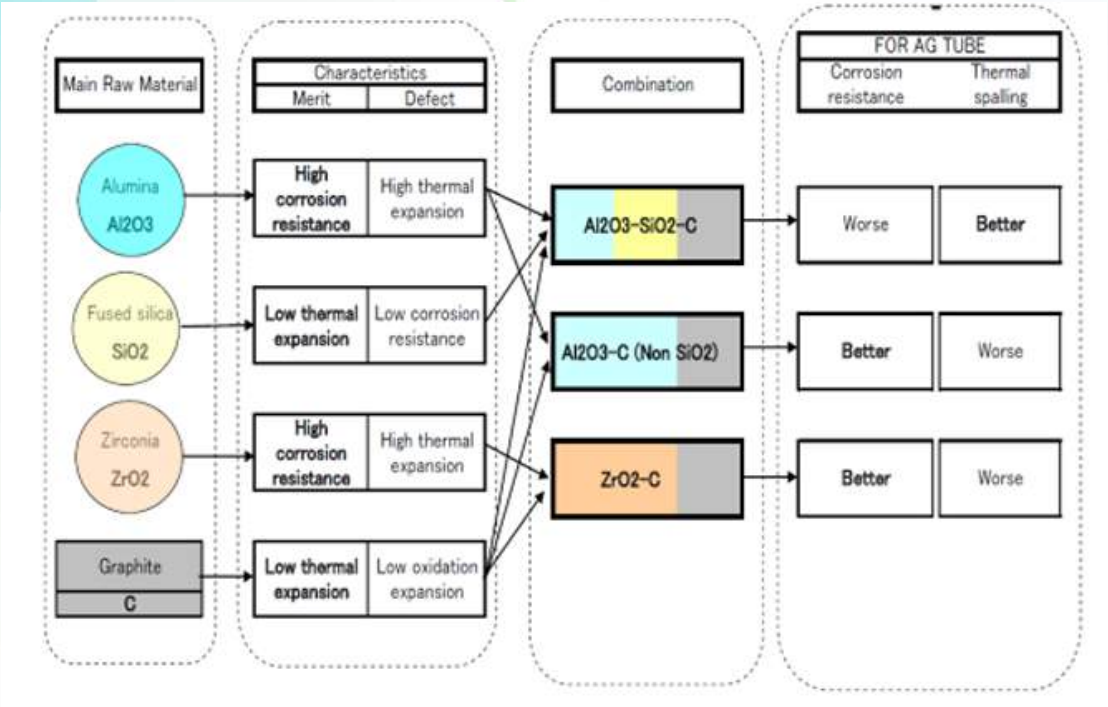


Fig 7 Corrosion Resistance vs Thermal Spalling

According to the table, it shows Zirconia is selected for High Corrosion Resistance and combined with Graphite to form ZrO2-C. This material gives better corrosion resistance, but worse Thermal Spalling properties. Thus, the preheating conditions should be at best during actual trial.

Lab Trial & Results

A laboratory trial was conducted for ZG Material between existing material sample & improved material sample. Test was carried out in a container containing Liquid steel at temperature similar to casting temperature, with mold powder on top. Both the sample were held with a holder and rotated on a constant speed for around 3Hrs. Figure 8 shows the trial setup. After the test, sample was taken out and cooled, the remaining thickness was measured and eroded thickness was calculated, as the original thickness was known.

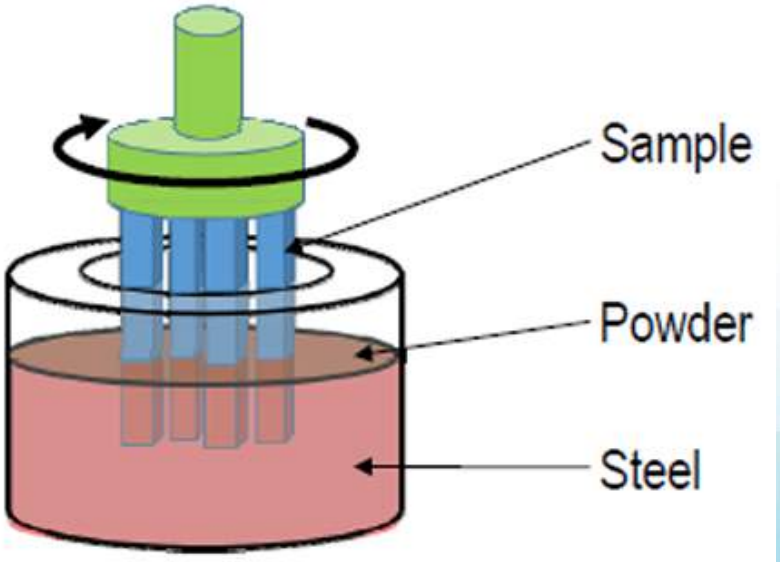


Fig 8 Lab Trial setup for corrosion comparison

The below table shows the results, comparing the corrosion index in (mm/min). Measurement-Before means measurement of sample before test, and Measurement-After means measurement of sample after the test. Corrosion (mm) is calculated by *Corrosion (mm) = Measurement (Before – After)*

Sample No	Material	Measurements		Corrosion	
		Before	After	(mm)	(mm/min)
1	Existing	20.10	10.65	9.45	0.0525
2	Material	20.08	10.56	9.52	0.0529
3	Improved	20.02	13.26	6.76	0.0376
4	Material	19.97	13.47	6.50	0.0361

The Lab results show better corrosion resistance with improved material. Trial under actual operational conditions was to be conducted to evaluate actual results.

Customer Operational Data Collection

Before proceeding for actual trial at customer site, we needed to analyse the operational data for regular SEN, so that it can be compared with the data collected during trial of Improved SEN. The following operational data was collected, which could be directly affected by the performance of SEN.

1. Mold Level Fluctuations – Metal in the mold moves up and down and form a wave during casting. The difference between the crest and peak for the wave is known as Mold Level Fluctuation. The value of Mold Level Fluctuation should be within desired range, if the fluctuation increases, it could lead to entrapment of non-metallic inclusions, hampering the quality of steel caster. If the fluctuations are at a higher value, the liquid steel could spill out from mold. This situation forms a severe hazard to the Operators standing nearby. If the Mold Level fluctuation is within range, it signifies that flow coming out from the SEN it stable and good.

2. Tundish & SEN Preheating Duration & Temperature – Preheating duration & temperature plays a crucial role before casting to specifically avoid thermal spalling, for Alumina Graphite Refractories. Since the improved SEN have higher erosion resistance properties & lower thermal spalling properties, thus SEN Preheating duration & temperature should be good enough, as per standards specified below in Figure 9.

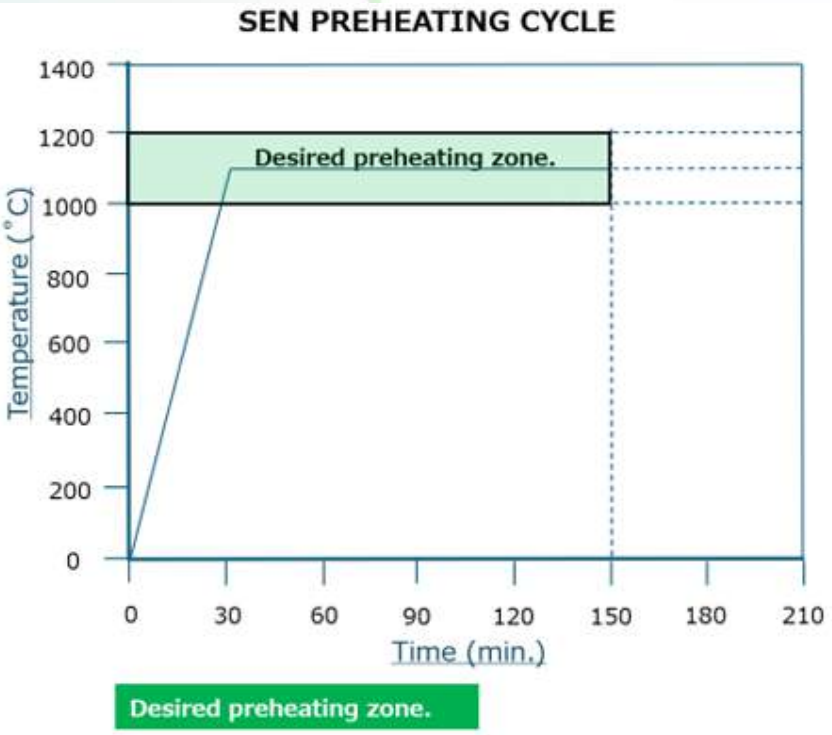


Fig 9 Desired SEN Preheating Curve

3. Ramping Duration & Ramping distance – Actual Ramping duration & Ramping distance gives the total expected sequence life of SEN. The actual value of Ramping duration & distance was noted and accordingly improvement in ramping duration was to be proposed with improved SEN.

4. Tundish lifting error study – Tundish is placed on Tundish Car at Casting Platform; the car moves forward and backward to move the tundish from one position to another. Hydraulic Cylinders are mounted on Tundish Car, which moves up & down to move Tundish up and down to facilitate the ramping process. Figure 11 shows the general arrangement of Tundish Car with Hydraulic Cylinder & Tundish. These hydraulic cylinders move up and down to facilitate Ramping Process, it is important for all the cylinder to move up or down equally. If there is variation in movements, then the Tundish along with the SEN will get tapered towards one side, causing repeated erosion again on the eroded area. Repeated erosion can cause completed erosion of the ZG wall and eventually cause puncture / failure. This variation in the movement of lifting equipment is termed as Lifting Error. It should always be monitored and should be within specified range for failure free casting.

Thus, monitoring customer operation data was essential to evaluated performance of the improvement implemented.

Phases of Trial

Actual site trial was conducted at Customer A site Thin Slab Caster. The shape of the improved SEN was kept similar; thus, application procedure was kept unchanged. Similar observation & checkpoints was maintained as normal SEN while fixing of SEN. The trial was planned in series of Phases to evaluate performance with every improvement planned. With every trial phase, the Ramping Methodology was improved up to maximum desired potential was achieved.

Trial Phase 1: Trial was planned with 2nos of Improved SEN in 1st Phase considering the SEN as Regular SEN. Ramping Methodology was decided to be followed same, as regular

& Operational data was recorded to analyse any abnormal behaviour of SEN, if any. Casting was started & completed smoothly. The SEN was collected for evaluation of ZG Band. Operational data was summarized and compared with the data for regular SEN and found that there was no abnormal deviation observed. The data compared is mentioned below.

1. Mold Level Fluctuation
2. Heat Flux Value
3. Casting Speed
4. Throughput
5. MBS Position

The retrieved SEN was cooled for detailed evaluation. The following parameters were analysed in the SEN.

1. ZG Band Eroded Thickness
2. Left Over Thickness at ZG Band
3. SEN Port & Body condition evaluation

ZG Band Eroded Thickness is calculated by subtracting the ZG Band minimum Left-Over Thickness by the ZG Band Original Thickness. Upon diving the maximum eroded thickness by Ramping Duration (in min) & Heats, Erosion Rate in mm/min & mm/Heat would be derived respectively. Figure 10 shows the explanation of Left-Over Thickness, Eroded Thickness & Erosion Rate.

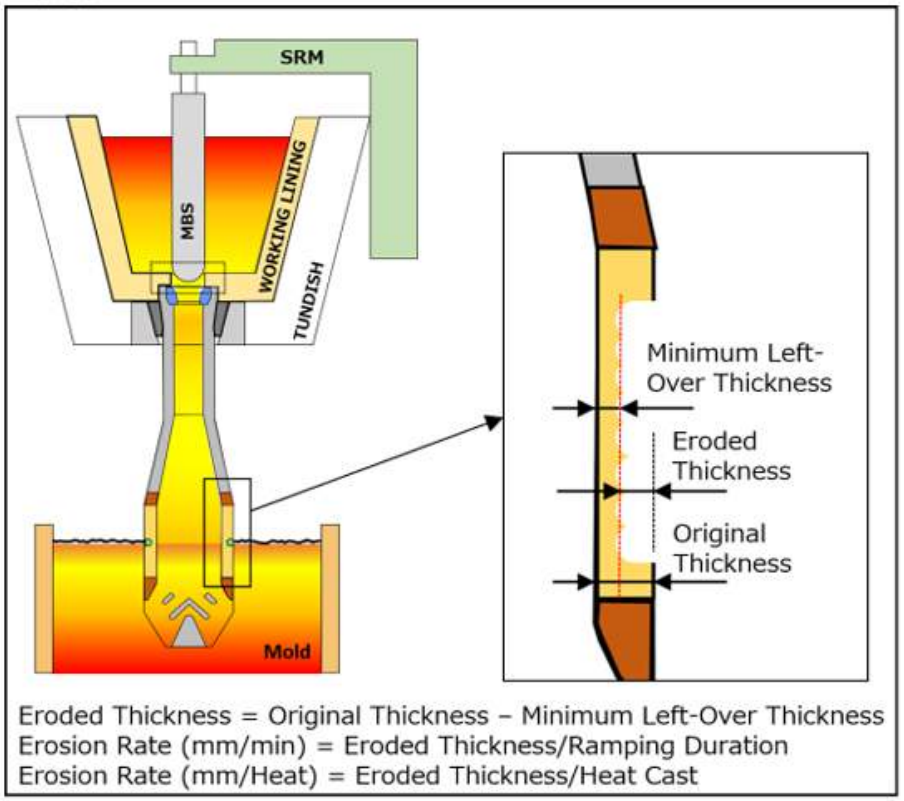


Fig 10 Left Over Thickness, Eroded Thickness & Erosion Rate

With the measurements & calculations, it was observed that Improved SEN had lesser erosion rate than regular SEN. The below table shows comparison of 1. Improved SEN vs 2. Regular SEN.

SEN Type	Casting Duration (mins)	Heats	SEN Measurements			Erosion Rate	
			Original Thickness	Max. Eroded	LOT	mm per min	mm per heat
1	1586	31.5	33.5	17	16.5	0.12	0.54
2	1510	31.6	33.85	20.46	13.39	0.15	0.66

Thus, it was justified with 1st Phase Trial that Improved material showed better & lesser erosion rate. 2nd Phase Trial was planned with improved Ramping Duration.

Phase 2 Trial: With the aim of increasing sequence life of tundish by Improved SEN, this trial was planned with increased Ramping duration per band. The ramping duration with Regular SEN was 140 mins and total 13 nos of Ramping Bands could be taken. It was planned to increase the ramping duration gradually. The duration should be such that ZG Band could be used up-to maximum possible extent, with predefined minimum Left-over Thickness. Gradually increasing the Ramping duration and evaluating the Operational Parameter, Eroded Thickness and erosion rate of the SEN, it was observed that maximum Ramping Duration per band could be increased up-to 160mins, with minimum required Left Over Thickness. Ramping Duration per band was improved by 14.28%, and same extent could be extended to Tundish Sequence Life enhancement by approximately 14%. Operational data recorded was compared for Improved SEN with extended Ramping Duration vs Regular SEN and found that there was no abnormal deviations or issues reported. All the SEN cast completed successfully without having any issue reported to refractory. Figure 11 contains some sample pictures of SEN after Casting.



Fig 11 Improved SEN after casting

Conclusion

SEN plays a major role in defining the sequence life of Thin Slab Caster Tundish. To improve the sequence life of tundish, SEN performance needs to be improved. Identification of bottleneck and improvement plan to mitigate the bottleneck could be best possible way. SEN ZG Band Erosion is the bottleneck for this scenario. Various studies & Lab Trial was conducted to improve performance of ZG Band. Material quality was improved and the results were analysed by Lab Trial & Actual site trial. Eventually the actual site trial showed improvement in the performance of SEN by approximately 14% in terms of duration, and eventually the same is extended to the Tundish Sequence Life Enhancement by 14%.

References

1. Harmuth, H.; Xia, G. Interaction Steel/Slag/Submerged Entry Nozzle and its Impact on Refractory Wear: Thermochemical Process Simulation. ISIJ International, Vol. 55, No. 4, 2015, pp. 775-780.

2. Nakamura, Y.; Ando, T.; Kurata, K.; Ikeda, M. Effect of Chemical Composition of Mold Powder on the Erosion of Submerged Nozzles for Continuous Casting of Steel. Transactions of the Iron and Steel Institute of Japan, Vol. 26, No. 12, 1986, pp. 1052-1058

3. Zhang, S.; Yuan, H.; Gan, M.; Wang, Q.; He, S. Wetting and Erosion of ZrO_2-Graphite Refractory by CaO-SiO_2 and CaO-Al_2O_3-Based Mold Slags for Submerged Entry Nozzle. Metallurgical and Materials Transactions B, Vol. 50B, 2019, pp. 1322-1333

SUCCESSFUL IMPLEMENTATION OF TRM IN RH DEGASSER UNIT - A UNIQUE AND COLLABORATIVE APPROACH TOWARDS PERFORMANCE IMPROVEMENT, HIGHER RELIABILITY & PRODUCTIVITY, OPTIMIZED INVENTORY CONTROL

Rajesh Ghosh[1], Subhajit Chatterjee[1], Bibhas Karmakar[1], Soumen Jana[1], Sunanda Sengupta[1], Prasanta Kumar Naik[1], Somak Chattopadhyay[2], Niladri Shekhar Raut[2], Amit Khokhar[2]

1. TRL Krosaki Refractories Limited, Belpahar, Odisha
2. Jindal Steel Limited, Raigarh, Chhattisgarh

Corresponding Author's email: rajeshghosh@TRL Krosakirosaki.com

Abstract

RH degasser is a secondary steel refining unit used for producing high purity special steels for various applications.In India about 20% of steel produced through RH degasser route and it is in increasing trend.

Jindal Steel Limited, Raigarh, renowned for its innovation in steelmaking, has entrusted TRL Krosaki Refractories Limited (TRL Krosaki) with the responsibility of Total Refractory Management (TRM) for SMS-2, including the RH unit. This collaboration underscores Jindal Steel Limited's commitment to operational excellence and reflects the confidence placed in TRL Krosaki's expertise in delivering comprehensive refractory solutions. This contract is unique because TRL Krosaki will be responsible for the complete RH vessel lining, dismantling and maintenance of full RH Vessel (including RH Snorkel, Lower Vessel, Upper Vessel etc.). TRL Krosaki will also need to adhere to the minimum guaranteed life requirements along with fulfilling other key performance criteria (KPI) in place.

As part of the TRM implementation, TRL Krosaki introduced modified snorkel brick quality, enhanced gunning material with proper maintenance practices, improvement upon existing design etc. which collectively strengthened RH snorkel performance.The collaborative improvement journey delivered significant operational gains:

i. 20% improvement in Snorkel & Lower Vessel life
ii. 100% RH down by operational planning during TRM period
iii. 25% improvement in specific gunning consumption

During this improvement journey, TRL Krosaki achieved some record-breaking milestones, such as achieving the highest RH snorkel life and the highest single-month RH production in Jindal Steel Limited. This case study demonstrates that a collaborative improvement journey can significantly enhance operational performance and set new benchmarks in productivity and efficiency.

Keywords: Steelmaking, RH Degasser, Total Refractory Management (TRM), Life Improvement, Snorkel

1. Introduction

RH degassing process is extensively used to produce special steels like rail steel, electrical steel used in transformer core, steels made for manufacturing seamless pipes for oil and gas transportation, high tensile steel plates etc. The quality of these grades must be very consistent and free from gaseous inclusions, mainly Hydrogen[3].

The RH Degassing unit consist of two numbers of refractory Snorkels – Inlet Snorkel (or Up leg Snorkel) and Outlet Snorkel (or Down leg Snorkel). Leg brick (or Throat brick) installed above RH Snorkel. Snorkels are immersed in the liquid steel bath of the Steel Ladle placed underneath. Inlet Snorkel

consists of Argon gas (Ar) purging system through specialized nozzles.

Jindal Steel Limited, Raigarh, is one of India's leading integrated steel manufacturing facilities. The Steel Melting Shop-2 (SMS-2) is equipped with modern secondary metallurgical units, including RH degassers, enabling the production of value-added and specialty steel grades. To improve refractory performance and operational efficiency of the RH unit, Jindal Steel Limited adopted a Total Refractory Management (TRM) model and entrusted TRL Krosaki Ltd. with complete refractory management of the RH vessel system, including snorkels, lower vessel, upper vessel, alloy chute, and associated maintenance activities. Total Refractory Management (TRM) is a performance-based service model in which the refractory supplier assumes complete responsibility for the installation, maintenance, inspection, monitoring, and performance optimization of refractory systems, while ensuring the highest standards of safety, quality, reliability, and operational efficiency.

2. Key Challenges present before the TRM Project

Before implementing the Total Refractory Management (TRM) project, the plant faced several operational, maintenance, safety, and performance-related challenges:

a. Fragmented Responsibility: Multiple agencies were involved in refractory supply, installation, and maintenance, leading to unclear accountability for refractory performance.

b. Frequent Refractory Failures: Premature wear and unexpected refractory failures resulted in production interruptions and increased maintenance requirements.

c. High Furnace and Vessel Downtime: Extended shutdown periods for refractory repairs adversely affected plant availability and productivity.

d. Manpower Management Issues: Challenges in manpower planning, skill availability, deployment, supervision, and productivity impacted execution quality.

e. Safety Risks During Refractory Activities: Refractory installation and maintenance activities involved working at heights, confined spaces, hot work, and material handling, posing significant safety challenges.

f. Inconsistent Quality of Installation: Variations in workmanship and adherence to standard procedures led to inconsistent refractory performance.

g. Higher Refractory Consumption and Cost: Suboptimal maintenance practices and premature lining failures resulted in increased refractory consumption and operating costs.

h. Limited Data-Driven Decision Making: Absence of centralized performance tracking and analytics restricted opportunities for continuous improvement.

i. Coordination Challenges: Ineffective coordination among operations, maintenance, procurement, and contractors led to delays and execution inefficiencies.

These challenges highlighted the need for a single-point, performance-based refractory management model, leading to the adoption of the TRM Project with clear accountability for safety, quality, cost, and refractory performance.

3. Project Objective and Scopes

The objective of TRM is to maximize refractory life, reduce downtime, improve equipment availability, and deliver measurable value through continuous performance monitoring and accountability.

Key Features of TRM:

- End-to-end refractory management
- Performance & availability-based accountability
- Continuous condition monitoring and inspection
- Maintenance planning and lifecycle optimization
- Reduction in refractory consumption and operational costs
- Improved equipment reliability and plant productivity
- Adequate deployment of skilled manpower, seamless workforce mobilization and site access control.
- Strict compliance with safety standards and procedures
- Proper housekeeping of refractory installation areas

This model shifts the focus from merely supplying refractory materials to delivering guaranteed performance outcomes and sustainable operational improvements.

4. Performance Improvement

For fulfil the project objectives, the 1st priority was to improve the equipment availability by improving the Snorkel and Lower vessel life.

a. Snorkel and Lower Vessel Brick quality
b. Maintenance material
c. Installation procedures

TRL Krosaki and Jindal Steel Limited have extensively studied the previous failures and identified the key areas of improvement:

d. Preheating Practices
e. Operational Practices

Based on the study we have made the following improvements:

a. Snorkel and Lower Vessel Brick Quality Enhancement:

Elevated sheer stress in RH Snorkel is the major reasons for higher erosion of Inlet bricks[8]. Fused grains of Mag-chrome co-clinker were used here along with high purity magnesia and ultra-low silica chromite along with specialized additives were used for improvement in brick quality in RH Snorkel by enhancing solid solution in-between magnesite and chromite grains[1].

Figure 1: Microstructure of improved brick suggested formation of secondary spinel and higher solid solution percentage observed in improved quality DBMCbrick



Figure 2: Improvement in strength in DBMC brick



Significant improvements in the microstructure, CCS (Fig. 2), Pore size distribution (Fig.3) has been observed in the brick quality.

b. Improvement in Maintenance material and Maintenance Practices:

In the case of continuous process equipment in steel making cold repair is not possible, so monolithic repair is considered for zonal repair and continuation of service of the equipment[7].We have also improved our gunning mass by altering chemical composition with better stickability and retention.

Table 1: Chemical analysis of Old gunning Mass vs Improved Gunning Mass

Chemical Components (%)	Old Gunning Mass	Improved Gunning Mass
SiO_2	7.8	4.89
Al_2O_3	1.02	0.93
Fe_2O_3	1.59	1.44
CaO	3.6	11.6
MgO	80.9	72.22
LOI	6.69	6.74

High purity raw materials are used to get superior properties and less impurities. This gunning mass has less gelation time with good stickability and high HMOR value for better corrosion resistance[2]. (Fig. 4 and Fig. 5). With improvement in gunning material, the maintenance practice also improved by implicating regular and situation-based gunning practice focusing on the Inlet Snorkel[6].

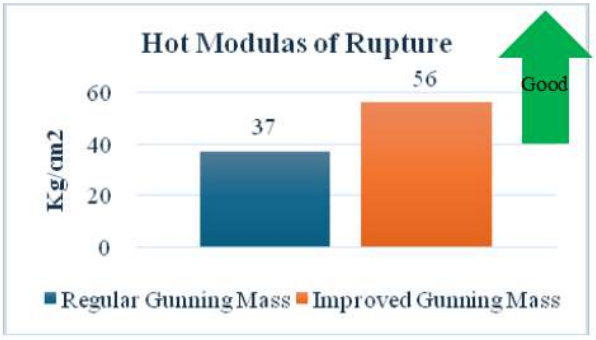
Figure 3: Enhancement of <1µm pore sizes with similar total porosity help us to achieve higher spalling and slag corrosion resistance under high stress



Figure 4: Improvement of water demand in Gunning Mass



Figure 5: Improvement of Hot Strength (HMOR) in the Gunning Mass



c. Installation Procedure:

To ensure faster and flawless installation, a proper Installation SOP has been developed and implemented. TRL Krosaki and Jindal Steel Limited jointly prepared the SOP and successfully deployed it across the installation process. To enhance understanding and adherence among the installation team, a visual SOP in the local language has also been developed and implemented, highlighting all key checkpoints and critical installation requirements.

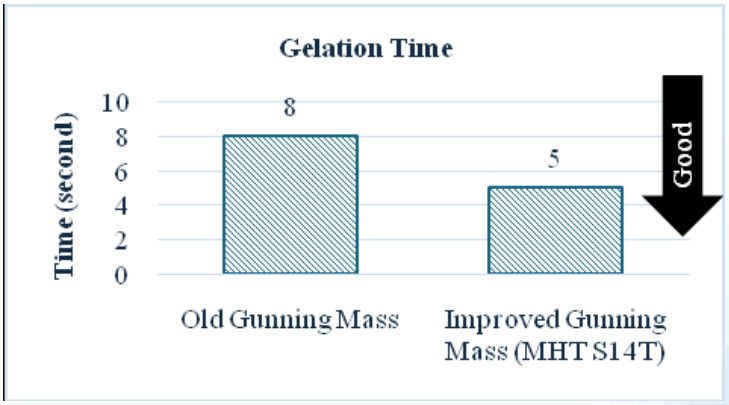
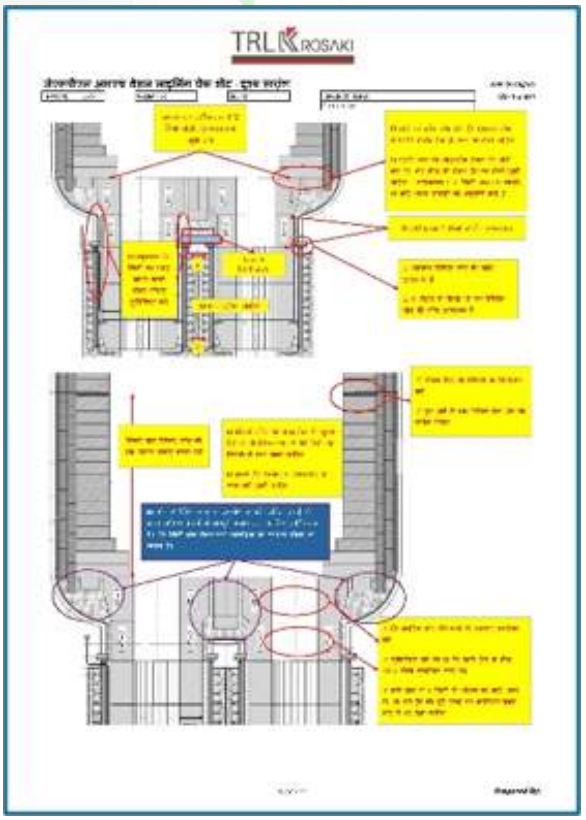


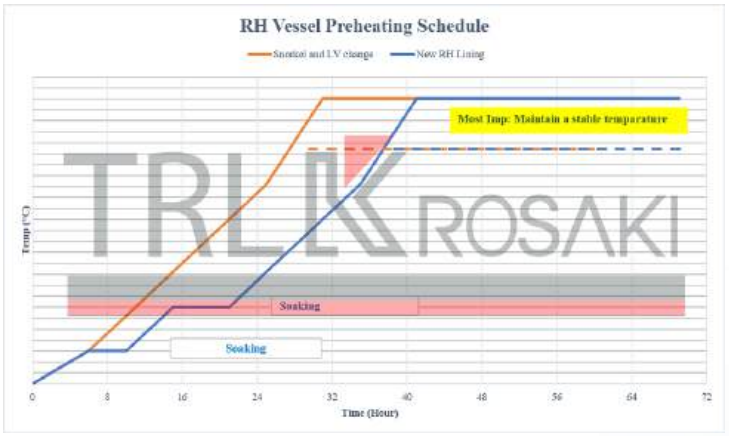
Figure 6: Development and implementation of visual SOP in local language



d. Preheating Practices:

Jindal Steel Limited has accepted the recommendation to modify its RH vessel heating schedule and has switched to a preheating fuel with a higher calorific value to ensure optimal heating of the RH vessel refractories[5].

Figure 7: Standardization of RH Preheating Practice by implementation of preheating schedule



e. Operational Discipline:

RH Refractory Life is very much dependent on the operational practices followed[4]. Jindal Steel Limited has optimised their operational practices to utilise the maximum potential out of the RH Refractories. The following changes help to improve the Snorkel life

- Regular RH production
- Scope of Snorkel gunning in every 1~2 heats
- Optimised treatment time
- Optimised Lift gas flow rate

5. Strengthening Safety Practices

Manpower and process safety were among the key focus areas of the TRM. With the objective of achieving our "Injury Free 2026" target, several proactive measures and safety initiatives were implemented throughout the contract period. The key safety improvements and initiatives undertaken during the TRM period are listed below:

- Strict adherence to PPE (Personal Protective Equipment) requirements in RH vessel and preheating areas.
- Reinforcement of Lockout-Tagout (LOTO) practices during maintenance and inspection activities.
- Enhanced safety briefings and toolbox talk before critical jobs.
- Improved barricading and access control around hot work and refractory installation zones.
- Standardization of safe operating procedures (SOPs) for RH vessellining, heating and vacuum operations.
- Identification and closure of safety observations and near-miss incidents through regular audits.
- Training and competency development programs for operators, supervisors, and maintenance personnel.
- Improved housekeeping in work areas to reduce slip, trip, and fall hazards.
- Strengthened permit-to-work (PTW) compliance for confined space entry, hot work, and maintenance activities.
- Reinforced Working at Height (WAH) safety practices through mandatory use of full-body harnesses, inspection of lifelines and anchorage points, verification of work platforms and scaffolding, and stricter supervision of elevated work activities.
- Better communication and coordination between operations, maintenance, and refractory teams during shutdowns and vessel preparation.
- Implementation of emergency response drills and review of emergency preparedness procedures.

6. Results

The strong technical partnership between Jindal Steel Limited and TRL Krosaki played a crucial role in delivering several key achievements through the TRM, contributing to improved operational performance, safety, and refractory management.

We have compared the key improvement parameters for one year duration during the pre-TRM period vs TRM period. The improvements are as follows:

a. Snorkel Life: 27% improvement in Snorkel Life
b. RH Heat % in SMS and monthly RH Production: 100% increase in TRM period
c. By Plan Snorkel Outage: 100% increase in TRM period
d. Specific Gunning Consumption: 25% reduced in TRM period
e. Snorkel & Lower Vessel relining duration: 30% reduced in TRM period
f. Lost Time Injury (LTI): Zero (0) during TRM period
g. Injury: Zero (0) during TRM period
h. Fatality: Zero (0) during TRM period

7. Conclusions

The TRM project demonstrates how a structured improvement strategy can generate sustainable business value. By integrating reliability engineering, improved refractory material, site condition monitoring, and workforce engagement, the customer achieved improved equipment life, higher productivity, and lower operating costs.TRL Krosaki has ensured 100% equipment availability with the same number of RH vessels by efficient installation process and improved life. During the entire TRM period the site has not witnessed any Lost Time Injury (LTI), all the near miss incidents recorded, reported and communicated with the entire team. Timely action, proper PPEs and preventive measures ensure zero harm to the manpower.

Figure 8: Key improvement outcomes of RH TRM project; at top left: Improvement in Snorkel Life; top right: Increment in Number of RH Heats/month; bottom left: Reduction of Specific gunning consumption; bottom right: Reduction in Refractory Lining Duration



Apart from the KPIs; we (TRL Krosaki and Jindal Steel Ltd – Raigarh) have also achieved some record-breaking figures as mentioned below – as on 31st Aug 2026.

i. Highest RH Snorkel Life – 111 heats
ii. Highest Treatment duration in a Snorkel – 1554 minutes
iii. Highest ever RH heat in a single day operation
iv. Highest RH heat production in a single month operation

References

1. New Generation Semi-Rebonded Magnesia Chrome Refractories for RH Degasser (UNITECR 2021)
2. Krosaki Harima Technical Reports (2012)
3. Refractory for Secondary Refining of Steel (Subir Biswas & Debasish Sarkar)
4. Recent Advances and Future Prospects of Refining Technology (Nippon Steel Technical Report Apr-1994)
5. Nippon Steel Technical Report (April 1994) on recent advances in ultralow carbon steel refining technology by vacuum degassing process.
6. Mechanisms of wear of refractory materials in snorkels of RH degasser and the possibilities for their reduction (English) by Czapka, Z. / Skalska, M. / Zelik, W.
7. Development of Basic Gunning Mixes: AISTech 2019 — Proceedings of the Iron & Steel Technology Conference 6–9 May 2019, Pittsburgh, Pa., USA
8. A holistic approach to enhance RH snorkel performance based on computational fluid dynamics (CFD) study (UNITECR 2025)

INTEGRATED REFRACTORY SOLUTION FOR A 140-TON ALUMINUM REVERBERATORY FURNACE (NOVELIS ULSAN) CASE STUDY

Woong Kim (Sales Manager, Calderys Korea)
Won seok Yoon (Hansung, CEO)

Calderys Korea

Introduction/ background of the case/issue; roles of involved organizations

1. Introduction

Integrated Refractory Solution for a 140-ton Aluminum Reverberatory Furnace (Novelis Ulsan): From Global Design Collaboration to Partner-Driven Installation and Commissioning

2. Background of the cast

Aluminum recycling processes are increasingly important due to growing demand for sustainable production and a circular economy. To achieve global carbon neutrality and ESG management, meet the demand for low-carbon products, and secure cost competitiveness and supply chain stability, Ulsan Aluminum (a joint venture between Novelis and Kobe Steel) pushed forward with building a new 140-ton reverberatory furnace designed to process contaminated aluminum scrap involving high temperatures and chemical loads. The Ulsan Aluminum project underwent precise design reviews to meet high-efficiency energy-saving and eco-friendly standards, proceeding through open competitive bidding with multiple companies during the contracting and execution stages. The roles and execution details by organization for this project are as follows:

3. Roles of involved organization

Calderys Korea: Oversaw the entire turnkey scope of the refractory system, including installation and dry-out (generated about 2.2 billion KRW / roughly 1.5 million EUR in revenue in 2024).

Calderys India: Performed engineering.

Calderys Taiwan: Handled material supply. Calderys Japan & Taiwan Supervisors: Provided on-site support.

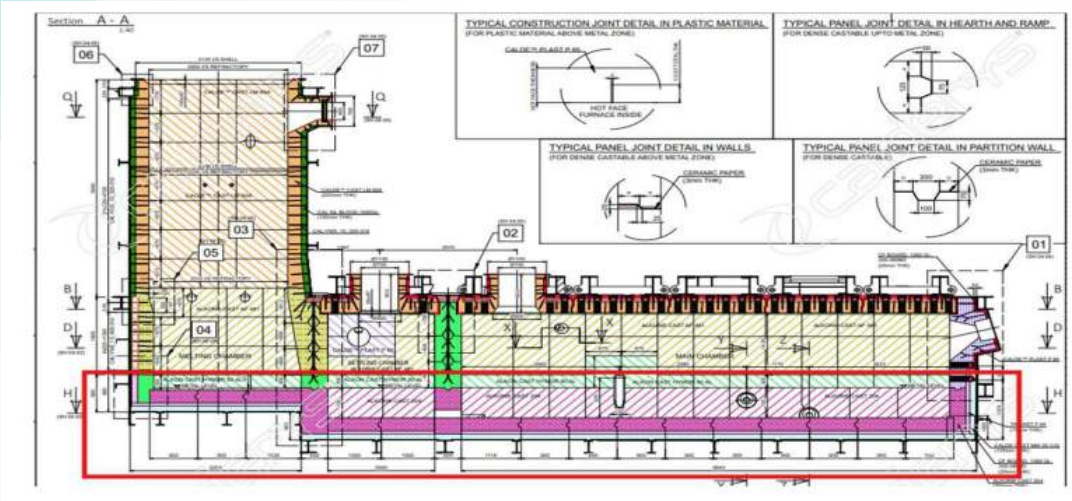
Define the case/ problem/ original practice

1. Conventional Practices and Challenges: Aluminum recycling equipment is exposed to harsh environments such as contact with molten aluminum, chemical corrosion by slag, thermal shock, and mechanical impact from charged scrap. In particular, the core challenges are controlling local overheating and chemical reactions caused by charging contaminated scrap, and dealing with the harsh environment around the belly band.

2. Requirements by Specific Zone: Each zone inside the reverberatory furnace including the melting chamber, main chamber, settling chamber, and pumpbox requires a customized lining configuration to resist mechanical wear and thermal shock.

3. Limitations in Construction Experience: In particular, there was no prior construction experience for a 140-ton reverberatory furnace domestically.

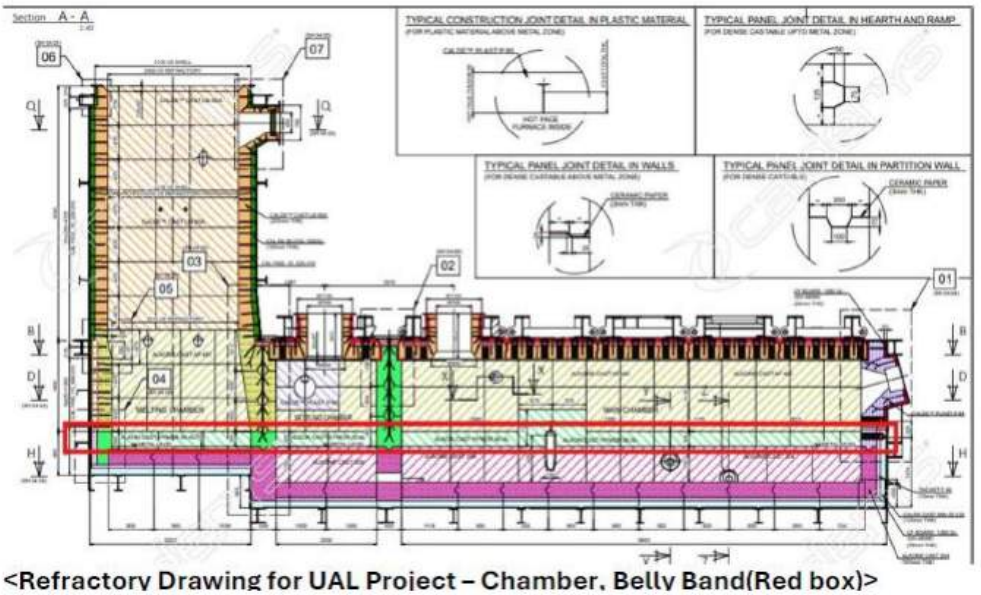
Define the case/ problem/ original practice



1.Melting Chamber: Initial scrap melting zone with high impurities, severe chemical corrosion, and mechanical impact from falling scrap.

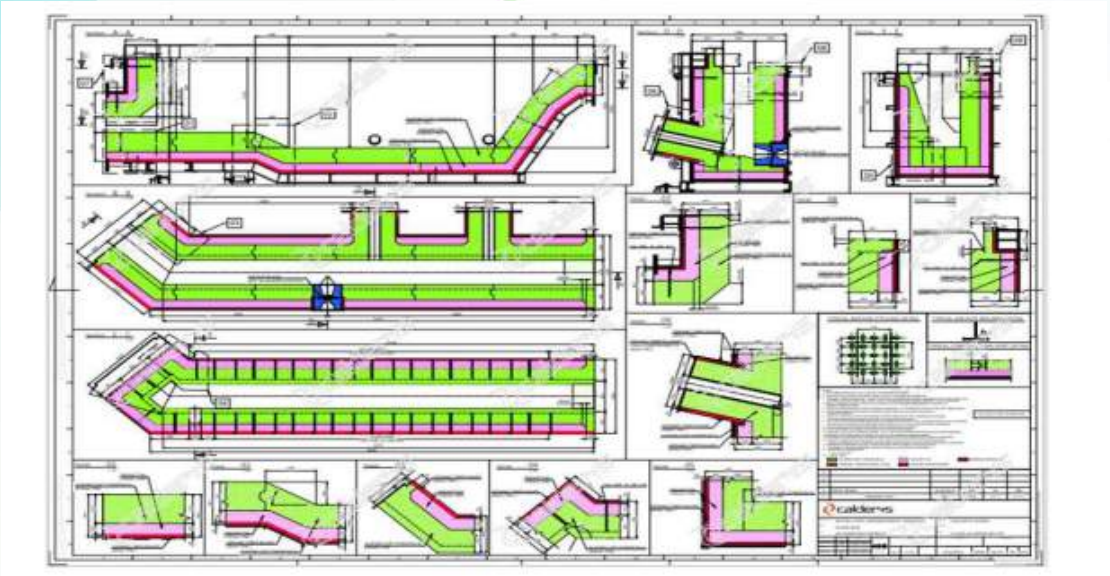
2.Settling Chamber: Impurity stabilization zone demanding high corrosion resistance against prolonged static contact with slag.

3.Main Chamber: Stable flow zone toward the Pump Box, requiring resistance to thermal and mechanical fatigue from sloshing.



<Refractory Drawing for UAL Project – Chamber, Belly Band(Red box)>

4. Belly band: The Belly Band zone is where the free surface level of molten aluminum periodically rises and comes into contact with the refractory lining. It experiences extreme conditions, including sloshing motion of molten metal, chemical attack, thermal shock, and mechanical impact.



5. Pump box: The Pump Box temporarily stores molten aluminum discharged from the Main Chamber before it is transferred to the Holding Furnace. It serves as a critical connection point for aluminum flow within the system. Internally, it is exposed to molten aluminum at high temperatures and undergoes frequent inflow and outflow cycles. Therefore, its refractory lining must withstand chemical corrosion from molten metal, repeated thermal cycles, and mechanical impact.- Temperature: up to 800°C,Outer Shell Temperature: approx. 60°C.

Benchmarking/ comparison/ major challenge

1. Key Challenge: Since a single-lining structure struggles to withstand extreme temperature gradients and mechanical-chemical stresses, a segmented multi-layer structural design tailored to the operating conditions (such as temperature and load) of each zone is essential.

2. Comparative Analysis: Unlike conventional blanket approaches, optimized refractory materials and thicknesses were differentiated and applied to each zone—such as the reverberatory furnace Roof, Hearth & Ram, Upper Wall, Preheat Shaft, Regenerator Box, and Pipe Work—based on HTC (Heat Transfer Coefficient) criteria established at UAL.

3. Simulation-Based Verification: Pre-verification processes were conducted by crosscomparing simulation data across zones to reduce heat loss rates and maximize durability compared to conventional designs.

Technical improvement/ development/ solution/action plan

Multi-Layer Functional Refractory Design:

•Corrosion & Attack Mitigation (Hot Face, Belly band): Applied a specialized refractory with 84% high-purity corundum and BaO-based components in the belly band to effectively suppress interfacial reactions and penetration by molten aluminum.

•High-Temperature Structural Stability (Roof): Utilized a mullite-based low cement castable in the roof section, exhibiting a hot compressive strength exceeding 210 MPa at 1500°C, ensuring long-term load-bearing capacity without sagging under severe radiant heat.

•Thermal Stress Dispersion: Incorporated a 3-to-4 layer composite structure combined with a low apparent porosity (15%) to dissipate thermal stress across extreme temperature gradients and prevent internal gas permeation.

•Mechanical Restraint & Expansion Control: Deployed SS310 Y-shaped anchors and precisely engineered expansion joints to accommodate dimensional changes and maintain structural tightness, minimizing lining deformation and cracking caused by thermal expansion.

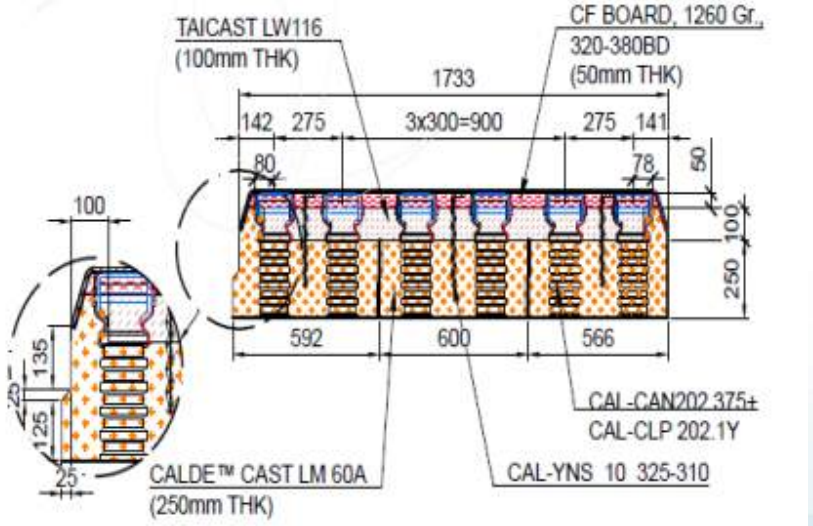
Roof: Applied CALDE CAST LM 60 A and others to secure high-temperature strength and thermal shock resistance.

•High Temperature Structural Integrity
•Prevents sagging and ensures long-term load-bearing capacity in roof applications through a significant increase in hot compressive strength up to 210 MPa at 1500°C.

•Thermal Shock Resistance via Mullite Matrix
•Suppresses cracking and spalling under frequent thermal cycling based on a mullite-based structure with 60.5% Al2O3.

•Gas Permeation Control and Sealing
•Minimizes internal degradation from hot process gases using a low apparent porosity of 15% and maintains structural tightness with controlled linear change (+0.6% at 1500°C).

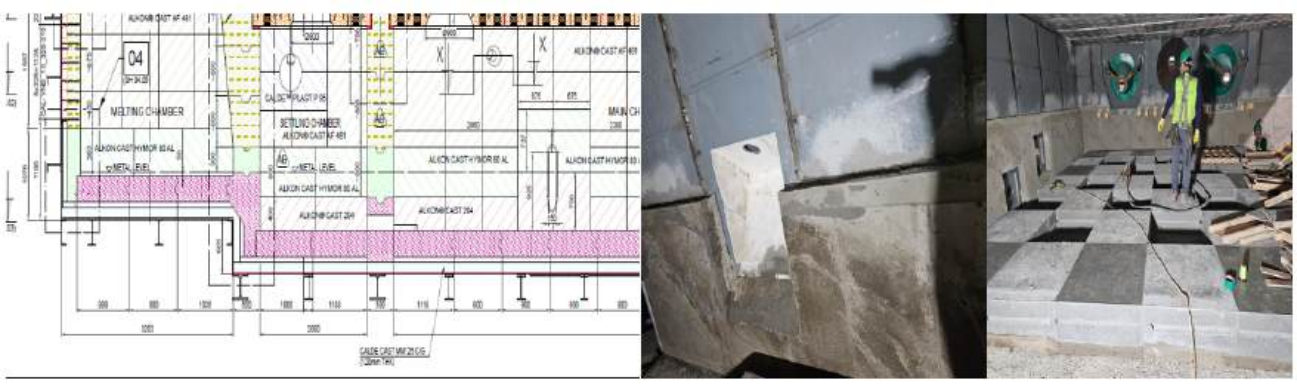




Zone-Specific Custom Material Application:

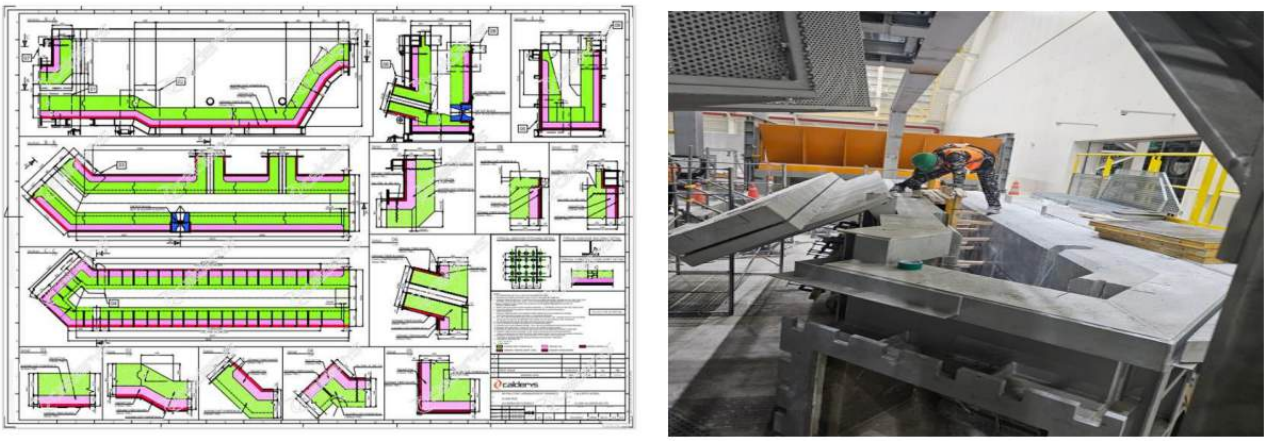
Hearth & Lower Wall(Belly band): Prevention of molten aluminum penetration through the interfacial reaction suppression effect of high-purity 84% corundum and specialized BaO-based components, while minimizing structural collapse caused by thermal shock

in harsh belly band environments based on high-temperature cold crushing strength exceeding 130 MPa and a stable linear change rate (-0.2%).



Zone-Specific Custom Material Application:

Pump box: Applied ALKON® CAST HYMOR 80 AL (250 mm)A high-performance low-cement castable using brown fused corundum aggregates.Exhibits excellent non-wettability with molten aluminum, suppresses corundum growth, and resists reactions with high-alloy aluminum.



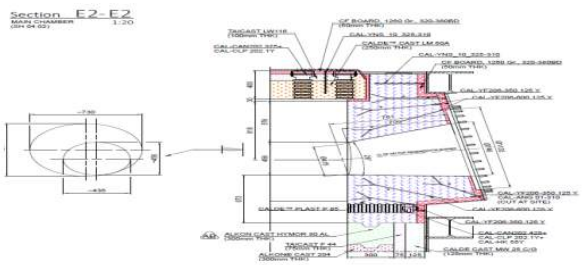
Zone-Specific Custom Material Application:

•**Burner:** Applied CALDE PLAST P 85 exhibits excellent thermal shock resistance and dimensional stability even under direct flame.

•**High Thermal & Chemical Resistance:** Withstands up to 1650°C utilizing an 84.0% high alumina bauxite composition to prevent corrosion from high-velocity combustion gases.

•**Superior Thermal Shock Resistance:** Achieves a compressive strength of 80 MPa at 1200°C, mitigating cracking and spalling from frequent thermal cycling and flame impingement.

•**Dimensional Stability & Tightness:** Maintains a stable linear change (+0.1% at 1200°C) with chemical-inorganic ramming to prevent joint openings and minimize heat loss around burners.



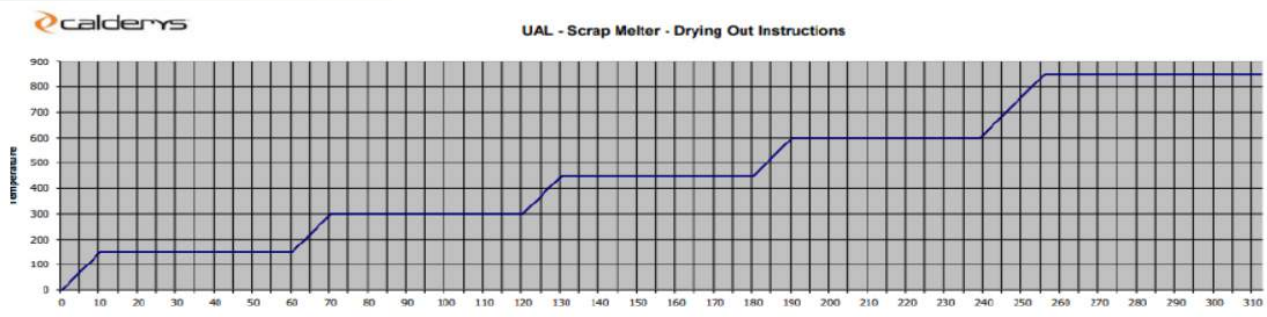


Custom Drying Process (Dry-out):

•**Tailored Dry-out Schedule:** Established a systematic 312-hour drying process that successfully prevents lining damage caused by moisture vaporization during initial heat-up.

•**Prevention of Critical Spalling:** Applied dedicated 50-hour holding periods at the critical spalling risk zones of 300°C and 450°C to effectively control internal vapor pressure build-up.

•**Overcoming Operational Constraints:** Successfully broke through thermal-hydraulic heating limitations within an automated pressure-controlled multi-chamber environment through close collaboration with a specialized dry-out contractor.



Pump box: A separate burner is used to perform the drying process in alignment with the reverberatory furnace drying schedule.

Regen box: Performs an independent 35-hour drying process using separate heating pads.

■ 공사명 : UAL RECYCLING CENTER PROJECT Refractory Installation for Scrap Melter 내화물 건조



Dry Out 현장 사진 (Furnace) | Dry Out 현장 작업 사진

Dry Out 온도 Monitor | Dry Out 현장 사진 (Pump Box)

Safety & Partnership: Achieved zero accidents over an 8-month construction period, earning high trust from Ulsan Aluminum, and successfully collaborated with partner company Hansung.



Benefit/ Value Addition & Conclusion

•The multi-layer refractory design and optimized dry-out protocol validated in this study establish a robust engineering benchmark to enhance the service life and operational stability of similar aluminum high-temperature furnaces.

•Successfully executing an integrated engineering approach—encompassing design, material selection, construction, and drying—elevated the technical reliability of furnace lining operations and established a practical standard applicable across broader aluminum recycling facilities.

•Furthermore, routine maintenance inspections and post-mortem analyses provide critical empirical data for continuous monitoring, laying the foundation for ongoing advancements in customized high-temperature refractory solutions.

•We have successfully secured a proprietary dry-out engineering reference optimized for large-scale 140-ton reverberatory furnaces structured with complex chambers.

•Co-developed a new turnkey business model by transforming our core customer into a capable contractor, establishing an integrated solution framework spanning engineering, material supply, construction, and dry-out.

NEXT-GENERATION RAPID HEATING THROUGH CASTABLES: ENHANCING PERFORMANCE AND SUSTAINABILITY THROUGH SUPERIOR CORROSION RESISTANCE AND REDUCED CARBON EMISSIONS

Sougata Roy[1], Subhadeep Chatterjee[1], Minakshi Dash[1], Sagar Dey[1], Sajal Goldar[1], Arup Kumar Samanta[1], Prasant Kumar Naik[1], G. Bhattacharya[2], E. Chabas[2], C. Wöhrmeyer[2], F. Lacoue[2]

[1]TRL Krosaki Refractories Limited, Belpahar, Odisha

[2]IMERYS S.A., France

Email: asamanta@trlkrosaki.com

Abstract

The development of next-generation trough castables focuses on achieving rapid heating capabilities and superior slag corrosion resistance, addressing both operational efficiency and environmental sustainability. Recent innovations involve the adoption of a cement-free system leveraging an advanced “No Cement” Castable (NCC) binder. This binder, a single-component solid powder with very low CaO content, facilitates superior application performance by providing fast dry-out and maximizing refractoriness. The faster drying and pre-heating cycles significantly reduce the risk of steam explosion and shortens installation and repair times, enabling earlier commissioning of troughs. Laboratory trials demonstrate that this castable maintain general physical properties like cold crushing strength, bulk density, permanent linear change, thermal spalling resistance to desired levels. In several aspects this castable is showing superior properties over the existing trough castables. The specific improvements are in permeability, oxidation resistance and slag corrosion resistance particularly against aggressive slags with varying basicity. The improved castable shows reduced corrosion depths and enhanced oxidation resistance, extending service life and reducing maintenance frequency. Importantly, the faster heating schedules directly contribute to lower CO_2 emissions by minimizing energy consumption during pre-heating, aligning with industry goals for carbon neutrality. This holistic approach not only optimizes throughput and cost-effectiveness but also supports the steel industry’s transition toward more sustainable practices by lowering the overall carbon footprint of refractory operations.

Introduction

Blast furnace trough refractories play an important role in ensuring uninterrupted transportation and separation of molten iron and slag before further processing. The refractory lining of troughs is continuously exposed to severe thermal, chemical and mechanical conditions including molten slag attack, oxidation, abrasion and repeated thermal cycling. Consequently, the service life and performance of trough castables have a direct impact on hot metal throughput, maintenance frequency, productivity and overall operational cost.

Trough castables are generally based on calcium aluminate cement (CAC) bonded Al-SiC-C systems. Although these castables provide satisfactory installation characteristics and mechanical strength, the presence of hydraulic cement results in the formation of calcium aluminate hydrates which contain considerable amounts of chemically bonded water. During the initial dry-out and pre-heating process, both physically and chemically combined water must be removed carefully to avoid excessive vapour pressure generation that may lead to steam explosion and catastrophic lining failure. Therefore, prolonged drying and pre-heating schedules are generally adopted, which increase furnace downtime and energy consumption while contributing to higher CO_2

emissions. Recent studies[1,2,3] have shown that drying remains one of the most critical stages during the commissioning of refractory castables and often determines the success of lining installation.

Several efforts have been made to overcome the limitations associated with conventional cement-bonded castables. One approach involves the use of drying additives such as polymeric fibres, metallic powders and permeability-enhancing agents to improve water evacuation from the refractory matrix[4,5]. These additives create additional pathways for vapour release and help to reduce the risk of explosive spalling during rapid heating. However, the effectiveness of such approaches is still limited by the presence of hydrated cement phases which continue to require controlled heating schedules.

In recent years, significant attention has been directed towards the development of "No Cement" Castable (NCC) technologies. Cement-free binder systems (refer to table no.1) based on colloidal silica, microsilica-gel bonding and other advanced inorganic binders have demonstrated superior drying behaviour, lower CaO content, enhanced refractoriness and improved thermo-mechanical properties compared with low-cement castables. Peng and Myhre[6,7]reported fast dry-out characteristics in microsilica-gel bonded castables. Furthermore, novel NCC binder systems have shown superior high temperature strength, improved oxidation resistance and enhanced corrosion resistance under severe operating conditions.Among the different NCC binder systems, colloidal silica provides the highest dry-out efficiency, although it comes with the complexity of handling a two-component system, low initial strength and lower control of setting.

Along with rapid heating capability, corrosion resistance remains a major challenge for blast furnace trough applications. Slag infiltration and dissolution of refractory constituents at the metal-slag interface are major factors limiting campaign life. Several researchers[9,10] have reported that reduction of CaO content and optimization of matrix chemistry significantly improve resistance against slag attack by reducing the formation of low melting phases and minimizing slag penetration. Recent developments in Al_2O_3-SiC-C castables have further demonstrated that suitable microstructural modifications can simultaneously enhance both corrosion resistance and thermal shock resistance[11].

Apart from technical performance, sustainability has become a key driver for the refractory industry. The steel industry is actively pursuing carbon-neutral manufacturing practices, creating increasing demand for refractory materials that can contribute to lower energy consumption and reduced greenhouse gas emissions. Rapid-heating and without drying castable technologies have recently emerged as effective approaches to reduce fuel consumption associated with drying and pre-heating operations. Industrial investigations have demonstrated[12,13] that advanced binder systems can significantly shorten repair turnaround times while contributing to substantial reductions in CO_2 emissions.

Considering these requirements, the present work focuses on the development of a next-generation rapid-heating trough castable based on an advanced cement-free binder system. The objective is to achieve superior permeability, improved steam explosion resistance, enhanced slag corrosion resistance and lower energy consumption during commissioning. The performance of the developed castable has been evaluated in comparison with conventional trough castables through measurements of physical properties, steam explosion behaviour and slag corrosion resistance. Furthermore, the potential contribution of this technology towards reduced carbon emissions and sustainable ironmaking operations has been assessed.

Background

A systematic laboratory investigation[14] was previously conducted to evaluate the feasibility of replacing conventional CAC-bonded Alumina-SiC-C castables with a special binder-based system. Based on the overall laboratory performance, the special binder-based composition containing a minimum level of CAC was selected for further development and industrial validation, as it provided the best balance of workability, mechanical strength, thermal stability, steam explosion resistance, and slag corrosion resistance.

Parameter	Conventional	Special Binder
Binder system	CAC based	CAC free/negligible
CaO content	Relatively higher	Very low
Drying requirement	Conventional schedule	Rapid-heating compatible
Steam explosion resistance	Moderate	Improved
Slag corrosion resistance	Standard	Enhanced
Sustainability	Baseline	Improved

Tab.1: Comparison of Conventional and Special Binder Technology

The Special Binder-Based Batch demonstrated the most balanced thermo-mechanical performance among the trial formulations. It exhibited the highest CCS at high temperatures while maintaining comparable CCS and CMOR values to other batches up to 1100°C, indicating improved strength development through the combined effect of the special binder and a controlled amount of CAC.The batch also showed better dimensional stability, with lower positive PLC at 1500°C compared to the conventional CAC-bonded castable, suggesting reduced formation of expansive calcium aluminate phases.In the steam explosion test, the Special Binder-Based Batch remained intact at 1000°C and exhibited only minor surface damage at 1300°C, whereas the conventional castable suffered severe explosive spalling. These results highlight its potential to reduce drying and preheating requirements while ensuring safe and reliable operation.

The slag corrosion study was conducted at 1550°C using blast furnace slag further demonstrated the superiority of the modified binder system. Progressive reduction in corrosion depth was observed with decreasing CAC content, and the CAC-free formulation exhibited the best corrosion resistance (~18% improvement). The improved performance was attributed to the lower lime content in the refractory matrix, which minimized the formation of slag-reactive phases and enhanced resistance against chemical attack.

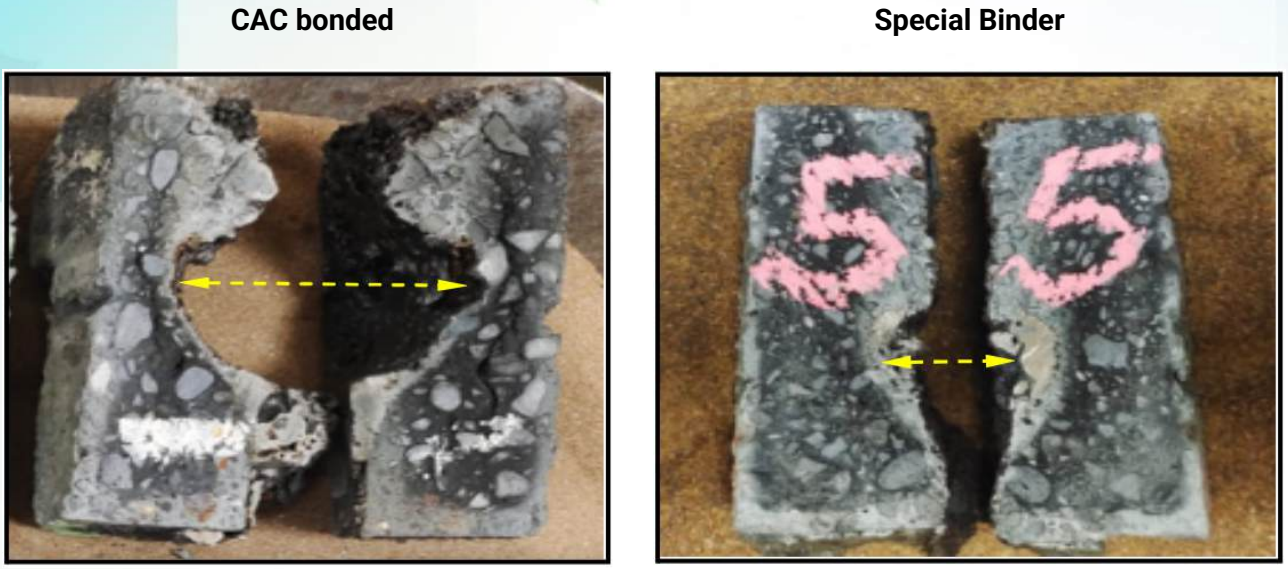


Fig.1: Appearance after Slag Corrosion Test

Also, XRD analysis confirmed the formation of the desired refractory phases, namely corundum, mullite, and silicon carbide, indicating that the special binder system did not adversely affect the phase composition or high-temperature stability of the castable.

A key benefit of CAC elimination was demonstrated through the steam explosion resistance study. While the conventional CAC-bonded may suffer severe explosive spalling under rapid heating conditions, the CAC-free composition remained intact, highlighting its potential for reduced drying and preheating requirements, lower installation time, and reduced carbon emissions.Based on the laboratory findings, the special binder-based castable system was identified as a promising alternative to conventional formulations, offering two major advantages:

1. Improved slag corrosion resistance, leading to enhanced durability and service life.
2. Reduced carbon footprint, through the potential reduction of preheating temperature and drying/preheating duration.

Accordingly, the field trial program was planned in two phases. Phase-1 was conducted using the standard heating cycle (as per current practice) to validate the corrosion resistance benefits, while Phase-2 is intended to evaluate the full potential of the technology, including both improved corrosion resistance and reduced preheating requirements. The results presented in this paper are based solely on the extended field trial outcomes of Phase-1, whereas Phase-2 is planned for future implementation.

Materials and Experimental procedures:

Based on the initial laboratory investigations, a special binder-based castable (SB-1) was developed and selected for field evaluation. Subsequently, as part of a collaborative development program between **TRL Krosaki and Imerys**, an advanced no-cement castable (NCC) technology (SB-2) was evaluated in parallel with the aim of further improving dry-out performance, permeability, operational safety, and sustainability beyond the capabilities of SB-1. Prior to field implementation, the physico-chemical properties of SB-2 were assessed and compared against both the CAC-bonded castable (CAC) and the established special binder-based castable (SB-1).

Novel NCC binder technology from Imerys (SB-2):

The Imerys NCC binder (SB-2) addresses key limitations inherent in common NCC binders, such as inconsistent setting, reduced mechanical strength, and logistical complexities for two component colloidal silica based castables. This single component powder solution streamlines job-site application while enhancing both drying and refractory performance[15].

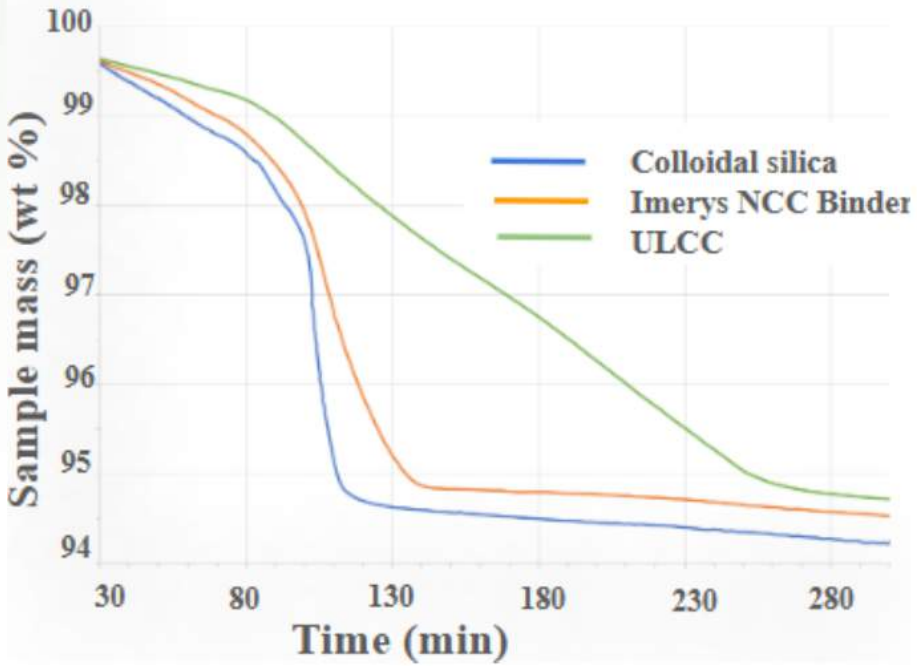


Fig. 2: Macro thermo-gravimetric analysis (TGA) of colloidal silica, Imerys NCC binder and alumina cement bonded ULCCtested on a 10 cm^3 cube

As a hydraulic binder with minimal CaO content and integrated additives, it simplifies castable design and storage by requiring only the addition of water. It offers distinct advantages over conventional NCC binders, including predictable demoulding times, improved green mechanical strength, and high refractoriness derived from mullite formation after firing. Furthermore, its drying profile is comparable to that of colloidal silica solutions (Fig. 2), facilitating moisture release below 150°C and effectively minimizing the risk of explosive steam spalling.

By combining formulation flexibility with operational efficiency, this NCC binder represents a significant advancement in refractory castable technology, successfully balancing technical performance with ease of use.

Flow results and setting time (Table 2) indicated that the SB-1 formulation showed optimum workability among all with same amount of casting water with optimum setting time, demonstrating that the special binder system could provide adequate dispersion and placement properties comparable to conventional castables. Good flowability is essential for proper mould filling, compaction, and uniform lining quality during installation. Long setting time was observed for the SB-2 formulation, which was later adjusted with an accelerated version of the NCC binder, the results of which were not discussed in this paper.

Parameters	CAC	SB-1	SB-2
Water (%) for casting	7	7	7
Setting time	2 hrs	3 hrs	47hrs
Vibration Flow (mm)			
T=0 min	205	215	184
Permeability (mD)			
110°C	0.234	>5	>5
200°C	0.828	>5	>5
US Results			
1500m/s velocity time (min)	330	430	4726
2700m/s velocity time (min)	785	Not observed	6789
3500m/s velocity time (min)	1133	Not observed	Not observed

Tab.2: Comparison of properties

Ultrasonic stiffness (US) measurements were used to monitor the development of internal bonding and hardening with time. The results (Fig. 4)showed that the cement bond developed the highest strength (final US velocity 3000m/s), followed by SB-2 (final US velocity 2750m/s despite taking long hours), whereas SB-1 showed a significantly lower US velocity (1400m/s), indicative of a very low strength development. Controlled stiffness development ensures safe demoulding and handling while maintaining the advantages of non-cement bonding systems.



Fig.3: Castable samples after 24h at 110°C for permeability test

The samples for permeability test after drying at 110^0C for 24 hours are shown in Fig. 3. Permeability studies showed improved gas and moisture evacuation characteristics in the both SB-1 and SB-2 formulations. The enhanced permeability facilitates the escape of water vapor during the drying and heat-up stages, thereby reducing internal pressure build-up and minimizing the risk of explosive spalling. This is one of the key advantages of this technology.

Results of Ultrasonic Stiffness (US) versus H_2 Degassing

The test is particularly relevant for Al_2O_3-SiC-C castables containing very small amount of metallic aluminium powder, this metallic aluminium powder is incorporated in Al_2O_3-SiC-C castables to improve dry-out safety through controlled hydrogen gas generation. In the alkaline environment created during mixing, aluminium reacts with casting water as follows:

$$2Al+6H_2O \rightarrow 2Al(OH)_3+3H_2\uparrow$$

The controlled evolution of H_2 gas creates a network of fine interconnected micro-channels within the castable matrix. These channels increase permeability and provide pathways for the rapid escape of water vapor during heating, thereby reducing

internal steam pressure and minimizing the risk of explosive spalling. The dosage of aluminium powder is carefully optimized to generate sufficient permeability without adversely affecting strength, dimensional stability, or overall castable integrity.

Here the relationship between ultrasonic stiffness (US) development and hydrogen (H_2) degassing behavior was investigated to understand the evolution of the castable microstructure during setting and drying. This evaluation is particularly important for no-cement based formulations, where achieving sufficient green strength while maintaining safe moisture removal is critical.

The ultrasonic stiffness (US) results provided information on the rate of bond formation and hardening within the castable matrix. An increase in US indicates progressive development of the internal structure and gain in mechanical integrity. Simultaneously, H_2 degassing measurements were used as an indirect indicator of pore connectivity and gas transport capability within the castable body.The study demonstrated that the optimized binder formulations were capable of developing adequate stiffness while still allowing efficient gas release through the pore network. This is a significant advantage because, in refractory castables, rapid stiffness development can sometimes restrict gas evacuation and increase the risk of pressure build-up during heating. H_2 degassing happened rapidly for both CAC and SB-1 bonded castables as observed from the sharp US peaks and H_2 vol. release within a few hours of casting (Fig. 4). CAC bonded castable continued developing strength afterwards and reached a good final US velocity (3000m/S), whereas SB-1stabilized at a very low US velocity (1400m/S). SB-2 showed H_2 degassing much later after the final strength development (US velocity 2750m/S).

The correlation between US and H_2 degassing suggests that the advanced binder technology promotes the formation of a permeable microstructure that permits continuous gas escape even as the castable gains strength. As a result, internal vapor pressure during dry-out can be reduced, leading to a lower risk of explosive spalling and enabling faster, safer heat-up schedules

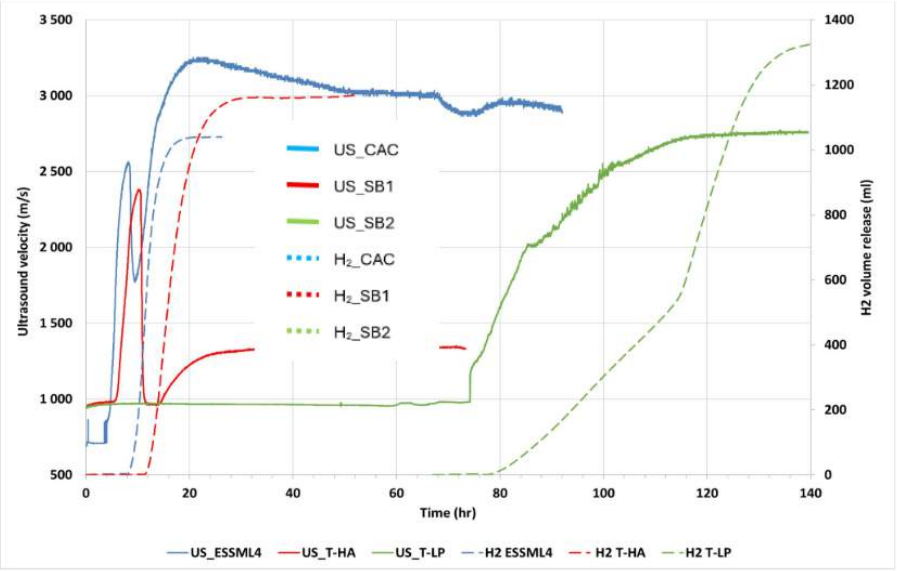


Fig. 4: Ultrasonic Stiffness vs H_2 Degassing

These results provided strong technical evidence supporting the use of advance binder technology for applications requiring rapid commissioning, improved operational reliability, and lower overall energy consumption

Results of Macro Thermo Gravimetric Analysis (TGA) (50°C/h)

Macro Thermogravimetric Analysis (Macro TGA) was conducted at a heating rate of 50°C/h to evaluate the moisture removal behavior and thermal stability of the castable systems during heating. This test simulates the drying and preheating conditions experienced by refractory linings in actual service and provides valuable information on mass loss associated with free water evaporation, dehydration, and decomposition reactions.

The sample appearance (surface& cross section) is shown in Fig. 5 after Macro TGA. Theresults (Fig. 6) showed that the both SB-1 and SB-2 formulations exhibited rapid weight-loss behavior during heating compared withCAC-bonded systems. Reduction in calcium aluminate hydrate formation decreased the amount of chemically bound water in the castable matrix, resulting in lower water release during heating and improved dry-out performance.

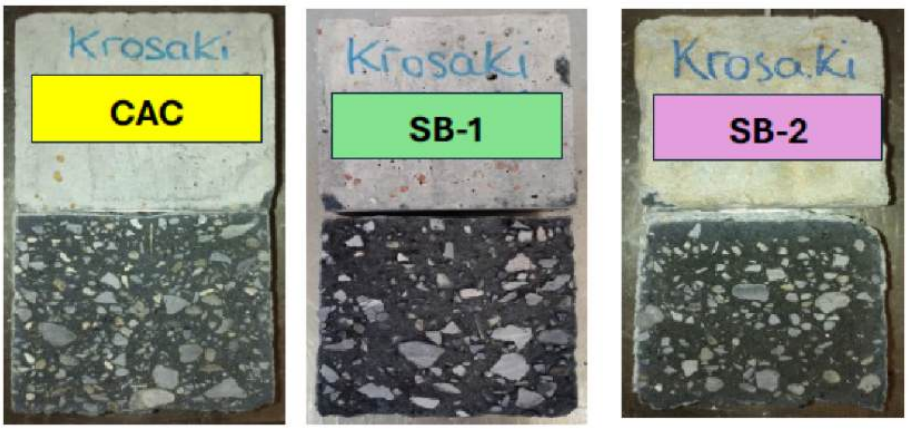


Fig. 5: Appearance of sample surface (top) and cross-section (bottom) after Macro-TGA analysis

A rapid weight-loss profile indicates that moisture can escape without generating excessive internal vapor pressure. The Macro TGA findings therefore support the improved permeability and H_2 degassing results observed best for the SB-1 technology.

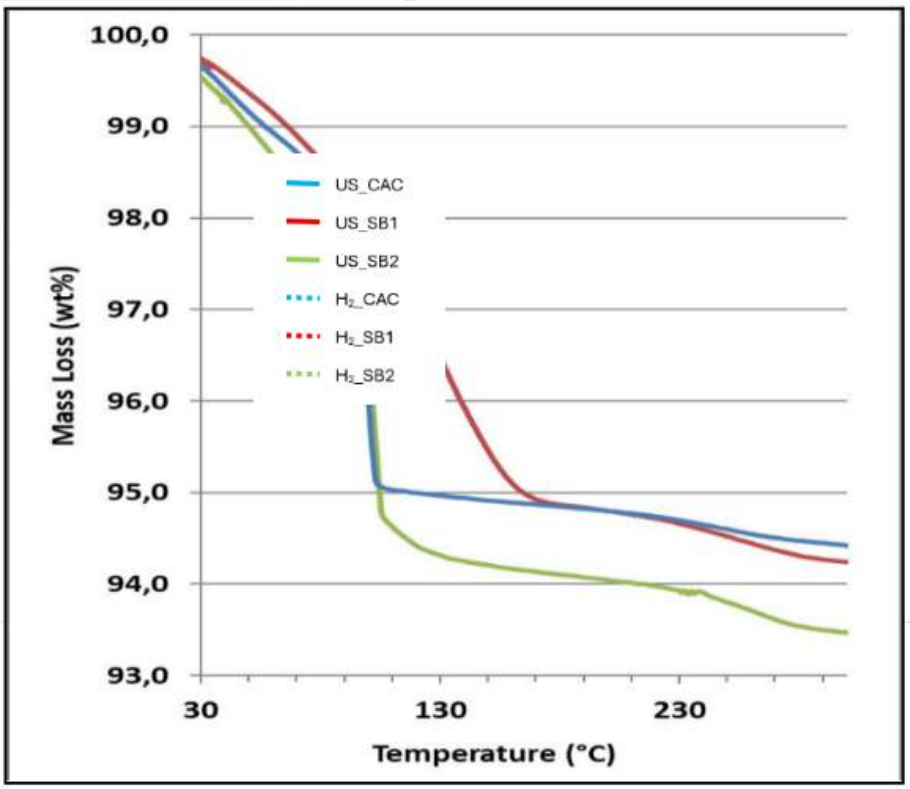


Fig.6: Macro TGA Analysis

Furthermore, the study confirmed that the advanced binder systemspromote safer and more efficient moisture removal while maintaining structural integrity during heating. The lower mass-loss rate associated with the advanced binder-based formulation suggests the possibility of accelerated drying and preheating schedules, which can reduce commissioning time, energy consumption, and overall carbon footprint.These results further validate the suitability of the advance binder technology as a next-generation refractory solution combining operational safety, installation efficiency, and sustainability

Industrial Trial Outcomes

With the initial progress of lab trials for SB-1, it was selected for the first phase of field trials. Subsequently, industrial trials were conducted in an operating blast furnace runner system to assess the performance of SB-1 under actual service conditions. Multiple trial locations, representing different wear and corrosion mechanisms, were selected to comprehensively evaluate its in-service behaviour

Trial Location	Material used (MT)	Throughput Achieved
Waterfall TH-03	2	~67,000 THM
Waterfall TH-04	2	~58,000 THM
Slag Runner Junction 01 & 04	5	~225,000 THM
Slag Runner Junction 02 & 03	4	~196,000 THM

Tab.3: Industrial Trial Summary

The selected locations exposed the castable to varying combinations of slag attack, molten metal turbulence and mechanical wear, providing a comprehensive assessment of field behaviour.

Field Performance Assessment

Performance in Waterfall Areas: The waterfall region is recognized as one of the most aggressive locations within the trough system due to the combined effects of high turbulence, mechanical impact and slag attack.

The SB-1 castable was installed at waterfall locations associated with TH-03 and TH-04. After operation, both locations exhibited satisfactory structural integrity. However, sidewall erosion levels were observed to be somewhat higher than existing benchmark materials.

At TH-03, approximately 200 mm sidewall erosion was reported after achieving nearly 67,500 THM throughput. Similarly, TH-04 exhibited approximately 170 mm erosion after achieving approximately 57,600 THM throughput.

The results indicate that while the castable provides acceptable service performance, additional optimization focused on impact and turbulence resistance may further improve life in waterfall applications.



Fig. 7:After application appearance of waterfall TH-04

Performance in Slag Runner Junction Areas

Among all trial locations, the most promising results were achieved in slag runner junction applications.

SB-1 trial quality was installed at the junctions connecting runner sections associated with TH-01 & TH-04 and TH-02 & TH-03. Following extended operation, both trial locations remained in good condition and exhibited only minor erosion.

parameters	Junction 1 & 4	Junction 2 & 3
Hot Metal Throughput (THM) at Inspection	2,25,252 THM	1,96,833 THM
Condition of Slag Runner Junction	Good	Good

Initial lining thickness (mm)	400 mm
Erosion Observed	~250 mm (with regular quality) ~180 mm (with SB-1 quality)
Overall Assessment	SB-1 Demonstrated Better Corrosion Resistance Compared to Regular Quality

The junction associated with TH-01 & TH-04 achieved approximately 225,252 THM throughput, while the TH-02 & TH-03 junction reached approximately 196,833 THM throughput. During subsequent inspections, only about 180 mm bottom erosion was observed and the overall lining condition remained satisfactory.



Fig. 8: After application appearance Slag runner 01&04 junction



Fig. 9: After application appearance Slag runner 01&04 junction

Compared with conventional materials used previously in similar locations, SB-1 demonstrated superior resistance against slag attack and excellent structural stability.These results strongly support the laboratory findings related to enhanced corrosion resistance and confirm the suitability of the technology for high-slag-contact applications.The industrial trial program provided valuable insights into the relationship between laboratory performance and field behaviour.Since the specialbinder-based formulation SB-1 design was originally optimized to improve slag corrosion resistance, so superior performance in these locations was expected and subsequently confirmed.

The waterfall applications introduced additional mechanical and operational variables. Higher turbulence, localized impact loading and installation sensitivity contributed to increased wear relative to benchmark materials. Nevertheless, the trials successfully identified key opportunities for further improvement.

The field observations also validated the importance of installation characteristics. While corrosion resistance remained excellent, improved flowability and controlled setting kinetics will be critical for maximizing performance in complex geometries.

These findings demonstrate the value of industrial trials in translating laboratory innovations into commercially successful technologies.

Sustainability Benefits

Sustainability has become an increasingly important performance metric for refractory materials.

The elimination of hydraulic cement from the SB-1 formulation with introducing special advanced binder-based technology will definitely reduce dependence on traditional drying schedules because the binder system contains significantly lower levels of chemically bonded water. Consequently, shorter drying and pre-heating cycles can potentially be implemented during the next installation and repair operations in phase-2.

The ability to reduce fuel consumption directly supports ongoing efforts within the steel industry to minimize greenhouse gas emissions and progress toward carbon-neutral manufacturing.In addition, improved corrosion resistance in suitable applications can extend campaign life and reduce refractory consumption, further contributing to environmental sustainability.

Future Development Work

Although the present study successfully demonstrates the industrial validation of the SB-1 technology, further optimization efforts are underway, along with the evaluation of the SB-2 composition aimed at achieving improved performance and controlled setting characteristics.

Future work will focus on:

- Improving casting flowability with optimized setting characteristics.
- Enhancing resistance against turbulent flow conditions.
- Increasing impact and abrasion resistance in waterfall applications.
- Detailed microstructural investigation of worn lining samples.
- Correlation of field performance with laboratory corrosion mechanisms.

These developments are expected to expand the applicability of cement-free rapid-heating technology across a broader range of blast furnace trough environments.

Conclusions

A next-generation cement-free rapid-heating trough castable, developed through systematic laboratory investigations, was successfully validated under industrial operating conditions. The castable exhibited excellent slag runner junction performance, achieving throughput levels of approximately 196,000 THM and 225,000 THM while maintaining satisfactory residual lining thickness. The waterfall trial highlighted opportunities for further optimization in installation characteristics and localized erosion resistance. Future work will focus on reducing the preheating cycle and further enhancing material properties. Compared with CAC-based castables, the advanced cement-free binder system offers strong potential for reduced drying and preheating requirements, subject to further field validation. Overall, the technology represents a promising next-generation refractory solution, delivering improved corrosion resistance, enhanced operational efficiency, and a lower carbon footprint.

References

[1] Peng, H.; Myhre, B. “Dring Behaviour and Explosion Resistance of No-Cement Refractory Castables”. Refractories Worldforum11 (2019) [4].

[2] Peng, H.; Myhre, B. “Improved explosion resistance of low cement refractory castables using drying agents”. International Journal of Ceramic Engineering & Science, 2022.

[3] Luz, A. P.; Moreira, M. H.; Salomão, R.; Braulio, M. A. L.; Pandolfelli, V. C. “Drying behavior of dense refractory castables”. Part 2: Drying agents and design of heating schedules. Ceramics International, [48] 2965 – 2987 (2022)

[4] Moreira, M. H.; Dal Pont, S.; Ausas, R. F.; Luz, A. P.; Cunha, T. M.; Parr, C.; Pandolfelli, V. C. “Main trends on the simulation of the drying of refractory castables”. Review. Ceramics International, 2021, 47 (20), pp.28086-28105.

[5] M. H.; Tengattini, A.; Dal Pont, S.; Pandolfelli, V. C. “Permeability enhancing drying additives– A perspective from in-situ analysis”.Zenodo proceedings, October 2023

[6] Peng, H. “Novel Binder Systems for No-Cement Castables: A Comprehensive Evaluation of Mechanical Strength and Hot Properties”. Journal of Ceramic Science and Technology, 16 [3] 153-160 (2025).

[7] Ramult, J.; Wiśniewska-Tobiasz, K.; Prorok, R.; Madej, D. “Fundamental Investigations on the High-Temperature Corrosion of Spinel-Forming Alumina Castables by Steel

Slags". Applied Sciences, Vol 12, Issue 2, 2022.

[8[Yilmaz, S. "Corrosion of high alumina spinel castables by steel ladle slag". Ironmaking & Steelmaking, 2006.

[9] Schnabel, M.; Buhr, A.; Dutton, J. "Rheology of High-Performance Alumina and Spinel Castables".NovyeOgneupory (New Refractories), Issue No – 3, Pages 119 – 126, 2017.

[10] Orsolini, H. D.; Sako, E. Y.; Galesi, D. F.; da Silva, B. M. G.; Alves, W.; Januário, N. F. "Reducing CO2 emissions with a zero-drying castable for blast-furnace trough and runners". Proceedings of ABM International Annual Congress / ABM Week, DOI: 10.5151/5463-5463-35049.

[11] Maeno, S.; Goda, K.; Goto, K. "Improved Corrosion Resistance and Thermal Shock Resistance of Al_2O_3-SiC-C Castable for Main Runner of Blast Furnace by Composite Addition of TiO_2 and Metallic Si Powder". Krosaki Harima Technical Report, 2025.

[12] Weber, K.; Pezennec, E.; Laugier-Werth, A.; Joos-Bloch, M. "Calculation of the Product Carbon Footprint of Refractory Materials". UNITECR 2025, Cancún, Mexico, 30 October 2025.

[13] Zetterström, C.; Schneider, P. "Reducing the Carbon Footprint of Calcined Alumina for the Refractory Industry". UNITECR 2025, Cancún, Mexico, 30 October 2025.

[14] Roy, S; Chatterjee, S; Samanta, A. "Development of new generation cement-free, water based castable: a sustainable approach towards carbon neutrality". IREFCON 2024, Goa, India

[15] Lacoue, F; Collomb, Q; Liu, C; Wöhrmeyer, C. "A new approach to achieve robust and easy to use NCC.". UNITECR, Francfort, Germany, 2023

THE BEHAVIOUR OF DIFFERENT ALUMINOSILICATE REFRACTORIES EXPOSED TO HYDROGEN AND CARBON MONOXIDE

Anamaria Soare[1], Johannes Boersma[1],
Christoph Wöhrmeyer[2], Frederic Lacoue[2], Elodie Chabas[2], Goutam Bhattacharya[2]

[1] Gouda Refractories BV, Gouda, The Netherlands, [2]Imerys SA, Paris, France

Corresponding author's email: anamaria.soare@goudarefractories.com

Abstract

Driven by the global imperative for industrial decarbonization, hydrogen is poised to become a vital fuel and reactant in high-temperature processes, particularly as its cost competitiveness against natural gas improves. While pure alumina and zirconia are known for superior hydrogen resistance at high temperatures compared to aluminosilicates, the latter are essential in many applications, such as andalusite-based refractories, due to their excellent thermal cycling and creep resistance. This paper presents an investigation into the alteration processes of a selection of industrially manufactured aluminosilicate bricks and castables provided by Gouda Refractories. These materials, varying in aggregate type, binder composition, porosity, and other physical properties, were exposed to both hydrogen and hydrogen-carbon monoxide atmospheres in a specialized multi-atmosphere chamber furnace at Imerys. Macroscopic, microscopic, and mechanical property investigations are utilized to investigate potential alteration phenomena and their underlying mechanisms. The discussion is focused on the potential performance of different aluminosilicate refractories in Direct Reduced Iron (DRI) production using either hydrogen or a mix of natural gas and hydrogen as reactants.

Keywords: Aluminosilicates, hydrogen, carbon monoxide, corrosion

1. Introduction

As part of their potential decarbonization roadmaps many steelmakers are investigating options to use hydrogen as a reductant for the transformation of iron ore into direct reduced sponge iron (DRI) [1,2]. Although this move to hydrogen might take more time and money (Capex and Opex) than predicted a few years back, it remains a very interesting decarbonisation technology option, especially when hydrogen becomes available at a reasonable price vs natural gas, and produced at large scale based on renewable electricity [3,4]. It is known from thermodynamic calculations and experiments that the reaction of SiO_2 in the refractories with hydrogen at temperatures well above the DRI operating temperature creates SiO gas, resulting in a depletion of silica and creation of a more porous and fragile alumina rich zone at the outer rim of the refractory material. However, DRI production usually happens at temperatures below 1100°C where SiO_2 is thermodynamically stable [5] while at temperatures above approximately 1130°C the reaction starts to shift to the right side of the equation (1) as for example shown in a simulation with Factsage for a hydrogen atmosphere containing H_2O with a partial pressure of 10^{-4}atm [6].

$$SiO_2(s)+H_2(g)\rightleftharpoons SiO(g)+H_2O(g) \qquad (1)$$

Although not very likely, due to operational conditions the temperature in the DRI kiln might exceed 1100°C for a short period of time which could then start to have an effect on the stability of aluminosilicate refractories. To evaluate such an extreme and unlikely condition for a DRI shaft kiln, 1200°C has been selected in this study as the test temperature for a range of aluminosilicate refractories exposed to 100% hydrogen and a mix of 50 vol.% hydrogen and 50 vol.% carbon monoxide.

2. Test materials and test conditions

This study is investigating a range of different aluminosilicate refractory bricks and castables, industrially produced and provided by Gouda Refractories, The Netherlands, and containing different aggregates, having different densities, porosities, mineralogies, purities, and different binder systems. The tested aluminosilicate refractories and their product concepts are shown in Tab. 1. Castables with an Al_2O_3 content ranging from 48 to 75%, respectively 49 to 84% for bricks, have been selected. The test program comprises dense refractory castables and bricks (DRC, DRB), and insulating castables and bricks (IRC, IRB). The main type of aggregate is listed as well for each refractory product. Amongst the castables, products have been selected with a regular cement content (RC), and deflocculated castables with either a low or ultra low calcium aluminate cement content (LC, ULC).

Castables	Main raw material
DRC-48-LC	Chamotte
DRC-51-RC	Chamotte
IRC-53-RC	LW-Chamotte
IRC-56-RC	LW-agg & Perlite
DRC-60-LC	Andalusite
DRC-61-ULC	Andalusite
DRC-74-LC	White Fused Mullite
DRC-75-LC	Sintered Mullite (70%)
DRC-75-RC	Bauxite

Bricks	Main raw material
DRB-49	Mullite (47%)
IRB-55	Chamotte
DRB-61	Andalusite
DRB-62	Andalusite
DRB-81	Fused Mullite
IRB-84	Bubble alumina

Castables:
DRC = Dense refractory castable
IRC = Insulating refractory castable
XX = Al_2O_3 content (wt.%)
RC = Regular cement castable
LC = Low cement castable
ULC = Ultra low cement castable
Bricks:
DRB = Dense refractory brick
IRB = Insulating refractory brick
XX = Al_2O_3 content (wt.%)

Table. 1: Test materials and product concepts

The brick samples have been prepared by drilling cylinders with a height of 50 mm and a diameter of 50 mm from industrially produced and fired bricks, followed by a

drying step to remove water from the samples. For castables, cubes with a side length of 50 mm have been prepared by cutting larger prisms, and subsequently pre-fired at 1200°C in air with a dwell time of 6h to remove all water from the system and to transform the CaO-containing phases into non-hydratable compounds to avoid humidity pick-up prior to the exposure to the hydrogen atmosphere. For each product two samples have been exposed to a 100% hydrogen atmosphere and as well a mix of 50 vol.% hydrogen and 50 vol.% carbon monoxide. The mix of H_2 and CO might become relevant during an initial transition phase towards decarbonized DRI when green H_2 might not be sufficiently available and eventually mixed with natural gas. The samples have been placed on a shelf (Fig.1) and introduced into the furnace at the Imerys Technology Center. To prepare for the test, the air in the furnace chamber is evacuated by flushing it with nitrogen till an oxygen concentration of less than 1% is reached and then the furnace is heated up within 3 h to 1200°C under a continuous gas flow of 2 l/min N_2 and 10 l/min H_2 (Tab. 2). During the holding time of 80 h at 1200°C the hydrogen flow has been adjusted to 3 l/min. At the end of the test a controlled cooling within 3h from 1200°C to 20°C is done under constant nitrogen flow of 5 l/min. In case of the trial with a mix of hydrogen and carbon monoxide, flow rates have been modified as shown in Tab. 2. The gas inlet is at the bottom of the furnace and the outlet with an after-burner at the top of the furnace.



Fig. 1 Shelf with brick and castable samples (left) and special chamber furnace for H_2 and H_2/CO exposure at 1200°C, 80h (right)

Temperature (°C)	Time (h)	N2 (l/mn)	H2 (l/mn)
20-1200	3	2	10
1200	80	-	3
1200-20	3	5	-

Temperature (°C)	Time (h)	H2 (l/mn)	CO (l/mn)
20-1200	4	5	5
1200	80	3	3
1200-20	4	3	3

Tab. 2 Gas flow rates before, during and after the exposure to H_2 or H_2/CO

4. Results and Discussion

Fig. 3 and Fig. 4 show the measured weight changes after the 80 h test cycles at 1200°C in 100% hydrogen (3 l/min) and 50% hydrogen (3 l/min) & 50% carbon monoxide (3 l/min). With the exception of the castables DRC-75-LC and DRC-75-RC all other castables and bricks show a very small weight loss of less than 0.7 %.

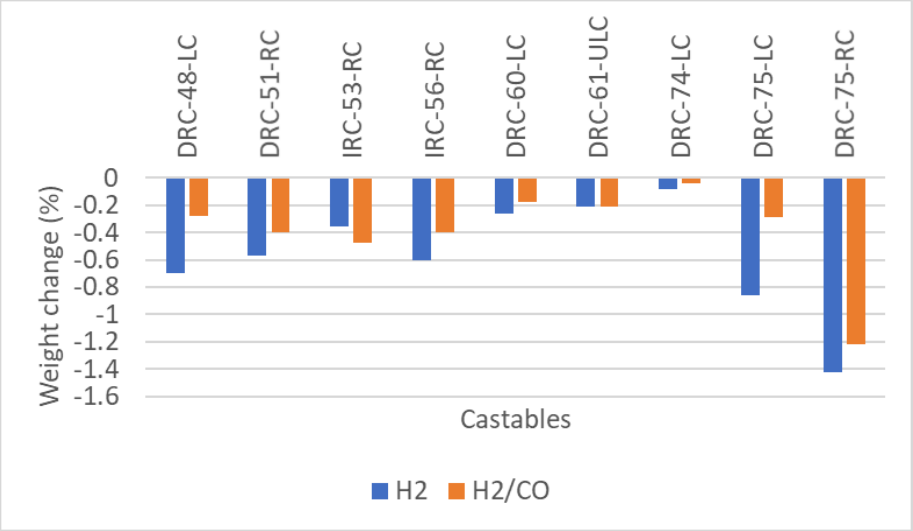


Fig. 2: Weight change of aluminosilicate castables after 80 h exposure to H_2 or H_2/CO at 1200°C

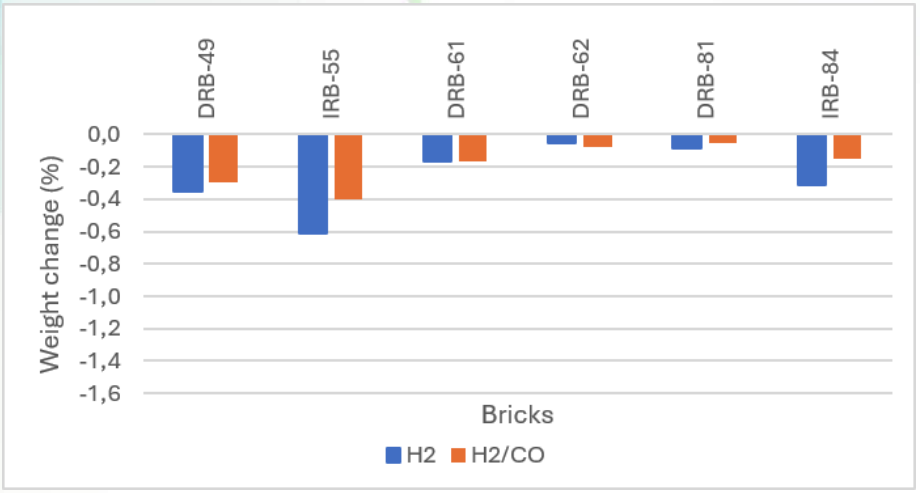


Fig. 3: Weight change of aluminosilicate bricks after 80 h exposure to H_2 or H_2/CO at 1200°C

The castables seem to have a slightly higher weight loss than the bricks. Both castables and bricks lose slightly more weight when exposed to pure hydrogen than to the mixed H_2/CO atmosphere. Nevertheless, it's worth noting that the two castables with the highest total alumina content show the highest weight loss in hydrogen and DRC-75-RC as well in H_2+CO atmosphere.

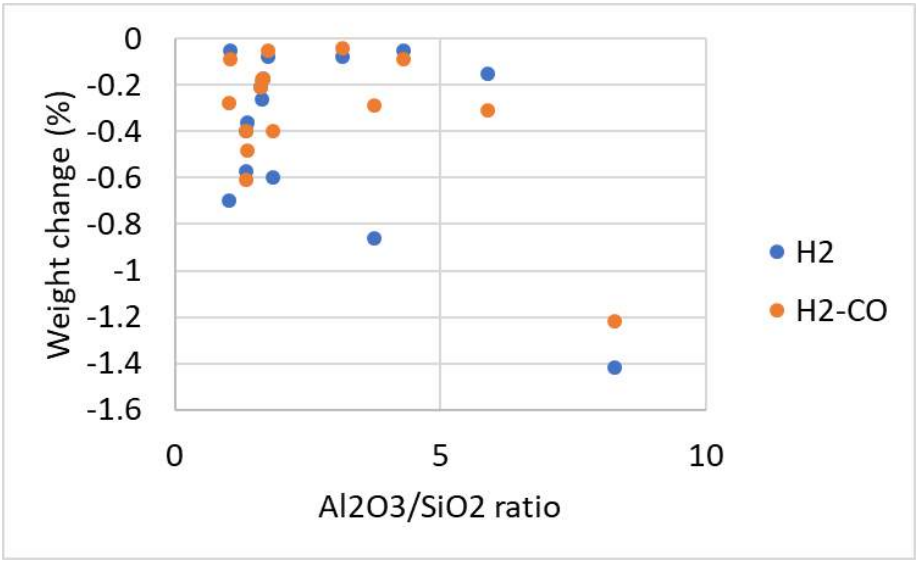


Fig. 4: Weight change and Al_2O_3/SiO_2 ratio of aluminosilicate refractories

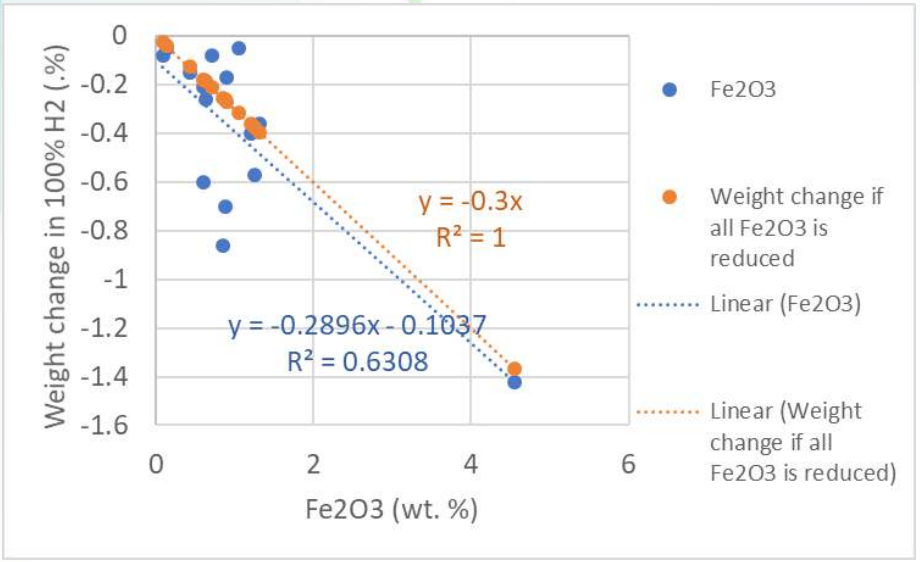


Fig. 5: Correlation between Fe_2O_3 content of aluminosilicate refractories and weight change in H_2 atmosphere

However, looking at the full set of results, the measured weight losses don't correlate with the Al_2O_3/SiO_2 ratio, neither for pure H_2 nor H_2/CO (Fig. 4). From that finding one can conclude that a reaction to SiO-gas is most likely not the main cause for the observed weight losses at 1200°C and that other parameters seem to have a more dominant effect.

Since iron oxide can easily be reduced at 1200°C, the next obvious assumption is that there might be a correlation between weight loss and Fe_2O_3 content. As can be seen in Fig. 5 there is a certain relationship between the total Fe_2O_3 content in the original material and the weight loss after treatment in reducing atmospheres. However, compared to the theoretical maximal weight loss that would result from a complete reduction of Fe_2O_3 to metallic iron some data points are higher than the theoretical value, some fit perfectly the calculated number while others have a lower weight reduction than theoretically possible, although the later ones are at very low level of weight loss where measurement accuracy might not be good enough to conclude. However, the Linear of the measured values is very close to the theoretical weight loss as shown in Fig. 5. Those refractories that show a clearly higher weight loss (between 0.6 and 0.9%) than expected from the Fe_2O_3 reduction seem to be furthermore impacted by other aspects. The material DRC-75-LC with 0.85% Fe_2O_3 and a weight change of -0.86% behaves obviously somewhat differently. In this case the relatively high weight loss can most likely be attributed to the specific mineralogy of the aggregate that was used in this castable. It contains some TiO_2 in the form of rutile. It is assumed that rutile was reduced by hydrogen. Contrary to that, the sample DRC-75-RC, although having a high TiO_2 content (2.93 wt.%) compared to DRC-75-LC (2.12 wt.%), is fitting the theoretical weight loss that is expected from the complete reduction of Fe_2O_3 only. This might be due to a different mineralogy in DRC-75-RC (bauxite based) since its high amount of TiO_2 most likely originates from tialite (Al_2TiO_5). Tialite seems to be more resistant to hydrogen than rutile (TiO_2). Nevertheless, due to the high iron oxide content in the initial bauxite-based material (4.55% Fe_2O_3), this castable shows by far the highest weight loss of all tested samples, well correlated with its Fe_2O_3 content. Another product that exhibits a

relatively higher weight loss (-0.6%) that cannot only be explained by the reduction of Fe_2O_3 is a light weight castable. IRC-56-RC with a bulk density below 1 g/cm^3, contains only little Fe_2O_3 and TiO_2, but a high amount of Na_2O and K_2O. It is assumed that these alkali oxides, probably present within a glassy phase, have been partly reduced and vaporized during the hydrogen treatment at 1200°C. Furthermore, due to the high porosity, the inner surface was probably more easily and faster accessible for the hydrogen attack than in the case of the dense refractories. The chamotte containing castable DRC-51-RC is slightly deviating as well towards a higher weight loss (-0.75%) than expected from Fe_2O_3 reduction only. In this case it can probably as well be attributed to a somewhat elevated TiO_2 content (1.57 wt.%).

Three products show very low weight loss (below 0.2%), and even less than expected considering their Fe_2O_3 content between 0.7 and 1.1 wt.%. They are all fired bricks and contain very dense aggregates, two of them are andalusite based (DRB-61 and DRB-62) and one contains a dense mullite-rich aggregate with 47% Al_2O_3. These three materials achieve a similarly low weight loss as the even more pure white fused mullite based products (castable DRC-74-LC and brick DRB-81) and the bubble alumina containing brick (IRB-84).

In line with the overall small weight changes, also the cold crushing strength does not change significantly after the exposure to hydrogen or H_2+CO compared to the samples fired in air (Fig. 6). However, to be noted that the dwell time in air was only 6h, while the treatment in the reducing atmospheres lasted 80 h. The addition of carbon monoxide did not have an impact on strength compared to pure hydrogen at 1200°C. However, it need to be further investigated, what would happen at lower temperatures, eg. at the inlet of the DRI shaft kiln, where the equilibrium of the equation (2)

2 CO = CO2 + C (2)

would shift to the right side, potentially creating carbon deposits in the structure, catalysed by iron-containing phases. This obviously represents a risk of crack formation and strong weakening of the refractory material especially when the iron content is high as for example in the case of the bauxite containing refractory materials. Contrary to that, the equilibrium is fully on the left side of reaction (2) at the tested temperature of 1200°C.

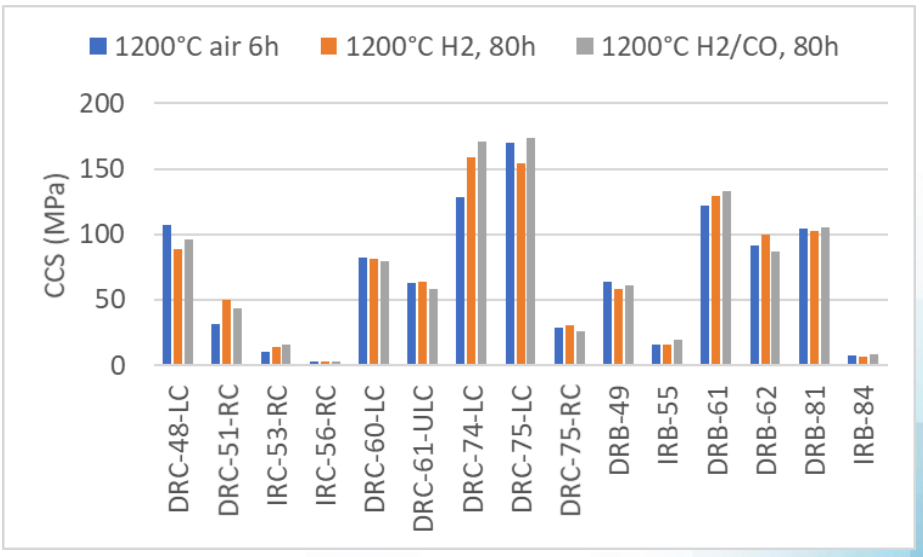


Fig. 6: Cold crushing strength (CCS) of the test specimens after firing at 1200°C in air (6h) and H_2 (80h) respectively H_2/CO (80h)

5. Conclusions

At usual operating temperatures of DRI (<1100°C), hydrogen seems to have little impact on the stability of SiO_2. Even at the test temperature of 1200°C there is no obvious relationship between weight loss and silica content in the refractory materials during the 80h test cycle. For the selection of suitable refractory materials for DRI-H_2 it is important to focus on the impurities in the refractory materials, particularly Fe_2O_3. Without surprise, not only the iron oxide of the ore but also the Fe_2O_3 in the refractory lining can be reduced by hydrogen, forming small metal particles inside the refractory products. But also other impurities are prone to reduction by hydrogen, like TiO_2, especially if present as rutile, while tialite seems to be more resistant against hydrogen at 1200°C. Dense high purity bricks and castables based on aluminosilicates like andalusite and white fused mullite raw materials and an engineered microstructure have shown the lowest weight loss of all tested samples and are excellent candidates for hydrogen-based DRI operations which usually operate well below the here tested 1200°C. Further investigations are required to investigate the effect of H_2/CO atmospheres at lower temperature where CO reacts to CO_2 and C with a potential carbon deposit inside the refractory structure. Furthermore, microstructure investigations of the corroded samples are planned to investigate the reaction mechanisms, the size and distribution of the reaction products like Fe and Ti and potential changes at the grain boundaries after a long term exposure to hydrogen and carbon monoxide.

Acknowledgment

We thank all contributors to this cooperative study at Gouda Refractories and at the Imerys Technology Center for their excellent support and fruitful discussions.

References:

1. M. Finn: Green steel revolution: Complete guide to hydrogen-based DRI/EAF production. 03/2026. https://oxmaint.com/industries/steel-plant/green-steel-hydrogen-dri-eaf-production-guide
2. J. M. Marguttiet al. : Towards green steel from hydrogen-based direct reduction of low-grade iron ores: Techno-economic and greenhouse gas emissions assessment. International Journal of Hydrogen Energy, Volume 235, 20 May 2026, 155073. https://www.sciencedirect.com/science/article/pii/S0360319926017118
3. IEA's Global Hydrogen Review 2026. https://www.iea.org/reports/global-hydrogen-review-2026
4. F. Rosner et al: Green steel: design and cost analysis of hydrogen-based direct iron reduction. Energy Environ. Sci., 2023, 16, 4121. https://pubs.rsc.org/ee/article/16/10/4121/807435/Green-steel-design-and-cost-analysis-of-hydrogen
5. I.N. Chakraborty: Refractories for hydrogen environments. Iron & Steel Review, Vol 67, No 7, p 206-226, Dec 2023
6. H. Jansen et al. 12th Freiberg Refractory Forum, Germany, Dec 2021.

DEVELOPMENT OF A HIGH STRENGTH NO-CEMENT CASTABLE WITH ENHANCED INTERMEDIATE TEMPERATURE PROPERTIES

S. D. Majumdar[1], R.P. Samal[1], N. Mukherjee[1], A. Bajoria[1], R. Ghosh[2] and A. Mukherjee[2]

1. IFGL Refractories Limited, India,
2. Elkem South Asia Private. Limited, India

Corresponding author's e-mail: sachidulal.majumdar@ifgl.in, riya.ghosh@elkem.com

Abstract

No Cement Castables (NCC) are recognized for their superior high-temperature performance compared to Low Cement Castables (LCC) and Ultra-Low Cement Castables (ULCC). They offer higher refractoriness, enhanced slag resistance, and faster, safer dry-out behavior. However, the conventional additives used in NCC systems-such as silica sol and hydratable aluminaexhibit limited strength development at low and intermediate temperatures, which restricts their broader industrial application. To address these limitations, a specially designed microsilica based additive, has been developed. This additive improves flow characteristics, ensures uniform microsilica dispersion, and promotes mullite formation at significantly lower temperatures in the range of 600–900 °C, while maintaining superior performance at higher temperatures. By overcoming the inherent drawbacks of traditional NCC formulations, this additive expands the applicability of NCC systems, enabling consistent strength development and reliable performance across the entire temperature range. Castables formulated using this modified NCC system have been successfully implemented in tundish dams, well blocks and Monobox at Integrated steel plants.

Keywords: No Cement Castable, Microsilica based Additive, NCC, Mullite Refractories

1. Introduction

No-cement castables (NCCs) are widely used as monolithic refractories because the elimination of cement can reduce the formation of calcium containing phases and provide favorable high temperature properties [1,2]. However, the absence of hydraulic cement bonding can result in relatively low green and dried strength, which may create difficulties during demoulding, handling, transportation, and installation, particularly for large and complex precast refractory components [1,2].

To overcome these limitations, alternative additive systems such as colloidal silica and microsilica-gel additives have been developed for NCCs. Silica-based additives provide bonding without introducing cement-derived calcium phases and can improve the setting behaviour and mechanical properties of cement-free castables [3,4] . It will improve setting behaviour and mechanical properties in silica-bonded NCC systems, while further studies demonstrated the potential of microsilica-gel bonding for developing cement-free castables with improved processing and strength characteristics [3,4] . Recent work has further highlighted the development of microsilica-gel-bonded NCCs as an alternative to conventional cement-bonded systems [5].

Despite these developments, achieving sufficient early-stage strength while maintaining the required intermediate- and high-temperature performance remains a challenge. The development of ceramic bonding and phase evolution within the matrix during heating is particularly important for the mechanical performance of

NCCs. Mullite is an important alumino-silicate phase in refractory systems because of its high-temperature stability and favorable thermo-mechanical properties [6] . Controlled development of mullite within the matrix can contribute to improved ceramic bonding and structural integrity during heat treatment.

In the present study, a microsilica based additive system was developed for a high-strength NCC. The objective was to improve the green and ovendried strength while maintaining the high temperature performance of the castable. The developed formulations were evaluated in terms of flowability, setting behaviour, bulk density, cold crushing strength (CCS), permanent linear change (PLC), and hot modulus of rupture (HMOR). Microstructural and mineralogical analysis were also carried out to investigate phase evolution and its correlation with mechanical properties. The influence of the additive on strength development at different thermal stages was systematically assessed and further evaluated through industrial trials in tundish well blocks, tundish dams, and monobox applications under actual operating conditions

2. Experimental

2.1 Raw materials characteristics

The castable formulations were prepared using alumina- and alumino-silicate–based raw materials, selected to achieve an optimized balance between particle packing, matrix densification, and high-temperature phase development. The general characteristics of the raw material categories, including chemical composition, particle size range, and true density, are summarized in Table 1. The high-alumina aggregates formed the coarse-grained skeleton of the castable, contributing to its overall mechanical integrity, while alumina fines enhanced matrix densification and mechanical strength. Aluminosilicate aggregates and fines were incorporated to improve thermal stability and to promote in-situ mullite formation during firing. The selected raw materials were also designed to provide adequate reactivity and compatibility with the developed microsilica based additive system. All raw materials were used as received without further treatment.

Table 1 General raw material categories used in the present study

Raw material	Chemistry (wt.%)	Particle size range	True density (g·cm^{-3})
High-alumina aggregate	Al_2O_3 > 95	1–5 mm	3.0–3.2
Alumina fines	Al_2O_3 > 95	< 45 μm	3.8–3.9
Alumino-silicate aggregate	Al_2O_3: 55–65, SiO_2: balance	0.1–1 mm	2.6–2.8
Alumino-silicate fines	Al_2O_3: 55–65, SiO_2: balance	< 45 μm	2.6–2.8

2.2 Additive characteristics

Two types of microsilica based additive were investigated in this study. The additives were formulated to promote microsilica dispersion, matrix cohesion, fill the interstitial voids between the larger refractory aggregates and strength development during setting and

thermal treatment. Their chemical characteristics are summarized in Table 2.

The additives control the surface charge of ultrafine, amorphous microsilica particles upon water addition. As the castable sets, the microsilica particles undergo a coagulation and gelation process and link together via siloxane bridges (SiO-Si), creating a rigid three-dimensional microsilica-gel network across the matrix, which will act as the primary additive before any high temperature ceramic bonding occurs.

Table 2 Characteristics of microsilica based additive

Parameters	Type 1	Type 2
SiO_2 (Wt %)	55-70	50-65
Al_2O_3 (Wt %)	25-40	20-35
Additive content (Wt %)	5-15	8-18
BD in kg/m^3	300-550	8-18
pH (10% solution)	9-10	8-10

2.3 Formulation and preparation

Three batches of castable mixes were prepared for comparison. The first batch consisted of a conventional low-cement castable (N-0), while the second (N-1) and third batches (N-1+) incorporated Type-1 and Type-2 microsilica based additives, are no cement castables respectively as mentioned in Table 3.

The dry raw materials were homogenized in a Hobart mixer at 60–80 rpm for 3–5 min. Mixing water (4.5–6.0 wt.%) was then added gradually, followed by the addition of the microsilica based additive, and mixing was continued at 90–150 rpm for 3–5 min to obtain a uniform and flowable castable. The fresh mix was cast into standard CCS and HMOR moulds (IS 1528) under light vibration to remove entrapped air. The specimens were cured under ambient conditions.

Table 3 Typical compositional ranges of tested batches

Raw material	N-0	N-1	N-1+
	Wt %		
Alumina coarse aggregate	20-25	20-25	20-25
Alumina intermediate aggregate	35-40	35-40	35-40
Alumina intermediate aggregate	10-20	10-20	10-20
Alumino-silicate intermediate aggregate	5-10	5-10	5-10
Microsilica	5-15	5-15	5-15
HAC	0-5	-	-
Microsilica based additive	-	0-3	0-3

2.4 Laboratory testing and characterization

Flowability was determined using a standard flow cone and vibration table in accordance with ASTM C230/C230M. Bulk density (BD), cold crushing strength (CCS), and permanent linear change (PLC) were evaluated after drying at 110 °C for 24 h and firing at 1000 °C and 1550 °C for 3 h, as per IS 1528 guidelines. Hot modulus of rupture (HMOR) was measured at 1400 °C with a 30 min dwell using a three-point bending furnace (IS 1528). Phase evolution and microstructure were characterized by XRD (Bruker D8 Advance, CuKα) and SEM-EDS (Hitachi SU3900), respectively. These analyses were used to evaluate the changes in phase formation, bonding characteristics, and mechanical properties with increasing temperature. The results were correlated to assess the effect of the modified additive on NCC performance.

3. Results and Discussion

3.1 Comparison of Test Properties between LCC and NCC Systems

Table 4 Comparison laboratory test properties

Parameters	N-0	N-1	N-1+
Water addition (%)	6	4.2	5.5
Flow (%)	110	110	90
Setting Time (Min)	350	150	120
Bulk Density at 110 °C/24 hr (g/cc)	2.52	2.67	2.66
PLC at 1550 °C/ 3 hr (%)	-0.15	-0.31	+0.39
HMOR at 1400°C/ 30 min (kg/cm^2)	12	33	48
CCS at Green Stage (kg/cm^2)	30-40	80	96

Parameters	N-0	N-1	N-1+
CCS at 110 °C/ 24 hr (kg/cm^2)	312	354	575
CCS at 600 °C/ 24 hr (kg/cm^2)	388	442	682
CCS at 800 °C/ 24 hr (kg/cm^2)	422	495	968
CCS 1000 °C/ 3 hr (kg/cm^2)	737	528	1160
CCS 1550 °C/ 3 hr (kg/cm^2)	1344	1342	1348

Table 4 compares the laboratory properties of LCC (N-0) and the developed NCC formulations (N-1 and N-1+). The NCC systems exhibited improved setting behaviour, density, and mechanical properties compared with N-0. The setting time decreased from 350 min for N-0 to 150 and 120 min for N-1 and N-1+, respectively, enabling faster demoulding. The bulk density increased from 2.52 g/cc to 2.67 and 2.66 g/cc, indicating improved matrix packing and densification.

The PLC values at 1550 °C remained within a narrow range (−0.15 to +0.39%), confirming good dimensional stability. A substantial improvement was observed in HMOR at 1400 °C, increasing from 12 kg/cm² for N-0 to 33 kg/cm² for N-1 and 48 kg/cm² for N-1+. The superior HMOR of N-1+ indicates enhanced high-temperature bonding and structural integrity, attributed to the combined effects of improved microsilica dispersion, matrix packing, and progressive ceramic bonding.

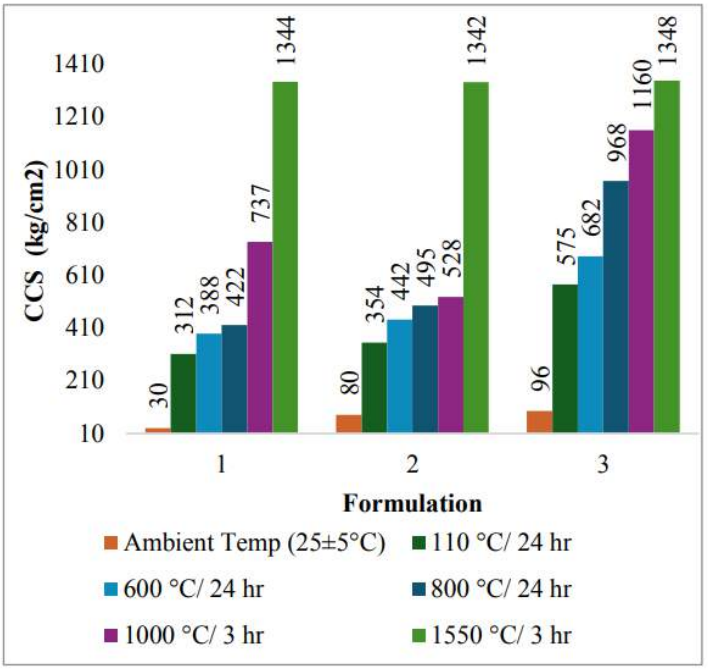


Figure 1 CCS at different Stage of Thermal Treatment

Figure 1 illustrates the evolution of CCS of N-0, N-1, and N-1+ at different thermal treatment stages. At the green stage, N-1 and N-1+ exhibited significantly higher CCS values of 80 and 96 kg/cm², respectively, compared with 30– 40 kg/cm² for N-0. After drying at 110 °C, the CCS increased to 312, 354, and 575 kg/cm² for N0, N-1, and N-1+, respectively. The higher strength of the NCC formulations is attributed to improved microsilica dispersion, three dimensional siliceous gel-network formation, and enhanced particle packing, which increase matrix cohesion and particle-to-particle

contact. With increasing temperature, CCS increased further, particularly for N-1+, reaching 682 kg/cm² at 600 °C, 968 kg/cm² at 800 °C, and 1160 kg/cm² at 1000 °C. This progressive strengthening is associated with matrix consolidation and the development of alumina– silica-rich transient phases, which promote interparticle ceramic bonding and initiate mullite formation. At 1000 °C, N-1 showed a lower CCS of 528 kg/cm², indicating differences in the evolution of intermediate bonding phases. After firing at 1550 °C, all formulations exhibited comparable CCS values of approximately 1340– 1350 kg/cm², demonstrating that the developed additive system enhances green and intermediate temperature strength without compromising the final high-temperature strength. Overall, the strength development results from a multi-stage bonding mechanism involving gel formation and particle packing at lower temperatures, followed by progressive ceramic bonding and mullite development at intermediate temperatures.

3.2 Mineralogy analysis by X Ray Diffraction (XRD)

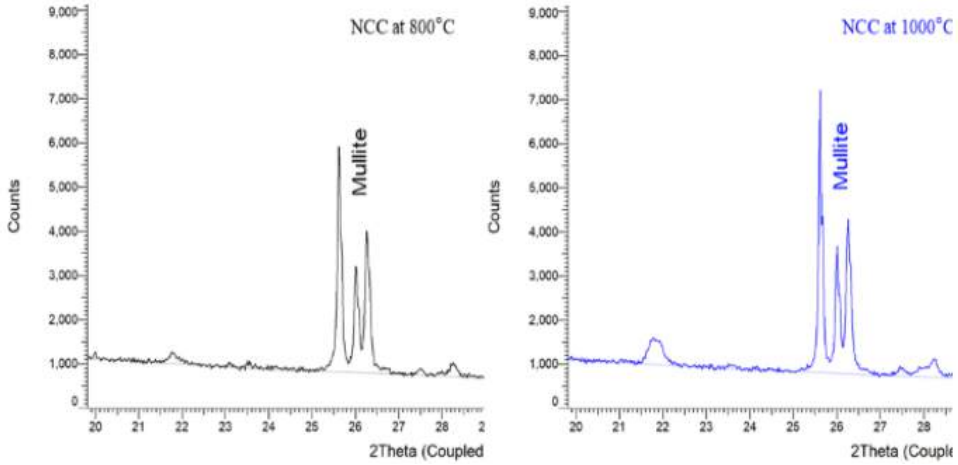


Figure 2 XRD patterns of NCC samples fired at 800 °C and 1000 °C

Table 5 Quantitative XRD phase analysis of the NCC formulation after heat treatment at different temperatures

Sl No.	Phase Name	Formula	110 °C	800 °C	1000 °C
1	Mullite	$3Al_2O_3 \cdot 2SiO_2$	26.55	27.18	31.39
2	Corundum	Al_2O_3	43.78	43.55	49.41
3	β alumina	$NaAl_{11}O_{17}$	3.23	2.65	2.21
4	Cristobalite	SiO_2	2.21	2.21	2.75
5	Rutile	TiO_2	2.75	0.30	0.30
6	Monoclinic Zirconia	ZrO_2	0.50	0.49	0.51
7	Albite	$NaAlSi_3O_8$	0.16	0.25	2.29
8	Amorphous	-	24.84	24.75	11.09

The XRD patterns in Figure 2 show the phase evolution of the NCC matrix with increasing temperature. As shown in Table 5, mullite content changes slightly from 26.55% at 110 °C to 27.18% at 800 °C, indicating its presence mainly from the initial alumino-silicate raw materials. At 1000 °C, mullite increases to 31.39%, accompanied by a reduction in the amorphous phase from 24.75% to 11.09%, indicating enhanced crystallization and increased mullite formation. This phase development correlates with the improved CCS of N-1+ at 1000 °C (1160 kg/cm²), suggesting enhanced matrix bonding and intermediate-temperature strength. The development of this in-situ mullite phase correlates well with the enhanced mechanical properties measured at intermediate temperatures, demonstrating the effective role of the additive in promoting phase evolution and associated strengthening mechanisms within the system.

3.3 Microstructure study by Scanning Electron Microscope (SEM)

SEM micrographs of NCC specimens fired at 800 °C (Figure 3-A, B) and 1000 °C (Figure 3-C, D) reveal the formation of a distinct transient spongelike/whisker-type microstructure (transient alumino-silicate phase) within the matrix. This morphology is attributed to the controlled thermal decomposition of the microsilica based additive, which facilitates localized silica-rich regions and short-range viscous flow during intermediate temperature exposure between 800 and 1000 °C. This microstructural evolution is clearly evident in the SEM micrographs presented in Figure 3.

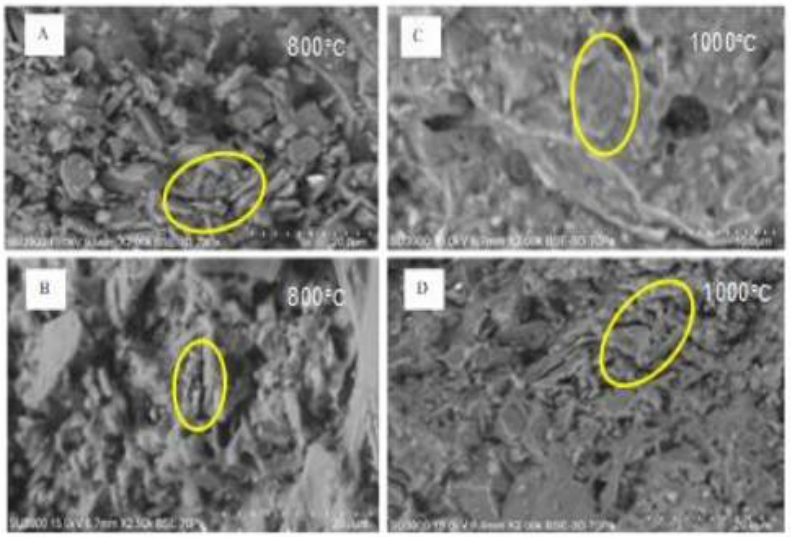


Figure 3 SEM images of NCC samples fired at 800°C and 1000°C

EDS analysis of the selected regions in Figure 3 shows that the whisker-like features observed at 800 °C (Figure 3-A, B) and 1000 °C (Figure 3-C, D) are enriched in Alumina and Silica as shown in Figure 4, suggesting the formation of alumino silicate phases. In conjunction with the XRD results, these observations indicate the development of mullite during intermediate temperature treatment. The formation of these phases and the resulting inter-particle bonding are considered to contribute to the improved CCS of the additive-modified NCC at intermediate temperatures.

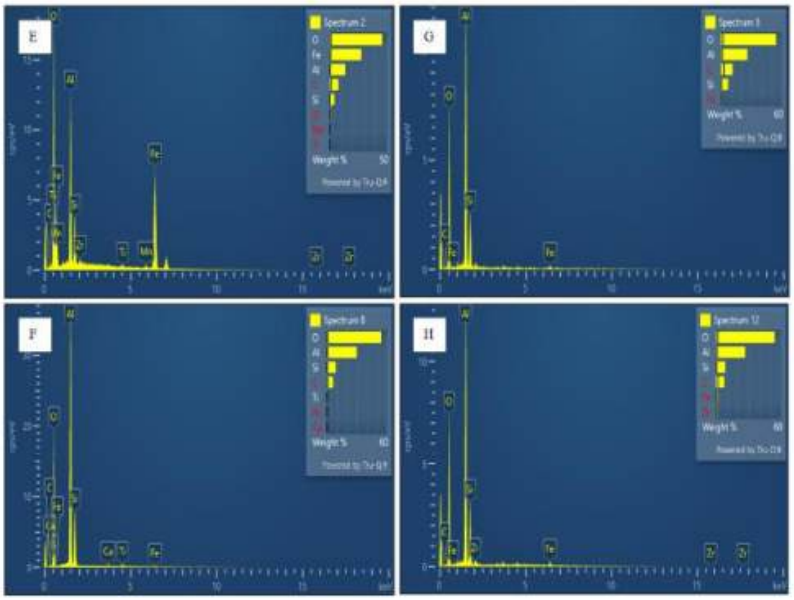


Figure 4 EDS analysis of NCC samples fired at 800°C and 1000°C

4. Industrial Trials and Performance Evaluation

4.1 Phase 1 trial of tundish well block at integrated steel plant-1

No cement castable used to cast tundish well blocks for billet casting applications. The cast material exhibited excellent green handling strength, enabling safe demoulding and installation without damage. During steel casting operations, the tundish well blocks performed satisfactorily for a duration of 6 hours. Postoperation inspection following deskulling revealed no visible abnormalities, such as cracking, spalling, or excessive wear as shown in Figure 5. This confirms the material's suitability for service conditions.



Figure 5 NCC Tundish wellblock after casting operation

4.2 Phase 2 trial of NCC dam at integrated steel plant-2

In phase 2, NCC dams were evaluated under actual tundish conditions for 4 hours. Post-casting inspection showed no erosion, cracking, or displacement, confirming good structural integrity and thermal resistance as shown in Figure 6.



Figure 6 NCC DAM after casting operation

4.3 Phase 3 trial of NCC monobox at integrated steel plant-3

NCC monobox was evaluated under continuous casting conditions over an extended 12-hour operational sequence. The monobox exhibited exceptional dimensional stability and zero abnormal metal splashing. Post casting inspection revealed no liquid steel or slag penetration into the refractory matrix as clearly observed in Figure 7.

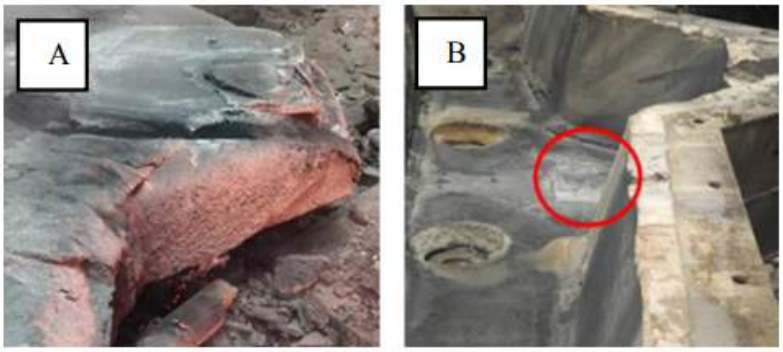


Figure 7 NCC Monobox after casting operation

5. Conclusions

The developed no-cement castable (NCC) demonstrated significant improvement in green and intermediate-temperature strength while maintaining comparable high-temperature performance to the conventional LCC system. The enhanced strength development is attributed to the combined effects of the microsilica-based additive, including improved microsilica dispersion, three-dimensional siliceous gel network formation, enhanced particle packing, and progressive ceramic bonding during thermal treatment.

Among the investigated formulations, N-1+ (NCC) exhibited the most favourable overall performance, with CCS values of 96 kg/cm² at the green stage, 575 kg/cm² after drying at 110 °C, 682 kg/cm² at 600 °C, 968 kg/cm² at 800 °C, and 1160 kg/cm² at 1000 °C. At 1550 °C, N-1+ maintained a CCS of 1348 kg/cm², comparable to the LCC system(N-0), confirming that the additive-induced improvement in early and intermediate-temperature strength was achieved without compromising the final fired strength.

The increase in intermediate-temperature strength was supported by the observed alumina–silicarich phases in SEM–EDS and progressive mullite development by XRD, with mullite content increasing from 26.55% at 110 °C to 31.39% at 1000 °C. These results indicate that progressive ceramic bonding and mullite formation contribute significantly to the strength development at intermediate temperatures.

The developed NCC also showed improved high temperature load-bearing capability, with HMOR increasing from 12 kg/cm² for LCC to 48 kg/cm² for N-1+ at 1400 °C. Successful industrial trials in tundish well blocks, tundish dams, and Monobox applications further validated its practical performance.

Overall, the developed microsilica-based NCC provides a multi-stage strengthening mechanism, A B involving early-stage gel bonding and particle packing followed by intermediate-temperature ceramic bonding and mullite development. The combination of high early strength, enhanced intermediate-temperature performance, and reliable high-temperature properties demonstrates its potential as an effective alternative to conventional LCC systems for demanding refractory applications.

Acknowledgements

The authors gratefully acknowledge the support and facilities provided by the R&D department, as well as the plant operation and quality control teams, during the preparation, testing, and characterization of the materials. The authors also thank colleagues for their valuable discussions and assistance throughout the course of this work. Additionally, the authors acknowledge the technical service teams for their support during the industrial trials.

References

1.Lee, W. E., and Vieira, W., "Castable Refractories," in Refractory Engineering and Technology in the Steel Industry, Iron & Steel Society, 2005.

2.Chesters, J. H., Refractories: Production and Properties, 3rd ed., The Iron and Steel Institute, London, 1973.

3. H. Peng and B. Myhre, "Comparison of Setting Behaviour and Mechanical Properties of Various Silica Bonded No-Cement Castable," China's Refractories, Vol. 26, No. 1, pp. 8–12, 2017.

4. H. Peng and B. Myhre, "Microsilica-Gel Bonded Refractory Castable with Improved Setting Behaviour and Mechanical Properties," Refractories Worldforum, Vol. 3, pp. 69–75, 2015.

5. H. Peng, "Recent Progress in Microsilica-Gel Bonded No-Cement Castables," Ceramics International, Vol. 49, No. 14, Part B, pp. 24566– 24571, 2023.

6. H. Schneider, J. Schreuer, and B. Hildmann, "Structure and Properties of Mullite—A Review," Journal of the European Ceramic Society, Vol. 28, pp. 329–344, 2008.

MATRIX DEVELOPMENT OF LOW CEMENT SELF-FLOW CASTABLES FOR BF BLOWPIPE APPLICATION

Sachidulal Majumdar[1],Neelendu Mukherjee[1] Sourojit Pal[2], Shankha Chatterjee[2]

[1]IFGL Refractories Limited, India
[2]Almatis Alumina Pvt. Ltd., India

*Corresponding author e-mail: sachidulal.majumdar@ifgl.in

Abstract

The low cement (LC) castables are being used in various critical iron and steel applications since quite long. Such types of castable's matrix designing is formulated by using aggregate superfines up to -45 micron particles and reactive alumina, while primarily installed by using vibration technique in iron and steel applications. However, the criticality of shape/ size/ application zone demanded the development of self-flow nature of LC castables. This paper illustrates the development of LC self-flow castable for blast furnace blowpipe application. Blast furnace blowpipe application require good thermal conductivity, high thermal shock resistance and good flexural strength properties along with control over porosity and porosity distribution. The modification of matrix formulation plays key criteria against previously used vibration type castable in other regular applications, by using high purity and consistent setting control of cement, higher dosage of different type of reactive alumina, and right choice of additives. The optimization of matrix's PSD (Particle Size Distribution) is very necessary for getting good sinterability in castable. The optimum selection of matrix components impart required thermal conductivity and thermal shock resistance. This paper also explains the development process that reduced mixing water demand in targeting high self-flow behaviour and also achieve good thermos-mechanical properties by using special additives. Incorporation of such versatile additives also assure required setting and demoulding time demands. In many occasion, castable business go through long lead time factor between production and application, spread over quite different ambient conditions (summer/ winter/ dry/ humid). This development also explains how the used additives meet all demands of setting and demoulding times at various ambient conditions and still provide self-flowability at reduced water demand condition.

Keywords: Alumina matrix enhancement, Blast furnace blowpipe, Self-flow Castable

Introduction

Demand of Self-flow castable is increasing day by day as there are number of areas in high temperature processing plants which are extremely complex in geometry and hence prohibits usage of mechanical forces during casting and installation of the material. These are the areas which demands for good flowability of the castable because vibro-setting is impossible due to the complexity of installation. In absence of good flowability of the castable, blowpipe lining will suffer heavily, whereas, a highly dense castable with good flowability will also cause problem due to higher energy loss through the castable and red-hot zone formation in blowpipe and efficiency loss in hot blast.

BF blowpipes inject hot air blast (exceeding 1200°C) into the furnace and hence require a highly specialized refractory lining. Blow pipes have a narrow, tapered annular space between the outer steel shell and the inner bore. Mechanical vibrators cannot fit into these tight gaps. Any void in a blowpipe lining creates a hotspot that can cause catastrophic steel shell failure. Blowpipes experience rapid temperature swings during furnace start-ups and shutdowns. The hot air flows through the pipe at very high velocity

and as a result the lining is subjected to heavy abrasion. The outer shell temp can also rise if the thermal conductivity of the lining material is high.

Conventional Low Cement Castable (LCC) cause development of air pockets, voids, honeycombing. But self-flow castable does not cause the above shortcomings. Self-flow castable flows by gravity, and fills all complex, critical and narrow, thin gaps. Due to presence of ultra fine particles, it provides optimized particle packing. it helps to obtain very high strength due to this dense packing.

Further in blow pipe the castable should have optimal Thermal Conductivity (TC)for not reducing thermal efficiency of blow pipe hot gas. to reduce the heat loss. The TC of high-alumina castable is quite high (around 3 W/mk at 1200ºC) and it has to bring down to the level of below 2 W/mk. For the same, alumina content needs to be kept at 60-70% level.The self-flowingability in castablecan be easily obtained using densehigh-aluminaaggregate of more than85%.In case of lower alumina containing castable with about 60-70%, normally porous and dense aggregates are mixed, which makes it rather difficult to obtain self-flowing property, due to the higher water absorption of the porous aggregates.

Thus, obtaining the castable self-flowability is significantly more difficult in an alumino-silicate system than in a high-alumina system due to fundamental differences in aggregate porosity, water demand, and packing mechanics. The scope remains only with matrix improvement to develop desired rheology of a castable,which dictates its self-flowing capabilities and also provides desired setting, required strength, demanded thermal efficiency and necessary thermal shock resistance.

Alumino-silicate aggregates: Commonly sourced from natural minerals like calcined clay, fireclay, pyrophyllite or andalusite etc. These materials contain inherent micro-porosity and rough surface textures. They absorb a portion of the mixing water into their pores, taking it away from the matrix where it is needed to facilitate the flow. Alumino-silicate systems contains a mixture of different mineral phases (such as mullite, quartz, and cristobalite). Each phase exhibits different surface charges (Zeta potential) and hydroxyl groups when exposed to water. This mineralogical diversity makes it incredibly complex to find a suitable dispersing agent (deflocculated additive) that can successfully neutralize all surface charges simultaneously to prevent particle clustering. Further it may be mentioned that Alumino-silicate fines are typically obtained via mechanical grinding, resulting in highly irregular, angular particle shapes that physically interlock and resist gravitational flow.
High Liquid Viscosity and Gelation is also responsible to reduce the flow in silica system. When the alumino-silicate system come in contact of water, minor amounts of soluble silica or silanol(Si-OH) groups can dissolve into the aqueous phase.This dissolution increases the intrinsic viscosity of the fluid medium and can initiate partial, premature gelation or network formation. This chemical friction quickly raises the yield stress of the fresh mix, stopping it from self-levelling.

Alumina aggregates: High-purity synthetic materials like tabular alumina are highly dense, crystalline, and virtually non-porous. They absorb negligible water, leaving almost the entire added water to act as a lubricant between particles.Synthetic alumina system is chemically homogenous because the particles share uniform surface chemistry, a single surfactant or deflocculant can easily create uniform electrosteric repulsion, drastically lowering viscosity and initiating free flow.

Considering the shortcomings experienced with alumina silicate or naturally occurring alumina system, focus was given to select the right type of alumina silicate aggregate, correct type of matrix former and suitable dispersants.

In self-flow castable with alumina silicate aggregate, it is necessary to counter the rough surfaces. Surface roughness increases interparticle friction, which severely restricts self-flow behaviour. To take care, it is needed to introduce Silica Fume: A highly spherical material which acts as microscopic ball

bearings that roll between the rough aggregate grains. Further, introduction of sub-micron calcined/ reactive alumina enhances the densification after sintering, fill the void spaces and also lubricate the contact zones between rough aggregates during installation. The above concept also neutralizes the varying surface charges (positive in alumina edges and negative in silica faces) which causes aggregate clumping and unwanted flocculation and finally good flow is obtained.

Flocculation can be avoided by using special dispersant additives. The special additives acts as electrosteric repulsive forces which reduces water demand drastically and also aids to self-flow behaviour.

Considering above criteria, a developmental activity was undertaken to develop a self-flow-lacement castable with alumina between 60 to 70%, having a mix of dense alumina and porous alumino-silicate aggregates with matrix combination of high-alumina cement, silica fume, calcines/reactive alumina and dispersants.

Experimental

Alumino- silicate based self-flow castable was prepared using calcined pyrophyllite, WTA, calcined alumina, reactive alumina, silica fume, cement and dispersants. The physical and chemical properties of the used raw materials are mentioned in table 1. Continuous particle size distribution model was used with distribution coefficient q= 0.21 using coarser size of 5-6 mm and finest below 0.045 mm.A reference to previously proven Anderson packing coefficient, q of 0.21 is followed. Further, it is required to increase the proportion of fine matrix particles (below 45 μm) to completely encapsulate the coarse aggregates for better flowability.

	Chemical parameters	**Physical parameters**
WTA	99.6% Al_2O_3, 0.25%Na_2O	3.60 g/cc BSG, 1.2% AP
Pyrophyllite	42% Al_2O_3, 50% SiO_2, 0.8%Fe_2O_3	2.50 g/cc BSG, 3.8% AP
Calcined Alumina CA	99.7% Al_2O_3, 0.12%Na_2O	1 m^2/g BET, 5μm d50
Reactive Alumina RA	99.7% Al_2O_3, 0.0.8%Na_2O	3m^2/g BET, 2.2μm d50
Cement CA14	71% Al_2O_3, 28%CaO	13 μm d50
Silica Fume	94% SiO_2, 2.5% LOI	98% < 45 μm
Dispersing Aluminas	91-96% Al_2O_3, 3-7% LOI	2.5 μm d50

Table 1 – Major chemical and physical properties of raw materials used

The table 2. shows the concepts used with different distributions of aggregates along with calcined alumina, reactive alumina, high alumina cement, silica fume and additives.As

aggregate was not part of this paper, only variances in matrix alumina is discussed here in this paper with a purpose to see the differences in water demand, flowability, fired density and strengths, thermal conductivity and thermal spalling resistance.Four different castable concepts were selected to be evaluated based on the expectations that has to affect castable rheology and thus change castable water demand and flowability, and successively other fired properties.

Material	Grade	CA	CA+DA	RA+DA	CA+RA+DA
Pyrophyllite	3-5	X	X	X	X
	1-3	XX	XX	XX	XX
	0-1	X	X	X	X
WTA	1-3	X	X	X	X
	0-1	X	X	X	X
	0-0.2	X	X	X	X
	-325	X	X	X	X
Calcined alumina CA		XX	XX		Xx
Reactive Alumina RA				XX	X
CA 14Cement		X	X	X	X
Silica fume		X	X	X	X
Additive	MADS1		x	x	x
	MADW1		x	x	x

Table 2: Formulation concept of Blast Furnace Blowpipe castable

The raw materials were dry mixed in Hobart mixer.Minimum mixing water was added till the mix attains flowability. The prepared castable composition was characterized for self-flowability using self-flow cup (without vibration or tap) and after 30 secs and thereafter at intervals of 30 and 60 minutes.

Next the mixed batches were casted in mouldof 40*40*160 mm sizes. The mixes were allowed to cure within the mould for 24 hrs. under temperature and humidity controlled conditions. After demoulding, they were allowed to air dry for 24 hrs., followed by oven drying at 110 ºC/ 24 hrs. The dried samples were then fired at 1000 and 1400 ºC/ 5 hrs. All the samples were then tested for BD, PLC, CCS, CMOR, and HMOR (at 1400 ºC/ 0.5hr, using pre-fired bars at 1400 ºC/ 5 hrs).

Results and discussions

The rheological properties are given in table 3.The batch CA resulted at very high water demand with higher wet-out time but still didn't execute any self-flow behaviour. The higher apparent porosity of pyrophyllite grains absorbed some mixing water and relatively coarser median particle size calcined aluminalacks submicron particles required to fill micro-voids for flowability without vibration. As a result, adequate flow could not be obtained in batch CA.

Test result		CA	CA+DA	RA+DA	CA+RA+DA
Water demand	%	12	8	5	6
Wet-out time	sec	70	45	30	35
Self-flow10 min.	mm	No flow	160	210	200
Self- flow 30 min.	mm	-	150	200	195
Self-flow 60 min.	mm	-	135	180	175

Table 3:Physical properties of test castables

Water demand drastically reduced in batch CA+DA due to presence of dispersing aluminas. These alumina based additives are superfine in nature as well as accomplish with electrosteric repulsive forces. As a result it reduced water demand, however the self-flow behaviour was at very minimum level to be used for application installation.

The role of reactive alumina on water demand and flowability got evident from batch RA+DA with further reduction of mixing water demand, reduction of wet-out time and superior flowability till 60 mints of mixing. The figure-1 below shows the self-flow behaviour at F10 for the batches CA, CA+DA and RA+DA. The figure 2-6 explains the fired properties of the batches.



Fig. 1(A, B, C): Self flow at F10 for batches CA, CA+DA, RA+DA

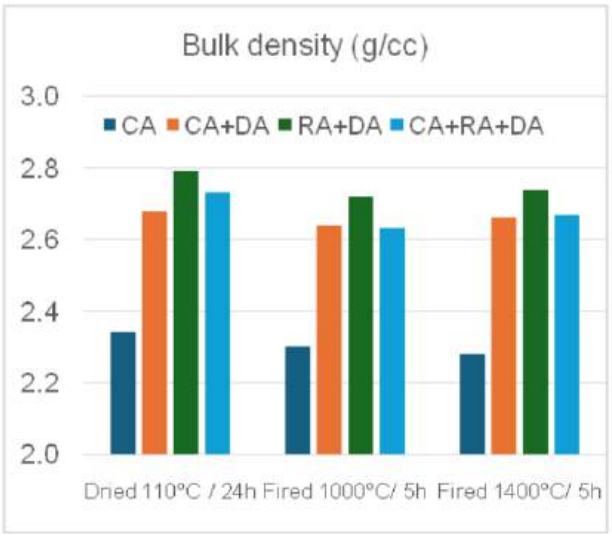


Fig.2: Bulk density of the batches

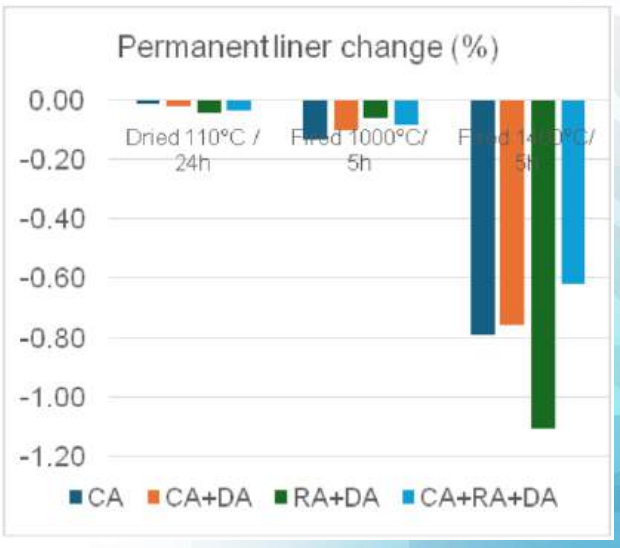


Fig. 3: Permanent liner change of the batches

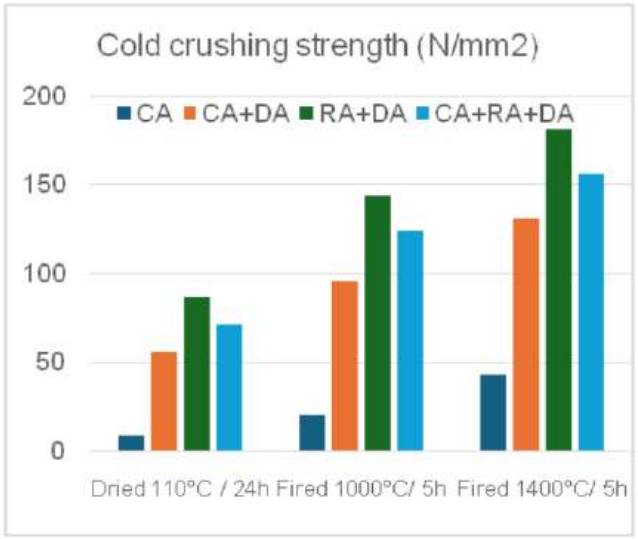


Fig. 4: Cold crushing strength of the batches

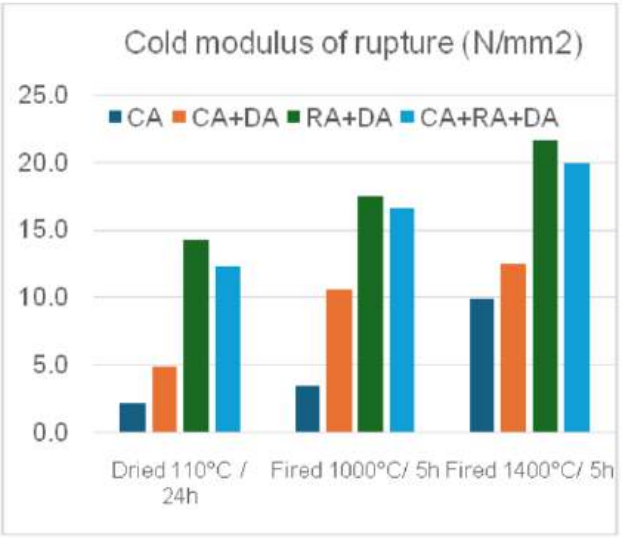


Fig. 5: Cold modulus of rupture of the batches

Batch RA+DAresulted further reduction in water demand and improvement in flowability due to presence of significant amount of sub-micron particles as well as bi-modal particle size distribution. The fired properties with batch RA+DA were also better dur to the same reason which resulted strong sintering and as a result increased density and improved the strength properties.

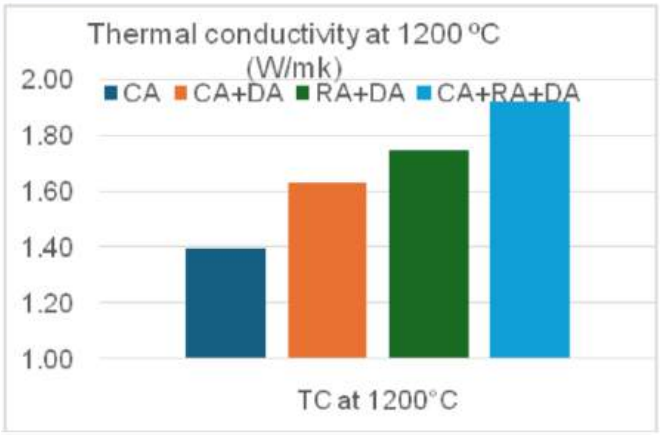


Fig. 6: Thermal conductivity of the batches

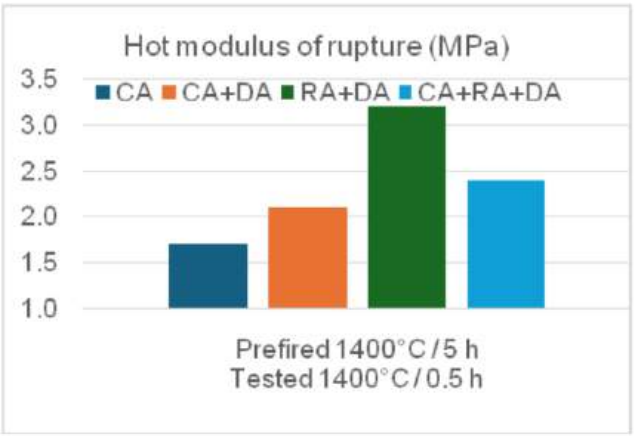


Fig. 7: Hot modulus of rupture of the batches

As seen in figures 6 and 7, thermal conductivity and hot modulus of the batches also followed similar trend to other properties. And introduction of reactive alumina with dispersing aluminas (batch RA+DA) gave best property. However, the thermal conductivity has approached towards 2 W/mk value at 1200 °C (around operating temperature in blast furnace blow pipe application) and could be a technical hindrance for the long term usage of the application.

It indicated a technical tread-off was necessary and the batch CA+RA+DA was tried. This had resulted a marginal increase in water damand to 6% with slight reduction in rheological properties compared to batch RA+DA, but acceptable fired properties and moderate permanent liner change due to partial reduction of sinterability. And as a result, a balanced hot modulus of rupture with reduced thermal conductivity was achieved as shown in the above figures.

Based on the trials, batch CA+RA+DA is selected as an optimum selection for blow pipe castable. This is having ~70% alumina content, good flowability till 60 mints with just 6% water addition and resulted moderately high cold and hot strengths with <2 W/mk thermal conductivity at 1200 ºC and best suitable for the service of particular castable.

Conclusion

- Blast furnace blow pipe castable is very critical application for balanced properties requirements for low cement 60-70% alumina containing self-flow castable with reduced water demand.
- Self-flow castable was designed with the use of pyrophyllite and WTA as aggregates.
- With calcined alumina alone and micro silica, adequate flow was not obtained.
- Dispersing aluminas prove to be very efficient for reducing castable mixing water drastically and still providing good self-flow properties.
- With reactive alumina and dispersing alumina combination, best flowability and strength features were obtained but thermal conductivity was also higher due to maximum sinterability of the choosen batches.
- A mix of calcined and reactive alumina proved to be optimal option for balanced sinterability for achieving strengths as well as thermal conductivity.
- In low cement 60-70% alumina containing castable category with silica fume, balanced optimal properties obtained using bimodal reactive alumina, calcined alumina and dispersing aluminas in matrix.

INFLUENCE OF CALCINED ALUMINA CHARACTERISTICS ON THE ABRASION RESISTANCE OF CASTABLE

Ankita Das[1], Saumen Sinha[1], Sourojit Pal[2], Shankha Chatterjee[2]

[1]Calderys India Refractories Limited, Nagpur, India

[2]Almatis Alumina Pvt. Ltd., Kolkata, India

Corresponding author's e-mail: ankita.das@calderys.com

Abstract

Refractories used in petrochemical industries are subjected to extremely adverse conditions. Especially for refractories used in units like SRU, the lining must endure severe wear due to high velocity gas streams and entrained solid particles. Hence, abrasion resistance becomes a crucial performance parameter to ensure durability and integrity of such refractory linings. Abrasion, defined as loss of mass due to mechanical friction on the surface, is mainly governed by grain pull out and is primarily associated with the integrity of the matrix and the strength of the aggregate-matrix bonding.

It is often assumed that refractories exhibiting favorable bulk physical properties, such as high density and strength, will inherently demonstrate superior abrasion resistance; however, this is not always the case. The matrix is actually more critical than the aggregates in improving wear resistance of the material. Enhanced interfacial bonding strengthens the matrix and improves grain retention, as a result, tendency of grain detachment during abrasion is reduced. The present study highlights the significant variation in abrasion resistance of castable compositions with similar aggregates, but different matrix characteristics. To investigate this, two types of calcined alumina with different particle size distributions were incorporated into comparable formulations to understand their influence on matrix characteristics and eventually on abrasion resistance through microstructural analysis. Both the compositions were processed under controlled conditions and evaluated for physical and mechanical properties.

Comparative testing shows that the addition of a special calcined alumina reduced the abrasion loss by approximately 30%, with a substantial improvement in the aggregate-matrix bonding. The findings demonstrate that abrasion resistance in refractory systems is predominantly governed by matrix characteristics and bonding rather than strength of the aggregates alone. Additionally, consistency in the properties of the calcined alumina is crucial for achieving the desired performance and ensuring long-term durability of the lining under service conditions.

Keywords: Abrasion loss, Calcined alumina, Matrix characteristics, Particle size distribution

1. Introduction

Refractories play a critical role in petrochemical industries, since they are extremely important to provide thermal insulation as well as protection against the severe operating conditions, including high temperature and chemical corrosion. Additionally, segments that deal with continuous movement of particles can be subjected to extreme abrasion. High-velocity particle flow can erode the refractory surface, leading to material loss, dimensional instability, and premature failure. Such degradation can expose the underlying equipment to elevated temperatures and corrosive process environments, and may cause unplanned shutdowns, increased maintenance costs, and reduced plant efficiency.

In this context, there is an increasing demand for improved abrasion resistant refractories for petrochemical applications. Refractories used in FCCU, cyclones, ducts, risers, hydrogen transfer lines must retain their structural integrity under prolonged mechanical stress, including at lower temperatures prior to the completion of ceramic bond formation or sintering. As a result, although conventional refractory properties such as refractoriness and chemical stability remain the primary criteria, improved abrasion resistance of the lining becomes a major requirement of the process.

It is often assumed that the type and properties of the coarse aggregate are majorly responsible for enhancing the abrasion resistance characteristics of a refractory material, since the aggregates constitute a major portion of the composition. However, abrasion resistance cannot be enhanced by focusing on the aggregates alone. The bonding and strength of the matrix play an important role in determining the resistance of the refractory to grain pull-out and eventual material loss. A strongly bonded matrix can effectively hold the aggregate particles in place and reduce grain detachment under abrasive conditions. Therefore, abrasion behavior, in reality, is influenced by the combined effects of composition, particle-size distribution, packing characteristics, matrix development, and microstructural bonding, rather than by physical properties alone. The particle-size distribution of microfine alumina is an important but relatively less explored parameter in this context. A calcined alumina with sufficiently broad and continuous distribution of particles, can reduce interparticle voids by filling pores of different sizes, resulting in higher packing density and increased particle–particle contact. These improved packing and bonding characteristics of the matrix may in turn have an influence on the abrasion resistance of the material.

Previous studies have demonstrated that the particle-size distribution of alumina can significantly influence packing and densification behavior, although the reported trends in conventional physical properties such as bulk density and strength are not always consistent. Hai Tang, Yingheng Shi, and Wenjie Yuan reported that submicron alumina with a broader particle-size distribution exhibited higher packing density [1]. Similarly, studies employing colloidal processing have shown that alumina compacts with comparable mean particle sizes, but different particle-size distributions can exhibit significant differences in green density and early-stage densification, with broader particle-size distributions demonstrating favorable behavior [3]. Due to the void filling ability of a suitably broad particle size distribution, enhanced sintering as well as grain growth has been observed [2].

The objective of the present case study is to investigate the influence of particle-size distribution of microfine alumina on refractory matrix development and, ultimately, on abrasion resistance. Particular emphasis is placed on understanding how a broader particle-size distribution contributes to matrix integrity and improved wear performance, and on establishing the relationship between alumina particle-size distribution, microstructure, and abrasion behavior.

2. Experimental Procedures

2.1. Raw Material Characterization

Two high alumina based conventional castable compositions were formulated with commercially available high purity alumina aggregates using effective particle packing. An indicative composition of the trials can be found in Table 1. Two different types of commercially available calcined aluminas, C1 & C2, were used in the formulation to evaluate their influence on matrix distribution and packing efficiency and, consequently, on the mechanical properties of the refractory. C1 represents a narrower particle size distribution, while C2 (Almatis) exhibits a relatively broader distribution, which is expected to offer improved packing and enhanced microstructural bonding. The

details of their respective properties are given in Table 2. The trials were designed to evaluate the influence of matrix distribution on the abrasion resistance of the material, aiming to enhance the microstructural bonding in the refractory compositions.

Raw Material	T1	T2
Alumina Aggregate	XX	XX
Cement	S	S
Additives	A	A
C1	**Y**	**-**
C2	**-**	**Y**
Mixing water %	Z	Z

Table 1 General information on the designed high alumina castable compositions.

Parameter	C1	C2
d10 (µm)	0.91	0.88
d50 (µm)	2.75	3.00
d90 (µm)	8.59	12.63
Specific Surface Area (m2/gm)	1.2	0.8

Table 2 Properties of the selected calcined aluminas, C1 & C2

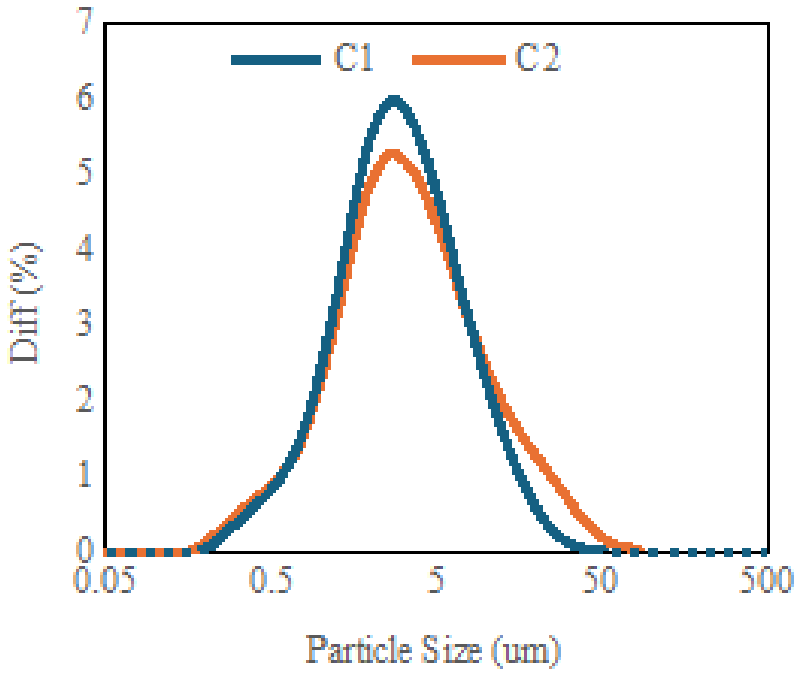


Fig 1. Particle Size Distribution of Calcined Aluminas

2.2. Sample Preparation & Method of Analysis

The two high alumina compositions were developed to study the influence of raw material selection and particle size distribution on the matrix bonding and mechanical properties of the final refractory structure.

The dry castable mix was homogenized for 1 min and then mixed for another 4 minutes in a mixer by adding minimum required water for obtaining suitable flow. The test specimens were prepared by vibration casting following the ASTM C 862 standard and cured at room temperature for 24 hours. After demolding, the specimens were dried at 110℃ for 24 hours. For evaluation of high-temperature physical properties such as BD, MOR, & PLC, specimens were fired at 815°C and 1100°C respectively with a soaking time of 5 hours in each case according to ASTM C 865. Cold abrasion resistance of the castable specimens was also evaluated (114*50*50 mm size specimens, pre-fired at 815 °C for 5 h) as per the ASTM C 704 standard. The microstructure of the samples was observed in an optical microscope at 100X magnification after firing the specimens at 815 °C for 5 hours.

3. Results and discussion

The bulk density of the two castable compositions with different calcined alumina, fired at different temperatures, is presented in Fig 2. It can be observed that the formulation with the broader distribution of calcined alumina demonstrated higher density across different firing temperatures.

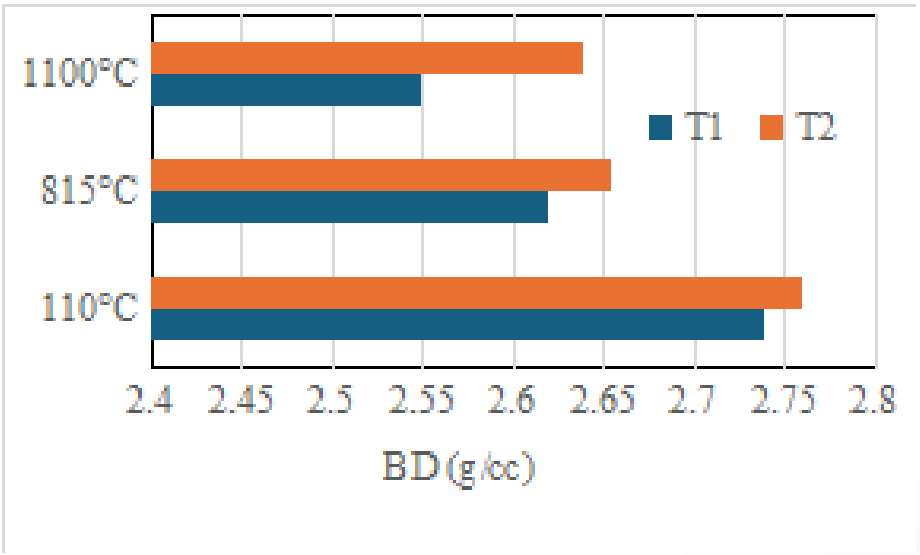


Fig 2. Bulk Densities of test specimens after firing at 110°C, 815℃ and 1100°C

This observation was consistent with the changes in modulus of rupture (MOR) of the samples as shown in fig 3. The higher MOR of T2 indicates a more homogeneous bonding with enhanced particle-particle contact, attained by a slightly broader distribution of particles in C2.

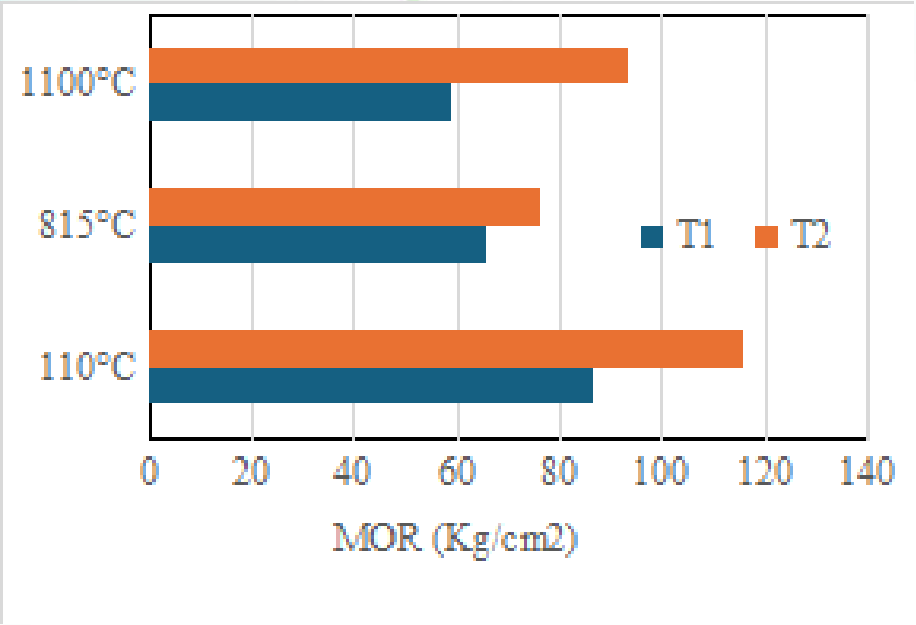


Fig 3. MOR of test specimens after firing at 110°C, 815℃ and 1100°C

The improvement in MOR can also indicate a more homogeneous matrix distribution, reducing the formation of localized large pores or internal defects that may act as severe stress concentrators under tensile loading. This was also indicated in the microstructure of the samples fired at 815°C for 5 hours as shown in Fig. 4.

a. b.

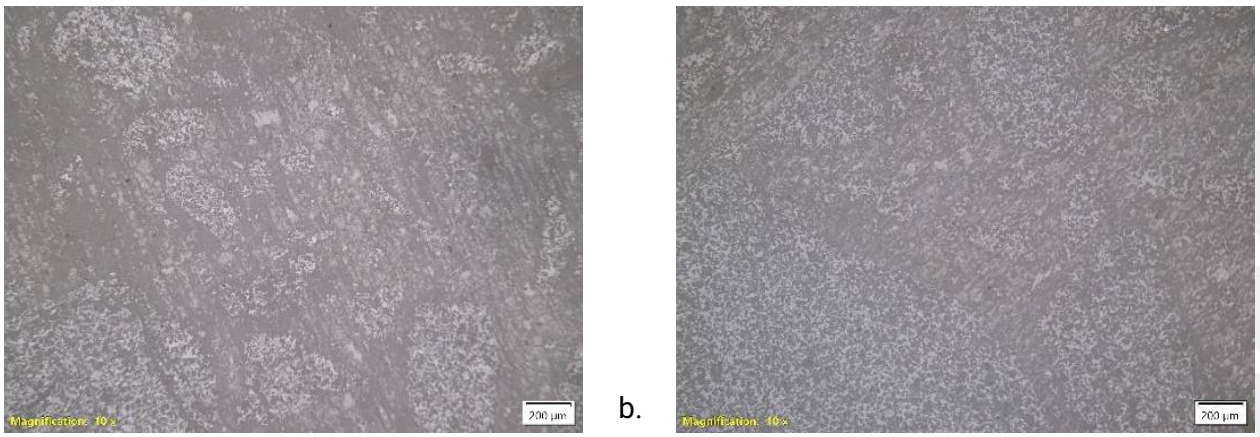


Fig 4. Microstructure of samples fired at 815℃ for 5 h: a) T1, b) T2 sample

The most important difference between the samples of T1 and T2 lies in the degree of matrix refinement and uniformity rather than in a drastic difference in the aggregate skeleton, as expected. T1 contains localized regions with noticeably different matrix textures. This indicates potentially less uniform packing. T2, in contrast, exhibits a more continuous bonding matrix, with improved filling of the spaces between the coarse aggregate particles. Regarding porosity, both T1 and T2 show predominantly fine, dispersed porosity rather than large, continuous pore channels. However, in T1, the pores appear to be distributed more irregularly, with local concentration in comparatively heterogeneous matrix regions and along some aggregate–matrix boundaries, whereas, T2 shows a finer and more uniformly distributed pore structure, with fewer localized pore-rich zones and better filling of the inter-aggregate spaces. This more homogeneous matrix in T2 is

expected to have enhanced the mechanical response of the material.

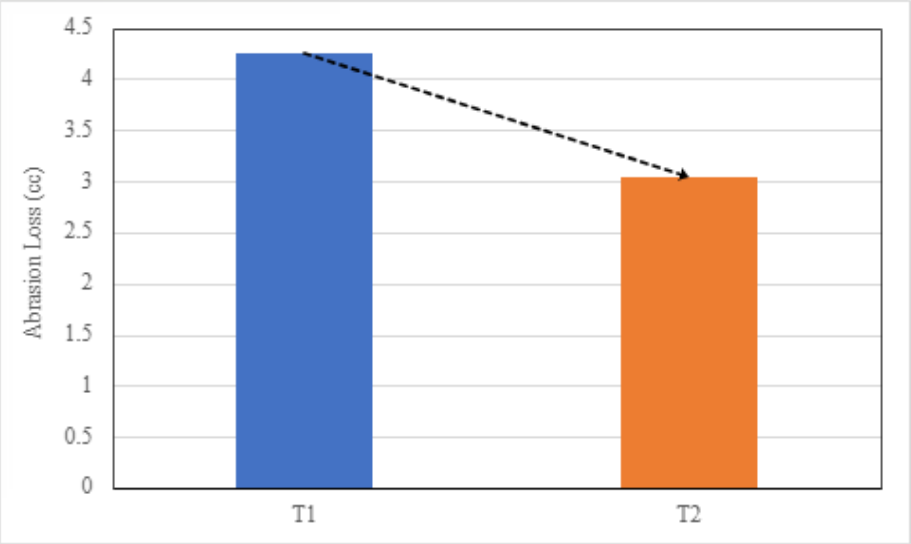


Fig 5. Abrasion loss of test specimens after firing at 815℃ for 5 hours

A noticeable reduction of around 30% is found in the abrasion loss for the samples of T2, sintered at 815°C for 5 hours. The comparative results are shown in Fig. 5. This result helps us to understand the influence of particle size distribution on wear resistance of the refractory. A suitably broader particle size distribution of the second calcined alumina enhanced density and interparticle bonding between the aggregate and the matrix. This densely packed and continuous matrix exhibited a lower tendency of grain detachment during abrasion.

4. Conclusion

The particle-size distribution (PSD) of the calcined alumina powders plays an important role in improving the packing efficiency and consequently the densification of the refractory matrix. A densely packed matrix is achieved when particles of progressively smaller sizes occupy the void spaces generated between coarser particles. Therefore, a calcined alumina with slightly broad and continuous distribution of particles, can reduce interparticle voids by filling these sites, resulting in higher packing density, increased particle–particle contact, and increased matrix homogeneity. This in turn helped reducing the loss of material under abrasive conditions.

References

1. Tang, H., Shi, Y., & Yuan, W. (2022). Influence of powder characteristics on the sintering behaviour of reactive alumina powders. *Processing and Application of Ceramics*, *16*(1), 1-6.
2. Ma, J., & Lim, L. C. (2002). Effect of particle size distribution on sintering of agglomerate-free submicron alumina powder compacts. *Journal of the European Ceramic Society*, *22*(13), 2197-2208.
3. Yeh, T. S., & Sacks, M. D. (1988). Effect of particle size distribution on the sintering of alumina. *Journal of the American Ceramic Society*, *71*(12), C-484.

MICROSTRUCTURAL ENGINEERING OF ZIRCONIA–MULLITE REFRACTORY USING A SPECIAL REACTIVE ALUMINA FOR ENHANCED HIGH TEMPERATURE PERFORMANCE

Avishek Mitra[1], Ankita Das[1], Dr Saumen Sinha[1], Shankha Chatterjee[2]

[1]Calderys India Refractories Limited, Nagpur, India

[2]Almatis Alumina Pvt. Ltd., Kolkata, India

Abstract

Zirconia–mullite refractories are commonly used in high temperature industrial applications owing to their ability to exhibit excellent thermal stability, corrosion resistance, and mechanical strength. However, conventional zirconia-mullite compositions often face issues such as relatively high porosity, moderate creep resistance, and restricted thermo-mechanical stability during prolonged exposure to elevated temperatures. Considering these limitations can affect the performance of refractories by reducing the service life and durability in demanding application conditions, optimization of the microstructure can be a promising way forward in overcoming this issue.

In the present development, microstructural modification of zirconia-mullite refractories was achieved by incorporating a special reactive alumina (Almatis) with the objective of inducing enhanced densification, improved inter-particle sintering, and overall improved high-temperature properties. This study also investigates the characteristics of two types of microfine alumina to understand their influence on matrix bonding and densification. The newly developed composition was processed under controlled conditions and evaluated for the physical, mechanical, thermo-mechanical, and chemical properties. Key physical parameters such as bulk density, apparent porosity, and mechanical strength were tested to understand the influence of reactive alumina.

According to the attained results, conventional compositions developed using regular microfine alumina did not provide the required densification, due to its relatively lower reactivity and limited sintering activity. However, incorporation of a special reactive alumina significantly improves matrix densification and promotes stronger bonding within the zirconia–mullite system. This leads to a reduction in porosity and a corresponding increase in bulk density and mechanical strength. Furthermore, improved microstructural homogeneity and refined grain bonding contribute to enhanced resistance against thermo-mechanical degradation under high-temperature conditions. The modified composition also exhibits improved chemical stability, indicating better resistance to aggressive environments.

Overall, the findings highlight the critical role of a special reactive alumina in tailoring the microstructure and enhancing the performance of ZIRCONIA-MULLITE refractories. The improved densification and bonding achieved through this approach make the developed material a promising candidate for high-temperature industrial applications requiring superior durability and reliability.

Keywords: Creep, Glass, Reactive Alumina, Zircon Mullite

1. Introduction

Zirconia–mullite refractories are multiphase oxide materials that had been developed for applications which require high refractoriness, mechanical integrity, chemical resistance and dimensional stability during prolonged exposure to elevated temperatures. Such bricks are mainly used in glass manufacturing plants in forehearths, distributors, feeders and glass-forming components such as plungers, spouts, tubes, stirrers, channels and orifice rings. Refractory components in these zones must retain their dimensions while exposed continuously to molten glass, static mechanical load and temperatures nearly 1400-1500°C. Zirconia–mullite materials are suitable for such service because of a mullite–alumina framework and a dispersed zirconia-bearing phase. Mullite ($3Al_2O_3.SiO_2$) shows good performance at high-temperature structural applications because of its low thermal-expansion coefficient, good chemical stability and retention of strength at elevated temperatures [1]. Dispersed zirconia can additionally help in restricting crack propagation, improving fracture behaviour and microstructural evolution. But its effect on long-term creep depends strongly on the zirconia form, distribution and grain-boundary chemistry [2,3].

Zircon Mullite can be produced by the reaction sintering of zircon and alumina. Zircon initially dissociates to zirconia and silica, Equation (1):

$$ZrSiO_4 \rightarrow ZrO_2 + SiO_2 \quad ¿------(1)$$

The liberated silica subsequently reacts with alumina to form mullite, Equation (2):

$$3Al_2O_3 + 2SiO_2 \rightarrow 3Al_2O_3 \cdot 2SiO_2 \quad ------(2)$$

The overall reaction is shown in Equation (3):

$$2ZrSiO_4 + 3Al_2O_3 \rightarrow 2ZrO_2 + 3Al_2O_3 \cdot 2SiO_2 \quad --(3)$$

This transformation does not occur through a single instantaneous reaction. Zircon dissociation, local silica-rich liquid or amorphous-phase formation, alumina dissolution, mullite nucleation and zirconia precipitation occur simultaneously. The alumina particle size, reactivity, dispersion and impurity content strongly influence the rate of mullite formation, matrix densification and final zirconia distribution [4].

Studies on mullite–zirconia composites show that creep is governed by microstructure, diffusion paths, grain-boundary phases and mullite morphology rather than by oxide chemistry alone [5,6]. Creep resistance is very important in glass-plant applications because the furnace and its feeder components remain under load for prolong period. Even small continuous deformation can change the geometry of a plunger, spout or orifice, cause joint opening or misalignment, disturb glass-flow control and create local stress concentrations.

The present study isolates the influence of alumina grade by comparing two zirconia–mullite refractory compositions having nearly identical chemistry but containing different microfine alumina sources. A conventional microfine alumina (CA) was replaced with a special reactive alumina (ASA) to determine how differences in specific surface area, particle-size distribution, impurity level and sintering activity affect the matrix development. Apparent porosity, bulk density, cold crushing strength, modulus of rupture, hot modulus of rupture, permanent linear change and compressive creep at 1450°C were measured. The objective was to establish a mechanism-based relationship between alumina characteristics, microstructural densification, ceramic-bond development and the resulting high-temperature mechanical stability.

2. Experimental

Commercially available high purity alumina and zircon with different size fractions were used as major raw materials. Two different batches of bricks were manufactured using two different types of alumina. In T-B, calcined alumina named CA was used while in T-A, reactive alumina ASA was used.

The special reactive alumina (ASA) differed significantly from the conventional calcined alumina (CA) in terms of fineness, surface area and purity. ASA had a much higher specific surface area of approximately 7.2 m²/g, compared with only 1.2 m²/g for CA. ASA also have a finer particle-size distribution $(D_{50}=0.6\ \mu m, D_{90}=2.0\ \mu m)$ than CA $(D_{50}=2.9\ \mu m, D_{90}=7.45\ \mu m)$. The finer ASA particles can more effectively fill the interstitial spaces between coarse grains, increase particle-particle contact area and shorten the diffusion distance during firing. This promotes stronger sintering, faster reaction with zircon-derived silica and more uniform secondary mullite formation. ASA also contained higher Al_2O_3 purity and lower impurity, especially Na_2O content, approximately 0.08% compared with 0.40% in CA. This in turn reduces the possibility of forming alkali-rich, low-viscosity grain-boundary phases.

The set of trial samples consisting of two different recipes were shaped into bricks by using industrial hydraulic press with a specific pressure of 1.8 Ton/cm^2 and samples were dried at 110°C for 24 hrs. After drying, the samples were fired at 1550°C with predetermined heating schedule and soaking time in laboratory furnace. The fired samples underwent testing as per the industrial testing practices.

Parameter	ASA (Used in T-A)	CA (Used in T-B)	Technical significance (ASA vis-à-vis CA
Specific surface area (m²/g)	7.2	1.2	6 times higher surface-area
D50 (µm)	0.6	2.9	79.3% smaller median size
D90 (µm)	2.0	7.45	73.2% fewer coarse matrix particles
Al_2O_3 (%)	99.8	99	Higher refractory-oxide purity
Na_2O (%)	0.08	0.40	80% lower alkali impurity
Fe_2O_3 (%)	0.02	0.03	Comparable low iron impurity

Table 1 Properties of CA vs ASA

After firing, specimens were cut from comparable locations of the bricks and tested for apparent porosity (AP), bulk density (BD), cold crushing strength (CCS), modulus of rupture (MOR), hot modulus of rupture (HMOR) and creep in compression using standard refractory-testing practices.
Creep testing was carried out at 1450°C for 50 hours under constant compressive load. The creep deformation between 20 and 50 h was calculated as per Equation 4:

$$Z_{20-50} = |\varepsilon_{50} - \varepsilon_{20}| \quad ---- \quad (4)$$

A target of $Z_{20-50} < 0.30\%$ was selected for evaluating dimensional stability under prolonged high-temperature load. Each reported property represents the average of parallel specimens.

3. Results and discussion

The special reactive alumina, ASA, exhibited a specific surface area of $7.2\,m^2\,g^{-1}$, approximately six times that of the conventional alumina, CA. ASA also had a substantially finer particle-size distribution, with lower D_{50} and D_{90} values. This combination increases the number of matrix-aggregate contacts and increases the surface free energy available for sintering. For an idealised spherical particle, the capillary pressure (ΔP) driving pore shrinkage and neck formation may be expressed as Equation 5:

$$\Delta P \approx \frac{2\gamma}{r} \quad ------ \quad (5)$$

where γ is the solid–vapour or grain-boundary surface energy and r is the effective particle radius. Reduction in particle radius therefore increases the sintering pressure and simultaneously shortens the diffusion distance required for lattice, grain-boundary and surface transport. Consequently, ASA is expected to promote earlier neck development, improved pore elimination and stronger ceramic bonding during firing [1,9].

Alumina fineness also controls the kinetics and spatial uniformity of mullite formation. During zircon dissociation, the released silica must diffuse and react with alumina. A finer and more uniformly distributed alumina increases the interfacial contact area between Al_2O_3 and silica-bearing reaction products. This reduces local chemical gradients, suppresses the formation of isolated alumina-rich or silica-rich regions and favours a more continuous secondary-mullite bond. Reaction-sintering studies have shown that alumina precursor characteristics and the scale of Al_2O_3–SiO_2 mixing significantly influence zircon decomposition, mullite nucleation, densification and final phase distribution [2–4].

The lower Na_2O content of ASA is also important. Sodium has limited solubility in the mullite lattice and preferentially enters residual silicate-rich intergranular phases. Although a small amount of such liquid can assist initial densification, excessive alkali lowers the viscosity and refractoriness of the grain-boundary phase. Thus, it promotes viscous flow and grain-boundary sliding during high-temperature loading [10]. ASA therefore provides a favorable combination of high sintering reactivity and reduced alkali-derived glass formation.

Property	Relative change in T-A	Technical interpretation
Apparent porosity (%)	7.2% lower	Reduced pore volume
Bulk density (g/cm³)	1.1% higher	Improved densification
CCS (MPa)	10.6% higher	Stronger compressive network
MOR (MPa)	22.0% higher	Lower tensile flaw severity
HMOR at 1400°C (MPa)	38.1% higher	Stronger hot ceramic bond
PLC at 1600°C/ 6 h (%)	31.4% less expansion	Improved reaction completion
Creep $Z_{20\text{-}50}$ at 1450°C / 50 h (%)	35.7% lower	Reduced time-dependent creep

Table 2 Fired-property comparison T-A & T-B

T-A showed a 7.2% lower apparent porosity and a 1.1% higher bulk density than T-B. As the coarse zirconia–mullite aggregates occupy most of the brick volume, the increase in bulk density was small. The ASA mainly affects the fine matrix between these coarse grains. Even a small reduction in matrix porosity can significantly improve strength because pores reduce the effective load-bearing area and act as points of stress concentration. The relationship between strength and porosity can be explained by the

Ryshkewitch–Duckworth equation (6):

$$\sigma = \sigma_0 exp(-bP) \quad ------ \quad (6)$$

where σ is the measured strength, σ_0 is the theoretical strength of a pore-free material, P is porosity and b is a material constant. This equation shows that ceramic strength decreases rapidly as porosity increases [12].

The cold crushing strength increased by 10.6% while the modulus of rupture increased by 22%. The percentage improvement in MOR was greater because flexural failure is highly sensitive to large pores, cracks and weak grain-boundary paths on the tensile side of the specimen. The finer ASA particles improved matrix packing and sintering, reduced connected pores and created more contact points between particles. As a result, the applied load could be transferred more effectively through the matrix. Similar improvements in porosity, bulk density, CCS and hot strength have been reported when reactive alumina promotes faster bond formation and improved mullite–corundum development [13].

T-A showed a 38.1% higher HMOR at $1400^{\circ}C$ than T-B. This improvement is more important than the increase in room-temperature strength because HMOR directly reflects the stability of the refractory bond at service temperature. At $1400^{\circ}C$, the load-bearing capacity depends on the strength of the mullite–corundum–zirconia interfaces, the amount and viscosity of grain-boundary liquid, and the resistance of the matrix to grain-boundary sliding.

The better HMOR of T-A can be explained by the characteristics of ASA. Its finer particle size and higher surface area increased the number of particle contacts during firing and promoted stronger ceramic-neck formation. ASA also contained considerably less Na_2O than CA. Sodium is only weakly incorporated into the mullite structure and generally remains in silica-rich grain-boundary phases. These alkali-rich phases soften at high temperature and allows the grains to move more easily under load [14–15]. Therefore, the lower Na_2O content of ASA reduced the formation of weak glassy films, while its higher reactivity produced a more continuous mullite-bearing bond. Both effects contributed to the higher HMOR of T-A.

The permanent linear change after heating at $1600^{\circ}C\ for\ 6\ hours$ decreased from +0.35% for T-B to +0.24% for T-A. Positive PLC indicates that some expansion-producing reaction or structural rearrangement continued during the test. The lower positive PLC of T-A suggests that more of the sintering and mullite-forming reactions had already been completed during the original firing process. Consequently, less residual reaction remained to occur during reheating.

The creep curves for T-A and T-B were obtained under the same test conditions of $1450^{\circ}C$ for 50 h. Both specimens reached approximately $1450^{\circ}C$ after about 2.5 hours, allowing a direct comparison of their deformation behaviour. T-A showed a lower maximum expansion, $dL_{max} = 0.524\%$, compared with 0.709% for T-B. More importantly, T-A showed less accumulated compressive deformation throughout the test. The measured values were:

Creep parameter	T-A	T-B
Z_5 (%)	0.405	0.672
Z_{20} (%)	0.728	1.144
$Z_{49.99}$ (%)	1.002	1.57
$Z_{20\text{-}50}$ (%)	0.274	0.426

Table 3 Parameters extracted from the corrected creep curves

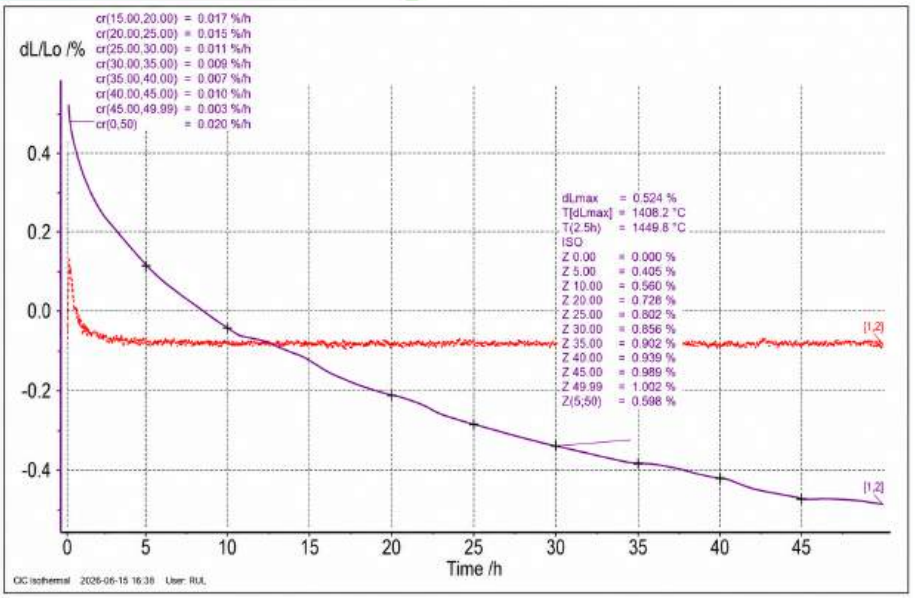


Figure 1 Creep graph for T-A

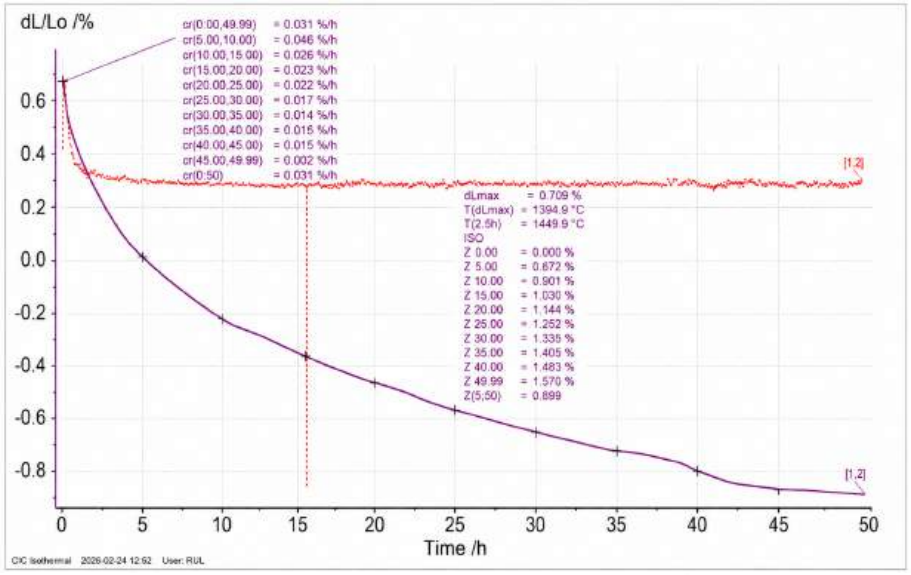


Figure 1 Creep graph for T-B

The most important value for long-term performance is Z_{20-50}, because the initial part of the test includes thermal expansion, rapid pore closure and primary creep. Deformation between 20 and 50 h represents the more stable high-temperature creep. T-A showed a Z_{20-50} value of 0.274%, which was approximately 35.7% lower than the value of 0.426% recorded for T-B. The corresponding average creep rates between 20 and 50 h were:

The lower rate of T-A shows that its deformation resistance was maintained during the later part of the test and was not limited only to the initial heating stage.

ASA reduced these deformation mechanisms in several ways. Its finer particles improved packing and reduced connected porosity. Its higher surface area increased sintering activity and formed stronger ceramic necks between matrix particles. More uniform contact between alumina and zircon-derived silica also promoted a more continuous mullite bond. In addition, the lower Na_2O content reduced the amount of low-viscosity alkali-rich glass at the grain boundaries. As a result, the matrix became less susceptible to viscous flow and grain-boundary sliding at $1450^{\circ}C$.

Very fine particles can sometimes increase diffusional creep if they produce an excessively fine final grain structure. However, this effect was not dominant in T-A. The observed reduction in creep shows that improved densification, stronger bonding and lower grain-boundary glass had a greater influence than any possible fine-grain contribution. Since the zirconia content of T-A and T-B was almost identical, the creep improvement cannot be attributed to zirconia quantity. It is therefore mainly related to the microstructural engineering produced by ASA, particularly stronger ceramic bonding, reduced connected porosity, lower alkali-rich glass content and more uniform mullite formation.

4. Conclusion

i) The special reactive alumina (ASA) has 6 times higher surface area, 79.3% lower D50, 73.2% lower D90 and 80% lower Na_2O than the conventional alumina (CA).

ii) At nearly constant Al_2O_3-ZrO_2-SiO_2 chemistry, T-A achieved lower apparent porosity, higher density, 10.6% higher CCS and 22.0% higher MOR, demonstrating improved matrix consolidation.

iii) The 38.1% HMOR improvement shows that the main benefit persisted at service temperature and is consistent with a stronger, less glass-sensitive ceramic bond.

iv) The creep testing at 1450°C showed 35.7% lower $Z_{20\text{-}50}$ deformation, 33.5% lower $Z_{5\text{-}50}$, and 35.5% lower overall creep rate for T-A.

v) Controlled PLC indicates improved dimensional stability. Reactive-alumina selection is therefore an effective route to improve zirconia-mullite refractory performance without increasing zirconia content.

References

[1] F. Temoche, L.B. Garrido and E.F. Aglietti, "Processing of mullite–zirconia grains for slip cast ceramics," Ceramics International, 31 (2005) 917–922.

[2] C. Aksel, "Mechanical properties and thermal shock behaviour of alumina–mullite–zirconia and alumina–mullite refractory materials by slip casting," Ceramics International, 29 (2003) 311–316.

[3] C. Aksel, "The microstructural features of an alumina–mullite–zirconia refractory material corroded by molten glass," Ceramics International, 29 (2003) 305–309.

[4] T. Ebadzadeh and E. Ghasemi, "Influence of starting materials on the reaction sintering of mullite–ZrO_2 composites," Materials Science and Engineering A, 283 (2000) 289–297.

[5] P. Descamps, S. Sakaguchi, M. Poorteman and F. Cambier, "High-temperature characterization of reaction-sintered mullite–zirconia composites," Journal of the American Ceramic Society, 74 (1991) 2476–2481.

[6] D. Glymond, M. Vick, M.-J. Pan, F. Giuliani and L.J. Vandeperre, "Creep of mullite zirconia composites," Journal of the European Ceramic Society, 35 (2015) 3607–3611.

[7] S.B. Gürel and A. Altun, "Reactive alumina production for the refractory industry," Powder Technology, 196 (2009) 115–121.

[8] ISO 3187:1989, Refractory products—Determination of creep in compression, International Organization for Standardization.

[9] Kothari, N.C., "The Effect of Particle Size on Sintering Kinetics in Alumina Powder," Journal of Nuclear Materials, Vol. 17, No. 1, 1965, pp. 43–53.

[10] W.G. Fahrenholtz and D.M. Smith, "Densification and microstructure of sodium-doped colloidal mullite," Journal of the American Ceramic Society, 77 (1994)

1377-1380.
[11] Delia, D.J., Lee, H. and Carty, W.M., “Surface Area Reduction During the Sintering of Alumina,” Journal of the American Ceramic Society, Vol. 106, No. 9, 2023, pp. 5178–5186
[12] Ryshkewitch, E., “Compression Strength of Porous Sintered Alumina and Zirconia,” Journal of the American Ceramic Society, Vol. 36, No. 2, 1953, pp. 65–68
[13] S. Ghose, C. Saigal, A. Maldhure and S.K. Das, “Effect of reactive alumina on the physico-mechanical properties of refractory castable,” Transactions of the Indian Ceramic Society, 72 (2013)
[14] C. Wolf, R. Kauermann, H. Hübner, J.A. Rodrigues and V.C. Pandolfelli, “Effect of mullite-zirconia additions on the creep behaviour of high-alumina refractories,” Journal of the European Ceramic Society, 15 (1995) 913-920.
[15] P. Descamps, S. Sakaguchi, M. Poorteman and F. Cambier, “High-temperature characterization of reaction-sintered mullite-zirconia composites,” Journal of the American Ceramic Society, 74 (1991) 2476-2481

RESEARCH ON SLAG ADHESION TREATMENT TECHNOLOGY IN THE MELTING AND CASTING INDUSTRY

ZHOU Haixiang[1], WU Linlin[2], ZHAN Zan[2], CHEN Yuxin[1], WU Guanghua[1]

1. Calderys China, Tangshi Street, Tangshi Town, Zhangjiagang, 215618 Jiangsu
2. HuangshiDongbei Casting Co., Ltd., Guanghu Road, Luoqiao Street, Daye City, 435100 Hubei

Corresponding author's e-mail: sachidulal.majumdar@ifgl.in, riya.ghosh@elkem.com

Abstract

In the melting and casting production using medium-frequency induction furnaces, slag tends to form a hard and difficult-to-remove slag adhesion layer on refractories and other locations.The slag adhesion problem not only affects the normal operation of equipment, but also may lead to potential safety hazards, increase maintenance costs, and reduce casting quality.Among them, chemical slag adhesion is particularly difficult to remove because it forms compounds with a high melting point, even higher than that of the refractories.This paper mainly analyzes the characteristics of chemical slag adhesion, proposes solutions and conducts preliminary attempts, achieving obvious effects.The study shows that the main cause of slag adhesion is the enrichment of Al_2O_3 in the medium-frequency furnace slag near the furnace lining and its combination with SiO_2 and MgO to form high-melting-point phases.The high-melting-point phases are mainly $MgO{\cdot}Al_2O_3$ spinel and $Al_2O_3{\cdot}SiO_2$ mullite.The designed slag agent contains 30–60% of $3CaO{\cdot}Al_2O_3$ phase and 20–60% of $12CaO{\cdot}7Al_2O_3$ phase, which achieves a balance between slag dissolution performance and protection against refractory erosion.The designed addition amount of the slag agent is about 80–120% of the slag adhesion weight or at least 40% of the surface slag weight in the medium-frequency furnace.Industrial tests show that the slag agent can effectively remove slag adhesion and protect the refractories.

Keywords: Flux, induction furnace, adhesion slag, refractory protection

1. Introduction

Similar to the expansion of the iron and steel industry, China's casting output reached 50.75 million tons in 2024, accounting for approximately 45% of the global total, ranking first in the world for more than 20 consecutive years. Melting scrap steel in an intermediate frequency furnace followed by casting is a common practice in the foundry industry. In the melt-casting industry, slag adhesion refers to the phenomenon where molten metal or slag adheres to the inner walls of equipment (such as iron ladles, steel ladles, desulfurization tools, etc.) at high temperatures, forming a hard and difficult-to-remove slag layer [1].This not only impairs normal equipment operation but also introduces potential safety hazards, increases maintenance costs, and degrades casting quality.

Based on formation mechanisms, slag adhesion can be classified into chemical slag adhesion, physical slag adhesion (mechanical adhesion), and cold steel anchoring slag adhesion. Chemical slag adhesion mainly occurs when molten slag reacts chemically with refractory materials at high temperatures to form low-melting-point compounds that firmly attach to equipment surfaces. Physical slag adhesion arises when high-temperature molten slag splashes into low-temperature zones (e.g., the upper ladle wall) due to splashing, liquid level fluctuations, or slag skimming, then condenses and adheres. In addition, entrapped unmelted metal particles in the slag form a composite "cold steel + slag" structure, which significantly strengthens bonding strength and leads to anchoring slag adhesion.

In recent years, competition in the foundry industry has intensified, with growing focus on production efficiency, cost control, and quality. Therefore, the removal of slag adhesion has become one of the key common issues in the melt-casting industry. The latter two types of slag adhesion are relatively easy to remove, typically by manual stripping or heating-assisted slag skimming. In contrast, chemical slag adhesion is extremely difficult to remove because it forms high-melting-point compounds—even higher than the melting point of the refractory itself. This paper analyzes the characteristics of chemical slag adhesion, proposes solutions, and conducts preliminary trials with remarkable results.

2. Slag Adhesion in Melt-Casting

2.1 Process Conditions and Slag Adhesion Phenomenon

An 8-ton intermediate frequency furnace (furnace lining: acidic refractory, SiO_2 > 85%) is used to melt iron for gray iron casting. As shown in Figure 1, a continuous slag ring forms at approximately 1/4 to 1/3 of the furnace height, which thickens progressively. This reduces the iron tapping capacity and heating efficiency of the furnace, and may even cause excessive bottom temperature, accelerating erosion of the bottom lining. Each campaign lasts more than 300 heats, with a tapping temperature around 1500 °C. The slag ring on the furnace wall reaches a diameter of 0.94 m and thickness of 350 mm, with an estimated weight of 800–900 kg (formed over ~100 heats), averaging about 9 kg of slag adhesion per heat. Part of the slag ring can be removed with a pneumatic pick, showing a clear interface between the slag ring and the refractory lining.

2.2 Composition Analysis of Slag Adhesion

Chemical composition (by XRF) and phase analysis were performed on both free molten slag and furnace wall-adhered slag. As shown in Table 1, the main components of both samples are SiO_2, Al_2O_3, and MgO. The adhered slag contains less SiO_2 but higher Al_2O_3 than free slag. MgO and Al_2O_3 are notably enriched in the adhered slag, indicating significant accumulation. As shown in Table 2, phase analysis of the adhered slag reveals that, in addition to glassy phase, the main crystalline phases include quartz, CA6, spinel, α-Al_2O_3, plagioclase (calcic feldspar and albite), and magnetite. Among them, the quartz phase increases slag viscosity, promoting adhesion to the furnace wall, while the spinel phase drastically strengthens the bonding strength of the adhered slag.

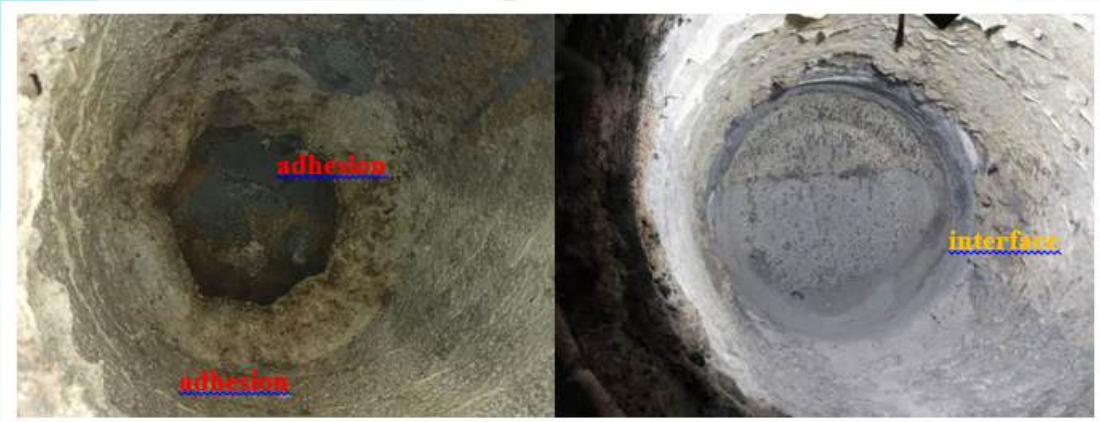
Table 1 Composition of slag and adhesion on furnace wall

	Na_2O	MgO	Al_2O_3	SiO_2	K_2O	CaO	MnO	Fe_2O_3
Adhesion without Fe	1.50	2.11	78.02	13.11	0.94	1.79	0.35	0.78
Surface slag	0.912	7.7	31.9	46.3	1.17	4.5	1.15	4.04

Table 2 Metallurgical phases of adhesion on furnace wall

	Glass	Cristobalite	Quartz	CA_6	C_3A	α-Al_2O_3	C_2S_beta	MA Spinel	Magnetite
Adhesion	8.1	4	3.5	12.8	1.4	9.7	8	44.2	8.4

Index: C = CaO, M = MgO, S= SiO_2, A = Al_2O_3.



a）adhesion b）after treatment

Fig. 1. Slag adhesion on the wall of Induction Furnace

2.3 Melting Property Analysis of Slag Adhesion

As shown in Figure 2, the melting curve of the furnace lining adhesion was calculated using FactSage 7.3 software. Near 1300 °C, the liquid phase decreased significantly, and MA spinel phase precipitated. Even above 1500 °C, the liquid phase formation was still no more than 50%, resulting in strong adhesion. In practice, the temperature of the molten slag or the temperature near the furnace lining is lower than that of the molten iron, which easily leads to adhesion

.

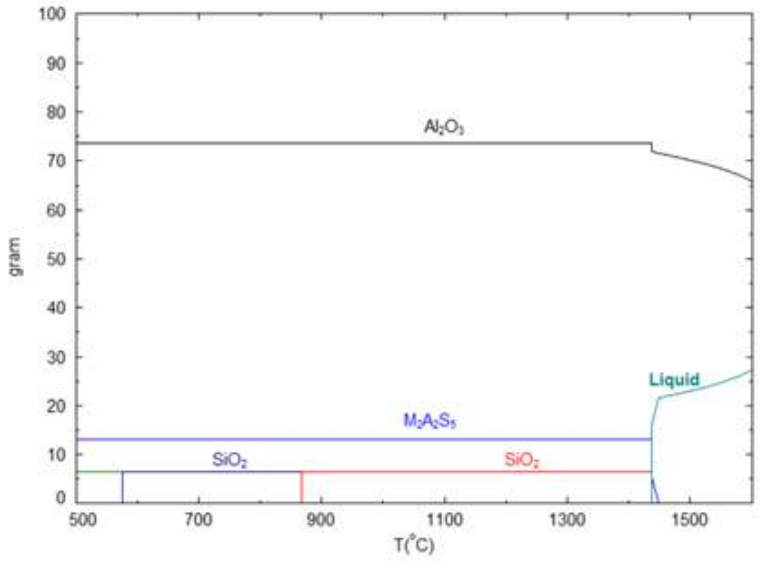


Fig.2 Melting curve of adhesion

The enrichment of Al_2O_3 in the molten slag near the furnace lining is believed to be the main cause of adhesion. Owing to the high Al_2O_3 content in the formed slag, it readily reacts with SiO_2 in the slag and the surface of the furnace wall refractory, as shown in Reactions (1)–(5)[2]. New adhesive layers form after the reactions and attach to the base furnace lining, gradually building up in thickness.

$Al_2O_3 + SiO_2 = A_3S_2$ (Mullite, melting point 1850℃) (1)

$[Al] + SiO_2 = A_3S_2 + [Si]$ (2)

$Al_2O_3 + SiO_2 + MgO = M_2A_2S_5$ (Cordierite, melting point 1470℃) (3)

$Al_2O_3 + MgO = MA$ (Spinel, melting point 2250℃) (4)

$SiO_2 + MgO = M_2S$ (Magnesium olivine, melting point 1890℃) (5)

To remove the adhered slag, the temperature should be increased while adjusting the chemical composition of the adhered material.

3. Design Principle of Slag Agent

3.1 Principle of Adhered Slag Removal

The SiO_2-Al_2O_3-CaO phase diagram and SiO_2-Al_2O_3-MgO ternary phase diagram were calculated using FactSage 7.3 software, as shown in Figure 3. In the phase diagrams, the smallest red region represents the 100% liquid phase zone at 1300 °C; the area enclosed by the blue line represents the 100% liquid phase zone at 1400 °C; the area enclosed by the green line represents the 100% liquid phase zone at 1500 °C; and the largest area enclosed by the red line represents the 100% liquid phase zone at 1600 °C.

Based on the chemical composition and phase analysis of the molten slag, the adhered material on the furnace wall is dominated by mullite (A_3S_2) phase or Al_2O_3 phase. These phases remain solid at or below 1600 °C and tend to adhere firmly to the furnace lining.

According to the lever rule, increasing the CaO and MgO contents in the system can raise the liquid phase fraction, and CaO exhibits a more significant effect. Considering that lime and pure MgO particles have high melting points and are difficult to distribute uniformly, a low-melting-point slag containing CaO and MgO should be used as the slag agent to increase the liquid phase fraction. It can also be seen from the above phase diagrams that increasing the temperature can significantly increase the liquid phase fraction.

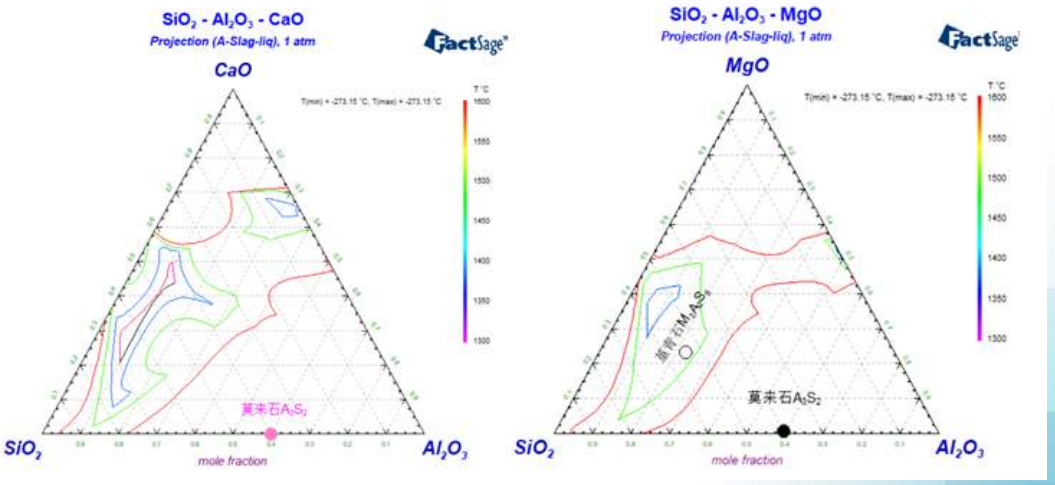


Fig.3 Ternary diagram of SiO2-Al2O3-CaO (Left) SiO2-Al2O3-MgO (Right)

3.2 Slag Flux Design

The design of the slag flux should aim to increase the CaO content of the system. However, CaO has an extremely high melting point (as shown in Table 3), so it cannot melt or mix effectively in a short time. Without fully contacting the molten slag, it rises with the liquid level and adheres to the furnace lining, easily causing non-uniform erosion of the lining. Therefore, the slag flux should be designed to have a relatively low melting point and low CaO activity.

The chemical composition design of the slag flux is listed in Table 4. The slag flux is designed to contain 30–60% C_3A phase and 20–60% $C_{12}A_7$ phase. According to the CaO activity data in Table 3, the erosion ability of this slag flux to the SiO_2-based furnace lining is only about 1/10 that of lime. The $C_{12}A_7$ phase promotes melting [3,4], and the C_3A phase reacts with mullite (A_3S_2) phase or Al_2O_3 phase, as shown in Reactions (6) and (7).

C3A + A = C12A7 (6)
C3A + A3S2 = L（Liquid） (7)

These reactions typically occur between **1300–1450 °C**, and the reaction rate decreases with decreasing temperature. According to the experimental results, when the temperature rises to **1400 °C or higher**, a large amount of molten slag floats up (accompanied by massive formation of $C_{12}A_7$), which is related to this mechanism.

Table 3 Melting points of different phases

Phase	$C_{12}A_7$	C_3A	CA_6	MA	CaO
Melting point	**1415**	1530	1830	2000	2020
1450℃, CaO activity	**0.061**	0.131	0.012	-	1.000

Table 4 Constituents of flux

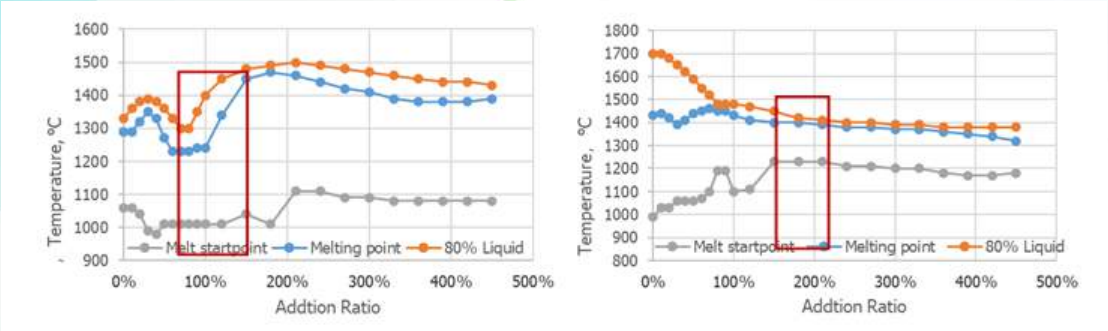
	CaO	Al_2O_3	SiO_2	MgO	CaF_2	$Na_2O + K_2O$	H_2O
Typical	45	35	3.5	2.5	1.5	1.5	0.4
Range	> 40	> 32	< 7.0	< 5.0	< 6	< 5	< 1.5

3.3 Slag Modification and Calculation of Adhered Slag Removal

The adhered slag on the furnace lining mainly consists of high-melting-point phases in the liquid slag that precipitate and adhere to the lining as the temperature drops. Therefore, lowering the melting temperature of the adhered slag and increasing the liquid phase fraction at the same temperature can help the molten steel dissolve it.

As shown in Figure 4, FactSage 7.3 was used to calculate how the addition ratio of different slag fluxes (listed in Table 4) affects the initial melting temperature, the melting point (50% liquid phase), and the temperature for 80% liquid phase of the surface slag and the adhered slag.Based on the initial melting temperature of the surface slag (Figure 4a), adding approximately 40% slag flux can significantly reduce the initial melting temperature and thereby reduce adhesion.

For the adhered slag on the furnace lining (Figure 4b), about 80%–120% addition is required to lower the temperature for 80% liquid phase to below 1500 °C. Furthermore, the liquid phase fraction can rise above 50% only when the temperature is increased to above 1400 °C.



a) surface slag b) adhesion

Fig.4 Change of melting Characteristics of surface slag and adhesion with different fluxes addition ratio. Calculated by FactSage7.3

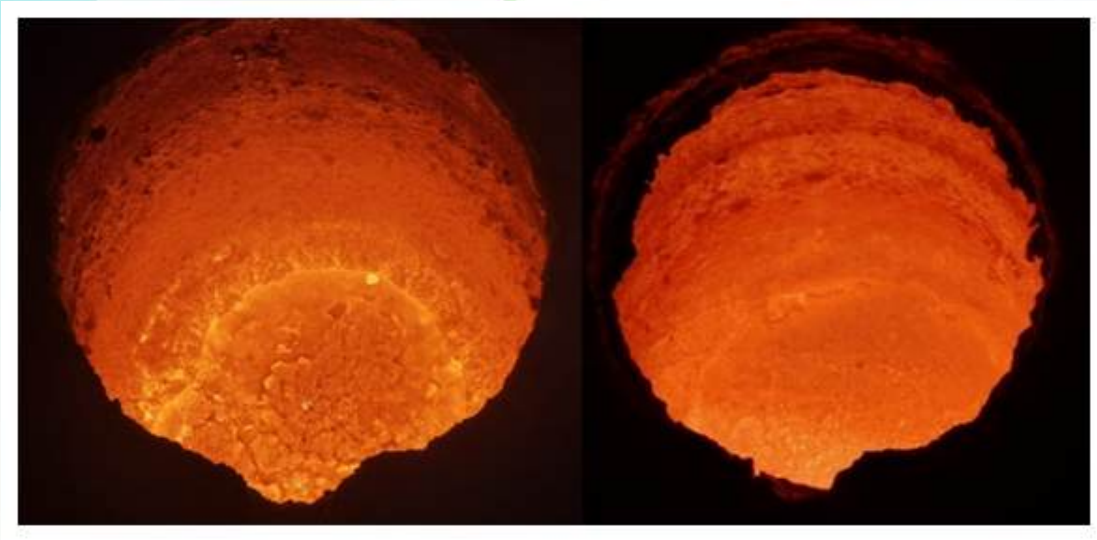
4. Industrial Application Results

Industrial trials of the slag flux were carried out on a medium-frequency furnace with adhered slag in a foundry. The furnace campaign was ≥ 140 heats during the test. As shown in Table 5, the slag flux was added to the furnace bottom, and the furnace was heated normally to above 1500 °C, causing a large amount of molten slag to float up. Thereafter, heating and holding were performed at 1430–1490 °C.

In the 1st heat, part of the adhered slag at the furnace bottom near the tapping hole and the lower furnace wall was removed.In the 2nd heat, the edges of the large adhered slag became bright and transparent.In the 3rd heat, the adhered slag at the furnace bottom was almost completely removed (see Figure 5).

Table 5 Industrial trial record of flux

Order	Additionkg	Charging Position	Temperature, ℃	Holding time, min	Slag Removal Effect	Refractory Erosion
1	10	Furnace bottom (before charging)	1551	0	Partial removal at tapping side; furnace wall smoothed	Relatively low
2	10		1562	8	Adhered slag loosened with bright edges	No obvious erosion
3	5		1571	21	Slag ring generally cleaned	No obvious erosion



a）before treatment　　b）after treatment

Fig. 5 The adhesion slag disappeared by flux process

5. Conclusions

1) The enrichment of Al_2O_3 from molten slag near the furnace lining and its combination with SiO_2 and MgO to form high-melting-point phases is the main cause of slag adhesion.

2) The high-melting-point phases are mainly $MgO•Al_2O_3$ spinel and $Al_2O_3•SiO_2$ mullite.

3) The slag flux contains 30–60% $3CaO•Al_2O_3$ phase and 20–60% $12CaO•7Al_2O_3$ phase. The design of the slag flux balances slag dissolution efficiency and protection against refractory erosion.

4) The designed addition amount of the slag flux is approximately 80–120% of the adhered slag mass, or no less than 40% of the surface molten slag in the furnace.

5) Industrial tests show that the slag flux can effectively remove adhered slag while protecting the refractory.

References

[1] Zhang Guanghe. Factors affecting furnace lining service life and solutions [C]. Proceedings of the 10th Annual Conference of China Foundry Association, 2012: 350-362.
[2] Li Wenchao (Ed.). Physical Chemistry of Metallurgy and Materials, 2nd ed. Beijing: Metallurgical Industry Press, 2001.
[3] Huang Xihu (Ed.). Principles of Iron and Steel Metallurgy, 2nd ed. Beijing: Metallurgical Industry Press, 2002.
[4] Shen Yishen, Li Baowei, Wu Maolin. Fundamentals of Metallurgical Transport Phenomena, 3rd ed. Beijing: Metallurgical Industry Press, 1996.

FROM VARIABILITY TO CONSISTENCY: THE IMPACT OF STABILISED MICROSILICA ON CASTABLE PERFORMANCE

Suparna Basu[1] , Sumit Samanta[1] , Santanu Basak[1] , Ankita Mishra[2] , Arindam Mukherjee[2]

[1]Calderys India Refractories Limited. Nagpur, India; [2]Elkem South Asia Pvt. Ltd. Nagpur, India

Email: suparna.basu@calderys.com; ankita.mishra@elkem.com

Abstract

The performance of low-cement and ultra -lowcement castables is influenced by several factors, including raw material consistency, manufacturing conditions, storage, and installation practices. Among the key matrix components, microsilica plays a vital role in controlling particle packing, flow behaviour, water demand, setting characteristics, and overall castable performance. While high-purity microsilica generally provides stable behaviour, lower and mid-purity grades can exhibit variability arising from fluctuations in production conditions, leading to inconsistent rheology and increased sensitivity to storage
.
This study compares a stabilised microsilica grade with conventional as-produced microsilica grades of similar chemical purity in a standard aluminosilicate low-cement castable formulation. The materials were evaluated for flow properties, water demand, setting behaviour, and batch-to-batch consistency. By combining historical quality-control statistics with castable performance over time, the work demonstrates how stabilised microsilica can improve robustness beyond what is indicated by chemical purity alone. Results demonstrate that the stabilised microsilica delivers more predictable flow characteristics, lower variability in workability, and improved rheological consistency across batches. These improvements enhance the robustness of the castable system, contributing to more reliable installation performance and greater process consistency in refractory manufacturing.

Keywords: Microsilica, rheology, consistency

1. Introduction

Microsilica is a co-product of silicon smelting process, consisting of amorphous, sub-micron SiO_2 spheres roughly 0.1-0.4 µm in diameter, finer than cement and matrix fines used in monolithic refractories. Microsilica contributes to efficient particle packing between cement and fine aggregate in a castable, self-flow behaviour at minimal water addition and mullite formation through reaction with alumina in the matrix during firing.

Purity of the microsilica matters, but batch-tobatch stability of the whole property set particle size distribution, coarse residue, loss on ignition (LOI), moisture, pH, and impurity oxides (Fe_2O_3, CaO, MgO, Na_2O, K_2O, carbon) keeps a given formulation valid from one castable manufacturing batch to the next.

As produced, microsilica collected directly from a furnace's baghouse or electrostatic precipitator on any given day reflects that day's operating campaign charge mix, quartz source, furnace temperature and collection efficiency. These operating shifts produce real lot-to-lot variation. High purity microsilica grades demonstrate stable characteristics, as furnace parameters are managed to prioritize microsilica quality over silicon production (yield), whereas mid to lower purity grades are markedly more sensitive to production condition fluctuations.

In this study, the term stabilised or engineered microsilica refers to a microsilica grade that has undergone controlled post-production selection, processing, and quality adjustment to reduce normal batch-to-batch variability compared with

conventional as-produced microsilica. While as produced microsilica directly reflects the operating conditions of the silicon furnace at the time of collection, including variations in raw materials, furnace campaign, off-gas handling, and collection efficiency, stabilised microsilica is designed to achieve a more consistent property profile. This may include improved control of chemical composition, impurity levels, particle size distribution, bulk density, pH, moisture, and other parameters relevant to castable rheology and setting behaviour. The objective is therefore not only to obtain a given SiO_2 purity, but to deliver a more predictable and reproducible microsilica performance in refractory castable formulations, particularly with respect to water demand, flow behaviour, setting response, and storage stability. This variability has two distinct downstream consequences. For the castable manufacturer, variation in coarse fraction or specific surface area changes the particle packing model, forcing repeated adjustment of water demand or dispersant dosage in the castable batch, holds and rework that add cost and reduce line throughput. For the application site, wet-out time, self-flow, vibration flow and hardening time define the working window for application, variability in the microsilica affects the casting efficiency and water addition at site above the specified limit leads the uncertainty in the performance life of the castable and crew confidence. This paper evaluates the engineered microsilica and as produced lots and impact of batch-to-batch consistency in the microsilica and its impact on castable placement behaviour, relative to two as produced comparator grades of similar chemical purity. By integrating historical quality-control statistics with castable storage performance, the study assesses whether stabilised microsilica improves formulation robustness beyond the information provided by chemical purity alone.

2. MATERIALS AND METHODS

2.1 Microsilica grades evaluated

Microsilica A: as-produced 95% SiO_2 content densified microsilica

Microsilica B: as produced 93.5% SiO_2 content undensified microsilica

Microsilica E: an engineered or stabilised 95% SiO_2 content microsilica.

The grades were selected to compare the influence of engineered stabilisation against conventional as-produced microsilica having comparable silica purity.

2.2 Batch-to-Batch consistency evaluation

Historical quality-control data covering production batches received during 2024-2026 were compiled. Parameters were selected such as SiO_2, total alkalis ($CaO + MgO + Na_2O + K_2O$), Fe_2O_3, pH, bulk density as their influence on castable rheology, setting behaviour and long-term performance.

The statistical evaluation included, mean, median, standard deviation, Coefficient of Variation (CV%) and Interquartile Range (IQR). Box-and-andwhisker plots were generated to compare distribution characteristics of the three grades.

2.3 Castable evaluation and storage performance study

The three microsilica grades were evaluated in two castable formulations: an 80% alumina lowcement castable (LCC) and a SiC-based lowcement castable. The formulations were assessed for key rheological properties, including water demand, wet-out time, flow consistency, and setting time, as well as mechanical performance through cold crushing strength (CCS) measurements after firing at 110°C, 1100°C, and 1550°C. The same castable formulations were subsequently used to investigate the

influence of microsilica type over time. Prepared castable mixes were stored under normal plant storage conditions for a period of six months. Storage performance evaluated on the initial day of manufacture (D0) and subsequently at thirty-day intervals up to six months, enabling assessment of changes in rheological and strength properties over time and the effect of microsilica consistency on castable storage stability.

3. RESULTS AND DISCUSSION

3.1 Batch-to-batch chemical and physical consistency

The box-plot analysis demonstrates that the three microsilica grades exhibit distinctly different consistency profiles rather than a simple ranking of performance.

For SiO_2, both MS A and MS E showed narrow distributions and very low relative variability, whereas MS B exhibited a noticeably wider spread. The CV was approximately 0.44% for MS A, 0.90% for MS B and 0.40% for MS E. These results indicate that SiO_2 consistency is comparable between MS A and MS E, while MS B is more sensitive to batch-to-batch variation.

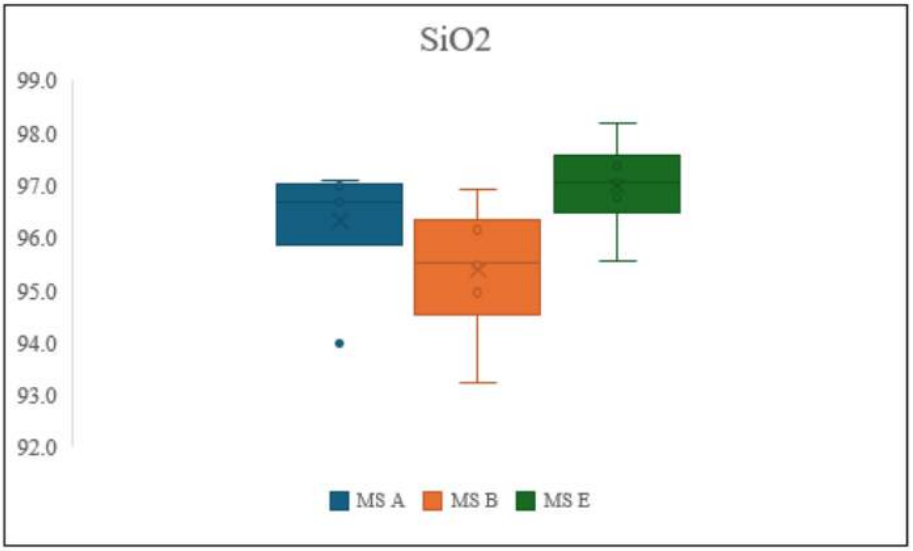


Figure 1: The distribution of SiO_2 content for MS A, MS B and MS E

The average Fe_2O_3 levels were approximately 0.102%, 0.118%, and 0.073% for MS A, MS B and MS E, respectively. For Fe_2O_3, MS E exhibited the lowest average content. However, MS E showed the narrowest Fe_2O_3 distribution. The CV values were approximately 21%, 38%, and 41% for MS A, MS B and MS E, respectively. The need to distinguish between impurity level and batch consistency, as a lower concentration does not automatically indicate lower variability.

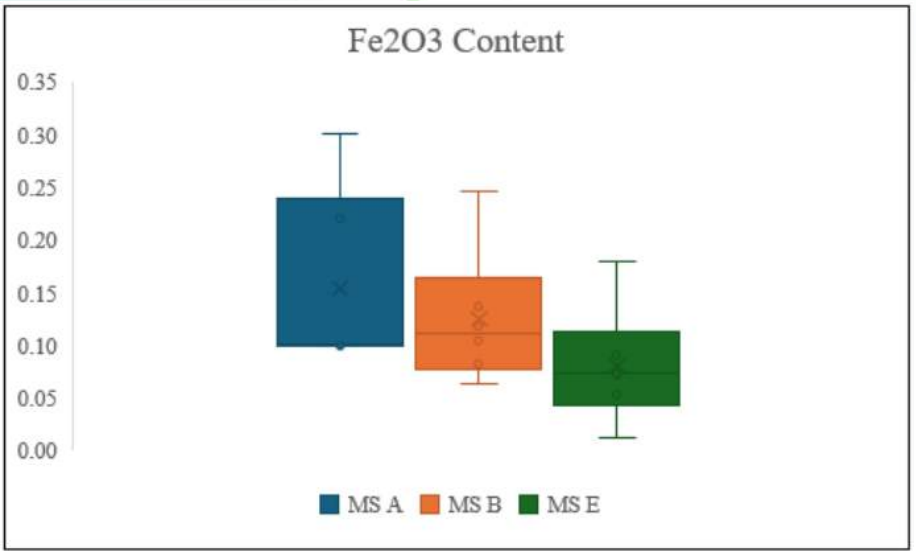


Figure 2: The distribution of Fe_2O_3 content for MS A, MS B and MS E

The pH distributions of all three grades remained within a relatively narrow range. The average pH values were 7.33, 7.68 and 7.18 for MS A, MS B and MS E, respectively. MS A with narrowest pH distribution with a CV of approximately 1.8%, while MS B and MS E showed similar relative variation near 4.9%. Therefore, pH is unlikely to be a major differentiating factor among the grades.

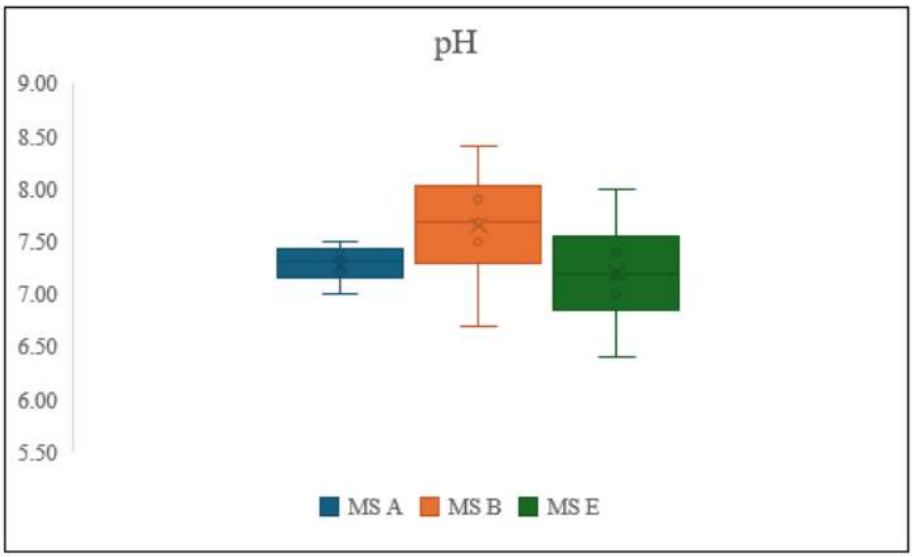


Figure 3: The distribution of pH for MS A, MS B and MS E

The total alkali distribution revealed a different trend. MS E generally exhibited lower alkali levels than rest grades while maintaining a moderate distribution width. MS B showed the broadest spread, indicating greater process variability.

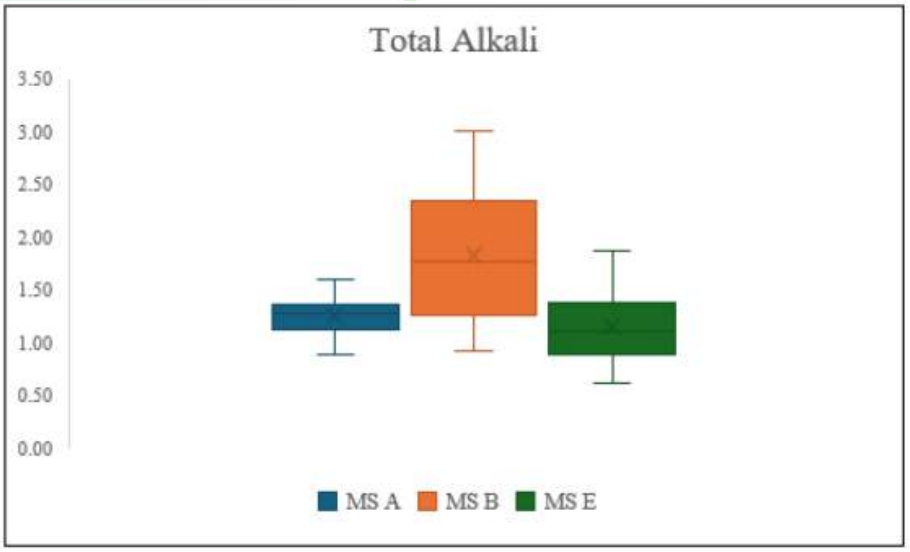


Figure 4: The distribution of total alkali content for MS A, MS B and MS E

Bulk density showed the largest difference among the materials because MS A is a densified product while MS B and MS E are undensified grades. Consequently, average bulk density values should not be interpreted as an indicator of quality. Instead, the relative spread of the distributions is more informative. The bulk-density CV values were approximately 3.1%, 9.3%, and 3.5% for MS A, MS B and MS E, respectively. Within the undensified materials, MS E showed a narrower distribution than MS B.

The carbon content results indicate differences among three microsilica grades. MS A exhibited the highest median carbon content with values concentrated within a relatively narrow range, indicating good consistency, whereas MS B showed an intermediate carbon level with a broader distribution, suggesting higher batch-tobatch variability. MS E presented the lowest median carbon content, although some variability was also observed.

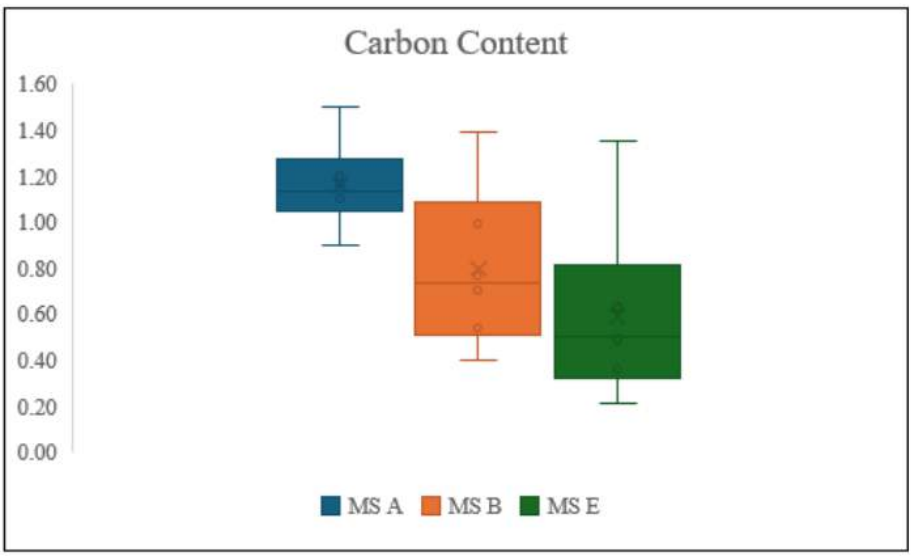


Figure 5: The distribution of carbon content for MS A, MS B and MS E

Particle size distribution was determined using Malvern Mastersizer 3000 laser diffraction analyzer. Samples were dispersed in deionized water and subjected to ultrasonic treatment (5 min at 100% amplitude) to achieve primary particle deagglomeration before measurement.

Grade	BET (m2/g)	Particle Size Distribution		
		D10 (%)	D50 (%)	D90 (%)
MS A	26.69	0.035	0.186	7.63
MS B	23.38	0.119	0.356	10.00
MS C	20.40	0.158	0.375	1.31

Table 1: Comparison of BET Surface Area and Primary Particle Size Distribution of Microsilica

The PSD results showed that MS A had the finest primary particles, with a D50 of 0.186 µm, whereas MS B and MS E exhibited D50 values of 0.356 µm and 0.375 µm respectively. The higher BET surface area of MS A (26.69 m^2/g) is consistent with its finer particle size. In contrast, MS E exhibited the lowest BET value (20.4 m^2/g), indicating lower exposed surface area and potentially reduced moisture adsorption during storage. The low D90 value of MS E (1.31 µm) suggests a narrower particle size distribution compared with MS A and MS B. Overall, MS E combines a lower specific surface area with a relatively uniform particle size distribution, which may be advantageous for long-term storage stability.

3.2 Effect of storage on castable performance

Before assessing the storage performance, it is important to recognise that small variations in microsilica properties can strongly influence castable placement behaviour. Changes in bulk density and particle packing affect powder dispersion, matrix filling, and the amount of water required to achieve a given flow. Variations in alkali content and pH may alter the surface chemistry of the fine-particle matrix and influence the efficiency of dispersants, thereby affecting wet-out time, flow development, and setting response. As a result, even microsilica grades with similar SiO_2 purity may show different sensitivity to storage performance and different robustness in water demand, workability, and hardening behaviour.

The storage performance of the three microsilica grades was evaluated in two low-cement castable systems for up to six months. The study included an 80% alumina LCC and a SiC-based LCC, with changes in casting water, initial flow, wet-out time, setting time, and cold crushing strength monitored at monthly intervals.

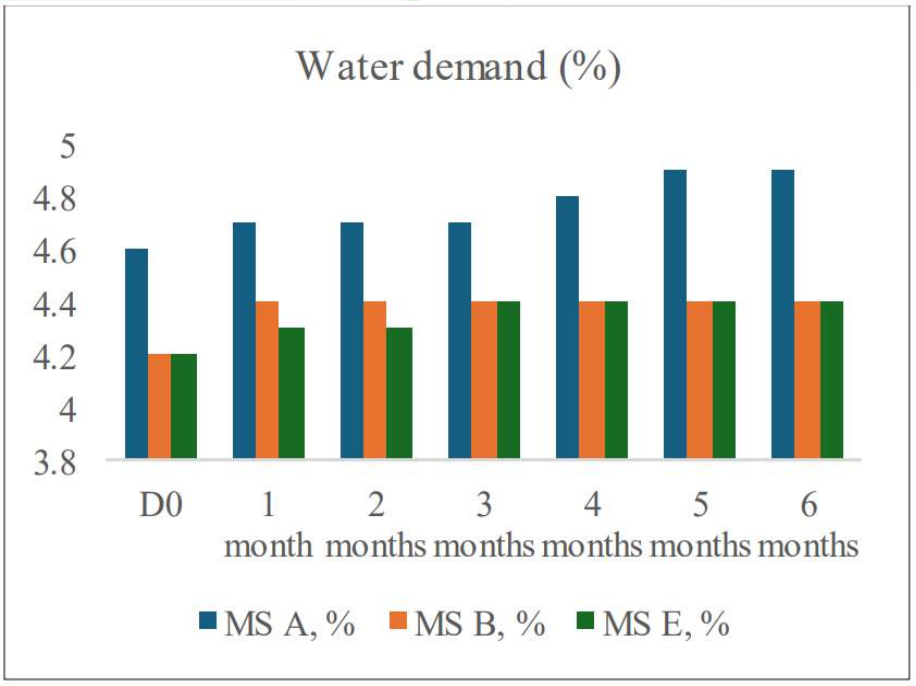


Figure 6: Effect of storage on water demand of the 80% alumina low-cement castable containing MS A, MS B and MS E

In the 80% alumina LCC, the castable containing MS A showed the highest change in placement characteristics during storage. Its water requirement increased from 4.6% to 4.9%, while initial flow decreased from 108% to 98%. More notably, the setting time increased from 110 to 350 min and the wet-out time increased from 60- 90s to 240-260s after six months. These results indicate a progressive reduction in mixing and setting responsiveness during storage. The higher carbon content of MS A (Figure 5) necessitates a greater water addition to achieve the optimum flow consistency, which consequently leads to the deterioration of the thermo-mechanical properties of the castables formulated with MS A

The MS B and MS E castables showed comparatively smaller changes in water requirement, increasing from 4.2% initially to 4.4% after six months. MS B maintained flow between 108% and 122%, although its setting time varied during the first two months before stabilizing at approximately 110-120 min from the third month onward. MS E showed the most consistent setting response. After an initial increase to 185 and 170 min during the first two months, its setting time remained between 100 and 105 min from three to six months. Its initial flow also remained within 100-115% over the six-month storage period. Therefore, among the three microsilica grades, MS E provided the most stable combination of flow and setting behaviour in the aged 80% alumina castable.

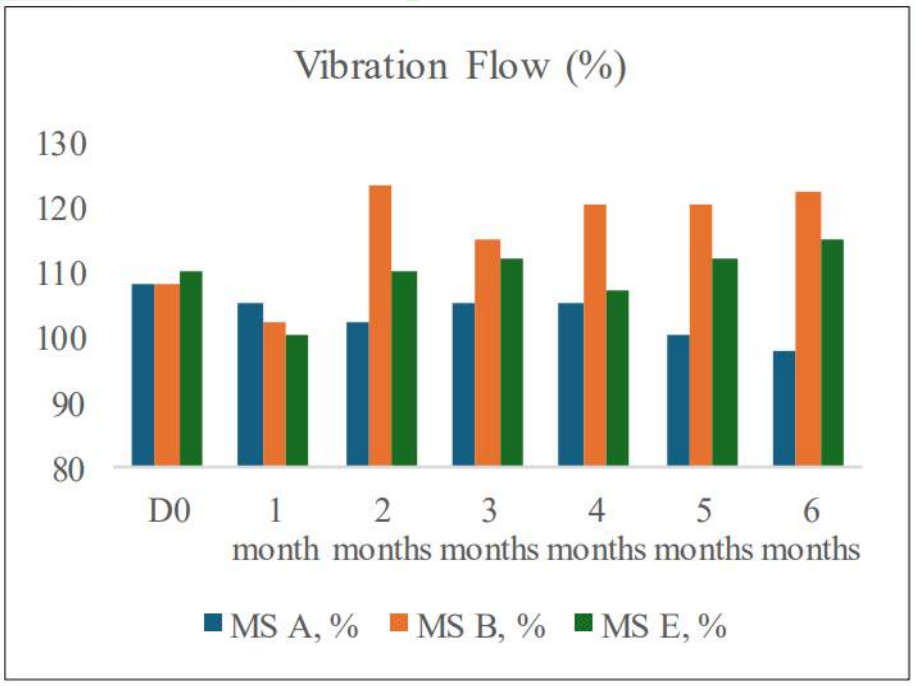


Figure 7: Effect of storage on flow consistency of the 80% alumina low-cement castable containing MS A, MS B and MS E

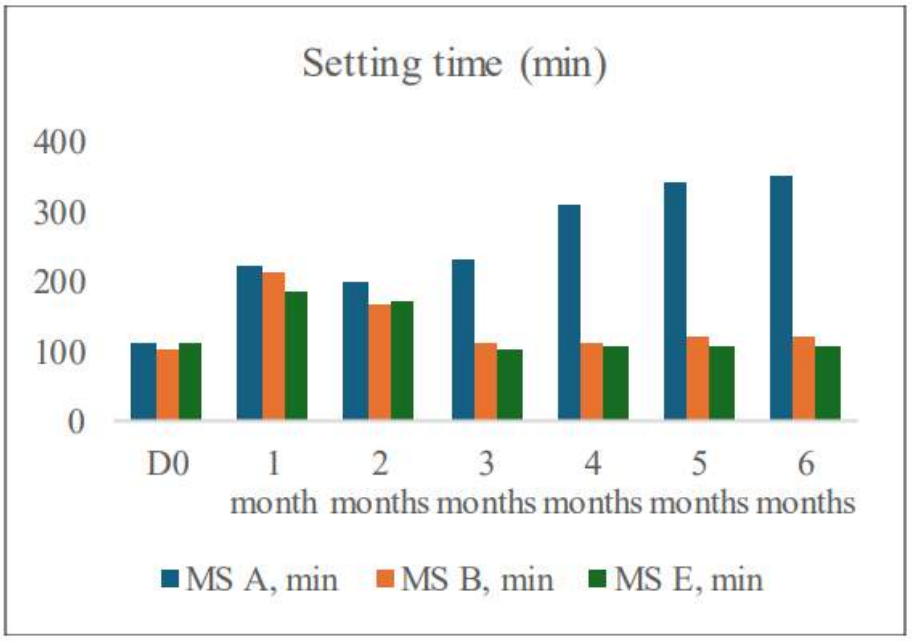


Figure 8: Effect of storage on setting time of the 80% alumina low-cement castable containing MS A, MS B and MS E

A similar, although less pronounced, trend was observed in the SiC-based LCC. The water requirement remained essentially unchanged for all three compositions, allowing a more direct comparison of flow and setting behaviour. After six months, the setting time of the MS A castable increased from 120 to 200 min, while MS B increased from 120 to 210 min. In comparison, MS E changed from 100 to 130 min and remained within a relatively narrow range of 120-150 min throughout the six-month period. Initial flow remained usable for all three grades, but MS E showed the most consistent balance between flow, wet-out, and setting response.

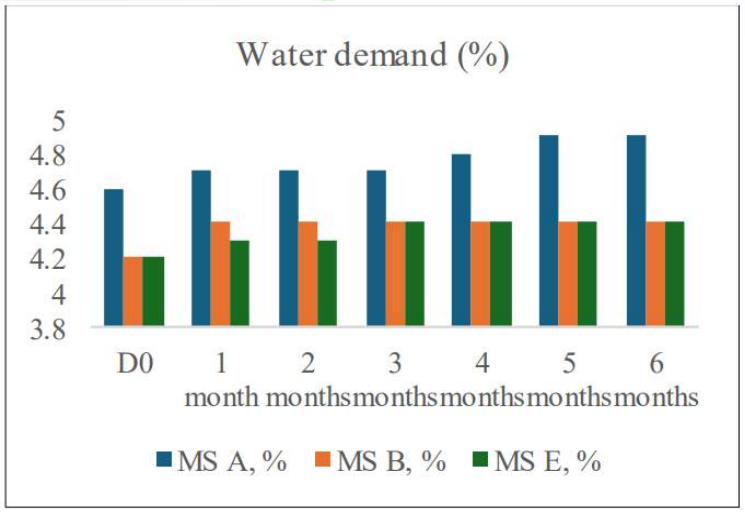


Figure 9: Effect of storage on water demand of the SiC-based low-cement castable containing MS A, MS B and MS E

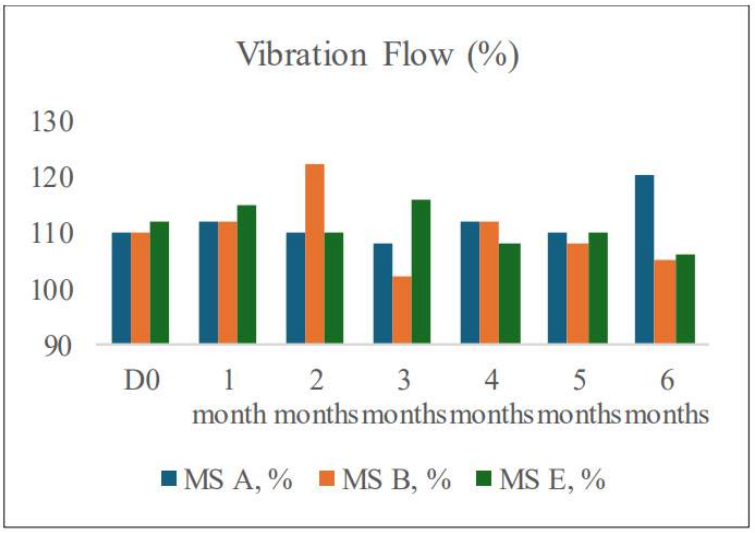


Figure 10: Effect of storage on flow consistency of the SiC-based low-cement castable containing MS A, MS B and MS E

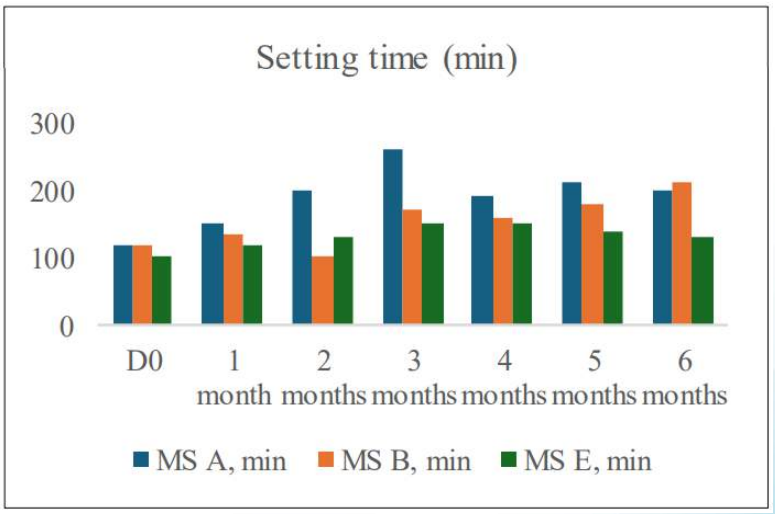


Figure 11: Effect of storage on setting time of the SiCbased low-cement castable containing MS A, MS B and MS E

The dried CCS at 110°C decreased during storage in both castable systems, although the magnitude of reduction depended on microsilica grade. In the 80% alumina LCC, the six-month CCS retention values were approximately 77%, 85%, and 89% for MS A, MS B, and MS E, respectively. In the SiC-based LCC, the corresponding retention values were approximately 75%, 82%, and 91%. Thus, MS E exhibited the highest retention of dried strength in both castable systems. This can be attributed to the lower carbon content, narrower particle size distribution, and lower specific surface area of MS E, which render it less sensitive to moisture and interactions with other chemical constituents in the castable matrix during storage

The strength response after firing at 1100°C was less affected by prolong storage than the dried strength. After six months, the 80% alumina LCC retained approximately 94%, 94%, and 96% of its initial 1100°C CCS for MS A, MS B, and MS E, 0 100 200 300 400 D0 1 month 2 months 3 months 4 months 5 months 6 months Setting time (min) MS A, min MS B, min MS E, min 3.8 4 4.2 4.4 4.6 4.8 5 D0 1 month 2 months 3 months 4 months 5 months 6 months Water demand (%) MS A, % MS B, % MS E, % 90 100 110 120 130 D0 1 month 2 months 3 months 4 months 5 months 6 months Vibration Flow (%) MS A, % MS B, % MS E, % 0 100 200 300 D0 1 month 2 months 3 months 4 months 5 months 6 months Setting time (min) MS A, min MS B, min MS E, min respectively. In the SiC-based castable, the sixmonth CCS at 1100°C was approximately 92-100% for all grades. Results indicate that the fired strength of castable 80% alumina LCC & SiCbased castable broadly maintained within the variability of the available measurements.

Storage had a stronger influence on fresh-state properties and dried strength than on fired strength. MS E provided the most consistent setting response and the highest six-month driedstrength retention in both formulations. The results support the use of stabilized microsilica where predictable installation behaviour after extended storage is required.

4. CONCLUSIONS

Batch-to-batch statistical analysis revealed distinct consistency profiles for the three microsilica grades. MS A and MS E showed comparable SiO_2 consistency, whereas MS B exhibited a wider compositional spread. MS E demonstrated lower total alkali levels and lower variability than MS B, although MS A remained more consistent for selected parameters such as pH and Fe_2O_3. MS A exhibited the finest primary particle size and highest BET surface area, while MS E showed the lowest BET value and narrowest particle size distribution. These characteristics suggest that MS E may offer improved stability during prolonged storage. MS A exhibited the highest and most consistent carbon content, whereas MS E showed the lowest carbon level.

Impact of storage had a stronger influence on fresh-state properties than on fired mechanical properties. In both castable systems, MS E exhibited lower drift in setting behaviour and higher dried-strength retention during six months of storage.

The results indicate that engineered stabilisation improves overall predictability and storage robustness of castable performance, while acknowledging that individual quality parameters may still be more consistent in specific as produced grades.

REFERENCES

[1] Sandberg, B.; Myhre, B. Microsilica - A Versatile Refractory Raw Material. Presented at the Indian Refractories Congress 1994, Jamshedpur, India, 14-16 February 1994.

[2] Microsilica in Alumina -Based Ultra-Low Cement Castables: The Effect of Microsilica Additions on Flow. Presented at the XXIII ALAFAR Congress, Puerto Vallarta, Mexico, 6-10 November 1994.

[3] Myhre, B. Microsilica in Refractory Castables: How Does Microsilica Quality Influence Performance? Presented at UNITECR 2005, Orlando, USA, 8-11 November 2005.

[4] Peng, H.; Myhre, B.; Roszinski, J.O. Influence of Microsilica on Properties of Bauxite-Based Castables. Presented at the 5th International Symposium on Refractories (ISR 2007), Beijing, China, 11-12 April 2007.

[5] Myhre, B.; Fan, H. Gel Bonded Castables Based on Microsilica as Binder. Presented at UNITECR 2011, Kyoto, Japan, 30 October-2 November 2011.

[6] Peng, H. Recent progress in microsilica -gel bonded no-cement castables. Ceramics International 49 (2023), 24566-24571. DOI: https://doi.org/10.1016/j.ceramint.2022.12.187

ADVANCED REFRACTORY SOLUTIONS FOR COKE DRY QUENCHING: A FOCUS ON HIGH-PERFORMANCE ANDALUSITE BRICKS

S. Adak[1], A.K. Das[1], R. Prakash[1], M. Gugalia[1], G. Bhattacharya[2], M. Szepizdyn[2], C. Wöhrmeyer[2], P. Panigrahi[3]

([1]Mahakoshal Refractories Pvt. Ltd., Katni (India), [2]Imerys S.A, France, [3]Tata Steel, India)

Corresponding author's e-mail: goutam.bhattacharya@Imerys.com

Abstract

Coke Dry Quenching (CDQ) technology is vital for modern, energy-efficient coking operations, yet it creates a harsh environment for standard refractory linings. The process subjects refractories to intense thermal cycling, mechanical abrasion, and chemical stress, often leading to premature degradation. This paper presents high-performance andalusite-based refractory bricks as a solution.

The technical advantages of andalusite, which serves as a unique *in-situ* mullite precursor were explored in this application. During high-temperature service, andalusite transforms into an interlocking network of primary mullite, while simultaneously reacting to form a dense secondary mullite matrix. This unique microstructure provides critical benefits including superior dimensional stability by counteracting ceramic shrinkage and enhanced thermal shock resistance through a network of energy-dissipating micro-cracks.

This study compared andalusite-based bricks against conventional sintered mullite compositions across key physical and thermo-mechanical parameters, including bulk density, strength, permanent linear change, thermal expansion, refractoriness under load, creep in compression, and resistance to thermal shock and CO atmosphere. The results demonstrate that the andalusite-based formulation provides significantly better resistance to the thermal shocks in CDQ chambers. The practical efficacy of this solution was further validated by successful long-term performance in a live CDQ chamber at the Tata Steel Meramandali plant. These findings confirm that andalusite-based refractories offer a reliable, durable, and sustainable choice for running coking quenching operations.

Keywords: Coke Dry Quenching (CDQ), Andalusite, Mullite, Thermal shock resistance

1. Introduction

Coke Dry Quenching (CDQ) technology has emerged as a key component of modern coking operations offering a significant technological breakthrough over conventional Wet Quenching (WQ). CDQ improves energy efficiency in coking plants by capturing heat from hot coke using a circulating gas, usually nitrogen, to cool the coke and generate high-pressure steam. This process saves energy that would otherwise be wasted [1]. Furthermore, it provides superior environmental performance by eliminating dusty steam clouds and the discharge of contaminated quench water, while also yielding a more uniform, dry coke product that optimizes downstream blast furnace performance [2].

However, the operational environment of a CDQ chamber is challenging to refractory. Refractory linings must withstand service temperatures of approximately 1000°C from hot coke. Intensive thermal cycling involved in the cooling process often acts as the primary reason for refractory degradation. Furthermore, the lining faces persistent mechanical abrasion from the movement of hot coke and chemical attacks from circulating hot nitrogen gas.

This paper explores the development and industrial application of high-performance andalusite-based refractory bricks. Through a collaborative initiative between Mahakoshal Refractories and Imerys, different compositions including a sintered mullite and andalusite bricks were examined and the performance of the developed andalusite bricks was evaluated in a live CDQ chamber at the Tata Steel Meramandali plant, aiming to demonstrate their superior resistance to thermal and chemical degradation.

2. The Role of Andalusite in Refractory Design

Andalusite (Al_2SiO_5) is a unique natural raw material that offers distinct technical advantages for CDQ refractories, primarily due to its transformation behavior at high-temperatures. It functions as an *in-situ* mullite precursor. During the initial firing of the refractory brick, andalusite grains undergo a phase transformation at high temperatures (typically starting around 1300°C), converting into an interlocking network of needle-like primary mullite crystals (around 80% by weight) and a capillary network filled with silica-rich amorphous phase (~20% by weight) (Fig. 1).

The newly formed mullite is topotactically oriented in relation to the host crystal, maintaining structural alignment during growth. Specifically, the *c*-axis of the neoformed mullite develops parallel to the *c*-axis of the original andalusite lattice (Fig. 2 & 3). Concurrently, the exuded glassy phase occupies interconnected capillary channels that remain structurally elongated along this shared crystallographic axis. Due to this unique microstructure, mullitised andalusite behaves like a typical composite material deflecting the microcracks at the mullite-glass interface increasing the thermal shock resistance [3].

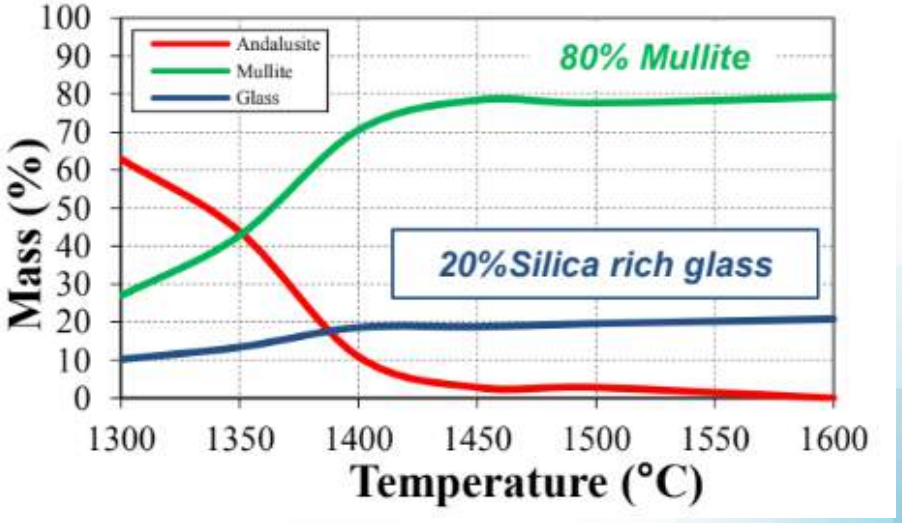


Fig. 1: Phase transformation of andalusite as a function of sintering temperature [4]

This transformation provides a rigid, thermally stable structural backbone. The resulting microstructure is further strengthened by the formation of secondary mullite. The silica-rich glassy phase reacts with fine alumina particles in the matrix: 3 Al_2O_3 + 2 SiO_2 → $3Al_2O_3 \cdot 2SiO_2$ (Mullite).

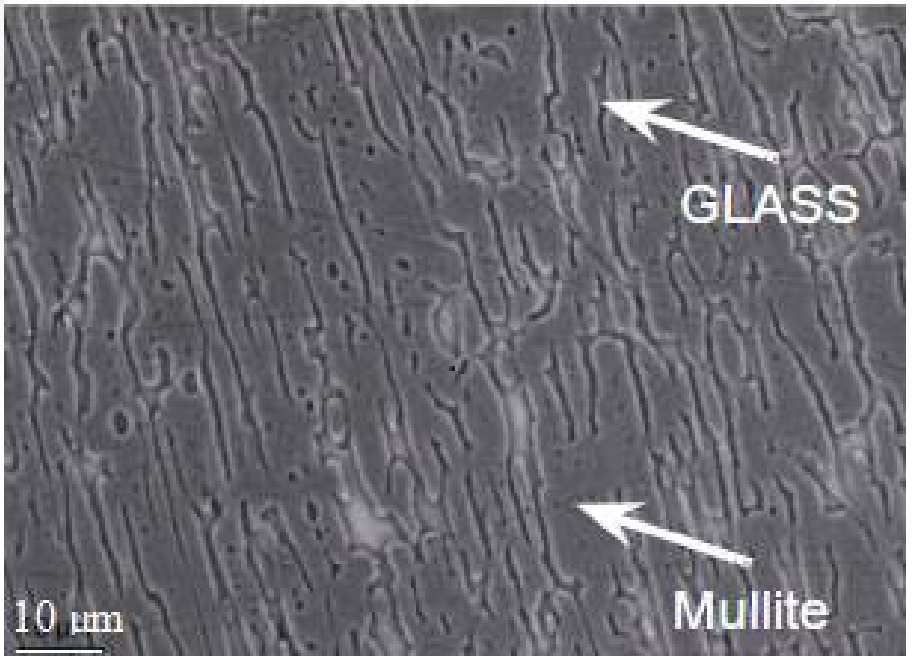


Fig. 2: Mullitized andalusite parallel to C axis after sintering at 1550℃

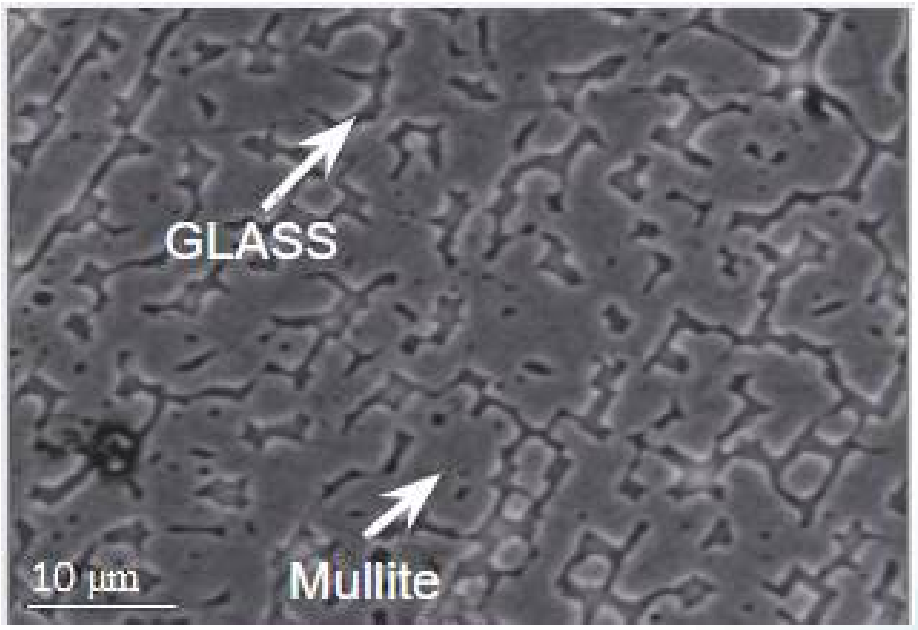


Fig. 3: Mullitized andalusite perpendicular to C axis after sintering at 1550℃

This secondary reaction creates a dense mullite network that bonds the primary mullite grains, effectively bridging the granular structure. While the primary mullite formed via the thermal transformation of andalusite provides a stable, needle-like scaffold resistant to deformation, the secondary mullite formed through the reaction between the silica-rich glass and alumina reinforces the matrix to enhance overall density, strength, and chemical resistance. This multi-stage reinforcement mechanism, combining the primary mullite backbone with a dense secondary mullite matrix, ensures the refractory body possesses both the flexibility required for thermal shock resistance and the density necessary for long-term durability.

The exceptional thermal shock resistance of andalusite-based refractories also stems from its unique expansion properties. Andalusite undergoes a gradual, controlled volume expansion as it transforms into mullite, unlike materials that exhibit sharp contractions or sudden volume changes. This anisotropic expansion creates a network of microcracks within the refractory matrix. These microcracks function as energy dissipaters; they arrest crack propagation by absorbing the stress generated during the rapid thermal cycling typical of CDQ operations. By inhibiting the coalescence of these micro-fissures into damaging macro-cracks, the material maintains its structural integrity despite aggressive and cyclic thermal loads.

3. Experimental Procedures

Two brick compositions were prepared to compare their chemical and thermomechanical properties: one containing 55–60% Imerys Andalusite Purusite P57 and the other using sintered mullite (60% alumina). Sintered mullite was selected for its chemical similarity to andalusite. Raw Bikaner clay served as the binder for both compositions. Bricks were prepared by pressing in a 630T Electric Screw Press and sintered in a 100m long Tunnel Kiln at 1550°C. Samples for each test were cut and prepared from the fired bricks.

The chemical composition of the brick samples was determined using wet chemical analysis according to ISO 21587-1 and ISO 21587-2. The apparent porosity and bulk density was tested via the Archimedes method (ASTM C20) on cube samples with each side 75mm.

Mechanical strength was assessed using ASTM C133. Cold modulus of rupture (CMOR) was tested on 152 × 25 × 25 mm^3 prisms at a loading rate of 0.774 kN/min and Cold compressive strength (CCS) was measured using 51 mm^3 cubes at a loading rate of 24.3 kN/min.

Permanent linear change (PLC) was evaluated using 228 × 114 × 64 mm^3 prisms held at 1500°C for 4 hours and 1600°C for 2 hours followed by measuring the difference in length on heat treatment. Pyrometric cone equivalent (PCE) was tested according to ASTM C24, using finely ground brick (<212 µm) samples at a heating rate of 150°C/h and the brick samples were measured against standard Orton Cones. Refractoriness under load (RUL) was measured following EN 993-8, using cylindrical samples (50 mm diameter and length with 12mm internal bore diameter) under a 0.2 MPa load at a 5°C/min heating rate. Creep in compression was tested at 1350°C for 50 hours, under a load of 0.2 MPa using the same sample size as RUL with a heating rate of 10°C/min up to 500°C and 5°C/min thereafter till 1350°C.

Thermal expansion was tested at 1000°C following IS 1528-19. The sample (50 mm long, 10 mm diameter) was placed in a fused silica tube placed inside a furnace and

heated at 5–10°C/min. The change of length was measured via a transducer at every 5-minute interval and temperature using a thermocouple.

Thermal spalling resistance was tested according to IS 1528-3 using both air and water quenching:

- **Air Quenching:** Prismatic samples with 75 mm height and 50 mm square base were placed in a furnace at room temperature and heated to 1000°C and held for 30 minutes. The hot prism samples were then unloaded and air-cooled for 10 minutes on a brick floor free from air draughts. After examining for any damage due to the thermal shock, the samples were reloaded into the furnace at 1000°C, if the damage was not significant. The number of cycles each brick withstood was noted.
- **Water Quenching:** The furnace was preheated to 950°C and the dried cylindrical samples (50 mm diameter and height) were inserted into the furnace and held for 15 minutes followed by offloading and plunging into running water for 3 minutes. The samples were then dried at 110°C for 30 minutes before returning to the furnace. The number of cycles sustained without damage was recorded.

Finally, the CO-disintegration test was conducted at 500°C for 100 hours according to ASTM C288, using 228 × 76 × 76 mm^3 bars and the conditions of the bar was noted at the end of the test and categorized from A to D, where A indicates completely unaffected, and D signifies for a destructive condition, when the specimen breaks into two or more pieces, or when hand pressure can cause breaking. B and C refer to intermediate categories.

5. Results and Discussion

The experimental investigation evaluated two refractory brick compositions: T-1, an Andalusite-based composition, and T-2, a sintered mullite-based composition.

5.1 Chemical Composition

The chemical analyses of the two compositions, presented in Table 1, indicate that both materials satisfied the minimum requirement of 60% Al_2O_3 and 1% Fe_2O_3 max. Andalusite based composition had slightly lower Al_2O_3 %, although it contained lower impurities - Fe_2O_3, TiO_2 and other fluxing impurities (CaO + MgO, Na_2O + K_2O), ensuring its higher refractoriness.

Chemistry (wt %)	Specification	Andalusite (T-1)	Sintered Mullite (T-2)
Al_2O_3	60 min.	67.4	69.1
Fe_2O_3	1.0 max.	0.87	0.91
TiO_2	-	0.39	1.03
CaO + MgO	-	0.25	0.31

$Na_2O + K_2O$	-	0.53	0.59

Table 1: Chemical analysis of the brick samples

5.2 Physical Properties

Both compositions exhibited similar CCS and CMOR, which exceeded the adequate strength for the structural demands of a CDQ chamber as given in the product specification for CCS (>400kg/cm^2) and CMOR (>80kg/cm^2) of the bricks. Andalusite based bricks showed higher bulk density (2.81g/cm^3) than those with sintered mullite (2.68g/cm^3) (Fig. 4). Higher bulk density comes from the lower apparent porosity created by andalusite via formation of a dense microstructure with primary and secondary mullite. The product composition was designed to withstand the mechanical abrasion inherent in coke handling operations.

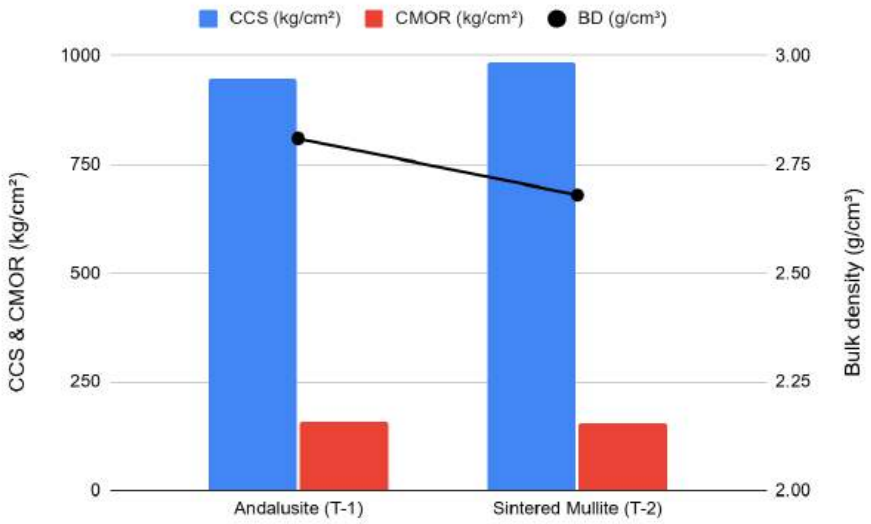


Fig. 4: Comparison of the andalusite and sintered mullite bricks in terms of CCS, CMOR and bulk density

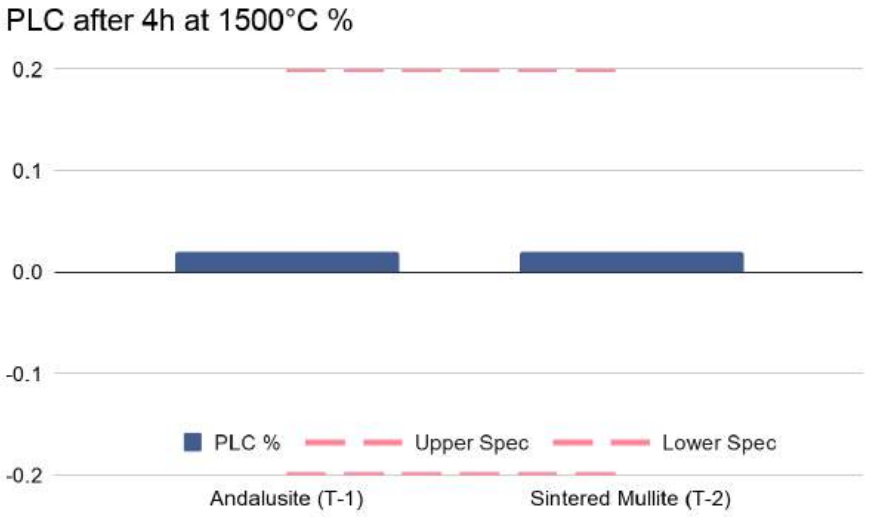
5.3 Thermo-Mechanical Stability

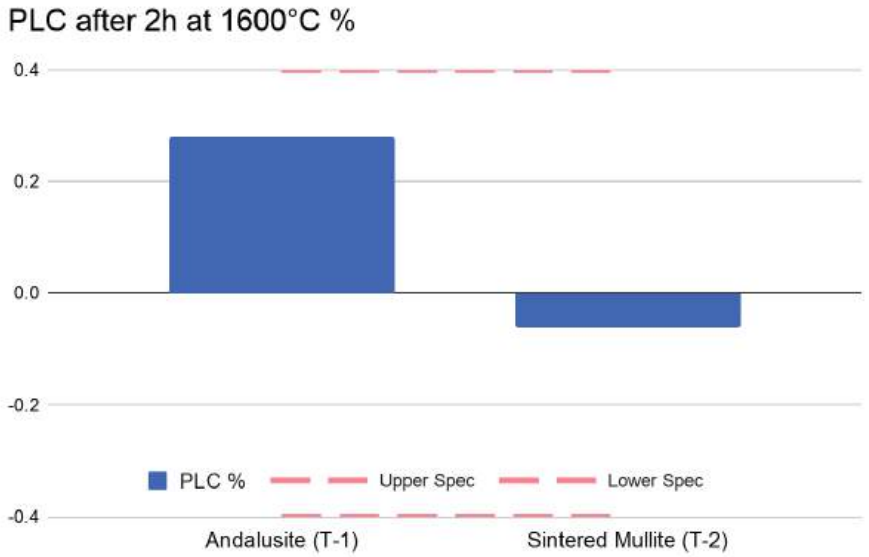
A critical difference between the two compositions was observed in the permanent linear change (PLC) and thermal expansion shown in Fig. 5.

While both materials exhibited stability at 1500°C, distinct behaviors appeared at 1600°C. The andalusite-based bricks (T-1) developed a positive expansion, confirming the active *in-situ* mullitisation process [4], whereas the sintered mullite (T-2) showed a contraction, which, over time, can lead to joints opening within the lining, increasing vulnerability to gas penetration. Furthermore, the andalusite-based brick showed slightly lower thermal expansion at 1000°C, a characteristic essential for minimizing internal stress and mitigating crack initiation during the rapid thermal cycling typical of CDQ operations.

High-temperature property comparisons (Table 2) further validate the superiority of andalusite composition. The T-1 bricks showed greater stability under Refractoriness Under Load (RUL) testing, with only -0.34% deformation 1625°C, compared to the -0.5% deformation observed for T-2 at 1619°C. Both

materials performed similarly in creep in compression tests and PCE values and exceeded the specification.





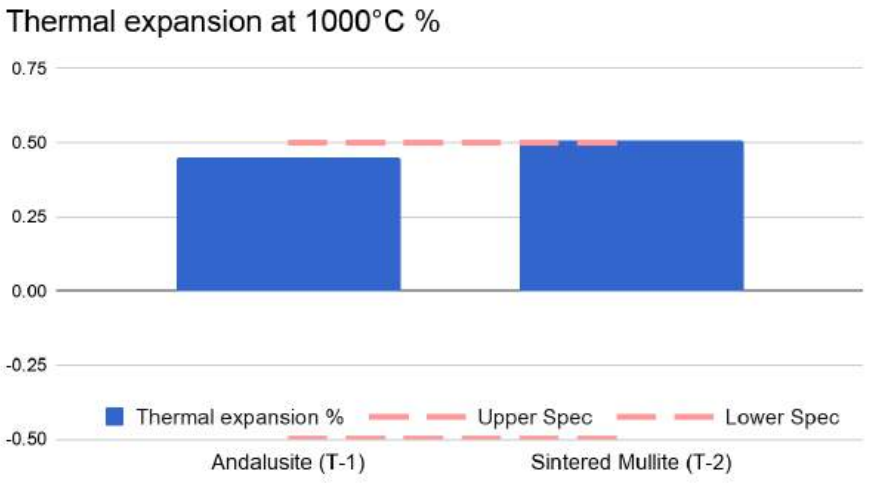


Fig. 5: Comparison of the andalusite and sintered mullite bricks in terms of PLC after 4h at 1500°C, 2h at 1600°C and thermal expansion at 1000°C

Properties	Specification	Andalusite (T-1)	Sintered Mullite (T-2)
PCE (Orton Cone/°C)	37 min/1820°C	+ 37	+ 37
RUL ($T_{0.5}$°C)	1580°C min for -0.5% deformation	At 1625°C, -0.34% deformation	At 1619°C, -0.5% deformation
Creep % at 1350°C, 0-50h	- 1.0 max.	-0.14	-0.11

Table 2: Comparison of the high temperature properties (PCE, RUL and Creep in compression) between the andalusite and sintered mullite bricks

5.4 Resistance to thermal shock and CO gas

The most significant functional advantage of the andalusite-based bricks lies in their thermal shock resistance (Table 3). While both compositions withstood air quenching tests, the water quenching test revealed a dramatic performance gap. The T-1 bricks consistently withstood 30 cycles, whereas the T-2 bricks failed significantly earlier (3–11 cycles).

This disparity is attributed to the unique microstructural architecture of the andalusite-based bricks. *In-situ* conversion of andalusite into an interlocking network of needle-like mullite crystals, reinforced by secondary mullite, effectively creates a tortuous path for micro-crack propagation [5]. By absorbing the energy generated during rapid thermal shocks, the T-1 microstructure prevented the coalescence of macro-cracks, thereby ensuring extended structural integrity. Both compositions demonstrated excellent resistance to CO-disintegration (Category A), confirming that both matrices were sufficiently dense and chemically inert to prevent carbon deposition at 500°C (Table 4).

Thermal shock	Specification	Andalusite (T-1)	Sintered Mullite (T-2)
Spalling Resistance in Air at 1000°C	30 Cycles min.	+ 50, + 50, +50	+ 50, + 50, +50
Spalling Resistance in Water at 950°C	-	+30, +30, +30	+3, +11, +10

Table 3: Comparison of thermal shock resistance between the andalusite and sintered mullite bricks

	Andalusite (T-1)	Sintered Mullite (T-2)
CO disintegration test at 500°Cfor 100 hrs.	A (No Change, No C deposition)	A (No Change, No C deposition)

Table 4: Comparison of CO disintegration test between the andalusite and sintered mullite bricks

6. Industrial Application: Tata Steel Meramandali

Andalusite bricks were installed in the coke dry quenching facility at Tata Steel, Meramandali plant and after completion of the service life repeat order was executed.

7. Conclusion

The experimental investigation and industrial application detailed in this paper demonstrated that andalusite-based refractory bricks offer a superior technical solution for the demanding operational environment of Coke Dry Quenching (CDQ) chambers. The critical advantage of this refractory lies in the function of andalusite as an *in-situ* mullite precursor. The controlled phase transformation of andalusite into an interlocking network of primary mullite, reinforced by a secondary mullite matrix derived from silica-rich glassy phases, creates a highly stable, dense, and chemically inert microstructure.

This unique microstructural architecture effectively mitigated the primary challenges associated with CDQ operations. The material's controlled, positive volume expansion on heat treatment successfully counteracted traditional ceramic shrinkage, resulting in superior dimensional stability. Furthermore, its significantly lower and uniform thermal expansion, combined *in-situ* formed micro-cracks, provided exceptional resistance to thermal spalling and crack propagation under the aggressive thermal cycling inherent to the CDQ process. Comparative testing confirmed the outperformance of the andalusite-based bricks over conventional sintered mullite compositions across key thermo-mechanical parameters, specifically in permanent linear change (PLC) stability, refractoriness under load (RUL), and thermal shock resistance.

The practical efficacy of this solution was further validated by its successful installation and operational performance at the Tata Steel Meramandali plant.

8. References

[1] S.Mweemba, M.Zhang, C.Han, H.Gu , J. Xu, L.Sun: Thermomechanical analysis of a coke dry quenching furnace. Energy Vol.325, 2025

[2] G.Bisio and G.Rubatto: Energy saving and some environment improvements in coke-oven plants, Energy, Vol.25, 2000, p. 247-265

[3] M-L.Bouchetou, J-P.Ildefonse, J.Poirier and P. Daniellou: Mullite grown from fired andalusite grains: the role of impurities and of the high temperature liquid phase on the kinetics of mullitization and consequences on thermal shocks resistance, Ceramics International, Vol.31, 2005, p.999-1005

[4] D.Frulli: Production and properties of refractory raw materials based on andalusite and mullite—influence of impurities in the refractory behavior, Refractories Worldforum, Vol.8(3), 2016, p.1–4.

[5] Wang, L., Zhang, Y., & Liu, H. (2019). Microstructural evolution and mechanical properties of andalusite-based refractories during high-temperature service. *Ceramics International*, 45(8), 10245-10252.

DEVELOPMENT OF INDIGENOUS GUNNING MASS FOR EOF (ENERGY OPTIMISED FURNACE) AND ESTABLISHING ITS PERFORMANCE FOR THE HOT MAINTENANCE

Pravash Gourav[1], Saumen Sinha[1], Raja Sarkar[1], Abhinandan Kapase[1], Jagadish Kumar M [2]

Calderys India Refractories Ltd [2] , Jai Raj Steel [2]

Abstract

Energy Optimized Furnaces (EOFs) are primary steelmaking reactors based on combined oxygen blowing, where hot metal, preheated scrap, and fluxes are charged and refined. Oxygen is injected through supersonic lances and submerged tuyeres, generating intense bath stirring due to CO evolution and post-combustion. The process utilizes exothermic oxidation heat and off-gas energy for scrap preheating, improving overall energy efficiency.

These operating conditions create highly aggressive slag–metal interaction and severe refractory wear at critical zones such as tuyeres, tap holes, slag line, and stadium. Among these, the tuyere zone is the most critical due to continuous oxygen injection and localized high reaction intensity.

Earlier, gunning materials for such applications were predominantly imported. CALDE MAG GUN EOF was developed under the 'Make in India' initiative at Calderys Bhubaneswar Refractory Works, the world's largest single-site refractory and casting flux plant.

CALDE MAG GUN EOF is designed with optimized granulometry and binder system to achieve fast sintering, strong adhesion, and high resistance to slag corrosion and erosion under dynamic EOF conditions. To ensure high-temperature stability and high corrosion-erosion resistance, a CaO/SiO_2 ratio greater than 2 was used for the input DBM. This case study elaborates on the physical and chemical properties of the gunning mass. Slag corrosion behaviour of the gunning mass was theoretically calculated using factsage software using refractory –metal-slag interaction model. Formulation resulting ~20% lower amount of slag with comparable viscosity at 1600 C as calculated by factsage has given desired performance. Product was successfully used in a 40MT EOF whose details will be provided, gunning mass performance data will also be showcased in this case study.

Keywords: EOF, Magnesia, Sintering, Steelmaking, Gunning mass, Campaign life, Refractory wear

1. **Introduction**

The Energy Optimizing Furnace (EOF) is a hybrid steelmaking technology that combines the concepts of the Basic Oxygen Furnace (BOF) and Electric Arc Furnace (EAF). It is intended for small to medium-sized Indian steel plants and offers improved energy efficiency, flexible raw material processing, and lower electrical consumption [1]. Due to extreme mechanical, chemical, and thermal stresses, refractory gunning repair is essential. Operational factors including oxygen flow, the ratio of Scrap to hot metal, vessel design, and tap-to-tap time all affect gunning mass performance.

JSW Salem, Hospet Steel, SLR Metaliks, and Jairaj Ispat are the four EOF units that are currently in operation in India; each operates under different process and maintenance conditions.

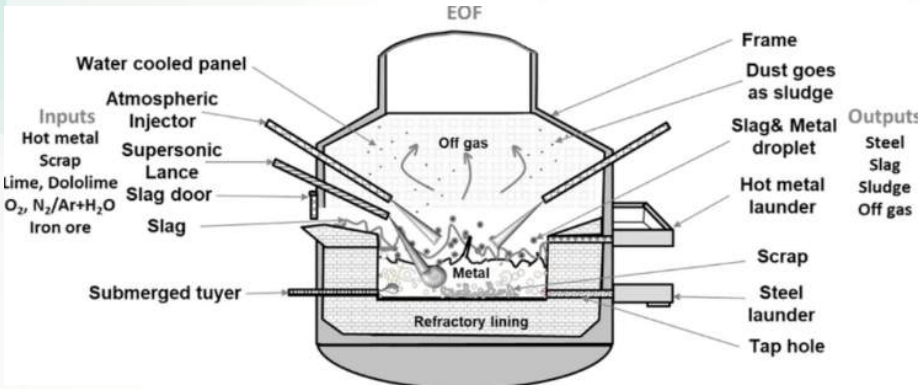


Figure 1 Schematic diagram of EOF Furnace [2]

The EOF uses a unique combined oxygen practice, featuring submerged side tuyeres to inject oxygen directly into the molten bath and supersonic lances from above. This creates localized zones of extreme thermal energy, severe chemical corrosion from a foamy slag high in iron oxide (FeO), and aggressive physical agitation (pool boiling) [1]. The area around the submerged tuyeres and the hearth bottom suffers accelerated wear. Magnesite-based gunning mixes are pneumatically sprayed (via specialized machines) in tuyere & stadium area to patch and rebuild thickness without full cooldown or relining. This is done through the slag door of EOF. EOF gunning allows to patch these high-wear zones (tuyere zone) without waiting for the furnace to cool down.

EOF Gunning was developed locally at Calderys Bhubaneswar Refractory works (BRW) with technical collaboration with Calderys Europe and Taiwan plant. This product has following advantages:

(a) Premium dead burned magnesia (DBM) with optimized CaO/SiO_2 ratio:

To ensure high-temperature stability and high corrosion-erosion resistance, a CaO/SiO_2 i.e C/S ratio greater than 2 is used in CALDE MAG GUN EOF gunning Products, It promotes the formation of high-melting phases such as dicalcium silicate (M.P 2130°C) instead of low melting phase monticellite(C/S<1.5), merwinite(C/S – 1.5-1.85) etc and contributes to the corrosion resistance of EOF gunning. The presence of low-melting silicates accelerates chemical corrosion by dissolving MgO into the liquid slag. If low-melting silicates exist at grain boundaries, they act as a solvent, accelerating chemical corrosion by dissolving the MgO into the liquid slag [3]. By keeping impurities (SiO_2, Al_2O_3, FeO) low and controlling their ratio to favor high-temperature dicalcium silicates or pure magnesia bonds formation in EOF gunning, our formulation minimizes the formation of a low-viscosity liquid phase at operating temperatures, maintaining the high corrosion and erosion resistance of EOF gunning [3]. This high-temperature phase provides the structural integrity needed to withstand the harsh thermal environment of the EOF furnace.

(b) Optimized grain size distribution(GSD) for adhesion and minimal rebound:

The particle size engineering of the gunning mass directly controls the balance between adhesion, buildability, and rebound loss. Calderys formulation achieves a rebound loss of below 5-10% in EOF tuyere applications—a benchmark performance metric that reduces material waste and lowers the cost per heat of gunning maintenance.

(c) Application-specific binder additive:

Calderys engineers the binder chemistry—drawing on phosphate, silicate, or sulphate-based systems—to match the specific curing mechanism and operating temperature profile of the EOF environment.

This ensures the gunning mass develops appropriate bond strength at intermediate temperatures while sintering effectively at operating conditions.

(d) Superior sinterability:

The formulation is engineered to sinter rapidly and densely, forming a compact microstructure that resists slag penetration and corrosive attack. This is particularly important at the tuyere zone, where the combination of oxygen injection, liquid metal contact, and thermal cycling creates the most aggressive wear conditions in the furnace.

This paper will discuss the development work of EOF gunning mass based on thermomechanical properties at different temperatures and fact sage analysis.
This paper will also include the field trial feedback of EOF Gunning mass and its successful application at Tuyere & Stadium zone.In a breakthrough commercial deployment, Calderys reduced lead time from 90 days (import) to just 15 days—an 83% improvement—eliminating supply chain risk for an Indian steel producer.

2. Experimental

The main objective of this project is to develop the CALDE MAG GUN EOF domestic products which gives the high corrosion & erosion resistance, good stickability & durability and high sinterability for Tuyere & Stadium Zone of EOF furnace. As discussed, product formulation design was based on the selection of raw materials and binder-additives system with control GSD of gunning mix. Several investigations and trials were conducted with different types of binder concentration and additives to obtain the optimum physical, chemical & thermal properties of gunning products. DBM raw materials have been used as a base material for this gunning product. Hybride Binder System has been selected for the EOF gunning product to minimize the rebound loss, good sinterability and excellent spalling resistance.

Gunning mix samples were prepared for testing with water addition in Hobart mixer. Prisms (160*40*40) were made by ramming method. After 24 hours of natural air drying, prisms were demolded. Demolded samples were kept inside the oven for 24hrs of drying at 110 °C temperature. After oven drying(110°C/24hrs) bulk density, cold crushing strength & MOR testing has been carried out. Samples were fired at 1550°C/3hrs. After Firing bulk density, cold crushing strength & MOR testing has been carried out. Grain size distribution is determined according to Indian standard methods



Figure 2 Gunning Prism after Ramming



Fig 3 Gunning Prism after drying at 110°C/24hrs



Fig 4 Gunning Prism after firing at 1550°C/3hrs

3. Results and discussion

(a) Chemical Composition

PRODUCTS	MgO	CaO	Fe2O3
CALDE MAG GUN EOF	85-90	02-03	0.5-1.5

Table 1 Chemical Composition of EOF GUUNNING

(b) Grain Size Distribution

GSD is determined according to Indian standard from 6.3 mm to -0.063 mm. CALDE MAG GUN EOF has a combination of coarse and fines aggregates. Fine grains possess high specific surface area, which is vital for the rapid sintering and activation of chemical binders. This allows the gunning masses to instantly adhere and set on hot furnace walls during mid-campaign repairs.

(c) Cold Crushing Strength (CCS)

Cold Crushing strength of the refractory prism was measured at room temperature after drying and firing at 110 °C & 1550 °C respectively. High CCS value is the indication of good strength development. During drying of samples at 110 °C free water is released and it showed little weight loss. CCS value at 110 °C temperature was low since ceramics bonding didn't form. Above 1300 °C temperature formation of ceramic bond starts so the CCS value of EOF gunning products is high after firing at 1550°C/3hrs.



Fig 5 CCS at 110°C/24hrs & 1550°C/3hrs of EOF Gunning

(d) Bulk Density (B.D)

Bulk density of gunning products has been determined after firing at 1550 °C/2hrs. This is measured by water boiling method based on Archimedes' principle.

$$BD = \frac{D\rho}{W-S} 100$$

D=Dried Weight, W=Soaked Weight, S=Suspended Weight, $\rho = Density\ of\ liquid$

PARAMETERS	CALDE MAG GUN EOF
BULK DENSITY (gm/cc)	2.60

Table 2 B.D of EOF Gunning

(d) Permanent Linear Change (PLC)

Permanent Linear Change OF CALDE MAG GUN EOF has been determined after firing at 1550 °C for 3hrs. Due to its superior raw material base % PLC of CALDE MAG GUN EOF was <2.0% at 1550 °C/3hrs.

(e) FACT SAGE of EOF GUNNING

Study of EOF gunning material with process slag (70:30 ratio) was done using thermodynamic simulation (FACT SAGE 8.2) at three different temperatures. From fact sage analysis it is found that as operation temperature of EOF is increased from 1500 °C to 1600 °C amount of liquid phase formation is increased by 2-3 % after interaction with slag

MgO	Al_2O_3	SiO_2	MnO	FeO	CaO
13	04	20	06	22	45

Table 3 Chemical Analysis (%) of Slag:

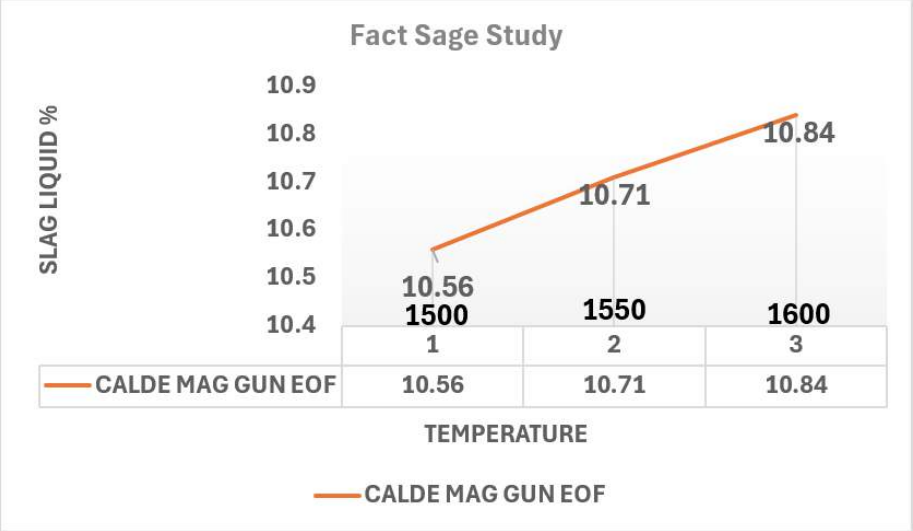


Fig 6 Fact Sage Study (refractory slag interaction) at three temperatures

4. Installation & Customer Trial Feedback

4.1. OPERATING PARAMETERS OF EOF

EOF Gunning mass performance in Energy Optimizing Furnaces (EOFs) is influenced by both operational practices and slag chemistry. Longer campaign life and extended gunning intervals indicate reduced refractory wear, lower maintenance frequency, and decreased gunning mass consumption, aided by optimal setting time for stronger bonding and denser repairs. Conversely, high hot-metal ratios and elevated sulphur & FeO content accelerate wear and weaken refractory integrity. Operational factors—such as tap-to-tap time, oxygen-blowing duration, and heats per day—further affect performance, with shorter cycles and higher heat counts increasing thermal stress. Evaluating total daily operational time provides a realistic measure of thermal exposure, supporting accurate assessment and optimization of gunning mass efficiency.

Parameter	Jai Raj Ispat
Heats/Day	25
Tap-to-Tap Time (min)	50 - 55
Oxygen Blow Time (Mins)	30 - 35
Daily Output (Tons)	1000
Production (Million Tons/Year)	0.43 *
EOF Capacity (MT)	40
Number of EOFs	1
Gunning Setting Time (Mins)	10

Table 4 Operating Parameters of EOF

Input (%)	Jai Raj Ispat
Hot Metal	84.00
Scrap	4.30
DRI	1.08
Pig Iron	1.08
Coke	2.30
Lime	0.1

Table 5 Charge Details of EOF

Oxide (% Mass)	Jai Raj Ispat
FeO	23.0
SiO_2	18.4
CaO	45.4
MgO	13.3
S	1.0
Basicity	2.47

Table 6 Indicative Slag Chemistry of EOF

EOF gunning mass at Jairaj Steel experienced higher wear rate and lesser life due to it contained higher Hot Metal charge (84.00%) and high S (1 %) & FeO (23%) in slag.

Plant	Jai Raj Ispat
Slag Zone Bricks	MgO-C
Metal Zone Bricks	MgO-C
Campaign Life (Heats)	1000

Table 7 Working Lining of EOF

Working Lining of EOF furnace is MgO-C brick for slag & metal zone.

Metric	Jai Raj Ispat
Gunning Mass (kg/ton of liquid steel)	4.5
Gunning Interval (Tuyere (Heats)	6 – 8
Daily Consumption (Tons)	5.4
Yearly Consumption (Tons)	1971

Table 8 EOF Gunning Mass Consumption

4.2. FIELD TRIAL

Application of EOF Gunning was done at Tuyere & Stadium area of the furnace. During Gunning, 3-5% of rebound loss was observed. EOF Gunning was successfully used which gives 10 to 12 heats. It has excellent sinterability and durability.

Products	Soaking Time	Heat Life
CALDE MAG GUN EOF	15 Mins	11
CALDE MAG GUN EOF	13 Mins	10
CALDE MAG GUN EOF	12 Mins	09
CALDE MAG GUN EOF	08 Mins	08
CALDE MAG GUN EOF	12 Mins	09
CALDE MAG GUN EOF	15 Mins	12

Table 9 Field Trial Feedback of Tuyere Zone

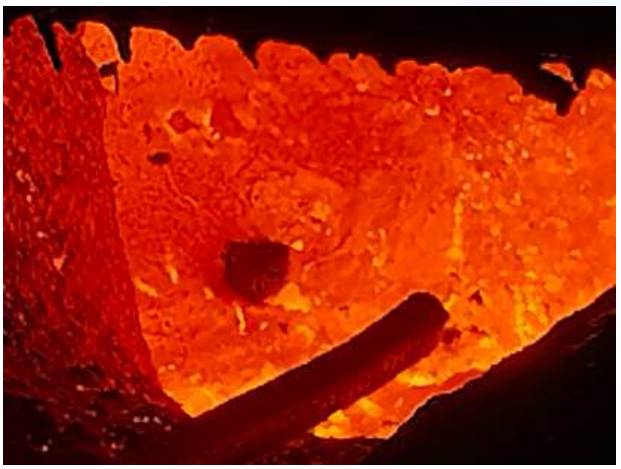
Products	Soaking Time	Heat Life
CALDE MAG GUN EOF	3-5 Mins	08
CALDE MAG GUN EOF	2-3 Mins	07
CALDE MAG GUN EOF	2-3 Mins	08
CALDE MAG GUN EOF	1-2 Mins	06
CALDE MAG GUN EOF	2-3 Mins	07
CALDE MAG GUN EOF	2-3 Mins	08

Table 10 Field Trial Feedback of Stadium Zone

At Tuyere No. 2, with a tuyere life of 150 heats and a furnace bottom life of 516 heats at the time of application, a gunning quantity of 400 kg delivered a gunning life of 11 heats—consistent with the proven performance range of 8–12 heats per gunning cycle targeted for this application.



95 % residual after 1st heat



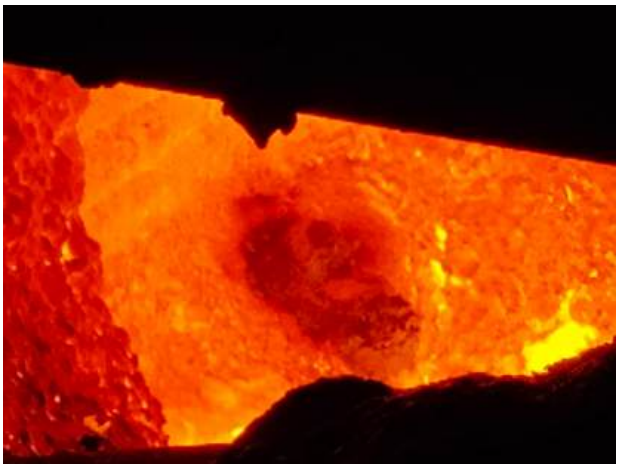
90 % residual after 2nd heat



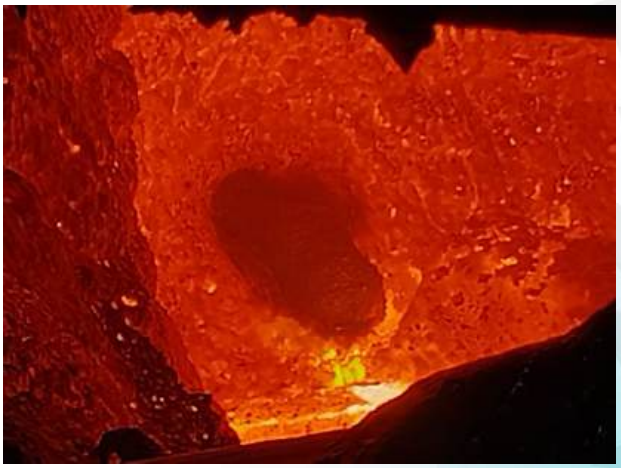
85 % residual after 3rd heat



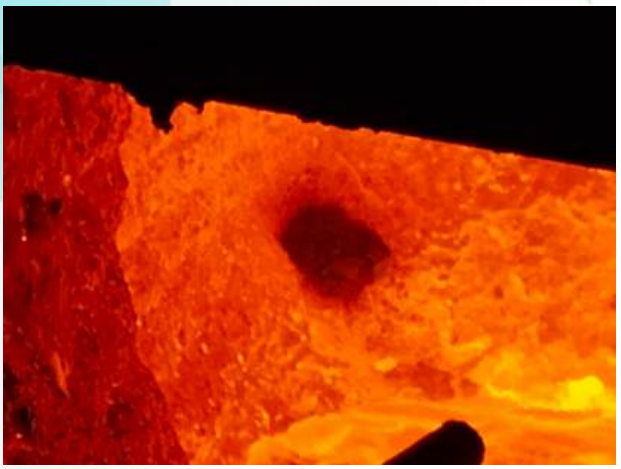
75 % residual after 4th heat



70 % residual after 5th heat



65 % residual after 6th heat



55 % residual after 7th heat



45 % residual after 8th heat



35 % residual after 9th heat



20 % residual after 10th heat



10 % residual after 11th heat

Fig 7 Sequential tuyere residual images from Heat 1 through Heat 11, demonstrating the progressive, controlled wear profile of Calderys EOF gunning material (Tuyere No. 2, Gunning Quantity: 400 kg, Gunning Life: 11 heats)

5. Conclusion

CALDE MAG GUN EOF was developed domestically in India. Based on the lab trial analysis (CCS, B.D, PLC) and thermodynamic modeling (fact Sage 8.2) CALDE MAG GUN EOF is being tries at Indian Steel Plants, with performance 08-12 heats for tuyere Zone and 07-08 heats for Stadium zones.

The successful development and commercial deployment of EOF basic monolithic gunning material from the Calderys plant in Odisha marks a significant milestone—not only for Calderys in India, but for the Indian steel industry as a whole. Domestic EOF operators can now have access to a locally manufactured, globally benchmarked basic monolithic gunning solution, produced to the highest standards of quality and consistency. The achievement reflects a convergence of strategic investment, R&D capability, and operational commitment. Calderys has demonstrated that world-class refractory performance for one of steelmaking's most demanding applications can now be delivered in India—with the responsiveness, technical support, and commercial flexibility that only local manufacturing can provide.

References

1. S. Burde, The EOF: Latest Achievements and Developments, Steel Tech, Kolkata, India, 2014.

2. Malaiyappan Vidhyasagar, Deepoo Kumar, ”A Static Model for Energy-Optimizing Furnace ”, Steel Research International 93 (2022).

3. Almeida, Rodolfo Arnaldo Montecinos de, et al. "MgO Saturation Analysis of $CaO-SiO_2-FeO-MgO-Al_2O_3$ Slag System." Materials Research 21.1 (2017).

4. M. Rivenet, N. Ruchaud,” A basic gunning material interfaces study Alumina volatility in water vapor at elevated temperatures”, Journal of the European Ceramic Society 20 (2000).

ENHANCING REHEATING FURNACE CAMPAIGN LIFE THROUGH OPTIMIZED REFRACTORY ANCHOR DESIGN AND STANDARDIZATION

Biswajit Pal*, Arko Chakraborty, Umesh Chandra Deep, Tapas Kumar Pal, Santanu Saha,

Sujat Ali Khan

Tata Steel Limited, India

Mail id: biswajit.pal@tatasteel.com, arko.chakraborty@tatasteel.com, umesh.deep@tatasteel.com, tapas.pal1@tatasteel.com, santanu.saha@tatasteel.com, sujat.khan@tatasteel.com

Abstract

In Reheating Furnaces role of anchor design is very crucial in extending the lifespan of furnace linings. The holding mechanism is paramount in ensuring the refractory lining remains intact under extreme thermal and mechanical stresses. Different anchor designs offer varying degrees of effectiveness in securing the lining and preventing premature failure. Optimizing anchor design directly translates to increased furnace uptime, reduced maintenance costs and improved overall operational efficiency. Selecting the right anchor configuration, material and installation technique is vital for maximizing the longevity of the furnace lining.

This project proposes a comprehensive analysis and optimization of the refractory anchor systems currently employed in Tata Steel's reheating furnaces. The core objective is to move beyond a one-size-fits-all approach and develop a data-driven methodology for selecting the optimal anchor design, material composition and installation protocol for specific furnace zones and operating conditions.

Keywords: Reheating Furnace, Refractory Anchors, C-Clamp Anchor, Campaign Life, SS310, Thermal Modelling, Refractory Reliability

1. Introduction

The reheating furnace is one of the most critical units in the hot rolling process. It is responsible for heating slabs, blooms or billets to the required rolling temperature while maintaining thermal uniformity and operational efficiency.

The refractory lining protects the furnace shell from extreme temperatures and serves as a thermal insulation barrier. In monolithic refractory systems, metallic anchors provide structural support and ensure that the refractory remains securely attached to the furnace shell throughout its operating life. These anchors are continuously exposed to severe thermal cycling, mechanical loading and oxidizing furnace atmospheres.

Failures of refractory anchors can result in:

- Refractory cracking and spalling
- Lining detachment
- Hot spots on furnace shell
- Increased heat losses
- Unplanned shutdowns
- Inconsistence performance
- Increased maintenance costs
- Safety hazards

The core problem is the premature failure of furnace linings due to non-standardized and suboptimal refractory anchor systems. Therefore, optimization of the anchor system is essential for maximizing furnace campaign life and ensuring reliable operation.

2. Problem Definition

Existing Situation

A study conducted during planned shutdowns and refractory inspections identified several recurring anchor-related failures across reheating furnaces.

Observed Issues

- Non-standardized anchor designs across different furnace zones.
- Common anchor specifications used irrespective of operating temperature.
- Premature oxidation and deformation of anchors.
- Cracking around anchor locations.
- Localized refractory spalling.
- Frequent emergency repair requirements.

Root Cause Analysis

The primary causes identified were:

1. Inadequate anchor design selection.
2. Improper material grade for high-temperature service.
3. Improper anchor spacing and density.
4. Lack of standardized installation procedures.
5. Limited monitoring of anchor performance during campaigns.

Problem Statement

The absence of a standardized and scientifically optimized refractory anchor design methodology results in premature refractory failure, reduced furnace campaign life, increased maintenance expenditure and production losses due to unplanned shutdowns.

3. Project Objectives

The key objectives of the project were:

- Increase refractory campaign life.
- Improve lining structural integrity.
- Minimise refractory spalling and detachment.
- Standardize anchor design across all reheating furnaces.
- Optimize anchor material selection based on furnace operating temperature.
- Improve furnace availability.
- Reduce annual refractory maintenance costs.
- Establish best practices for installation and inspection.

4. Benchmarking and Technical Challenges

4.1 Existing Practice

Current anchor selection is largely based on historical practices rather than engineering design principles.

Parameter	Existing Practice
Anchor Shape	Multiple non-standard designs
Anchor Material	Common stainless steel grades
Anchor Pitch	Uniform spacing
Installation	Contractor-dependent
Inspection	Limited monitoring

The study identified considerable scope for furnace reliability improvement through systematic anchor optimization and standardization.

4.2 Existing Anchor Performance

The existing SS310 round rod anchors are exposed to temperatures of 1100-1150°C at the anchor tip, which is at or beyond the material's recommended service limit of SS310 stainless steel. Sustained exposure to these temperatures causes accelerated oxidation, thermal softening and creep deformation, resulting in a progressive loss of mechanical strength and load-bearing capacity. The weakened anchors are unable to effectively support and retain the 230 mm plastic working lining, leading to refractory bulging, sagging, spalling, and localized lining detachment. Consequently, refractory campaign life is reduced, necessitating frequent repairs and increasing the risk of unplanned furnace shutdowns.

Parameter	Existing Condition
Total Lining Thickness	500 mm
Plastic Working Lining	230 mm
Anchor Type	Round Rod Anchor
Anchor Material	SS310
Anchor Tip Distance from Hot Face	300 mm
Estimated Tip Temperature	1100-1150°C
SS310 Recommended Service Temperature	~1100°C
Failure Mode	Oxidation, Softening, Creep Deformation
Result	Lining Instability & Premature Failure

4.3 Thermal Modelling Study

Thermal modelling of the original lining configuration indicated anchor tip temperatures of 1105°C under normal lining conditions (Fig-1) and 1123°C after incorporating microporous backup insulation (Fig-2). Both values exceeded the recommended maximum continuous service temperature of SS310 (~1100°C), making the anchors susceptible to oxidation, thermal softening, and creep deformation (Fig-3).

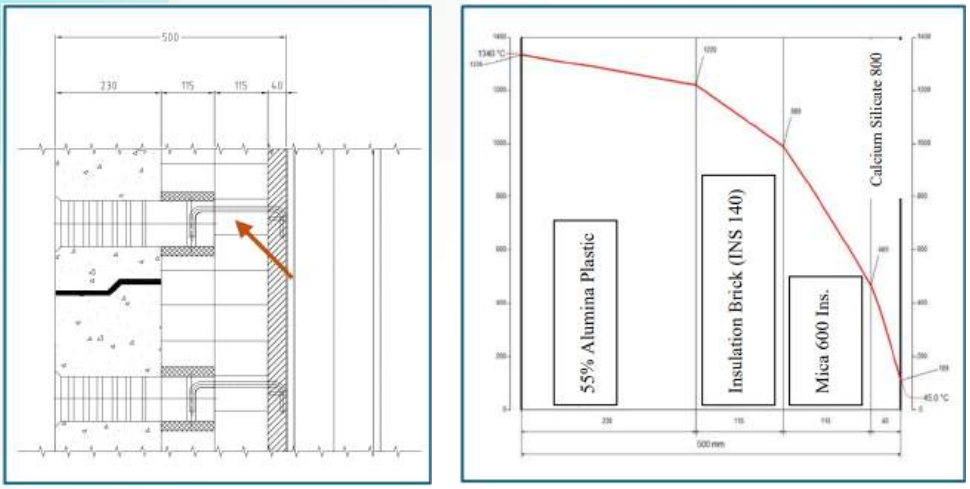


Fig-1 Existing Lining Configuration & Round Rod Anchors

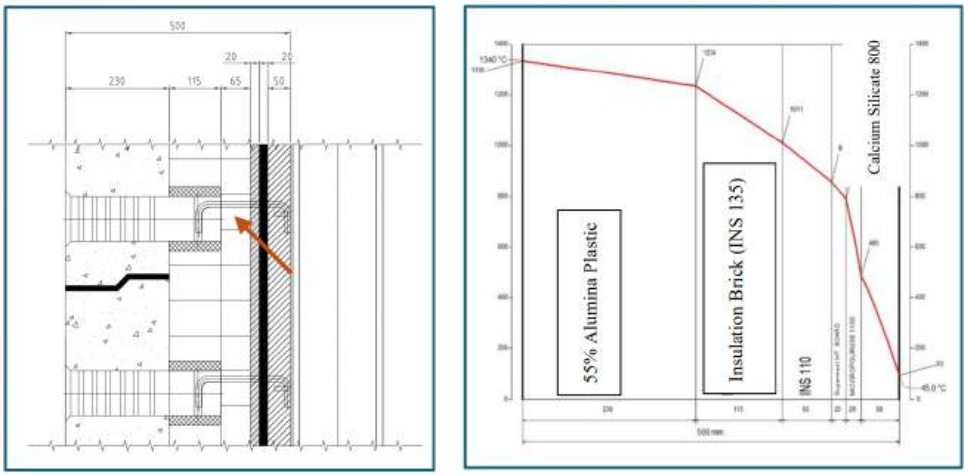


Fig-2 Existing Lining Configuration with Microporous Insulation & Round Rod Anchors

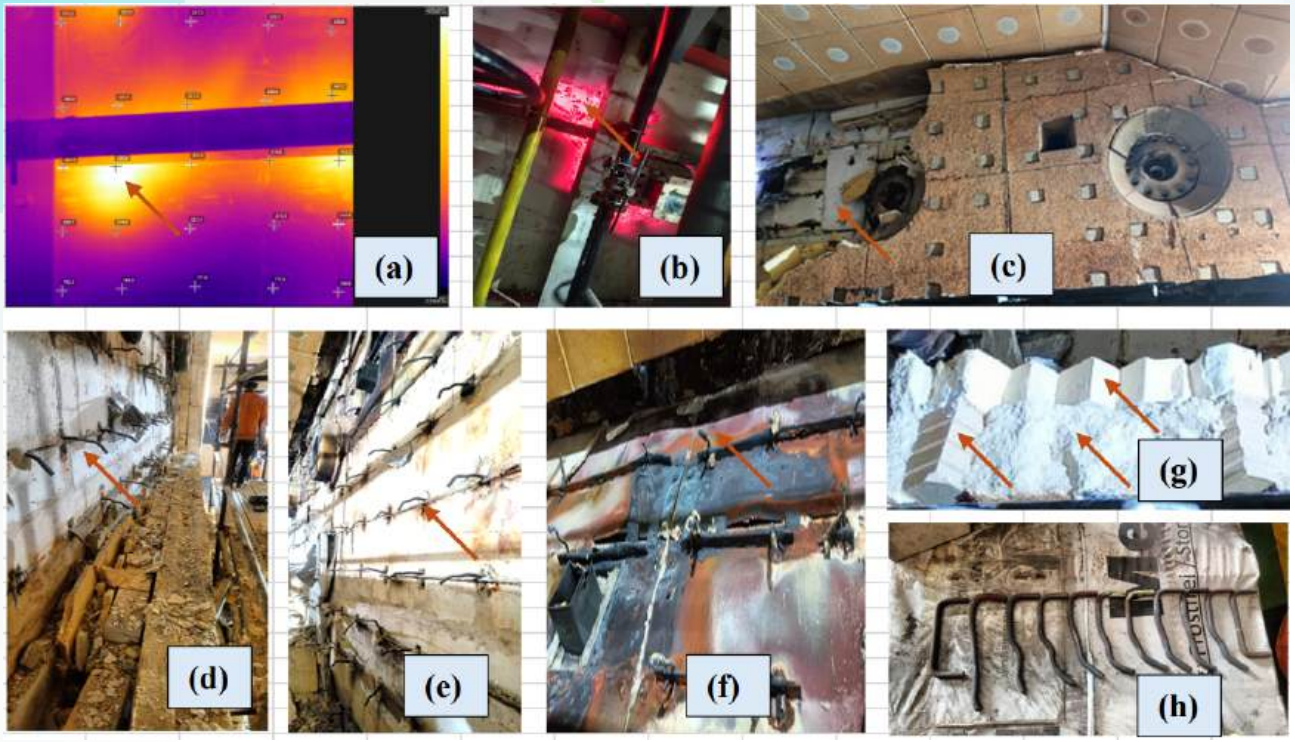
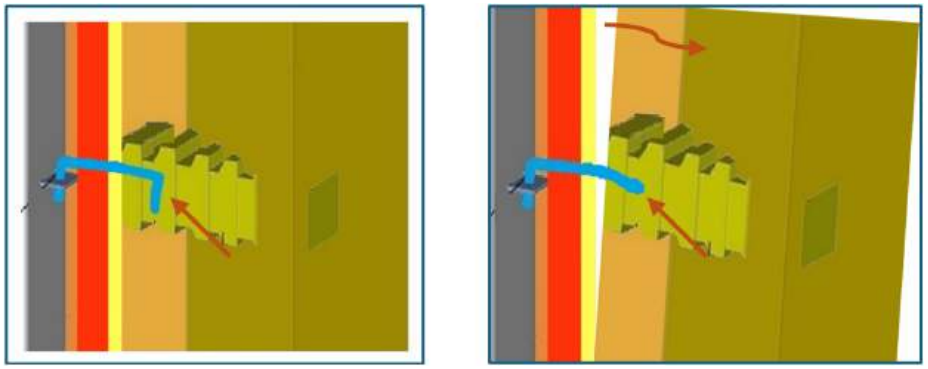


Fig-3 Failure analysis of the existing refractory anchoring system.
(a) Thermography of shell temperature indicating a hot spot
(b) Inside lining partially collapsed at the corresponding location
(c) Extensive lining failure resulting emergency shutdown
(d) (e) (f) Dismantled lining showing oxidized and deformed SS310 round rod anchors
(g) Plastic refractory, anchor bricks and back up insulations remaining intact
(h) Comparison between deformed rod anchor vs original anchor, confirming degradation



Modelling results showing anchor deformation due to elevated operating temperatures, resulting in loss of load-bearing capacity, refractory bulging, and localized lining detachment.

5. Technical Improvement and Design Optimization

To address this limitation, the anchor system was redesigned using a combined Rod + CClamp anchor arrangement and the anchor brick length was increased by 45 mm, resulting in an anchor brick length equivalent to approximately 80% of the total lining thickness (Fig-4 & 5). This modification increased the distance of the metallic anchor from the furnace hot face and significantly reduced the operating temperature of the anchor.

Parameter	Existing Design	Modified Design
Anchor Type	Round Rod	Rod + C-Clamp
Total Lining Thickness	500 mm	500 mm
Plastic Working Lining	230 mm	230 mm
Anchor Brick Length	Existing	+45 mm Increased
Anchor Tip Distance from Hot Face	300 mm	350 mm
Anchor Face Temperature	1100-1150°C	~950°C
SS310 Service Limit	~1100°C	~1100°C
Oxidation Risk	High	Low
Creep Deformation Risk	High	Low
Refractory Holding Capability	Moderate	High
Lining Stability	Poor	Excellent

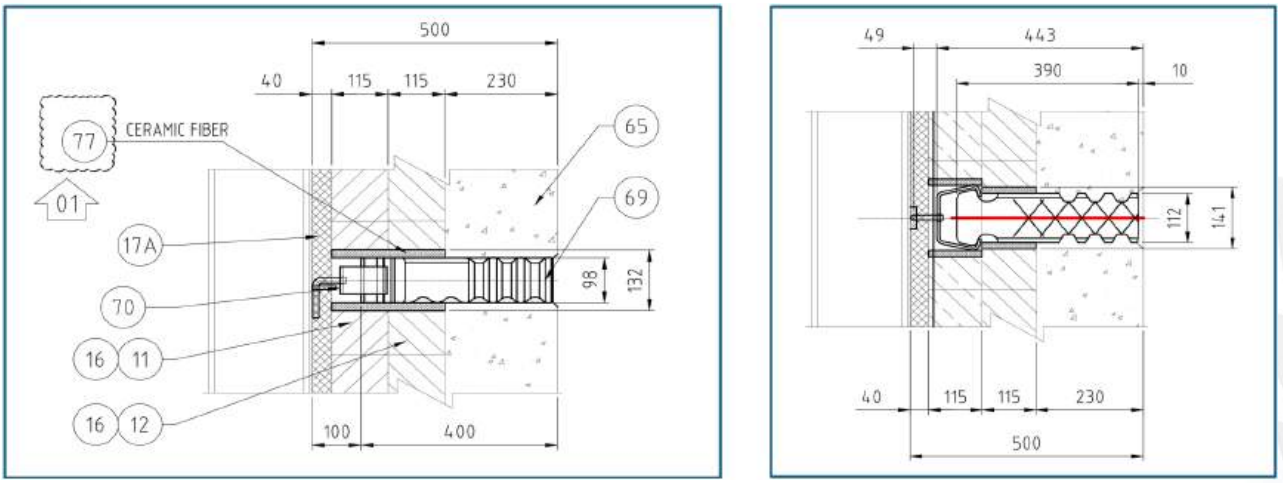


Fig-4 Modified lining configuration with Rod + C-Clamp anchors and increased anchor brick length, providing improved refractory holding, lower anchor temp. and enhanced lining stability.

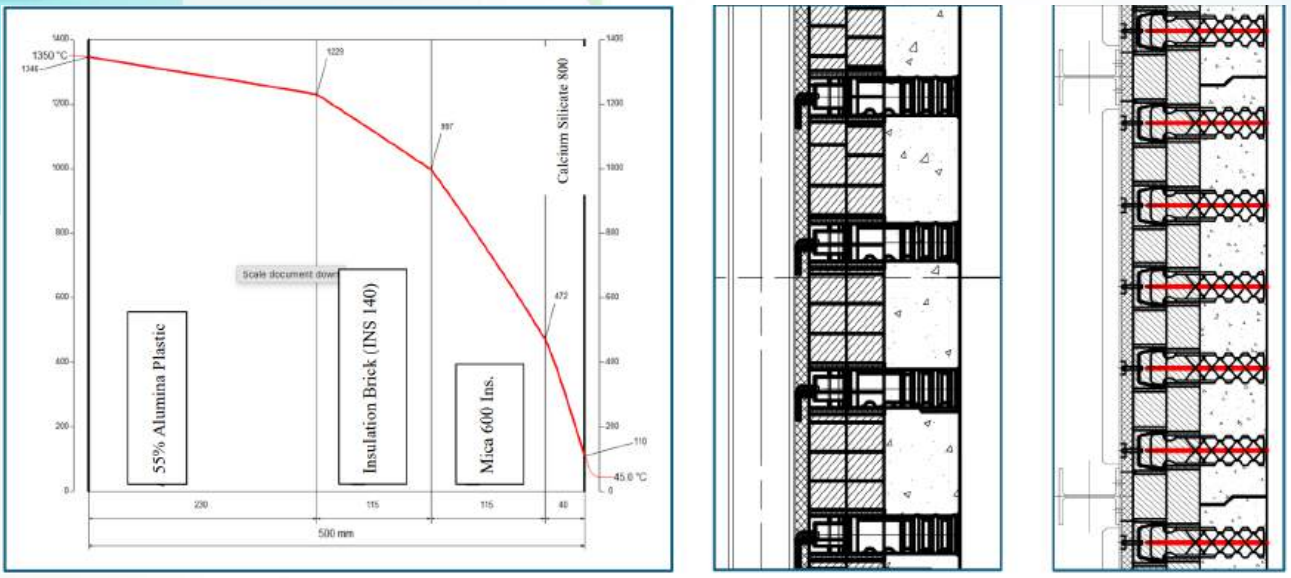


Fig-5 Thermal modelling of the modified lining system and standardized horizontal and vertical Rod + C-Clamp anchor pattern.

Comparative Assessment of Anchor Designs

Parameter	Round Rod Anchor	Rod + C-Clamp Anchor
Holding Strength	Moderate	High
Refractory Retention	Limited	Superior
Load Distribution	Localized	Uniform
Resistance to Sagging	Moderate	High
Thermal Stress Accommodation	Lower	Higher
Structural Stability	Prone to Deformation	Improved Rigidity
Anchor Operating Temperature	Higher	Lower
Oxidation & Creep Susceptibility	Higher	Lower
Campaign Life	Lower	Higher
Maintenance Requirement	Frequent	Reduced
Drawing Details (Bricks + Anchor)	Fig-6	Fig-7

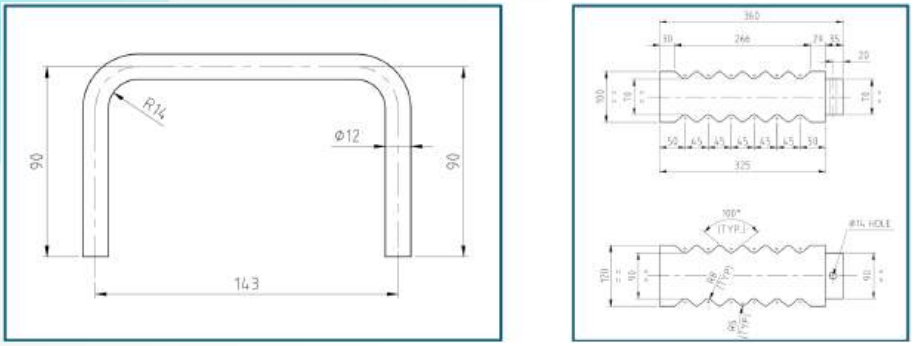


Fig-6 Conventional SS310 round rod anchor and anchor brick arrangement used in the existing furnace lining.

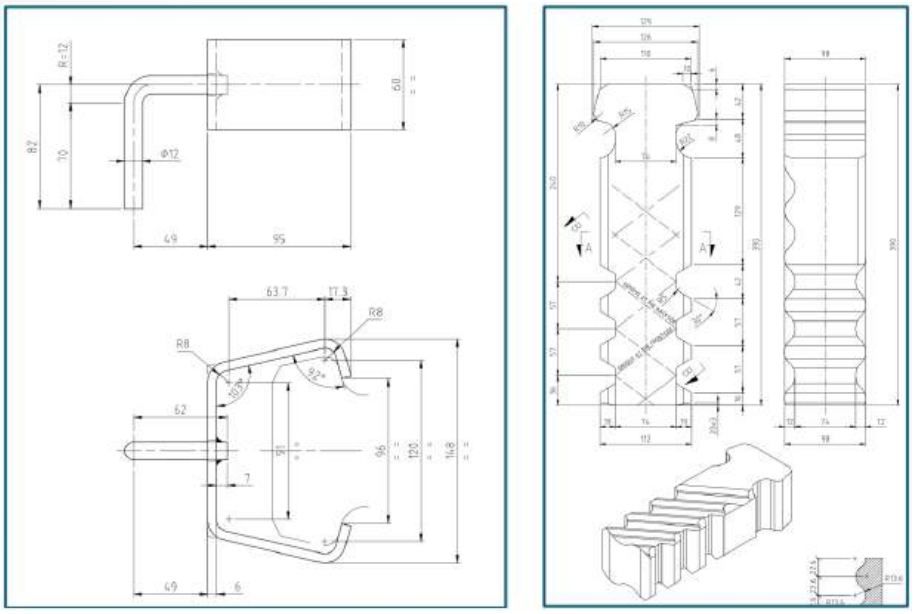


Fig-7 Modified SS310 Rod + C-Clamp anchor with extended anchor brick arrangement implemented in the furnace lining. The design reduces anchor temperature exposure, enhances refractory holding capability and improves lining stability, resulting in longer campaign life and reduced maintenance requirements.

The combined Rod + C-Clamp anchor design provided enhanced mechanical interlocking, improved load distribution and superior resistance to thermal and mechanical stresses. The increased anchor brick length relocated the metallic portion of the anchor to a lower temperature zone, substantially reducing oxidation and creep-related degradation (Fig-8).

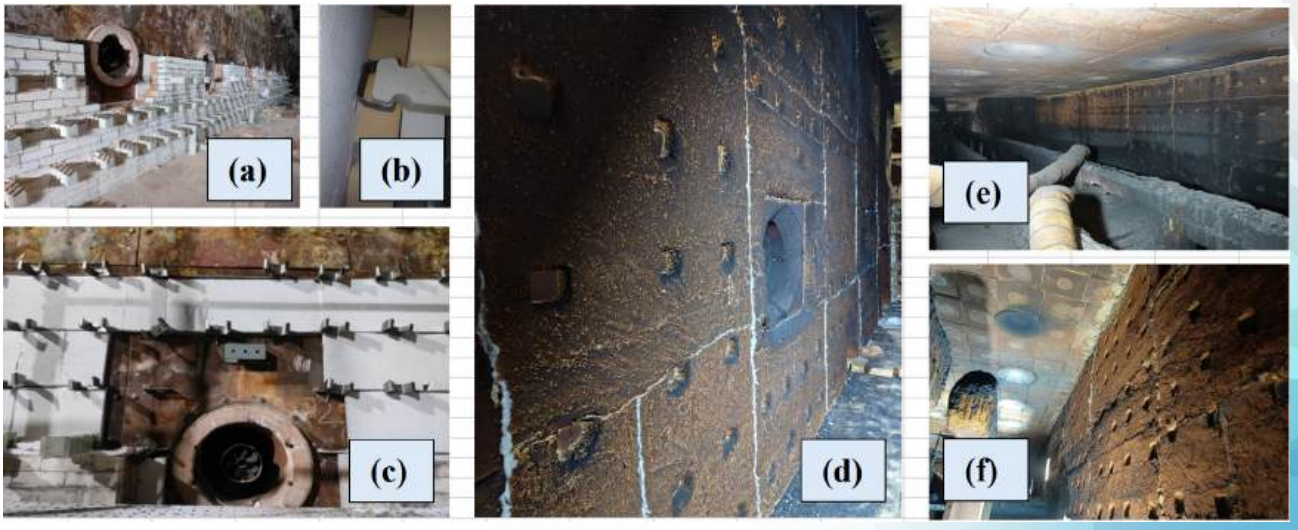


Fig-8 Implementation of the modified anchor and lining condition after two years of successful service.

6. Results and Performance Evaluation

Implementation of the optimized anchor design resulted in significant improvement in refractory performance and furnace reliability.

Performance Indicator	Before Implementation	After Implementation
Refractory Campaign Life	12-15 Months	>36 Months
Anchor Failure Rate	High	Negligible
Emergency Repairs	Frequent	Minimal
Furnace Availability	<90%	>98%
Maintenance Frequency	High	Significantly Reduced
Lining Stability	Poor	Excellent

Key Outcomes

- Reduction of anchor operating temperature from 1100-1150°C to ~950°C.
- Elimination of anchor exposure above the SS310 service temperature limit.
- Significant reduction in oxidation, thermal softening, and creep deformation.
- Enhanced refractory anchorage through improved mechanical interlocking.
- Prevention of refractory bulging, sagging, and localized detachment.
- Extension of furnace campaign life from 12-15 months to more than 36 months.
- Improvement of furnace availability to greater than 98%.
- Reduction in maintenance interventions and refractory consumption.

7. Conclusion

The refractory anchor system is a critical component governing the long-term performance of reheating furnace linings. Analysis of existing furnace performance indicates that premature refractory failures are often linked to non-standardized anchor design, inappropriate material selection and inconsistent installation practices.

The study established that refractory lining failures in reheating furnaces were primarily associated with the exposure of conventional SS310 round rod anchors to temperatures exceeding their recommended service limit, leading to oxidation, thermal softening, and creep deformation.

Through the development of a standardized Rod + C-Clamp anchor system and optimization of anchor brick length, the anchor operating temperature was reduced to approximately 950°C, well within the acceptable range for SS310. The enhanced anchor geometry improved refractory retention and lining stability, eliminating major causes of bulging, sagging, and spalling. As a result, refractory campaign life increased from 12-15 months to over 36 months, furnace availability improved to above 98%, and maintenance requirements were substantially reduced.

The project demonstrates an effective, sustainable, and replicable approach for improving reheating furnace reliability through optimized refractory anchor design and standardization contributing directly to operational excellence and asset reliability.

PERFORMANCE ENHANCEMENT OF SEN THROUGH GEOMETRIC MODIFICATION OF THE SLAG ZONE.

Sourav Banerjee*, Suvendra Mishra*, Sishir Nayak*, Bhabani Shankar Sahoo*; Yougojoti Nayak*, Manoranjan Beura *, S D Mazumdar *.

Santanu Saha**,(santanu.saha@tatasteel.com), ApurbaDey**,(apurba.de@tatasteel.com), Taposh Mandal**.PrasantaPanigrahi**,(PPANIGRAHI@TATASTEEL.COM),Sabyasachi Mishra **, (sabyasachi.mishra2@tatasteel.com), ShrinathKoushik** , (shrinath.koushik@tatasteel.com)

Abstract

A novel Submerged Entry Nozzle (SEN) has been developed along with Technical Team of Tata steel RED to enable continuous casting operations for up to 24 hours on slab casters, eliminating the need for tube-changing mechanisms during the casting campaign. The design innovation based on a differentiated zirconia (Zr) erosion band, engineered with variable cross-sectional geometry along its length to compensate for non-uniform erosion rates observed across different zones of the nozzle during prolonged service. By tailoring the dimensional profile of the Zr band to the localized erosion behavior, a near-uniform residual wall thickness is maintained throughout the 24-hour casting window, ensuring consistent steel flow characteristics and structural integrity. To accommodate the tundish furniture was developed in conjunction, providing the requisite mechanical support and sealing performance required under extended operating conditions. The proposed solution offers a significant operational advantage to steel producers by extending the casting sequence length, reducing refractory material consumption per heat, improving productivity through the elimination of scheduled nozzle change interruptions, and lowering associated safety risks. This integrated approach — combining erosion-adaptive refractory design with compatible tundish hardware — represents an advancement in long-sequence casting technology for high-throughput slab caster operations at Tata Steel Meramandli.

1. Introduction

The Submerged Entry Nozzle (SEN) is a critical refractory component in continuous slab casting, governing steel flow distribution into the mould while preventing reoxidation of the liquid steel stream. SEN service life is predominantly limited by erosion of the zirconia (Zr) band at the slag-line region, arising from chemical dissolution by mould flux and mechanical wear under high-velocity flow conditions. This erosion is markedly non-uniform along the nozzle length, driven by localized variations in flow dynamics, slag–refractory interaction, and thermal gradients across different functional zones.

Conventional SEN designs incorporate a Zr band of uniform cross-section, which is inherently governed by the zone exhibiting the highest erosion rate. Once this critical section reaches its minimum permissible wall thickness, casting time comes to an END, regardless of the residual condition elsewhere along its length. This constraint necessitates scheduled tube changes during long casting sequences, resulting in process interruptions, elevated refractory consumption, reduced productivity, and increased operational safety risk.

* IFGL Refractories Limited.
** Tata Steel Limited, Meeramanadali

To address this limitation, a geometrically optimised SEN has been developed to enable 24-hour, Tube-Change – System -free casting on slab casters. The design employs a differentiated Zr erosion band with a variable cross-sectional profile engineered to match zone-specific erosion rates, thereby sustaining a near-uniform residual wall thickness and consistent flow characteristics over the full campaign duration. Compatible

tundish furniture was co-developed to ensure adequate mechanical support and sealing under the extended operating regime. This paper presents the design basis, development, and performance validation of this erosion-adaptive SEN system, deployed at Tata Steel Meramandli.

MATERIALS AND METHODS

Raw Materials and Batch Preparation

The primary raw materials employed in this study comprised fused alumina and calcined alumina, used as aggregates within a selected particle size range, along with carbon and select functional additives. Batches were formulated by combining varying proportions of the Alumina aggregates, Carbon, and additives to achieve the desired compositional characteristics.

All dry constituents, including an aromatic binder, were homogeneously blended using an mixer for a controlled duration. A liquid binder system was then introduced, followed by continued mixing to ensure uniform distribution. Carbon was subsequently incorporated, and mixing was extended further to allow evaporation of excess volatile constituents and to achieve a homogeneous batch consistency.

The mixture obtained from the blending stage was processed through a drying unit to have a controlled size distribution and to regulate volatile matter content in preparation for downstream processing. The material was subsequently aged under controlled atmospheric conditions for a defined period to stabilize its properties prior to consolidation.

Consolidation and Thermal Treatment

The aged granulated mixture was consolidated using an isostatic pressing technique to produce cylindrical specimens of representative dimensions for the evaluation of physical properties. The resulting green bodies were subjected to a controlled heat treatment, followed by a subsequent process at an elevated temperature to achieve the desired final properties.

2.3. Characterization Techniques

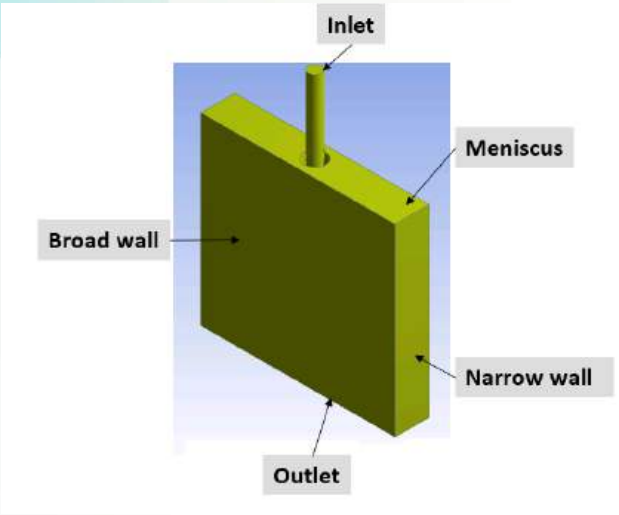
Elemental and phase characterizations of the raw materials were conducted via X-ray fluorescence (XRF; Bruker S8 Tiger) and X-ray diffraction (Bruker D8 Advance, evaluated using Topas software) with Cu-Kalpharadiation, respectively. Microstructural and morphological analyses were performed using a scanning electron microscope (SEM; Hitachi SU3900).

Background-Technical Challenge with Performance Validation: Field Trial Results

In the present work, influence of changes in SEN design on the final flow dynamics particularly the flowdynamics of molten metal is being studied using an analytical tool called CFD (computational fluid dynamics). The flow velocity and temperature profile over the flow domain is optimized by regulating the SEN design. The final validation of modified design is being carried out by field trials at TATA-Meramandali. Details of initial assumptions and parameters considered to make a comparative analysis using CFD software is being described below. Picture (Figure - 1) below shows a schematic representation of initial 3D model used for CFD analysis.

Here flow of hot metal through SEN to top offunnel shaped copper mold, acts as an inlet.Whereas, the left and right end of Cu mold is represented as narrow walls.The front and back end of Cu mold is represented as broad walls respectively. The bottom of Cu mold where initial solidification of molten

metal takes place is shown as outlet. The top surface of molten metal is termed as meniscus.As shown in figure – 2 below, for



Mesh size for CFD analysis

CFD study tetrahedral dominated cells with prism layer on walls have been considered.

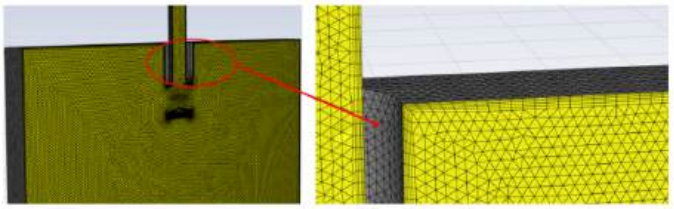


Fig -1. 3D model for CFD Analysis **Fig - 2**

Figure-3(a) and (b)shows the SEN with minimum and maximum dipping height of 230 mm and 330 mm from SEN bottom respectively. Mold flux height is shown as 90mm from mold top. The mold size considered for this flow simulation study is 1650mm * 230mm with a throughput of 5.3 Ton/minute.

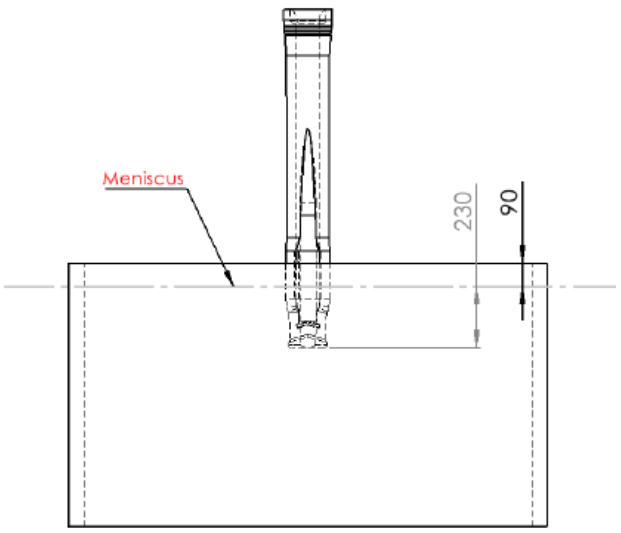


Fig-3(a). Minimum dipping condition of SEN.

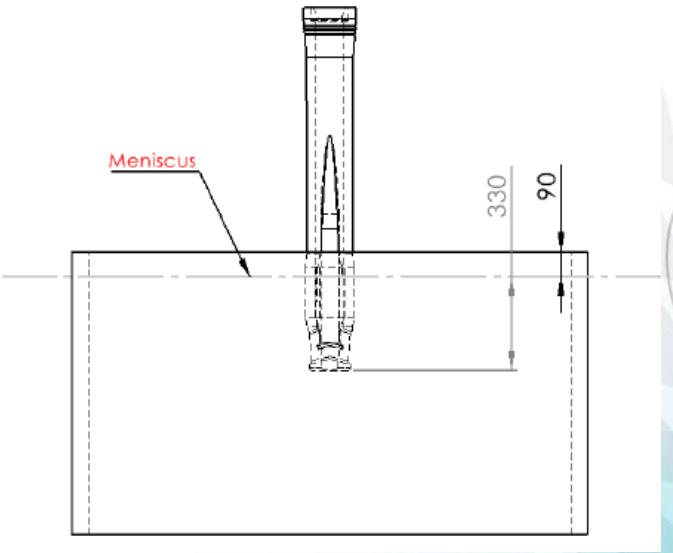


Fig-3(b). Maximum dipping condition of SEN

Figure 4 (a) and (b) below shows the velocity contour of both old and proposed new design SEN at center plain with 230mm immersion respectively. While the upward flow (primary flow) velocity have got reduced in proposed new design SEN (figure 4 (b)), the downward flow (secondary flow) velocity have got intensified with proposed new design SEN. However, the comparative velocity contour at center plan for both old and new design SEN at 330mm immersion[Figure 5 (a) and (b)] shows a significant difference in velocity plot.

While the old design (i.e. figure 5(a)) shows significant flow is in the upward direction with a major primary loop formation but the new proposed design (i.e. figure 5(b)) shows the secondary loop to be significantly intense with only a faint line forming the primary loop. This reduction in primary flow is assumed to reduce the surface turbulence and subsequently reducing slag line erosion of SEN, while maintaining the temperature at meniscus to facilitate mold flux melting.

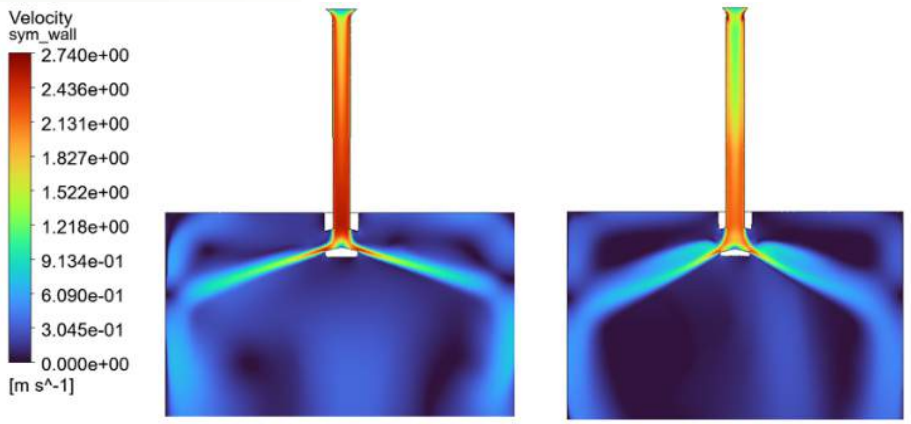


Fig. 4 (a) Old design with 230mm dipping **Fig. 4 (b) Proposed design with 230mm dipping**

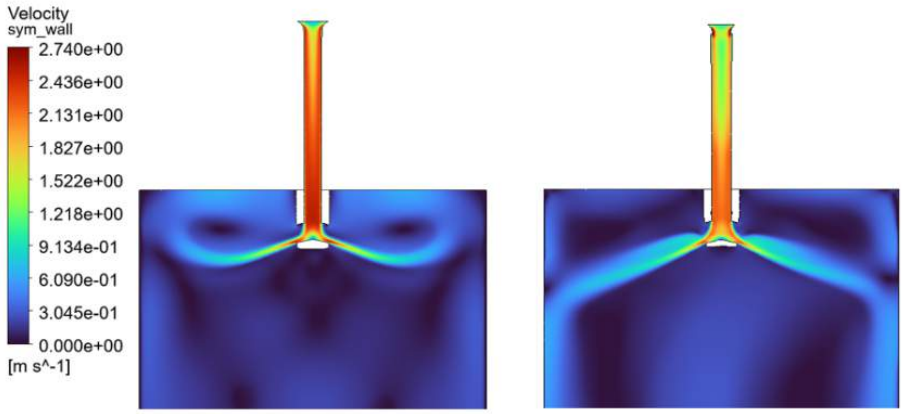
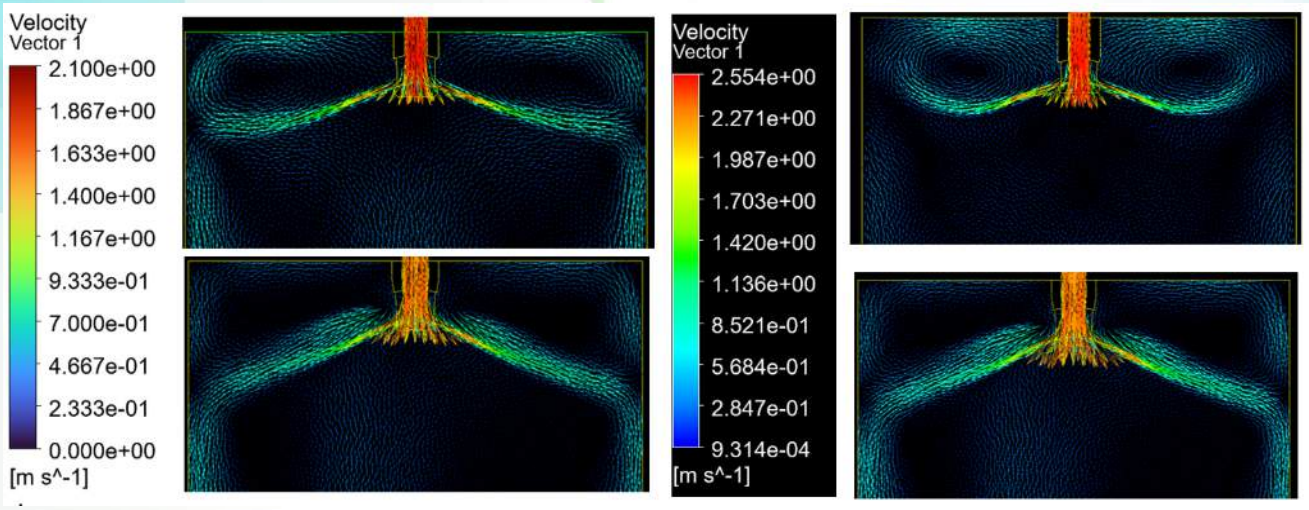


Fig. 5 (a) Old design with 330mm dipping. **Fig. 5 (b) Proposed design with 330mm dipping.**

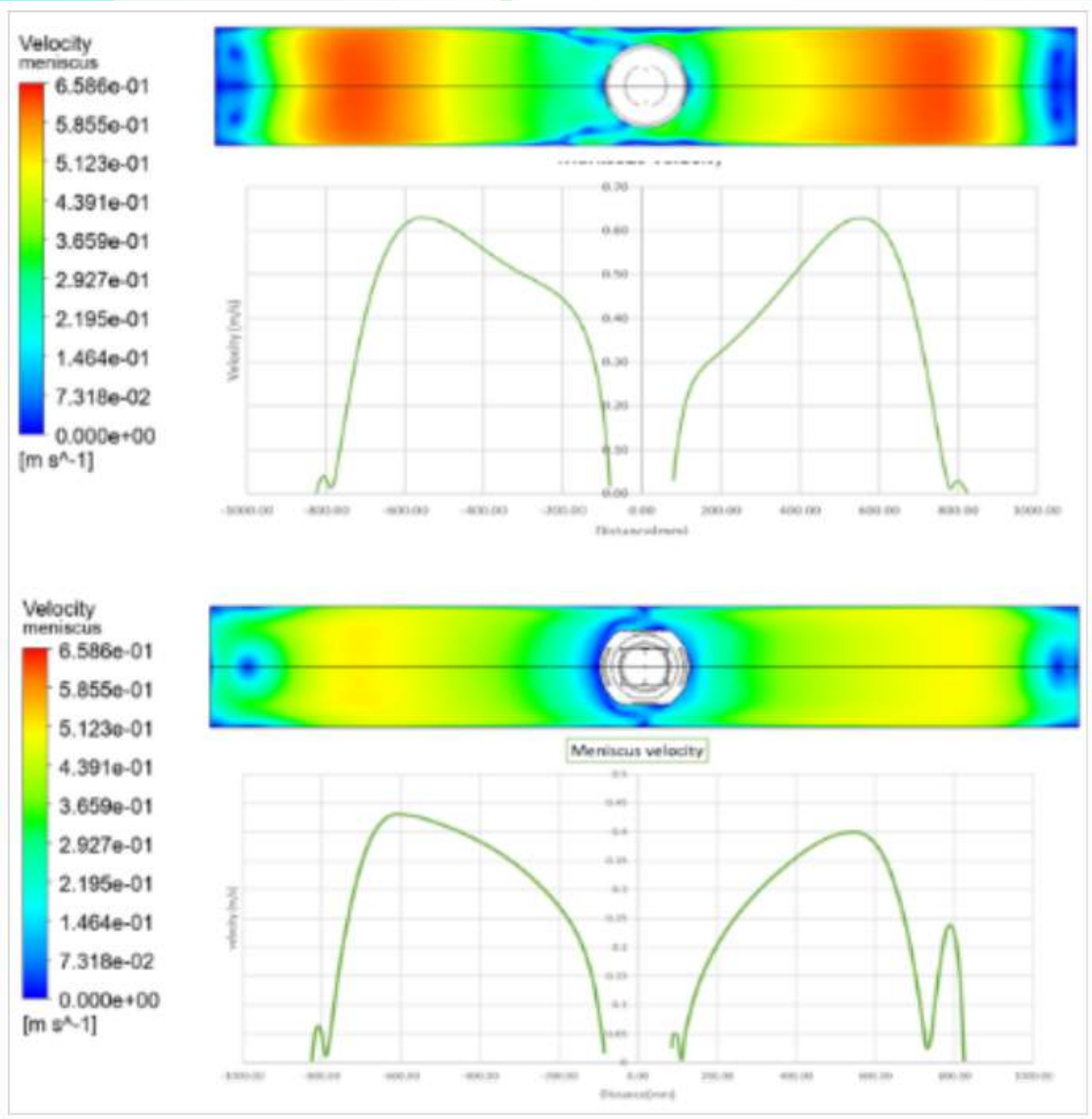
A similar trend was also observed for comparative velocity vector plot at center plane (y = 0). The velocity vector plot at 230mm immersion shows higher upward flow with existing SEN design. Whereas the proposed SEN design shows maximal flow is downward (secondary loop).

Same event got repeated even at 330mm immersion of SEN. The secondary flow being prominent with proposed design and a faint line of primary flow reaching the surface, good enough to melt the mold flux. While the velocity vector plot of existing design shows just the reverse with very little or no downward (secondary) flow.Besides the primary flow is even found to be not reaching the mold wall, resulting in a dead zone.



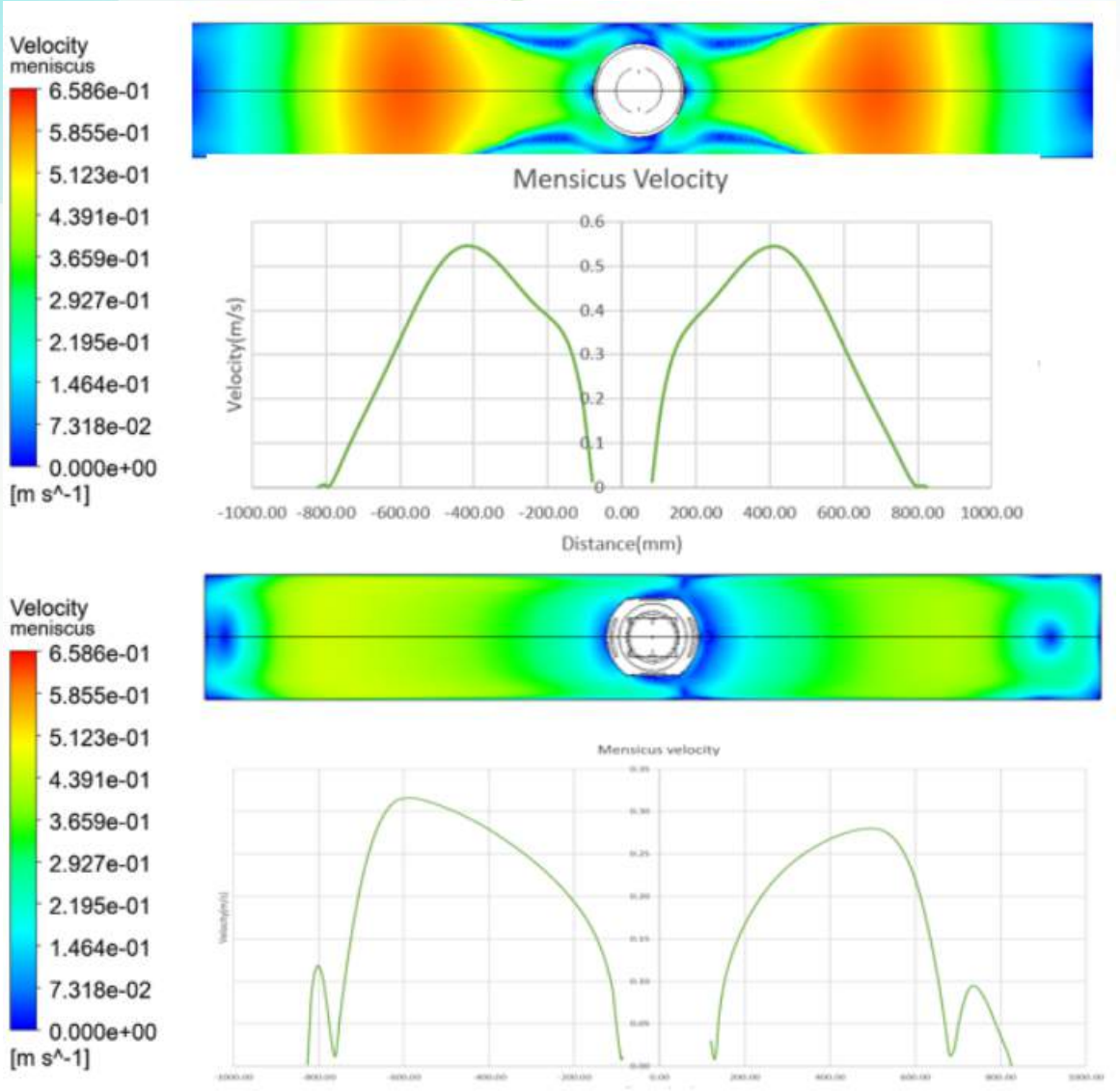
SEN Design	Immersion (mm)	Max Velocity (m/s)	Remark
Existing SEN	230	0.61	Max Velocity at Meniscus is in the higher range.
Proposed SEN	230	0.44	Max Velocity at Meniscus is in the optimize range.

Picture below shows the meniscus velocity at 230mm SEN immersion. While the velocity distribution looks symmetrical with both the old and new design, but the maximum meniscus velocity is found to be more with the old existing design rather than with the proposed one.The proposed SEN design significantly reduces the maximum meniscus velocity from 0.61 m/s to 0.44 m/s, representing an approximate 28% drop in peak velocity. Thus, suggesting lesser turbulence with proposed design.This reduction strongly indicates a more stable fluid flow and a lower risk of mold powder entrainment.



The figure below illustrates the meniscus velocity at a330 mmSEN immersion depth.Consistent with previous findings at 230mm immersion, the maximum meniscus velocity is higher with the existing design (0.56 m/s)than with the proposed design (0.33 m/s). However, the velocity distributionremains symmetricalfor both configurations, indicating reduced surface turbulence at both the maximum and minimum SEN dipping positions.

In continuous steel casting, a peak velocity of > 0.5 m/s is quite high and frequently leads to severe meniscus fluctuations, slag trapping, and subsequent surface defects on the cast product. Bringing this peak down with the proposed design brings the system much closer to the ideal operational window (typically targeted below 0.3–0.4 m/s), effectively mitigating turbulence-induced quality issues while maintaining a symmetrical flow profile and safeguarding the refractory from erosion related issue by enhancing refractory performance.



SEN Design	Immersion (mm)	Max Velocity (m/s)	Remark
Existing SEN	330	0.56	Max Velocity at Meniscus is in the higher range.
Proposed SEN	330	0.33	Max Velocity at Meniscus is in the optimize range.

Figure10 and Figure 11 below shows the temperature contour at central plane (y=0) along with meniscus temperature profile for 230mm and 330mm SEN dipping respectively.Figure 10 (a) shows the molten steel jet shoots aggressively upward and outward toward the surface, creating, uneven temperature "arms" near the top. This produces localized hotspots at left corner under the meniscus line while leaving the right-sidesurfacecomparatively cooler.Same was not observed for the new proposed design [i.e. Figure 10 (b)].The redesigned geometry redirects the flow more in the downward direction (secondary loop). Thus, delaying and narrowing the hot material spread, it shields the topmost surface layers from direct, concentrated thermal impact.

The bottom part of Figure 10(a) and (b) shows the temperature distribution at meniscus both for older SEN design and proposed SEN design respectively.Figure 10 (a) bottomshows the surface temperature distribution is comparatively uneven. Asymmetric thermal plumes reach out the

surface from the center nozzle, creating broad hot zones across the meniscus. Whereas proposed design, Figure.10 (b) bottom shows temperature profiles with a uniform, cooler background temperature profile. It successfully eliminates wide thermal variations across the surface area. Similar result was also seen with 330mm SEN dipping [i.e. Figure 11 (b)].

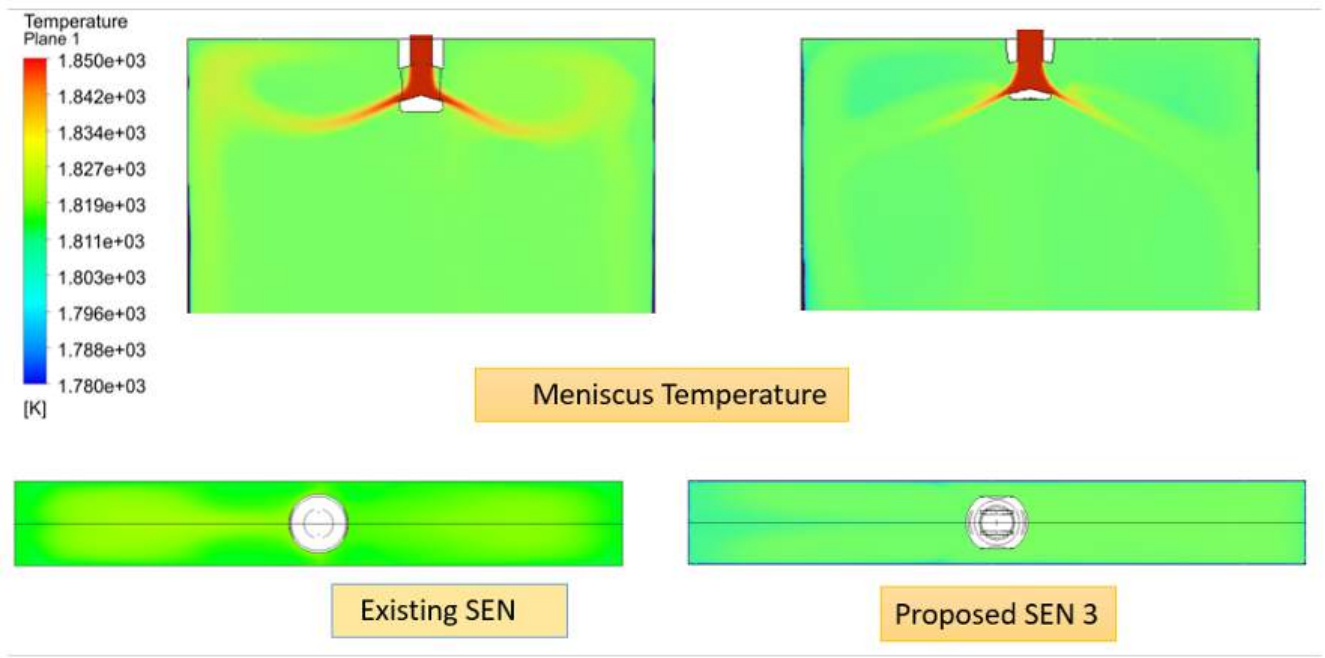


Fig. 10. Temperature profile with 230mm SEN dipping for (a) old and (b) proposed design.

Figure 11. shows the temperature profile for both the SEN at 330 mm dipping. Figure 11(a) shows asymmetrical temperature distribution within mold. The jets leaving the SEN exit ports travel deeply into the mold, forming narrow, circular paths generating a dead zone.Since thered projection is directed deeper into the strand, it fails to deliver adequate heat to the upper mold area. Thus, two distinct, cool upper recirculation loops appear as blue/green zones. Bottom part of figure 11 (a) shows the temperature profile at meniscus level to be nonuniform with a distinct variance in temperature. Whereas on the contrary the bottom part of figure 11 (b) shows a uniform temperature distribution.

3. Proposed SEN Final Performance (Right)

Figure 11 (b) features a flatter, widerport delivery with more uniform distribution of temperature, both inside and on the meniscus of mold. The hot steel is also found to be evenly distributed across the upper mold volume, eliminating the severe cool zones seen in the original design.

- **Meniscus Profile:** The top-down view (bottom right) reveals a significantly warmer and highly uniform meniscus profile. The surface maintains a steady, higher green thermal band (1.819×10^3 K), reducing variation across the mold width.

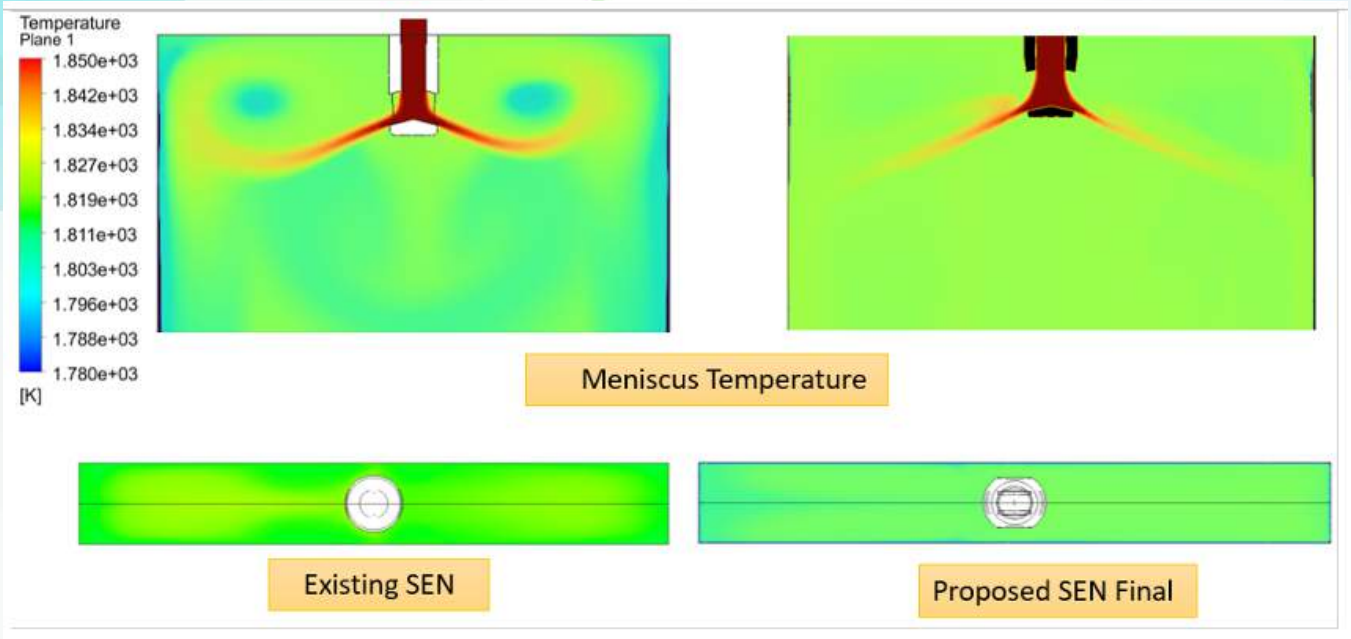


Fig. 11. Temperature profile with 330mm SEN dipping for (a) old and (b) proposed design.

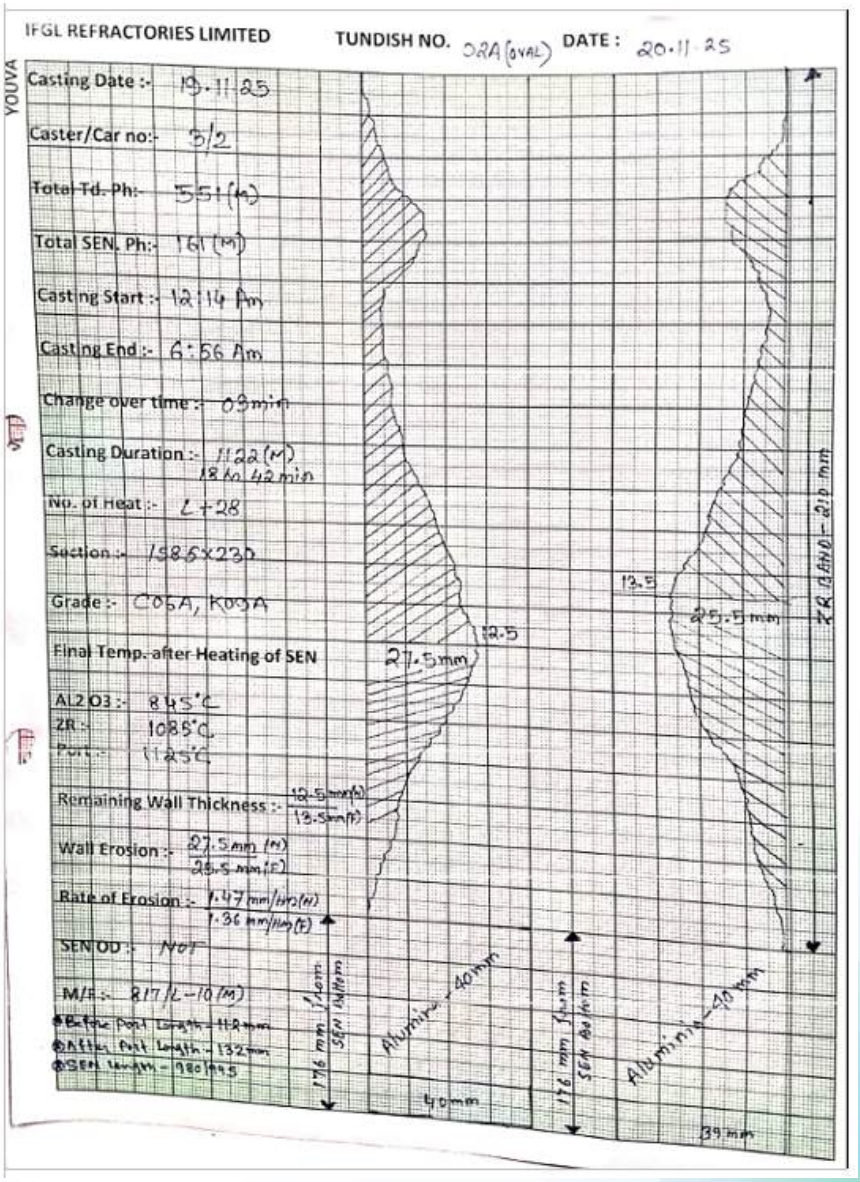


Fig. 12. Erosion Profile of proposed design SEN

The performance of the developed erosion-adaptive SEN was validated through field trials, with erosion-profile data captured as shown in Figure 12 across the casting campaign. The newly developed SEN demonstrated a substantially extended service life, sustaining a casting duration of approximately 18 h 42 min over L+28 heats. This performance was underpinned by a low and controlled rate of erosion, measured at approximately 0.0245 mm/min and 0.226 mm/min (equivalent to ~1.47 / 1.36 mm per hour), reflecting the enhanced resistance of the differentiated Zr erosion band to slag-line dissolution and mechanical wear.

Residual wall thickness measurements taken across the nozzle length ranged between approximately 12.5 mm and 13.5 mm, confirming that adequate structural margin was retained even after prolonged exposure to the casting environment. Notably, the erosion values recorded at different height zones (30 mm, 40 mm, and 50 mm regions) were found to be comparable rather than concentrated at a single critical section, indicating that the variable cross-sectional profile of the Zr band effectively compensated for the non-uniform erosion tendencies typically observed in conventional uniform-band designs. Furthermore, the trial was completed with satisfactory results, and tundish operating parameters, remained within stable and expected ranges throughout the campaign. These results collectively validate the design intent of achieving near-uniform wall-thickness retention and confirm the SEN's suitability for extended casting time and it'll give an opportunity to caster to run the tube-change-free casting operations.

Based on the erosion-profile data captured as shown in Figure 12 for this geometric developed SEN , here are five positive key performance indicators (KPI):

1. Extended campaign life achieved and its having more potential too .
2. Low and controlled erosion rate.
3. Adequate residual wall thickness remained favourable for higher sequence.
4. Near-uniform erosion profile along the Zr band length.
5. Stable performance under actual operating conditions.

CONCLUSION

1. Proposed SEN show good velocity & Temperature distribution across Meniscus. It may help to produce better and cleaner steel.
2. Looking at the velocity contour it is anticipated,the Slag line erosion of refractory due to abrasion may be reduced.
3. The above study has been validated by field trial showing substantial reduction in slag band erosion and subsequent improvement in SEN performance.

ACKNOWLEDGEMENT

The authors gratefully acknowledge the Management of IFGL Refractories Limited and the Management, Operations, and Refractory Departments of Tata Steel, Meramandali, for their valuable support and for providing the opportunity to carry out this study. The authors also thank both organizations for granting permission to present this paper at the seminar.

REFERENCE

- Tiwari, J.N., et al. "Effect of Nano-oxides and antioxidants on corrosion and erosion behaviour of submerged nozzle for longer sequence casting of steel," *UNITECR, Vol.* 3, pp. 516–519 (2009)
- Sen, A., Prasad, B., Sahu, J.K., Sahoo, N., Tiwari, J.N. "Development of sub entry nozzles having high corrosion and erosion resistance," *IREFCON, pp.* 204–209 (2012).
- "Studies & Optimisation of Various Types of Zirconia to Minimise Crack Propagation & Improve Corrosion & Erosion Resistance of Slag Band of Sub-Entry Nozzle, *"UNITECR Proceedings* (2013).
- Kim, H., et al. "Dissolution Behavior of Zirconia Refractories During Continuous Casting of Steel".
- Kuroda, T., Mizobe, A., Kurisu, J. "Flow optimization in the mould by port design improvement of submerged entry nozzle," *UNITECR* (2011).
- "Fracture Characteristics of Isostatic Pressed Submerged Entry Nozzle,"Key *Engineering Materials*, Vol. 290.

A CASE STUDY ON LANCE PERFORMANCE IMPROVEMENT AT TATA STEEL KALINGA NAGAR THROUGH CUSTOMER COLLABORATION

Samik Sarkar[1], Subhadip Ghosh[2], Sourav Ghosh[3], Saiyan Behera [4]

[1] Production, Calderys India Refractories Ltd., Katni, India
[2] Iron and Steel Sales, Calderys India Refractories Ltd., Jamshedpur Branch, India
[3] Refractory, Tata Steel KPO, Kalinga Nagar, India
[4] CFD Engineer, NPD ,Calderys India Refractories Ltd., Butibori, India

Corresponding author: samik.sarkar@calderys.com

Abstract

With the global growth in steel production, the demand for high-quality steel has increased significantly. Steel producers are therefore increasingly focused on optimizing manufacturing costs without compromising product quality, while simultaneously maximizing refractory service life. In this context, this paper presents a case study in which customer-driven value-added feedback enabled Calderys India Refractories Limited to improve the service life of a ladle furnace lance at Tata Steel's Kalinga Nagar site. Plant observations identified a localized region of accelerated refractory wear, which was subsequently analyzed in relation to the lance operating conditions and the hydrodynamic environment generated by argon injection. Based on the identified wear pattern, a targeted refractory modification was implemented at the critical region rather than uniformly along the lance. The modified design increased the lance campaign life to as high as 12 heats, exceeding 200 minutes of operation. The case demonstrates how customer–vendor collaboration, supported by plant-level observations and refractory engineering, can be translated into a targeted value-added solution for improving refractory performance and operational reliability.

Keywords: Refractory, LF lance, CFD, refractory wear, secondary steelmaking

1. Introduction

The steel industry is continuously working to improve product quality, reduce production costs, and maintain reliable plant operation. Steelmaking has evolved from conventional open-hearth and converter processes to secondary steelmaking, where temperature adjustment, alloying, homogenization, desulphurization, and inclusion control are carried out before casting. With increasing production and tighter quality requirements, the reliability of secondary steelmaking equipment and consumables has become increasingly important. India is following the same trend, with a target of around 300 MTPA crude steel capacity by 2030 under the National Steel Policy. Refractories play an important role in this system, as their performance affects process continuity, maintenance, productivity, and cost.

At Tata Steel Kalinga Nagar, Calderys India Refractories Limited supplies refractory lances for applications such as desulphurization, argon stirring, CAS-OB, and ladle furnace operations. While the desulphurization lances have achieved service lives above 1500 min, different applications have different operating conditions and performance challenges. Plant observations and customer feedback therefore provide important inputs for understanding wear and improving lance design. The present work began with customer feedback on the performance of an emergency ladle furnace lance and focuses on identifying the cause of its localized refractory wear and developing a practical modification. The ladle furnace (LF) is used for temperature adjustment, alloying, chemical homogenization, and bath conditioning before casting. Molten steel is generally maintained at 1550–1600 °C, while argon stirring helps in bath mixing, refining, and inclusion flotation. Gas injection creates

a rising plume that entrains molten steel and produces upward, lateral, and recirculating flow in the ladle [1]. Normally, this stirring is provided through bottom purge plugs. If a plug fails or becomes ineffective, a top-submerged lance can be used to provide argon stirring and continue the LF treatment.

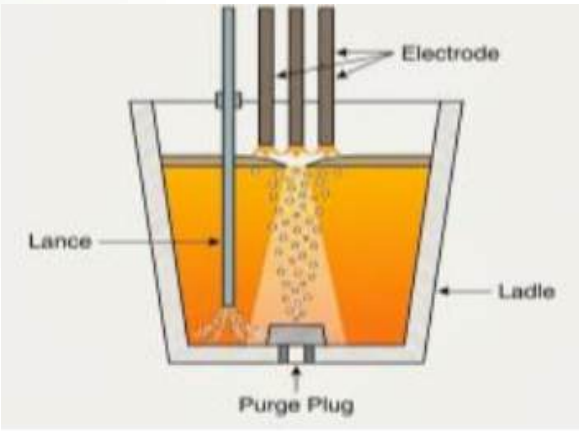


Fig 1: Basic Schematic of a ladle furnace

The lance operates under severe conditions, with its refractory exposed to molten steel at 1550–1600 °C as well as the gas–liquid flow generated by argon injection. Thermal exposure, chemical interaction with steel and slag, and flow-induced erosion can act simultaneously. Repeated heating and cooling can generate thermal stresses and cracks, while chemical interaction can weaken the refractory surface. Flowinduced erosion can then remove the weakened material. Both flow-induced erosion and reactioninduced corrosion have been reported as important refractory degradation mechanisms in ladle refining [2]. The lance geometry also affects its wear. Unlike a ladle wall, a submerged cylindrical lance is surrounded by molten steel around its circumference, so different sections can experience different flow conditions. Its inclined position further changes the exposure of each section to bath circulation and the argon plume. The resulting flow field can therefore vary significantly along the submerged length. In this study, plant observations, post-service wear measurements, analytical assessment, and CFD modelling were used to investigate the wear behavior of an emergency LF lance. The predicted flow behavior was then compared with the actual wear profile to understand the likely contribution of flow-induced erosion. Based on the combined findings, the lance design was modified by providing additional refractory thickness in the critical wear region to improve service life.

Wear phenomena in gas-stirred systems: insights from the literature

Refractory wear in gas-stirred steelmaking vessels is generally understood as the combined action of thermal, chemical, and hydrodynamic mechanisms rather than as independent processes acting in isolation. Inert-gas injection generates forced convection, turbulence, wall shear, and enhanced mass transfer, which can influence refractory erosion [4] .The rising plume entrains the surrounding molten steel and produces upward, lateral, and recirculating flow [1] bubble expansion during ascent, together with coalescence and breakup, further modifies the surrounding liquid flow, allowing the hydrodynamic influence of the plume to extend beyond its immediate path. In CFD-based wear studies, the erosion rate of the lining refractory is estimated from the wall shear stress and turbulence intensity, while the corrosion rate is assessed from the refractory diffusion coefficient and the slag property at high temperature with the most severe wear found where rapidly rising bubbles act on the wall [2] Chemical interaction additionally alters the refractory surface: dissolution of oxide refractories in

slag is controlled by mass transfer in the slag, and the rate decreases as the slag approaches refractory saturation [2]. Thermal stresses from repeated thermal cycling contribute to thermal spalling, with the time between heats having a significant effect [3].

The literature therefore predicts that wear is strongest where high turbulence, high wall shear, and intense mass transfer coincide typically in the vicinity of the rising plume and provides the basis for interpreting a non-uniform wear pattern on an immersed lance.

Lance wear rate measurement and CFD

Post-service measurements showed that the maximum refractory wear occurred at approximately 2300 mm from the lance top, around 300 mm below the bath surface and approximately 3000 mm from the main argon plume. After an average of three heats, corresponding to 60–70 min of cumulative operation, the original lance diameter of 200 mm reduced to 138– 149 mm at this location.

$$\Delta R = (D_o - D) / 2 \text{ ------(1)}$$

(where (D_o) is the original lance diameter and (D) is the diameter measured after service) The measurements from four used lances (Table 1) show a clear localized wear zone around 2300 mm. The diameter was comparatively unchanged above 2000 mm and partially recovered towards 2800–3300mm The corresponding apparent radial loss was approximately 0.39–0.50 mm/min, calculated over the available service duration. Since intermediate measurements were not available, this represents an average dimensional loss rather than an instantaneous wear rate.

Lance no	0	1200	2000	2300	2800	3300	5000
1	200	200	196	185	140	165	180
2	200	200	197	190	145	172	183
3	200	200	195	182	138	175	186
4	200	200	193	181	149	168	182

Table 1: Diameter in millimeter as observed in lances from top of casting zone till plume after use.



Fig : 2 Lance wear and bending tendency

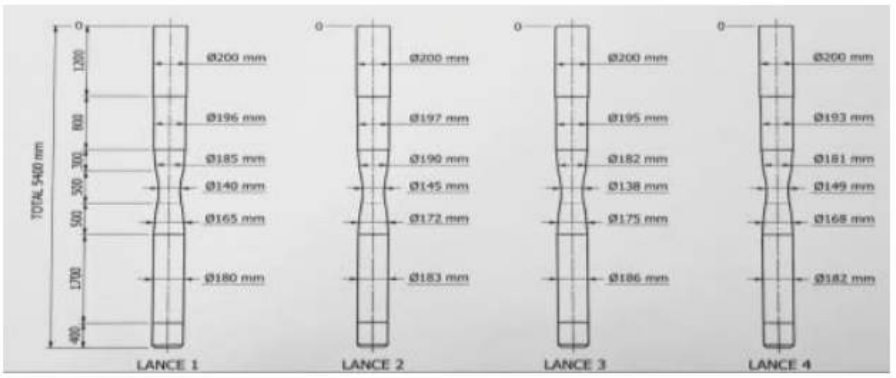


Fig : 3 Lance Erosion profile measurement

To investigate the origin of this localized wear, a three-dimensional CFD model was developed based on the actual ladle geometry and lance position. The steel–argon interaction was modelled using a Eulerian approach in ANSYS Fluent software, with molten steel treated as the continuous phase and argon as the dispersed phase.The standard k–ε turbulence model, with bubble-induced turbulence, was employed to describe the turbulent flow generated by argon injection. Velocity, wall shear stress, and turbulence intensity along the lance surface were evaluated to identify regions subjected to higher hydrodynamic loading. The simulation was carried isothermally at 1800 K. The fluid properties at 1800 K used for the analysis are listed in Table 2.

Property	Steel	Slag	Argon
Density, kg/m³	7020	3500	0.568
Viscosity, kg/(m·s)	0.006	0.030	2.125×10^{-5}

Table 2: Fluid properties at 1800K

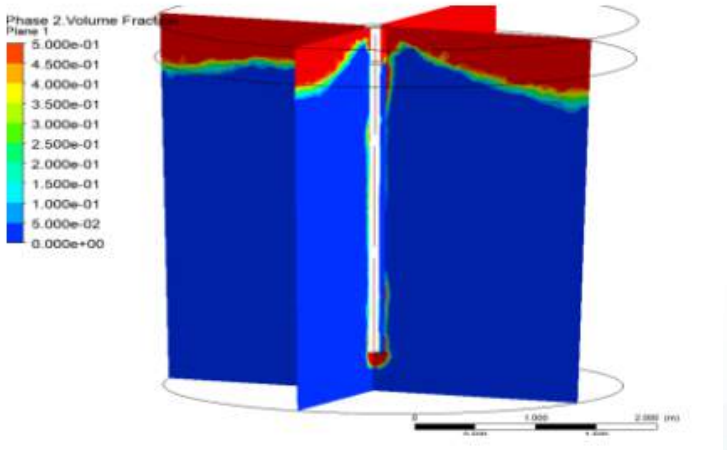


Fig : 4 Volume fraction Contour of argon gas

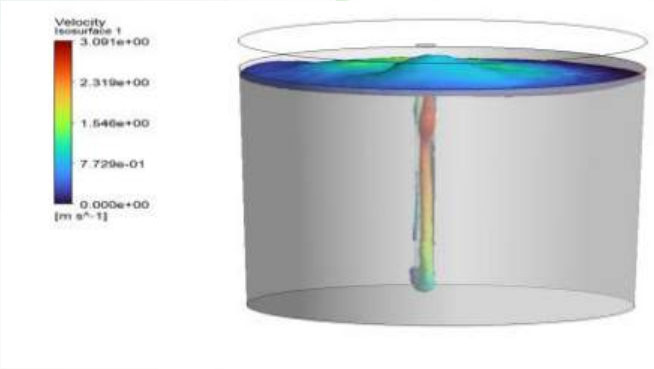


Fig : 5 Iso-surface of argon plumes

The simulations showed that the argon plume established a circulation pattern extending well beyond the immediate plume region. The lance intersected this circulating flow, resulting in increased wall shear and turbulence along the experimentally identified wear zone. The location of the predicted high-flow-intensity region was consistent with the measured reduction in lance diameter, while regions experiencing lower flow intensity showed comparatively lower wear. This agreement between the simulated flow field and the measured wear profile supports flow-induced erosion as a significant contributor to the localized refractory degradation.

Implementation and results

Based on the measured wear profile and CFD results, the refractory design was modified locally rather than changing the refractory composition or redesigning the complete lance. A change in composition would require additional development time and plant trials to stabilize the new formulation. After discussion with Tata Steel, t was decided to address the identified high-wear positions by increasing the refractory diameter from the original 200 mm to 230 mm, providing an additional 15 mm radial sacrificial allowance. The modified section was extended from approximately 2300 to 3300 mm from the lance top, covering the region where the highest refractory wear and elevated flow-induced loading were observed.



Fig5: Pre Implementation lance life

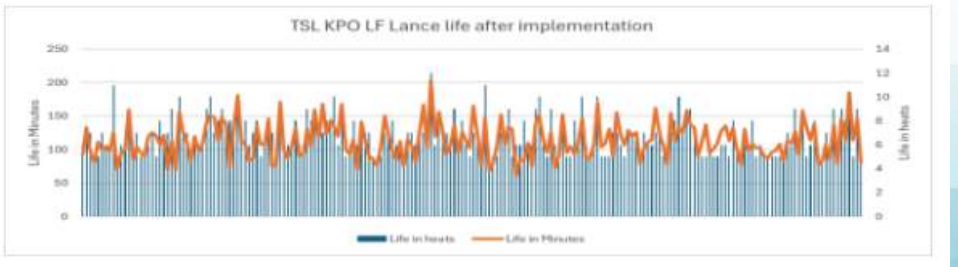


Fig6: Lance life after implementation

The modified lance design was subsequently evaluated through plant trials, and the performance data were analyzed in terms of service life in heats and cumulative operating time. The recorded lance life ranged from 5 to 12 heats, with operating times ranging from 61 to 203 min. The overall average was 6.73 heats and 113.3 min.

Conclusion

1. The emergency LF lance exhibited localized refractory wear, with maximum degradation around 2300–2800 mm from the lance top. Post-service measurements showed a diameter reduction from 200 mm to 138–149 mm after approximately 3 heats (60–70 min).

2. CFD analysis showed higher flow intensity, wall shear stress and turbulence in the region corresponding to the measured wear zone, indicating flow-induced erosion as a significant contributor to the observed degradation, along with thermal and chemical effects.

3. Based on the localized wear pattern, the refractory diameter was increased from 200 to 230 mm over the 2300–3300 mm section, providing an additional 15 mm radial sacrificial allowance while retaining the existing refractory composition and lance construction.

4. Plant validation of the modified design showed 5–12 heats and 61–203 min of service, with an average of 6.73 heats and 113.3 min, compared with the previous average of approximately 4.5 heats.

5. Based on future performance and customer feedback, further optimization may be attempted for better resolution.

6. The study demonstrates that field-wear measurements combined with CFD analysis with customer collaboration can guide targeted refractory design modifications and improve lance service life.

References

[1] Mazumdar, D., and Guthrie, R. I. L., "The Physical and Mathematical Modelling of Gas Stirred Ladle Systems," ISIJ International, 35(1), 1– 20, 1995. DOI: 10.2355/isijinternational.35.1.1.

[2] Wang, Q., Liu, C., Pan, L., Zhu, H., Li, G., and Wang, Q., "Numerical Understanding on Refractory Flow-Induced Erosion and ReactionInduced Corrosion Patterns in Ladle Refining Process," Metallurgical and Materials Transactions B, 53, 1617–1630, 2022.

[3] Johansen, Stein & Løvfall, Bjørn & Duran, Tamara. (2024). A pragmatical physics-based model for predicting ladle lifetime. Journal of the Southern African Institute of Mining and Metallurgy. 124. 93-109. 10.17159/2411-9717/2680/2024.

[4] Rajeev Singh, Dipak Mazumdar, A. K. Ray, Mathematical Modeling and Validation of Wall Shear Stress in Gas Stirred Vessels, ISIJ International, 2008, Volume 48, Issue 7, Pages 1033-1035.

STUDY ON THE INFLUENCE OF PROCESS PARAMETERS ON STEEL TEEMING LADLE REFRACTORY PERFORMANCE IN SECONDARY STEEL MAKING PROCESS USING ANALYTICAL TOOLS

Author: Bipin Kumar Singh, Goutam Pal, Raja Mohan Singh, Amitava Mukhopadhyay, Atul Yadav, Mallikarjuna Math

Abstract

In secondary steelmaking, refractory-lined vessel performance is critically influenced by operating parameters such as tap bath oxygen concentration, aluminium de-oxidation practice, sulphur removal, argon purging behaviour, and purging timing. These parameters govern steel cleanliness as well as the chemical, mechanical, and thermo-mechanical degradation mechanisms of refractory linings. Higher tap oxygen levels promote the formation of alumina (Al_2O_3) inclusions, which may adhere to refractory surfaces and contribute to nozzle clogging, inclusion build-up, and localized refractory wear. Aluminium addition, widely used for de-oxidation, further influences inclusion chemistry by forming solid alumina and reacting with MgO-based refractories to generate spinel ($MgO{\cdot}Al_2O_3$) phases. This transformation can cause volume expansion, internal stress development, cracking, and spalling. Sulphur removal also add on process time and purging. Argon purging supports inclusion flotation, bath homogenization, and slag-metal reactions; however, excessive or poorly controlled purging can induce turbulence, localized erosion, and wear near purging plugs and slag-line regions. Optimized purging during alloying enhances inclusion removal, while excessive late-stage purging may form slag-eye openings, promote atmospheric re-oxidation, and reduce ladle refractory integrity.

Keywords: Collaborative, Operational Parameters, Steel Teeming Ladle Refractory, Secondary Metallurgy, Analytical Tools

Introduction

Secondary steelmaking plays a crucial role in modern steel making by enabling precise control of chemistry, temperature, and cleanliness. During this process, molten steel is treated in refractory-lined vessels termed as ladles, in which various operations like de-oxidation, sulphur removal, alloying, inclusion modification, and Argon gas stirring are performed. The performance and service life of the refractory lining are very crucial as it is continuously exposed to severe chemical, thermal, and thermo-mechanical stresses that may lead to refractory erosion/degradation.

Tap bath oxygen ppm is one of the primary factors determining the extent of de-oxidation reactions (exothermic) in the ladle & that generate the excessive localized energy impact on the refractory health. The elevated dissolved oxygen levels promote the formation of Al_2O_3 inclusions following Al ingot addition. These alumina inclusions are initially dispersed throughout the molten steel bath and are subsequently removed through argon stirring, which facilitates their flotation toward the slag layer.

Argon purging is essential for achieving the desired steel cleanliness; however, incomplete removal may result in the accumulation of solid alumina particles within the steel. To further modify and control the morphology of these inclusions, calcium treatment is carried out through CaFe wire injection. Calcium reacts with solid alumina inclusions to form calcium aluminate, which exhibit improved floatability and also reduce nozzle clogging tendency also to promote bath homogenization, temperature equalization, inclusion flotation, and slag-metal reactions. Properly controlled argon stirring enhances metallurgical efficiency and facilitates the removal of

non-metallic inclusions from the molten steel. Other hand the excessive/high purging will induce severe bath turbulence that accelerates zonal refractory erosion, particularly in regions surrounding the purging plug, metal zone, transition and slag line. Such conditions can significantly impact on refractory service life and lead to ladle availability in day-to-day production or productivity.

Objective

The objective of this study is to evaluate the influence of key secondary steelmaking parameters on steel ladle refractory performance. Operational data like, tap-bath oxygen ppm, aluminium consumption, sulphur removal, argon consumption, process time, and Ca-Fe wire addition are analysed using analytical tool, Microsoft Power BI. The study aims to identify process deviations, find out correlations among these variables, and determine their potential association with refractory wear/erosions and campaign life. The findings are intended to support improved process control, optimization of ladle metallurgy practices, and enhancement of refractory lining life without compromising standard operating practices, steel cleanliness and quality.

Data Collection

Eight months of Level 2 process data, from August 2025 to March 2026, are collected. The dataset contained tap-bath oxygen ppm, aluminium consumption, argon consumption, process time, CaFe wire addition, sulphur removal and other operational parameters. The datas are filtered, cleaned, and organized according to the study requirements before being imported into Microsoft Power BI.

Heat	Route	Start	End	Process Time	Al Bar	Plug 1 Ar	Plug 2 Ar	Stir Ar
AB3033XZ	SH3;LF3;LF1;CCM1	31.07.2025 21:18	31.07.2025 22:30	77.9	18	16	17	33
CD2032EF	SH2;LF2;LF5;CCM3	31.07.2025 22:17	31.07.2025 23:59	122.7	1	7	8	15
GH4033IJI	SH4;LF4;CCM2	31.07.2025 22:20	31.07.2025 23:20	88.5	18	32	39	71
MN4033IP	SH3;LF3;CCM2	31.07.2025 22:25	01.08.2025 00:07	107.8	21	19	19	37
RS4033PL	SH4;LF4;LF5;CCM3	31.07.2025 23:24	01.08.2025 01:04	113.9	4	13	14	28

Table – 1: Raw data level - 2

After cleaning and filtering, the datasets are imported into Microsoft Power BI to verify correlations among tap bath oxygen ppm, Al consumption, Ar consumption, Sulphur removal, total process time, and Ca-Fe wire addition, with erosion rate of slag zone refractory.

Results

Following graphs & tables are obtained with Microsoft Power BI tools.

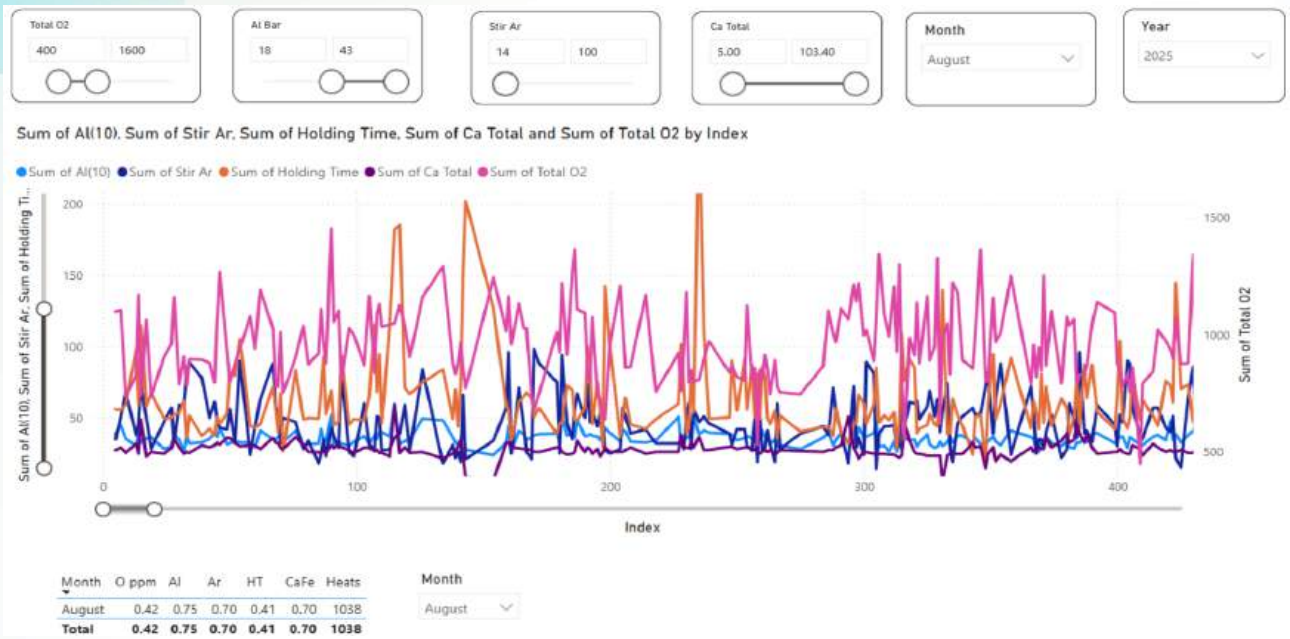


Figure-1: Correlation visualization of Aug 25

Month	O ppm > 950		AL > 3.2		Stir Ar > 50		Process Time > 66		CaFe > 25		LF IN_S > 0.02		LF IN_S > 0.02; PT >66		Life	ER SZ
Aug 2025	435	42%	264	25%	736	71%	414	40%	702	68%	820	79%	331	32%	60	2.62
Sep 2025	392	37%	324	31%	773	73%	463	44%	502	47%	862	81%	372	35%	57	2.82
Oct 2025	333	34%	421	42%	699	70%	431	43%	505	51%	820	83%	350	35%	57	2.90
Nov 2025	344	35%	417	43%	670	69%	397	41%	333	34%	777	80%	320	33%	57	2.97
Dec 2025	401	33%	400	33%	841	69%	428	35%	361	30%	946	78%	327	27%	63	2.62
Jan 2026	300	56%	184	34%	319	60%	218	41%	200	37%	297	56%	119	22%	63	2.59
Feb 2026	289	51%	277	49%	346	61%	173	31%	145	26%	376	67%	114	20%	63	2.58
Mar 2026	321	57%	259	46%	392	69%	157	28%	202	20%	515	91%	137	24%	65	2.44
Apr 2026	299	59%	220	43%	316	62%	177	35%	368	72%	444	87%	151	30%	63	2.56

Table – 2: Deviation of parameters (Heat Counts with threshold values)

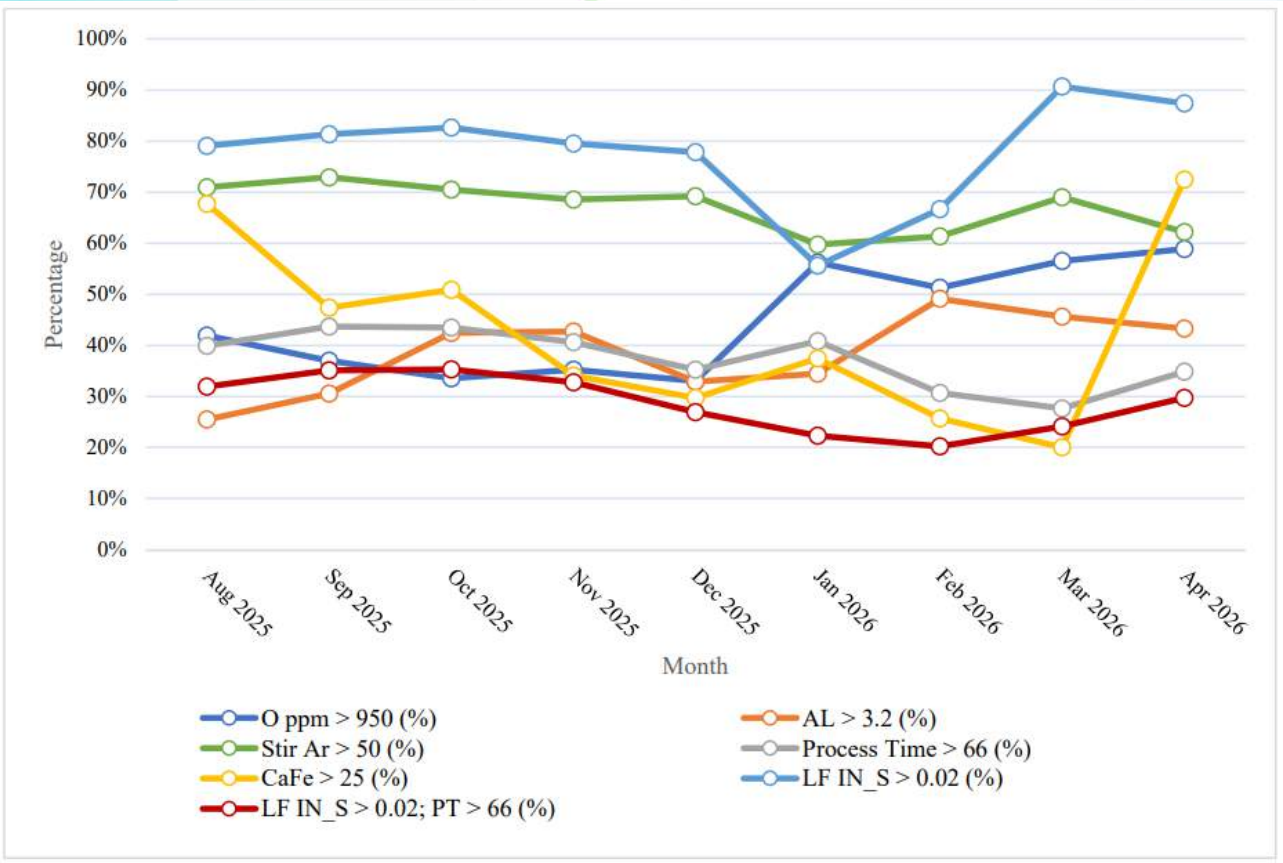


Figure-2: Graph of deviated parameters

Discussions & Correlations

From the table and graph it is observed that when the dissolved oxygen concentration exceeded 950 ppm, aluminium addition was not at par with the oxygen ppm level, indicating that the oxygen– aluminium relationship was influenced by additional process variables rather than only controlled by the nominal deoxidation requirement. In contrast, argon consumption, LF treatment time, and sulphur concentrations above 0.02% showed positive correlations with increased slag zone erosion rate. This pattern suggests that high-sulphur heats were associated with longer and more intensive refining conditions, during which extended argon stirring and increased process duration may have promoted reoxidation, slag–metal interaction, and additional oxygen transfer. From refractory perspective, these conditions are relevant because prolonged high-temperature exposure and gas stirring can increase the time available for MgO–C oxidation, slag penetration and mechanical erosion. Higher O ppm can be a reason of removal of carbon from MgO–C bricks increases porosity and reduces resistance to slag infiltration, while purging turbulence can produce localized wear near gas-entry regions. Therefore, the observed association between oxygen, argon consumption, treatment time, and sulphur should be interpreted as a combined process-exposure effect rather than as evidence that oxygen ppm alone caused the refractory degradation. The effect should be verified by comparing brick residual thickness, decarburized-layer depth, slag-infiltration depth, and wear location across heats with oxygen concentrations below and above 950 ppm, while adjusting for treatment time, argon flow, slag chemistry and temperature.

Further analysis with Advanced Excel tool is done for correlation of sulphur removal and tap O ppm with erosion rate of slag zone.

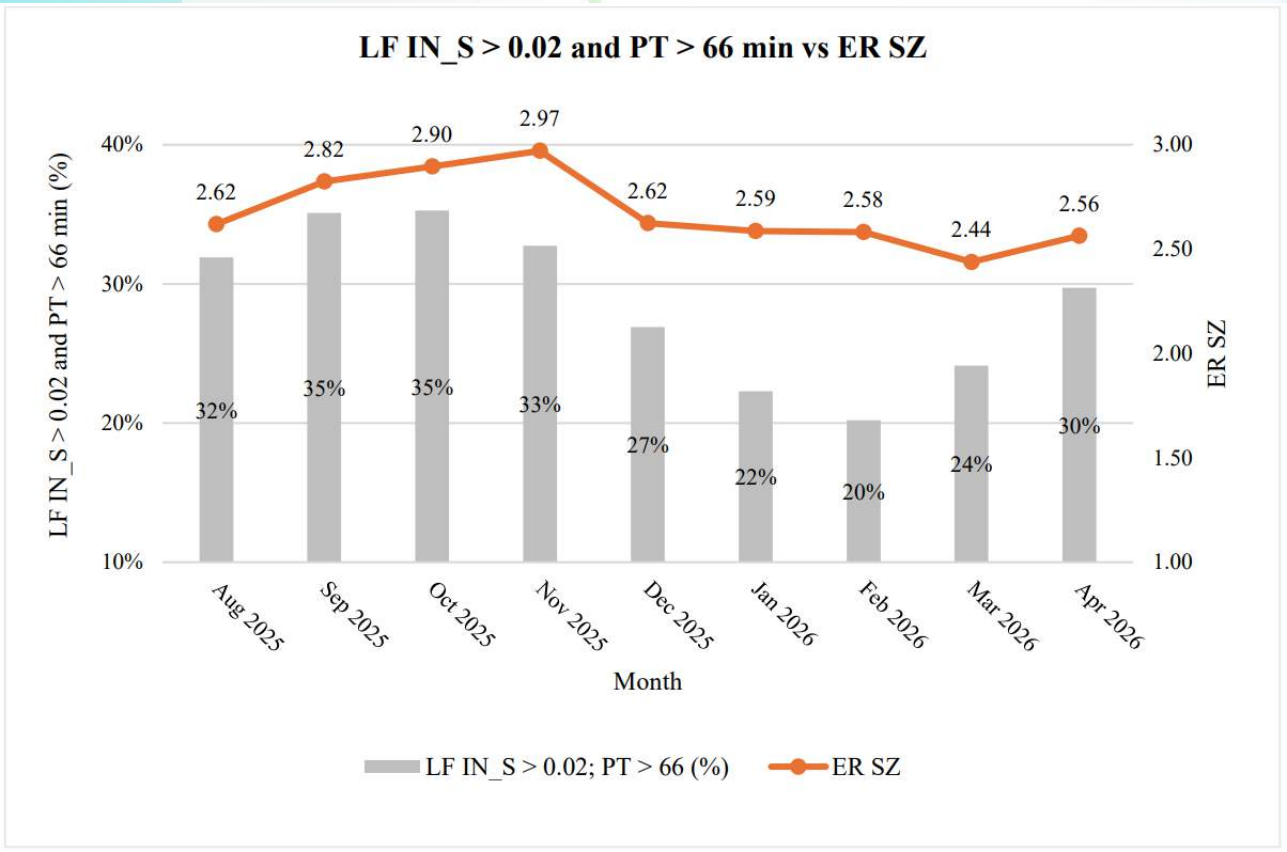


Figure – 3: Correlation of Sulphur removal with Slag Zone Erosion Rate

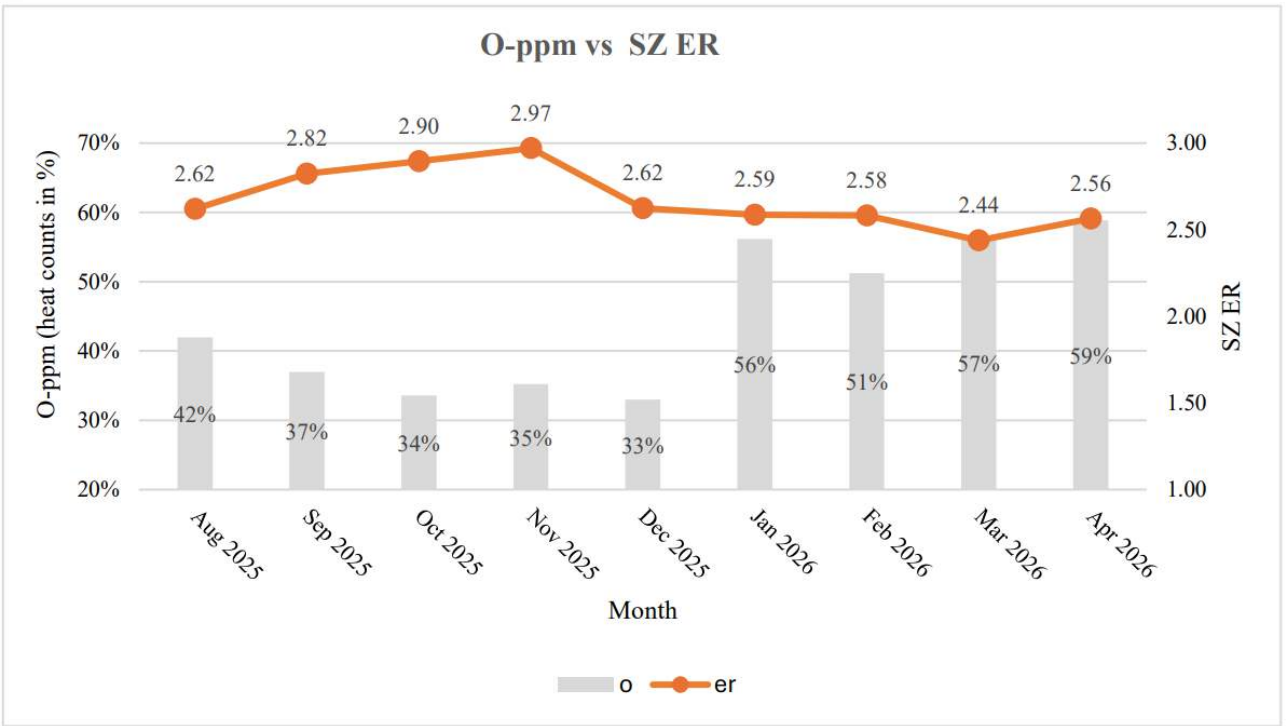


Figure – 4: Correlation of O-ppm with Slag Zone Erosion Rate

Figure-3 shows that when the incoming sulphur content is greater than 0.02 for heats simultaneously erosion rate is higher. And as the sulphur content greater than 0.02 is lesser consequently erosion rate comes down. This clearly depicts the impact of sulphur content and how it affects the refractory of steel teeming ladle.

Figure-4 does not show the trend of more slag zone erosion rate when O ppm is higher than 950.

Conclusions

The present study establishes that steelmaking process conditions have a significant influence on steel teeming ladle refractory performance. Analysis of Level-2 process data indicates that tap-bath oxygen, aluminium consumption, sulphur-removal requirements, argon purging, and treatment time collectively affect the refractory degradation in different zones.

Higher oxygen potential and aluminium addition can promote oxide formation and refractory–slag interactions, while intensive or prolonged argon purging may increase hydrodynamic erosion, particularly in the slag-line and purging-plug regions. Higher sulphur-removal requirements were also associated with increased process intensity and slag-zone erosion.

The study therefore highlights the importance of integrated control of oxygen, deoxidation, sulphur removal, argon-purging practice, and treatment duration for improving refractory campaign life without compromising steel cleanliness and process productivity. The identified trends provide a basis for establishing an optimized operating window and developing predictive refractory-performance models using advanced statistical and data-analytics techniques.

Further Study

Further study should focus on optimizing operational parameters affecting ladle refractory life, particularly:

- Optimization of tap oxygen level to minimize re-oxidation and alumina formation.
- Standardization of aluminium addition quantity, sequence, and timing.
- Optimization of argon flow rate, pressure, and purging duration for effective inclusion flotation with minimum refractory erosion.
- Establishment of optimum purging timing during alloying and before casting.
- Control of slag basicity, FeO/MnO content, and slag carryover to minimize chemical corrosion.
- Correlation of steel temperature, holding time, and ladle turnaround time with refractory wear.
- Monitoring slag-line and purging-plug wear against actual operating conditions.
- Development of an operational control window linking oxygen, aluminium, sulphur, argon, slag, temperature, and holding time with ladle refractory life.

The objective is to establish standard operating practices (SOPs) that maximize refractory campaign life without compromising steel cleanliness and productivity

Acknowledgement

The authors gratefully acknowledge the Management of JSW Dolvi Works for providing the necessary facilities, resources, and institutional support for this study. The authors also sincerely acknowledge the valuable technical contributions and cooperation of the SMS, Refractory, Process, and Quality teams in providing operational inputs and supporting data collection and analysis.

References

1. Nag, M., Agrawal, T., Nag, B., Singh, B., & Biswas, S. (2019). Study and post mortem analysis of steel ladle porous plug to improve bottom purging efficiency for cleaner steel. Engineering Failure Analysis, 101, 447–455. DOI: 10.1016/j.engfailanal.2019.03.017. — Highly relevant to argon flow, purging practice, plug degradation and thermomechanical failure.

2. Tabatabaie-Hedeshi, S. M., Bavand-vandchali, M., & Naghizadeh, R. (2020). Characterization and postmortem analysis of Al_2O_3-MgO-C refractories used in steelmaking ladle furnaces. Engineering Failure Analysis, 116, 104697. DOI: 10.1016/j.engfailanal.2020.104697. — Directly supports post-mortem evaluation, spinel formation, slag corrosion and refractory degradation mechanisms.

3. Leite, F. C., Luz, A. P., & Pandolfelli, V. C. Characteristics and wearing mechanisms of MgO-C refractories for steel ladle slag line. — Useful for MgO-C slag-line wear, oxidation and corrosion mechanisms.

4. Bhattacharyya, A., Roy, S., & Sarkar, R. (2026). Al_2O_3-MgO-C Refractory for Iron & Steel Industry – An Overview. Transactions of the Indian Institute of Metals, 79. DOI: 10.1007/s12666-026-03820-1. — Useful as a recent review covering AMC refractories, in-situ spinel formation, volume expansion and thermo-mechanical behaviour.

DEVELOPMENT OF MINI-AUTOMATIC FLUX FEEDER FOR SMALL AND MEDIUM STEEL PLANTS

An intelligent, accurate and cost-effective solution for controlled mould-flux feeding

Dhananjoy Ghosh, Shantanu Deshpande, Chandan Sharma, Deep Mehta

Department of Technical, Operation, Sales and Service, Calderys Steelcasting India Pvt. Ltd.

Author: dhananjoy.ghosh@calderys.com

Abstract

The role of mould flux in continuous casting is critical for lubrication, heat transfer, protection of the steel surface and stable mould–strand conditions. Improper or inconsistent flux feeding can contribute to longitudinal, transverse and star cracking, gas or slag entrapment, deep oscillation marks and sticker-type breakouts. Manual feeding is operator dependent and may result in variation in quantity, timing and distribution. This paper presents the development of a compact Mini-Automatic Flux Feeder (Mini-AFF) for small and medium steel plants. The system combines controlled feeding with flow-sensor feedback, load-cell based material control and an optional flux preheating arrangement. The development focuses on accurate and repeatable delivery, lower risk of over- or underfeeding, reduced routine operator intervention, cost-effective automation and more resource-efficient operation. The paper also documents field application experience in which a stickering issue at Tata Steel KPO was reported as solved following AFF implementation in 2024 and a cracking issue at JSPL Raigarh was reported as solved following AFF implementation in 2025.

Keywords: continuous casting; mould flux; automatic flux feeding; Mini-AFF; flow sensor; load cell; pre-heating; powder consumption.

1. Introduction

Mould flux is a functional consumable in continuous casting. Its behaviour at the mould–strand interface influences lubrication and heat transfer, while the flux layer also provides protection of the liquid steel surface. Consequently, stable and adequate powder coverage is an important part of casting practice. Literature identifies mould-flux properties and casting conditions as important factors in surface quality, oscillation-mark formation, flux consumption and breakout-related behaviour [1–4]. In small and medium steel plants, however, mould powder is often added manually. Manual addition requires operator judgement and repeated intervention near the hot casting area. Variability in feeding can make it difficult to maintain a repeatable operating condition.

The objective of the Mini-AFF development is therefore to provide a compact automatic solution that measures and controls flux delivery while remaining practical for smaller installations. The design emphasizes accurate feeding, feedback, maintainability, operator safety and economical deployment.

2. Mini-Automatic Flux Feeder: Development Concept

The Mini-AFF is designed as a compact automatic mould-flux feeding unit. The basic process consists of controlled flux storage, optional pre-heating, material-weight monitoring, controlled conveying, flow measurement and delivery through a mould-powder distributor. The combination of measurement and control changes the feeding task from intermittent manual addition to a repeatable process operation.



Figure 1. Mini-Automatic Flux Feeder (Mini-AFF) developed for compact and controlled mould-flux feeding.

3. Technical Features and Engineering Functions

3.1 Automatic feeding in place of manual feeding

A defined feed-rate set point is used to control powder delivery. This reduces dependence on operator timing and judgement and improves repeatability between heats.

3.2 Accuracy through flow-sensor feedback

The actual delivery rate is monitored and compared with the selected feed-rate requirement. Feedback enables correction of deviations caused by changing conveying conditions or powder behaviour.

3.3 Flux pre-heating system

Where required by the selected flux and plant practice, controlled pre-heating can improve powder handling and reduce the influence of ambient moisture. Heating temperature must be selected according to flux specifications and safe operating limits.

3.4 Load-cell control

Load-cell measurement provides feeder inventory information and supports material-balance verification. It can also provide low-level indication and help compare material consumption with commanded feeding.

3.5 Consistent feeding with lower powder consumption

Stable feeding reduces the tendency for over- and under-feeding. The aim is not a fixed universal consumption value, but repeatable delivery of the required quantity for the selected casting condition.

3.6 Operator health and working-condition improvement

Automatic feeding reduces routine manual powder handling and the frequency of operator intervention near the hot mould area, supporting a safer and more ergonomic work environment.

3.7 Cost-effective automation

The compact architecture targets small and medium plants where a large automation package may not be economically suitable. Modular components also support easier maintenance.

3.8 Eco-friendly and resource-efficient operation

Better control can reduce unnecessary powder use and associated material handling. The resulting environmental benefit should be quantified using actual plant consumption and rejection data.

Parameter	Manual Flux Feeding	Mini-Automatic Flux Feeder
Feed-rate control	Operator dependent	Set-point based with feedback
Repeatability	Variable	Controlled and repeatable
Process feedback	Primarily visual	Flow sensor + load-cell information
Powder use	Risk of over/under-feeding	Better opportunity for optimized consumption
Operator intervention	Frequent	Reduced routine intervention
Working condition	Exposure to heat/dust and manual handling	Improved operator working condition
Automation cost	Low initial equipment cost	Higher initial investment, lower process dependence

Table 1. Functional comparison of manual and Mini-AFF mould-flux feeding

5. Mould-Powder Distributor and Controlled Delivery

The distributor is the final material-delivery element between the feeder and the mould. Its purpose is to transfer the controlled flux stream into the required mould region with a stable and repeatable distribution pattern. Distributor geometry, installation position and operating practice must be selected for the specific mould and casting arrangement.

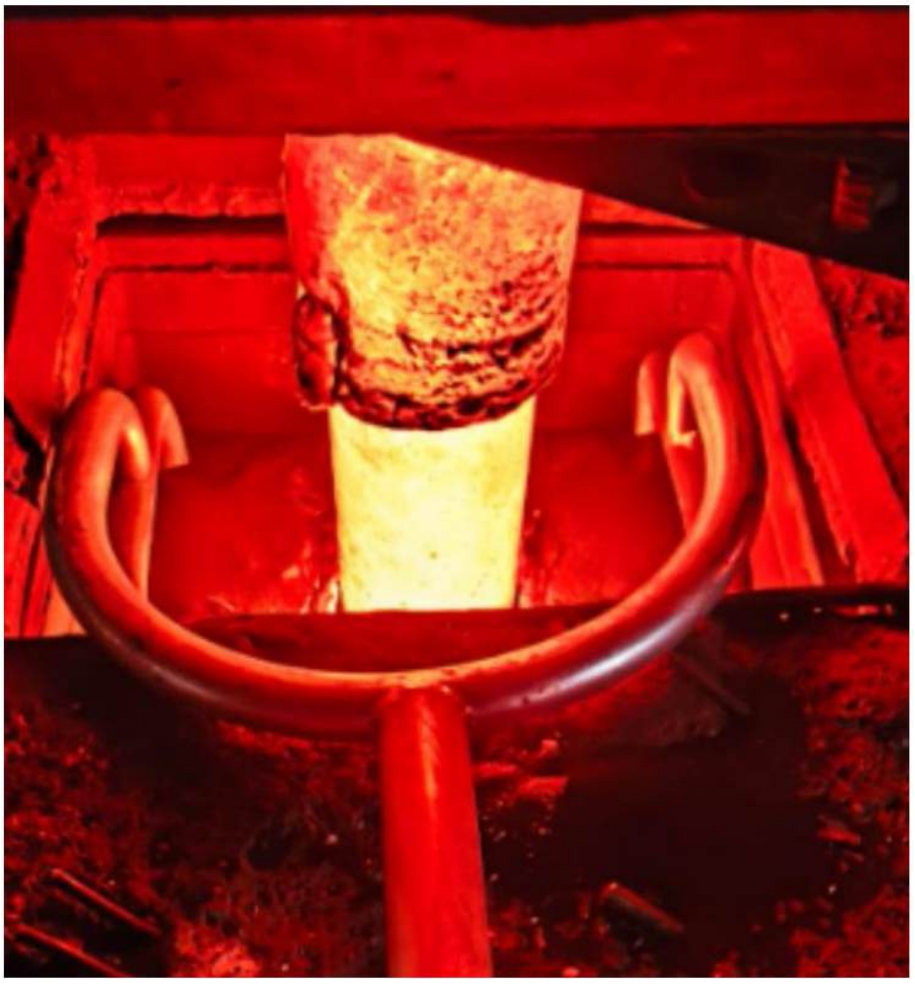


Figure 2. Actual mould-powder distributor photograph at the casting area. The distributor provides the final controlled delivery path for mould flux toward the mould.

6. Mini-AFF Control Architecture

The control philosophy combines two complementary measurements. Flow feedback indicates the rate at which powder is being delivered, while the load cell provides feeder inventory information. The controller can use the measured values to maintain the selected operating condition and provide alarms or operator indications when the material balance or delivery condition deviates from the intended range.

Flux Pre-heating	Load Cell (Weight)	Flow Sensor (Delivery)	Control Panel (Control)	Mould Flux Distributor
→	→	→	→	Controlled mould flux delivery

Figure 3. Simplified Mini-AFF control architecture: material storage → weighing → flow measurement → control → mould distribution.

7. Field Application and Results

The following cases represent plant application experience reported for AFF installations. They are presented as field observations rather than controlled laboratory trials; casting speed, steel grade, mould design, flux chemistry and other process variables can also influence defects.

7.1 Tata KPO – Stickering issue (2024)

A stickering issue at Tata KPO was reported as solved following implementation of an AFF machine in 2024. Controlled and consistent flux delivery was used as part of the casting-practice improvement, supporting stable mould–strand conditions.

7.2 JSPL Raigarh – Cracking issue (2025)

A cracking issue at JSPL Raigarh was reported as solved following implementation of an AFF machine in 2025. Consistent mould-flux feeding supported the effort to stabilize mould conditions and improve casting surface quality.

8. Discussion

The principal technical benefit of Mini-AFF is the conversion of an operator-dependent consumable addition into a measurable process variable. The feeder can be configured around the required flux feed rate, while the flow sensor provides direct information on delivery and the load cell provides material-balance information. This combination offers a stronger basis for repeatable operation than fixed manual addition.

For small and medium steel plants, the compact design is also important. Automation must provide measurable process value without introducing excessive complexity. The Mini-AFF development therefore focuses on essential control functions, modular construction and ease of operation. Pre-heating is treated as an application-specific option rather than a universal requirement.

9. Conclusions

A Mini-Automatic Flux Feeder has been developed as a practical solution for controlled mould -flux feeding in small and medium steel plants. The system addresses the main limitations of manual feeding through automatic delivery, flow-sensor feedback, load-cell based material control and optional flux pre-heating. These functions support more consistent powder delivery, lower risk of over- or under-feeding, reduced routine operator intervention and a more resource-efficient operating approach. Field experience reported at Tata KPO in 2024 and JSPL Raigarh in 2025 indicates that AFF implementation can contribute to resolving casting problems associated with unstable mould-flux practice, including stickering and cracking. Future work should quantify feed-rate accuracy, powder consumption, defect frequency, maintenance cost and return on investment using standardized plant data.

10. References

1. Mills, K. C., Fox, A. B., Li, Z. and Thackray, R. P., “Performance and properties of mould fluxes,” Ironmaking & Steelmaking, 32(1), 26–34, 2005.
2. Saraswat, R., Fox, A. B., Mills, K. C., Lee, P. D. and Deo, B., “The factors affecting powder consumption of mould fluxes,” Scandinavian Journal of Metallurgy, 33, 85–91, 2004.
3. Sridhar, S., Mills, K. C. and Mallaband, S. T., “Powder consumption and melting rates of continuous casting fluxes,” Ironmaking & Steelmaking, 29(3), 2002.
4. Litsin, K. V., Baskov, S. N. and Morkovnik, D. A., “A model of automated mold flux feeding into the crystallizer of a continuous casting machine,” CIS Iron and Steel Review, 26, 33–38, 2023.
5. Tata Steel KPO plant application record, Automatic Flux Feeder implementation and reported stickering issue resolution, 2024.
6. JSPL Raigarh plant application record, Automatic Flux Feeder implementation and reported cracking issue resolution, 2025.

ZONE-SPECIFIC AL_2O_3–SIC–C REFRACTORY SYSTEMS FOR TORPEDO LADLES: WEAR MECHANISMS, FIELD INVESTIGATION AND REFRACTORY OPTIMISATION

Alok Patro, Saumen Sinha, Bhushan Bobde, Tuhin Patranabish, R Basavraj

Calderys India Refractories Limited, Nagpur, India

Abstract

A torpedo ladle has to survive thermal cycling, slag corrosion, hot-metal penetration and mechanical impact all at once, over years of service and thousands of fill-and-empty cycles. This paper looks at where torpedo refractory practice currently stands, focusing on the alumina–silicon carbide–carbon (Al_2O_3–SiC–C, or ASC) brick systems that have become the standard working lining almost everywhere. It draws on the underlying wear chemistry, characterisation of zonespecific ASC grades, and field wear data recorded on a torpedo at a major steel unit in India. The results support zone-specific grade selection as a practical approach for lining design, along with a few potential improvement measures such as window repair, hotmetal heel, micro-porous insulation and no-cement spout castable.

1. Introduction

The torpedo ladle car (TLC) carries molten hot metal from the blast-furnace cast house to the steelmaking shop, and on many plants, it also doubles as a hot-metal pretreatment vessel for desiliconisation, desulphurisation or dephosphorisation. A large modern torpedo holds 300–420 t of hot metal at 1,350– 1,525°C, and over one campaign it will go through well over a thousand fill-and-empty cycles before it needs relining. Every hour a torpedo spends out of service for relining is an hour of transport capacity lost between ironmaking and steelmaking, so campaign life and relining turnaround time have a direct impact on plant productivity and operating cost, and are therefore important from both refractory and operational perspectives.

Lining practice has moved a long way since the 1970s. Early linings were high-alumina brick impregnated with pitch, later chamotte brick, and both were vulnerable to reaction with FeO- and CaO-bearing slag — the slag simply reacted with the SiO_2 in the brick to form low-melting compounds that corrode the lining faster. Resin-bonded Al_2O_3–SiC–C brick, developed from the late 1980s onward, solved enough of that problem that it is now the default working lining for torpedo and hot-metal ladles worldwide, mainly because it resists corrosion better, with controlled wetting with molten iron or slag, and tolerates thermal shock far better than what came before it.

Torpedo Ladle Design and Service Conditions

A torpedo ladle is a mobile, refractory-lined steel shell: a cylindrical barrel with two conical (venturi) end sections, and a mouth/spout on the upper barrel where hot metal goes in and comes out. The lining itself is built up in layers — insulation board or brick against the shell, a high-alumina safety backup layer, and the Al_2O_3–SiC–C working lining at the hot face. At the mouth and spout, monolithic castables and pre-cast shapes take over from brick, simply because the geometry is awkward, and that area needs replacing far more often. Zonal lining is required because the different regions of the torpedo are exposed to different types and levels of thermal, chemical, and mechanical stress. A single brick grade cannot provide the required performance across all service zones.

Material Science of Al_2O_3–SiC–C Working Linings

The three main constituents of an ASC brick have different roles in determining its performance. Al_2O_3 provides the main refractory matrix and contributes to high-temperature stability and corrosion resistance. SiC and carbon are important for thermal-shock resistance, thermal conductivity, and non-wetting behaviour. The balance between these constituents therefore needs to be selected according to the service zone. SiC (6–20%) raises thermal conductivity, which helps the brick shed thermal stress quickly, and it protects the neighbouring carbon phase from oxidising away. Flake graphite or free carbon (3–15%) is what stops the brick wetting with molten iron and slag in the first place, and it is the single biggest contributor to thermal-shock resistance — but carbon starts oxidising above roughly 600–700°C in air, so it needs protecting with antioxidants (Si, B4C, Al metal) and by the SiC itself. Lose that protection and the carbon burns out, leaving a porous surface that hot metal and slag walk straight into.

Field post-mortems and lab work keep pointing to the same four wear mechanisms in ASC linings. The first is chemical corrosion: aggressive components in the slag work their way into the brick's open pores and react with the Al_2O_3/SiO_2 already there. Textbook treatments usually centre on FeO — FeO and CaO reacting with the brick to reform low-melting phases such as fayalite ($2FeO{\cdot}SiO_2$, melting around 1,210°C) and hercynite ($FeO{\cdot}Al_2O_3$, ~1,550°C). That is a real pathway where the slag actually carries meaningful FeO, but it is worth being precise about which slag is under discussion: the operating slag chemistry measured for this study (§5) is dominated by CaO, SiO_2, Al_2O_3 and MgO, with FeO at only 0.40% on average, so an FeO-driven mechanism is not automatically the right explanation here without further evidence. A calcium-aluminosilicate pathway — anorthite ($CaO{\cdot}Al_2O_3{\cdot}2SiO_2$, ~1,550°C) or similar calcium-aluminate/spinel-type interfacial products — sits closer to what the bulk chemistry actually supports for this slag, though which phases actually form at the brick/slag interface can't be settled from bulk composition alone; that needs XRD and SEM/EDS on the worn brick itself, which was outside the scope of the data available here. The second mechanism is metal infiltration: hot metal gets drawn into the open porosity by capillary action, and the densified layer that results in different thermal expansion from the bulk brick, so it spalls off the next time the lining heats and cools. Third is plain thermal spalling — a brick without enough SiC/C simply can't take the repeated heating and cooling of fill-and-empty cycles without cracking. Fourth is carbon oxidation in the free-board and roof area, and during any idle period, which leaves a porous surface ready to be infiltrated the moment metal or slag contact starts again.

Characterisation of ASC Refractory Grades

The ASC refractory system evaluated in this study comprises three zone-specific alumina–silicon carbide–carbon grades for torpedo-ladle service: Slag Zone, Metal Zone and Impact Zone. All three are alumina–silicon carbide–carbon bricks with a carbonceramic bond, manufactured by dry pressing, with a specified maximum service temperature of 1550 °C.

Table 1: Typical Properties of ASC Grades

Property	Slag Zone	Metal Zone	Impact Zone
Al_2O_3 (%)	68.0	64.0	63.0
SiC + C (%)	20.5	19.0	19.0
Bulk density (g/cm³)	2.93	2.93	2.88
Apparent Porosity (%)	4.6	6.2	7.6
CCS (MPa)	38.2	35.6	38.2
Maximum service temperature (°C)	1550	1550	1550

Source: Product datasheets for the respective ASC grades

One clear difference between the three grades is apparent porosity. The Slag Zone grade has the lowest typical value at 4.6%, followed by the Metal Zone at 6.2% and the Impact Zone at 7.6%. This difference is relevant when considering liquid penetration, although apparent porosity alone is not sufficient to explain refractory performance. Pore structure, carbon distribution, SiC content, matrix characteristics, and the actual service conditions also need to be considered.

The three grades are selected according to the service zone rather than using one common chemistry throughout the lining. The Slag Zone combines the highest typical Al_2O_3 and SiC + C levels with the lowest apparent porosity, while the Metal and Impact Zone grades have different combinations of these properties.

The earlier laboratory comparison also showed that differences in ASC formulation were reflected in apparent porosity and mechanical properties after coking. This supports considering the chemistry and physical structure together rather than using a single property as an indicator of performance.

The field inspection helps to check how this zonal approach performs under the actual operating conditions of the torpedo. It provides the opportunity to see how the selected ASC grades perform under the actual combination of slag contact, hot-metal exposure, thermal cycling and local flow conditions present in the torpedo.

Field Wear Investigation

The present study was carried out on a 380-t-class torpedo ladle, 13.6 m long, with 78 brick-ring layers— 21 in each conical section, 36 in the cylindrical section, and two in each circular end wall. The working lining comprised zone-specific ASC grades for the slag, metal and impact zones. Two separate operating records were available for the study period: the first minor-repair inspection was carried out after 511 heats, while a separate operating log contained 556 trips over the monitored period.

Duty cycle and thermal-cycling frequency

Over the 183-day logging window, the TLC made 556 trips, or about 3.04 trips per day. These trips represent repeated thermal cycling of the lining under the operating conditions recorded during the period. Hotmetal temperature at the runner averaged 1,492.5°C (σ = 23.0°C, range 1,402–1,554°C). The median loaded (iron-zone) time was 313

min, or about 5.2 hours, while the median total turnaround was 442 min, or about 7.4 hours. A meaningful minority of trips exceeded 1,000 minutes (Figure 1), extending the range of loaded exposure time.

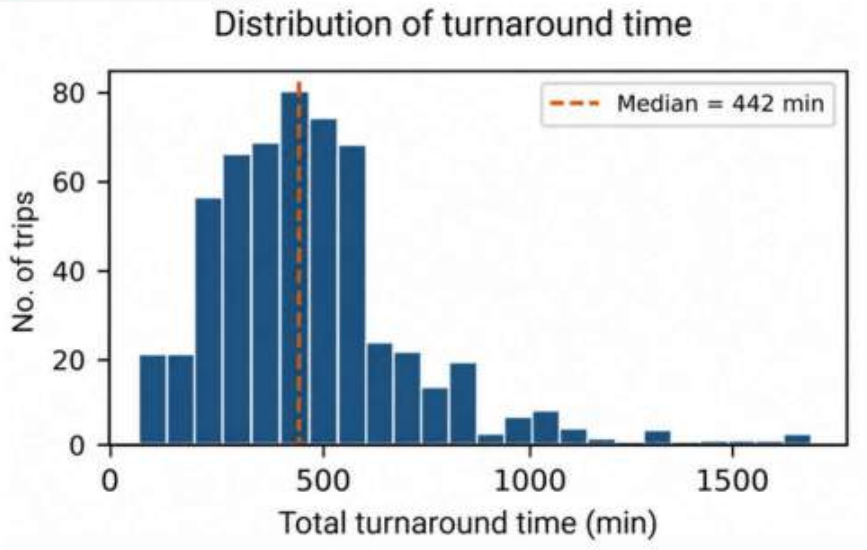


Figure 1. Distribution of TLC total turnaround time

The average cycle time varies with the furnace supplying the torpedo. Furnace B and Furnace D show higher loaded times of around 423 and 408 minutes, respectively, while Furnace A and Furnace C show lower loaded times of around 275 and 272 minutes. Furnace E falls between these ranges, with an average loaded time of about 330 minutes. The total turnaround time also varies between the different furnaces. The data indicate that a torpedo operating predominantly with Furnace B or Furnace D experiences substantially longer periods of sustained thermal and chemical exposure in each cycle than one operating with Furnace A or Furnace C. Therefore, refractory wear and campaign life should be evaluated not only on the number of trips, but also on the cumulative loaded exposure time. Treating all cycles as equivalent may not accurately represent the actual refractory exposure.

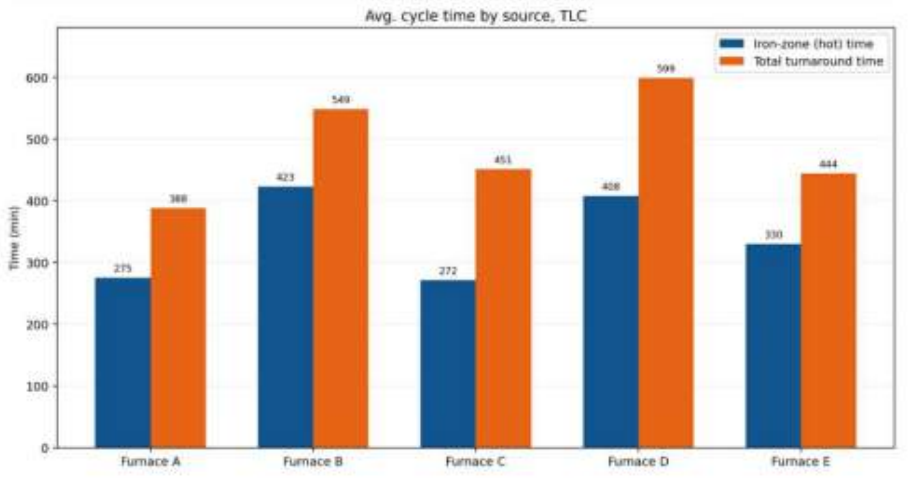


Figure 2. Average loaded (iron-zone/idle) time and total turnaround time by charging source, TLC.

Hot-metal and slag chemistry

Over a 38-day period, the hot-metal and slag chemistry from Furnace C, Furnace D and Furnace E remained stable. The average slag FeO was about 0.40%, with values ranging from 0.26–0.57%, while average basicity (B2) was around 1.02, varying between 0.99 and 1.06. Al_2O_3 and MgO in the slag were around 16.4% and 7.5%, respectively. There was no clear upward or downward trend in FeO or basicity; the values mainly fluctuated within this narrow range. However, the day-to-day variation in FeO can still influence the actual corrosion rate, so average values alone may not capture the complete picture.

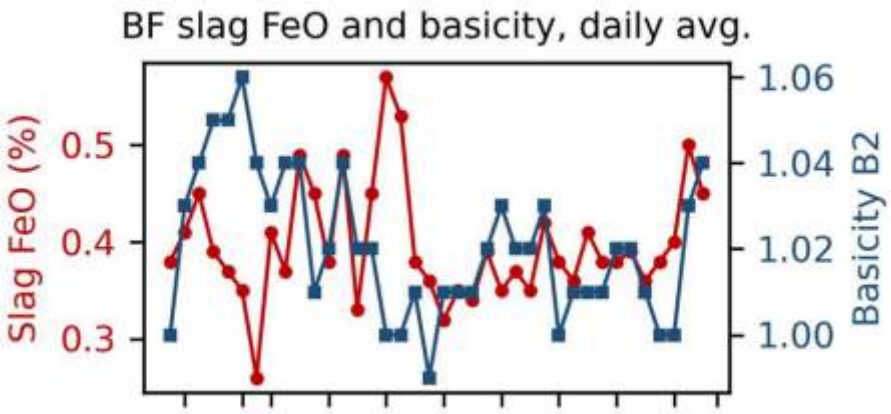


Figure 3. Daily-averaged blast-furnace slag FeO and basicity (B2).

The available hot-metal chemistry data indicate an average Si content of about 1.43%, with higher values occurring intermittently. Such variations can influence the silica content of the slag and therefore the chemical load on the slag-zone refractory.

Measured wear profile

During the first minor-repair inspection of TLC, the residual brick thickness was measured at every third ring in four directions around the ladle circumference: spout, bottom, and the two pouring sides (1 and 2), named based on the blast-furnace groups filling each side. Measurements were taken on both the drive and non-drive sides and averaged for each ring and direction, as shown in Figure 4. The lowest wear was observed at the bottom/conical face, at around 0.03– 0.07 mm/heat, where metal and slag interaction is limited. The highest wear was seen on the Pouring side 2, at around 0.18–0.37 mm/heat, with the maximum wear just below the spout. The spout direction also showed a noticeable increase in wear at the last ring, which is closer to the slag-metal interaction zone.

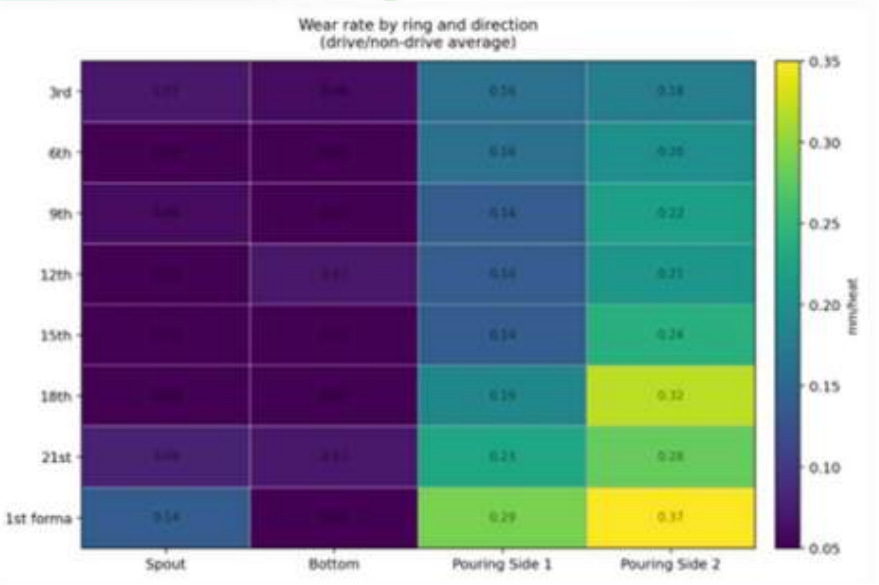


Figure 4. Ring-wise refractory wear rate at the first minor repair.

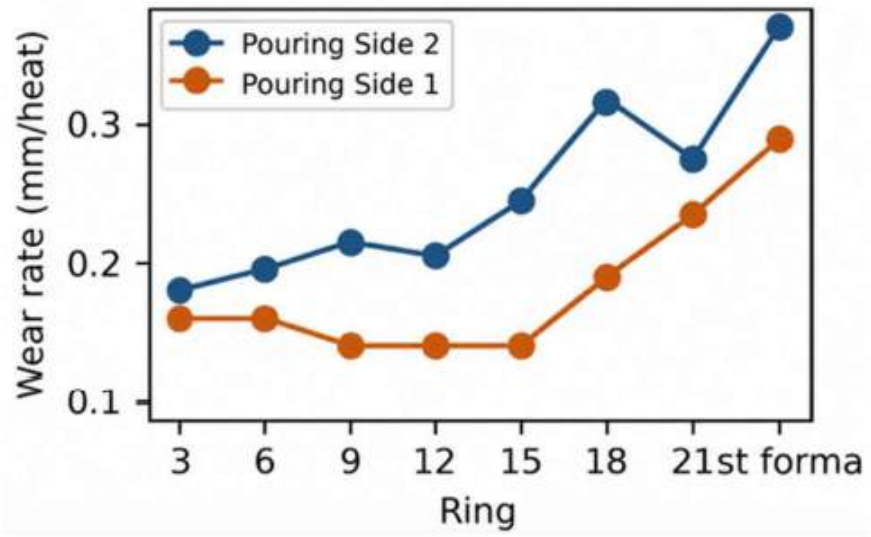


Figure 5. Pouring-side wear rate

Two distinct wear patterns were observed during the inspection. 'Rat holes' of around 85–90 mm depth were mainly found near the cone-to-cylinder joint, suggesting localized wear under transport and sloshing conditions. A separate wider wear band was observed along the slag-metal interface. The wear in this area did not follow the staggered brick-joint pattern, suggesting that the joint configuration was not the primary control on the observed wear. Used-brick analysis is required to distinguish the relative contributions of chemical corrosion and mechanical erosion. A separate spot measurement just below the spout on the Pouring Side 2 showed 70 mm residual thickness, corresponding to a wear rate of 0.45 mm/heat over 511 heats. This was the highest local wear observed during the inspection; however, since it was a single-point measurement, it has not been included in the ring-wise wear map. At the first minor repair, the residual thickness in other areas of the slag zone was around 90–120 mm against an as-installed thickness of 343–345 mm, while the generic specified residual thickness is ~120-150 mm at 500–525 heats. Used brick analysis will be carried out to determine the detailed wear mechanism.

Performance Enhancement Strategies

Based on reported plant experience, one of the major factors influencing torpedo campaign life is the way refractory repairs are carried out during service, rather than only the initial brick quality. The 'window repair' approach involves regularly inspecting the known high-wear areas, such as the slag line, the area below the spout and the lower freeboard, and repairing only the affected areas using shotcrete, gunning or additional brick thickness instead of waiting for a complete reline. A published study on a 350-t-class torpedo reported an increase in average campaign life from around 1,217 to 1,953 cycles with this approach, along with around 30% reduction in hot-metal handling cost. These are reported results from another integrated steel plant and should not be considered as a direct indication of the performance of the investigated torpedo. Another practice that can help reduce wear is maintaining a hot-metal heel of around 10–15 t at the bottom of the torpedo instead of completely draining it at the steel shop. The heel helps cushion the incoming hot-metal stream and reduces the direct impact on the bottom and impact-pad area. In the same study, the impact-pad bricks in ladles operated with heel practice reportedly required no repair even at a campaign life of 2,034 cycles, with around 80–95 mm residual thickness still remaining.

Heat-transfer calculations across the lining also indicate that there could be a benefit from improving the insulation. Replacing the conventional insulating brick/board with a micro-porous board, having a thermal conductivity of around 0.023–0.030 W/m·K compared with around 0.24 W/m·K for the standard material, can reduce the shell temperature by about 100–150°C under the same hot-face conditions. This is important because shell temperature is often one of the limiting factors for continuing a torpedo campaign. In one documented 320 t case, the calculated reduction in shell temperature was estimated to increase the campaign from around 1,350 to 1,845 trips, or about 37%, without increasing the overall lining thickness. Another area worth considering is the use of silica-solbonded no-cement castable (NCC) for the mouth/spout area. In reported trials, the Al_2O_3–SiC NCC showed higher cold crushing strength (927–962 vs. 780–867 kg/cm²) at 1000/1400 °C and much better corrosion resistance against furnace slag (26.5% vs. 72.2%) compared with the existing low-cement castable. The same is already implemented at one major steel plant.

Future R&D Directions

- Used brick sample analysis to understand root cause behind brick wear

- Modification of the antioxidant system can be explored to improve carbon protection at higher temperatures. Further ASC formulation optimization can also be considered, with a balance between carbon retention, thermal-shock resistance and slag corrosion.

- Digital wear-prediction tools can be developed by combining shell thermography with a calibrated heat transfer model and furnace-wise duty-cycle data from Figure 2. This can help move window-repair planning from a fixed schedule to a condition-based approach, based on the actual lining condition and exposure.

- SiC-based shotcrete can be evaluated for window repairs in high-wear areas, especially around the slag line and the spout/cone-cylinder region. The higher SiC content is expected to improve resistance to slag attack, abrasion and thermal shock, while allowing local repairs without waiting for a complete relining. A controlled trial on TLC can help assess its impact on wear rate, repair frequency, and overall campaign life.

Conclusion

The main wear mechanisms in torpedo refractories are slag corrosion, hot-metal infiltration, thermal spalling and carbon oxidation, although their contribution varies across different zones of the vessel. The observations show why different refractory grades are required for different zones of the torpedo. The operating log covering 556 trips also shows significant differences in thermal exposure depending on the furnace source, while the slag chemistry remained relatively stable with some day-to-day variation. The measured wear pattern points to slag-zone corrosion, particularly around the spout and cone-cylinder region, as the main area currently affecting lining life. The improvement measures discussed in this study, including window repair, hot-metal heel practice, insulation improvement, no-cement castable and SiCbased shotcrete, are based mainly on experience and results from other plants. Their actual benefit on TLC should therefore be established through controlled trials and monitored through wear rate, repair frequency and campaign life.

REFERENCE

1) Gupta, R. B., “A techno-economic balance for zonal lining of torpedo ladles,” Steel Times International, October 2017.

2) Sahu, B., Singh, M. K., Singh, A., Panigrahi, P., Agrawal, T., Khan, S. A. and Singh, B., “A novel approach to reduce torpedo ladle relining turnaround time,” REFIS 4.0, Tata Steel, Jamshedpur.

3) Anand, A., “Optimization of 320T torpedo ladle BOM for higher life,” Vocational Training Project Report, Tata Steel, Jamshedpur (2015).

4) Calderys India Refractories Limited, “Internal Characterisation Study”

5) Calderys India Refractories Limited, “Comprehensive torpedo ladle refractory solutions,” technical proposal.

OPTIMISATION OF ALUMINA-SPINEL CASTABLE FOR USE IN PRECAST BOTTOM FOR LARGE CAPACITY STEEL LADLE

Nathan Leicht[1], Phil White[1], Andreas Buhr[2], Shankha Chatterjee[3]

[1]Shinagawa Refractories Australia Pty. Ltd., NSW, Australia
[2]Almatis GmbH, Frankfurt, Germany
[3]Almatis India Pvt. Ltd., Kolkata, India

Corresponding author's e-mail: nathan.leicht@shinagawa.com.au

Abstract

This paper discusses the relationship between particle size distribution, matrix selection and cement content on thermal and mechanical performance of alumina spinel castables. It forms part of the development and implementation of high purity alumina-spinel precast refractory shape for a large capacity steel ladle bottom. Refractory design arising from proper selection of aggregate, in-situ or pre-formed spinel, matrix and binder to achieve optimum balance of key parameters such as porosity, strengths and wear resistances, are discussed here. The critical castable factors of water demand, flowability, setting parameters are discussed along with selection of proper casting, de-moulding and drying parameters of a large precast shape. The success in this particular refractory is an outcome of balanced and optimum selection of castable material quality (aggregate, matrix and binder) and manufacturing parameters of the precast refractory shape with the overall aim to achieve target service life as a component of the ladle repair program.

1. Introduction

Steel ladle refractory lining has gone through many changes over time. With the current challenges include increasing demand of inclusion-free clean steel production, the high purity alumina based lining has taken the driving trend for the steel ladle bottom. The common forms of such modern trend are high purity alumina-spinel, in the form of in-situ casting or precast refractory shapes. The major factors for deriving selection of lining quality lie with steel and slag metallurgy, treatment methodology and operating parameters such as treatment time, holding time, tapping temperature, alloying elements, heats per ladle per day etc. In addition to these, achieving higher performance (life or heats) for large capacity steel ladle remains a major challenge.

The bottom refractory of a steel ladle is subjected to severe thermo-mechanical and chemical stresses during secondary steelmaking. It must therefore possess high load-bearing capacity, hot strength, erosion resistance, thermal-shock resistance, and volume stability over prolonged service. Carbonbonded Magnesia-Carbon (MgO-C) and Alumina-Magnesia-Carbon (AMC) bricks are commonly used for such demanding applications. However, the presence of carbon can be a significant limitation in the production of ultra-low-carbon and other special steel grades because of the possibility of carbon pickup from the refractory to steel.

The challenge becomes more critical with increasing ladle capacity. In this context, large precast refractory blocks offer an attractive alternative to conventional brick construction. Replacement of multiple bricks by a large monolithic component reduces the number of joints and associated weak interfaces, potentially improving lining integrity. Precast blocks can also facilitate localised repair and partial replacement, thereby providing opportunities for service-life extension and improved refractory material sustainability.

For large-shaped precast components such as ladle bottoms, selection of the castable is a critical starting point. Low-cement castable (LCC), ultra-low-cement castable (ULCC), and

no-cement castable (NCC) technologies are well established in the refractory industry. LCC remains widely preferred because of its favourable combination of mixing, casting, setting, handling, and green-strength characteristics. These attributes become particularly important when manufacturing large and complex precast shapes.

Alumina-spinel castables are attractive for critical refractory applications because of their excellent high-temperature mechanical properties. During firing and service at temperatures typically between 1400 and 1700°C, significant phase evolution occurs in the $CaO–Al_2O_3–MgO$ system. Formation of ternary CAM phases and their interaction with CA_6 (hibonite), alumina, and spinel can promote strong microstructural bonding[1]. The development of platy or hexagonal phases and their growth into alumina-rich regions enhances interconnection between matrix and aggregate, contributing to high hot strength and structural integrity.

Raw-material selection and matrix design are critical to achieving the required performance. High-purity synthetic alumina aggregates, such as tabular alumina, white fused alumina, or their combination, are generally preferred. Although both materials can provide approximately 99.5% Al_2O_3 purity, they differ in microstructure, porosity, pore distribution, and impurity distribution, particularly in fine fractions. For large precast components, suitably selected coarse and super-coarse aggregates can improve packing density and contribute to thermal-shock and spalling resistance.

The spinel component can be introduced as pre-formed $MgAl_2O_4$ spinel or generated in situ. Pre-formed spinel provides better control of expansion and volume stability, whereas in-situ spinel formation can offer advantages in microstructural development and bonding. However, the latter requires careful control of raw-material reactivity, impurities, and associated volume changes.
Particle-size distribution plays a decisive role in packing, rheology, water demand, and casting behaviour. High and sustained flowability is particularly important for large ladle-bottom precasts to ensure complete filling and homogeneous consolidation. Optimised particle packing can reduce wet-out time and water addition, thereby improving density and thermo-mechanical properties. However, excessive densification can adversely affect thermal-spalling resistance; hence, an optimum balance is essential.

The matrix comprising reactive alumina/spinel, cement, and chemical additives governs rheology, setting, and cured strength. Cement selection strongly influences flowability and setting kinetics, while modern polymer- and alumina-based dispersing aluminas enable improved rheological and setting control. Adequate cured strength after approximately 24 hours is essential for safe demoulding and handling.

Large ladle-bottom precasts may be manufactured either at the refractory plant or at the steel plant, depending on mixing, casting, handling, drying, and preheating facilities. A hybrid route, involving casting and controlled drying at the refractory manufacturer's facility followed by prefiring at the steel plant, can provide operational flexibility.

Thus, successful development of large alumina-spinel precast ladle bottoms requires an integrated approach involving raw-material selection, particle packing, matrix engineering, rheological control, controlled drying, and thermal treatment. Such carbon-free refractory solutions can potentially improve steel cleanliness, reduce joints, enhance thermo-mechanical reliability, extend ladle life, and contribute to more sustainable refractory utilisation.

2. Formulation Design and Test Methods

Test mixes were formulated with a view to reducing the thermal shock when in service in a steel ladle bottom, however the importance of erosion and corrosion resistance remains key to performance. As such the use of high density, high alumina aggregates were selected for the range of castables in the test program along with addition of preformed alumina-magnesia spinel. Castable design examined how increasing the proportion of top-size aggregate influenced overall performance, with particular focus on density, strength and resistance to thermal shock.

	STD	M1	M2	M3	M4
Tab. Alum. up to 15 mm	✓	✓✓	✓✓	✓✓	✓✓
Spinel AR78 Fines	✓✓	✓	✓	✓	✓
React. Alum. CL 370	✓				
React. Al-Sp E-SY 2000		✓	✓	✓	✓
70% CAC CA-670	✓	➜Increasing➜			
Additives ADS+ADW	✓	✓	✓	✓	✓
PE Fibre	✓	✓	✓	✓	✓

Table 1: Compositions of castables

The effect of cement content was also assessed, as cement level can influence setting behaviour, strength development, and susceptibility to steam spalling during initial heating. To promote a more open matrix, reactive alumina-spinel E-SY2000 was incorporated as a replacement for the standard CL370 reactive alumina. This substitution was intended to modify the fine-particle packing and improve the thermal shock resistance. In Mods 1 to 4, the cement content was progressively increased to determine its influence on steam spalling resistance and overall castable properties.Table 1 describes the variations in formulation design assessed in the work.

	PSD	Al_2O_3 %	MgO %	BET m^2/g	d50 µm
CL 370	Bi-modal	99.8	0.02	3.0	2.6
E-SY 2000	Broad	88.3	11.2	2.3	1.7

Table2: Difference in matrix reactive aluminas

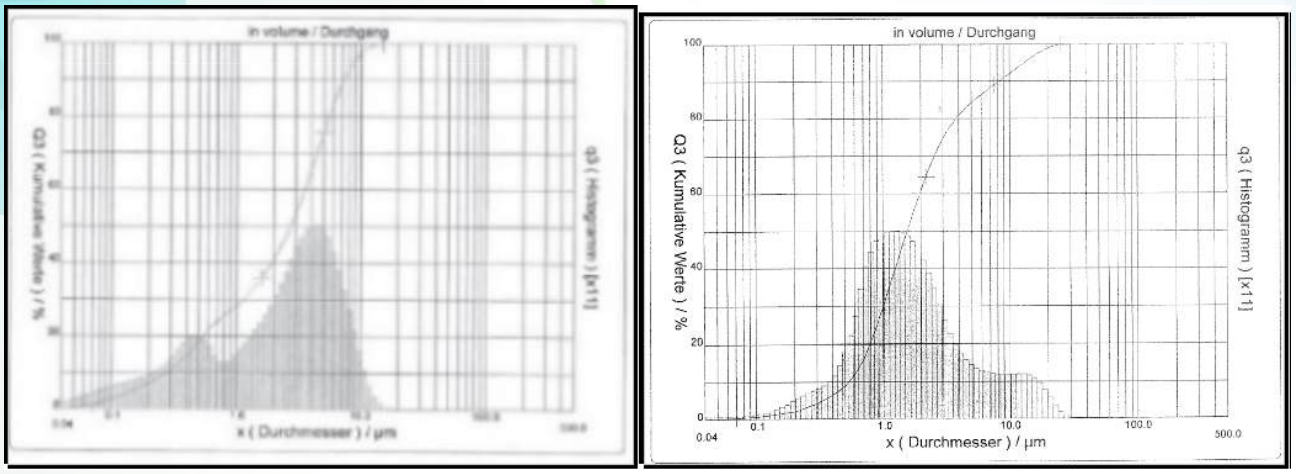


Figure 1: PSD of CL 370 (left), E-SY 2000 (right)

The castables were initially prepared in the laboratory by drymixing for 1 minute, followed by the addition of the required amount of water and wet mixing for 4 minutes. Vibration flow was measured at different time intervals and the exothermic reaction during cement setting was evaluated using the heat of hydration method. Test bars were prepared for the different mix recipes, as shown in Table 1. The bars were first cured at ambient temperature for 24 hours, then dried at 110°C for 24 hours, and subsequently fired at 1000°C for 5 hours and 1500°C for 5 hours, respectively. After cooling, the bars were tested for bulk density (BD), cold crushing strength (CCS), cold modulus of rupture (CMOR), and permanent linear change (PLC). Most tests were carried out in accordance with the Australian Standards AS 1774 series methods. Steam spall testing was conducted as per ISO 16334 test method with samples being cast and cured at 23°C for 24 hours before being placed in a protective cage. The sample and cage are then introduced into the live kiln at 1000°C with the integrity of the sample being determined after 20 minutes in the kiln. Thermal shock resistance will be determined as per AS1774.24 whereby test samples are thermal cycled five times between room temperature and 1000oC. The average MOR of these samples is compared to the average MOR of control samples and the Retained Strength Index is calculated. Results were not available for paper submission but will be presented at the conference.

3. Results and Discussion

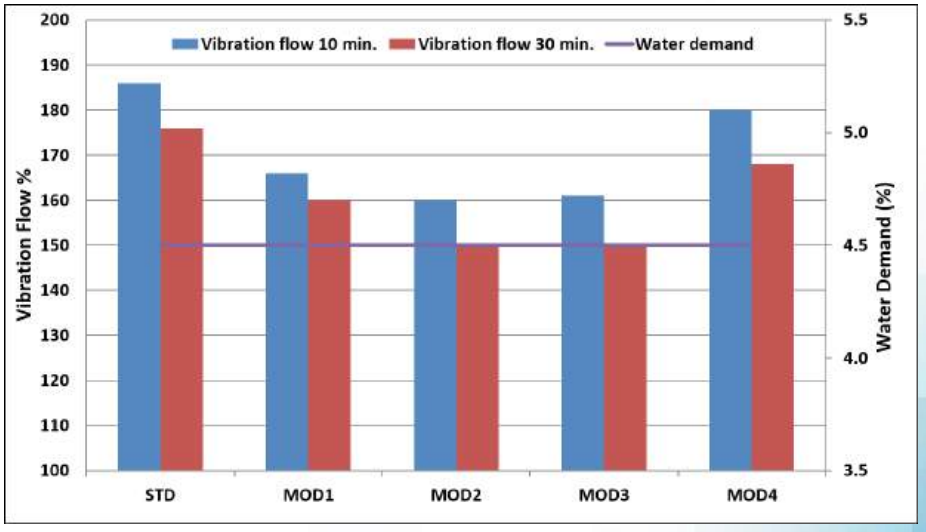


Figure 2: Water demand and flow values

Water addition remained constant at 4.5% and resulted in some differences in measured flow values due to the change in particle size distribution at the coarse end and the use of E-SY2000 when compared to the finer particle sized CL370 reactive alumina. All variants achieved an acceptable retained flow value at 30 minutes indicating that casting characteristics will be maintained for the duration of a casting period. Exothermic reaction results show that all tests have a suitable working and setting time however for situations where working and setting time adjustments are required, the ratio of setting accelerator (W-type) and setting retarder (S-type) can be adjusted.

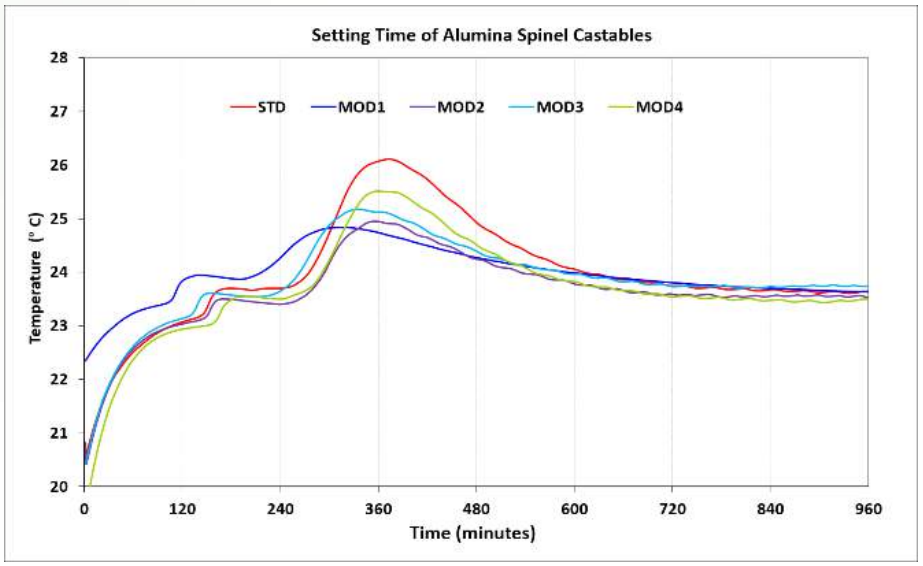


Figure 3: Setting time characteristics

The planned reduction of bulk density has been achieved with all MOD mixes lowering the bulk density when compared to the STD as shown in Figure 4. PLC largely remains unaffected by the variations with all MOD mixes indicating good volume stability up to 1500°C (fig. 5).

Figures 6 and 7 indicate that for the MOD mixes both the cold compressive strength and cold modulus of rupture have been reduced compared to STD after drying 110°C and firing to 1000 and 1500°C. Within the set of MOD castables, the MOR is relatively stable however the CCS shows a gradual strength increase as the cement content is increased.

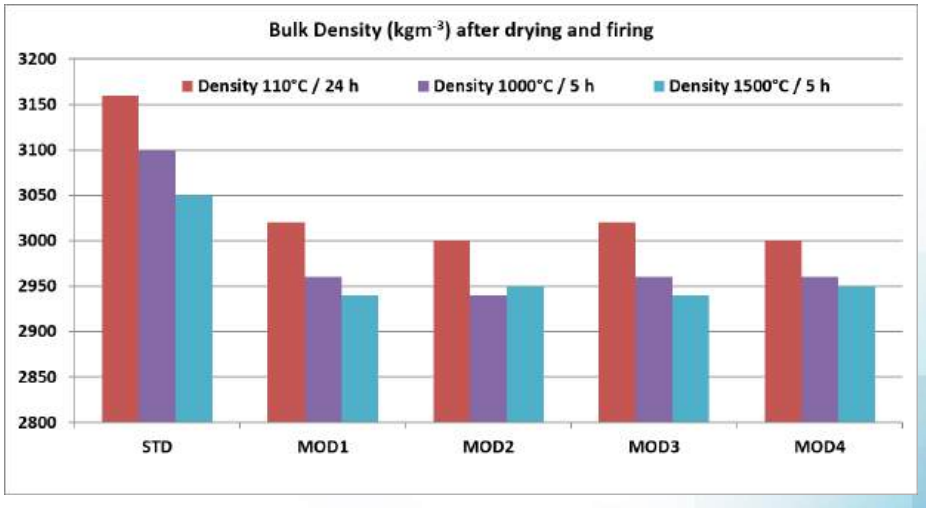


Figure 4: Bulk Density of test castables

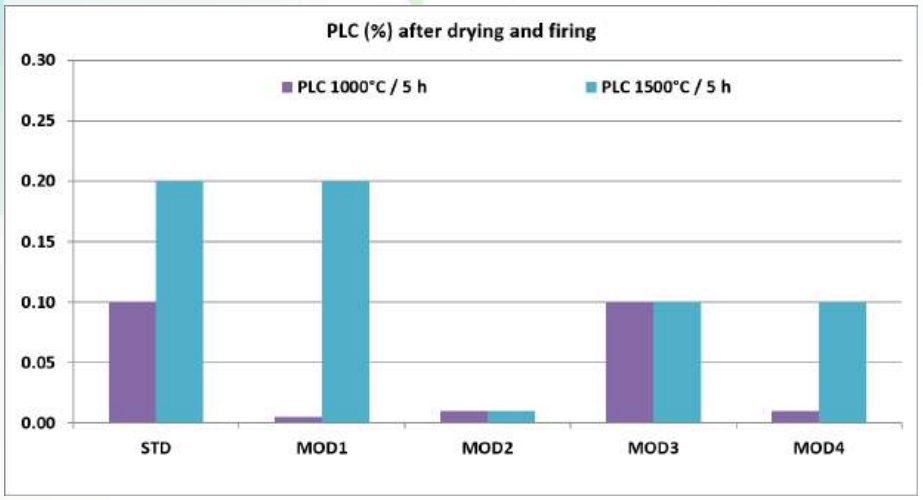


Figure 5: PLC of test castables

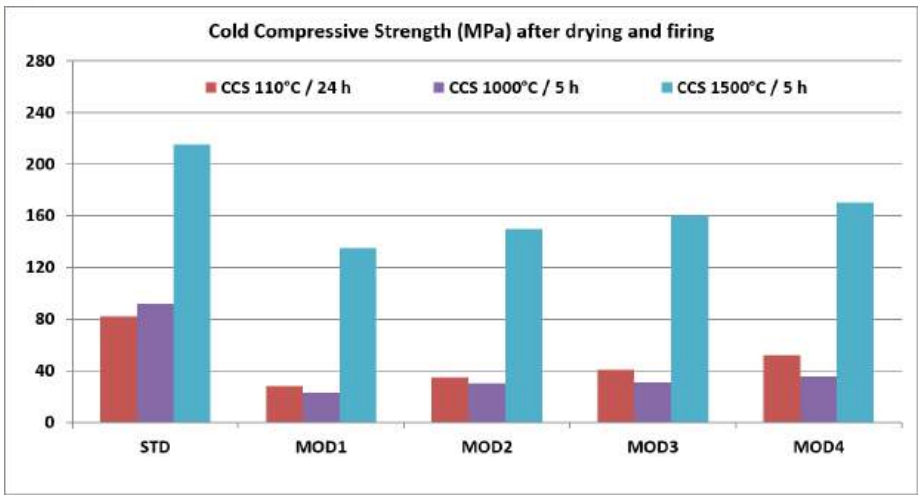


Figure 6: CCS of test castables

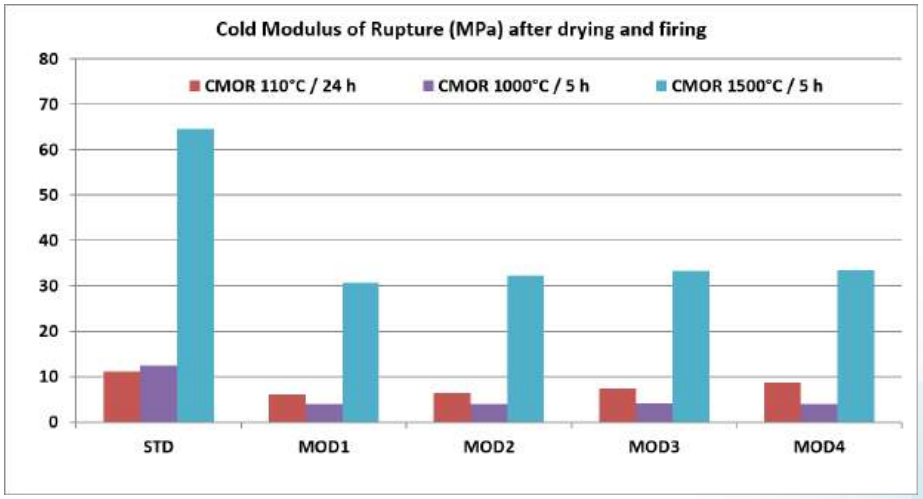


Figure 7: Cold MOR of test castables

Steam spall test result is summarised in Table 3 and shown visually in Figure 8. Results were clear that the LCC variants were successful in withstanding the harsh test environment of the spalling test were the ULCC variants did not generate sufficient green strength in the first 24 hours of curing to pass the test conditions.

	STD	M1	M2	M3	M4
Condition	Pass	Fail	Fail	Fail	Pass

Table 3: Steam Spall results of test castables



Figure 8: Typical result of steam spall test pass (left) and failed (right)

4. Conclusion

Alumina-spinel LCC and ULCC castables are important for improving the performance of steel ladle precast bottom components. Aggregate type, matrix design, and use of pre-formed spinel addition must be carefully controlled to achieve suitable rheology and placement behaviour.The open structure, combined with dispersed spinel in the matrix can successfully deliver the targeted properties of mechanical strength. Thermal spalling resistance will be reported at the conference. However, low and ultra-low cement contents must be considered as critical components in the overall formulation design. Reliable in-service performance also depends on the practical ability to manufacture and dry large precast shapes, which must be considered during formulation development.

References

1. S. Klaus, A. Buhr, M. Bauer, et. Al.: Formation of hexa-aluminate solid solution phases in spinel containing castables – mineralogical investi-gations in the system $CaO-Al_2O_3-MgO$, 62. Intl. Colloquium on Refr., 2019, Aachen, 90-94.

MEETING THE 2200 °C+ CHALLENGE IN CARBON BLACK REACTORS WITH DEVELOPMENT OF ADVANCED ZIRCONIA REFRACTORY

Dr. P M Sivaram[1], G. Bhattacharya[2], Ranjan Dey[1], S Panneerselvam[1], Imran Khan[1], R. Soth[2], C. Wöhrmeyer[2], Subhasis Gangopadhyay[1], Prabhakar Jha[1], C R Manoj Kumar[1], B Raghavendra Pai[1]

(1. Carborundum Universal Limited, Chennai, Tamil Nadu, India; 2. Imerys SA, France)

Corresponding author's e-mail: sivarampm@cumi.murugappa.com

Abstract

The drive for increased efficiency and premium-grade production in carbon black manufacturing demands hard black reactor temperatures reaching more than 2200°C, significantly exceeding the current 1800°C. This extreme thermal environment causes severe structural degradation in traditional alumina linings, necessitating the development of advanced zirconia-based refractories. Quantifiable benefits include a projected 1% improvement in product yield for every 100°C increase in flame temperature, potentially leading to a 4% higher yield at operating temperatures around 2200°C. A novel zirconia refractory with optimized phases was developed to withstand this critical environment. Fused zirconia raw materials are used to ensure extremely low impurity levels, exhibit sufficient melt crystallization, high density, and maintain stabilized phase qualities. The developed zirconia refractory underwent detailed examination for phase analysis, reversible thermal expansion, microstructure, and structural and thermal properties. The comprehensive test results are highly promising, validating the exceptional applicability of this high cubic-phase zirconia refractory for ultra-high temperature application.

Keywords: Zirconia refractory, carbon black reactors, high temperature, zirconia phases

1. Introduction

Carbon black is a critical material used in tyre, paint, ink, batteries, electronics, plastics, composites and other industries as additive, feed stock, conductive material etc. Carbon black materials are produced from heavy petroleum products by partial combustion or thermal decomposition at high temperatures ranging from 1500°C to 2300°C. These carbon black materials are classified into hard black and soft black based on their sizes and produced in Tread and Carcass reactors respectively. Hard black materials are ultra fine in size (1 to 30 nm) and produced at high temperatures ~1850°C and above. The zones, temperature profiles, criticalities and hot face refractories used are given in figure 1 and table 1. In a tread reactor, the most severe refractory exposure is generally in the combustor, throat/choke and post-choke regions because of peak temperature, high gas velocity, reducing atmosphere, feedstock cracking, particle erosion and water-quench thermal shock. Alumina refractories are employed in such situation due to their high temperature stability and wear resistance property.

Carbon black yield/productivity depends on the temperature of process. Typical tread reactors running at 1850°C peak temperature yield 56% [1]. For every increase in 100°C, yield can be improved by 1%. However, alumina refractories are limited to 1850°C design temperature and demand the need of alternative refractories. For temperatures more than 2200°C, zirconia refractories are an ideal choice. More applications of zirconia refractory are found in glass furnace, metallurgy (crucibles, nozzles, slide gates, furnace linings), and as kiln furniture and lining in specialty kilns. However, the temperature is limited to 1650°C.

Zirconia has emerged as the premier refractory material for these demanding hot-face zones due to its superior material characteristics, notably its exceptionally high melting point exceeding 2700°C, high-temperature structural strength, and outstanding chemical inertness [2] against aggressive process gases. Furthermore, Zirconia offers significantly lower thermal conductivity, over 40% lower than dense pure alumina (~4 W/mK) at 2000°C [3], providing an efficient thermal barrier that retains valuable heat while protecting the outer steel shell. Pure zirconia undergoes allotropic phase transformations from monoclinic to tetragonal at ~1173°C and cubic at ~2370°C causing volume changes of 5–6% that can lead to catastrophic mechanical failure. To mitigate this, zirconia is "stabilized" with dopants like Calcia, magnesia, or yttria. However, fully stabilized cubic zirconia lacks phase-transformable grains and is thus prone to thermal shock cracking due to a high coefficient of thermal expansion (~10.5 to 11×10^{-6} K^{-1}) and low thermal conductivity. Consequently, refractory-grade partially stabilized zirconia (PSZ), such as MSZ (Magnesia stabilized) and CSZ (Calcia stabilized), is engineered to retain a multi-phase microstructure capable of absorbing the stress generated during cracking by strategically allowing controlled transformation into the monoclinic phase from tetragonal [4]. Under thermal stress, this microstructure can induce a phase transformation and intergranular microcracking, which effectively dissipates thermal strain energy and arrests macrocrack propagation, thereby enhancing thermal shock resistance [5]. For carbon black reactors, PSZ with a balanced monoclinic and cubic crystal microstructure is preferred over fully stabilized options, as it provides the essential thermal shock resistance required for dynamic reactor cycling. A detailed analysis of the physical, thermal and material characteristics of zirconia refractory is conducted to understand its applicability in high temperature Carbon black applications.

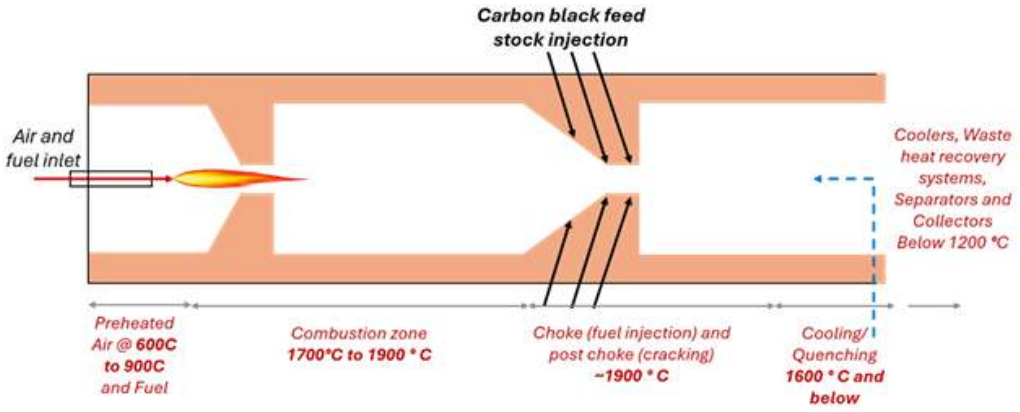


Figure 1 Schematic diagram of Combustion and reaction zone in Tread reactor

Table 1. Critical parameters at different zones in Tread reactor

Zones	Preheated Air	Combustion zone	Choke and Post Choke	Cooling/ Quenching	Dryer, Waste Heat recovery and other collection zones
Temperature	600 °C to 900 °C	1700°C to 1900°C	~1900°C	~1200°C to 1600°C	<1200°C
Criticality	Less critical	High temperature	High temperature	Thermal shock	Less critical

			and erosion		
Type of hot face refractories used	Mullite	High Alumina	High Alumina	High Alumina with thermal shock resistance	Alumina-Silicate

2. Methodology

2.1 Raw material processing and parameters

Table 2. Critical parameters at different zones in Tread reactor

Chemical analysis (weight %)	**Calcia Stabilized Zirconia - CSZ (ZCO GW-1)**	**Monoclinic Zirconia (ZCO RA)**
ZrO_2+ HfO_2	95.5	99.2
Fe_2O_3	0.05	0.03
SiO_2	0.1	0.14
Al_2O_3	0.21	0.2
TiO_2	0.12	0.11
CaO	3.72	Trace

The zirconia bricks were manufactured primarily using Calcia-stabilized fused zirconia (ZCO-GW-1) from the Imerys Yingkou Plant in China. During production, monoclinic zirconia and lime were fused in an electric arc furnace, followed by casting the molten material into ingots. The stabilization levels for these grades ranged between 77% and 82%. A minor proportion of monoclinic zirconia (ZCO-RA) was incorporated into the composition to optimize the mix. X-ray fluorescence (XRF) analysis, presented in Table 2, confirmed the high purity of both components, which is essential for ensuring stability under the extreme thermal conditions of carbon black reactors.

2.2 Refractory sample manufacturing

Calcia stabilized zirconia of sizes coarse, medium and fines produced by IMERYS Co. Ltd., are mixed with temporary binders, and stabilizers in planetary mixer. The wet mix was formed as 230X115X75 (mm) bricks in a vibro compaction press. The bricks formed were dried in electrical drier to remove the moisture in the sample and fired in batch kilns at +1700°C. Heating and cooling of refractory in kiln are critical. Calcia-stabilized zirconia raw material consists predominantly of the cubic phase (70% to 90%) (irreversible), with a minor fraction of monoclinic phase (10% to 20%) by weight.

2.3 Property evaluation

This zirconia bricks developed are subjected to physical, thermal and microstructural tests. Physical properties such as bulk density and apparent porosity are measured using boiling water method. Structural properties like cold crushing strength and modulus of rupture are measured using universal testing machine in samples with size 50X50X50 (mm) and 150X25X25 (mm) respectively. Thermal conductivity was

measured using water calorimetry method in samples of size 230X115X75 (mm) as per ASTM C 202, and reversible thermal expansion (RTE) is carried out as per ASTM E 228-06 respectively, to understand the thermal stability of the refractory and compared with samples available in market.

2.4 Microstructural characteristics

Scanning electron microscopy (Make: JEOL, Model: JSM IT100), X-ray diffraction (Make: Bruker D8 Advance, Panalytical X-Pert3), Raman spectroscopy (Make: XploRA PLUS) are conducted to understand the microstructure, phase pattern of the refractory developed. The resulting properties and characterization of the developed zirconia sample (ZR) are benchmarked against commercially available zirconia refractory samples (ZC).

3. Results and discussion

3.1 Physical properties

Bulk density, Apparent porosity for the developed zirconia refractory and commercially available samples are compared and given in Table 3. Both samples are with similar bulk density and apparent porosity. However, the cold crushing strength of the developed zirconia sample ZR is 73% higher than the commercially available zirconia sample ZC. Similarly, modulus of rupture of ZR is 50% more than ZC. Better particle packing, distribution of coarse and fine material used in the developed refractory (ZR) and the in-situ stabilization help in achieving higher crushing strength and modulus of rupture in ZR. Microstructural analysis can help in visualizing the distribution of coarse and fine materials in the developed refractory sample and discussed in the below sections

.

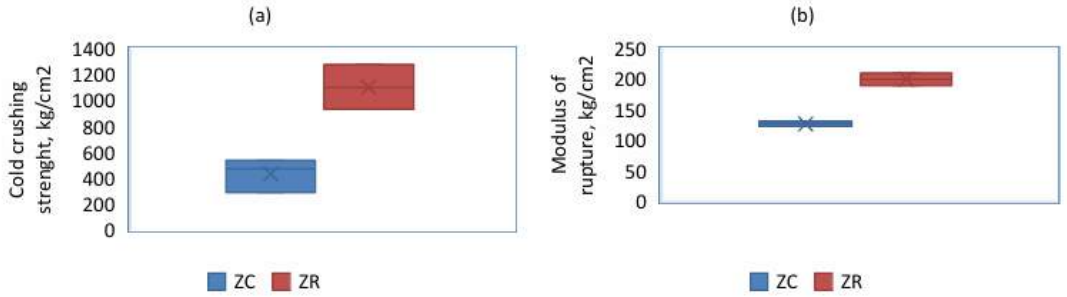


Fig 2. (a) Cold crushing strength and (b) modulus of rupture of the refractory samples

Table 3 Bulk density and Apparent porosity

Properties	Units	Testing standards	Zirconia refractory (ZR)	Commercially available zirconia refractory (ZC)
Bulk density	g/cc	ASTM-C20 (2005)	4.52 to 4.56	4.5 to 4.53
Apparent porosity	%	ASTM-C20 (2005)	19.1 to 19.3	19.3 to 19.8

3.2 Thermal propertie

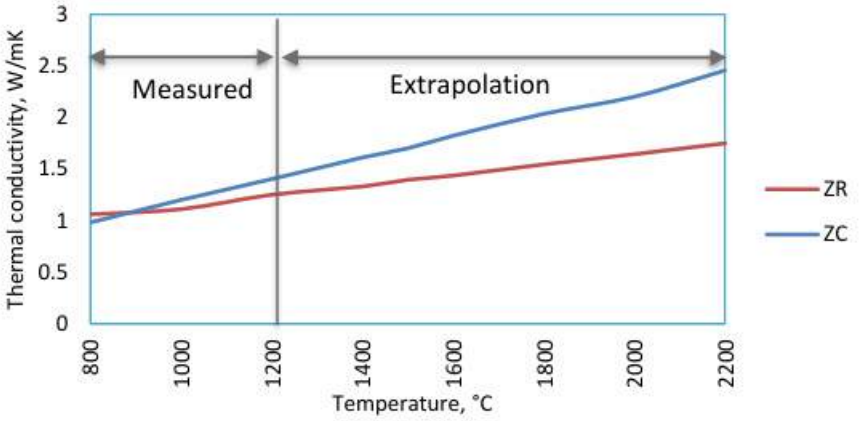


Fig 3. Thermal conductivity chart of refractory samples

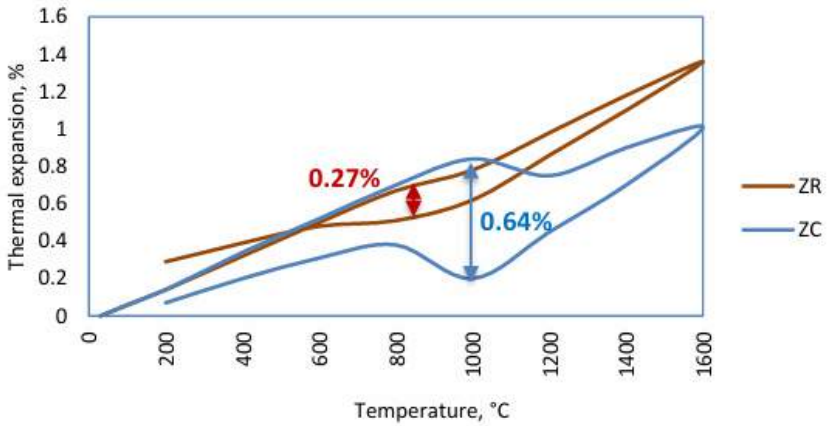


Fig 4. Reversible thermal expansion profiles of zirconia refractory samples

Thermal conductivity was measured using ASTM C202 (Water calorimetric method) for both ZR and ZC samples. Thermal conductivity of ZR is 1.06 W/mK and more than ZC (0.98 W/mK) at temperature 800°C and shown in Figure 3. When heated to higher temperature, the thermal conductivity of ZC increases and more than ZR. This indicates the presence of stable phases in the developed zirconia refractory (ZR). Further from figure 4, the thermal expansion coefficient of ZR is 30% higher than ZC. However, the reversible thermal expansion has delta ~0.27% in the developed zirconia and ~0.64% in the ZC sample between 800°C to 1200°C. Higher delta indicates the phase transition between monoclinic to tetragonal while heating and vice-versa while cooling. Heating of ZC sample above 1170C, the monoclinic crystal structure moves to tetragonal structure which is rigid and conducts heat effectively than the developed zirconia sample (ZR) and the same was reflected in figure 3. Further, thermal shock test conducted in a 50X50X50 (mm) sample in a furnace at 1000C. Due to lower monoclinic phase and reversible thermal expansion coefficient in the ZR sample, the crack initiated between 20th to 28th cycle and completely broke between 70th to 80th. This result indicates the structural stability of the developed refractory material in planned or unplanned shutdown scenario.

3.3 Microstructural characteristics

The microscopic image shows the even distribution of grains for both the refractory samples (ZR and ZC). More micro fines (10µm) are visible in sample ZC than ZR. Comparatively coarser grits used in sample ZR helps in achieving higher cold crushing

strength and lower reversible thermal expansion coefficient. Figure 6 shows the XRD peaks of the refractory samples. Primary peaks of zirconia monoclinic phase are identified at 2θ angles 28.2° and 31.5°; and a double peak at 24.08°.

Primary peak of cubic phase is identified in 2θ angle 30.2° followed by other secondary peaks at 35.1°, 50.2° and 60.0°. Phase analysis was carried out for both refractory samples (ZR and ZC) using full width half maxima technique from the XRD data. The refractory samples ZR and ZC are with 82% and 61% cubic respectively, and the remaining are monoclinic phases. Competitively, Monoclinic phase in sample ZC is 50% higher than sample ZR and aligns with the 30% higher RTE value (Fig. 4) of ZC sample. The reduced monoclinic phase fraction in the zirconia (ZR) sample is attributed to the incorporation of a stabilizing agent during processing. This promotes in situ stabilization and the conversion of monoclinic zirconia into the cubic phase. The resulting stabilized cubic phase remains thermodynamically stable, rendering the transformation effectively irreversible. Higher monoclinic phase will result in phase conversion, expand and contract during heat up and cooling and require slow ramp to avoid cracking of refractories while application.

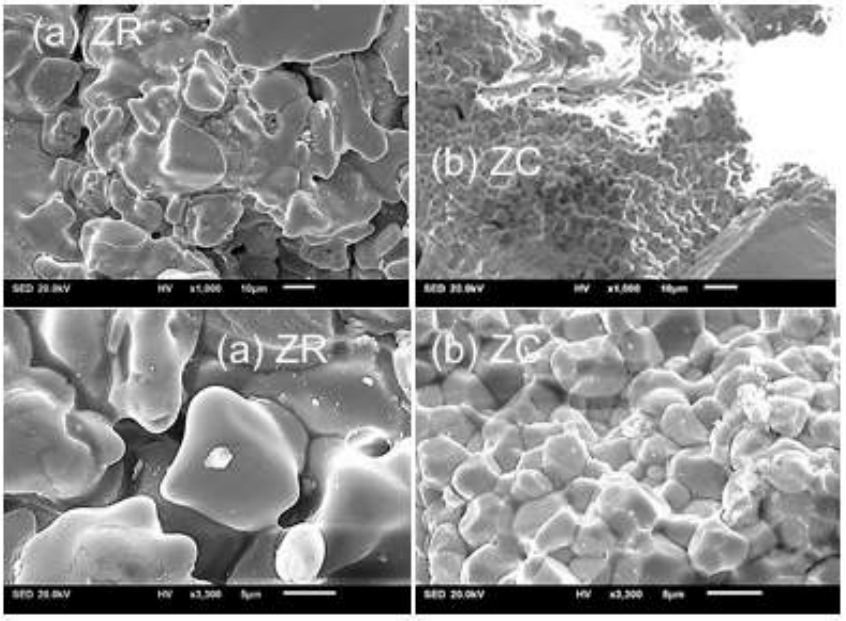


Fig 5. Scanning Electron Microscopic images for (a) ZR and (b) ZC

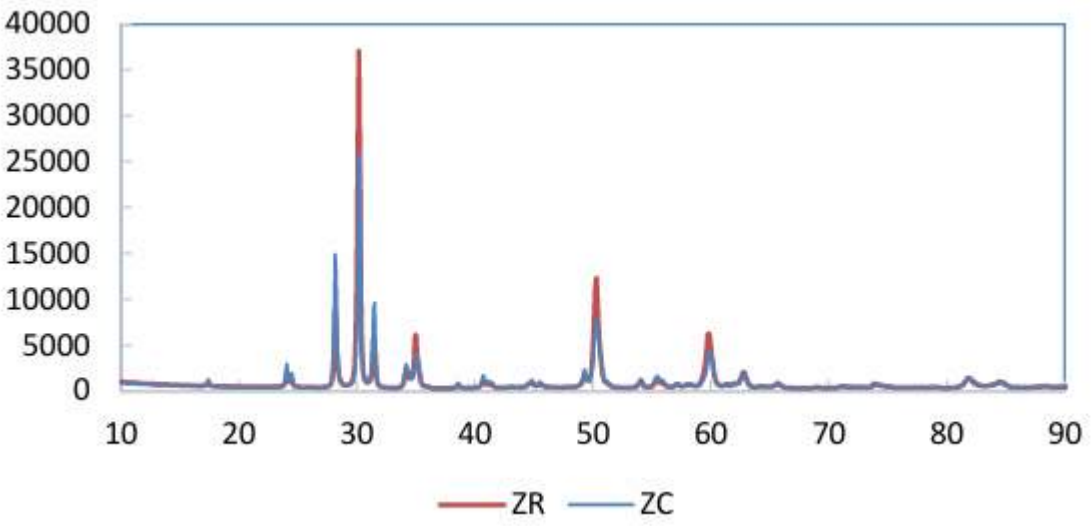


Fig 6. XRD chart of the refractory samples Z and ZM

Raman spectroscopy on the zirconia refractory samples (ZR and ZC) is conducted to check the monoclinic phases presence. Monoclinic phase is identified by its doublet formation between 180 cm-1 and 190 cm-1 and other peaks at 267 cm-1, 335 cm-1, 380 cm-1 [6]. These peaks are observed in sample ZM and reflect more presence of monoclinic phase and can be related with the results of XRD analysis. The peaks in sample ZR are broad and not intense and indicate less monoclinic phase which is achieved by in-situ stabilization of zirconia material. Peaks at 505 cm-1 and 580 cm-1 represent tetragonal phase. Broad peaks observed between 900 cm-1 to 1050 cm 1are cubic in nature. Similar cubic patterns are observed in both ZR and ZC samples.

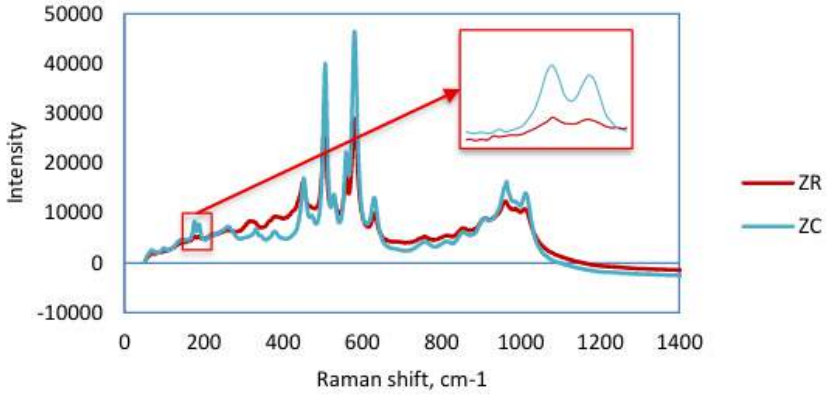


Fig 7. Raman spectrum for the zirconia refractory samples with zoomed image of monoclinic doublet in sample ZC

4. Conclusion

Zirconia refractory for temperatures more than 2200°C is successfully developed and tested for its application feasibility. Following conclusions are drawn from the above study.

• The developed Zirconia refractory exhibits a cold crushing strength 70% higher than that of the commercially available zirconia refractory. Its room-temperature modulus of rupture is also 50% higher, owing to greater compactness, in-situ stabilization, and high-temperature bond formation.

• Scanning electron microscopy images show that the developed refractory has larger grain size proportionately than the commercial counterpart, contributing to its higher structural strength.

• The developed Zirconia refractory is less thermally conductive and has lower differences of thermal expansion rate when compared with the commercial Zirconia refractory and can avoid cracks in sudden heating and cooling of carbon black reactors and reduce surface heat losses. These properties are due to the compactness, in-situ stabilization i.e., more conversion of monoclinic to cubic phases during firing.

• The phases of the developed and commercial zirconia refractory are quantified by X-ray diffraction technique. The cubic phase is around 82% and 61% in the developed zirconia refractory and the counterpart sample respectively. Further, Raman spectroscopy results also highlight more monoclinic phases in the commercially available zirconia refractory than the developed one.

These results demonstrate that the developed zirconia exhibits superior structural and thermal properties compared with commercially available zirconia. Further research is needed to understand the periodic behavior of refractory at high temperature and high erosion environment.

References

1. Rabishwar Roychowdhury, Brahmanada Mukhopadhyay: An improved process for the manufacture of carbon black by furnace process and an improved high volume high temperature (hvht) reactor for carrying out said method, WO2000020514A2, 1999

2. J.D.Lee: Concise Inorganic Chemistry, 4th Edition, ELBS with Chapman & Hall, London, UK,1991,p 690

3. T.Perrey: "Maximizing Reactor Performance: The Benefits and Challenges of Zirconia Refractories in Carbon Black Production," Carbon Black 2024 - Perspectives in Asia Pacific, Kolkata, India

4. J.Kim, H.Jeon, K.Jo, H.Lee and H.Lee: Phase Transformation Behavior, Mechanical Properties Under Thermal Stress, and Slag-Induced Erosion of 2–4 mol% CeO2-Doped CaO-Stabilized Zirconia. Materials, Vol.18, p.64

5. A.Priesea, A.Börger: "A Comparison of different lime stabilized zirconia powders made under different production conditions," India International Refractories Congress 2014, Kolkata, India

6. Bincy Cyriac: Analytical Approaches to Characterizing Zirconia-Based Compounds for Advanced Applications, Zirconia and Other Advanced Ceramics - Fabrication, Challenges and Applications, 2025

ENERGY SAVING SOLUTIONS – THE REFRACTORIES DESIGN, PROCUREMENT AND INSTALLATION FOR AN ETHYLENE CRACKING FURNACE

Sharmila Bose & Raj Kataria

Furnace Department
Technip Energies India Ltd., Noida (Delhi), India

Email: sharmila.bose@ten.com

Abstract

An Ethylene Cracking Furnace represents the critical core of petrochemical processing, facilitating high temperature thermal cracking reactions. These units operate at temperatures ranging from 1100°C to 1225°C. The Cracking unit consists of multiple furnaces having a complex refractory lining system. To achieve the long life of the refractory lining system in the furnaces, the improvement in refractory and insulation design detail required for the multi-layer Insulating Brick and Block lining system of the lower wall up to 6-meter height with steel support system. This zone is subjected to thermal flux due to the proximity of multiple burner assemblies and sight doors causing refractory failure for the deformation of metal support system and hot spots. Improper thermal management at the tube-pulling and access door interfaces lining with ceramic fiber blanket covering multiple retainer plates often leads to the deformation of the retainer plates, resulting in heat transfer and subsequently causing hot spots. All the issues analyzed by the Refractory experts based on the field inspection done on actual cases and considered as design challenges improvement required in the Radiant section to stabilize the refractory lining system from stress-induced spalling, structural deformation and different penetration sites of doors and burners to achieve desired results.

Keywords: Retainer, Deformation, Ethylene Cracker, Mockup and Quality Control

1. Introduction

An Ethylene Cracking Furnace Unit (Fig.1, twin cell Radiant Section) consists of multiple furnaces with complex multi-layer refractory lining having bricks and blocks up to 6-meter height at radiant section. The rest (upper walls) of the radiant section lining has ceramic fiber modules and ceramic fiber blanket lining. Several burners are mounted at floor and on the side walls of the Cracking Furnace, that combust a mixture of air and fuel, usually methane and hydrogen obtained in the cold section and flue gas generated. Several sight doors are made with bricks at the lower radiant wall and ceramic fiber materials at the end walls and upper radiant walls to view coils/supports/burner flames inside the radiant fire box. Large number of cutouts on furnace shell leads the sources of heat losses and generate hot spots due to disturbance in continuity of the lining. Typically, the furnaces are designed based on Licensor specifications and run at operating temperatures 1100°C to 1225°C or higher. Proper refractory & support plate design, engineering, material selection and sourcing, material quality and skilled application perfection which help to reach the expected operating temperature in furnace with significant energy savings with increase in production.



Fig.1: Ethylene Cracker Furnaces

1. Furnace Refractory Lining Design - Critical Factors

There are various critical factors which should be considered during design and detailing of radiant section refractory lining to avoid any hot spots and high heat losses.

a) In ethylene cracking furnace with brick and block lining reaching approximately 6 meters in height, adequate support bracket (lintel plate and rib plate) to be provided to bear the weight of the lining and ensure structural stability. The elevation difference(Fig.2) between support plates should be maintained within a very tight tolerance (0 to 7 mm max.) to prevent misalignment and ensure proper load distribution.

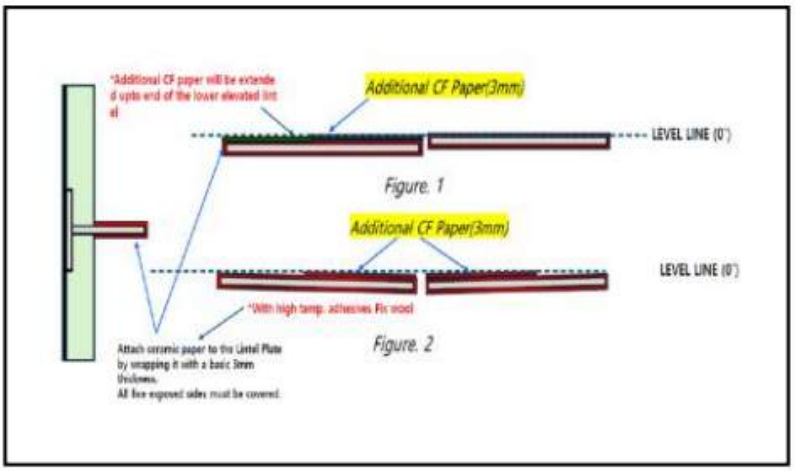


Fig.2: Dealignment adjustment with Ceramic Fiber paper

b) Bulging of the furnace (Fig.3) shell impacts negatively with the adherence of the refractory lining and disrupts the alignment of the multi-layer refractory lining. Gaps between these layers to be strictly avoided. Therefore, the shell's bulging to be maintained within a very narrow range of 5-10 mm. If shell bulging within limits is unavoidable, appropriate corrective measures should be implemented during refractory installation to ensure proper performance.



Fig.3: Undulation of shell plate

c) Proper refractory material, brick hooks and ancillaries quality and placement plays an important role in refractory lining performance in operation.

d) The layout detailing and positioning of expansion joint (Fig.4) locations of the bricks and the blocks lining shall be done as per Licensor's standard and specification. Any cutouts or notching required on the backup insulation block/board for brick holder adjustment shall be within 75 mm from the edge of block/board.



Fig.4: Expansion Joint staggering and plate support

e) Retainer plate design for the Tube pulling doors and the access doors of the end walls of Radiant section are very critical and based on lining thickness.

Lining Thickness	Retainer Plate Width less than total Lining thickness
Less than 300 mm	25 mm
300 mm to 400 mm	50 mm
More than 400 mm	100 mm

f) Sight door construction done with insulating brick lining design and detailing for lower radiant walls are critical because the thickness of the lining get reduced near the cutout location and causes high heat losses and can damage the shell.

2. Resolution Of The Refractory Lining Detail Design And Engineering

Detail Engineering should be done with proper resolution of the critical factors over regular standard information of refractory lining which are indicated below.

a. A robust structural bracket support (Fig.5) to be designed at the brick and block lining location of the radiant lower wall up to 6-metre height. The material of the support plate to be selected based on the operating temperature. The structural bracket support to be wrapped with 3 to 6 mm thick ceramic fiber paper of 1425oC grade to protect from direct heat conduction to shell. To nullify the alignment variations of the support plates, different thickness of ceramic fiber paper to be wrapped prior to brick and block installation. High temperature adhesives shall be used to fix properly the ceramic fiber paper with metal support plate.

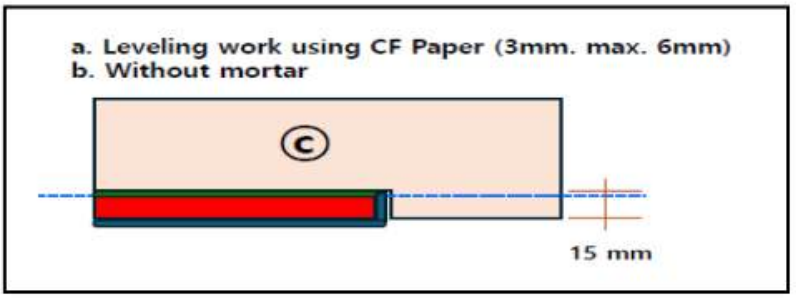


Fig.5: Ceramic fiber paper wrapping on support steel plate

b. The maximum permitted mortar joint thickness of the brick lining is 3 mm. For dimensional adjustments mortar should not be used of higher thickness. No mortar shall be applied between brick and ceramic fiber paper (Fig.6).

c. If any gap occurs even after increasing the ceramic fiber paper thickness up to 6 mm (max.) and mortar between the bricks up to 3 mm (max.), then to address width of brick (114 mm) can be used to make the height as required (in lieu of standard 76 mm brick height) after cutting to fit at site (fig. 6), as standard brick sizes are supplied/available.



Fig.6: Ceramic fiber paper for gaps

d. If bulging or unevenness is found of the shell plate, then plate shall be packed with ceramic fiber blanket or paper prior to the installation of insulation block lining. In this way, the gaps generated due to shell deformation shall be nullified before refractory application.

e. Ceramic paper / ceramic blanket / ceramic coatings(Fig.7) shall be used if any gap observed at interface of cold face and hot face lining.



Fig.7: Ceramic Coating used as filler and hardness

f. At the expansion joint locations (Fig.8), be sure to use specified expansion gap thick plywood during brick construction for achieving uniform expansion gap throughout the refractory lining thickness and height. Thermal expansion gaps to be maintained within 2 to 3mm tolerance range. Ceramic fiber blanket of 128kg/m3 density and 1425oC grade to be compressed by 30 to 40% to fill the gap.



Fig.8: Expansion joint of the brick lining

g. Slot cutting size of the brick hook area should be 45degree for the smooth movement through cleat.

h. During detail design of the brick lining care to be taken that no expansion joint should fall at brick joint area. The brick hook location should be placed mostly within the middle location of the brick. The mortar joint thickness should be 3 mm max. The mortar joint should not be applied at interface of cold layer and hot layer of brick lining. Each layer of the brick lining should be separated and free from the adjacent layering of the bricks and block lining.

i. Retainer plate (Fig.9) width is very critical at radiant access door and tube pulling door. At high temperature due to direct heat, the retainer plates would warp in serpentine manner. To avoid deformation of retainer, the retainer plate the width should be reduced by 100 mm for the refractory lining thickness of more than 400 mm. The ceramic fiber blanket HTZ grade shall be wrapped over the retainer plate (welded on door openings) of full

thickness which causes reduction in retainer tip temperature and protects from the direct effect of the heat.



Fig.9: Ceramic fiber blanket at Tube pulling door

j. The retainer plate of the Tube pulling door and access door (Fig.10) should be wrapped with U fold or S fold ceramic fiber blanket of HTZ grade 128kg/m3 density vertically throughout the height of Radiant End wall. Vertical U or S fold height should be maximum 600 mm to insert full depth of the lining thickness. If not possible, filling the gap with ceramic bulk fiber may require of certain extent based on the feasibility of ceramic fiber blanket insertion. Horizontal U fold of 30 to 32mm should be inserted after every 600 mm vertical height which shall take care of the vertical shrinkage of the U or S fold.



Fig.10: U fold insertion pattern of Ceramic Fiber Blanket

k. For ceramic fiber lining area Vacuum formed ceramic fiber board (Fig.11) of minimum 320-350kg/m3 density is preferred to use. If Ceramic fiber blanket or module is used for sight door construction, then coating materials obtained from the combination of polycrystalline ceramic fibers and sintered refractory oxides to be applied on the hot face to avoid any gap generation and act as surface hardener.

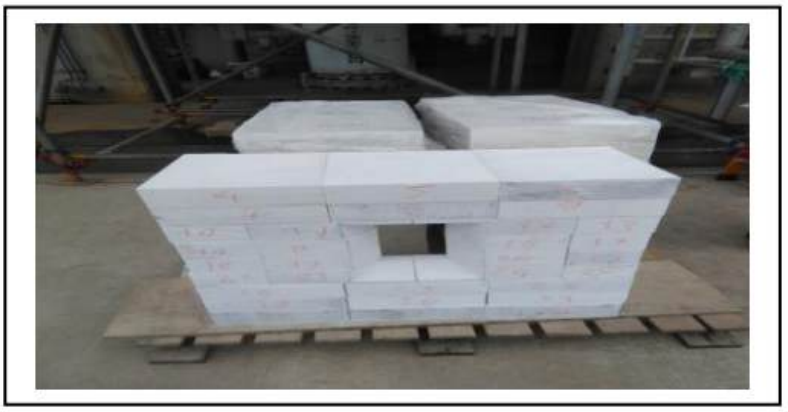


Fig.11: Brick lined Sight Door

l. The brick lining detail layout adjacent to the sight door and burner block should be done most critically. The normal shaped bricks 230x114x76mm along with special sizes of 230 x114x114mm shall be required for proper design and detailing Fig.7: Ceramic Coating used as filler and hardness Fig.8: Expansion joint of the brick lining Fig.9: Ceramic fiber blanket at Tube pulling door Fig.10: U fold insertion pattern of Ceramic Fiber Blanket Fig.11: Brick lined Sight Door Fig.6: Ceramic fiber paper for gaps packing the brick layout. No gap should be generated at the corner area of the sight door or burner block lining with the surrounding brick lining.

m. Sight door (Fig.11) at the lower Radiant wall be constructed with Insulated Brick lining and Chemical bonded high strength mortar. The reduced thickness of the lining near to the cut-out location which causes high heat loss and elevated shell temp. This also affects the shell and sometime deformed the shell. To reduce the heat loss backup insulation with lower thermal conductivity should be implemented behind the insulating brick lining.

3. Critical Factors For The Application Of Refractory Linings

Effective application of refractory lining based on the detail design and drawings lead to cause heat losses reduction and increases the production capacity by achieving effective heat storage and maintain the operating temperature inside the furnace. For effective application the most critical factors that should be taken care of are indicated below.

a) Skilled Mesons and Supervisors shall be engaged with clear understanding about the Drawings and details provided by the design detail engineering team for the lining.

b) Erection philosophy should be planned for the lining of Radiant section in sequence prior to initiating Refractory Installation.

c) All the Refractory material sources including sight doors and burner blocks shall be checked before starting the lining.

Inspection shall be done 100 percent for the notching locations. If any notching location observed at the edge of the block is less than 75 mm then the cleat location to be shifted locally.

d) During insulating block lining the notching shall be marked prior to installation.

e) The variation of support plates shall be checked prior to installation of the insulation block. All the support plate and Rib shall be wrapped with 3 to 6mm thick Ceramic Fiber paper of 1425oC (HTZ) grade (Fig.12 and 13) with special adhesive fixing ceramic fiber paper with Metal plate. Leveling shall be done

with the rectification done with ceramic fiber paper.

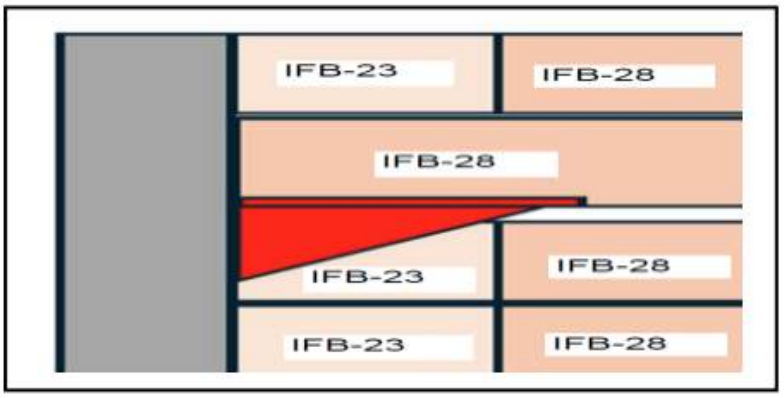


Fig 12: Type-1 Brick lining at Rib support

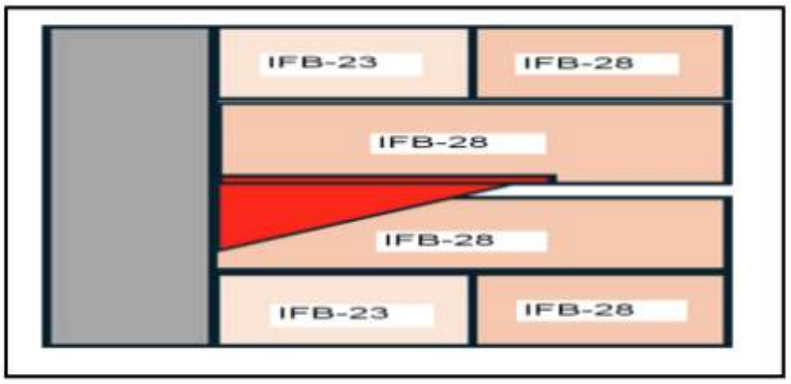


Fig 13: Type-2 Brick lining at Rib support

f) If any bulging observed at the Furnace shell then the condition to be rectified. Proper contact between the refractory lining with shell plate is mandatory. Rectification can be done in various manner.

1. Furnace shell to be changed.
2. Ceramic fiber paper to be inserted between the block and shell
variation with suitable adhesive.
3. Ceramic fiber blanket to be inserted to fill the gap between the furnace shell and the block.
4. Pumpable ceramics can be used to fill the gap.

g) After installation of Insulating block all the notching location shall be properly filled with ceramic fiber loose wool or blanket tightly. If any surface crack is observed on the hot face of the insulating block, then coating materials obtained from the combination of polycrystalline ceramic fibers and sintered refractory oxides to be applied on the hot face to avoid any gap generation and act as surface hardener.

h) The different grades of Insulating bricks shall be installed for the brick lining as middle layer and hot face layer. The middle layer brick shall be Grade 23 (IFB2300) based on the licensor specification. The mortar joint shall be at the bottom and side location. No mortar at the interfaces of brick and block lining.

No mortar between brick and lintel plate. Proper contact to be maintained between brick and block lining. If any gap found to be filled with ceramic fiber paper or coating

materials obtained from the combination of polycrystalline ceramic fibers and sintered refractory oxides to be applied on the hot face to avoid any gap generation and act as surface hardener.

i) The Hot face insulating brick lining shall be Grade 28 (IFB2800). No mortar at the interfaces of brick-to-brick lining. Proper contact to be maintained between brick and block lining. If any gap found to be filled with ceramic fiber paper or coating materials obtained from the combination of polycrystalline ceramic fibers and sintered refractory oxides to be applied on the hot face to avoid any gap generation and act as surface hardener.

j) The Lintel to be set under the brick with no mortar. If the measured dimension observed is less than the slot dimension indicated 18mm, then brick installation shall be done as per Type-1 (fig.12). If the measured dimension is found more than the slot dimension (indicated exceeds 18mm) then brick installation shall be done as Type-2 (Fig.13 & 14). After the installation of the brick the thermal expansion gap dimension to be maintained as specified (i.e. 13 -15 mm.in general). Brick to be cut to fit the thermal expansion regulation gap size. The Insulating brick to be cut to get fit at the rib support.

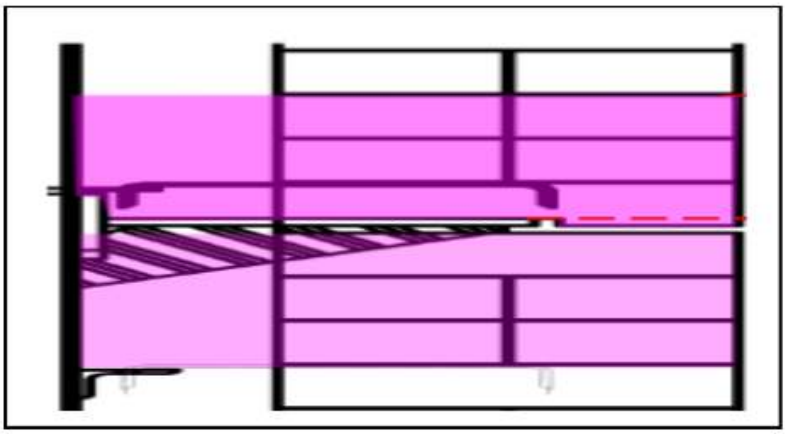


Fig .14: Lintel and Brick detail

k) At the expansion joint area of the brick lining (Fig.16 & Fig.17): The creation of expansion gaps is very important for the Brick lining. Plywood can be used for constructing uniform expansion gap throughout the lining thickness. The expansion gap to be filled tightly with HTZ Ceramic Fiber density 128 kg/m3. The HTZ ceramic fiber blanket to be compressed by 30 to 35% in thickness to fill the gap tightly. No mortar should be applied at the joint location of the brick adjacent to the expansion gap as indicated in the Fig(16 and Fig.17).

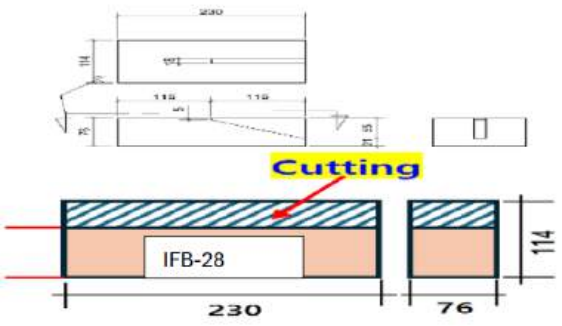




Fig.15: Shaping of Bricks at the Lintel and Support plate

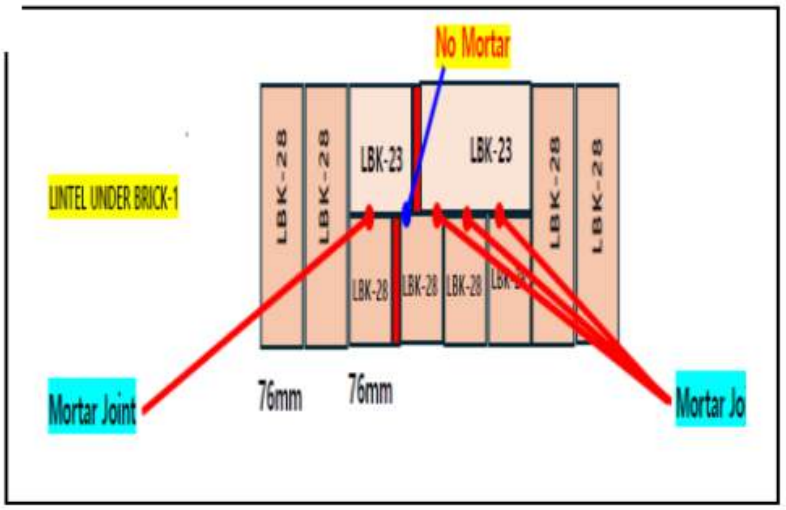


Fig.16 : Expansion Gap construction



Fig17: Brick lining near expansion joint and expansion joint construction

l) Peep door block at the lower radiant wall to be constructed by Insulating Fire bricks of Grade 2800 mortared with strong chemical bonded mortar (Fig.18). The bricks sizes to be designed based on the shapes and sizes of the peep door. To reduce the heat losses at the peep door at cut out location ceramic fiber blanket or board shall be installed at the backup lining with required thickness. Peep hole insert block anchor shall be used to hold the brick with backup ceramic fiber lining.



Fig18: Brick lining around the Sight/ Peep door area and Burner block area

4. Common Observation During Furnace Dry-Out Monitoring

Controlled dry-out (Fig.19) is necessary for refractory lining, before exposed to operation (high service temperature). The total dry-out of the furnace is done up to 550oC with slow rate of increasing temperature and given appropriate soaking time. Temperature measurement is done through temperature elements installed on the Equipment.

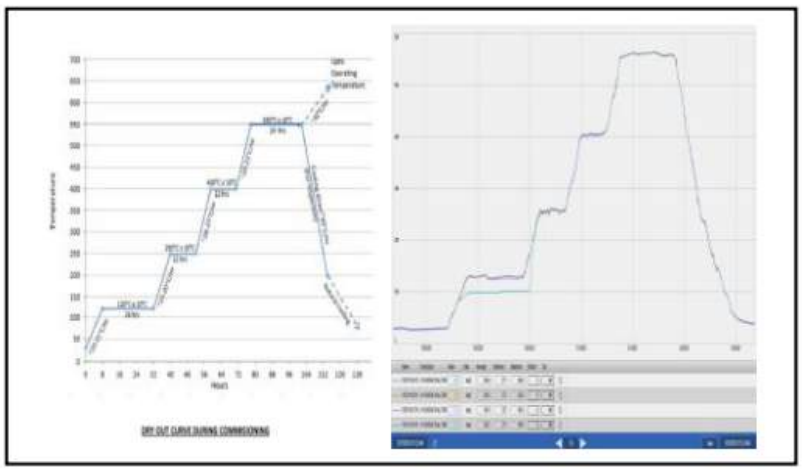


Fig19: Dry-out curve after complete lining

5. Conclusions & Summary

The multi-layer brick and block refractory lining system, extending up to 6 meters in height for the Ethylene Cracking Furnace radiant section, is the most critical lining system in terms of stability and performance. To achieve the goal proper detail Engineering and application of the refractory and steel support system are required. Very skilled fabrication required for avoiding undulation of the shell and alignment variation of the steel support system.

Quality of the refractory materials and steel support plates, ribs and ancillaries plays a very important role for facing thermal flux due to the proximity of multiple burner assemblies.

Refractory application in this critical zone must be carried out with very strict supervision and quality control as per relevant API standards mentioned in the reference list . Retainer plate design and installation also play an important role in the Radiant end wall tube pulling door and access door. Ceramic fiber blanket lining at the retainer plate location should be applied strategically with proper compaction to minimize heat loss and protect the plate from bending. Proper engineering, documentation, material selection and sourcing, along with skilled application under strict supervision, are essential to achieve effective refractory lining in the most critical area of the Ethylene Cracking Furnace, thereby reducing energy loss and increasing production rate.

6. Acknowledgments

The authors express their deep sense of gratitude to their Company Management, for their continued support and for giving permission for submission of this Technical Paper and Oral presentation at the IREFCON 2026. Further the authors acknowledge with gratitude the information used from various references listed here-with and also otherwise as well. Also, the authors are thankful to the IREFCON 2026 Organizing & Selection Committee for their support /feedback and opportunity provided.

7. References

1. API STANDARD 560, 2016 - Fired Heaters for General Refinery Service.
2. ASTM C680-23a - Standard Practice for Estimate of the Heat Gain or Loss and the Surface Temperatures of
Insulated Flat Cylindrical and Spherical Systems by use of Computer Program.
3. ASTM C892-19 - Standard Specification for High Temperature Fiber Blanket Thermal insulation.
4. ASTM C401 - Standard Classification of Alumina and Alumina Silicate Castable Refractories
5. Next generation Steam Cracking Reactor Concept - Marco van Goethem.
6. API STANDARD 936, 2024 - Refractory Installation Quality Control - Inspection and Testing Monolithic
Refractory Linings and Materials
7. API Standard 982, 2023 - Inspection and Assessment of Refractory Linings
8. API Standard 975, 2025 - Refractory Installation Quality Control-Inspection and Testing of Refractory Brick
Systems and materials

MODULAR REHEATING FURNACE INSULATION WITH REDUCED DOWNTIME, FUEL CONSUMPTION AND CARBON FOOTPRINT

Julie Hardy, Aditya Vishwakarma, Dr Sankar Kannabiran

Monocon International Refractories Ltd. Old Denaby, Doncaster, DN12 4LP, United Kingdom

Abstract

An advanced modular insulation system based on microporous calcium aluminate aggregates can provide a cost effective and reliable solution for the insulation of reheating furnace post and beam structures. It offers reduced installation and preheating times with reliable performance that maximises furnace uptime and productivity along with significant energy savings. This paper discusses the results of thermal modelling which demonstrate significant reductions in energy losses to the cooling water, in the range of 20-66%, along with the resulting reductions in fuel consumption and carbon dioxide emissions. It also discusses case studies which demonstrate the practical benefits of reduced installation time and extended service life.

1. Introduction

High-purity calcium aluminate aggregates were first commercially developed during the 1990's [1] and have found use as an effective insulating material in a variety of industrial applications. They can be used to produce effective alternatives to AES Wool, refractory ceramic fibre and other traditional insulating materials. Careful blending of these aggregates with high purity calcium aluminate cements and suitable additives allows us to create a range of highly insulating castables, which have good volume stability, excellent resistance to thermal shock and can be used up to a maximum service temperature of 1500°C. Typical properties for these materials have previously been described by the authors [2] By maintaining a high purity and silica-free chemistry then we can ensure that no low melting point phases are formed in the presence of iron oxides [3] See Fig. 1. This provides high resistance to mill scale when compared to most conventional refractories, making it an excellent choice for use in reheating furnace applications. These materials can then be combined with other refractory materials and a carefully engineered anchor system to provide an effective modular tube insulation system (K-BLOK) for use in both walking beam and raised beam pusher furnaces for steel reheating applications. See Image 1.

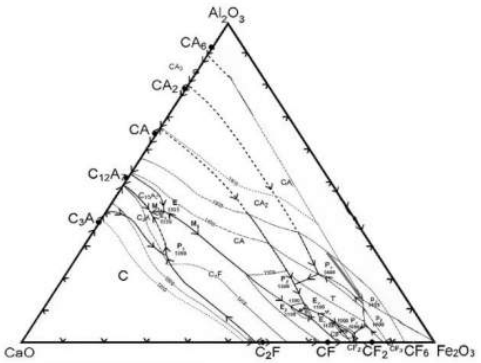


Fig. 1: Phase Diagram of CaO-Al_2O_3-Fe_2O_3 System.



Image 1: Typical layout of K-BLOK modular tube insulation

2. Thermal Modelling

Thermal modelling is carried out on a wide range of product and furnace designs using NASTRANS Inventer. See Image 2. This enables us to optimise reductions in energy loss through the refractory to the tube cooling water. In posts this reduction can be as high as 66% when compared with dense precast, cast in-situ or rammed solutions. In beams then this percentage is typically somewhat lower due to the presence of high conductivity alloy rider castings, but the overall savings are still very similar.

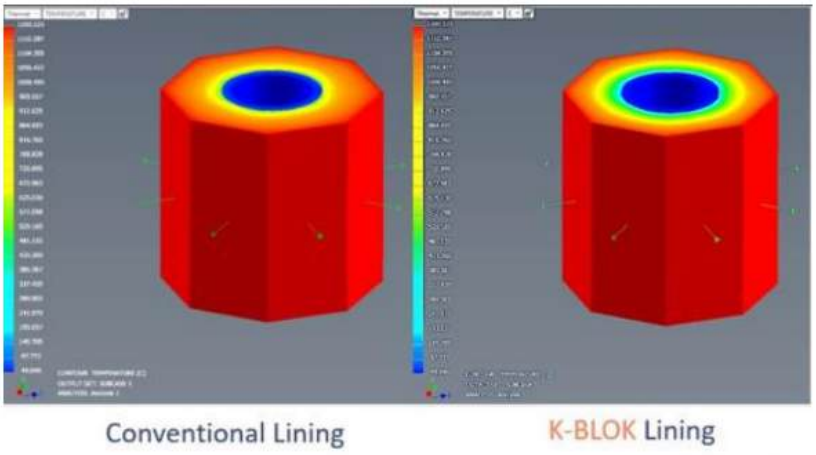


Image 2: Comparison of conventional and K-BLOK temperature profiles

This modelling allows us to calculate reductions in energy loss, fuel consumption and CO_2 emissions for each furnace configuration, fuel mixture and combustion efficiency factor of the furnace. Cost savings can then be calculated based on local fuel costs and CO_2 surcharge etc. See Fig. 2. Feedback from field trials is then used to refine the calculations based on real life data.

Annual Saving Model	Unit	Existing Construction	K-BLOK Construction	Reduction
Energy loss/furnace	MWh	16,880.00	14,540.00	2,340
Energy loss/furnace	GJ	60,768	52,344	8,424
Fuel Equivalent	t	3,093	2,664	429
Fuel Equivalent	SCM	4,283,139	3,689,386	593,753
CO_2 Equivelent (from 30% methane 70% corex top gas)	t	5,041	4,342	699
Combustion efficiency factor*	%	55.00%	55.00%	55.00%
Fuel Equivalent	t	5,623	4,843	7,546,197
7,546,197	t	9,165	7,895	1,271
Assumes 55% Furnace Combustion Efficiency				

Fig. 2: Typical comparison of fuel consumption and CO2 emissions for a 150 TPH walking beam furnace

Significant savings in both fuel consumption and CO_2 emissions are achievable. This can lead to large cost savings, even in large integrated plants where by product gasses are typically the main fuel source. These cost savings are even greater in plants where the furnaces are fueled using natural gas and in areas where CO_2 surcharges are applied.

3. Design

The modular design has been optimised with feedback from several years of field trials. Typical features include a single point stud fixing which requires only one weld for each block, while ensuring that each block is independently supported in case of damage to other blocks, while also allowing for the expansion and contraction of the beams during service. Our primary design philosophy is that we must ensure reliable performance while offering rapid installation and repair times. Annual Saving Model Unit Existing Construction K-BLOK Construction Reduction Energy loss/furnace MWh 16,880.00 14,540.00 2,340 Energy loss/furnace GJ 60,768 52,344 8,424 Fuel Equivalent t 3,093 2,664 429 Fuel Equivalent SCM 4,283,139 3,689,386 593,753 CO_2 Equivalent (from 30% methane 70% corex top gas) t 5,041 4,342 699 Combustion efficiency factor* % 55.00% 55.00% 55.00% Fuel Equivalent t 5,623 4,843 779 Fuel Equivalent SCM 7,787,525 241,328 7,546,197 CO2 Equivalent t 9,165 7,895 1,271 Assumes 55% Furnace Combustion Efficiency Newer designs have the option of a solid stainless steel shell against the tube to help protect the blocks from water leakage and a reverse taper fixing hole which retains the filling material in case of high vibration.

4. Case Studies

Case Study 1

K-BLOK post insulation modules were installed in the heating zone of a 250 TPH walking beam furnace and subjected to 12 months of normal operation. The K-BLOK exhibited minor surface discolouration, but it showed no reaction with millscale and no signs of deterioration. The high alumina plastic refractory installed above and below was starting to show heavy surface reaction with mill scale and part of this had already failed due to cracking. Precast shapes produced from a high alumina low cement castable were also installed in this furnace and they were showing significant deterioration and cracking after 18 months service.See images 3,4 and 5. These blocks remain in good condition and are still in service after 48 months.



Image 3: K-BLOK after 12 Months

Image 4: LCC block after 18 Months

Image 5: K-BLOK after 36 Months

Case Study 2

K-BLOK post and beam insulation modules were installed in the soak/discharge area of a 250 TPH walking beam furnace. Installation was found to be quick and easy compared with ramming, cast insitu or conventional precast shapes. This was a traditional problem area in this furnace due to the proximity of burner ports and cold air currents from a camera ports. Traditional refractory linings in this area would typically need extensive repairs after 18 months of service. Inspection of the K-BLOK after 18, 24 and 36 months showed no deterioration and no need for repairs. See Images 6 &7.



Image 6: K-BLOK after 18 Months

Image 7: K-BLOK after 36 months

Case Study 3

K-BLOK was installed in the posts of a 150 TPH raised skid pusher furnace. The installation of both posts was carried out within two hours, even though the installation team were unfamiliar with the K-BLOK system. Only 16 welds were required to complete each post compared with 64 welds required for a competitor's precast system and over 144 welds for conventional plastic or castable refractory. An unplanned inspection was carried out after around 9 months due to other problems with the furnace and one of the blocks was damaged during the shutdown. A new block was simply screwed onto the existing stud so that it was possible to replace the damaged block in a few minutes rather than hours. The remaining blocks showed no deterioration so it was decided to extend the trial during the planned shutdown after 12 months. Further blocks were installed in the posts, pusher beam and cross beams. See images 8, 9 and 10.



Image 8: Post Installation **Image 9: Post Repair** **Image 10: Installation of further K-BLOK**

5. Conclusions

The K-BLOK modular insulation system has been continuously refined over a period of several years, with close attention to material performance, optimised design and feedback from real world case studies. It has progressed from early small-scale trials and the gradual replacement of existing linings into full furnace supply. It provides reliable and trouble free performance when compared with traditional solutions and offers significant savings in terms of reduced installation and repair times, fuel savings and reduction in CO_2 emissions.

REFERENCES

[1] D. van Garsel, V. Gnauk, G.W. Kriechnaum, I StinneBen. New Insulating Raw Material for High Temperature Applications. Internationalen Feurfest-Kolloquium, Aachen 1998

[2] Julie Hardy, Dr Sankar Kannabiran,. Continuous Development and Practical Experiences with Microporous Calcium Aluminate Insulating MaterialsInternationalen Feurfest-Kolloquium, Aachen 2025

[3] De la Iglesia, P.G., García-Moreno, O., Menéndez, J.L. et al. Exploring the limits of Fe3+ solid solution in calcium hexaluminate. Journal of Materials Research 38. 2023.

A PRE-CAST CERAMIC-STEEL COMPOSITE OFFERING A UNIQUE COMBINATION OF PROPERTIES TO SOLVE ENGINEERING PROBLEMS IN INDUSTRY

L. W. Marston, J. Peat and S. Abdullahi

Fiberstone Products Limited, Pinxton, Nottingham, NG16 6NT, United Kingdom

Corresponding author's e-mail:

Abstract

Non-ferrous metallurgical processes, particularly within the primary and secondary aluminium **industries**, present severe service conditions for refractory materials. Components used in aluminium cast houses and smelters—such as **l**aunders, tap blocks, door blocks, skimmers, thermocouple protection tubes, and metal transfer systems—must operate under conditions of molten aluminium exposure, aggressive fluxes and salts, thermal shock, mechanical abrasion, and cyclic heating and cooling. Conventional monolithic refractories provide good chemical stability and thermal insulation but remain inherently brittle and susceptible to crack formation, spalling, and accelerated wear under these combined stresses.

This paper presents Fiberstone™, an advanced ceramic–metal composite (CMC) developed as a high-performance refractory solution for demanding industrial environments. The material is manufactured by infiltrating a dense network of stainless-steel melt-extract fibres with specially engineered ceramic slurries, producing a pre-cast composite capable of containing up to approximately 16% fibre by volume. This architecture combines the refractoriness and corrosion resistance of ceramic materials with the toughness and crack-arresting behaviour of metallic reinforcement, providing significantly improved resistance to fracture, thermal shock, and mechanical loading compared with conventional castable refractories.

Fiberstone™, demonstrate substantial improvements in fracture toughness, flexural strength, and energy absorption relative to both traditional refractory castable's and low-dosage fibre-reinforced systems. Crack propagation within the composite is controlled by a combination of fibre pull-out, fibre plastic deformation, and crack bridging mechanisms, which collectively increase the fracture energy of the material and significantly reduce the likelihood of catastrophic brittle failure.

The paper places particular emphasis on applications in aluminium smelting and casting operations, where refractory components are frequently exposed to molten aluminium, cryolite-containing environments, dross formation, and high thermal gradients. Several case studies are presented illustrating the successful use of Fiberstone in aluminium plant equipment including launder systems, molten metal transfer channels, skimmers, stirrers, and structural refractory components. In these applications, the composite material demonstrates improved durability, reduced cracking, and extended service life compared with conventional refractory solutions.

Keywords: ceramic-steel composite, fibre reinforcement, fracture toughness, refractory

1. Introduction

Refractories are among the oldest engineered materials still in widespread industrial use. They are strong, chemically resistant and generally good thermal insulators, but inherently brittle under combined mechanical and thermal stress. Reinforcement with stainless steel fibres has been shown to extend refractory life by improving toughness and flexural strength, thereby slowing crack initiation and growth [1].

Conventionally around one percent of fibre by volume is introduced during mixing. While beneficial, this level is limited by the difficulty of mixing and placing castables at higher fibre contents — yet it is at higher fibre volumes that toughness and flexural strength rise towards values approaching those of metals.

An alternative route overcomes this constraint: a pre-formed network of stainless steel fibres are placed into a mould and infiltrated with a ceramic slurry, producing a consolidated ceramic-steel composite. This slurry-infiltration route is economical and versatile in component size and shape. Components from around 100 g to several tonnes have been produced, with fibre contents up to sixteen per cent by volume achieved by controlling fibre aspect ratio — yielding a composite combining metallic and ceramic behaviour that neither class provides alone. The material has been applied across the iron, steel, aluminium, cement and petrochemical industries.

2. The Composite Material

The composite consists of a network of melt-extracted stainless steel fibres, typically 0.5–0.7 mm diameter, distributed through a ceramic matrix selected to suit the service environment — ranging from mullite-based systems for general use to high-alumina systems for superior abrasion resistance and high-temperature strength. Melt-extracted fibres have irregular cross-sections and a rough surface, giving an intermediate fibre-matrix bond strength central to the toughening behaviour described below (Fig. 1).



Fig. 1 Composite microstructure: (a) macrograph showing fibres in the matrix, (b) fibre cross-section, (c) fracture surface

2.1 Manufacture

Fibres, with any fixings, are placed into a mould and infiltrated with slurry under vibration for full consolidation. The green component is dried at low temperature (~30°C overnight) then fired at ~450°C to consolidate the matrix, with porosity controlled to a few per cent (Fig. 2).

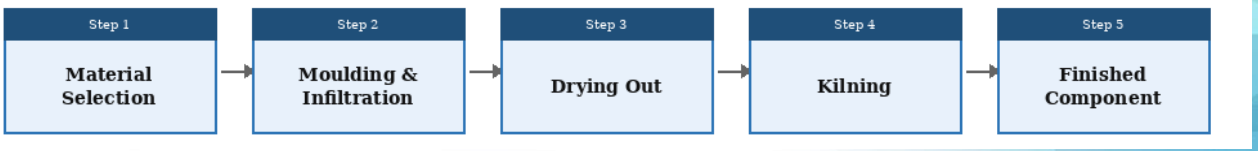


Fig. 2 The pre-cast manufacturing sequence

3. Key Properties

Conventional castable refractories have low fracture toughness and fail abruptly once a crack initiate. In the composite, fibres crossing a developing crack continue to carry load and absorb energy through progressive debonding and frictional pull-out, and through plastic deformation of fibres before they fail [2–4], the balance between the two governed by the fibre-matrix bond strength (Fig. 3).

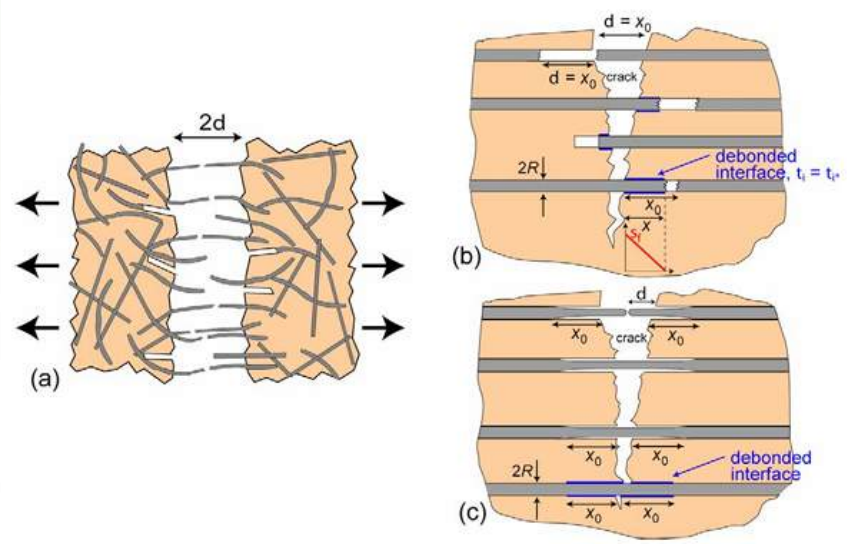


Fig. 3 Fracture process: (a) geometry, (b) fibre pull-out, (c) fibre plastic deformation

Fracture energies measured by IZOD testing at the University of Cambridge [5] lie in the range 25–60 kJ/m², against ~0.5 kJ/m² for the unreinforced ceramic — roughly one hundred times more energy absorbed before failure, placing the composite closer to hardwood and mild steel than conventional ceramic (Fig. 4). Larger-diameter fibres favour higher toughness [5].

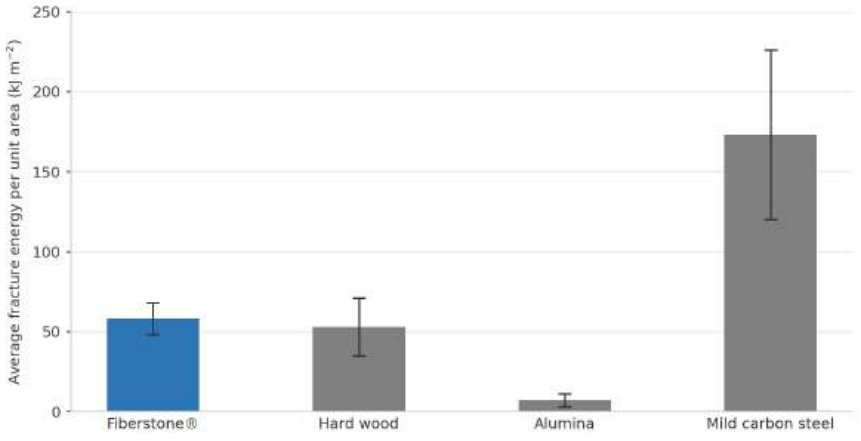


Fig. 4 Fracture energy vs hardwood, alumina and mild steel (IZOD)

In load-deflection testing, the composite sustains load well beyond first crack — reaching a peak load ~3.5 times greater than a castable with 4% stainless fibre, and continuing to carry load beyond 5 mm deflection where the unreinforced castable fails abruptly (Fig. 5).

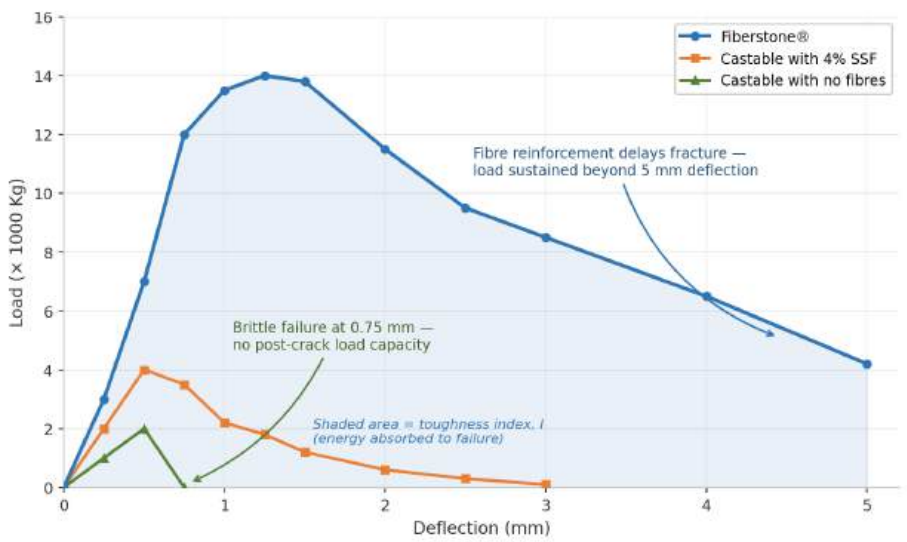


Fig. 5 Load-deflection: unreinforced castable fails abruptly; the fibre network delays fracture

The composite retains useful strength well above the continuous service range of steelwork, with negligible creep under sustained load. Thermal shock and fatigue resistance is favoured by a high strength-to-modulus ratio combined with low thermal expansion [6], both of which the composite exhibits. Verified properties are summarised in Table 1.

Property	Value	Source
Fracture energy (IZOD)	25–60 kJ/m²	Cambridge
Compressive strength	116–143 MPa	DIFK
Flexural str., 20°C	45 MPa	FPL
Flexural str., 1000°C	12.3 MPa	DIFK
Creep, 600–1000°C	~0 %/h	DIFK
Thermal exp., 1020°C	1.15%	DIFK
Max service temp.	1700°C	FPL
Peak load vs 4% fibre	3.5×	FPL

Table 1 Independently verified properties (304-type stainless fibres)

A further chemical advantage applies in aluminium service: where molten aluminium penetrates a silica-bearing refractory it reduces the silica to corundum and free silicon, generating internal stresses that crack and spall the lining. A high-alumina matrix is based on the thermodynamically stable oxide phase, so this reaction has no driving force [7], removing the corundum-growth pathway that degrades conventional aluminosilicate refractories.

4. Applications Across Industrial Sectors

The combination of toughness, strength, thermal shock and chemical/abrasion resistance suits the composite to components conventional refractories or steelwork struggle to sustain. Representative components across the sectors are listed in Table 2; selected service examples follow.

Sector	Representative components
Iron	Ladle spouts, torpedo throats, launder covers, tuyere covers, mud gun tips, slag spouts, rabbler blades, tundish parts, RH snorkels
Steel	Induction furnace top blocks, ladle lip rings, cover inserts, kiln nose rings
Aluminium	Door blocks, lintels, jambs, launders, tap blocks, stirrers, impellers, skimmers, nose rings, thermocouple tubes
Cement	Kiln nose rings, air cannon nozzles, damper blades, tyre fingers, retaining rings
Ferro-alloys	Ladle spouts, lip rings, rim blocks, mix/charge chutes

Table 2 Representative composite components by sector

4.1 Aluminium — rotary furnace nose ring

A rotary aluminium melting furnace nose ring, operating continuously at 900–1000°C across a thermal gradient from ambient in a varying acid-to-alkali atmosphere, saw the conventional castable reach 75% wear within three months. A composite nose ring, fitted as a bolted veneer over the most severely stressed 30% of the section, showed no detectable wear at three months; at six months, after a loading accident, it retained 90% of its depth with the seal fully intact; at nine months it survived a full furnace reline undamaged. Total service life exceeded 21 months — around seven times the conventional castable (Fig. 6).

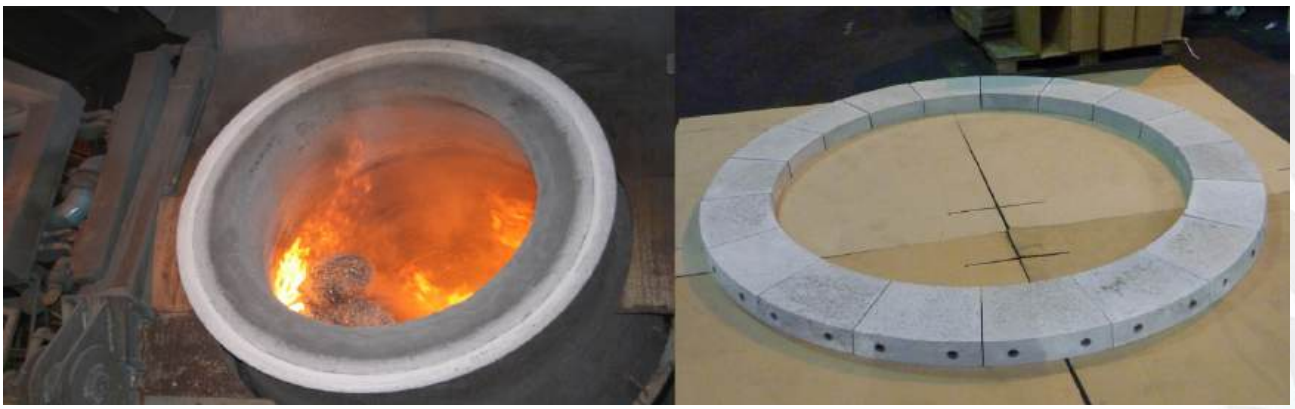


Fig. 6 Composite aluminium nose ring assembled prior to installation (left) and in service (right)

4.2 Steel — rotary kiln nose ring

At a metal recovery operation, precast refractory nose rings had achieved a best life of ~3 months before failing and collapsing, damaging the steel casing. A composite nose ring assembly fitted to a replacement casing subsequently survived eighteen cold-to-hot campaigns above 1200°C in near-continuous use, surpassing the original six-month target and prompting a repeat order.

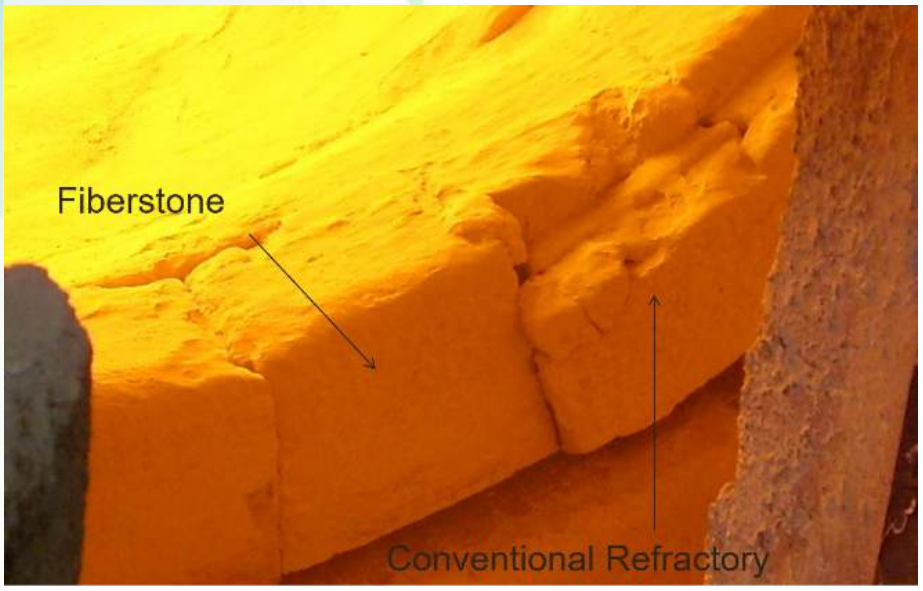


Fig. 7 Composite section alongside a conventional refractory section in the same kiln casing

4.3 Cement — air cannon nozzles

At a cement works, composite air cannon nozzles replaced steel structures that had lasted three to four months; the composite nozzles remained in service beyond eleven months, substantially reducing maintenance and downtime (Fig. 8).



Fig. 8 Composite air cannon nozzles ready for installation (left) and a nozzle in service in a cement kiln cooler (right)

4.4 Ferro-alloys — ladle spout

A ferro-alloy ladle spout, subject to constant thermal cycling and erosion at every tap, achieved 7–8 months in service using a previous fibre-reinforced product; a composite spout of the same geometry extended this to approximately one year (Fig. 9). At the same plant, a composite rim block replaced a cast steel component that had lasted 3–6 months, and a composite mix chute replaced a water-cooled steel chute, in continuous service since 2004.



Fig. 9 Composite ferro-alloy ladle spout components

5. Conclusions

Ceramic-steel composites provide a combination of toughness, strength, refractoriness, thermal shock and fatigue resistance, and corrosion/abrasion resistance that conventional materials find difficult to match, in precise, retrofittable shapes from small parts to multi-tonne components.

Independent and accredited testing confirms fracture energies of 25–60 kJ/m² — roughly one hundred times unreinforced ceramic — alongside retained hot strength, negligible creep and a 1700°C maximum service temperature [5,6]. Service evidence across the iron, steel, aluminium, cement and ferro-alloy sectors demonstrates substantial, repeatable extensions in component life relative to conventional refractories and steelwork.

Many industrial components fail not because a crack forms, but because it cannot be controlled once it does. Selecting critical components for fracture toughness and damage tolerance, rather than temperature capability alone, offers a route to improved reliability across high-temperature industrial processes.

Acknowledgements

The authors thank the Department of Materials Science and Metallurgy University of Cambridge, for independent fracture testing, and DIFK, Germany, for accredited mechanical and thermal testing.

References

1. M. Marston and P. Rooney: Internal Report, The Effect of Fibre Dosage Levels on the Performance of Castable Refractory Materials, Unpublished work, Fiberstone Products Ltd, 2002.
2. M.F. Ashby, F.J. Blunt and M. Bannister: Acta Metallurgica, Vol.37, 1989, p.1847.
3. M. Rühle and A.G. Evans: Progress in Materials Science, Vol.33, 1989, p.85.
4. D.A.W. Kaute, H.R. Shercliff and M.F. Ashby: Acta Metallurgica et Materialia, Vol.41, 1993, p.1959.
5. S.R. Pemberton, E.K. Oberg, J. Dean, D. Tsarouchas, A.E. Markaki, L. Marston and T.W. Clyne: Composites Science and Technology, Vol.71, 2011, p.266.
6. G.E. Dieter: Mechanical Metallurgy, 3rd Edition, McGraw-Hill, New York, USA, 1988, p.430.
7. E. Adabifiroozjaei, P. Koshy and C.C. Sorrell: Journal of the Australian Ceramic Society, Vol.51, 2015, p.139.

RIP IT OUT AND START AGAIN: NO LONGER A SIDESHOW, RECYCLING REFRACTORIES IS OUT OF THE SHADOWS

Mike O'Driscoll

Director, IMFORMED, UK | mike@imformed.com | www.imformed.com

Abstract

The refractories industry is facing some challenging headwinds, especially in Europe, but certain factors, including bright spots expected from steel market performance in India, the Middle East and eventually the USA, should contribute to an overall positive outlook to 2040. Indeed, world refractory consumption is projected to increase by 25% by 2040. Among the key trends anticipated to dominate the next decade will be increased use of recycled refractory material, with the rate of refractory recycling perhaps by up to 50% or more. This will be driven in part by the continued risk of volatility in certain refractory raw material availability, limited sources, vulnerable supply chains, influenced by geopolitical and trade issues. No more an esoteric sideshow practiced by a few players under the radar. Recycling refractories is now in the mainstream and expected, indeed required, to contribute much more to future refractory design, material selection, and assist in the overall drive to the Circular Economy. This paper highlights the drivers and the industry's recent response.

Note: accompanying tables and charts for this paper will be in the PowerPoint presentation.

The Big Picture

The future for the refractory minerals sector (and of mining in general), is being shaped by a New Order of geopolitical and environmental factors. Examples of the former include recent and ongoing conflicts, and the US tariffs impact. Of the latter, recycling is one of the two environmental missions of the refractory industry's time right now; the other is decarbonisation. Get these right and the industry will be more resilient to the challenges to come plus making much needed improvements to our environment.

While refractory mineral recycling will be an important contributor to the Circular Economy and assist in climate protection, significantly, it will also evolve as an essential alternative source of refractory raw materials. This will present opportunities in mineral recycling project developments and increased innovation and supply of pertinent processing and sorting technologies.

This new era of refractory mineral recycling is already underway and gaining momentum. But it is not plain sailing, mindsets need to be adopted and correct processes employed. Key questions include:

- How to go about getting involved in this sector?
- Whether to vertically integrate? Invest for an in-house business/plant?
- What kind of processing/sorting technology is required?
- Partner with/acquire an independent recycler? Join forces with same-sector end-use players?
- What kind of logistics are involved? Permits for handling/transport? Costs?
- Crucially: making grade acceptable, consistent, & economic for customers?

Refractory mineral recycling key drivers

The primary drivers, which may be interlinked, responsible for accelerating refractory mineral recycling, and in particular its growing requirement for domestic markets, maybe summarised as below:

1. Environment & market awareness of it: climate change; CO_2 reduction; overall drive for the "Circular Economy"; sustainable development of raw materials; and, crucially, mineral-bearing end product manufacturers (ie. the mineral consumers – the refractory manufacturers) increasingly needing to show "evidence" of "green credentials" in their raw material sourcing and production (eg. sustainability, CO_2 footprint).

2. Cost factors: rising cost of primary refractory mineral mining and processing, energy, logistics, waste treatment, landfill, future environment legislation penalties.

3. Limited primary sources: risky overreliance on supply/trade from limited overseas sources; for certain minerals, shortage of commercially developed mineral resources and processing plants.

4. Supply chain vulnerability: logistics stress; geopolitical impact; vulnerability particularly spotlighted by Covid-19 pandemic, Russia-Ukraine war, US trade tariff issues, US-Iran conflict, China-Taiwan?

5. China in change: relevant owing to China's mainstay as world refractory mineral supplier – overreliance by global consumers?; domestic supply issues impacted by wide range of factors = unpredictability in export availability and prices; end of an era for low-cost import reliance? Time to de-risk? = boost to alternative refractory mineral source development outside China, including recycled materials as an option.

6. "Criticality" of minerals recognised:"critical" and "strategic" mineral awareness now more mainstream; increasing government awareness/action/support/investment to include recycling programmes; of course, recognition of refractories and refractory raw materials as "critical materials" is required to assist such state support for refractory recycling initiatives, and this remains an ongoing issue.

7. Recycling technology more economic/established: evolved from somewhat esoteric, expensive mineral processing sideshow to mainstream processing line; advances in processing and sorting technology; opportunities now sensed and sought after; and significantly, more primary mineral miners increasing mine waste recycling efforts.

Refractory recycling: challenges & benefits

Recent technological advances have demonstrated that refractories containing recyclates can still perform, eg. MgO-C bricks can perform with up to 30% recycled material. However, there remain some key challenges:

• Security of consistent availability and "quality" of waste refractory supply to recycler
• Price remains main driver for customers; so primary benefits for end users should be that refractories with recycled material should cost less than their "standard" version, plus they should also have a lower Product Carbon Footprint (PCF), but this is challenged by…
• Costs of demolition, logistics, processing and sorting; especially processing, where the higher the share of recyclate = higher quality recyclate required = higher degree of processing = higher cost and impact on PCF.
• Waste and recycled material handling legislation remains unharmonised across borders. Certain waste law revisions and the EU Carbon Border Adjustment Mechanism (CBAM) have cost and movement limiting ramifications.

• Lack of acceptance from some end users and incentive by refractory producers – mindsets need to change.

PCF reduction benefit

Raw materials used to manufacture refractory bricks can account for up to 90% of their total carbon footprint, so a real objective in benefit of using recycled refractories should be cost savings by reduction of Scope 3 emissions. Indeed, the cement industry has found 11% less CO_2 per tonne of finished product using refractory bricks containing recycled raw materials.

Work by Dr Kathrin Weber, Head of Research & Development, Refratechnik Cement GmbH, has shown that the World Refractories Association (WRA) calculation method provides a standardised, comparable and simplified way of calculating the PCF of refractories.
Moreover, Weber demonstrated that using recycled raw materials has a significant impact on the PCF. In a magnesia-spinel brick, replacing half of the dead burned magnesia (DBM) with recycled DBM reduced the PCF by approximately 31-38%.

However, Weber urged that attention must be paid to after-use treatment, such as washing and drying. The higher the share of recycled materials the higher the quality standards required, and thus more energy-intensive processing is required.

Refractory sector examples: glass, cement

Expertise is required in tackling both the sorting and processing of the wide range of spent refractories, which vary greatly according to their end use, type, exposure, and contaminants.

In glass refractories for example, regenerators (checkers) yield spent material containing magnesia, alumina, and zircon, with the main contaminants being alkali vapour condensation, sulphate formation, dust infiltration, and chlorite penetration.

Whereas the glass furnace crown refractories, containing silica and high alumina, are subjected to alkali vapours, alkali sulphates, chlorites, and SOx gases.

• Expand trial installations in stable, low-risk kiln zones
• Encourage cement plants using recycled brick solutions
• Assess feasibility of a region-wide formation of recycling hubs

The cement industry is cautiously using more refractories containing recycled material. For example, Heidelberg Materials used just 0.4% “recycled” bricks during 2021-24, but in 2025-26 this value grew to 2.1%.

Much of Heidelberg’s spent bricks are consumed as alternative kiln feed. In Europe 15-20% is sold to recyclers, while in the USA as much as 40% waste bricks are sold to recyclers.

To enhance a much needed boost to using recycled refractories in the cement sector, Dr. Volker Wagner, Global Refractory Manager, Heidelberg Materials AG recommended that refractory manufacturers should:

• Evaluate potential of widening the recycling concept to all kind of materials (alumina bricks, monolithic refractories)

While cement manufacturers should:

- Expand trial installations in stable, low-risk kiln zones
- Encourage market entry of additional refractory suppliers for recycled brick solutions
- Assess feasibility of a region-wide tendering model for demolished bricks to generate plant-level revenue
- Evaluate relevance of Scope 3 emissions in corporate sustainability strategy

Such recommendations, could, and perhaps should be similarly applied to other refractory sectors.

Recycling activity reboot

While refractory recycling has been ongoing for some decades, it is only since around 2021 that activity has really started to increase, and worldwide. Initially, this was mainly led by the small group of well-established independent refractory recyclers (mostly in Europe) which have been operating for some years, happy in keeping a low profile…until now.

These are now expanding and are being followed by initiatives from large and medium-sized refractory manufacturers, as well as a few emerging new independent recyclers.

Europe remains leading the pack in refractory recycling, while catching up fast are India, China, Turkey, and South Korea. In the USA, refractory recycling remains at an early stage.

India

India's 2.2m tpa refractory industry, which is set to grow, remains facing an acute raw material challenge, whereby some 40% of its refractory mineral demand (particularly bauxite, magnesia) is reliant on imports, especially from China. Domestic refractory mineral development is limited, and so increased recycling is surely a primary objective for the industry, and this has been reflected in recent developments.

Established independent recyclers Chaitanya Refractory Pvt Ltd, Global Recycling, and Jai Balajee Trading Co., and refractory major TRL Krosaki, have all increased their activities. In June 2026,Valoref India inaugurated its plant, while RHI Magnesita launched MINPRO, a refractory recycling JV with Khemka Refractories Pvt. Ltd based in Odisha.

Europe

Long established recycler Horn & Co. Group, Germany,has been at the forefront of Europe's expansion in refractory recycling through Horn & Co. Minerals Recovery. In 2021 Horn formed a ground-breaking JV with Refratechnik (Refratechnik Horn Produktions GmbH) to use recycled material in MgO-C brick manufacture (in 2025 the JV was integrated completely in Refratechnik Steel GmbH).

This was followed in 2022 with the founding of MIRECO, a recycling JV between RHI Magnesita and Horn & Co. Minerals Recovery. A new recycling plant was constructed in Veitsch, Austria, and new sites and expanding activities by MIRECO have come on stream recently in France, Kosovo, Poland, Sweden, and Turkey. MIRECO acquired Italian recycler Trezzi Refrattari in 2024.

In March 2026, Horn acquired PAHAGE Refractories which is active in recycling.MIRECO now has 12 recycling sites in Europe and expects to recycle >250,000 tonnes in 2026.

Glass refractory experts REF Minerals, Latvia, acquired Czech demolition company SEBOREF, in 2022, and in 2024announced building a second processing plant at the site at Dolni Rychnov.

Valoref, France (part of Saint-Gobain) has significantly upped its activities since 2022 with subsidiaries recently established in India and China, and plans for North and South America. In 2025, Valoref acquired Alfaref, a ceramic waste recycler in Germany.

USA

In the USA, where expensive logistics and cheap landfill remain challenging factors, the refractory recycling sector is in its early days, but this needs to ramp up.

The USA relies on significant import volumes of refractory minerals, particularly from China: Bauxite, 100% (net import reliance), from China, Guyana; Graphite, 100%, China, Canada, Mozambique, Mexico; Fused alumina, >95%, China, Canada, Brazil, Austria; Chromium, >79%, South Africa, Kazakhstan, Finland, Canada; Silicon Carbide, 74%, China, Brazil; Alumina, 71% from Brazil, Jamaica, Australia, Canada; Magnesia, 52%, China, Israel, Brazil, Canada.

Glenn Hunter & Associates, with recycling plants in Ohio and Indiana, has dominated the fledgling US independent refractory recycling sector for many years. But over the last two years there has been increased activity from HarbisonWalker International and RHI Magnesita. In 2025, RHI Magnesita acquired established US recycler BPI Inc. to bolster its US recycling efforts.

Wrap-up

All this has triggered the evolution of a new mine-to-market supply chain option for consumers of refractory minerals, with the intermediate stages of the mineral processor and the trader extending their activities to encompass specific refractory waste stream sourcing and recycling.

However, in order to make the entire recycling loop function, both efficiently and economically, there needs to be continuous and growing alliances and collaboration between each of the refractory recycling supply chain stages, especially with the refractory waste providers (ie. steel, glass, cement plants etc.).

In particular, there must be a mindset on the part of refractory manufacturers to raise the degree or ease of recyclability of the spent end product, as well as ensuring increasing volumes of recycled material maintain the desired performance of the product.

References

Dr. Jennifer Astoveza (2026) “The hard truths about recycling and the road to circularity”*

Celio Cavalcante (2026) “North American refractory recycling strategy & market outlook”*

Kevin Christmann et al (2024) “Case studies of high recycling containing MgO-C bricks in high performance steel applications”, Bulletin 2024 The Journal of Refractory Innovations, RHI Magnesita

Werner Odreitz (2026) “Glass refractory recycling developments”*

Dr. Volker Wagner (2026) “Recycling in the cement industry”*

Dr Kathrin Weber (2026) “Impact of Secondary Raw Materials on the Product Carbon Footprint of Refractories”*

** presentation from Mineral Recycling Forum 2026, Cannes, 15-17 April 2026 organised by IMFORMED | Conference details & Proceedings PDF available – contact: maria@imformed.com| Coming up: Mineral Recycling Forum 2027, Cannes, 12-14 April 2027, CALL FOR PAPERS, Full Details: www.imformed.com*

WAKE UP AND SMELL THE COFFEE: PREVENTING ODOUR EMISSIONS FROM REFRACTORIES AT TATA STEEL IJMUIDEN

Warbout Tesselaar, Hein van der Velden, Frida Hameka, Chris Kooij, Patrick Tijsen

Tata Steel IJmuiden, The Netherlands

Corresponding author's e-mail: warbout.tesselaar@tatasteeleurope.com

Abstract

Carbon-bonded refractories release volatile substances when they are first exposed to high temperatures. Some of these volatiles can be harmful or unpleasant, occasionally leading to odour issues for nearby villages or for workers on the shop floor. In line with Tata Steel's core values of integrity and responsibility, multiple initiatives are underway, or already implemented, to reduce or even completely eliminate the release of refractory-related emissions to the environment.

Using torpedo cars, steel ladles and BOS vessels as examples, this work highlights recent progress in measuring, understanding and reducing such emissions. Each installation requires a tailored approach to achieve optimal results. In many cases, modifying the refractory materials to be inherently low-emission or free from harmful volatiles offers the most effective - or sometimes the only - solution. This underlines the importance of accelerating the development of cleaner refractory materials for every application, without compromising their performance.

Keywords: carbon-bonded bricks, emissions, safety, health and environment, measurement techniques.

1. Introduction

Carbon-bonded bricks have been a favourite among steelmakers worldwide for many years. Their excellent resistance to slags, thermal stresses and mechanical impact results in a high value in use, which is very difficult to match with other materials. The favourable properties of these bricks are very dependent on the binder system. Tar- and pitch-based binding systems were most common in the past, but the high content of carcinogenic polycyclic aromatic hydrocarbons (PAH) in these systems have necessitated a shift towards (phenolic) resin binders in recent years.

After production bricks are usually cured at 200 – 250ºC to let theresin form an organic polymer network which gives the material its green strength. Final brick properties are only achieved during first heat-up of the bricks in service, when the binder system breaks down into coke, eventually forming a carbon network that holds the brick together. In the case of phenolic resin binders 40 to 70% of the initial binder content(3 – 5% of total brick) remains as carbon network in the final brick, with the remaining 30 to 60% leaving the system as gases[1]. Most of these gases are not harmful, but small amounts of phenol, BTX and PAH are formed. The exact amounts of different volatiles are not only influenced by the type of binder (resol vs. novolac), but also by the composition of the rest of the brick and external factors like the amount of oxygen available during heating. For most resins the amount of harmful components is low enough for the material to be considered non-toxic[1]. However, the large scale on which these bricks are applied in installations like BOF, EAF and ladles means that the total amount of gases emitted during first heating is still considerable. Some of the emitted components can present nuisance because of their strong odour, even at concentrations far below legal limits.

Tata Steel strives to be not only a good employer but also a good neighbour, therefore multiple projects are ongoing to identify areas for improvement, understand the mechanisms involved and reduce or even eliminate emissions wherever possible.Materials, lining design and heating conditions can differ significantly between installations, necessitating a tailored approach. This paper will show developments on quantifying emissions and application of various solutions in the fields of torpedo cars, steel ladles and BOS vessels at Tata Steel in IJmuiden.

2. Measurement techniques

Sustainable reduction of emissions requires reliable and reproducible analytical methods to establish baseline emission levels and quantify the effectiveness of improvement measures. Emissions from refractory materials can be evaluated under controlled laboratory conditions or directly in industrial installations. Laboratory testing is particularly useful for comparing materials and identifying the temperatures at which volatile compounds are released, whereas field measurements are required to assess actual emission routes and potential exposure of workers and nearby residents.

2.1 Laboratory emission measurements

Laboratory emission measurements were performed using ThermoGravimetric Analysis (TGA). Small samples weighing approximately 50 – 100 mg were heated from ambient temperature to 1000°C at a constant heating rate of 25 K/min under an inert gas atmosphere. Continuous mass-loss measurements were used to determine the thermal decomposition behaviour of the refractory binder system.

To characterise the emitted volatile compounds, a continuous slipstream of the TGA off-gas was passed through a thermal desorption adsorption tube throughout the entire heating cycle. As a result, all compounds released between room temperature and 1000°C were collected in a single sample, providing an integrated representation of the overall emission profile of the material.

After sampling, the adsorption tubes were analysed by Thermal Desorption Gas Chromatography Mass Spectrometry (TD-GC-MS). During thermal desorption, the retained compounds are released from the tube and transferred to the gas chromatograph, where individual components are separated before identification and quantification by mass spectrometry. The method enables the determination of a broad range of volatile organic compounds, including phenols, benzene, toluene, ethylbenzene, xylenes (BTX), polycyclic aromatic hydrocarbons (PAH), and other aromatic degradation products.

The combination of thermogravimetric analysis and TD-GC-MS provides both the total mass loss of the material and the chemical composition of the released volatiles. This allows direct comparison of different refractory materials and binder systems with respect to their emission potential under controlled laboratory conditions.

2.2 Field emission measurements

While laboratory measurements provide insight into emission potential, industrial conditions are more complex because emitted gases may undergo combustion, dilution, adsorption or removal by gas-cleaning systems before reaching the environment. Therefore, field measurements were performed to determine actual emission pathways and exposure risks.

Gas samples were collected using adsorption tubes connected to calibrated sampling pumps.

Sampling durations were typically between 5 and 10 minutes, providing sufficient sample volume while maintaining adequate time resolution to identify variations during the process cycle. The collected samples were analysed using the same TD-GC-MS method as described for laboratory measurements, ensuring direct comparability between laboratory and industrial data.

The combination of laboratory TGA-TD-GC-MS measurements and industrial sampling campaigns enables identification of both the emission potential of refractory materials and the fate of emitted compounds within the production process.

3. BOS vessels

Magnesia-carbon bricks are by far the most common choice for BOS vessels, with IJmuiden being no exception. In the past these bricks were mostly produced on site in a dedicated brick plant, but since its closure more and more externally produced materials are being used.

Total lining weight of the IJmuiden converter is around 850t. Most of this consists of MC bricks that emit gases when first exposed to temperature, which will mostly be during the initial firing of the lining and the first heats after that.Even though most of the emitted gases will be burnt in the vessel, there is still a risk of odour nuisance for workers in the steel plant and in some cases even for residents of villages near the steel plant, since some of the components are malodorous at very low concentrations.

To reduce exposure of people to any of these emissions, a strategy is followed which is based on two pillars: understanding and improving.

3.1 Understanding: measuring emissions

Before any measures can be taken to reduce emissions it is important to understand the mechanisms involved as well as establish a baseline that enables quantification of the effect of any improvements measures.

The mechanisms behind formation of volatile compounds from resin binders are quite well known and some modelling has been done on emission rates over time in a BOF[2]. After leaving the bricks however, the emitted gases can take various paths. Volatile compounds traveling towards the hot face of the brick have a high chance of further combustion, especially during initial firing and during oxygen blowing in the subsequent heats. Gases leaving the vessel via the cold face (e.g. through holes in the shell) or via the hot face when there is less oxygen available (e.g. between heats) might not react further and therefore pose a higher risk of causing odour issues. After leaving the vessel there are again various paths the gases can follow, as there are three separate extraction systems. The primary extraction system has various cleaning systems before gas reaches the stack, including wet gas scrubbing, lowering the amount of volatiles reaching the environment. The secondary and tertiary extraction systems only remove solid particles, so volatiles entering these systems can reach a larger area surrounding the plant.

To establish the distribution of volatiles over the different exit routes and over time, an extensive measurement programme was started, in which gases are sampled in five different locations at various moments in time during the start of a new vessel campaign. The following sampling locations were used:

1. Primary off-gas extraction system, above vessel (before scrubber)
2. Primary off-gas extraction system, stack (after scrubber)
3. Secondary extraction system (extracts gases around vessel during charging and tapping)
4. Tertiary extraction system (extracts gases from top of building above the vessels)
5. Atmosphere in vicinity of vessel during tapping

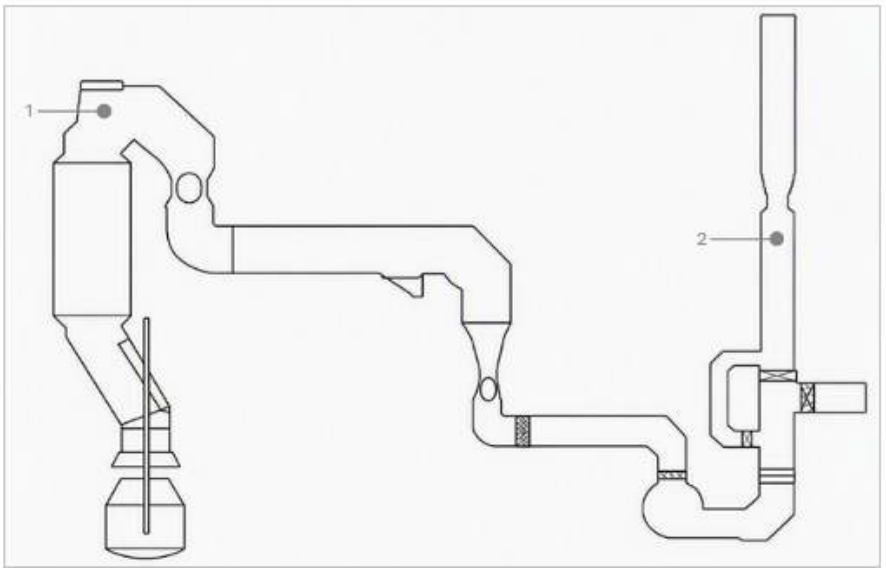


Figure 1: Primary off-gas extraction of BOS vessels with sampling locations 1 and 2

Sampling is done by pumping small amounts of gas through an adsorption tube. Samples are analysed afterwards using Thermal Desorption Gas Chromatography with Mass Spectrometry (TD-GC-MS), as described in chapter 2.

The use of sampling tubes means that there is a trade-off between granularity and completeness of the data. To catch all details it would be required to perform a high number of back-to-back measurements, as emissions could change over short periods of time. However, the number of samples tubes available as well as the time required to measure and analyse afterwards poses a limit to the number of samples that can be taken in practice. It was therefore decided to perform measurements at three key process moments for a selected number of heats, where most emissions are to be expected. The duration was chosen as 5 – 10 minutes per sample to get a balanced result:longer sampling masks any peaks whereas shorter sampling increases the risk of not catching short-term emission peaks at all. During a sampling window all sampling locations are measured at the same time.

The following process phases were defined for sampling:

• Charging: from start of scrap charging until 10% of main blow
• Blowing: from 40% to 90% of main blow
• Tapping: from end of main blow until start of slag tipping

With five sampling locations and three samples per heat, a maximum of five heats per campaign can be measured with the available sampling tubes. It was known from past experience that the highest risk of odour nuisance occurs around heats 4 – 10 of a new vessel. The objective is therefore to perform at least 3 measurements during the first 10 heats, with at least one in heats 4 – 10.One or two more samples are then taken in the days after to check whether emissions are indeed decreasing.

This method has now been applied multiple times to establish a good baseline.The most important findings for these campaigns are:
• Highest amounts of total emissions occur during the first 5 heats, with highest

concentrations in primary extraction system above the vessel.

• After 30 – 40 heats emissions of all components are lower, but not zero.
• PAH, BTX and other aromatic compounds are mostly found in primary extraction system, much less elsewhere. Highest concentrations occur during first heat. Concentrations in stack (after scrubber) are significantly lower than right above the vessel (before scrubber).
• Amount of phenolic and PAH compounds is low compared to other compounds (~2.5% of total).
• Phenolic compounds are mostly found in the secondary extraction system and close to the vessel.
• There is a peak in phenolic compounds in heats 4 – 8.

These findings indicate that the most likely route for odour nuisance is phenolic compounds coming through openings in the vessel shell and/or from the converter mouth (during tapping and charging) and exiting the plant through the secondary extraction system. Phenolics emitted through the primary extraction system are mostly burnt or washed out by the scrubber and therefore pose a much lower risk of leading to odour nuisance.Preventing fumes from leaving the vessel therefore has good potential as a first step in reducing odour emissions to the environment.

Emissions of PAH and BTX are mostly passing through the primary extraction system, which means part will be washed out by the scrubber. The fact that during oxygen blowing most of the off-gas will go to gas recovery further lowers the emissions of these components to the environment.

In general the first 10 – 15 heats of a new vessel are critical when it comes to preventing odour nuisance.

3.2 Improving: reducing emissions in practice

As with all health, safety and environment issues, the best way to solve the problem is by eliminating it at the source. In this case that means preventing emissions by applying alternative materials. Tata Steel's main refractory suppliers for converters were therefore asked to propose alternative lining materials with low or no emissions.

Maximum impact would result from using materials that do not emit any malodorous or harmful components during heating. This could be achieved by replacing the current phenolic binder system with a different binder. Although such binders do exist, the application in MgO-C bricks is mostly still in the development stages[3],[4]. Properties of MgO-C bricks with such alternative binding systems are often less favourable than those of standard resin-bonded bricks and application of these bricks could have a dramatic effect on vessel life and therefore production capacity.Although some positive results have been achieved in ladles, there are no known examples of emission-free bricks being applied in a converter on industrial scale.

More progress has been made with so-called low-emission MgO-C bricks. These are produced in the same way as normal resin-bonded bricks, but receive an additional heat treatment after curing to remove most of the volatile materials. At first glance this might seem like moving the problem elsewhere instead of solving it, however this preventive heat treatment by the supplier can be done in a tailored furnace where the escaping gases can be further treated to prevent harmful or odorous components from entering the environment, which is often difficult or even impossible to do when bricks are first heated after installation.Of course the heat treatment does have some environmental and financial implications because of the additional energy required in the process. It should be noted thatMC bricks can only be pre-fired to approximately 600 – 650ºC. Higher temperatures would lead to a high drop in strength, causing a very high risk of damage during transport and installation. As a result there will still be some emissions upon first firing, when the bricks reach temperatures higher than the pre-firing temperature, hence the term "low-emission".

Samples of low-emission bricks were requested from three different suppliers and evaluated in Tata Steel's refractory testing facilities according to the standard procedure for selecting converter materials[5].The objective was to identify materials with a ranking for suitability similar to or higher than the currently used materials, to enable a plant trial with minimal risk. Based on this evaluation the different suppliers were ranked and a first plant trial was conducted with the highest ranking concept to establish its performance in practice.

Evaluation of performance is done by comparing wear rates in different areas between the low-emission lining and regular linings of the same supplier. Wear rates are calculated based on laser scans for the first 2000 heats of a campaign, since during this period no reactive maintenance (e.g. gunning or patching,which could mask actual brick wear) is done yet. Determining wear rate is performed per area by fitting a linear trend to all measurements for that area, using the minimum thickness for each measurement. An example for one area is shown in Figure 2.

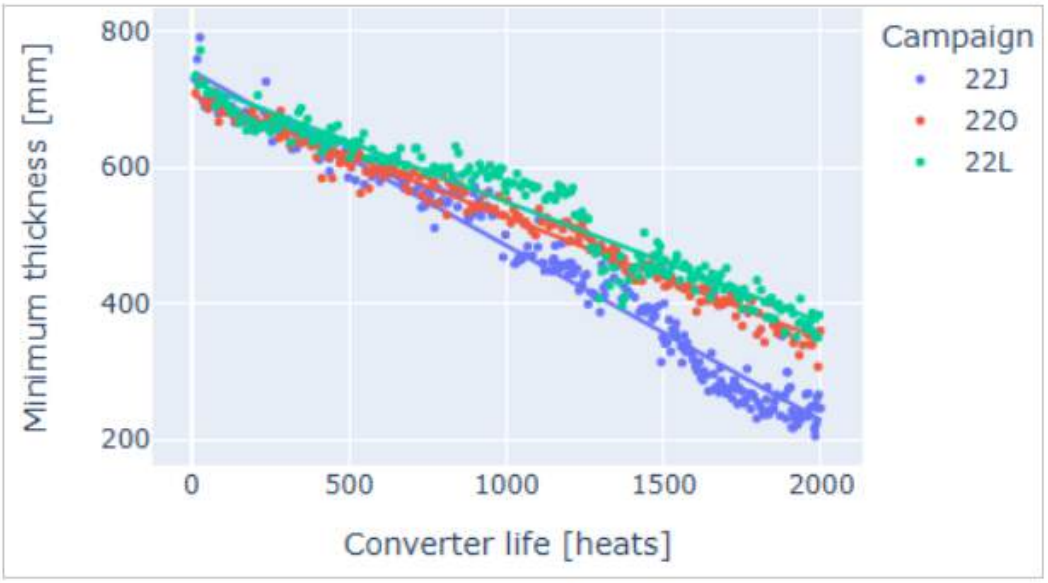


Figure 2: Minimum thickness of SE knuckle, including linear trends, for first 2000 heats of three campaigns

The dataset consists of three campaigns: two with standard bricks and one with low-emission bricks. Although more campaigns with standard bricks are available, these are not used as they occurred longer ago and therefore difference in process between then and now are likely to play a significant role. The two selected reference campaigns occurred shortly before and after the campaign with low-emission bricks. The wear rates for the two reference campaigns are averaged per main area and compared with those of the low-emission campaign. The results are shown in Figure 3.

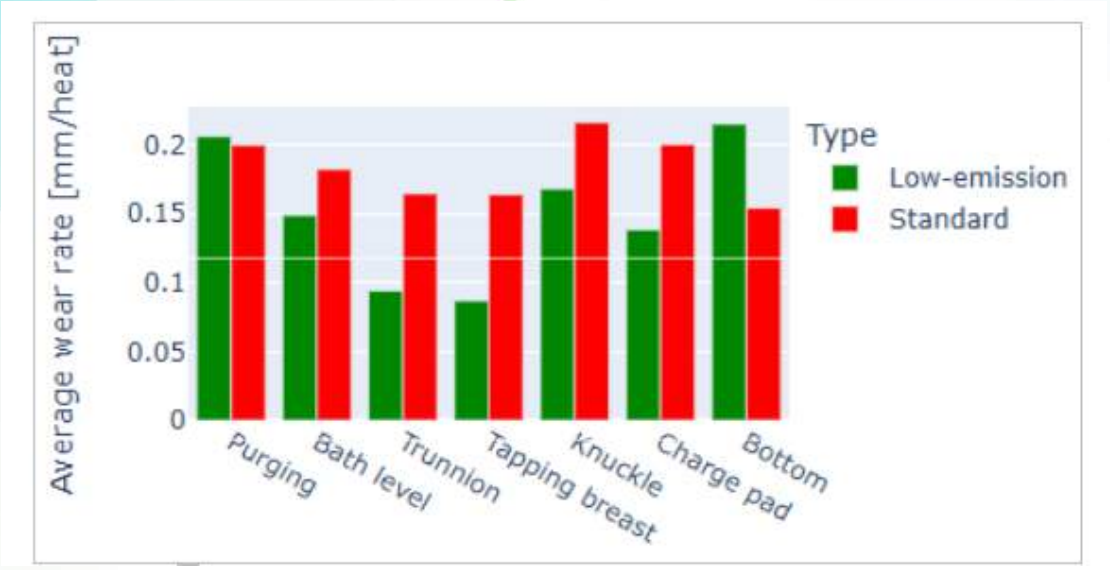


Figure 3: Wear rates per area for standard and low-emission bricks

On average the low-emission bricks have lower wear rate for most areas. This might be a result of the brick properties or of process conditions being slightly different between campaigns. Only the bottom has (significantly) higher wear. The bottom itself is currently not a bottleneck and therefore a slight increase in wear could be acceptable, however the thickness in the purging areas (around the multi-hole plugs) is sometimes limiting and can requires switching off multi-hole plugs to ensure safe continuation of the campaign. Higher wear in the bottom, particularly around the MHP's, is therefore not acceptable. Based on these results the supplier has proposed a different bottom quality which, according to the TSIJ evaluation method, should perform slightly better than the original one. A second trial lining, which will include the improved bottom material, is scheduled for installation in November 2026. Emission measurements, as described in the previous paragraph, will be performed during the initial heats of this campaign.

4. Steel ladles

For many years the standard wear lining concept for IJmuiden steel ladles has been as follows: resin-bonded alumina – magnesia – carbon (AMC) bricks in the bottom, fired alumina-spinel bricks in the barrel and resin-bonded MC bricks in the slagline. The large size of this ladle (~335t capacity) means that roughly 24t of resin-bonded bricks are installed. Although this is much less than the amount of bricks in a converter and furthermore heating takes place in a fully enclosed dryer with afterburner, the fact that around 5 new ladles are being built and heated every week means there is still a small residual risk of odour nuisance.

It should be stressed that any possible improvement should be evaluated not only for its potential to lower emissions but also its potential effect on value in use. Even small changes in wear rates of critical areas can result in major effects[6], not only affecting ladle life and refractory cost, but potentially also increasing the risk of a costly breakout.

In IJmuiden the wear rate of the slagline is currently often limiting ladle life. Alternatives materials tend to have higher wear rates in the slagline than MC bricks[7]. Furthermore development of emission-free MC bricks is still in the development stages, as mentioned in chapter 3. It was therefore decided to focus efforts on replacing the resin-bonded bricks in the bottom by an emission-free alternative.Monolithic bottom linings have become an established alternative for resin-bonded bricks[8] and show good value in use in various steel plants.Switching from

bricks to an in-situ cast lining has the disadvantage of required high initial investment for equipment such as mixers and suitable drying stands. To establish the potential of monolithic material it is therefore much more attractive to start with precastpieces.

Besides eliminating emissions from this part of the lining, switching from bricks to precast pieces has other advantages as well:

• Reducing thermal losses through the bottom of the ladle and reducing shell temperatures.
• Reducing repair times: can be completed in 1.5 – 2 hours with 3 people, whereas bricked lining usually takes 8 hours with 2 people+ 1.5 hours with 3 people).
• Improving working conditions during lining, since 250 mm bottom bricks are difficult to handle.
• Reducing amount of small repairs on the safety lining as the absence of joints prevents steel intrusion.

Various alumina-spinel materials were tested and evaluated for suitability. Together with the supplier a design was developed where the complete bottom can be built using only four pieces. The gaps between the pieces and the gaps around purge plugs and well block are then filled with alumina-spinel castable. Due to the small amount of castable cast in-situ there was no need for new mixers or drying stands. To allow for potentially higher wear rates of the precast impact pad, especially for the initial trials, the design was made with 300 mm thickness in the impact pad and 250 mm thickness for the rest of the bottom, where the bricked design has a thickness of 250 mm throughout the whole bottom.

Various optimizations of working methods and materials have been done over an extended trial period and at the moment of writing the wear rate of the precast design is approximately 10% higher than that of the bricked design. This does not negatively affect ladle life, sine the precast design has 50 mm extra thickness. Tapping on the joint between the precast blocks is considered to have a significant contribution to the higher wear rate.Therefore alternative designs using different shapes are currently being investigated. Furthermore, new materials are also being qualified for plant trials.It is expected that an optimized precast design will have similar or even lower wear rate compared to the bricked design, enabling reduction of lining thickness in the impact pad back to 250 mm to restore ladle capacity.

5. Torpedo cars

Another installation that relies heavily on resin-bonded bricks is the torpedo cars. In IJmuiden the complete wear lining of the 450t torpedo cars consists of resin-bonded ASC bricks (alumina – silicon carbide – carbon). During heating, as well as during the first 10 heats of a repaired torpedo car, odorous emissions sometimes occur. Since heating takes place in the open air, this means that nearby residents as well as Tata Steel staff can experience odour nuisance. This not only contradicts Tata Steels ambition of being a good neighbour, but also affects availability of the torpedo cars[9].

Suppliers were asked to supply alternative materials with no or low emission. These materials were evaluated in the lab for emissions by heating samples in TGA equipment and sampling the emissions in adsorption tubes at 9 different temperature intervals between 20ºC and 1000ºC. The components sampled were then determined using the analysis method described in chapter 2. Resulting amounts of phenolic and PAH compounds are shown in Figure 4 and 5.

Sample 94857 and 12987 are regular ASC bricks. Sample 120202 was used as a reference, since this is a fired brick. Although this obviously has the lowest emissions, trials in the past have shown that wear rates of such a material are too high for practical use in the torpedo car. Sample 130613 is an ASC brick with alternative binding system.

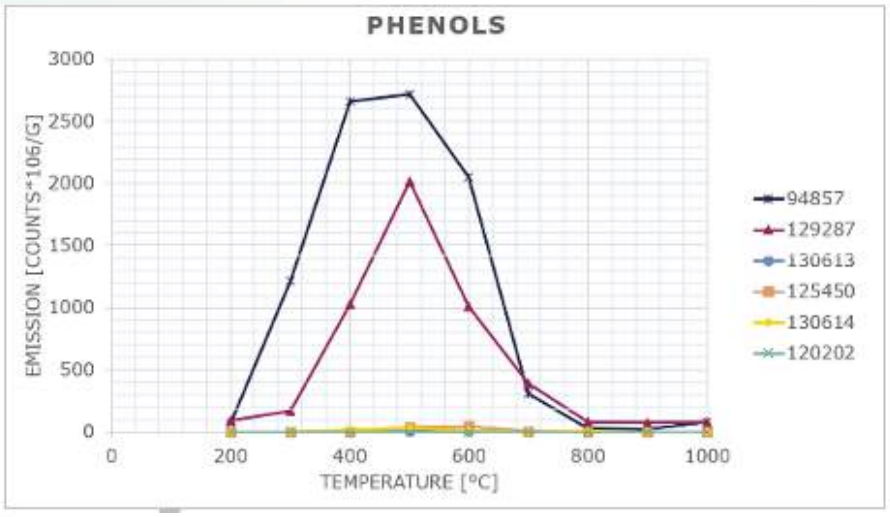


Figure 4: emissions from various torpedo car materials[9]

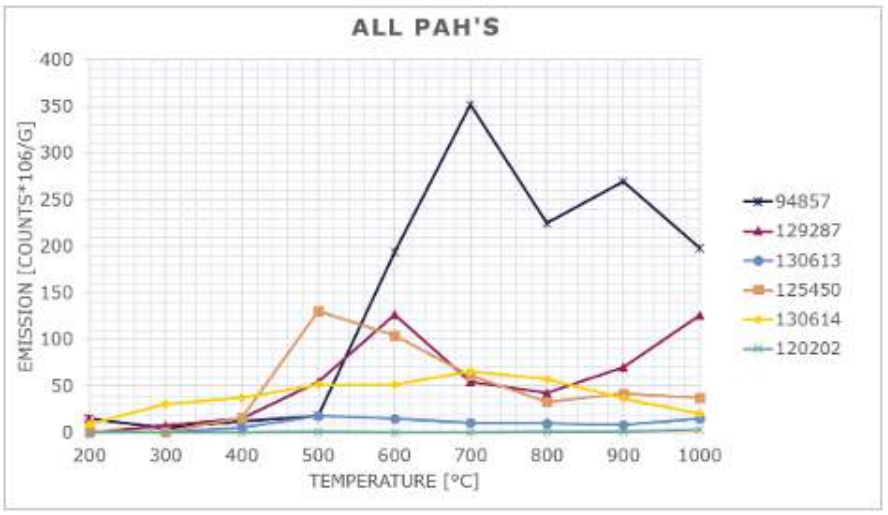


Figure 5: emissions from various torpedo car materials[9]

It can be seen that this has very low emissions compared to all other resin-bonded materials, almost matching the fired brick. This material was therefore selected for trials in practice.Emissions were also measured in practice for various materials to check results, which confirmed the ASC brick with alternative binding system indeed has the lowest emissions. Extended trials have shown that performance of this material is similar to previously used regular ASC materials and therefore it was decided to convert the complete fleet of torpedo cars to this material.

6. Conclusions

Reducing emissions from refractory materials is a very important topic for Tata Steel IJmuiden as it not only limits the risk of odour nuisance experienced by employees or neighbours but also results in less potentially harmful materials emitted to the environment.

Measuring emissions, both in the lab and in practice, is the key to understanding the emission mechanisms and pathways. The combination of laboratory TGA-TD-GC-MS measurements and industrial sampling campaigns enables identification of both the emission potential of refractory materials and

the fate of emitted compounds within the production process.

Tailored solutions are needed for each installation, as availability and suitability of alternative materials depends strongly on the application and type of refractory material. For certain materials, very similar alternatives are available, where only the binder is different and performance is not affected, as was the case for the ASC bricks in the IJmuiden torpedo ladles. In some cases replacing resin-bonded bricks with fired or monolithic materials is the best and easiest solution, as shown for IJmuiden steel ladles.The most difficult material to replace is MC brick, as there are little emission-free materials available and these come at the cost of having substantially higher wear rates. For the moment the most likely solution is using low-emission pre-fired bricks. Although these show promising performance, their side-effects (such as increased overall energy consumption) mean that they should be considered a temporary solution. Working together with refractory suppliers to develop emission-free MC bricks with good performance should be the way forward for Tata Steel to reach its goal of being the best(-smelling) neighbour.

References

1. A. Da Luz, R. Salomão, C. Bitencourt, C. Renda, A. Lucas, C. Aneziris and V. Pandolfelli(2020). Thermosetting resins for carbon-containing refractories: Theoretical basis and novel insights. Open Ceramics, 3.

2. S.K. Dinda andK. Chattopadhyay(2020). Numerical modeling of volatile organic compounds (VOC) emissions during preheating of magnesia-carbon bricks in a basic oxygen furnace. Metal, 10. 1277.

3. D.K. Gunasekar, J. Hubalkova, S. Dudczig, G. Schmidt, F. Kerber, T. Schemmel, P. Gehre and C.G. Aneziris (2026).Development of sustainable MgO–C refractories using MgO–C recyclates and a novel eco-friendly fructose–tannin binder crosslinked with citric acid.Advanced Engineering Materials, 28

4. Tengteng Shi et al (2019), Preparation and properties of MgO-C refractories using sucrose as binder, IOP Conf. Ser.: Mater. Sci. Eng. 678 012092

5. H. Visser, R. Siebring, and W. Tesselaar(2024). How to select the best refractories for the converter? A systematic improvement method. Proceedings of the International Colloquium on Refractories 66, 134-137, ISBN 978-3-9826104-0-5

6. R. Siebring, S. Sinnema, and W. Tesselaar(2017). Bridging the gap between refractory supplier and the refractory user in the steel plant. refractories WORLDFORUM 9, 71-75

7. H.W. Jansen and H.G. Daldrup(2004). Refractories in steel ladles: materials and design. AISTech Conference Proceedings 2004, Vol. 1

8. L. Akselrod and V. Garten (2018). An alternative lining of steel ladles: technical and economic aspects. Ferrous Metallurgy. Bulletin of Scientific , Technical and Economic Information. 72-80

9. F. Hameka, C.J. Kooij, J. van der Plas and J.J. Liefhebber(2025). Reducing odour nuisance during heating of the torpedo ladle at Tata Steel in IJmuiden. Poster presentation at International Colloquium on Refractories, Aachen 2025

NEXT-GENERATION LADLE GATE SLIDE PLATE WITH MULTIFUNCTIONAL ADDITIVE FOR OXYZEN-RICH CALCIA-TREATED STEEL CASTING

Sovan Khan, Subhadeep Chowdhury, Ryotaro Kimura, Arup Kumar Samanta, Hiroshi Nagata, Sunanda Sengupta, Prasant Kumar Naik

TRL Krosaki Refractory Limited, Belpahar-768218, Odisha, India

Corresponding author's email – sovan.khan@trlkrosaki.com

Abstract

Continuous casting is a critical metallurgical process in which molten steel, after stringent chemical control and thermal homogenization, is delivered into a water-cooled mold to produce semi-finished billets, blooms, or slabs. The ladle gate slide plate (LGSP) acts as a precision refractory flow-control component, regulating molten steel discharge from the ladle to the tundish via collector nozzle and ladle shroud and thereby ensuring casting stability and optimized flow regulation. Conventional alumina–carbon and alumina–zirconia–carbon LGSP perform satisfactorily during casting of mild steel grades with relatively non-aggressive slag chemistries. However, during casting of medium-carbon, oxygen-rich, calcia-treated steel grades, these materials undergo accelerated degradation. The presence of CaO-rich inclusions, high oxidation potential, and severe thermal cycling promotes molten metal penetration, slag-induced chemical dissolution, microstructural deterioration, and localized erosion within the throttling zone, leading to reduced service life and increased operational risk.

The present study investigates the degradation mechanisms governing LGSP performance under calcia-saturated slag environments with the objective of developing a next-generation refractory solution suitable for modern continuous casting conditions. Emphasis is placed on improving resistance to chemical corrosion, oxidation, and thermal shock under repeated thermo-mechanical cycling. Based on the findings, an advanced magnesia–carbon LGSP incorporating multifunctional performance-enhancing additives was developed and evaluated. The engineered matrix, combined with a tailored carbon architecture and antioxidant additives, exhibits significantly improved resistance to slag infiltration and oxidation while maintaining microstructural stability. Industrial evaluation demonstrates a substantial improvement in service performance compared with conventional alumina-based LGSP. The developed magnesia–carbon LGSP offers a robust and reliable solution for the continuous casting of high-purity calcia-treated steel grades.

Keywords: Continuous casting; Calcia-treated steel; Ladle gate slide plate; Throttling zone; Magnesia–carbon; Multifunctional additives

1. Introduction

Continuous casting is a technologically intensive steelmaking process that integrates refractory engineering, fluid dynamics, heat transfer, and solidification metallurgy to transform molten steel into semi-finished products with high productivity and quality consistency (fig.1). Refractory flow-control components, including slide gate assemblies, ladle shrouds, tundish nozzles, and submerged entry nozzles, play a critical role in regulating steel flow and suppressing reoxidation. Simultaneously, the tundish functions as an active metallurgical vessel that promotes inclusion removal, temperature homogenization, and flow optimization. Controlled solidification within the water-cooled mould and subsequent secondary cooling govern shell development, internal soundness, and strand integrity. Therefore, casting performance is fundamentally governed by the interplay of refractory reliability, transport phenomena,

thermal gradients, and solidification kinetics, which collectively influence steel cleanliness, operational stability, and product quality.

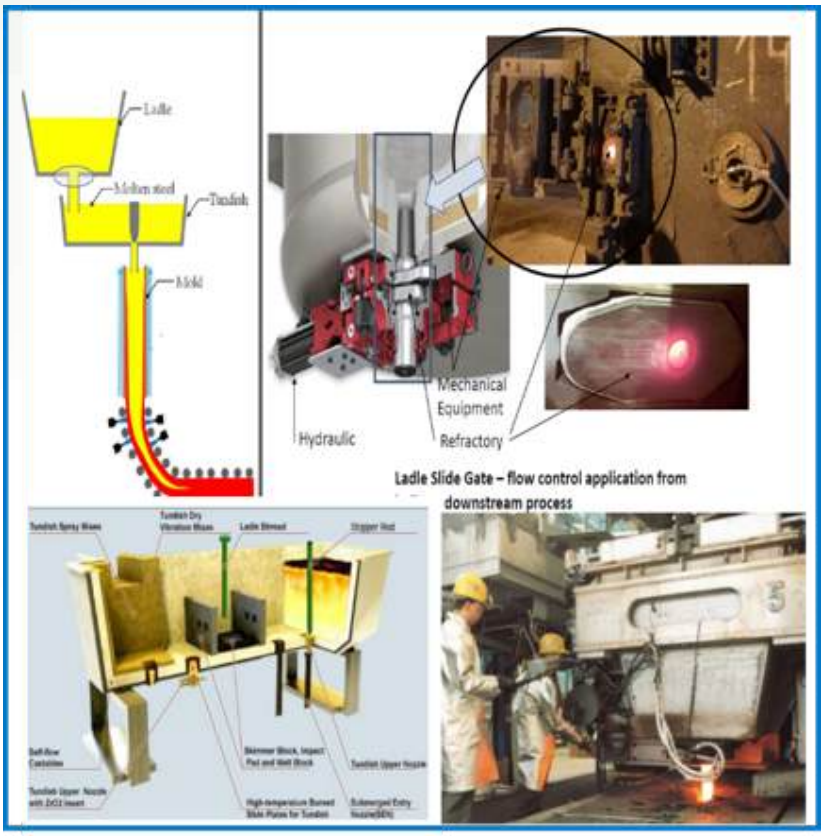


Fig 1: Schematic of continuous casting process along with cross section of slide gate assembly and tundish along with application photographs.

A ladle gate slide plate is a key component of the flow control refractory system used in continuous casting to regulate the flow of molten steel from the ladle to the tundish. It is installed at the bottom of the steel ladle and is connected to the nozzle system through a collector nozzle. The flow of molten steel is controlled by the horizontal movement of the slide plate, which opens or closes the flow passage. By adjusting the opening area, the slide gate system ensures a controlled and consistent flow of steel through the ladle shroud into the tundish during the casting process (fig.2). During operation, particularly during molten steel transfer from the ladle to the tundish, the slide plate is subjected to severe thermochemical and mechanical stresses. The refractory surface experiences intense corrosion by molten steel and slag at extremely high temperatures, while the continuous movement of the slide gate mechanism causes significant mechanical wear and erosion. In addition, the slide plate must possess excellent resistance to thermal spalling because the casting process involves repeated heating and cooling cycles as it is intermittent operation. To withstand the combined effects of corrosion, erosion and thermal shock, specialized carbon-containing refractory compositions are commonly used. Depending on the steel grade and casting conditions, alumina-carbon (Al_2O_3-C), alumina-zirconia-carbon (Al_2O_3-ZrO_2-C), and magnesia-carbon (MgO-C) slide plates are widely employed in continuous casting operations. These materials provide an optimal combination of high-temperature strength, corrosion resistance, thermal shock resistance, and wear resistance, ensuring reliable flow control and extended service life.

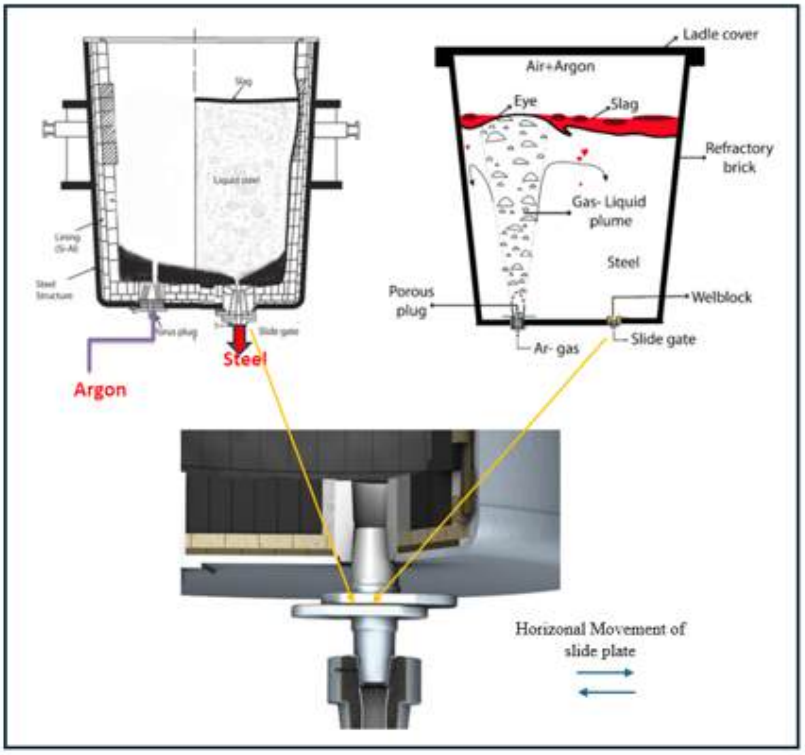


Fig 2. Schematic cross section of ladle showing location of slide gate and slide gate assembly

In the current steelmaking scenario, steel producers are increasingly adopting calcium treatment to modify non-metallic inclusions and improve steel cleanliness, castability, as well as mechanical properties, according to specific application requirements. However, calcium treatment significantly alters the chemistry of inclusions and secondary refining slags, often resulting in the formation of calcia-rich (CaO-rich) slags with higher corrosivity toward refractory materials. These highly aggressive slags intensify the chemical attack on the slide gate refractory system, particularly the slide plates and nozzles, during continuous casting operations. Under such severe operating conditions, conventional alumina-carbon (Al_2O_3-C), alumina-zirconia-carbon (Al_2O_3-ZrO_2-C), and magnesia-carbon (MgO-C) slide plates experiences accelerated wear and degradation, leading to reduced service life and lower heat endurance. Consequently, there is a growing need for the development of refractory compositions with enhanced resistance to calcium-bearing slags, improved thermal shock resistance, and superior wear performance to meet the requirements of modern steelmaking practices.

This study systematically investigates the wear and degradation mechanisms of ladle gate slide plates exposed to calcia-saturated slags generated during the production of calcium-treated steels. Particular attention is directed toward understanding the coupled effects of chemical corrosion, carbon oxidation, slag infiltration, thermal spalling, and mechanical abrasion, which collectively limit refractory service life in modern continuous casting processes. To address these challenges, a new MgO-C refractory formulation was developed by tailoring the matrix composition and incorporating multifunctional additives capable of enhancing corrosion resistance and microstructural stability. The optimized system promotes the formation of a dense and chemically stable microstructure while simultaneously suppressing oxidative degradation and improving resistance to thermal cycling. Comprehensive laboratory investigations and plant-scale trials revealed markedly improved performance compared with conventional LGSPs.

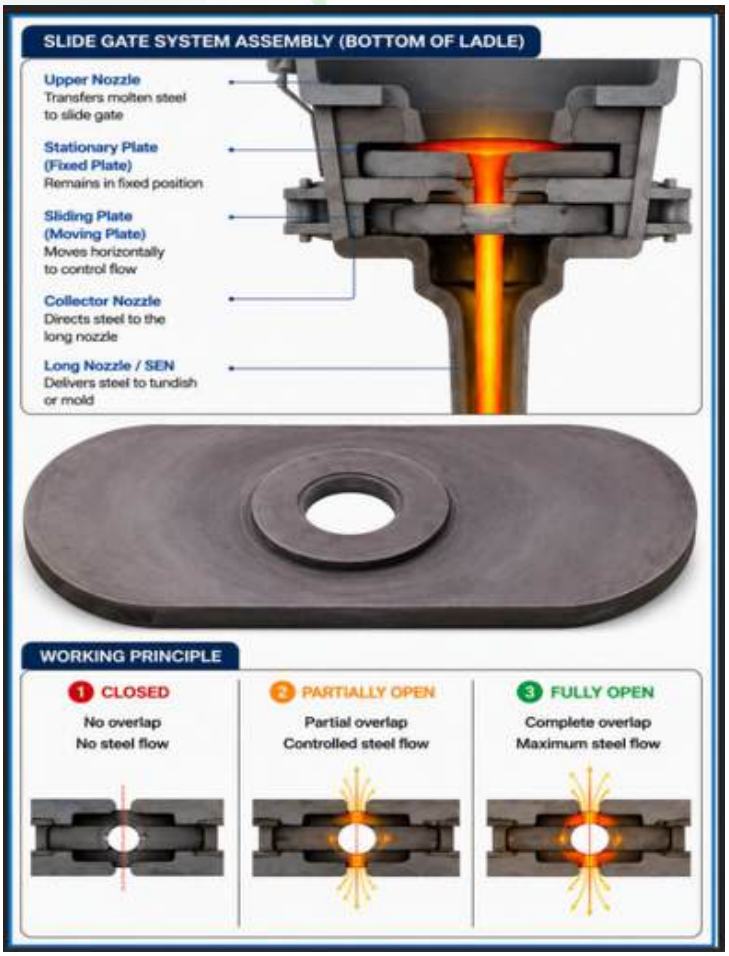


Fig 3: Slide plate & Working principal

Experimental procedure

Raw materials & Mix preparation

The developed slide plate was designed using a high-purity magnesia-based engineered matrix in combination with selected synthetic raw materials to achieve enhanced resistance to corrosion, abrasion, and microstructural degradation under severe metallurgical conditions. A carefully tailored combination of antioxidant additives was incorporated to improve oxidation resistance, while a high-purity multifunctional synthetic additive was employed to enhance microstructural integrity, mechanical strength, thermal spalling resistance, and slag corrosion resistance. The synergistic interaction of these additives enabled the matrix to withstand aggressive calcia-rich basic slag attack while maintaining excellent thermomechanical stability. Furthermore, a novel multi-stage high-speed Eirich mixing process ensured efficient constituent dispersion, optimized binder distribution, and superior microstructural homogeneity, resulting in improved durability, reliability, and overall service performance of the developed slide plate. Following the mixing process, the batch was conditioned in a temperature-controlled air-conditioned environment for 48h to improve workability. This curing treatment helps in achieving superior green strength and improved the dimensional stability of the plates.

Ladle gate slide plate

After the aging process, the formulated batch was compacted into slide plates using a hydraulic press at a pressure of 1.8-2.0 t/cm² to obtain the desired shape, density, and dimensional accuracy. The slide plates were manufactured according to the specified

geometry required for industrial application, with the bore diameter precisely designed and controlled to meet site-specific operational requirements and casting performance demands.The prepared green slide plates were subjected to a controlled thermal processing route comprising drying, followed by coking under a reducing atmosphereSubsequently, the coked slide plates were impregnated with tar under autoclave to reduce open porosity and improve density of the matrix in the refractory body. Following tar impregnation, the slide plates were processed through shot blasting, grinding, casetting (fixing of a metal casing), air drying, baking, and final finish grinding. These post-processing treatments were carried out to obtain the desired surface flatness, and dimensional precision required for sliding gate applications. Since the slide plates are subjected to continuous horizontal sliding during operation to control molten steel flow, superior surface quality is essential to minimize frictional wear,prevent leakage of steel and maintain stable performance.

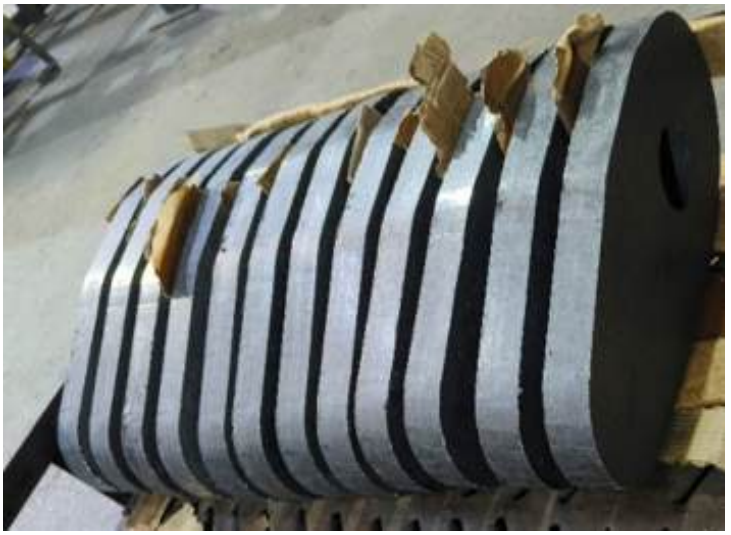


Fig 4: Green Slide Plate after pressing

The physical, thermal, thermo-mechanical, and corrosion-resistance properties of the newly developed next-generation slide plate were systematically evaluated. The performance of the developed slide plate was compared with that of commercially used conventional slide plate materials, namely alumina-carbon (Al_2O_3-C), alumina-zirconia-carbon (Al_2O_3-ZrO_2-C), and magnesia-carbon (MgO-C) slide plate. Comparative investigations were conducted in terms of physical properties, thermal behavior, thermo-mechanical performance, and resistance to slag corrosion. In addition, detailed microstructural and morphological characterization was carried out to elucidate the influence of the engineered matrix design on the overall performance of the developed material.

Results & Discussion

The physical, thermo-mechanical, and thermo-chemical properties of conventional MgO-C, Al_2O_3-C, and Al_2O_3-ZrO_2-C slide plates were systematically evaluated and compared with newly developed slide plate material using advanced characterization techniques and industry-standard testing methods. The investigation encompassed the determination of key physical properties, thermal stability, oxidation resistance, corrosion resistance against calcia-rich slags, and high-temperature performance.

DTA-TGA

DTA-TGA analysis of green mixes comprising conventional MgO-C, Al_2O_3-C, Al_2O_3-ZrO_2-C, and the developed slide plate composition was performed under oxidizing conditions to evaluate their thermal stability and oxidation resistance. As illustrated in Fig.5, all compositions exhibited pronounced thermal reactions within 500-800°C, primarily associated with carbon oxidation, constituent decomposition, and consequent mass loss. Al_2O_3-C demonstrated the highest thermal stability, characterized by the lowest weight loss (~3.7%) and delayed degradation onset. The developed composition exhibited superior oxidation resistance compared with conventional MgO-C, resulting in reduced mass loss (~5.5%). In contrast, Al_2O_3-ZrO_2-C showed the highest weight loss (~8.5%), indicating comparatively lower oxidation resistance. Accordingly, the thermal stability followed the sequence: Al_2O_3-C > Developed > MgO-C > Al_2O_3-ZrO_2-C.

Physical Properties

The physical properties of conventional MgO-C, Al_2O_3-C, and Al_2O_3-ZrO_2-C slide plates were evaluated and compared with a newly developed slide plate composition (fig.6). The developed material exhibited a modulus of rupture (291.92 kg/cm²) higher than MgO-C and Al_2O_3-C and comparable to Al_2O_3-ZrO_2-C. It also showed the lowest apparent porosity (3.50%), indicating a dense microstructure with enhanced resistance to slag penetration and oxidation. The bulk density (2.95g/cc) and cold crushing strength (870 kg/cm²) were comparable to those of commercial slide plate materials, demonstrating adequate mechanical (fig.6) integrity for industrial applications. crushing strength (870 kg/cm²) were comparable to those of commercial slide plate materials, demonstrating adequate mechanical integrity for industrial applications. Among the investigated compositions, Al_2O_3-ZrO_2-C exhibited the highest bulk density and cold crushing strength, Overall, the newly developed slide plate demonstrated a well-balanced combination of strength, density, and low porosity, suggesting improved performance under severe thermo-mechanical and thermo-chemical operating conditions. These results indicate that the developed composition is a promising alternative to conventional slide plate materials for continuous casting applications.

High Temperature Properties

The high-temperature properties of conventional MgO-C, Al_2O_3-C, and Al_2O_3-ZrO_2-C slide plates were compared with those of the newly developed composition through hot modulus of rupture (HMOR) and oxidation resistance measurements (fig. 7). The developed slide plate exhibited the highest HMOR at 1400°C (190 kg/cm²), indicating superior strength retention under severe thermal conditions. Furthermore, the developed composition demonstrated the lowest oxidation losses at both 1000°C (18.52%) and 1400°C (42.13%), reflecting improved resistance to carbon oxidation. Although Al_2O_3-C showed the highest HMOR at 1000°C (232 kg/cm²), the developed material provided the best overall balance between mechanical stability and oxidation resistance.

Spalling Resistance

The thermal shock resistance of conventional MgO-C, Al_2O_3-C, Al_2O_3-ZrO_2-C, and the developed slide plate was assessed using a high-temperature spalling test at 1400°C with repeated air-quenching cycles to simulate severe service conditions (Fig. 8). Specimens were subjected to cyclic heating and rapid cooling, and the onset of crack formation was used as the failure criterion. Significant differences in thermal spalling behavior were observed among the investigated compositions. MgO-C exhibited crack

initiation after six cycles, while Al_2O_3-C and Al_2O_3-ZrO_2-C sustained eight cycles before failure. Notably, the developed slide plate withstood nine thermal shock cycles prior to crack formation, indicating superior thermal shock resistance, enhanced crack tolerance, and improved thermo-mechanical stability under aggressive thermal cycling conditions.

Corrosion Resistance

The slag-corrosion behavior of conventional and newly developed slide plate refractories was investigated under calcia-rich slag conditions at 1600-1650°C for 2h. The corrosion resistance was assessed in terms of average material degradation following slag exposure. Among the evaluated compositions, the developed slide plate exhibited the lowest average corrosion loss (22.78%), demonstrating superior performance compared with MgO-C (25.37%), Al_2O_3-C (27.30%), and Al_2O_3-ZrO_2-C (36.07%) materials (fig 9). The results indicate that the developed slide plate possesses superior thermo-chemical stability and corrosion resistance compared with conventional slide plate materials. Such performance is expected to translate into improved reliability and extended service life in ladle gate systems operating under calcia-treated steel casting conditions, where refractory degradation by highly basic slags remains a critical challenge.

The comprehensive evaluation demonstrates that the developed slide plate significantly outperforms conventional MgO-C, Al_2O_3-C, and Al_2O_3-ZrO_2-C materials. The superior performance is attributed to the synergistic effect of the engineered matrix design and multifunctional additive system, which collectively promote matrix densification, enhance thermal conductivity, improve oxidation resistance, and suppress slag penetration. These combined effects result in superior thermo-mechanical stability, enhanced thermal shock and spalling resistance, and improved corrosion resistance, establishing the developed slide plate as a promising next-generation refractory solution for demanding calcia-treated steel casting applications.

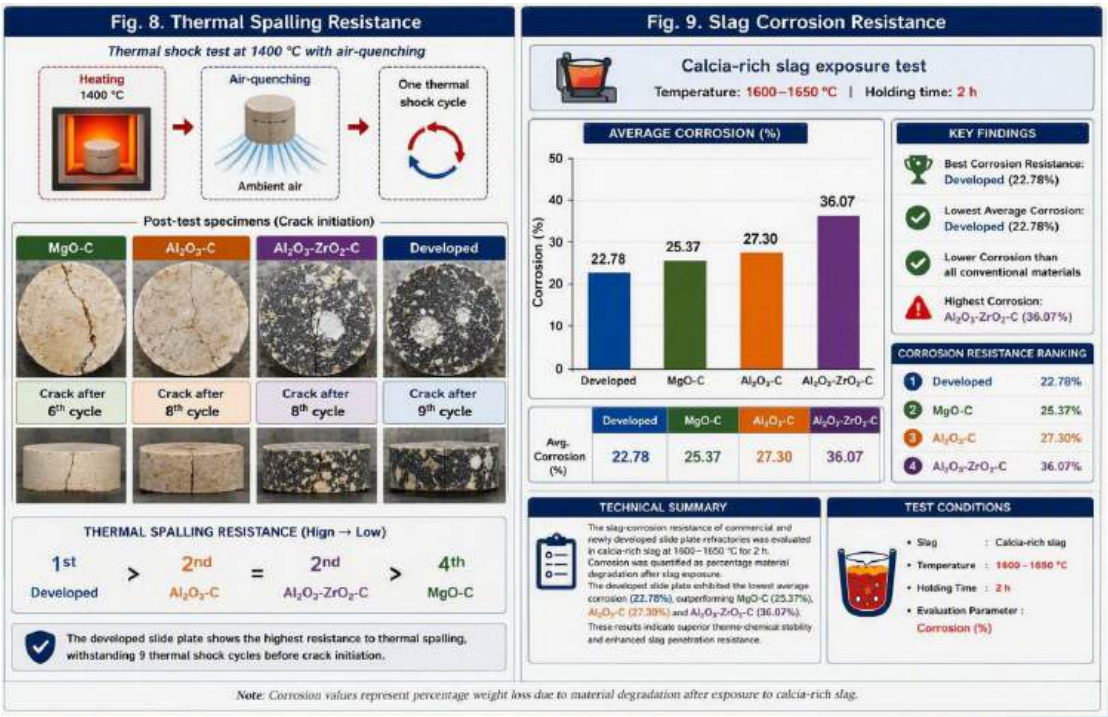
Field Trial

The developed slide plate was validated through industrial trials in the ladle gate slide plate system of a steel plant operating under calcia-treated steel casting conditions.The field evaluation was conducted in a 160-t ladle system at casting temperatures of 1560-1615 °C with a casting duration of 55-60 min per heat. The steel chemistry comprised 30-35 ppm Ca, 1.1-1.3 wt% Mn 0.05 wt.% Si, and 0.06 wt.% C. The field-trial results demonstrated that the developed slide plate achieved the highest service life (4 heats), surpassing Al_2O_3-C and MgO-C slide plates (3 heats each) as well as Al_2O_3-ZrO_2-C (2 heats), thereby confirming its superior durability and operational performance under industrial casting conditions.

The enhanced service life is attributed to its improved thermo-mechanical stability, superior resistance to thermal shock and slag-induced degradation, and enhanced structural integrity, validating the effectiveness of the proposed material design for demanding calcia-treated steel casting applications.


Fig. 5. TG-DTA Analysis and Thermal Stability under Oxidizing Conditions
(a) MgO-C
(b) Developed
(c) Al_2O_3-C
(d) Al_2O_3-ZrO_2-C
Major reactions 500–800 °C
Temperature (°C)
TG (%) – Thermogravimetric analysis (mass change)
DTA (μV/mg) – Differential thermal analysis
TG-DTA SUMMARY
Composition | Weight Loss at 1400 °C (%) | Major Reaction Range (°C) | Relative Thermal Stability
MgO-C | ~6.5 | 500–800 | Moderate
Developed | ~5.5 | 500–800 | High
Al_2O_3-C | ~3.7 | 500–800 | Highest
Al_2O_3-ZrO_2-C | ~8.5 | 500–800 | Lowest
OVERALL THERMAL STABILITY (High → Low)
1st Al_2O_3-C > 2nd Developed > 3rd MgO-C > 4th Al_2O_3-ZrO_2-C
All compositions exhibit major thermal reactions in the range of 500–800 °C. Al_2O_3-C shows the lowest mass loss (~3.7%) and the highest thermal stability, while Al_2O_3-ZrO_2-C shows the highest mass loss (~8.5%) and the lowest stability.

Fig. 6. Physical Properties of Slide Plates (Room Temperature)
Properties | Unit | MgO-C | Developed | Al_2O_3-C | Al_2O_3-ZrO_2-C | Best Value
MOR (Modulus of Rupture) | kg/cm² | 287.27 | 291.92 | 289.54 | 295.11 | Al_2O_3-ZrO_2-C
Bulk Density (B.D.) | g/cc | 2.93 | 2.95 | 3.25 | 3.27 | Al_2O_3-ZrO_2-C
Apparent Porosity (A.P.) | % | 3.69 | 3.50 | 3.55 | 3.76 | Developed (Lowest)
Cold Crushing Strength (CCS) | kg/cm² | 860 | 870 | 900 | 1100 | Al_2O_3-ZrO_2-C
Modulus of Elasticity (MOE) | GPa | 42.88 | 40.44 | 40.81 | 39.67 | MgO-C
Note: Best value for each property is highlighted in bold.
MOR (kg/cm²)
B.D. (g/cc)
A.P. (%)
CCS (kg/cm²)
MOE (GPa)
MgO-C
Developed
Al_2O_3-C
Al_2O_3-ZrO_2-C
Fig. 7. High-Temperature Properties of Slide Plates
Properties | Unit | MgO-C | Developed | Al_2O_3-C | Al_2O_3-ZrO_2-C | Best Value
HMOR @1000°C | kg/cm² | 220 | 230 | 232 | 227 | Al_2O_3-C (232 kg/cm²)
HMOR @1400°C | kg/cm² | 180 | 190 | 185 | 182 | Developed (190 kg/cm²)
Oxidation @1000°C | % | 20.61 | 18.52 | 19.41 | 19.04 | Developed (18.52 %)
Oxidation @1400°C | % | 47.45 | 42.13 | 45.16 | 44.17 | Developed (42.13 %)
OVERALL ASSESSMENT
The developed slide plate exhibits superior high-temperature performance, retaining the highest mechanical strength at 1400°C while showing the lowest oxidation loss at both 1000°C and 1400°C. This indicates enhanced thermal stability and oxidation resistance compared with conventional slide plate compositions.
HMOR @1000°C (kg/cm²)
HMOR @1400°C (kg/cm²)
Oxidation @1000°C (%)
Oxidation @1400°C (%)
KEY FINDINGS
Highest HMOR @1000°C: Al_2O_3-C (232 kg/cm²)
Highest HMOR @1400°C: Developed (190 kg/cm²)
Lowest Oxidation @1000°C: Developed (18.52 %)
Lowest Oxidation @1400°C: Developed (42.13 %)
Note: HMOR – Hot Modulus of Rupture; Oxidation values represent percentage weight change after exposure at respective temperatures.


Fig. 8. Thermal Spalling Resistance
Thermal shock test at 1400 °C with air-quenching
Heating 1400 °C
Air-quenching
Ambient air
One thermal shock cycle
Post-test specimens (Crack initiation)
MgO-C
Al_2O_3-C
Al_2O_3-ZrO_2-C
Developed
Crack after 6th cycle
Crack after 8th cycle
Crack after 8th cycle
Crack after 9th cycle
THERMAL SPALLING RESISTANCE (High → Low)
1st Developed > 2nd Al_2O_3-C = 2nd Al_2O_3-ZrO_2-C > 4th MgO-C
The developed slide plate shows the highest resistance to thermal spalling, withstanding 9 thermal shock cycles before crack initiation.
Fig. 9. Slag Corrosion Resistance
Calcia-rich slag exposure test
Temperature: 1600–1650 °C | Holding time: 2 h
AVERAGE CORROSION (%)
Corrosion (%)
22.78
25.37
27.30
36.07
Developed
MgO-C
Al_2O_3-C
Al_2O_3-ZrO_2-C
KEY FINDINGS
Best Corrosion Resistance: Developed (22.78%)
Lowest Average Corrosion: Developed (22.78%)
Lower Corrosion than all conventional materials
Highest Corrosion: Al_2O_3-ZrO_2-C (36.07%)
CORROSION RESISTANCE RANKING
1 Developed 22.78%
2 MgO-C 25.37%
3 Al_2O_3-C 27.30%
4 Al_2O_3-ZrO_2-C 36.07%
Avg. Corrosion (%) | Developed 22.78 | MgO-C 25.37 | Al_2O_3-C 27.30 | Al_2O_3-ZrO_2-C 36.07
TECHNICAL SUMMARY
The slag-corrosion resistance of commercial and newly developed slide plate refractories was evaluated in calcia-rich slag at 1600 – 1650 °C for 2 h. Corrosion was quantified as percentage material degradation after slag exposure.
The developed slide plate exhibited the lowest average corrosion (22.78%), outperforming MgO-C (25.37%), Al_2O_3-C (27.30%) and Al_2O_3-ZrO_2-C (36.07%). These results indicate superior thermo-chemical stability and enhanced slag penetration resistance.
TEST CONDITIONS
• Slag : Calcia-rich slag
• Temperature : 1600 – 1650 °C
• Holding Time : 2 h
• Evaluation Parameter : Corrosion (%)
Note: Corrosion values represent percentage weight loss due to material degradation after exposure to calcia-rich slag.

Conclusion

I. A next-generation MgO-C slide plate incorporating an engineered matrix design and multifunctional additives was successfully developed for calcia-treated steel casting applications, exhibiting a superior balance of physical, thermo-mechanical, and thermo-chemical properties.

II. The developed composition demonstrated enhanced high-temperature performance, characterized by improved hot strength retention, reduced oxidation loss, and superior thermal shock resistance, resulting in delayed crack initiation and propagation during thermal cycling.

III. Corrosion evaluation under calcia-rich slag conditions revealed the lowest corrosion loss among the investigated materials, confirming its enhanced resistance to slag penetration and thermo-chemical degradation.

IV. The improved performance is attributed to the synergistic interaction between the engineered matrix architecture and multifunctional additive system, which promoted matrix densification, improved thermal conductivity and oxidation resistance, stabilized the microstructure, and suppressed slag infiltration.

V. Industrial trials validated the laboratory findings, with the developed slide plate achieving the longest service life under calcia-treated steel casting conditions, establishing its potential as a next-generation refractory solution for demanding steelmaking operations.

Reference

I. Duan, J., Han, B., Wei, J., Chen, C., Miao, Z., Wang, H., Li, N., & Chen, J. Corrosion Mechanism and Microstructure Evolution of Industrial Used Al_2O_3-ZrO_2-C Slide Plates. Materials Today Communications, Vol. 39, Article 108796, 2024.

II. Tsutsui, Y., Katou, K., & Umeda, S. Magnesia-Carbon Refractories for Converters. Nippon Steel Technical Report, No. 125, pp. 83-92, 2021.

III. Lüle, G.M., & Lüle Şenöz, G.M. A Study of Comparison Different Al_2O_3-ZrO_2-C Slide Gate Plates for the Casting Al-Killed Steel. Journal of Materials and Electronic Devices, Vol. 1, No. 1, pp. 25-31, 2020.

IV. Krasnyanskaya, I.A., et al. Influence of Slag Chemistry on the Wear Mechanisms of MgO-C Refractories. CIS Iron and Steel Review, Vol. 27, pp. 20-30.

V. Bahtli, T., Bostanci, V.M., Hopa, D.Y., & Yasti, S.Y. The Effect of Carbon Sources on the Thermal Shock Properties of MgO-C Refractories. Universal Journal of Materials Science, Vol. 6, No. 5, pp. 139-147, 2018.

VI. Xue, L., Zhang, T., & Wang, W. Corrosion Behaviors of Al_2O_3 and ZrO_2 Refractories in Contact with High-Basicity Refining Slag. The Minerals, Metals & Materials Series, pp. 171-181, 2020. Relevant for understanding refractory corrosion under highly basic and calcium-containing slags.

VII. Chen, Q., Li, Y., Zhu, T., Xu, Y., Li, Y., & Wang, X. Improved Thermal Shock Resistance of MgO-C Refractories with Addition of Calcium Magnesium Aluminate (CMA) Aggregates. Ceramics International, Vol. 48, 2022. Covers thermal shock resistance improvement in MgO-C refractories used in steelmaking.

DRIVING EFFICIENCY: A NOVEL APPROACH TO BULLNOSE REFRACTORY PERFORMANCE AND RELIABILITY IN WALKING BEAM FURNACES

Kshitish Kumar Jena*, Pritam Sarkar, Biswanath Nag, Biswajit Pal, Dirk Dürrschmid

Department of Refractories Mills & Kiln, Tata Steel, Jamshedpur, India

Author's Email: kshitish.jena@tatasteel.com

Abstract

This technical paper details a comprehensive initiative to significantly enhance the reliability and performance of bullnose refractories that are used in a recuperative type walking beam furnace of a Hot Strip Mill (HSM). The 31 pieces of inverted camel-hump shaped bullnose structures, critical for flue gas control, historically experienced crack generation, particularly originating from ceramic anchors with a square-shaped diameter. A comprehensive strategy was put in place to tackle these issues. In terms of refractory material, different approaches were tested ranging from phosphate-bonded ramming material over SiC-containing low cement castable (LCC) to conventional andalusite-based LCC. Laboratory analyses of post-mortem samples confirmed that chemical attack, e.g., alkali-bursting, was not the dominant wear mechanism. A root cause analysis identified crack initiation at the corners of anchors with a square-shaped diameter. This led to a strategic switch from square- to round-shaped diameter ceramic anchors, demonstrating their enhanced suitability and performance in mitigating stress concentrations within the bullnose refractory body. To accommodate the thermal expansion characteristics of the best performing andalusite-based LCC, the thickness of expansion joints between bullnoses during installation was purposefully enlarged, preventing crack formation due to thermal gradients and restraint. Overall, this report elaborates on the investigative work, laboratory findings, and on-site modifications undertaken to achieve a substantial improvement in the overall performance and operational reliability of the bullnose refractory system in the HSM recuperative furnace.

Keywords: Bullnose, Refractory, Thermal Stress, Ceramic Anchor

1. Introduction

In modern steel production, refractories are indispensable for high-temperature processes, particularly in the reheating furnaces of Hot Strip Mills (HSM). Their thermo-mechanical strength is crucial for preheating steel slabs to ~1300 °C before rolling. These furnaces utilize mixed gases (CO & LD gas) and recuperators for efficient heat recovery from flue gases, preheating combustion air. A key component within these furnaces is the "bullnose," a camel-hump shaped refractory structure that extends from the roof, separating preheating and heating zones [2-3]. This structure, vital in Recuperative Type Walking Beam Furnaces (typically 31 units in HSM), precisely controls flue gas flow, enhancing heat transfer and ensuring uniform slab heating.

The bullnose refractory is alumina silica based that forms mullite at elevated temperature. This mullite phase provides thermal shock resistance to the bullnose structure against the temperature fluctuation and protects from cracking & dislodgement. However, the compatibility of bullnose refractory with its anchor refractory plays a critical role to protect from dislodging. The ceramic anchor is the part of bullnose structure, rectangular in shape and have multiple jaws on its surface that holds all the refractories together and provides strength to the bullnose refractories.

As part of a design optimization program, both the geometry of the ceramic anchors and the expansion concept of bullnose

refractory were systematically improved. The objective was to reduce the thermomechanical stresses acting within the structure and thereby significantly increase the long-term durability of the system.

The following paper describes the underlying damage mechanism together with the implemented design modifications and their influence on the mechanical behaviour of the assembly.

2. Background and Root Cause Analysis

Bullnose is part of the roof refractories positioned at the middle part of the RHF. It controls the hot flue gas flow inside the furnace and increases the retention time of this gas by obstructing its movement. Just below this bullnose structure, a 6- foot wall exists which further narrows the gaps between bullnose and wall at the middle of RHF. In recent past years, the cracking and dislodging phenomenon has been observed in the bullnose refractories which could be anticipated for the following reasons:

A. Thermo-mechanical stress generated from operational process.
B. Chemical reactions with bullnose refractory material
C. Structural stability of bullnose refractory

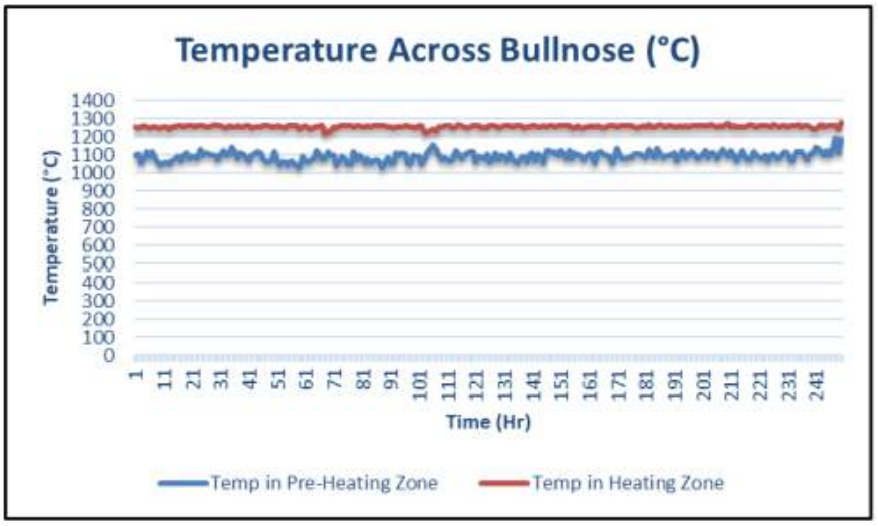
2.A. Thermo-mechanical stress generated from operational process

The reheating furnace at HSM uses mixed gases to preheat the slabs upto 1300°C based on the predetermined heating schedule. The operational environment imposes severe thermal stress on these refractories. Furnaces cycle from 1300 °C down to 500 °C during monthly maintenance shutdowns, and even below 50 °C during major annual shutdowns. Repeated heating and cooling cycles generate thermal expansion throughout the entire assembly of bullnose. At the same time, the steel frame, ceramic anchors and refractory castable exhibit different thermal and mechanical properties, resulting in stress development within the composite structure.

When analysing the temperature profile of the running furnace, we observed that the bullnose is exposed to a temperature gradient. Because it separates the preheating and heating zones, the refractory on either side of the bullnose is subjected to different temperatures, resulting in an average of 150 °C thermal differential across its body.

Geometric discontinuities at ceramic anchors represent extremely critical areas in refractory structures. The sharp transitions at these anchors lead to localised stress concentrations within the surrounding refractory castable. Consequently, elevated tensile stresses develop locally, even though the overall structure is predominantly subjected to compressive loading.

Because refractory castable is significantly more vulnerable to tensile stresses than compressive ones, these highly stressed zones become the primary sites for microcrack initiation, ultimately compromising structural integrity.



Graph-1: Temperature profile around bullnose

2.B. Chemical reactions with bullnose refractory material

The bullnose refractory, typically alumino-silicate based, forms a protective mullite phase at elevated temperatures, offering thermal shock resistance. But the problem of corrosion that originated from the reaction of alumina (present in bullnose refractory) with alkali oxides in presence of silica, led to sagging and failure of bullnose refractory prematurely[1]. It's further validated that the sodium oxide which was an alkali oxide coming from the mould powder used in caster operation reacted with the bullnose refractory and formed low melting phase such as sodian anorthite (sodium aluminosilicate) at 1270°C[1]. The phase formation resulted in volume expansion in the refractory thereby generation of stress and sagging of bullnose structure.

2.C. Structural stability of bullnose refractory

The compatibility between the bullnose refractory and its anchoring system is critical to preventing dislodgement. Each block incorporates a Ushaped steel frame (1) serving as the primary load-bearing structure. To increase its stiffness, the frame is reinforced by an internal web plate (2), which also provides the mounting interface for the ceramic anchors (3). The ceramic anchors are inserted through the steel frame and mechanically fastened to the web plate (4). Thermal insulation boards (5) are installed on both sides of the steel frame. The refractory castable (6) is subsequently applied onto the insulation layers and is permanently retained by the geometry of the ceramic anchors. The resulting symmetrical design forms a mechanically stable composite assembly capable of withstanding the severe thermomechanical loading encountered during furnace operation.

The sharp corners of rectangular ceramic anchors in the bullnose structure act as stress concentration points. During thermal cycling, non-uniform distribution of thermal expansion stress initiates cracks at these anchor edges. These cracks propagate into the adjacent refractories, ultimately causing crack interconnection and refractory spalling or dislodgement.

The sharp corners of rectangular ceramic anchors in the bullnose structure act as stress concentration points. During thermal cycling, non-uniform distribution of thermal expansion stress initiates cracks at these anchor edges. The cracks then extend into neighbouring refractories, link up, and ultimately cause spalling or dislodgement of the bullnose lining. Additionally, thermal expansion of bullnose blocks accumulates across the furnace width, if not adequately accommodated. These resulting compressive forces increase mechanical

loading, which promotes the propagation of existing microcracks. Repeated cycles progressively extend the cracks until local spalling occurs, reducing service life.

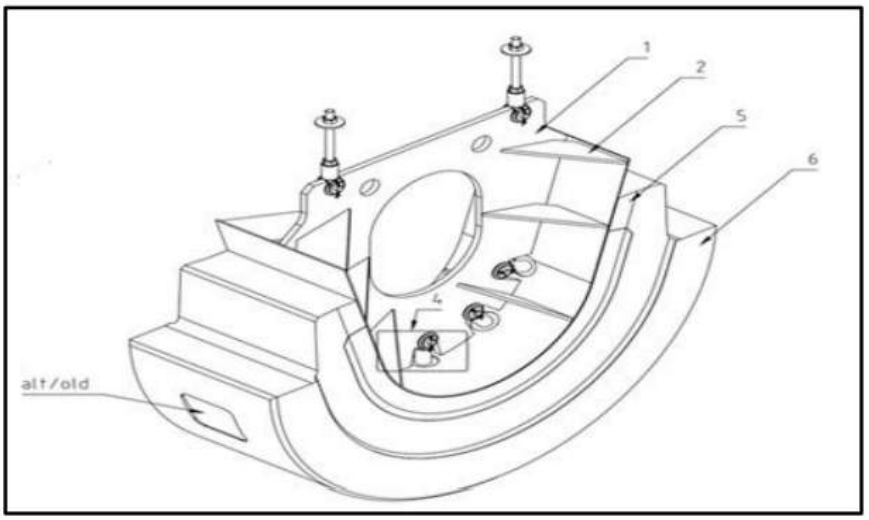


Figure 1

3. Results and Discussion

To mitigate challenges concerning material and structural stability alongside thermo-mechanical stress, several upgradation and practical skill initiatives were implemented periodically, as outlined below:

3.1. Material Quality Upgrade

The chronology of upgradation of bullnose refractory material was started from andalusite-based phosphate-bonded ramming mix KORUDUR A to andalusite-based calcium aluminate cement (CAC) bonded dense castable BEKAFIX A. The process of manufacturing bullnose blocks includes ramming of premix mass into shapes and then heat treated at approximately 400°C before shipping it to customer. However, due to low CCS i.e., 10-20 MPa after heat treatment, the bullnose couldn't sustain the shape during sea shipping. To address the issue, the material quality was upgraded to andalusite-based calcium aluminate cement (CAC) bonded dense castable BEKAFIX A that exhibited improved in CCS.

Although this improved CSS could facilitate the overseas transport without damages. However, in service the bullnose showed crack development after short service life. To address this issue, further the quality of material was changed to andalusite based LCC BEKAFIX AS LC, which exhibits lower PLC, but performance was still unsatisfactory.

Root cause analysis indicated that the primary wear mechanism in refractory roofs is alkalibursting, which occurs when alkalis interact with the refractory material at the hot face. This interaction triggers expansive mineral reactions that promote hot-face spalling. Since material expansion was clearly a critical issue for the bullnose, a silicon carbide (SiC)-containing, alkali-resistant LCC (BEKAFIX 52 S6 LC) was introduced. Following this implementation, the bullnose refractory has demonstrated a marked improvement in performance.

Table-1: Material upgradation in Bullnose

Parameter	KORUD UR A	BEKAF IX A	BEKAF IX AS LC	BEKA FIX 52 S6 LC
Type	Phosphate-bonded ramming mix	Andalusite based dense castable	Andalusite based LCC	SiC containing LCC, alkali resistant
BD, dried (g/cm³)	2.58	2.40	2.48	2.50
CCS, dried (MPa)	10-20	50	91	89
CCS, (MPa)	30	20	85	95
PLC (%)	1.6	1.8	0.2	0.2

3.2. Anchor Design Modification

To reduce localized stress concentrations, the geometry of the ceramic anchors was fundamentally redesigned. The original anchors (Figure 2) featured predominantly angular geometries with relatively small transition radii. This configuration created pronounced notch effects, resulting in elevated local stresses within the surrounding refractory castable.

As part of the design optimization, the original anchor geometry was replaced by tapered, smoothly rounded ceramic anchors (Figure 3). The continuous geometric transitions provide a more uniform transfer of mechanical loads between the ceramic anchor and the refractory castable. As a result, localized stress concentrations are significantly reduced and the maximum tensile stresses in the anchoring region are lowered.

Consequently, the probability of microcrack initiation decreases, leading to improved longterm durability of the entire assembly.



Figure 2



Figure 3

3.3. Optimization of Expansion Joints

The investigated refractory separation wall consists of 31 individual precast modules, each having a width of 396 mm. In the original design, expansion joints approximately 4 mm wide were already provided between adjacent modules, allowing thermal expansion of the individual components to be accommodated.

The practice of usage of adhesive tape and ceramic fibre blankets between bullnose blocks has reduced expansionary stress. Precise and adequate thickness of expansion provisioning is to be ensured to avoid heat leakages and hot spot issues. To improve the expansion concept, six additional expansion joints with a width of 10 mm were evenly distributed across the entire furnace width (Figure 4). This subdivides the refractory separation wall into several independent expansion sections. Thermally induced movements can therefore be accommodated locally within each section, preventing the build-up of high compressive forces across the entire assembly. Consequently, restraint stresses are significantly reduced, resulting in lower local tensile stresses within the refractory castable and effectively slowing the propagation of existing microcracks.

Operational experience, however, showed that thermal movements accumulated across the entire furnace width, resulting in considerable restraint forces within the complete assembly. Expansion provisioning is paramount to reduce mechanical stress generated due to expansion and contraction.

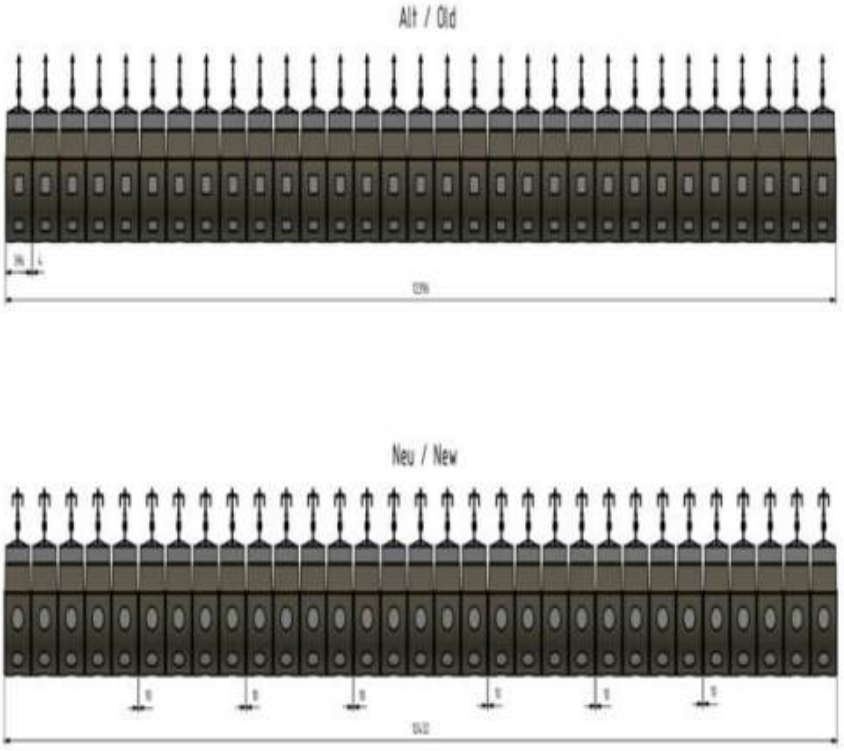


Figure 4

4. Conclusion

Detailed analysis revealed that bullnose cracking, and dislodgement were driven by chemical reaction, thermal cycling, and structural stress. The original alumino-silicate refractory reacted with alkali oxides in the mould powder, forming low-melting phases that degraded the blocks. Additionally, temperature fluctuations and mismatched expansion rates between the steel frame, ceramic anchors, and refractory castable induced high thermo-mechanical stresses. To address this, the refractory was upgraded to an alkali-resistant, SiC-bearing low-cement castable (BEKAFIX 52 S6 LC). To improve structural load transfer, the anchor profile was modified from square to rounded, reducing localized stresses, and slowing microcrack growth. Finally, longitudinal stresses were relieved by introducing six 10 mm expansion joints across the furnace width, creating independent expansion segments. These combined actions have improved bullnose stability and long-term performance.

5. References

[1] Ashish Chaudhary, Failure analysis of bullnose refractory in reheating furnace of Hot Strip Mill, 2016

[2] J Heinlein, Energy Saving in Walking Beam Furnaces at Arcelormittal (Bremen, Germany) by A New Concept for Skid Pipe Insulation, 2014

[3] Michal Švantner, Continuous walking-beam furnace 3D zonal model and direct thermal-box barrier-based temperature measurement, 2020

[4] Guishi Cheng, Corrosion, permeation, and mass transfer mechanisms of alkali metals in corundum refractories, 2024

[5] G.G. Roy, S. Ghosal, G. Saha, An Overview of Design Development of Walking Beam Furnace, 3rd International Conference on Refractories at Jamshedpur, 2013.

[6] S. R. Zamyatin, Modern refractory materials for lining of heating furnaces, Published: September 1990, Volume 31, pages 585–588 (1990)

[7] H.-H. Cheng, Y.-L. Hsu, C.-H.Wang, F.-Y. Hsia, T.-T. Ou, Control Method for Low Oxygen Concentration in Reheating Furnace, China Steel Technical Report, No. 24, 2011, pp. 20–27.

DEVELOPMENT OF CHROME BEARING HIGH ALUMINA BRICK FOR SETTLING CHAMBER OF EAF BY USING GREEN RAW MATERIALS – A SUSTAINABLE APPROACH TOWARDS MANUFACTURING OF COST-EFFECTIVE HIGH-END REFRACTORIES

Aakash Dalui, Jyoti Prakash Nayak, Biswajit Ghosh, Hiroshi Nagata, Prasant Kumar Naik
TRL Krosaki Refractories Limited, Belpahar, Odisha, India

Corresponding author: aakash.dalui@trlkrosaki.com

Abstract

The Electric Arc Furnace (EAF) has emerged as a cornerstone of modern steelmaking, offering a sustainable and flexible alternative to traditional blast furnace methods because they melt steel scrap and direct reduced iron (DRI) using electrical energy, thereby reducing overall energy use and greenhouse-gas emissions compared with conventional blast-furnace routes. Within the EAF off-gas system, the settling chamber is a large-volume enclosure that lowers gas velocity to enable gravitational separation of coarse particulates. This component experiences severe service conditions, including high dust loading near the inlet, thermal gradients during gas cooling, attack by volatile species, and repeated thermal cycling.

Accordingly, the lining—typically >85% Al_2O_3 high-alumina firebrick—must provide strong resistance to slag corrosion/erosion, thermal shock, and mechanical damage under fluctuating redox conditions. To address these requirements, TRL Krosaki Refractories Limited developed a chrome-bearing high-alumina brick specifically for settling-chamber applications. The formulation incorporates green raw materials (GRMs) as a major recycled constituent, blended with selected aluminous raw materials to reduce dependence on prime resources while supporting waste minimization goals. The fired bricks exhibit improved cold crushing strength, modulus of rupture, and thermal-shock endurance, translating to longer service life relative to conventional high-alumina linings. These results demonstrate that sustainable refractory design can enhance operational reliability while contributing to broader carbon-footprint reduction initiatives.

Keywords: Green raw materials; Chrome-alumina; Thermal shock; EAF.

Introduction

Electric Arc Furnace (EAF) steelmaking has become a key technology for sustainable steel production due to its efficient utilization of steel scrap and direct reduced iron (DRI), resulting in lower energy consumption and reduced greenhouse gas emissions compared with conventional blast furnace routes. The performance and reliability of EAF auxiliary systems are critical for ensuring uninterrupted operations under demanding service conditions. Among these, the settling chamber in the off-gas handling system plays an essential role in reducing gas velocity and facilitating the removal of coarse dust particles. However, refractory linings in this zone are exposed to severe thermal, chemical, and mechanical stresses, leading to premature degradation.[1] To address these challenges, a chrome-bearing high-alumina refractory brick incorporating substantial quantities of green raw materials (GRMs) was developed. This study evaluates its physical, mechanical, and thermal-shock properties and demonstrates its potential to enhance lining life while supporting sustainability and carbon-footprint reduction objectives.

Experimental Study

The principal raw materials employed in this investigation were fused corundum, High dense bauxitic aggregates, along with major alu-chrome GRMs with conventional binders.

Table 1 : Batch composition of bricks

Raw Material	Trial-1 (%)	Trial-2 (%)
Fused Corundum	*	*
High Dense Bauxite	**	*
Alu-Chrome Green Raw Material	*	**

Trial-1 was formulated predominantly with bauxitic-grade raw materials, incorporating a comparatively lower proportion of Alu-Chrome GRMs. In contrast, Trial-2 consisted primarily of Alu-Chrome GRMs with a reduced bauxitic content. The two formulations were designed to achieve a balanced compositional profile while maintaining the targeted performance characteristics, with the additional objective of developing a cost-effective refractory solution for steelmakers operating through the Electric Arc Furnace (EAF) route. Both formulations were manufactured using a high-capacity 1600-ton hydraulic press and subsequently fired at 1460°C in a tunnel kiln to ensure adequate densification and phase development.

Characterization of Products

The developed refractory bricks were comprehensively characterized to evaluate their physical, mechanical, and high temperature properties in accordance with relevant DIN standards. Apparent porosity (AP), bulk density (BD), cold crushing strength (CCS), and permanent linear change (PLC) were measured to assess the fundamental structural integrity, density characteristics, and thermal stability of the materials. Furthermore, the hot modulus of rupture (HMoR) was determined to evaluate the mechanical strength and load-bearing capability of the bricks under elevated-temperature conditions. In addition, X-ray diffraction (XRD) analysis was conducted to identify and quantify the crystalline phases present in the refractory matrix.

Thermal shock resistance (TSR) was evaluated in accordance with the DIN standard testing procedure, involving repeated heating cycles to 950°C followed by rapid water quenching. This method was employed to simulate severe thermal cycling conditions and to assess the resistance of the developed refractory compositions to crack initiation and propagation under abrupt temperature fluctuations. Hot abrasion resistance was assessed at 1250°C using a silicon carbide (SiC) jet abrasion test, with volumetric and mass losses recorded after specified exposure durations. The microstructural evolution and phase assemblage within the brick matrix following abrasion testing were examined using scanning electron microscopy (SEM).

Results & Discussion

Physical and chemical properties analysis of both products have been evaluated and summarized in Table 2 & Table 3 respectively.

Table 2: Physical Properties analysis of the brick samples

Properties	Unit	T-1	T-2
A.P.	(%)	14.3	12.4
		14.1	12.9
B.D.	(gm/cc)	2.91	2.98
		2.92	2.96
CCS	(kg/cm2)	675	776
		732	748

The physical property results in Table 2 indicate that T-2, containing a higher proportion of Alu-Chrome GRMs and lower High Dense Bauxite, exhibited superior densification compared to T-1. T-2 showed lower apparent porosity (12.9%) and higher bulk density (2.96 g/cm³) than T-1 (14.1% AP and 2.92 g/cm³ BD), indicating the formation of a more compact microstructure after firing.

Similarly, T-2 achieved a slightly higher cold crushing strength (748 kg/cm²) compared to T-1 (732 kg/cm²). The improved strength is attributed to its lower porosity and enhanced ceramic bonding resulting from the higher Alu-Chrome GRMs content. Overall, the results suggest that increasing the Alu-Chrome GRMs content promotes densification and mechanical strength, making T-2 a more suitable candidate for demanding EAF steelmaking environments requiring high resistance to abrasion and mechanical wear.

Table 3: Chemical analysis of the brick samples

Constituents (Wt.%)	T-1	T-2
Al_2O_3	84.49	85.62
Fe_2O_3	0.95	0.51
TiO_2	1.34	1.21
Cr_2O_3	4.40	7.01
Others	8.82	5.65

The chemical analysis in Table 3 confirms that both formulations are high-alumina refractories, containing more than 84 wt.% Al_2O_3. T-2 exhibited slightly higher Al_2O_3 (85.62 wt.%) and Cr_2O_3 (7.01 wt.%) contents compared to T-1 (84.49 wt.% Al_2O_3 and 4.40 wt.% Cr_2O_3), owing to the higher incorporation of Alu-Chrome GRMs. Additionally, T-2 contained lower Fe_2O_3, TiO_2, and other impurity oxides, indicating a comparatively purer composition. The increased alumina and chromium oxide contents, together with reduced impurities, are expected to enhance refractoriness, slag resistance, and high-temperature stability, making T-2 more suitable for demanding EAF steelmaking applications.

Table 4: High-temperature properties of brick samples

Properties	Unit	T-1	T-2
RUL (ta)	°C	1622	1657
PLC at 1550°C/3hrs.	(%)	+0.17	+0.11
HMoR at 1500°C	Kg/cm2	124	152
Thermal Shock Resistance at 950°C/Water.	Cycle	+30	+35
Abrasion Loss	cc	0.23	0.18

The thermal property results in Table 4 indicate that T-2 exhibited superior high-temperature performance compared to T-1. T-2 achieved a higher refractoriness under load (RUL) value of 1657°C, compared to 1622°C for T-1, demonstrating better load-bearing capability at elevated temperatures. The lower permanent linear change (PLC) of +0.11% in T-2, compared to +0.17% in T-1, indicates enhanced dimensional stability during thermal exposure.

The hot modulus of rupture (HMoR) at 1500°C was significantly higher for T-2 (152 kg/cm²) than T-1 (124 kg/cm²), reflecting improved mechanical strength under service conditions. Furthermore, T-2 exhibited better thermal shock resistance, withstanding more than 35 cycles compared to more than 30 cycles for T-1, indicating greater resistance to crack formation during rapid temperature fluctuations. The abrasion loss was also lower for T-2 (0.18 cc) than T-1 (0.23 cc), suggesting enhanced wear resistance. Overall, the higher Alu-Chrome GRMs content in T-2 contributed to improved thermal stability, hot strength, thermal shock resistance, and abrasion resistance.[2]

XRD Analysis

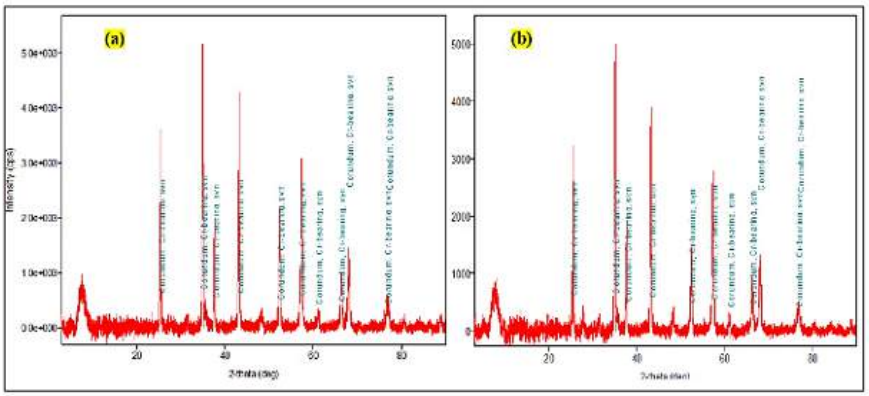


Figure 1: XRD Pattern of (a) Trial -1 and (b) Trial -2 product.

Fig.1 shows the XRD patterns of Trial-1 and Trial-2 exhibited nearly identical diffraction peaks, confirming the formation of the same crystalline phases in both samples. No significant peak shift was observed in Fig.1(a) to Fig.1(b), indicating structural stability and phase reproducibility. The sharp diffraction peaks demonstrate good crystallinity, while the absence of major secondary-phase reflections suggests high phase purity.

Thermal Shock Resistance

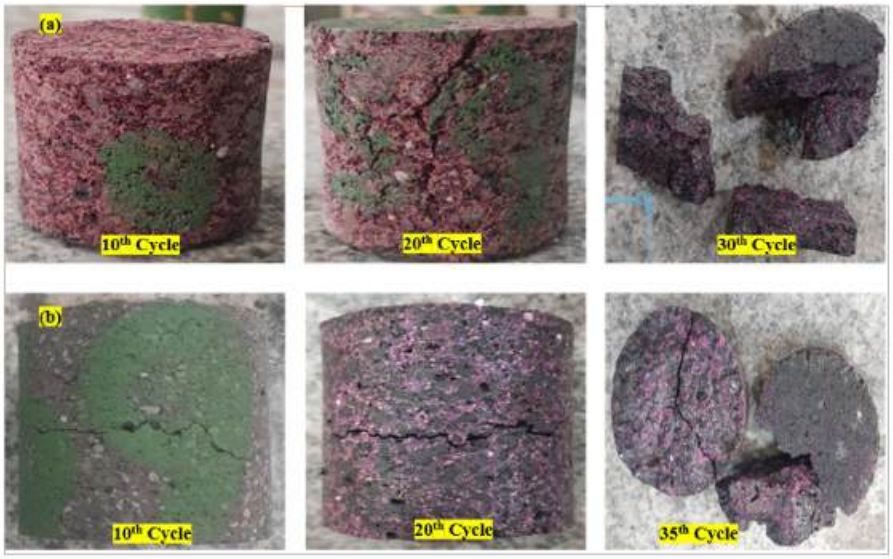


Figure 2: Brick samples after Thermal Shock Test (a) Trial-1 and (b) Trial-2 product

The superior thermal shock resistance in Fig.2 observed for Trial-2 (>35 cycles) compared to Trial-1 (>30 cycles) indicates its enhanced resistance to thermal spalling under severe heating and cooling conditions. This improvement can be attributed to the higher proportion of Alu-Chrome GRMs in T-2, which increased the Cr_2O_3 content of the refractory matrix and promoted the formation of stable alumina-chromia phases. These phases contribute to improved structural stability under severe thermal cycling.

The denser microstructure of T-2, evidenced by its lower apparent porosity and higher bulk density, helped reduce stress concentration sites and restricted crack initiation during rapid temperature fluctuations. Furthermore, the higher hot modulus of rupture (152 kg/cm²) indicates better retention of mechanical strength at elevated temperatures, enabling the refractory to withstand thermally induced stresses more effectively.

Consequently, T-2 exhibited reduced surface spalling and better crack-arrest capability, leading to greater thermal shock resistance and indicating superior suitability for EAF applications subjected to frequent thermal cycling.[3]

Hot Abrasion Test



Figure 3: Status of brick samples (a) Trial-1 and (b) Trial-2 product after Abrasion Test

The sample condition after hot abrasion test carried out at 1250°C in Fig.3 demonstrated improved wear resistance for T-2, which exhibited a lower volumetric loss (0.18 cc) than Trial-1 (0.23 cc). This enhancement is attributed to the higher Alu-Chrome GRMs content, which increased the Cr_2O_3 concentration and promoted the formation of hard, wear-resistant Corundum (α-Al_2O_3) and alumina-chromia phases within the refractory matrix. In addition, T-2 showed lower apparent porosity and higher bulk density, resulting in a denser microstructure with stronger ceramic bonding and reduced grain pullout under abrasive conditions. The higher hot modulus of rupture further contributed to maintaining mechanical integrity at elevated temperatures. Consequently, T-2 exhibited superior resistance to SiC-induced erosion, indicating its suitability for severe high-temperature wear environments encountered in EAF service conditions.

Microscopical Analysis:

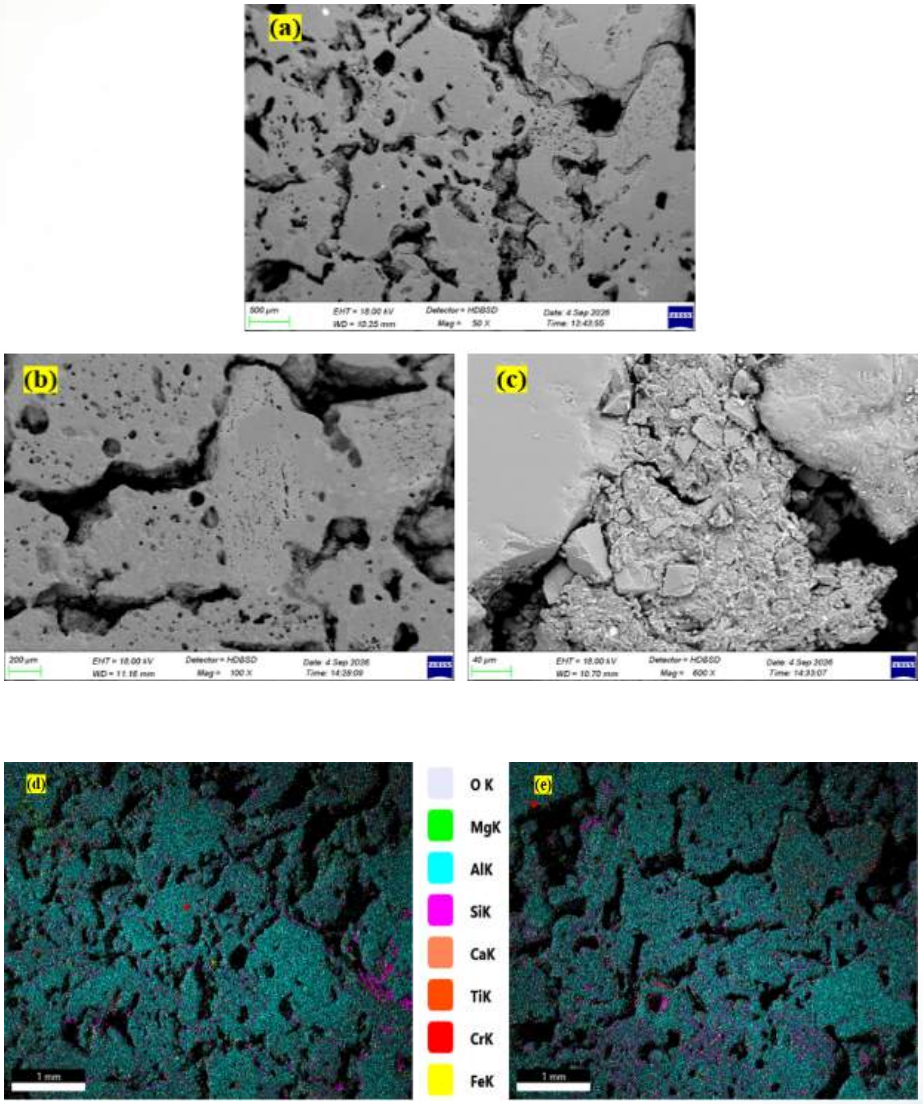


Figure 4: Microscopy analysis (a) Trial-1 and (b), (c) indicating Trial-2 product after abrasion test and EDS Analysis (d) & (e) represents elemental colour mapping for Trial-1 & Trial-2 respectively

SEM micrographs in Fig.4 (a) show a homogeneous distribution of Alu-Chrome grains throughout the refractory matrix inside T-1 whereas Fig.4 (b) & (c) exhibited well-packed grains inside T-2 with limited intergranular voids, confirming good densification even after abrasion. Distinct grain boundaries were observed to be tightly

bonded by a continuous ceramic matrix inside T-2, suggesting the development of strong interparticle bonding and effective sintering.

EDS elemental mapping in Fig.4 (d) & (e) further confirmed the uniform distribution of Al and Cr across the microstructure of T-1 & T-2 respectively, indicating the presence of alumina-chromia phases. The intimate contact between Alu-Chrome grains and the surrounding matrix is expected to enhance load transfer, improve crack-arrest capability, and reduce grain pullout under service conditions. Such a dense and strongly bonded microstructure contributes to the improved hot strength, abrasion resistance, and thermal spalling resistance observed for the developed refractory composition.

The SEM and XRD analyses confirmed the presence of a dense corundum-rich matrix along with chromia-containing phases, which collectively enhance the intergranular bonding and wear resistance. Consequently, the synergistic effect of higher alumina-chromia phase content, improved densification, and enhanced hot strength resulted in the superior abrasion resistance observed in T-2, making it a promising composition for EAF settling chamber applications subjected to severe abrasive conditions.[4]

Conclusion

The comparative evaluation of T-1 and T-2 demonstrated that increasing the Alu-Chrome GRMs content at the expense of conventional bauxite significantly improved the overall performance of the refractory. XRD analysis confirmed the presence of stable Chrome containing Corundum (Al_2O_3) phases, while SEM-EDS studies revealed a uniform distribution of Alu-Chrome grains and the development of a dense, strongly bonded microstructure. Consequently, T-2 exhibited lower porosity, higher bulk density, improved hot strength, superior hot abrasion resistance (0.18 cc), and enhanced thermal spalling resistance (>35 cycles) compared with T-1.

The improved performance is attributed to the formation of a robust alumina-chromia matrix, which enhanced densification, mechanical integrity, wear resistance, and resistance to thermal shock. In addition to delivering superior thermo-mechanical properties, the partial replacement of bauxite with Alu-Chrome GRMs provides a cost-effective and sustainable utilization of recycled alumina-chrome material without compromising product quality.

Overall, the results indicate that T-2 is the most suitable composition for the intended EAF refractory application, offering enhanced service performance, improved durability under severe operating conditions, and a favourable cost-performance balance.

Reference

1. Lee, W. E., & Zhang, S. (1999). Melt corrosion of oxide and oxide-carbon refractories. International Materials Reviews, 44(3), 77-104.

2. Routschka, G., & Wuthnow, H. (2008). Pocket Manual Refractories. Vulkan-Verlag GmbH, Essen, Germany.

3. Schacht, C. A. (Ed.). (2004). Refractories Handbook. CRC Press, Boca Raton, Florida, USA.

4. Parr, C., & Wohrmeyer, C. (2014). Advances in alumina-chromia refractory technology for high-temperature industrial applications. Refractories Worldforum, 6(2), 71-78.

DEVELOPMENT OF A HIGHER-SERVICE-LIFE COLLECTOR NOZZLE

S. Chowdhury[1], Dr. A. K. Samanta[1], R. Kimura[1], H. Kazuaki[1], H.Nagata[1], P. K. Naik[1], D. Yoshitsugu[2], J. Amano[2]

[1]TRL Krosaki Refractories Limited, Belpahar - 768218, Odisha, India
[2]Krosaki Harima Corporation, Kitakyushu, Japan

Abstract

Flow control refractories are essential for regulating molten-steel flow in continuous casting, but these refractories are used under harsh conditions.Collector nozzles are subjected to severe and repeated thermal shocks, which can lead to crack initiation. Such failures disrupt casting stability, increase nozzle-related interruptions, and adversely affect steel cleanliness and productivity.

This study reports the development of a high-spalling-resistance, unburnt collector nozzle through optimized raw-material selection.

The new formulation incorporates a high-expansion raw material that undergoes controlled expansion during phase transformation, providing a crack-arresting effect within the refractory matrix.

The product was further validated in industrial trials at multiple integrated steel plants, where results confirmed superior field performance in terms of extended service life, improved casting stability, and a significant reduction in nozzle-related casting interruptions. Owing to its low-temperature curing process and enhanced durability, the developed collector nozzle also contributes to reduced greenhouse-gas emissions by minimizing the need for high-temperature firing and reducing refractory consumption through fewer replacements.

Keywords: Collector nozzle, Spalling, high-expansion raw material, crack-arresting effect

1. Introduction

A slide gate mechanism is installed at the bottom of a steel ladle. After completion of secondary refining of steel in steel ladle, the liquid steel is transferred from steel ladle to tundish through the slide gate. The flow of molten steel is controlled by opening and closing the slide plates. Slide gate works on the principle of the parallel displacement of plates.

The flow-control system consists of a well block, ladle nozzle, slide plates, and collector nozzle, as shown in Fig. 1.

During tapping when the molten steel is passing through the slide plates it is subjected to the attack by the molten steel in the sliding surface. Additionally, during ladle operation, the collector nozzle is exposed to repeated heating and cooling cycles which can lead to spalling and crack propagation.

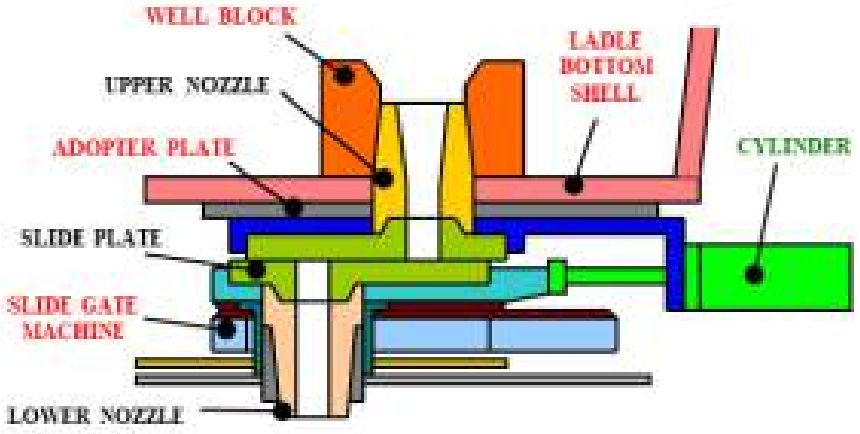


Fig 1. Arrangement of flow-control products

Table 1 Required properties of flow-control products

	Purpose	**Required properties**
Plate	Control flow rate (Start and Stop casting)	a) Strength against face pressure b) Spalling resistance against thermal shock c) Corrosion resistance against steel or lancing
Upper or Ladle Nozzle	Connect to Ladle or to Tundish	Corrosion resistance against steel, slag or lancing
Lower or Collector Nozzle	Control steel flow	Spalling resistance against thermal shock

2. Collector nozzle problem at the customersite

Previously, customers were predominantly producing conventional steel grades under relatively stable operational conditions, with consistent ladle temperatures, holding times, casting sequences, and flow control practices. Based on these operating conditions, we successfully supplied alumina-carbon-based unburnt collector nozzles containing silica to various steel plants, and the performance was found to be satisfactory over an extended period.

One of the key advantages of silica-containing refractory materials is their thermal behaviour at elevated temperatures. Above approximately 600°C, silica exhibits relatively low thermal expansion and improved dimensional stability. As a result, the refractory can accommodate the thermal strains generated during repeated heating and cooling cycles encountered in ladle and continuous casting operations. This characteristic helps in minimizing the development of thermal stress within the collector nozzle and reduces the tendency for crack initiation and spalling under normal operating conditions.

However, with the increasing production of special steel grades, wider variations in steel

temperatures, prolonged holding times, frequent casting interruptions, higher superheats, and more aggressive operating practices, the thermal and mechanical loads acting on the collector nozzle have increased significantly. As a result, typical problems such as rathole formation and severe cracking are often observed in the bore region and beneath the collar portion of the collector nozzle shown in Fig. 2 and the mechanism of rathole formation is shown in Fig. 3.

It was necessary to reassess the refractory composition and design to ensure enhanced thermal shock resistance and operational reliability.

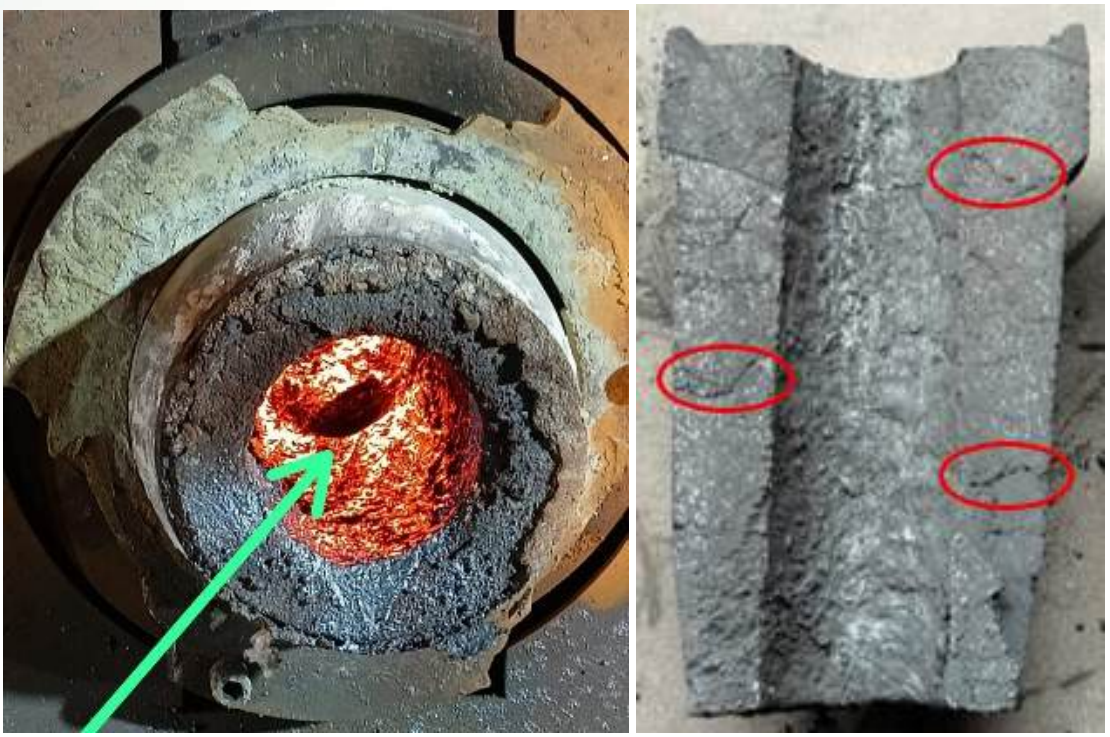


Fig 2. Rathole formation (left) and crack formation (right) after use

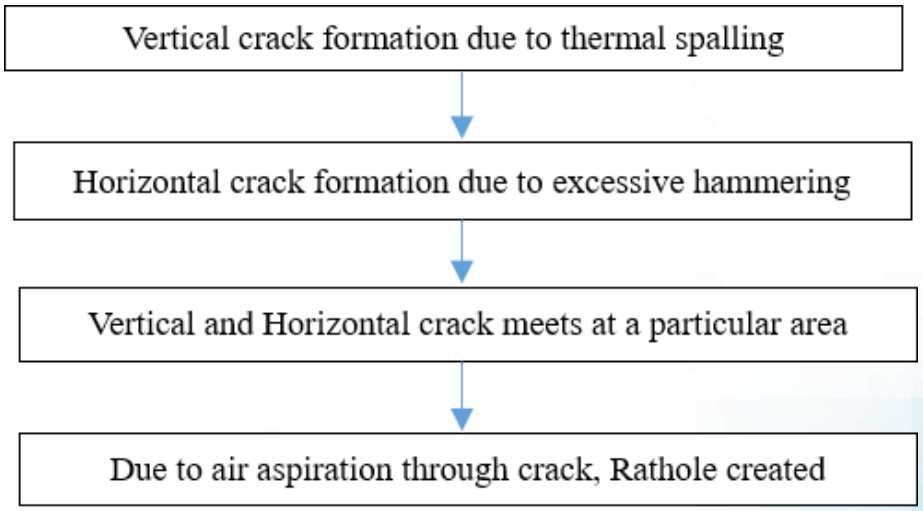


Fig 3. Mechanism of rathole formation

3. Concept of Crack Arrestor in Unburnt Collector Nozzle

To address crack-related failures and extend service life, a new universal unburnt collector nozzle was developed. A key feature of this nozzle is the inclusion of a high-expansion raw material (Fig.4), which significantly improves its overall spalling resistance. The controlled expansion behavior helps to arrest crack propagation within the refractory structure. As a result, vertical cracks initiated from the outer surface during thermal cycling are prevented from extending continuously toward the bore area (Fig.5). This interruption in crack growth minimizes the likelihood of vertical and horizontal crack interconnection, which is a primary cause of premature nozzle failure, as shown in Fig. 3.

Consequently, it is expected that the formation of through-cracks and rathole defects is significantly reduced.

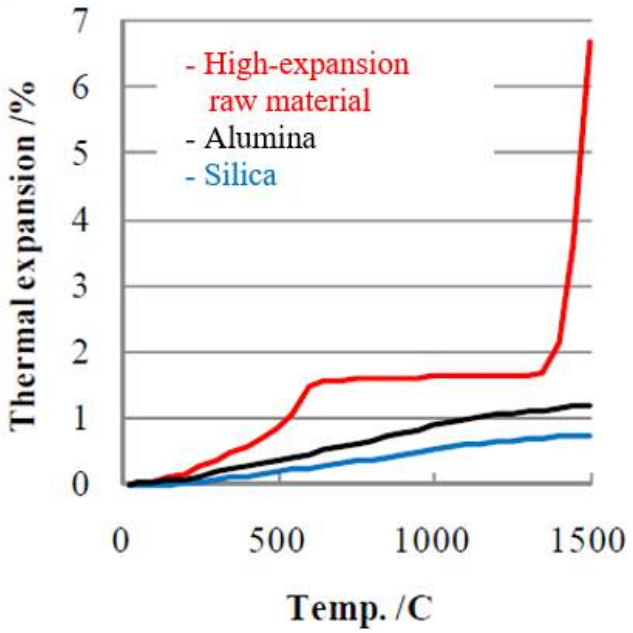
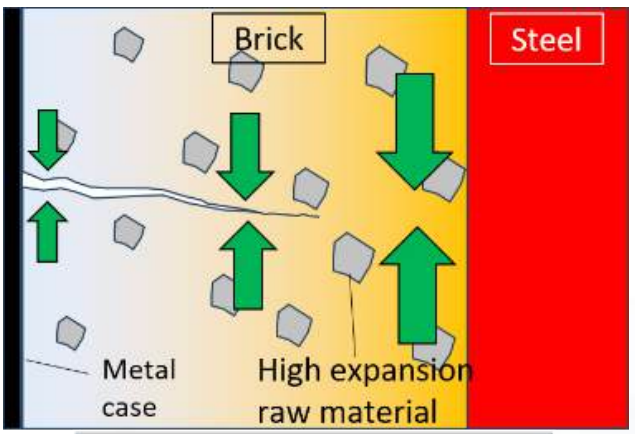


Fig 4. Thermal expansion behavior of raw material



The expansion of the raw material inhibits crack propagation.

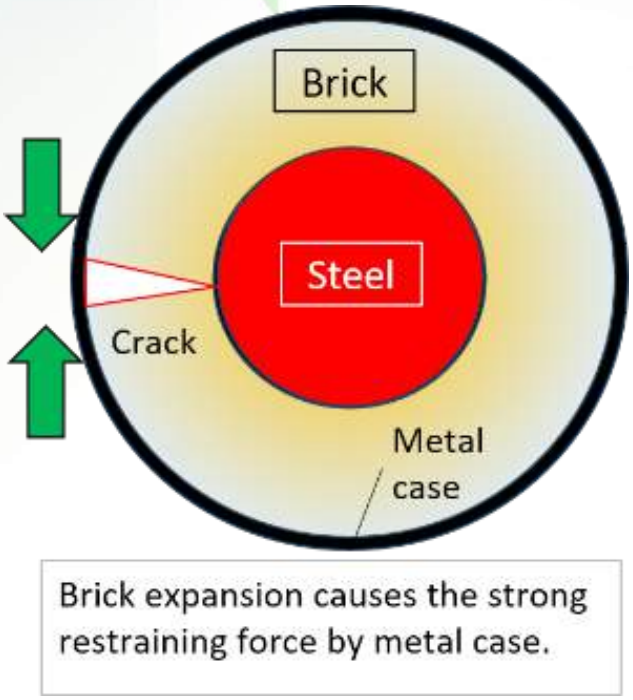


Fig 5. Crack-arresting mechanism of the developed nozzle

4. In-house Experiment

In a high frequency induction furnace, corrosion resistance was evaluated by measuring the amount of material corroded by FeO, as shown in Table 2 and Fig. 6.The spalling resistance test was conducted in an electric furnace and the test pieces were heat-treated at 1200°C for 15 min followed by water quenching for 3 min.

Table 2 Properties and test results

Type		Conventional	Developed
Feature		Standard	Crack Arrestor
Chemistry (%)	Al_2O_3	79.2	77.2
	SiO_2	17.5	19.6
Physical	AP (%)	6.1	5.5
	BD	2.87	2.97
Corrosion depth (mm) (at 1600 deg C x 2hrs) *Lower value is better		10.85	10.09
Spalling resistance (at 1200 °C x 15mins → Water quenching x 3mins * max.13 cycles)		Cycle of initial crack appearance 8 (Fine crack)	Cycle of initial crack appearance - (No crack)

	Conventional	Developed
Corrosion test		
Spalling test (Cross section after 13 cycles)		

Fig. 6 Sample appearance after test

The developed collector nozzle exhibited higher spalling resistance than the conventional nozzle due to the presence of the high-expansion raw material. Its corrosion resistance was comparable to that of the conventional nozzle.

5. Field Trial Results

In the field trial, both the conventional and developed collector nozzles were tried under identical operating conditions. The comparison is shown in Fig.7 and Fig.8.

Fig.7shows that rathole formation occurred in the conventional collector nozzle, whereas no rathole formation was observed in the developed nozzle under the same operating conditions. Furthermore, Fig.8shows that in the conventional nozzle, all the cracks generated during operation were connected to the bore, providing a direct pathway for rathole development. In contrast, although crack formation was observed in the developed nozzle, none of the cracks were connected to the bore. As a result, the likelihood of rathole formation was significantly reduced in the developed nozzle.

This improved crack pattern and enhanced structural integrity translated into superior field performance. At both Customer Site A and Customer Site B, the developed nozzle consistently outperformed the conventional nozzle. With this developed design we have achieved an average service life of 4 heats and 6 heats, respectively, compared with 2.5 heats and 4 heats for the conventional nozzle. These results clearly indicate that the developed nozzle offers improved resistance to rathole formation and enhanced operational durability, leading to a substantial increase in service life under actual plant operating conditions.



Fig.8 Cracks connected to the bore in the conventional nozzle (left) and no crack connection to the bore in the developed nozzle (right)

Table 3 Service life of nozzles (heats)

Customer Site	Conventional (Avg Life)	Developed (Avg Life)
A	2.5	4
B	4	6

6. Conclusion

We analysed the performance of both collector nozzles under identical operating conditions and found that the developed nozzle consistently outperformed the conventional nozzle. The improved performance can be attributed to the presence of an expansive raw material in the developed nozzle, which acts as a crack-arresting mechanism. During operation, thermal stresses generated by factors such as prolonged holding time, extended preheating duration, temperature fluctuations, and casting conditions can initiate vertical cracks within the nozzle body. In the developed nozzle, the expansive component helps restrict the propagation of these cracks, preventing them from extending toward the bore.

Once the vertical crack is arrested and unable to reach the bore, the possibility of rathole formation is significantly reduced. Although horizontal cracks may still develop due to excessive hammering or mechanical impact during nozzle installation, these cracks remain isolated because they do not intersect with the arrested vertical cracks. As a result, a continuous crack network leading to the bore is not formed, thereby minimizing the likelihood of rathole development and improving the overall service life of the collector nozzle.

Based on the performance evaluation, the crack-arrestor collector nozzle is particularly suitable for steel plants operating under severe and unstable casting conditions, where frequent thermal cycling, extended holding periods, and operational fluctuations increase the risk of crack propagation. Conversely, under relatively stable operating conditions, where thermal and mechanical stresses are well controlled, the conventional collector nozzle remains a suitable option.For customers, the developed nozzle contributes to an extended service life and reduced refractory consumption, thereby improving their profitability while reducing CO_2 emissions associated with refractory manufacturing.

References

1) Subir Biswas and Debasish Sarkar, “Introduction of refractories for Iron and Steel making”, pp 359-367 (2020)

EFFECT OF SILICON CARBIDE ON THE PROPERTIES OF HIGH-DENSITY SILICA BRICKS FOR COKE-OVEN APPLICATIONS

Deeptayan Banerjee, Tapas Mahata, Vikash Kumar, Jyoti Prakash Nayak, Biswajit Ghosh, Hiroshi Nagata and Prasant Kumar Naik

Corresponding author's e-mail: deeptayan.banerjee@trlkrosaki.com

Abstract

Silica refractories are valued for their high refractoriness, structural rigidity, and volume stability at elevated temperatures. Their performance is largely governed by silica phase transformations during firing (quartz to tridymite and cristobalite). With growing demand for high-density silica bricks that provide longer campaign life and improved mechanical integrity in coke-oven service, modification of conventional compositions using suitable additives is of increasing interest. Silicon carbide (SiC), in particular, is expected to promote matrix densification and enhance strength because of its inherent thermal and structural characteristics.

In this study, different SiC powder size fractions were added at an optimized level to a base silica composition to evaluate their influence on the properties of high-strength, high-density silica bricks. All batches were benchmarked against a reference composition without SiC. The samples were characterized by X-ray fluorescence (XRF) for chemical analysis, X-ray diffraction (XRD) for phase identification, and residual quartz estimation to assess the extent of silica transformation. Microstructural features and SiC distribution within the matrix were examined using scanning electron microscopy (SEM).

Key physical and mechanical properties were assessed in terms of apparent porosity (AP), bulk density (BD), and cold crushing strength (CCS). High-temperature performance was further evaluated through reversible thermal expansion and creep resistance tests to understand thermo-mechanical stability under service-relevant conditions.

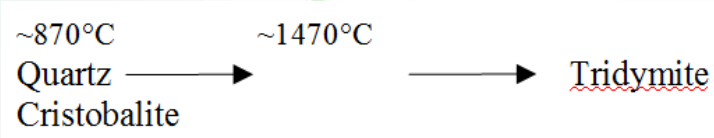
This work aims to establish the relationship between SiC particle size and the overall performance of high-density silica refractories. The findings provide guidance on selecting SiC fineness and distribution to improve densification, reduce porosity, and enhance mechanical strength, supporting the development of durable silica bricks for extended coke-oven campaigns.

Keywords: Silica refractories, Silicon carbide

1. Introduction

Silica refractories constitute the predominant lining material for high-temperature industrial infrastructure, most notably in heavy-duty coke-oven batteries, glass-melting tanks, and hot-blast stoves. Their wide adoption stems from unique thermal and mechanical characteristics: exceptional load-bearing capacity at temperatures approaching their fusion point (> 1650°C), high resistance to thermal spalling above 600°C, and robust volume stability driven by completed silica polymorph transformations during initial synthesis.

The performance of quartzite-derived refractories is intrinsically linked to phase transformations occurring during high-temperature firing. Natural quartz (α-quartz) undergoes reconstructive phase transformations into metastable tridymite and cristobalite polymorphs.



Because reconstructive phase shifts involve the breaking and reforming of Si—O covalent bonds, significant volumetric expansion occurs during the conversion of dense quartz (ρ ~2.65 g/cm3) into lower-density polymorphs such as tridymite (ρ ~2.28 g/cm3) and cristobalite (ρ ~2.33 g/cm3). Uncontrolled phase conversion leads to severe cracking, low bulk density, and excessive open porosity. Consequently, mineralizing agents are routinely incorporated into quartzite formulations to promote liquid-phase development at lower temperatures, accelerating conversion to stable tridymite/cristobalite networks and improving matrix sintering[1].

In modern steelmaking, coke ovens face demanding operational conditions: higher coking rates, increased mechanical abrasion from pushed coke charges, aggressive thermal cycling, and harsh chemical attack. To extend campaign life and improve thermal efficiency, there is a growing industrial demand for high-density, high-strength silica refractories.

A promising strategy to enhance standard silica brick formulations is the addition of non-oxide ceramic powders, specifically Silicon Carbide (SiC)[1]. Silicon carbide possesses high intrinsic hardness, high thermal conductivity, low thermal expansion, and excellent abrasion resistance. However, incorporating SiC into an oxidizing silicate processing environment introduces complex thermodynamic and kinetic phenomena. At elevated firing temperatures (> 1000°C), SiC undergoes passive oxidation:

$$SiC\ (s) + 2O_2\ (g) \rightarrow SiO_2\ (s) + CO_2\ (g) \quad (1)$$
$$SiC\ (s) + O_2\ (g) \rightarrow SiO_2\ (s) + CO\ (g) \quad (2)$$

This oxidation process involves a substantial positive molar volume change (~100%) as the dense SiC converts into amorphous or crystalline SiO_2. Depending on particle size, temperature, and atmospheric conditions, this localized expansion can either beneficially fill matrix or induce micro-cracking and gas-driven bloating due to CO/CO_2 entrapment[1][2].

Although, the general benefits of non-oxide additives are recognized, systematic investigations examining how varying SiC particle size distributions affect densification mechanisms, micro-porosity formation, stress-transfer interfacial bonding, and thermal expansion in silica bricks remain limited. This study evaluates the effect of three distinct SiC powder fineness grades (F1, F2, and F3) on the physical properties, mechanical strength, phase development, and microstructural evolution of high-density silica refractories designed for coke-oven service.

2. Materials and Procedures

2.1 Raw Material Selection and Batch Formulation

High-purity natural quartzite raw materials were crushed, ground, and classified into three primary grain-size fractions: coarse, fines and dust. Three fixed mineralizing and binding additions (designated as Additive 1, Additive 2, and Additive 3) along with an organic binder were incorporated in consistent, identical weight percentages across all test batches to promote liquid-phase formation during firing.

Commercial SiC powder was added at a constant weight fraction A% across three batches (T1, T2, T3), alongside a standard

control batch (batch G) synthesized with 0% SiC. The variable parameter across experimental batches was the grain size fineness of the added SiC powder, defined by fineness hierarchy F3<F2<F1.

Table 1 Experimental Formulation Matrix

Material Component	Batch G	Batch T1	Batch T2	Batch T3
Coarse Aggregate	X	X	X	X
Fines Aggregate	Y	Y	Y	Y
Dust Aggregate	Z	Z	Z	Z
Mineralizing Additives+ Organic Binder	√	√	√	√
SiC F1	-	A	-	-
SiC F2	-	-	A	-
SiC F3	-	-	-	A

2.2 Component Shaping and Industrial Firing

The homogenized mixtures were pressed in a semi-automatic screwpress to achieve a constant green bulk density in all the four batches. Dried bricks were fired in an industrial tunnel kiln following standard silica plant thermal cycles, peaking at typical quartz to cristobalite/tridymite conversion temperatures.

2.3 Characterization

Post-firing, the batches were subjected to detailed characterization:

• Apparent Porosity (AP) and Bulk Density (BD) as per ISO 5017:1998
• Cold Crushing Strength as per ISO 10059-2:2003
• X-ray Diffraction (XRD) for phase identification and analysis of Residual Quartz by Rigaku™SmartLab™ XRD Analyzer
• Reversible Thermal Expansion at 1000°C as per ISO16835:2014
• Refractoriness Under Load (Ta) as per DIN 51064:1981
• Creep in Compression as per EN 993-9
• Microstructure by ZEISS™ EVO 18™ Scanning Electron Microscope

3. Results and Discussion

3.1 Physical and Mechanical Trends

The measured properties of fired bricks are summarized in Table 2.

Table 2 Physical, mechanical, and thermal properties of fired bricks

Property	Batch G	Batch T1	Batch T2	Batch T3
Apparent Porosity (%)	19.2 , 18.4	17.2 , 17.0	14.4 , 14.7	15.1 , 15.0
Bulk Density (g/cm3)	1.86, 1.89	1.93 , 1.94	1.96 , 1.97	1.94 , 1.95
Cold Crushing Strength (kg/cm2)	357, 362	380 , 374	476 , 520	757 , 780
RTE at 1000°C (%)	1.25	1.28	1.26	1.30
Residual Quartz (%)	0.40	0.43	0.25	0.29
CIC at 1500°C, 0.2MPa, 5-50 hours (%)	-0.020	-0.025	-0.016	-0.012
Linear expansion	↑	↑	↑	↑↑

3.1.1 Comparative Densification Analysis (AP and BD)

• Batch G (Control – 0% SiC): This represents the baseline standard, displaying high porosity and low bulk density governed purely by the packing and conversion kinetics of raw quartzite aggregates.
• Batch T1: This batch yields physical properties better than Batch G (~9% and ~3% improvement in AP and BD respectively). F1 particles act as inert inclusions, providing no densification benefit over the baseline.
• Batch T2: This batch shows a distinct improvement over the control, achieving maximum densification (~22% and ~5% improvement in AP and BD respectively). F2 particles fill interstitial matrix voids while undergoing localized $SiC \rightarrow SiO_2$ volume expansion that plugs micro-voids.
• Batch T3: This batch maintains significantly lower porosity and higher density (~20% and ~4% improvement in AP and BD respectively).

3.1.2 Compressive Strength Comparison (CCS)

Mechanical strength demonstrates a remarkable shift relative to Batch G.

• Batch T1 yields minimal strength gain over Batch G (~5% improvement), confirming that unreacted coarse SiC provides negligible reinforcement.
• Batch T2 increases CCS due to matrix compaction (~40% improvement).
• Batch T3 achieves an extraordinary strength of more than double the result of Batch G, driven by high specific reactivity that establishes a robust chemical bond across the matrix[1][2].

3.2 Reversible Thermal Expansion (RTE) at 1000°C

The Reversible Thermal Expansion evaluated up to 1000°C reveals distinct behaviour driven by SiC particle fineness and oxidation kinetics.

• Batch T1 exhibits a slight increase over Batch G. F1 grains mostly remain chemically inert and unbonded where unconstrained differential expansion between the aggregate

grains and silica matrix slightly elevates bulk expansion.

• Batch T2 achieves thermal stability close to the Batch G. The F2 particles are tightly entrapped within the matrix without generating excess oxidation products, maintaining a dense, structurally coherent framework that restrains expansion.

• Batch T3 exhibits the highest RTE. The ultrafine F3 grains have a much larger specific surface area, promoting extensive high-temperature oxidation during firing (equation (1)) and the formation of crystalline cristobalite scales[2][3]. During subsequent dilatometric reheating, the newly formed, finely dispersed cristobalite undergoes a sharp α→β displacive inversion with significant volume expansion, thereby increasing the bulk reversible expansion[4].

3.3 Creep in Compression (CIC)

• Batch G: This batch represents the baseline deformation of a standard quartzite-derived silica matrix governed by the viscosity of the intergranular glassy film.

• Batch T1: This batch displays the highest deformation where poorly bonded F1 grains create boundary voids that accelerate localized shear and viscous grain displacement under load.

• Batch T2: This batch shows improved resistance due to higher bulk density and mechanical entrapment of F2 grains, which reduce compressible voids.

• Batch T3: This batch shows superior creep resistance due to the chemically anchored highly viscous transition layer(discussed later under section 3.5) pins F3 grains across boundaries, arresting high-temperature grain-boundary sliding[5][6].

3.4 Post-firing Linear Expansion

Dimensional measurements were recorded before and after tunnel kiln firing to determine linear expansion.

• Batches G, T1 and T2: Linear expansion remained consistent, governed primarily by the density decrease during quartz conversion (ρ ~2.65g/cm^3) into tridymite (ρ ~2.28g/cm^3) and cristobalite (ρ ~2.33g/cm^3). In batch T2, local expansion of F2 SiC was accommodated within matrix pores, maintaining baseline growth[1].

• Batch T3: This batch exhibits a distinctly higher expansion. The high specific surface area of F3 accelerates passive oxidation ($SiC \rightarrow SiO_2$) and promotes secondary cristobalite devitrification, which further creates expansion and amplifies reversible thermal dilation via displacive transformation of α and β cristobalite[2].

3.5 Microstructural Analysis (SEM/EDS)

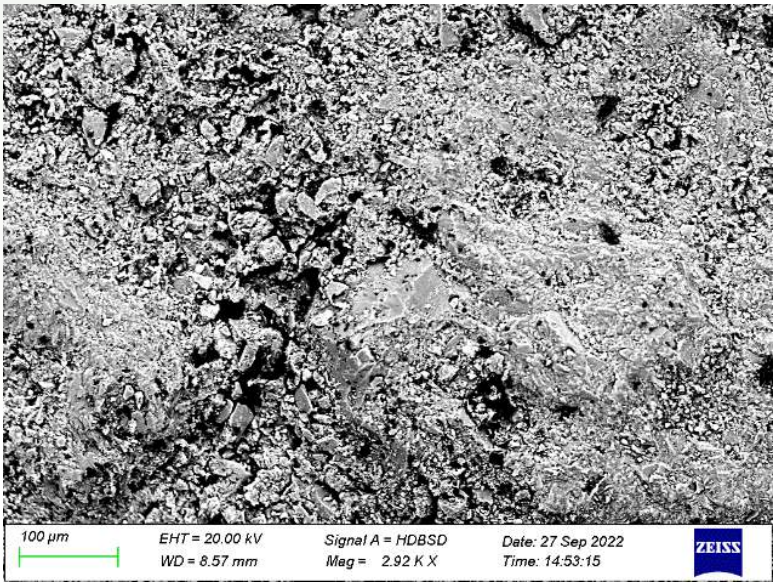


Figure 1 SEM of sample from Batch G (100µm)

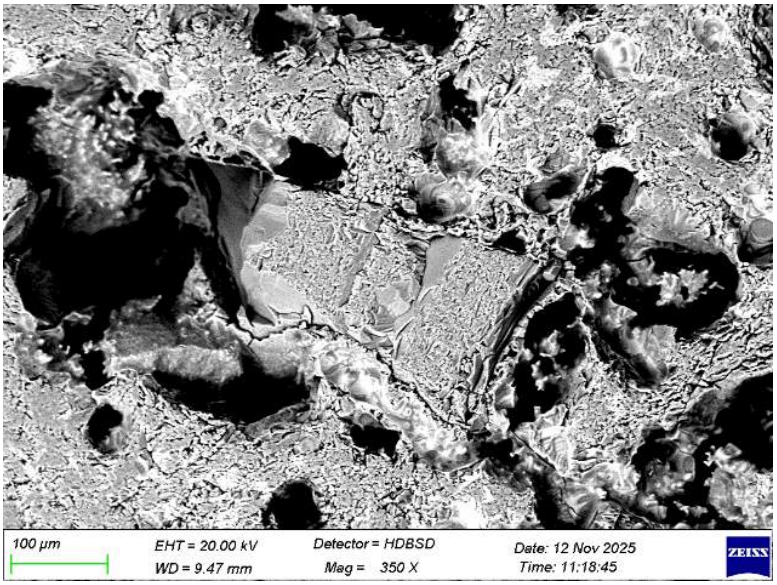


Figure 2 SEM of sample from Batch T1 (100µm)

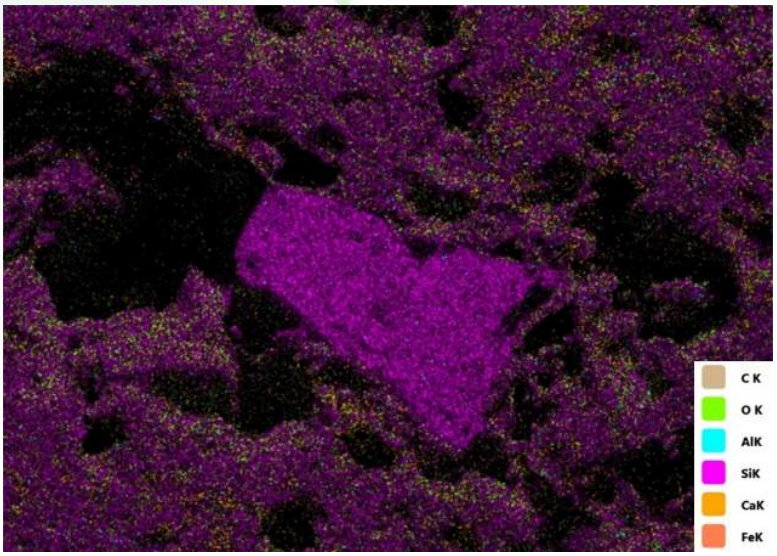


Figure 3 EDS colour mapping of Figure 2confirms inert SiC F1 grain

Table 3 Elemental analysis of the area marked in yellow in Figure 2 (all figures are approximations)

Element	Wt%
C	42.3
O	8.5
Si	49.2

Batch T1 Microstructure (Inert Inclusion): SEM/EDS confirms F1 grains retain sharp crystalline boundaries with Table 3 confirming low oxygen content (~8.5 wt%). They behave similarly to unbonded inclusions (Figure 2), offering almost no microstructural advantage over Batch G.

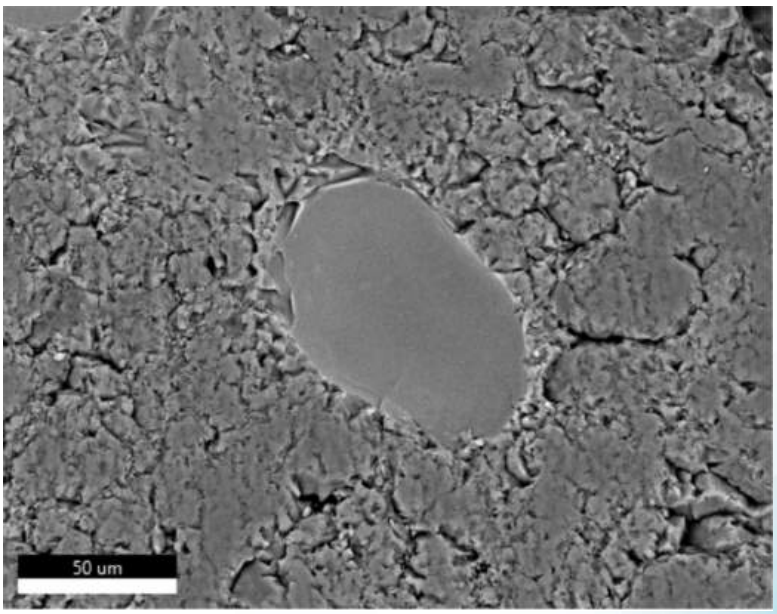


Figure 4 SEM of sample from Batch T2 (20µm) shows tightly entrapped SiC grain within matrix

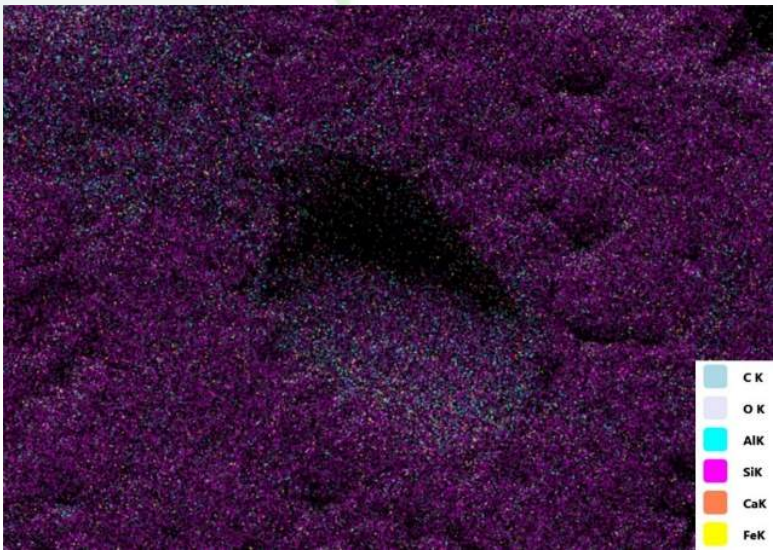


Figure 5 EDS colour mapping of Figure 4 confirms oxidation of SiC particle

Table 4 Elemental analysis of the overall scan area in Figure 4 (all figures are approximations)

Element	Wt%
C	13.2
O	47.7
Si	35.9

• Batch T2 Microstructure (Mechanical Entrapment): F2 grains are tightly entrapped within matrix pockets (Figure 4). Surface oxidation of SiC forms a localized SiO_2 layer whose volumetric expansion plugs surrounding micro-pores, superior to the open-pore network of Batch G. This further decreases the Apparent Porosity as observed in Table 2.

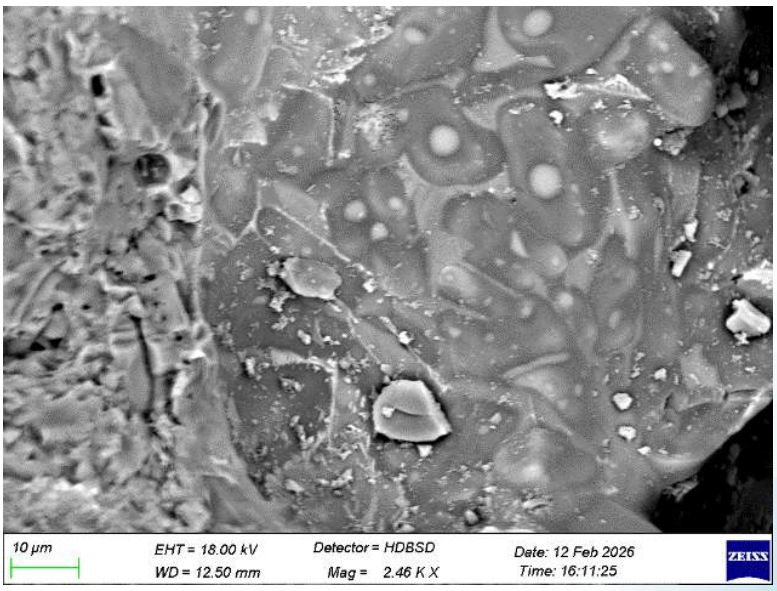


Figure 6 SEM of sample from Batch T3 (10µm)

Batch T3 Microstructure (Chemical Anchoring): High-magnification SEM and extensive reaction zones (Figure 6).

Table 5 Elemental analysis of the area marked in yellow in Figure 6 (all figures are approximations)

Element	Wt%
C	23.6
O	20.9
Si	55.4

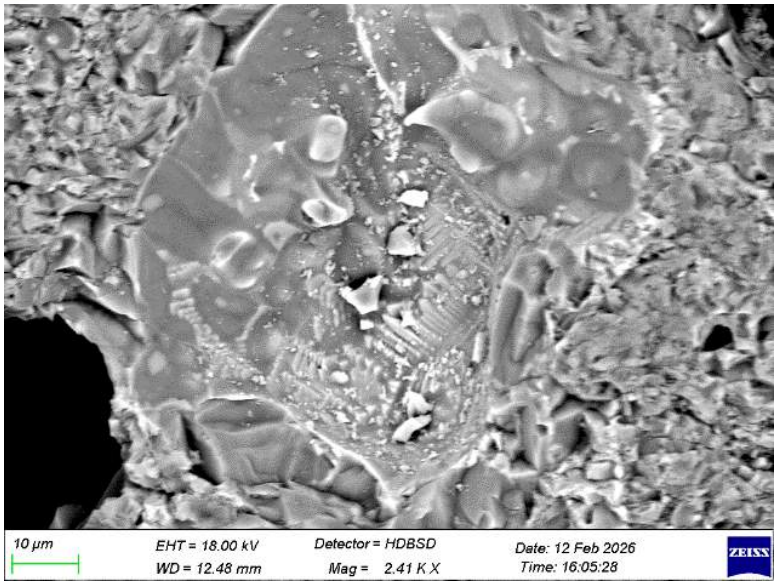


Figure 7 Showing F3 grains anchored to the matrix

• F3 grains in Batch T3 form a non-stoichiometric highly viscous silicon oxycarbide (SiO_xC_{4-x}) transition layer that acts as a chemical bridge, anchoring particles deeply within the matrix (Figure 6 and Figure 7)[2][5][6].

Micro-elemental analysis confirms distinct interfacial oxidation states across grain sizes. F1 grains exhibit minimal oxidation (Table 3), reflecting unreacted SiC core. F3 grains develop intermediate oxygen levels (Table 5) corresponding to the formation of a chemically bridging silicon oxycarbide transition layer. The high surface reactivity also allows a substantial portion of nascent silica to dissolve into the mobile liquid phase rather than remaining as an isolated thick oxide shell. F2 grains show the highest localized oxygen concentration (Table 4)due to the formation of a distinct, stoichiometric SiO_2 reaction shell that tightly seals the particle within matrix pores[2].

3.6 Phase Development and XRD Analysis

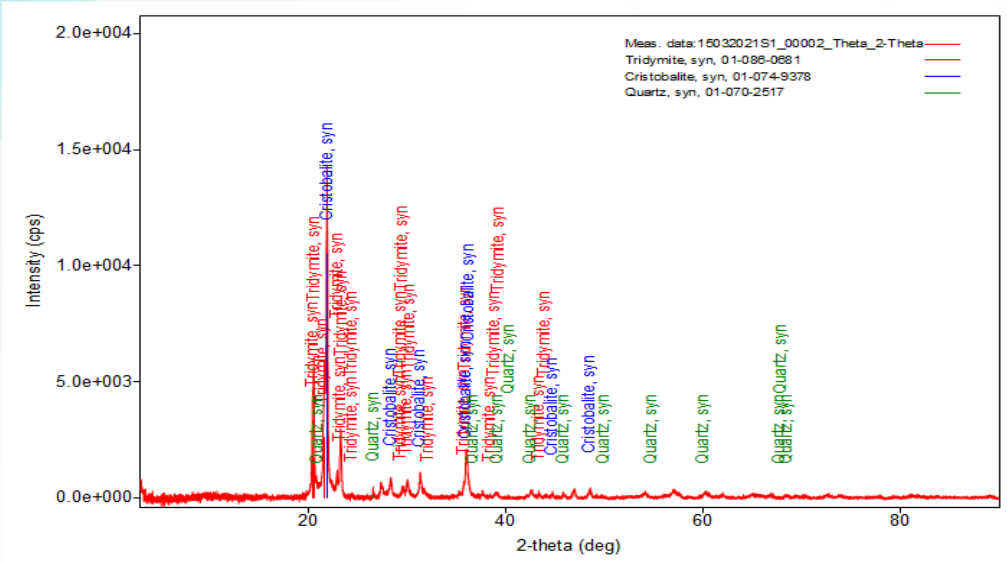


Figure 8 XRD Analysis of Batch G

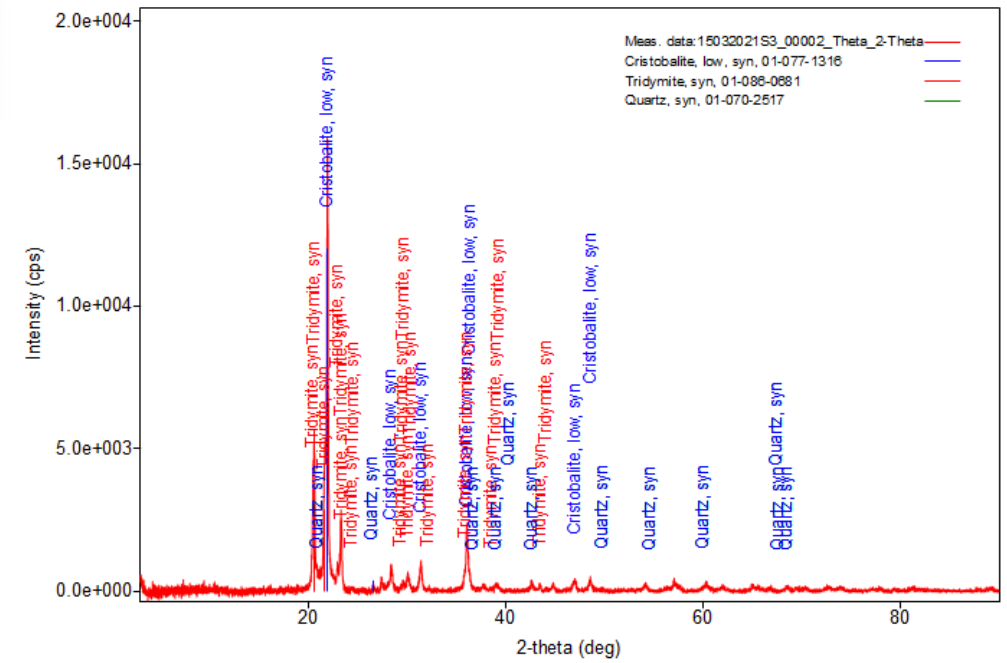


Figure 9 XRD Analysis of Batch T1

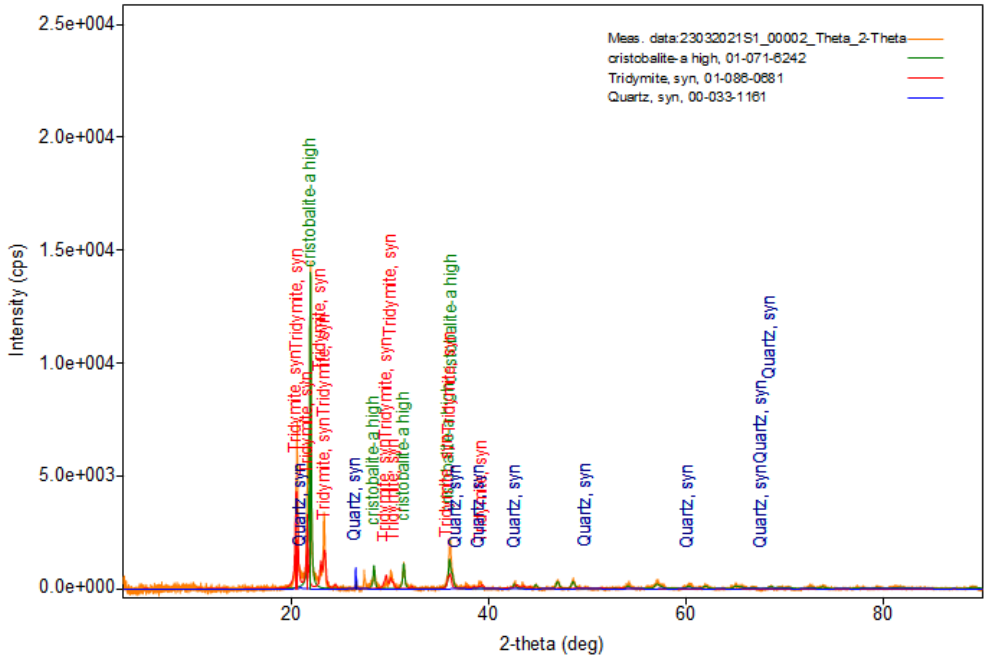


Figure 10 XRD Analysis of Batch T2

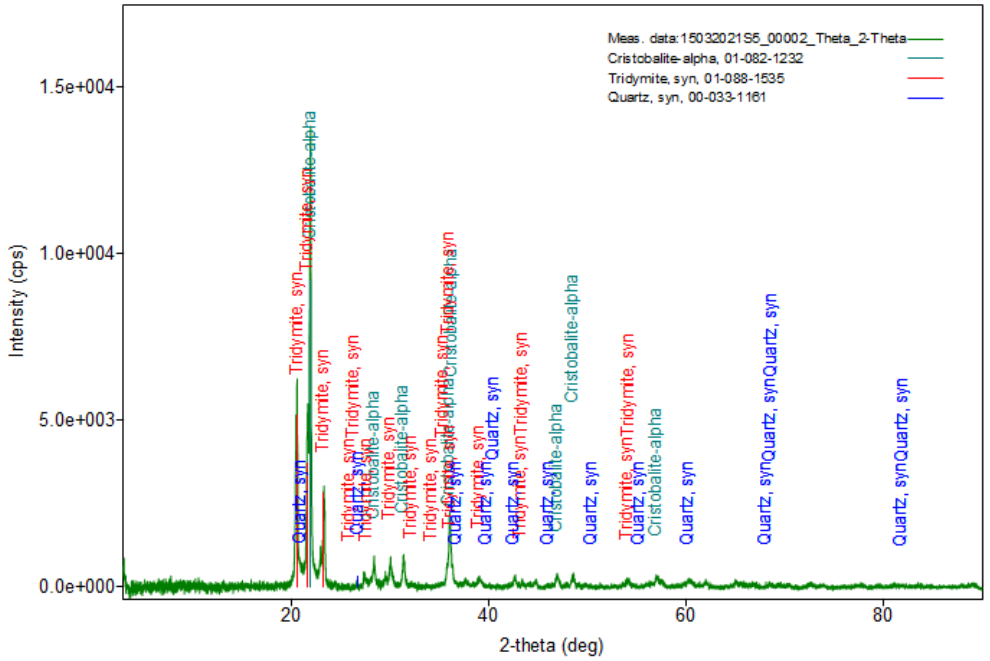


Figure 11 XRD Analysis of Batch T3

• Dominant Mineral Phase: All batches developed tridymite as the predominant crystalline phase, accompanied by cristobalite as a secondary minor phase. This confirms that the firing schedule and mineralizer system have successfully triggered the reconstructive transformation of raw quartz.

• Residual Quartz: Low residual quartz contents (Table 2) confirm near-complete quartz inversion.

• Impact of SiC Fineness: The consistency of the major tridymite and minor cristobalite phases indicates that introducing SiCdoes not disrupt the primary silica phase transformation kinetics regardless of grain fineness.

4. Conclusion

4.1 Densification with Controlled Expansion (F2)

Incorporating intermediate SiC grade optimizes bulk physical properties, achieving the lowest apparent porosity and the highest bulk density. This densification is driven by efficient multi-fraction particle packing coupled with localized SiC SiO2volumetric expansion, which effectively seals the interstitial micro voids.

4.2 Mechanical Reinforcement with Chemical Anchoring (F3)

F3 SiC gives the highest Cold Crushing Strength and superior creep resistance among all the four batches. The high specific area promotes the formation of a non-stoichiometric silicon oxycarbide transition layer that acts as a chemical bridge, pinning the grains within the silicate bond to improve load transfer and crack propagation resistance.

4.3 Inefficiency of Coarse Inclusions (F1)

F1 SiC remains almost microstructurally inert during firing, exhibiting low interfacial reactivity, wide perimeter boundary voids, high apparent porosity, and minimal strength enhancement, offering minimal functional advantage over standard composition.

4.4 Phase Stability and Thermal Expansion

Quantitative XRD confirms that primary silica polymorph conversion into tridymite and cristobalite proceeds without any interruption across all batches. While F2 maintains stable reversible thermal expansion at 1000°C through matrix densification, F3 exhibits higher post-firing expansion and elevated reversible thermal expansion at 1000°C due to accelerated oxidation kinetics and widespread secondary cristobalite devitrification.

References

1. E. Karamian, H. Gheisari, V. Kadkhodari and A. Monshi: International Journal of ISSI 12 (2015), No.1, p.37-41

2.Maxime J-F. Guinel and M. Grant Nortona: J. Mater. Res., Vol. 21, No. 10, Oct 2006, p.2551-2563

3. Linus U. J. T. Ogbuji: Journal of the American Society, 80 [6], 1997, p.1544-1550

4. Ritwik Sarkar: Refractory Technology Fundamentals and Applications, Version Date: 20160822, CRC Press, Boca Raton, FL 33487-2742

5. D. Scott Mackenzie: Thermal Processing, January 2024, p.24-25

6. Tanguy Rouxel, Gian-Domenico Soraru and Jean Vicens: Journal of the American Society, 84[5], 2001, p.1052-1058

DEVELOPMENT OF HYDRATION RESISTANT MAGNESIA BASED BRICKS FOR STEEL AND CEMENT INDUSTRIES

Avishek Mitra, Ankita Das, Dr. Saumen Sinha

Calderys India Refractories Limited, Nagpur, India

Abstract

Magnesite and magnesia–spinel bricks are widely used in steel and cement industries due to their excellent refractoriness, high corrosion resistance, and thermal stability in basic environments. These refractories are highly hydrophilic and readily absorb atmospheric moisture, leading to hydration of free MgO and formation of brucite, which causes volumetric expansion and internal stress. This hydration-induced degradation results in cracking, powdering, and loss of mechanical strength, ultimately reducing product durability and leading to premature rejection during storage and service in steel and cement industries.

This study focuses on developing magnesite and magnesia–spinel bricks with improved hydration resistant properties through a hydrophobic surface coating that produces a lotus-effect behavior upon contact with water. The coating creates a water-repellent micro-structured surface that minimizes moisture adhesion and prevents water penetration into the brick matrix, thereby suppressing brucite formation, volumetric expansion, and strength degradation during storage.

Keywords: Magnesite, brucite, hydration resistant, sorptivity

Introduction

As periclase provides higher refractoriness and chemical compatibility with clinker liquid phases, Magnesia based fired refractory bricks are used in cement rotary kilns and lime kilns. High-temperature service mechanisms do not control the storage durability of these refractories. They are controlled by a low temperature reaction. Generally, when these Magnesite bricks come in direct contact with water or atmospheric condensation, dissociative adsorption, Mg^{2+} dissolution and hydroxide nucleation occurs which ultimately leads to the formation of brucite [1-4]. This brucite formation process gets accelerated by the presence of fine periclase, defect-rich grain boundaries, lime-bearing secondary phases and connected open porosity. In magnesia-spinel bricks, the preformed spinel ($MgAl_2O_4$) is one of the main components. This spinel is comparatively stable. But the continuous periclase phase and microcrack network remain the potential hydration pathways.

$$MgO(s) + H_2O\ (l \text{ or } v) \rightarrow Mg(OH)_2(s)$$

The damage occurs mainly because of the density difference between periclase and brucite. The density of periclase (ρMgO) is 3.58 g cm^{-3} and that of brucite (ρbrucite) is 2.36 g cm^{-3}. The molar volumes are also 11.26 and 24.71 $cm^3\ mol^{-1}$, respectively.

The molar volume expansion ratio (Ω) is expressed by the following Equation (1):

$$\Omega = \frac{V_{m,Mg(OH)_2}}{V_{m,MgO}} = 2.19$$

The corresponding theoretical volumetric expansion is expressed by Equation (2):

The complete conversion of MgO to Mg $(OH)_2$ can theoretically produce about 119.5% local volume expansion. In fired refractory bricks, the surrounding grains tend to constraint this expansion and thus generate excessive internal tensile stresses, microcracking, edge spalling, powdering, and loss of mechanical strength.

Even partial conversion to brucite can generate enough tensile hoop stress which leads to the opening of pre-existing microcracks and thus, progressive loss of cold strength. The aim of this development was not to change the MgO inside the brick. We tried to prevent water from reaching the reactive sites by making the exposed surface water-repellent and thus reducing moisture penetration.

2. Experimental

Commercial fired magnesia-based bricks were taken. One piece was kept as it is (ref) while the other had been treated (HR). The treatment was applied to the finished refractory; its chemistry, loading, solvent system, curing route and application equipment are commercially confidential.

The water-repellent behaviour of the brick surfaces was evaluated using the sessile-drop method. A water droplet was placed on the brick surface, and the apparent contact angle was measured from the droplet image.

Whole-brick water uptake had been determined by measuring the initial mass (m_0) and final mass after 1 h, (m_1). Water Absorption Reduction (WAR) was calculated by Equation (3):

$$WAR\ (\%) = [(\Delta m_{ref} - \Delta m_{HR})/\Delta m_{ref}] \times 100,$$

where $\Delta m = m_1 - m_0$

m_{ref} = Mass of reference sample

m_{HR} = Mass of HR treated sample

The capillary uptake was measured by exposing one face of area A. The bricks' exposed surfaces were kept in contact with water and the mass gain was recorded after every 10-minute intervals up to 60 minutes. Cumulative water absorption (CWA) and sorptivity were calculated by Equation (4):

$$CWA(t) = [m(t) - m_0]/A;$$

$$CWA(t) = S\sqrt{t} + b$$

where S is the initial sorptivity and b represents rapid surface filling and experimental offset. m_0 is the initial mass and m(t) is the mass at time t. This method is an adaptation of the square-root-of-time capillary approach rather than a claim of full compliance with ASTM C1585. The ASTM procedure was developed for hydraulic-cement concrete [7].



Figure 1 Treated vs untreated sample

Accelerated hydration tendency was calculated for 168 hours at 90 °C and 95% relative humidity. The mass change (W_2 after, W_1 before) was recorded in every 24 h. Cold crushing strength (CCS) was measured before (C_1) and after exposure (C_2). From these data, two internal screening metrics, Hydration Resistance Index (HRI) and Hydration Damage Factor (HDF) are identified. These are Equation (5) & (6) respectively.

$$HRI = (C_2/C_1) / [(W_2 - W_1)/W_1];$$
$$HDF = 100/HRI$$



Figure 2 Treated sample after 30 hrs in 100% humidity at 90°C°

3. Results and Discussion

3.1 Surface Wetting Behaviour

The water contact angle of HR treated brick is 3 times (> 115°C) more than the untreated one.

A contact angle below 90° indicates that water can spread and wet the surface. Therefore, the untreated brick is hydrophilic and is expected to absorb water readily through its open pores and microcracks.

A contact angle above 90° indicates resistance to wetting. Therefore, the treated brick can be described as hydrophobic according to the static contact-angle criterion.

The effect of contact angle on water entry into pores can be explained using the Young–Laplace equation (7)

$$\Delta P_c = \frac{2\gamma_{LV}\cos\,\theta}{r_p}$$

where:

- ΔPc is the capillary pressure,
- γLV is the surface tension of water,
- θ is the contact angle, and
- rp is the effective pore radius.

For the untreated brick,

$$\Delta P_{c,\,untreated} = \frac{1.633\gamma_{LV}}{r_p}$$

The positive value means that the pore surface generates capillary suction, which promotes spontaneous water entry into the brick.

For the treated brick:

$$\Delta P_{c,\,treated} = -\frac{0.885\gamma_{LV}}{r_p}$$

Similarly, the negative value indicates that the direction of the capillary pressure is reversed. So, instead of drawing water into the pores, the treated surface creates a capillary barrier against spontaneous entry of water.

The most important effect of the treatment is that it changes the brick surface from Capillary suction to Capillary resistance. This provides a clear explanation for the lower water uptake of the treated brick.

The apparent solid–water contact fraction can be estimated using the Cassie–Baxter relation (8):

$$f_s = \frac{\cos\,\theta_{CB} + 1}{\cos\,\theta_Y + 1}$$

Taking the untreated contact angle as a first-order approximation of the Young contact angle for HR treated brick:

$$f_s \approx 0.307$$

Thus, the estimated apparent solid-contact fraction is approximately 31%.
The corresponding apparent air or non-contact fraction is:

$$f_{air} = 1 - f_s$$
$$f_{air} = 1 - 0.307 = 0.693$$

Therefore, from this result, we can say that approximately 69% of the apparent area beneath the droplet may behave as an air-supported or non-wetted region.

3.2 Whole-Brick Water Uptake and Sorptivity

The water uptake for HR treated brick is much lower than the reference brick. There is also a reduction in apparent porosity by 10.4%. But the water gained after one hour decreased from 161 g to 9 g. This reduction is 94.4%. When expressed relative to the initial brick sample mass, the one-hour water gain decreased from 3.28% to 0.17%.

A similar trend was observed in the capillary water-absorption results. The cumulative water absorption at 10 minutes decreased from 3.93 to 0.04 kg m^{-2}, while the value after 60 minutes decreased from 4.28 to 0.08 kg m^{-2}. The reported sorptivity also decreased from 0.08 to 0.01 kg m^{-2} $min^{-1/2}$, a reduction of almost 87.5% in the rate of capillary water transport.

The much larger reduction in water uptake compared with the relatively small change in apparent porosity indicates that the improvement was not caused mainly by lower bulk porosity. Instead, the treatment significantly restricted the initial wetting of the brick and reduced the accessibility of pore entrances and connected capillary pathways. The treatment therefore acted as an effective barrier to moisture entry while leaving the overall bulk pore structure largely unchanged.

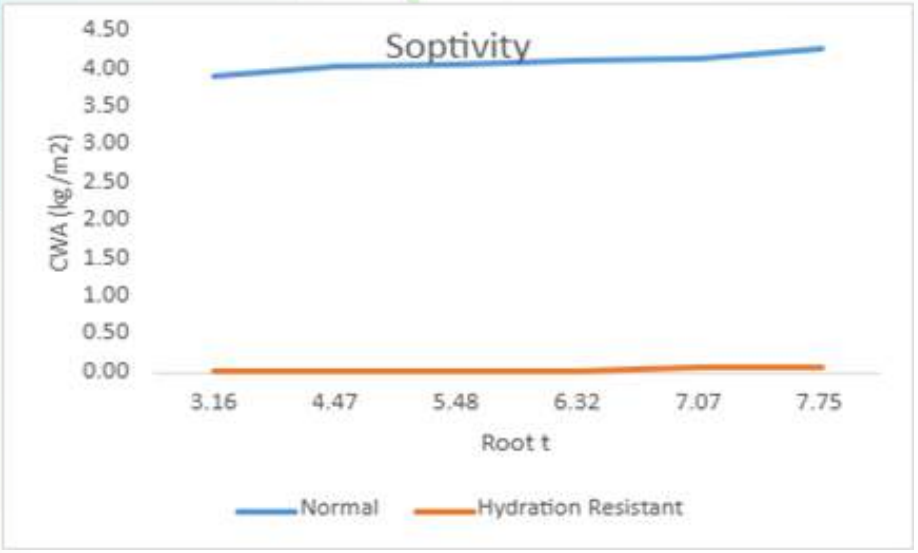


Figure 3 Sorptivity analysis

3.3 Accelerated Hydration Kinetics and Mechanical Integrity

When the bricks were exposed to 90°C and 100% relative humidity, there was a continuous mass gain for the untreated reference brick. Its cumulative mass gain increased from 0.72 g after 24 h to 2.42 g after 168 h. The mass gain was almost linear, showing continued moisture uptake and hydration throughout the test period.

The hydration-resistant brick showed only 0.02 g mass gain by 48 h, after which no further measurable increase was recorded up to 168 h.

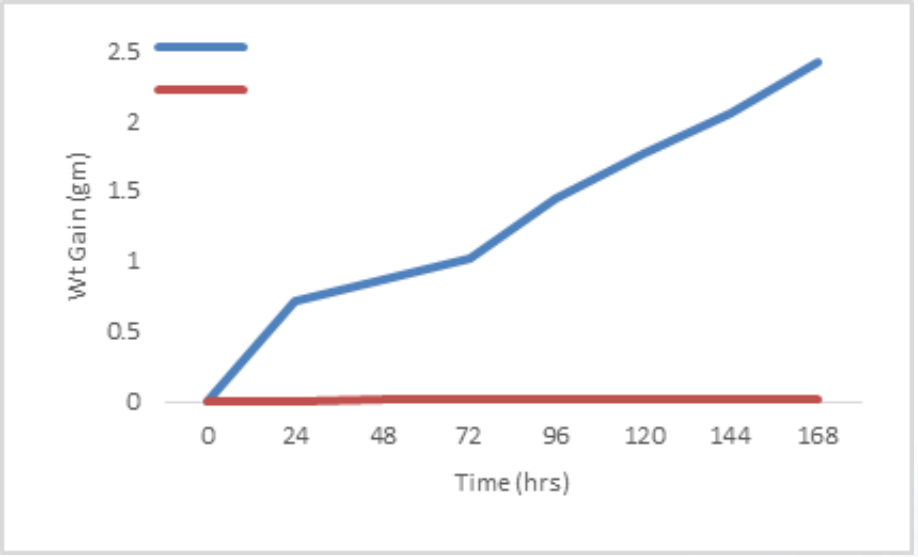


Figure 5 Cumulative mass gain of the reference and hydration-resistant bricks at 90°C and nominal 100% RH.

Except the mass change, the decrease in CCS of reference reduced from 647 to 587 kg cm^{-2} while the CCS reduction of treated brick is only 5 kg cm^{-2}. The treated brick shows a CCS retention of 99.2%. Therefore, the treatment reduced the strength loss by approximately 91.7%.

These results indicate that the treatment has strongly restricted the water entry into the brick and suppressed internal hydration reactions. In untreated magnesia bricks,

moisture can react with MgO to form brucite, which is accompanied by volume expansion and crack development. The high strength retention of the treated brick suggests that this hydration-induced damage was effectively limited.

The calculated HRI of reference brick is 71.4 while that of HR treated brick is 9872.6, an apparent 138-fold improvement. This very high value is strongly influenced by the extremely small mass gain of the treated brick.

Parameter	Reference	Hydration-resistant	Relative result
Normalized mass gain (%)	1.271	0.01	-99.21%
CCS retention (%)	90.7	99.2	+8.5 percentage points
Absolute CCS loss (kg cm^{-2})	60	5	-91.70%
Hydration Resistance Index	71.4	9872.6	138×
Hydration Damage Factor	1.401	0.01	-99.30%

Table 1 Mass gain and cold crushing strength of the reference and HR treated bricks after 168 h accelerated humidity exposure

3.4 Proposed Protection Mechanism and Industrial Relevance

These results suggest that the treatment protects the brick mainly by reducing the movement of water into its pore structure. The treated surface has lower attraction to water and may trap small air pockets beneath the water droplet. This reduces the time that water remains at pore openings and limits continuous water flow into the brick.

As a result, less water reaches the periclase grains inside the brick. This slows the reaction of MgO with moisture and reduces the formation of brucite.

This treatment does not need to survive at the final service temperature. Its main purpose is to protect the brick before use, especially during manufacturing, palletization, monsoon storage, transportation, lining installation, and the period before controlled drying or kiln heat-up.

4. Conclusion

i) The confidential engineering route changed the apparent water contact angle by 3 times in HR treated brick. The surface meets the static-angle criterion for hydrophobicity.

ii) One-hour water gain decreased from 161g to 9 g, while capillary absorption at 60 min decreased from 4.28 to 0.08 kg m^{-2}.

iii) After 168 h at 90 °C and 100% RH, normalized mass gain was reduced by 99.21%. The CCS retention also increased from 90.7 to 99.2%. For the treated brick, the absolute strength loss was reduced by 91.7%.

iv) The results show that the treatment protects the periclase by blocking pore openings and reducing moisture movement into the brick without changing the overall chemistry of the bricks.

References

[1] R. Salomão, L.R.M. Bittencourt and V.C. Pandolfelli, "A novel approach for magnesia hydration assessment in refractory castables," Ceramics International, 33(5) (2007) 803-810.

[2] R. Salomão and V.C. Pandolfelli, "Magnesia sinter hydration-dehydration behavior in refractory castables," Ceramics International, 34(8) (2008) 1829-1834.

[3] T. dos Santos Jr., J. dos Santos, A.P. Luz, C. Pagliosa and V.C. Pandolfelli, "Kinetic control of MgO hydration in refractory castables by using carboxylic acids," Journal of the European Ceramic Society, 38(4) (2018) 2152-2163.

[4] M. Pettauer et al., "Hydration of MgO: Reaction kinetics and pH control on brucite crystal morphology," Crystal Growth & Design (2024).

[5] R.N. Wenzel, "Resistance of solid surfaces to wetting by water," Industrial & Engineering Chemistry, 28(8) (1936) 988-994.

[6] A.B.D. Cassie and S. Baxter, "Wettability of porous surfaces," Transactions of the Faraday Society, 40 (1944) 546-551.

[7] ASTM C1585-20, Standard Test Method for Measurement of Rate of Absorption of Water by Hydraulic-Cement Concretes, ASTM International, West Conshohocken, PA (2020).

[8] J.R. Philip, "The theory of infiltration: 4. Sorptivity and algebraic infiltration equations," Soil Science, 84(3) (1957) 257-264.

DEVELOPMENT OF AN ADVANCED ALKALI–SULFUR CORROSION RESISTANT MAGNESIA SPINEL REFRACTORIES IN HIGH AFR CEMENT KILNS

Avishek Mitra, Ankita Das and Dr Saumen Sinha

Calderys India Refractories Limited, Nagpur, India

Abstract

The dependence on alternative fuel & raw material is increasing day by day in the cement rotary kiln. It has significantly altered the internal chemical environment of the kiln by intensifying alkali, chloride, and sulfur circulation, leading to more aggressive conditions for refractory linings.

This study focuses on the influence of different types of magnesite on the alkali–sulfur corrosion resistance of magnesia-based bricks under high alternative fuel rate conditions, with specific attention towards failure mechanisms associated with refractory quality. Bricks were formulated using multiple grades of dead-burned magnesite characterized by variations in purity, density, and microstructural characteristics. These samples were evaluated for their physical and thermal properties along with laboratory corrosion tests simulating alkali–sulfur-rich environments at elevated temperatures. The degradation behavior and extent of chemical attack was assessed by measuring penetration depth, phase evaluation, and microstructural study.

Keywords: Magnesia Spinel, high AFR, cement rotary kiln, alkali-sulfur corrosion

Introduction

The use of alternate fuels and alternative raw materials are increasingly steadily in Indian Cement Industry. The traditional use of coal or petroleum coke is partly being replaced by waste-derived fuels, biomass, used tires, and other combustible wastes. Similarly, a portion of conventional cement raw materials is also being replaced by suitable industrial-by-products. These changes help to reduce the consumption of fossil fuels, resulting in a much environmentally friendly impact on cement production. But these alternative fuels and raw materials also introduce additional sulfur, chlorine, sodium and potassium into the kiln system. As a result, a kiln operating with a high alternative-fuel rate, or high AFR, might have a more chemically aggressive atmosphere than a kiln operating mainly with conventional fuels.

Sulfur, chlorine, and alkalis are the main volatile or circulating elements in a cement kiln. At high temperatures, compounds such as potassium chloride, sodium chloride and alkali sulfates partially evaporate. These vapors generally tend to move towards the colder parts of the kiln and preheater with the gas stream. When the temperature of these zones decreases, these vapors condense on raw-meal particles, kiln deposits, and refractory surfaces. These condensed compounds again return to the hotter part of the kiln with the solid material, where they may evaporate again. An internal alkali–chloride–sulfur cycle is created by the repeated cycle of evaporation, condensation, and return. Even if the total input of these elements is moderate, this repeated circulation can produce a much higher local concentration inside the kiln. Choi and Glasser demonstrated that the vapor pressures and thermal stability of sulfate phases strongly control sulfur circulation in cement kilns [1].

This sulfur circulation is further increased by the combustion behaviour of alternative fuels. Firstly, alternative-fuel particles are often larger and less uniform than pulverized coal. They also vary in moisture, volatile matter, and burning rate. During condensation, they release carbon monoxide, hydrogen, and hydrocarbon gases, thus

creating a temporary reducing atmosphere near the material bed. Under such reducing conditions, the calcium sulfate and alkali sulfates decompose to release SO_2. These released SO2 again react with calcium and alkalis, thus strengthening the internal sulfur cycle [2]. The refractory lining is therefore exposed simultaneously to alkali and sulfate condensation, clinker-liquid infiltration, redox fluctuation, thermal shock, abrasion, mechanical loading and repeated coating formation and loss.

Today, most of the cement rotary kilns are using magnesia–spinel bricks in transition and burning zones. Periclase provides high refractoriness and chemical compatibility with the basic kiln environment, and magnesium aluminate spinel is used to improve thermal-shock resistance and structural flexibility. There is a high difference between the thermal expansion co-efficient of periclase and spinel. This causes controlled microcracking, which in turn reduces the crack propagation and also improves the thermal shock resistance [3].

The performance of magnesia–spinel bricks depend not only on their bulk MgO and Al_2O_3 contents. It also depends on some important factors like the purity and crystal size of the magnesia aggregate, the amount and distribution of CaO and SiO_2 bearing impurities, grain-boundary chemistry, pore size and pore connectivity. Based on previous examinations, it can be said that the alkali salts and clinker liquid mainly enter the brick through connected pores, cracks and weak aggregate–matrix interfaces. Once it enters the refractory, the Ca, Si, Al, and Fe bearing liquids react with the refractory matrix and grain boundaries. By these reactions, many low-melting phases like mayenite (C12A7), gehlenite (C2AS), merwinite (C3MS2), calcium sulfoaluminate and complex calcium–magnesium–aluminosilicate are formed [4,5]. Continuous formation, melting, and solidification of these phases cause densification, brittleness, crack development and structural spalling.

In the present study, the effect of magnesia aggregate quality on alkali–sulfur corrosion resistance has been studied. Trial A was produced using conventional dead burnt magnesia (DBM), while the base raw material for Trial B was high-purity synthetic magnesia. Their performance against AFR attacks was tested through physical-property testing, gas permeability, pore-size distribution, accelerated alkali–sulfur exposure, X-ray diffraction, and optical microscopy. The study aims to find out whether use of high purity sintered magnesia with improved grain-boundary chemistry and less connected pore structure can provide better corrosion resistance under high-AFR cement-kiln conditions.

2. Materials and Experimental Methods

Two trial magnesia–spinel bricks were prepared using the same basic particle-size grading and the same amount of spinel addition. They were pressed in industrial 630T ESP and fired at the same temperature. The only difference between the two formulations was the type of magnesia aggregate used. Trial A was produced using conventional DBM, while Trial B was made from different source high-purity magnesia (HM).

HM contains higher MgO purity and approximately 70% lower silica content than DBM. This difference in chemistry was also observed in the fired bricks. The Al_2O_3 contents of both bricks were almost similar. The CaO and Fe_2O_3 contents were also comparable. Chemically, the main difference between the two bricks was lower silica percentage and higher CaO/SiO_2 ratio of Trial B.

As Trial A and Trial B contain the same amount of spinel (confirmed by XRD), so the difference in their corrosion behaviour cannot be explained by spinel percentage alone. It is mainly related to the higher purity of HM, lower silica content, improved secondary-phase chemistry, and differences in pore and grain-boundary structure.

Apparent porosity and bulk density were measured by the ASTM C20. The Cold crushing strength was determined at room temperature by ASTM C133. Gas permeability

was measured to evaluate the connectivity of the open-pore network by ISO 8841. Mercury-intrusion porosimetry was used to determine the cumulative connected-pore volume and pore-size distribution. The results were used to compare the internal pore structures of Trial A and Trial B and to understand their influence on corrosion resistance. Alkali–sulfur resistance of the brick samples was evaluated by using an internally developed high-temperature laboratory test designed to imitate the combined action of alkali vapors, sulfur-bearing species and salt condensation experienced in high-AFR cement kilns. The detailed test arrangement and operating procedure are proprietary and are therefore not disclosed in this paper. The weight and cold crushing strength of the samples were measured before and after the alkali-sulfur test. The corrosion behaviour was calculated using percentage mass gain and cold crushing strength retention. It is considered that higher mass gain is an indication of greater penetration and reaction of alkali–sulfur-bearing compounds within the refractory. An Alkali–Sulfur Resistance Index (ASRI) was also used to compare the two samples. A higher ASRI value indicates better resistance to alkali-sulfur attack.

X-ray diffraction analysis was carried out using Cu Kα radiation over a scanning range of 5–90° 2θ. The XRD results obtained before and after alkali–sulfur test were background-corrected and normalized for comparison. The graphs were interpreted mainly on a semi-quantitative basis. Optical microscopy was used to determine the magnesia aggregate morphology, periclase crystal structure, secondary-phase distribution, aggregate–matrix interfaces, pores, and cracks.

3. Results and discussion

The physical properties and alkali-sulfur corrosion-test results of Trial A and Trial B are given in Table 2. The two bricks had almost similar apparent porosity and bulk density. Apparent porosity was 15.50% for Trial A and 15.30% for Trial B, while bulk density was 3.04 and 3.05 g cm^{-3}, respectively. These small differences show that in both samples, the overall level of open porosity was similar. Apparent porosity alone therefore cannot explain the large difference observed in alkali–sulfur resistance.

A clearer difference was found in gas permeability. Trial A showed a permeability of 22.1% higher than Trial B. This data shows that the open pores in Trial B were less connected than Trial A. This is very important because the corrosive gases, condensed alkali salts and clinker liquid do not move through the total pore volume uniformly. Their penetration mainly depends on the continuity of the larger pore volume, internal cracks, and weak grain-boundary regions. A brick may therefore have moderate apparent porosity but still show good corrosion resistance when the pores are poorly connected and non-continuous.

Trial A had a higher initial cold crushing strength than Trial B. But, after the alkali–sulfur test, the final CCS values were almost similar. From here it can be said that although Trial B started with lower strength, it retained a larger part of its original load-bearing structure during the test. The CCS retention of Trial A was 66.01% and that of Trial B is 76.98%. This shows a lower strength loss in Trial B after an alkali-sulfur attack.

After the alkali-sulfur test, the difference in weight gain was even clearer. The weight gain of Trial A is around 1.68% while that of Trial B is only 0.57%. Trial B showed a 66.1% reduction in weight gain. Since the test samples were exposed to alkali- and sulfur attack, weight gain represents the combined effect of salt penetration, condensation, and chemical reaction within the accessible pore structure. The lower weight gain of Trial B shows that less corrosive material entered or remained inside the sample. The improvement was therefore not limited to mechanical strength. It was directly related to lower chemical penetration.

Table 1. Physical properties and alkali–sulfur test response

Property	Unit	Difference of Trial B properties from Trial A
Apparent porosity (AP)	%	-1.30%
Bulk density (BD)	g cm^{-3}	0.30%
Initial CCS	kg cm^{-2}	-13.70%
Gas permeability	10^{-12} m^2	-22.10%
Mass gain after ASRI	%	-66.10%
Final CCS	kg cm^{-2}	0.60%
CCS retention	%	16.60%
CCS loss magnitude	%	-32.30%
ASRI	-	18.50%

The Alkali–Sulfur Resistance Index increased by 18.5% in Trial B. The higher ASRI of Trial B was a combined effect of lower weight gain and better strength retention. From these results, it can be said that the HM-based brick showed better overall resistance to alkali-sulfur attack, even though the two samples had almost similar apparent porosity, bulk density, and spinel content.

The mercury-intrusion porosimetry results show why the two bricks samples behaved differently despite having nearly identical apparent porosity. The total cumulative intrusion volume was 0.0632 mL g^{-1} for Trial A and 0.0477 mL g^{-1} for Trial B. Thus, the connected-pore volume measured by mercury intrusion was 24.5% lower in Trial B. The difference became clearer when the coarse-pore fractions were examined. The volume of pores larger than 1 µm decreased from 0.05249 mL g^{-1} in Trial A to 0.03631 mL g^{-1} in Trial B, a reduction of around 30.8%. For pores larger than 10 µm, the reduction was 37.2% in Trial B. The volume of very coarse pores (above 100 µm) decreased from 0.00823 to 0.00311 mL g^{-1}, corresponding to a reduction of 62.3%.

These coarse pores (above 100 µm) might be more harmful during service. They provide rapid entry paths for vapors and liquids. They can also act as storage sites for condensed salts. Once these pores are filled, there is a continuous contact between the corrosive phase and the refractory matrix. The corrosive reaction can continue along connected pores and grain boundaries. The lower volume of coarse connected pores in Trial B is consistent with its lower gas permeability. The two measurements describe different aspects of the same structure. While mercury intrusion porosimetry measures the volume and size of accessible pore, the permeability shows the ease with which a fluid can pass through the complete sample. The results indicate that Trial B showed better alkali-sulfur resistance not only because of its slightly lower porosity. Its pores were less connected, which made it more difficult for alkali- and sulfur-bearing materials to enter the brick. As a result, less reaction product formed inside Trial B. This explains its lower weight gain and better strength retention after testing.

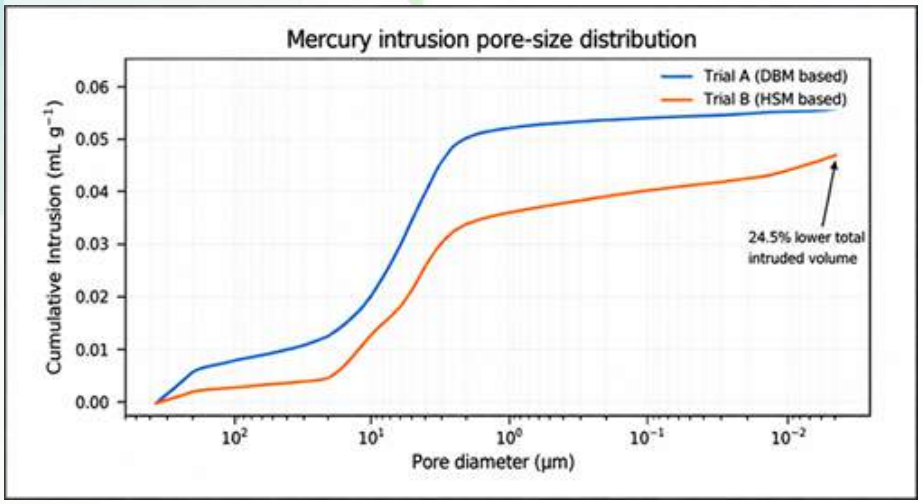


Figure 1 Cumulative MIP pore-volume curves

The optical micro photographs show clear differences between the two magnesia aggregates. The conventional DBM aggregate used in Trial A has a relatively fine and irregular polycrystalline structure. Several bright intergranular films, patches, and boundary discontinuities are visible. These regions are likely to contain the minor Ca, Si, and Fe bearing phases present in the DBM. In comparison, aggregate used in Trial B contains larger, well-developed polygonal periclase crystals. Direct contact between adjacent periclase crystals is more extensive, and the internal structure appears cleaner.

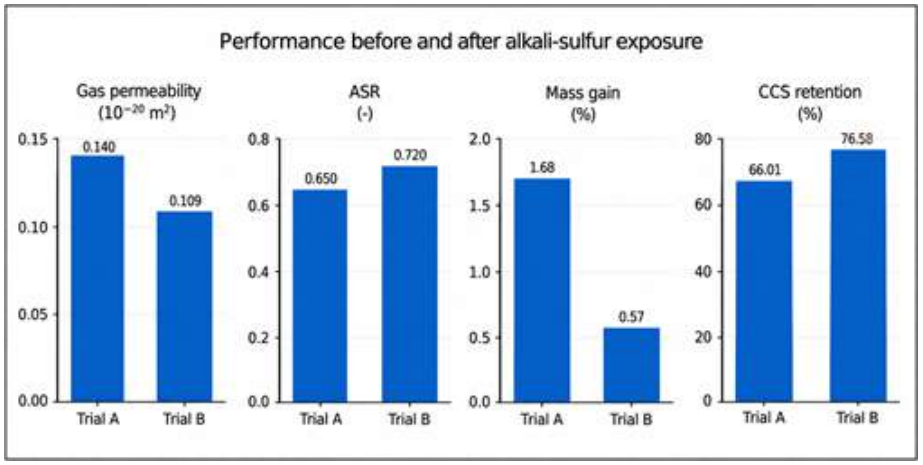


Figure 2 Transport and corrosion-performance comparison

Large periclase crystals are beneficial because they reduce the total grain-boundary area available for impurity segregation. Fine-grained polycrystalline DBM contains a relatively high density of periclase grain boundaries. Secondary Ca–Mg–silicate phases are commonly located in these intercrystalline regions. At elevated temperature, some of these phases can form low-melting liquids, while pores and grain boundaries provide preferential pathways for penetration and reaction of alkali- and sulfur-bearing species. Consequently, degradation may initially involve the intergranular/secondary phases before substantial attack or dissolution of the main periclase grains [14-17].



Figure 3 Micro photograph of aggregate in Trial B at 100X



Figure 4 Micro photograph of aggregate in Trial A at 100X

XRD results showed that periclase (MgO) and magnesium aluminate spinel ($MgAl_2O_4$) were the main crystalline phases in both bricks before alkali–sulfur test. There is no major difference in the basic phase composition between Trial A and Trial B. The main MgO reflections were observed near 36.9°, 42.9°, 62.3°, 74.7° and 78.6° 2θ. The characteristic spinel reflections were present near 19.0°, 31.3°, 36.9°, 44.8°, 55.7°, 59.4°, and 65.3° 2θ. Some MgO and spinel peaks overlap, particularly near 36.9°, and this was considered during interpretation.

After the alkali–sulfur test, the main periclase and spinel peaks were still clearly visible in Trial B. This shows that the basic MgO–spinel structure remained stable and there was no major breakdown of the refractory phase system. Some weak additional peaks and a small increase in background intensity were observed. These changes may be because of the formation of small amounts of new reaction products or poor crystalline phases at the exposed surfaces and grain boundaries.

The post-test graphs of Trial A and Trial B were also compared after background correction and normalization to the strongest MgO peak near 42.95° 2θ. Trial A showed stronger relative peaks at approximately 31.3°, 36.9°, 59.4°, and 65.3°, which are mainly associated with spinel. The likely explanation is that MgO was more strongly attacked in the reacted region. When the MgO contribution decreases, the remaining spinel peaks appear stronger relative to the main

MgO peak. Peak overlap with newly formed reaction phases may also contribute to higher relative intensity.

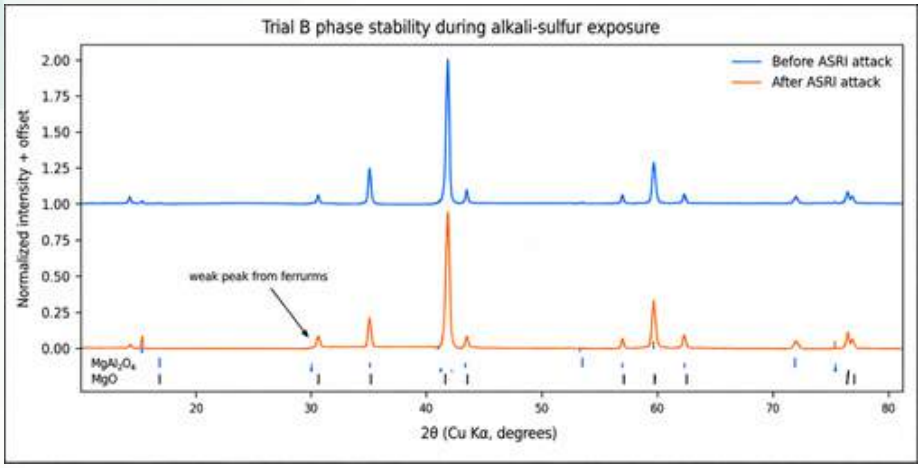


Figure 5 Normalized Trial B XRD patterns before and after the ASRI test.

Trial A also showed a larger amount of residual intensity outside the main MgO and spinel peak positions. This shows greater phase disturbance and the possible formation of additional crystalline or poorly crystalline corrosion products. In comparison, the post-test XRD graph of Trial B remained cleaner and was still mainly represented by the original MgO–spinel phase system.

The XRD results confirm the physical and microstructural observations. Trial A showed higher weight gain, more strength loss, and may be higher concentrated Ca–Si–Fe-bearing secondary phases. Its stronger post-test phase of redistribution is therefore consistent with a more severe alkali–sulfur attack. Trial B retained a more stable MgO–spinel structure, supporting its lower weight gain and higher residual strength.

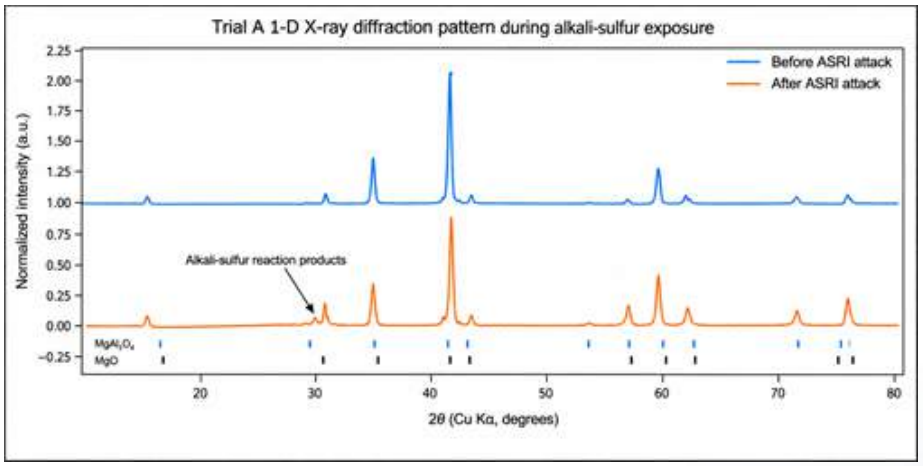


Figure 6 Normalized Trial A XRD pattern before and after the ASRI test.

4. Conclusion

The better performance in ASRI Test of Trial B is due to two related factors:

a) lower penetration of corrosive species
b) more stable matrix chemistry.

Trial A has higher gas permeability and a larger volume of connected coarse pores. This allows alkali salts and clinker liquid to penetrate more easily into the brick. It also

contains higher SiO_2, compared with Trial B. These silica-rich areas react readily with CaO and alkalis, producing low-viscosity liquids along grain boundaries.

After cooling, the liquid solidifies brittle alkali and sulfate-bearing phases. Repeated heating and cooling then cause cracking along the reacted grain boundaries. This explains the higher weight gain of 1.68% and the lower CCS retention of 66.01%.

The corrosion process in Trial A can therefore be described as:

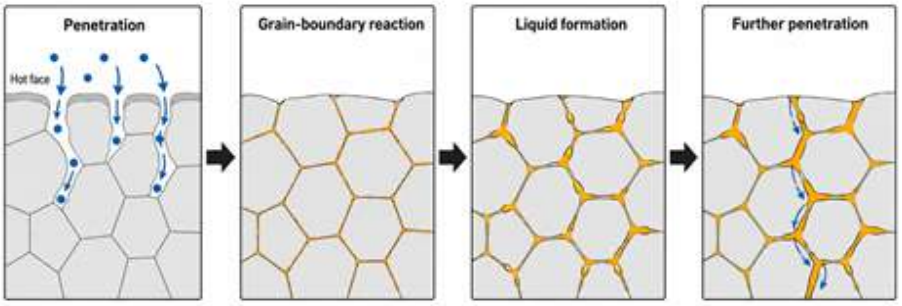


Figure 7 Corrosion mechanism for Trial A

Trial B has lower permeability and fewer connected coarse pores. This restricts the movement of alkali- and sulfur-bearing species into the brick. The aggregate also contains larger and cleaner periclase grains. Its lower silica content reduces the amount of reactive grain-boundary material available for low-melting phase formation. As a result, the reaction zone is thinner and less continuous. Less salt enters the sample; less reaction liquid forms, and the MgO–spinel skeleton remains better connected. Trial B therefore showed only 0.57% weight gain and retained 76.98% of its original CCS.

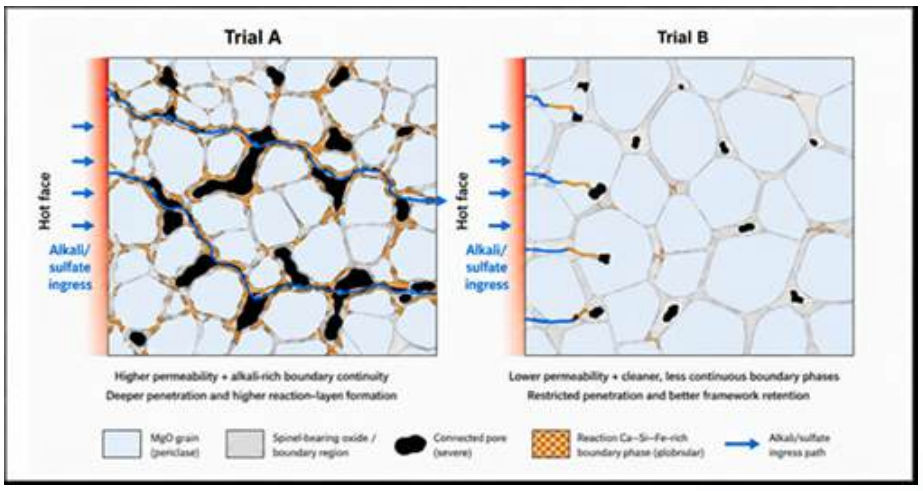


Figure 8 Corrosion Pathway for Trial A & Trial B

Overall, Trial B develops an effective reaction–transport barrier. Its less connected pore network reduces chemical penetration, while its cleaner and lower-silica grain boundaries reduce liquid-phase formation. These two effects together provide better alkali–sulfur corrosion resistance than Trial A.

References

[1] Choi, G.-S., and Glasser, F. P., "The Sulphur Cycle in Cement Kilns: Vapor Pressures and Solid-Phase Stability of the Sulphate Phases," Cement and Concrete Research, Vol. 18, No.

3, 1988, pp. 367–374. DOI: 10.1016/0008-8846(88)90071-3.

[2] Cortada Mut, M. M., Nørskov, L. K., Glarborg, P., and Dam-Johansen, K., "SO_2 Release as a Consequence of Alternative Fuel Combustion in Cement Rotary Kiln Inlets," Energy & Fuels, Vol. 29, No. 4, 2015, pp. 2729–2737. DOI: 10.1021/ef502746f.

[3] Ghosh, A., Sarkar, R., Mukherjee, B., and Das, S. K., "Effect of Spinel Content on the Properties of Magnesia–Spinel Composite Refractory," Journal of the European Ceramic Society, Vol. 24, No. 7, 2004, pp. 2079–2085. DOI: 10.1016/S0955-2219(03)00353-4.

[4] Szczerba, J., "Chemical Corrosion of Basic Refractories by Cement Kiln Materials," Ceramics International, Vol. 36, No. 6, 2010, pp. 1877–1885. DOI: 10.1016/j.ceramint.2010.03.019.

[5] Belgacem, S., Galai, H., and Tiss, H., "Qualitative and Quantitative Investigation of Post-Mortem Cement Refractory: The Case of Magnesia–Spinel Bricks," Ceramics International, Vol. 42, No. 16, 2016, pp. 19147–19155.

[6] Nielsen, A. R., Larsen, M. B., Glarborg, P., and Dam-Johansen, K., "High-Temperature Release of SO_2 from Calcined Cement Raw Materials," Energy & Fuels, Vol. 25, No. 7, 2011, pp. 2917–2926.

[7] G. Pacheco, G.E. Gonçalves, V.F.C. Lins, Qualitative and quantitative coating tests: a comparison in magnesia–spinel refractory bricks, Ceramics 3 (2020) 144–154. https://doi.org/10.3390/ceramics3010014.

[8] ASTM C577, Standard Test Method for Permeability of Refractories, ASTM International, West Conshohocken, PA.

[9] E.W. Washburn, Note on a method of determining the distribution of pore sizes in a porous material, Proceedings of the National Academy of Sciences 7 (1921) 115–116.

[10] T. Matsui, T. Ikemoto, Z. Nakagawa, Effect of pore structure on slag penetration into alumina sintered body, Taikabutsu 59 (2007) 280–287. https://doi.org/10.60431/taikabutsu.59.6_280.

[11] T. Richards, V. Athavale, J.D. Smith, R.J. O'Malley, High-temperature confocal scanning laser microscopy analysis of dead-burned magnesia aggregates, International Journal of Ceramic Engineering & Science 5 (2023) e10175.

[12] Z. Guo, Y. Ma, M. Rigaud, Sinterability of macrocrystalline and cryptocrystalline magnesite to refractory magnesia, International Journal of Ceramic Engineering & Science 2 (2020) 303–309.

[13] C. Ota, Studies on the microstructure of dead-burned sea-water magnesia, II, Journal of the Ceramic Association, Japan 69 (1961) 216–224.

[14] Richards, T., Athavale, V., Smith, J., & O'Malley, R. (2023). High temperature confocal scanning laser microscopy analysis of dead-burned magnesia aggregates. International Journal of Ceramic Engineering & Science, 5(3), e10175.

[15] Guo, Z., Ding, Q., Liu, L., Zhang, X., Luo, X., & Duan, F. (2021). Microstructural characteristics of refractory magnesia produced from macrocrystalline magnesite in China. Ceramics International, 47(16), 22701–22708.

[16] Wagri, N. K., Carlborg, M., Eriksson, M., Ma, C., Broström, M., & Andersson, B. M. (2023). High temperature interactions between K-rich biomass ash and MgO-based refractories. Journal of the European Ceramic Society, 43(8), 3770–3777.

[17] Fonseca, D., Gregurek, D., & Nunes, E. H. M. (2020). Application of a novel and simple TEST to evaluate the corrosion resistance of magnesia-based refractories to sulfur gases. Ceramics International, 46(16), 26160–26167.

WATER-FREE, QUICK-DRYING AND HIGH STRENGTH SOL-BONDED GUNNING MASS FOR ENERGY-EFFICIENT LIME KILN APPLICATIONS

Subhadeep Chatterjee, Sougata Roy, Minakshi Dash, Sagar Dey, Rajeswar Pramanik, Shamshad Ansari, Siddhartha Roy, Arup Kumar Samanta, Prasant Kumar Naik

TRL Krosaki Refractories Limited, Belpahar, Odisha

Email: asamanta@trlkrosaki.com

Abstract

Global decarbonization targets are accelerating the shift towards low-energy, low-emission manufacturing routes and shorter installation-to-startup timelines across process industries. In refractories, this trend is evident in the rapid adoption of "no-firing" products and in efforts to minimize dry-out and heat-up cycles for monolithic linings. Conventional gunning masses typically require water addition at site, which can prolong drying, increase risk of steam spalling during heat-up, and potentially introduce moisture-related damage to the backup lining and shell-side insulation.
To address these challenges, TRL Krosaki has developed a Sol-bonded gunning mass for lime kiln applications with three key performance requirements: (i) quick drying to reduce commissioning time, (ii) high strength and (iii) elimination of added water to help protect the backup lining from moisture exposure. The newly developed material is supplied as a water-free system using sol bonding, enabling gunning without on-site water addition and supporting a more controlled and faster dry-out strategy. Beyond operational benefits, the approach aligns with sustainability goals by targeting reduced energy demand during dry-out/heat-up and by enabling faster return to service.

This paper presents the material concept, installation approach, and expected operational advantages for lime kiln service, including implications for turnaround duration, drying-related failure risk, and lining reliability. Field implementation learnings and a performance
discussion framework (drying behaviour, heat-up sensitivity, and lining integrity) is also outlined to support broader adoption of water-free gunning solutions in high-availability kiln operations.

Keywords: Sol bonded gunning, quick drying, Carbon footprint

1. Introduction

The refractory industry is continuously being driven by global sustainability initiatives, energy conservation requirements, and the need to reduce carbon emissions associated with maintenance and production activities. Along with decarbonization efforts across process industries, refractory users are also demanding shorter shutdown durations, faster commissioning schedules, and improved asset availability. Consequently, significant attention has been directed toward the development of monolithic refractory systems that can minimize drying and heat-up times while maintaining mechanical integrity and service performance. Conventional refractory gunning masses and castable generally require the addition of water during installation, followed by controlled drying and preheating schedules to prevent steam-related failures. Such practices increase energy consumption, prolong downtime, and contribute indirectly to greenhouse gas emissions. Calcium aluminate cement (CAC) for so long has been the dominant bonding system for monolithic

refractories because of its ability to provide rapid setting and adequate green strength. However, the presence of CaO in refractory formulations is associated with several inherent limitations. During service, reactions between CaO, Al_2O_3, and SiO_2 it may generate low-melting phases, adversely affecting refractoriness and thermo-mechanical stability. Furthermore, CAC-bonded systems contain both free and chemically combined water, necessitating carefully controlled drying schedules to prevent explosive spalling caused by the generation of internal steam pressure during heat-up. These concerns have encouraged researchers to explore alternative bonding technologies capable of eliminating or reducing the dependence on calcium aluminate cement[1,2].

Over the last two decades, considerable progress has been made in the development of low-cement, ultra-low-cement, and no-cement refractory technologies. Among these alternatives, colloidal sol-based systems have emerged as one of the most promising solutions. Silica sol, alumina sol, mullite sol, and spinel sol binders form three-dimensional inorganic networks through gelation mechanisms rather than hydraulic reactions. As a result, sol-bonded refractories exhibit lower CaO content, superior refractoriness, improved corrosion resistance, and significantly enhanced after drying characteristics compared with conventional cement-bonded systems[3,4]. The absence of calcium aluminate hydrates substantially reduces the risk of vapor-pressure-related damage during heat-up, enabling faster and safer commissioning schedules.

A major advantage of sol-bonded refractory systems is their ability to achieve rapid moisture removal owing to their highly permeable gel structures and lower bound-water content. Peng and Myhre[5] demonstrated that microsilica-gel bonded no-cement castable exhibit superior dry-out behaviour and explosion resistance as compared to conventional or low-cement castable. Industrial-scale studies showed that cement-free castable could withstand accelerated heat-up rates without suffering explosive damage, thereby offering substantial reductions in drying and preheating duration. Similar observations were reported by Piippo et al., who demonstrated that increasing CAC additions adversely affects drying behaviour and increases the tendency for drying-related damage. These findings clearly indicate that cement-free refractory designs can support rapid start-up practices while improving operational reliability [6].

The industry has simultaneously witnessed increasing utilization of gunning refractories because of their installation flexibility, reduced labour requirements, and ability to eliminate formwork. Traditionally, gunning materials require water addition at the nozzle to facilitate adhesion and placement. Although effective, nozzle water addition increases variability in installation quality and introduces additional moisture that subsequently requires removal while drying. In response to these challenges, advanced dry-gunning technologies have been developed. Komatsubara et al. reported[7] the development of the SIG (Shinagawa Improved Gunning) technology, in which a binder solution was introduced instead of conventional water. The system exhibited substantially higher mechanical strength together with superior quick-drying characteristics and reduced requirements for forced drying. Such developments demonstrate the growing acceptance of alternative binder technologies for reducing energy consumption and improving sustainability of refractory installation practices.

Lime kilns represent one of the industrial areas where rapid installation and fast commissioning can provide significant economic benefits. Monolithic linings employed in lime kiln zones are frequently exposed to thermal cycling, abrasion, and mechanical stresses. Downtime associated with drying and preheating of repaired linings directly affects the plant productivity and operating cost. Conventional water-containing gunning materials can prolong the commissioning cycles and increase the possibility of steam-related damage to the working lining, backup lining, and insulation components. Therefore, technologies that eliminate or significantly reduce water addition while maintaining high

mechanical performance are increasingly attractive for lime kiln applications.

Recent reviews on colloidal binder technologies[3,8] have identified sol-bonded refractory systems as an important pathway toward sustainable refractory engineering. Compared with traditional CAC-bonded products, colloidal binder systems generally require less water, exhibit shorter drying times, improve thermal shock resistance, and generate fewer drying-related defects. Furthermore, the reduction or elimination of cement contributes to lower carbon emissions associated with refractory production and installation. These benefits are aligned with global efforts directed toward carbon neutrality and improved resource efficiency across process industries.

Despite the substantial body of work available on silica-sol bonded castable and no-cement refractory systems, published information concerning water-free, sol-bonded gunning masses designed specifically for lime kiln applications remains limited. Most previous studies have concentrated on castable rather than gunning materials, and information regarding the combined achievement of water-free installation, rapid drying, high strength development, reduced steam-spalling risk, and improved commissioning efficiency remains scarce. Therefore, the development of a water-free, quick-drying, high-strength sol-bonded gunning mass represents a significant advancement in monolithic refractory technology, addressing both operational and sustainability challenges encountered in modern lime kiln operation specifically in roof application. The sol-bonded gunning mass not only accelerate the pre-heating process but also restricts the damage of back up insulation refractory while apply hydraulic bonded gunning mass.

Recent work carried out at TRL Krosaki Refractories Limited on the development of cement-free, Sol-bonded gunning mass. The study demonstrated that elimination of CAC improved resistance to steam explosion and slag corrosion while contributing towards shorter drying and pre-heating schedules. Improved corrosion resistance was attributed to the reduction of CaO-containing phases, while the improved explosion resistance arose from the absence of calcium aluminate hydrates responsible for excessive steam generation during rapid heating. The work also highlighted the role of alternative calcium-free binder in achieving the carbon neutrality objectives through lower energy requirements during commissioning.

2. Experiment

Two different compositions(HB & GB) have been designed for this study. HBis a conventional cement bonded 50% alumina-based gunning massand GB is the TRLK's newly developed gunning massbonded with silica sol.

In both the cases 15 kg sample was prepared and dry mixing was carried out in a high intensity Hobert mixer for five minutes. For HB batch water was added & for GB batch liquid silica sol was added followed by wet mixing for 3 minutes.Three different sizes of samples were prepared for the evaluation of different properties. For measurement of CCS, CMOR, AP, BD and PLC sample size was 160 mm X 40 mm X 40 mm and for measurement of thermal spalling resistance cube samples of size 50 mm height and 50 mm width were prepared. For measurement of HMOR the sample size was 150 mm X 25 mm X 25 mm.

All samples were dried at110^{0}C with 24 hrs soaking time. For measurement of CMOR, CCS, AP, BD and PLC at higher temperature, firing of samples was carried out at 1000^{0}C and 1200^{0}C with a soaking time of 3hrs. HMOR was measured at 1200^{0}C and 1400^{0}C after pre-firing the samples at 1200^{0}C &1400^{0}C respectively. XRD was carried out to understand about the formation of different mineralogical phases after firing at 1200^{0}C and 1400^{0}C. Samples for spalling test werepre-fired at 600^{0}C before conducting the thermal spalling test at 1200^{0}C by water quenching.

Apart from the evaluation for different physical properties one special test was also carried out i.e. alkali resistance test. Alkali resistance is crucial for lime kiln refractories because volatile alkali compounds (such as

sodium and potassium from the feed and fuel) chemically attack the lining, causing destructive expansion, cracking, and premature structural failure.

Alkali resistance test specimens were prepared from both the conventional gunning mass (HB) and the newly developed sol-bonded gunning mass (GB). Each specimen has an outer diameter of 80 mm, a height of approximately 75 mm, and a central cavity measuring 40 mm in diameter and 40 mm in depth. After casting, the specimens were dried at 110°C for 24 hours and subsequently fired at 1200°C for 5 hours. Before alkali resistance test, 38 g of sodium carbonate (Na_2CO_3) was placed into the central cavity of each specimen. The cavity was then covered with a lid of approximately 80 mm × 25 mm and sealed using an air-setting mortar to prevent the escaping of alkali vapours during testing.The sealed specimens were thereafter fired at 1100°C for 5 hours and then allowed to cool to room temperature. After cooling, the lid was removed, and each specimen was cut into two equal halves for visual inspection and evaluation.

3. Results & Discussions

The typical chemical composition for two different gunning masses is shown in Table-1.

Material Name	HB	GB
Type of Binder	Cement	Silica Sol
Al_2O_3	50	50
Fe_2O_3	1	1
CaO	5.1	0.45

Table-1 Chemical composition of two different gunning masses

All physical properties like AP, BD, CCS, CMOR, PLC etc. were measured after drying the samples at 110^0C for 24 hrs and after firing at different temperatures.
The variation in AP is shown in **Fig.1**.There is increase in AP in HB batch while firing the samples at higher temperature against the AP measured after drying at 110^0C for 24 hrs. This is quite normal as the removal of both physically and chemically combined water takes place with increasing temperature creating pores in the body.

Whereas in case of GB batch the porosity is higher at 110^0C for 24hrs as compared to HB batch due to lack of hydraulic bonds & free water evaporate early & leaving behind an open highly permeable network. But with increase in temperature, it maintains a highly stable porosity as silanol (—Si—OH) groups seamlessly undergo dehydration and condensation (Si—O—Si) network without collapse along with highly reactive nano-silica initiates early, uniform sintering and prompts in-situ mullite formation, sealing pores and densifying the matrix.

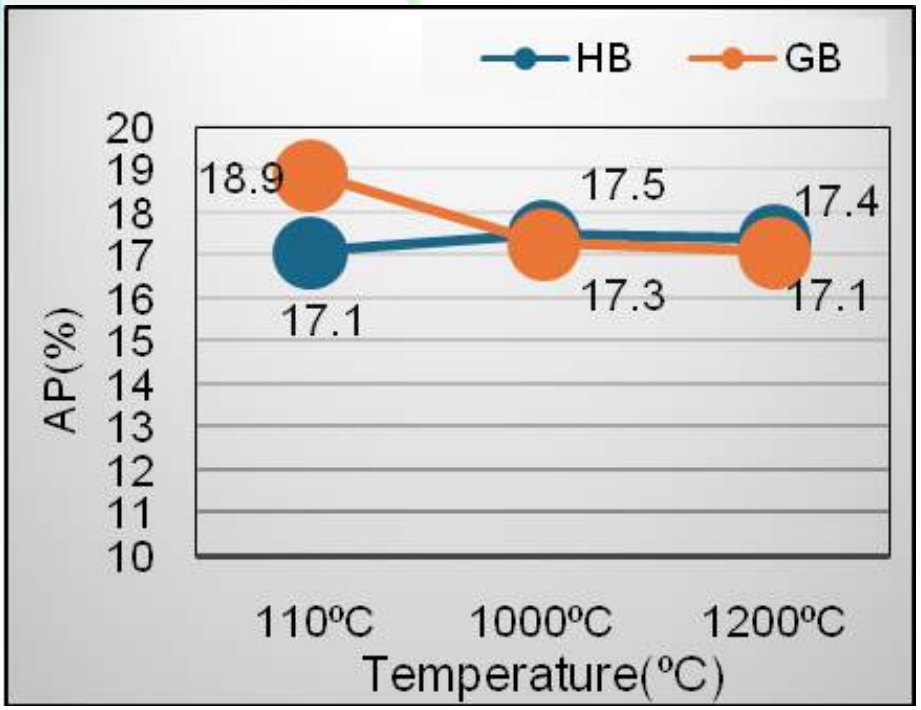


Fig:1-Variation of AP with temperature

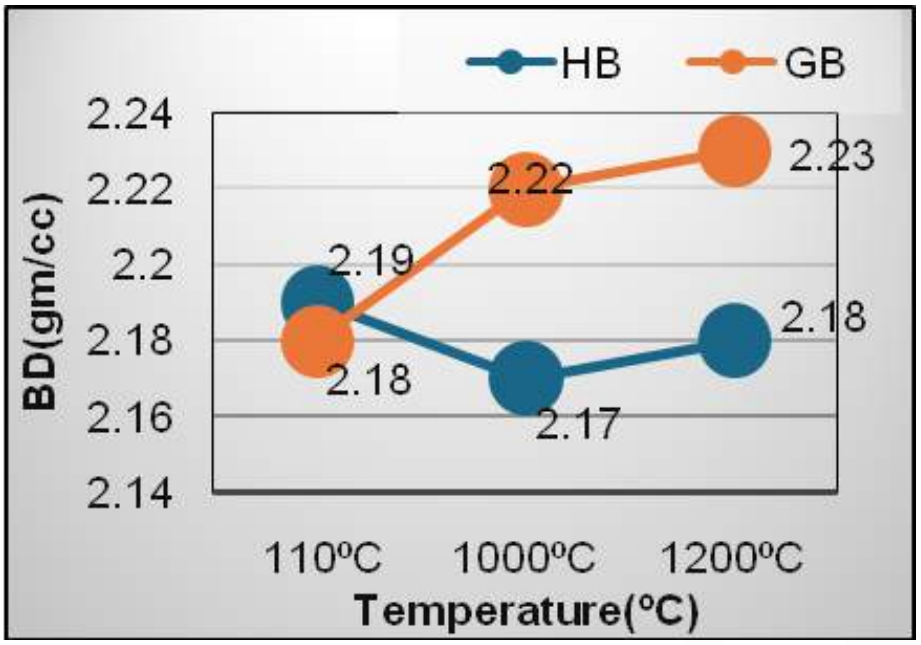


Fig:2-Variation of BD with temperature

In Case of BD (**Fig.2**),HB batch shows higher BD at 110^{0}C for 24 hrs because the calcium aluminate cement forms rigid hydraulic hydration phases that tightly pack the matrix space.Whereas GB batch shows slightly lowerBD as because the binding mechanism relies on the gelation of nano-silica particles via siloxane bonds which leaves a highly uniform, finely distributed capillary network upon moisture removal. But with increase in temperature, BD increases due to nano particle packing along with better high temperature sintering.

In case of GB batch, the CCS & CMOR (**Fig.3a & 3b**)is lower than conventional cementbonded gunning mass (HB) but moderate to withstand green strength of the body.While at higher temperatures strength remains stable and continuously increases

for GB as nano-silica reacts with the matrix fines to initiate microstructural co-sintering.

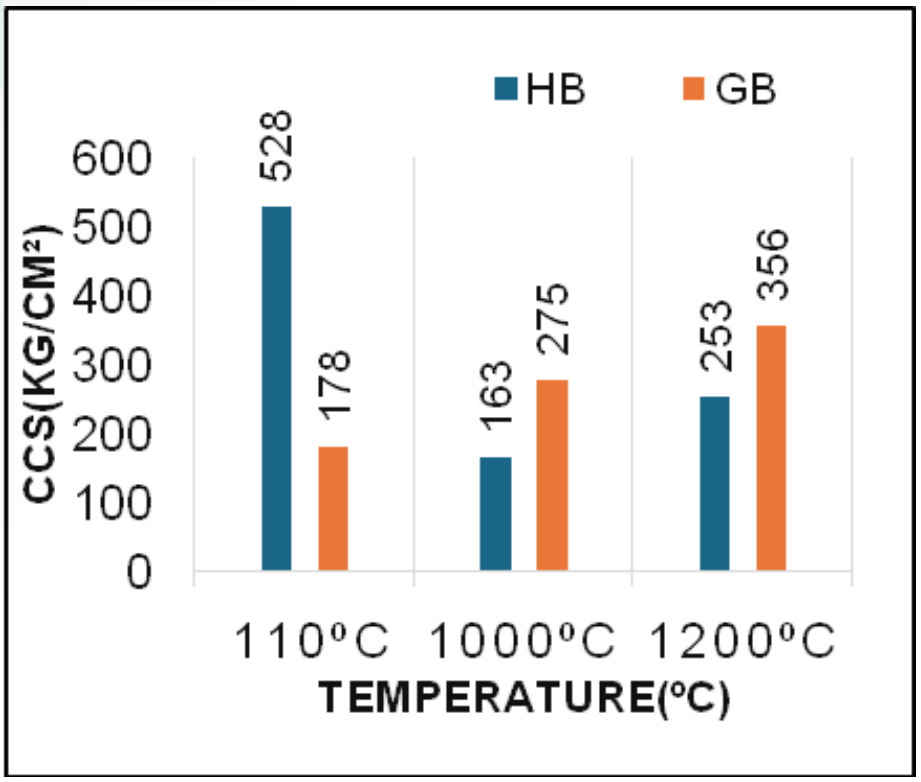


Fig:3 (a)-Variation of CCS with temperature

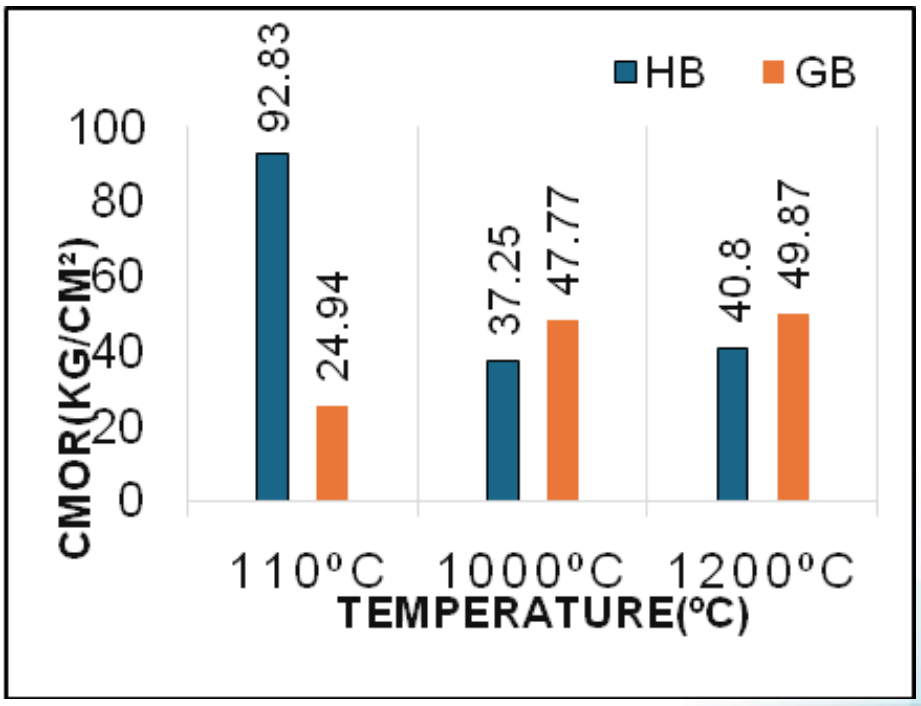


Fig:3 (b)-Variation of CMOR with temperature

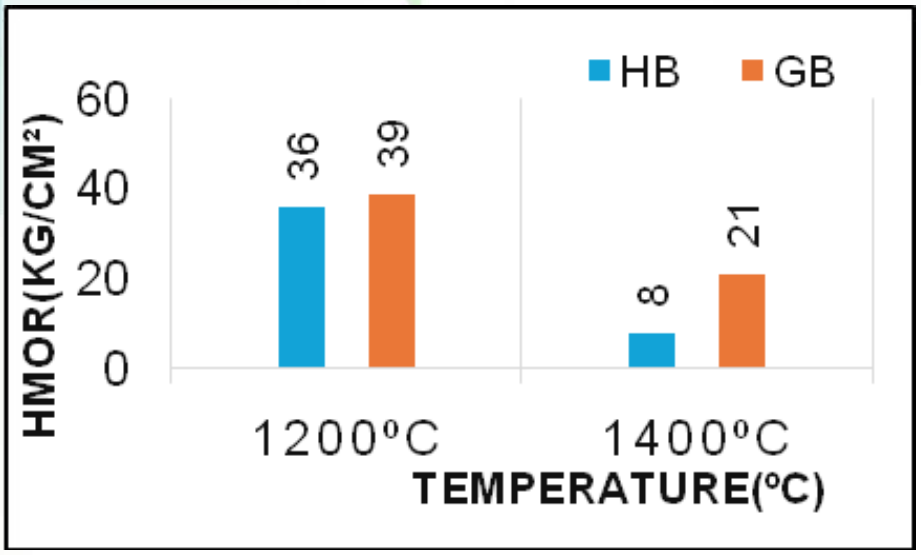


Fig:4-Variation of HMOR with temperature

Fig-4 shows HMOR of gunning masses measured at two different temperatures (1200^{0}C & 1400^{0}C). Samples were pre-fired at 1200^{0}C & 1400^{0}C before measuring HMOR. While comparing silica sol bonded gunning mass (GB) against a traditional cement-bonded gunning mass (HB), the Hot Modulus of Rupture (HMOR) profiles differ significantly. GB batch shows higher HMOR values at both 1200^{0}C & 1400^{0}C than compared to HB batch. The primary cause for this difference is the presence of calcium Oxide (CaO) in the cement, which reacts with silica and alumina to form low-melting liquid phases (like anorthite and gehlenite) at higher temperatures in case of HB batch. But in case of GB batch,there is no possibility to form any low eutectic compounds due to absence of CaO. At 1200^{0}CHMOR is moderate for HB as initial sintering begins and new calcium aluminate phases develop but in case of GB, solid-state sintering accelerates in-situ mullite formation and starts to lock the matrix. But at higher temperatures (1400^{0}C) there is a sharp drop in HMOR in HB batch as CaO acts as a flux. It creates a glassy liquid phase or low melting phase that causes the gunning massto soften and lose its high temperature strength abruptly. But in GB batch the absence of calcium prevents the formation of low-temperature eutectics and the interlocking mullite network yields superior high-temperature rigidity that will further be confirmed by XRD analysis.

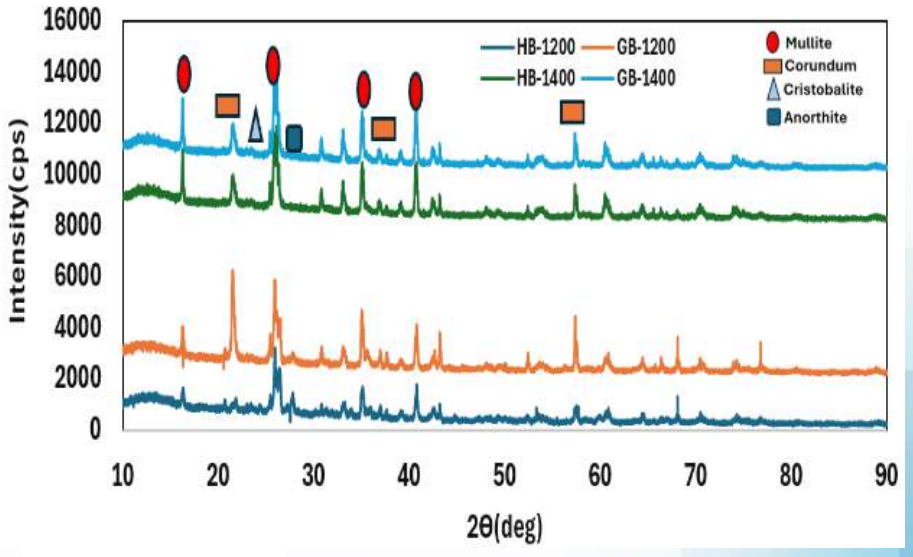


Fig:5- XRD pattern of HB and GB after firing at 1200ºC and 1400ºC

The mineralogical phases present in the samples were identified by XRD analysis after firing at 1200ºC and 1400ºC (Fig. 5). For the HB batch fired at 1200°C, the major phases identified are corundum and mullite, along with low-melting phases such as anorthite. Upon increasing the firing temperature to1400°C, the intensity of these low-melting phases increased significantly. On the other hand, the GB batch fired at 1200°C exhibited corundum, mullite, and cristobalite as the predominant phases, with a considerably lower quantity of low-melting phases. Even after firing at 1400°C, the intensity of the low-melting phases remained minimal, with only a partial transformation of cristobalite to mullite observed. This behavior indicates superior high-temperature phase stability of the GB batch compared to the HB batch.

3.1 Thermogravimetric analysis

One of the main objectives of this study is to develop a gunning mass with quick drying property as compared to conventional gunning mass for the reduction of carbon footprint. The main reason for drying process is the removal of water components from the gunning mix after application.

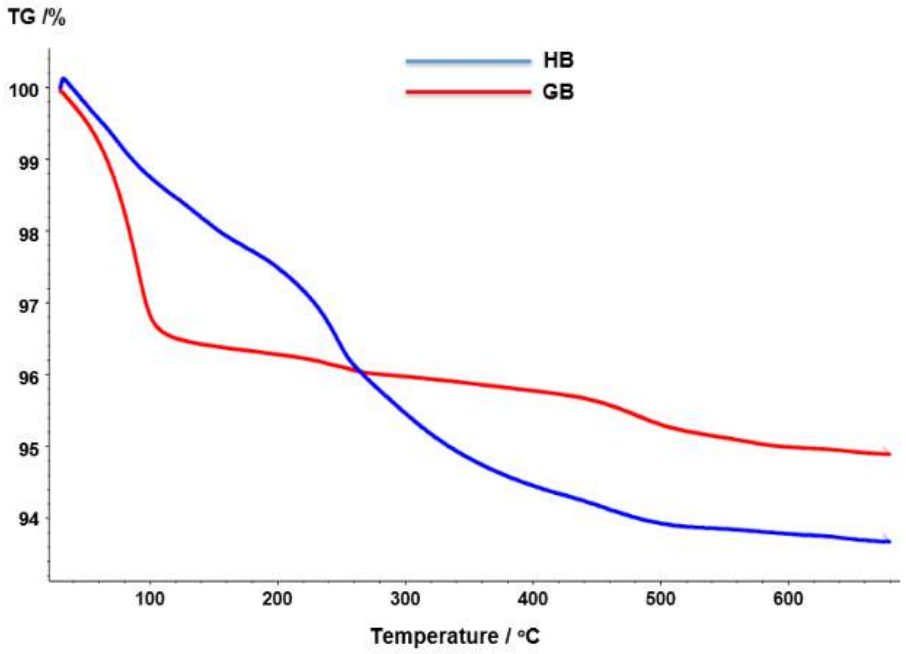


Fig:6-Variation of TG of HB & GB batch composition with temperature

Thermogravimetric analysis (TGA) was conducted after curing the samples for 24 h under 90% relative humidity. As shown in Fig. 6, the GB curve exhibits a major mass loss associated with water evaporation and completes the drying process at approximately 110°C. In contrast, the HB curve shows a significantly lower mass loss of about 1.2 wt.% within the same temperature range, indicating a slower release of water vapor compared with GB. The presence of crystalline hydrate phases formed during hydration before drying, as well as in-situ hydration reactions occurring under hydrothermal conditions during drying, results in lower permeability in HB and restricts the easy escape of free water. Consequently, the HB curve displays a lower mass-loss rate (lower slope), and complete drying occurs only at higher temperatures after the release of both free water and chemically bonded water from calcium aluminate hydrates. On the other hand, the GB curve shows a steeper mass-loss slope and achieves near-complete drying at around 110°C. These results correlate well with the higher permeability of GB compared with HB, which facilitates faster moisture removal during drying.

3.2 Permeability Test

The drying of monolithic refractories must be carried out gradually at a controlled heating rate to minimize the risk of explosive spalling. During heating, the evaporation of free and chemically bound water generates internal vapour pressure within the refractory body. If the generation rate of vapour pressure exceeds the rate at which vapour can escape through the pore structure, excessive internal pressure may develop, leading to cracking and explosive spalling. Therefore, the development of a gunning mass with high permeability is essential for safe and rapid drying.

The permeability of the HB and GB gunning masses, after heating at approximately 110ºC for 24hrs and 250ºC for 3hrs, is shown in fig.7.

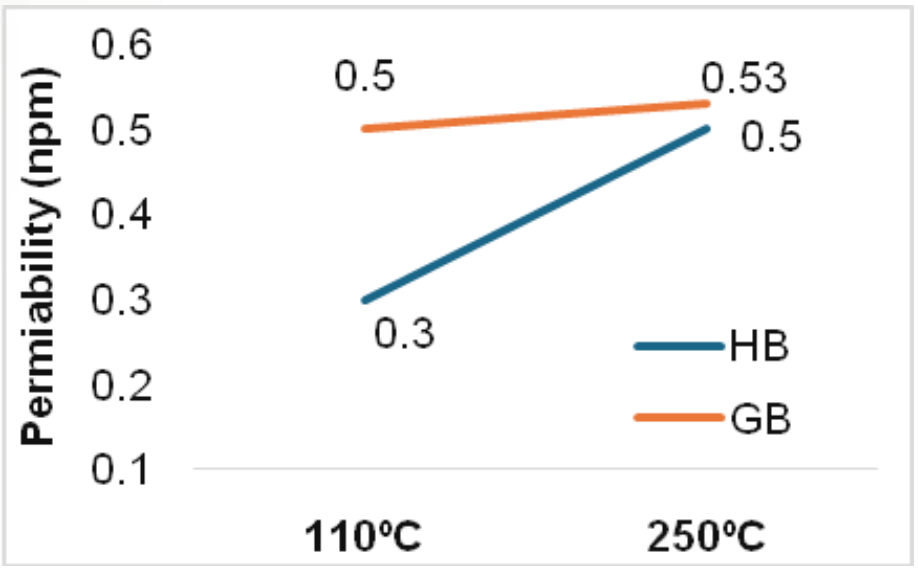


Fig:7-Comparison of permeability between HB and GB

It is observed that the GB gunning mass exhibits significantly higher permeability than the HB gunning mass. The higher permeability is due to the absence of HAC in GB formulation. Consequently, the formation of calcium aluminate hydrates, which can contribute to pore blockage and reduce vapour transportation. In case of GB gunning mass, the pore structure remains more open, providing easier pathway for vapour escape. This leads to higher permeabilityandimproved drying characteristics.

3.3 Spalling test

Spalling resistance in lime kiln roof gunning is crucial because it prevents the refractory lining from fracturing, flaking, or collapsing under extreme operational stress.Any failure in its structural integrity can trigger catastrophic equipment damage, product contamination, and costly unplanned downtime.Lime kilns undergo intense heating and cooling cycles (start-stop operations), shutdowns, flame variations and the introduction of cold raw limestone.So, a superior spalling resistance gunning mass is always recommended to achieve expected performance.

Thermal spalling behavior was studied through water quenching method from 1200^0Cto water. Appearance of samples after 20 cyclesis shown in Fig.8.



Fig:8-Appearance of sample after 20 cycles

In conventional gunning mass (HB) some cracks appear after 20 cycles whereas Sol-bonded gunning mass (GB) remained free from visible cracks. Subsequently, Cold Crushing Strength (CCS) was measured both for HB & GB samples after completion of 20cycles. The GB specimen achieved a CCS value of 180 kg/cm², whereas the HB specimen attained a CCS value of 105 kg/cm². The higher retained CCS confirm that GB can better withstand severe temperature fluctuations.

3.4 Alkali resistance test

Alkali-resistant gunning mass is commonly recommended for lime kiln applications specially for roof application because lime kilns are exposed to significant alkali attack from the raw materials, fuel ash, and process vapours. Ordinary refractory gunning mass can deteriorate rapidly under these conditions. During lime production, alkali compounds such as Sodium oxide (Na_2O), Potassium oxide (K_2O) become volatile at operating temperatures and penetrate the refractory lining.These alkalis react with gunning mass and form low-melting compounds that weaken the structure,cause expansion and cracking,accelerate wear and structural spalling. So,roof gunning mass should have the resistance against alkalies.

Photographs of outer surface and cross section of sample specimen after alkali resistant test are shown in the Fig.9 and Fig.10. The alkali components have deeply penetrated in the crucible sample made of conventional gunning mass (HB),crack on the outer surface of the sample, namely, bursting. On the contrary, penetration of alkali components into the test piece made of newly developed gunning mass (GB) is shallow with no cracks initiated on the outer surface.



Fig:9-Photograph of outer surface after alkali resistance test



Fig:10-Photograph of cross section of sample after alkali resistance test

4. Field trial

After getting encouraging lab trial results, field trial was conducted in an integrated steel plant A with improved gunning mass quality (GB). An overview of lime kiln at plant A is shown in the Fig.11.

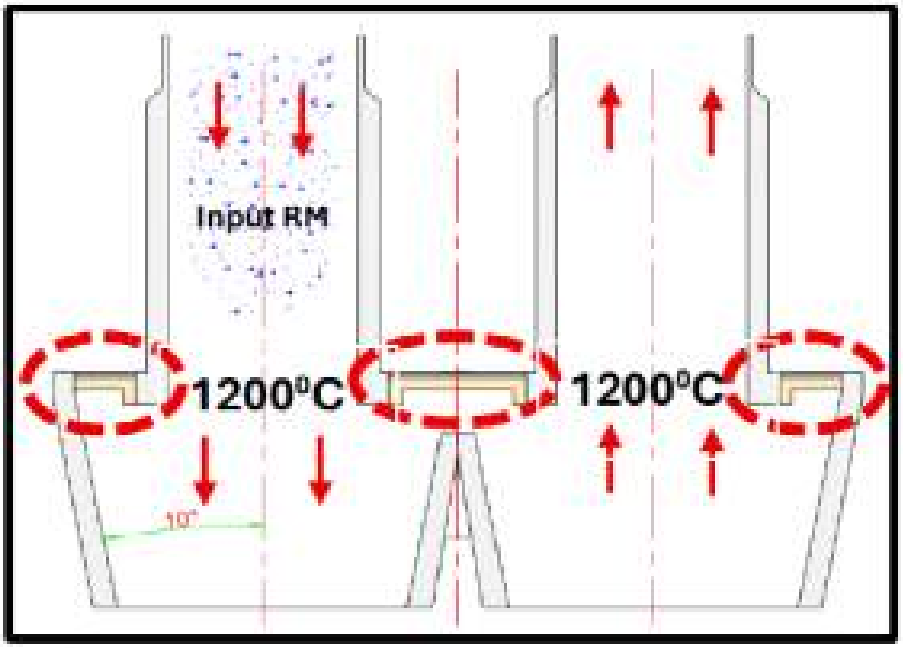


Fig:11-Overview of lime kiln at plant A

The gunning mass was applied over an insulating mix with an average thickness of around 200-250 mm on the roof of the lime kiln. Rebound loss in the gunning operation was roughly 10%, which is better than that of conventional cement bonded gunning material (HB). Fig.12 shows gunning panelwork on the roof of the lime kiln from the inside of the furnace.

As shown in the Fig.13. with conventional cement bonded gunning material, powdery gunning refractory is admixed with water at the gunning nozzle. In the gunning operation it is necessary for gunning refractory materialto coagulate immediately after dissolution of blended binder into admix water. Furthermore, in case where dissolution of blended binder into admix water does not take place evenly, dispersion of binder in the relined body becomes uneven, resulting in inhomogeneity of mechanical strength. For these reasons an excessive amount of water tends to be admixed.

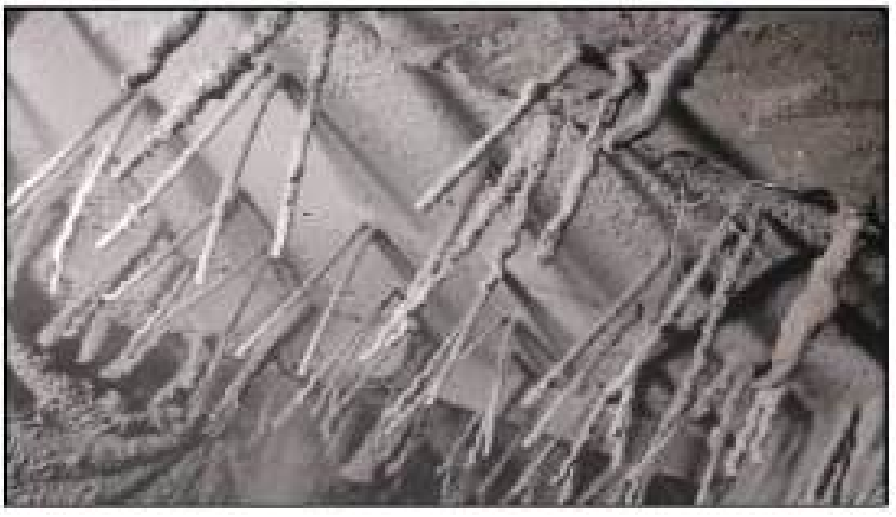


Fig:12-Gunning panel work on the roof of the lime kiln from the inside of the furnace

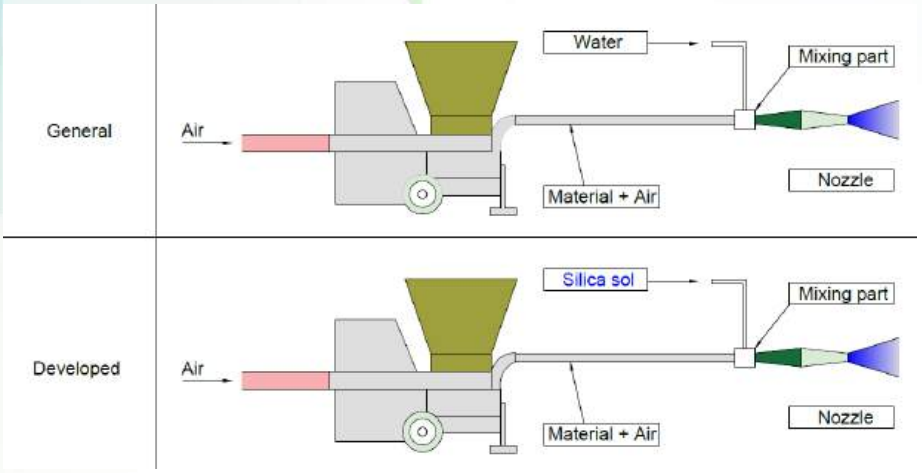


Fig:13-Comparison of conventional & sol bonded gunning mass

To overcome these limitations, silica sol was employed as the bonding system instead of a cement-water binder. A small quantity of gelling agent incorporated in the dry mix reacts rapidly with the silica sol to form a uniform gel network, providing adequate green strength and improved homogeneity throughout the installed lining.

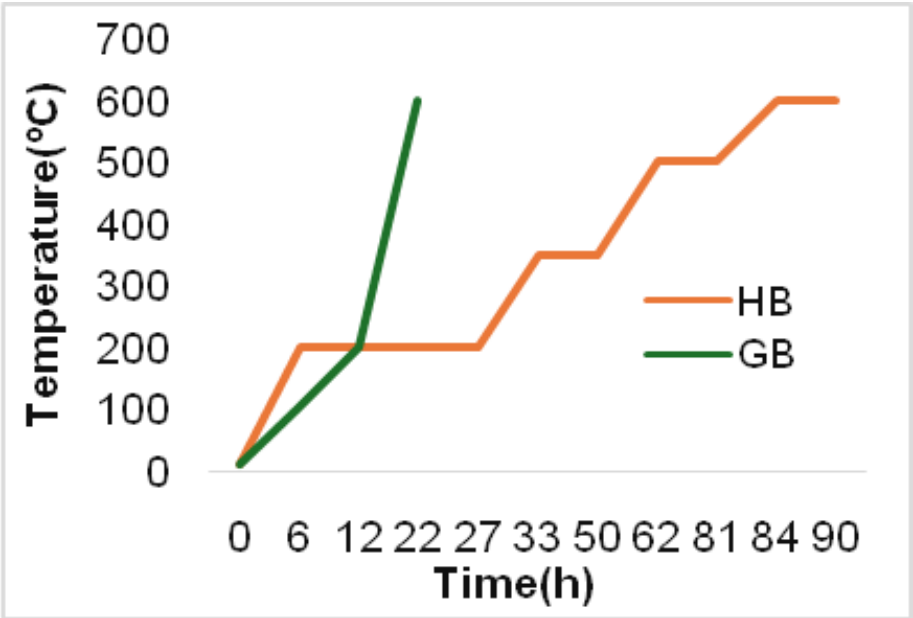


Fig:14-Comparison of drying profile between HB & GB

Fig.14.is the comparison of drying profile between HB and GB. For conventional gunning mass the body is so dense that drying need to be conducted gradually with a slow heating rate for a long time to avoid explosive spalling incident during drying time. As a result, approximately 90 hours (about 4 days) are required to complete the drying process.

To develop a monolithic gunning refractory with quick gunning nature it is important to avoid explosive spalling even during rapid drying. In other words,it is important to develop a gunning refractory with high permeability. TRLK's newly developed gunning mass is more permeable than conventional gunning mass as it is cement free.

After curing,the gunned body of TRLK's newly developed gunning mass had rapidly heated as shown in Fig.14for removal of water component. The total drying time was approximately 22 hours, which is significantly shorter than that of the conventional material and represents a reduction of nearly 75%

compared with the 90-hour drying cycle.Despite the accelerated heating schedule, no explosive spalling was observed during drying. These results demonstrate that the improved permeability of the TRLK cement-free gunning mass enables safe and rapid dry-out while maintaining the integrity of the installed lining.

5. Conclusion

A cement-free, silica sol-bonded gunning mass for lime kiln roof applications was successfully developed and evaluated against a conventional cement-bonded gunning mass. The developed material exhibited higher permeability, faster moisture release, and significantly improved resistance to explosive spalling during heat-up. Thermogravimetric and permeability studies confirmed that the absence of calcium aluminate hydrates facilitates rapid drying and safer commissioning.

The silica sol-bonded improved gunning mass also demonstrated superior high-temperature performance, thermal shock resistance, and alkali resistance. XRD results indicate the formation of a stable mullite-corundum microstructure with reduced low-melting phases, resulting in improved hot strength and thermo-mechanical stability. In addition, the material showed lower alkali penetration and better durability under conditions representative of lime kiln service.

A key advantage of the developed technology is the elimination of on-site water addition during gunning, leading to improved lining homogeneity, reduced rebound loss, and reduced risk of moisture-related damage to backup insulation. The material can be installed using conventional gunning equipment with minimal modification.

Overall, the newly developed TRLK silica sol-bonded gunning mass offers a combination of rapid dry-out, high permeability, excellent alkali and thermal shock resistance and superior high-temperature strength. and proven field performance. These advantages make it a generation refractory solution for high-availability lime kiln operations, enabling shorter shutdowns, improved lining reliability, and reduced energy consumption during commissioning.

6. References

[1] M. Singh, “Effect of Mullite Formation on Thermo-Mechanical Properties of Refractory Castables,” Ceramics International, Vol. 45, No. 12, 2020.

[2] D. Zhao, “Thermo-Mechanical Behavior of Cement-Free Castables with Enhanced Mullite Formation,” Journal of Advanced Ceramics, 2019.

[3] M. Cichocki, J. Angelkort, N. Fröse et al., “The Binding of Non-Cement Refractory Castables Using the Technology of In-Situ Sol-Gel Formation,” Intocast AG, 2023.

[4] E. Brochen, C. Dannert, M. Thiesen et al., “Thermomechanical and Thermochemical Behaviour of Silica- and Spinel-Sol-Bonded High-Alumina Refractory Castables,” Journal of Ceramic Science and Technology, 2025.

[5] H. Peng and B. Myhre, “Drying Behaviour and Explosion Resistance of No-Cement Refractory Castables,” Refractories WORLDFORUM.

[6] A. Piippo, K. Ruotanen, V.-V. Visuri et al., “Experimental Study on the Effect of Calcium Aluminate Cement Addition on the Drying and Physical Properties of Refractory Castables Containing Colloidal Silica,” Materials, 17(21), 5308, 2024.

[7] K. Komatsubara, H. Nishiguchi and R. Yamada, “Dry Gunning Material SIG with High Durability and Quick Drying Properties,” Shinagawa Technical Report.

[8] Kandulna and Dana, “Replacing CAC: A Review of Colloidal Binders for Monolithic Refractories,” Ceramic Tech Today, 2026

GUNNING ROBOTS FOR THE HOT REPAIR OF EAF, LADLE AND RH SNORKEL

Christian Wolf, Velco GmbH, Germany

Abstract

Refractories are used to protect the steel making aggregate from the hot steel melt. Due to the steel making process this refractory lining is subject to wear. Using gunning robots this lining can be repaired very efficiently and according to the highest standards for operational safety. This paper describes the recent developments in robotic gunning of EAF, ladle and RH degassers with the help of integrated TV cameras and laser scanners.

1. Ladles

The refractory wear at ladles is mainly in the slag zone and the lip area. At plants with secondary metallurgy the slag zone wears out even more quickly. Sometimes the top of the lining, the lip ring, becomes damaged due to slag removal with a breaking out machine. Consequently, a ladle can be put back into operation very quick after a hot gunning repair focused only on the slag zone.

The most convenient location to carry out a hot repair is the tilting stand, where the slide gate is repaired. It is possible to use a manual gunning lance but this results in high physical stress for the worker.

When using a gunning robot the gunning repair is:

- Quicker, because of higher gunning rates.
- More efficient, because of the well directed jet.
- Easier because there is no physical stress for the worker.

Velco has built different solutions for this task, depending on the plant layout and if the ladle is in horizontal or vertical position. One version is a fixed installation consisting of a rotating lance that can move in and out, running on a beam structure. For each repair stand one robot is required (Fig. 1)

The second version is a gunning lance which is mounted on an electric trolley that can drive from a parked position to one, or more repair positions. Fig. 2 shows a manipulator at a ladle with a liquid content of approximately 150t of steel, for the repair of ladles which are in a tilting stand, at voestalpine in Linz, Austria.



Fig. 1 Stationary ladle gunning installation



Fig. 2 Mobile lance trolley for ladle gunning

Fig. 3 shows the newest development for horizontal ladle gunning installed at a German steel plant. The robot swings away when the ladle is set in position.

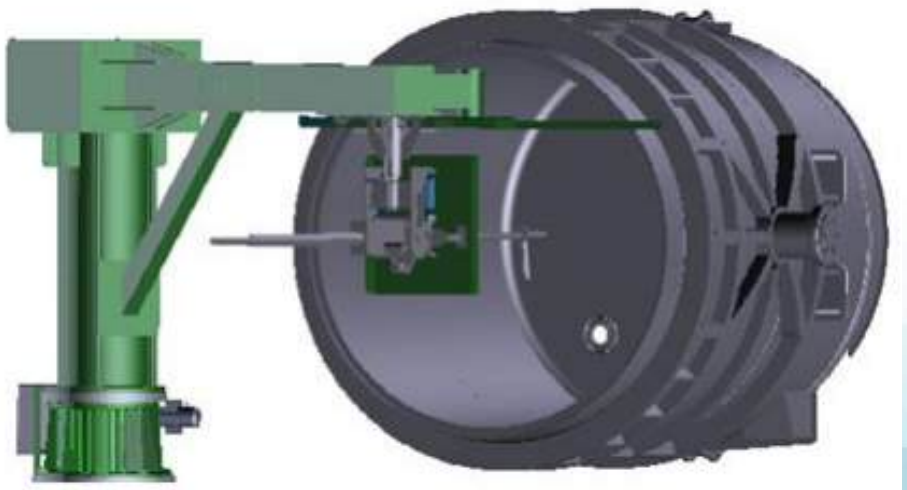


Fig 3 Stationary ladle gunning installation for horizontal ladle

2. RH-Degassers

The high quality demands of the automobile industry, leads to an increase in the proportion of melts routed via the vacuum degasser. Snorkel lifetime is an important factor in achieving high availability, of the RH-degasser. Due to the reaction with steel and slag, the snorkel wears out both internally and externally. Often the outside lining is damaged by slag removal with scrapers or de-bricking machines. It is of primary importance to keep the system safe and to avoid break outs of hot metal, but the service time is limited as the sequences of the steel plant have priority. Any unplanned exchange of the snorkels should be avoided. Outside gunning is a common practice. However, the workplace is exposed to heat and the operator likes to stay away from the snorkel, so the gunning is not always well directed and has high rebound losses.

Some steel plants have a service car to which a platform for hand gunning is attached. So the distance is smaller and the rebound lower. Nevertheless, inside gunning is not possible because of the danger of dripping hot steel or slag from the RH-vessel.

Hence, using a gunning robot is beneficial for outside repairs, because the gunning is better directed and the physical stress on the workers is eliminated. A robot is essential for the inside repair of the RH snorkel. If gunning is performed well, consumption is in the range of 0.5kg/t steel. Typically gunning takes place after 6 to 8 treatments.

Most robots have two gunning lances, one for inside and one for the outside repair. Lances and lifting arm are based on a frame that can rotate by 180° (Fig. 4 a, b). One lance can repair the inside of snorkel A, while the other is doing the outside repair of the snorkel B. When this is finished, the main base rotates, so snorkel A is repaired on the outside and snorkel B is repaired on the inside.

The operator can either use automatic programs or may control the maintenance process via a radio remote control (manually).





Fig .4 a, b Gunning manipulator with 2 lances

The advantage of placing the scraper and the gunning robot on the same service car is the time saving in handling. The complete operation of snorkel cleaning and inside/outside gunning can be performed in approx. 12 -15 min. (Fig 5).

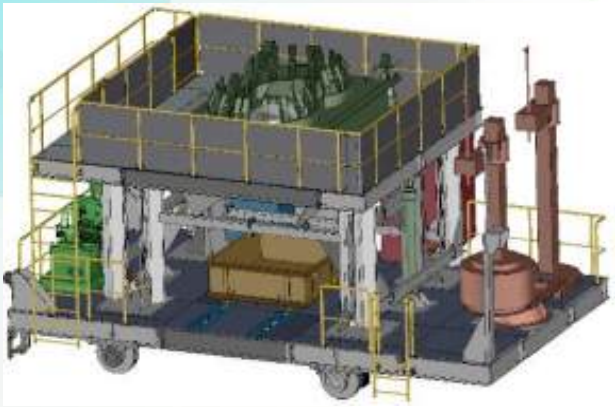


Fig. 5 service car with scraper and gunning robot (picture SMS group)

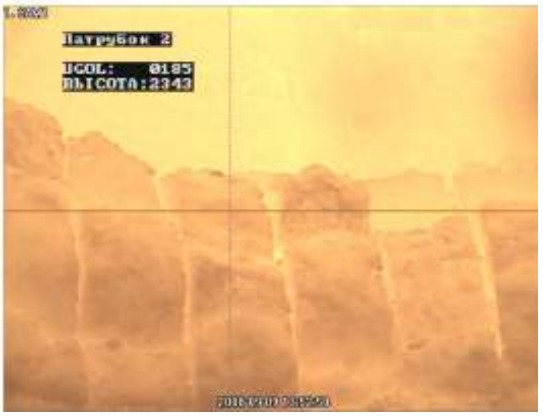


Fig. 6 Inside picture of RH-snorkel using camera

For the inspection and documentation of the wear pattern it is possible to attach a camera on the robot. A video can be made of the snorkel or the lower vessel area. Using positioning encoders, the area of robot in the video can be exactly determined (Fig. 6)

High performance RH degassing installations are in DUPLEX RH design with 2 vessels, one treatment position, two stand-by positions and fast vessel exchange system.

Instead of blocking the treatment position for the gunning repair, customer can install two gunning robots at the standby positions. As the repair time is not time critical a single lance design is sufficient. Fig.7 a, b, c) shows installation at Big River Steel in AR/USA. The gunning robot is put on a moveable trolley car, which moves away from the snorkels during snorkel cleaning.



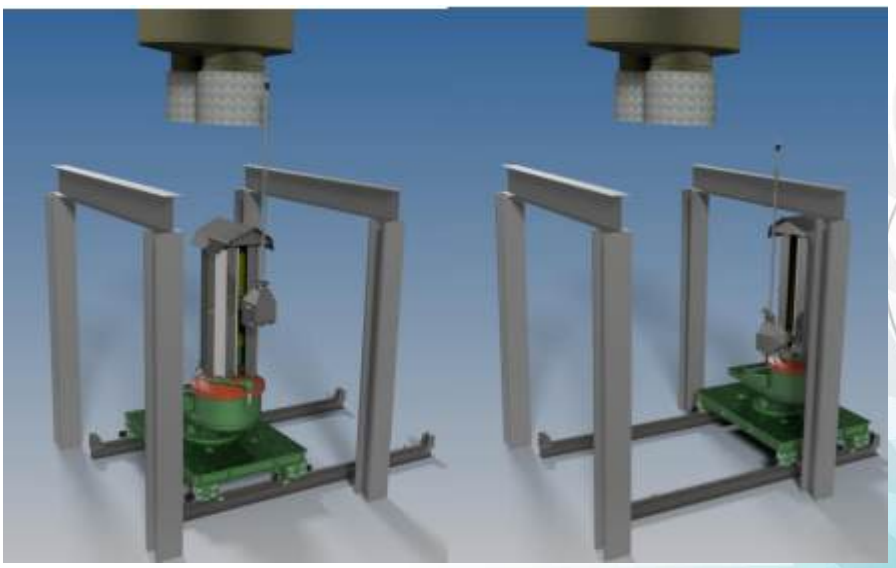


Fig. 7 (a + b) gunning robot on trolley car

c) for snorkel cleaning the robot moves away

3. Electric Arc Furnaces

In the past 25 years Velco has supplied 24 gunning robots for electric arc furnaces. However, due to the different layouts of the melt shops no two robots are alike. It has to

checked for collisions with T&P robot, oxygen lance or door ram.

In between the vessel exchange sequences, hot gunning is the preferred solution to keep the furnace operative. When using hand lancing a pipe of typically 6 to 8m in length is introduced through the slag door. The gunning rate is only 60 to 80 kg/min. Handling the pipe is hard work and not all areas at the furnace can be reached, especially close to the slag door.

There is the option to install a CCTV camera in the gunning head (Fig. 8 - 10), so that it is possible to watch and record the gunning repair. The operator can stay safely in the pulpit. safely in the pulpit.

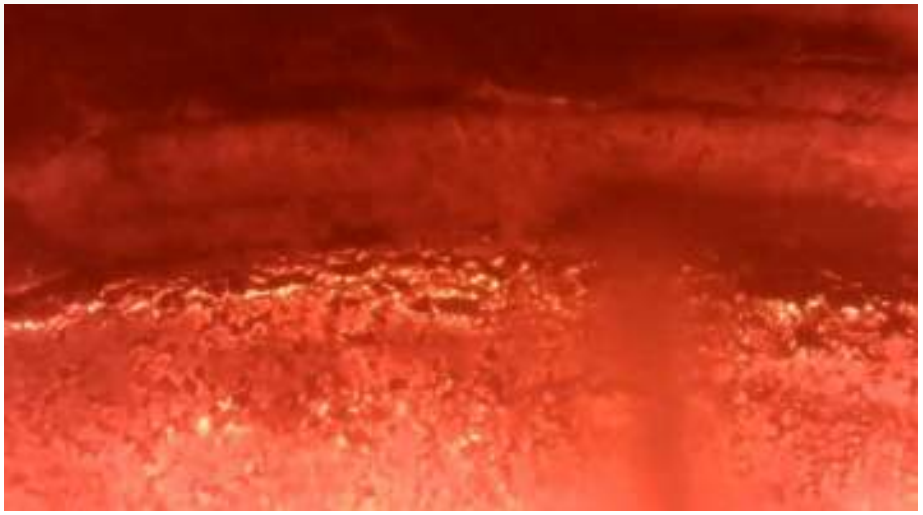


Fig. 8 Video of gunning with Camera in gunning robot head





Fig. 9 and 10 Air cooled camera in gunning head

The new design developed in 2021 is called METOP. It has a pure mechanical lift system by an electro-mechanical cylinder. No hydraulic required Fig. 11.



Fig. 11 Metop at customer site in Egypt

Next step of improvement is the use of pre-programmed gunning programs. The operator can pre-select areas to be gunned on a touch screen. He can save different gunning programs depending on the gunning strategy and furnace life. The robot then automatically repairs only the selected locations (Fig. 12)

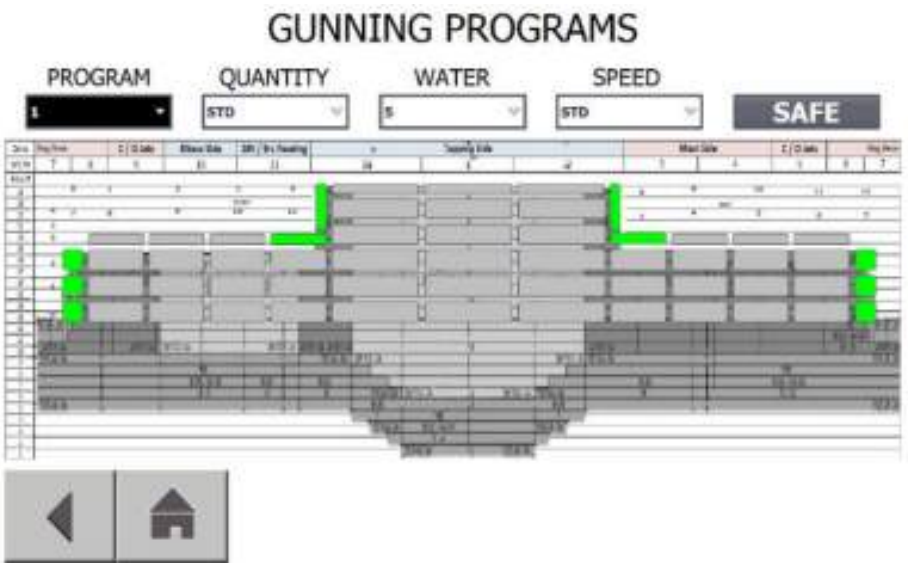


Fig. 12 Zone selection for automatic gunning

Even the application of bottom material is possible with the gunning robot. This addition can be with Joystick control or pre-programmed Fig. 13.



Fig. 13, addition of bottom material (before and after sintering)

Lucchini Industries Steel Plant in Lovere /Italy was looking for a new gunning manipulator to improve operational safety, but had no space near the electric arc furnace. They decided for the crane held gunning manipulator PNEUTOP. Which is parked approx. 40m away from the furnace in a special structure. For the gunning repair, the manipulator is picked up by the overhead crane (Fig.14) and lowered from the top into the furnace. The PNEUTOP is connected to a pressure vessel machine



Fig. 14 PNEUTOP robot moved by a crane



Fig. 15 hot gunning repair with PNEUTOP

The refractory gunning material is supplied in BIG BAGs that are filled into the pressure vessel via a filling hopper. Via a radio remote control the operator moves the lance to the desired location, starts and stops the pressure vessel machine and controls the gunning water flow.

Using the gunning manipulator the repair is quicker and the operational safety is improved (Fig. 15).

4. Laser Scanner

In cooperation with IMSI (Industrial Measuring Systems Inc., Toronto, Canada) it has been developed a design where a high speed laser scanner with its own swing arm is attached to the boom of the gunning robot. The laser arm is mounted very compact onto the gunning robot boom and requires no extra space on the shop floor. During parking and gunning operation the laser and the arm head towards the robot base. Only for the measurement the arm swings over the furnace shell (fig. 16).

The laser is protected against heat and dust by enclosures, heat shields and air cooling. The laser scans the shape of the refractory lining, compares with the initial brick lining and gives recommendations where gunning should take place. So the gunning repair can be performed automatic. The furnace refractory is scanned immediately after the lining and this result is compared with the worn out areas to identify the zones for the gunning repair (Fig 17).



Fig. 16 Gunning robot METOP with attached laser scanner

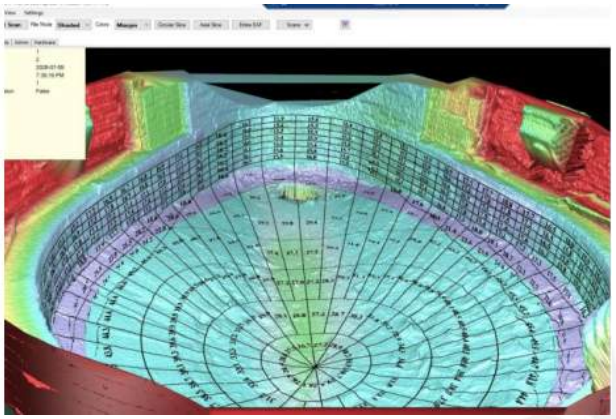


Fig 17. Scan of EAF with new lining, grid pattern

5. Conclusions

Gunning robots help to increase productivity and the safety for the repair of the refractory lining. In combination with cameras and laser scanner they bring a new level of operational safety to the steel mill.

ENERGY EFFICIENT MAGNESIA CARBON BRICKS SOLUTION FOR STEEL LADLE

Avishek Mitra, Tuhin Patranabhish, Suvankar Mondol, Raja Sarkar, Dr. Saumen Sinha

Calderys India Refractories Limited, Nagpur, India

Abstract

Magnesia carbon (MgO-C) bricks are commonly used in steel ladles because they have very good thermal shock resistance and high resistance to slag and corrosion. Good ladle refractories also help to keep molten steel hot for a longer time, which reduces the need for reheating and saves electricity and fuel to lower operation costs as well as to reduce environmental impact.

This paper presents a new steel ladle lining concept to reduce CO_2 emissions and support sustainable steel production using optimized refractory design. The study focuses on the development of MgO-C bricks with nano carbon as well as reclaimed material, designed to reduce energy used during ladle operation and lower CO_2 emissions (LCA of refractory solution). Introduction of a small amount of nano carbon causes a significant reduction in the requirement of graphite, leading to a marked reduction in the emission of greenhouse gases. This approach supports sustainable steelmaking with better efficiency and environmentally friendly refractory lining.

Keywords: Magnesia Carbon, steel ladle, nano carbon, CO emission

Introduction

Magnesia–carbon (MgO–C) refractories are widely used in steel ladles because of their high refractoriness, resistance to basic slags, good thermal-shock resistance and low slag wettability. Conventional MgO–C bricks are mainly composed of fused magnesia, flake graphite, phenolic resin binders and antioxidants such as Al, Si or B_4C [1]. Magnesia provides the structural and chemical resistance, while graphite improves thermal-shock and slag-penetration resistance. During heating, the resin forms a carbonaceous bond, whereas antioxidants help retard carbon oxidation.

A major challenge of conventional MgO–C refractories is their relatively high carbon content. During steelmaking, carbon is oxidized and generates gaseous carbon species, particularly CO.

At high temperature, carbon can also participate in carbothermic reduction of magnesia:

$$MgO + C \quad Mg\ (g) + CO\ (g)$$

These reactions cause carbon loss, increased porosity, and weakening of the refractory matrix. Therefore, reducing the carbon content of MgO–C bricks offer a potential route to lower CO-emission potential, provided that corrosion resistance, strength, and service life are maintained.

Nano-carbon is one promising approach for developing low-carbon MgO–C refractories. Because of its very small particle size and high specific surface area, nano-carbon can be distributed more effectively throughout the refractory matrix than conventional flake graphite. Previous studies have shown that relatively small additions of nano-carbon can compensate for a substantial reduction in graphite and can improve coked strength, oxidation resistance and corrosion behavior [2–4]. Thus, the key objective is not only to reduce total carbon, but to improve the efficiency of carbon utilization within the refractory structure.

In the present work, the conventional slag-zone grade S-1 contains about standard graphite content, whereas the developed S-2 contains less than 50% graphite together with 1 wt.% nano-carbon. This represents a major reduction in conventional graphite while retaining a fine carbon phase within the

matrix. The lower carbon content is expected to reduce the amount of carbon available for oxidation and therefore decrease the potential generation of CO during service.

A second sustainability route was applied to the metal-zone refractory. The developed M-2 contains recycled MgO–C material, replacing a significant portion of virgin fused magnesia and graphite used in the conventional M-1 grade. Recycling spent MgO–C refractories can reduce virgin raw-material consumption, refractory waste, and the environmental burden associated with primary raw-material production [5,6].

Accordingly, this study evaluates two complementary approaches for a more energy- and resource-efficient steel-ladle lining: low-carbon, nano-carbon-containing MgO–C bricks for the slag zone and recycled-material-containing MgO–C bricks for the metal zone. The developed S-2 and M-2 grades are compared with the conventional S-1 and M-1 grades in terms of physical, mechanical, oxidation, and corrosion properties. The objective is to determine whether lower carbon content and increased recycled-material utilization can reduce CO-emission potential and virgin raw-material demand while maintaining satisfactory refractory performance.

2. Materials and Experimental Methods

Four resin-bonded MgO–C brick qualities were investigated in this study. Two qualities were intended for the ladle slag zone and two for the metal zone. S-1 was the conventional slag-zone reference brick, whereas S-2 was developed as a low-carbon MgO–C grade using a modified carbon system containing nano-carbon. Similarly, M-1 represented the conventional metal-zone MgO–C brick, while M-2 was developed using a significant proportion of recycled MgO–C refractory material. The experimental comparison was designed to determine whether the modified S-2 and M-2 grades could provide performance equivalent to or better than their respective conventional references while reducing virgin carbon and raw-material consumption. The four grades and their intended functions are summarized in Table 1.

All four qualities were manufactured through the same industrial production route. After mixing, the batches were shaped using an industrial 630 T ESP press and subsequently tempered at 230°C for 24 h. This ensured that the comparative evaluation was based primarily on the differences in material design rather than on differences in the brick manufacturing process.

The basic physical and mechanical properties were evaluated after tempering. Apparent porosity (AP), bulk density (BD), and cold crushing strength (CCS) were measured according to the applicable ASTM methods/IS 1528. Modulus of rupture (MOR) was also determined at room temperature to assess the flexural strength of the resin-bonded structure. Fixed carbon was measured to characterize the carbon level of the different qualities. The measured properties were used to compare the initial compactness, strength, and carbon characteristics of the reference and developed bricks.

To evaluate the behavior of the carbon-bonded matrix after thermal treatment, a second set of specimens was coked at 1000°C for 3 h. After coking, AP, BD, CCS and MOR were again determined, together with the percentage weight change. The coked properties are particularly important for MgO–C refractories because decomposition of the phenolic-resin binder and development of the carbon bond significantly modify the pore structure and mechanical behavior of the brick. Comparison between the tempered and coked properties was therefore used to assess the structural stability of the different carbon systems after high-temperature exposure.

Oxidation resistance was investigated by exposing the samples to air at 1000°C for 1, 2 and 3 h. After each exposure period, percentage weight change and decarburized-layer thickness were measured. The CCS and MOR of the oxidized specimens were also determined to evaluate the extent

to which oxidation affected the residual mechanical integrity of the refractory. Decarburization thickness was considered a direct comparative measure of the progression of the oxidation front into the brick; a lower value indicates more effective restriction of oxygen penetration and carbon oxidation. The combination of weight change, decarburization depth, and residual strength therefore provides a more complete assessment of oxidation resistance than weight change alone.

Corrosion performance was evaluated under conditions representative of the intended ladle zones. The S-1 and S-2 slag-zone grades were tested at 1650°C for 2 h, whereas the M-1 and M-2 metal-zone grades were tested at 1600°C for 2 h. Slag corrosion testing was conducted at 1650°C to ensure complete slag melting, adequate fluidity, and representative refractory–slag reaction kinetics. Metal corrosion testing was performed at 1600°C, where the steel is fully molten and sufficiently superheated to simulate typical steel–refractory contact conditions. After testing, the dimensions of the resulting cavity and affected interface region were measured. Overall specimen dimensions, main cavity length, maximum cavity width, and approximate affected-zone dimensions were used as comparative parameters. Smaller cavity dimensions and a more restricted affected zone were considered indicative of improved resistance to penetration, dissolution, and refractory degradation.

Optical microscopy was carried out on the four brick qualities at 50× magnification to support the interpretation of the physical, oxidation, and corrosion results. The microstructures were examined with particular attention to magnesia-aggregate morphology, aggregate–matrix interfaces, carbon-rich matrix regions, pores, and cracks. The S-1/S-2 comparison was used to assess the microstructural effect of the modified low-carbon system, while the M-1/M-2 comparison was used to evaluate the influence of recycled refractory incorporation.

3. Results and discussion

The slag-zone grade S-2 shows a clear improvement over S-1 in both tempered and coked conditions despite its substantially lower carbon content. In the tempered state, AP decreases from 4.6 to 2.2% (−52.2%) and BD increases from 2.97 to 3.13 g/cm³ (+5.4%). At the same time, CCS increases by 66.7% and MOR by 35.3%, although fixed carbon decreases by 59.2%. This combination of lower porosity, higher density, and improved strength indicates that the modified low-carbon matrix of S-2 develops a more compact and mechanically efficient structure. The results suggest that refractory performance is governed not only by total carbon content but also by the distribution and effectiveness of the carbon phase within the matrix.

After coking at 1000°C for 3 h, the superiority of S-2 is maintained. Its AP remains lower than S-1 (10.2 versus 12.0%), while BD remains higher (3.01 versus 2.86 g/cm³). More importantly, coked CCS increases from 318 to 522 kg/cm² (+64.1%) and MOR from 4.71 to 9.17 MPa (+94.5%). Since coking represents the development of the carbon-bonded refractory skeleton after resin pyrolysis, these results are more representative of the structural condition experienced during ladle service. The strong coked-state performance confirms that the substantial reduction in carbon does not weaken S-2; instead, the modified matrix produces a denser and stronger post-pyrolysis structure.

For the metal-zone grades, M-2 shows a different response due to the incorporation of recycled MgO–C material. In the tempered condition, AP increases from 2.8 to 3.9%, BD decreases from 3.07 to 2.92 g/cm³, and CCS and MOR decrease by 22.2% and 30.2%, respectively, relative to M-1. This behavior is consistent with greater heterogeneity and additional interfaces introduced by recycled refractory particles. However, after coking, M-2 develops improved mechanical properties: CCS increases from 340 to 362 kg/cm² and MOR from 5.95 to 6.70 MPa (+12.7%) compared with M-1. Thus, although the recycled grade shows somewhat inferior

tempered properties, its post-coking load-bearing structure is fully adequate. Overall, S-2 demonstrates a significant improvement over S-1 with much lower carbon content, while M-2 achieves coked-state properties comparable to or better than M-1 despite the high recycled-material addition, supporting the suitability of both developed grades for steel-ladle application.

Table 1. Physical properties and alkali–sulfur test response

Property	S-1	S-2	M-1	M-2
Tempered				
AP (%)	4.6	2.2	2.8	3.9
BD (g/cm³)	2.97	3.13	3.07	2.92
CCS (kg/cm²)	427	712	532	414
MOR (MPa)	19.56	26.46	23.01	16.07
Fixed carbon (%)	14.2	5.8	10.4	10.1
Coked at 1000°C				
AP (%)	12	10.2	10.8	13.8
BD (g/cm³)	2.86	3.01	2.97	2.82
CCS (kg/cm²)	318	522	310	362
MOR (MPa)	4.71	9.17	5.95	6.7

S-2 exhibits a substantially improved oxidation response compared with S-1. After 1, 2 and 3 h at 1000°C, the decarburized-layer thicknesses of S-2 are 1.80, 2.49 and 4.17 mm, respectively, compared with 2.66, 3.26 and 8.55 mm for S-1. The difference becomes particularly pronounced with prolonged exposure; after 3 h, S-2 shows a 51.2% lower decarburization depth, indicating a markedly slower inward progression of the oxidation front. For comparative assessment, the parabolic index , calculated from the 3 h data, decreases from 24.37 mm²/h for S-1 to 5.80 mm²/h for S-2, corresponding to a 76.2% reduction.

The improved performance of S-2 indicates that the modified low-carbon matrix restricts oxygen ingress more effectively despite its much lower total carbon content. The superior oxidation resistance of S-2, despite its lower carbon content, is attributed to reduced oxygen permeability through a denser matrix, more uniform carbon distribution, and a more effective antioxidant system, which together suppress oxygen transport and carbon oxidation. The denser structure observed for S-2 is also consistent with a lower accessible pore network, which can reduce oxygen transport toward the interior carbon phase and delay development of the decarburized zone.

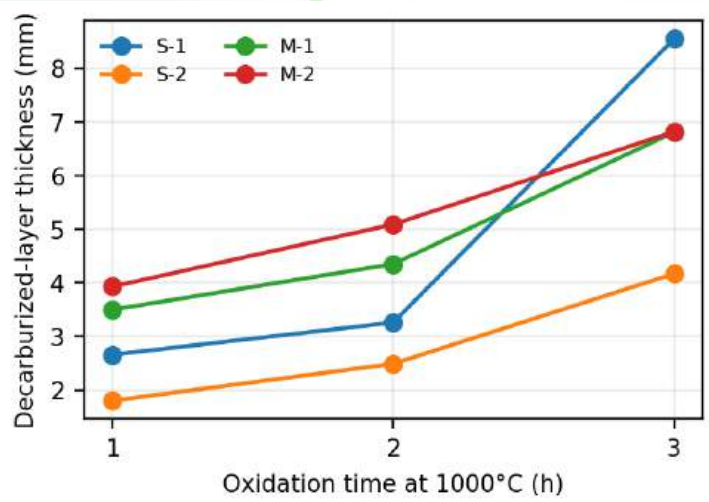


Fig 1: Oxidation response at 1000°C vs measured decarburized-layer thickness

Mass-change measurements also confirm the oxidation test findings. However, the non-monotonic mass changes observed for S-1 and the metal-zone grades indicate that specimen mass is influenced by several competing mechanisms, including carbon oxidation, formation of solid oxidation products and possible material loss from the surface. Consequently, mass change alone should not be interpreted as a direct measure of carbon consumption. In the present study, decarburization depth together with residual mechanical strength provides a more reliable engineering assessment of oxidation-induced degradation. Overall, the significantly lower oxidation-front penetration of S-2 confirms that substantial carbon reduction can be achieved without sacrificing, and in this case, while improving oxidation durability.

The post-oxidation mechanical properties further differentiate the two slag-zone grades. After 3 h of oxidation at 1000°C, S-2 retains a CCS of 209 kg/cm² and MOR of 5.05 MPa, compared with only 71 kg/cm² and 2.27 MPa, respectively, for S-1. When normalized with respect to the corresponding coked-state strength, S-2 retains 40.0% of its coked CCS, whereas S-1 retains only 22.4%. MOR retention follows the same trend, with values of 55.1% for S-2 and 48.2% for S-1. These results confirm that the lower-carbon S-2 matrix is not only more resistant to oxidation-front penetration but also preserves a considerably larger fraction of its load-bearing structure after carbon degradation. The higher absolute residual CCS and MOR indicate that oxidation-induced pore formation and matrix weakening are less severe in S-2.

The metal-zone grades show a less distinct separation. After 3 h of oxidation, the decarburization depths of M-1 and M-2 are essentially identical at 6.81 and 6.82 mm, respectively. At the same exposure time, M-2 retains 47.9 kg/cm² CCS and 2.35 MPa MOR, compared with 61.2 kg/cm² and 2.65 MPa for M-1. However, at 2 h M-2 shows a higher residual CCS of 125 kg/cm², compared with 84.7 kg/cm² for M-1. The absence of a consistent advantage across all exposure periods indicates that M-2 should be considered broadly equivalent rather than superior to the conventional metal-zone grade.

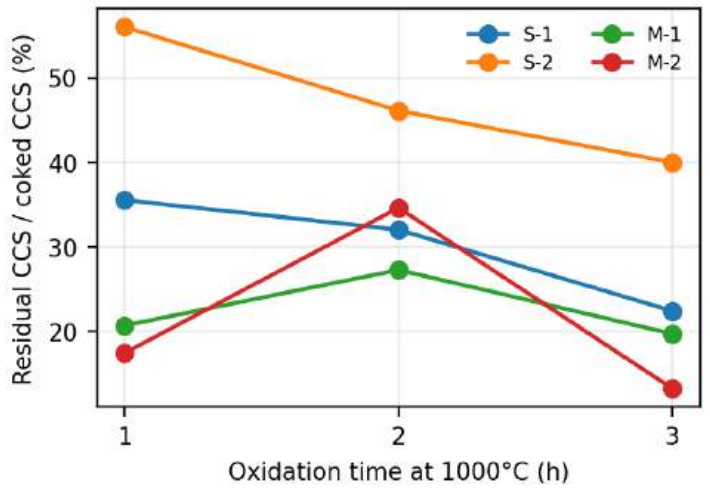


Fig 2: Oxidation vs Residual CCS

The greater scatter observed for M-2 is consistent with the more heterogeneous structure expected from a refractory containing a substantial recycled MgO–C fraction. Variations in recycled aggregate condition, residual carbon, pre-existing pores, and recycled particle/matrix interfaces can locally influence oxidation penetration and crack development. Nevertheless, the comparable decarburization depth and overall residual-strength response indicate that incorporation of recycled material does not cause a major deterioration in oxidation performance

.

The static corrosion test further confirms the improved slag-zone performance of S-2. A synthetic slag containing 34.2% CaO, 24.8% Fe_2O_3, 17.5% SiO_2, 9.2% Al_2O_3 and 8.9% MgO, with minor TiO_2 (1.3%), MnO (1.4%), Cr_2O_3 (0.8%) and V_2O_5 (0.2%), was used for the static corrosion test. For the metal corrosion test, steel scrap was used as the metallic charge to evaluate the interaction of the refractory with molten metal under test conditions. Relative to the initial cavity depth, the depth increased by approximately 60% for S-1 and 36% for S-2, corresponding to about a 40% reduction in net penetration depth for S-2 compared with S-1. Overall, S-2 shows the most significant improvement in resistance to slag penetration.

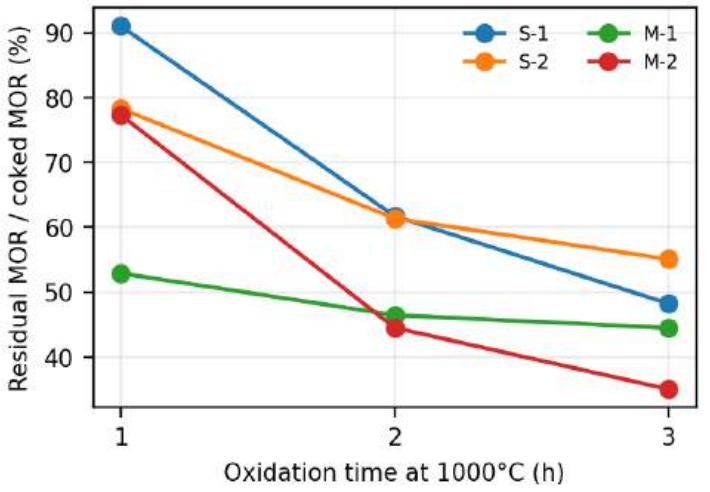


Fig 3: Oxidation vs Residual MOR

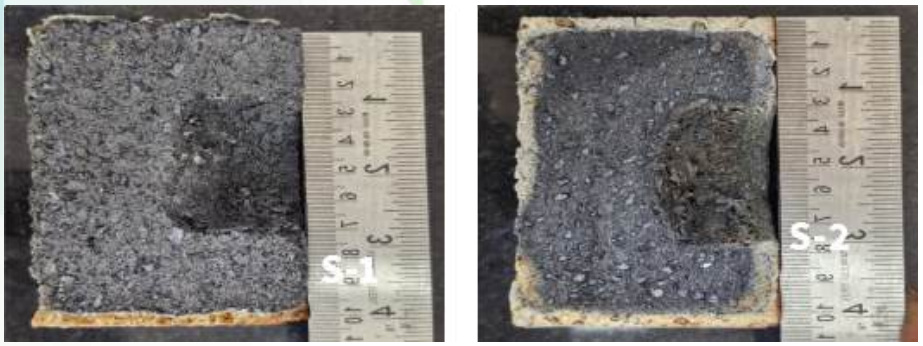


Fig 4: Static Slag Corrosion Samples

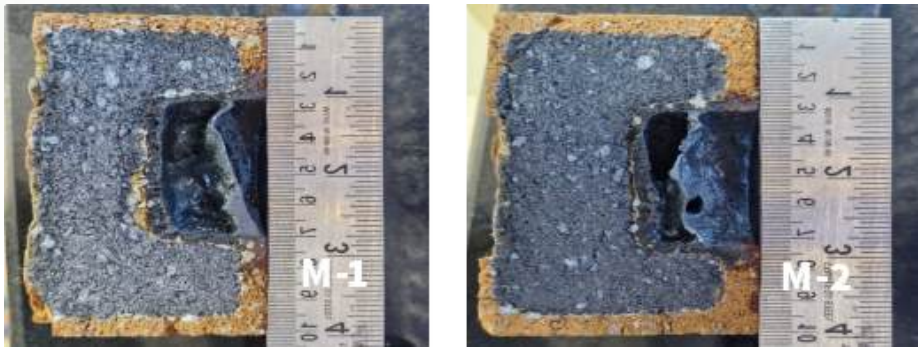


Fig 5: Static Metal Corrosion Samples

The improved corrosion geometry of S-2 is consistent with its lower apparent porosity, higher coked strength and reduced decarburization depth discussed earlier. A denser and mechanically stronger matrix can restrict slag penetration and slow the progressive opening of pathways created by carbon oxidation. The smaller cavity and interface-zone dimensions therefore support the conclusion that the low-carbon S-2 composition maintains, and in this test improves, resistance to slag-induced degradation despite its substantially lower carbon content.

For the M-series, the depth increased by approximately 52% for M-1 and 48% for M-2, giving only about a 7.7% reduction in net penetration depth for M-2 compared with M-1. Importantly, this comparable behavior is achieved despite the incorporation of recycled MgO–C material, supporting the technical feasibility of the recycled grade for metal-zone application.

4. CO Emission Modelling

The combined CO_2e reduction achieved by replacing the S-1 and M-1 configuration with S-2 and M-2 is approximately 35.07 t CO_2e per ladle. The larger contribution comes from the M-2 configuration, mainly due to the increased use of reclaimed raw materials and the corresponding reduction in virgin raw-material consumption. These results show that the transition from Case 1 to Case 2 can significantly reduce the overall carbon footprint associated with the refractory lining.

5. Conclusion

i) S-2 is an energy-efficient slag-zone formulation with superior overall performance compared with regular S-1, showing improved strength, lower porosity, reduced carbon content, and better oxidation/corrosion resistance.

ii) S-2 also exhibits significantly lower decarburization and slag-corrosion damage than S-1, indicating improved durability and

service potential.

iii) M-2 is an energy-efficient metal-zone formulation incorporating recycled MgO-C. Compared with regular M-1, it maintains comparable oxidation resistance while offering improved coked strength and slightly better corrosion performance.

iv) Overall, replacing S-1/M-1 with the energy-efficient S-2/M-2 system reduced CO_2e emissions by approximately 35.07 t per ladle, mainly through higher reclaimed-material use and lower virgin raw-material consumption.

6. References

[1] R. Kundu and R. Sarkar, "MgO-C refractories: A detailed review of these irreplaceable refractories in steelmaking," Interceram, 70(3) (2021) 46–55.

[2] M. Bag, S. Adak and R. Sarkar, "Study on low carbon containing MgO-C refractory: Use of nano carbon," Ceramics International, 38 (2012) 2339–2346.

[3] M. Bag, S. Adak and R. Sarkar, "Nano carbon containing MgO-C refractory: Effect of graphite content," Ceramics International, 38 (2012) 4909–4914.

[4] S. Behera and R. Sarkar, "Low-carbon magnesia-carbon refractory: Use of N220 nanocarbon black," International Journal of Applied Ceramic Technology, 11(6) (2014) 968–976.

[5] M.F. dos Santos et al., "Enhanced numerical tool to evaluate steel ladle thermal losses," Ceramics International, 44 (2018) 12831–12840.

[6] K. Moritz et al., "Magnesia-carbon refractories from recycled materials," International Journal of Ceramic Engineering & Science, 4 (2022) 53–58.

[7] K. Christmann et al., "Case studies of high-recycling containing magnesia-carbon bricks in high-performance steelmaking applications," RHI Magnesita Bulletin (2024).

[8] L. Horckmans, P. Nielsen, P. Dierckx and A. Ducastel, "Recycling of refractory bricks used in basic steelmaking: A review," Resources, Conservation and Recycling, 140 (2019) 297–304.

[9] RHI Magnesita, "Technical product data for MgO-C grades SYNCARBON C F1T05X, ANCARBON F6T10 and ANCARBON F3T14," RHI Magnesita technical datasheets (2017–2018), thermal conductivity at 1000°C.

TAILORING 80% ALUMINA CEMENTS FOR HIGH-PERFORMANCE REFRACTORY CASTABLES

G. Bhattacharya, C. Wöhrmeyer, C. Parr
(Imerys S.A, France)

Corresponding author's e-mail: goutam.bhattacharya@Imerys.com

Abstract

80% alumina calcium aluminate cements (CAC) are widely used for high-temperature refractory applications, particularly valued for their purity and capacity to form dense microstructures. However, optimizing refractory systems requires a comprehensive understanding of how different cement grades perform in practical applications. This study compares three distinct 80% alumina CACs: Secar® XT, Secar® 80, and Secar® Plenium. Mineralogy and physical properties of these cements in both sand mortar and model castable systems reveal how their mineralogy and specific surface areas lead to distinct rheological and mechanical behaviors. Reactivity is the key factor in determining suitability for specific applications. Secar® XT, with its high reactivity, is well-suited for rapid-hardening repairs such as patching and gunning. In contrast, Secar® Plenium offers superior flow retention and lower water demand, making it ideal for casting and shotcreting. Secar® 80 acts as a versatile middle ground, bridging the performance differences between the two. These results provide a practical framework for manufacturers to select the most appropriate binder for their monolithic refractory needs.

Keywords: 80% alumina cement, Mineralogy, Reactivity, Performance flexibility

1. Introduction

80% alumina calcium aluminate cements (CAC) are favored in high-refractoriness applications due to their higher purity and low water demand, which enable the formation of dense, sub-micron microstructures [1]. These materials mitigate the characteristic 'low strength' observed in 70% alumina CAC-bonded castables between 800°C and 1100°C by accelerating the formation of the calcium dialuminate (CA_2) phase at the time of castable heat up. Consequently, 80% alumina CAC imparts a stable mineralogical and microstructural matrix, enhancing abrasion resistance and resistance to metal penetration.

These cements have been utilized extensively in monolithic refractory systems for many decades. When formulated with high-purity alumina aggregates, such as white fused or tabular alumina, a simple regular castable with 20% CAC (80% alumina) can withstand service temperatures up to 1800°C, primarily due to the absence of silica. Despite a significant CaO content (~4%), these systems facilitate the in situ formation of calcium hexaluminate (CA_6, melting point 1870°C) through reaction between calcium aluminate phases (CA and CA_2) and the fine alumina of the composition. 80% alumina CACs are particularly valued in non-ferrous applications including petrochemical, glass, and carbon black industries where high purity is desired. Adoption patterns vary by region; notably, in Japan and Korea, these materials are widely employed in deflocculated castables, particularly for steel ladle monolithics.It is preferred in dry-gunning applications due to their high reactivity, making them suitable for rapid-hardening. In India, however, the market penetration has been limited despite its potential, largely due to the lack of domestic production.

This study characterizes the performance of three 80% alumina CAC products - Secar® XT, Secar® 80, and Secar® Plenium, which demonstrate diverse reactivity profiles. Through an analysis of their mineralogical composition and physical properties, this investigation evaluates their behavior in a model castable composition and determines their suitability for specific refractory applications..

2. Materials and Experimental Procedure

Chemical analysis of the three 80% alumina CAC products (Table 1) shows that Secar® 80 and Secar® Plenium possess comparable Al_2O_3 and CaO%, whereas Secar® XT has slightly lower Al_2O_3 levels and a higher CaO content.

Table 1: Typical Chemical analysis of the three 80% alumina CACs

Chemistry (wt%)	Secar® XT	Secar® 80	Secar® Plenium
Al_2O_3	80.0	81.1	81.8
CaO	19.2	17.5	17.4

Despite minor variations in chemical composition (<2% variance for individual constituents) among the cements, X-ray diffraction (XRD) analysis revealed significant divergence in their mineralogical profiles (Fig. 1). Secar® XT occupies a distinct position near the top right corner in the CA/CA_2 versus $C_{12}A_7/CA$ plot, indicative of a more reactive phase assemblage, whereas Secar® 80 and Secar®Plenium display similar characteristics. The Blaine specific surface area of the cements follows the order: Secar® XT>Secar® Plenium>Secar® 80 (Fig. 2).

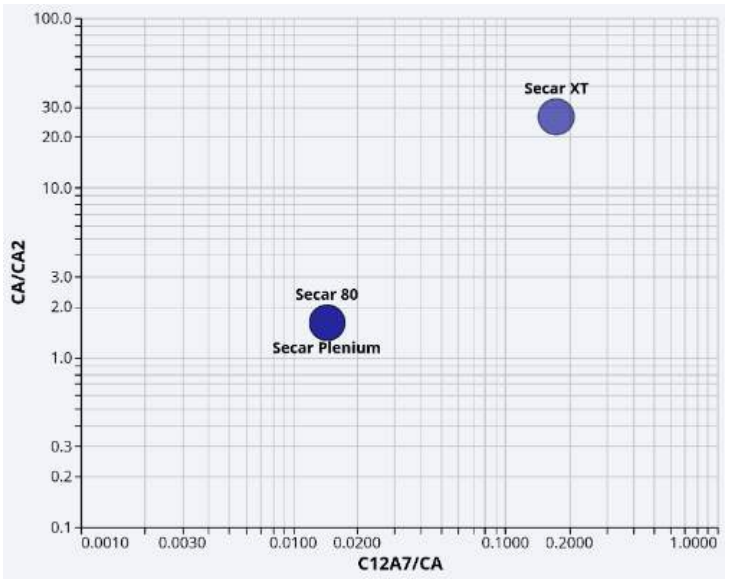


Fig. 1: Mineralogical ratio comparison for 80% alumina CACs

CA = $CaO.Al_2O_3$, CA_2 = $CaO.2Al_2O_3$, $C_{12}A_7$ = $12CaO.7Al_2O_3$, A = Al_2O_3

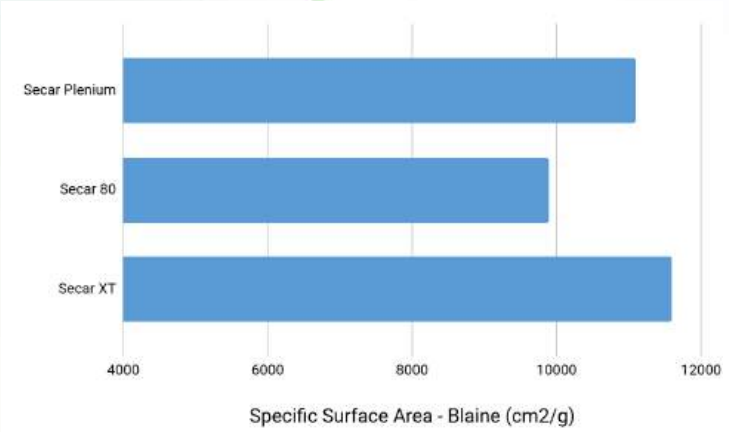


Fig. 2: Typical Blaine specific surface area values for the three 80% alumina CACs

Two compositions were evaluated to characterize the cements: a standard sand mortar and a tabular alumina based regular castable.

Sand mortar

Mortars were prepared using European standard sand compliant with EN 196-1 and ISO 679 (Table 2). The water-to-cement ratio was optimized to maintain consistency within testing limits. Physical properties, including tap flow, Vicat set time, and compressive strength, were assessed. Tap flow was determined using an ASTM C230 flow cone and a shock table; flow % was quantified by the average increase in diameter following 25 drops immediately after mixing, with further measurements of flow at specific intervals for the flow decay. Initial and final set times were measured using an automatic Vicat apparatus according to EN 196-3, and compressive strength was evaluated using 160 × 40 × 40 mm prisms in accordance with EN 196-1 after curing at 20°C and >90% relative humidity, demoulding and breaking the prism in two halves from the middle.

Table 2: Mortar compositions for testing 80% alumina cements

	Secar® Plenium	Secar® 80	Secar® XT
European Standard Sand (g)	1350	1350	1350
Cement (g)	500	500	500
Water (g)	160	180	180
Water/Cement (W/C)	0.32	0.36	0.36

Regular castable

The cements were evaluated using a tabular alumina-based regular castable composition (Table 3). After wet mixing, the castable's vibration flow was assessed using an ASTM C230 flow cone, with measurements taken from initial mixing until complete flow decay. Prisms (160 × 40 × 40 mm) were cast, demolded after 24h curing at 20°C, and dried 24 h at 110°C. Subsequently, samples were fired at temperatures ranging from 500°C to 1550°C. The Cold Crushing Strength (CCS) was determined for cured, dried, and fired specimens. Apparent porosity was evaluated using the water boiling method using Archimedes principle, and the Hot Modulus

of Rupture (HMOR) was assessed after firing samples at 1450°C for 30 minutes.

Table 3: Model castable composition to compare 80% alumina CAC

Raw material	Wt %
Tabular alumina 0-6 mm	85
80% alumina CAC	15
Total	100

3. Results and discussion

Sand mortar

While initial flow for all three cements were comparable, Secar® Plenium achieved this despite a lower water-to-cement (w/c) ratio. After 30 minutes of mixing, flow retention for Secar® Plenium was significantly higher than for the other two cements (Fig. 3) and Secar® 80 showed much higher flowability than Secar® XT. Setting characteristics further differentiated the products: Secar® XT and Secar® 80 exhibited accelerated Vicat setting, whereas Secar® Plenium demonstrated significantly long set times. As shown in Fig. 3, these performance profiles correspond to distinct reactivity levels, with Secar® XT showing the highest reactivity—indicated by rapid setting and minimal flow retention—followed by Secar® 80, whereas SecarPlenium showed long setting and high flow retention.

Compressive strength development (Fig. 4) correlates with these setting observations. At 8h, Secar® XT achieved the highest compressive strength of the 3 cements, followed by Secar® 80, while Secar® Plenium showed no strength, consistent with its extended setting time. Despite comparable final set times for Secar® XT and Secar® 80, the higher 8h compressive strength of Secar® XT points to more rapid early hardening. By 24h, all three cements developed significant compressive strength, following the order: Secar® XT >Secar® 80 >Secar® Plenium.

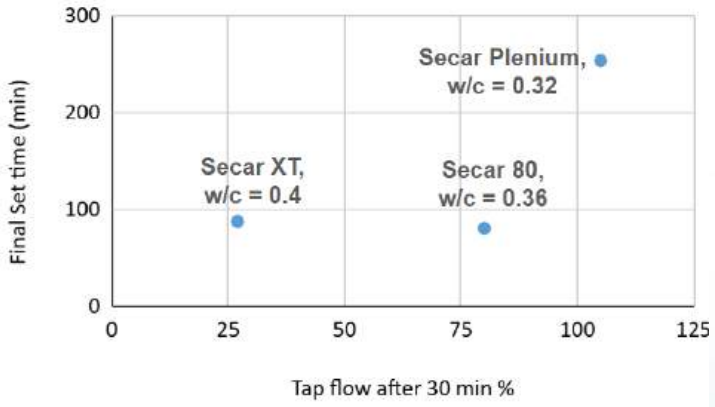


Fig. 3: Relationship between final setting time (min) and tap flow after 30 minutes for the 80% alumina cement based mortars (Table 1)

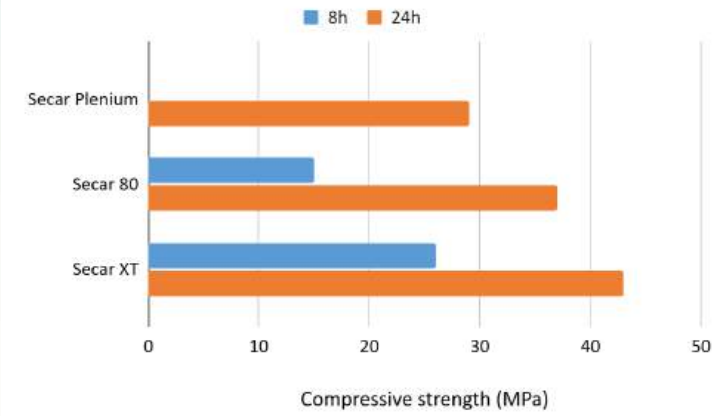


Fig. 4: Comparative compressive strength of mortars with the three 80% alumina CACs, measured after 8h and 24h of curing at 20°C

Application test in a regular castable

Water demand of the regular castables was optimized to achieve a consistent initial vibration flow of approximately 100%. Secar® Plenium showed high flowability, requiring only 5.5% water, whereas Secar® 80 and Secar® XT needed 6.7% and 7.0% water, respectively (Fig. 5). For a 7% water addition, Secar® Plenium exhibited very high flow compared to the other cements. Consistent with observation in standard sand mortar, Secar® Plenium with an adapted water addition of 5.5% retained flow over a long duration despite its lower water demand, reaching "no flow" after 2h. Conversely, Secar® XT displayed very rapid flow decay, faster than Secar® 80. The prolonged working time and reduced water demand of Secar® Plenium are attributed to its specific integrated additive system, whereas the accelerated flow decay of Secar® XT results from the higher reactivity of its relatively higher $C_{12}A_7$ mineralogical phase (Fig. 1). This is further corroborated by the exothermic profiles (Fig. 6), where Secar® Plenium exhibited a delayed exothermic peak at 785min from mixing compared to the more reactive Secar® 80 (550 min) and Secar® XT (456 min) based compositions.

After 24h curing, all three cements achieved comparable cold crushing strength (CCS), despite the significantly lower water demand for Secar® Plenium (Fig. 7). This observation likely reflects the slower initial reactivity imparted by its integrated additives. While this lower reactivity is more pronounced in the sand mortar composition, indicated by relatively lower 24h compressive strength compared to Secar® 80 and Secar® XT, the model castable formulation appears to leverage the accelerating effect of fine alumina offsetting this effect [2]. Secar® Plenium samples exhibited significantly higher CCS values, after 24h drying at 110°C and firing 6h at 800°C, 1100°C, and 1500°C, primarily due to the lower water-to-cement ratio and the resulting lower apparent porosity (Fig. 8). Above 1100°C porosity of Secar® Plenium based castable started increasing (Fig. 8) probably due to the early onset of expansive CA_6 formation thanks to its higher surface area. Apparent porosity of the other 2 cements decreased between 800°C and 1350°C, attributed to sintering, before increasing due to expansive calcium hexaluminate (CA_6) formation [3]. Secar® 80 displayed elevated strength between 110°C and 800°C, potentially linked to its higher calcium dialuminate (CA_2) content, which hydrates at higher temperatures. Above 600°C, a decline in CCS was observed for all compositions, consistent with the dehydration of calcium aluminate hydrates. The minimum strength for Secar® 80 occurred at 1100°C, while Secar® XT reached this minimum at 800°C, likely due to its higher specific surface area facilitating accelerated ceramic bond formation.

Secar® Plenium and Secar® 80 yielded comparable hot modulus of rupture (HMOR) at 1450°C, whereas Secar® XT achieved

higher hot strength (Fig. 9). This difference may not be fully attributed to the liquid phase content, as both Secar® 80 and Secar® Plenum demonstrated increased HMOR values when tested at 1500°C compared to 1450°C.

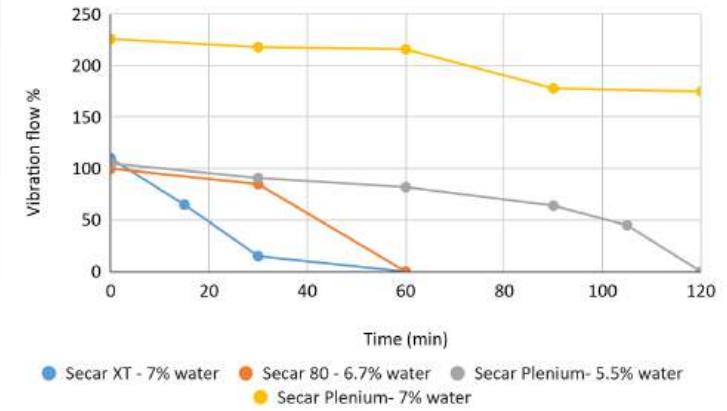


Fig. 5: Evolution of vibration flow over time for 80% alumina CACs in a model regular castable composition.

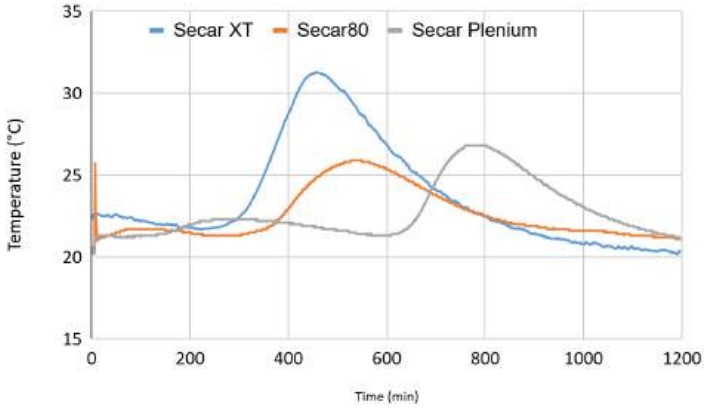


Fig. 6: Exothermic Peak Time (min) of the model regular castable with the three 80% alumina CAC

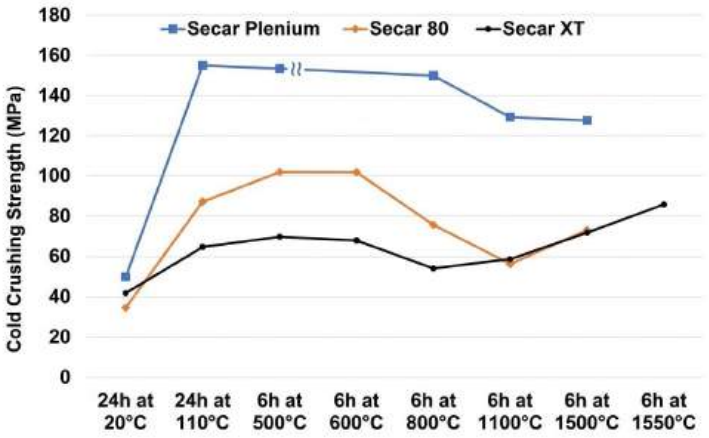


Fig. 7: Effect of heat treatment temperature on the cold crushing strength (CCS) of model regular castables bonded with the three 80% alumina CACs.

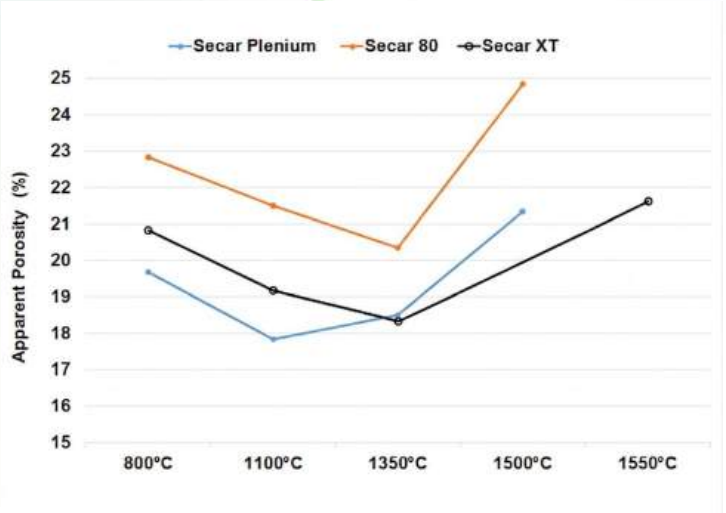


Fig. 8: Evolution of apparent porosity in model regular castables bonded with the three 80% alumina CACs as a function of firing temperature.

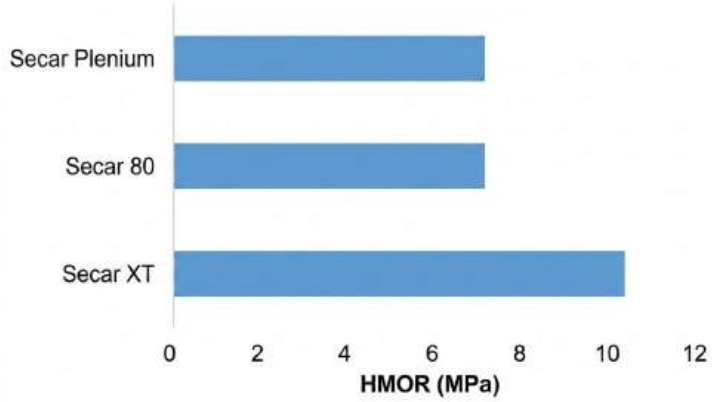


Fig. 9: Hot Modulus of Rupture (HMOR) after 30min at 1450°C of the model regular castable with the three 80% alumina CAC

Applications

The application suitability of the three 80% alumina calcium aluminate cements—Secar® XT, Secar® Plenium, and Secar® 80—is dictated by their distinct reactivity profiles and physical properties. Secar® XT, characterized by its highest reactivity, is particularly well-suited for patching and gunning applications, though its use in casting requires adaptation to accommodate its shorter working time. In contrast, Secar® Plenium is optimized for casting and shotcreting, where its superior deflocculation and reduced water demand promote enhanced dried and fired strength. Secar® 80 functions as a versatile intermediary, offering a balanced reactivity that permits its effective use across a broad spectrum of casting, dry-gunning, and patching applications.

4. Conclusion

This investigation confirms that the three 80% alumina calcium aluminate cements (CAC): Secar® Plenium, Secar® 80, and Secar® XT exhibit distinct performance characteristics driven by variations in their mineralogical composition, specific surface area, and integrated additive systems. Secar® XT demonstrates the highest reactivity, attributed to its highest $C_{12}A_7$ content and high specific surface area, which facilitates rapid hardening and provides early strength in both mortar and castable systems, although with fast flow decay. Conversely, Secar® Plenium is characterized by significantly delayed reactivity and superior flow retention, alongside a reduced

water demand resulting in consistently higher cold crushing strength (CCS) across a wide temperature range (110°C to 1500°C). Secar® 80 acts as an intermediate performer, exhibiting enhanced strength development between 110°C and 800°C, likely linked to its higher calcium dialuminate (CA_2) content. Across all formulations, apparent porosity reduces initially due to sintering up to 1100°C–1350°C, followed by an increase at higher temperatures due to in-situ formation of expansive calcium hexaluminate (CA_6).

References

[1] C.Wöhrmeyer, H.Fryda, C.Parr, J.M.Auvray and V.Guillaumin, Mineralogy and microstructure evolution along the curing, drying and firing process of calcium aluminate bonded refractory castables. Proc. Int. Refractory Colloquium, EUROGRESS, Aachen, Germany, 2009

[2] G. Bhattacharya, B. Valdelièvre, C. Wohrmeyer and C. Parr, Effect of calcined and reactive alumina on placing and hardening properties of castables, Secar® Gazette, Vol. 6, April 2013

[3] J. Pelletier, C. Wöhrmeyer and C. Zetterström, Critical factors affecting the performance of refractory repair materials and the influence of calcium aluminates, Proc. 54st Annual Symposium on Refractories, The St. Louis Section and Refractory Ceramics Division of the American Ceramic Society, St. Louis, Missouri, USA, 2018

ENERGY SAVING IN STEEL LADLES WITH INNOVATIVE LINING CONCEPTS

Andreas Buhr[1], Shankha Chatterjee[2], Reinhard Exenberger[3], Georg Grimm[3], Rinus Siebring[4], Warbout Tesselaar[4], Danny Schreiber[5], Antti Piippo[6], Eeva-Liisa Pisilä[6], Jerry Dutton[7]

1. Almatis GmbH Frankfurt, Germany, 2.Almatis Alumina Private Ltd. Kolkata, India, 3. voestalpine Stahl Gmbh Linz, Austria 4. Tata Steel Europe IJmuiden, The Netherlands, 5. Badische Stahlwerke Kehl, Germany, 6. SSAB Steel Raahe, Finland, 7. Stourbridge, United Kingdom

andus.buhr@almatis.com

Abstract

The paper discusses the impact of the steel ladle wear lining on temperature loss of steel in the ladle.

Carbon-free alumina-spinel refractories provide a clear advantage over carbon containing linings such as MgO/C due to significantly lower thermal conductivity. The new development of lower bulk density alumina aggregate ECO-TAB® and testing results from different steel works are reported.

1. Introduction

From the various requirements of steel ladle linings, energy saving has gained importance in recent years and is gaining increased focus in steelworks (fig. 1). Temperature loss of steel in the ladle also depends on the refractory lining. Specifically designed lining concepts with thermally insulating layers to reduce heat transport to the steel shell were introduced in the 1990s and have now become standard practice

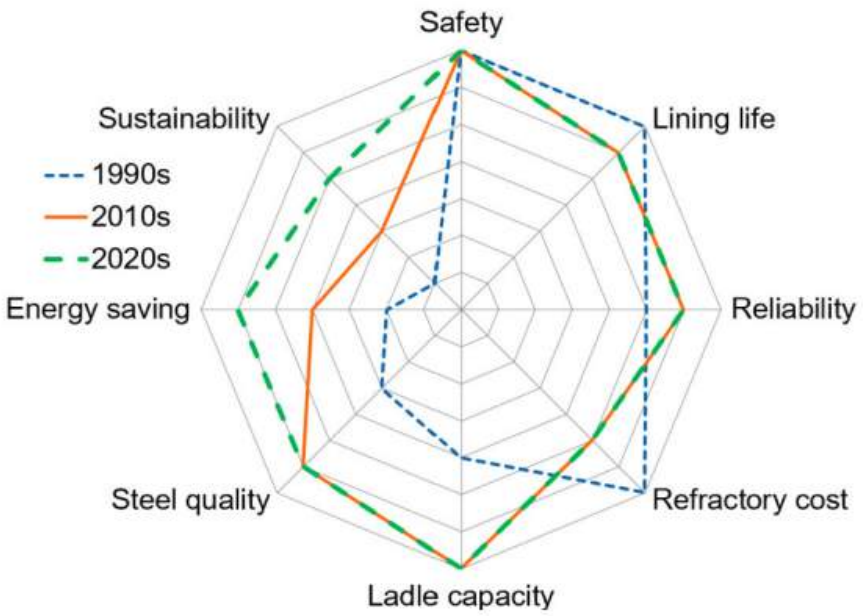


Figure 1 Requirements on steel ladle lining[1]

However, there is also heat loss at the hot face of the lining during the time when the ladle is empty (fig. 2). The heat lost due to cooling of refractories on the hot face will be taken from the next charge of steel, This needs to be addressed by either increasing the tapping temperature into the ladle or reheating the steel by ladle furnace or

aluminothermic heating. The cost for such steel temperature loss is in the range of 0.1€ per Kelvin per tonne of steel.

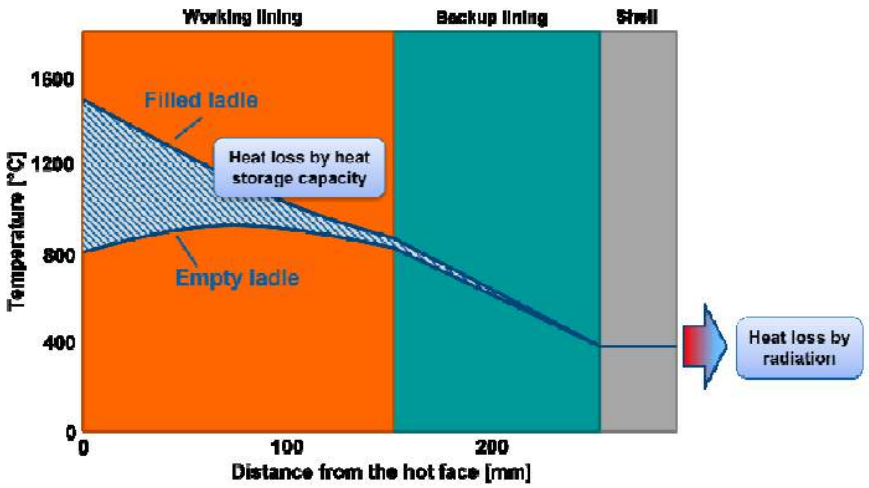


Figure 2 Schematic drawing of the temperature change in the refractory lining of a steel ladle during operation. Drawing after Ogata et al.[2]

2. Steel temperature loss

The amount of heat loss of the refractory wear lining depends on the thermal conductivity and heat capacity of this layer. Here, carbon-free aluminaspinel linings provide a clear advantage over carbon bonded graphite containing basic refractory bricks (tab. 1).

Table 1 Properties of wear lining material

	MgO/C	Alumina – Spinel (5% MgO)		
	Brick	Fired brick	Castable Tabular	Castable ECO-TAB®
Carbon [%]	10-15	-	-	-
BD [g/cm³]	2.9	3.1	3.04	2.87
BD [g/cm³]	8-10	3	2.9	2.6

Fig. 3 shows calculated steel temperature losses from tapping to casting in the Tata Steel Europe IJmuiden ladle model with different lining concepts in the steel ladle. The MgO/C brick wear lining with microporous insulation has 11 K higher temperature loss when compared with a fired alumina-spinel brick lining using the same insulation. Based on 0.1 € per K per tonne of steel, that would mean a higher production cost of 1.1 € per tonne of steel using MgO/C rather than alumina-spinel in the lining.

A comparison of electric power consumption in the ladle furnace with different ladle lining concepts in the side wall was presented by voestalpine Stahl Linz[4]. A steel grade that required intensive secondary metallurgy treatment was selected for this comparison. Even with an additional insulation layer, the power consumption was 4.6 kWh per tonne of steel higher for the MgO/C brick lining compared to the alumina-spinel castable lining. Assuming an industrial power price of 0.1 €/kWh, that means a higher production cost of 0.46€ per tonne of steel.

Such higher cost due to energy losses with carbon containing lining must be taken into account when evaluating the specific refractory cost for steel ladle lining concepts which are typically in the range of 1.5-2 € per tonne of steel.

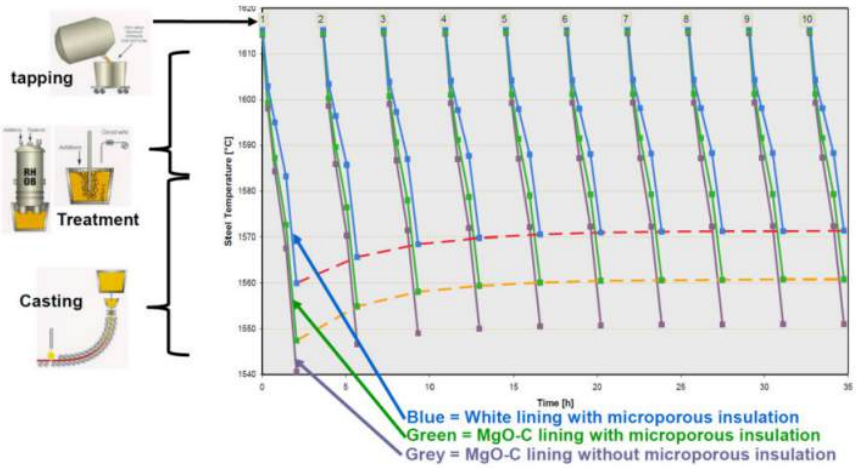


Figure 3 Steel temperature loss with different lining concepts during the first ten heats [3]

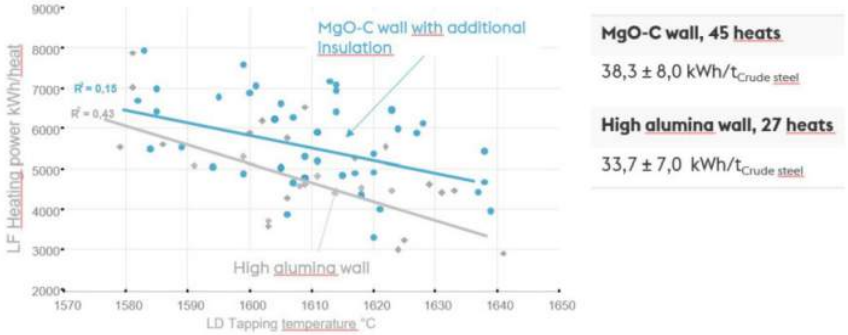


Figure 4 Electric power at ladle furnace for HIC steel grade[4]

3. New development ECO-TAB®

Alumina-spinel refractories can be further improved in the effort towards lower energy losses, by reducing bulk density and thermal conductivity. Here, the main aggregate in the refractories plays a key role. Therefore the idea was to develop a new sintered alumina aggregate with lower bulk density than tabular alumina T60/T64 or white fused alumina but with comparable wear resistance for ladle wear lining. This would result in a reduced weight steel ladle wear lining leading to a higher tapping weight when the crane weight limit is reached. In addition, it would reduce the thermal conductivity and heat capacity of the wear lining resulting in lower heat losses of steel in the ladle.

The idea of a new sintered alumina aggregate was discussed in the Stage-Gate process which is used for new product developments within Almatis. The question raised was whether the value created in the steel ladle application would be sufficient for all stakeholders in the business: Almatis as the raw material producer, refractory producers as customers, and steel plants as end users. In 2016, the motivation and advantages of applying a sophisticated steel ladle model at Tata Steel Europe IJmuiden were discussed in the keynote lecture at the International Colloquium on Refractories in Aachen, Germany[5]. The model allows a quantitative assessment of the economic impact from refractory changes in the ladle lining. The

general value proposition of the new aggregate idea was interesting for Tata Steel IJmuiden and therefore it was evaluated in the ladle model for the plant in IJmuiden[6] .

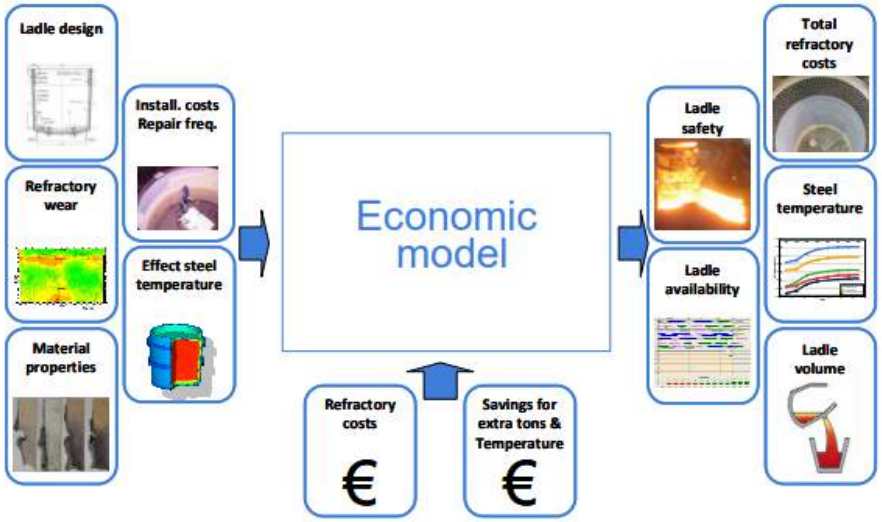


Figure 5 Schematic overview of Value in Use (ViU) model inputs and output[5]

The model evaluation of the potential new lower density Alumina-Spinel fired brick based on the new lower density refractory aggregate provided a potential gain in value high enough to justify the business case for the development of the lower density alumina aggregate. This modelling was an essential contribution to making the development decision in the Almatis Stage-Gate process. Details are discussed by Buhr et al[6] .

Table 2 Typical data of Tabular and ECO-TAB®

		T60/T64	ECO-TAB®
Bulk density	g/cm3	3.55	3.3
Open porosity	%	2	11
Water absorption	%	0.5	3.5
Al2O3 content	%	99.5	99.5

The new lower density aggregate ECO-TAB® (tab. 2) was launched at UNITECR 2023[7]. First industrial experience was gained in 2023 at a trial at Badische Stahlwerke (BSW) in Kehl, Germany. The slag line wear lining of the 109 ton steel ladle was made with a spinel forming ultra-low cement castable based on ECO-TAB® instead of regular tabular alumina. Despite a slightly higher water demand of about 1%, the wear and slag infiltration was comparable to the standard castable and cleaning prior to relining went very well (fig. 6).



Figure 6 ECO-TAB® castable after 91 heats at BSW and cleaning prior relining

In 2024 SSAB Raahe Finland started rigorous testing of a new spinel-forming ladle castable based on ECO-TAB® .Detailed results were reported at UNITECR 2025[8]. Initial repair tests indicated that the new castable maintained the same wear resistance as the regular castable. Subsequent trials, which included a complete lining of the bottom and side-wall (excluding the slag line), confirmed the comparable wear behaviour of the new castable (fig. 7).

Extended trials provided the statistical basis to evaluate the impact of the new castable on heat losses. Fig. 8 shows that the cooling rate of steel in the ladle was reduced by 0.01K/min. With 100 min residence time in the ladle, the overall temperature loss was reduced by 1K. This practical industrial result is in the same range as the result the Tata Steel Europe IJmuiden model predicted for their steel ladle when replacing the regular aluminaspinel fired brick by the ECO-TAB® based hypothetical brick. 1K lower temperature loss with cost of 0.1€ per K per ton of steel indicates a potential annual energy cost saving of around €260,000 (2.6 million tonnes steel production per year at Raahe). The lower density of the ECOTAB® castable[8] potentially reduces the material consumption by about 5%.



Figure 7 Used steel ladle with ECO-TAB lining after 82 heats at SSAB Steel Raahe[8]

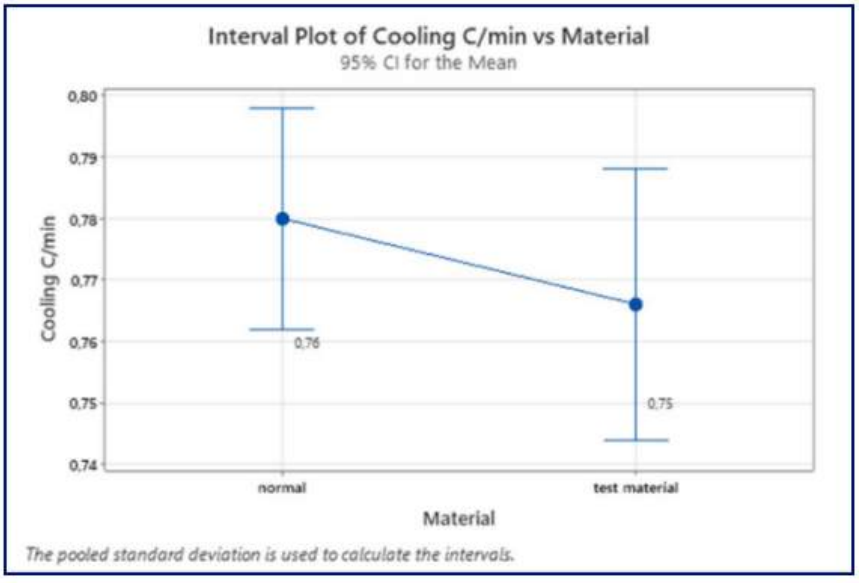


Figure 8 Cooling rate in °C/min for fully relined ladles (test material = ECO-TAB castable) at SSAB Steel Raahe[8]

4. Conclusion

Energy saving by reduced steel temperature loss in the steel ladle is a relevant economic factor when comparing and developing advanced ladle lining concepts. Carbon free refractories provide a clear advantage here due to lower thermal conductivity. New developments with reduced bulk density aggregate ECO-TAB® enable further improvement of alumina-spinel lining concepts. Lower temperature loss, lower material consumption, and potentially higher steel tapping all have a relevant economic impact for the steel works.

References

1. A. Buhr: Trends in Clean Steel Technology and Steel Ladle Lining, presentation at Seminar Steel Ladle Lining, 16-18 June 2026, Düsseldorf, Germany, www.steel-academy.com.

2. M. Ogata, M. Namba, S. Uchida and E. Maeda: Saving Energy by using Working-lining Refractories with Low Thermal Conductivity, Journal of the Technical Association of Refractories, Japan, pp. 181-184, 2015.

3. R. Siebring: Economics in Refractories Usage, presentation at Seminar Steel Ladle Lining, 16-18 June 2026, Düsseldorf, Germany, www.steelacademy.com.

4. R. Exenberger, G. Grimm: Steel Ladle 25 Years Experience in Capacity Increase, Refractories, and Recycling, UNITECR 2023, Frankfurt/Germany, pp. 371-373.

5. R. Siebring, W. Tesselaar: Refractories in a rapidly changing steel economy, ICR Aachen, 28-29 September 2016, pp. 11-16.

6. A. Buhr, S. Klaus, H.L. Groß, R. Siebring, W. Tesselaar, J. Dutton: The value of modelling for raw material development, UNITECR 2025, Cancun/Mexico, pp. 503-506.

7. S. Klaus, A. Buhr, H.L. Groß, D. Schmidtmeier, W. Zwijnenburg, J. Dutton: ECO-TAB® - a new aggregate for steel ladle lining, UNITECR 2023, Frankfurt/Germany, pp. 374-377

8. E.L. Pisilä, S. Vatanen, S. Hyttinen, H. Pärkkä, A. Piippo, K. Ruotanen, A. Buhr, S. Klaus, J. Dutton: New aggregate ladle castable at SSAB Raahe, UNITECR 2025, Cancun/Mexico, pp. 316-319.

ENHANCED CORROSION RESISTANCE OF LOW-CARBON MgO-C BRICKS FOR SECONDARY REFINING FURNACES BY FERROCHROME ADDITION

Hayate KAWANO, Koichi SHIMIZU, and Masayuki EGAMI
(Technical Research Laboratories, KROSAKI HARIMA CORPORATION, Japan)

Corresponding author's e-mail: kawano.wbi.hayate@krosaki.co.jp

Abstract

Ferrochrome (Fe ≥60 mass% Cr mother alloy), a ferroalloy, was added to low-carbon MgO-C bricks to extend their use in heavily corroded zones of secondary refining furnaces for steel under low-basicity slag. Adding 3 mass% ferrochrome together with 3 mass% graphite to the MgO-C bricks reduced the slag corrosion depth by 64%, achieving corrosion resistance close to that of burnt MgO-Cr_2O_3 bricks while preserving the bricks' original superior resistance to FeO. This improvement was attributed to a protective layer of Cr-enriched slag, a spinel solid solution, and CO bubbles formed at the slag-refractory interface through the in-situ reaction of Fe-Cr carbides with slag. The ferrochrome-enhanced grade is thus recommended as part of the low-carbon MgO-C lineup for RH degasser linings used in corrosive, low-basicity slag and during oxygen-blowing operations, to consolidate linings into eco-friendly materials with energy savings, a low carbon footprint, and high durability.

Keywords: Steelmaking, RH degasser, Low-basicity slag, In-situ reaction

1. Introduction

In the steelmaking process, the operating conditions of secondary refining furnaces have become increasingly severe due to growing demands for higher process efficiency and superior steel product quality. To meet stricter requirements for steel cleanliness and productivity, secondary refining processes such as RH degassing are increasingly operated at higher temperatures and with more intensive oxygen blowing and alloy addition. Low-basicity slag with high SiO_2 content generated during Silicon-addition refining, and high-temperature FeO splash caused by oxygen blowing, lead to wear of the refractory lining. Under such conditions, the lining refractories are required to exhibit strong resistance to slag corrosion, high temperature FeO, and thermal spalling. Burnt magnesia-chrome (MgO-Cr_2O_3) bricks have traditionally been widely used as the lining of secondary refining furnaces because of their excellent corrosion resistance against slag. Since these bricks are damaged by structural spalling caused by slag penetration, they have transitioned from highly porous direct-bonded bricks to semirebonded and rebonded bricks in which a lower porosity suppresses slag penetration. However, achieving dense microstructures requires firing at temperatures above 1700 °C, and the resulting high CO_2 emission during manufacturing has become a serious environmental concern. To mitigate these environmental effects, magnesia-carbon (MgO-C) bricks, which require a lower heat-treatment temperature, have been widely developed. Because of the low wettability of carbon by molten slag, MgO-C bricks suppress structural spalling, and the high thermal conductivity of carbon provides excellent thermal service performance. In secondary refining, however, carbon pickup by the molten steel and heat loss from the vessel must be minimized, spurring the development of low-carbon MgO-C bricks. Ishii et al.1) developed an MgO-C brick containing 3 mass% graphite and reported that its performance in the lower vessel of an RH degasser surpassed that of conventional $MgOCr_2O_3$ bricks. Terada et al.2) developed MgO-C bricks containing 2-7 mass% graphite and demonstrated that heat loss decreased with decreasing graphite content. De Melo et al.3) developed a low-carbon MgO-C brick (<1.8 mass% carbon) utilizing a specially

designed graphite. When installed in RH vessel throats, the developed bricks exhibited superior service performance compared with MgO-Cr_2O_3 bricks. Furthermore, carbon pickup from the refractory was negligible and did not affect steel quality. As reviewed above, reducing the graphite content mitigates heat loss and carbon pickup during secondary refining. However, although graphite suppresses slag penetration owing to its low wettability, it is readily oxidized by FeO, which can adversely affect the FeO corrosion resistance of the refractory. To achieve an optimal balance between these competing effects, a series of low-carbon MgO-C bricks were developed, as described below. We have developed low-carbon MgO-C bricks 4) for secondary refining furnaces(Fig. 1). Although graphite offers several advantages, the need to suppress heat loss during secondary refining has



Fig.1 Appearance of MAGreenXTM (carbon content is 2mass%).

driven the demand for refractories with reduced graphite content. MAGreenX™ was developed to meet this requirement. These bricks offer three value propositions:

(i) reduced heat loss during operation owing to low thermal conductivity
(ii) improved service life due to high resistance to high-temperature FeO
(iii) reduced CO_2 emissions during production.
These characteristics enhance operational efficiency and environmental performance in secondary refining processes.

Figure 2 shows the corrosion depth of a lowcarbon MgO-C brick (MAGreenXTM, A: 2 mass% carbon) and a burnt magnesia-chrome brick, evaluated by a drum rotating corrosion test using high-temperature FeO, high-basicity slag, and low-basicity slag (the detailed test conditions are described in Section 2.2). For the slag corrosion tests, the low-basicity slag consisted of 30 mass% SiO_2, 30 mass% CaO, 20 mass% Al_2O_3, and 20 mass% FeO, corresponding to a basicity (CaO/SiO_2 ratio) of 1. The high-basicity slag consisted of 15 mass% SiO_2, 45 mass% CaO, 20 mass% Al_2O_3, and 20 mass% FeO, corresponding to a basicity of 3. The product exhibits corrosion resistance superior to that of the burnt MgO-Cr_2O_3 brick for high-temperature FeO and high-basicity slag, whereas it is inferior to the MgO-Cr2O3 brick for low-basicity slag. Therefore, to broaden the application of the low-carbon MgO-C bricks, it is necessary to improve their corrosion resistance to low-basicity slag.

In this study, therefore, to extend the application range of low-carbon MgO-C bricks for RH degassers, their corrosion resistance to lowbasicity slag was improved while preserving their characteristic advantages on the superiority in corrosion resistance to high-temperature FeO.

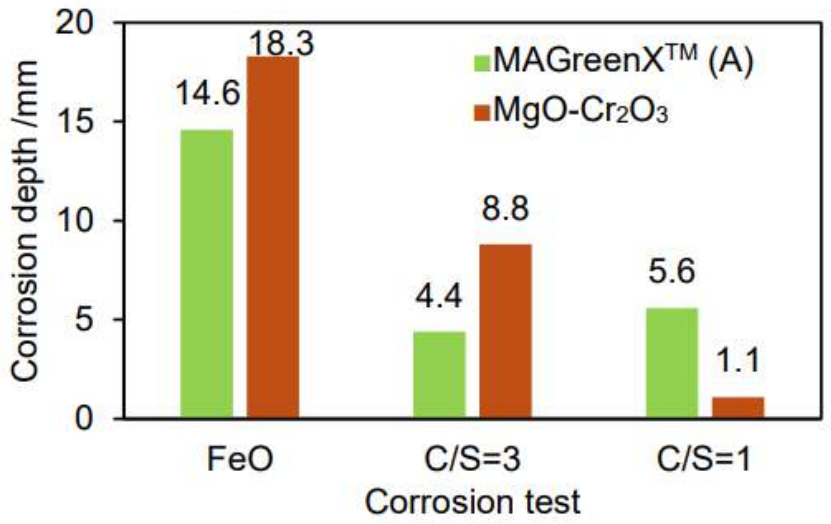


Fig.2 Comparison of corrosion depth of MAGreenX™ and burnt magnesia-chrome brick, evaluated using a drum-rotating corrosion test with high-temperature FeO, high-basicity slag and low-basicity slag.

2. Development of an Improved Grade

2.1 Ferrochrome as an in-situ reactive additive

It had been reported [5] that adding ferrochrome (Fe-Cr alloy) to burnt magnesia-chrome bricks improved corrosion resistance by forming the $MgCr_2O_4$ spinel, which fills interparticle gaps during firing and densifies the microstructure. In the present work, this concept was applied to an unfired, low-carbon MgO-C brick. The aim was to use a small quantity of ferrochrome as an in situ reactive additive that generate a protective layer at the slag-refractory interface during operation, thereby improving the resistance to slag of the MgO-C bricks.

2.2 Sample preparation and evaluation methods

Raw materials with phenolic resin as a binder were molded to 230×100×110 mm using a vacuum hydraulic press, and then dried at 250 °C for 5 h. Apparent porosity and bulk density of each fabricated brick were measured after drying and after heat treatment at 1400 °C under carbothermal reduction, using the Archimedes method in accordance with JIS R2205 on test pieces measuring 20×20×80 mm. The elastic modulus was determined through calculating the propagation velocity of ultrasonic waves. Table 1 shows the composition of the test bricks and their physical properties. A low-carbon MgO-C brick containing >90 mass% electro-fused MgO was used as the base brick (A). Ferrochrome powder (Cr ≥60 mass%) was fixed at 3 mass%, and graphite was added at 0 and 3 mass% (B-0, B-3). A conventional semi-rebonded fired MgO-Cr_2O_3 brick (SRB) was used as a reference material.

Table 1 Composition and mechanical properties for the test bricks heat-treated at 250 ℃×5 h (i)and 1400 ℃×10 h

Test brick			A		B-0		B-3		SRB
Composition /mass %	Base		MgO-C						MgO-Cr_2O_3
	Additive	Ferrochrome (Cr >60 mass%)	-		3				
		Additional Graphite	-				3		
Condition			i	ii	i	ii	i	ii	
Bulk density /g·cm−3			3.23	3.21	3.26	3.27	3.22	3.24	3.22
Apparent porosity /%			3.5	7.7	4.1	8.5	3.2	7	14.2
Elastic modulus /GPa			85.6	71.8	85.2	88.5	76.5	68.4	48.3

Slag corrosion resistance was evaluated using a rotary furnace lined with test pieces on the inner wall, each with a trapezoidal cross-section. The central part of the drum furnace was heated with an oxygen-propane gas burner and maintained at 1700-1750 °C while the drum rotated. Then, 2 kg of slag was charged; the drum was rotated for 30 min; the slag was discharged; and new slag was charged.

This sequence was repeated 10 times for a total of 5 h. The slag composition was SiO_2: 30 mass%, CaO: 30 mass%, Al_2O_3: 20 mass%, FeO: 20 mass%, and the basicity (CaO/SiO_2 ratio) was 1. After the test, the corrosion depth was calculated by averaging six points on the cross-section of the test piece where material had been removed by wear. The corrosion index was calculated to compare the corrosion resistance of the test bricks, expressing each brick's measured corrosion depth as a ratio to the corrosion depth of the reference brick (A), which was set to 100. The lower the corrosion index, the higher the corrosion resistance.

FeO corrosion resistance was evaluated using the same apparatus and cross-section, positioned at the center of the drum furnace, as in the slag corrosion test. Oxygen blowing in the RH degasser was simulated by blowing oxygen from a steel lance into the center of a rotary furnace. Oxygen blowing for about 2 min 30 s and FeO slag exchange were repeated 10 times, resulting in a total test time of about 25 min. After the test, the evaluation method was the same as that used in the slag corrosion test. The corrosion depth was measured, and a corrosion index was calculated to compare the test bricks.

Thermal shock resistance was evaluated by subjecting the material to three repeated cycles of 90 s immersion in molten iron at 1600 °C, followed by 30 s of water-cooling at 20 °C. Crack formation and the number of cycles until spalling were visually assessed.

3. Results

3.1 Slag corrosion resistance

Figure 3 shows the appearance of the specimens cut surface after the slag corrosion test, along with the corrosion depth and index. Corrosion depth decreased with the addition of 3 mass% ferrochrome, resulting in a 31% reduction relative to the base brick. In B-3, containing 3 mass% ferrochrome and 3 mass% graphite, the

corrosion depth was reduced by 64%. Although the corrosion depth remained higher than that of the burnt MgO-Cr_2O_3 brick, the difference was markedly reduced.
These results indicate that the combined addition of ferrochrome and graphite enhances the corrosion resistance of MgO-C bricks in lowbasicity slag regions in RH degassers.

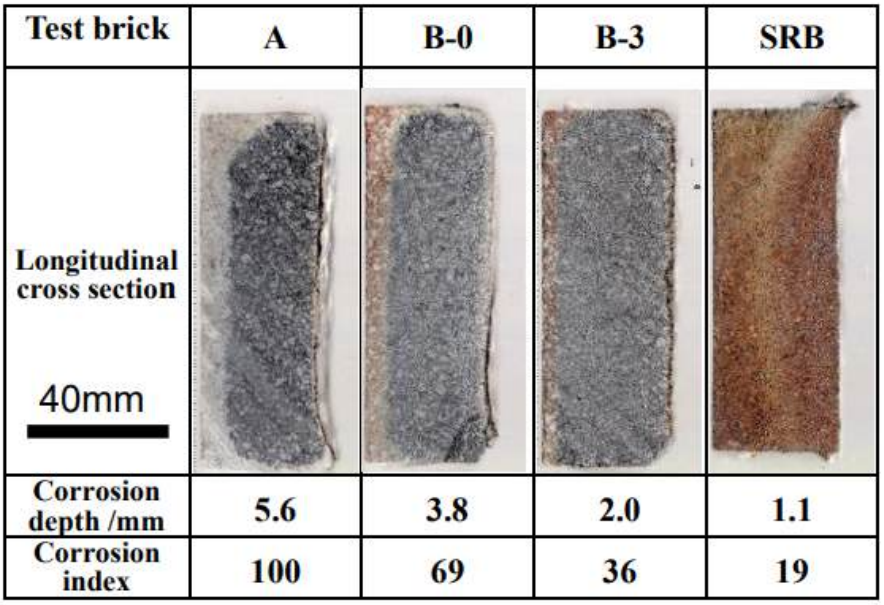


Fig.3 Results of the rotating drum slag corrosion test, showing appearance of the specimen cut surface used to measure the corrosion depth for the test bricks A, B-0, B-3, and SRB.

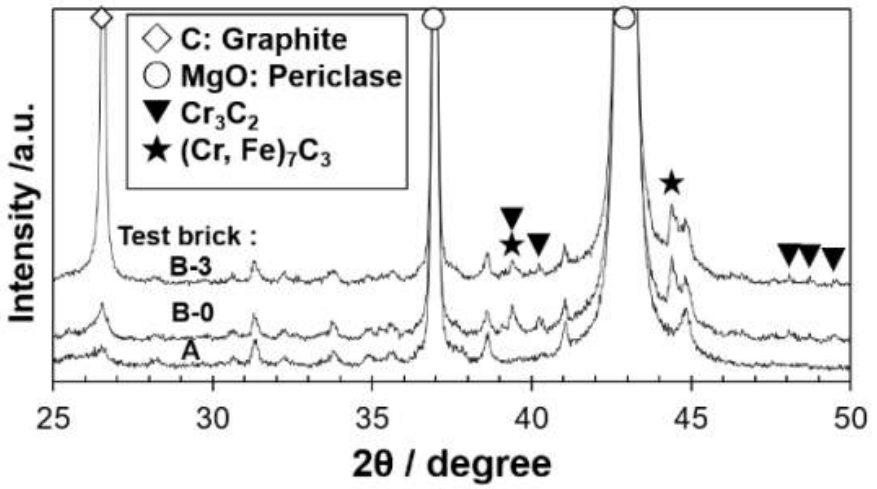


Fig.4 XRD patterns of the test bricks A, B-0, and B-3, taken at a position 20mm from the contact surface with slag in the rotating drum slag corrosion test.

These results indicate that the combined addition of ferrochrome and graphite enhances the corrosion resistance of MgO-C bricks in lowbasicity slag regions in RH degassers.

Figure 4 shows the XRD patterns of the test bricks at a distance of 20 mm from the contact surface with slag in the rotating drum slag corrosion test. In all ferrochrome-containing specimens, chromium carbides Cr_3C_2 and $(Cr, Fe)_7C_3$ were confirmed.

Figure 5 shows SEM-BEI (back-scattered electron image) and EPMA elemental mapping of the test bricks after the slag corrosion test. In B-0 and B-3, to which ferrochrome was added, Cr-enriched compounds were observed in the contact

surface layer with slag. These compounds are considered to have been formed by the reaction between the added ferrochrome and the slag. In addition, in B0 and B-3, gas bubbles were observed within the reaction products between ferrochrome and slag.

3.2 FeO corrosion resistance

Figure 6 shows the results of the FeO corrosion test. All test bricks exhibited superior FeO corrosion resistance compared to the burnt $MgOCr_2O_3$ brick SRB. No deterioration in FeO corrosion resistance was observed with the addition of ferrochrome or graphite. In general, adding graphite or other raw materials to MgO-C bricks raises concerns about oxidation and the formation of low melting-point phases, which may reduce the corrosion resistance to FeO. In the present case, however, because the added amounts of ferrochrome and graphite were small, oxidation and the formation of low-melting phases were avoided.

3.3 Thermal shock resistance

Figure 7 shows the appearance of the specimens after the thermal shock test, along with the number of cycles to spall. Spalling occurred during the second cycle in test brick B-0, which contained ferrochrome, and in B-3, where graphite had been added to reduce the elastic modulus. In contrast, test brick A exhibited no significant cracking even after the third cycle.

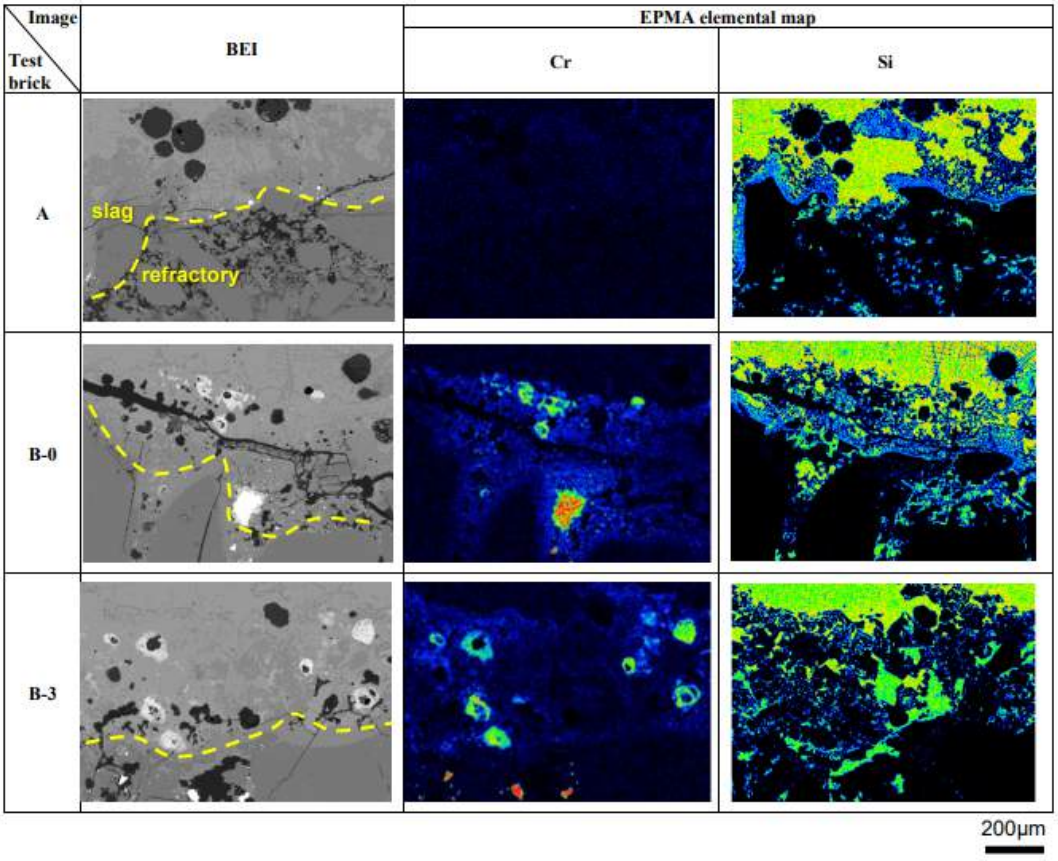


Fig.5 SEM-BEI (back-scattered electron images) and EPMA elemental mapping of the test bricks A, B-0, and B-3 after the rotating drum slag corrosion test, showing slag contact surface in the upper side of each BEI. The yellow lines in the images also indicate the reaction surface.

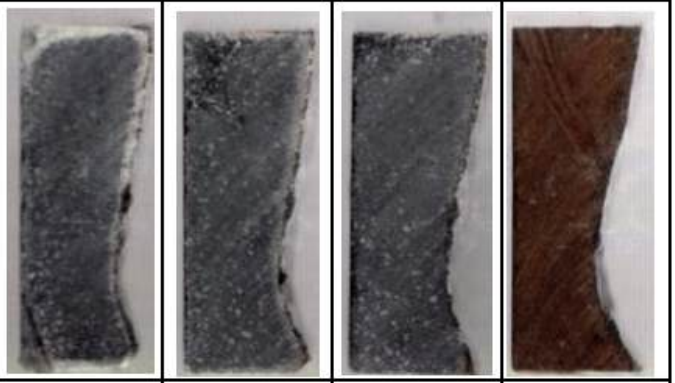
Test brick	A	B-0	B-3	SRB
Longitudinal cross section 40mm				
Corrosion depth /mm	14.6	14.6	13.6	18.3
Corrosion index	100	100	93	125

Fig.6 Results of the FeO corrosion test, showing the appearance of specimen cut surface used to measure corrosion depth for test bricks A, B-0, B-3, and SRB.

Test brick	A	B-0	B-3	SRB
Appearance after test 40mm				
Number of cycles to spall	>3	2	2	3

Fig.7 Results of the thermal shock test, showing the appearance of test pieces after testing and number of cycles to spall for the test bricks.

This behavior is attributed to the formation of chromium carbides and iron-chromium composite carbides produced by reactions involving ferrochrome. Although the overall elastic modulus of the bricks was reduced by the addition of graphite, the locally formed high elastic modulus carbide phases acted as stress concentrators, thereby promoting embrittlement and reducing thermal shock resistance.

4. Discussion

4.1 Improving mechanism of corrosion resistance

The results of SEM-BEI, EPMA and XRD analyses indicate that ferrochrome initially reacts with surrounding carbon to form (Fe, $Cr)_7C_3$ and Cr3C2. Spinel solid solution with the composition (Fe, Mg)(Cr, $Al)_2O_4$ is also expected to form through the reaction between the slag and (Cr, $Fe)_7C_3$/ Cr_3C_2. During this reaction process, the oxidation of carbon in the carbide is expected to produce CO gas. The bubbles observed within the Fe-Cr residue at the slag interface after the corrosion test, as shown in Fig. 5, can be attributed to CO gas formation. Furthermore, a portion of the chromium carbide dissolves into the slag as CrOx, increasing the Cr content in the slag with rising temperature. As a result, distinctive microstructures develop near the slag contact surface, with residual Cr-carbide particles serving as cores surrounded by a spinel solid solution.

An increase in the Cr content within the slag tends to increase its viscosity [6] due to the enhanced formation of Cr-containing oxides. The spinel solid solution formed under these conditions is believed to increase the apparent viscosity by dispersing as fine solid particles, suspended in the molten phase, throughout the slag. Furthermore, the dispersion of CO gas bubbles forms a gas-liquid mixture within the slag, thereby increasing the apparent viscosity and suppressing convection and mass transport. Consequently, a high-viscosity interfacial layer composed of Cr-enriched slag, spinel solid solution, and CO gas bubbles form at the slag contact surface of the low-carbon MgO-C brick. This layer is believed to act as an effective protective barrier, inhibiting further dissolution of the refractories. The test bricks in which graphite was added to a ferrochrome-containing brick (test brick B-3) exhibited corrosion resistance approaching that of the burnt magnesia-chrome brick SRB. This enhanced corrosion resistance is attributed to reduced wettability at the slag-solid interface, increased CO gas generation through reactions with MgO, and viscosity-increasing effects.

4.2 Potential application to RH degassers

Table 2 summarizes the relative performance of the base brick A, the ferrochrome-enhanced grade (B-3), and the conventional burnt MgO-Cr_2O_3 brick (SRB). Due to their high MgO content, low carbon MgO-C bricks generally exhibit superior resistance to FeO compared with MgO-Cr_2O_3 bricks. In zones dominated by thermal shock spalling, the conventional grade remains the preferred material. The developed material B-3 Table 2 summarizes the relative performance of the base brick A, the ferrochrome-enhanced grade (B-3), and the conventional burnt MgO-Cr_2O_3 brick (SRB). Due to their high MgO content, lowcarbon MgO-C bricks generally exhibit superior resistance to FeO compared with MgO-Cr_2O_3 bricks. In zones dominated by thermal shock spalling, the conventional grade remains the preferred material. The developed material B-3.

Test brick / Resistance to;		SRB	MAGreenX™	
			A	B-3
		$MgO-Cr_2O_3$	MgO-C	A+FeCr +C
Corrosion against	Slag(C/S=1)	○	△	○
	FeO	△	○	○
Thermal shock		△	◎	△

◎: excellent, ○: good, △: inferior,

Table 2 Comparison of the relative performance of test brick B-3 with the comparative bricks of SRB and the base MgO-C, assessing resistance to corrosion and thermal shock

5. Conclusion

In this study, ferrochrome was added to lowcarbon MgO-C bricks to extend their use in heavily corroded zones under low-basicity slag. Adding 3 mass% ferrochrome and 3 mass% graphite reduced the slag corrosion depth by 64%, by approaching the performance of burnt $MgOCr_2O_3$ bricks while preserving the superior FeO corrosion resistance of MgO-C bricks. This improvement was attributed to a protective layer of Cr-enriched slag, a spinel solid solution, and CO bubbles formed at the slag-refractory interface through in-situ reaction of Fe-Cr carbides with slag. The ferrochrome-enhanced grade is thus recommended as part of line-up for RH degasser linings subjected to severe slag corrosion under low-basicity slag and during oxygen-blowing operation, enabling the consolidation of linings into eco-friendly materials with energy savings, a low carbon footprint and high durability.

References

1) H. Ishii, S. Takeshita, K. Sasaki, E. Maeda, and S. Tanaka: Taikabutsu, 53 [2]78-79 (2001).

2) S. Terada, D. Hara, Y. Murakami, and T. Fukuda: Taikabutsu, 73 [5]171-179 (2021).

3) L. S. de Melo, R. D. da Mota Araújo, W. S. Moraes, J. A. Coelho, G. F. Coimbra, L. A. Vieira, S. L. Cabral Silva, L. R. Martins, C. G. Pires, and S. E. Soares: Proc. AISTech 2025, Nashville, TN, USA, p 2671.

4) Y. Tomita, T. Anan, K. Goto, and K. Morikawa: Proc. UNITECR2023, Frankfurt, Germany, p 364.

5) K. Asano, Y. Otsuki, K. Goto, H. Shikano, H. Yamamoto, and K. Tamaki: Taikabutsu, 44 [1]2-9 (1992).

6) D. Yang, F. Zhang, J. Wang, Z. Yan, G. Pei, G. Qiu, and X. Lv: Journal of Materials Research and Technology, 9 [6] 14673-14681 (2020)

ADVANCING CEMENT-KILN RELIABILITY WITH DUAL-STAGEBONDED NO-CEMENT CASTABLES: ENHANCED THERMAL-SHOCK AND ALKALI RESISTANCE

Hong Peng[a]*, Zixin Liao[a,b]
[a]Innovation Materials, Elkem Silicon Products, Kristiansand NO-4621, Norway
[b]State Key Laboratory of Advanced Refractories, Wuhan University of Science and Technology, Wuhan 430081, China

*Corresponding author: hong.peng@elkem.com

Abstract

Cement-kiln refractories are exposed to rapid thermal cycling and alkali-rich atmospheres, which accelerate cracking, penetration, and lining degradation. This study evaluates a microsilica-gel-bonded no-cement SiC–mullite castable (NCC-SZ) as a low-CaO alternative to low-cement (LCC-SF) and ultra-low-cement (ULCC-SF) references. The proposed dual-stage bonding concept combines an installation-stage silica-gel network for early handling strength with in-situ mullite ceramic bonding during firing. NCC-SZ retained practical castability, achieved sufficient green strength for demoulding after 24 h, and developed improved high-temperature flexural strength, reaching approximately 19 MPa after firing at 1400 °C. It also showed the highest thermal-shock resistance, retaining approximately 48% and 34% of its initial CMOR after one and three water-quench cycles, respectively. Static alkali-corrosion testing showed the lowest alkali-penetration fraction for NCC-SZ, while SEM and XRD confirmed reduced matrix alteration beyond the reaction zone and identified kalsilite as the main alkali-reaction product. These results demonstrate that dual-stage microsilica-gel-to-mullite bonding is a promising route for durable no-cement castables in cement-kiln zones exposed to combined thermal shock and alkali attack.The improved resistance to thermal shock and alkali attack may contribute to enhanced lining durability and operational reliability in cement-kiln service.

Keywords: no-cement castables; microsilica-gel bonding; mullite formation; thermal-shock resistance; alkali resistance.

1. Introduction

Monolithic refractory castables are essential linings in cement-kiln systems, where preheater cyclones, riser ducts, calciners, tertiary-air ducts, kiln hoods, and transition zones are exposed to thermal cycling, alkali-rich atmospheres, abrasive dust flows, and combined thermo-mechanical stresses [1–4]. The increasing use of alternative fuels and secondary raw materials further intensifies alkali circulation, accelerating chemical infiltration, cracking, spalling, and premature lining failure. Next-generation cement-kiln refractories must therefore combine reliable installation and early strength with improved resistance to rapid heat-up, thermal shock, and alkali corrosion.

Calcium aluminate cement (CAC)-bonded low-cement and ultra-low-cement castables are widely used because of their robust hydraulic setting and practical installation behaviour. However, CaO from CAC may react with alumina and silica during firing or service to form calcium aluminate and calcium aluminosilicate phases, which can promote low-melting phase formation, reduce refractoriness, increase permeability, and impair long-term structural stability under alkali-bearing kiln conditions [5]. Reducing or eliminating cement from the matrix is therefore a key strategy for improving refractory durability in aggressive cement-kiln environments.

Cement-free silica-based bonding systems offer a promising route to low-CaO castables. Dry microsilica-gel bonding provides practical advantages in storage, handling, and formulation flexibility compared with liquid silica-sol binders, while enabling a dual-stage

bonding mechanism [6–10]. An initial silica-gel network supports setting and green strength during installation, whereas firing promotes reactions between reactive silica and alumina to form a mullite-rich ceramic bond. This concept is particularly relevant for SiC–mullite castables, where SiC contributes thermal-shock and abrasion resistance and mullite provides refractoriness, low thermal expansion, and chemical stability [11–12].

Although silica-based no-cement binders have been studied previously, limited comparative data are available for microsilica-gel-bonded SiC–mullite castables under combined thermal-shock and alkali-penetration conditions relevant to cement-kiln service. In this study, a microsilica-gel-bonded no-cement castable (NCC-SZ) was benchmarked against low-cement (LCC-SF) and ultra-low-cement (ULCC-SF) references to determine how binder chemistry and cement reduction affect fresh-state behaviour, strength development, thermal-shock resistance, alkali-corrosion response, and microstructural evolution. The objective was to assess whether the dual-stage microsilica-gel-to-mullite bonding concept can provide a practical route for advancing cement-kiln reliability through enhanced thermal-shock and alkali resistance.

2. EXPERIMENTAL

2.1 Castable formulation and bonding concepts

Three SiC–mullite castables with the same aggregate framework but different bonding systems were studied: LCC-SF, ULCC-SF, and microsilica-gel-bonded NCC-SZ (Table 1). All contained 24 wt.% SiC, 44 wt.% mullite, and 7 wt.% tabular alumina, with alumina fines, Kerphalite, microsilica(Elkem Microsilica® 971U), and binder-specific additives forming the matrix. LCC-SF and ULCC-SF contained 6 and 3 wt.% CAC, respectively, with SioxX®-Flow; ULCC-SF also contained SioxX®-Set. NCC-SZ contained 3 wt.% SioxX®-Zero and only 0.5 wt.% CAC, used mainly as a Ca^{2+} source to initiate microsilica coagulation and silica-gel bonding. A water addition of 5 wt.% was used for all formulations.

Table 1.Overall compositions of the SiC–mullite castables with different bonding systems (wt%).

Raw material / additive	LCC-SF	ULCC-SF	NCC-SZ
SiC aggregate, 0–2 mm	24	24	24
Mullite aggregate, 0–6 mm	44	44	44
Tabular alumina, 45 µm	7	7	7
Alumina fines, D50 = 2.8 µm	7	10	10.5
Kerphalite, 0–0.055 mm	5	5	5
Elkem Microsilica® 971	6	5	5
Calcium aluminate cement, 70 wt.% Al_2O_3	6	3	0.5
SioxX®-Flow	1	1	-
SioxX®-Set	-	0.5	-
SioxX®-Zero	-	-	3

2.2 Sample preparation and characterization

Dry constituents were mixed for 4 min at 60 rpm, followed by addition of 5 wt.% water and a further 4 min of mixing. Specimens were vibration-cast as 40 mm × 40 mm × 160 mm bars for mechanical/physical testing and 100 mm × 100 mm × 60 mm crucibles for alkali testing, cured for 24 h at 20 °C and >90% relative humidity, demoulded, and dried at 110 °C for 24 h. Bars were fired at 815, 1000, or 1400 °C for 12 h, while crucibles were prefired at 1100 °C for 6 h.

Workability was assessed by self-flow and vibration-flow tests (ASTM C230), setting by ultrasonic pulse velocity, and cold modulus of rupture (CMOR), cold crushing strength (CCS), bulk density, and apparent porosity after drying or firing. Thermal-shock resistance was evaluated by water quenching after prefiring, with damage assessed after one and three cycles. Alkali resistance was tested by charging prefired crucibles with an equal-mass K_2CO_3–KCl–K_2SO_4 mixture, heating at 1100 °C for 5 h, and quantifying the affected cross-sectional areas. Alkali-affected microstructures and phases were examined by FE-SEM/BSE, EDS, and XRD using Cu Kα radiation over 2θ = 10–80°.

3. RESULTS AND DISCUSSION

3.1 Workability and green-bond development

The first requirement for replacing cement-bonded systems is to ensure that the alternative binder maintains adequate workability and develops sufficient early stiffness for demoulding and handling. Figure 1 compares the flowability of the three SiC–mullite castables. LCC-SF, ULCC-SF, and NCC-SZ exhibited comparable vibration-flow values of approximately 89%, 90%, and 87%, respectively, showing that the microsilica-gel-bonded NCC-SZ retained practical castability despite the substantial reduction in CAC content. The self-flow values followed the same trend, with the cement-bonded systems showing slightly higher particle mobility than NCC-SZ, reflecting the influence of binder chemistry on early rheology.

The ultrasonic pulse-velocity curves further illustrate the distinct early bonding mechanisms, as shown in Figure 2. LCC-SF and ULCC-SF developed stiffness rapidly as a result of CAC hydration, whereas NCC-SZ exhibited a more gradual increase associated with Ca^{2+}-induced microsilica coagulation and silica-gel network formation. Nevertheless, NCC-SZ reached final setting after approximately 10 h and could be demoulded after 24 h of curing, confirming that the microsilica-gel network provides sufficient early integrity for handling and subsequent firing. This early-strength development is essential for practical installation in cement-kiln applications.

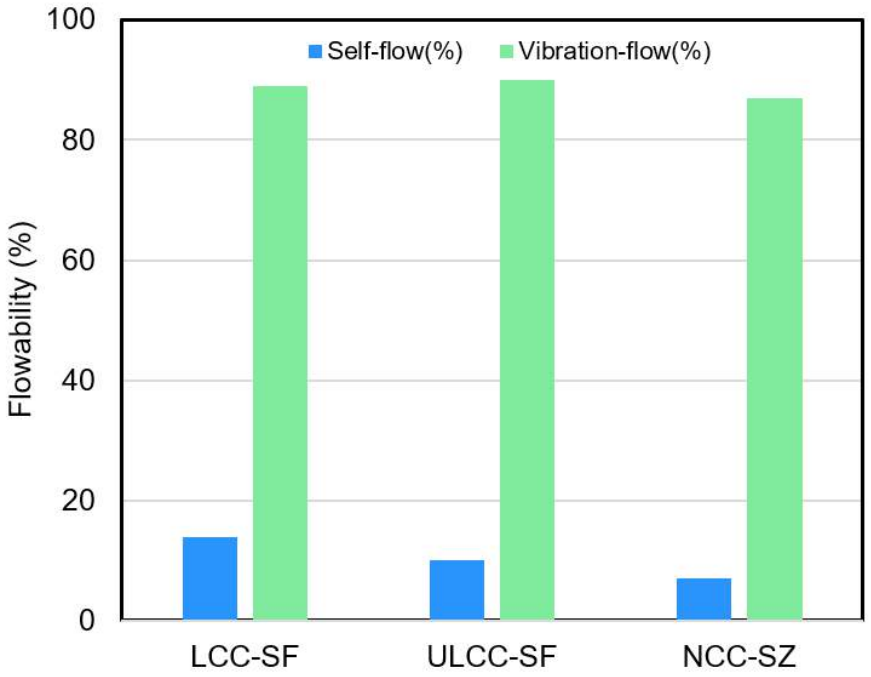


Fig. 1: Flowability of SiC–mullite castables with different bonding systems: self-flow and vibration flow.

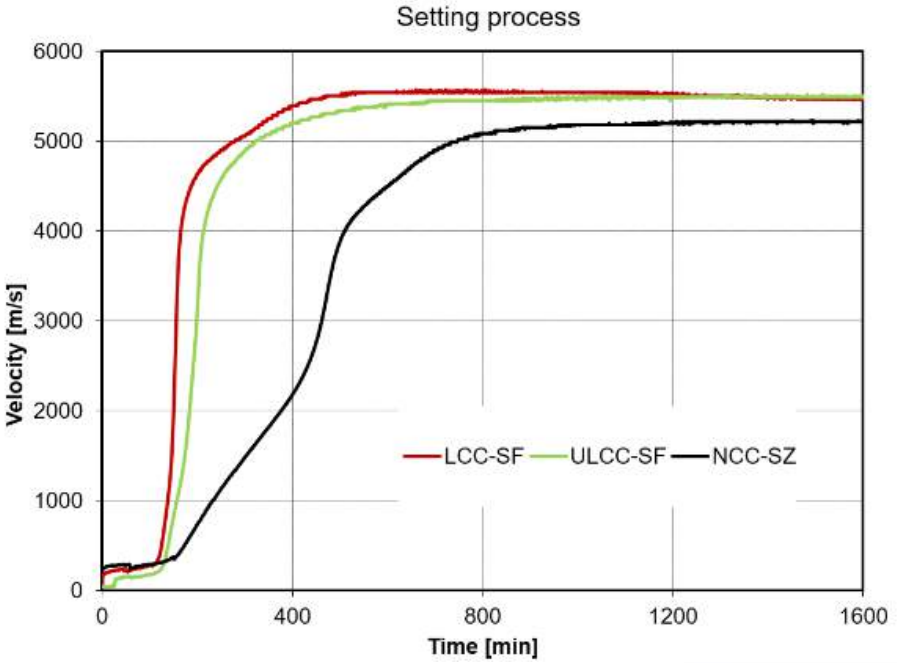


Fig. 2: Setting and hardening behaviour of SiC–mullite castables after 24 h curing at 20 °C and >90% relative humidity.

3.2 Mechanical properties and physical characteristics

Figures 3 and 4 summarize the mechanical and physical-property evolution of the SiC–mullite castables after drying and firing. After drying and firing at 815 °C, the CAC-bonded LCC-SF and ULCC-SF showed higher CMOR than NCC-SZ, reflecting the stronger early contribution of hydraulic cement bonding. With increasing firing temperature, however, the response became increasingly controlled by high-temperature binder-phase evolution rather than by density or apparent porosity alone.

The CAC-bonded castables reached maximum CMOR values of approximately

28–29 MPa after firing at 1000 °C but decreased to 11–13 MPa at 1400 °C, despite the lower porosity obtained by high-temperature sintering. This strength loss indicates that flexural performance was governed mainly by phase changes in the bonding matrix. Calcium aluminosilicate-rich liquid or glassy phases formed in CAC-containing systems may increase matrix brittleness and promote crack propagation [5].

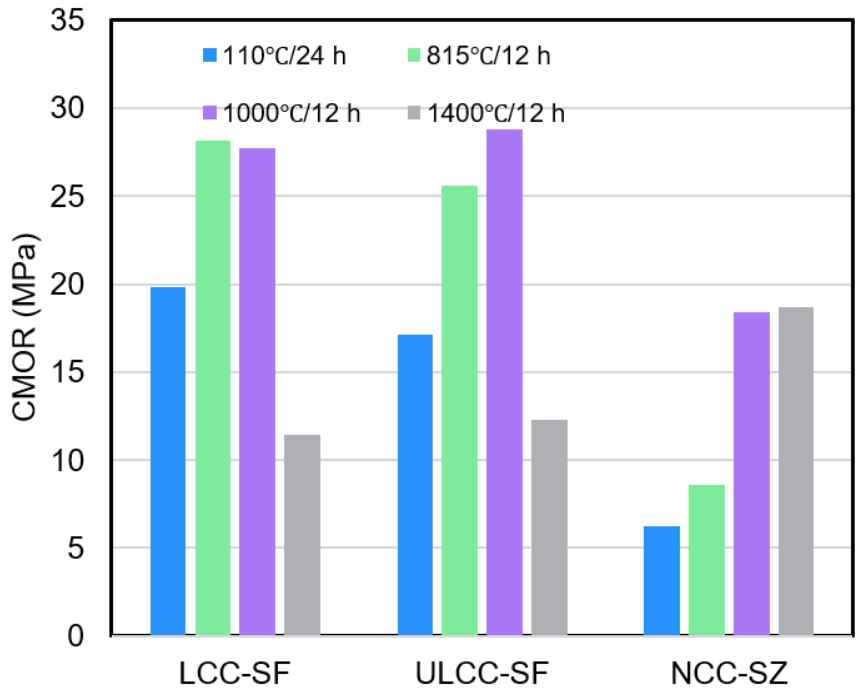
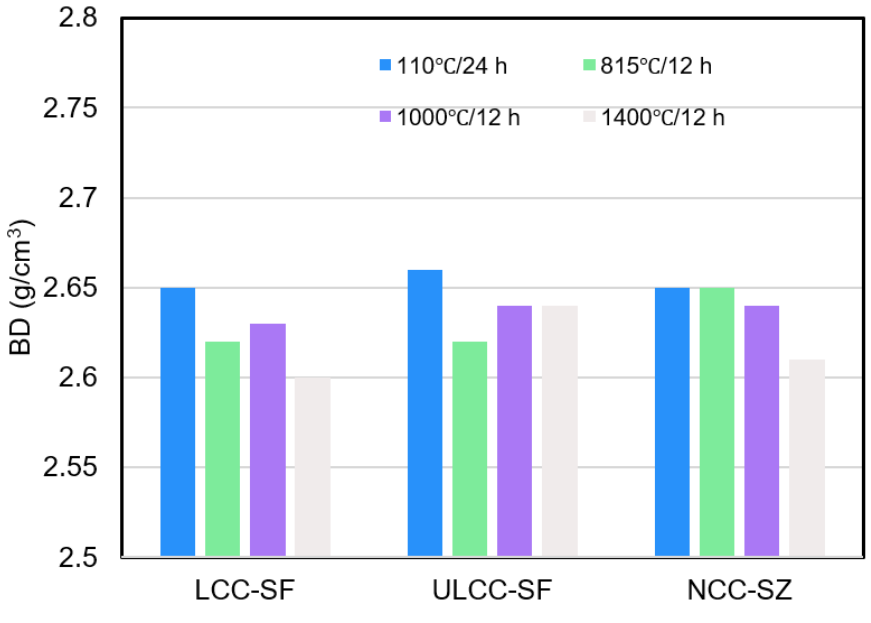
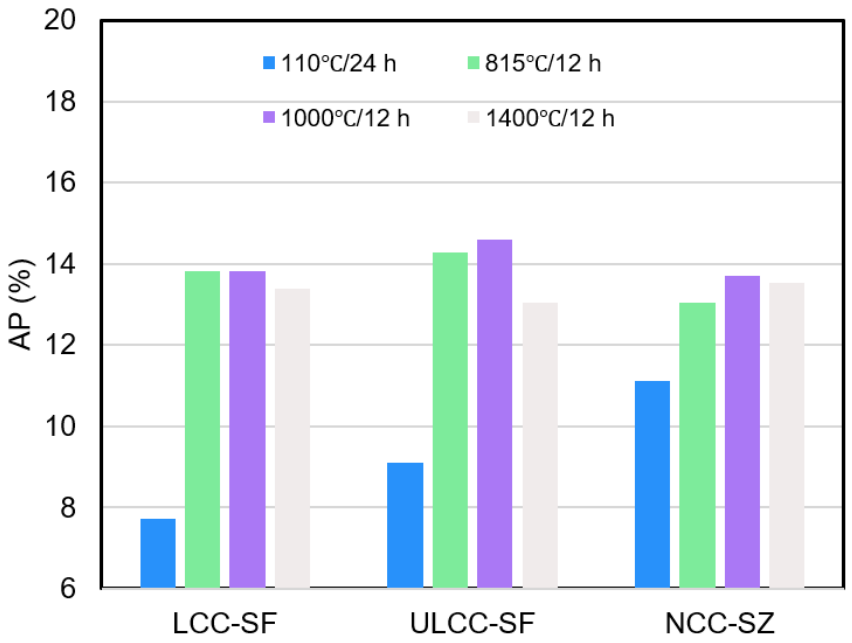


Fig. 3: CMOR of SiC–mullite castables after drying at 110 °C for 24 h and firing at 815, 1000, and 1400 °C for 12 h.



(a)



(b)

Fig. 4: Physical properties of SiC–mullite castables after drying and firing: (a) bulk density (BD) and (b) apparent porosity (AP).

In contrast, NCC-SZ showed continuous strength development with firing temperature, increasing from approximately 6 MPa after drying to about 19 MPa after firing at 1400 °C. Bulk density remained similar for all formulations (2.60–2.66 g/cm³), while apparent porosity increased at 815–1000 °C and decreased again at 1400 °C. The improved high-temperature CMOR of NCC-SZ therefore cannot be explained by densification alone, but is attributed to the formation of a mullite-rich ceramic bond in the microsilica-gel-bonded matrix [8–10]. This confirms that reducing CaO and promoting microsilica-gel-to-mullite bonding improves the high-temperature mechanical stability of SiC–mullite castables.

3.3 Thermal-shock damage and CMOR retention

Because cement-kiln linings undergo repeated heating and cooling, CMOR retention after water-quench cycling was used to assess thermal-shock damage (Fig. 5). All formulations showed strength loss after cycling, confirming microcrack formation during rapid temperature changes; however, the extent of degradation depended strongly on the binder system.

NCC-SZ retained approximately 48% of its initial CMOR after one cycle and 34% after three cycles, compared with only 26%/15% for LCC-SF and 32%/17% for ULCC-SF. This demonstrates the superior thermal-shock resistance of NCC-SZ relative to the CAC-bonded references.

The improved CMOR retention is attributed to the low-CaO microsilica-gel-bonded matrix, which likely limits calcium aluminosilicate-rich glassy phases and promotes a mullite-rich ceramic bond. This matrix reduces brittleness and slows crack initiation and propagation under repeated thermal cycling.

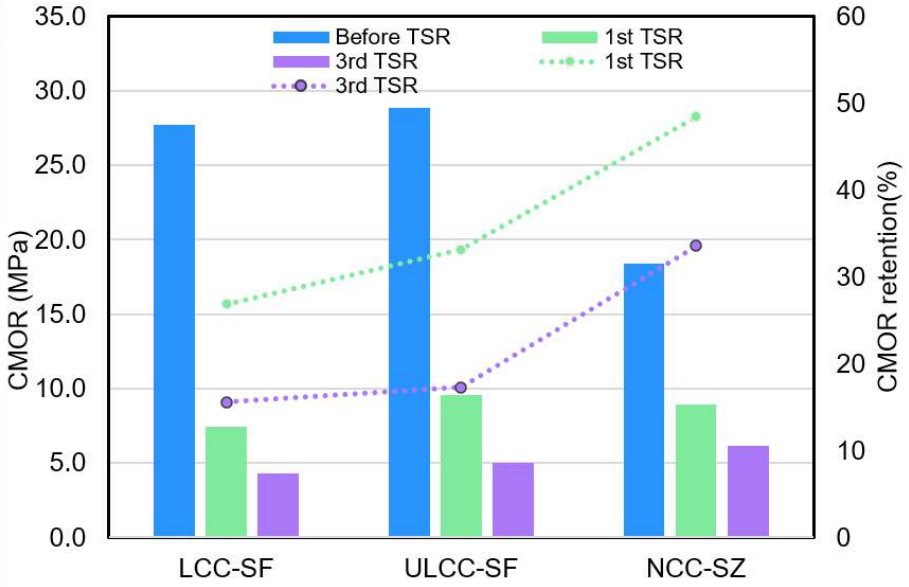


Fig. 5: CMOR retention of SiC–mullite castables after repeated water-quench thermal-shock cycles following prefiring at 1000 °C for 5 h.

3.4 Alkali-penetration behaviour and reaction products

Alkali resistance was evaluated by combining macroscopic cross-sectional analysis, SEM observations, and XRD phase characterization after static corrosion testing at 1100 °C for 5 h in an equal-mass K_2CO_3–KCl–K_2SO_4 mixture. As shown in Fig. 6, all specimens remained structurally intact after exposure, with degradation primarily localized around the alkali cavity. Three distinct regions could be identified from the cross-sections: a near-alkali reaction zone, an intermediate penetration zone, and a far-alkali zone. The reaction-zone area was similar for all formulations, ranging from 265 to 305 mm² (7.4–8.5% of the cross-sectional area). In contrast, the extent of the penetration zone was strongly dependent on binder chemistry. LCC-SF exhibited the largest penetration zone (2493 mm², 69.3%), followed by ULCC-SF (1807 mm², 50.2%), whereas NCC-SZ showed the smallest affected area (1761 mm², 48.9%). These results indicate that the microsilica-gel-bonded NCC-SZ castable provided the highest resistance to alkali ingress under the present test conditions.

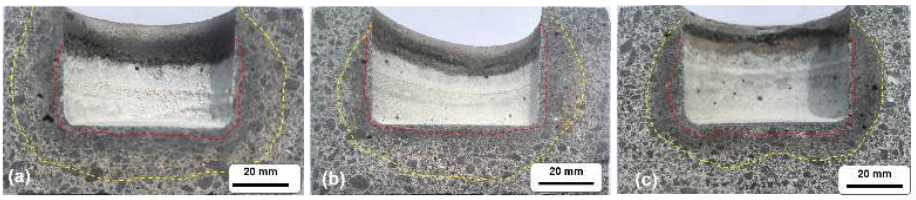


Fig. 6: Cross-sections of SiC–mullite castables after static alkali-corrosion testing at 1100 °C for 5 h using an equal-mass K_2CO_3–KCl–K_2SO_4 mixture: (a) LCC-SF, (b) ULCC-SF, and (c) NCC-SZ.

Low-magnification BSE images of representative cross-sections are shown in Fig. 7. The images generally support the regional division identified in Fig. 6, with the most pronounced microstructural alteration occurring adjacent to the alkali source and gradually decreasing toward the interior. However, the transitions between the near-alkali, penetration, and far-alkali regions are less distinct in the BSE micrographs than in the macroscopic cross-sections. In addition, condensed alkali-bearing deposits partially obscured the BSE contrast in some areas, making precise delineation of region boundaries difficult. Complementary SEM/EDS observations from the far-alkali

region (not shown) detected potassium-, chlorine-, and sulfur-containing deposits, indicating that volatile alkali species generated during testing condensed within the crucible environment. These deposits likely originated from a combination of alkali transport through the refractory and condensation of alkali vapours within the crucible, potentially including vapours escaping through minor openings around the crucible lid. Therefore, Fig. 7 should be regarded primarily as qualitative microstructural evidence supporting the macroscopic observations of Fig. 6 rather than as a basis for quantitative determination of penetration depth. Nevertheless, the microstructural alteration appeared less extensive in NCC-SZ than in LCC-SF and ULCC-SF, consistent with the penetration-area measurements shown in Fig. 6.

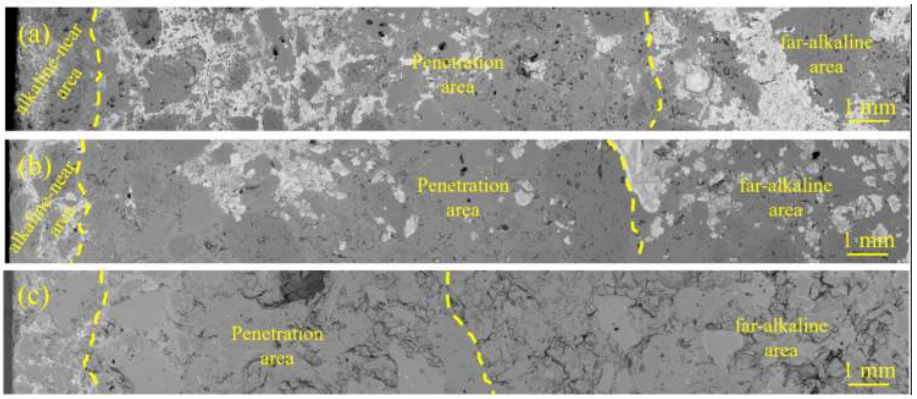


Fig. 7: Cross-sectional BSE micrographs after alkali-corrosion testing at 1100 °C showing the near-alkali, penetration, and far-alkali regions in (a) LCC-SF, (b) ULCC-SF, and (c) NCC-SZ.

XRD patterns obtained from the near-alkali regions are shown in Fig. 8. Kalsilite ($KAlSiO_4$) was identified as the predominant alkali-reaction product in all three castables, indicating that the fundamental reaction mechanism was similar irrespective of the bonding system. The formation of kalsilite confirms the reaction between potassium-bearing species and aluminosilicate phases in the castable matrix. Residual mullite, α-SiC, corundum, and quartz were also detected, together with minor amounts of anorthite in the CAC-bonded compositions. The similar phase assemblages observed in the reaction zones suggest that differences in alkali resistance were not primarily associated with the reaction products formed, but rather with the ability of the matrix to restrict alkali transport into the refractory body.

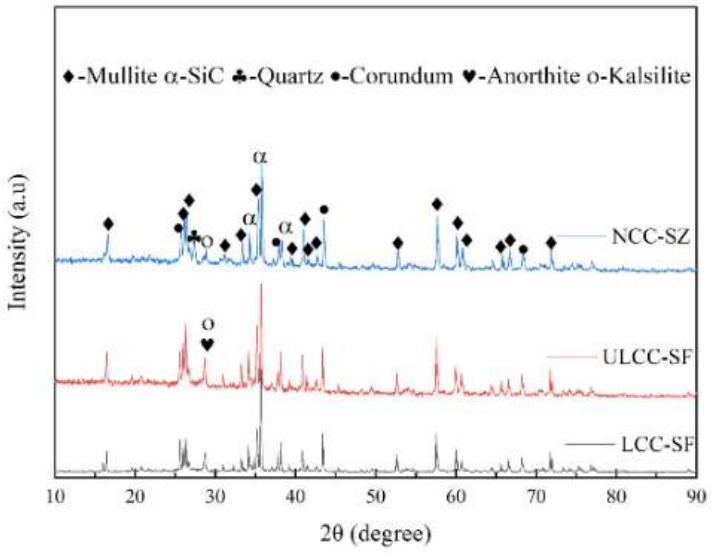


Fig. 8: XRD patterns of the near-alkali regions after alkali-corrosion testing at 1100 °C: (a) LCC-SF, (b) ULCC-SF, and (c) NCC-SZ.

Overall, the macroscopic, microstructural, and phase-analysis results indicate that NCC-SZ exhibited the highest resistance to alkali attack among the three formulations. All castables showed comparable near-surface reaction behaviour and formed similar alkali-reaction products, with kalsilite identified as the principal reaction phase. However, NCC-SZ exhibited the smallest penetration-zone fraction in the cross-sectional analysis and the least extensive internal microstructural alteration. These observations suggest that the microsilica-gel-bonded system was more effective than the CAC-bonded formulations in limiting alkali transport into the refractory body. While condensed alkali-bearing deposits introduce some uncertainty in the interpretation of local microstructural features, the conclusions regarding relative alkali resistance are primarily supported by the clearly distinguishable penetration zones observed in the macroscopic cross-sections (Fig. 6).

4 CONCLUSIONS

This study demonstrates that dual-stage microsilica-gel-to-mullite bonding is a viable route for developing SiC–mullite no-cement castables for cement-kiln service. NCC-SZ retained practical castability and sufficient green strength for demoulding after 24 h while developing superior high-temperature performance through mullite-rich ceramic bonding, reaching approximately 19 MPa CMOR after firing at 1400 °C. Compared with the CAC-bonded references, NCC-SZ also showed the highest thermal-shock resistance, with CMOR retention of approximately 48% and 34% after one and three water-quench cycles, respectively.

In static alkali-corrosion testing, NCC-SZ exhibited the lowest alkali-penetration fraction and the least extensive internal microstructural alteration. Macroscopic cross-sectional analysis revealed substantially smaller alkali-affected areas in NCC-SZ than in the CAC-bonded formulations, indicating more effective resistance to alkali ingress. XRD analysis identified kalsilite as the principal alkali-reaction product in all castables, suggesting that the observed differences in alkali resistance were mainly related to the ability of the matrix to restrict alkali transport rather than to differences in reaction products. Although condensed alkali-bearing deposits locally complicated the interpretation of low-magnification BSE images, the overall conclusions are consistent across the macroscopic, microstructural, and phase-analysis results.

Overall, NCC-SZ offers a promising combination of installation reliability, high-temperature strength, thermal-shock damage tolerance, and resistance to alkali penetration, making the microsilica-gel-bonded system a strong candidate for cement-kiln zones exposed to combined thermal and chemical attack. These improvements in resistance to thermal-shock damage and alkali ingress are expected to contribute to enhanced lining durability and service reliability, with the potential to reduce maintenance interventions, improve kiln availability, and lower the overall cost of refractory ownership.

ACKNOWLEDGEMENTS

This work received financial support from Elkem Silicon Products in Norway through the Elkem Graduate Student Internship Program at Wuhan University of Science and Technology (WUST) and from the Federation for International Refractory Research and Education (FIRE). The authors also acknowledge the long-standing collaboration between Elkem, FIRE, and WUST, which enabled this research.

REFERENCES

[1] J. Szczerba, E. Śnieżek and V. Antonovič, “Evolution of refractory materials for rotary cement kiln sintering zone,” Refractories and

Industrial Ceramics, vol. 58, pp. 426–433, 2017.

[2] B. Ren, Y. Li, M. Nath, Q. Wang and Y. Xu, “Enhanced alkali vapor attack resistance of bauxite–SiC refractories for the working lining of cement rotary kilns via incorporation of andalusite,” Ceramics International, vol. 44, no. 18, pp. 22113–22120, 2018.

[3] D. Madej and J. Szczerba, “Detailed studies on microstructural evolution during the high-temperature corrosion of SiC-containing andalusite refractories in the cement kiln preheater,” Ceramics International, vol. 43, no. 2, pp. 1988–1996, 2017.

[4] I. Recio Dominguez, J. Gómez-Millán, M. Alvarez, S. De Aza, L. Contreras and A. H. De Aza, “Build-up formation and corrosion of monolithic refractories in cement kiln preheaters,” Journal of the European Ceramic Society, vol. 30, pp. 1879–1885, 2010.

[5] L. Pan, Z. He, Y. Li, T. Zhu, Q. Wang and B. Li, “Effects of cement content on the microstructural evolution and mechanical properties of cement-bonded corundum castables,” Ceramics International, vol. 46, pp. 4634–4642, 2020. doi: 10.1016/j.ceramint.2019.10.193.

[6] M. R. Ismael, R. D. dos Anjos, R. Salomão and V. C. Pandolfelli, “Colloidal silica as a nanostructured binder for refractory castables,” Refractories Applications and News, vol. 11, no. 4, pp. 16–20, 2006.

[7] M. Nouri-Khezrabad, M. A. L. Braulio, V. C. Pandolfelli, F. Golestani-Fard and H. R. Rezaie, “Nano-bonded refractory castables,” Ceramics International, vol. 39, no. 4, pp. 3479–3497, 2013. doi: 10.1016/j.ceramint.2012.11.028.

[8] H. Peng and B. Myhre, “Comparison of setting behaviour and mechanical properties of various silica-bonded no-cement castables,” China’s Refractories, vol. 26, no. 1, pp. 8–12, 2017.

[9] H. Peng and B. Myhre, “Microsilica-gel bonded refractory castables with improved set-behaviour and mechanical properties,” Refractories Worldforum, vol. 7, no. 3, pp. 69–75, 2015.

[10] H. Peng, “Novel binder systems for no-cement castables: A comprehensive evaluation of mechanical strength and hot properties,” Journal of Ceramic Science and Technology, pp. 1–8, 2025.

[11] H. Schneider, J. Schreuer and B. Hildmann, “Structure and properties of mullite—A review,” Journal of the European Ceramic Society, vol. 28, pp. 329–344, 2008. doi: 10.1016/j.jeurceramsoc.2007.03.017.

[12] H. Peng, S. Zhang, Q. Wang and Y. Li, “Development of microsilica-gel bonded castable for nose ring application,” Refractories Worldforum, vol. 15, no. 3, pp. 20–29, 2023.

COMPARATIVE EVALUATION OF HYDRATION BEHAVIOUR IN MAGNESIA BASED REFRACTORIES

Sirshendu Das, Soumendu Das, Adyasha Ipsita Khuntia, B. Ghosh, Prasant Kumar Naik.

TRL Krosaki Refractories Ltd.

Abstract

Magnesia refractories are utilised in a wide range of applications, including calcination kilns, high-temperature molten salt electrolysis, metal smelting, and slag processing, owing to their excellent high-temperature performance and chemical stability. However, hydration of magnesia-based refractories remains a key challenge that impacts handling, storage stability, and in-service reliability. To address this issue, various strategies have been employed to enhance hydration resistance, such as surface treatments and the application of glassy coatings on MgO grains through siliceous additives. This study presents a comparative evaluation of the hydration behaviour of magnesia (MgO) and magnesia–spinel bricks, with the aim of elucidating the impact of spinel addition and raw material selection on hydration resistance. Furthermore, the effectiveness of anti-hydration treatments and their influence on the thermo-mechanical properties of these refractories are analysed. All samples were exposed to controlled ambient humidity and water conditions, and variations in physical properties—including weight gain, bulk density, apparent porosity, and cold crushing strength—were systematically assessed. Phase evolution and microstructural alterations before and after hydration were characterised using X-ray diffraction and scanning electron microscopy. The results indicate that magnesia bricks are highly prone to hydration than Magnesia Spinel, as due to lower free MgO content and dense microstructure, which limits moisture penetration and brucite development. The results regarding spinel addition percentage, selection of raw materials, and anti-hydration treatment contribute valuable insights to enhancing the durability of magnesia-based refractories for various industrial applications.

Keywords: MgO-C Refractories, Hydration behaviours, Hydration resistancestudy, XRD SEM-EDSstudy.

1. Introduction

Magnesia-based refractories are extensively utilized in steelmaking converters, electric arc furnaces, ladles, cement kilns, and non-ferrous metallurgical processes owing to their excellent refractoriness, high-temperature strength, and superior resistance to basic slags. Despite these advantages, hydration of MgO remains one of the primary challenges affecting the shelf life, handling characteristics, and long-term performance of basic refractories. The hydration reaction of periclase (MgO) with atmospheric moisture results in the formation of brucite [$Mg(OH)_2$], which is associated with significant volumetric expansion. This expansion generates internal stresses within the refractory matrix, leading to crack formation, structural deterioration, and subsequent loss of mechanical properties. Several approaches have been investigated to improve hydration resistance, including optimization of raw material selection, incorporation of spinel or chrome-bearing phases, microstructural

densification, and application of anti-hydration surface treatments. Among these, the use of fused magnesia, magnesia-chrome aggregates, and protective coatings has shown considerable promise in reducing moisture penetration and suppressing brucite formation. However, the effectiveness of these approaches depends strongly on the refractory composition and microstructural characteristics. The present study aims to comparatively evaluate the hydration behaviour of various magnesia and magnesia-chrome refractory compositions subjected to controlled humidity conditions. Special emphasis is placed on understanding the influence of raw material selection, anti-hydration dipping treatment, and frit coating on physical and mechanical property retention. Furthermore, the hydration mechanisms are correlated with microstructural changes and phase evolution to identify effective strategies for improving hydration resistance in basic refractory systems.

2. Experimental

Different grades of commercial magnesia, magnesia spinel and magnesia-chrome refractory were selected for the investigation. These grades are manufactured from fused magnesia, dead burnt magnesia, fused magnesia chrome, Spinel etc. All the grades are high temperature fired. To increase hydration resistance all the grades undergo special salt impregnation treatment. Beside the original, salt impregnated variants, third was also designed with adding some special additive.

The samples were tested for hydration resistance as per ASTM C456 (Reapproved 2008) standard. 50X50X50 mm cube size samples were kept in an autoclave at 80psi and 162°C temperature for five hours. After colling samples are taken out and physical observations are noted. Sem and XRD analysis are done to identify new phases that evolved during hydration.

Results and Discussions

Figure: 1 clearly shows effectiveness of the anti-hydration treatment and incorporation of the additive against the hydration. Anti hydration treatment is effective for Sample M-1 & 2, but incorporation Al_2O_3 reduces the effectiveness of that treatment and MA-2 becomes hydrated partially due to presence of higher percentage of Al_2O_3. But effectiveness of additive to increase hydration resistance is proven in all four samples.

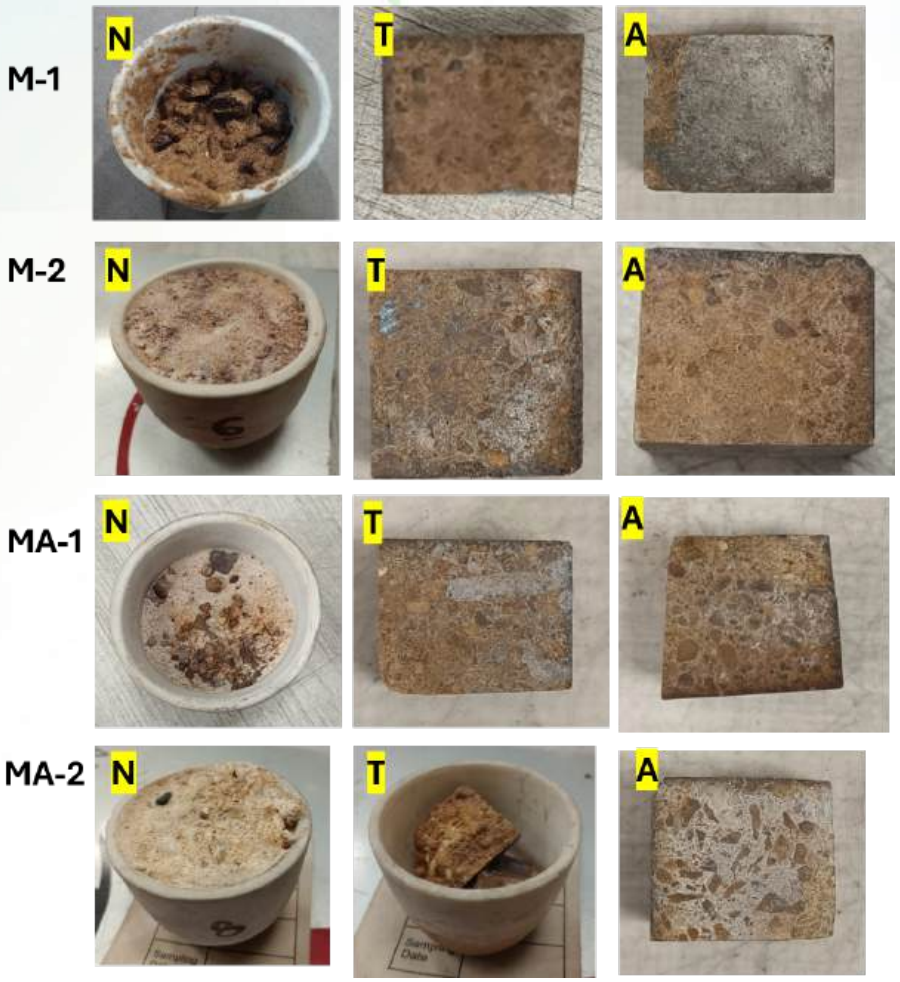


Figure-1: Condition of the different samples after hydration test. N represents normal sample; T represents anti hydration coated sample & A represents samples with special additives.

The hydration assessment revealed significant differences among the investigated formulations. Untreated magnesia-based compositions containing large fractions of free MgO exhibited visible hydration after hydration. The presence of reactive MgO provided favourable conditions for brucite formation, resulting in localized expansion and deterioration of matrix integrity.The dipping treatment significantly improved hydration resistance in almost all investigated compositions. Samples subjected to anti-hydration dipping exhibited lower susceptibility to visible hydration compared with their untreated counterparts. The protective surface layer generated during dipping effectively reduced direct contact between atmospheric moisture and exposed MgO particles.

The beneficial effect of dipping is believed to originate from partial sealing of open pores and microcracks. By reducing permeability, the treatment delayed moisture ingress and suppressed brucite formation within the refractory body. This improvement was particularly noticeable in high-MgO formulations that otherwise exhibited severe hydration in the untreated state.

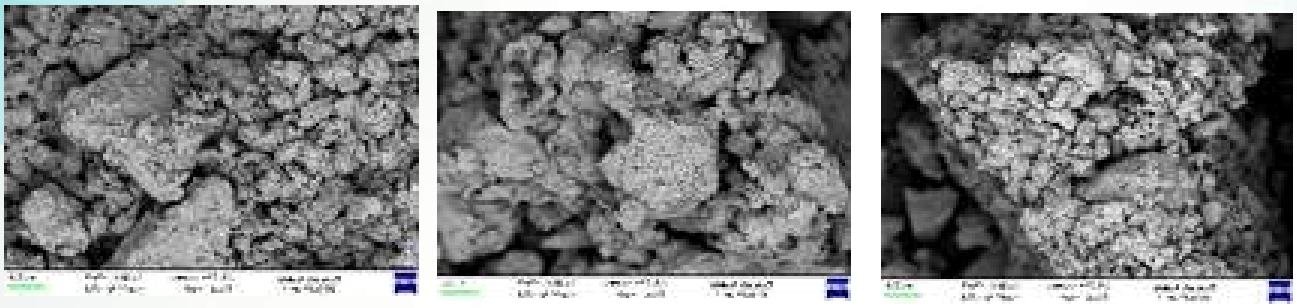


Figure-2: Microstructure of M-1& 2 after hydration test.

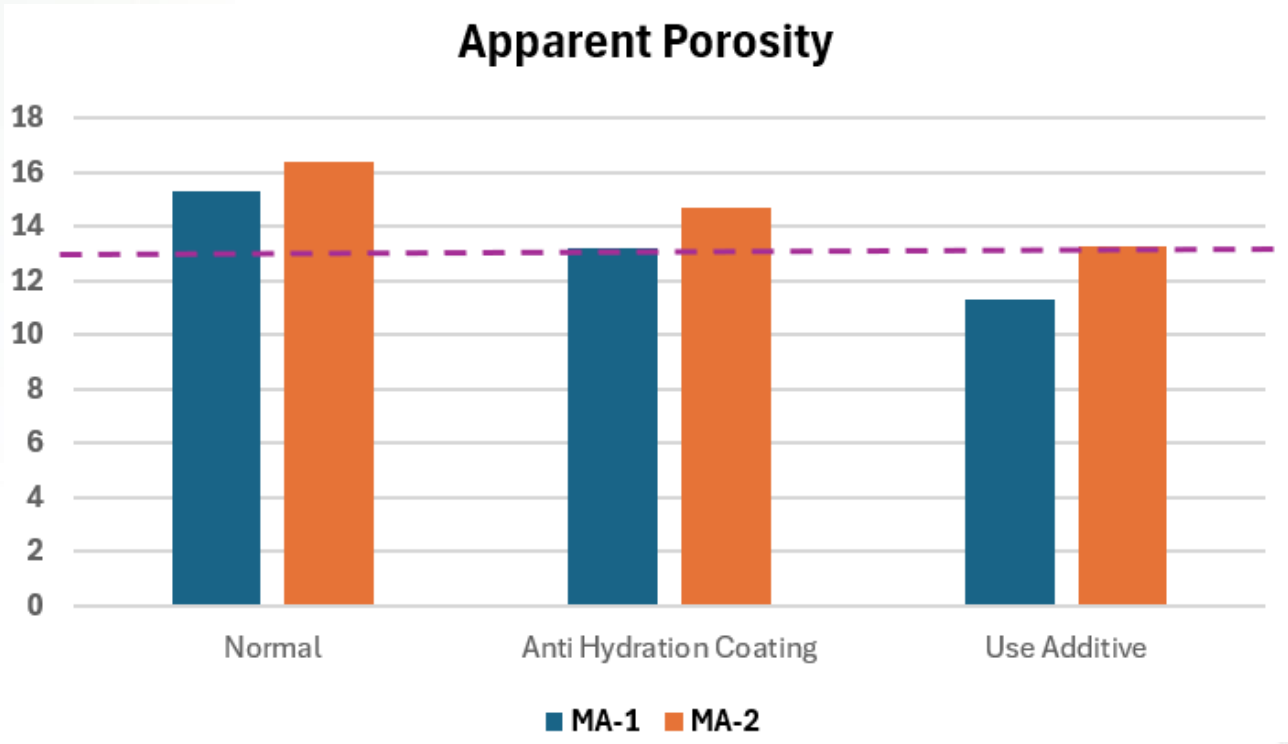


Figure-3: Apparent Porosity of MA-1 and MA-2.

Figure-3 explains the role of Alumina on the hydration resistance of magnesite refractory. At high temperature it reacts with MgO grains to form spinel which precipitate at the grains boundary and improved hydration resistance. But formation of spinel accompanying with volume expansion that increase the structural porosity when Alumina percent is beyond 10% and reduces the hydration resistance.

A strong relationship was observed between hydration resistance and microstructural density. Compositions possessing lower apparent porosity and higher bulk density exhibited superior resistance to humidity-induced degradation. The denser microstructure restricted capillary transport of moisture and minimized direct access of water vapors to MgO grains. Consequently, hydration reactions remained largely confined to the outer surface.

Among all protection methods, additives containing specimens exhibited the highest resistance against humidity attack. It increases the solubility of C_2S in the glass

phase and promotes a continuous glassy surface layer that acted as a highly effective barrier against moisture penetration. This coating sealed open pore channels and significantly reduced water diffusion into the refractory interior.

The superior performance of these refractories having glassy coating around the periclase grains demonstrates that moisture transport is a key factor controlling hydration degradation. Once water penetration is effectively restricted, even highly basic refractory compositions can maintain structural integrity during prolonged exposure to humid environments. The results confirm the importance of surface engineering in enhancing stability and handling reliability of magnesia-based refractories.

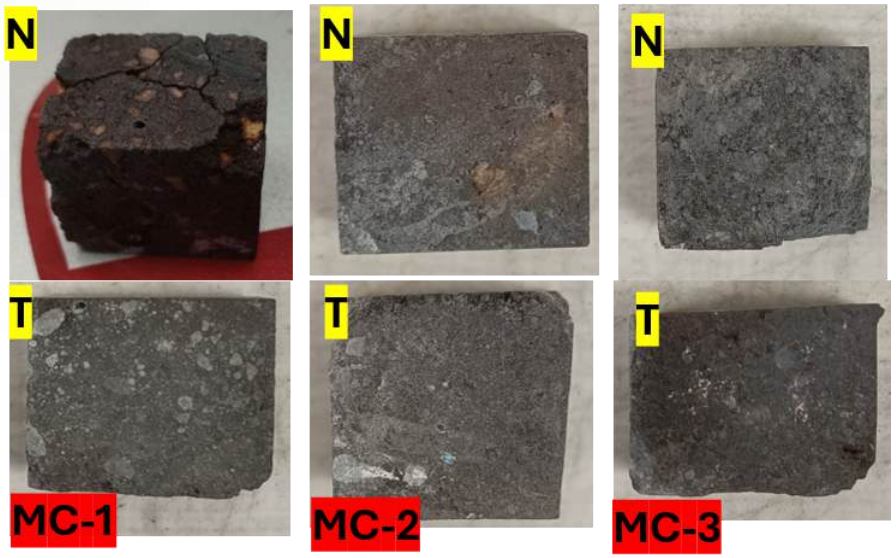


Figure-4: Condition of the different Magnesia chrome samples after hydration test. N represents normal sample; T represents anti hydration coated sample.

The hydration assessment of Magnesia chrome sample revealed significant differences among the investigated formulations. The improved behavior of chrome-containing compositions can be attributed to their reduced effective free MgO content and more stable mineralogical structure. Magnesia-chrome aggregates possess a dense fused microstructure that restricts water penetration and lowers the hydration reaction rate. Furthermore, chrome-bearing phases improve grain-to-matrix bonding and reduce the availability of highly reactive surfaces. Among three samples MC-3 shows best hydration resistance than MC-2 and MC-1. Normal sample of MC-1 developed some cracks after hydration test due absence of fused materials and higher porosity. But these effects is minimized in MC-2 and MC-3 due to presence of Fused grains reduces the porosity. Presence of Cr_2O_3increases the surface energy and promotes sintering that's helps to risk of hydration and formation of $MgO\text{-}Cr_2O_3$ does not hydrate due to strong direct bonding between grains.

3. Conclusions

The present investigation demonstrates that hydration resistance of basic refractories is governed primarily by free MgO reactivity, pore structure, and moisture accessibility. Untreated magnesia-rich compositions showed higher susceptibility to hydration because of brucite formation and the associated expansion-induced damage. Magnesia-chrome phases, dense microstructures, and protective surface treatments interrupt this cycle by reducing either MgO reactivity or moisture accessibility. As a result, hydration progression becomes substantially slower, ensuring better physical and mechanical property retention.

Anti-hydration dipping treatment effectively improved resistance by creating a protective barrier that reduced water access to MgO grains. Among all evaluated protection methods, frit coating provided the highest level of hydration resistance through the formation of a dense glassy surface layer that sealed open pores and minimized moisture diffusion.

4. Reference

1. N. Kamochi, Y. Miyamoto, T. Kishi and K. Takeda, “Hydration Resistance of Magnesia Refractories and Effect of Surface Coating Treatment,” *Taikabutsu Overseas*, Vol. 18, No. 2, 1998, pp. 18-25.
2. P. Pilate, A. Buhr and C. Parr, “Influence of Magnesia Raw Materials on Hydration Behaviour of Basic Refractories,” *UNITECR Proceedings*, Orlando, USA, 2001.
3. E. García, J. M. Rincón and M. Romero, “Effect of Glass-Forming Additives on Hydration Resistance of Magnesia Refractories,” *Ceramics International*, Vol. 35, 2009, pp. 2525-2531.

ROLE OF ANTIOXIDANTS ON THE THERMOMECHANICAL PROPERTIES OF MAGNESIA CARBON REFRACTORIES

Sirshendu Das, Soumendu Das, B. Ghosh, Prasant Kumar Naik.

TRL Krosaki Refractories Ltd

Abstract

MgO-C refractory is widely used in steel making applications, mainly in steel ladles, LD converters, electric arc furnaces and in secondary steel making due to their excellent thermal shock & slag corrosion resistance. Graphite plays a pivotal role in MgO-C due to its excellent non-wetting behaviour against Slag& Metal and high thermal conductivity which enhance the thermal shock resistance of MgO-C. But due its least oxidation resistance at elevated temperatures remains a critical limitation affecting thermomechanical performance. Different metal powder and oxide, carbide & Nitride are used to slow down the oxidation rate of graphite and improve thermomechanical strength at elevated temperature. In this study the role of antioxidant additives like Al, Si, SiC, B4C & Al-Mg on the thermomechanical properties of MgO–C refractories are studied. These antioxidants in different combination were incorporated into MgO–C recipe, and their effects on oxidation resistance, hot modulus of rupture, elastic modulus, permanent linear change, and thermal shock resistance were systematically evaluated.Formation of different phases due to presence of different additives at high temperature also studied through XRD and SEM analysis, and their role on high temperature property are also studied. The findings from this study are helpful for selection and optimization of antioxidants which play a decisive role in enhancing the thermomechanical stability and service performance of MgO–C refractories under severe steelmaking conditions.

Keywords: MgO-C Refractories, metal powder, thermomechanical properties, XRD SEM-EDS, XRF study.

1. Introduction

Magnesia-carbon (MgO-C) refractories are extensively utilized in steelmaking vessels such as steel ladles, LD converters, electric arc furnaces (EAFs), and secondary refining units due to their excellent resistance to slag corrosion, superior thermal shock resistance, and outstanding non-wetting characteristics against molten steel and slag. The exceptional performance of MgO-C refractories is attributed to the synergistic combination of fused magnesia and graphite. Graphite provides high thermal conductivity, low thermal expansion, and excellent non-wetting behaviour, while magnesia offers superior chemical compatibility with basic steelmaking slags. Carbon plays a vital role in MgO-C refractories by filling pore spaces and minimizing slag penetration.However, the primary limitation of graphite-containing refractories is the oxidation of carbon during service. Carbon oxidation occurs through direct oxidation below 1400°C and indirect oxidation above 1400°C, leading to graphite depletion, increased porosity, reduction in mechanical strength, and accelerated refractory wear. The loss of carbon generates interconnected pore channels, which facilitate slag penetration into the refractory matrix and accelerate degradation. To mitigate this limitation, various antioxidants such as aluminum (Al), silicon (Si), silicon carbide (SiC) and boron carbide (B_4C), additives are incorporated into MgO-C formulations. These antioxidants preferentially react with oxygen and form secondary ceramic phases including spinel ($MgAl_2O_4$), forsterite (Mg_2SiO_4), monticellite ($CaMgSiO_4$), silica-rich phases, and borate compounds. The formation of these phases not only enhances oxidation resistance but also significantly influences mechanical strength, thermal shock resistance, and

elastic behaviour at elevated temperatures. In the present investigation, eight MgO-C refractory formulations containing different antioxidant combinations were developed and evaluated. The objective of the study was to examine the influence of Al, Si, SiC, and B_4C-based antioxidant systems to establish correlations between phase formation and thermomechanical performance. The study aims to identify the most effective antioxidant combination for enhancing the service life and overall performance of MgO-C refractories operating under severe steelmaking conditions.

2. Experimental

Total 8 no of batches were made using various fraction of fused magnesia, graphite, antioxidants, additives, and binder (shown in Tab.1). All the materials were mixed thoroughly in an inclined mixer and pressed in a high-capacity electric screw press (650 MT) and tempered in a Tempering Kiln.

Batch No	A1	A2	A3	A4	A5	A6	A7	A8
Fused Magnesia	MgO >97.3							
Graphite	12-14%							
Al	✓				✓		✓	✓
Si		✓				✓		
SiC			✓		✓	✓		
B4C				✓			✓	✓
Binder	2.5-3%							

Tab. 1: Batch Composition

The tempered bricks were cut into different shapes and tested for different thermomechanical properties like Apparent porosity, bulk density, cold crushing strength both at atmospheric & elevated temperature, HMOR, MOE, spalling resistance etc were tested. SEM and XRD analysis also done from coked sample to corelate the different phases with the changes in the property at high temperature.

3. Results and Discussions

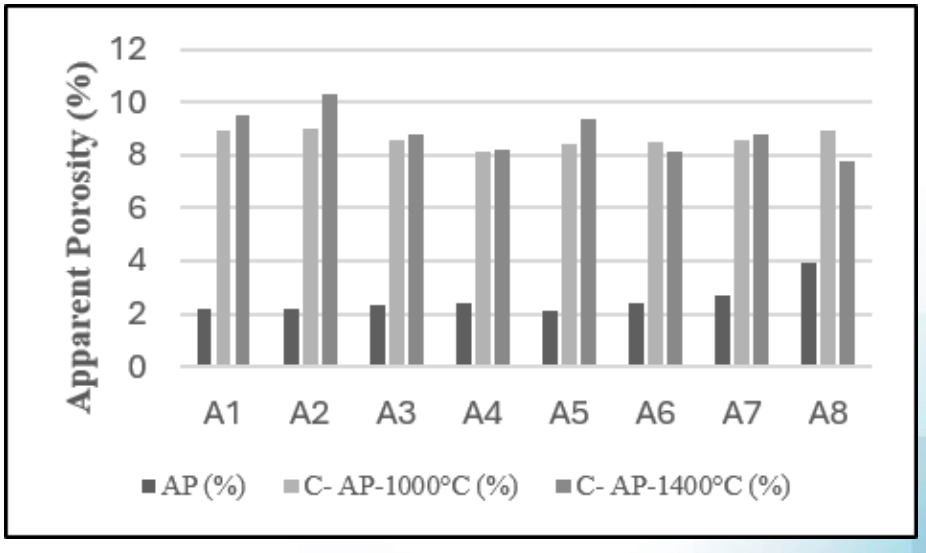


Fig. 1: Apparent Porosity measured at room temperature and after coking at 1000˚C and 1400˚C.

Among the eight trial batches (A1 to A8), the physical properties remained largely comparable, indicating that variations in antioxidant type had minimal influence on particle packing and compaction behaviour. The A6 batch (Si + SiC) exhibited the highest bulk density, suggesting improved packing efficiency and matrix compactness. Following coking at both intermediate and elevated temperatures, all batches showed increased porosity and reduced density due to resin decomposition, graphite oxidation, and microstructural pore development. However, the extent of degradation varied significantly with antioxidant chemistry. Among all formulations, A6 maintained the highest coked bulk density at 1000°C and 1400°C, indicating excellent structural stability. Similarly, A8 showed the lowest apparent porosity after coking at 1400°C (7.8%), demonstrating the effectiveness of B_4C in minimizing oxidation-induced pore formation.In contrast, the A1 (Al) andA2 (Si) batches developed comparatively higher porosity after coking, which increased stress concentration sites and promoted crack propagation, ultimately affecting mechanical performance.

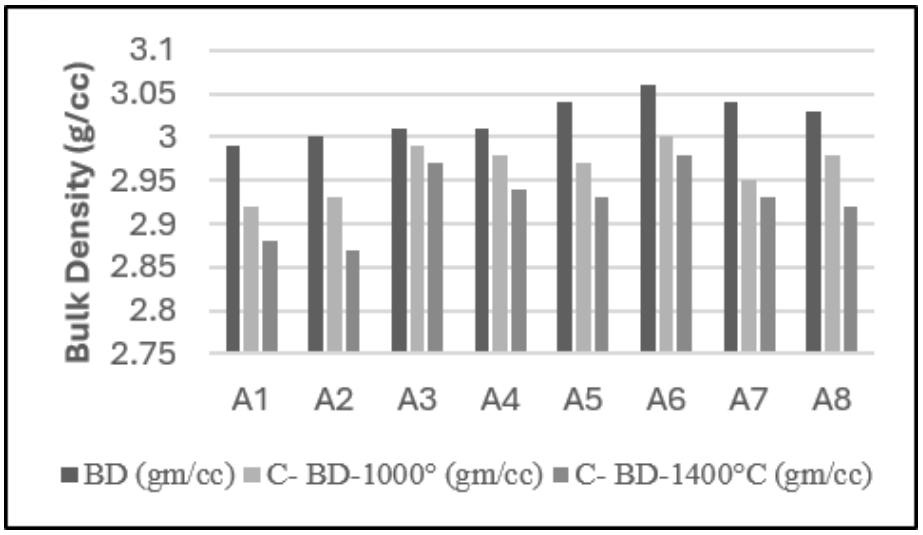


Fig. 2: Bulk Density measured at room temperature and after coking at 1000˚ C and 1400˚ C.

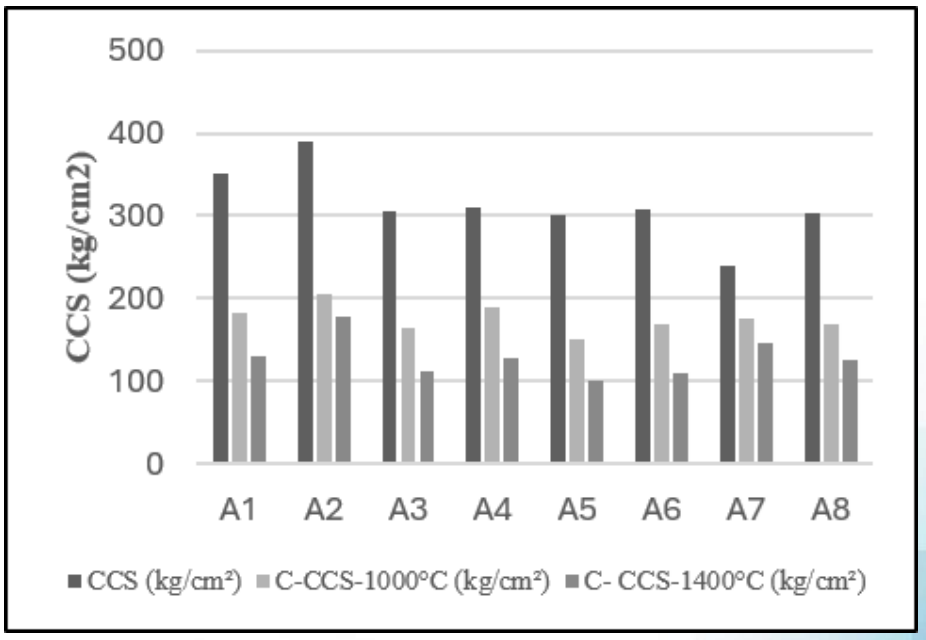


Fig.3: Cold Crushing Strength measured at room temperature and after coking at 1000˚C and 1400˚C.

The influence of antioxidant chemistry became more pronounced after coking. The A2 batch (Si) exhibited the highest retained CCS at both coking temperatures, indicating the formation of strong magnesium silicate bonding phases that enhanced matrix strength and inhibited crack initiation. The A7 batch (Al + B_4C) also showed excellent strength retention despite its relatively lower green strength, highlighting the effectiveness of B_4C in preserving graphite and limiting pore formation during firing. Although all batches experienced strength reduction after high-temperature(1400°C)exposure, the superior retained strength of A2 and A7 confirms the beneficial role of silicon- and boron-based antioxidants in maintaining structural integrity under severe thermal conditions.

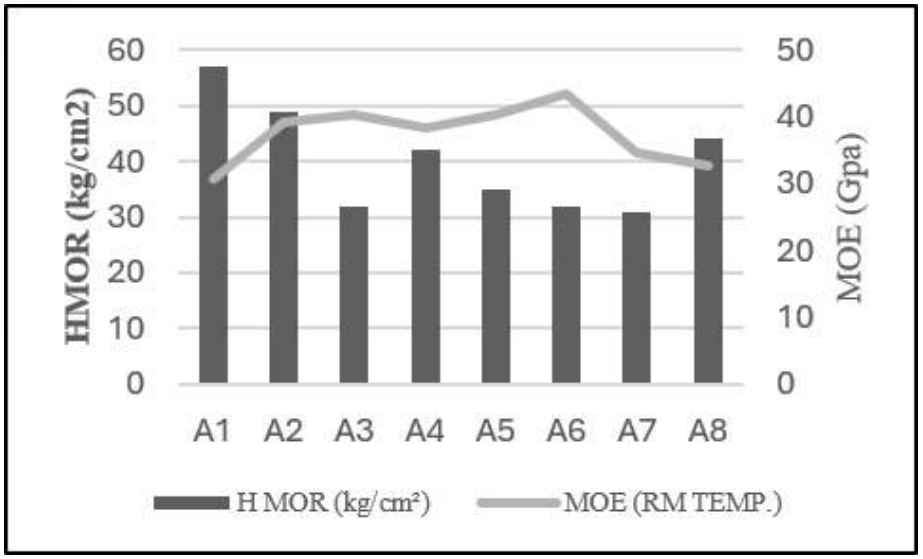


Fig. 4: Hot Modulus of Rupture & Modulus of elasticity measured at room temperature and 1400˚C

The Hot Modulus of Rupture (HMOR) values and hot strength was highest inA1, followed by A2 and A8. The enhanced HMOR observed in aluminium-containing formulations can be attributed to the development of spinel-based ceramic bonding phases, which provide structural integrity and maintain strength under elevated-temperature conditions.The Modulus of Elasticity (MOE) value in silicon and silicon carbide generally exhibited higher MOE values, indicating the formation of a comparatively stiffer and more compact microstructure. Although increased stiffness can enhance resistance to mechanical loading, excessively rigid structures may become more susceptible to thermal stress and crack propagation during thermal cycling.

Sample	Major Phase	Minor Phase
A1	Periclase, Graphite	Spinel, metallic Al
A2	Periclase, Graphite	Forsterite, metallic Si
A3	Periclase, Graphite	SiC
A4	Periclase, Graphite	Spinel, Forsterite
A5	Periclase, Graphite	Spinel, SiC
A6	Periclase, Graphite	SiC, Monticellite
A7	Periclase, Graphite	Spinel, Monticellite

A8	Periclase, Graphite	Spinel, B4C

Tab. 2: Phase analysis by XRD of different MgO-C samples
Fig. 5: Oxidation resistance of trial sample at 1400˚ C for 3 hrs

The oxidation and thermal shock resistance results highlighted the significant influence of the antioxidant system on refractory performance. B_4C-containing compositions exhibited superior oxidation resistance, which can be attributed to the formation of borate-rich reaction products that seal pores, restrict oxygen ingress, and protect graphite from oxidation.

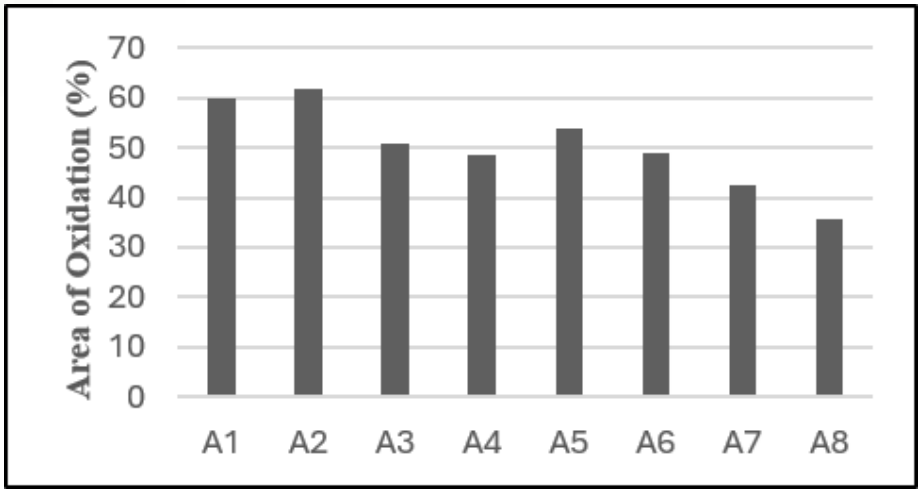


Fig. 5: Oxidation resistance of trial sample at 1400˚ C for 3 hrs

The development of a protective surface layer further enhanced carbon retention and reduced the extent of the oxidized zone. In contrast, SiC-containing formulations demonstrated the best thermal shock resistance due to their higher thermal conductivity, which minimizes thermal gradients during rapid heating and cooling. Additionally, SiC promotes crack deflection and stress redistribution, improving resistance to thermal stress damage. However, the glassy phases generated from B_4C oxidation tend to increase matrix stiffness, reducing the material's ability to accommodate thermal stresses.

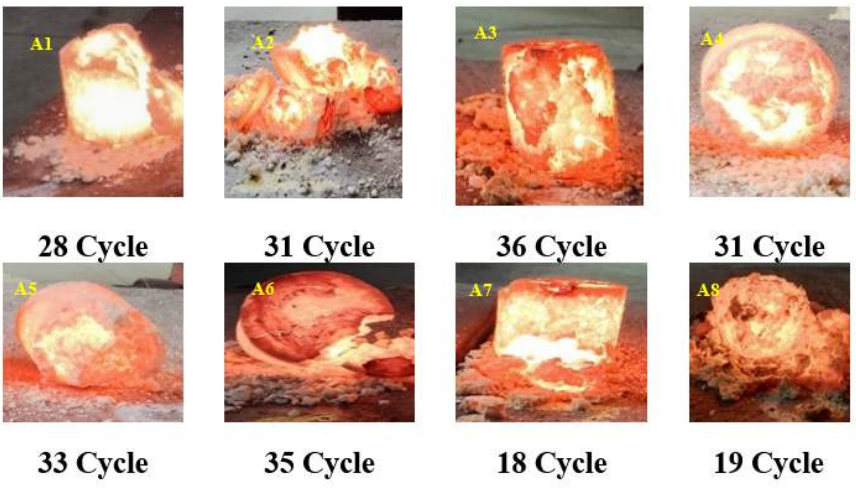


Fig. 6: Thermal shock resistance of trial sample at 1400˚ C

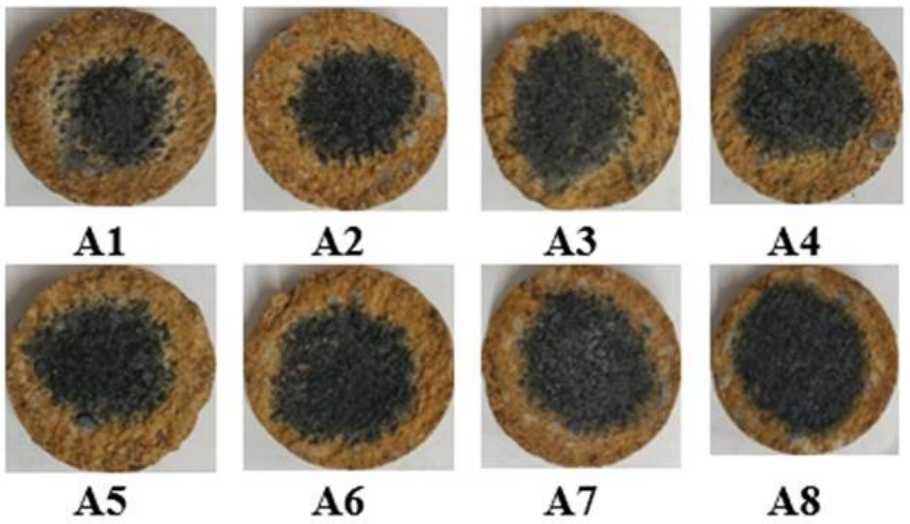


Fig. 7: Photographs showing the oxidation test samples.

XRD and SEM analyses revealed that antioxidant chemistry significantly influenced phase evolution and microstructural development after coking at 1400°C. Periclase remained the dominant phase in all formulations, while secondary phases varied according to the antioxidant system. Al-containing compositions showed the formation of $MgAl_2O_4$ spinel, which enhanced ceramic bonding and high-temperature strength. Silicon-containing samples developed forsterite phases that improved matrix densification and cold strength, whereas SiC-bearing compositions retained SiC particles that contributed to thermal shock resistance through improved thermal conductivity. Monticellite was detected in Si-SiC systems, and its excessive formation may be responsible for reduced hot strength. SEM observations confirmed the presence of spinel, forsterite, SiC, and boron-containing phases distributed within the matrix.

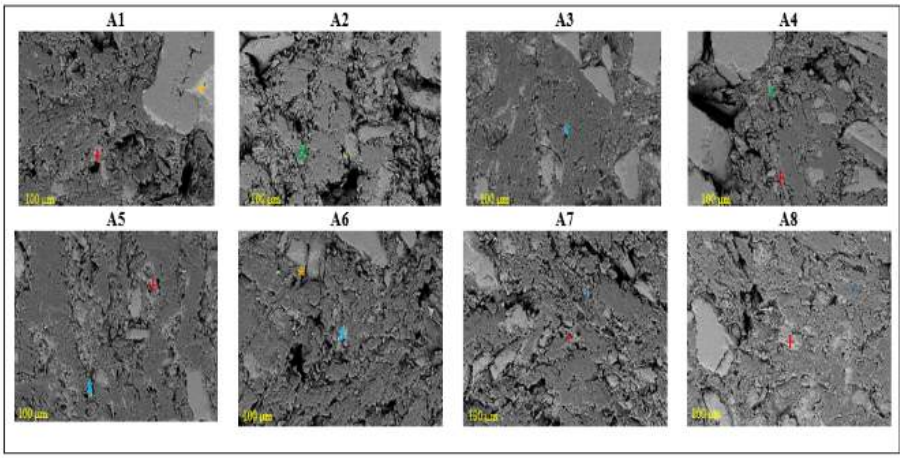


Fig. 8 SEM analysis of trial sample +: Spinel, *: Monticellite; ^: Metallic Si; #: Forsterite, $: SiC, ●: B4C.

The Al-B_4C compositions exhibited a denser microstructure with fewer oxidation-induced pores and higher graphite retention, indicating effective pore sealing by borate phases and superior oxidation resistance. It is strongly correlate with the improved thermomechanical performance observed in the B_4C-containing formulations.

4. Conclusions

The present study demonstrates that the selection of antioxidant systems has a significant influence on the overall performance of MgO-C refractories. Aluminum-containing formulations showed improved high-temperature strength through the formation of stable ceramic bonding phases, while silicon and silicon carbide additions enhanced microstructural rigidity and thermal shock resistance. SiC-based compositions exhibited superior resistance to thermal cycling due to their ability to reduce thermal stress development and promote crack deflection. Boron carbide proved to be the most effective antioxidant, significantly improving oxidation resistance by forming protective reaction products that limit oxygen penetration and preserve carbon within the refractory matrix. However, the increased stiffness associated with these reaction products resulted in comparatively lower thermal shock resistance. The results therefore indicate a clear performance trade-off between oxidation resistance and thermal shock resistance.

Overall, the findings suggest that no single antioxidant system provides optimum performance for all service requirements. A balanced antioxidant design combining strength retention, oxidation protection, and thermal shock resistance is essential for achieving enhanced durability and reliable performance of MgO-C refractories under severe operating conditions.

5. Reference

I. Gokce, A., Gurcan, C., and Aksel, C., "Effect of Antioxidants on Oxidation Behaviour of MgO-C Refractories," Ceramics International, Vol. 33, No. 4, 2007, pp. 533-540.

II. Luz, A.P., Pandolfelli, V.C., and Aneziris, C.G., "Review of Carbon-Containing Refractories and Their Oxidation Mechanisms," Ceramics International, Vol. 44, 2018, pp. 19447-19463.

III. Yamaguchi, A., and Zhang, S., "Role of Aluminum and Silicon Additives in MgO-C Refractories," Journal of the European Ceramic Society, Vol. 16, 1996, pp. 775-779.

IV. Uchida, S., and Bradt, R.C., "Oxidation Protection Mechanisms of Boron Carbide in Carbon-Bonded Refractories," Journal of the American Ceramic Society, Vol. 72, No. 1, 1989, pp. 16-21.

V. Singh, V., Sarkar, R., and Banerjee, G., "Microstructural Evolution and Phase Development in Antioxidant-Containing MgO-C Refractories," Ceramics International, Vol. 42, 2016, pp. 16572-16

INNOVATIVE COLD-START REFRACTORY TECHNOLOGIES FOR CONTINUOUS CASTING WITHOUT FUEL-GAS PREHEATING: AN APPROACH TOWARD ENHANCED ENVIRONMENTAL SUSTAINABILITY

S.Palit, S.Karmakar, S.Ali, H.Suzuki, K.Haren, T.Sadano, H.Nagata

TRL Krosaki Refractories Limited, Belpahar, Odisha, INDIA

Corresponding author's e-mail: sudipta.palit@trlkrosaki.com

Abstract

The Submerged Entry Nozzle (SEN) is a critical refractory component in continuous casting, providing a protected channel for molten steel from the tundish to the mold. Conventional SENs consist of an Alumina-Graphite (AG) body and a Zirconia-Graphite (ZG) slag-line region and require fuel-gas preheating to prevent thermal shock during casting start-up.

To address the limitations associated with fuel consumption, CO_2 emissions, and operational dependency on preheating systems, Krosaki Group developed a **Cold-Start SEN** capable of direct operation without preheating with adequate corrosion resistance. Thermal shock resistance was enhanced through increasing fused silica content and optimization of particle-size distribution (granulometry).

Thermal shock performance was evaluated using a severe water-quenching test ($\Delta T \geq 1000°C$), which confirmed excellent resistance to cracking and spalling. Industrial trials further validated stable start-up and reliable casting without fuel-gas preheating. The technology improves operational flexibility, reduces fuel consumption and CO_2 emissions, and supports sustainable continuous casting operations.

Keywords: Submerged Entry Nozzle, Thermal Shock Resistance, Fused Silica, Particle Size Distribution.

1. Introduction

Continuous casting has become the predominant steel solidification technology, accounting for more than 90% of global steel production due to its superior productivity, yield, and product quality. Among these refractory components, the Submerged Entry Nozzle (SEN) performs a critical function by safely transferring molten steel from tundish to mold while maintaining a protective barrier against atmospheric oxidation and maintaining steel cleanliness.

Consequently, conventional SENs manufactured from Alumina-Graphite (AG) body materials and Zirconia-Graphite (ZG) slag-line materials require preheating prior to service. Typically, SENs are preheated between 1000-1200°C for several hours before use. However, preheating requires fuel gas, increases operating costs and CO_2 emissions, and reduces operational flexibility during schedule changes or emergency nozzle replacement.

To address these challenges, the Krosaki Group developed a Cold-Start SEN capable of direct operation without fuel-gas preheating. The present study describes the material design, thermal shock evaluation, and industrial validation of this innovative refractory technology for sustainable continuous casting operations.

2. Experimental

2.1 Design Philosophy of Cold-Start SEN

The primary challenge in developing a Cold-Start SEN is to withstand the severe thermal shock generated when molten steel is introduced into a nonpreheated nozzle.

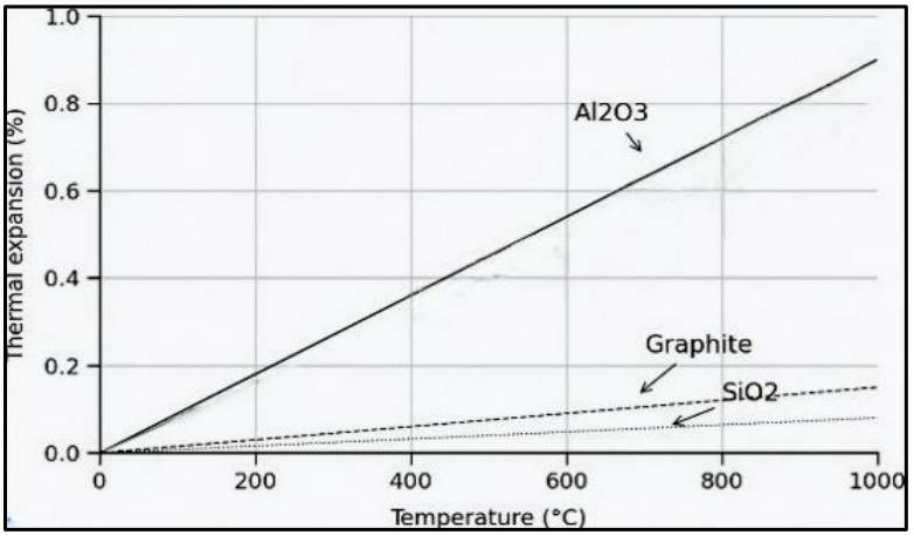


Fig. 1: Temperature v/s Thermal expansion % relationship [1]

.

As shown in Fig. 1, fused silica and graphite exhibit significantly lower thermal expansion than conventional alumina-based refractory constituents. Therefore, incorporation of fused silica reduces the overall thermal expansion of the body material and consequently lowers the thermal strain generated during rapid heating.

In addition to compositional optimization, the particle size distribution was redesigned by shifting the granulometry towards a coarser structure. The resulting increase in porosity and reduction in elastic modulus improved the material's ability to accommodate thermally induced stresses during casting start-up. Thus, the development concept combined the thermal expansion reduction effect of fused silica with the stress-relief effect of optimized granulometry to achieve superior thermal shock resistance required for Cold-Start SEN operation.

2.2 Material Preparation

Since the SEN consists of a multilayer refractory structure comprising an Al_2O_3-C body material and a ZrO_2-C powder-line material, the present development was primarily focused on improving the thermal shock resistance of the Al_2O_3-C body material, which is exposed to the most severe thermal gradients during casting start-up.

Based on the above design philosophy, three material concepts were prepared and evaluated, namely Preheated Type, Intermediate Type, and Cold-Start Type. The chemical composition and physical properties of developed materials are summarized in Table 1.

Sample		Preheated	Intermediate	Cold Start
Composition & Properties		Conventional		Newly Developed
Composition /mass%	Free C	23	27	30
	Al_2O_3	70	56	42
	Fused SiO_2	-	13	25
	Others	7	5	3
Apparent porosity / %		10.9	12.5	13.7
Thermal Expansion at 1000°C /%		0.43	0.31	0.23
Thermal Spalling Resistance Index (S/E *α)		0.88	1.56	2.32

Table 1: Chemical composition and physical properties of developed materials.

The compositions were designed by progressively increasing the levels of fused silica and free carbon, as shown in the mix-mapping diagram (Fig. 2).

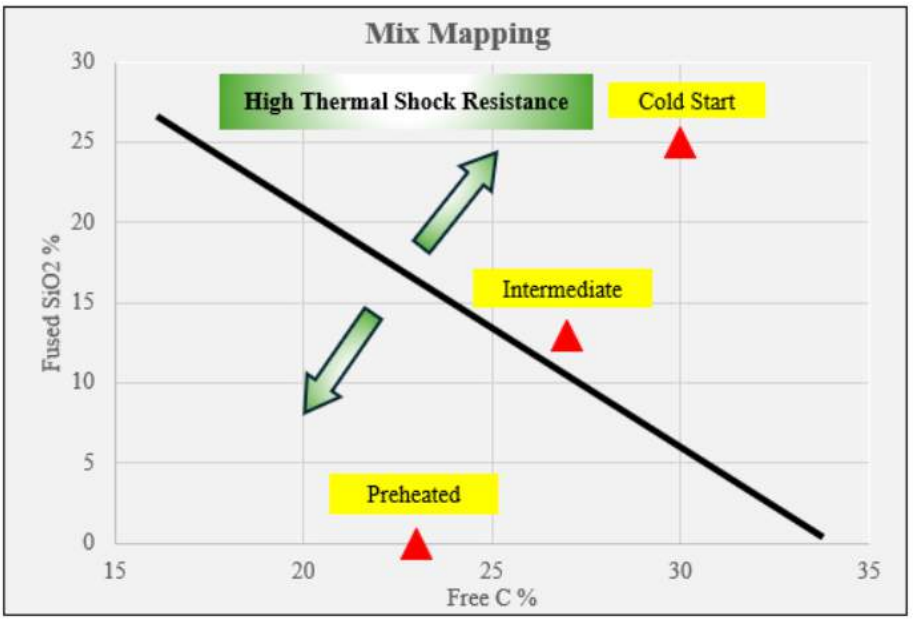


Fig. 2: Fused Silica% vs Free C% mapping of Body Materials for Cold-Start SEN Development.

Further improvement was achieved through optimization of particle size distribution. As shown in Fig. 3, the conventional Preheated material contained a relatively high fraction of medium-sized particles, whereas the Intermediate and Cold-Start compositions were progressively shifted toward a coarser granulometric structure. This modification resulted in a more open microstructure with increased apparent porosity (Table 1) and reduced elastic modulus. The resulting decrease in thermal stress during rapid heating improved the material's ability to withstand severe thermal gradients. Therefore, while fused silica primarily contributed to lowering thermal expansion,

granulometry optimization contributed to thermal shock resistance through microstructural stress relaxation.

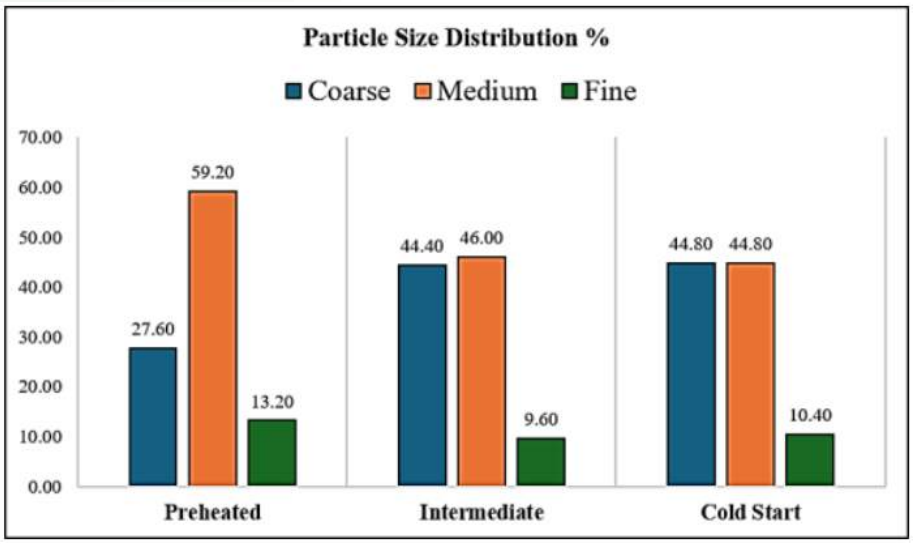


Fig. 3: Particle size distribution (%) of Preheated vs Intermediate vs Cold Start types.

The combined optimization of fused silica content and particle size distribution enabled the development of a Cold-Start SEN material exhibiting significantly improved thermal shock resistance while maintaining the structural integrity required for continuous casting applications.

3. Results and Discussion

3.1 Thermal Shock Resistance Evaluation

Thermal shock resistance was evaluated using a simplified thermal spalling resistance index based on the parameter proposed by D.P.H. Hasselman [2] . The index was used for relative comparison among the developed compositions and was calculated as:

Thermal Spalling Resistance Index =

$$S / E \times \alpha \quad (1)$$

where S is the Cold Modulus of Rupture (MPa), E is the Modulus of Elasticity (GPa), and α is the thermal expansion rate (%) measured at 1000°C. Higher index values indicate better resistance to thermal shock damage. The calculated indices are presented in Fig. 4.

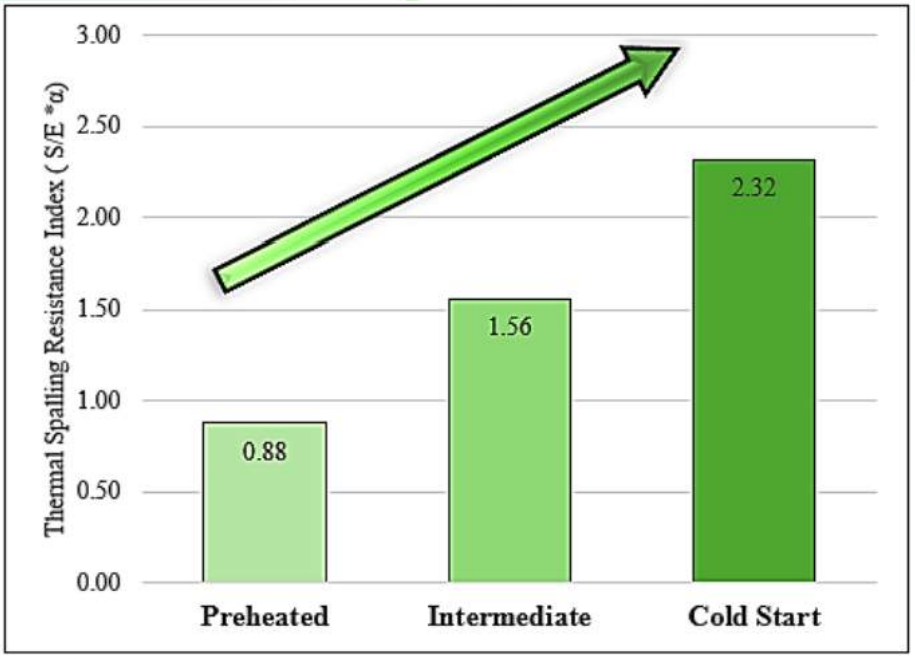


Fig. 4: Comparison of Thermal Spalling Resistance Index of Developed Materials.

Fig. 4 shows a continuous increase in thermal spalling resistance from Preheated to the ColdStart composition. The improvement is attributed to two complementary mechanisms. Firstly, the incorporation of fused silica reduced the thermal expansion coefficient (α), thereby lowering thermal strain generated during rapid heating. Secondly, optimization of particle size distribution shifted the structure towards a coarser and more porous microstructure, which decreased the elastic modulus (E) and improved stress accommodation. The combined reduction in α and E resulted in a significant increase in the thermal spalling resistance index and consequently improved resistance to thermal shock damage.

3.2 Thermal Spalling Test

While the thermal spalling resistance index provides a theoretical assessment of thermal shock behavior, a severe thermal spalling test was conducted to evaluate the materials under practical conditions representative of casting start-up.

As reported previously for Cold-Start SEN development, cylindrical specimens measuring 180 mm diameter × 200 mm height, with an open upper end and closed bottom, were prepared from the developed body materials. The specimens were heated uniformly for an hour in an electric furnace to the specified high temperature and subsequently subjected to rapid water quenching from the outer surface. This method generated a severe radial temperature gradient similar to that experienced by an SEN during direct contact with molten steel without preheating.The schematic diagram and actual thermal spalling test procedure are shown in Fig. 5.[3]

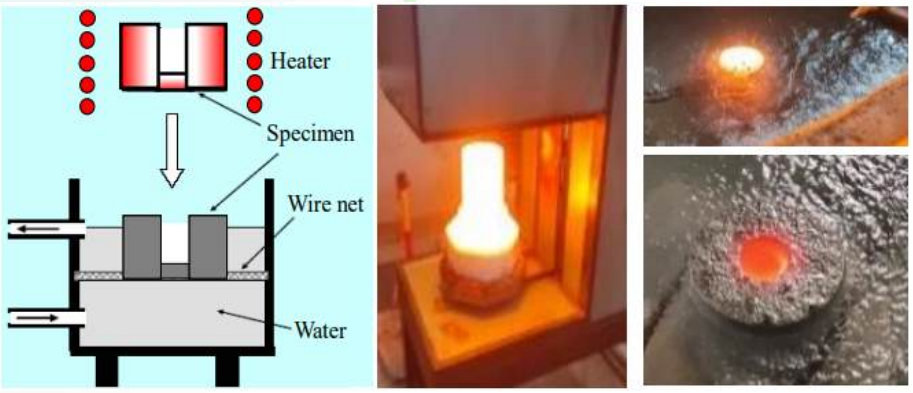


Fig. 5: Schematic diagram of thermal spalling test

After each quenching cycle, the specimens were visually examined for crack formation and the procedure was repeated until thermal damage was observed.The observations were summarized in Table 2.

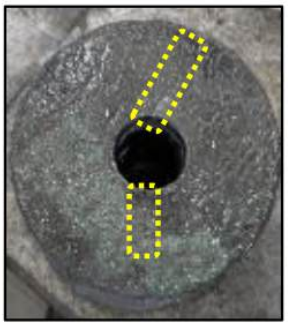
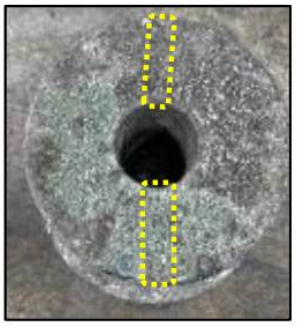
Temp. (°C)	Sample No.	Body Mix		
		Preheated	Intermediate	Cold Start
At 1200°C	1st Sample	○⇒×	○⇒○⇒×	○⇒○⇒○
	2nd Sample	○⇒×	○⇒○⇒×	○⇒○⇒○
At 1400°C	1st Sample	×	○⇒×	○⇒○⇒○
	2nd Sample	×	○⇒×	○⇒○⇒○
			○ *No crack*	× *Crack observed*
Result of Spalling Test		 Cracks appear at 1st cycle	 Cracks appear at 2nd cycle	 No Cracks appear at 3rd cycle

Table 2: Thermal Spalling results of developed materials.

4. Industrial Validation and Operational Benefits

Following laboratory qualification, the Cold-Start SEN was evaluated under actual production conditions at continuous casting facilities. The nozzles were installed directly without fuel-gas preheating and exposed immediately to molten steel during casting start-up.

Stable casting initiation was achieved without thermal shock-related failures, and no evidence of cracking, abnormal wear, or structural deterioration was observed during operation. Service lives exceeding 400 minutes were successfully achieved under normal slab caster operating conditions. Post-service inspection of the used SENs confirmed satisfactory wear characteristics

and structural integrity, validating the effectiveness of the optimized material design.

Customer	Customer A	Customer B	Customer C
Type of Casting Mould	Slab Caster with 1850 -2050 Mould section	Slab Caster with 1850 -2050 Mould section	Slab Caster with 1850 -2050 Mould section
Avg Service life of used SEN (n=50)	417 min	480 min	550 min
Photographs of Used SEN			

Fig. 6: Photographs of used Cold start SEN [4]

An additional advantage of the Cold-Start SEN is its immediate availability for use, eliminating the waiting time associated with conventional preheating. This improves operational flexibility and enables rapid response during emergency nozzle replacement or clogging incidents. Although fuel-gas preheating is unnecessary, moisture control remains important for safe operation. Therefore, SENs are stored in an electrically heated drying chamber maintained at approximately 200°C for a minimum of 12 hours prior to use.[5] This ensures safe deployment while preserving the operational flexibility offered by Cold-Start technology.

5. Environmental Sustainability and Economic Benefits

The elimination of fuel-gas preheating through Cold-Start SEN technology contributes directly to the reduction of greenhouse gas emissions in continuous casting operations. To quantify this benefit, a theoretical calculation was carried out assuming a typical changeable slab caster SEN weighing 22.1 kg.

Assuming an average specific heat capacity of 1.1 kJ/kg·K, an ambient temperature of 25°C (298 K), and a conventional preheating temperature of 900°C (1173 K), the heat energy required for SEN preheating can be estimated as:

$Q = mCp\Delta T$ (2)

Q = 22.1 × 1.1 × (1173 − 298)

$Q \approx$ 21,271 kJ

Assuming propane is used as the preheating fuel, with a calorific value of 46,000 kJ/kg, the theoretical fuel requirement is approximately 0.46 kg Propane per SEN. Considering a practical burner efficiency of 60%, the actual propane consumption increases to approximately 0.76 kg per SEN.

Based on the combustion reaction:

$C_3H_8 + 5O_2 \rightarrow 3CO_2 + 4H_2O$ (3)

The combustion of 0.76 kg propane produces approximately 2.28 kg of CO_2. Therefore, each ColdStart SEN used in place of a conventionally preheated SEN can avoid approximately 2.28 kg of direct CO_2 emissions associated with the preheating process.

Considering the large number of SENs consumed annually, the cumulative environmental benefit is significant. In addition to reducing fuel consumption and direct CO_2 emissions, the Cold-Start SEN minimizes refractory losses associated with discarded preheated nozzles, thereby supporting both operational efficiency and steel industry decarbonization efforts.

6. Conclusions

An advanced Cold-Start Submerged Entry Nozzle technology has been successfully developed through the combined optimization of fused silica addition and particle size distribution in the Al_2O_3- C body material. The reduction in thermal expansion achieved by fused silica incorporation, together with the improved stress accommodation resulting from a coarser granulometric structure, significantly enhanced thermal shock resistance.

Both thermal spalling index evaluation and severe water-quenching tests confirmed the effectiveness of the developed material design. Industrial trials further demonstrated stable casting performance without fuel-gas preheating.

The developed Cold-Start SEN provides improved operational flexibility while reducing fuel consumption and associated CO_2 emissions, contributing to more sustainable continuous casting operations.

References

[1] Schacht, C.A. (Ed.). Refractories Handbook. Marcel Dekker, New York, 2004.

[2] Hasselman, D.P.H.,"Elastic Energy at Fracture and Surface Energy as Design Criteria for Thermal Shock," Journal of the American Ceramic Society, Vol. 46, No. 11, pp. 535-540, 1963

[3] S. Fujimoto, H. Shikano, and T. Kaneko, "Spalling Test Method for Graphite-Containing Nozzles," Taikabutsu, vol. 35, p. 144.

[4] S.Palit, S.Ali, G.Pandey, K.Haren,T.Sadano, A.Banik, H.Nagata, S.Sengupta.; "Advance cold start submerged entry nozzle for stable and flexible casting operations: a holistic approach towards carbon neutrality".

[5] T. Kuroda, T. Takasu, J. Amano, et al., "Advanced Cold-Start Submerged Entry Nozzle (SEN)," Krosaki Harima Technical Report, no. 164, 2016.

HIGH TEMPERATURE HYDROGEN RESISTANCE OF SYNTHETIC ALUMINA BASED CASTABLES

Andreas Buhr, Sebastian Klaus, Almatis GmbH, Frankfurt, Germany
Isabelle Henn, Universität Koblenz, Germany
Shankha Chatterjee, Almatis Alumina Pvt. Ltd., Kolkata, India

Abstract

Hydrogen is emerging as a key element in the decarbonisation of steel manufacturing and other high-temperature industrial processes, serving as an alternative to carbon-based reactants and fossil fuels. However, hydrogen's reactivity poses a challenge due to its potential to degrade refractory materials by reduction of oxidic minerals. The resistance of refractory oxides to hydrogen attack is primarily governed by their thermodynamic stability. Synthetic alumina-based materials, known for their excellent resistance to hydrogen corrosion, have shown promising results in high-temperature environments such as in the petrochemical industry or gas turbines.
Prior research has demonstrated the stability of synthetic alumina refractories, whereas silica fume containing castables showed significant strength loss when exposed to hydrogen atmospheres. This study extends the investigation to assess the performance of synthetic alumina-based and silica fume containing castables. It focuses on findings obtained at a temperature of 1400°C in comparison to 1150°C, the common temperature used in converters for direct reduction of iron ore. Also, treatment with lower hydrogen purity was included to cover the potential reactivity of industrial hydrogen quality. The results provide important insights into optimising refractory material performance in hydrogen-rich industrial settings.

Keywords: Alumina, Castable, Hydrogen, Refractory, Strength loss

1. Introduction

The European industry faces significant challenges to achieve the goals of the European Green Deal Industrial Plan. This ambitious plan aims to enhance the competitiveness of EU net-zero industry and support the fast transition to climate neutrality. To achieve this, the EU must reduce greenhouse gas emissions and balance remaining ones with removals, effectively minimizing the net impact on the climate. While some sectors, like the cement production industry, are facing challenges to avoid carbon emissions, experts are exploring technologies such as carbon capture and storage (CCS) or carbon capture and utilization (CCU). Other industries, particularly those using carbon as a reactant gas, search for alternative solutions to meet the European target. Part of this solution is to replace carbon by other reducing gases such as hydrogen.

In integrated steel plants around 1.9 mt of CO_2 are emitted for each mt of steel produced. The major contributor, around 90%, comes from the blast furnace in which CO (formed in the Boudouard reaction from coking coal) is used as reducing gas for iron reduction leading to direct CO_2 emission (Eq. 1). The alternative concept is to use hydrogen as reactant gas instead of CO with zero greenhouse gas emission (Eq. 2).

$$Fe_2O_3 + 3CO\ (g) \rightarrow 2Fe + 3CO_2\ (g) \quad (1)$$
$$Fe_2O_3 + 3H_2\ (g) \rightarrow 2Fe + 3H_2O\ (g) \quad (2)$$

The iron ore is reduced in DR (direct reduction) units, typically shaft kilns, running at temperatures around 1000°C under a hydrogen atmosphere. In a second step the produced iron sponge (direct reduced iron, DRI) then has to be melted in furnaces, e.g. electric arc furnaces.

Since the DRI shaft kilns are running under hydrogen atmospheres, the refractory lining is exposed to hydrogen with the risk of weakening, or in the worst case, destruction by reduction of incorporated oxides. Silica for example is well known to be reduced in hydrogen atmospheres (Eq. 3).

$$SiO2 + H2\,(g) \rightarrow SiO\,(g) + H2O\,(g) \quad (3)$$

Common refractory materials used in the reduction region of DRI shaft kilns are non-basic high-alumina products based on raw materials like corundum, bauxite, fireclay and mullite [1]. A recent investigation by thyssenkrupp Steel showed strong hydrogen attack for common refractories which are currently applied in Claus plants for blast furnace gas desulphurisation, and the authors suggest to reduce the silica content as much as possible [2].

Henn et al. [3] showed that hydrogen attack of silica containing materials appears on both matrix and aggregate grains. Choi et al. [4] confirmed reduction of SiO2 and other impurities such as Na2O, K2O and Fe2O3 under hydrogen conditions resulting in weakening of refractory bricks.

Synthetic alumina based material are already well known for their high resistance against hydrogen exposure and are therefore well established in industries such as in the petrochemical industry [5, 6] or gas turbines [7].

Stability of alumina at temperatures exceeding 1000°C was reported by P. Walls [8]. However, the new applications for carbon replacement by hydrogen, demand other conditions such as elevated temperatures and high gas flow. Research is needed to further understand the durability of alumina based refractories to ensure long life in future applications. A joint research project including university, steel, refractory, and raw material producers was established to investigate how the lifetime of linings can be predicted based on lab testing.

MATERIALS AND METHODS

The vibratable tabular alumina castables according to composition shown in Tab. 1, were mixed and cured at 20°C for 24h in the Almatis Ludwigshafen application laboratory. After curing the 230x64x54 mm test bars were dried for 5h at 400°C and then transferred to the University of Koblenz for the hydrogen corrosion test in a chamber furnace located at the German Institute for Refractories (DIFK). Due to the limited size of the furnace, the test bars were cut into 150x25x25 mm bars. The corrosion test using 100% hydrogen (purity 5.0; 1 atm.) was performed for 200h at 1400°C to accelerate the relatively slow phase transformation which occurs in contact with hydrogen. The silica containing castable was also tested for 200 hours at 1150°C using 100% hydrogen (purity 5.0; 1 atm.) and for 200 hours at 1400°C using a technical grade of hydrogen (purity 3.0; 1 atm.). The test bars were placed in the furnace as shown in Fig. 1. In addition, a reference castable sample fired at 1400°C for 5h in a common lab furnace was created for each recipe as a reference and for comparison with the hydrogen treated specimens.

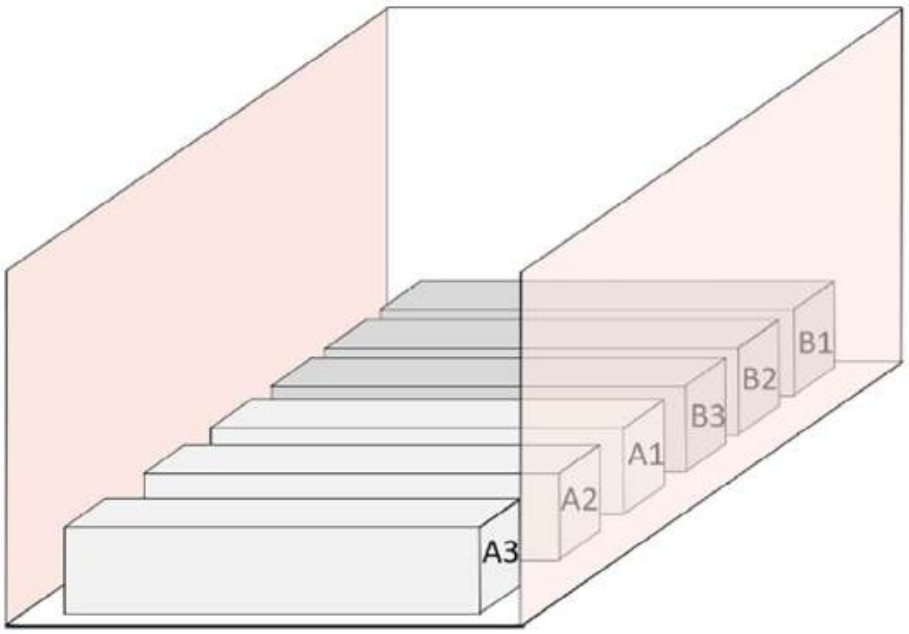


Fig. 1: Schematic drawing of the furnace installation. The heating elements were located left and right of the samples (red highlighted wall sections) [9].

Tab. 1: Composition of investigated tabular alumina castables.

Raw Material	CC	LCM	LC	NC
T60/T64 Tabular	%	%	%	%
0 – 6 mm		74	75	75
0 – 5 mm	73			
-45 MY LI	7	8		
-20 MY			7	7
Matrix				
CT 9 FG		8		
CL 370			13	
Silica fume				
Mikrosilica 971 U		5		
Binder				
CA-25 C	20			
CA-14 M		5	5	
Alphabond 300				3
Additives				

Dispersing Aluminas		1	1	1
Liquid				
H_2O	7.5	4.5	4.4	4.6

The castable named “CC” is a conventional castable with 20% CAC-80. These types of castables typically show lower density and increased porosity due to a non-optimised matrix concept and high water demand.

A silica fume containing low cement castable (“LCM”) was chosen to investigate the impact of SiO2 in the system when exposed to hydrogen. “LC” is a well optimised low cement castable with 13% reactive alumina CL 370 to increase its density, reduce water demand and consequently the open porosity. CL 370 is a bimodal reactive alumina providing the necessary amount of submicron particles to replace silica fume. In the latest test, the cement content was replaced with 3% Alphabond 300 and 2% T60/T64 -45MY LI to have a comparison for the stability of cement phases in hydrogen conditions (“NC”). Alphabond 300 is a calcia free binder consisting of hydratable alumina.

The hydrogen treatment was done at the DIFK and further testing was carried out at the University of Koblenz as part of the joint research project mentioned before.

RESULTS AND DISCUSSION

Effect of hydrogen treatment on mass and strength loss

The mass loss for the tabular alumina based castables is presented in Fig. 2. For comparison, the mass loss is calculated to the change in mass per unit area g/cm2 as shown on the right y-scale. As the exposed surface area plays a role for the hydrogen attack, it makes sense reflecting it in the unit for mass loss.

The matrix optimised pure alumina castable NC has the lowest mass loss - 1.2%. The cement free castable shows high resistance against hydrogen corrosion due to its maximum alumina content.

The conventional castable shows the highest mass loss of about 4%. The higher porosity of this sample due to the non-optimised matrix and the higher cement content leads to stronger hydrogen attack.

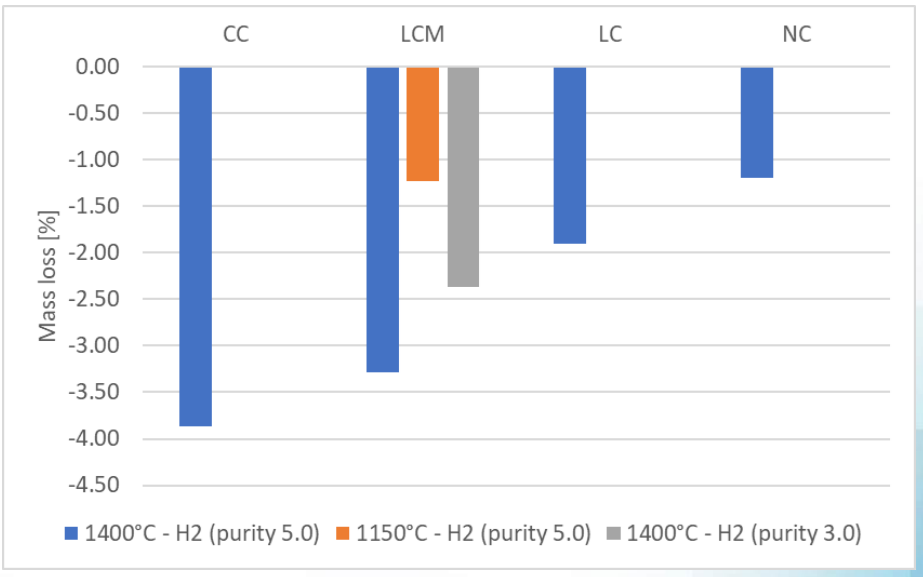


Fig. 2: Mass loss of alumina-based castables.

In comparison, the low cement castable (LC) shows lower mass loss of 2% in total. Matrix and cement content optimisation leads to a reduction in mass loss. If fumed silica is introduced to the system the mass loss increases from 2% (LC) to 3.3% (LCM) indicating reduction of SiO2 to SiO. The mass loss is only 1.2% for the LCM when a temperature of 1150°C is applied. This indicates a slower reduction of SiO2 to SiO.

Fig. 3 shows the cold modulus of rupture (CMoR) for the reference samples and the hydrogen treated ones.

Firstly, it is interesting to observe that all castables, except the silica fume containing LCM, show an increase in CMoR after hydrogen treatment. This effect is explained by further sintering during the hydrogen treatment at 1400°C with a very long sintering time of 200h.
So, it can be noted that despite the mass loss during hydrogen treatment no loss in strength properties is generally to be expected for silica fume free castables.
The situation is different for the silica fume containing castable LCM. The CMoR drops steeply after the hydrogen treatment from 30 down to only 10 MPa. This gives a strong indication that the silica fume containing matrix is highly corroded and disintegrated when in contact with hydrogen. The CMoR drops to 13 MPa when a lower purity grade of hydrogen was used.

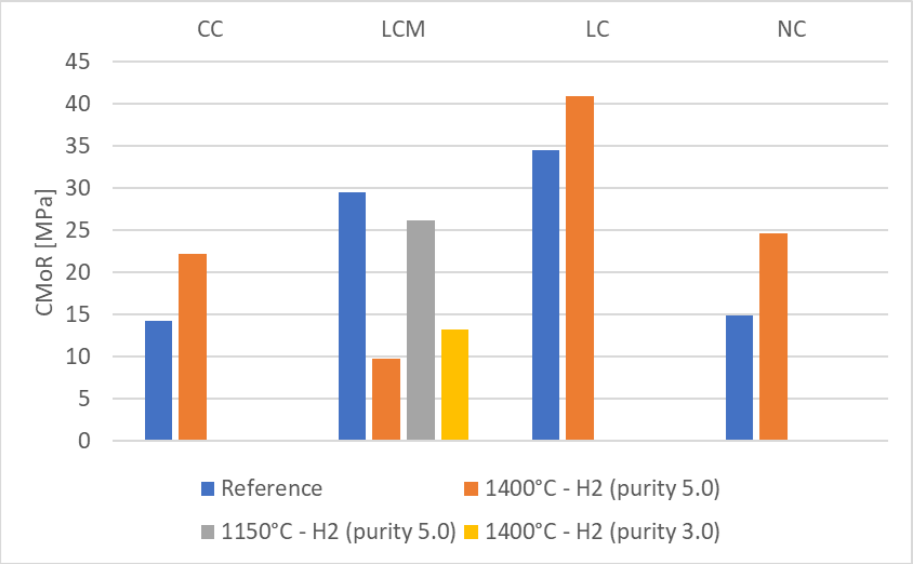


Fig. 3: Initial and residual cold modulus of rupture of alumina-based castables.

When the LCM is exposed to hydrogen at 1150°C the CMoR is only 10% lower than the reference strength. Because the reduction of silica is slower the strength loss is also not as severe as when the sample is exposed to hydrogen at 1400°C for 200 hours. It can be expected that the corrosion will further impact the strength when silica containing castables are exposed to hydrogen for longer periods. In many refractory applications pieces will be exposed to hydrogen for much longer times and a failure could be expected at an earlier stage.

The results show that measurement of mass loss alone is not sufficient to judge the destruction of refractories due to hydrogen attack. The silica fume containing castable LCM shows a similar mass loss as the conventional castable CC. However, while CC keeps its strength after hydrogen attack, LCM loses two thirds of its strength, here shown as cold modulus of rupture.
The loss in mass and CMoR for the castables LC and LCM in comparison to an andalusite based castable (~60% Al2O3) and a mullite fireclay brick (~60% Al2O3) are shown in Fig. 4.
The andalusite castable and the mullite brick exhibit very similar mass and strength loss. The silica fume containing castable LCM has a significant lower mass loss but much

severe loss in strength due to SiO2 disintegration. This clearly shows that the grain and mineralogical phase assembly of the silica containing part matters for the hydrogen corrosion resistance. For the LCM castable the silica is present in the matrix only. The andalusite castable and mullite brick have silica incorporated in the andalusite or mullite coarser aggregates. Their matrix are apparently attacked less by hydrogen when compared to LCM. Matrix disintegration causes critical loss in strength properties because the bonding effect is no longer present.

The optimised castable LC based on synthetic alumina has the lowest mass loss and exhibits no strength loss - in contrast to the other materials. It does, however, show, a clear gain in strength after 200 h treatment time with hydrogen.

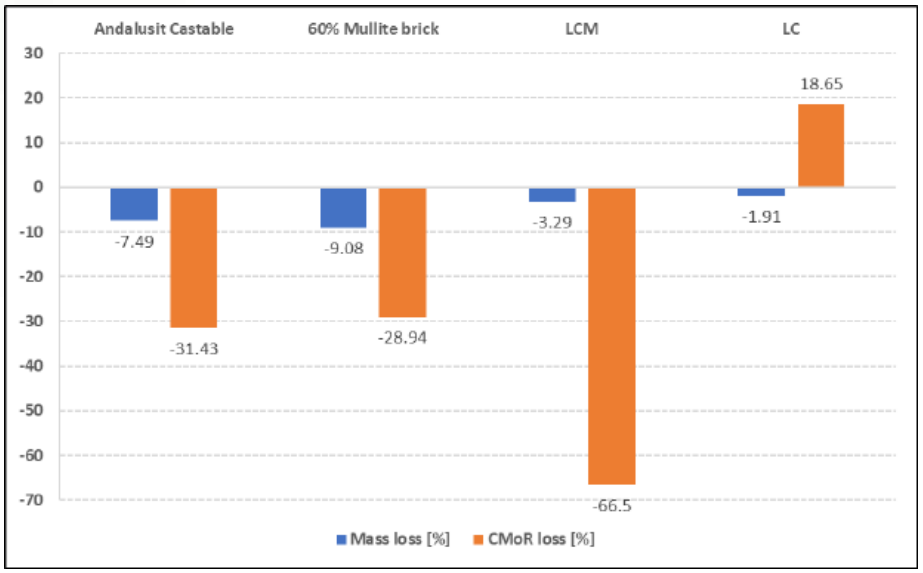


Fig. 4: Loss in mass and CMoR for the mixes LC & LCM in comparison with Andalusite castable and Mullite brick.

SEM investigations

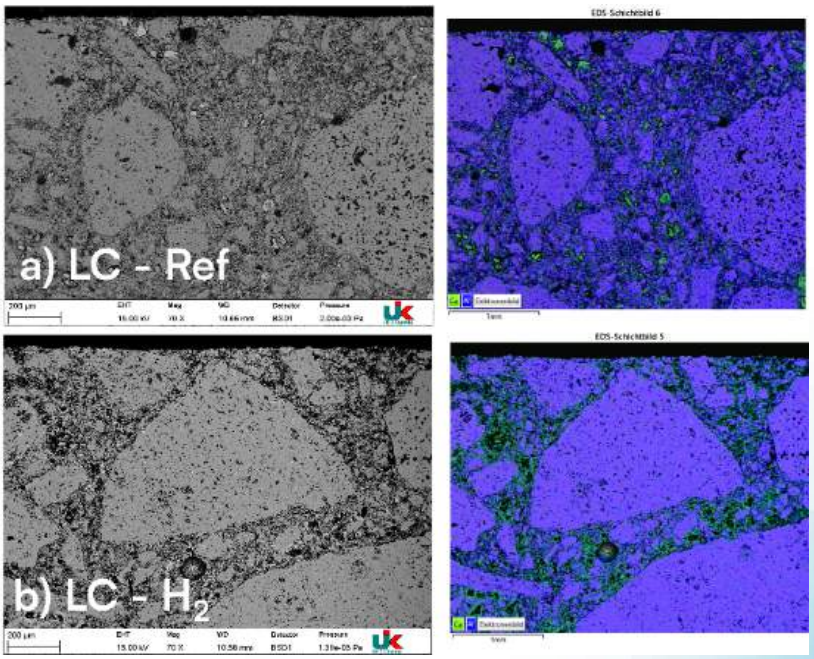


Fig. 5: SEM pictures and element mapping of the pure alumina based castable LC without (a) and with hydrogen treatment (b); Ca green, Al blue.

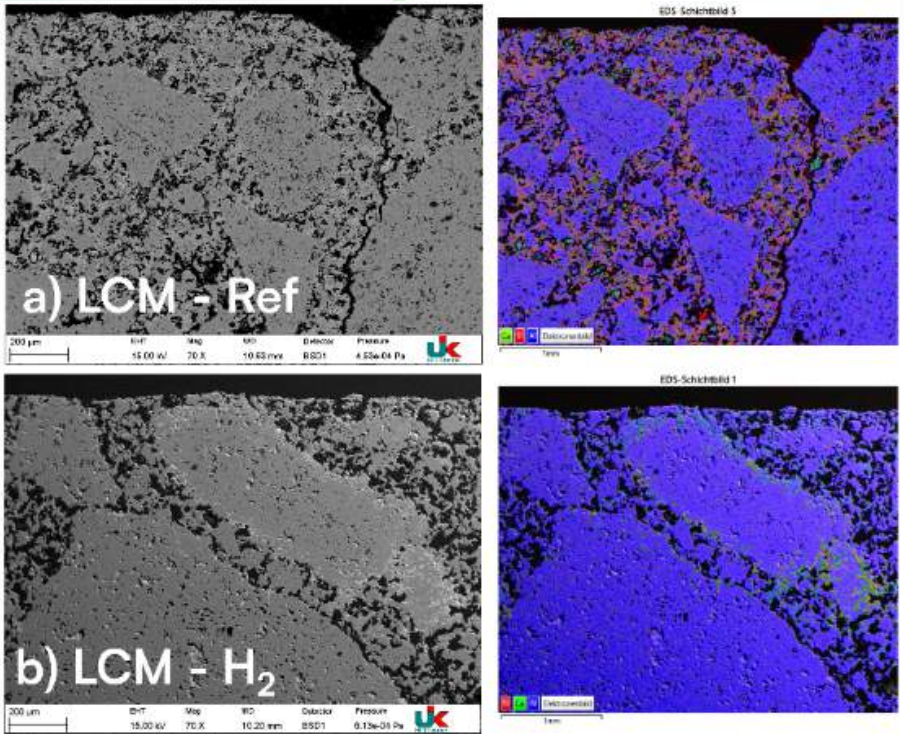


Fig. 6: SEM pictures and element mapping of the silica fume containing castable LCM without (a) and with hydrogen treatment (b); Ca green, Al blue, Si red.

The SEM images of the LC castables (a)without and (b)with hydrogen treatment are shown in Fig. 5. The reference sample was fired at 1400°C for 5h for comparison purposes. The section shows the top surface of the test bars which is most exposed to hydrogen during the 200h of treatment time.

Tabular grains are clearly visible surrounded by a fine matrix consisting of reactive alumina and calcium aluminates. The larger Ca-rich grains visible in a) are remaining calcia rich calcium aluminate phases close to CaO·2Al2O3 (CA2) composition as measured with point EDX. The other fine matrix compounds consist of alumina and CaO·6Al2O3 (CA6).

The sinter reaction after 200h hydrogen treatment at 1400°C is clearly visible in b). The matrix consists of alumina finely distributed with secondary formed CA6. The continued sintering in combination with the hydrogen resistance of alumina and calcium aluminate phases explains the increase in strength as shown in Figures 3 and 4. A microstructural damage of the LC castable after hydrogen treatment is not visible.

The reference castable LCM (Fig. 6a) shows a silica-rich matrix embedding larger Tabular Alumina aggregates. After hydrogen treatment the matrix has been clearly reduced in silica content. Silica SiO2 is reduced to SiO during hydrogen treatment according to Eq. 3 and evaporation resulting in a continuous decrease in silica content and weakening of the matrix structure. The tabular alumina grains show no change during exposure to hydrogen but the castable strength has drastically suffered due to loss of matrix integrity.

Change in colour by hydrogen treatment

It is well known that the oxidisation level of oxides influences the colour of materials. Choi et al. [4] for example reported a significant darkening of different refractory materials after treatment in hydrogen atmospheres. The authors report a reversible effect when the samples are re-fired in oxidation conditions.

As such, the investigated samples also show a change in colour. Both, matrix and Tabular alumina grains darken after exposure to hydrogen. It is assumed that the darkening is caused by reduction of Fe2O3 or traces of other elements.

The change in colour of the castables LC and LCM is shown in Fig. 7. It is clearly visible that the matrix and Tabular Alumina aggregate compounds darken in hydrogen atmospheres. The test bars shown are broken in half as they have also been used for the cold modulus of rupture testing.

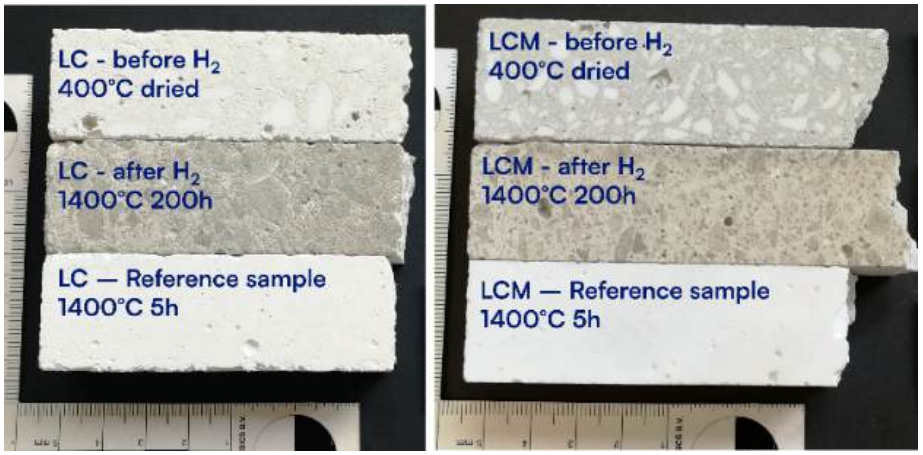


Fig. 7: Macro images of castables LC and LCM castable before, after hydrogen treatment and in the fired reference state. Darkening due to hydrogen treatment.

While both samples clearly change in colour, the strength losses after hydrogen treatment are significantly different. LCM loses ~67% whereas LC gains ~19% in CMoR due to further sintering during hydrogen treatment. This shows that discoloration alone cannot be used as indicator for strength loss of refractory materials after hydrogen attack.

CONCLUSION

The results show that silica containing refractory materials weaken during time in contact with hydrogen at the tested temperatures of 1400°C and 1150°C. The 5% silica fume containing castable exhibits a loss of CMoR strength of 67% and 10 respectively %. The loss of strength is less pronounced with increasing synthetic alumina content in the matrix.The silica-free castables based on synthetic alumina even show a strength increase when exposed to hydrogen at 1400°C. Matrix optimisation and porosity reduction lead to further H2-corrosion resistance. The lowest mass loss is detected for the castable containing the calcia free hydratable alumina Alphabond 300.The SEM investigations prove the evaporation of formed SiO during hydrogen treatment and weakening of silica containing matrix formulations. The silica free LC castable shows no destruction of microstructure after 200 hours of hydrogen treatment.Also, it became clear that evaluation of mass loss or colour change alone, is not suitable to assess the potential severity of hydrogen attack on the refractory material. Instead, a combination of test methods including residual strength tests are advised to be performed

REFERENCES

[1]E. J. E. Ospino, G. Hebenstreit, S. Postrach, D. Gavagnin and T. Janssen, "Challenges for the Refractory Industry to Support the Foreseen Large-Scale Transition to DRI Shaft Kilns" Iron & Steel.

[2]K. Kursch, B. Kohnen and M. Weinberg, "Transformation to hydrogen-based steel making and refractory challenges at thyssenkrupp Steel Europe (tkSE) AG in Duisburg" (18thUNITECR), Frankfurt, 2023.

[3]I. Henn, A. Sax and P. Quirmbach, "Hydrogen induced attack of Al2O3-SiO2 refractories – application of SEM techniques and thermodynamics" (18thUNITECR), Frankfurt, 2023.

[4]S. Choi, R. Park, G. Yang and Y. Kim, "Investigation of Refractory Bricks and Oxide Materials Heated in Hydrogen Reduction Conditions" China's Refractories, vol. 2, pp. 22-26, 2024.

[5]A. Buhr, B. J. Baier, J. M. Aroni and R. W. McConnell, "Raw material concepts for SiO2 free high strength castables in the temperature range to 1200 °C" in 25th ICR, Aachen, 2002.

[6]P. Tassot, E. Bachmann and R. Johnson, "The Influence of Reducing Atmospheres on Monolithic Refractory Linings for Petrochemical Service" (UNITECR), Cancun, 2001.

[7]H. Grote, R. Anton, A. F. Rentaria, C. Nikasch and I. Krausz, "Status and challenges of hydrogen containing fuels on porous ceramic materials and protective systems in the energy industry" (18thUNITECR), Frankfurt, 2023.

[8]P. Walls, "Switching to hydrogen based fuels and their effect on refractory linings and processes" (18thUNITECR), Frankfurt, 2023.

[9]A. Razavi, I. Henn, A. Sax and P. Quirmbach, "X-ray computed tomography study of microstructure weakening by high-temperature hydrogen attack on refractories" International Journal of Ceramic Engineering & Science, vol. 6, no. 3, p. 6:e10211, 2024.

[10]J. Sperber, "H2-Change: Refractories under attack of challenging atmospheres during transformation process" (18thUNITECR), Frankfurt, 2023.

MULTIFUNCTIONAL ADDITIVE SOLUTIONS FOR OPTIMIZING SILICA FUME-BASED CASTABLE SYSTEMS

[1]Sourojit Pal, [1]Shankha Chatterjee, [2]Andus Buhr
[1]Almatis Alumina Pvt Ltd India, [2]Almatis GmbH

*Corresponding author e-mail: Sourojit.Pal@almatis.com

Abstract

The use of fine matrix fillers such as silica fume and reactive alumina are essential in low-cement (LC) and ultra-low-cement (ULC) castables, but require efficient additives to achieve optimal dispersion, low water demand, and controlled rheology. Additives must also provide reliable setting and working times under varying temperature and placement conditions, while ensuring homogeneous dosing, reproducible strength development, and high mechanical and hot performance. Aging resistance of dry-mixed castables and the possibility of adjusting setting behavior during installation are additional requirements.This paper compares widely used traditional organic and inorganic additives with advanced additives, such as dispersing aluminas containing highly efficient polymers. Their influence on workability, water demand, and setting behavior is evaluated using a silica-fume-based low-cement vibration castable. In addition, short-term aging tests are conducted on dry-mixed castables containing different additive systems. The results demonstrate the advantages of advanced additive technologies in achieving improved processing reliability, castable performance, and robustness under varying application conditions.

Keywords: Alumina castable additive, Castable setting and rheology control, Dispersing alumina, Silica-fume containing castable

1. Introduction

Dispersing aluminas are dispersing agents designed as a pre-mixes of alumina backing and one or more active organic ingredient, which improve dispersion and allow controlled setting characteristics.Kriechbaum et al.[1], in 1996, first described a group of newly developed fine materials, the 'Matrix Advantage System' (MAS), which consisted of Reactive Alumina, Reactive Alumina/Spinel, Calcium Aluminate Cement and Dispersing Aluminas, namely ADS 1 and ADW 1.

Following the success of this new and unique performing product line, market demand led to the development of Dispersing Aluminas specifically targeted at silica fume containing Low Cement Castables.With the same concept of setting behavior control led to the development of M-ADS 1 and M-ADW 1 in 2000 by Van Garsel et al.[2]. In2007, a stronger retarding grade was required for silica-containing castable and thus M-ADS 3 was developed. The product line of Dispersing Aluminas for silica fume containing castables is shown in Tab. 1.The recommended total amount is about 1% for low cement and 0.7% for ultra-low cement castables.

By keeping the total amount unchanged, the rheological performance of dispersing aluminas remains stable no matter which ratio of S/W is used [2]. Figure 1 demonstrates the set control by varying the M-ADS 1 / M-ADW 1 ratio in a low cement castable with 5% silica fume.

Product	M-ADS 1	M-ADS 3	M-ADW 1
Effect	Retarding	Strong retarding	Accelerating
Chemical Composition [%]	typical		
Al_2O_3	91	95	96
Na_2O	1.40	1.40	0.10
B_2O_3	1.30	2.50	0.55
CaO	0.02	0.02	0.02
L.O.I. at 1050°C	7.0	8.0	2.7
Particle Size D50 Cilas [µm]	2.6	2.6	2.6
Particle Size D90 Cilas [µm]	9.0	9.0	9.0

Tab. 1: Typical product data - Dispersing Aluminas for silica fume containing castables

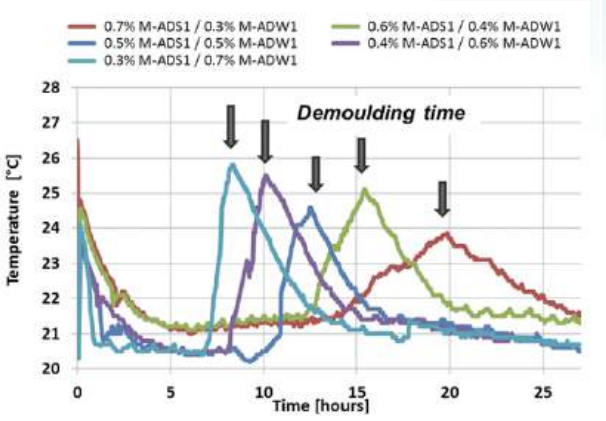


Fig. 1: Dispersing Alumina combinations and their influence on castable setting. Exothermic reaction of a LC castable with 5% silica fume

2. Experiment

2.1 Test castables

Two low cement vibration castables with 5% (VIB 5M) and 3% (VIB 3M) of a 94% grade silica fume were selected for the test series. In addition to dispersing aluminas, sodium-tripolyphosphate (STPP) and sodium-hexametaphosphate (SHMP) were also chosen, as they are still widely used as additives in silica fume containing castables. For the adjustment of working and setting time, citric acid was added. Test mix compositions and test results for selected additive dosages are given in table 2.In addition, some tests were done with castables containing only 3% instead of 5% silica fume. The amount of tabular -45MY Li was then increased by 2%.

The castable components were dry mixed in a Hobart mixer type A200 at speed 1 for one minute and for another four minutes after the addition of water. The flow properties after 10, 30, and 60 minutes were measured by the cone test.The setting behaviour was determined by the exothermal method (EXO) and partially by measuring the ultrasonic velocity (US). Both methods and terminology were described in detail by Gierisch et al. [3].

Tab. 2: Typical product data - Dispersing Aluminas for silica fume containing castables.

Mix			VIB 5M DA	VIB 5M STPP	VIB 5M STPP/CA	VIB 5M SHMP	VIB 5M SHMP/CA
Components [%]							
T60/T64	up to 6 mm		82	82	82	82	82
Alumina	CT9 FG		8	8	8	8	8
Silica fume	94% SiO2		5	5	5	5	5
Cement	CA-14 M		5	5	5	5	5
Additives	M-ADS1		0.4	-	-	-	-
	M-ADW1		0.6	-	-	-	-
	STPP		-	0.1	0.1	-	-
	SHMP		-	-	-	0.05	0.05
	Citric acid		-	-	0.03	-	0.03
H_2O			4.5	5.0	5.0	5.0	5.0
VIB-Flow	10 min	[cm]	22.5	22.7	23.0	23.8	23.0
	30 min	[cm]	23.0	17.8	23.5	23.5	23.3
	60 min	[cm]	21.8	10.0	23.0	23.0	23.0
EXO	Start 1		66'/21.8°C	n.d.	n.d.	n.d.	n.d.
	Start 2		8.1h/20.6°C	4.3h/20.8°C	9.8h/20.8°C	6.0h/20.9°C	25.0h/20.6°C
	Max		10.1h/25.5°C	6.2h/22.4°C	13.0h/22.9°C	8.9h/23.2°C	30.2h/22.8°C
CCS	20°C / 24 h	[MPa]	24	29	26	34	14
C MoR	20°C / 24 h	[MPa]	5	4	5	4	3

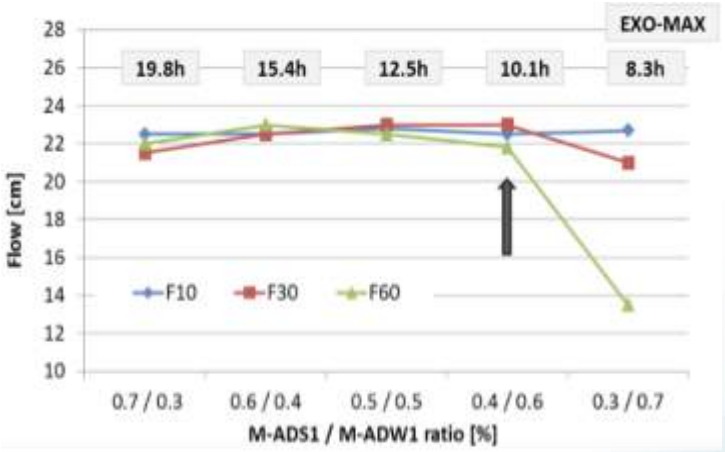
Test bars were prepared and tested according to the European standard DIN-ISO 1927 part 5 and 6. Cold crushing strength (CCS) and cold modulus of rupture (CMoR) were measured after 24 hour curing at 20°C.

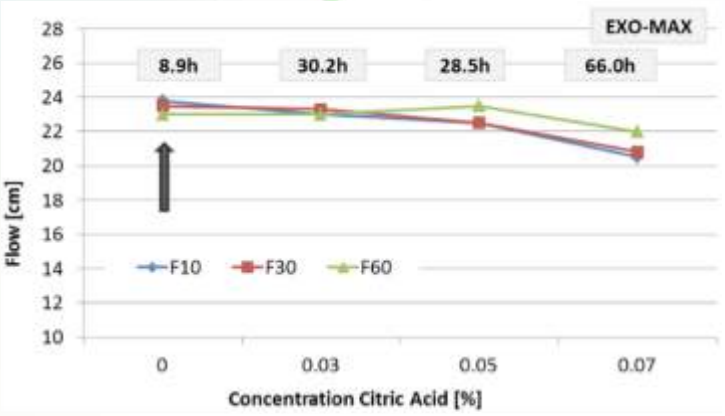
For the investigation of the storage stability, 5 kg batches of dry mixed castables were used. Selected mixes were stored in an open bucket in a climate cabinet at 20°C and 65% relative humidity for 1, 7, and 14 days. The setting behaviour (EXO) was tested for fresh and aged test mixes. The cement hydration with silica fume, phosphate, and citric acid was investigated with a calorimeter, (designed at the University of Erlangen), at a consistent temperature of 23°C ± 0.1°C. The calorimetric test method is described in detail by Kuzel [4].

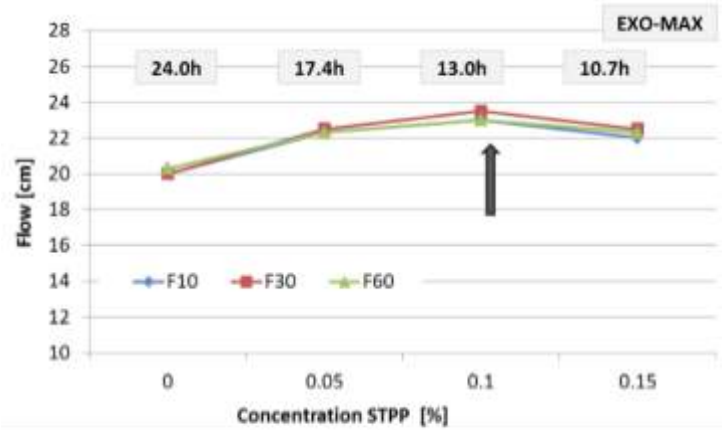
2.2 Determination of additive dosage

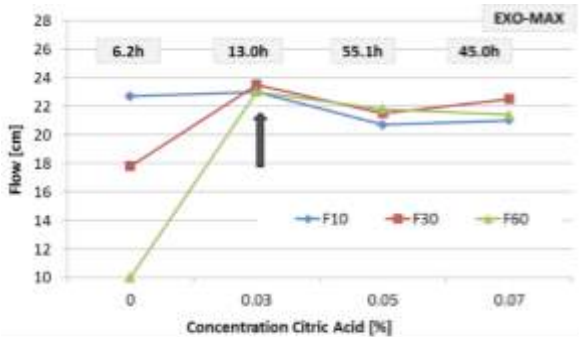
Additive and water additions were adjusted to comparable vibration flow at lowest possible water addition. Focus was not only on flow after 10 and 30 minutes, but also after 60 minutes, to ensure a working time which is sufficiently long for on-site installations. For the dispersing alumina different M-ADS 1 / M-ADW 1 ratios were tested. For the phosphates two series of tests were performed. Firstly, different phosphate additions were tested at a fixed citric acid addition of 0.03%, and in a second test the citric acid dosage was varied while keeping the phosphate content constant. Results for VIB 5M are shown in figures 2 – 6. The time of EXO Max is also given in the figures. Arrows are indicating the mixes shown in table 2.

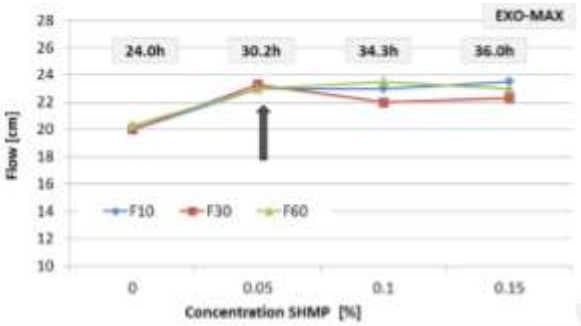
When using dispersing aluminas M-ADS 1 and M-ADW 1 stable flow properties are achieved for both test castables at a low water addition of 4.5%. Only at a high M-ADW 1 content does flow decay occur at 60 minutes due to an early setting start. By the adjustment of the M-ADS/W ratio the de-moulding time (EXO Max) is steered in the range of 8.3 – 19.8 hours for VIB 5M and 4.4 – 10.4 hours for VIB 3M. If longer working and setting times are required, the replacement of M-ADS 1 by the stronger retarding M-ADS 3 enables further extension without risking ultra-long or never setting times. For the strength tests a dispersing alumina ratio of 0.4% M-ADS 1 and 0.6% M-ADW 1 was selected. The test castables containing phosphate additives generally require a higher water demand of 5% when compared to M-ADS/W (4.5%). The 0.5% higher water addition which is required for the phosphate dispersed mix might result in lower strength values after firing at 800°C/5hwhen compared to the dispersing alumina system as reported by Schnabel et al. [2].











VIB 5M dispersed with STPP shows an acceleration of the cement hydration with increasing amounts of STPP (figure 3). Without addition of citric acid and 0.1% STPP in the mix, flow decay already occurs after 30 minutes and there is no flow at 60 minutes. By the addition of citric acid flow up to 60 minutes can be achieved. However, the cement hydration is very sensitive to the amount of citric acid as can be seen from the EXO Max times in figure 4. EXO Max increases from 13 hours at 0.03% to about 50 hours at 0.05 - 0.07% citric acid. Slight over-dosages of citric acid in practice would result in an increasingly retarded cement reaction and delayed strength development.

Contrary to STPP, SHMP acts as a retarder in VIB 5M (figure 5). Good flow properties are achieved at a dosage level of 0.05% SHMP even without the addition of citric acid (figure 6). How ever, when citric acid is added for the extension of working and setting time, EXO Max becomes significantly longer (30 instead of 9 hours with addition of 0.03% citric acid

and even 66 hours at 0.07% citric acid). Experiments with polyphosphates are not part of this paper, but were also performed in extended test series. They showed a similar trend as SHMP. In general all the phosphate systems in this work showed a high sensitivity for citric acid additions which are often applied in practice to steer the working time of the castables. Late cement hydration and strength development are disadvantages.

2.3 Castable setting and strength development

After placing a castable into a mould or a former, the process of strength development is of high importance. Within a specific time period, sufficient strength has to be developed for de-moulding and further processing.

VIB 5M–DA shows good workability over a period of more than 1 hour and achieves de-moulding strength (EXO Max) relatively shortly after the end of working time. EXO Max occurs after about 8 – 10 hours for the selected additive ratio of 0.4% M ADS 1 and 0.6% M-ADW 1. Good green strength of 24 MPa is achieved after 24 hours (table 2). VIB 5M containing only phosphate additives STPP and SHMP show comparable EXO Max and green strength results. However, to avoid flow decay with STPP and to achieve extended working times with phosphates in general, the addition of citric acid is often required. As a consequence the strength development is delayed. Citric acid additions in the range of 0.03 – 0.07% only slightly increase the working time, but significantly retard the cement hydration and strength development. For e.g., the addition of 0.03% citric acid retards the EXO Max peak of VIB 5M-SHMP to 30h and 0.07% to 66h. Such long de-moulding times are often not acceptable for both on-site installations and pre-cast shape production.

Figure 7 shows cold crushing strength at 20°C after 24 hours curing and EXO Max of all additive packages tested in VIB 3M. It is clear that a late EXO Max results in low curing strength after 24h. Castables with an EXO Max above 24 hours have insufficient green strength for de-moulding, handling and transport. Mechanical damage of the cast piece or lining is very likely and may often be discovered at a later stage during drying or firing of the material. M-ADS/W dispersed castables achieve high green strengths due to a reliable early exothermal reaction for all adjusted ratios.

The impact of citric acid on the cement hydration was further investigated with heat flow calorimetry under tightly controlled conditions using a paste based on tabular alumina -45MY Li and containing 20% cement, 10% reactive alumina RG 4000, 3% silica fume, and 0.1% polyphosphate. Citric acid was added in the range of 0 – 0.08%. The heat flow curves show two distinct peaks, a smaller sharp peak (I) within the first hours and a later broader peak (II) which comes from the main cement reaction (figure 8).

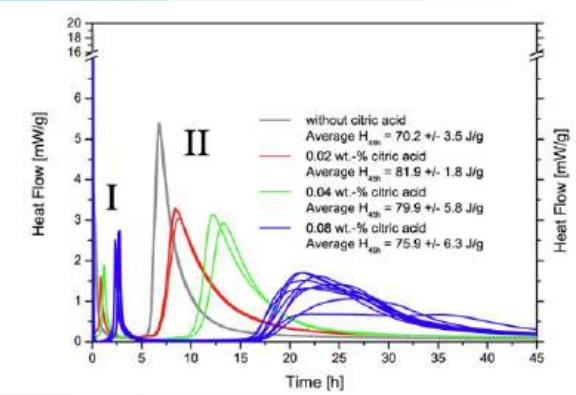


Fig. 8: Heat flow of test paste with 3% silica fume, 0.1% poly phosphate and different additions of citric acid.

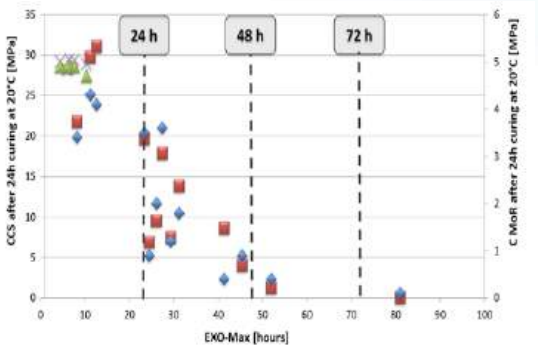


Fig. . 7: Curing strength after 24h vs. EXO Max tested in VIB 3M.

The first peak is caused by a reaction of phosphate in combination with cement, but it is not related to hydration of the cement and produces only a small amount of heat and therefore strength in technical castables. It is this reaction which leads to a “stiffening” [1] and the end of workability of refractory castables dispersed with phosphate additives. This stiffening usually occurs rather quickly within the first hour(s) after casting and is often considered as the start of setting and the cement hydration. However, it is obvious that the cement hydration only occurs hours later. As shown in figure 8, this first reaction can be retarded by citric acid with a roughly linear relationship between citric acid amount and retardation achieved. This makes the use of citric acid as a retarder so popular in the industry. However, the citric acid also has a retarding effect on the main reaction (II) but here the relationship is far from being linear. Small increases of citric acid result in strong retardation of the main reaction and at 0.08% citric acid the intensity of the reaction also becomes weaker. This is shown by a broader and flat peak in figure 8. This confirms the observations made with the test castables at increasing amounts of citric acid, where EXO Max becomes very long and sometimes not easy to detect because of the flat broad peaks. This indicates a hampered sub-optimal cement hydration reaction.

In order to check the strength development of phosphate dispersed castables in comparison to M-ADS/W castables, strength testing of castables with 97% grade silica fume and selected additive systems (table 2) was performed parallel to ultrasonic and exothermic reaction measurements during curing (figure 9 and 10). For the dispersing alumina castable the increase in ultrasound velocity correlates well with the strength development (figure 9). The phosphate/citric acid castables show a stepped increase of US velocity where a first increase to 3-4000 m/s can not be related to a measurable cold crushing strength which only appears after further increase of US velocity which takes place after 20 to 24 hours. The CCSlevel of these castables after 24 hours curing is significantly lower when compared to the dispersing alumina castable, and only after 48 hours curing are they on the same level.

It becomes obvious, that the stiffening reaction with phosphates is sufficient to increase the US velocity significantly but still no real strength development is taking place. Therefore US measurements of phosphate castables must be evaluated and considered with care and focus should be made on the subsequent increase of US velocity. The EXO measurement provides reliable data for the strength development.

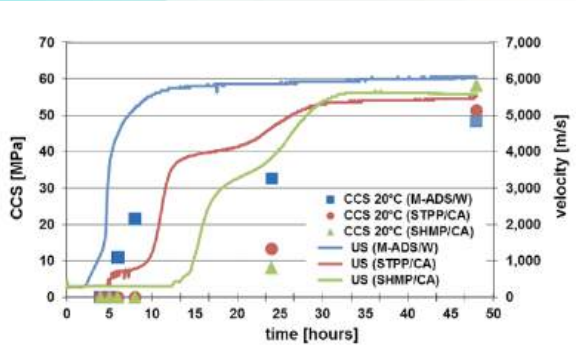


Fig. 9: VIB 5M - Ultrasonic velocity and CCS at 20°C/24h

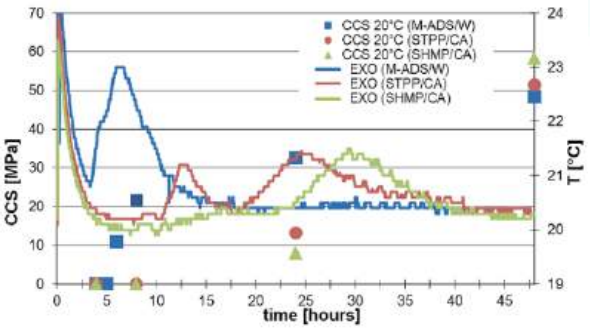


Fig. 10: VIB 5M - Exothermal reaction and CCS at 20°C/24h

Figure 10 shows how well the EXO peak correlates with the strength development. For dispersing alumina castables the US and EXO curves correlate well and the increase in the curves comes from the main cement reactions from which the strength develops.

Short term aging tests up to 14 days were performed for the test castables with dispersing alumina and test mixes containing STPP or SHMP with and without 0.03% and 0.05% citric acid addition. The setting was measured with the EXO method for the fresh dry mix and for dry mixes aged up to 14 days at 20°C and 65% relative humidity. Figure 11 compares the EXO Max results of the test mixes. VIB 5M dispersed with M-ADS/W shows an early EXO Max for the fresh mix which remained stable over 14 days open storage.The same applies for the 0.1% STPP containing mix without citric acid. Castable with 0.05% SHMP started at a longer EXO Max which increased slightly over storage time. The castables containing STPP or SHMP plus citric acid as retarder already show a long EXO Max at the starting point.

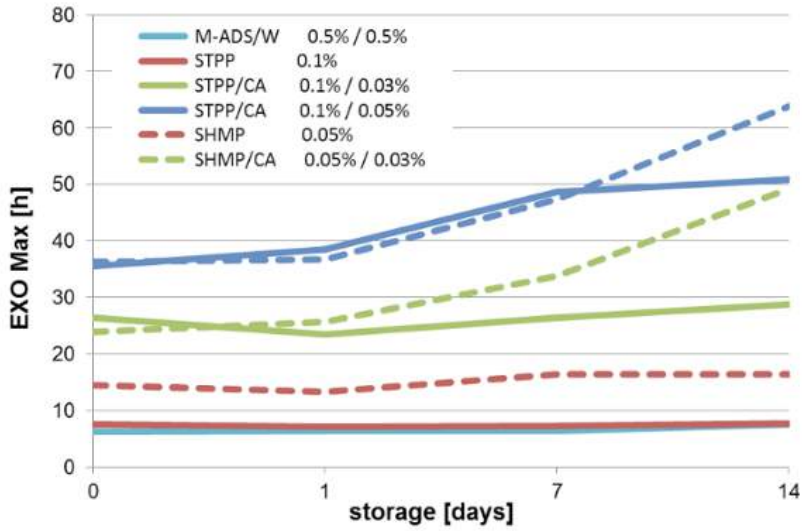


Fig. 11: VIB 5M – Short term aging of dry mix up to 14 days

After 14 days storage the working time has changed significantly, e.g. from initially 36 hours to 64 hours for the mix with 0.05% SHMP and 0.05% citric acid.

The change in castable behaviour over a short storage period for the phosphate/citric acid systems is very critical and increases the risk of failure during installation. Quality control (QC) testing is not able to monitor the

changes happening during storage be cause the testing is normally performed during or shortly after manufacturing.

3. Conclusion

Traditional additive systems for silica fume containing low cement castables such as different phosphates in combination with citric acid have been compared to the modern polymer based dispersing alumina system M-ADS/W. In addition to the flow behaviour at different dosing levels the cement hydration and strength development has also been investigated with regard to the practical requirements for monolithic linings and pre-cast shape manufacturing. Also, other important practical aspects such as the aging resistance of dry mixed castables during storage has been discussed. Phosphate based additive systems are low cost solutions when compared to dispersing aluminas, but they have several disadvantages with regard to control of working time and strength development, sensitivity to slight over-dosages of citric acid, and lower storage stability especially when containing citric acid.

Overall, dispersing aluminas provide a much more robust system which strongly contributes to reliable castable performance and avoids installation failures and the frustrating consequences of such failures which may lead to complaints. The higher price of this modern solution is therefore money well spent when the cost/performance ratio is taken into account, especially for more demanding applications where reliable performance is essential.

References

[1] Kriechbaum, G,; Stinnessen, I.; Gnauck, V., Laurich, J.O.; Routschka, G.; van der Heijden, J.: “The Matrix Advantage System, a new approach to low moisture LC selfleveling alumina and alumina spinel castables”: 39th International Colloquium on refractories, Aachen, Germany (1996) p. 211-218

[2] van Garsel, D., van der Heijden, J.; Kockegey-Lorenz, R.; Kriechbaum, G.: “New developments in calcium aluminate cements and in dispersing aluminas for microsilica-containing castable systems”: XIII. Conference on Refractories, Prague 2000, p. 1-6

[3] Gierisch, D.; Buhr, A.; Dutton, J.; Hsler, M.; Franz,B.: Ag Gierisch, D.; Buhr, A.; Dutton, J.; Hsler, M.; Franz, B.: Aging behaviour of Alphabond and Calcium Aluminate Cement bonded castables, 49. International Colloquium on refractories, Aachen, Germany (2006).

[4] Kuzel, J.H.: An efficient conduction-type calorimeter, TIZ 108 (1984) 46-48 (50-51). [5] Alphabond 300 – Global Product Data, Almatis GP-RCP/015/ R04/0812, available under www.almatis.com

EXPERIENCE OF COMPENSATOR DESIGN AND PERFORMANCE FOR BLAST FURNACE STOVE AT TATA STEEL

Goutam Ghosh, Biswanath Nag, Navneet Singh, Santanu Saha, Sujat Ali Khan

Iron Making Refractory, One Refractory, Tata Steel, Jamshedpur, INDIA

Corresponding author's e-mail: goutam.ghosh2@tatasteel.com

Abstract

Hot blast stove refractories play a critical role in achieving stable blast furnace operation, high hot blast temperature, and extended campaign life. Proper design of the hot blast system, particularly expansion joints and compensator arrangements, is essential to accommodate thermal expansion, prevent refractory damage, and ensure system reliability. Multiple refractory lining concepts and compensator designs are available for hot blast systems; however, their performance varies under actual operating conditions.

In this study, a comparative evaluation of different refractory lining designs and expansion joint configurations for hot blast stoves at Tata Steel was carried out. Key design parameters such as thermal expansion behaviour, stress distribution, installation practices, operating temperature fluctuations, and maintenance requirements were analyzed. The study highlights the advantages and limitations of various design approaches and identifies critical factors influencing long-term performance and reliability. The findings provide practical guidance for selecting appropriate compensator designs and refractory expansion joint concepts for modern high-temperature hot blast systems in large blast furnaces.

Keywords: Blast Furnace Stove, Compensator, Expansion Joint, Bellows, Thermal Expansion

1. Introduction

A hot blast compensator is a specialized expansion joint massive thermal growth of the piping system that carry extreme heat and air from stove to blast furnace. The metallic bellows is the flexible element of a compensator that absorbs thermal expansion generated in hot-blast ducts during operation.

When the hotblast duct is heated, its length increases due to thermal expansion. If this expansion is restrained, large compressive forces develop in the system, causing damage to the duct, refractory lining, supports, and anchors. A schematic diagram of expansion joint is given in Fig. 1

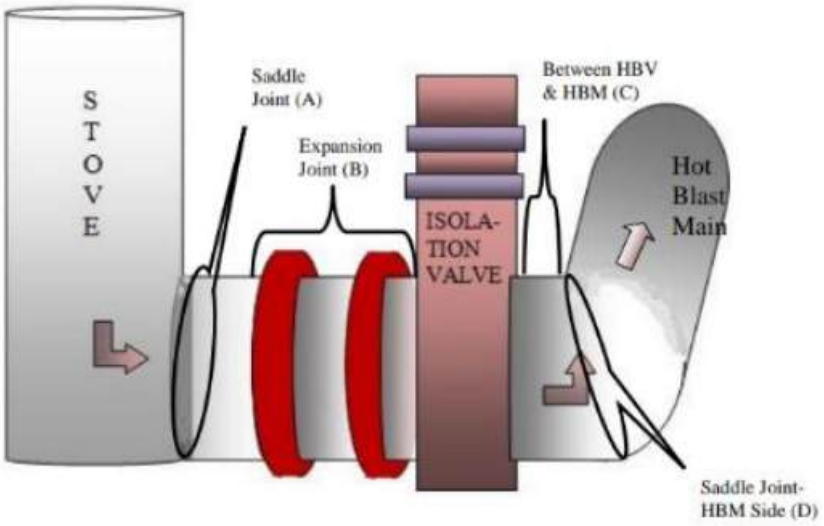


Figure 1 A Schematic diagram of expansion joint assembly in blast furnace stove

The bellows absorbs this movement through its corrugated (convoluted) structure. At Ambient Temperature, the bellows remains in its neutral position, and no significant deformation is present. During Heating the duct expands longitudinally, the corrugations of the bellows compress like a spring, the expansion movement is absorbed within the folds of the bellows instead of being transferred to the ducting system. During Cooling the duct contracts, the bellows extends back toward its original shape, thermal stresses are relieved without damaging the connected equipment. As a result, thermal stresses in the duct are significantly reduced, refractory crushing and cracking are minimized, loads on supports and anchors are lowered, the risk of duct buckling is eliminated, and system reliability and service life are improved. The design, fabrication, and operation of expansion bellows used in hot blast stove systems were evaluated with reference to EJMA Standards

1.1 Working Principle

The bellows converts thermal expansion movement into controlled elastic deformation of its corrugations. The metallic bellows functions as a flexible spring element that accommodates thermal expansion and contraction of the hot-blast duct. Its corrugated geometry allows the convolutions to elastically compress and extend in the axial direction. During heating, the thermal growth of the duct is absorbed by compression of the bellows convolutions, while during cooling the bellows returns toward its original configuration. This controlled deformation prevents excessive thermal stresses from being transmitted to the refractory lining, duct supports, anchors, and connected equipment, thereby ensuring safe and reliable operation of the hotblast system. Consequences of operating without a compensator are uncontrolled thermal expansion can cause buckling of the hot-blast duct, high compressive forces may damage the internal refractory lining, leading to cracking and premature failure, excessive expansion loads can overstress pipe supports, anchors, and associated structural components, resulting in mechanical failure and system instability. During operation, thermal expansion of the hot-blast duct is absorbed by the corrugated metallic bellows. The bellows compress and extend axially, reducing thermal stresses in the piping system and preventing damage to the refractory lining, supports, and associated structures. The Key Functions of expansion below are absorption of the axial thermal expansion, reduction of the thermal stresses in the ducting system. It dampens vibration and mechanical shock and accommodates minor installation misalignment. This

enhances system reliability and operational safety.

1.2 Inspection and Testing

Purpose of Inspection and Testing are to ensure structural integrity and fabrication quality, to verify compliance with design and operational requirements, to identify defects before installation and commissioning, to enhance the reliability and service life of the compensator system. To ensure the integrity and reliability of the compensator, the following inspections and tests are carried out:

- **Visual Inspection:** Examination of all components for surface defects, deformation, cracks, welding irregularities, and dimensional conformity.
- **Dye Penetrant Testing (DPT):** Non-destructive testing of welded areas to detect surface cracks, porosity, and other discontinuities.
- **Hydrostatic/Pneumatic Pressure Testing:** Verification of pressure-retaining capability and leak tightness under specified test conditions.
- **Dimensional Inspection:** Measurement and verification of critical dimensions, tolerances, flange alignment, and overall geometry against design specifications.

2. Design Methodology

The design of a hot-blast stove compensator requires the integration of mechanical flexibility, thermal expansion accommodation, refractory protection, and long-term operational reliability. At Tata Steel, the compensator design methodology is based on process requirements, expected thermal growth of the hot blast duct, operating temperature, pressure conditions, and maintenance considerations.

3. Failure mechanism

Failure of compensators can result in hot blast leakage and loss of process efficiency, Damage to adjacent ducting and support systems, premature refractory deterioration, increased maintenance costs and unplanned shutdown and reduced reliability and availability of the blast furnace hot-blast system.

3.1 Failure Modes Observed in Compensators

Fig. 2 and Fig. 3 represents the details mechanical shell damage and thermography to identify the damage in the expansion joint. The following failure mechanisms have been observed in hot-blast stove compensators during service:

- **Thermal Fatigue Cracking:** Repeated heating and cooling cycles induce cyclic stresses in the bellows, leading to crack initiation and propagation over time.
- **Over-Compression Failure:** Excessive axial movement beyond the design limit can cause permanent deformation or buckling of the bellows.
- **Erosion Damage:** High-velocity dust-laden hot blast gases may erode the internal refractory lining and metallic components, reducing service life.
- **Refractory Lining Failure:** Cracking, spalling, or displacement of refractory materials can occur due to thermal stresses, mechanical loading, or improper expansion allowance. • Weld Failure: Defects in fabrication, thermal cycling, and stress concentration at welded

joints can result in crack formation and weld rupture.

• **Pressure Thrust Failure:** Inadequate restraint of pressure-induced forces can lead to excessive loading on the compensator, connected ducting, and support structures.



Figure 2 Shell damage found during application of the compensator

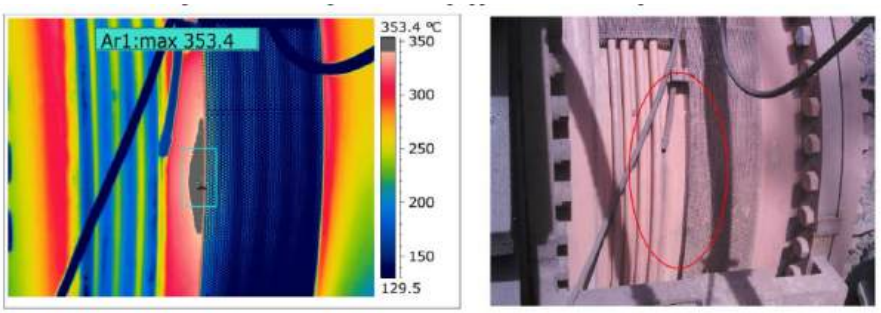


Figure 3 Thermography measurement for detection of the compensator failure

4. Main Components of an Expansion Bellows Compensator

A compensator is a metallic expansion joint designed to provide axial flexibility and accommodate thermal expansion in hot-blast duct systems.

4.1. Metallic Bellows

• The primary flexible element of the compensator.

• Manufactured from heat-resistant alloy steel to withstand high operating temperatures.

• The corrugated construction enables axial compression and extension, thereby absorbing thermal expansion.

4.2. Refractory Lining

• Protects the metallic shell and bellows from direct exposure to hot-blast temperatures.

• Minimizes heat loss and enhances the service life of the compensator.

4.3. Outer Shell

• Provides structural strength and pressure containment.

• Protects the internal components from mechanical damage and external influences.

4.4. Flanges and Weld Ends

• Facilitate secure connection of the compensator to the hot-blast ducting system.

• Ensure proper alignment and leak-tight operation under service conditions.

5. Refractory lining of expansion bellow

5.1 OEM supplied expansion bellow

It is a “single bellow” compensator can absorb axial expansion, reduces thermal stress in ducting, dampen vibrations, and compensates minor misalignment. Advantage of OEM supplied expansion bellow are simple design, cost-effective, easy installation, and lower maintenance as bellow compensator. compared to double bellow compensator. Refractory brick lining design includes simple arch brick lining with 2 layer 1 layer of dense brick as working lining insulation. It has both horizontal and vertical expansion joints (50mm) using ceramic fiber blanket. Dense Arch locking brick as working lining will prevent sliding in vertical direction, control expansion direction, strengthen transition area as it is a high-stress zone, and avoid gas penetration path. Fig. 4 presents the lining pattern of the OEM supplied expansion bellow.



Figure 4 Refractory lining of the OEM supplied expansion below

5.2 Inhouse developed expansion bellow

A double bellow compensator is a metallic expansion joint connected spool piece. It is designed to absorb higher axial movement & lateral displacement compared to an OEM supplied compensator. Expansion bellow is made from heat-resistant alloy steel, corrugated structure allows axial movement, refractory Lining, insulate and protect shell from extreme heat. The outer Shell Provides pressure containment along with flange and weld ends for the connection to ducting system. Working principle include both bellow compress and extend during application, center spool shifts laterally, stress is distributed between 2 bellows and overall spring rate reduces. Advantage over “Single bellow” compensator are higher axial movement, lateral movement is limited as single bellow and expensive than single bellow one. Refractory Brick Lining Design: insulation and Hysil board is used of the retainer as per required ID. till the height, 2 layer of working Tongue & Groove brick lining, PCPF brick lining towards outer retainer, ceramic blanket inserted in the inner side of the two-bellow area. Finally having a layer of 84% alumina conventional castable at the face of the both side of the flange, supported with 70 mm anchors. Double bellow design to be selected for the long hot blast ducts run, large thermal growth, significant lateral displacement, high misalignment possibility, and lower spring load required. Advantage of 2 retainer plate design are maximum lateral displacement, improved flow dynamics (Low pressure drop), and reduced “Thermal Bridging”. Limitations of 2 bellow compensator are no of bricks and materials is more than single one, retainer is to be temporary cut for key, additional casting to be done at both side which can lead to lower thermal shock resistance.

5.3 Comparison between OEM supplied and inhouse developed expansion bellow

Fig. 5 and Fig. 6 presents the drawing and picture of expansion bellow after refractory lining of the OEM supplied and inhouse developed expansion bellow respectively. Table 2 provides the comparative analysis of the OEM supplied and inhouse designed expansion bellow for stove.

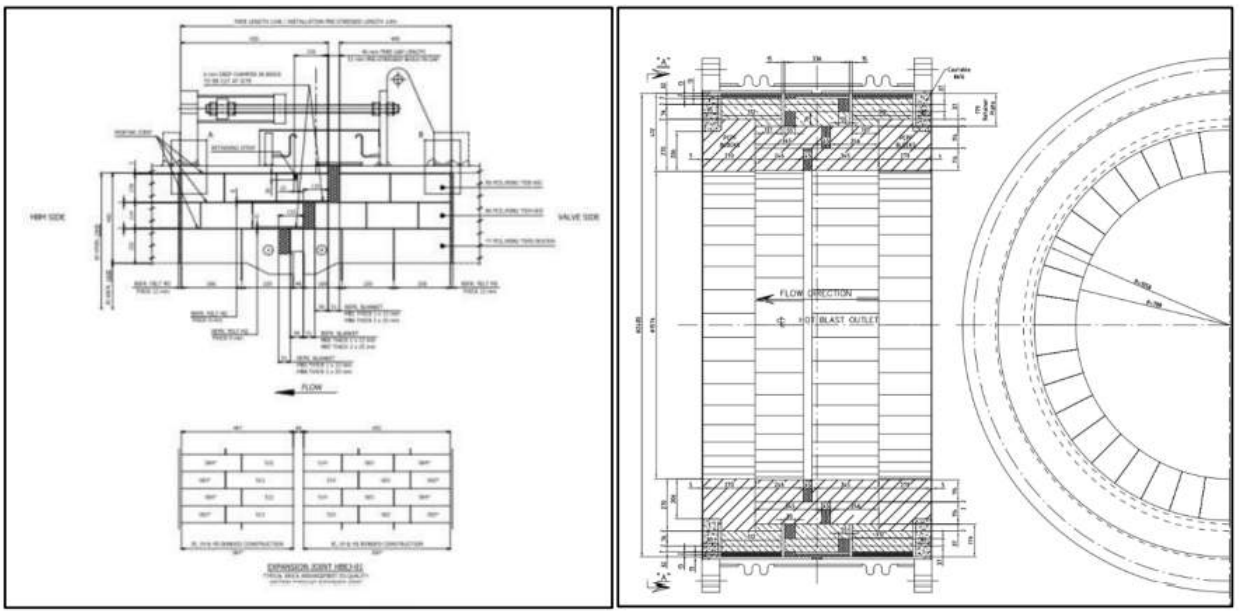


Figure 5 Drawing of the OEM supplied and inhouse made expansion bellow design



Figure 6 Refractory lining in the OEM supplied and inhouse designed expansion bellow.

Table 2: Comparison of the different compensator design

OEM supplied Compensator	In-house refurbished compensator
One bellow	Two bellow
Axial (Compression/extension) movement	Axial + Lateral movement
Simple design with no retainer plates	Complex design with 2 retainer plates
PCPF brick not used during lining	PCPF brick used during lining
Refractory brick key fixing retainer plate not present is easy due to	Refractory brick key fixing retainer plate not present is easy due to
Anchor welding and castable patching not required at face side of both the flange	Anchor welding and castable patching required at face side of both the flange due to complex design
High stress on joints during compression	Distributed stress across two flexible points
Misalignment tolerance is low	Misalignment tolerance is high
Lighter is overall weight	Heavier in overall weight
Mech. & Refractory maintenance and cheaper	Mech. & Refractory maintenance is expensive
Failure risk under large movement is higher	Failure risk under large movement is lower
Center spool not required	Center spool required
Fabrication and bricks lining time is shorter	Fabrication and bricks lining time is higher
Vibration absorption is moderate	Vibration absorption is Better

6. Conclusions

Both compensator concepts can perform satisfactorily when selected according to operating requirements. Single-bellow compensators are suitable where movement requirements are limited, and maintenance simplicity is important. Double-bellow compensators are preferred for applications involving large thermal expansion, lateral displacement, and higher reliability demands. Optimised compensator selection, combined with appropriate refractory lining design, can significantly improve stove availability and campaign life.

References

1. Expansion Joint Manufacturers Association (EJMA). (2020). Standards of the Expansion Joint Manufacturers Association (11th ed.). EJMA, White Plains, NY, USA. https://www.ejma.org/ejmastandards/

2. Primetals Technologies. (2024). Hot Blast Stove Technology for Blast Furnace Ironmaking. https://www.primetals.com/en/portfolio/ironmaking/blast-furnace/hot-blast-stove

3. N. Kushnir, A. Babich: "Hot Blast Stove Operation and Maintenance Practices in Modern Blast Furnaces." Ironmaking & Steelmaking, 46(8), (2019) 743-752.

4. P. Chattopadhyay: Failure Analysis of Bellows in High-Temperature Service. Engineering Failure Analysis, 11(3), (2004)367-379.

5. M. Geerdes, H. Toxopeus, C. van der Vliet: Modern Blast Furnace Ironmaking. IOS Press. Chapters on hot blast stoves and hot blast systems (2009).

6. T. M.Link, R. Zauter: "Design and Life Assessment of Metallic Expansion Bellows under Cyclic Thermal Loading." International Journal of Pressure Vessels and Piping, 78(2-3), (2001) 131- 139.

ZIRCONIA: MAINTAINING THE STABILITY OF AN ESSENTIAL MINERAL IN REFRACTORY FORMULATIONS

R. Soth[1)], C. Wöhrmeyer[2)], C. Liu, G. Bhattacharya, E. Chabas

[1)] Corresponding author (ratana.soth@imerys.com), [2)] Presenting author

Imerys SA, Paris, France

Abstract

Zirconia is renowned for its exceptional resistance to slags and casting powders in the flow control process of modern steel production. The stabilization of its crystal structure—typically to the cubic or tetragonal phases through doping with oxides like CaO, MgO, or Y_2O_3 during electrofusion and subsequent controlled cooling and solidification of the zirconia raw material—is a well-established industrial practice. However, less is understood about how this stabilization and the related volume behavior of zirconia are maintained when incorporated into a formulated refractory product exposed to thermocyclic application. The degradation of stabilization, leading to a transformation from the desired tetragonal/cubic phases to the monoclinic structure, is a critical concern. This phase change causes undesirable volume changes and expansion-shrinkage hysteresis during thermocycling, which results in reduced strength and the formation and propagation of cracks. This paper will demonstrate that while the inherent stability of the zirconia raw material is crucial, the surrounding refractory matrix also plays a significant and complex role. Depending on its chemical composition, the matrix oxides can either enhance or compromise the stability of the zirconia phases, influenced by both the matrix chemistry and the initial stabilizing oxides within the zirconia raw material. We will analyze microstructural changes in formulated model zirconia refractories throughout thermal cycling, correlating these findings with the determination of mechanical properties, phase and volumetric evolution.

Keywords: Zirconia, Refractory, Phase stability, Thermocycling, Volume change, Monoclinic transformation, Slag resistance, Microstructural changes

1. Introduction

Zirconia refractories are key in continuous steel casting due to extreme thermal/chemical stresses [1-3]. Pure zirconia undergoes detrimental phase transformations (monoclinic to tetragonal at ~1170°C, cubic at ~2370°C) with critical volume changes causing microstructural failure [4]. To prevent this, zirconia is pre-stabilized with oxides like CaO, MgO, or Y_2O_3 [3,5,6]. However, pre-stabilized zirconia can destabilize under high thermal stress or when interacting with slag and steel melts. This paper brings additional data to a previous work [7] and investigates binder-aggregate microstructural interactions to achieve additional in-situ stabilization and enhanced thermal shock resistance.

2. Materials and methods

Three zirconia raw materials were evaluated: calcia partially stabilized zirconia (CSZ), magnesia partially stabilized zirconia (MSZ), and a prototype double magnesia-yttria partially stabilized zirconia (MYSZ) (Table 1). Two binders were tested: Calcium Aluminate-Spinel (CMA 72: 70 wt% MA spinel, 20 wt% CA, 10 wt% CA2) and a

magnesia-based binder (LP 552C: 81 wt% MgO, 19 wt% organic compounds).

	Stabilising oxide (wt%)		
Zirconia	CaO	MgO	Y_2O_3
CSZ	4		
MSZ		3	
MYSZ		1.8	2.5

Table 1. Zirconia materials and type of stabilizing oxides

Model refractories were formulated per Table 2 (water kept at 4.4 wt%). Prismatic specimens (40x40x160 mm3) were cast, dried at 110°C (24h), and fired at 1650°C (2h dwell, ±1°C/min rate). Thermal shock (TS) tests consisted of heating fired specimens to 950°C (2h hold), followed by compressed air quenching (1 bar, 2 min). CMoR (3-point flexion, 0.05 kN/s), CCS (2.4 kN/s), density and open porosity (Archimedes method) were measured at room temperature. Permanent linear change (PLC) was evaluated post-firing.

Zirconia MSZ or CSZ or MYSZ	-12+100 mesh	70	70
	-100 mesh	27.7	24
LP552C		2.3	
CMA 72			5
Refpac 500	Defloculating agent		1
Total		100.0	100.0
Water		4.4	4.4

Table 2. Formulation compositions in weight percent

3. Results and Discussion

Physical properties

CMA 72 formulations systematically showed higher density and lower open porosity compared to LP 552C series post-firing at 1650°C (Table 3). Moderate linear contraction (PLC ≤ -1.1%) occurred for all specimens between 110°C and 1650°C (Figure 1).

Refractories physical properties				
	Density (g/cm^3)		OP (%)	
	CMA 72	LP 552C	CMA 72	LP 552C
CSZ	4.39	4.05	20.7	27.9
MSZ	4.31	3.99	22.3	31.7
MYSZ	4.27	3.78	23.0	34.3

Table 3. Density and open porosity of refractories after 1650°C firing

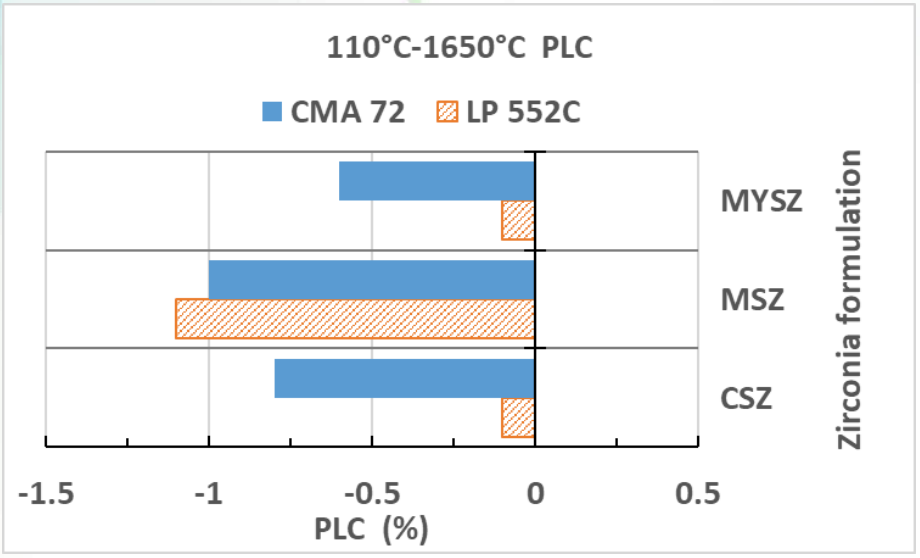


Figure 1. Permanent linear change of refractories between 110°C drying and 1650°C firing.

Microstructural investigation

SEM/EDS analyses on polished cross-sections revealed significant inter-phase reactions post 1650°C firing. In CMA 72 systems, zirconia grains are linked by MA-spinel and calcium aluminates (CA6, CA2) (Figures 2, 4). CSZ grains retained constant oxide contents (Figure 3), whereas in MYSZ formulations, CaO migrated from the CMA 72 binder into zirconia grains to form (Ca,Y)-ZrO_2 (Figures 4, 5).

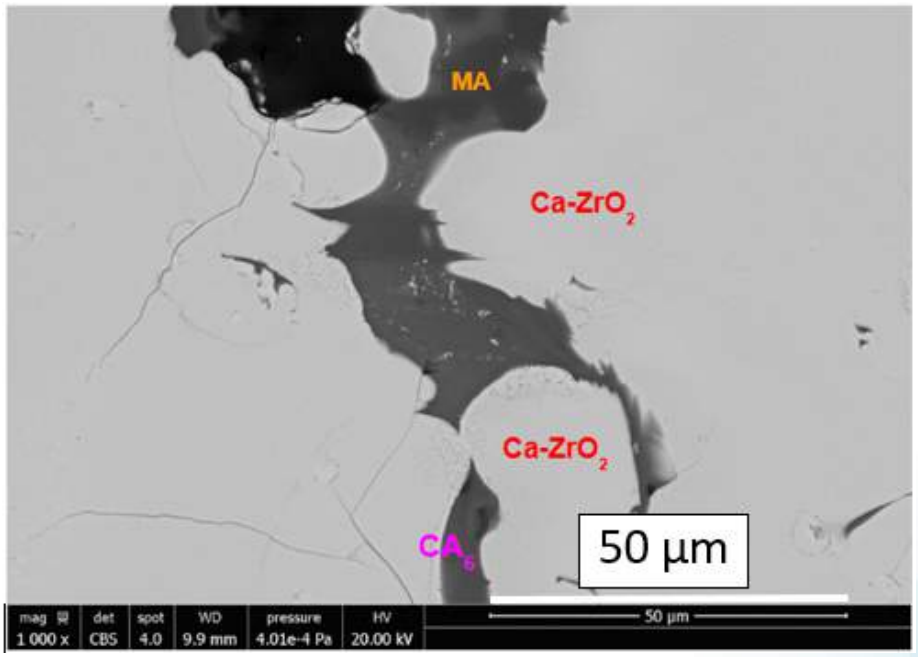


Figure 2. SEM microstructure of CSZ-CMA 72 after 1650°C firing focused on the matrix indicating MA-spinel and CA_6 interconnecting zirconia grains.

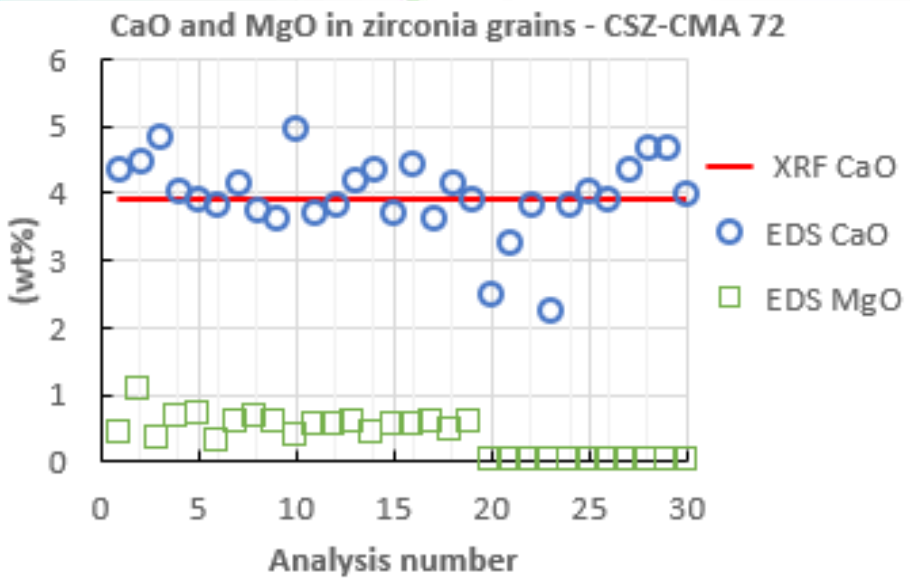


Figure 3. EDS CaO and MgO concentration in zirconia grains of CSZ-CMA 72 formulation.

For LP 552C systems, MgO migrated into the fine zirconia matrix and aggregate grain boundaries (Figure 6), inducing an enrichment of MgO in zirconia and a double in-situ stabilization across CSZ systems after firing at 1650°C. This phenomenon is also observed for the other two formulas, MSZ-LP 552C and MYSZ-LP 552C, but the results are not shown here.

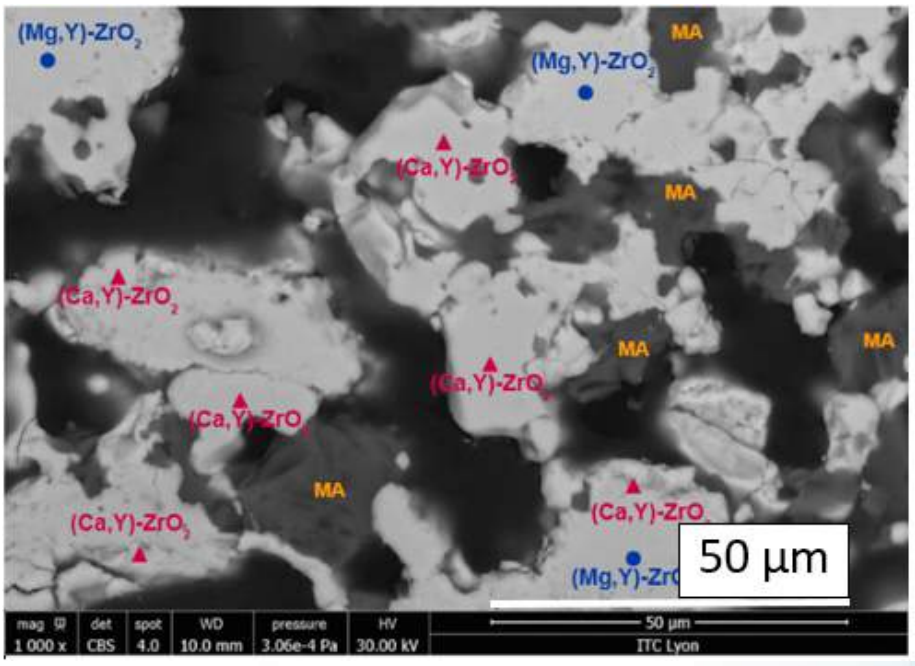


Figure 4. SEM microstructure of MYSZ-CMA 72 after 1650°C firing focused on the matrix indicating the presence of CaO entering the zirconia grains with (Ca,Y)-ZrO_2.

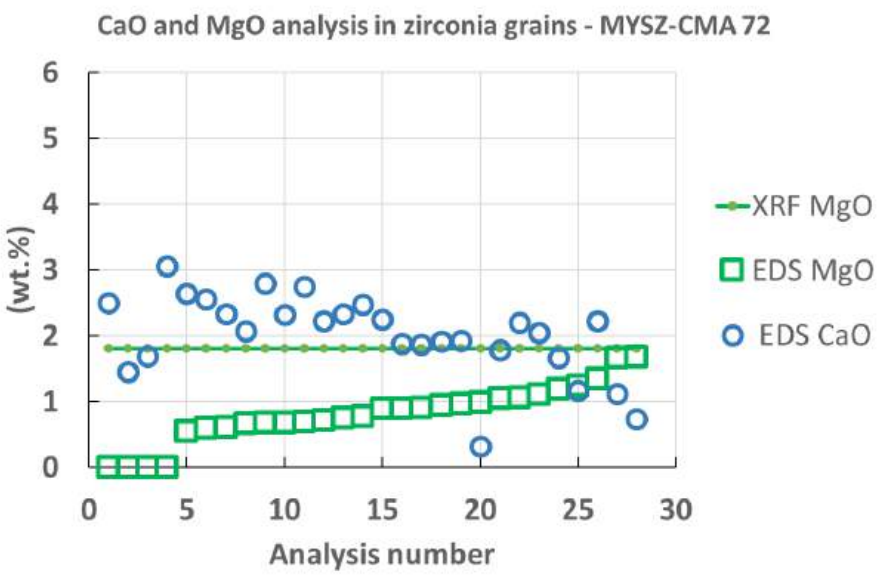


Figure 5. Incorporation of CaO in zirconia grains of MYSZ-CMA 72 formulation.

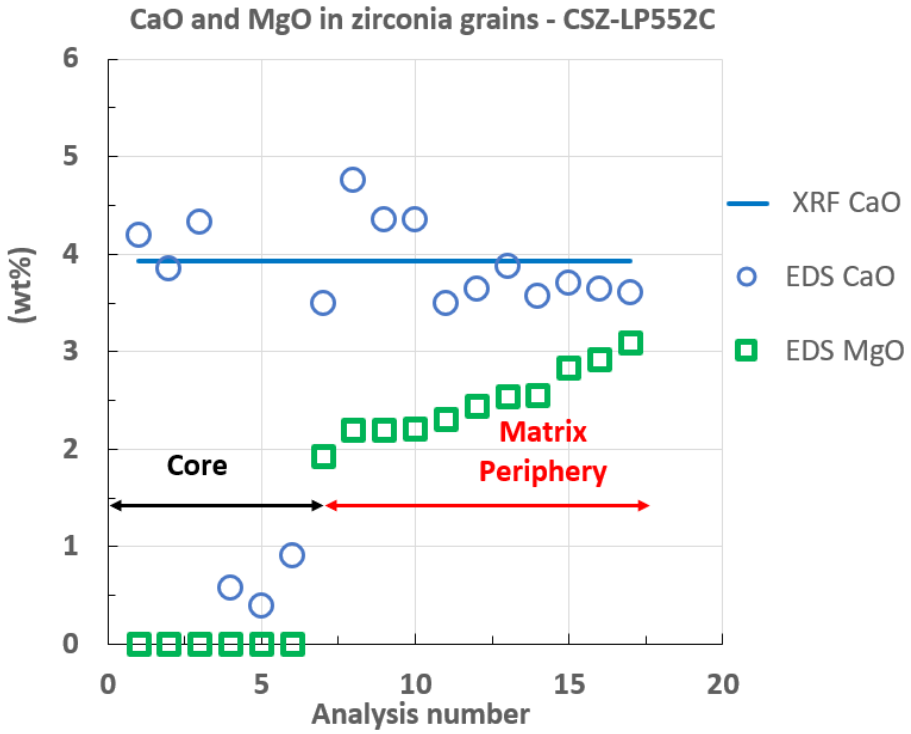


Figure 6. Presence of MgO in zirconia grains at the coarse grain core and periphery or in the matrix of CSZ-LP 552C formulation.

Phase composition change over heat treatments

Zirconia phase quantity by X-ray diffraction (XRD) shown in the graphs below has been normalized to 100% of zirconia in the formulation.

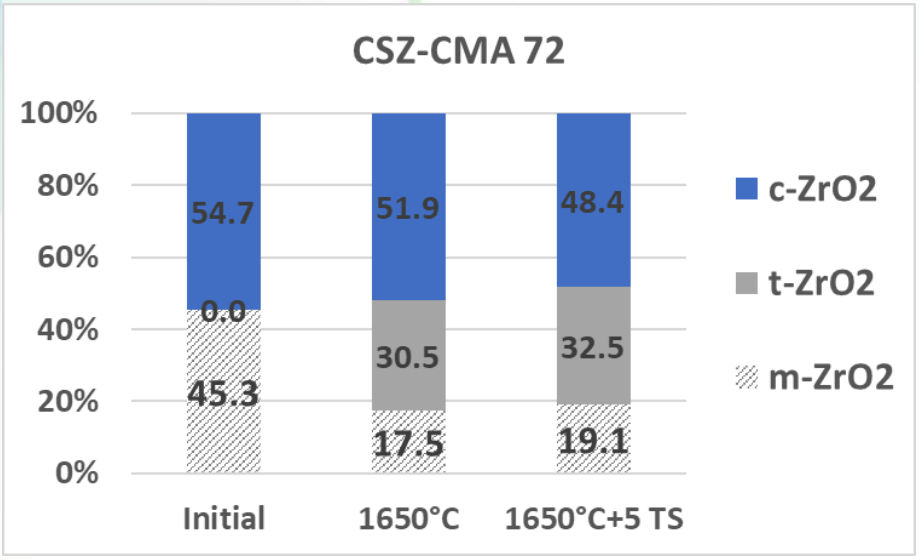


Figure 7. Zirconia phase evolution over heat treatments for CSZ-CMA 72.

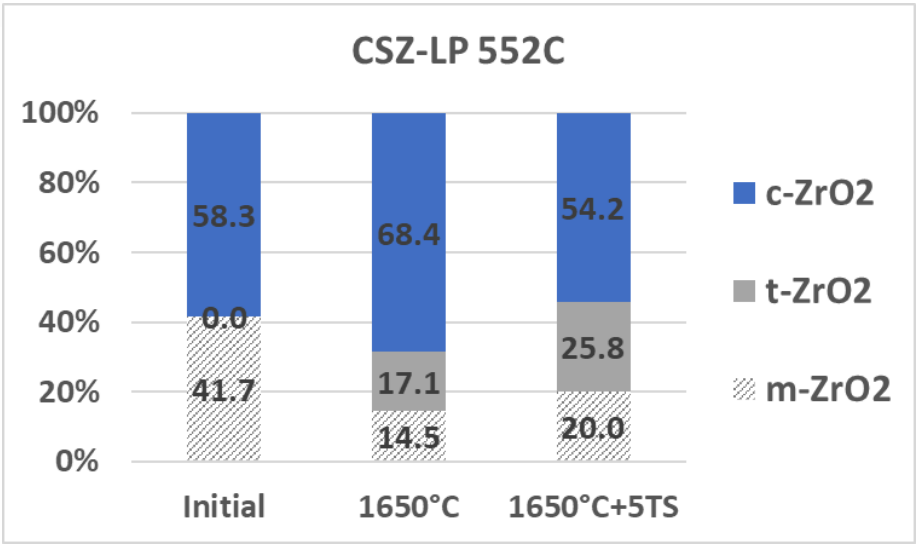


Figure 8. Zirconia phase evolution over heat treatments for CSZ-LP 552C.

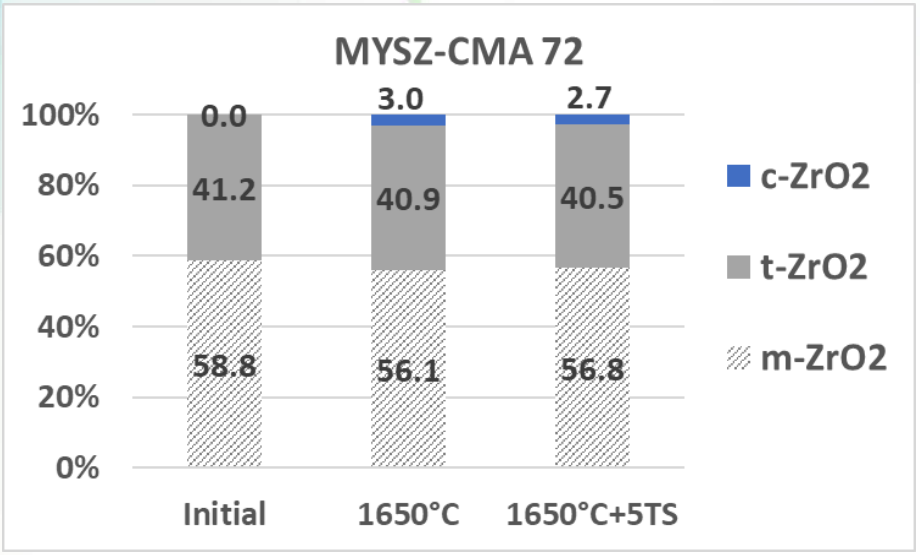


Figure 9. Zirconia phase evolution over heat treatments for MYSZ-CMA 72.

Firing at 1650°C promoted monoclinic-to-tetragonal/cubic transformation, reinforcing zirconia stabilization (Figures 7-10). Following 5 thermal shock cycles at 950°C, phase compositions remained remarkably stable with minor cubic phase degradation into tetragonal/monoclinic forms. Initial CMoR was higher for CMA 72 series, matching its lower porosity and higher density (Table 3). After 5 thermal shocks, residual flexural strength remained high: 40-60% for CMA 72 and 57-84% for LP 552C series (Figures 11, 12).

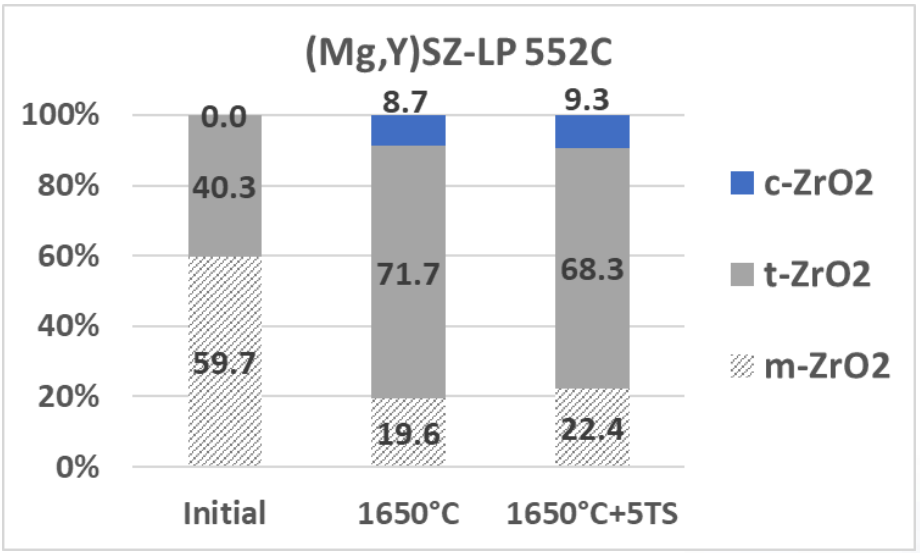


Figure 10. Zirconia phase evolution over heat treatments for MYSZ-LP 552C

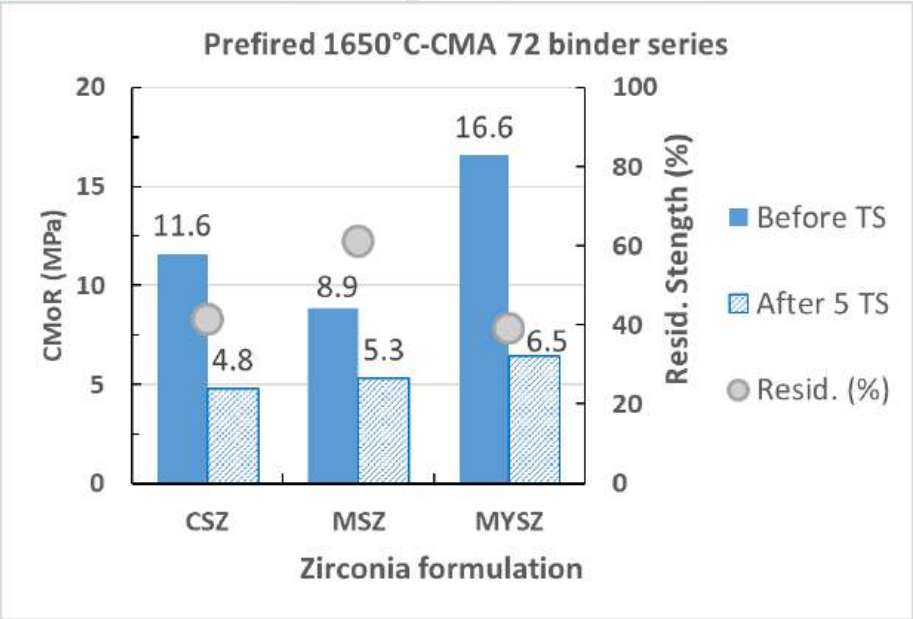


Figure 11. CMOR of CMA 72 series before and after 5 thermal shocks.

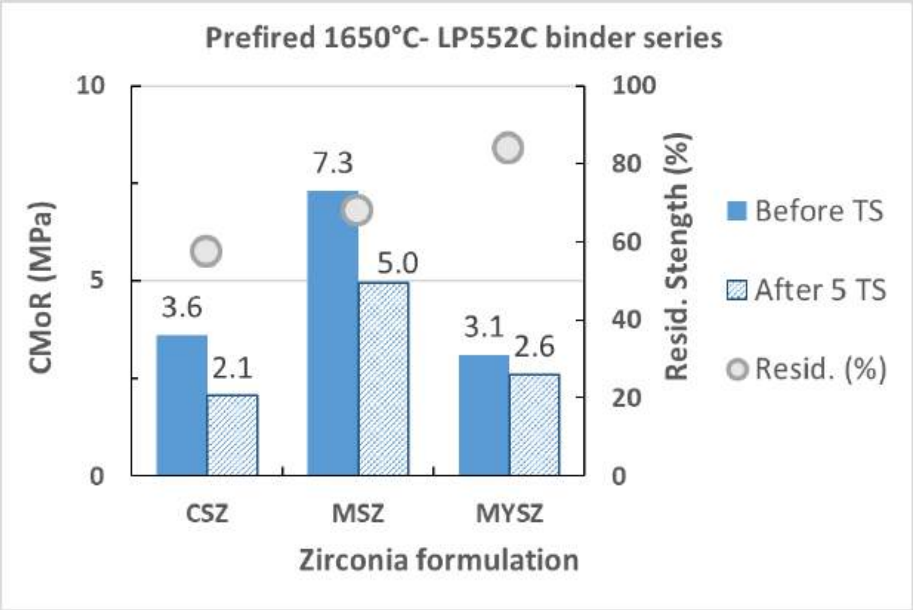


Figure 12. CMOR of LP 552C series before and after 5 thermal shocks.

4. Conclusion

Binder-aggregate oxide migration (CaO from CMA 72, MgO from LP 552C) during firing has been evidenced by SEM-EDS and XRD. This phenomenon has led to in-situ additional zirconia stabilization. Consequently, an initial mono-stabilized zirconia may become double-stabilized through this mechanism resulting in increased stabilisation. This stabilization reinforcement enhances high-temperature phase stability and maintains high residual mechanical strength following thermal cycling.

Further works may be focused on the effect of grain size distribution and of the ratio of

stabilized-to-monoclinic zirconia on the thermal shock resistance, while maintaining the resistance to slag corrosion.

Acknowledgment

The authors thank all contributors from the Imerys Technology Centers in Lyon, France, and Tianjin, China for the contribution to this work.

References

1. C.G. Aneziris, E.M. Pfaff, H.R. Maier, Fine grained Mg±PSZ ceramics with titania and alumina or spinel additions for near net shape steel processing, J. Eur. Ceram.Soc. 20 (2000) 1729–1737.
2. C.G. Aneziris, E.M. Pfaff, H.R. Maier, Corrosion mechanisms of low porosity ZrO2 based materials during near net shape steel casting, J. Eur. Ceram. Soc. 20 (2000) 159–168.
3. C. Heuer, S. Dudczig, C. G. Aneziris, R. Soth , A. Priese, C. Wöhrmeyer , C. Parr, Effect of stabilizer and binder on the phase formation in zirconia castables for application in secondary steel industry, Open Ceramics 16 (2023) 100455, https://doi.org/10.1016/j.oceram.2023.100455.
4. J. R. Kelly and I. Denry, Stabilized zirconia as a structural ceramic: an overview, Dental Materials, vol. 24, no. 3, pp. 289– 298, 2008.
5. C. E. Curtis, Development of zirconia resistant to thermal shock, Journal of The American Ceramic Society, October 200630(6):180-196, DOI:10.1111/j.1151-2916.1947.tb18886.x.
6. A. G. Karaulov, A. A. Grebenyuk, I. N. Rudyak, Effect of stabilizing additions on the thermal shock resistance of zirconia products, January 1967, Refractories 8(1):53-58.
7. C. Wöhrmeyer, R. Soth, G. Bhattacharya, An overview about zirconia for refractories and internal & external stabilization systems, IREFCON, 13th-15th November 2024, Goa, India.

SYSTEMATIC EVALUATION OF RECLAIMED MATERIALS FROM INDUSTRIAL SOURCES FOR LOWCEMENT CASTABLE

Parul Kumari, Kazi Asif Ahmed, Subhasis Das, Bhavna Kumari, Gaurav Sinha

Calderys India Refractories Ltd, Katni, India

Corresponding author's e-mail: gaurav.sinha@calderys.com

Abstract

The increasing demand for refractories has intensified the need for alternative raw materials, promoting the use of Reclaimed materials as partial substitutes for virgin resources without compromising performance. This study evaluates the feasibility of incorporating Reclaimed bricks and castable from industries such as iron and steel, sponge iron, cement, and aluminium into lowcement castable (LCC) formulations. The Reclaimed materials were characterized based on their physical and chemical properties. Emphasis was placed on understanding the influence of pH and leachable alkali content on the rheological and physical behaviour of LCCs. Four formulations—based on chamotte, bauxite, tabular alumina, and synthetic aggregates—were investigated. A comparative analysis between virgin and Reclaimed material-based castable was conducted to assess performance variations. The results indicate that apparent porosity, total alkali, and leachable alkali significantly affect castable rheology and overall properties, highlighting the importance of controlled selection of Reclaimed materials for sustainable refractory production.

Keyword: Reclaimed, LCC

1. Introduction

The mineralogical characteristics of raw materials are subject to wide variation depending on their geological origin [1]. Increasing depletion of mineral deposits coupled with raising carbon footprints from mining and raw material processing activities has increased strain on supply-chain leading to the adoption of Reclaimed materials as partial replacements for virgin inputs. The broader challenge of using reclaimed material is the presence of impurities introduced from diverse industrial processes and service conditions. Prolonged exposure to aggressive operating conditions leads to infiltration of alkali fumes, slags, Sulphur-chlorine bearing species, and other corrosive compounds, altering the chemical composition, pH, and microstructure. These changes directly affect critical properties including apparent porosity, leachable alkali content, rheological behavior, and overall thermo-mechanical performance. In this work Reclaimed bricks and castable from industries such as iron and steel, sponge iron, cement, and aluminum are thoroughly investigated. These materials were incorporated into low-cement castable (LCC) formulations, and their performance was evaluated with particular emphasis on rheology, setting behavior, and comparative analysis against equivalent formulations prepared using virgin raw materials.

1.1 Apparent Porosity in LCC

In castable system added water readily reacts with hydraulic binder, then gradually fills the intergranular and interparticle pores. Excess water forms a thin coating over their surfaces, acts as a lubricant, enabling the castable to flow under applied energy [2]. LCCs are engineered for low water content with high packing density. Raw materials with relatively high porosity increase water demand of the castable which undermine the effectiveness of deflocculant, directly impact on setting time due to dilution of cement hydration kinetics and rheological behavior of castable - leads to reduced strength, poor

structural integrity, and higher susceptibility to microcrack propagation particularly during thermal cycling. Furthermore, higher porosity promotes pore coalescence and connectivity, increasing permeability of liquids and gases and thereby reducing resistance to chemical attack [3]

1.2 Effect of excess Alkali and pH on Zeta Potential

In castable formulation, matrix comprises particles <0.15 mm. Presence of excess leachable alkali in raw materials destabilized the matrix electrokinetic potential [4]. During water addition, partial ionization occurs, releasing cations into the slurry. The ionization behavior is governed by electro-positivity of the released cations. Due to their high surface to volume ratio, finer particles exhibit a higher surface charge density, resulting in strong interparticle repulsive forces. This enhanced repulsion promotes better dispersion within the castable matrix. However, these electrostatic repulsive forces are opposed by short-range attractive van der Waals forces, which become dominant when particles approach one another closely. Figure 1 illustrates that overall rheology is thus determined by the balance between these opposing interactions.

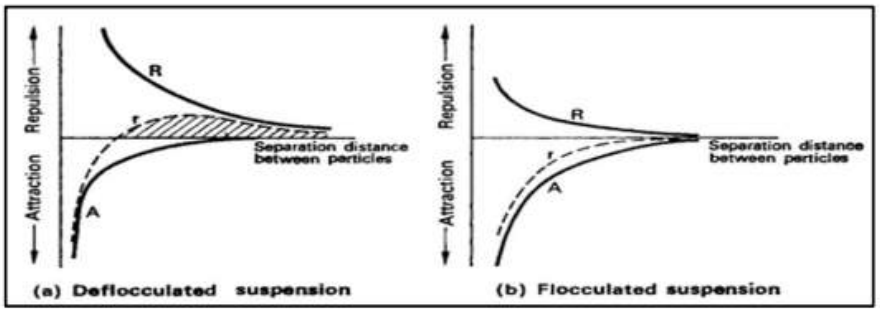


Figure 1 Variation of inter-particle forces [5].

The individual van der Waals and electrostatic repulsive forces as solid lines, with their resultant as a dotted line in figure 2, forming a distinct energy barrier. When particles are sufficiently separated, repulsive interactions dominate, preventing close contact. However, if external energy is applied through increased temperature, changes in ionization, or pH modification - the energy barrier can be surpassed. Attractive van der Waals forces become dominant, causing particles to adhere firmly and irreversibly [6]. To understand the atmosphere surrounding charged fine particles, double layer theory is used. Microfine particles in the castable system typically possess a negative surface potential. Figure 2 represents electropositive particles that are attracted and attached firmly around the surface of negatively charged particles. This counter-ion layer is known as stern layer Additional positive ions approaching the negative ions are now repelled by the Stern layer. Thus, the concentration of positive ions decreases with distance, until it reaches equilibrium. In a similar way, negative ions are repelled by negative charge particles. Where these excess electropositive ions are more loosely associated through electrostatic forces and continuously exchange with the surrounding solution is known as diffuse layer. The attached counter-ions in the stern layer and the charged atmosphere in the diffuse layer refer as double layer [5].

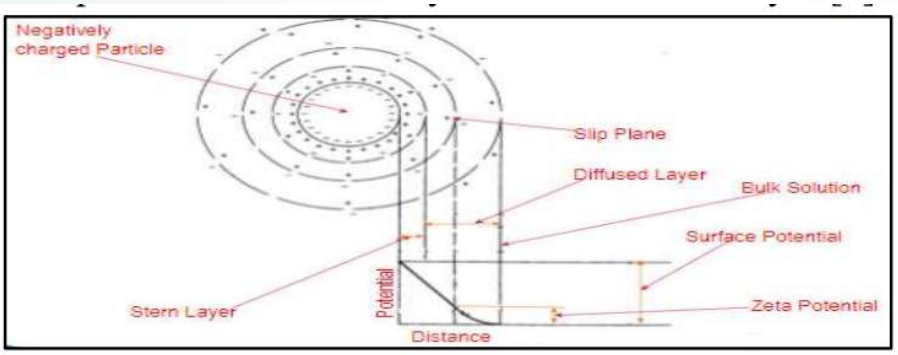


Figure 2 Schematic of electrical double layer [7]

The double layer is formed to neutralize the electrokinetic potential between the surface of the charged particle and any point in the mass of the suspending liquid. This voltage difference is in millivolts and is referred to as zeta potential, can be described by equation

1. A charged particle moves with a fixed velocity in a voltage field. The particle's mobility is related to the dielectric constant and viscosity of the suspending liquid and to the electrical potential at the boundary between the moving particle and the liquid.

$$\tau = 4\pi ed/D \qquad (1)$$

Where, τ is the zeta-potential, e is the surface density of charge on the particle, d is the double layer thickness, D is the dielectric constant of the liquid medium [8]. Excess alkali in the system reduces the thickness of the electrical double layer, making system less stable. Figure 3 represents when Na^+ exceed optimum level, the castable– water mix exhibits increased viscosity due to particle flocculation. Both TPP (sodium tripolyphosphate) and PP (polyphosphate) exhibit a minimum viscosity near 0.1 wt%, representing the optimum dosage for maximum dispersion. Beyond this point, double layer compresses induce particle flocculation. This over doping negatively impacts workability and overall rheology [8].

PH also governs the system's zeta potential by influencing the degree of ionization and net surface charge of fine particles. Each oxide has an isoelectric point (IEP). When the system pH is below the IEP, particles adsorb anions and become positively charged, yielding a positive zeta potential. When the pH is above the IEP, particles attract cations and develop a negative surface charge, resulting in a negative zeta potential. As shown in Figure 4, achieving a highly dispersed suspension requires the system pH to be maintained far from the IEP, either strongly acidic or strongly basic to maximize the magnitude of the zeta potential and enhance electrostatic repulsion between particles [6].

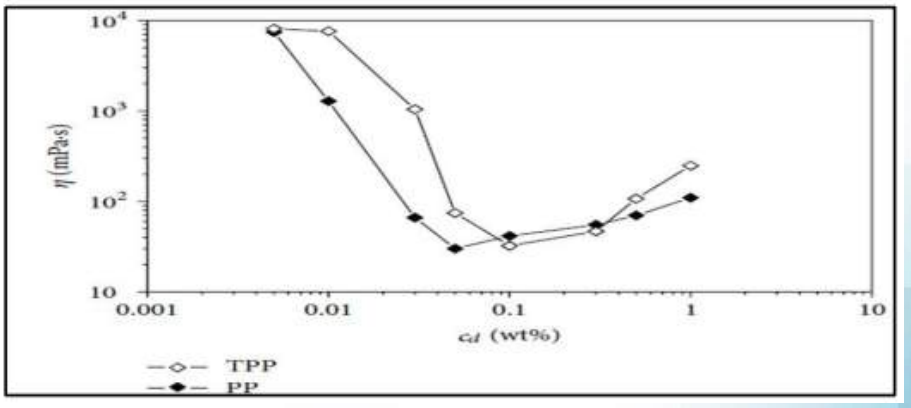


Figure 3 Viscosity vs. deflocculant concentration for TPP and PP in a castable system [4]

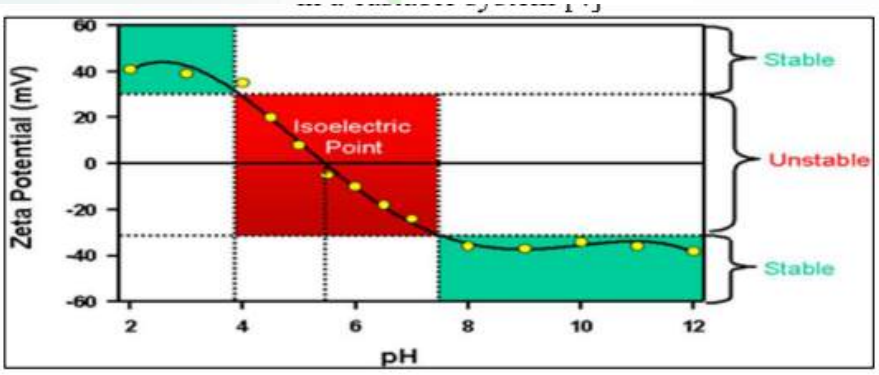


Figure 4 Effect of pH on Zeta Potential of a castable system [6]

1.3 Role of alkali in high alumina cement hydration

High alumina cement dissolves in water, releasing Ca^{2+} and $Al(OH)^{4-}$ ions, which increases the system pH. The $Al(OH)^{4-}$ ions form a protective film around calcium aluminate phases, temporarily inhibiting their hydration; however, in highly alkaline environments, this film gradually dissolves [9]. Leachable alkalis are not chemically bound within the material structure. When dissolved in water, they release Na+ /K+ ions, elevating and accelerating calcium aluminate hydration. Excess microfine silica may react with these alkalis to form a gel layer around cement grains, restricting water penetration and delaying the setting process.

2. Experimental

Four sets of LCCs formulations are presented in Tables 1 - 4. In each set, a control (C) was prepared using virgin or synthetic raw materials to serve as a baseline. Particle size fractions were categorized as: +1 mm coarse, 0.15–1 mm middling, and <0.15 mm fines, collectively forming the matrix. Trials conducted by replacing C% of the base raw material in the matrix with the same proportion of reclaimed materials. Dry constituents were mixed in a Hobart A200 planetary mixer for 1 minute. Fixed water% used for similar category of castable as per IS 10570, after which the mix was wet blended for 3 minutes. Rheology was measured immediately after mixing (T0) and after 30 minutes (T30) according to EN ISO 1927-4. Setting time was determined by using a Vicat needle compressibility of the castable over time. Physical properties of the castable were also evaluated as per IS 10570. Leachable alkalis were determined by boiling fines in distilled water at 100°C for 3 hours, following IS 12107 Part 9. Chemical composition was analyzed using X-ray fluorescence (XRF) with a Bruker ‘S8 Tiger II.

Table 1 Chamotte based formulation

Raw Material - Fraction	CH1 (C)	CH2	CH3
Calcined Chamotte - Coarse + Middling	A + B	A + B	A + B
Calcined Chamotte - Fines	C	-	-
Brick Grog Fines - Aluminum	-	C	-
Porcelain Grog Fines - Insulator	-	-	C
High Alumina Cement + Microsilica with phosphate based Deflocculating system	D + E	D + E	D + E

Table 2 Bauxite based formulation

Raw Material - Fraction	BX1 (C)	BX2	BX3
Calcined Chamotte - Coarse + Middling	A + B	A + B	A + B
Calcined Chamotte - Fines	C	-	-
Castable Grog 1 Fines – I&S	-	C	-
Brick Grog 1 Fines - I&S	-	-	C
High Alumina Cement + Microsilica with phosphate based Deflocculating system	D + E	D + E	D + E

Table 3 WTA based formulation

Raw Material - Fraction	WT1 (C)	WT2	WT3
WTA - Coarse + Middling	A + B	A + B	A + B
WTA - Fines	C	-	-
Castable Grog 2 Fines – I&S	-	C	-
Brick Grog 1 Fines – I&S	-	-	C
High Alumina Cement + Microsilica with phosphate based Deflocculating system	D + E	D + E	D + E

Table 4 Synthetic Aggregate based formulation

Raw Material - Fraction	SN1 (C)	SN2	SN3	SN4
60% Al_2O_3 Synthetic Aggregate - Coarse +Middling	A + B	A + B	A + B	A + B
60% Al_2O_3 Synthetic Aggregate -Fines	C	-	-	-
Castable Grog 3 Fines - – I&S	-	C	-	-
Brick Grog 2 Fines - – I&S	-	-	C	-
70% Brick Grog - Cement	-	-	-	C
High Alumina Cement + Microsilica with phosphate based Deflocculating system	D + E	D + E	D + E	D + E

3. Result and discussion

The impact of reclaimed raw materials on low cement castable properties was evaluated by comparing their pH and leachable alkali content.

Table 6: Results of Chamotte based formulation

Matrix system Industry	Chamotte Based Virgin	Brick Grog Fines Aluminum	Porcelain Grog Fines Insulator
Workability drops after 30 minutes (%)	22	18	21
Setting time (minutes)	155	175	135
pH value of raw material	8.39	8.35	10.19
Total Leachable alkali of raw material (%)	0.076	0.156	0.143

Total Leachable alkali of raw material (%)

Matrix system Industry	Bauxite Fines	Castable Grog 1 Fines I&S	Brick Grog 1 Fines I&S
Workability drops after 30 minutes (%)	24	28	44
Setting time (minutes)	105	180	80
pH value of raw material	8.49	9.27	9.13
Total Leachable alkali of raw material (%)	0.091	0.108	0.109

Table 8: Result of WTA based formulation

Matrix system Industry	WTA Fines	Brick Grog 1 Fines I&S	Castable Grog 2 Fines I&S
Workability drops after 30 minutes (%)	29	44	32
Setting time (minutes)	105	80	95
pH value of raw material	8.48	9.13	9.06
Total Leachable alkali of raw material (%)	0.134	0.109	0.096

Table 9: Result of Synthetic Aggregate based formulation

Matrix system Industry	Synthetic Aggregate Fines	Castable Grog 3 Fines I&S	Brick Grog 2 Fines I&S	70% Brick Grog Cement
Workability drops After 30minutes (%)	24	100	28	100
Setting time (minutes)	95	1300	225	1185
pH value of raw material	8.38	8.9	9.23	8.6
Total Leachable Alkali of raw material (%)	0.172	2.126	0.114	2.05

Tables 6–9 present the rheology and workability characteristics of the LCC formulations, along with the corresponding pH values and leachable alkali contents of the virgin and reclaimed raw materials. It is evident that refractory castable behavior is governed by multiple factors rather than any single property. Figure 8 shows the relationship between leachable alkali content with setting time and the 30-minute workability drop, revealing a critical threshold at approximately 0.172% leachable alkali. At or below this level, alkalis do not significantly disturb the electrical double layer of the castable system. However, above this threshold, a sharp increase in setting time and a substantial loss of workability are observed. As alkali content increases, more positive ions are released into the system, compressing the electrical double layer around particles. This reduces the zeta potential [Equation 1] weakens electrostatic repulsion, allowing van der Waals forces to dominate and draw particles closer together. Consequently, particle flocculation occurs, forming clusters that restrict particle mobility and increase viscosity. In the case of 70% Brick Grog – Cement and Castable Grog 3 Fines having exceptional high leachable alkali content 2.05% and 2.126% respectively resulted into zero initial workability at the constant water level. Furthermore, excess leachable alkali reacts with micro silica to form a gel around calcium aluminate cement grains. This gel layer impedes water penetration and delays the hydration of calcium aluminate phases, thereby extending the setting time of the castable.

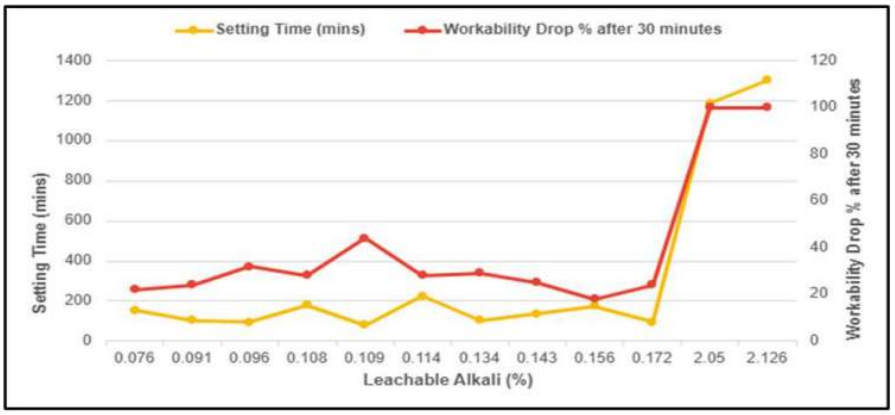


Figure 8: Impact of leachable alkali of raw material fines on workability and setting time of LCC

Figure 9 at two specific pH values 8.59 and 8.90, a drastic increase in setting time and a sharp decline in 30-minute workability is observed. These anomalies are primarily attributed to the inclusion of 70% Brick Grog–Cement and Castable Grog 3 Fines, which contain exceptionally high leachable alkali levels of 2.05% and 2.126%, respectively. Excluding these two outliers, it becomes evident that up to pH of 9.13, pH

variation has minimal influence on castable setting time. However, a slight upward trend in workability loss is noticeable as the pH of the fine raw materials increases. Elevated pH enhances interparticle interactions, promoting particle agglomeration and consequently increasing the workability drop. Beyond pH 9.23, a consistent reduction in setting time is observed. This accelerated setting is attributed to the increased alkalinity of the medium, in which $Al(OH)^{4-}$ begins to dissolve more readily, thereby promoting the hydration of calcium aluminate cement.

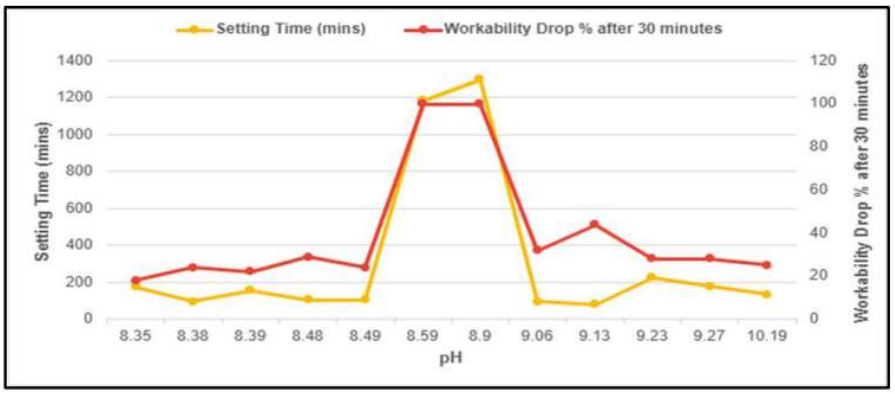


Figure 9: Impact of pH of raw material fines on workability and setting time of LCC

To validate this effect, 50 ml each of 1N NaOH and 1N KOH were combined to prepare a 100 ml alkaline solution. Three chamotte-based control formulations were then prepared at a fixed water content to evaluate rheological behavior. The water types used were normal tap water, 3.5% alkaline mix water, and 17.5% alkaline mix water.

Table 10: Result of the Chamotte based formulation for different percentages of alkaline water.

Chamotte Based - Formulation	Normal Tap Water	3.5% Alkaline Solution Mix Water	17.5% Alkaline Solution Mix Water
Water (%)	A	A	A
Water (%)	7.64	10.52	12.67
Workability drops after 30 minutes (%)	27	45	100
Setting time (minutes)	110	85	50

The results follow a similar trend: increasing pH sharply reduced castable workability and shortened setting time. As soluble Na^+ and K^+ ions in the alkaline mixing water accelerated CAC hydration kinetics. In Figures 8 and 9, one notable deviation is observed for the WTA based formulation containing Brick Grog 1 Fines I&S. Although this reclaimed material exhibited a pH of 9.13 and a leachable alkali content of 0.109 substantially lower than those of the reclaimed material with the highest pH (10.19) and alkali content (2.146), it showed a much higher 30- minute workability drop of 44%. To investigate this behavior, the free lime content of all fine raw materials was examined. Brick Grog 1 Fines – I&S was found to contain 0.042% free lime, whereas the other materials contained less than 0.02%. Higher free CaO increases the concentration of Ca^{2+} ions in solution, which is particularly influential in systems containing reactive phases such as $C_{12}A_7$. The increased Ca^{2+} concentration accelerated

$C_{12}A_7$ hydration, forming the exothermic peak and significantly reduce workability [13].

5. Conclusion

This study evaluates the influence of pH, leachable alkali, and free lime in raw materials on the performance of low cement castable.

- Castable behavior is governed by multiple factors including pH, leachable alkali, and free-lime content of raw materials.
- Variations in pH and leachable alkali content effect on zeta potential & CAC hydration, influencing workability and rheology of castable.
- The presence of free lime promotes exothermic reactions after water addition effecting workability and setting behavior of castable.
- Reclaimed materials should be selected based on controlled pH, leachable alkali, free lime, and known processing history to ensure consistent workability and setting.
- Integrating recycled materials without compromising product performance demands adjustments to standard formulations; for example, deflocculant dosage must be fine-tuned based on the leachable alkali content of the aggregates.

6. Reference

1. Kingery, Bowen, Uhlmann, “Introduction to Ceramics” 2nd Edition, p 6.

2. I. N. Chakraborty, “Monolithic Refractories”, Calderys India Refractories Ltd Nagpur India

3. Ritwik Sarkar “Refractory Technology Fundamentals and Applications”, 2nd Edition, p 25.

4. Zeta Potential: A Complete Course in 5 Minutes, Zeta Meter Inc https://ipls.gatech.edu/wp-content/uploads/2016/07/Zetapotential-excerpt.pdf

5. F. Moore, Maclaren, “Rheology of Ceramic Systems” 1965

6. Zeta potential - An introduction in 30 minutes by Malvern Instruments Limited.

TAILORING LOW-CEMENT CASTABLE RHEOLOGY VIA MICROSILICA PROPERTIES

Bhavna Kumari, Gaurav Sinha, Ram Prosad Pal, Subhasis Das and Pratanu Nag

Calderys India Refractories Ltd, Katni, India

Corresponding author's e-mail: gaurav.sinha@calderys.com

Abstract

Microsilica is an essential component in low cement castables (LCCs), significantly influencing their rheological behaviour and overall performance. This study investigates the effect of microsilica properties on LCC characteristics by examining seven different types of commercially available microsilica grades. Key parameters such as pH, mean particle size, carbon content, and leachable alkali content were evaluated for each variant. The prepared LCC formulations were assessed for both rheological and mechanical properties. The results demonstrate that variations in microsilica characteristics notably affect the flow behaviour, and strength performance of LCCs. Among the studied factors, leachable alkali content, mean size, pH, and carbon content were identified as critical contributors governing the rheological and physical properties of the castables. This study highlights the importance of selecting appropriate microsilica to optimise LCC performance.

Keywords: Low Cement Castables, microsilica, rheology, physical properties.

1. Introduction

Low-cement castables (LCCs), typically containing less than 5 wt.% calcium aluminate cement (CAC), are widely used in high-temperature applications due to their low porosity, high thermo-mechanical properties, and corrosion resistance. Reduced cement content minimizes low-melting calcium-containing phases, thereby improving refractoriness under load, hot strength, and slag resistance [1]. However, the low cement level increases sensitivity to particle packing, water demand, and rheology, making flowability control essential for effective mixing and placement [2]. Microsilica which is a by-product of silicon and ferro-silicon industries with colour variation which is strongly correlated with its carbon content that exists in various forms like coke residue, silicon carbide, tar-related substances, or carbon black [3]. Microsilica is a key ultrafine component in LCCs. Its amorphous SiO2 particles fill interparticle voids, improve packing and densification, and contribute to reduced permeability and enhanced microstructure [4]. However, its high specific surface area strongly affects water demand and rheology. Commercial microsilica grades can vary significantly in particle size, loose bulk density (LBD), pH, impurity level, and leachable alkali content due to differences in production and processing [5]. These variations influence interactions with mixing water, dispersants, and cement hydrates, affecting flowability, setting behaviour, and storage stability [6]. Thus, microsilica replacement may require castable reformulation even at similar SiO2 contents. Although its role in LCC packing and hydration is well established, the combined influence of microsilica physicochemical characteristics on LCC rheology remains comparatively less studied [7,8]. In this study, seven commercially available microsilica grades (MS A–MS G) were evaluated in an identical LCC formulation. The microsilicas were characterised in terms of pH, leachable alkali content, mean particle size, and carbon content. Their effects on wetting time, initial flow (T0) and setting time (ST) were investigated. The objective was to identify the microsilica parameters most strongly associated with fresh-state behaviour, providing practical criteria for microsilica selection and qualification in industrial LCC formulations.

2. Experimental

Castable Preparation

To conduct a systematic study, seven low-cement castable formulations (Samples A–G) were prepared using seven different microsilica grades (MS1 to 2 MS7). The microsilica grades differed in pH, leachable alkali content, carbon content, and mean particle size, while all other raw materials, including aggregates, calcium aluminate cement (CAC), reactive alumina, additives, and dispersants, were kept constant to isolate the effect of microsilica properties on castable performance like flow, setting time, and other relevant properties. All tests were conducted in accordance with EN ISO 1927, with the castable materials, mixing water, and laboratory temperature maintained at 18 ± 2 °C and the relative humidity controlled at 90-95% throughout the testing period.

Mixing, Flow Measurement, Setting Time determination and other related details

Mixing was carried out using a Hobart A200 mixer. The dry constituents were initially mixed for 1 min, followed by wet mixing for 3 min after the addition of water. The water addition was maintained at 4.2 wt.% for all formulations throughout the study. Flow was determined in accordance with EN ISO 1927 using a truncated-cone mould having a bottom diameter of 100 mm, a top diameter of 70 mm, and a height of 80 mm. The filled mould was placed on a vibrating table operated at 50 Hz with an amplitude of 0.5 mm for 30 s. The flow measured immediately after mixing was designated as T0, while the flow measured 30 min after water addition was designated as T_{30}. Setting time (ST) was determined using a Vicat initial-setting needle. The freshly mixed castable was filled into a plastic cup and vibrated for 20-30 s on a flow table at an amplitude of 0.75 mm to ensure proper consolidation. Excess material was then removed using a trowel to obtain a level surface. The Vicat needle was subsequently used at regular intervals to assess the penetration resistance of the castable. The setting time was defined as the elapsed time from water addition at which the Vicat needle could no longer penetrate the castable through the full depth of the specimen.

Microsilica Characterization

Leachable alkali content was determined by boiling the microsilica samples in distilled water for 3 h. The concentrations of Na_2O and K_2O in the resulting extract were determined in accordance with the procedure specified in IS 12107, Part 9. The total leachable alkali content was calculated as the combined concentration of Na_2O and K_2O and reported on a weight-percent basis (wt%). The mean particle size of each microsilica grade was determined using a Horiba Partica LA-960 V2 laser diffraction particle size analyser. The carbon content of the microsilica samples was obtained from the supplier-provided test certificates, where it was determined using a LECO carbon analyser.

3. Result and Discussion

Figure 1 shows the relationship between leachable alkali content (LA; Na2O + K2O), microsilica pH, and wetting time (WT).

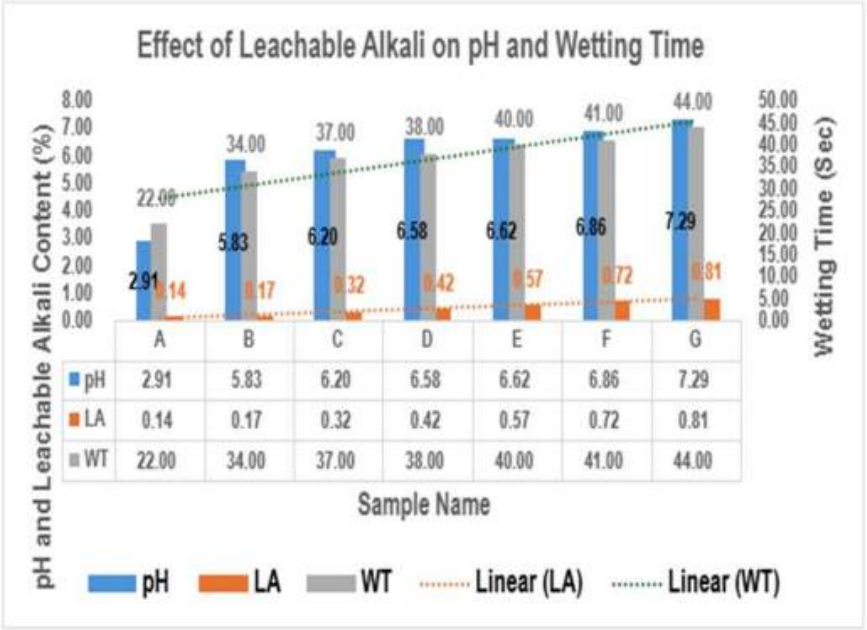


Figure 1: The effect of leachable alkali content on pH and wetting time on low cement castable

Here, a clear positive correlation is observed, with the most pronounced change from sample A to B, where LA increases from 0.14 to 0.17%, pH from 2.91 to 5.83, and WT from 22 to 34 s. At higher LA levels, the increase in pH becomes more gradual, indicating a tendency toward alkaline saturation. WT progressively increases from 22 to 44 s as LA rises from 0.14 to 0.81%, indicating slower wetting at higher leachable alkali levels.

Leachable Na^+ and K^+ from microsilica increase the ionic strength of the pore solution, compressing the electrical double layer around microsilica particles and reducing the magnitude of the negative zeta potential. The resulting decrease in electrostatic repulsion promotes particle flocculation and increases interparticle interactions, leading to higher yield stress and viscosity. Consequently, the castable exhibits reduced flow and poorer workability at higher levels of leachable alkali. Therefore, Na/K species alter surface chemistry, surface charge, ionic strength, and particle-water interactions, thereby affecting wetting kinetics and dispersion.

Nevertheless, LA is not the sole controlling factor, as particle size, agglomeration, amorphous SiO_2, carbon content, LBD, surface area, and other soluble ions like Ca^{2+} may also contribute. Overall, leachable alkali content is one of the important chemical parameters influencing microsilica wetting and rheological behaviour of low-cement castables.

Figure 2 shows a clear dependence of LCC flow and setting time on the mean particle size of microsilica. Increasing the mean particle size from 0.70 to 5.53 µm resulted in a reduction in initial flow from 151.7% to 98.3%, while the setting time increased from 110 to 450 min. Thus, finer microsilica produced higher flowability and shorter setting time, whereas coarser grades showed the opposite trend.

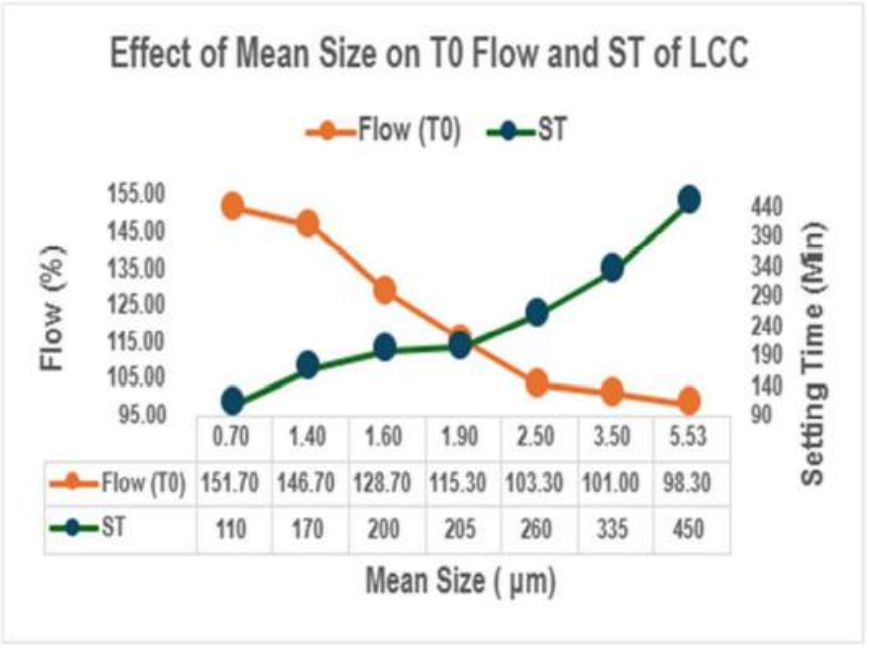


Figure 2: Effect of Mean Size on T0 Flow and ST of LCCs

At a constant LCC composition and water addition, the higher flow of finer microsilica may be attributed to its ability to fill smaller interparticle voids more effectively, improving particle packing and reducing water demand. The larger specific surface area of finer particles may also enhance their interaction with the aqueous phase and CAC hydration products, promoting faster development of the setting structure. The effect becomes particularly pronounced above approximately 2 µm. However, the influence of particle size cannot be completely isolated from other grade-dependent properties, including pH, leachable alkali, amorphous silica content, and carbon content. Overall, the results demonstrate that microsilica particle size can significantly influence both the rheology and setting behaviour of LCCs under otherwise constant formulation conditions. Figure 3 shows a clear relationship between microsilica carbon content and the rheology and setting behaviour of the seven LCCs. As carbon content increases from 0.30% to 1.40%, the initial flow decreases, with the most pronounced reduction occurring between 0.40% and 1.00%. The hydrophobic nature of carbon reduces particle wetting and alters water distribution within the matrix. At the fixed water addition of 4.2%, higher carbon content reduces the freely available water for particle lubrication and affects water/admixture distribution around the cementitious phase, thereby increasing apparent viscosity and reducing flow.

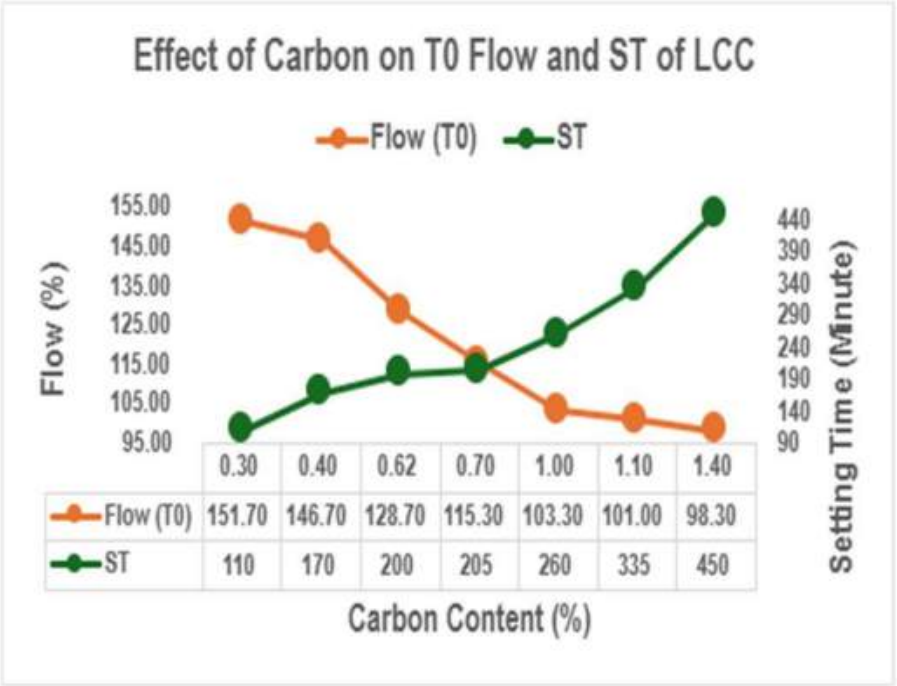


Figure 3: Effect of carbon content on T0 flow and setting time of LCCs

In contrast, setting time increases with carbon content, becoming particularly pronounced between 1.00% and 1.40%, where it increases from 260 to 450 min. This indicates that higher carbon content adversely affects wetting and water availability, thereby delaying the hydration and setting reactions. Figure 4 shows a clear inverse relationship between Flow (T_0) and Setting Time (ST) with increasing leachable alkali. Flow decreases from 151.7% at 0.14% alkali to 98.3% at 0.81%, while ST increases from 110 to 450 min. At approximately 0.42% alkali, the flow and ST are 115.3% and 205 min, respectively. Above this level, the increase in ST becomes more pronounced, reaching 335 min at 0.72% and 450 min at 0.81%. This behaviour can be attributed to changes in the aqueous-phase chemistry caused by soluble alkalis.

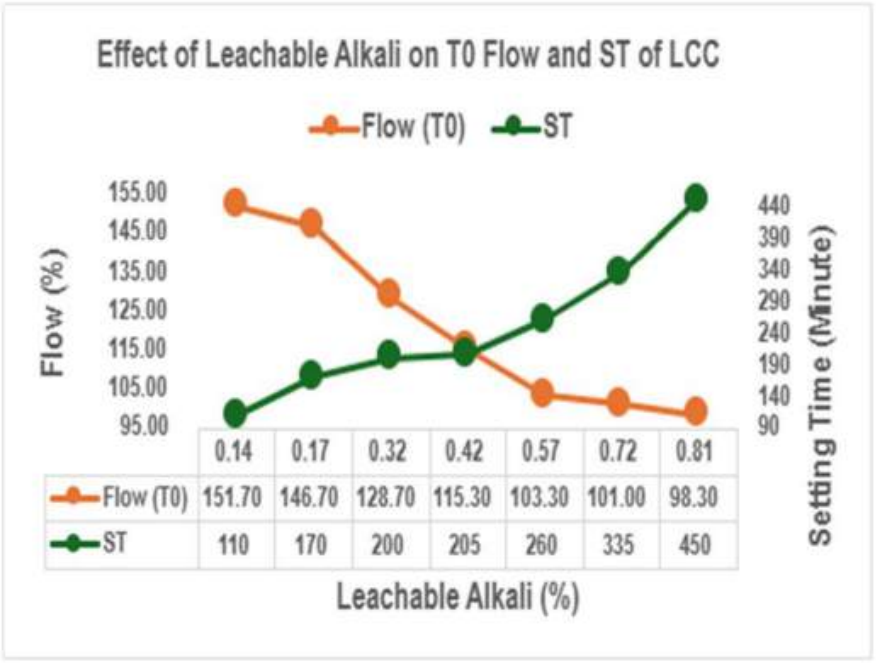


Figure 4: Effect of leachable alkali on T0 flow and setting time of LCC

Upon water addition, microsilica interacts with hydronium ions (H_3O^+), while CAC dissolves and releases Ca^{2+} and aluminate species, predominantly $Al(OH)^{4-}$, progressively increasing the system pH. At elevated alkalinity, interactions among dissolved species and particle surfaces can modify CAC dissolution and hydration kinetics, promote particle flocculation and reduce the free water available for lubrication [9-11]. Consequently, Figure 4 shows flow reduction with increasing leachable alkali. Here, higher leachable alkali increases pore-solution ionic strength, compresses the electrical double layer, reduces electrostatic repulsion, and promotes microsilica flocculation, thereby increasing yield stress and viscosity and reducing castable flow. At the same time, higher microsilica fineness and alkali concentration can promote the formation of silica-rich reaction products or gels, which may restrict water transport and ion diffusion and thereby retard the development of the continuous reaction-product network responsible for setting [12]. Thus, reduced flowability does not necessarily indicate faster setting as flow is primarily governed by rheology and particle interactions, whereas setting time reflects the development of a load-bearing hydration/reaction network. The temperature was maintained constant to isolate the influence of microsilica characteristics on these behaviours.

4. Conclusions

The present study demonstrates that microsilica characteristics significantly influence the rheological and setting behaviour of low-cement castables (LCCs), even at constant composition and fixed (4.2 wt.%) water addition. Here the synergistic effects of pH, leachable alkali, mean particle size, carbon content have been graphically demonstrated on wetting, particle interactions, water distribution, and CAC hydration for seven different commercially available microsilica grades (MS A–MS G). Their combined control is therefore essential for achieving consistent LCC rheology and setting behaviour.

4. References

1. R.Rasheeduzzafar: Cement and Concrete Research, Vol.21, 1991, p.1035.

2. M.A.L.Braulio: Journal of the Technical Association of Refractories, Vol.28, p.180.

3. A.Srivastava: Ceramics International, Vol. 40, 2014, P.14061.

4. S.M. Martinovic: Processing and Application of Ceramics, Vol.3, p.191.

5. S.Kumar:Ceramics International, Vol. 29, 2003, P. 139-144.

6. A. Kudžma: Case Studies in Construction Materials, Vol.22, 2025, p.4701.

7. D. Zemánek: Materials, Vol. 15, 2022, p.5918.

8. W.E. Lee: Castable refractory concretes, Vol. 46, 2013, p.145.

9. T.Chotard: Cement and Concrete Research, Vol.31, 2001, p.405.

10. G.Trtnik: Ultrasonics, Vol.54, 2014, p.66.

11. Z.A.Munir: Journal of Materials Science, Vol.14, 1979, p.640.

12. E. John: Journal of Materials Science, Vol.58, 2023, p.9805.

LANCE: DELIVERING CUSTOMISED SOLUTIONS FOR DIVERSE CUSTOMER NEEDS

Subhasis Das[1], Samik Sarkar[2] , Bhavna Kumari[1], Gaurav Sinha[1]

[1]Quality & Process Control, Calderys India Refractories Ltd, Katni, India
[2]Production, Calderys India Refractories Ltd, Katni, India

Corresponding author's e-mail: gaurav.sinha@calderys.com

Abstract

In the pursuit of cleaner steel, the desulphurization lance is not merely a consumable, but a critical, process specific tool whose performance is shaped by each plant's unique operating conditions. Variations in hot metal chemistry, slag properties, and injection practices mean that no two steel plants function identically. Addressing this complexity requires a tailored approach. Key operational parameters like input sulphur, required sulphur, Injection Compound Dosage, Injection Time, etc govern the performance of lances. Dosage quantity of CaO and Mg and their ratio also have a defining impact on how the lances perform in terms of Life. By systematically analysing operational parameters, process constraints, and performance objectives, customized lance solutions can be developed. This approach includes close collaboration with customers, data collection, and analysis.

Keywords: Lance, Refractory, Desulphurization.

Introduction

Among the impurities in hot metal, sulphur is particularly detrimental because it promotes hot shortness, weakens grain-boundary cohesion, and increases susceptibility to cracking during solidification. With the increasing use of lower grade, sulphur-rich raw materials, effective hot metal desulphurization (HMDS) has become essential for high-quality steel production.

Current HMDS is typically performed by co-injecting magnesium and lime into molten iron through a refractory-lined lance comprising a seamless steel pipe protected by a monolithic refractory lining. During operation, the lance is repeatedly immersed in hot metal at 1350–1420°C and exposed to severe thermal shock, chemical attack from the slag, and thermo-mechanical stresses. Its performance and service life are therefore governed by both refractory properties and the surrounding process conditions. Magnesium acts as the primary desulphurizing reagent and reacts rapidly with dissolved sulphur to form MgS. The MgS formed in the metal is transferred to the slag but in the presence of oxygen, this MgS can decompose according to Eq. (2), releasing sulphur back into the metal. CaO promotes sulphur stabilization through conversion of MgS to the more stable CaS phase, as represented by Eq. (3). The principal reactions can therefore be represented as. [1]

$$[Mg] + [S] = MgS\ (s) \quad (1)$$
$$MgS\ (s) + ½\ O2(g) = MgO\ (s) + [S] \quad (2)$$
$$MgS\ (s) + (CaO) = (CaS) + (MgO) \quad (3)$$
$$CaO(s) + [S] = CaS\ (s) + [O] \quad (4)$$

Where reaction (1) is 20 times as fast as reaction (4) The resulting HMDS slag is a continuously evolving multiphase system containing CaO, MgO, CaS, residual MgS and other constituents. Its liquid fraction, solid fraction, viscosity and phase distribution change during injection and mixing. Schrama et al. reported that a minimum (B2) (CaO / SiO_2) of approximately 1.1 is required in industrial practice to maintain adequate sulphur-removal capacity. At the same time, slag viscosity depends on the complete slag composition, temperature and solid fraction rather than on basicity alone.

These slag characteristics also influence refractory corrosion. The refractory matrix at

the hot face interacts with the liquid fraction of the slag, and the amount and viscosity of the liquid generated at the slag–refractory interface influence penetration, dissolution and matrix degradation [4]. Low viscosity liquid promotes transport into refractory pores and dissolution of susceptible matrix phases. However, viscosity and sulphur-removal capacity must be considered together because reducing slag viscosity by lowering basicity can also reduce sulphur capacity.

For this reason, reagent addition data alone cannot establish the actual slag environment at the refractory interface. The practical CaO / Mg ratio indicates reagent practice but does not directly quantify free CaO, liquid fraction, solid fraction or viscosity after treatment. Direct characterization of post-desulphurization slag is required to determine the actual chemical environment. The measured slag chemistry can then be combined with the refractory 1 matrix chemistry in thermodynamic calculations to determine the liquid fraction and viscosity relevant to slag attack to the refractory, so slag viscosity is a critical parameter. Low-viscosity slags favor settling of entrained metal droplets and reduce iron losses during skimming, but they also enhance slag penetration into the refractory, dissolution of binding phases, and matrix degradation. Fluxes such as fluorspar and cryolite are added to improve slag fluidity and metal recovery, but at the expense of accelerated refractory wear. Thermodynamic Simulation Software like Factsage can help simulate equilibrium conditions which can help design lance refractory as per operating condition.

2. Operational observations with Lance life

We shall be discussing in this paper one such prominent established customer station where performance behaviors changed as per operating condition. Lance life was taken as a baseline and then set against what happened through 2023 to 2025 December. This comparison quickly revealed that the period from August to September 2025 marked a clear shift towards a harsher desulphurization practice. Magnesium additions climbed around 79-92 kg per heat, and average injection times stretched to 11.3–12.6 minutes.

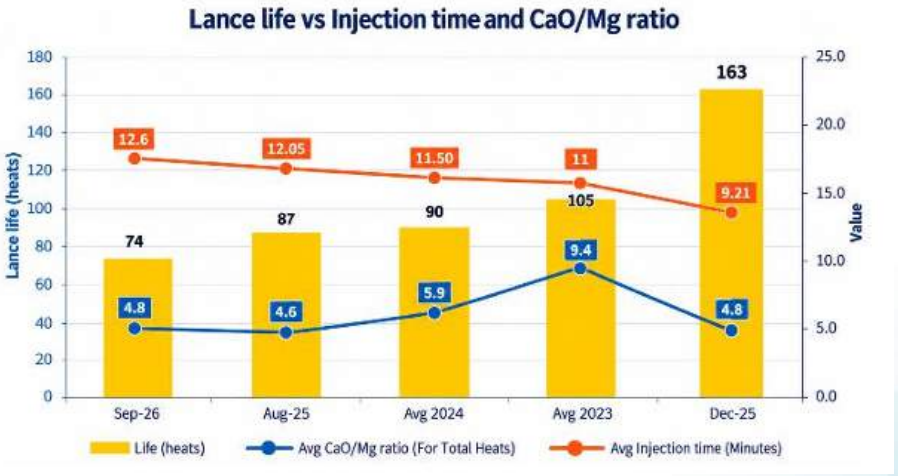


Fig. 1. Trend of lance life with injection time and injected compound ratio

As compared to Year 2023-2024, the input sulphur levels increased. Mg injection was increased to counter the increased input sulphur. This led to decreased in the CaO / Mg ratio to 4.6–4.8. In December 2025, as the initial S levels dropped, the plant softened the treatment intensity. Magnesium consumption was reduced to about 64–70 kg and injection times were shortened to 9.0–9.6 minutes while the injection ratio

remained comparable thus reducing the CaO to 350 kg per heat in average from that of 450+ kg of previous tenure when the performance was lower.

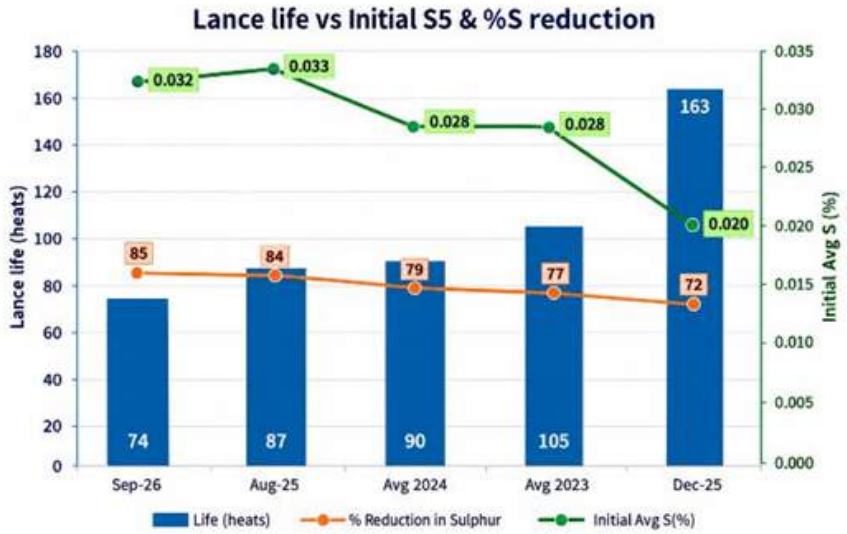


Fig. 2. Trend of lance life with initial S% and Sulphur % drop.

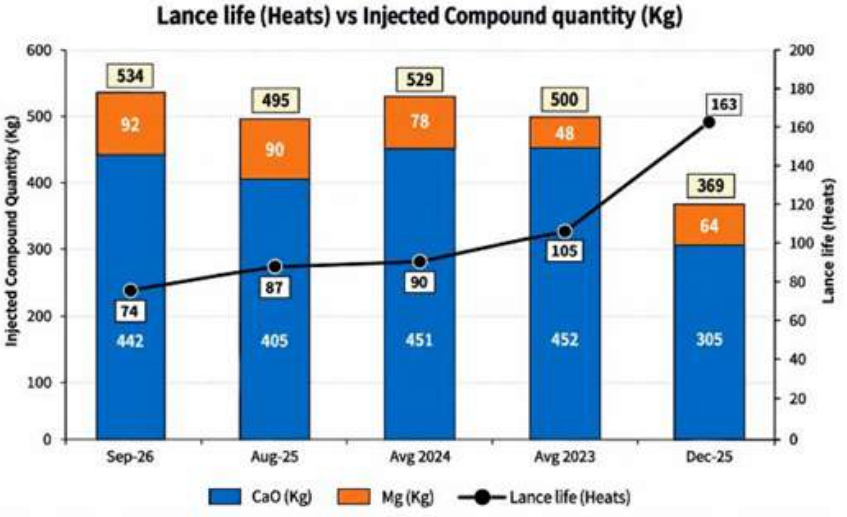


Fig. 3. Trend of lance life with Injection compound

also shows a change in treatment reduction. The initial sulphur level was approximately 0.028% during 2023–2024, increased to approximately 0.033% during August–September 2025, and decreased to approximately 0.020–0.022% in December 2025. Final sulphur levels remained comparable between the August–September and December campaigns, at approximately 0.005 0.006% which indicates the Sulphur drop requirement had dropped in December 2025 to 77% compared to 84 % Sulphur drop in August - September 2025 , which led to higher injection time to disperse the additional desulphurization reagents added. Since the bath volume remained same the excess unreacted CaO reacted within the slag zone of lance pipe and rapid and continuous MgS formation near the plume increased the localized temperature causing a thermal load and eventual failure along with the fact that individual heats became longer. The overall CaO + Mg injection quantity also dropped during this December 2025 campaign .

3. Analysis and experimentation

Effective lance design and material selection require integration of systematic analysis of operating parameters, direct characterization of industrial slag, and thermodynamic assessment of slag–refractory interactions. The first element is systematic evaluation of process parameters. Previous failure analyses across multiple HMDS stations have identified key variables governing lance life, including the proportion of CaO mono-injection heats within the first 20 heats of a campaign; average and maximum injection time during the initial heats; injection compound and dosage; and the required sulphur reduction. The severity of the initial 10–20 heats are critical, as severe early-stage treatment conditions can significantly reduce the probability of achieving long lance life, whereas lances subjected to less severe conditions during campaign initiation generally show improved performance. The second element is direct slag characterization. Reagent addition data alone cannot adequately describe the evolving chemistry, phase distribution, liquid fraction, or physical properties of industrial HMDS slags. Direct slag analysis is therefore essential for establishing the actual environment responsible for refractory degradation. Such characterization enables the slag composition and properties at individual HMDS stations to be incorporated into refractory selection, As a basic slag is required for effective desulphurization the unreacted CaO in post desulphurization slag can influence the interface slag- refractory interaction and can also lead to matrix leaching into the slag as free CaO attacks the Al_2O_3 in the matrix and dissolves it weakening the refractory bonding in that area. Interaction of the matrix with CaO-rich slag promotes greater liquid formation and lower liquid viscosity, accelerating refractory dissolution and penetration. Slag samples were collected from a steel plant desulfurization station. Refractory specimens for the cup test were prepared. In this study we have calculated the chemistry of the refractory matrix (150 µm constituents of the castable) and have the slag chemistry collected from the customer site. Interacted the 70% of the matrix chemistry with the 30% of the slag chemistry in a thermodynamic simulation software Factsage 8.2 at a temperature of 1400°C. By using the chemistry of the liquid generated through refractory-slag interaction, the viscosity was calculated in the Factsage 8.2 viscosity module, and the results are reported in Table 1.

Product	Theoretical liquid formation at Factsage (wt%)	Factsage liquid viscosity (PaS)	Wear Volume (cm^3)
A	81.6	2.7	394.85
B	22.0	5.7	112.63
C	19.0	5.8	80.26
D	18	5.5	74.11

Table 1: The extent of wear at different products due to slag interaction determined by Factsage and experiment

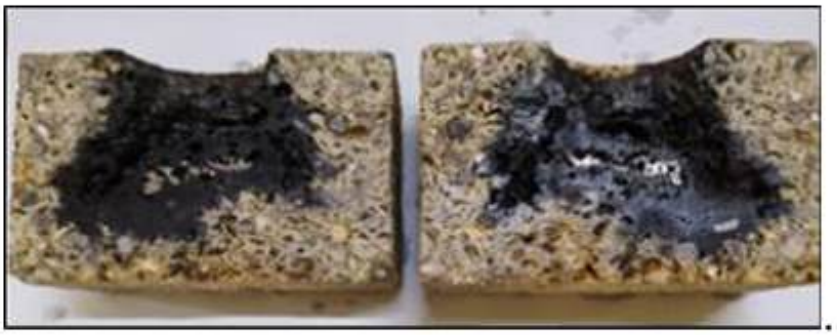


Fig 4 Product A after cup test at 1400°C for 10 hrs.

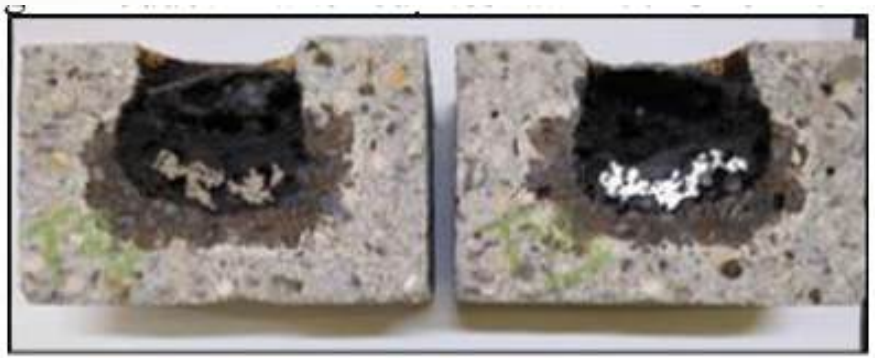


Fig. 5. Product D after cup test at 1400°C for 10 hrs

From the figures and the reported data from table 1, it was evident that the liquid was forming at the boundary of slag and refractory.

Factsage calculated Slag Generation: A > B > C > D
Factsage calculated Viscosity: A < D < B < C
Wear volume at cup test: A > B > C > D

This test demonstrate that refractory corrosion is governed primarily by the liquid fraction formed at the slag–refractory interface and the viscosity of the resulting liquid phase. A higher liquid fraction increases the extent of slag–refractory interaction, while lower viscosity facilitates penetration into refractory pores, dissolution of binding phases, and accelerated matrix degradation. Increasing temperature further reduces liquid viscosity, thereby promoting penetration and refractory wear. The cup test results support this relationship: Product A, which generated the highest liquid fraction (81.6 wt.-%) and lowest liquid viscosity (2.7 Pa·s), exhibited the highest wear volume, whereas formulations producing lower liquid fractions and higher viscosities showed significantly lower wear, consistent with the thermodynamic predictions. On the other hand, a separate thermal contribution arises from the MgS formation reaction during desulphurization:

$$Mg(s)+[S]\rightarrow MgS(s)$$

The standard enthalpy of formation for magnesium sulfide (MgS) is approximately -274.4 kJ/mol. The strongly negative enthalpy of MgS formation indicates a highly exothermic Mg–S reaction. As this reaction occurs within the rising Mg–reagent plume, it can be said that it generates localized heat in the metal zone. Higher Mg consumption increases the amount of Mg participating in the reaction and may intensify this localized thermal exposure. Combined with continuous plume flow and prolonged injection duration, the resulting thermal and chemical loading can accelerate refractory degradation and contribute to metal-zone puncture.

4. Conclusion

I. Lance life was strongly associated with the overall HMDS treatment severity, reflected by reagent consumption, CaO / Mg ratio, initial sulphur level, required sulphur reduction, and injection duration.

II. CaO mono-injection heats within the first 20 heats of a campaign was associated with reduced lance life, identifying the early campaign period as a critical stage for lance degradation.

III. Longer injection duration increased the cumulative exposure of the lance to thermal, chemical attack. The August–September 2025 campaign, with higher Mg consumption and longer injection times, showed substantially lower lance life than the December 2025 campaign.

IV. The wear location changed with operating conditions. Lance puncture was observed in the slag zone during 2023, while the region shifted towards the metal zone during August–September 2025.

V. Higher liquid formation combined with lower liquid viscosity increased refractory penetration and erosion. Product A generated the highest liquid fraction (81.6 wt%) and had the lowest calculated liquid viscosity (2.7 Pa·s), corresponding to the highest measured wear volume (394.85 cm^3)

VI. Mg–S reaction activity provides an additional thermal contribution to metal zone exposure. Higher Mg throughput, when combined with prolonged injection, increases the quantity of Mg participating in the reaction and can intensify localized thermal loading around the reagent plume.

5. References

1. Sinha G, Ahmed KA, Kumar R, Kumari B, Bachhar S. Study of lance performance in terms of hot metal desulphurisation process parameters. Calderys India Refractories Limited.

2. Schrama FNH, Beunder EM, Panda SK, et al. Optimal hot metal desulphurisation slag considering iron loss and sulphur removal capacity part I: fundamentals. Ironmak Steelmak. 2021;48(1):1-13.

3. Choi, Ja-Yong & Kim, Dae-Jung & Lee, Hae-Geon. (2001). Reaction Kinetics of Desulfurization of Molten Pig Iron Using CaO-SiO2-Al2O3-Na2O Slag Systems.. ISIJ International. 41. 216-224. 10.2355/isijinternational.41.216.

4. Ahmed KA, Sinha G, Kumar R. Optimisation of lance corrosion: a thermodynamic approach. Calderys India Refractories Limited.

5. Irons GA, Guthrie RIL. The kinetics of the ladle desulphurization of hot metal with Mg vapor. Can Metall Q. 1976; 15:325-3.

6. Yang, Jian et al. “Simultaneous Desulfurization and Deoxidation of Molten Steel with in Situ Produced Magnesium Vapor.” Isij International 47 (2007): 418 426.

OPTIMIZATION OF SEN SLEEVE FOR RECORD BREAKING SEQUENCE CASTING AT JSW JFE STEEL THIN SLAB CASTER

Nitin Saxena, Sudeep Jagtap, Satish Srivastava, Prakash Sappa

JSW JFE Steel, Sambalpur works, Odisha

Nagarjuna Vangara, Suvadip S, Arijit Bhattacharyya, Kishan Kumar, Anup Kumar

Vesuvius India limited, Kolkata

Email: Nagarjuna.Vangara@vesuvius.com

Abstract

In the highly competitive landscape of integrated steel manufacturing, maximizing the sequence length of continuous casting is a primary driver for operational efficiency, yield improvement, and cost reduction. The primary bottleneck identified in achieving ultra-long sequences was the premature erosion and mechanical fatigue of the SEN sleeve at the JSW JFE Steel, Sambalpur works.

To address this issue, the Vesuvius and JSW JFE team jointly implemented a two-fold improvement strategy. First, the physical dimensions of the SEN sleeve were modified, specifically increasing the extension length of the sleeve. Second the material of the sleeve component was upgraded to a "Dura sleeve mix". This upgraded sleeve mix offers superior resistance to chemical corrosion and thermal shock compared to standard compositions which enable to cast longer sequence casting time consistently.

Keywords: Submerged entry nozzle, Dura sleeve mix, chemical corrosion etc...

Introduction

The JSW JFE Steel CSP at Sambalpur works, Orissa in India commissioned in 2007 year with a rated annual production capacity of 2.7 MTPA, produces strip up to 1350 mm wide. The steel grades produced are low carbon and high value-added grades for the cold rolling applications, and with final applications such as Auto and White goods sectors. Right from the commissioning of caster, Vesuvius supplies tundish permanent and working lining materials, tundish furniture and alumina graphite refractories (SEN, stopper and ladle shroud). To achieve longer sequence lengths, thereby reducing the process down time associated with sequence exchange time, which helps in increasing the caster productivity, yield and reduction in cost. In addition to this, the higher sequence length has an impact on sustainability by reducing the Carbon footprint.

2. Background

The demand for steel production is increasing at JSW JFE Steel. The authors focused extensive research effort in highlighting the role of SEN design and material for highest casting time with minimum erosion and then improving the utilization of the caster. With the present SEN R3 -Std (Fig-1) helping in the flow stability in thin slab casters for which casting flow rate exceeds 3tpm.

Prior to the improvement initiatives, the typical casting duration was approx.28 hrs. A systematic study of process conditions, operational practices like mold level behavior, tundish slag management and sequence limiting factors was undertaken to identify opportunities for improvement. Based on the findings metallurgical and operational measures were implemented to improve casting stability and extend sequence

duration.

This article summarizes improvements taken by JSW JFE Steel and Vesuvius jointly to achieve extended casting time of more than 32hrs in a single sequence. The effectiveness of the implemented measures is evaluated by comparing the pre improvement and post improvement casting hours with particular emphasis on sequence duration, process stability and operational reliability.

The following table consists of basic machine parameters of casting machine.

Parameters	Values
Process route	BF-- >EAFLFCSP
No of Casters	2
Year of commissioning	2007
Slab thickness	59mm (mold exit)
Slab width	800-1350mm
Cast speed	6.0 max
Throughput	2.8 to 3. 2 tpm
Steel Grade	Low Carbon, Value added Grade
Avg seq length	35 heats
Ladle capacity	110 tons

Table 1: Casting machine parameters



Figure 1: R3 std SEN

3. Effect of increased Zr Sleeve length on Casting sequence

The zirconia sleeve used in the submerged entry nozzle (SEN) plays an important role in protecting the refractory system from direct exposure to molten steel and maintaining the integrity of the steel-flow path during continuous casting. During extended casting sequences, progressive refractory wear can alter the flow characteristics and reduce the reliable operating life of the SEN assembly. As part of the sequence-length improvement initiative, the zirconia sleeve length was increased from 220 mm to 250 mm, providing an additional 30 mm of refractory length. The modification was implemented to increase the effective refractory life and provide a greater safety margin against progressive wear during long-duration casting. Following implementation of the modification, an improvement of approximately 2.5 additional casting hours per sequence was achieved. This directly contributed to the overall increase in achievable casting sequence length. From an operational perspective, the additional ~2.5 hours of casting per sequence contributes to improved caster availability, productivity and reducing number of sequence breaks in a month. When combined with other process improvements, this modification supported the overall increase in casting duration from 28 hours to 34 hours approximately 21% increase.

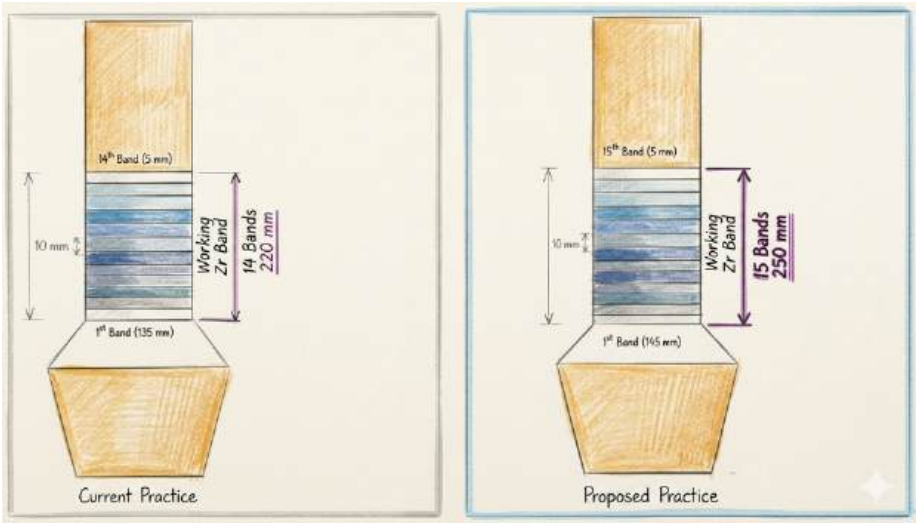


Figure 2 : Before and after SEN sleeve length increased from 220mm to 250mm (Ref.)

4. Effect of Dura sleeve Mix in Zr sleeve on Casting duration

During longer casting sequences, submerged entry nozzle (SEN) is strongly influenced by refractory degradation due to continuous exposure to molten steel, mold flux, slag, thermal cycling and chemical interaction with the surrounding materials. Progressive wear of the SEN sleeve can eventually become a limiting factor for sequence length. To improve the refractory life of the SEN, a Dura Sleeve refractory mix was incorporated in the zirconia sleeve system. The objective of this modification was to improve the resistance of the sleeve against high-temperature erosion, chemical corrosion and thermal degradation during prolonged casting.

The development of the Dura Sleeve material by Vesuvius has been grounded in extensive research and analysis, incorporating insights from both open literature and the company's archival data. Postmortem examinations of used industrial pieces have underscored the critical importance of particle packing and the compaction ratio of the zirconia-carbon mix in mitigating erosion and corrosion rates. To enhance the material's performance without compromising its thermal shock resistance, a series of model mixes were devised using a design of experiment software, aimed at achieving a denser zirconia-carbon composition with optimized open porosity (Fig :3).

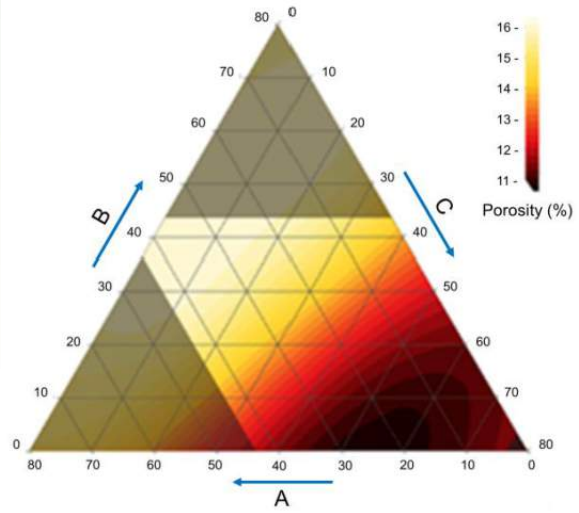
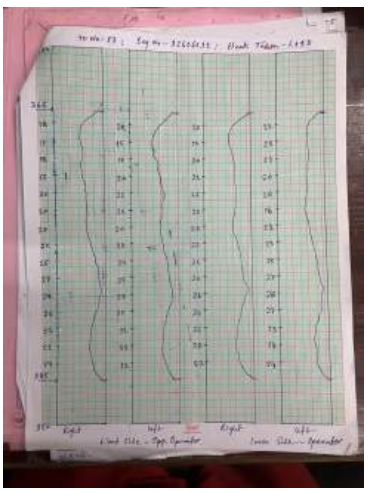


Figure 3: Optimization of the materials composition versus open porosity of the model mixes.

During the Dura sleeve development the comprehensive physical, thermal, and mechanical tests—including assessments of density, porosity, pore size distribution, thermal expansion, and mechanical strength were conducted at various temperatures to evaluate the performance of the optimized mix against a reference sample. This research resulted in a carbon zirconia mix with excellent results in relation to chemical corrosion that were industrially tested at various steel plants before adopting to the JSW JFE Steel, and which observed 20% performance improvement overall.

On 13 June 2026 at SMS 1, CSP Caster -1, Car -1 in Tundish Number 17, having sequence number 12606011 sequence was completed as per plan comprising highest cast duration of 2050 min (34hrs 10 min) & 59 Heats.





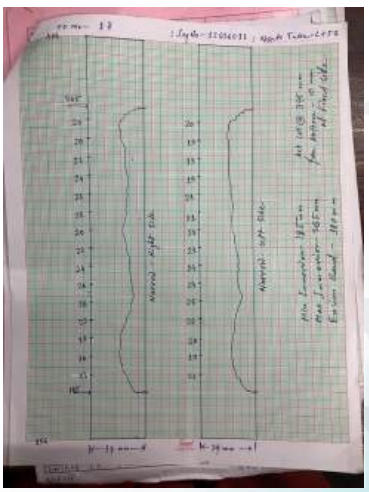


Figure 4: SEN condition after 34hrs 10 mins and 59 heats casting on 13th June 26 (Highest ever)

Figure 5: Post Casting SEN Left over thickness profiles on broad side and narrow side

5. Mold level control: operational challenges and improvement

Stable mould-level control is one of the critical requirements for maintaining consistent casting performance and for the longer sequence in a thin-slab caster. The mould level is continuously monitored using a radioactive source and scintillation-counter-based measurement system, with the measured signal being used for automatic mold-level control.

During the earlier operating period, deterioration of the radioactive source activity and degradation of the scintillation counter resulted in a reduction in the quality and reliability of the level-measurement signal. The low source count rate reduced the signal-to-noise ratio of the measurement system, making the detected signal more susceptible to fluctuations and measurement uncertainty.

As a consequence, the measured mould level showed significantly higher fluctuations than the desired operating range. Mould-level variation was observed in the range of approximately ±4–6 mm, against the targeted control band of ±2 mm.

The increased fluctuation disturbs the steel flow pattern near meniscus, increased possibility of slag entrainment and to increase the erosion of the SEN wall thickness which eventually becomes bottleneck for the high casting time.

As a permanent corrective measure, the aging radioactive source was replaced in June 2025. The improvement was reflected directly in the operating trend, with mould-level fluctuations reducing from approximately ±4–6 mm to around ±2 mm. This improvement was particularly important for the thin-slab caster, where stable mould-level control is essential for maintaining consistent meniscus conditions at higher casting speeds

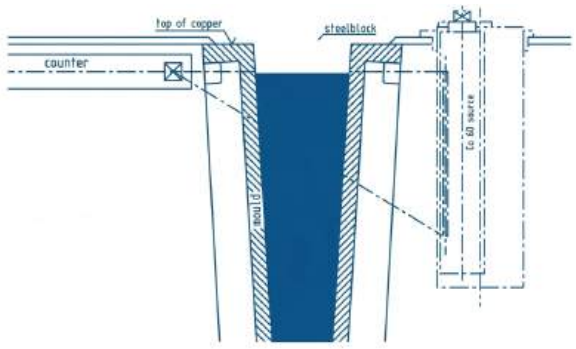


Figure 6: Mold level control system

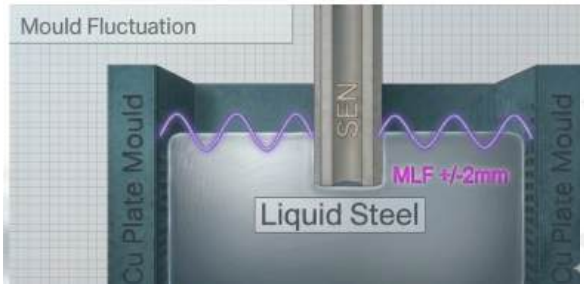


Figure 7: level fluctuation in mould (Ref).

6. Tundish slag off practice: Operational improvement

At present, JSW JFE steel operations team has no ladle slag detection system as such, the detection of the ladle slag at end of the ladle while casting is still in conventional method and then always there is chance of the slag carries from the ladle to tundish at every heat. To address this concern, team has implemented a stringent tundish slag-off practice in a regular interval, and the addition of tundish flux every 3 heats.

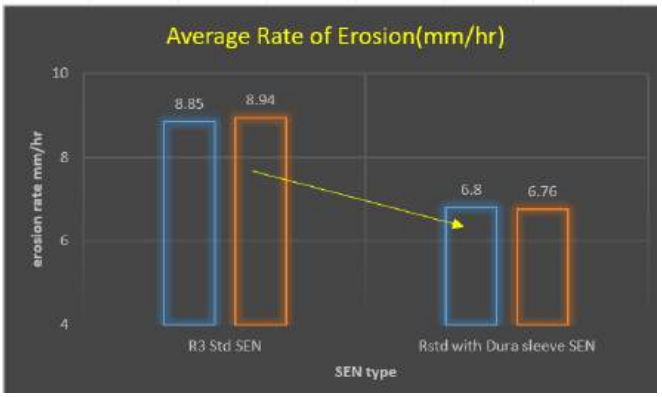
Purpose of the Work instruction: Due to long sequences or late detection of the slag, the ladle slag comes into the tundish. This slag must remove often, otherwise it may cause problem in casting.

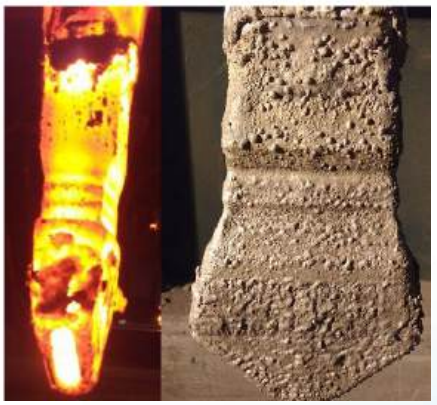
1. Increase the tundish level slowly above working level
2. Allow the slag to flow through launder into the slag box
3. Continue till the liquid metal starts streaming through the launder
4. After complete de-slagging bring back the tundish level to the working level
5. Add fresh tundish covering fluxes (5 kg) to prevent reoxidation
6. Check and clean the launder for any jam
7. Do de-slagging after every 3 heats / mixed grades/critical grades
8. Measure the tundish slag height in regular intervals



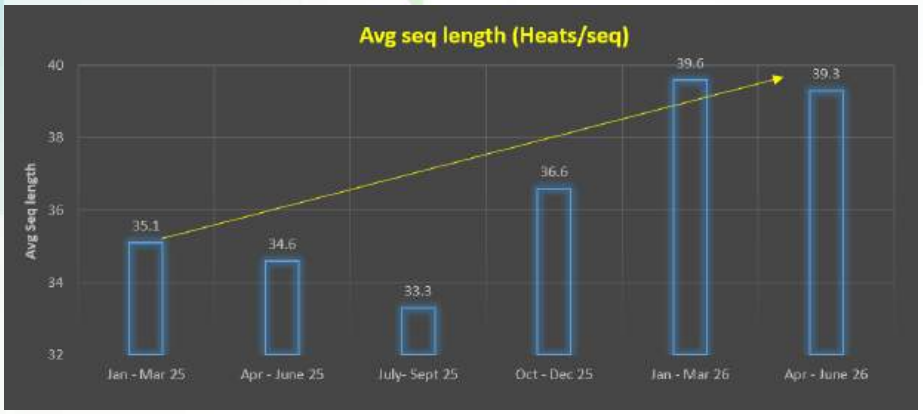
7. Results and discussion

The average rate of erosion with R3 std and R3 std dura sleeve SEN has been compared in Graph- 1. As shown in the graph below approximately 24% reduction in avg sleeve erosion observed from 8.9 to 6.8mm/hr. With this encouraged initial results JSW JFE Steel converted 100% SEN into the dura sleeve-based material and then the avg sequence length increased from 35 to 39.6 heats (13% increase in avg sequence length) and casting hours from 28 to 34 hours (21%increase in avg casting duration).





Graph 1: Avg erosion rate comparison between R3 SEN with R3 Dura sleeve SEN



Graph 2: Trend graph of Avg sequence length quarte wise

8. Conclusion

• R3 Std SEN with Dura sleeve mix and Zr sleeve length combine shown significant improvement in the erosion which helps to run cast at longer sequences.

• JSW JFE Steel has successfully cast sequence of 59 heats for a casting time of 34 hours 10 minutes using the R3 SEN.

• Replacing the Co-60 radioactive source with the new one shown improvement in the mold level stability while casting

• JSW JFE Steel and Vesuvius continue to focus with its highly trained operator further analyzing the process to cast more heats per sequence to reduce tundish consumption.

9. Acknowledgements

The authors wish to thank JSW JFE Steel management team, caster operating team, refractory team for the excellent support and their guidance while conducting the trials and their valuable insights.

We also extend our deep gratitude to the Vesuvius sales, M&T, Production, quality, and technical teams for their relentless efforts towards this project.

10. References

[1] H. Hasmukhrai Shah, N. Sinha, A. Kumar, C. Bhanu, P. Goswami, J. Richaud; Tundish and SEN Development for casting long sequences of wide slabs at TATA LD3 CSP®– India, METEC ESTAD 2015

[2] Sahai Y, Burval M, "Validity of Reynolds and Froude similarity criteria for water modeling of melt flow in tundishes", Proc. Electric Furnace Conference, ISS-AIME, Vol. 50, pp.469-474, 1992.

[3] V. Dhawan, S. Bhattacharjee, J. Richaud; Tundish refractor y optimization for yield, process and productivity improvements at Bhilai Steel Plant – India, METEC ESTAD 2015

[4] Richaud,J , Baehren, G, 25 years of refractory development for thin slab application, 28th European continuous Casting Conference, pp638-650

[5] Andrzej warchal , Julien berton, continuous cast sequence improvement with dura sleeve MTSP at Arcelor mittal PECEM, 54th steel making and Nonferrous Metallurgy

PHOSPHATE FREE RAMMING MASS FOR MONOBLOCK TUNDISH NOZZLE PLATE (MTNP) APPLICATION

Satyananda Behera[1], Akshay Bauskar[1], Amorie Patrick[2], Evgeny Popov[3] and Severine Romero Baivier[4]

[1]Vesuvius Refractory India Private Limited, India
[2]Vesuvius Research, Pittsburgh, USA
[3]Vesuvius Japan Inc
[4]Vesuvius Europe SAS

*Mail: Satyananda.Behera@Vesuvius.Com

Abstract

The mono block tundish nozzle plate (MTNP) plays a crucial role in continuous steel casting, where thermal stability, erosion resistance, and cleanliness directly impact casting performance and steel quality. Traditionally, dry ramming masses used for monoblock tundish nozzles contain inorganic binders to ensure adequate strength and sinterability. However, the presence of those binders often leads to undesirable reactions at high temperatures, such as increased corrosion, gas evolution, and potential contamination of molten steel. In this study, a dry ramming mass was developed to address these limitations while maintaining equivalent or superior performance characteristics. A novel binder system was formulated to achieve optimal particle packing, green strength, and high-temperature stability. The developed composition was evaluated through laboratory-scale tests, including bulk density, cold crushing strength, slag corrosion resistance, crystalline phase and microstructure. Additionally, trials were conducted on a customer site to validate the material's operational reliability and performance during casting. Results demonstrated that this formulation exhibited improved density, compressive strength, structural integrity, and reduced slag adherence. This development provides a high-performance alternative to conventional materials, supporting cleaner steel production and enhanced tundish nozzle reliability.

Keywords: Dry ramming mass, tundish nozzle, refractory development, continuous casting, clean

1. Introduction

In recent years, the need to produce clean steel has led to longer residence times for molten steel in tundishes, imposing new requirements on the refractory materials used in steelmaking. To extend the service life of the working lining, steel plants commonly replace nozzle well blocks and perform localized repairs for tundishes, nozzle replacement is the standard method for extending service life. Currently, plastic refractories are commonly used to fill the gaps around tundish nozzles. However, these plastic refractories suffer from high porosity, relatively low material quality, and poor slag resistance, posing significant safety risks [1]. Consequently, steel plants are seeking to replace them with high-performance ramming masses. Based on an analysis of the application areas and functional requirements, the ramming mass should possess the following properties: 1) Ready for direct on-site use without the need for mixing; 2) Appropriate strength—sufficient to secure the well block for safe operation while allowing for future excavation and repair; 3) Good slag resistance; 4) Good bonding with the overlying working lining. Based on these considerations, this study developed a magnesia-based ramming mass designed to fill the areas around tundish nozzles, meeting the operational requirements of steel plants. [3]

2. Ramming mix design

The selection of raw materials and particle size distribution directly affects the installation and service performance of ramming mixes. Currently, the plastic refractory used for the tundish nozzle area is a magnesia based system, while the castable for the working lining is a magnesia-Olivine; considering factors such as cost and performance, a magnesia-based ramming mix was ultimately selected. In addition to the primary raw materials, additives such as plasticizers, retarders, expansion agents, and binders are included. Furthermore, to ensure the ramming mass develops moderate sintering strength during use, small amounts of sintering aids were incorporated. The optimal dosages of binders and sintering aids were determined by comparing the compressive strengths of specimens prepared with varying amounts of these additives.

3. Experimental work

In this study, four mixes A, B, C &D with different doses of specific type of binders (says Y) were added to the mix with content x, 2x, 3x, and 4x % respectively where x=0.5 along with the standard plastic ramming mix with plastic binder were prepared using a Hobart mixer. The test samples were prepared by using a sand rammer of diameter 50mm and 50mm height. The temperature-dependent properties of the obtained samples were studied between 110°C/24h to 1500°C/5h. The bulk density (BD), cold crushing strength (CCS) and permanent linear change (PLC) of the fired samples was analyzed. Minerology and microstructure of the fired samples was characterized by using XRD and SEM techniques. Further, the corrosion behavior of the newly developed ramming sample was studied using an static cup test with standard plastic binder ramming mass sample.

4. Results and Analysis

a. Density Study

Figure 1 presents the bulk density values of four experimental mix compositions (A, B, C, and D) measured after drying at 110°C for 24 h and after firing at 1500°C for 5 h. The results are compared with a standard plastic-bonded ramming mass. The drying density increased progressively from 2.37 g/cm³ for Mix A to 2.60 g/cm³ for Mix D, indicating a clear influence of the non-plastic additive content on the packing characteristics of the material. Similarly, the fired density increased from 2.43 g/cm³ for Mix A to 2.70 g/cm³ for Mix D following firing at 1500°C. The standard plastic mass exhibited drying and fired densities of 2.58 g/cm³ and 2.66 g/cm³, respectively.

The observed increase in density with increasing non-plastic additive concentration suggests an improvement in particle packing efficiency and reduction in pore volume within the matrix. Non-plastic additives generally possess lower shrinkage characteristics during drying and can fill inter-particle voids more effectively, resulting in a denser green structure. Consequently, the packing density of the unfired body improves, leading to higher measured bulk density after drying [4].

A similar trend was maintained after firing at 1500°C. The increase in fired density indicates enhanced sintering and consolidation of the refractory matrix. During high-temperature treatment, diffusion-driven mass transport mechanisms promote particle bonding, neck formation, and pore elimination. Mixes containing higher levels of non-plastic additives appear to facilitate these densification mechanisms, producing a more compact microstructure with reduced residual porosity.

Among all compositions, Mix D exhibited the highest density values, achieving 2.60 g/cm³ after drying and 2.70 g/cm³ after firing. These values are slightly higher than those of the standard plastic mass, which recorded 2.58 g/cm³ and 2.66 g/cm³ under the respective conditions. The higher density obtained in Mix D indicates that the optimized proportion of non-plastic additives contributed positively to particle packing and sintering efficiency, ultimately leading to improved densification.

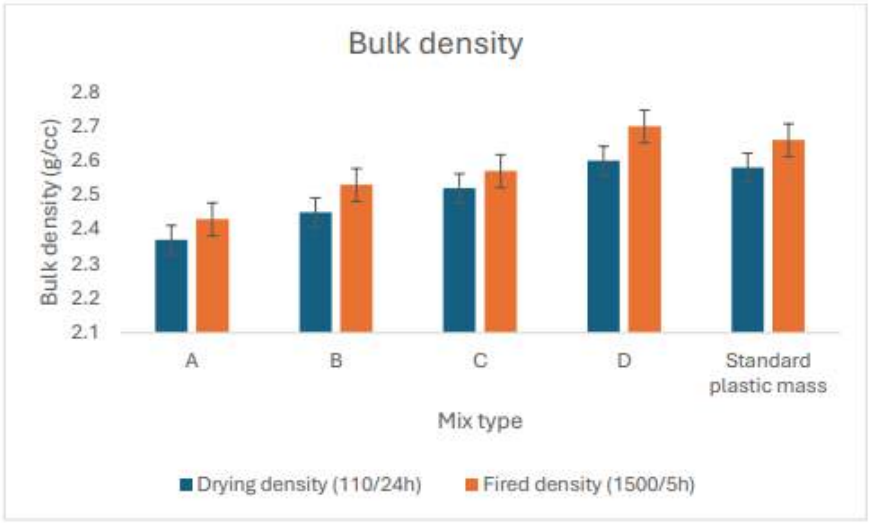


Fig 1: Bulk density at 110 deg C/24h and 1500 deg C/5h

b. Cold crushing strength (CCS)

Figure 2 illustrates the cold crushing strength (CCS) of the newly developed non-plastic binder-containing ramming mass compositions and compares their performance with that of the conventional plastic-bonded ramming mass. The CCS values show a progressive improvement from Mix A to Mix D, indicating that the incorporation of the non-plastic binder system significantly influences the mechanical integrity of the refractory matrix. This trend closely follows the variation observed in the bulk density measurements, suggesting a strong relationship between densification and strength development. The bulk density increased from 2.37 g/cm³ to 2.60 g/cm³ in the dried condition and from 2.43 g/cm³ to 2.70 g/cm³ after firing, with Mix D exhibiting the highest densification among all compositions.

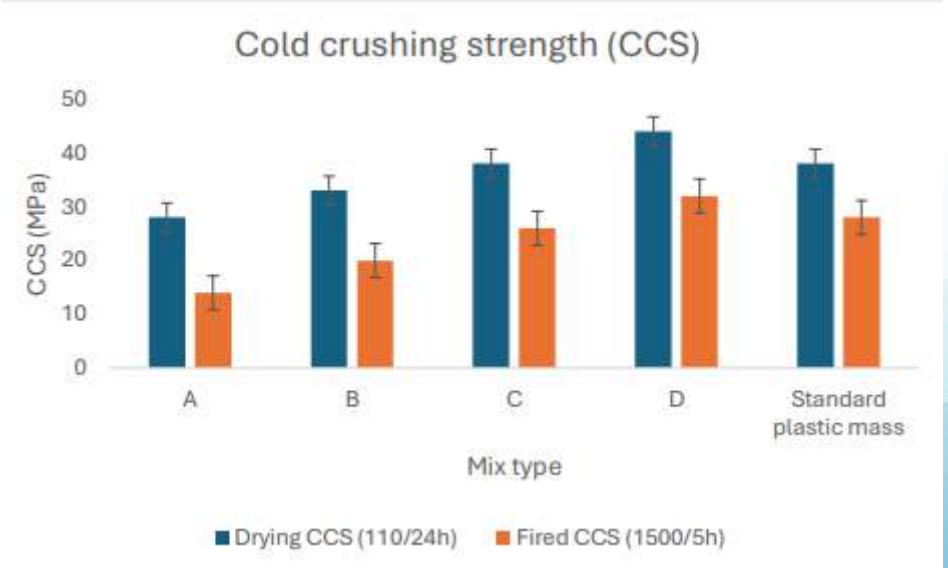


Fig 2: CCS at 110 deg C/24h and 1500 deg C/5h

The increase in CCS can be directly correlated with the enhanced bulk density and reduced porosity of the refractory body. In ceramic and refractory systems, cold crushing strength is highly dependent on the degree of particle packing, bond formation, and pore distribution within the matrix. As the non-plastic binder content increased, better particle arrangement and packing efficiency were achieved, resulting in a denser microstructure. The improved packing reduced the number of voids and structural defects that typically act as stress concentration sites during compressive loading. Consequently, the resistance of the material to fracture under compression increased, leading to higher CCS values.

The superiority of the non-plastic binder-containing compositions can also be attributed to the microstructural changes occurring during firing. At elevated temperatures, sintering promotes diffusion-driven neck growth between adjacent particles, strengthening the inter-particle bonds and reducing open porosity. The higher fired densities observed for the developed mixes indicate that sintering proceeded more effectively, producing a compact and mechanically robust structure. As a result, the fired specimens were able to sustain higher compressive loads before failure. This confirms that the non-plastic binder not only contributes to green strength and packing during processing but also facilitates effective densification during high-temperature exposure Among all the investigated compositions, Mix D exhibited the highest bulk density and correspondingly the highest CCS. This finding demonstrates the positive correlation between density and mechanical strength. A denser refractory structure contains fewer interconnected pores and microcracks, thereby increasing the effective load-bearing cross-sectional area. The reduction in porosity minimizes crack initiation and propagation under compressive stress, resulting in enhanced crushing strength. Therefore, the superior CCS of Mix D can be primarily attributed to its highly consolidated microstructure and improved ceramic bonding developed during firing

When compared with the standard plastic-bonded ramming mass, the newly developed non-plastic binder system exhibited comparable or superior strength characteristics. The standard plastic mass achieved a fired density of 2.66 g/cm³, whereas Mix D attained a slightly higher density of 2.70 g/cm³. The corresponding improvement in CCS indicates that the alternative binder system is capable of developing an equally strong, if not stronger, refractory network. This suggests that the non-plastic binder effectively replaces the conventional plastic binder without compromising the structural performance of the ramming mass.

The observed correlation between bulk density and CCS confirms that densification is one of the primary factors governing mechanical performance. As density increased from Mix A to Mix D, a corresponding increase in CCS was observed, demonstrating that improved particle packing, reduced pore volume, and enhanced sintering collectively contributed to strength development.

C. Permanent Linear Change (PLC)

The Permanent Linear Change (PLC) values of the developed non-plastic binder-containing ramming mass compositions (A-D) and the standard plastic ramming mass after firing at 1500°C for 5 hours are presented in the graph. All compositions exhibit negative PLC values, indicating that the specimens underwent linear shrinkage during high-temperature exposure due to sintering, particle rearrangement, binder decomposition, and densification of the refractory matrix.

The results demonstrate a gradual increase in shrinkage from composition A to D. Composition A exhibited the lowest PLC value (-1.9%), less sintering among all the investigated formulations. The reduced shrinkage suggests that the developed binder system effectively maintained the structural framework of the refractory body during

firing, thereby minimizing excessive densification and volume contraction.



Fig 3: PLC at 1500 deg C/5

d. Microstructure Analysis

The following microstructure is the microstructure of the non plastic binder ramming mass after firing at 1500 deg C/5h.

Fig 4A shows the there is an optimum formation of matrix phases which helps for grain growth. Fig 4B is the high resolution of the same surface.

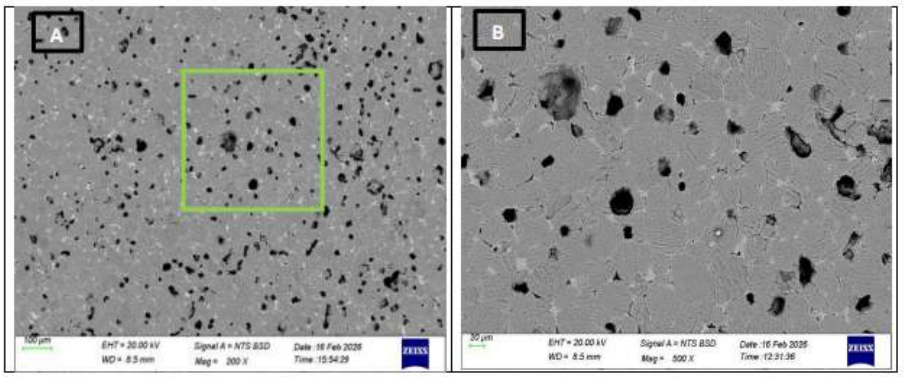


Fig 4: Microstructure of polished surface of the non plastic binder ramming mass fired at 1500 deg C/5h

Figure 4 presents the polished microstructure of the newly developed non-plastic binder containing ramming mass after firing at 1500°C for 5 h. The micrographs reveal the development of a well-bonded microstructure characterized by the formation of an optimum matrix phase between the aggregates. As shown in Figure 4A, A B C D Standard plastic mass PLC (1500/5h -1.9 -1.99 -2.1 -2.2 -2.1 -3 -2.5 -2 -1.5 -1 -0.5 0 PLC (%) Axis Title PLC (1500/5h) A B the matrix phase is uniformly distributed around the coarse grains, promoting effective inter-particle bonding and facilitating grain growth during high-temperature firing. The formation of this continuous matrix contributes significantly to the densification of the refractory body by reducing intergranular voids and enhancing particle packing.

The high firing temperature promotes diffusion-controlled mass transport, resulting in the growth of grains and improved coherence between the aggregate particles and the matrix phase. The microstructure

exhibits a compact morphology with limited pore concentration, indicating effective sintering of the refractory system. Such microstructural evolution is responsible for the increased bulk density observed in the developed composition and demonstrates the ability of the non-plastic binder to generate a stable ceramic bond without the need for traditional plastic clay binders.

Figure 4B, which represents a higher magnification image of the same region, provides further evidence of strong grain-to-grain bonding and matrix formation. The enlarged view shows that the matrix phase has penetrated and bridged the interfaces between adjacent silica grains, resulting in enhanced contact area and improved mechanical interlocking. The absence of extensive microcracking and the reduced porosity suggest that thermal stresses generated during firing were effectively accommodated by the developed bonding phase. The observed grain growth is indicative of advanced sintering and contributes to the formation of a rigid microstructural framework. This framework enhances load transfer across the microstructure and minimizes stress concentration sites, thereby improving the cold crushing strength of the fired ramming mass. The dense and coherent microstructure developed in the non-plastic binder system confirms the effectiveness of the binder chemistry in promoting ceramic bonding, densification, and structural integrity at elevated temperatures. Overall, the microstructural features observed in Figures 4A and 4B demonstrate that the non-plastic binder facilitates the formation of an optimum bonding matrix and controlled grain growth during firing. These characteristics are directly responsible for the improved densification behavior and superior mechanical performance of the developed silica ramming mass compared to conventional binder systems.

e. Static Corrosion Test

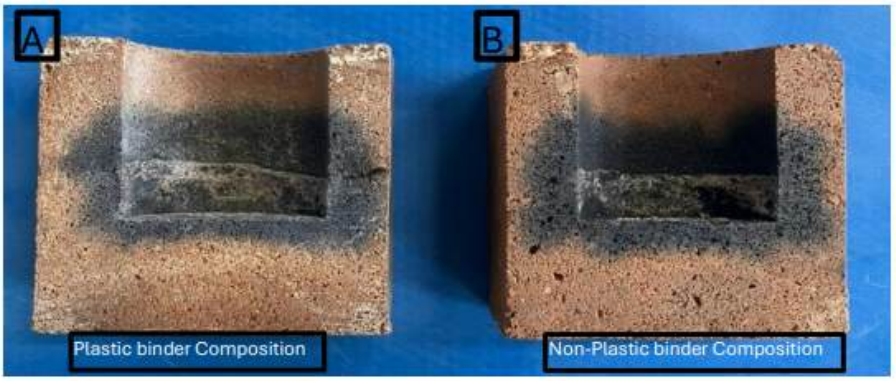


Fig 5: Static corrosion test of plastic and non-plastic binder (Composition D) ramming mass

The corrosion resistance of the developed non-plastic binder ramming mass was evaluated by a static cup corrosion test using tundish slag of basicity 3 at 1500°C for 5 h. After completion of the test, the specimens were sectioned vertically, and the extent of slag penetration was assessed from the exposed cross-sections. Figure 5A shows the corrosion profile of the conventional plastic binder-containing ramming mass, whereas Figure 5B represents the non-plastic binder formulation (Composition D).

The post-corrosion examination revealed that both compositions exhibited very similar corrosion characteristics. The slag attack was concentrated predominantly in the slag-contact region, with corrosion penetration extending to approximately 20% of the cup depth at the bottom and about 30% along the side walls.

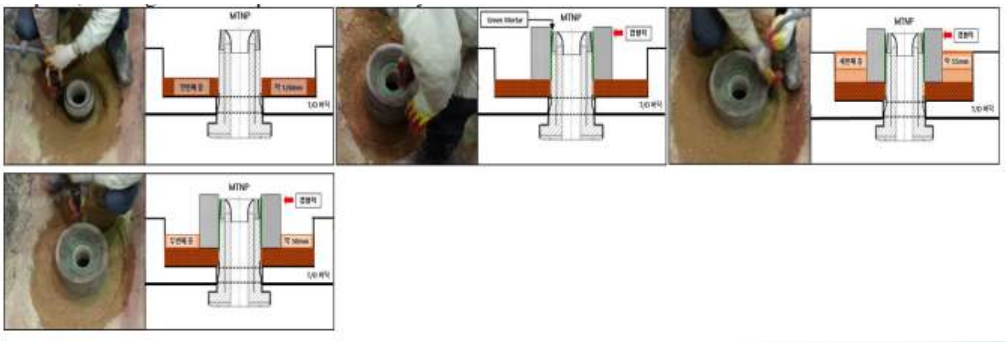
The relatively higher penetration observed at the side walls can be attributed to prolonged slag contact and enhanced dissolution of the refractory matrix in the vertical direction. Nevertheless, no significant difference in the

corrosion pattern or penetration depth was observed between the two compositions.

The comparable corrosion behavior indicates that the removal of the plastic binder does not adversely affect the resistance of the ramming mass against highly basic tundish slag. The excellent performance of Composition D can be correlated with the formation of a dense ceramic-bonded matrix during firing, as evidenced by the microstructural analysis. The improved sintering characteristics and development of magnesium silicate bonding phases contribute to reduced open porosity and restrict slag infiltration into the refractory body. Furthermore, the strong grain-to-matrix bonding formed during high-temperature exposure enhances the stability of the refractory structure and minimizes degradation under corrosive slag conditions.
The results clearly demonstrate that the non-plastic binder-based ramming mass (Composition D) exhibits corrosion resistance equivalent to that of the conventional plastic binder-containing composition. The similar corrosion penetration depths and attack profiles observed in both specimens confirm that the newly developed binder system maintains adequate chemical stability and structural integrity in contact with basic tundish slag, making it a promising alternative for tundish lining applications.

5. Trial Validation

To validate the laboratory findings under actual plant operating conditions, the developed non-plastic binderbased ramming mass (Composition D) was evaluated in a commercial trial at customer X. The material was installed in the monoblock tundish nozzle plate (MTNP) area and monitored throughout the casting campaign. The trial was completed successfully without any operational difficulties during installation, tundish preparation, or casting operations. Post-trial inspection confirmed that the developed ramming mass maintained its structural integrity and provided satisfactory resistance against thermal, mechanical, and slag-related wear during service. The achieved service life met the customer's key performance indicator (KPI) of 7-10 heats per ramming, demonstrating performance equivalent to or better than the conventional plastic binder-based material. The successful plant trial validates the laboratory results related to improved densification, mechanical strength, and corrosion resistance, confirming that the newly developed non-plastic binder technology is a reliable and for MTNP applications. The field performance further establishes its suitability for industrial adoption, offering enhanced operational reliability.



6. Conclusion

The results of this study demonstrate that the newly developed non-plastic binder-based magnesia ramming mass is a viable alternative to conventional plastic binder-containing materials for monoblock tundish nozzle plate applications. Among the investigated formulations, Composition D exhibited the best overall performance, achieving higher bulk density and cold crushing strength than the standard plastic ramming mass, indicating improved densification and mechanical integrity.

Microstructural analysis revealed the formation of a dense ceramic-bonded matrix with strong grain-to-matrix bonding and controlled grain growth after firing at 1500°C, which contributed to enhanced structural stability and reduced porosity. Furthermore, static cup corrosion testing using tundish slag of basicity 3 showed corrosion resistance comparable to that of the conventional plastic binder system, with similar corrosion penetration at both the bottom and sidewall regions. These findings confirm that the elimination of the plastic binder does not compromise the physical, mechanical, or corrosion-resistant properties of the refractory. Therefore, the developed non-plastic binder technology offers a high-performance and environmentally sustainable solution for tundish nozzle applications, supporting improved refractory reliability and operational safety.

Reference

1. Chandra, K. Sarath, and Debasish Sarkar. "Refractories and failures." Ceramic Processing: Industrial Practices. CRC Press New York, 2019. 168-211.

2. Sarkar, Ritwik. Advanced Refractories for Iron and Steel Industries. CRC Press, 2025.

3. Mishra, S. K., et al. "Effect of blockage of outlet nozzle on fluid flow and heat transfer in continuously cast multistrand billet caster tundish." Canadian Metallurgical Quarterly 51.2 (2012): 170-183.

4. Behera, Satyananda, and Ritwik Sarkar. "Sintering of magnesia: effect of additives." Bulletin of Materials Science 38.6 (2015): 1499-1505.

HIGH PERFORMANCE HIGH FLEXIBILITY (HPHF) DURAFLEX LADLE SHROUD FOR LONG LIFE MULTIPLE COLD REUSE APPLICATION

Sudip Banerjee [1], Stephane Mazerat [2],
Shubhrajyoti Dey [3], Murali Sabhapathy [4],
Krushna Panda [5]

[1] Senior General Manager- ISO Refractories - Vesuvius India Limited
[2] Senior R&D Engineer, ISO Refractories- Vesuvius Group S.A./N.V.
[3] Regional Product Specialist- ISO Refractories - Vesuvius India Limited
[4] Business Development Manager- Vesuvius India Limited
[5] Account Manager, Sales- Vesuvius India Limited

Corresponding Author's e-mail address: sudip.banerjee@vesuvius.com

Abstract

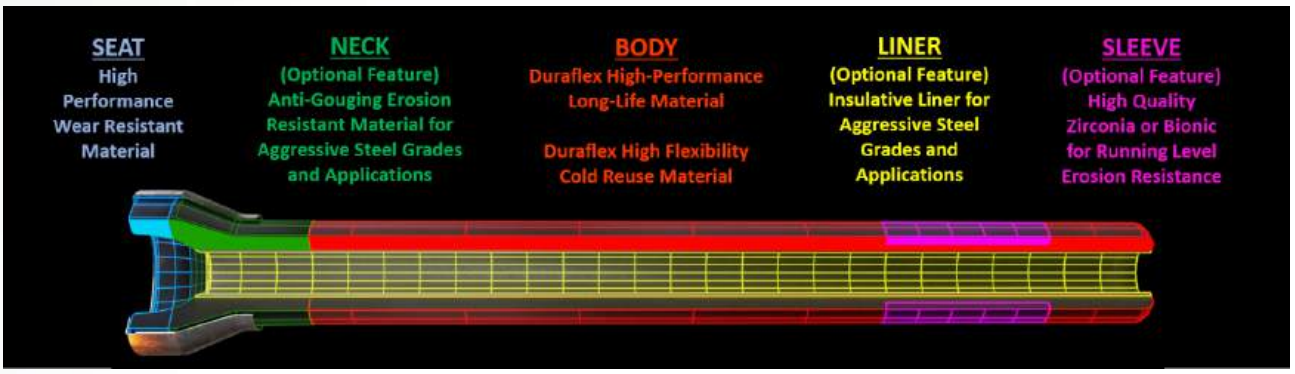
Ladle shroud is a flow control refractory which protects steel teeming from ladle to tundish from re-oxidation by ambient air. It's cleaned after every heat & hot reused in subsequent heats until its life or sequence length is over. Due to risk of thermal spalling shrouds are discarded in case of heat delay. Last shroud of the sequence is discarded as it can't be cold reused. Both situations increase consumption of shrouds resulting in wastage of refractory, disposal & increased carbon footprint. Shroud changing also poses ergonomical & safety risk since it's maneuvered manually in hot environment. High performance high flexibility ladle shroud, Duraflex aims to improve durability & thermal shock resistance. It can be cold reused multiple times without generating thermal crack. It improved shroud life manifold than conventional shroud. With reduction in consumption, this new ladle shroud is beneficial with respect to improving sustainability, safety, reliability & profitability.

Keywords: Ladle shroud, Duraflex, thermal shock, cold reuse

1. Introduction

Ladle shroud goes through thermal cycle during application which makes it vulnerable to thermal shock. With increasing casting duration, steel wets the shroud outside & inside surface penetrating inside the matrix. Material becomes stiffer and loses flexibility and when subject to thermal cycle it can't withstand the thermomechanical stress leading to crack formation or breakage. This is a serious limitation for extending shroud life. Hence Vesuvius has come up with a different alumina-graphite material having better thermal shock resistance & slower ageing feature enabling enhanced durability. It has two variants, one for longer straight life and another for longer life with multiple cold reuse.

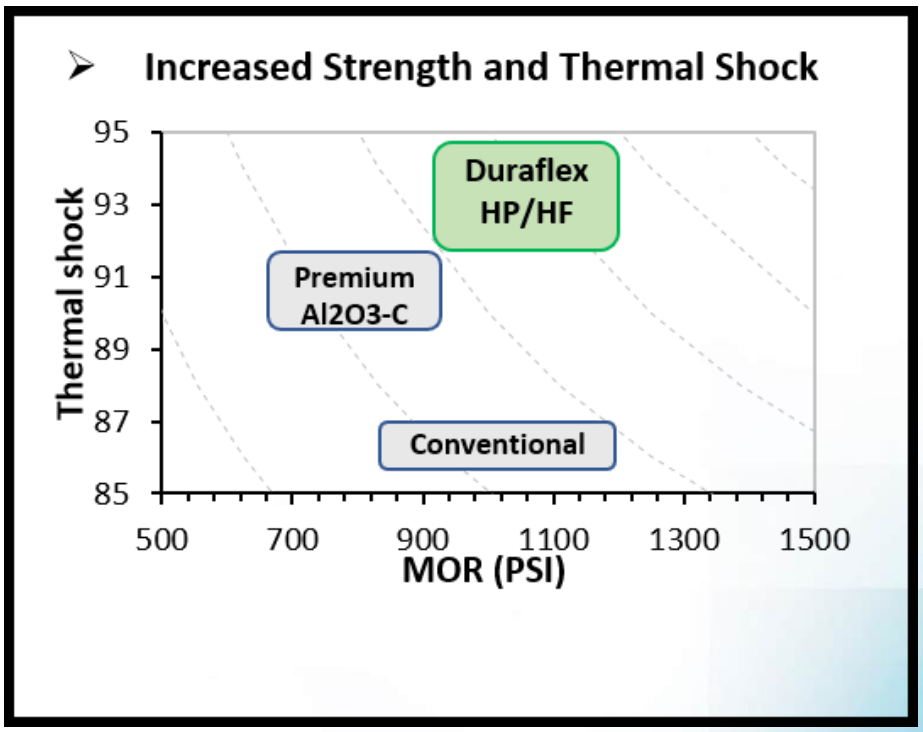




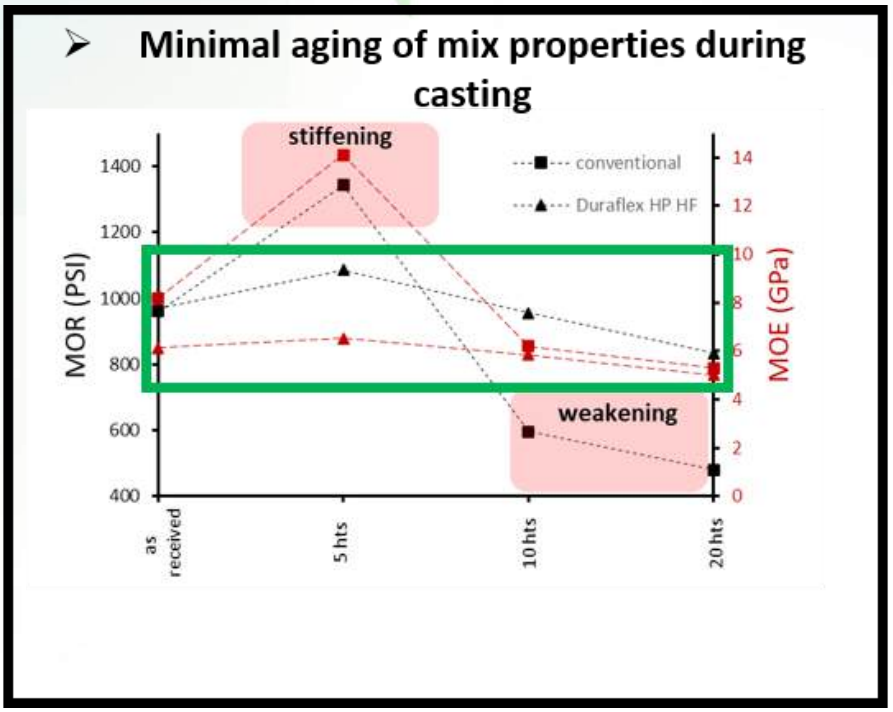
2. Technical background

Ladle shroud life limiting factors:

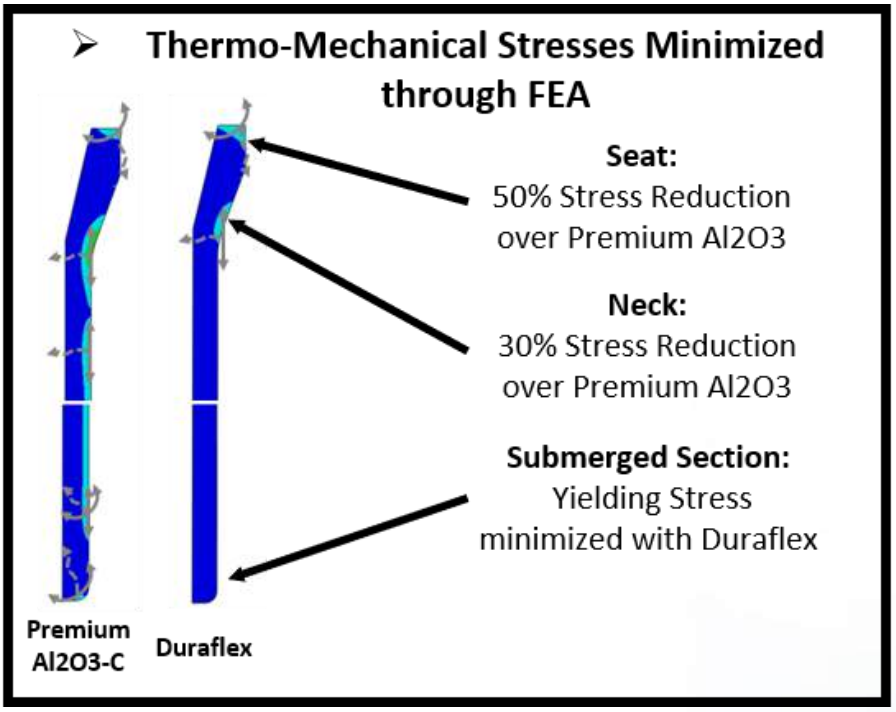
a) Thermal shock/ crack/ horse-shoe
b) Seat crack
c) Slag line corrosion
d) Gouging/abrasion



In the new material, both thermal shock and strength have been improved



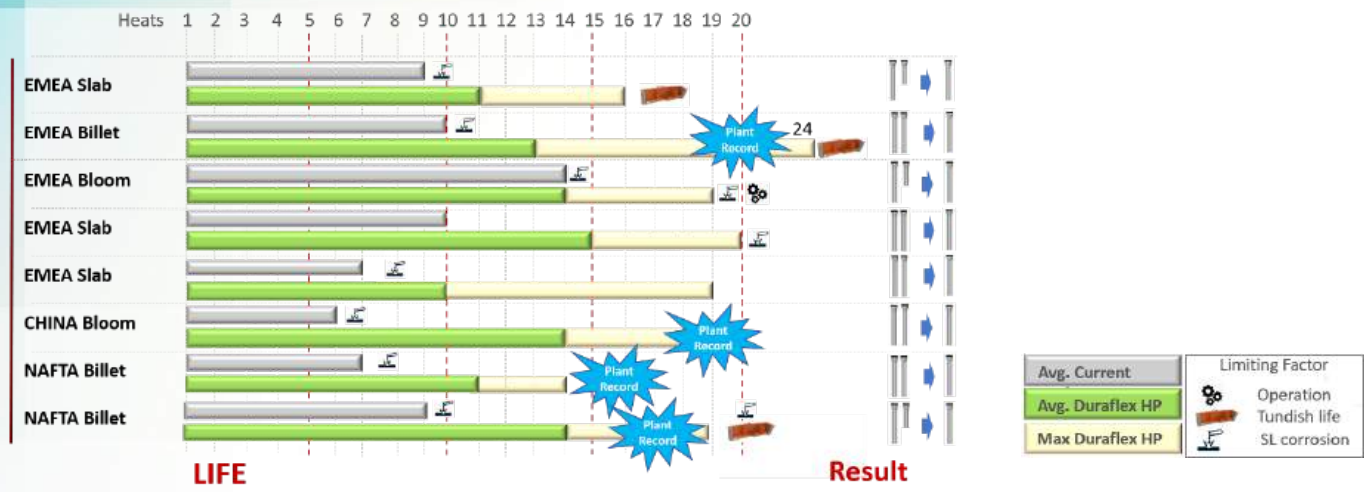
Since ageing consists of stiffening and then weaking of the material, the new material is with better ageing resistance



Properties of other parts of the shroud are also taken care of to avoid unwanted failures

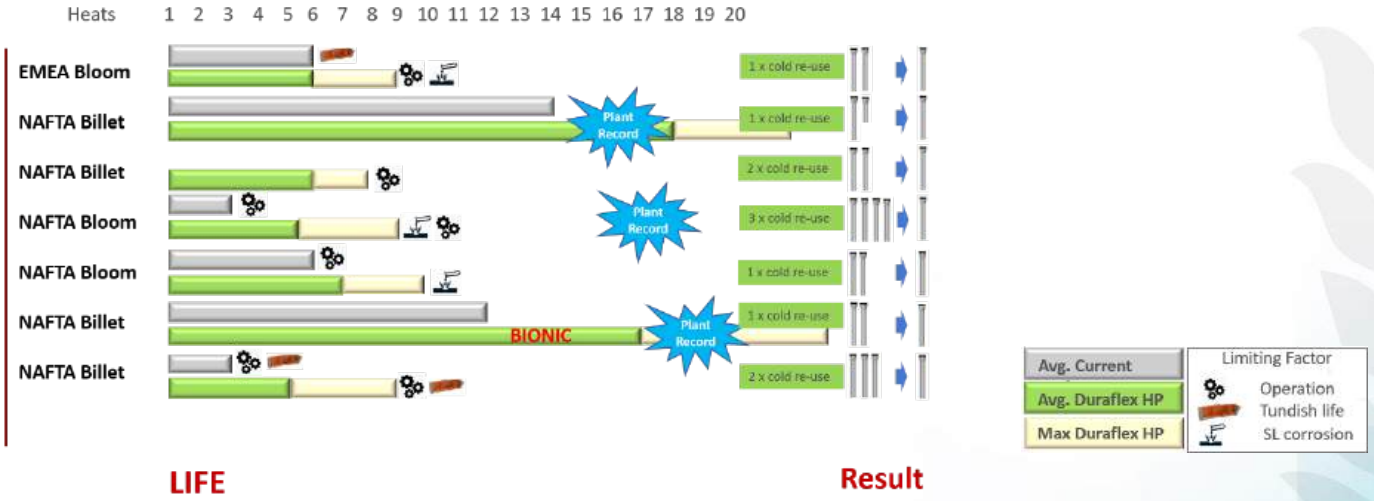
3. Field result

Both the variants have been tried at multiple steel plants and the comparative performance is given below.



Result of High performance Duraflex

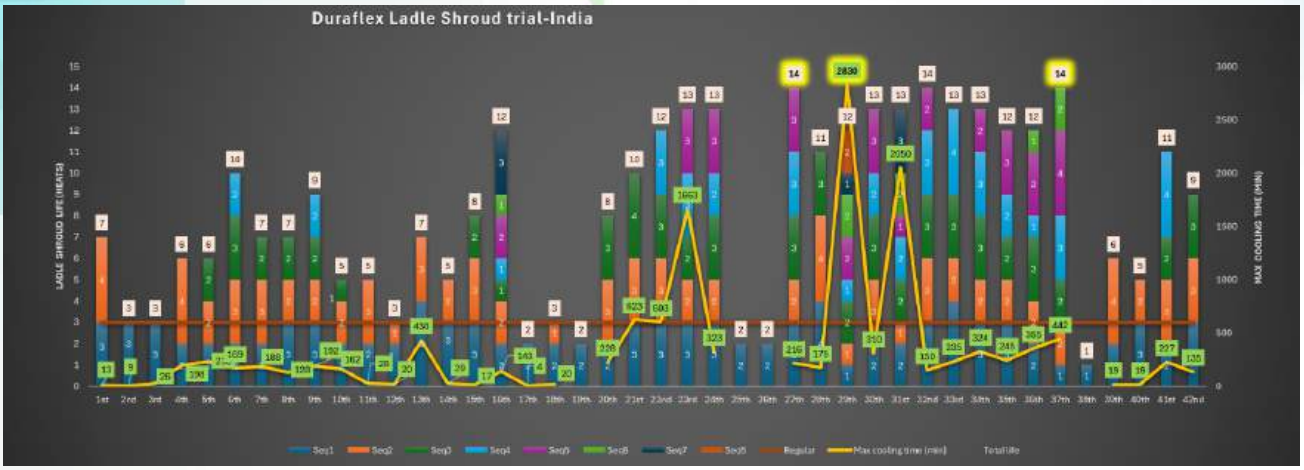
Duraflex life improved to 2.5 time compared to conventional shroud reducing shroud consumption per sequence from two to one



Result of High flexibility Duraflex

Duraflex could be cold reused 2-3 times compared to none in conventional shroud reducing shroud consumption per sequence from two/three to one

Field trial was done in one of the Indian steel plants where conventional shroud used to last for 3 heats only.



Convention shroud at this steel plant used to last for 3 heats and could not be cold reused.





Ladle shroud cross section after 12 heats casting; healthy remaining thickness of 18 mm

4. Conclusions

When Duraflex high flexibility ladle shroud was used,

a) Achieved avg life of 8 heats compared to avg life of 2.8 heats in conventional shroud
b) highest life achieved was 14 heats
c) highest number of cold reuse possible was 7 times
d) highest cooling time in between two uses was 2830 min

This demonstrates overall improvement in performance in terms of longevity as well as cold reusability. It also satisfied the benefits mentioned below.

a) Sustainability: with life increasing from 3 to 8 heats, total consumption would go down
b) Safety: With higher life, less frequent shroud change would be required
c) Reliability: Consistency of performance improved
d) Profitability: reduced specific consumption, hence more profitable for both steel plant & vendor

ACHIEVING BOTH THERMAL INSULATION AND DURABILITY WITH FIBER-ADDED CASTABLE REFRACTORIES

Kazuya Nakabo, Ryo Tsukada, Takahiro Kago and Tamiatsu Koyake

Research center
SHINAGAWA REFRA co., ltd., Okayama, Japan

Corresponding author's e-mail: nakabouk@shinagawa-ref.jp

Abstract

Reducing energy consumption is one of the most critical challenges facing modern industry. To address this issue, we developed a ceramic fiber blended castable refractory with low thermal conductivity and high slag resistance. To evaluate its performance for reheating furnace applications, numerical simulations and laboratory experiments were conducted. Heat loss in a skid pipe structure was analyzed using one-dimensional steady-state heat transfer calculations. The results indicated that the new refractory suppresses the temperature rise of cooling water, suggesting a reduction in heat loss. In addition, slag penetration tests using mill scale revealed superior slag resistance compared with conventional castable refractories. The improved durability is attributed to the characteristic microstructure of the developed material. These results demonstrate the potential of the new refractory to contribute to both energy savings and longer lining service life in reheating furnaces.

Keywords: reheating furnace, microstructure, scale attack resistance, thermal insulation

1. Introduction

A reheating furnace is a continuous industrial furnace used to heat semi-finished steel products to the required temperature before hot rolling. Most modern reheating furnaces employ a walking beam system[1]. Steel products are transported through the furnace by walking beams consisting of water-cooled pipes called skid pipes. The skid pipes are covered with refractory linings to reduce heat loss and protect the pipes from the high-temperature furnace atmosphere. Because the skid pipes are continuously cooled by water during operation, a significant amount of heat is lost through them. During reheating, an oxide layer known as scale is formed on the surface of steel products. The scale peels off during handling and accumulates around the skid pipes. At elevated temperatures, iron oxides contained in the scale penetrate and attack the refractory lining. Consequently, scale attack is one of the primary degradation mechanisms of skid pipe refractories. Therefore, skid pipe refractories are required to achieve both low thermal conductivity and high resistance to scale attack. To meet these requirements, various refractory materials have been developed and investigated. For example, dense castable refractories provide excellent durability because of their high resistance to scale attack. However, their thermal insulation performance is insufficient to meet the growing demand for energy conservation driven by carbon neutrality initiatives. In contrast, ceramic fiber products exhibit excellent thermal insulation performance[2]. However, its resistance to scale attack is inferior to that of castable refractories. As a result, its application is often limited to specific locations or requires protection by a veneering layer. To overcome these limitations, we developed a ceramic fiber blended castable refractory, referred to as "Fiber Castable". A proprietary fiber defibration and dispersion technology enables the incorporation of a large amount of ceramic fibers into the refractory matrix. As a result, a characteristic microstructure is formed, providing both low thermal conductivity and high resistance to scale attack. In this study, the microstructure,

resistance to scale attack, and thermal insulation performance of the newly developed refractory were investigated through microstructural observation, laboratory testing, and numerical heat transfer analysis. The applicability of the material to skid pipe linings in reheating furnaces was then evaluated.

Table 1 Typical properties of sample castable refractories

	Regular Castable	Regular Castable	Fiber Castable
Chemical composition / % Al_2O SiO_2	 61 33	 57 32	 61 28
Bulk density / kg·m-3	2250	1800	910
Apparent porosity / %	25	42	63
Water requirement / %	11	25	55

2. Materials and methods

2. 1 Sample materials

Three alumina-silica based castable refractories were evaluated in this study: the newly developed Fiber Castable (FC), a conventional Insulating Castable (IC), and a conventional Regular Castable (RC). The conventional materials were selected from products currently used for skid pipe linings in reheating furnaces. The typical properties of the investigated materials are summarized in Table 1.

2. 2 Microstructural Characterizations

The microstructure of FC was characterized using a digital microscope and scanning electron microscopy (SEM). Elemental distributions were analyzed by energy-dispersive X-ray spectroscopy (EDS). Specimens heat-treated at 110 °C and 1000 °C were examined. The observed microstructures were compared with those of IC and RC.

2. 3 Scale Attack Resistance

Scale attack resistance was evaluated using a crucible test. The experimental procedure is illustrated in Fig. 1. Crucible-shaped specimens (outer diameter: 70 mm; inner diameter: 30 mm) were prepared from the castables and dried at 110 °C. Subsequently, 20 g of mill scale generated in an actual reheating furnace was placed in each specimen, followed by heating at 1500 °C for 6 h. After the test, the extent of scale attack was quantified by measuring the penetration depth from the specimen cross-sections. In addition, the resulting microstructural changes were examined using SEM and EDS.

2. 4 Thermal Insulation Performance

The thermal conductivity of the investigated materials was measured using the hot-wire method. A pair of specimens with dimensions of 114 mm × 114 mm × 65 mm was used for each measurement. Thermal conductivity was measured at temperatures up to 1000 °C.

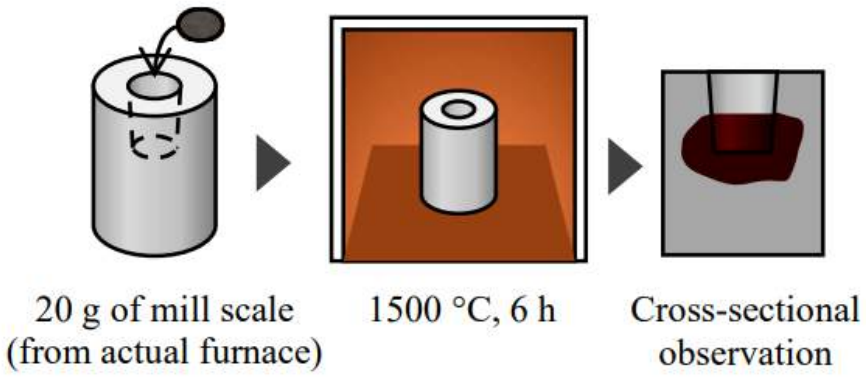


Fig. 1 Experimental procedure of crucible test for evaluating scale attack resistance.

The thermal insulation performance of the investigated refractories in a reheating furnace was evaluated using a one-dimensional steady-state heat transfer model of a skid pipe, as illustrated in Fig. 2. The overall thermal resistance was calculated from the measured thermal conductivity of the refractories and the heat transfer coefficients on both sides of the skid pipe. The calculation conditions are summarized in Table 2. The furnace atmosphere temperature, T_A, was assumed to be constant at 1300 °C. The heat transfer coefficient on the furnace side Ho was calculated from the StefanBoltzmann equation and an empirical correlation for natural convection[3]:

$$H_o = \varepsilon \cdot \sigma \cdot \frac{T_A^4 - T_S^4}{T_A - T_S} + 1.19 \cdot \left(\frac{T_A - T_S}{2 \cdot r_2}\right)^{0.25} \quad (1)$$

where ε is the emissivity, σ is the Stefan-Boltzmann constant, TS is the refractory surface temperature, and r2 is the outer radius. On the cooling-water side, the heat transfer coefficient was determined using the Dittus-Boelter equation[4]:

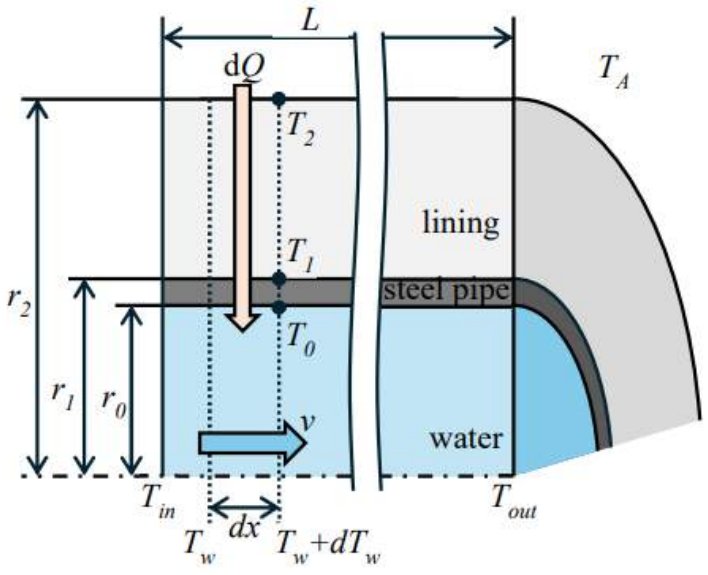


Fig. 2 One-dimensional steady-state heat transfer model for the skid pipe.

Table 2 Model parameters for the skid pipe heat transfer analysis

Steel pipe inner radius	r_0	0.077 m
Steel pipe outer radius	r_1	0.089 m
Refractory outer radius	r_2	0.17 m
Skid pipe length	L	10 m
Cooling water velocity	v	0.128 $m \cdot s^{-1}$
Water density	ρ	9.92×10^{2} $kg \cdot m^{-3}$
Water viscosity	μ	6.51×10^{-4} Pa·s
Water specific heat capacity	c_W	4.18×10^{3} $J \cdot kg^{-1} \cdot K^{-1}$
Water thermal conductivity	k_W	6.30×10^{-1} $W \cdot m^{-1} \cdot K^{-1}$
Furnace atmosphere temperature	T_A	1300 °C
Water inlet temperature	T_{in}	40 °C

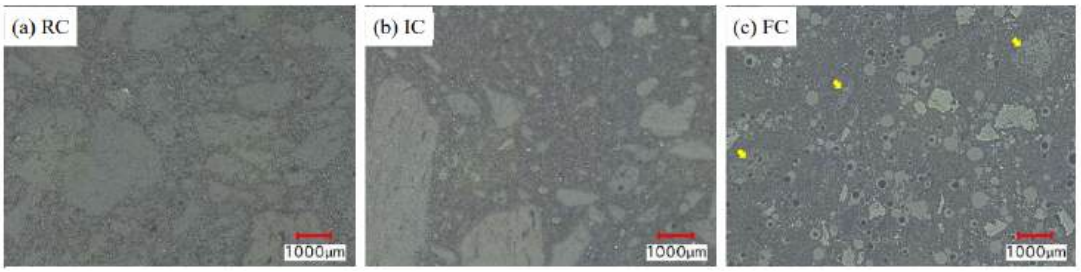


Fig. 3 Digital microscope images of investigated castables: (a) Regular Castable, (b) Insulating Castable, (c) Fiber Castable. Arrows indicate characteristic porous agglomerates.

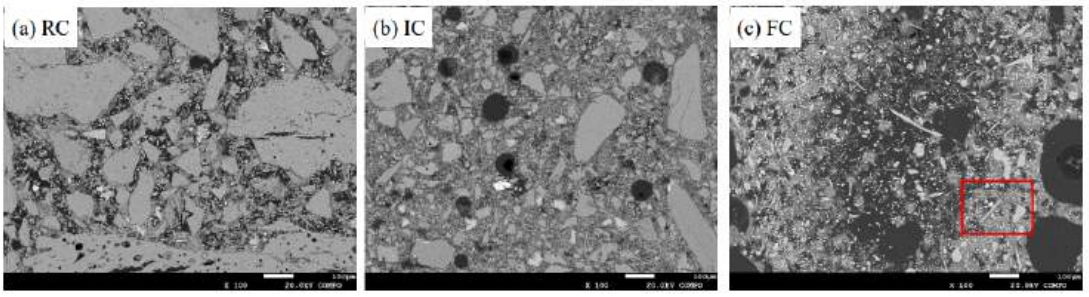


Fig. 4 SEM images of investigated castables; (a) Regular Castable, (b) Insulating Castable, (c) Fiber Castable.

$$Nu = \frac{H_i \cdot 2 \cdot r_0}{k_w} = 0.023 \cdot Re^{0.8} \cdot Pr^{0.4} \qquad (2)$$

where Nu, Re, and Pr are the Nusselt, Reynolds, and Prandtl numbers, respectively. The Reynolds and Prandtl numbers were calculated from the thermophysical properties of water and the flow conditions, using the inner diameter of the pipe as the characteristic length. The temperature rise of the cooling water was obtained by integrating the heat absorbed by the flowing water along the pipe length. The calculated outlet water temperatures were compared to evaluate the thermal insulation performance of the investigated materials. The thermophysical properties of water used in the calculations are summarized in Table 2. The properties were evaluated at 40 °C.

3. Results and Discussions

3. 1. Microstructural Characterization

Figure 3 shows digital microscope images of the investigated castables after drying at 110 °C. RC exhibited a microstructure in which aggregates were clearly distinguishable from the surrounding matrix. IC showed a relatively homogeneous matrix-rich microstructure containing dispersed pores. In contrast, FC exhibited numerous pores together with characteristic hollow regions approximately 1 mm in size.

Figure 4 shows SEM micrographs of the investigated castables. RC and IC exhibited conventional aggregate-matrix microstructures. In contrast, FC contained characteristic agglomerated regions with relatively dense shells surrounding hollow interiors. A higher-magnification image of the shell structure is shown in Fig. 5. The shell consisted of ceramic fibers and fine matrix particles. Numerous fiber cross-sections and elongated fibers were observed, indicating that the shell structure was formed by agglomerated ceramic fibers infiltrated by fine matrix particles.

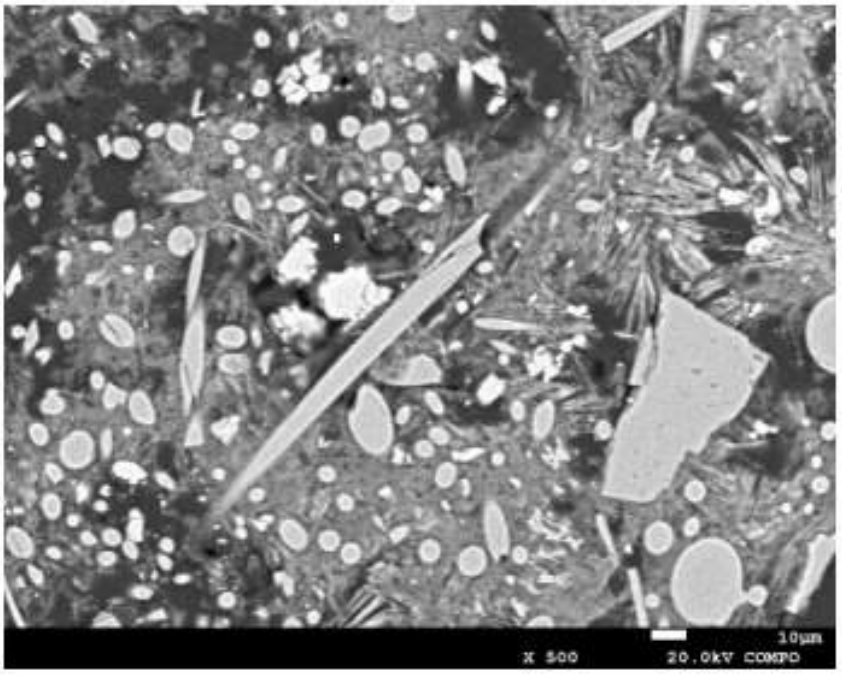


Fig. 5 Magnified SEM image of agglomerated region indicated in Fig. 4(c).

3. 2 Scale Attack Resistance

Figure 6 shows the cross sections of the specimens after the crucible test. Extensive penetration of molten scale was observed in both IC and RC. On the other hand, the penetration of molten scale into FC was significantly smaller than that observed in

either IC or RC. Figure 7 shows the penetration depth measured from the cross sections after the crucible test. FC exhibited the smallest penetration depth among the investigated materials. In contrast, IC and RC showed significantly larger penetration depth, indicating inferior resistance to scale attack.

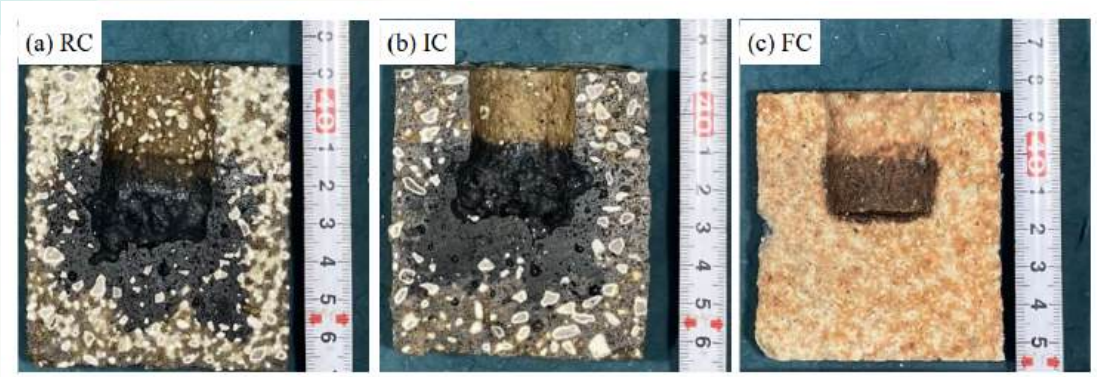


Fig. 6 Cross sections of the specimens after crucible scale attack test; (a) Regular Castable, (b) Insulating Castable, (c) Fiber Cast

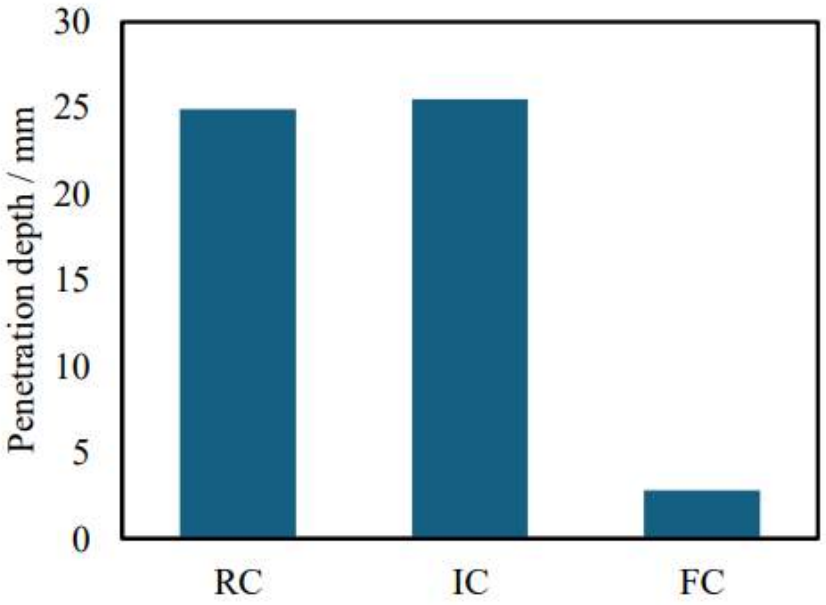
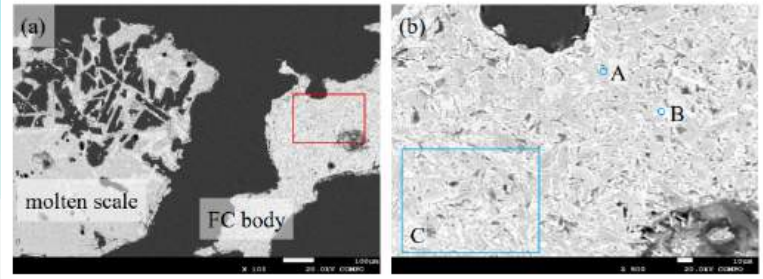


Fig. 7 Penetration depth measured from cross sections after crucible scale attack test (Fig. 6).

To investigate the origin of the superior scale resistance of FC, the microstructure near the molten scale/refractory interface was observed by SEM. As shown in Fig. 8, the characteristic shell-like structure derived from the fiber agglomerates remained after the crucible test. EDS point analyses were conducted for the grayish region (Point A) and the whitish region (Point B) shown in Fig. 8(b). In addition, area analysis was carried out for the shelllike structure. Point B exhibited a higher FeO content than Point A, while the area analysis indicated that the shell structure remained predominantly alumina-based even after exposure to molten scale. The retained shell-like framework is considered to contribute to the suppression of deep penetration.



(c)	Al_2O_3	FeO
Point A	87.7 %	11.5 %
Point B	31.6 %	67.8 %
Area C	73.8%	14.1 %

Fig. 8 Microstructural image of FC after crucible scale attack test; (a) SEM image of molten scale/refractory interface, (b) magnified of FC region indicated in (a), and (c) EDS point analysis results at locations A, B and C in (b).

3. 3 Thermal Insulation Performance

Figure 9 shows the thermal conductivities of the investigated castables. FC exhibited the lowest thermal conductivity over the measurement temperature range. At 1000 °C, the thermal conductivity of FC was approximately 56 % lower than that of RC and 40 % lower than that of IC. This reduction is attributed to the characteristic hollow agglomerate structure observed in Fig. 4, which introduces thermally insulating regions into the refractory matrix.

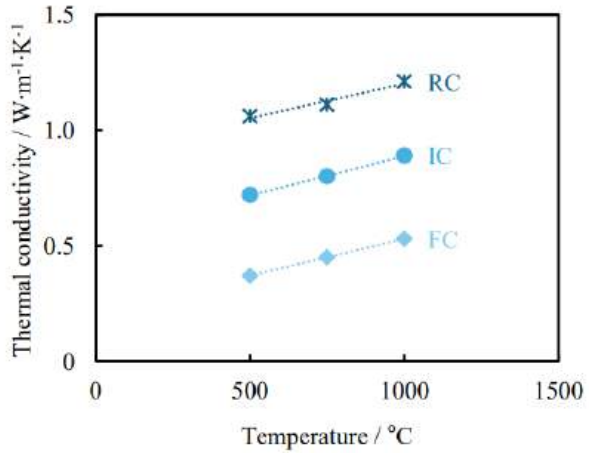


Fig. 9 Thermal conductivities of investigated castables.

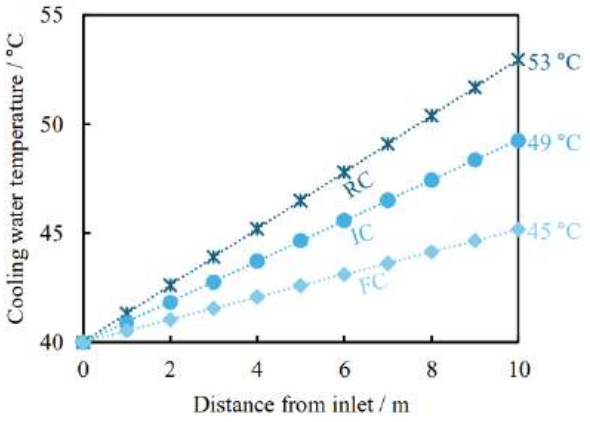


Fig. 10 Cooling-water temperature profiles calculated using the one-dimensional heat transfer model of the skid pipe

4. Conclusion

Fiber Castable (FC), developed for reheating furnace skid pipe applications, was investigated and compared with a conventional Regular Castable (RC) and a conventional Insulating Castable (IC).

FC exhibited characteristic hollow agglomerated regions approximately 1 mm in size. The shell structure of the agglomerates consisted of ceramic fibers and fine matrix particles.

FC showed the highest resistance to scale attack among the investigated castables. The penetration depth was significantly smaller than those of IC and RC. Although partial penetration of iron oxide into the structure was observed, the shell-like structure remained after the crucible test.

FC also exhibited the lowest thermal conductivity and the smallest cooling-water

temperature rise in the skid pipe heat transfer analysis.

These results demonstrate that FC has the potential to improve both the service life and thermal efficiency of reheating furnaces.

References

1. T. Motomachi, S. Miyagawa and A. Matsuo: Taikabutsu Overseas, 10 [4] 210–212 (1990).

2. H. Terajima, H. Ootsubo, N. Taki, M. Amano, K. Goto, E. Suzuki and K. Goto: J. Tech. Assoc. Refract. Jpn., 26 [4] 201–206 (2006).

3. Edited by The Technical Associations of Refractory Japan (TARJ): Refractory Handbook ver. 12, (2015) pp. 589.

4. F. Dittus and L. Boelter: Int. Comm. Heat Mass Transfer, 12 [1] 3–22 (1985).

DRY GUNNING MATERIAL "SIG (SHINAGAWA IMPROVED GUNNING)" WITH HIGH DURABILITY AND QUICK DRYING PROPERTIES

Natsumi Higashikawa, Kiyoyuki Komatsubara, Hidekuni Nishiguchi and Ryuta Yamada

Unshaped Refractories R&D Section, Research Dept. No.2, Research Center, Shinagawa Refra. Co., Ltd., JAPAN

Corresponding author's e-mail: higashikawan@shinagawa-ref.jp

Abstract

Dry gunning materials are widely used in industrial furnaces because of their ease of installation and reduced construction time. However, conventional dry gunning materials generally exhibit limited durability and require lengthy drying procedures owing to the use of cement hydration as the primary bonding mechanism. A novel dry gunning material, SIG (Shinagawa Improved Gunning), was developed by replacing water with a specially designed binder solution. The binder forms a chemical bonding network during drying and heating, resulting in superior hot strength and drying properties. Compared with a conventional dry gunning material, SIG exhibited approximately twice the modulus of rupture above 1000°C, 42% lower alkali penetration, 2.5 times higher adhesion strength, and 62% improved abrasion resistance. Steam explosion testing confirmed excellent drying performance without explosive spalling. Commercial application in a waste incinerator demonstrated a service life exceeding 24 months, more than twice that of the conventional material. Furthermore, SIG reduced drying duration by 67%, resulting in an estimated 70% reduction in drying energy demand. These results demonstrate that SIG contributes to both operational efficiency and environmental sustainability through enhanced durability, reduced maintenance downtime, and lower energy consumption.

Keywords: Dry gunning material, Waste incinerator, Durability, Quick drying, Binder solution

1. Introduction

Monolithic refractories are installed using various methods, including casting, gunning, spraying, and stamping. Among these methods, dry gunning has become increasingly popular because it eliminates the need for formwork installation and removal, thereby reducing construction time and labor requirements. In waste incinerators, dry gunning materials are frequently used for repair work and, in some applications, for initial lining, where installation of formwork is difficult. However, conventional dry gunning materials generally utilize alumina cement as a binder and suffer from limited hot strength, insufficient resistance to alkali attack, and the risk of explosive spalling during drying. These limitations often result in reduced service life and prolonged shutdown periods. To address these challenges, a new dry gunning material, SIG (Shinagawa Improved Gunning), was developed. SIG employs a binder solution mixed at the nozzle instead of water, enabling the formation of a strong chemical bond network within the installed lining. The objective of this work was to evaluate the characteristics of SIG and verify its performance through both laboratory testing and commercial application.

2. Concept of SIG Technology

Dry gunning materials are generally installed by pneumatically conveying dry material and mixing water at the nozzle. In such systems, bonding is achieved primarily through cement hydration. SIG adopts a different bonding concept. Instead of water, a specially designed binder solution is mixed with the dry material at the nozzle. During drying and

subsequent heating, the binder undergoes gel formation and develops a three-dimensional Si–O–Si network, resulting in the formation of a dense chemical bonding structure. This approach enables improved hot strength and drying performance while maintaining compatibility with conventional dry-gunning equipment. Only minor modifications, such as the addition of a binder feeding system, are required for practical application.

3. Experimental Procedure

3.1 Mechanical Strength

The modulus of rupture (MOR) after heating was evaluated for both conventional dry gunning material and SIG. Test specimens were heated to prescribed temperatures and subsequently tested according to standard bending-strength procedures.

3.2 Alkali Resistance

Alkali resistance was evaluated using potassium carbonate (K_2CO_3) as the corrosive agent. The specimens were exposed to K_2CO_3 at 1300°C for three hours and then sectioned to evaluate corrosion and penetration behavior.

3.3 Drying Performance

Drying performance was evaluated using a steam explosion test. Specimens were prepared by gunning material into a steel mold and curing for three hours at room temperature. The specimens were then directly inserted into a furnace maintained at 1000°C, and internal temperature changes were recorded.

3.4 Adhesion Strength

Adhesion strength was evaluated using specimens cut from the gunned lining. The bonding strength was measured by a three-point bending test.

3.5 Abrasion Resistance

Abrasion resistance was evaluated using a standardized abrasion test and expressed as a relative abrasion index, normalized to the conventional material.

4. Results and Discussion

4.1 Mechanical Strength

Figure 1 shows the modulus of rupture after heating. At low temperatures, SIG and the conventional material exhibited similar strength levels. However, a significant difference appeared after exposure to elevated temperatures. Above 1000°C, SIG showed approximately twice the MOR of the conventional material.

The improved hot strength is attributed to the chemical bonding network formed by the binder solution. Unlike cement-bonded systems, which experience strength limitations associated with dehydration of cement hydrates, SIG develops a stable bond structure through gel formation and Si–O–Si network development.

The superior hot strength is expected to improve resistance against wear and structural degradation during service in waste incinerators.

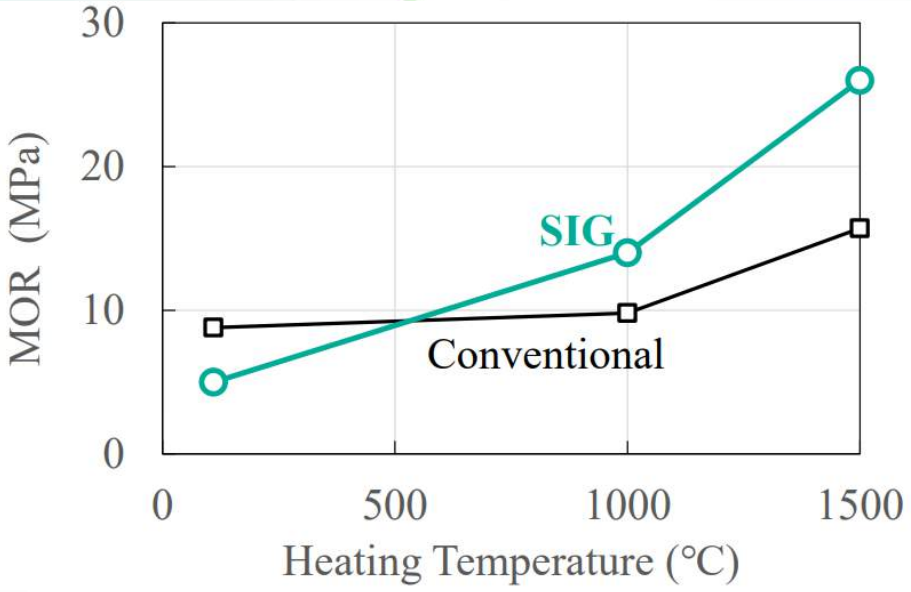


Figure 1. Modulus of rupture after heating for conventional dry gunning material and SIG.

4.2 Alkali Resistance

Figure 2 presents the results of the alkali corrosion test.

SIG exhibited a smaller corroded area and shallower penetration depth than the conventional material. The penetration index decreased from 100 to 58, corresponding to a reduction of approximately 42%.

The improved performance is attributed to the absence of cement-derived phases and the formation of a silica-rich matrix derived from the binder solution. These characteristics suppress alkali penetration and corrosion during high-temperature exposure.

Improved resistance to alkali attack is particularly important in waste-incinerator environments where alkali-containing deposits frequently interact with refractory linings.

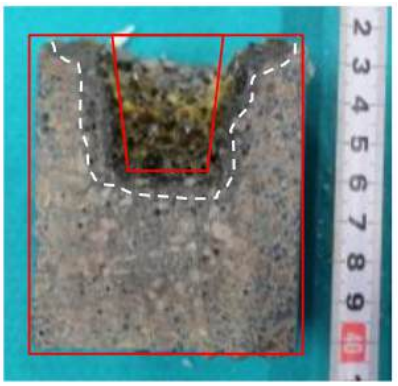
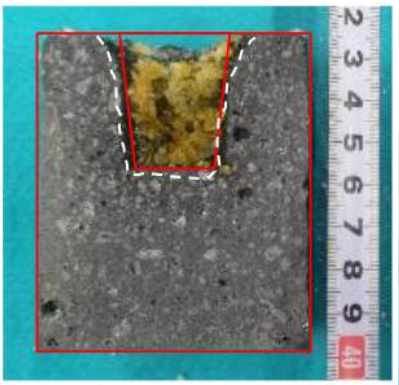
	Conventional	SIG
Cut section after alkali resistance test		
Penetration index	100	58

Figure 2. Cross-sectional appearance after alkali corrosion test using K_2CO_3.

4.3 Drying Performance

Figure 3 shows the results of the steam explosion test.
The specimens were cured for only three hours and directly inserted into a furnace maintained at 1000°C. No explosive spalling was observed despite these severe conditions.
The drying end point occurred at approximately 140°C, indicating rapid moisture removal and excellent permeability.

Figure 1. Modulus of rupture after heating for conventional dry gunning material and SIG. 0 10 20 30 0 500 1000 1500 MOR (MPa) Heating Temperature (℃) SIG Conventional Conventional SIG Cut section after alkali resistance test 100 58 Penetration index Figure 2. Cross-sectional appearance after alkali corrosion test using K_2CO_3. In addition, SIG has been successfully applied at lining thicknesses of up to 250 mm without a drying procedure in commercial operation.

These results demonstrate that SIG provides excellent drying performance and significantly improves maintenance efficiency.

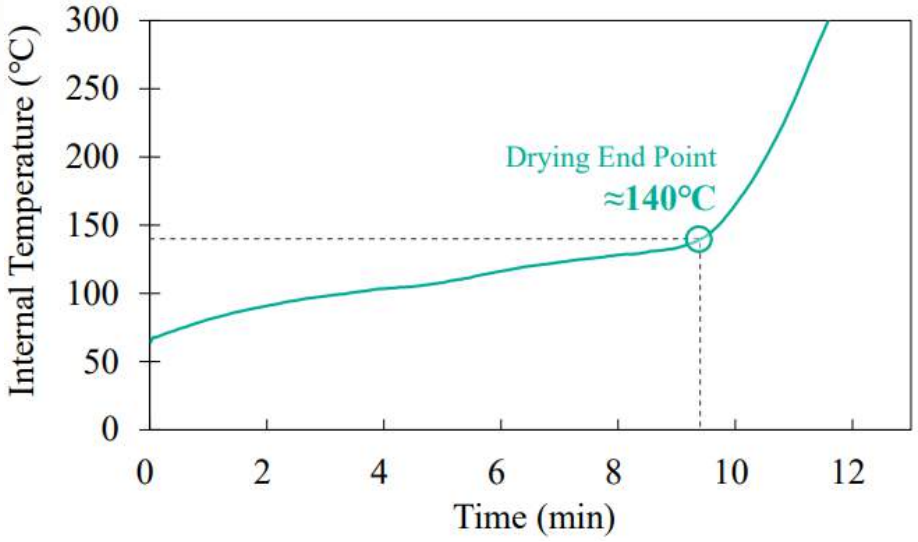


Figure 3. Internal temperature change during thermal explosion test.

4.4 Adhesion Strength

Figure 4 shows the adhesion strength results. The adhesion strength of SIG reached 14.2 MPa, whereas the conventional material exhibited 5.7 MPa. Therefore, SIG achieved approximately 2.5 times higher adhesion strength.

The strong bonding network formed within the lining contributes to improved structural integrity and reduces the risk of delamination during service. Enhanced adhesion is also expected to improve durability under thermal cycling and mechanical loading conditions.

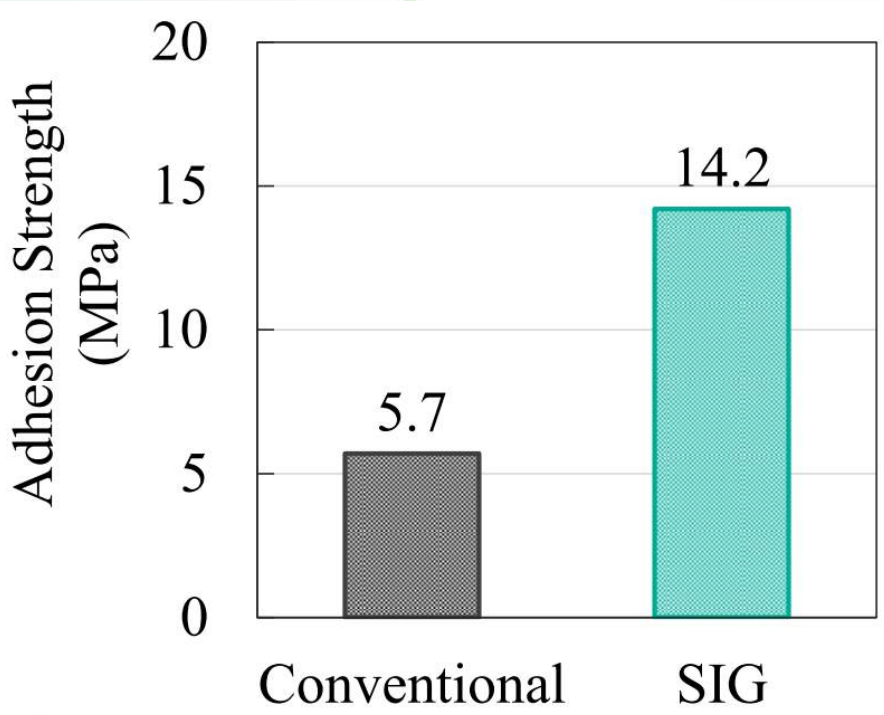


Figure 4. Adhesion strength of conventional dry gunning material and SIG.

4.5 Abrasion Resistance

Figure 5 shows the abrasion resistance results.

The abrasion index of the conventional material was normalized to 100, while SIG exhibited a value of 38. This corresponds to a 62% improvement in abrasion resistance.

The improved wear resistance can be attributed to the stronger bonding structure and higher hot strength of SIG. Together with superior alkali resistance, enhanced abrasion resistance contributes significantly to extended lining life under practical operating conditions. The effectiveness of these improvements was further verified through commercial application.

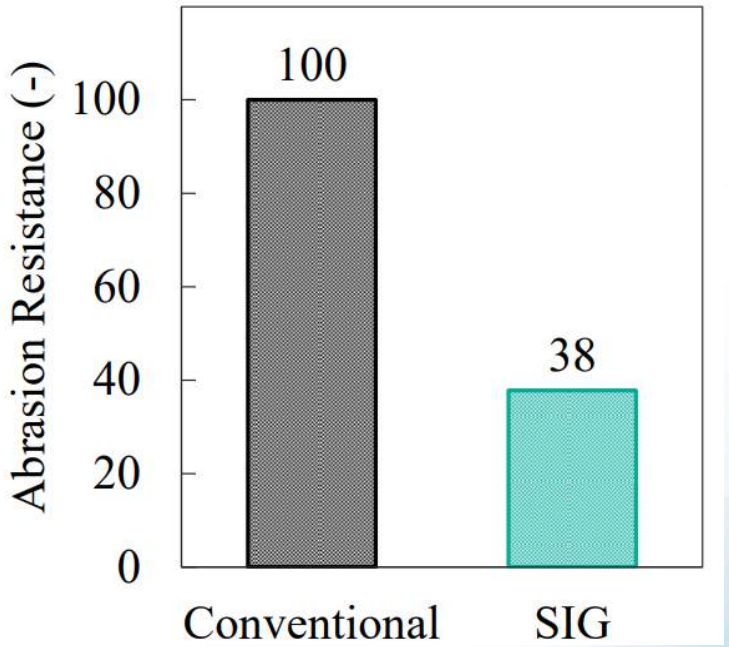


Figure 5. Relative abrasion resistance index of conventional dry gunning material and SIG.

5. Commercial Application

Laboratory evaluations indicated that SIG possessed superior hot strength, alkali resistance, drying behavior, adhesion strength, and abrasion resistance.
To verify these improvements under practical conditions, SIG was installed in a commercial stoker-type 0 50 100 150 200 250 300 0 2 4 6 8 10 12 Internal Temperature (℃) Time (min) Drying End Point ≈140℃ 100 38 0 20 40 60 80 100 Conventional SIG Abrasion Resistance (-) Figure 4. Adhesion strength of conventional dry gunning material and SIG. Figure 5. Relative abrasion resistance index of conventional dry gunning material and SIG. 5.7 14.2 0 5 10 15 20 Conventional SIG Adhesion Strength (MPa) waste incinerator operating at 950–1000°C with a lining thickness of 230 mm. The lining condition was evaluated during annual inspections.
The application conditions and service-life results are summarized in Table 1.
The conventional gunning material required replacement after approximately 12 months. In contrast, the SIG lining has remained in service for more than 24 months and continues to operate without replacement. At the time of writing, monitoring is ongoing and the final service life has not yet been reached. However, the achieved service life has already exceeded twice that of the conventional material.
These results confirm that the performance improvements observed in laboratory testing directly translate into enhanced durability under actual operating conditions.

Lining Material	Service life
Conventional	12 months
SIG	> 24 months (still in service)

Table 1. Service-life comparison in commercial application

6. Operational and Environmental Benefits

In addition to improved durability, SIG contributes to operational efficiency through its excellent drying performance.
By utilizing SIG, the drying schedule was shortened significantly, resulting in a reduction in maintenance shutdown time of approximately 67%.
Based on relative drying schedules, the estimated drying energy requirement was reduced by approximately 70%. Although this value was estimated from heating profiles rather than measured fuel consumption, it clearly demonstrates the potential for substantial energy savings.
Furthermore, recycled raw materials are actively utilized in SIG products. Depending on product grade, recycled material content ranges from approximately 20% to 50%.
The use of recycled materials reduces consumption of virgin mineral resources and lowers CO_2 emissions associated with material production.
Therefore, SIG contributes to sustainability through three approaches:

- Reduced drying energy consumption
- Extended service life and lower refractory consumption
- Utilization of recycled raw materials

7. Conclusions

A novel dry gunning material, SIG (Shinagawa Improved Gunning), was developed and evaluated. The following conclusions were obtained:

1. SIG exhibited approximately twice the hot strength of a conventional dry gunning material above 1000°C.
2. Alkali penetration was reduced by 42%, demonstrating superior alkali resistance.
3. Excellent drying performance was

confirmed without explosive spalling, even under severe drying conditions.
4. Adhesion strength increased by approximately 2.5 times and abrasion resistance improved by 62%.
5. Commercial operation demonstrated service life exceeding 24 months, more than double that of the conventional material. Lining Material Service life Conventional 12 months SIG > 24 months (still in service)
6. SIG contributes to sustainability through reduced maintenance time, estimated energy savings, and utilization of recycled raw materials.

Therefore, the developed dry gunning material demonstrated the potential to provide high durability, rapid start-up capability, and environmental benefits for waste-incinerator applications.

References

1. T. Iikuni, Y. Morimoto, D. Tanaka: Shinagawa Technical Report, 63 (2020) pp. 54-58.
2. Y. Oota, S. Komori, K. Asakawa: TAIKABUTSU, 72 [4] (2020) pp. 158-163.
3. O. Machinaga: TAIKABUTSU, 58 [9] (2006) pp. 476-483.
4. M. Nishimura, H. Sasaki, S. Nishida, M. Namba: Shinagawa Technical Report, 56 (2013) pp. 73-80.
5. E. Yoshizaki, H. Hirano, K. Moriguchi: TAIKABUTSU, 71 [3] (2019) pp. 126-130.
6. I. Matsubara, M. Nishimura, S. Nishida: TAIKABUTSU, 67 [12] (2015) pp. 618-619.

ENERGY SAVING IN STEELMAKING VESSELS USING A HYBRID REFRACTORY LINING SYSTEM

Toshikazu SETOGUCHI[1], Eriko KAWASHIMA[1], Kazunari TAKEMURA[2], Atsuhisa IIDA[2]

(1. Isolite Insulating Products Co., Ltd.; 2. Shinagawa Refra Co., Ltd.)

Corresponding author's e-mail: t-setoguchi@icf.isolite.co.jp

Abstract

A hybrid refractory lining material combining refractory bricks and microporous insulation materials has been developed. By integrating structural refractories with high-performance thermal insulation, this design provides thermal insulation while maintaining strength and durability equivalent to conventional refractory materials, thereby minimizing heat loss from the furnace shell. The use of this newly developed material offers four key benefits compared with conventional refractories and insulating materials: (1) reduced heat loss, (2) lower risk of molten steel leakage, (3) increased molten metal capacity, and (4) good installability. In actual furnace operations utilizing this material, a reduction in the shell surface temperature was confirmed, demonstrating that its insulation performance does not degrade even after long-term service. By accumulating performance data from commercial furnace applications and expanding its adoption, this material is expected to make significant contributions to energy conservation and environmental impact reduction.

Keywords: microporous, brick, thermal conductivity, Hybrid Refractory Lining Material

1. Introduction

In the steelmaking process, final products are manufactured through various stages, including the melting and reduction of iron ore in blast furnaces, refining processes to remove impurities, and continuous casting processes to solidify liquid steel into billets or slabs. Throughout these stages, steel exists in liquid form and is constantly maintained at temperatures above 1,500 °C. Consequently, heat losses occur through radiation and conduction from transfer vessels such as ladles and tundishes. Reducing these heat losses contributes to overall energy savings across the steelmaking process, enabling lower tapping temperatures in electric arc furnaces (EAF) and shorter processing times in secondary refining. Furthermore, driven by growing international demands for energy conservation and environmental protection, the effective utilization of thermal energy has become an urgent priority, with insulating refractories serving as an effective solution for this purpose. Insulating refractories possess excellent thermal insulation properties and high heat resistance, making them widely used for the inner and backup linings of various industrial furnaces. Conversely, dense refractory materials are used in areas in direct contact with or close to molten steel. Table 1 summarizes the physical properties of insulating refractories and refractory bricks [1][2]. Comparing the two reveals that insulating refractories exhibit extremely low thermal conductivity and superior insulation performance. However, due to their low bulk density and mechanical strength, there are concerns regarding damage during installation and degradation of insulation efficiency caused by heat leakage from damaged areas. To resolve these issues, a novel Hybrid Refractory Lining Material (HRL) was developed by integrating refractory bricks and insulating refractories. This material combines the high strength characteristic of refractory bricks with the high thermal insulation performance of insulating refractories. This paper reports the results of computer simulations and trials in an actual furnace using the newly developed HRL.

	Refractory Bricks	Microporous Insulation
Bulk Density (kg/m³)	2000	400
Compressive Strength (MPa)	600	0.6
Thermal Conductivity at 600°C (W/(m·K))	1-2	0.03–0.09

Table 1 Physical properties of insulating refractories and refractory bricks

2. Characteristics of Microporous Insulation Materials

Microporous insulation materials (hereinafter referred to as MP insulation) were selected as the thermal insulation component for HRL. Although various types of insulating refractories exist - such as insulating firebricks, ceramic fibers, and monolithic insulating refractories - demand for MP insulation has increased in recent years due to its superior thermal insulation performance compared with these conventional materials. Figure 1 shows the thermal conductivity of various insulating refractories alongside that of still air; it clearly demonstrates that MP insulation exhibits extremely low thermal conductivity compared with insulating bricks and ceramic fibers. The mechanism underlying the low thermal conductivity of MP insulation is illustrated in Figure 2 [3]. MP insulation is composed of ultrafine particles measuring less than 100 nm, inorganic fibers, and infrared scatterers. The use of ultrafine particles forms micropores smaller than the mean free path of air molecules, thereby suppressing both solid thermal conduction and gaseous convection heat transfer. Furthermore, the incorporation of infrared scatterers inhibits radiative heat transfer. Consequently, such high insulation performance is achieved by suppressing both solid conduction, which dominates in the low-temperature range, and radiative heat transfer, which becomes dominant in the high-temperature range. While many MP insulation products have maximum service temperatures around 1,000 °C, high-temperature grades capable of withstanding 1,200 °C and 1,400 °C are also available. In practical applications, MP insulation is primarily used as a backup lining material in temperature zones below 1,000 °C, on the steel-shell side of the lining in steelmaking vessels such as ladles, as well as in heat-treatment furnaces.

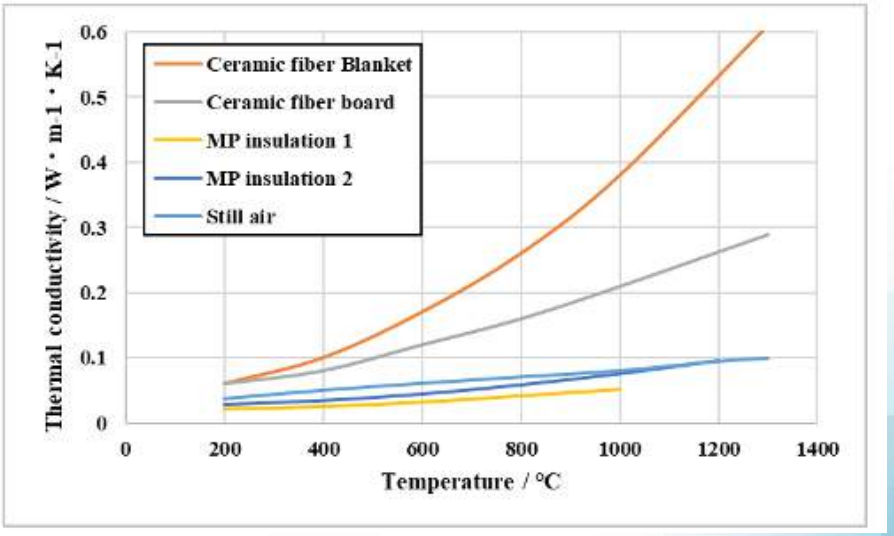


Figure 1 Thermal conductivity of various insulating refractories and still air

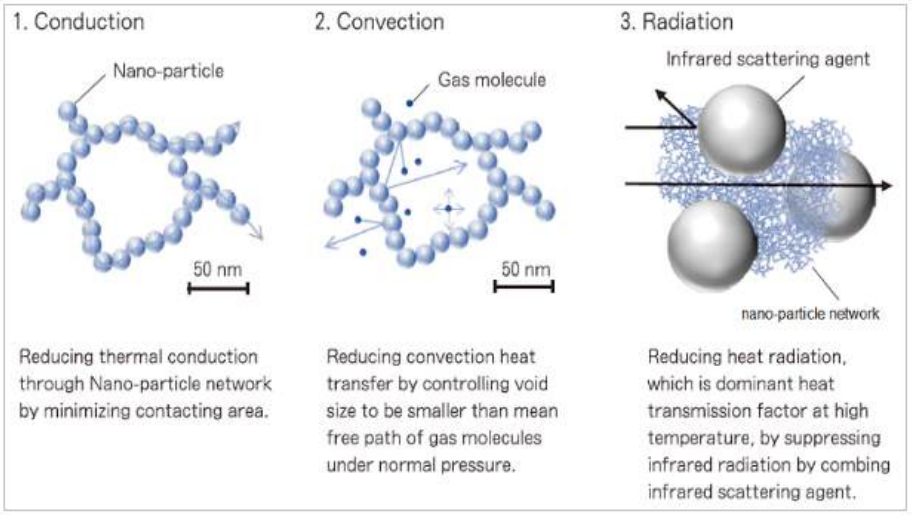


Figure 2 Low thermal conductivity mechanism of MP insulation

3. Hybrid Refractory Lining Material

The appearance of the developed product is shown in Figure 3. HRL is designed by incorporating MP insulation - which exhibits high heat resistance (1,200–1,400 °C) and low thermal conductivity - into the interior of refractory bricks. A recessed groove is formed in the base refractory brick, and the MP insulation is embedded within it. This structural configuration prevents mechanical damage to the MP insulation during installation and guards against collapse caused by compressive stress due to thermal expansion of the hot-face refractories when receiving molten steel. Consequently, it fully utilizes the high strength of the refractory bricks while simultaneously exploiting the excellent thermal insulation performance of the MP insulation, representing an innovative material that combines the advantages of both components.

The application of this novel material is expected to provide four primary benefits: (1) reduction of heat loss, (2) mitigation of molten steel leakage risk, (3) increase in molten metal capacity, and (4) good installability.

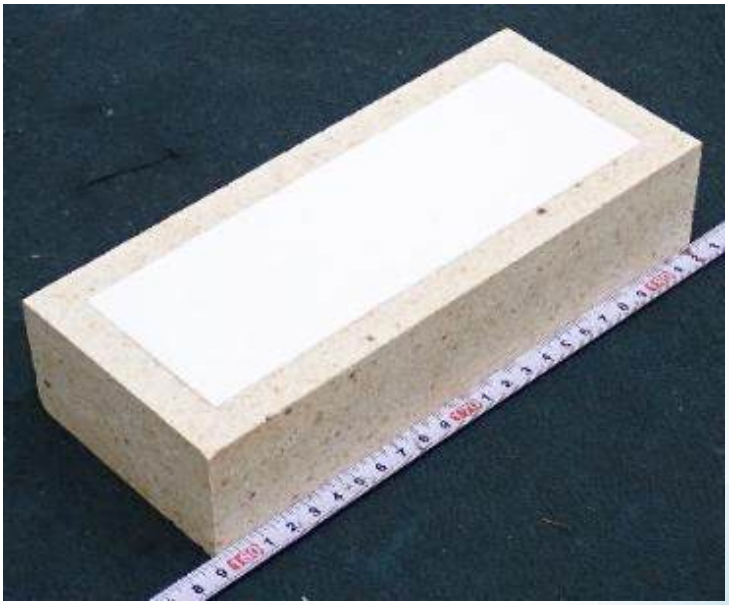


Figure 2 Low thermal conductivity mechanism of MP insulation

3.1 Investigation of Lining Configurations Utilizing HRL

Since HRL is a composite material consisting of MP insulation and refractory bricks, it is expected to yield lower shell temperatures than conventional linings using permanent bricks in steelmaking vessels. Consequently, if the shell temperature is maintained at the same level as when using conventional permanent bricks, the total lining thickness can be reduced by employing HRL. By thinning the lining structure, the allowable volume for molten metal increases, thereby enabling a higher processing capacity per charge (ch). Therefore, a simulation was conducted to determine the lining configuration for different MP insulation thicknesses in HRL, replacing conventional permanent bricks with HRL. The simulation results are shown in Figure 4, and the corresponding lining configurations are illustrated in Figure 5. For HRL Lining A, which incorporates an MP insulation thickness of 10 mm, an insulating brick thickness of 54 mm achieves the same shell temperature as that of the conventional permanent brick lining. Since the original insulating brick thickness is 65 mm, a thickness reduction of 11.5 mm is possible. Similarly, for HRL Lining B with an MP insulation thickness of 30 mm, an insulating brick thickness of 45 mm attains the equivalent shell temperature, allowing a thickness reduction of 20.3 mm. Considering a case where HRL is applied to the sidewall of a 200–300-ton ladle with a diameter of 4 m and an effective height of 3.3 m, HRL Lining B corresponds to an increase of approximately 2% in the allowable ladle volume.

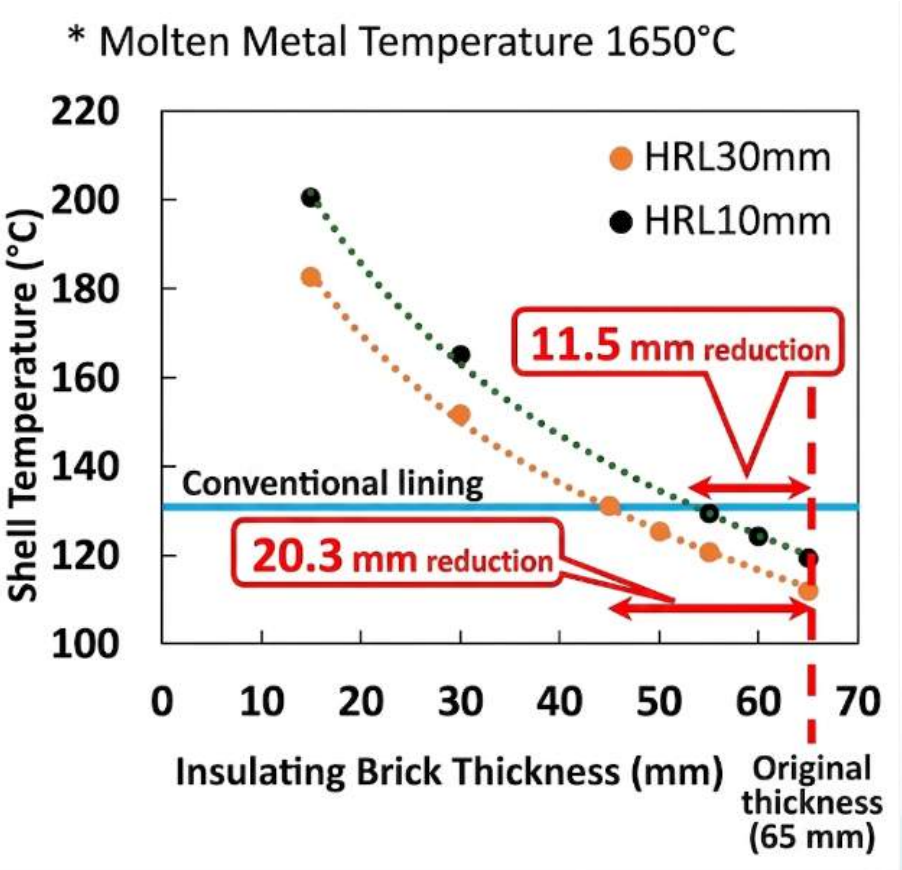


Figure 4 Steel shell temperature relative to insulating brick thickness for various MP insulation thicknesses



Figure 5 Ladle lining configurations incorporating HRL

3.2 Evaluation of Thermal Insulation Performance in an Actual Ladle

The thermal insulation effect in an actual ladle was evaluated by partially applying HRL and measuring the shell surface temperature at that location. The lining configuration of the ladle consisted of, from the inside outward, working lining refractories, semi-permanent bricks, HRL, and the steel shell. Temperatures were measured twice - during the 1st campaign (at 53 ch) and the 3rd campaign (at 389 ch) - and were compared with the shell surface temperatures measured at sections using conventional permanent bricks. The measurement results are summarized in Table 2.

	HRL area	Conventional area	Difference
1st campaign: 53 ch (°C)	154.6	170.6	16.0
3rd campaign: 389 ch (°C)	213.8	238.6	24.8

Table 2 Measured shell surface temperatures in actual ladle trials

In the 1st campaign, the shell temperature using conventional permanent bricks was 170.6 °C, whereas the shell temperature using HRL was 154.6 °C, representing a 16.0 °C reduction for the HRL section. In the 3rd campaign, the shell temperature for the conventional brick section was 238.6 °C compared with 213.8 °C for the HRL section, which was 24.8 °C lower. Thus, the thermal insulation effect of HRL was confirmed in both the 1st and 3rd campaigns. These findings demonstrate that HRL has sufficient heat resistance even when used at the same lining position as permanent bricks in ladles, while maintaining its thermal insulation performance over extended service.

3.3 Evaluation of Insulation Material Embrittlement

Although MP insulation exhibits almost no change in thermal conductivity over long-term use when exposed to heating temperatures below its continuous service temperature [4], exposure to high-temperature environments under compressive loading, such as those in actual furnaces, may cause embrittlement and structural collapse of the MP insulation, potentially increasing its thermal conductivity. Therefore, an evaluation was conducted to determine whether HRL degrades after extended service. The evaluation method involved heating one side of a sample recovered from an actual furnace to 1,400 °C, measuring the surface temperature of the opposite side, and calculating the temperature difference (Figure 6). Measurements were taken for three conditions: unused, after 1 campaign (178 ch), and after 3 campaigns (606 ch). The evaluation results are summarized in Table 3.

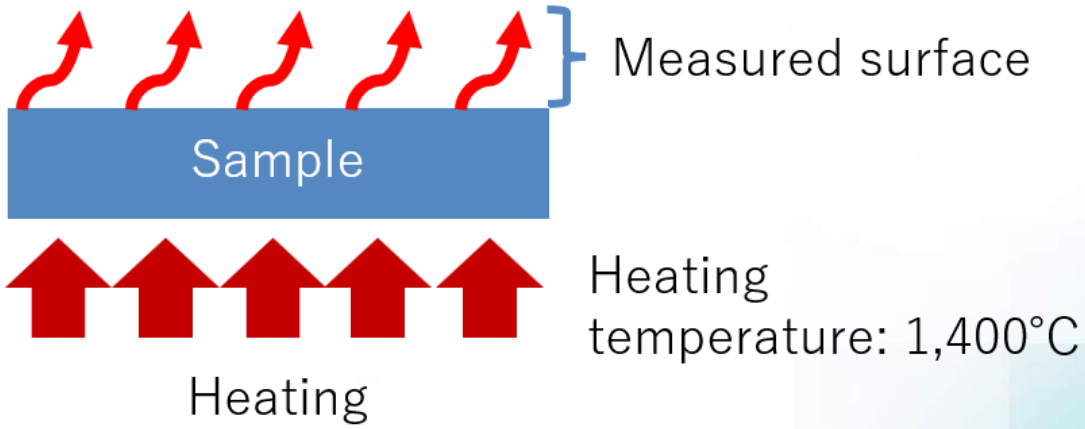


Figure 6 Schematic of the thermal evaluation method for samples recovered after service

	Unused	1st campaign (178 ch)	3rd campaign (606 ch)
Temperature (°C)	831	742	727
Temperature difference (°C)	569	658	673

Table 3 Thermal insulation performance of HRL samples after long-term service

For the unused sample, the opposite surface temperature was 831 °C, resulting in a temperature difference of 569 °C relative to the heated surface. In contrast, after 1 campaign, the opposite surface temperature was 742 °C with a temperature difference of 658 °C, and after 3 campaigns, the opposite surface temperature was 727 °C with a temperature difference of 673 °C. Thus, no degradation in thermal insulation performance was observed compared with the unused material. It is presumed that, because the MP insulation in HRL is protected by the surrounding permanent brick, physical compression-induced embrittlement and collapse of the MP insulation are effectively prevented, resulting in no degradation even after extended service.

4. Conclusions

The lining configuration when utilizing HRL, which combines permanent bricks with MP insulation, was evaluated via simulation. Furthermore, the thermal insulation performance in actual operational furnaces and the structural degradation of the thermal insulation material after extended service were evaluated, yielding the following key findings:

• Lining Configuration Simulation: Simulation of the lining configuration employing HRL suggested that, when maintaining the shell temperature equal to that of conventional permanent brick linings, the thickness of the insulating firebricks in the lining can be reduced by up to 20.3 mm.

• Thermal Insulation Performance in Actual Ladles: When HRL was applied to actual steelmaking ladles, the outer shell surface temperature was reduced by 16.0–24.8 °C compared with conventional permanent bricks, thereby confirming its significant thermal insulation effect.

• Long-Term Durability and Degradation Evaluation: Thermal evaluation was conducted by heating one side of samples recovered after extended service (up to 606 ch) and measuring the surface temperature on the opposite side. No degradation in thermal insulation performance was observed compared with the unused material, confirming that the insulation performance was maintained after long-term service.

Currently, trial applications of HRL in actual production furnaces are underway at multiple integrated steelmakers and electric arc furnace (EAF) steelmakers, with the objective of suppressing heat loss and expanding the internal vessel volume. Additional industrial trials are also scheduled with several other steel manufacturers. HRL represents an advanced hybrid material that combines the advantages of both structural refractories and thermal insulation refractories, offering substantial improvements over the limitations of conventional materials. By accumulating performance data from ongoing industrial operations and expanding the application of HRL, this technology is expected to make significant contributions to energy conservation and environmental impact reduction.

References

1. Shinagawa Refractories Co., Ltd., General Catalog.
2. Technical Association of Refractories, Japan (TARJ), Refractories Handbook, 12th revised ed., Technical Association of Refractories, Japan, p. 584 (2015).
3. M. Iida, K. Asakawa, Y. Shiraishi, and O. Kawasaki: Taikabutsu (Refractories), 73 [9] 418–425 (2021).
4. S. Suetake and A. Sueyoshi: Taikabutsu (Refractories), 70 [1] 7–10 (2018).

APPLICATION OF SHOTLESS CERAMIC FIBER AND LINING TECHNOLOGY IN COLD-ROLLING FACILITIES

Shinsuke SUETAKE, Atsuhiro KONDO
Isolite Insulating Products Co., Ltd.

Corresponding author's e-mail: atsuhirokondo@isolite.co.jp

Abstract

Surface defects on steel strips caused by dust generated from refractories in cold rolling mills are critical issues that significantly affect product quality. Particularly in vertical furnaces, dust falling from the roof and sidewalls tends to become trapped at the rolls, causing scratch defects. In the past, the surface layer of the refractories consisted of firebricks, which caused problems with dust generation. To suppress dust, designs using metal inner plates or alumina cloth on the furnace inner surface have become common; however, these designs still involve a high on-site installation workload and problems associated with degradation over time. This paper introduces a lining technology using shotless ceramic fiber (hereinafter referred to as CF) that maintains steel strip product quality by suppressing dust while reducing installation workload and addressing long-term degradation issues.

Keywords: Insulating Materials, Cold Rolling Facilities, Ceramic Fiber, Shotless CF

1. Introduction

In steel manufacturing, a cold rolling mill is a facility that further rolls steel strips obtained through hot rolling to produce cold-rolled steel strips with superior surface finish and high dimensional accuracy. Within this process, a continuous heat treatment (annealing) facility is used to restore the formability of strips that have undergone work hardening during cold rolling; refractory materials are used in this facility. In the continuous heat treatment process, energy saving aimed at reducing operational energy and carbon dioxide emissions is a critical challenge. Introducing refractory and insulating materials with low thermal conductivity and excellent thermal insulation (heat retention) properties into the furnace wall structure is an effective means of significantly reducing heat loss from the furnace body and achieving substantial energy savings. However, to ensure stable steel strip quality, material selection must consider not only thermal insulation characteristics but also compatibility with the furnace environment and operating conditions.

2. Characteristics and Types of Cold Rolling Facilities

Table 1 shows typical cold rolling facilities that require heat treatment. Each facility is designed to continuously process long steel strips at high speed. Within the line, the strips are guided and conveyed by rolls while advancing under appropriately controlled tension.

The temperature and atmosphere inside the furnace are primarily controlled to form the target microstructure and achieve the desired mechanical properties. Under these conditions, if foreign matter such as dust is suspended or accumulates inside the furnace, it can adhere to the surfaces of the steel strips and rolls, significantly degrading product surface quality. When hard dust particles become trapped at the contact interfaces (sliding and pressure-contact areas) between the rolls and steel strips advancing under high temperature and tension, the particles are pressed into the roll surface, forming microscopic irregularities. As the damaged roll surface repeatedly contacts and slides against the steel strip, continuous or periodic scratches and

indentation marks (roll pits) are induced on the strip surface along the direction of travel. Therefore, in the manufacture of high-quality steel strips, it is essential to prevent dust generation from furnace structures and insulating materials and maintain a high level of cleanliness inside the furnace.

Table 1 Typical heat treatment equipment

Abbreviation	Equipment
AL	Annealing Line
BAF	Batch Annealing Furnace
APL	Annealing and Pickling Line
CAL	Continuous Annealing Line
CGL	Continuous Galvanizing Line

3. History and Characteristics of Inner-Surface Refractories

Table 2 shows the historical transition and characteristics of materials used for the inner-surface refractories in conventional cold rolling facilities. In the early stages, firebricks were predominantly used for the furnace inner surfaces. While they offered excellent heat resistance, they were prone to chipping (loss of corners and edges) caused by mechanical impacts and thermal stress. This posed a high risk that detached dust and fragments could contaminate the furnace and adversely affect steel strip quality. Subsequently, inner metal plates were adopted, which reduced foreign matter contamination and decreased heat flux by approximately 40%, thereby improving energy efficiency. However, challenges remained, including dust generation from the underlying insulating materials due to thermal deformation and the high workload required for on-site fabrication, such as bending and welding. Alumina cloth suffered from fiber embrittlement under operating conditions (temperature and atmosphere), and the need for sewing during installation was also a drawback. Under these circumstances, shotless CF is expected to address these challenges while maintaining both energy-saving performance and dust suppression.

Table 2 Historical transition and characteristics of inner-surface refractory materials in conventional cold rolling

Refractory type	Firebricks	Inner metal plates	Alumina cloth	Shotless CF
Chronological order	Past	→	→	Present
Dust generation	Chipping	○	○	○
Heat resistance	○	Thermal deformation	Fiber embrittlement (Affected by temperature/atmosphere)	○
Installability	Heavy weight	On-site fabrication workload	Sewing workload	○

Refractory type	Firebricks	Inner metal plates	Alumina cloth	Shotless CF
Furnace wall configuration (Example)	Firebrick: 230 mm Insulating board: 20 mm	SUS inner plate: 1 mm CF: 250 mm	Alumina cloth: 0.5 mm CF: 250 mm	Shotless CF: 10 mm CF: 240 mm
Heat flux / $W \cdot m^{-2}$	700	400	400	400
Heat storage/ $W \cdot m^{-2}$	65,000	19,000	17,000	16,000

○: Good

4. Shotless Ceramic Fiber (CF)

Figure 1 shows CF fibers and shot. CF is a man-made inorganic mineral fiber produced through a fiberization process. During the fiberization stage of the melt in the manufacturing process, not all of the molten material is drawn into fibrous form; some unfiberized material remains as spherical or granular particles. These non-fibrous particles that fail to form fibers, or fibers that break during the fiberization process and become shortened, are generally referred to as “shot.”

CF is broadly classified into amorphous and crystalline types. Crystalline CF includes alumina fiber (hereinafter referred to as AF) with a maximum service temperature of 1600°C, while amorphous CF includes refractory ceramic fiber (hereinafter referred to as RCF) with a maximum service temperature of 1260–1500°C. Alumina fiber consists primarily of alumina and possesses high chemical stability and heat resistance.

Figure 2 shows a schematic of the AF fiberization process. AF is produced using a method known as the precursor method (sol-gel method). The spinning solution is prepared using a solution of aluminum-bearing salts as the primary raw material, to which an aqueous solution containing silicon and an organic polymer as a viscosity modifier are added; the mixture is then concentrated under reduced pressure. Subsequently, after adjusting the solution to a viscosity suitable for fiberization, it is spun as a precursor (inorganic polymer) in a chamber controlled at constant temperature and humidity, then drawn and dried to form precursor fibers. These fibers are then calcined in a furnace at 900–1200°C to remove water and organic components and crystallized to obtain the final fibers. This manufacturing method achieves a high fiberization rate, making it possible to suppress shot generation.



Fig. 1 Appearance of CF fiber and shot

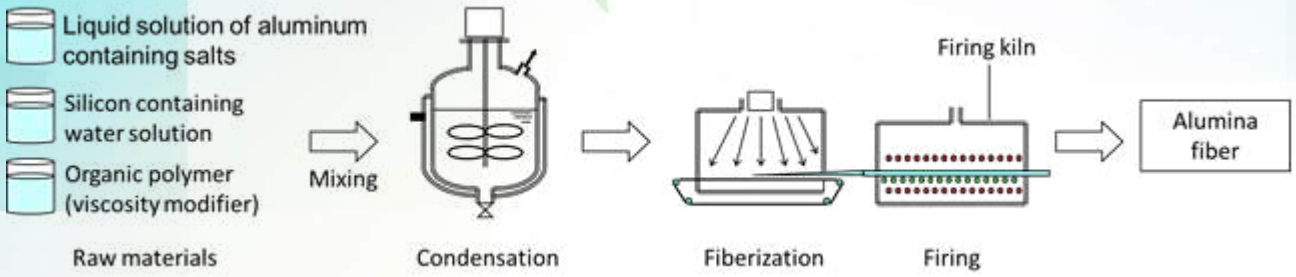


Fig. 2 Fiberization flow of the sol-gel process

5. Installation Methods

5.1 Lap Lining Method

Figure 3(a) shows a schematic of the lap lining method. The lap lining method is a type of paper-lining technique in which blanket-shaped CF is laminated parallel to the furnace steel shell. By overlapping both ends of the CF blankets at the furnace inner-surface layer, dust from the underlying insulating materials can be prevented from entering the furnace. Shotless CF is selected for the inner-surface layer, while various insulating materials can be selected for the inner layers based on their temperature limits and thermal insulation performance

5.2 Block Lining Method

Figure 3(b) shows a schematic of the block lining method. The block lining method uses block products in which CF is modularized into a cubic shape. Supporting anchors are embedded in the center of the block on the steel-shell side, and the blocks are fixed by attaching them to anchors welded to the steel shell. Because the supporting anchors are located on the steel-shell side and are not exposed to the furnace inner surface, heat transfer through the anchors can be suppressed. Since the block products are installed in a compressed state, they push against each other due to their resilient recovery after installation and during operation. This structure suppresses joint opening caused by volumetric shrinkage due to degradation over time. By forming shotless CF into blocks, a structure can be achieved that suppresses dust while simultaneously minimizing heat transfer from the supporting anchors.

(a) Paper lining method (Lap lining) **(b) Block lining method**

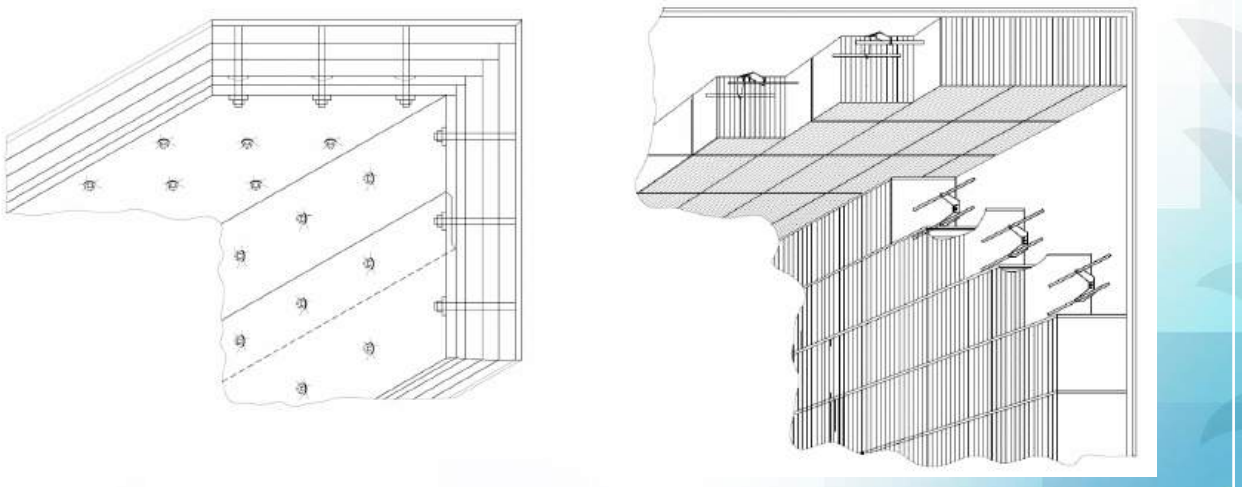


Fig. 3 Schematics of each installation method

6. Conclusions

This paper introduced a lining technology using shotless ceramic fiber (CF) and described its usefulness in maintaining steel strip product quality by suppressing dust while reducing installation workload and addressing long-term degradation issues in cold rolling mills.

1. Maintenance of Furnace Cleanliness and Improvement of Steel Strip Surface Quality

In cold-rolling heat treatment furnaces, dust generated from refractories becomes trapped between the steel strips and rolls, inducing surface defects such as scratches. To manufacture high-quality steel strips, it is essential to suppress dust generation and maintain a high level of cleanliness inside the furnace.

2. Superiority of Shotless CF

Conventional materials, including firebricks, have posed challenges regarding dust generation, installability, and heat resistance. Crystalline alumina fiber (AF) manufactured by the precursor method (sol-gel method) generates very little shot because of its high fiberization rate. This material is expected to address these conventional challenges while maintaining both energy-saving performance and dust suppression.

3. Optimization of Thermal Insulation and Dust Prevention through Lining Methods

The lap lining method, which overlaps blankets, can suppress the penetration of dust from underlying insulating materials into the furnace. Meanwhile, the modularized block lining method enables a structure that suppresses dust while simultaneously minimizing heat transfer from the supporting anchors.

It is expected that the implementation of this technology will contribute to improving steel strip quality, reducing repair costs, and further improving ease of maintenance in future cold rolling facilities.

APPLICATION OF CERAMIC FIBER IN REHEATING FURNACES AND ITS CONTRIBUTION TO CARBON NEUTRALITY

Shinsuke SUETAKE, Takayuki KANEKO
Isolite Insulating Products Co., Ltd.

Corresponding author's e-mail: t-kaneko@isolite.co.jp

Abstract

This paper describes recent applications of ceramic fiber (CF), particularly crystalline alumina fiber, to furnace walls (roofs and sidewalls), partition walls, skids, and burner walls of reheating furnaces. Compared with castable refractories widely used in the past, CF offers superior thermal insulation, with approximately one-fifth the density and one-third the thermal conductivity. Its excellent thermal shock resistance also helps prevent cracking and spalling under rapid temperature changes. In addition, the reduced number of anchors and formwork-free construction methods shorten installation periods and maximize equipment operating time (high availability). CF applications are described for furnace roofs, roof partition walls, skid pipe sections, and burner walls. The application of high-quality CF products represents an indispensable solution and can make a major contribution toward achieving a carbon-neutral society, an urgent challenge for industry.

Keywords: Steelmaking, Insulating Materials, Ceramic Fiber, Energy Saving

1. Introduction

In steel manufacturing, a reheating furnace is heating equipment used to heat steel slabs (semi-finished products obtained by casting) before they are rolled into thinner products. Slabs are conveyed through the furnace, which is maintained at a specified temperature by burner heating, and are then sent to the rolling equipment while red-hot. The walking-beam method is widely used for slab transport. In this method, moving and fixed beams alternately support and convey the slabs through repeated cycles of lifting, horizontal movement, lowering, and horizontal return to the initial position. This method helps prevent surface damage to the slabs.

Reheating furnace operating temperatures range widely, from relatively low temperatures of around 900°C to high temperatures exceeding 1300°C. During repairs, mist cooling is used to reduce the furnace temperature to ambient temperature. These large temperature fluctuations create severe conditions in which thermal spalling (cracking or peeling caused by thermal shock) can readily occur. Scale attack also occurs through chemical reactions with iron oxides such as FeO formed by oxidation of the slab surface, creating harsh conditions for the refractories. Furthermore, reducing heat loss from reheating furnaces as much as possible is extremely important for achieving carbon neutrality and requires improved thermal insulation.

2. Changes in Japanese Reheating Furnaces and Characteristics of CF

During the 1960s and 1970s, when many continuous reheating furnaces were constructed in Japan, refractory bricks were mainly used as lining refractories. Plastic refractories and refractory castables (unshaped refractories) came into use in the 1970s, and since the 1980s, efforts have continued to replace castable refractories with CF in various furnace sections for energy savings.

Table 1 shows the types of CF. CF is broadly classified into amorphous and crystalline types; the amorphous type is refractory

ceramic fiber (RCF), with maximum service temperatures of 1260-1500°C, while crystalline alumina fiber (AF) has a maximum service temperature of 1600°C. Both RCF and AF have been used since the early stages of CF application in reheating furnaces, but their roles have changed over time. Following the 2015 revision of the Industrial Safety and Health Act in Japan, RCF was designated as a Class 2 Specified Chemical Substance under the Ordinance on Prevention of Hazards Due to Specified Chemical Substances, and safer AF has since become the mainstream choice.

Table 1 Types of CF

Types of fibers		**RCF**	**AF**
Crystal system		amorphous	crystalline
Temperature grade (°C)		1260, 1400, 1500	1600
Chemical composition (wt%)	Al_2O_3	40-60	72
	SiO2	40-60	28
	Others	0-15	-

3. Application of CF in Reheating Furnaces

Table 2 shows the characteristics of various refractories. Because CF has a lower density and lower thermal conductivity than castable refractories, it stores less heat. Consequently, reductions in heat dissipation and heat-storage losses have proven effective for energy savings in various reheating furnaces. However, CF has lower mechanical strength and scale resistance than castable refractories.

Fig. 1 shows an outline of a reheating furnace. The furnace is divided into zones along its length from the charging side - preheating zone, heating zone, and soaking zone - each with different operating conditions. The preheating zone has a lower maximum temperature and lower combustion rate, whereas the heating and soaking zones experience heavier thermal loads. Examples of selection criteria include operating temperature, combustion rate, furnace pressure, exhaust gas, scale, and equipment vibration.

Because the loads on the refractories, energy-saving effects, and effects on steel slabs differ by location within the furnace, it is important to understand the conditions at each installation location and to design refractory materials and structures that maintain the required performance. Four main sections are described: (1) furnace walls (roof/sidewalls), (2) roof partition walls, (3) skids, and (4) burner walls.

Table 2 Types of Refractories

Refractory Type	Refractory Castable	Insulating Castable	CF	CF
Product Form	Monolithic	Monolithic	Blanket / Block	Vacuum-formed shape
Bulk Density (kg/m³)	2000-3000	1000-2000	100-200	200-300
Thermal Conductivity [W/(m·K)] at 1000°C	1.0	0.5	0.4	0.3
Insulation Performance	-	+	++	+++
Mechanical Strength	+++	+++	+	++
Scale Resistance	+++	+++	+	++

+++: Excellent, ++: Good, +: Average, -: Not applicable

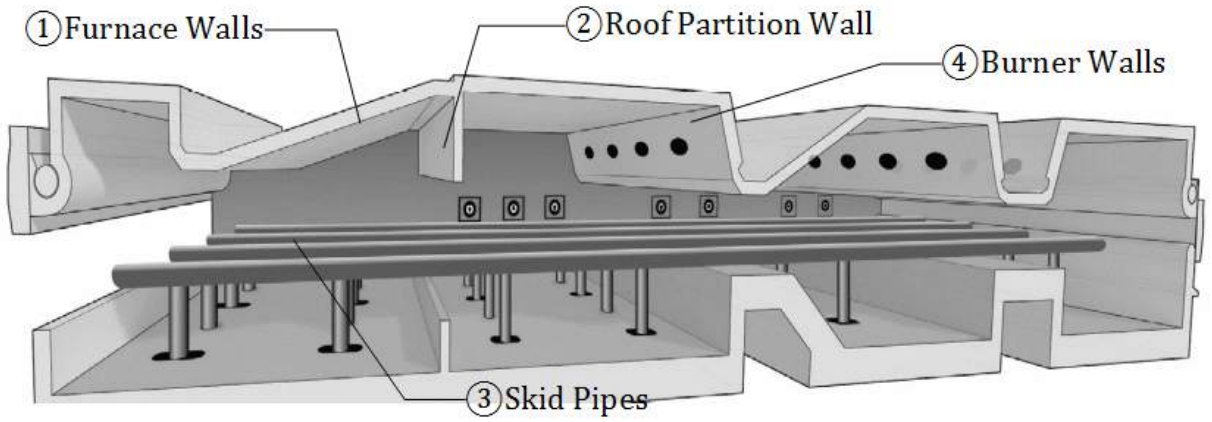


Figure 1 Furnace Sections

3.1 Furnace Walls (Roof / Sidewalls)

Furnace walls have the largest refractory heat-receiving surface area and volume in the furnace, so significant energy-saving effects can be expected. Cube-shaped modular CF block products are predominantly used for furnace walls.

Fig. 2 shows the appearance of a block product. The block product contains internal support anchors at the center of its cold face and is attached to anchors welded to the steel shell. Because the support anchors are not exposed to the furnace interior, heat transfer can be suppressed.

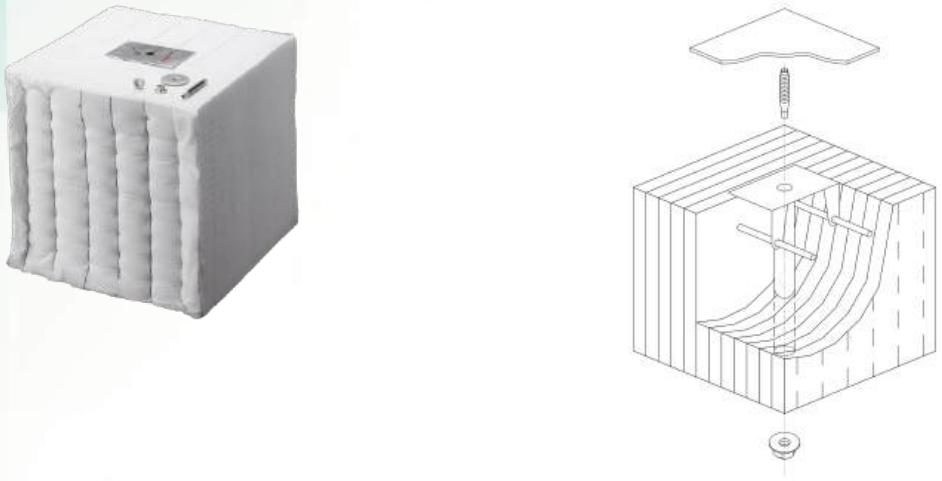


Figure 2 Structure and appearance of CF block product

Table 3 shows the results of steady-state heat-transfer calculations. Replacing refractory castables with CF block products is expected to reduce heat flux by about 20% and heat storage by about 92%. In actual furnaces, results differ from the calculations because of equipment specifications and operating conditions, but the performance has been demonstrated in many reheating furnaces in Japan.

Table 3 Steady-State Heat Transfer Calculation Results

	Refractory Castable Structure	CF Structure	Reduction (%)
Heat Flux (W/m^2)	1000	800	20
Heat Storage (MJ/m^2)	780	60	92

3.2 Roof Partition Walls

Roof partition walls separate zones with different operating conditions (preheating, heating, and soaking zones). Key environmental factors include (1) high thermal loads because three surfaces receive heat, and (2) direct contact with steel slabs during operational problems. Castable refractories were conventionally used with water-cooling systems to lower the temperature of the metallic anchors supporting the castables. This resulted in heat loss through the cooling water and unplanned repairs due to water leaks.

The CF products used for roof partition walls have the same structure as the CF block products described in Section 3.1 but are manufactured in elongated shapes. Because CF block products are lighter than castable refractories, water cooling for the support anchors is unnecessary, reducing heat loss and eliminating water-leak problems. However, stable operation is necessary because contact with steel slabs can cause damage.

3.3 Skid Pipes

Skid pipes support and transport steel slabs inside walking-beam reheating furnaces. They consist of heat-resistant steel pipes through which cooling water flows, with the outside protected by refractories. As with partition walls, heat is lost through the cooling water, and in some locations the pipes are close to burner flames, leading to damage from thermal spalling and equipment vibration. Skid pipes play a critical role in slab transport; if refractory damage exposes the pipe surface to the furnace interior, the pipe can soften, creating a major risk of an emergency plant shutdown.

Fig. 3 illustrates two CF installation methods: (a) vacuum-formed shape structures and (b) blanket structures. Vacuum-formed structures use semi-cylindrical CF products stacked in tiers, while blanket structures are installed by wrapping blanket-shaped CF products around the pipes with wire. Vacuum-formed structures require no welding to the water-cooled pipes, reducing heat transfer through support fixtures, suppressing deterioration and related problems in the pipes, and shortening installation time.

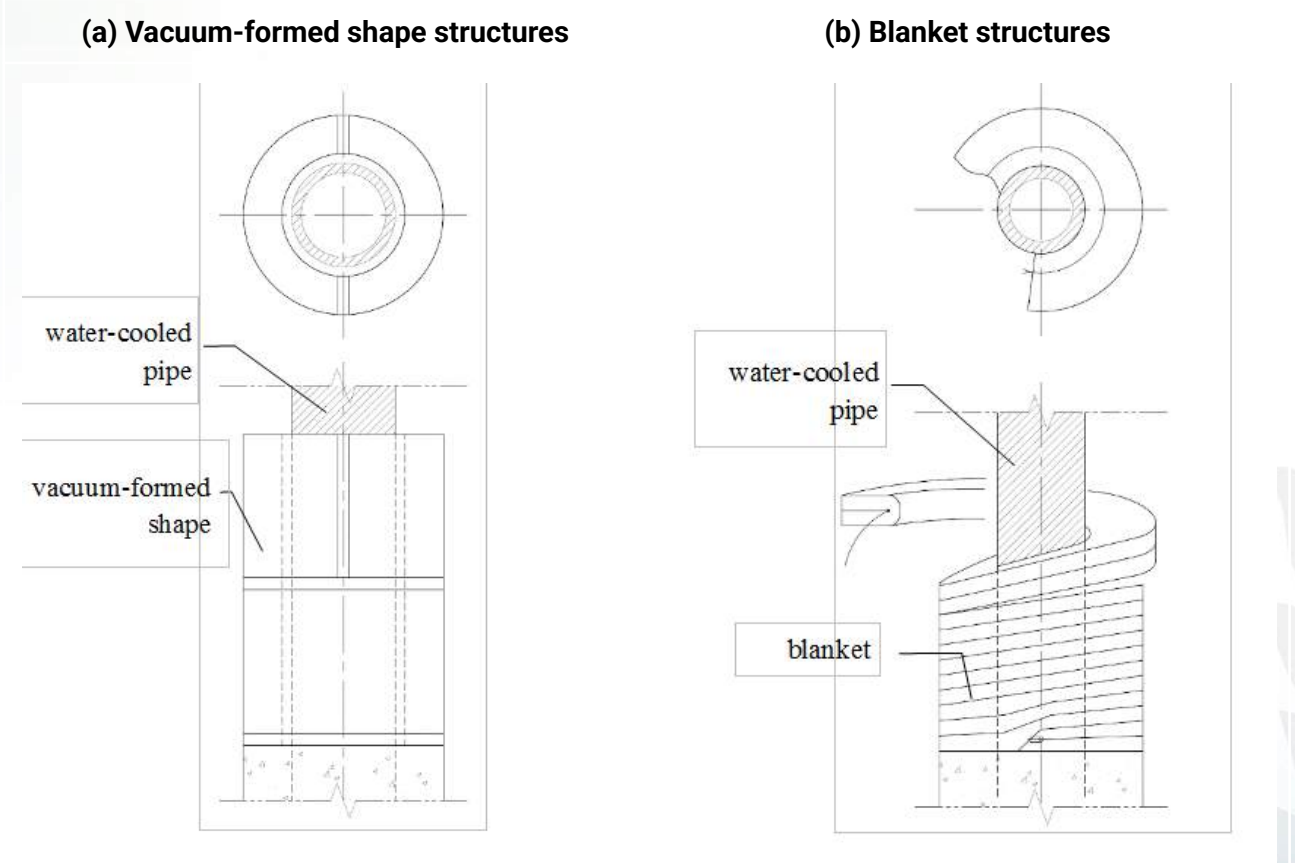


Figure 3 CF installation methods for skid pipes

3.4 Burner Walls

Burner walls refer to areas surrounding burners on roofs and sidewalls. Dense castable refractories are typically used here because high levels of heat resistance, thermal shock resistance, and resistance to high-velocity gas flow are required. Replacing them with CF products lowers thermal capacity and provides energy-saving benefits. Methods to improve resistance to high-velocity gas flow include the use of surface coatings or high-density CF blocks. Meanwhile, highly energy-efficient regenerative burners have higher gas velocities during heat recovery than

conventional burners, raising concerns about localized damage to CF blocks. When resistance to high-velocity gas flow is required for regenerative burners, installing a thin, high-density CF product at the hot-face layer reduces block wear while maintaining thermal insulation.

4. Conclusions

This paper presented CF applications in Japanese reheating furnaces by furnace section. In addition to direct energy-saving benefits, secondary advantages have also been achieved: the use of high-performance materials and efficient construction methods shortens installation periods and maximizes equipment operating time (improving productivity).

Going forward, optimization will continue by analyzing and evaluating individual factors in each furnace section while ensuring proper equipment maintenance.

BAUXITE–ZIRCON CASTABLE FOR ALUMINUM APPLICATIONS: NUMERICAL ANALYSIS OF RAPID DRYING BEHAVIOR

Hirotaka Goto and Kazuaki Komiya
Calderys Japan, Toyota city, Aichi, JAPAN

Corresponding author's e-mail: hirotaka.goto@calderys.com

Abstract

Calderys has created another fast-dry (FD) solution that enables a safe and short drying process without compromising physical properties. For aluminum refractory applications, a densely packed zircon matrix is desirable to prevent wetting and metal penetration. However, achieving both fast drying capability and a zircon including dense microstructure has been considered challenging.This work contributes to the development of a fast-dryable zircon-containing castable for aluminum smelting furnaces using the fast-dry solution. Moisture vaporized from the hydraulic bonding system within the castable matrix must be released to air at an appropriate rate, otherwise, destructive spalling occurs.A numerical calculation incorporating heat transfer, mass transfer, and pressure equations was implemented on an open-source platform to visualize moisture migration and vapor pressure distribution in an industrial-scale lining exceeds 200 mm in thickness.Therefore, consideration of vapor release from the dense zircon matrix is necessary before applying the fast-drying installation procedures.

Keywords: Aluminum refractory, Numerical analysis, Simulated drying behavior.

1. Introduction

Recent commodity price increases, including fuel costs, have imposed a heavy economic burden on small and medium-sized enterprises. In Japan, the enterprises play an essential role in aluminum recycling by melting scrap and promoting aluminum material circulation. Calderys provides fast-dryable monolithic refractory that enable shorter drying times without compromising lining lifetime, helping to reduce overall maintenance costs[1]-[4].

Refractory manufacturers provide fast-heating castable products to significantly reduce fossil fuel consumption and carbon emissions. In general, these products do not contain microsilica which typically improves abrasion resistance. Hence, they can achieve rapid heating acceptance but often at the expense of long-term durability.No-cement castables use silicate-, phosphate-, or gel-based bonding systems to form self-binding structures.Since moisture is not structurally bound within the crystalline matrix, it can be readily removed during the initial heating stage. Owing to this characteristic, no-cement castable exhibits favorable drying behavior. However, their installation typically requires the addition of a separate binder during mixing.

With leveraging computational simulations, reliable numerical calculations using finite-element methods are performed with Python tools like Jupyter Notebook, NumPy, and Matplotlib[5][6]. These calculations simulate moisture removal from castable under pore-pressure model during industrial scale drying out.

The pore-pressure model describes the development of open pores with dehydration in castable, it represents heat and mass transfer on coupled differential equations[7]-[10]. These equations are solved sequentially to evaluate temperature, air and vapor pressure at each element.

This study examines two materials distinguished by whether adapted the FD solution. Physical strength was assessed after drying, and fracture energy and stress were estimated. The pore-pressure model, grounded in coupled mass and energy conservation equations, elucidates pressure build-up during rapid heating. The numerical approach enhances analysis by indicating peak pressures and optimizing drying

schedules, both of which depend on denseness of matrix and thermal conductivity.

2. Experimental

2.1 Mix design and property measurement

For the comparison, we prepared a conventional bauxite-zircon low cement castable (LCC) as well as an FDimplemented formula. The mixes are compiled in Table 1.Kneading with water, the mix is casted in JIS specification shape (40×40×160 mm3), then cured for 24 hours in 90 %RH environment at 20 °C. After demolding, the samples are dried out at 110 °C, then cold crushing strength (CCS) is measured. For gas permeability measurement, the 50 mm diameter specimen is cast. It is dried out at 110 °C for 24 hours, then cut top and bottom into exact 50 mm-height. The permeability measurement is performed, following JIS R 2115. The flow rate of nitrogen gas is recorded when the sample gets 10, 20 and 30 kPa differential pressure.

Explosive spalling induced by pressure build-up occurs under tensile stressing environment[11]. Brittle fracture is modeled by the release of elastic strain energy at the crack edge[12]. The energy required to propagate the crack, known as fracture energy, can be quantified using mechanical strength[13].

Material (wt%)	FD	LCC
Bauxite	58	58
Zircon	30	30
70 %CAC	6	6
Calcined alumina, micro silica, anti-wetting agent	6	6
FD implementation	Yes	No
Water addition	4.8	4.8

Table 1 Mixing design for the measurement

2.2 Numerical modeling

The coupled differential equations governing heat and mass transfer in porous materials are formulated based on fundamental principles of mass and energy conservation, as detailed in references[7]-[10]. Mass migration is modeled using Darcy's law.

One-dimensional elements, representing monolayer lining up to 360 mm thick, were employed with spatial and temporal steps of 2 mm and 0.25 seconds, respectively. Boundary conditions included ambient pressure of 0.1 MPa at the outer surface and gas permeability of 10-14 m2 not to hinder vapor release.

As material parameters, thermal conductivity and gas permeability influence the maximum pore pressure. This simulation reveals the extent of pressure build-up during rapid heating, offering insight into the mechanisms driving explosive spalling in refractory materials under given aheating schedule.

The vapor pressure build-up model, incorporating moisture migration, is based on pore-pressure theory and was implemented in Python using NumPy.In the simulation, a lateral surface of the specimen were exposed to thermal loading ata heating rate of 60 °C/h from 30 °C to 700 °C. Matplotlib was used for

post-processing to visualize pressure distribution, moisture migration, and the drying front, and to animate the simulation results.

3. Result and discussion

The physical properties of the specimens after drying at 110 °C are summarized in Table 2. CCS value was160 MPa for both, also MoR value was 11 MPa, bulk density was 3.10. Measured value of gas permeability was 18 and 3×10-16 m2, respectively.

Calculate fracture stress from CCS and fracture energy using Glifiths equation. Brittle fracture is characterized by the release of elastic strain energy at crack tips, with the required fracture energy quantifiable through measurable mechanical strength. For concrete, fracture energy Gf can be estimated using the maximum aggregate diameter dmax and cold crushing strength f'ck, as shown in Eq.(1)[13]. Since explosive spalling occurs during drying at relatively low temperatures without mineral phase transformation, this estimation is suitable for the present analysis.

$$G_f = 10 d_{\max}^{1/3} f'^{1/3}_{ck} / 1000 \quad (1)$$

$$\sigma_C = \sqrt{2 G_f E / \pi c} \quad (2)$$

Table 2 presents the fracture energy, which can be converted to fracture stress using Eq.(2) based on Griffith's theory[12]. This conversion requires the Young's modulus E and the characteristic defect size c. In this analysis, typical values are assumed: E=80 GPa for LCC, with a defect size of $2c$=3 mm representing gas bubbles. Fracture propagation is driven by pressure build-up, as vaporization and insufficient vapor diffusion causes within the refractory matrix.

	FD	LCC
CCS (MPa)	160	160
Bulk density	3.10	3.10
Permeability (10^{-16} m^2)	18	3
Young's modulus (GPa)	80	80
Max. grain (mm)	6	6
Size of defect (mm)	3	3
Fracture energy (N/m)	0.099	0.099
Fracture stress (MPa)	1.8	1.8

Table 2 Physical property after drying at 110 °C

Before estimating pressure build-up behavior, intrinsic material parameters shown in Figure 1 should be considered. The upper part, water desorption and apparent porosity increasemonotonically withtemperature, and are assumed to be identical for both FD and LCC.The third parameter,thermal conductivity, is determined from the chemical composition and bulk density according to Routschka model[14].

Dewatering of refractory castable proceeds in three stages. The first stage (30-150 °C), prior to free water evaporation, exhibits high thermal conductivity due to water-filled open porosity. The second stage (150-300 °C) involves free water vaporization and hydrate decomposition, during which thermal conductivity decreases as liquid moisture is removed. After the transition stage, thermal conductivity stabilizes at the dried Routschka value.

Permeability increases as physically and chemically bound water is released, reaching 3×10^{-15} m^2.In the FD formulation, a permeable pore network develops with a relatively low heat input compared with the LCC.

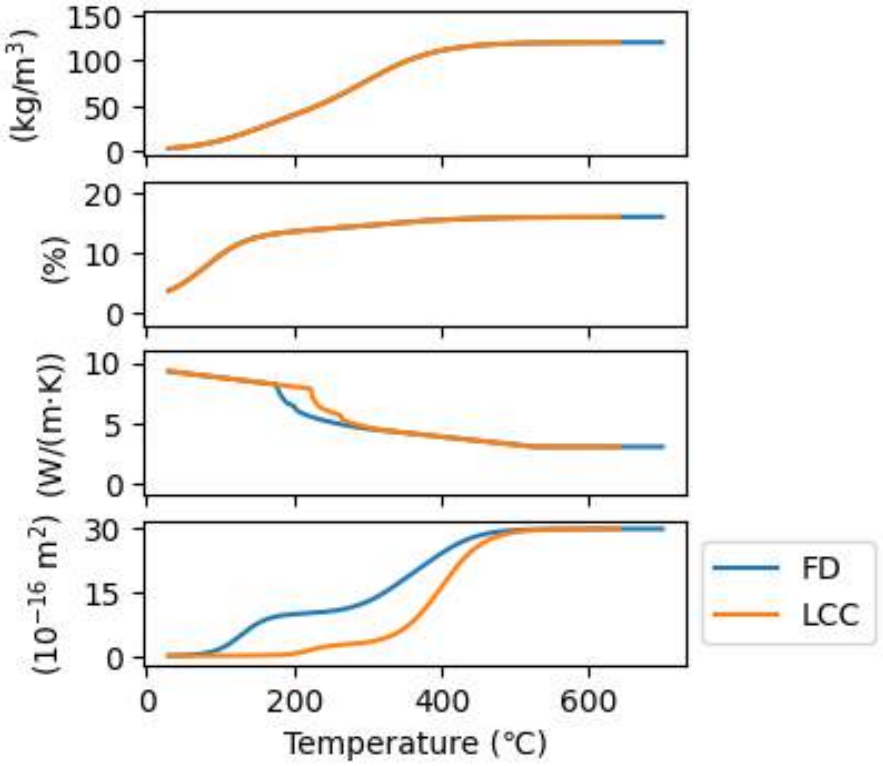


Figure 1Intrinsic material parameters: water desorption, apparent porosity, thermal conductivity, and gas permeability (from top to bottom)

Using these parameters, pressure build-up was simulated with the pore-pressure model.The model describes open-pore development during dehydration through three coupled equations governing heat and mass transfer. The computational simulations implemented with Python tools, provided visualizations of pressure evolution, moisture migration, and drying front progression.

Figure 2 displays the simulated temperature and pressure profiles for a 120 mm-thick specimen. The red lines indicate calculated fracture stress, and the legend digits note the depth from the heated surface in mm. The heating rate applied at the hot face was 60 °C/h to emphasize the differences between FD and LCC results. The selected thickness and heating rate are comparable to those used in previous researches.For the LCC, the simulation produced pressure profiles, shape and peak pressure,close to those reported in the literatures.

At a depth of 60 mm in the LCC, the pressure surpassed the fracture stress of 1.8 MPa, 4.4 hours after onset of heating. The corresponding temperature at the position was 205 °C. This is in good agreement with the previous explosive spalling cases.

The temperature profile displayed an inflection point near 200 °C, corresponding to the vaporization of physically bound water. At

this stage, thermal energy is consumed by the vaporization of physically bound water, including moisture migrating from adjacent cells, resulting in simultaneous pressure build-up.

Animated visualization of water distribution revealed the drying front advancing inward from the surface, providing insights into moisture migration and spalling mechanisms. The FD specimen exhibited temperature and pressure profiles similar to those of the LCC. However, owing to its high permeability, pressure was effectively mitigated, the peak pressure remained below 1.0 MPa.

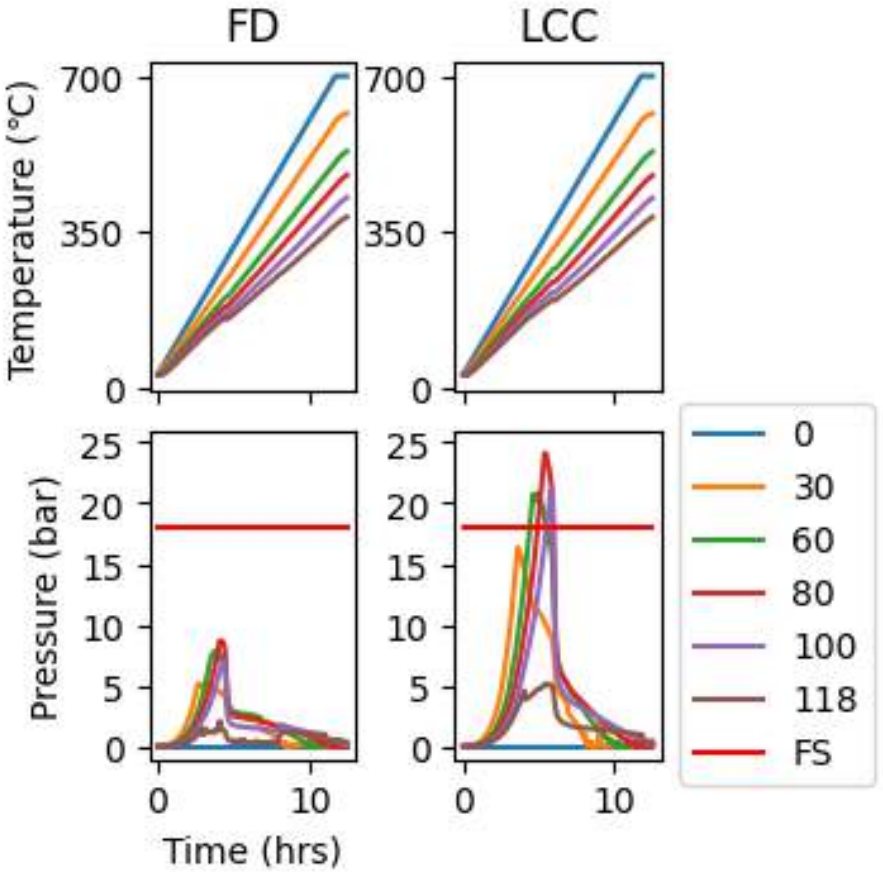


Figure 2 Calculated pressure build-up for FD and LCC specimens

The relationship between lining thickness and maximum pressure is summarized in Figure 3. The top and middle plots show temporal evolution of the maximum pressure within the entire lining, and the depth at which this maximum pressure occurs, respectively. The bottom plot shows the temperature at the location of the maximum pressure.The maximum pressure and the migration distance increase with lining thickness. However, the calculated pressure did not exceed the fracture stress of 1.8 MPa for any FD lining considered in this study. Although not shown in the figure, the maximum pressure calculated for the LCC exceeded this value, even for a lining thickness of 60 mm.

The pressure, position, and temperature curves followed similar trends regardless of lining thickness. In all FD calculations, the maximum pressure occurred at a temperature of approximately 178°C. For the LCC, although the curves exhibited a similar shape, the temperature converged to approximately 221°C.

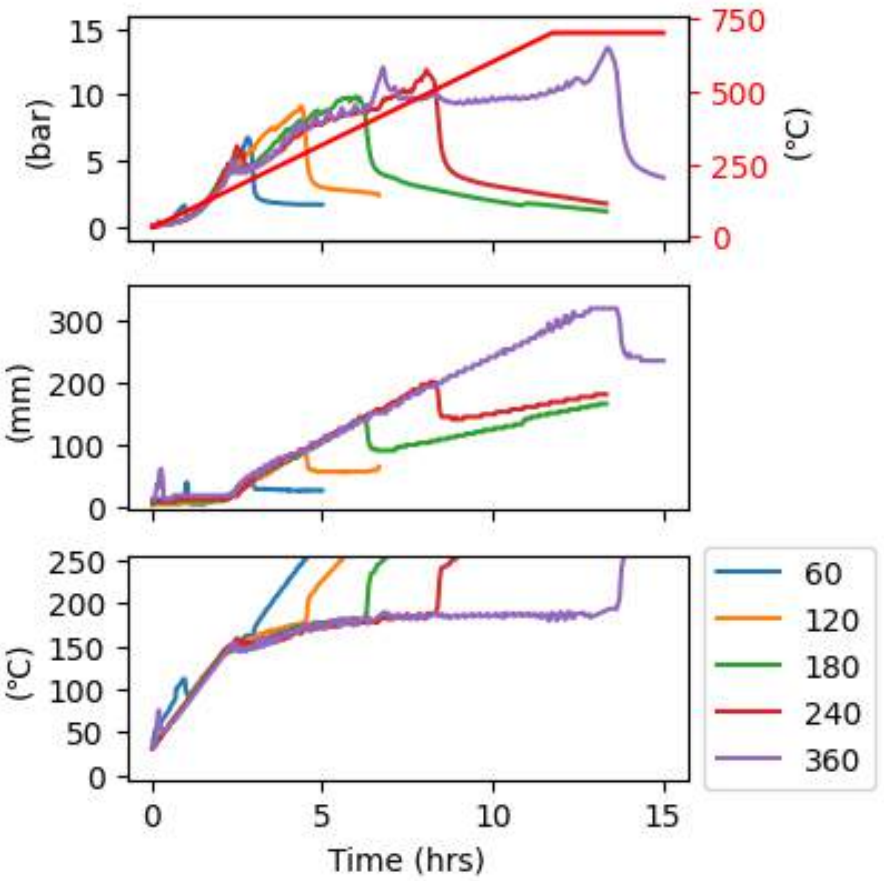


Figure 3 Maximum pressure, its position, and the temperature at which it occurs; red line in the upper indicates hot face temperature

The migration of the drying front is related to this converge behavior. Figure4presentsthe distributions of temperature, vapor pressure, water saturation in a 240 mm-thick lining. As the hot face temperature increases, vapor pressure progressively builds up within the lining. The bottom plot shows the water saturation, expressed as the mass of liquid water per unit volume, kg/m3. Immediately beneath the pressure peak, water saturation decreases sharply. This front migrates away from the hot face and corresponds to the liquid-vapor equilibrium interface, which is governed by vapor pressure and gas permeability.For the FD, the peak pressure reaches 9.58 bar at 178 °C, whereas for the LCC, it is 23.67 bar at 221°C. The values are consistent with saturation pressure predicted by Antonie equation. In the LCC, the pressure peak occurs at a temperatureapproximately 40° C higher than that of the FD, owing to its low permeability.

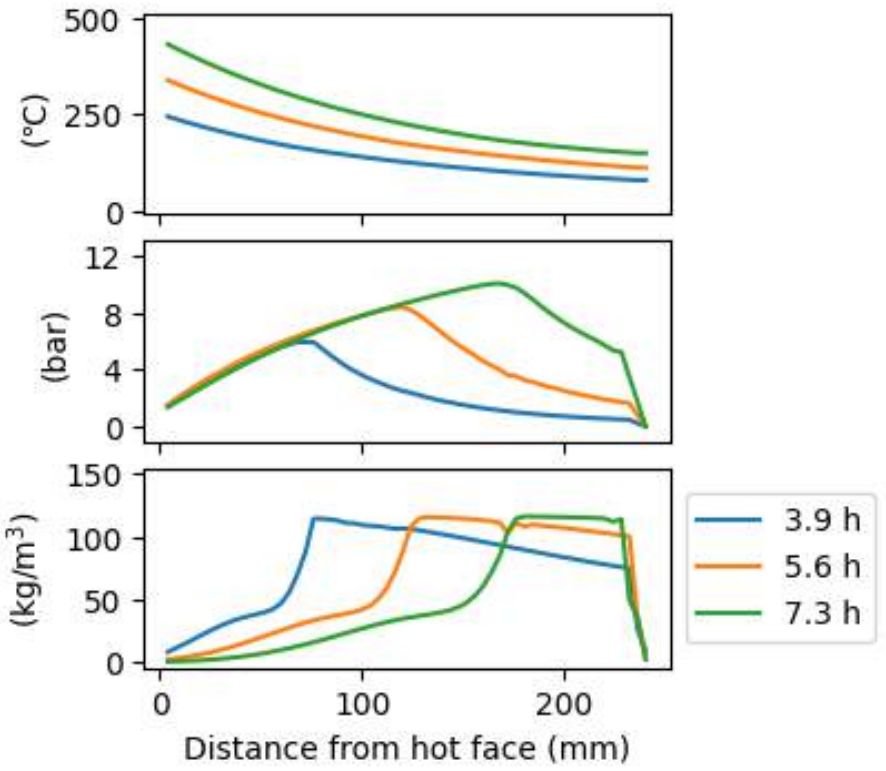


Figure 4 Distributions of temperature, vapor pressure, water saturation in 240 mm-thick FD lining

Figure 5 provides a detailed visualization of moisture transport. It compares the volume fractions of the vapor and liquid phases, together with their migration velocities, immediately before and after the reach of the pressure peak. The results are shown for a location 120 mm below the hot face in a 240 mm-thick lining.As shown in the middle plots, the volume fractions of the liquid and vapor phases undergo a reversal at that moment when the pressure peak appears.

At the beginning of heating, open porosity is filled with liquid water. As the temperature increase, additional porosity develops within the lining, reaching 14 vol% at around 200 °C(Figure 1).To fill the created pore, liquid water migrates from colder interior toward the heating side. In the bottom graph, negative and positive velocities denote transportation toward the hot and cold face, respectively.Prior to the pressure peaking event, liquid water migrates toward the hot face, whereas water vapor moves in the opposite direction to occupy the pore space vacated by the liquid phase.After the pressure peak is reached, the direction of vapor transport reverses and becomes oriented toward the hot face. Simultaneously, the liquid transport becomes negligible as physically bound water is fully vaporized. Therefore, low-temperature moisture release is critical for minimizing pressure build-up.

At the time of the peak pressure, the vapor migration velocity in the FD reached +2.1 mm/s at 178°C, which is approximately 5 times higher than that in the LCC at 221°C. The liquidwater velocity in the FD was -0.022 mm/s, about 10 times greater than that of the LCC. The superior permeability of the FD lining promotes both vapor release and liquid water transport, thereby mitigating pressure build-up and reducing the risk of destructive spalling.

In general, increasinggas permeabilitypromotesthe formation of higherdensity of microcracks, whichoften significant reduction in mechanical strength of refractory material.The cracks allow penetration of low surface tension liquid,such as molten aluminum, thereby compromising corrosion resistance. To evaluate the corrosion resistance of the FD formulation,a crucible test using A5083 aluminum (Al-Mg) alloy at 900 °C had been taken for 96 hours.The crucible exhibited neither corundum formation nor silica contamination of the alloy.

Without compromises for mechanical strength oranti-wetting performance, Caldery's FD solution provides the

bauxite-zircon dry mix for specifically designed for rapid dry-out applications.TheFD bauxite-zircon castable had already installed in an aluminum open well furnace with a thickness of 200 mm, then the first drying out reaching 700 °C was successfully completed within 18 hours.

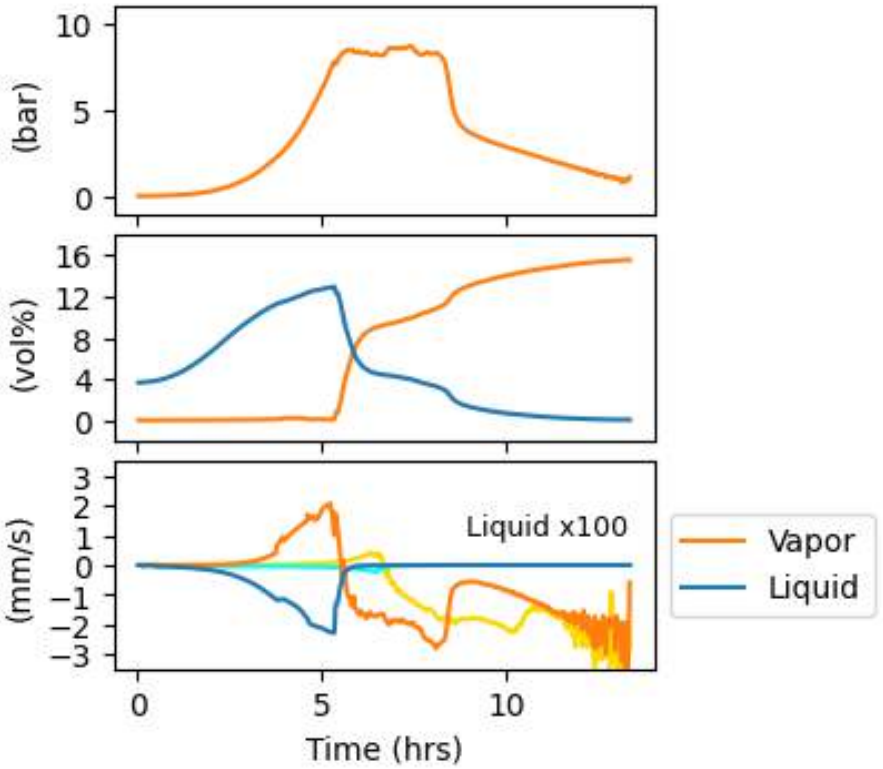


Figure 5 Pressure, volume fraction and velocity profiles at depth of 120 mm in 240 mm-thickFD lining; the lighter-colored curves in the bottom plot represent the LCC

4. Conclusions

This report investigates pressure build-up in industrial scale linings and evaluates fracture risk by comparing FD solution with LCC. It reveals temperature and internal pressure dynamics during rapid heating at 60 °C/h.This study also proposes moisture removal computations to assess the impact of the FD solution. The drying front temperature, corresponding to the liquid-vapor equilibrium interface, remained nearly constant at 180 ° C regardless of lining thickness. Gas permeability was identified as a key parameter governing the drying front temperature and influencing vapor and liquid transport velocities were 5 to 10 times higher than in LCC, and their effect on pressure build-up was quantitatively evaluated.

Calderys offers a wide range of monolithic products designed to reduce energy consumption and minimize environmental impact during the drying-out process, including CALDE® SOL CAST, Quick Dry (QD), SteadyDry (SD) and Fast Dry (FD).

Acknowledgement

We would like to express appreciation to our advisors, Bruno Touzo, Global Vice President of Calderys, Innovation&Technology, also Saumen Sinha, Calderys India, Jong-Won Shin and Uwe Klippel, Calderys Deutschland, for their support throughout the summarization process.

References

[1] B. Touzo, China's Refractories 33 [3], 30-36, (2024).
[2] U. Klippel, China's Refractories 24, 51-56, (2015).
[3] U. Klippel, Proc. UNITECR, Frankfurt, GERMANY, 215-218 (2023).
[4] https://calderys.com/sites/default/files/2025-01/PR_Calde%20Fast%20Dry_ENG_01162025.pdf
[5] E.T. Oliphant, Comput. Sci. Eng. 9 [3], 10-20, (2007).
[6] R. Landau, "Computational Physics: Problem Solving with Python 3rd Edition", Wiley-VCH, (2015).
[7] Z.B. Bazant and W. Thonguthai, Magazine of Concrete Research 31 [107], 67-76, (1979).
[8] R.T. Tenchev, Numer. Heat Transf. 39, 685-710, (2001).
[9] C.T. Davie, Numer. Heat Transf. Part A: Applications, 49 [8], 733-763, (2006).
[10] K.G. Fey, International Journal of Thermal Sciences 100, 108-125, (2016).
[11] Technical Association of Refractories, Japan, "Refractories handbook 12th edition", (2015).
[12] A.A. Griffith, Phil. Trans. Roy. Soc. A221, 163-198, (1921).
[13] Japan Society of Civil Engineers, "Standard Specifi-cations for Concrete Structures-2007, Design", (2010).
[14] G. Routschka, Interceram 37 [3], 24–33, (1988).

DEVELOPMENT OF A PLASTIC GUNNING MIX: A UNIQUE SYSTEM FOR MECHANIZED APPLICATION

Rajesh Bisen, Santosh Upadhyay and Dr. Saumen Sinha

Calderys India Refractories Limited, Nagpur

Abstract

Phosphate-bonded refractory plastics, preferred for 800°C–1400°C service, are conventionally installed by pneumatic ramming — a labour-intensive process demanding skilled manpower and extended furnace downtime. This paper presents the development and validation of Plastic Gunning 70P, a 70% alumina-based plastic mix for mechanized installation using a purpose-built rotary-wheel gunning machine. The formulation maintains stable Workability Index (17–23) over 180 days, substantially outperforming conventional rammed plastic which exits its usable window between 90 and 120 days. Comparative testing (IS 10570) confirms superior bulk density across all temperatures and near-equivalent CCS at 815°C and 1200°C. Thermomechanical properties are characterized across 260°C–1400°C per IS 10570 and EN 1927 Part 6. Gunning trials confirmed ~14% rebound loss and defect-free consolidation. Gunned panel CCS remains within 4% of lab-moulded values at 1400°C, establishing the viability of mechanized plastic installation for reheating furnaces, aluminium furnaces, and allied applications.

Keywords: Plastic refractory, mechanized installation, phosphate bond, reheating furnace.

1. Introduction

Refractory plastics occupy a distinctive niche in monolithic refractories, combining forming flexibility with the thermomechanical performance of dense phosphate-bonded systems. Their preferred service range of 800°C–1400°C suits the thermal cycling environments of reheating furnaces, boilers, and pelletizing indurating furnaces, where combined resistance to spalling, abrasion, and corrosion is essential. Conventional installation by pneumatic ramming demands skilled applicators, significant manpower, and extended furnace downtime — and the conventional rammed plastic's workability declines steeply with age, further constraining logistics and installation quality. Mechanized gunning offers faster, safer, and more reproducible installation; however, the rheological demands of plastic refractories — high binder content, stiff consistency, and moisture sensitivity — render them incompatible with conventional castable gunning equipment. The present work describes the development of a 70% alumina plastic gunning mix formulated for a rotary-wheel dry-gunning machine and reports its thermomechanical performance from laboratory characterization through gunning trial validation.

2. Material and Experimental

Plastic Gunning 70P is a 70% Al_2O_3 (min.) phosphate-bonded plastic mass. Product was developed with controlled plasticity and sufficient water retention without compromising green strength or dry out behavior. Design targets: rebound loss <15%; shelf life adequate for standard application requirements; and postgunning properties meeting or approaching those of the equivalent rammed plastic. Laboratory-molded samples were prepared by standard ramming in IS mold; gunned sample dimension was 230×180×64 mm. Test pieces (230×64×54 mm) were cut as per EN 1927 Part 6. Test methods are listed in Table 1.

Table 1 Test methods

Property	Standard	Firing Temp./Duration	Units
Bulk Density (BD)	IS 10570 / EN 1927-6	250, 815, 1200, 1400°C / 3h	g/cm³
CCS / MOR	IS 10570 / EN 1927-6	As above	kg/cm²
Perm. Linear Change (PLC)	IS 10570 / EN 1927-6	815, 1200, 1400°C / 3h	%
Workability Index (W.I.)	CALD 011- ENU	Ambient — fresh and aged	%

3. Results and Discussion

3.1 Workability Index (W.I) and Shelf Life

W.I. was tracked over 180 days for Plastic Gunning 70P and compared against conventional rammed plastic (Table 2, Fig. 1). The gunning mix maintains W.I. within its target range of 16–25% throughout, peaking at 23.4 on day 60 and ending at 17 on day 180 — still within limits. W.I. of the conventional rammed plastic falls to 30 by day 90, leaving only a 60–90day viable application window. The superior ageing stability arises of the plastic gunning mix is achieved due to formulation design, enabling standard warehousing and distribution in standard packing without logistic constraints.

Table 2 W.I. ageing: Plastic Gunning 70P vs. conventional rammed plastic

Material	1 st d	30th d	60th d	90th d	120th d	150th d	180th d	Limit
Plastic Gunning 70P	20.5	22	23.4	23	23	20	17	16–23
Conventional rammed plastic	60	40	34	30	14	-	-	30-60

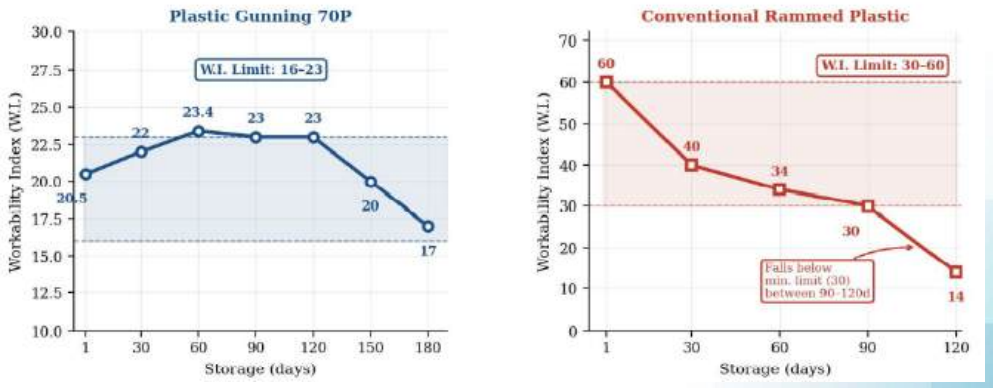


Figure 1 W.I. ageing behaviour: Plastic Gunning 70P remains within target range (16–23) for 180 days; conventional rammed plastic exits its usable range (30–60) between 90 and 120 days.

3.2 Comparative Properties: Plastic Gunning 70P vs. Conventional Rammed Plastic

Table 3 and Fig. 2 compare BD, MOR, CCS, and PLC of Plastic Gunning 70P against conventional rammed plastic (IS 10570). Plastic Gunning 70P consistently exhibits higher BD across all firing temperatures (2.52 vs. 2.48 g/cm³ at 260°C; 2.48 vs. 2.42 g/cm³ at 1200°C), reflecting a denser, more compact matrix achieved through the reformulated rheology. MOR remains superior at 260°C (+9 kg/cm²) and 815°C (+15 kg/cm²), converging at 1200°C (131 vs. 136 kg/cm²) — confirming equivalent high-temperature ceramic bond development.

CCS of Plastic Gunning 70P is markedly higher at 260°C (266 vs. 194 kg/cm², +37%), confirming the early-temperature strength advantage. At 815°C, CCS values are closely comparable (358 vs. 373 kg/cm²), indicating near-equivalent structural integrity at intermediate service temperatures. Both materials reach strong CCS at 1200°C (419 vs. 440 kg/cm²). PLC remains low and within acceptable limits across both materials through 1200°C, confirming dimensional stability in the working temperature range.

Table 3 Comparative Thermomechanical Properties: Plastic Gunning 70P vs. Conventional Rammed Plastic

Property	Firing Condition	Units	Plastic Gunning 70P	Conventional Rammed Plastic
Al_2O_3 content	-	%	69.5	67.7
Fe_2O_3 content	-	%	1.10	1.14
Bulk Density (BD)	260°C / 3h	g/cm³	2.52	2.48
	815°C / 3h	g/cm³	2.50	2.46
	1200°C / 3h	g/cm³	2.48	2.42
Modulus of Rupture (MOR)	260°C / 3h	kg/cm²	92	83
	815°C / 3h	kg/cm²	89	74
	1200°C / 3h	kg/cm²	131	131
Cold Compressive Strength (CCS)	260°C / 3h	kg/cm²	266	194
	815°C / 3h	kg/cm²	358	373
	1200°C / 3h	kg/cm²	419	419
Permanent Linear Change (PLC)	815°C / 3h	%	0.09	0.00
	1200°C / 3h	%	0.21	0.12

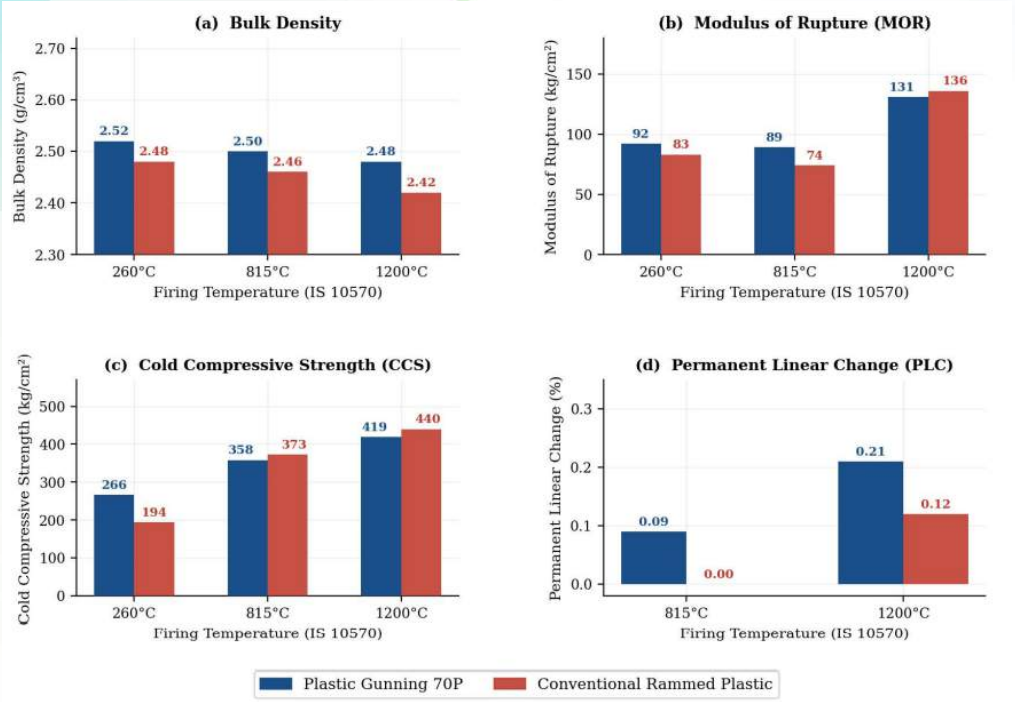


Figure 2 Thermomechanical property comparison: Plastic Gunning 70P vs. conventional rammed plastic (IS 10570).

3.3 GunningTrial

A gunning trial was conducted using a rotary-wheel dry-gunning machine; mix gunned into 230×180×64 mm molds, test pieces cut per EN 1927 Part 6 (Table 4). Rebound loss of ~14% was recorded — competitive with wet-process castable gunning. No choking or build-up was observed, and the lining exhibited satisfactory surface cohesion and consolidation throughout.

Table 4 Gunning trial parameters and observations (05.02.2026)

Parameter	Value / Observation
Gunning equipment	Rotary-wheel dry-gunning machine
Air pressure at nozzle	60–70 psi
Material applied / Rebound loss	~249 kg / ~14%
Choking / build-up	None observed
Lining consolidation	Satisfactory





Figure 3 Gunning machine setup (left) and gunned panel (right)

3.4 Lab-Molded vs. Gunned Panel: Property Comparison

Table 5 and Fig. 4 compares BD, MOR, CCS, and PLC of lab-moulded (EN 1927-6) and gunned panel cores across 260°C–1400°C. BD values track closely across all temperatures (2.38–2.48 g/cm³ for both), confirming consistent compaction density achieved through mechanized gunning. MOR of gunned samples at 260°C (60 kg/cm²) is marginally lower than lab-moulded (73 kg/cm²) — an expected characteristic of pneumatically applied monolithics attributable to lower compaction energy — but converges fully at 815°C (69 kg/cm² for both) before the gunned sample surpasses lab-moulded at 1200°C (94 vs. 73 kg/cm²), indicating progressive ceramic bond development. CCS of the gunned panel marginally exceeds the lab moulded at 815°C (356 vs. 349 kg/cm²), confirming equivalent structural integrity at intermediate service temperatures. At 1400°C, both samples demonstrate strong CCS (493 vs. 511 kg/cm²) with the gunned panel tracking within 4% of the lab-moulded value — a notably closer agreement than typically reported for gunned monolithics. PLC remains low and stable through 1200°C; the higher value at 1400°C (gunned: 1.25% vs. lab-moulded: 0.93%) reflects the natural progression of sintering shrinkage, both within acceptable bounds for reheating furnace applications.

Table 5 Properties: lab-molded (EN 1927-6) vs. gunned panel cores

Property	Firing Condition	Units	Lab-Molded (EN 1927-6)	Gunned Panel (R&D Trial)
Bulk Density (BD)	260°C / 3h	g/cm³	2.48	2.48
	815°C / 3h	g/cm³	2.45	2.47
	1200°C / 3h	g/cm³	2.41	2.42
	1200°C / 3h	g/cm³	2.40	2.38
Modulus of Rupture (MOR)	260°C / 3h	kg/cm²	73	60
	815°C / 3h	kg/cm²	69	69
	1200°C / 3h	kg/cm²	73	94
	1400°C / 3h	kg/cm²	121	92
Cold Compressive Strength (CCS)	260°C / 3h	kg/cm²	291	249
	815°C / 3h	kg/cm²	349	356
	1200°C / 3h	kg/cm²	478	419
	1400°C / 3h	kg/cm²	511	493
Permanent Linear Change (PLC)	815°C / 3h	%	+0.08	+0.13
	1200°C / 3h	%	+0.15	+0.00
	1400°C / 3h	%	+0.93	+1.25

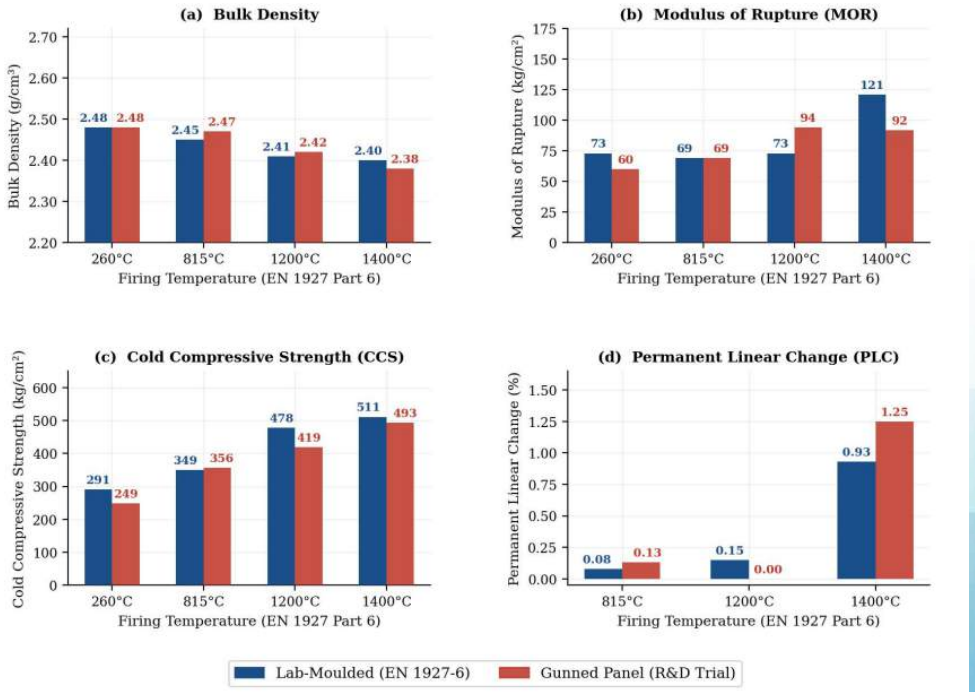


Figure 4 Thermomechanical properties: lab-molded vs. gunned panel samples

4. Conclusions

1. Plastic Gunning 70P (70% Al_2O_3, phosphate-bonded) has been successfully developed for mechanized refractory installation using a rotary-wheel dry-gunning machine, addressing the skilled-labour dependency, safety risks, and extended downtime inherent in conventional pneumatic ramming.

2. The gunning formulation maintains stable Workability Index (W.I. 17–23) over 180 days at ambient storage — substantially superior to conventional rammed plastic, which exits its usable W.I. window between 90 and 120 days. Comparative testing (IS 10570) confirms consistently superior bulk density across all firing temperatures (2.52 vs. 2.48 g/cm³ at 260°C through 2.48 vs. 2.42 g/cm³ at 1200°C), higher MOR and CCS at 260°C, and near-equivalent CCS at 815°C (358 vs. 373 kg/cm²) and 1200°C, confirming that the rheological reformulation does not compromise thermomechanical integrity at service temperatures.

3. The gunning trial (05.02.2026, EN 1927 Part 6) confirmed approximately 14% rebound loss, no choking, and satisfactory lining consolidation. BD values of lab-moulded and gunned panel samples track closely across 260°C–1400°C, confirming consistent compaction density. CCS of the gunned panel marginally exceeds lab-moulded at 815°C (356 vs. 349 kg/cm²) and tracks within 4% at 1400°C (493 vs. 511 kg/cm²) — a notably closer agreement than typically reported for gunned monolithics. MOR converges at 815°C and surpasses lab-moulded at 1200°C (94 vs. 73 kg/cm²), confirming progressive ceramic bond development in the gunned lining.

4. Plastic Gunning 70P represents a technically validated, commercially viable solution for mechanized refractory maintenance in reheating furnaces and boilers — combining the inherent performance advantages of phosphate-bonded plastic refractories with the installation efficiency, reduced manpower, and improved operational safety of mechanized gunning.

Acknowledgements

The authors acknowledge the project team and laboratory personnel involved in formulation development, characterization, and gunning trials, and the external partner institution for providing gunning machine access for trial validation.

References

Calderys/HWI Internal work, patent and database

PERFORMANCE BENCHMARK OF A SINGLE STRAND TUNDISH WITH SHROUD EXCHANGE MECHANISM 3085

Vimal Tiwari*, Prasanta Panigrahi*, Santanu Saha**, Apurba Kumar De*
Tata Steel Meramandali* Tata Steel Kalinganagar **

Soumen Nandi, Chinmoy Biswas, Subhajit Roy, H.Murty, Arijit Bhattacharyya
Vesuvius India Limited

E-Mail : Arijit.Bhattacharyya@vesuvius.com

Abstract

Tube Changing Devices are known for improving caster productivity. The SEM3085 Tube Exchange Mechanism, is not only a sustainable technology, but helps end-user in scaling up the tundish sequence rates significantly through usage of sophisticated technical features. Tata Steel Meramandali collaborated with Vesuvius and established a global performance benchmark of casting 50 heats with 34 hours and 03 minutes of sequence casting time with SEM3085 for a single strand tundish. A tonnage of 9484 tons was cast with single strand tundish in this sequence. The paper illustrates how this tundish performance benchmark was achieved with appropriate heat planning, strict operational discipline practices along with deployment of alternative refractory designs, different materials, SEM3085 machine and savings there out of, which additionally assist in engaging various environmental factors like reduction of energy consumptions. Work was carried out on all refractories, that get used in tundish and making them fit-for-use for very high sequence applications. This stands out as an example of how performance and sustainability can be met through joint, collaborative efforts.

Keywords: Productivity, SEM3085, Global Performance Benchmark

1. Introduction

The tundish-to-mould shrouding system is a critical element of continuous-casting metallurgy because it simultaneously supports production continuity, flow control and protection of liquid steel from atmospheric reoxidation. Its role has therefore evolved from that of a simple refractory tube to an integrated, monitored and exchangeable flow-control system.

Steelmakers have been using the Shroud Exchange Mechanism (still referred to as TCD, by many) for their continuous casting requirements. The machine itself has evolved over the last several decades with the significant objective of increasing casting sequence lengths at acceptable steel quality levels of grades being cast. While standard sequence lengths of (15 – 20) hours have got common, the challenge was to extend it further form refractory point of view.

From end-2021 onwards, TATA Steel Meramandali team had implemented SEM3085 in their tundish to improve productivity, safety, yield and quality in the process of steel casting of slabs. Through efficient production planning and casting, TSM gradually increased tundish sequence heats and soon touched around thirty heats' sequences in 2022 and even more in 2023. Some basic characteristics of the technicalities involved with this Shroud Exchange Mechanism have got outlined here.

Tube Changer – SEM3085

Hydraulically operated SEM3085 mechanism gets used in conjunction with the MBS control device. The main characteristics of

the SEM3085 tube changer mechanism, which play a role in steady performance are :-

- Double stroke feature – the second stroke is used to close the casting channel inside the mould, after casting ends. A separate blank plate is unnecessary. This improves safety (as no need to install the blank plate separately and no need to go near the machine for guiding it in) and this assists in quick operations.

- The refractory designs are robust and sturdier (vis-à-vis the previous machines like SEM2085) for matching high performance requirements.

- Installation procedures of refractory components have been modified vis-à-vis that, which got used in previous machines like SEM2085.

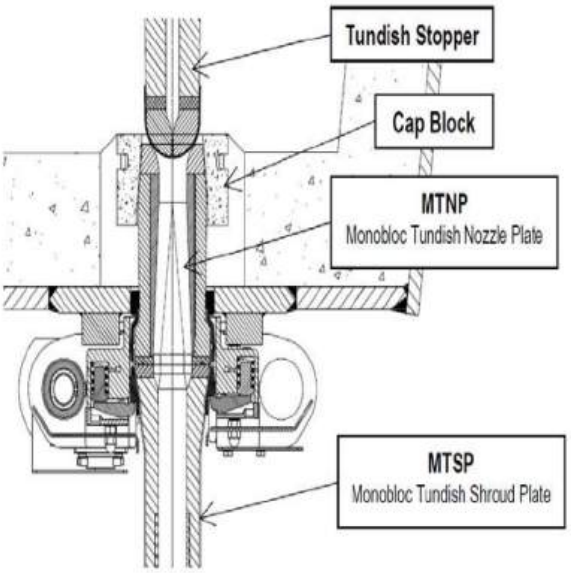
- Pressure distribution have been optimized for improved tightness in between the throttling surfaces.

Different refractories used are :-

Tundish Working Lining

TSM had already shifted from spray-mass lined tundish to dry-vibe lined tundish. It was done with the objectives of achieving of having less moisture in lining, not needing conventional tundish drying practise (just curing the dry-vibe with Dumag machine) and aiding in other two significant objectives of targeting high sequence followed by easy deskulling too. For targeting even higher sequencing - more than the standard of (15 – 20) hours, a different dry-vibe formulation, having 85% MgO was introduced at TSM in early 2026. This was used for some months, performance monitored and subsequently got used for the 50 heats' sequence.

The Refractory Stack-Up assembly has the following components :-



The MTNP (Monoblock Tundish Nozzle Plate) & MTSP (Monoblock Tundish Shroud Plate) are the two most critical refractory designs, that get used here.
The MTNP is a specific, monolithic design of tundish nozzle with a plate surface which is housed inside a rigid cast structure. Hard surface materials are on the plate surface to aid tube-change operation. The plate face that connects to the MTSP includes an argon shielding channel to protect against air aspiration. A special high purity seat mix,

which got developed, specifically for high sequence castings, has been incorporated here. This material has substantial high resistance to oxidation tendencies too and has aided in improving the casting duration.

Instead of a standard SEN, a tube is used which is exchangeable by nature. This is called MTSP ; the plate surface (at the top) and ports down below are joined by a common barrel. The plate surface is housed inside a rigid cast structure and remains in contact with that of MTNP. The tube is composed of hard plate surface material, high life aluminagraphite material on the barrel part and a very special zirconia-graphite has been used on the z-band. This z-band is named “Durasleeve”, which is designed for high-life. The DuraSleeve product was developed with the primary objective of improving the corrosion resistance of tundish shrouds while maintaining the level of thermal shock resistance required for demanding continuous casting applications. This development work was driven by the need to extend component service life under aggressive operating conditions, where refractory materials are simultaneously exposed to high temperatures, chemical attack, and rapid fluctuations. The resulting material design is based on a modified microstructural architecture characterized by increased density and a more controlled porosity distribution. By optimizing the balance between compactness and residual pore network, the new structure aims to limit corrosive penetration while preserving the ability of the material to accommodate thermal stresses. This combination of enhanced densification and tailored porosity contribute to improved in-service reliability without negatively affecting the resistance of the shroud to thermal shock during start-up, casting transitions, or other transient operating conditions. This material has provided a reduction in corrosion by (10 – 20)% at several steel plants, depending upon throughput, mould fluxes etc. With increase in z-band life, an attempt has been made to limit the number of tube changes (to the extent possible).

Monoblock Stopper – it is the flow regulation rod which helps in regulating the flow from tundish to mould. We had to adjust the materials and use necessary design for achieving the high sequence requirements of TSM. While the body part remains the high duty Alumina Graphite material, the nose tip has an advanced version of Magnesia-Graphite material. The design also has a calibrated pipe at the tip for back-pressure purposes.

Benchmark Development Approach

The benchmark was developed through staged sequence extension rather than a one-step attempt. Acceptance criteria included uninterrupted casting, stable flow control, positive shielding-gas backpressure, acceptable shell temperature, controlled refractory wear, safe tube exchange and trouble-free deskulling. A preceding 47-heats’ sequence (done on 27/08/25) provided the diagnostic baseline. It recorded 1,952 min of casting, normal stopper profile with low measured body wear, positive argon backpressure throughout the sequence, clean sealing channels and MTSP slag-band erosion rates close to 1.5 mm/h. Localized lining erosion near the launder side and tighter stopper shut-off during the tundish fly needed to be improved further. The resulting actions were higher-resistance zonal DVM lining, an upgraded high-purity MTNP seat and tighter control of stopper running.

Plant Results

On 28/03/26, TSM caster team planned and successfully executed a 50 heats’ TCD/SEM sequence with 3 MTSPs. The details of this tundish are mentioned below :-

- Caster = CCM 2
- Strand = 1
- Car = 02
- Tundish Type = Flat Bottom Design
- Tonnage = 9484 T
- Steel Grades = T12, T01A, C06A

- Section = 1560 by 230
- Casting Duration = 2043 minutes
- Average LS Life = 8.33 heats
- MTSP Life (mins) = 888, 568, 587
- Max shell temp = 272 degrees C

Mechanism-to-performance linkage

The performance outcome is consistent with four complementary design functions. First, the threepoint clamping concept and elastic loading distribute sealing force around the MTNP-MTSP interface. Second, hard sliding surfaces and the push-edge arrangement limit scratching and fin formation during exchange. Third, the inert-gas groove creates a monitored barrier against air aspiration. Fourth, the double-stroke shut-off gives an emergency flow interruption function without installing a separate blank plate. Together, these features connect long sequence capability with steel-quality protection, operational recoverability and operator safety Post casting, all refractories were checked (except for Turbo and bottom lining – these are not possible) – notably, the tubes surfaces, the z-band, plate surfaces and the stopper tip. The lining condition got checked too and no difficulty was encountered during deskulling. Some refractories were recovered for examination. Photos of some used refractories are shared down below :

MBS tip condition:-



MTSP – the slagzone & port regions.



MTSP – the slagzone & port regions



Plate Surface condition of MTSP refractory



General tundish look (post casting) :-



Steering Rod End



Integrated value of long-sequence casting

The main technical message should not be limited to the statement that 50 heats were cast. The evidence supports a broader conclusion - sequence extension is function of efficient production planning, refractory capability and system capability.

Horizontal Deployment of SEM3085 utilization

Building on the experiences gained, the Tata SteelVesuvius team have executed similar exercises at other locations too. On 31/07/26, the caster-team at TSK implemented a 46 heats' sequence (2350 minutes) for a double strand tundish. Similarly, on 9/06/26 the caster-team at TSJ implemented a 40 heats' sequence (1754 minutes) for a single strand tundish.

These kind of tundish performance-benchmarks are testament to joint collaborative efforts between the Tata team and Vesuvius.

References

1) Sustainability Initiatives in Steelmaking at Tata Steel BSL Subodh Padey, Saroj Kumar Banerjee, Siddhartha Misra, H. Mahesh Babu, Naresh Kumar Sharma Tata Steel BSL Limited (Formerly Bhushan Steel Limited), Narendrapur, Meramandali, Dhenkanal, Odisha 759121 5

2) Irefcon 2022 paper – Sustainability in Steel Manufacturing Process by Introduction of New Generation Technology H. Mahesh Babu, Dibakar Sahoo (TSM), Paromita Sarkar, Rijubak Dey, Avijit Sasmal (VIL)

Acknowledgement

The authors remain thankful to the refractory and caster-operation teams of TATA Steel Meramandali plant for overall guidance, production planning and successful usage of SEM3085. Authors also remain thankful to Vesuvius Global product development teams for development of machines and related products.

ADVANCING TROUGH REFRACTORIES WITH A NO-CEMENT BINDER SYSTEM

Ankita Mishra[1] , Izak Cameron[2]
[1] Elkem South Asia Pvt. Ltd. Nagpur, India; [2] Elkem Silicon Materials, Kristiansand, Norway
ankita.mishra@elkem.com; izak.cameron@elkem.com

Abstract

Blast furnace trough refractories have traditionally been based on ultra-low cement castables (ULCCs) because of their proven performance and reliable processing characteristics. However, increasing requirements for extended campaign life and reduced refractory consumption have encouraged the development of alternative binder technologies. This study evaluates a no-cement castable (NCC) formulated with brown fused alumina aggregates for trough applications in India. The conventional calcium aluminate cement binder was replaced with the SioxX®-Zero no-cement binder system while maintaining the same aggregate and matrix design.

A reference ULCC and the corresponding NCC were subjected to identical laboratory testing, including flowability, green strength development, cold and high-temperature strength (up to 1600°C), hot modulus of rupture, abrasion resistance and slag corrosion resistance. The NCC demonstrated comparable rheological behaviour, faster green strength development and significantly improved slag corrosion resistance. These results indicate that NCC technology can support longer trough service life, shorter turnaround times and reduced refractory consumption in blast furnace operations.

Keywords: Blast furnace, trough, NCC, SioxX®- Zero, corrosion resistance.

1. INTRODUCTION

India is the world's second largest producers of hot metal via the blast furnace (BF) route, with a growing installed base of large volume furnaces and an operating environment that places severe demands on trough refractories. The BF trough (or runner) system channels molten iron and slag at temperatures typically between 1500°C and 1700°C and exposed to repeated thermal shock, mechanical erosion and chemical attack by slag during every tap [1]. Historically, BF trough linings progressed from ramming masses and bricks to monolithic Al_2O_3-SiC-C castables, following the low-cement (LCC) and ultra-low cement castable (ULCC) binder systems become the industry standard due to their strength, slag resistance and installation efficiency [2]. The evolution of castable refractories in India mirrored the broader global development pathway.

No-cement castables (NCCs), based on microsilica-gel or colloidal silica binder systems, have emerged as an attractive alternative to calcium aluminate cement (CAC)-bonded ULCCs. By eliminating or drastically reducing CaO contribution from the binder, the formation of low-melting calcium-alumina-silicate phases at high temperature in NCCs was reduced, promoting mullite formation, and have been shown in the literature to offer faster dry-out, lower water demand and improved hot strength compared with conventional ULCC systems [3], [4] . A companion study by the present authors demonstrated these advantages for a tabular alumina-based trough castable using the SioxX®- Zero binder [5]. The present work extends that investigation to a brown fused alumina-based system representative of Indian trough practice, comparing a SioxX®-Zero-bonded NCC against a conventional CAC-bonded ULCC benchmark across rheology, mechanical strength and slag corrosion resistance.

2. MATERIALS AND METHODS

2.1 Raw materials and mix design

Indian trough castables are predominantly based on brown fused alumina or bauxite, which provide a favourable balance of refractoriness, mechanical strength and cost-effectiveness, supported by greater local saving availability and shorter supply-chain lead times. Two self-flow castable formulations were designed according to standard recipes utilised in India, a reference ULCC bonded with 70% calcium aluminate cement (CAC) with Polycarboxly Ether as dispersant, and a NCC formulation using Elkem SioxX®-Zero which plays dual role of binder and dispersant. Both castables were designed with identical aggregate and matrix constituents to isolate the effect of the binder system. Brown fused alumina was used as the principal alumina aggregate, together with silicon carbide (97% SiC) for slag and oxidation resistance. Carbon black and pitch pellets supplied carbon for bonding and thermal shock resistance. Reactive alumina, calcined alumina, and Elkem microsilica®971U formed the ultrafine matrix, with aluminium metal powder included as an antioxidant additive. Particle packing was optimised using the Andreasenmodel-based EMMA (Elkem Material Mixture Analyser) methodology, consistent with the mix design approach used in the companion tabularalumina study [5] . Raw materials were first dry mixed and thereafter wet mixed in a planetary mixer at laboratory room temperature (22 ± 2°C), with total wet mixing time of 5 minutes. To measure the rheological properties of castable i.e., self-flow, tap flow and vibration flow, a flow cone (ASTM C230) was used.

2.2 Test methods

2.2.1. Processing parameters – flowability & set time

To evaluate the flow characteristics of the castables, three initial flow measurements were conducted: self-flow, tap flow, and vibration flow. A new sample was used for each test to ensure consistency during initial flow measurements.

For self-flow, tap and vibration flow the spread of the castable on the table was measured after 90 seconds, 15 taps and 15 seconds respectively. The initial flow values were recorded as F_0. To assess flow after 30 minutes (F_{30}), the castable samples from initial flow were stored in a sealed plastic bag to prevent drying during the waiting period. Hardening time was determined using an ultrasonic IP 8 tester, which measured the velocity of sound (m/s) through the material over time.

2.2.4. Hot modulus of rupture (HMOR)

The samples used for hot modulus of rupture (HMOR) testing were casted in specimen of dimensions 150 × 25 × 25 mm. The sample were pre-fired at 1450°C for 24 hours and then tested at 1450°C after soaking for 1 hour.

3. RESULTS AND DISCUSSION

3.1 Flowability and setting behaviour

Both castables were designed to achieve comparable self-flow behaviour at equivalent water addition, consistent with the requirements of self-flow trough installation. The flowability results are shown in Figure 1. The NCC is showed flow performance comparable to the ULCC at initial (F0) measurement, together with a faster development of green strength ahead of demoulding, owing to the enhanced gelation mechanism of the SioxX®-Zero binder compared

2.2.5. Abrasion loss

The abrasion loss was conducted at room temperature (25°C) and elevated temperature (1000°C) as per ASTM C704 on pre-fired (1550°C) specimens with dimensions 114 × 114 × 65 mm.

2.2.6. Static slag corrosion test

The static slag cup test was performed using crucibles with external dimensions of 85 × 85 × 85 mm, featuring a central cavity of 45 × 45 × 45 mm. Crucibles were cast with both mixes and subsequently pre-fired at 1600°C for 5 hours prior to testing. A synthetic blast furnace slag was prepared with a CaO/SiO_2 ratio of 0.9 (Table 1). The cavity of each crucible filled to 80% of its volume with the slag and then subjected to a corrosion test at 1600°C for 5 hours.

Constituent Oxide	Composition (%)
CaO + MgO	39.08
$SiO_2 + TiO_2$	43.27
Al_2O_3	13.70
$K_2O + Na_2O$	1.45
Fe_2O_3	0.14
CaO/SiO	0.90

Table 1: Chemical composition of the synthetic blast furnace slag used for static corrosion testing

2.2.7. Scanning electron microscopy analysis (SEM)

Polished sections of the static corrosion samples were prepared by sectioning a piece of the sidewall and area of slag-refractory interaction. The corrosion samples were mounted in resin and coated with gold for SEM-EDS (Energy Dispersive X-Ray Spectroscopy) analysis. During EDS analysis, a backscattered electron image was captured and mapping was done to visualize compositional contrast and point analyses were performed on selected microstructural features to determine the atomic percentages of elements present in the various phases.

with the hydration-driven set of CAC. The setting time for both ULCC and NCC was 460 min and 220 min, respectively.

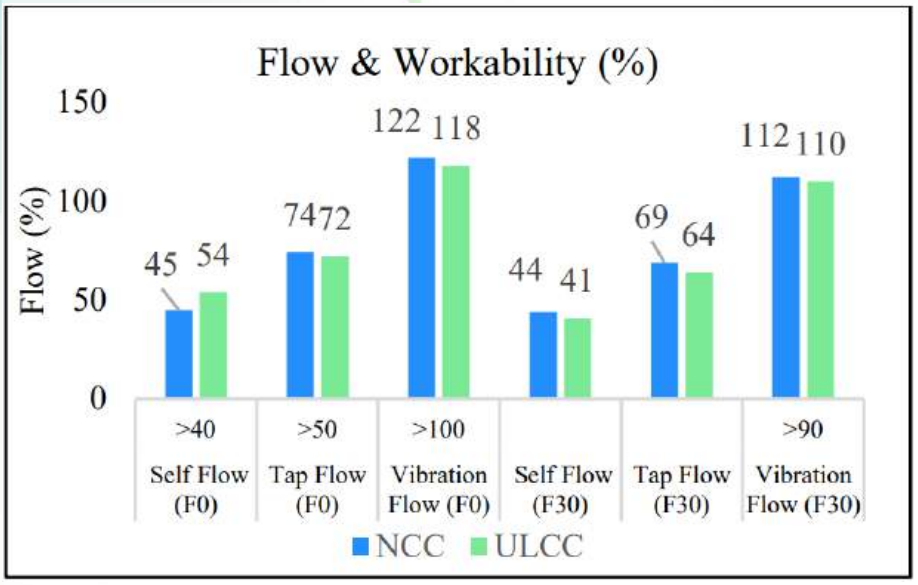


Figure 1: Initial and 30-minute flowability of ULCC and NCC trough castables

3.2 Cold modulus of rupture (CMOR) and cold crushing strength (CCS)

Cold compressive strength was evaluated after pre-firing samples at 110°C, 1000 °C and 1600 °C. Based on the mechanism established for the SioxX®-Zero binder system, the ULCC is retain a strength advantage at lower temperature due to the higher calcium aluminate cement content. The NCC is reached high strength at 1600°C as a result of its lower CaO content and consequent promotion of mullite phase bonding. Consequently, what can be seen is that the ULCC achieves higher values on both the CMOR and CCS. The cause of this could be due to castable fines requiring further optimization as direct replacement of CAC with SioxX®-Zero is not on a 1:1 basis.

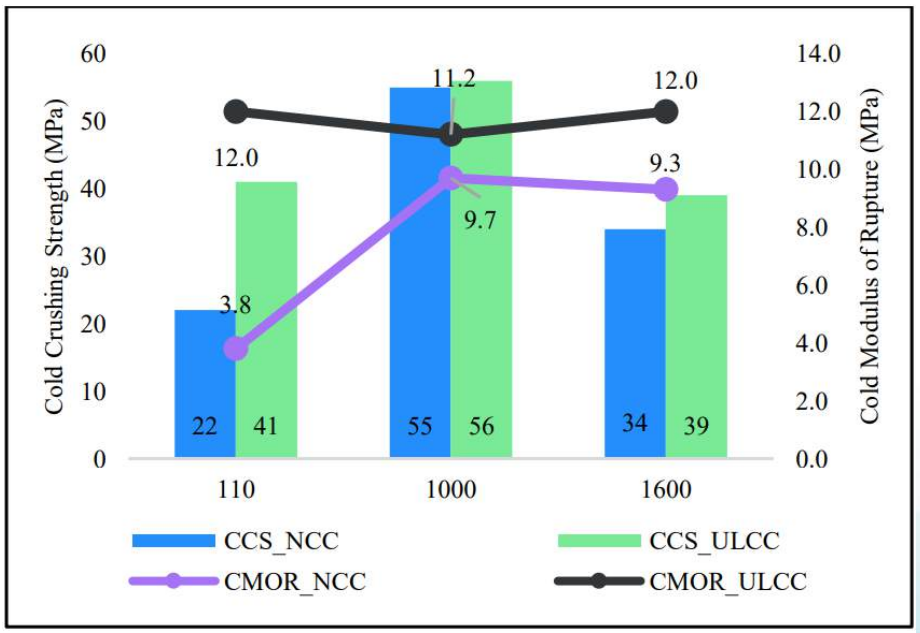


Figure 2: Mechanical property results of ULCC and NCC

3.3 Bulk density (BD) and apparent porosity (AP)

BD and AP were measured on the same specimens used for CMOR/CCS testing are shown in Figure 3. In the companion tabular alumina study, no significant difference in porosity was observed between binder systems, while the NCC showed a measurably higher bulk density at 1600°C a trend that, if confirmed here, would be consistent with a denser, better-sintered microstructure supporting the slag corrosion results in Section 3.6. The higher apparent porosity of the NCC version signifies that further water reduction is possible with optimised particle packing to enhance the microstructural features that translates to high temperature strength.

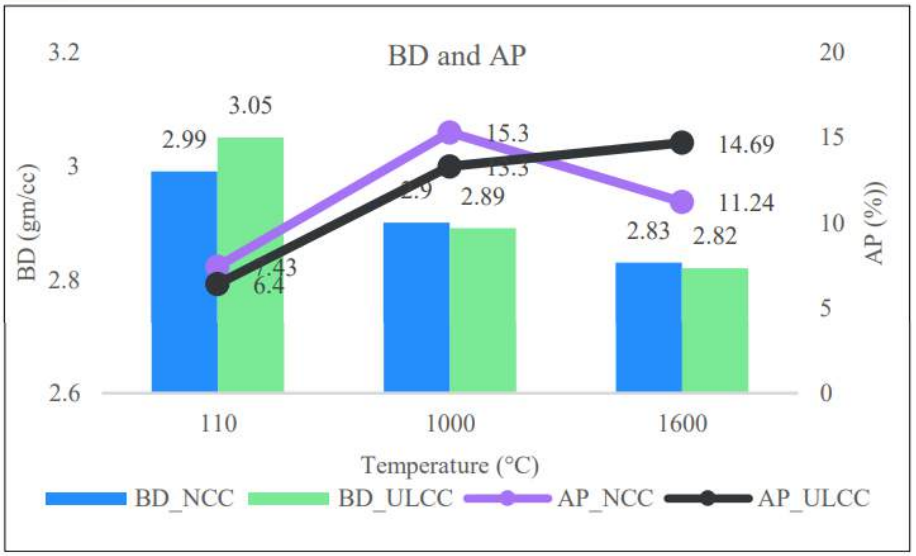


Figure 3: Bulk density and apparent porosity of ULCC and NCC

3.4 Hot modulus of rupture (HMOR)

HMOR was tested at 1450°C after a 1-hour soak, representative of trough operating conditions during tapping. Observed slightly higher hot strength in the ULCC compared to NCC i.e. 8.6 MPa and 9 MPa respectively.

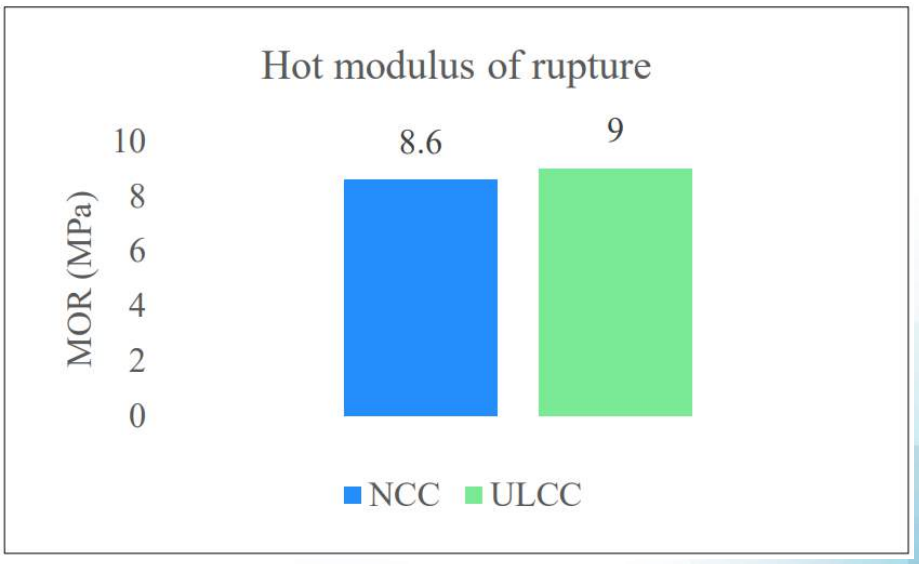


Figure 4: Hot modulus of rupture of ULCC and NCC

3.5 Abrasion loss

Abrasion resistance was evaluated at ambient (25°C) and elevated (1000°C) temperature on prefired specimens. As both mixes share an identical brown fused alumina and SiC aggregate system, abrasion loss was in a similar order i.e. 3.2% at 25°C and 5% at 1000°C between the two binder systems. Any difference attributable primarily to matrix bond strength rather than aggregate hardness.

3.6 Static slag corrosion analysis

The slag corrosion resistance is one of the most critical performance parameters for BF trough castables and was the primary focus of the microstructural investigation for this study. Crucibles of both the ULCC and NCC compositions were cast, pre-fired at 1600°C, and filled with the synthetic slag described in Table 1. The slag-filled samples were fired at 1600 °C and soaked for 5 hours before being sectioned for SEM-EDS analysis of the slag-refractory interface. Figure 5 illustrates the differences in slag penetration between the NCC and ULCC specimens, with the ULCC exhibiting a greater degree of corrosion. Cross-sections of the corroded samples, highlighting the affected regions, are presented in Figure 6. The penetration depth in each sample was assessed both visually and by SEM-EDS analysis.

The ULCC specimen showed significantly deeper corrosion penetration into the sidewall compared with the NCC specimen. Visual evidence of elephant footing was observed in the ULCC sample (highlighted in yellow in Figure 6), whereas no such feature was detected in the NCC sample. Furthermore, SEM-EDS analysis revealed a higher degree of alkali vapour penetration in the ULCC sidewall, while only limited penetration was observed in the NCC specimen. These observations are discussed in greater detail in this section.

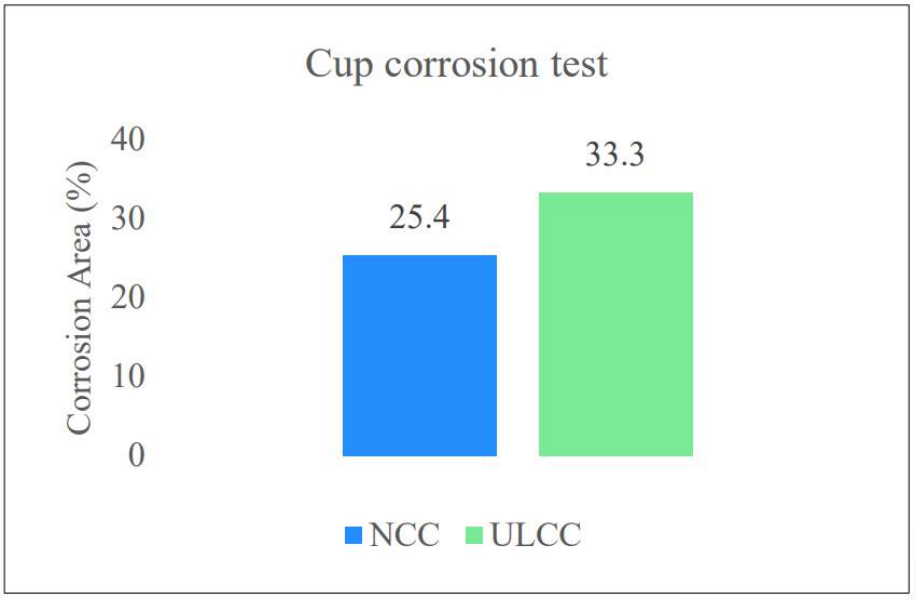


Figure 5: Corrosion area of ULCC and NCC after static slag-cup testing at 1600°C for 5 h



Figure 6: Cross-sections of ULCC and NCC specimens after static slag-cup testing

3.7 SEM-EDS microstructural analysis

3.7.1 ULCC

Elemental mapping of the ULCC post-mortem sample (Fig. 7) shows pronounced slag penetration inward from the exposed surface, tracked by the Ti and Ca marker elements. Ca is present throughout, consistent with its dual origin from both the slag and the CAC binder, while Ti present in the slag and some amount BFA aggregates as impurity more clearly delineates the penetration front. Ca-enrichment is particularly evident in regions coinciding with elevated Ti content, confirming active slag ingress rather than binder-only signal.

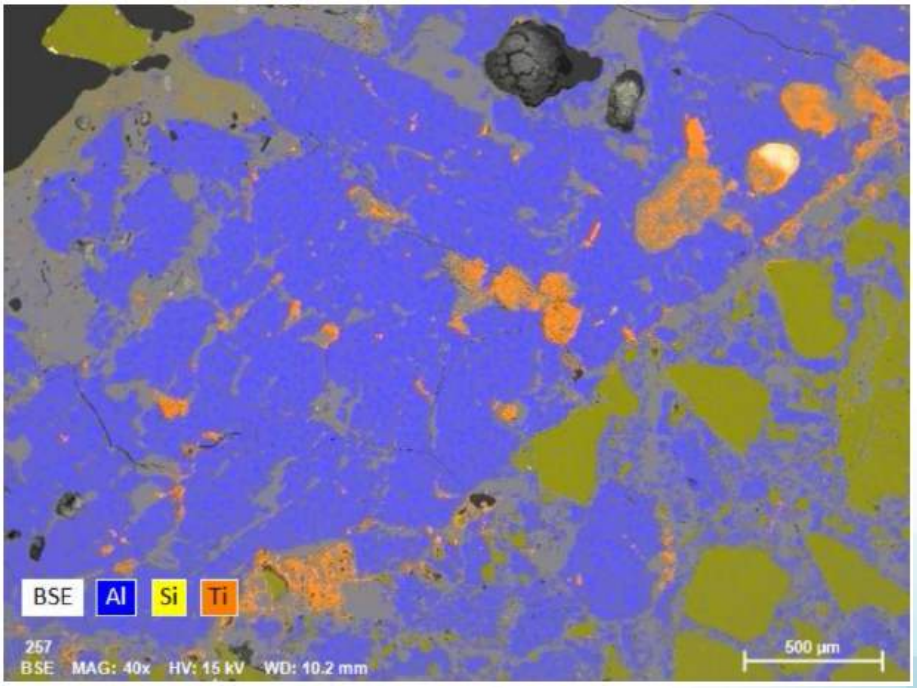


Fig. 7: SEM-EDS elemental map (Al – blue, Si – yellow, Ti – orange) of the ULCC post-mortem sample, showing slag penetration from the exposed surface tracked by the Ti marker.

Away from the immediate surface, backscattered electron imaging of ULCC reveals extensive microcracking accompanying deep slag penetration, with slag particles embedded well into the matrix of the castable, again identified through co-located Ti and Ca signal (Fig. 7).

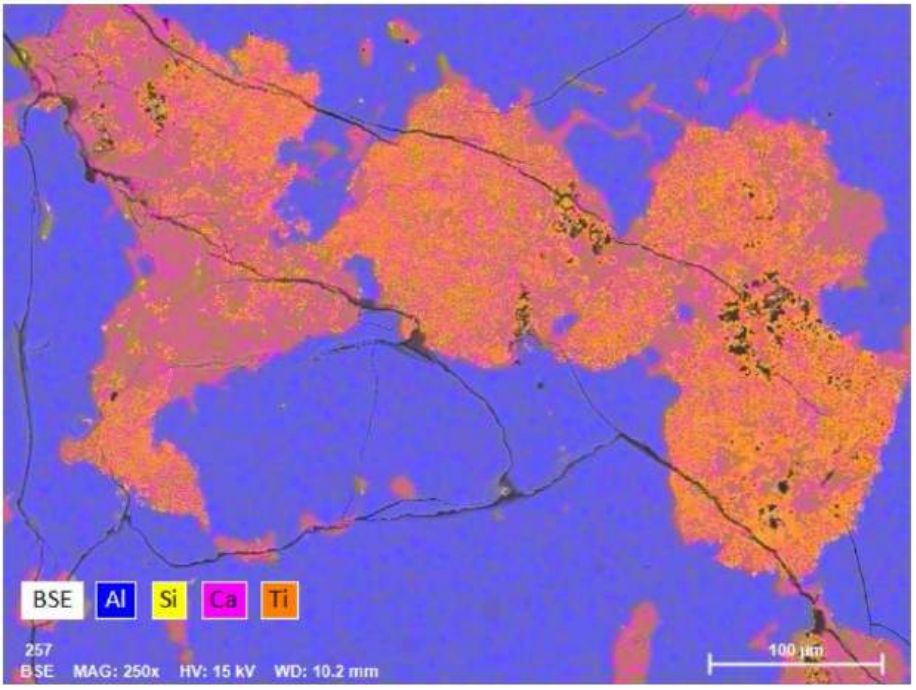


Fig. 8: SEM-EDS elemental map of the ULCC sample showing extensive cracking with slag particles (Ti, Ca) embedded deep within the matrix.

At the aggregate scale, slag in contact with SiC grains appears largely inert, consistent with the well-known chemical corrosion resistance of SiC in BF slag environments. In contrast, slag in contact with the fused alumina aggregate shows evidence of interaction at the grain boundary (Fig. 9), which is discussed further in the context of mullite morphology below.

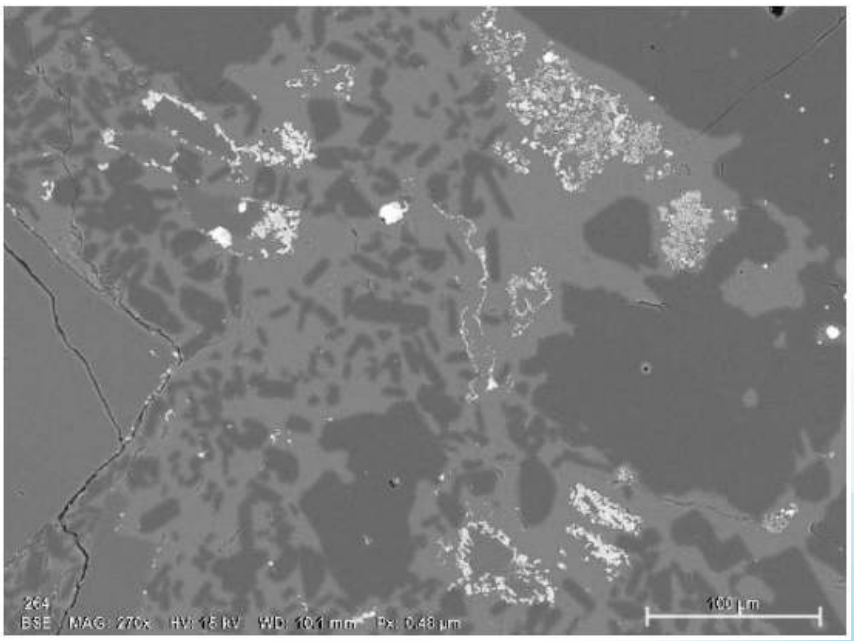


Fig. 9: Backscattered electron image showing slag interaction at a fused-alumina grain boundary in the ULCC sample

3.7.2 NCC

In marked contrast to the ULCC, the NCC sample shows slag ingress confined almost entirely to the immediate slag-line region, with negligible penetration into the bulk of the castable below the slag line (Fig. 10).

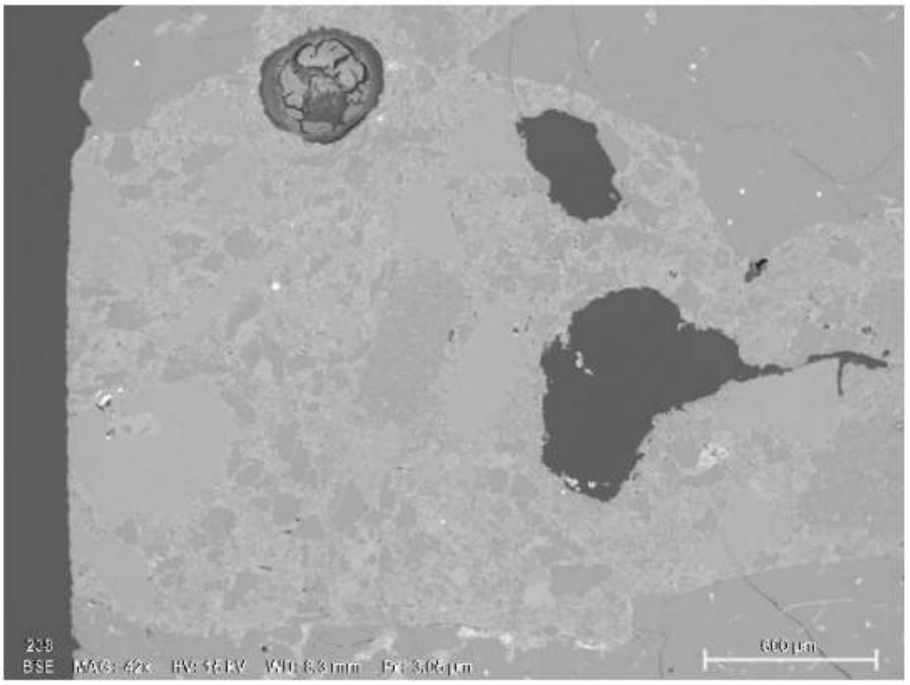


Fig. 10: Backscattered electron image of the NCC postmortem sample showing slag ingress confined to the slag-line region, with minimal penetration into the bulk matrix.

A elemental map taken of a wider area away from the slag line (Fig. 11) confirms this limited ingress where slag particles are present, they remain concentrated at the surface layer and are largely restricted to pre-existing cracks rather than penetrating the sound matrix shown predominantly by the Ti-markers.

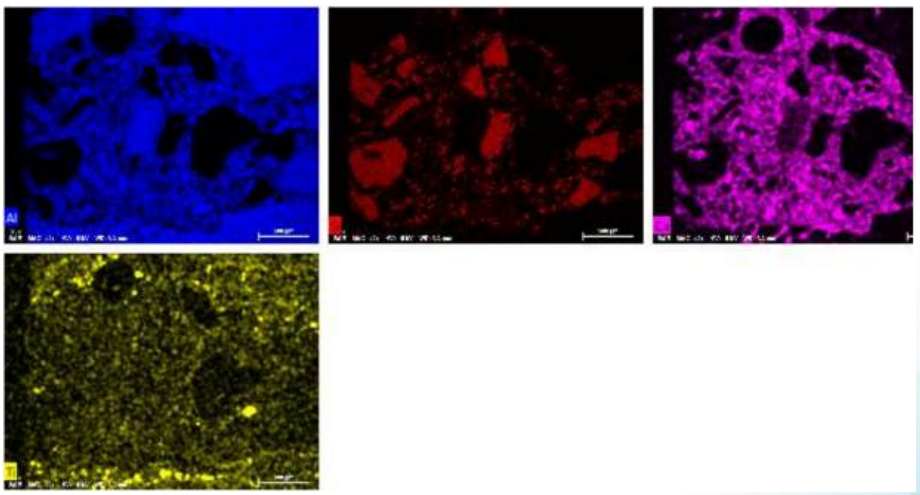


Fig. 11: SEM-EDS elemental map (Al – blue, Si – red, Ti – yellow, Ca - purple)of the NCC sample away from the slag line

The most significant microstructural difference between the two binder systems is the morphology of the mullite phase formed in the matrix on firing. In the NCC, well-defined, elongated, needle-like mullite crystals are observed (Fig. 12a), forming an interlocking network around the fused alumina aggregate (Fig. 12b).

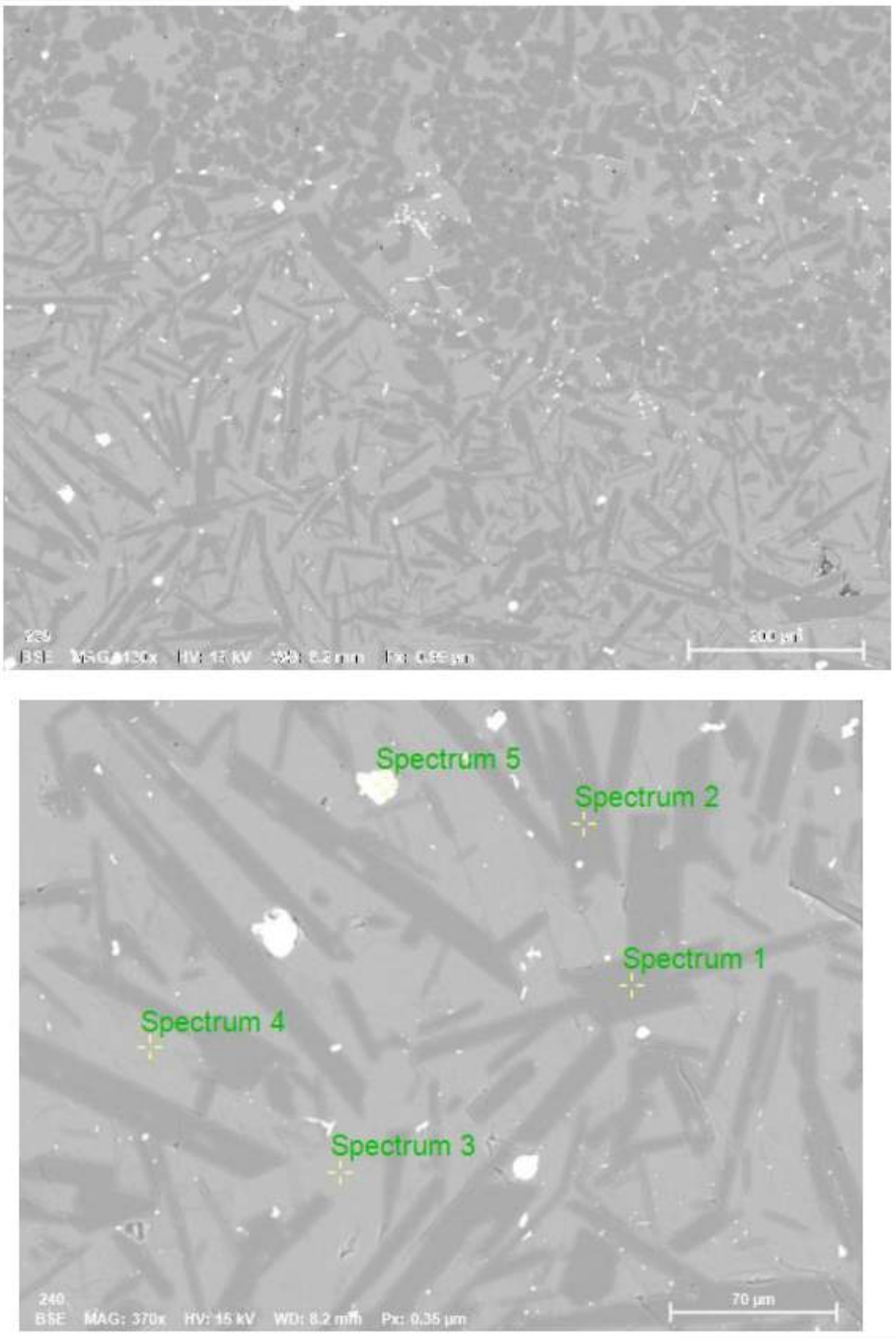


Fig. 12 (a) BSE image of the NCC matrix showing welldefined, elongated, needle-like mullite crystals. (b) BSE image with EDS spectrum locations showing a composite region of blocky fused-alumina grains and interlocking needle-like mullite in the NCC matrix; the mullite network correlates with the Ti-marker evidence of restricted slag ingress.

The elongated, interlocking mullite network observed in the NCC is consistent with the mechanism proposed in the companion tabularalumina study [5]. The lower CaO content of the SioxX®-Zero binder is reduced the formation of low-melting calcium-alumina-silicate liquid phases during high-temperature exposure, thereby promoting the development of a finer and more interconnected mullite bonding network. Such a microstructure is believed to act as a physical barrier to slag ingress along grain boundaries. In contrast, the CAC-bonded ULCC exhibits a comparatively coarser bond phase that is more susceptible to chemical dissolution and penetration by slag. These microstructural differences are consistent with the substantially lower slag penetration observed in the NCC relative to the ULCC.

4. CONCLUSION

A no-cement trough castable based on SioxX®-Zero and brown fused alumina aggregate representative of Indian raw-material practice was developed and benchmarked against a CAC-bonded ULCC reference with identical aggregate composition.

The NCC showed comparable initial flow behaviour and a substantially shorter setting time than the ULCC, indicating a potential advantage for demoulding and turnaround. However, the ULCC achieved higher CMOR, CCS and HMOR values, while abrasion loss was of a similar order for both systems. The bulkdensity and apparent-porosity results did not show a densification advantage for the NCC; rather, the higher apparent porosity suggests that further optimisation of water demand and particle packing is required.

The clearest performance benefit of the NCC was observed in static slag corrosion testing, where lower corrosion area, absence of elephant footing, reduced alkali vapour penetration and SEM-EDS evidence of restricted slag-associated elemental distributions were observed. The needle-like mullite network observed in the NCC matrix may have contributed to this improved corrosion resistance. Replicate testing, quantitative phase characterization, dry-out assessment, and industrial in-service trials of the trough castables are required to confirm the improvements observed highlighting the improvements translating into potential shorter turnaround time, longer campaign life and lower refractory consumption.

REFERENCES

[1] S. Carniglia, G. Barna, Handbook of Industrial Refractories Technology – Principles, Types, Properties and Applications, 1st Ed. William Andrew Inc., (2005), pp.71-75.

[2] W. Zhanmin, L. Zaigeng, Z. Ningsheng, Monolithic refractories for BF troughs. Luoyang Institute of Refractories Research.

[3] B. Myhre, The relationship between particle size distribution and superfines properties on rheology of refractory castables. IREFCON (2014), pp. 88-96.

[4] A. M. Rafei, T. S. Mansour, PhysicoMechanical and Microstructure Characteristics of Porous Mullite Ceramics, Silicon, 15, (2023), pp. 7157-7170.

[5] A. Mishra, I. J-P. Cameron, Design of Blast Furnace Trough Castable using SioxX®- Zero, ICR Proceedings, (2025)

DEVELOPMENT OF A READY-TO-USE REFRACTORY MORTAR WITH EXTENDED SHELF LIFE FOR STEELMAKING APPLICATIONS

Neelendu Mukherjee, Sachin Joshi and Sachi Dulal Majumdar

IFGL Refractories Limited, India

Corresponding author's e-mail: sachidulal.majumdar@ifgl.in

Abstract

Ready-to-use refractory mortars are increasingly preferred in steelmaking operations due to their ability to ensure consistent joint quality by eliminating on-site mixing variability. Despite these advantages, their industrial use remains limited, primarily because silicate-based binders tend to harden prematurely during storage, resulting in short shelf life. In the present study, a super-duty ready-to-use refractory mortar with a shelf life of up to six months is developed for steel ladle and tundish applications operating at temperatures up to 16000C.The formulation employs a carefully optimized alumino-silicate fine aggregate system combined with a modified silicate binder containing an organic reaction inhibitor to control premature polymerization. Laboratory characterization and phased industrial trials under closed tundish casting conditions are conducted to evaluate application behavior, bonding characteristics, dimensional stability, resistance to molten steel penetration, and service performance.The developed mortar retained stable rheology after prolonged storage and exhibited uniform sintering, negligible shrinkage, and complete resistance to metal penetration during service. Successful completion of a continuous 12-hour casting campaign confirmed its suitability for demanding steelmaking operations. The results demonstrate that extended shelf life can be achieved without compromising high-temperature joint performance.

Keywords: Monolithic refractories, Ready-to-use refractory mortar, Silicate-based binder, Extended shelf life, Tundish

1. Introduction

Monolithic refractories play an increasingly important role in modern steelmaking due to their installation flexibility, reduced downtime, and ability to form continuous linings and joints within monolithic systems[1], refractory mortars are critical auxiliary materials used for fixing and sealing interfaces in tundish and ladle assemblies such as well blocks, submerged entry nozzles (SEN), stopper systems, and slide gate components. These joints are exposed to severe thermal gradients, molten metal attack, and mechanical stresses during service[2]. Thus, the material properties of refractory mortars, including their resistance to these harsh conditions, are paramount for ensuring operational integrity and extending campaign life in steelmaking applications.

Conventional dry refractory mortars necessitate on-site water addition and mixing, rendering joint performance highly dependent on application practices. Variations in water addition and mixing directly impact joint density, shrinkage, and resistance to molten metal penetration[3]. In monolithic refractory technology, such variability undermines the objectives of reproducible microstructure and predictable thermomechanical performance. Ready-to-use refractory mortars offer a solution to these challenges by pre-mixing all components, including water, thereby ensuring consistency in rheology and curing characteristics upon application[4]. This pre-mixed format minimizes on-site preparation variables and improves the

overall quality and reliability of the refractory lining[5]. However, their wider industrial adoption has been limited by short shelf life due to premature hardening of silicate-based binders[6]. Extending shelf life without compromising high-temperature ceramic bonding remains a key challenge. The present work addresses this issue through formulation design and industrial validation. This study focuses on developing a super-duty ready-to-use refractory mortar that exhibits an extended shelf life of up to six months, specifically designed for high-demand steel ladle and tundish operations enduring temperatures up to 1600 °C.

2. Experimental Procedure

2.1 Raw Materials

The developed mortar formulation is designed as a fine-grained monolithic system to ensure dense joint packing, controlled thermal expansion, and effective sintering at service temperatures. A multimodal aluminosilicate aggregate system is selected to achieve progressive void filling and a stable joint microstructure[7]. The chemical composition and physical properties of the fine raw materials used are summarized in Table 1.

Raw material	Chemical composition (wt.%)	True density ($g \cdot cm^{-3}$)	Median particle size, d_{50} (μm)
Mullite fines	Al_2O_3: 70–75 SiO_2: 24–28 Fe_2O_3: ≤1.0	3.05–3.15	10–25
Quartz fines	SiO_2: ≥98.0 Al_2O_3: ≤1.0 Fe_2O_3: ≤0.5	2.63–2.66	15–30
Fused silica	SiO_2: ≥99.5 Al_2O_3: ≤0.2 Fe_2O_3: ≤0.05	2.18–2.22	5–15
Silica brick fines	SiO_2: 94–96 Al_2O_3: ≤1.5 Fe_2O_3: ≤1.0	2.30–2.35	15–30

Table 1 Chemical composition and physical properties of fine raw materials used in the developed ready-to-use monolithic mortar

The combination of crystalline phases (mullite and quartz) with amorphous fused silica provided controlled thermal expansion and reduced thermomechanical mismatch with adjacent refractories. A multimodal particle size distribution, with coarse particles forming the packing skeleton and finer fractions filling interparticle voids, improved packing density and overall stability[7], this optimized packing reduced green-state porosity and shrinkage during drying and heating, while promoting uniform ceramic bonding at high temperatures, thereby improving joint integrity and durability in tundish and ladle applications.

2.2 Binder chemistry and shelf-life control

A silicate-based binder is selected for the developed ready-to-use refractory mortar due to its ability to generate strong ceramic bonds at elevated temperatures. In conventional silicate-bonded mortars, however, alkali silicate binders undergo rapid polymerization at ambient conditions through silanol condensation reactions (1)

$Si–OH + HO–Si \rightarrow Si–O–Si + H_2O$

resulting in premature hardening and limited shelf life[6].To overcome this limitation, a Disaccharide-based organic reaction inhibitor is incorporated into the binder system. As illustrated schematically in Fig. 1, the inhibitor interacts with the alkali silicate binder during storage via hydrogen bonding to silanol groups (Si–OH) and complexation of alkali metal ions.These interactions suppress silanol condensation reactions, thereby inhibiting Si–O–Si network formation and stabilizing mortar rheology. Consequently, premature setting is averted, yielding an extended shelf life suitable for ready-to-use applications[8].During heating at 150–400°C, the Disaccharide-based inhibitor decomposes and volatilizes, restoring silicate binder reactivity. Above 1000°C, silicate condensation and reaction with aluminosilicate aggregates promote the formation of mullite and aluminosilicate glassy phases, resulting in effective ceramic bonding and joint sintering[7].The controlled transition from storage inhibition to high-temperature bonding provides both extended shelf life and reliable service performance. The resulting dense joint, low shrinkage, and resistance to molten steel penetration contribute to improved durability in industrial applications.

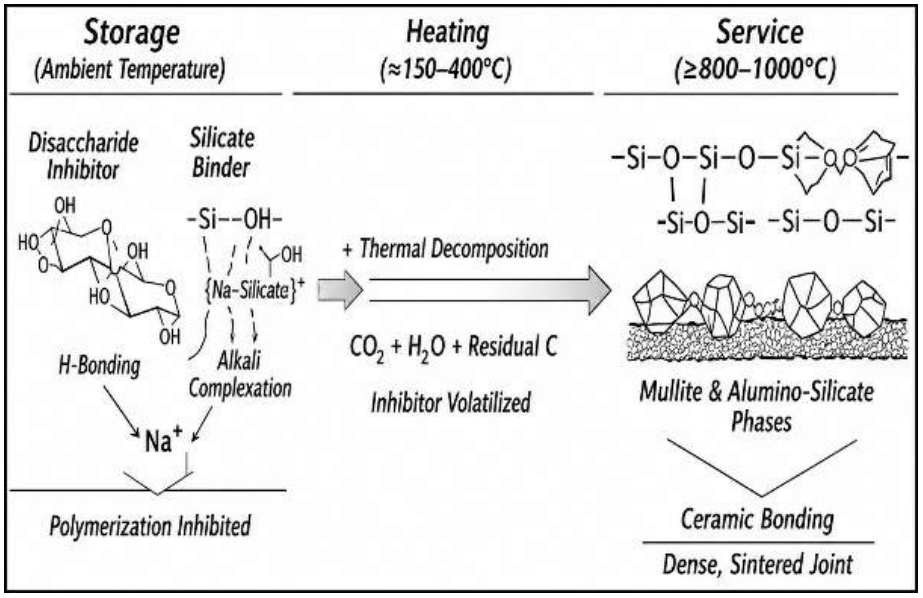


Figure 1 Schematic illustration of the Disaccharide-based organic inhibitor's mechanism in the alkali silicate binder system of the developed ready-to-use monolithic refractory mortar

2.3 Formulation Design

The formulation is designed to evaluate the effect of Disaccharide-based inhibitor concentration on shelf life and high-temperature bonding. In Table 2, the aluminosilicate fines and liquid silicate binder are kept constant, while the inhibitor content is varied from 1–6 wt.% in six formulations (T-1 to T-6). The aluminosilicate fines are fixed at 80 wt.% to maintain consistent refractory content and particle packing. This systematic variation enabled optimization of inhibitor concentration for controlling premature silicate polymerization while

maintaining effective ceramic bonding upon heating.

Component category	Constituent	T-1	T-2	T-3	T-4	T-5	T-6
		Wt.%					
Fine aggregate system	Alumino-silicate fines	80	80	80	80	80	80
Binder system	Liquid silicate binder	Constant					
Shelf-life control additive	Disaccharide-based inhibitor	1	2	3	4	5	6

Table 2. Experimental formulation matrix for Disaccharide-based inhibitor optimization

2.4 Sample preparation and test methods

Raw materials are weighed according to the formulations in Table 2. The aluminosilicate fines are homogenized, followed by gradual addition of the liquid silicate binder and Disaccharide-based inhibitor. The mixture is mechanically blended to obtain a homogeneous mortar and stored in airtight containers to prevent moisture exchange and contamination. The mortar is gently remixed before use, when required, to restore homogeneity[9]. Laboratory testing is conducted in accordance with relevant IndianStandards (IS 1528) and ISO standard to evaluate the thermo-mechanical behavior and refractoriness of the developed ready-to-use refractory mortar.To evaluate Flexural bonding strength of the mortar joint is determined using a three-point bending method in accordance with ISO 13765-4. Test specimens are prepared using refractory brick pieces of dimensions 57.5 × 25 × 25 mm, cut to the specified tolerances (±1 mm for length, ±0.1 mm for width, and ±0.2 mm for height). The bonding faces are kept smooth, clean, and free from cracks or dust to ensure proper adhesion.Prior to bonding, the test pieces aredried at 110 ± 5 °C until constant weight and then cooled to room temperature. A uniform layer of well-mixed mortar (~2 mm thickness) is applied on the bonding faces of two test pieces, which are then joined together while applying slight pressure and lateral movement to ensure proper contact and removal of excess mortar.The bonded specimens areair-dried for 24 hours, followed by staged oven drying (110 ^{0}C±5^{0}C) and subsequent firing under controlled heating conditions (5^{0}C/min) as per the standard. A total of five bonded specimens (10 pieces) are prepared for testing to ensure statistical reliability.The flexural bonding strength is calculated as the modulus of rupture using:
(2)

$$MOR = \frac{3PL}{2bd^2} \quad \frac{3PL}{2bd^2}$$

Where: P = Maximum load at fracture (N), L = Span length between supports (mm),
b = Specimen width (mm) and d = Specimen thickness (mm).The load is applied at a constant rate of 13 ± 1.3 N/s for dense refractory specimens of size 57.5 × 25 × 25 mm, in accordance withISO 13765-4. The load is applied at the center of the bonded interface until failure occurred.Permanent linear change is determined in accordance

with IS 1528 (Part 6) to assess dimensional stability after firing. Prismatic specimens of dimensions similar to MOR bars are prepared directly from the ready-to-use mortar. The initial length is measured at room temperature using a calibrated Vernier caliper. (3)

$$PLC = \frac{L_f - L_0}{L_0} \frac{L_f - L_0}{L_0} \times 100$$

Where, L_0= Initial length of the specimen before firing, L_f= Final length of the specimen after firing. The refractoriness of the ready-to-use mortar is determined by the Pyrometric Cone Equivalent (PCE) method in accordance with IS 1528 (Part 1). The material is used as received, without drying or water addition, and ground to pass a 212 µm IS sieve. Test cones are molded into standard tetrahedral shapes (25 mm height, 8 mm base). The cones are mounted at 82° angle alongside standard Orton cones, and the PCE is determined by comparative deformation during heating.Bulk chemical composition of the ready-to-use refractory mortar is determined by wavelength dispersive X-ray fluorescence (WDXRF) using the fused bead method, in accordance with IS 1528 (Part 9) and IS 12107. WDXRF analysis is employed due to its high accuracy and reproducibility for major oxides such as Al_2O_3 and SiO_2, which govern refractory bonding behavior.For analysis, the mortar sample is ground to pass a 212 µm IS sieve. A representative portion is mixed with a suitable flux and fused at high temperature to form a homogeneous glass bead, ensuring elimination of particle size, mineralogical, and matrix effects. The fused bead is analyzed using a calibrated
Wave dispersive X-ray fluorescence (WDXRF) spectrometer to obtain quantitative oxide compositions.Scanning electron microscope (SEM) coupled with Energy dispersive spectrometer (EDS) is used to examine microstructure and localized chemistry of the refractory mortar after firing up to 1400 °C. Grain morphology, porosity, and bonding phases are observed by SEM, while EDS provided elemental analysis at selected regions. Specimens are epoxy mounted, polished to 0.25 µm, coated for conductivity, and analyzed following ASTM E1508.

3. Result and Discussion

3.1 Shelf-life performance and inhibitor optimization

The Shelf life is strongly influenced by the Disaccharide-based inhibitor concentration. Lower levels (T-1 to T-3) resulted in premature silicate polymerization and rapid viscosity increase, whereas higher levels (T-4 to T-6) improved storage stability. Trial-5 shows the longest shelf life (>6 months) while maintaining good workability. Further inhibitor addition provided no significant benefit, indicating an optimum concentration range for effective polymerization control without affecting subsequent binder activation.In Fig. 2, shelf life increases progressively with inhibitor addition and reaches a plateau beyond ~4 wt.%. The dashed band (4–6 wt.%) indicates the optimum inhibitor range for extended storage stability without further significant improvement.

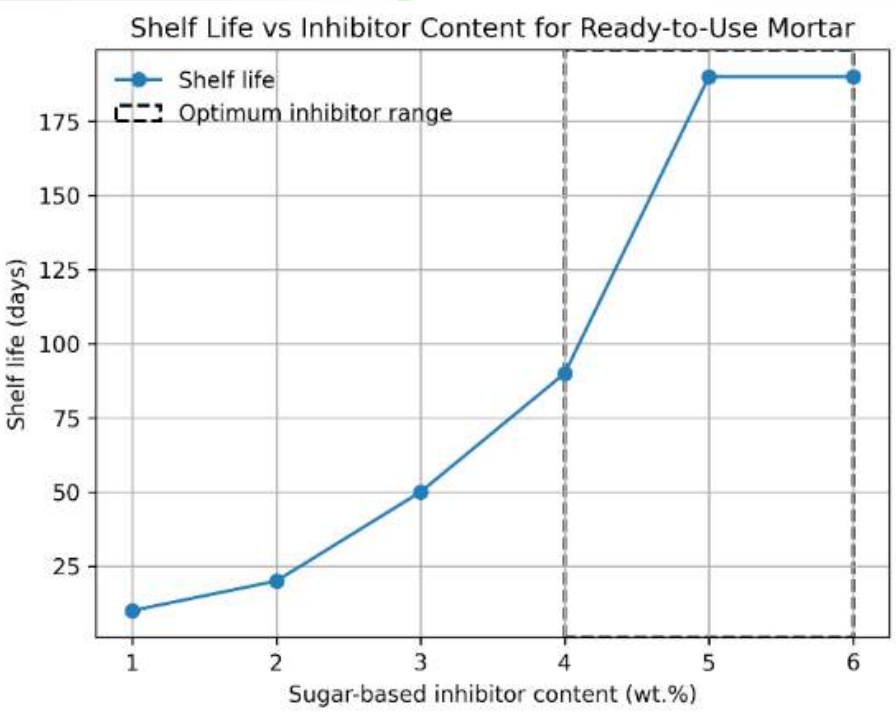


Figure 2 Shelf life of the ready-to-use refractory mortar as a function of Disaccharide-based inhibitor content

3.2 Laboratory Performance

The developed ready-to-use mortar exhibited good flexural bonding strength at room temperature, which further increased after firing at 1000 and 1400 °C, indicating effective silicate binder activation and ceramic bond formation. PLC results shows controlled dimensional change and good volume stability, attributed to optimized aggregate packing and balanced aluminosilicate chemistry. PCE testing confirmed suitable refractoriness for steelmaking applications, with no adverse effect from inhibitor incorporation.Fig. 3 shows strength retention and recovery at elevated temperatures indicate effective ceramic bonding, with Trial-5 showing pronounced strength development at 1400 °C.

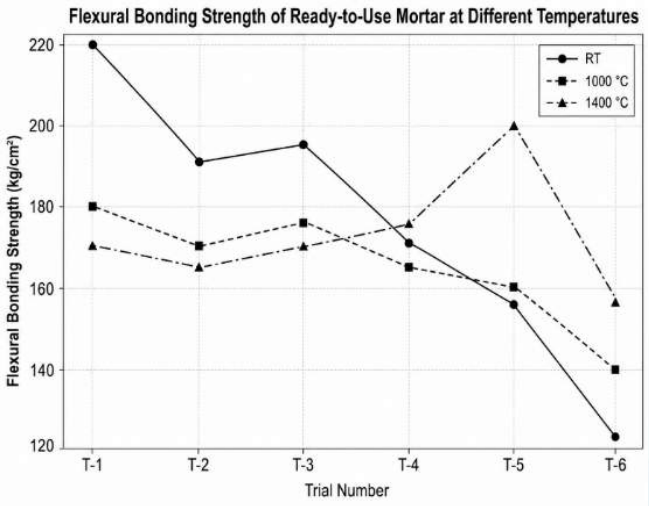


Figure 3 Flexural bonding strength of ready-to-use refractory mortar formulations at room temperature, 1000 °C, and 1400 °C

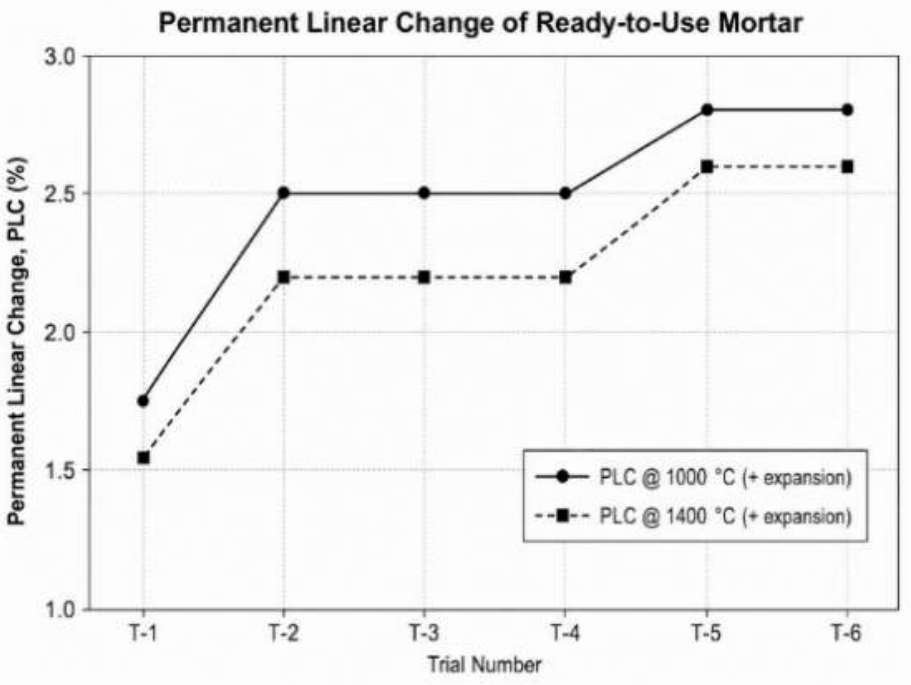


Figure 4 PLC of ready-to-use refractory mortar formulations after firing at1000 °C and 1400 °C. Positive values indicate expansion (+)

Laboratory evaluation indicated that the developed mortar exhibited a pyrometric cone equivalent (PCE) of Orton Cone No. 33, corresponding to a refractoriness of approximately 1743 °C, as determined in accordance with IS 1528 (Part 1).

3.3 Correlation with Industrial Performance

The industrial performance of the developed ready-to-use mortar is evaluated through phased trials conducted under closed tundish casting conditions. The trials progressed from short-duration campaigns to a full 12-hour casting cycle, enabling assessment under increasing thermal and operational severity. Across all phases, the mortar exhibited stable application behavior after storage, with satisfactory adhesion to refractory substrates following brief manual remixing where required.

Fig. 5 (a) shows Al-Paste A50 mortar after application to the Submerged entry nozzle (SEN) prior to casting, showing uniform coverage and good adhesion and in Fig. 5 (b), strand view after mortar application, confirming proper seating of the SEN and joint continuity before start of casting.



Figure 5 (a) Al-Paste A50 mortar after application to the submerged entry nozzle (SEN); (b) Strand view after mortar application

During casting, strands utilizing the developed mortar operated without difficulty. Casting stoppages, where encountered, are attributed to steel grade–related clogging and are not associated with mortar or joint failure.

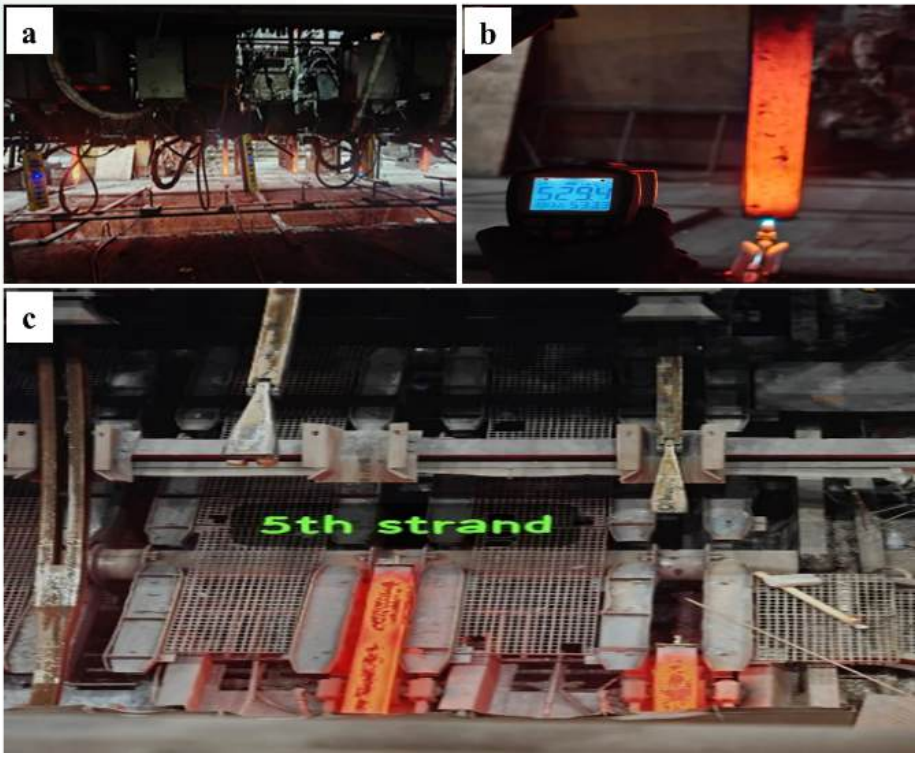


Figure 6 (a) Beginning of closed tundish casting operation after installation of the ready-to-use mortar joint; (b)Temperature monitoring during casting; (c) Fifth strand operation during casting

Fig. 6 (b) shows temperature monitoring during casting indicating stable thermal conditions at the joint region and in Fig. b (c), fifth strand operation during casting, confirming uninterrupted metal flow and stable strand performance.

According to the Fig. 7, the joint exhibits a uniformly sintered surface with no evidence of molten steel penetration at the interface between the well block and the submerged entry nozzle, indicating effective ceramic bonding and joint integrity after service.

Fig. 8 shows surface examination of the deskulled joints further confirmed effective ceramic bonding and structural integrity after service.

In Fig. 8 (a), macroscopic surface appearance of the deskulled ready-to-use mortar after closed tundish casting, showing a smooth, uniformly sintered surface with even reddish-brown coloration, indicative of consistent thermal exposure. No visible cracks or surface disintegration are observed, suggesting effective ceramic bonding and structural stability after service

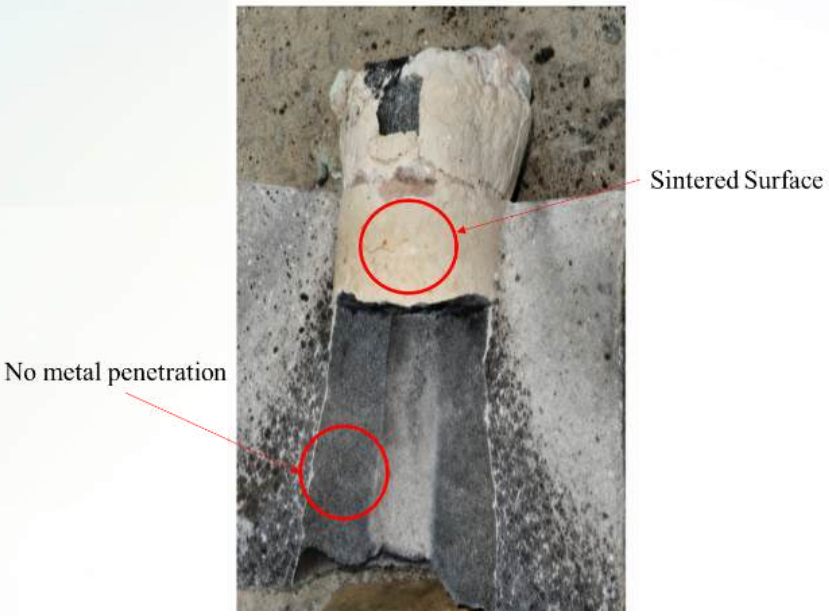


Figure 7 deskulled joint surface after closed tundish casting using the developed ready-to-use mortar

and in Fig. 8 (b), representative SEM micrograph of the mortar surface after casting, illustrating dense microstructure and low open porosity and Fig. 8(c) shows corresponding EDS elemental mapping of the joint region, confirming uniform distribution of major oxides and absence of metal penetration, the green region represents Al (aluminum), while the red region represents Si (silicon).

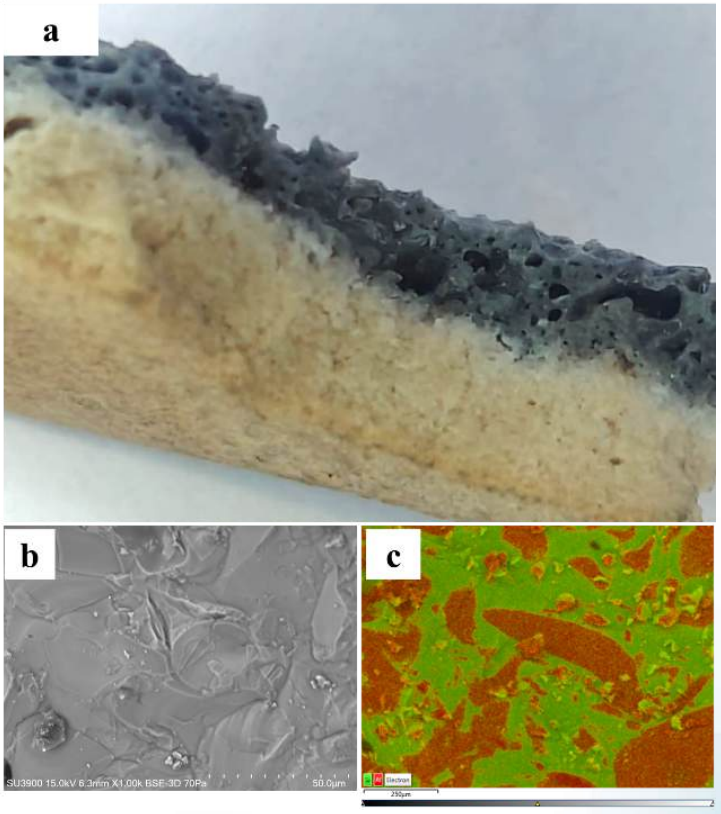


Figure 8(a) Macroscopic surface appearance of the deskulled ready-to-use mortar after closed tundish casting, (b) Representative SEM micrograph of the mortar surface after casting, (c) Corresponding EDS elemental mapping of the joint region

The final trial successfully completed the targeted 12-hour casting campaign, demonstrating that the extended shelf life achieved through binder inhibition does not adversely affect high-temperature joint performance.The industrial observations correlate well with laboratory results and confirm the suitability of the developed ready-to-use mortar for demanding closed casting operations.

4. Conclusion

A super-duty ready-to-use refractory mortar suitable for steelmaking applications is successfully developed by combining an optimized aluminosilicate fine aggregate system with a modified silicate binder chemistry. The incorporation of a Disaccharide-based organic reaction inhibitor effectively suppressed premature silicate polymerization during ambient storage, resulting in a shelf life of up to six months without adversely affecting high-temperature performance[8].

Laboratory testing confirmed that the developed mortar exhibited adequate refractoriness, controlled dimensional change, and strong ceramic bonding after firing at elevated temperatures. These properties are attributed to the optimized particle size distribution and balanced aluminosilicate chemistry of the formulation[7].Industrial trials conducted under closed tundish casting conditions further validated the laboratory findings. The mortar demonstrated stable application behavior after storage, satisfactory adhesion, and reliable joint integrity during a continuous 12-hour casting campaign. Post-casting inspections revealed uniformly sintered joints with no evidence of molten steel penetration or excessive shrinkage.The results indicate that the developed ready-to-use refractory mortar provides a reliable jointing solution for steel ladle and tundish operations, offering improved storage stability while maintaining robust service performance in demanding steelmaking environments.

Acknowledgement

The authors would like to acknowledge the support and facilities provided by the R&D and plant teams of IFGL Refractories, India, for enabling the development, laboratory evaluation, and industrial trials of the ready-to-use refractory mortar described in this study. The authors are grateful to the operations and casting teams for their cooperation during the closed tundish casting trials and for providing valuable practical inputs during industrial validation.The authors also acknowledge the assistance of the characterization and quality control teams for conducting material testing and microstructural analysis. AI-based tools are used only for language refinement; all experimental design, data generation, analysis, and interpretation are performed entirely by the authors.

References

1. M. Mobasheri, A. M. Hadian, Y. Mohammadi, B. Azimi, and M. Kamali, “The effect of plasticizers on rheological, physical and mechanical properties of low cement high alumina gunning refractories,” Research Square (Research Square), Dec. 2024, doi: 10.21203/rs.3.rs-5182459/v1.
2. J. C. G. de C. Bonaldo, “Modeling the link between microstructure, thermomechanical treatment and mechanical performance of refractory products,” HAL (Le Centre pour la Communication ScientifiqueDirecte), Jan. 2022, Accessed: Aug. 2025. [Online]. Available:https://theses.hal.science/tel-03651306
3. R. A. Heindl and W. L. Pendergast, “Some properties of heat-setting refractory mortars,” Journal of research of the National Bureau of Standards, vol. 30, no. 4, p. 303, Apr. 1943, doi: 10.6028/jres.030.022.

4. V. C. Miguel, D. Fini, V. S. Pinto, M. H. Moreira, V. C. Pandolfelli, and A. P. Luz, “Crack-free caustic magnesia-bonded refractory castables,” Ceramics International, vol. 47, no. 12, p. 17255, Mar. 2021, doi: 10.1016/j.ceramint.2021.03.036.
5. A. J. Barakat et al., “The effect of permeability enhancement on dry-out behavior of CA- and microsilica gel-bonded castables as determined by NMR,” Ceramics International, vol. 46, no. 9, p. 13556, Feb. 2020, doi: 10.1016/j.ceramint.2020.02.141.
6. S. A. Bernal, J. L. Provis, V. Rose, and R. M. de Gutiérrez, “Evolution of binder structure in sodium silicate-activated slag-metakaolin blends,” Cement and Concrete Composites, vol. 33, no. 1, p. 46, Sep. 2010, doi: 10.1016/j.cemconcomp.2010.09.004.
7. R. Torrecillas, M. A. Saínz, and J. S. Moya, “Alumina-alumina and mullite-mullite joining by reaction sintering process,” ScriptaMetallurgica et Materialia, vol. 31, no. 8, p. 1031, Oct. 1994, doi: 10.1016/0956-716x(94)90522-3.
8. L. Jin, G. Huang, Y.-Y. Li, X. Zhang, Y. Ji, and Z. Xu, “Positive Influence of Liquid Sodium Silicate on the Setting Time, Polymerization, and Strength Development Mechanism of MSWI Bottom Ash Alkali-Activated Mortars,” Materials, vol. 14, no. 8, p. 1927, Apr. 2021, doi: 10.3390/ma14081927.
9. M. S. de França, B. Cazacliu, F. A. Cardoso, and R. G. Pileggi, “Influence of mixing process on mortars rheological behavior through rotational rheometry,” Construction and Building Materials, vol. 223, p. 81, Jul. 2019, doi: 10.1016/j.conbuildmat.2019.06.213.

ADVANCED MOULD FLUX DESIGN FOR IMPROVED SURFACE QUALITY IN HIGH- AND LOW-SPEED CASTERS

Md Shamim Ahmed, Rahul Kumar, Mrityunjoy Pal, Manikanta Srinivas

Calderys Steelcasting India Private Ltd

Shamim.ahmed@calderys.com

Abstract

Continuous casting operations demand precise control of mould flux behavior to maintain optimal heat transfer and lubrication across a wide range of casting speeds. The dynamic interaction between molten steel, solidifying shell, and slag film becomes increasingly sensitive to flux characteristics as casting speed varies. This study focuses on the engineering of mould powder systems specifically tailored for lowspeed and high-speed casting conditions. At elevated casting speeds, the reduced residence time within the mould necessitates fluxes with controlled melting rates, low break temperatures, and stable liquid slag layers to ensure consistent lubrication and prevent shell sticking. The design strategy emphasizes controlling viscosity-temperature relationships and minimizing excessive crystallization to sustain a uniform liquid slag film under high thermal gradients. This work highlights the critical role of adaptive mould flux engineering in achieving consistent metallurgical performance under varying casting speeds.

Keywords: Slab caster, Break Temperature, Hot Stage Microscopy, Mould fluxes, Cuspidine.

Introduction

Continuous casting is the most widely adopted process to cast steel due to its high productivity and superior efficiency. During continuous casting, the formation and growth of the solidifying steel shell involve complex thermal and mechanical conditions within the mould.[1] To maintain stable heat transfer and suitable lubrication between the steel shell and the mould, mould flux plays the most important role. Mould flux has been added on the top of the mould above liquid steel, and this mould flux later transforms into sintered form and then, into mould slag. Mould flux characteristics are mainly governed by mould flux viscosity, break temperature, crystallization behaviour, melting point, and melting rate. [2] Mould flux design varies with the steel chemistry, casting speed of steel, and other caster operational parameters. At low casting speed, mould frequency is low, and negative strip time is on higher side, leads to more mould slag infiltration. However, at high casting speed, negative strip time decreases and subsequently, a drop of mould slag infiltration is there. Slag infiltration should be tuned with mould slag generation. And there is requirement of controlled melting rate of the mould flux for optimum slag generation as per requirement of the caster machine. Along with this, viscosity of the mould flux needs to be designed to obtain sufficient mould slag film to prevent steel shell to the mould. Break temperature of the mould flux is the point at which recrystallization starts from the mould slag within the mould.[3] This break temperature and crystallization tendency of the mould flux help in controlling the heat transfer within the mould. At high casting speed, mould slag film must sustain a balance between lubrication and heat transfer. Heat transfer needs to be in proper control, as higher heat transfer could lead to surface defects, like longitudinal cracks, while lower heat transfer could prevent the formation of thicker steel shells in the mould. [4] In this paper, the focus is on designing a single, but optimum mould flux for both low- and high-speed casting, with emphasis on melting rate, melting point, break temperature, viscosity, and crystallagraphic phases to achieve optimum slag generation,

stable slag film formation, and controlled heat transfer.

Experimental Work

The experiment for this study has been conducted with three granular mould fluxes, designated as A, B, and C. The compositions of these mould fluxes are shown in Table 1. The formulations of these mould fluxes were made using different selected raw materials to obtain the required chemical composition and other mould flux characteristics. The chemical composition of all three mould fluxes was determined using X-ray fluorescence (XRF) analysis through the fused bead method. The total carbon content of these fluxes was determined using the Carbon-Sulphur (CS) analyzer. The CO_2 content and crystal water were measured using CO_2/crystal-water (CW) analyzer.

Table 1: Chemical composition of different mould fluxes during the work

%	A	B	C
Basicity	0.88	0.82	0.78
MgO	2.70	3.20	3.70
Al_2O_3 + TiO_2	4.60	4.80	3.90
Na_2O + K_2O	8.50	11.2	11.5
F + MnO_2	8.10	9.10	10.40
C Total	5.60	6.40	5.80

The viscosity of the mould flux has been determined by the theoretical IRSID models (which has been described in equation 1), and the calculated results given in Table 2.

Eq (1): Viscosity(in Pa*s), $\eta = A.T.\exp(B/T)$

where A and B are constants determined by molar fractions of various oxides and fluorides, and T is the temperature [K].[5] (1 Pa*s = 10 Poise)

The break temperature of the mould flux has been determined by Sridhar et al method [3] (which has been described in equation 2), and the calculated results given in Table 2.

Eq (2): $(Tbr - 1180)(°C) = -3{\cdot}94\%Al_2O_3 - 7{\cdot}87\%SiO_2 + 11{\cdot}37\%CaO - 9{\cdot}88\%MgO + 24{\cdot}34\%Fe_2O_3 + 0{\cdot}23\%MnO - 308{\cdot}7\%K_2O + 6{\cdot}96\%Na_2O - 17{\cdot}32\%F$

The Hot Stage Microscopy has also been used for the measurement of the melting point and the flowing point of each mould flux, and the results have been shown in Figure 1 and Table 2. Thermodynamics Software FactSage 8.4 is also used for the calculation of crystallographic phases during recrystallization process of different mould fluxes.

Results & Discussion

The data generated during this work have been collated in Table 2.

Table 2: Characterization of different types of mould flux			
	A	**B**	**C**
Viscosity at 1300 °C (Poise)	1.60	1.10	0.70
Break Temperature (°C)	1104	1045	1008
Melting Point (°C)	1144	1086	1075
Melting Point (°C)	1145	1107	1094

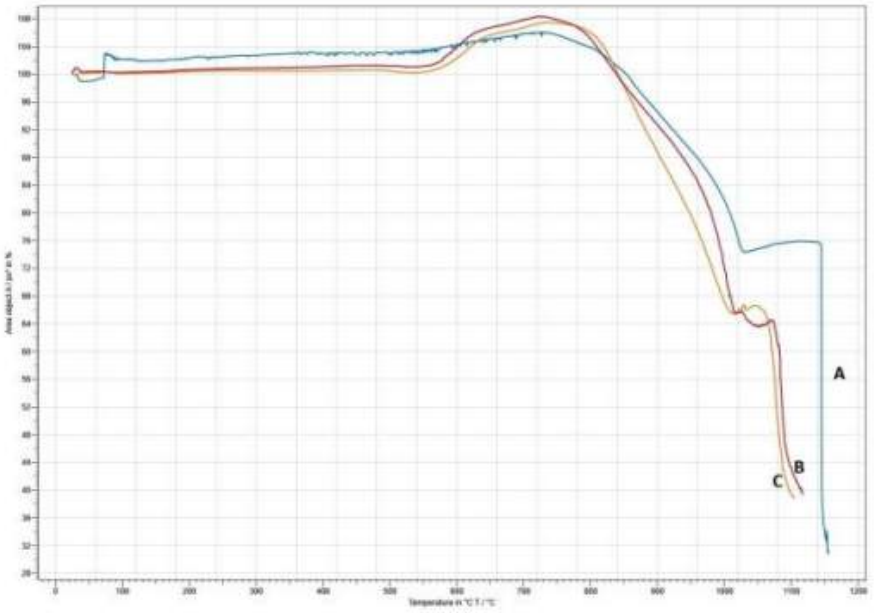


Figure 1: Melting behaviour of different fluxes determined by Hot Stage Microscopy

From Table 2, it is found that the viscosity, melting point and break temperature of the mould flux A is the highest amongst all the mould fluxes, and mould flux C has lowest viscosity, melting point and break temperature. The value of viscosity, break temperature and melting point in Flux B are in between all the three mould fluxes.

The amount of Crystallographic phases & Liquid Slag at 1000°C, which is determined by FactSage software, as given in Table 3.

Table 3: Crystallographic phases & Slag amount at 1000°C determined by FactSage software			
	A	**B**	**C**
Slag	62.7	69.1	72.4
Cuspidine	37.3	30.9	27.6

Cuspidine ($3CaO{\cdot}2SiO_2{\cdot}CaF_2$) is an important crystalline phase in mould flux films.[6] Higher cuspidine formation generally reduces heat transfer. From Table 3, it can be observed that cuspidine content of three mould fluxes A, B and C are in the sequence as A > B > C. The observed cuspidine content is also correlated with break temperature data of Table 2, and it can be pointed out that there is direct relation of cuspidine content and break temperature of mould fluxes. Higher break temperature could be related to lower cuspidine content in the mould flux, and subsequently reduction in heat transfer through the mould fluxes.

The field examination has been conducted with these three mould fluxes A, B and C for slab casting of Low Carbon Steel. With the use of these mould fluxes, trials in two cases have been executed; Case I and Case II are corresponding to Low and High casting speeds. The details of caster parameters, steel chemistry and mould flux performance for Case I and Case II are mentioned in Table 4, 5, 6 and 7, respectively. Several parameters have been considered for performance indicator of the mould fluxes for both Case I and Case II.

Table 4: Details of Caster parameters in two cases

Caster Parameters	Case I	Case II
Casting Speed, m/min	1.0	1.85
Section Size, mm2	1300 x 230	1270 x 230
Stroke Length, mm	7.0	7.0
Mould Water Flow Broad Face, L/min	4100	3900
Mould Water Flow Narrow Face, L/min	440	490

Table 5: Details of Steel Chemistry

%	Value
C	0.041
Mn	0.177
S	0.008
P	0.009
Si	0.15
Al	0.042
Ca	0.002
N	0.007

Table 6: Mould Flux Performance of different mould fluxes in Case I			
Performance Indicators	**A**	**B**	**C**
Cracks	No	No	No
Stickers	No	No	Yes
BPS Thermograph	Normal	Normal	Abnormal
Delta Temperature	Normal	Normal	High
Mould Heat Flux	Normal	Normal	High
Liquid slag pool depth (mm)	11-12	12-14	16-18
Slag Rim Formation	Soft & Normal	Soft & Normal	Hard & High
Mould Level Fluctuations (mm)	+/- 2	+/- 2	+/- 3

Table 7: Mould Flux Performance of different mould fluxes in Case II			
Performance Indicators	**A**	**B**	**C**
Cracks	No	No	No
Stickers	Yes	No	No
BPS Thermograph	Abnormal	Normal	Normal
Delta Temperature	Low	Normal	Normal
Mould Heat Flux	Low	Normal	Normal
Liquid slag pool depth (mm)	9-11	11-13	15-17
Slag Rim Formation	Unburnt	Soft & Normal	Soft & High
Mould Level Fluctuations (mm)	+/- 4	+/- 2	+/- 2

It is to be noted that Breakout prevention system (BPS) attached to the mould prevents the steel strand breakout and BPD thermograph gives an early indication if any abnormalities are present. BPS system measures the mould plate cold face temperature through thermocouples, and subsequently it identifies the sticker tendency and act for sudden reduction in casting speed, if required.

From Table 4, 6 and 7, it is observed that in case of low casting speeds i.e. Case I, mould flux A and B performs well, but mould flux C is showing abnormal behaviour and leads to increased heat transfer and high delta temperature, however, there are no cracks observed, but there is always some possibilities of crack generation in this scenario of high heat transfer; and there is also chance of mould flux entrapment. While in case of high casting speed i.e., Case II, mould flux B and C is Ok, but mould flux A shows inadequate flux behavior due to insufficient melting, unburnt slag is observed; this insufficient slag infiltration due to lower slag pool and high viscosity of the mould slag in mould flux A, also leads to lower heat transfer, BPS alarms and sticker formation. In case of Flux B, performance is good in both cases I and II i.e., at low casting and high casting speed, and it seems Flux B needs to

be preferred for a complete range of casting speed for low carbon steel slab casting.

Conclusion

This paper could be concluded with positive note as follows:

1. Flux B, with intermediate break temperature, looks most suitable mould flux for both low- and high-speed continuous casting, with respect to other fluxes.

2. Correlation between break temperature and cuspidine gives good direction regarding heat transfer through the mould flux, which could help in controlling heat transfer and preventing sticker formation in the mould.

3. Cuspidine content needs to be optimum to prevent longitudinal cracks; lower Cuspidine content increases possibilities of cracks due to increased heat transfer.

4. Higher carbon percentage in Flux B helps in controlling the slag rim at both low and high casting speed. Slag The hard slag rim generation provides an indication to bad BPS thermograph.

References

[1] Mills, K. C., & Fox, A. B. (2003). The Role of Mould Fluxes in Continuous Casting—So Simple Yet So Complex. ISIJ International, 43(10), 1479–1486.

[2] Mills, K. C., Fox, A. B., Li, Z., & Thackray, R. P. (2005). Performance and Properties of Mould Fluxes. Ironmaking & Steelmaking, 32(1), 26–34.

[3] Sridhar, S., Mills, K. C., Afrange, O. D. C., & others (2000). Break Temperature of Mould Fluxes and Their Relevance to Continuous Casting. Ironmaking & Steelmaking, 27(3), 238–242.

[4] Yuan, Z., & Zhu, L. (2022). Effect of Basicity on Crystallization, Heat Transfer, and Structure of Mould Flux for High-Speed Thin Slab Continuous Casting. Ironmaking & Steelmaking, 49(4), 375–397.

[5] V. Rusnakova, J. Kijac, G. Grimplini and G. Rusnak: Acta Metallurgica Slovaca, 16 (2010), 172- 180.

[6] Cicutti, C., Valdez, M., Prapakorn, K., & Cramb, A. W. (2011). Thermodynamic Modeling of Mineralogical Phases Formed by Continuous Casting Powders. Thermochimica Acta, 512(1–2), 129–133

UTILIZATION OF ALUMINIUM SALT SLAG FOR THE PRODUCTION OF CORDIERITE

Urbánek Jan[1], Mauermann Lukáš[1], Antoš Petr[1], Technopark Kralupy, University of Chemistry and Technology, Prague, CZECHIA

(1. Researcher, UCT Prague, Czechia)

Corresponding author's e-mail: urbanekj@vscht.cz

Abstract

The potential of high-temperature treatment of waste salt slag as an alternative to conventional wet processing was investigated. The objectives of the treatment were to remove hazardous non-oxidized compounds, separate chlorides and obtain a high-alumina raw material as the primary product. Based on the laboratory-scale results, the proposed processing technology was demonstrated at the pilot scale using a rotary kiln. The subsequent research was focused on the production of cordierite from salt slag via one-stage and two-stage processing routes.

Keywords: Salt slag, rotary kiln, high alumina, cordierite.

1. Introduction

Salt slag is a hazardous waste by-product generated during secondary aluminium production. Depending on the raw mix, the amount of salt slag produced per ton of secondary aluminium ranges from 200 to 500 kg [CITATION Tsa12 \l 1029]. Salt slag is usually a complex conglomerate containing metal oxides (Al_2O_3, MgO, FeO, and CaO), nitrides (AlN), chlorides (NaCl and KCl), fluorides (CaF_2 and NaF), carbides (Al_4C_3), sulfides, phosphides, soil, and other impurities[CITATION Kul26 \l 1029]. Due to the risk of atmospheric pollution (emission of toxic gases upon contact with water) and groundwater contamination (high salt content that can percolate and cause an increase in salinity), [CITATION Isa22 \l 1029] landfilling of this waste represents a significant economic and environmental burden. Its reuse may be limited by the energy and process demands associated with its treatment, transportation and storage[CITATION Gil16 \l 1029]. One available option is the wet process, which includes steps such as crushing and screening, water leaching and filtration, gas removal, and evaporation and crystallization.[CITATION Pad21 \l 1029] The resulting filter cake can be used as a source of high-alumina feedstock or as an inert filler, while the crystallized NaCl and KCl can be recycled as fluxes. The second approach, primarily examined in this work, is a high-temperature process. During thermal treatment of the slag, impurities are oxidized and chlorides are volatilized[CITATION Wal12 \l 1029] and subsequently captured in a filtration system. The fired product is an alumina-rich material, similar to the first route.

2. Materials and methods

The study involved two compositionally similar salt slags. One originated from a secondary aluminum production plant, while the other was collected from a landfill where salt slags from multiple secondary aluminum producers are deposited. They consist primarily of Al_2O_3 together with NaCl and KCl salts. Smaller amounts of SiO_2, MgO, metallic aluminum, and non-oxide phases, such as nitrides, are also present. Upon contact with water, the non-oxide phases undergo hydrolysis, releasing hazardous gases, primarily ammonia, along with other gaseous products.

The raw materials were first manually

crushed and then ground in a planetary ball mill. The resulting powder was placed in a corundum crucible and fired in a laboratory chamber furnace at temperatures ranging from 500 to 1400 °C for 3 h. After cooling, the chemical composition of the fired samples was analyzed by X-ray fluorescence (XRF). The chloride removal efficiency was evaluated based on the residual chlorine content. For comparison, a slag sample was also subjected to water leaching, yielding a filtrate and a filter cake. The chemical composition of the filter cake was used as a reference for evaluating the high-temperature treatment.

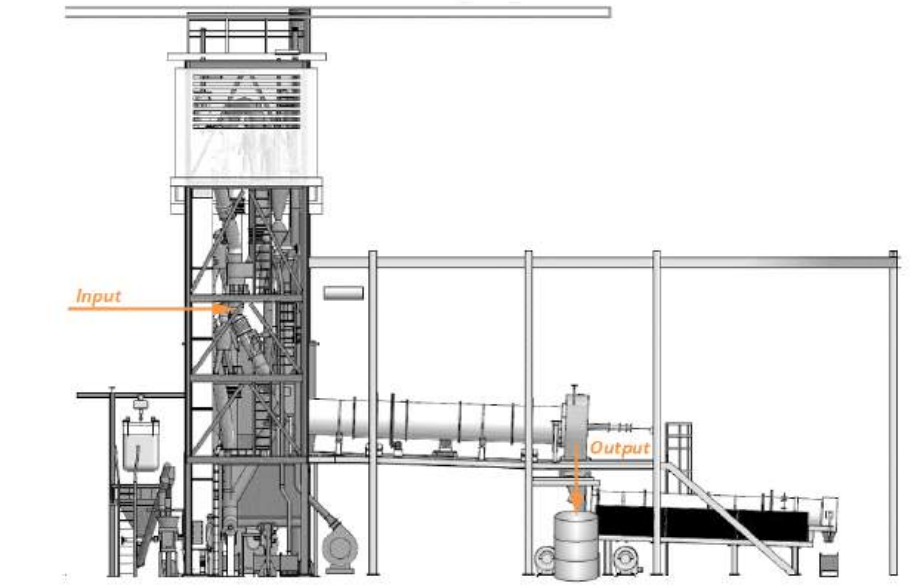


Figure 1 Pilot rotary kiln model

Based on the laboratory results, the high-temperature process was verified at the pilot scale using a pilot rotary kiln. A schematic of the kiln is shown in Figure 1. The raw material was first manually crushed, ground in a pin mill, granulated with water, and subsequently dried. The aim was to produce a high-alumina fired product and, as a by-product, a mixture of NaCl and KCl. During firing, the chlorides volatilize and are subsequently recovered from the flue gas using filters after cooling. To minimize chloride deposition in the gas ducts, limestone was added to the cooling chamber. Approximately 200 kg of granules were prepared and fired under these conditions. After cooling, the chemical composition was analyzed by X-ray fluorescence (XRF), and the phase composition was determined by X-ray diffraction (XRD).

The second part of the research focused on the processing of salt slag by firing and the subsequent or simultaneous formation of cordierite. A one- and two-stage process was investigated under laboratory conditions. In the two-stage process, the salt slag was first fired as described above. After cooling, the fired slag was ground and mixed with micro-milled sand or diatomaceous earth as SiO_2 sources and with talc or MgO as MgO sources. Water was added to the mixture, and spherical samples approximately 3 cm in diameter were manually shaped. The samples were then dried and fired at 1300 °C. In the one-stage process, the initial firing step was omitted, and the salt slag was directly mixed with the SiO_2 and MgO sources and subsequently fired. The presence and phase composition of the prepared cordierite were analyzed using X-ray diffraction (XRD).

3. Results and discussion

Firing of the salt slag samples resulted in the volatilization of NaCl and KCl chlorides and the oxidation of reactive non-oxide phases, including metallic aluminum and AlN. Although the two input salt slags exhibited similar chemical and phase compositions, their behavior during firing differed. The landfill-derived salt slag contained only trace amounts of chlorides after firing at 1300 °C, whereas the slag obtained directly from the secondary aluminum producer still contained more than 5 wt.% chlorides. The effectiveness of the thermal process was also demonstrated by results from pilot-scale firing in a rotary kiln (Table 1).

Fired product	
Oxide	**Content [%]**
Al_2O_3	70.6
SiO_2	9.9
MgO	7.0
Fe_2O_3	2.4
Na_2O	4.8
K_2O	0.5
CaO	3.1
Cl	0.1
Residue	1.6
∑Std	96.1

Kiln fly dust	
Oxide	**Content [%]**
Na	23.7
K	14.3
Cl	44.4
Ca	12.4
Si	1.8
Mg	0.7
Al	0.8
Fe	0.7
Residue	1.5
∑Std	105.3

Table 1 Chemical composition of fired product and kiln fly dust from pilot rotary kiln. ∑Std means the sum before standardization to 100 %

While the fired product contains only trace amounts of chlorine, the secondary product collected as bypass dust consists predominantly of NaCl and KCl together with the limestone added to the cooling chamber. The obtained product is comparable to that produced by wet leaching.

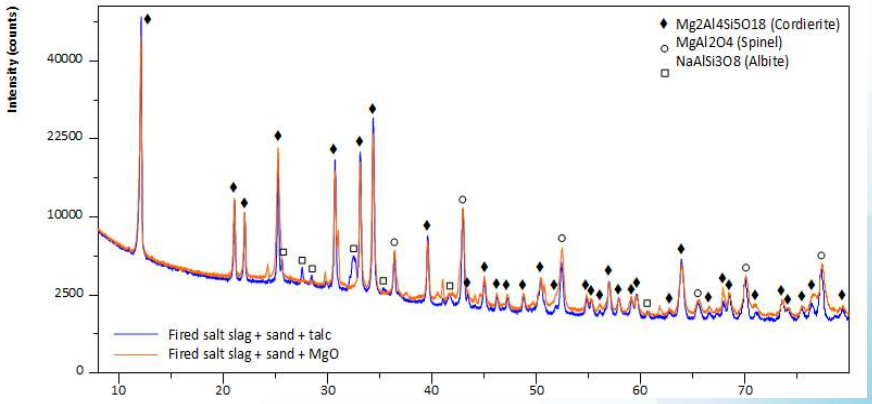


Figure 2 Diffractograms of fired mixture of pre-fired salt slag, micro-milled sand and MgO / talc

The obtained high-alumina raw material can be used for the preparation of cordierite, as demonstrated by the XRD patterns shown in Figure 2. Although different raw materials (talc, sand, diatomaceous earth, and MgO) were used in the starting mixtures, the resulting diffractograms are very similar. Cordierite could also be prepared by a single-stage process in which the salt slag was directly mixed with the other raw materials before firing. However, this approach makes the firing process more challenging due to the presence of chlorides. For example, rapid heating caused the samples to foam as a result of gas evolution.

4. Conclusions

The feasibility of thermal treatment of salt slag at both the laboratory and pilot scales has been verified. The results are comparable to those obtained by the conventional wet process, in which the slag is leached with water. This process produces a high-alumina feedstock with potential use in the production of refractory materials, although its wider use is hindered by the increased Na_2O content. Other potential applications include its use as a filler or as an additive in cement. The by-product is a mixture of NaCl and KCl, which can be recycled for secondary aluminum production. The study also confirmed the feasibility of using salt slag for cordierite production. The starting material can be either the high-alumina product obtained by thermal treatment of the slag or the untreated salt slag itself. This approach expands the possibilities for salt slag utilization and thereby increases its economic value.

References

1. P. Tsakiridis, „Aluminium salt slag characterization and utilization – A review," *Journal of Hazardous Materials*, pp. 217-218, 2012.
2. B. D. N. Kulikov, A. Kosovich, E. Partyko, Y. Mansurov, P. Yuryev, N. Stepanenko, Y. Baykovskiy, A. Durnopyanov, R. Blanev a M. Baranov, „Multistage Recycling of Aluminum Casting Slags: Metal Extraction and Salt Flux Regeneration," *Recycling, sv. 11, č. 52, pp. 1-21, 2026*.
3. I. Padilla, M. Romero, S. López-Andrés a A. López-Delgado, „Sustainable Management of Salt Slag," *Sustainability*, sv. 14, č. 4887, pp. 1-13, 2022.
4. A. Gil a S. Korili, „Management and valorization of aluminum saline slags: Current status and future trends," *Chemical Engineering Journal*, sv. 289, pp. 74-84, 2016.
5. S. K. Padamata, A. Yasinskiy a P. Polyakov, „A Review of Secondary Aluminum Production and Its Byproducts," *Recovery, Sorting, and Processing, of Secondary Aluminum*, sv. 73, č. 9, pp. 2603-2614, 2021.
6. D. Walker, W. Caley, S. Ferenczy a G. Kipouros, „ Modification of Steelmaking Slag by Additions of Salts from Aluminum Production," *High Temperature Materials and Processes*, sv. 31, č. 4-5, pp. 389-394, 2012.

DEVELOPMENT AND PERFORMANCE EVALUATION OF CALCIUM ALUMINATE CEMENT BONDED REFRACTORY SHOTCRETE FOR HIGH-TEMPERATURE APPLICATIONS

Polat, Buket[1], Nagar Alok[2]

[1]ÇİMSA ÇİMENTO
SANAYİ VE TİCARET A.Ş, TOROSLAR MAH. TEKKE CAD. YENİTAŞKENT – AKDENİZ, Mersin, 33013, TÜRKIYE
b.polat@cimsa.com.tr

[2]R 15 Ganesh Nagari, Koradi Road, Nagpur 441111 Maharashtra, INDIA
a.nagar@cimsa.com.tr

Abstract

This study focuses on the formulation of a refractory shotcrete designed for the internal metallic surfaces of industrial facilities, such as refineries, operating under harsh environmental conditions. A hydraulic binder system based on CAC 50 calcium aluminate cement was utilized to ensure robust resistance against acids, sulfates, and high-temperature exposure. The performance of the developed recipe was validated against stringent technical specifications, including a temperature resistance of at least 800^{0}C cold crushing strength > 35 MPa and an acid absorption rate < 1.5%. Furthermore, thermal conductivity was optimized to stay below 0.55 W/Mk at 350^{0}C while maintaining a bulk density of at least 1.6 g/cm^3. The dry method application technique was employed, focusing on the material's adhesion to metallic substrates and its post-drying dimensional stability. The results demonstrate that the proposed formulation meets and exceeds the minimum technical requirements for refractory applications, providing an effective solution for long-term industrial durability.

Keywords: Refractory shotcrete, calcium aluminate cement, refractory aggregate, high-temperature performance.

1. Introduction

Shotcrete is a method of placing concrete or mortar by projecting the material pneumatically at high velocity onto a receiving surface. In the dry-mix process, the cementitious constituents and aggregates are premixed and pneumatically conveyed through a hose, while water is introduced at the nozzle immediately before placement [1,2]. This process provides flexibility for intermittent placement and is particularly suitable for refractory materials [2,3]. These characteristics make dry-mix shotcrete attractive for the repair and lining of industrial units with complex geometries or restricted access. Refractory shotcrete differs from conventional structural shotcrete because the lining must retain adequate integrity under thermal exposure and, depending on the service environment, chemical attack. Calcium aluminate cement (CAC) is widely used as a hydraulic binder in refractory concretes. Unlike Portland cement systems, CAC does not generate portlandite during hydration, and CAC based refractory concretes can be combined with heat resistant aggregates to obtain improved high temperature performance [4]. The aggregate mineralogy is also important because it contributes to the refractory skeleton and affects the thermal stability of the composite [4,5]. heat-resistant filler is a commonly used aluminosilicate heat-resistant filler in CAC-bonded systems [4,5]. The objective of this study was to design and evaluate a deliberately simplified CAC-bonded dry-mix refractory shotcrete based on only three principal solid constituents: CAC 50, REGO heat-resistant refractory aggregate and heat-resistant filler. A relatively high CAC content of 35 wt.% was selected to provide a strong hydraulic bonding matrix while keeping the formulation simple. The material was assessed against target requirements for bulk density, cold crushing strength and

temperature resistance. Acid absorption resistance and thermal conductivity at 350 °C were included in the test program and were still under evaluation at the time of manuscript preparation.

2. Materials and Experimental Procedure

was used as the hydraulic refractory binder. REGO, with a particle size of 0-2 mm, was incorporated as a heat-resistant refractory aggregate, while a 3-5 mm heat-resistant filler formed the main refractory solid fraction. A key aspect of the formulation design was to obtain the required refractory performance using a simple three-component system with relatively high CAC content. The formulation ranges are presented in Table 1, while the selected chemical and physical characteristics of the raw materials are summarized in Table 2.

Table 1. Refractory shotcrete formulation

Raw material	Function
CAC 50	Hydraulic refractory binder
REGO	Fine refractory fraction
Heat-resistant refractory aggregate	Coarse refractory aggregate

CAC 50 was characterized by a high alumina content and a CA-dominant mineralogical composition, consistent with its use as a refractory hydraulic binder. The heat-resistant filler exhibited an aluminosilicate rich composition suitable for elevated-temperature exposure. The combination of a high CAC binder fraction with REGO and the heat-resistant filler was selected to provide a dense and mechanically stable refractory matrix while maintaining a relatively simple formulation.Table 2 Selected chemical and physical properties of the raw materials.

Table 2. Chemical and physical properties of the CAC 50 cement

Property	CAC 50
Al_2O_3, wt.%	53.17
CaO, wt.%	37.55
SiO_2, wt.%	4.81
Fe_2O_3, wt.%	1.22
A/C ratio	1.42
Blaine, cm^2/g	4140

The dry constituents were proportioned and blended to obtain a graded refractory mixture intended for dry shotcrete placement. In accordance with the dry-mix principle, the premixed solids are conveyed pneumatically and water is introduced at the nozzle during application [1,2]. The performance evaluation considered the requirements of at least 1.6 g/cm3 bulk density, at least 35 MPa cold crushing strength and temperature resistance of at least 800 °C. The test program also included acid absorption resistance (target

<=1.5%) and thermal conductivity at 350 °C (target <=0.55 W/mK). Detailed acid-exposure and thermal-conductivity results were not yet available and therefore are not interpreted in the present study.

3. Results and Discussion

3.1 Physical and mechanical performance

Despite the deliberately simple three-component formulation, the developed refractory shotcrete reached a bulk density of 2.3 g/cm^3, substantially above the minimum requirement of 1.6 g/cm^3. The measured cold crushing strength was 55 MPa compared with the specified minimum of 35 MPa, corresponding to approximately 57% higher strength than the target. The result is notable because the required mechanical performance was obtained without introducing a complex multi-component additive or filler system.

The formulation contains 35 wt.% CAC 50, representing a deliberately high hydraulic binder fraction for a refractory shotcrete. The remaining solid skeleton was kept simple, using only 5 wt.% REGO heat-resistant refractory aggregate (0-2 mm) and 60 wt.% heat-resistant filler (3-5 mm). This three component design was intended to minimize formulation complexity while providing sufficient fine material for matrix continuity and a heat-resistant coarse fraction. The measured density and strength indicate that this simplified, high-CAC approach was capable of producing a dense and mechanically coherent refractory composite.

3.2 High-temperature performance

High-temperature testing demonstrated that the developed material maintained its refractory integrity up to 1200 °C. This behavior is consistent with the use of CAC as a refractory hydraulic binder in combination with heat-resistant solid constituents. CAC-based refractory concretes are widely used at elevated temperatures, and their thermal performance depends strongly on both cement chemistry and the nature of the aggregate/filler system [4,5]. The high alumina content of the binder together with the aluminosilicate character of the heat-resistant filler contributes to a material system suitable for elevated temperature exposure.

The dominant crystalline phase in the CAC was CA, whereas the measured C12A7 content was low. At elevated temperatures, CAC hydrate bonds progressively transform, and ceramic bonding may develop depending on temperature and aggregate chemistry [5]. Because post-exposure phase evolution and microstructure were not characterized in the present work, the specific mechanism responsible for the observed high-temperature behavior cannot be assigned directly.

The experimental results demonstrate stable refractory performance under exposure up to 1200 °C.

3.3 Overall performance assessment

Table 3.Summary of refractory shotcrete performance

Property	Experimental result
Temperature resistance	1200 °C
Bulk density	2.3 g/cm³
Cold crushing strength	55 MPa

Table 3 shows that all currently completed performance tests satisfied the corresponding target values. The formulation exceeded the minimum temperature requirement by 400 °C and provided a substantial margin above the required cold crushing strength. However, a complete assessment for chemically aggressive and thermally insulating service requires completion of the acid absorption and thermal conductivity measurements. Accordingly, no conclusion regarding compliance with those two requirements is drawn at this stage.

4. Conclusions

A simplified CAC-bonded refractory shotcrete was formulated using only three principal solid constituents: 35 wt.% CAC 50, 5 wt.% REGO heat resistant refractory aggregate (0-2 mm), and 60 wt.% heat-resistant filler (3-5 mm). The relatively high cement content was intentionally selected to establish a robust hydraulic matrix while maintaining a low complexity formulation. The developed composite achieved a bulk density of 2.3 g/cm3 and a cold crushing strength of 55 MPa, exceeding the respective target values of 1.6 g/cm^3 and 35 MPa. Temperature resistance was demonstrated up to 1200 °C, compared with the minimum requirement of 800 °C. The results show that a high-CAC, three-component formulation can provide the density, mechanical integrity and thermal resistance required for dry-mix refractory shotcrete. Acid absorption resistance and thermal conductivity at 350 °C remain under evaluation.

References

1. American Shotcrete Association: What is the difference between shotcrete and Gunite, American Shotcrete Association, Farmington Hills, MI, USA.

2. ACI Committee 506: ACI PRC-506-22, Shotcrete - Guide, American Concrete Institute, Farmington Hills, MI, USA, 2022.

3. American Shotcrete Association: Dry-Mix Shotcrete, American Shotcrete Association, Farmington Hills, MI, USA.

4.K.L. Scrivener and A. Capmas: Calcium Aluminate Cements, in Lea's Chemistry of Cement and Concrete, 4th Edition, Butterworth-Heinemann, Oxford, UK, 1998.

5.Calcium-aluminate mortars at high temperatures: overcoming adverse conversion effects using clinker aggregates, Cement and Concrete Composites, 2017.

SUSTAINABLE USE OF RECYCLED SILICON CARBIDE IN MONOLITHICS: A VIABLE REPLACEMENT FOR VIRGIN SIC

Suparna Basu[1] , Sumit Samanta[2] , Sushavon Sarkar[3] , Souvik Palui[4] , Akash Kumar Patra[5] , and Santanu Basak[6]

Calderys India Refractories Limited, Nagpur, India

1. Director QPC, SWA-Calderys; 2. Deputy Manager QPC, Calderys, India; 3. General Manager CCR, Calderys, India; 4. Manager QPC, Calderys, India; 5. Deputy Manager QPC, Calderys, India; 6. Director QPC, SWACalderys

Corresponding Author's e-mail: suparna.basu@calderys.com

Abstract

The refractory industry is currently facing a significant increase in raw material costs, with a strong focus on sustainability and circular economy principles. Silicon carbide is extensively used in monolithic refractories due to its superior thermal conductivity, excellent thermal shock resistance, wear resistance, and Slag resistance. However, due to its high-cost exploration of alternatives, cost-effective material is required. This study investigates the feasibility of utilizing recycled silicon carbide as a partial replacement for virgin SiC in calcium aluminate cement (CAC)-bonded monolithic systems. Recycled SiC generated from dismantled SiC based refractories, was processed and characterized, for its polytype forms by XRD, chemical composition, particle size distribution, pH, leachable alkali, leachable lime, and impurity content. The performance of recycled SiC was evaluated in different CAC-bonded applications, including castables, gunning mixes, and ramming masses etc. Trial formulations incorporating recycled SiC were benchmarked against conventional compositions containing virgin SiC. Rheology, thermo-mechanical properties, abrasion resistance, thermal shock, and thermal conductivity of the trial recipes have been evaluated. The results show that recycled SiC can effectively replace virgin SiC up to an optimized level without compromising key performance parameters like rheological, placing characteristics, and thermo-mechanical properties. Additionally, the use of recycled SiC contributes to a significant reduction in material cost while supporting sustainable resource utilization and waste minimization.

Keywords: Reused SiC, monolithic refractories, thermo-mechanical properties and sustainable refractories

Introduction

The availability of refractory raw materials is increasingly constrained. Furthermore, geopolitical uncertainties and restrictions on the production of virgin refractory raw materials in China, driven by environmental regulations, pose a significant risk to the timely availability of some critical raw materials. Therefore, our focus is on re-using the used materials, termed as reused/recycled materials. Reused materials are collected from used or worn out refractory linings. Identifying a suitable reused material that can effectively replace virgin raw material is a key factor in ensuring product quality and operational consistency. It is essential to ensure that the principal constituent meets the specified purity requirements to maintain product quality and performance. Other contaminants need to be removed by proper processing and grading. Impurity levels in reused materials, particularly leachable alkalis and total alkali content, play a critical role in influencing the rheological behavior of castables, as well as their thermo-mechanical properties. Silicon Carbide (SiC) is one of the most essential refractory raw materials worldwide. Its unique characteristics, including high thermal

conductivity, excellent thermal shock resistance, and exceptional wear resistance, make it an ideal choice for a range of critical and specialized refractory applications. In this study, the effect of reused SiC with varying impurity levels on the properties of low-cement castables (LCC), widely used in the cement industry, was comprehensively evaluated.

Experimental Procedure

Five sets of LCC formulations have been designed using virgin and reused SiC with different alkali content (Table I). Formulation I is the reference one, formulated with virgin SiC, named as R1. Formulations II to V, named R2, R3, R4 and R5 respectively have been designed with partial replacement of virgin SiC with reused SiC of varied alkali content keeping the rest of the constituents unaltered. Table II illustrates the chemical constituents of virgin SiC and reused SiC. It is evident from the data that the total alkali content of virgin SiC and reused SiC is in the order of Reused SiC-3> Reused SiC-4> Reused SiC-2> Reused SiC1> Virgin SiC, whereas total leachable alkali content (leach Na_2O+leach. K_2O) is in the order of - Reused SiC-3> Reused SiC-2> Reused SiC-4> Reused SiC-1> Virgin SiC. The leachable alkali is determined by boiling 10 gms of 1-3 mm & 0-1 mm (1:1 ratio) in 300 ml distilled water for 3 hrs at 100°C, followed by filtration with Whatman No 40- filter paper. The filtrate is the stock solution for leachable alkali determination following the procedure as described in IS 12107 Part 9.

Table I: Recipes of the experimental sets

Ingredients	R1	R2	R1	R4	R5
Calcined Clay	a	a	a	a	a
Calcined Bauxite	b	b	b	b	b
CAC	c	c	c	c	c
Fume Silica	d	d	d	d	d
SiC	x	x-x'	x-x'	x-x'	x-x'
Recycled SiC-1	-	x'	-	-	-
Recycled SiC-2	-	-	x'	-	-
Recycled SiC-3	-	-	-	x'	-
Recycled SiC-4	-	-	-	-	x'
Deflocculant	m	m	m	m	m
Additive	n	n	n	n	n

Table II: Properties of Virgin SiC and Reused SiC

	Virgin SiC	Reused SiC-1	Reused SiC-2	Reused SiC-3	Reused SiC-4
SiC (%)	97.8	90.43	85.43	76	69.2
Fe_2O_3 (%)	0.21	0.29	0.37	0.32	0.23
Al_2O_3 (%)	0.07	1.98	0.2	1.31	1.81
SiO_2 (%)	-	6.92	13.6	21.0	26.80
pH (50% Aq Soln)	7.82	8.02	8.36	11.08	9.06
Leach. Na_2O (%)	0.0001	0.002	0.006	0.88	0.003
Leach. K_2O (%)	0.0003	0.0005	0.008	0.006	0.0006
Total Na_2O (%)	0.002	0.07	0.14	1.00	1.00
Total K_2O (%)	0.003	0.008	0.03	0.04	0.04

Dry constituents of LCC formulations were mixed using a Hobart A 200 planetary mixer for 5 minutes. Subsequently, the castables were mixed with water for an additional 5 minutes. The castable flow, immediately after completion of mixing with water (T0) was measured as per EN ISO 1927 - 4. Physical properties of castables were evaluated as per IS 10570. The cured test specimens were dried at 110°C for 24 hrs before heat treating at 1100°C for 3 hrs. Cold Crushing Strength (CCS), Cold Modulus of Rupture (MOR) and bulk density (BD) of the cured specimens as well as heat treated specimens were measured. Apparent Porosity (AP) measurement of the fired test specimens were conducted as per ACTM C 20. The abrasion resistance of the heat treated LCC was measured as per ASTM C 704. Specimens of dimension 115mm × 115mm × 75 mm were also made for each set of castables to test the alkali resistance properties, specimens were cured in the same way as described above and fired at 1100°C for 3 hrs before testing the alkali interaction with K2CO3 at 1100°C for 5 hrs and with 90%K2SO4+10%KCl at 1300°C for 5 hrs as per Calderys Test Procedure L-3/TP/064. Core drilling of the specimens makes it vulnerable to an alkali attack. The initial dimension of the core is measured to compare the alkali penetration after the test.

Results & Discussion

The results reported in Figure I illustrate the water requirement, initial flow consistency, and setting time of the mixes. The rheological properties were evaluated at a fixed water addition level across all castable sets. Experimental set formulated with virgin SiC, i.e. R1 exhibits highest flow consistency compared to the other set of castables. Set R4 exhibits the lowest flow consistency followed by R5. The reduction in flow consistency in the R4 set can be attributed to the higher leachable alkali content of the recycled silicon carbide used in the mix [Table I and Table II]. Higher leachable alkali content not only alters the pH of the castable wet mix but also influences its zeta potential [1], thereby significantly impairing the flow consistency. The higher leachable alkali content promotes the hydration of calcium aluminate cement by enhancing the dissolution of $Al(OH)_4^-$ through an increase in the system pH, thereby shifting the aluminate equilibrium toward soluble species [2],[7]. As a result, the R4 set exhibits earlier setting compared to the other experimental sets.

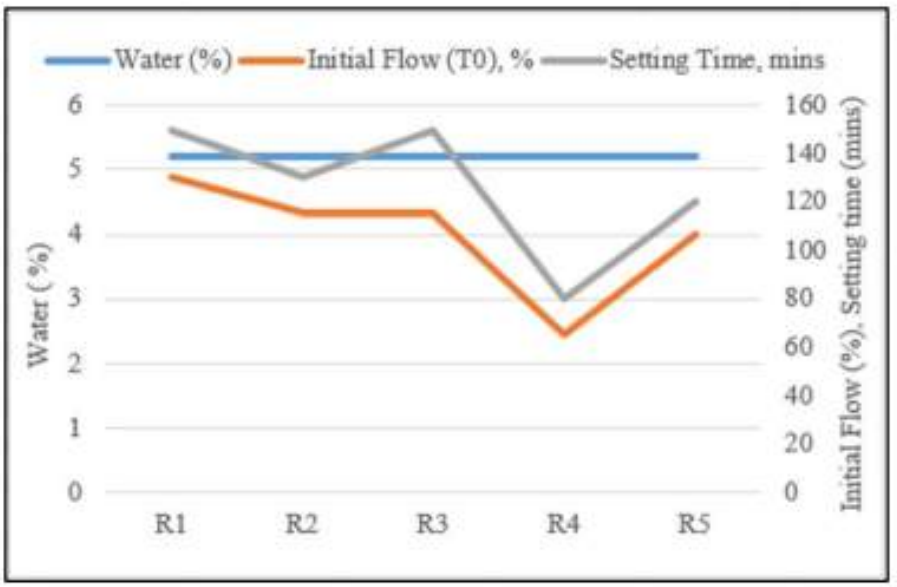


Figure. I: Water requirement, Initial Flow and Setting time

Figure II illustrates the dried properties of the experimental sets. CCS and CMOR of all the sets are comparable except R4. This R4 exhibits CCS, CMOR compared to the other formulations due to its higher Apparent Porosity (AP) [3], as well as due to the maximum levels of leachable alkali content of reused SiC used in R4. Higher leachable alkali levels adversely affect the rate of strength development [6] .

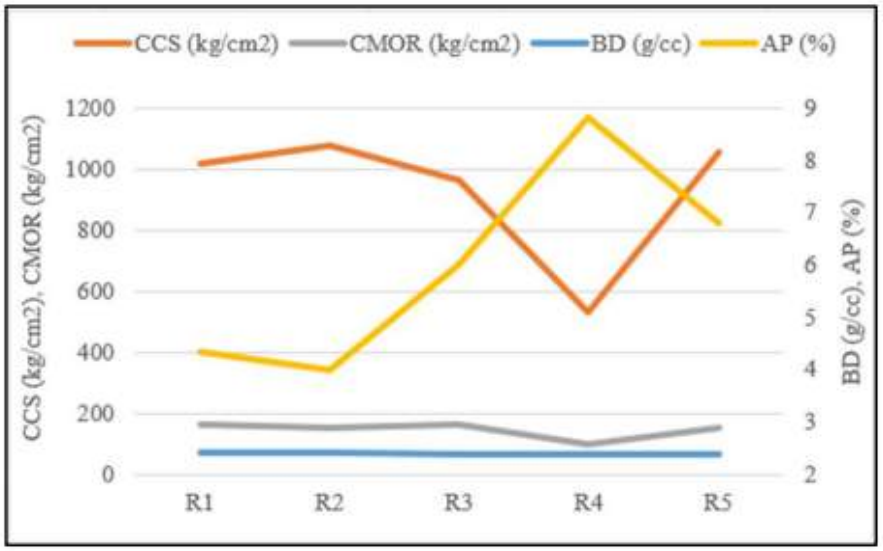


Figure II: Properties after drying at 110°C for 24 hrs

Thermo-mechanical properties of the experimental sets fired at 1100°C for 3 hrs are shown in Figure III. The R4 set exhibits lower mechanical strength followed by R5. Set R1 exhibits the highest CCS value. The XRD analysis of the fired specimens [Figure IV-a, b, c, d, and e] indicates that Set R1 exhibits the highest mullite concentration among all sets, which likely accounts for its superior mechanical properties [4]. Owing to the higher concentration of alkali oxides present in the recycled SiC used in Set R4, promotes the formation of lower melting feldspathic compounds, such as sanidine ($KAlSi_3O_8$) and sodium aluminum silicate ($Na_{0.875}Al_{0.875}Si_{0.125}O_2$), in higher proportions compared to the other sets. Being mechanically weaker and more brittle [5] than

mullite, the feldspathic phases formed in Set R4 contribute to its substantially lower CCS and CMOR. Similar to Set R4, the higher abundance of feldspathic phases in Set R5 leads to a noticeable reduction in CCS compared to Sets R1, R2, and R3. Flexural strength (CMOR) of set R4 is also the lowest among the other sets.

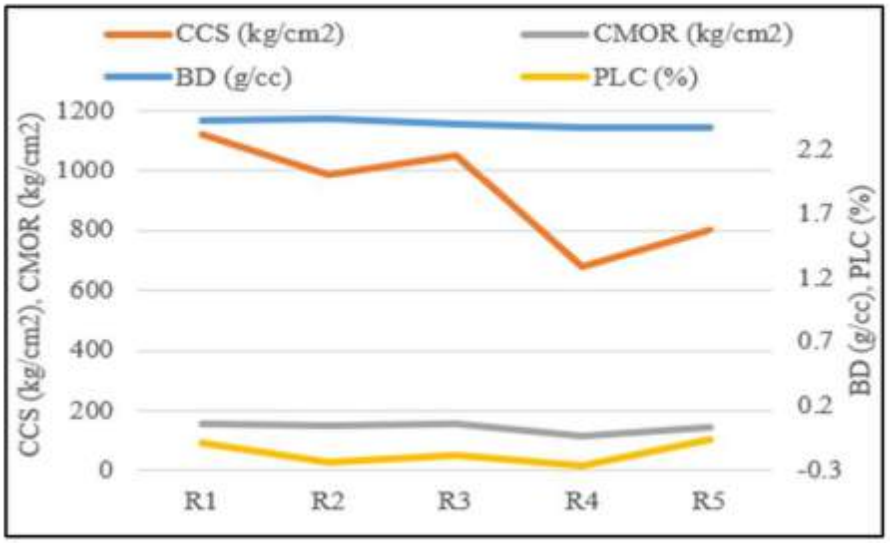


Figure III: Properties after firing at 1100°C for 3 hrs

Phase ID (11)	Chemical Formula	PDF-#	Wt% (σ)
Mullite (PO) (?)	Al2.22Si0.78O4.89	04-016-1586	42.7 (1.5)
Moissanite-6H (PO)	SiC	04-010-5698	26.8 (0.9)
Corundum (PO)	Al2O3	98-000-0174	10.5 (0.7)
Moissanite-4H (PO)	SiC	04-010-5697	5.9 (0.5)
Anorthite (PO)	(Ca2.133Na1.867)(Si10.003Al5.9	01-083-6377	4.9 (0.5)
Kaliophilite (PO)	KAlSiO4	00-011-0313	1.8 (0.4)
Cristobalite High (PO)	SiO2	98-000-0177	2.0 (0.3)
Qusongite (PO)	WC	04-016-3698	1.1 (0.1)
Sinoite (PO)	Si2N2O	04-015-7205	1.3 (0.2)
Nierite, syn | α-Si3N4 (PO)	Si3N4	04-005-5074	0.5 (?)
Sanidine (PO)	KAlSi3O8	04-017-1681	2.4 (?)

(a)

Phase ID (13)	Chemical Formula	PDF-#	Wt% (σ)
Mullite (PO)	Al4.59Si1.41O9.7	01-079-1455	37.7 (1.6)
Moissanite-6H (PO)	SiC	04-007-1548	28.1 (1.0)
Moissanite-4H (PO)	SiC	04-010-5697	8.5 (0.8)
Sinoite (PO)	Si2N2O	04-012-5691	3.9 (0.5)
Corundum (PO) (?)	Al2O3	98-000-0174	7.7 (0.7)
Orthoclase (PO)	KAlSi3O8	04-015-9317	2.1 (0.4)
Cristobalite low (PO)	SiO2	04-007-2134	1.4 (0.3)
Cristobalite High (PO) (?)	SiO2	98-000-0177	3.3 (0.5)
Qusongite (PO)	WC	04-004-6809	1.3 (0.1)
Rutile (PO)	TiO2	04-008-7847	2.3 (0.4)
Sanidine (PO)	KAlSi3O8	04-017-1681	1.7 (0.3)
Trinepheline (PO) (?)	NaAl(SiO4)	04-012-1728	1.1 (0.3)
Kaliophilite (PO)	KAlSiO4	00-011-0313	0.9 (0.5)

(b)



Phase ID (13)	Chemical Formula	PDF-#	Wt% (σ)
Moissanite-6H (PO)	SiC	04-010-5698	25.5 (0.7)
Mullite (PO)	Al4.59Si1.41O9.7	01-079-1455	33.5 (1.2)
Corundum (PO)	Al2O3	98-000-0174	11.5 (0.6)
Albite (PO)	NaAlSi3O8	04-007-5007	9.0 (0.7)
Moissanite-4H (PO)	SiC	04-010-5697	5.8 (0.4)
Sinoite (PO)	Si2N2O	04-012-5691	2.0 (0.3)
Cristobalite High (PO) (?)	SiO2	98-000-0177	1.5 (0.3)
Cristobalite low (PO)	SiO2	04-007-2134	4.2 (0.5)
Qusongite (PO)	WC	04-008-1622	1.3 (0.1)
Nierite (PO)	Si3N4	04-005-5074	0.6 (0.2)
Quartz (PO)	SiO2	04-005-4718	1.1 (0.3)
Potassium Aluminum Silicate (PC	KAlSiO4	00-050-0437	2.5 (1.0)
Orthoclase | potassium tecto-alur	KAlSi3O8	04-009-6197	1.4 (?)

(c)

Phase ID (11)	Chemical Formula	PDF-#	Wt% (σ)
Moissanite-6H (PO) (?)	SiC	04-010-5698	27.7 (1.5)
Mullite (PO)	Al4.59Si1.41O9.7	01-079-1455	31.9 (1.6)
Corundum (PO)	Al2O3	98-000-0174	9.3 (0.8)
Sanidine-high (PO)	KAlSi3O8	98-000-0377	11.7 (0.9)
Moissanite-15R (PO)	SiC	00-022-1301	0.8 (0.4)
Nierite | β-Si3N4 (PO)	Si3N4	04-026-8817	1.6 (0.3)
Sinoite (PO)	Si2N2O	04-015-7205	2.8 (0.4)
Cristobalite low (PO)	SiO2	04-007-2134	2.3 (0.4)
Cristobalite High (PO) (?)	SiO2	98-000-0177	8.0 (0.7)
Qusongite (PO)	WC	04-016-3698	1.0 (0.1)
Sodium Aluminum Silicate (PO)	Na0.875Al0.875Si0.125O2	04-010-3959	2.7 (?)

(d)

Phase ID (14)	Chemical Formula	PDF-#	Wt% (σ)
Mullite (PO)	Al4.59Si1.41O9.7	01-079-1455	32.8 (1.2)
Moissanite-6H (PO)	SiC	04-010-5698	30.5 (0.8)
Sanidine (PO)	KAlSi3O8	04-017-1681	8.1 (0.7)
Corundum (PO)	Al2O3	98-000-0174	6.9 (0.5)
Moissanite-4H (PO)	SiC	04-010-5697	6.7 (0.5)
Cristobalite low (PO)	SiO2	04-007-2134	5.1 (0.5)
Kaliophilite | facellite (PO)	*KAlSiO4	00-071-0879	0.1 (0.1)
Sinoite (PO)	Si2N2O	04-012-5691	2.7 (0.4)
Qusongite (PO)	WC	04-002-2679	0.9 (0.1)
Silicon (PO)	Si	98-000-0396	0.7 (0.1)
Silicon Oxide | silicon dioxide (PC	SiO2	01-082-1575	0.5 (0.2)
Potassium Aluminum Silicate (PC	KAlSi3O8	04-023-9697	1.4 (?)
Cristobalite High (PO)	SiO2	98-000-0177	2.9 (?)
Nierite, syn | α-Si3N4 (PO)	Si3N4	04-005-5074	0.6 (?)

(e)

Figure IV: XRD data of (a) R1, (b) R2, (c) R3, (d) R4 and (e) R5, fired at 1100°C for 3 hrs

Figure V illustrates the abrasion resistance properties, apparent porosity and CMOR of the experimental sets fired at 1100°C for 3 hrs. Abrasion loss is inversely proportional to the CMOR and directly proportional to the apparent porosity. The poor abrasion resistance exhibited by Set R4, followed by Set R5, can be attributed to the combined influence of lower bond strength (CMOR), greater concentration of feldspathic phases and higher apparent porosity. Set R1, R2, and R3 possess good abrasion resistance characteristics.

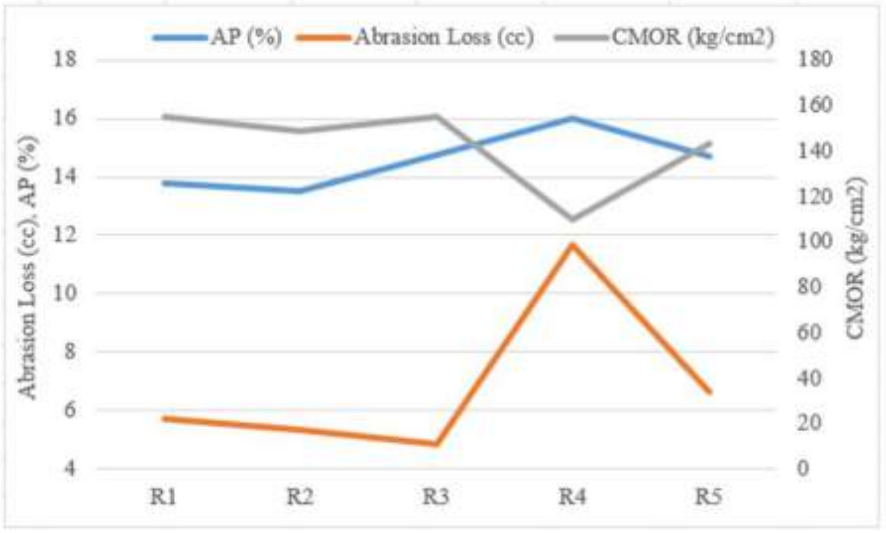


Figure V: Abrasion loss vs CMOR and Apparent Porosity after firing at 1100°C for 3 hrs

The suitability of the experimental castable sets for alkaline service conditions, representative of the riser duct and calciner environments in cement rotary kilns, was evaluated through alkali resistance test. The experimental sets exhibited greater susceptibility to the K_2CO_3 environment than to the K_2SO_4 + KCl environment (Figure VI). Set R1, R2, R3, and R5 are good in both conditions compared to the R4 set. Furthermore, the elevated apparent porosity of the R4 set accelerates molten alkali ingress, leading to the maximum penetration depth among the experimental castables. Photos of the specimens after alkali interaction are shown in Figure VII-a, b. A glossy surface has been observed in the cut surface of R1, R2 after interaction with K_2CO_3 and IN R1, R2, and R3 after interaction with K_2SO_4 + KCl.

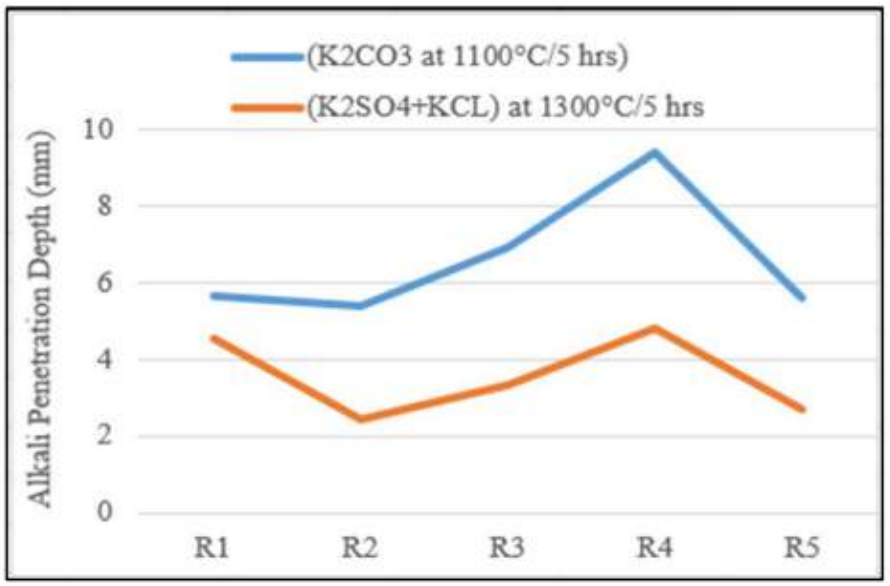


Figure VI: Alkali Penetration Depth

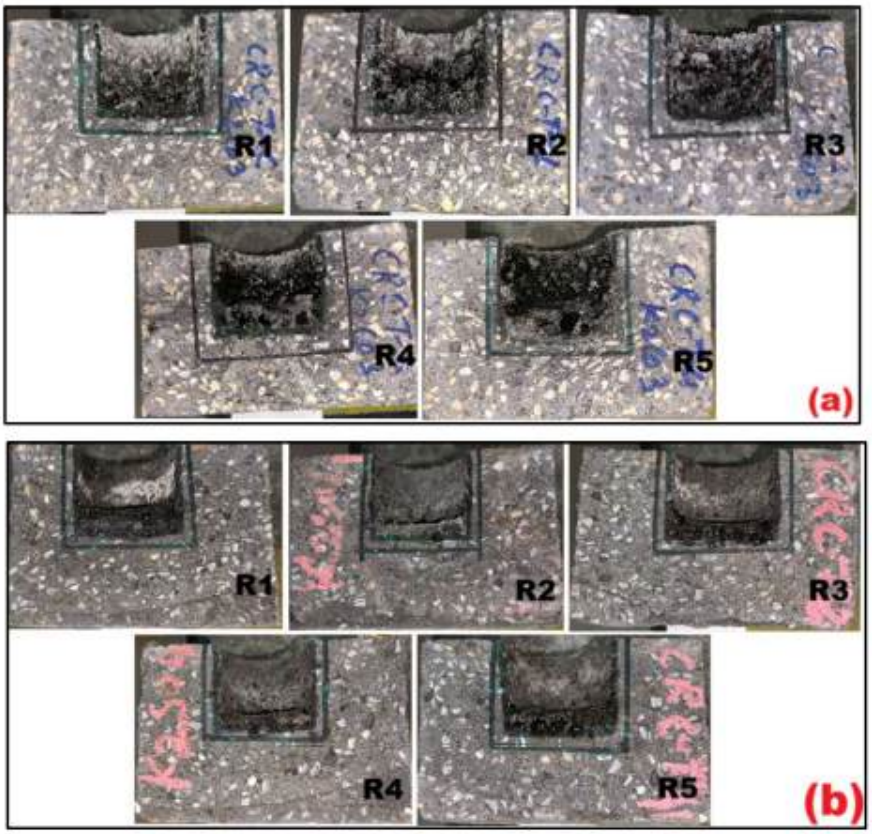


Figure VII: Photos of test specimens after alkali interaction with (a) K_2CO_3 at 1100°C/5 hrs and, (b) K_2SO_4 + KCl at 1300°C/5 hrs

Conclusion

1. Rheology as well as thermo-mechanical properties of R1, R2, R3 and R4 are superior compared to the R4 set.

2. The R4 Set exhibits poor abrasion resistance and alkali resistance properties.

3. The formation of a protective glassy layer in the R1, R2, and R3 sets enhances their resistance to alkali attack, making them suitable for service in alkaline environments

4. Reused SiC can be used as a replacement of virgin SiC upto a certain level.

5. The purity of reused SiC, along with the type and concentration of impurities present, plays a critical role in determining the properties and performance of the final product.

6. The impact of other impurity constituents like Leachable CaO, total CaO, MgO etc has not been taken into consideration in this study.

Castables prepared using the R1, R2, R3, and R5 recipes have been successfully evaluated in several cement plants, exhibiting satisfactory performance under operating conditions. However, R4 formulation is not evaluated under site conditions based on the outcome of this work.

Future Aspects

A similar investigation is underway on ASC-based BFT castables used in metal runner and slag runner applications to assess the feasibility of substituting virgin SiC with reused SiC.

Reference

1. A. Serrano-Lotinaa,1, R. Portelaa,*,2, P. Baezab,3, V. Alcolea-Rodrigueza,4, M. Villarroelc, P. ´ Avilaa,*,5, “Zeta potential as a tool for functional materials development”, Volume 423, 1 November 2023, 113862, CatalysisToday423(2023)113862, ScienceDirect

2. Matthew P Adams, Jason Henry Ideker, “Pore Solution Chemistry of Calcium Aluminate Cement Systems Undergoing Accelerated Conversion”, October 2015 Conference: The 14th International Congress on the Chemistry of Cement At: Beijing, CH

3. Hajar Ahmadi Moghadam and Seyed Mohammad Arab, “Effects of Heating Rate on the Thermal and MechanicalProperties of the BauxiteBased Low-Cement Refractory Castables”, Submitted March 12, 2020; in revised form August 16, 2020, JMEPEG _ASM International, https://doi.org/10.1007/s11665-020- 05079-z

4. "Towards improved mechanical strength and fracture toughness of mullite refractory ceramics: a review”, Journal of the Australian Ceramic Society, Sat, 5 Sep 2026 7:56:04 UTC.

5. Wikipedia https://en.wikipedia.org › wiki ›Sanidine

6. Ana Fernández-Jiménez, Teo Vazquez, Angel Palomo,” Effect of Sodium Silicate on Calcium Aluminate Cement Hydration in Highly Alkaline Media: A Microstructural Characterization” Journal of the American Ceramic Society, January 2011.

7. AZO material, Editorial Feature,” The Hydration of Calcium Aluminate Cements”, Sep 12, 2002

FUNDAMENTAL DESIGN APPROACH FOR SYNTHETIC SLAG TO CONTROL INCLUSIONS

Rahul Kumar[1] , Saurabh Tambe[1]

[1]Calderys Steeelcasting India Private Limited

rahul.kumar@calderys.com, saurabh.tambe@calderys.com

Abstract

The control of non-metallic inclusions is a key objective in steelmaking to ensure improved steel quality and process reliability. Synthetic slag plays a vital role in this process by facilitating inclusion absorption, modification, and separation from molten steel. This paper presents a fundamental design approach for synthetic slag with emphasis on achieving effective control. The importance of maintaining an optimal balance between slag reactivity and fluidity is highlighted to ensure efficient inclusion absorption and floatation. Additionally, the role of slag in modifying inclusion chemistry to form low-melting phases is examined from the thermodynamic perspective. The paper proposes a structured approach for designing synthetic slag compositions suitable for various steelmaking conditions. The study provides conceptual and practical guidelines to develop and implement effective slag systems for improved steel cleanliness.

Keywords: Synthetic Slag, Viscosity, Inclusions, FactSage.

Introduction

The demand of steel is in increasing trend for fulfilling the requirement of different sectors like construction, automobile, energy, defence, space etc. The selection of steel is the basis of their properties, governed by the content of carbon, other alloying elements, treatment procedures, and cleanliness of the steel. Non-metallic oxides act as inclusion in the steel matrix and impact the overall steel cleanliness. When the steel is treated during rolling, stresses build-up around the inclusion, resulting in cracks and loss in mechanical properties of the steel. It is noted that inclusion free steel is not possible, but the inclusion content should be controlled and modified as per the end properties requirements.[1] Some details about the maximum allowed impurity fraction and inclusion size in various steel grades are given in Table 1.[1]

Table 1: Typical steel cleanliness requirements for various steel grades[1]

Steel product	Maximum impurity fraction	Maximum inclusion size
Automotive Interstitial Free Steel	[C]≤30ppm, [N]≤30ppm	100µm
Drawn and Ironed cans	[C]≤30ppm, [N]≤30ppm, T.O.≤20 ppm	20µm
Line pipe	[S]≤30ppm,T.O.≤30ppm, [N]≤50ppm	100µm
Ball Bearings	T.O.≤10 ppm, [Ti]≤15 ppm	15µm
Tire cord	[H]≤2ppm, [N]≤40ppm, T.O.≤15 ppm	10µm - 20µm

Steel product	Maximum impurity fraction	Maximum inclusion size
Heavy plate	[H]≤2ppm, [N]≤30-40 ppm, T.O.≤20 ppm	13μm
Wire	[N]≤60 ppm, T.O.≤30ppm	20μm
Electrical steel	[N]≤30ppm	100μm

The practice of the modern secondary metallurgy process involves the slags forming with increased sulphide capacity, providing reliable protection of the metal from reoxidation and having a minimal effect on the refractory lining of the steel ladle [2 - 5]. In order to accelerate the formation of slag with the described properties, synthetic slags are used to ensure the rapid assimilation of additive materials[4- 7] .

CaF2-based materials can be used for this, however, their use leads to increased wear of refractories in the slag line [3-6]. Another way is to use Al_2O_3- containing materials, however, their use can lead to a slowdown in the formation of slag due to the slow melting of the latter [4,5] . Thus, the purpose of the paper to investigate fundamental design approach for the formation of synthetic slag, focussed on Calcium Aluminate based synthetic slag and to evaluate its effect on the processes of slag formation in a steel ladle.

Thermodynamics Calculation

A Calcium Aluminate Synthetic slag has been selected with composition CaO - 40 %; Al_2O_3 - 54 %; SiO_2 - 2.5 %; MgO - up to 2.5 %; TiO_2 - up to 1.5 %; Fe_2O_3 - up to 1.5 % for this study. To carry out thermodynamic modelling of the phase composition at different temperatures by the FactSage software, the actual composition of the synthetic slag was presented in the form of a ternary system CaO-Al_2O_3-SiO_2 (CaO - 41.0 %, Al_2O_3 - 56.0 %, SiO_2 - 3.0 %). It is important, CaO-Al_2O_3 diagram produced by the FactSage software includes 2 peritectic points, 3 eutectic points and 4 compounds (incongruently melting $(CaO)_3 \cdot Al_2O_3$, $CaO \cdot (Al_2O_3)_6$ and congruently melting $CaO \cdot Al_2O$, $CaO \cdot (Al_2O_3)_2$). This interpretation of the binary system CaO-Al_2O_3 impacts the ternary phase diagram CaO-Al_2O_3-SiO_2 (the compound $(CaO)_{12} \cdot (Al_2O_3)_7$ is ignored) [8]. The CaO-Al_2O_3-SiO_2 diagram is presented by Figure 1.

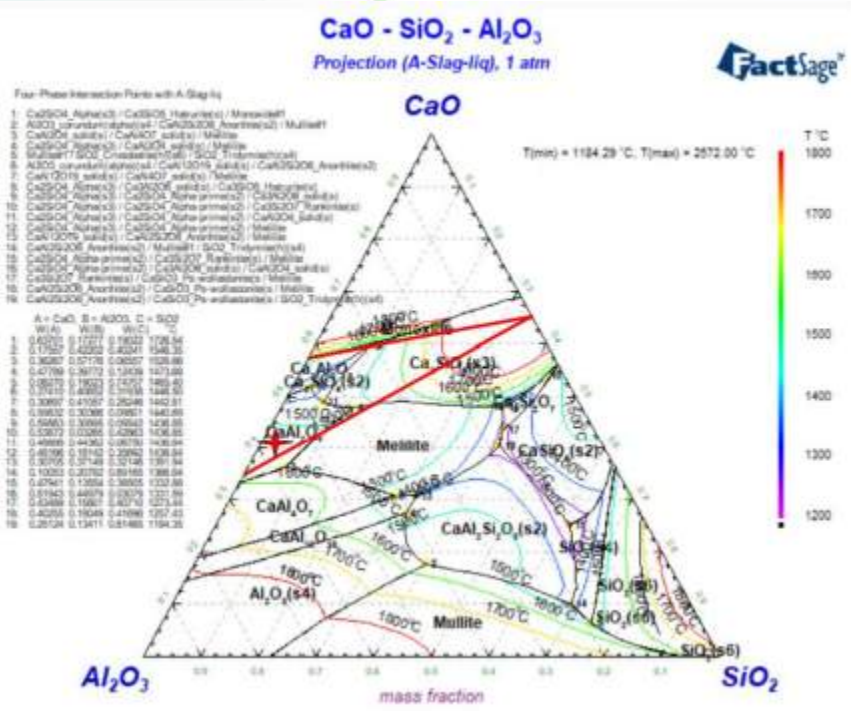


Figure 1: CaO-Al_2O_3-SiO_2 diagram produced by FactSage software

To study the melting process of the synthetic slag, the phase compositions of the system were calculated at temperatures of 1300 °C (fully solid system), 1331.59 °C (eutectic point), 1350 °C, 1400 °C, 1450 °C, 1500 °C and 1550 °C (fully liquid system). The results of calculations of the phase composition are presented in Table 2. Next, the calculation of the distribution of CaO, Al_2O_3 and SiO_2 between the available phases was done. The calculation results are presented in tables 3, 4, 5.

Table 2: Results of calculating the phase composition of the system by FactSage software

Temperature, °C	The content of phases in the system, wt. %			
	$(CaO)_2 \cdot SiO_2$	$CaO \cdot Al_2O_3$	$(CaO)_3 \cdot Al_2O_3$	Liquid slag
1300	8.6	80.3	11.1	-
1331.59	6.7	71.8	-	21.5
1350	6.4	70.9	-	22.7
1400	4.7	66.9	-	28.5
1450	-	56.5	-	43.5
1500	-	38.9	-	61.1
1550	-	-	-	100.0

Table 3 : Distribution of CaO between phases in the system by FactSage software

Temperature, °C	The amount of CaO contained in the phase			
	$(CaO)_2 \cdot SiO_2$	$CaO \cdot Al_2O_3$	$(CaO)_3 \cdot Al_2O_3$	Liquid slag
1300	13.7	69.5	16.8	-
1331.59	10.6	62.1	-	27.2
1350	10.1	61.4	-	28.5
1400	7.4	57.9	-	34.7
1450	-	48.9	-	51.1
1500	-	33.7	-	66.3
1550	-	-	-	100.0

Table 4 : Distribution of Al_2O_3 between phases in the system by FactSage software

Temperature, °C	Amount of Al_2O_3 contained in the phase			
	$(CaO)_2 \cdot SiO_2$	$CaO \cdot Al_2O_3$	$(CaO)_3 \cdot Al_2O_3$	Liquid slag
1300	-	92.5	7.5	-
1331.59	-	82.7	-	17.3
1350	-	81.7	-	18.3
1400	-	77.0	-	23.0
1450	-	65.1	-	34.9
1500	-	44.9	-	55.1
1550	-	-	-	100.0

Table 5 : SiO_2 distribution between phases in the system by FactSage software

Temperature, °C	Amount of SiO_2 contained in the phase			
	$(CaO)_2 \cdot SiO_2$	$CaO \cdot Al_2O_3$	$(CaO)_3 \cdot Al_2O_3$	Liquid slag
1300	100.0	-	-	-
1331.59	77.7	-	-	22.2
1350	73.9	-	-	26.1
1400	54.1	-	-	45.9
1450	-	-	-	100.0

1500	-	-	-	100.0
1550	-	-	-	100.0

Results and Discussion

According to the obtained data, the composition corresponding to the synthetic slag at a temperature of 1300 °C is represented by the following phases: $(CaO)_2 \cdot SiO_2$ (CaO - 65.1 %, SiO_2 - 34.9 %), $CaO \cdot Al_2O_3$ (CaO - 35.4%, Al_2O_3 - 64.5 %), $(CaO)_3 \cdot Al_2O_3$ (CaO - 62.3 %, Al_2O_3 - 37.7%). According to these conditions, the synthetic slag has the following phase composition: $(CaO)_2 \cdot SiO_2$ - 8.6 %; $CaO \cdot Al_2O_3$ - 80.3 %; $(CaO)_3 \cdot Al_2O_3$ - 11.1 %. In the composition of $(CaO)_2 \cdot SiO_2$ is 13.7 % of the total CaO and 100 % SiO_2. As part of $CaO \cdot Al_2O_3$ - 69.5 % and 92.5 %, respectively CaO and Al_2O_3. Composed of $(CaO)_3 \cdot Al_2O_3$ - 16.8 % and 7.5 %, respectively CaO and Al_2O_3.

The performed calculations show that the melting process begins when temperature starts to be 1331.59 °C. The chemical composition of the resulting liquid slag is determined by the elementary triangle $(CaO)_2 \cdot SiO_2$ - $CaO \cdot Al_2O_3$ - $(CaO)_3 \cdot Al_2O_3$ of the diagram. The appearance of liquid slag is accompanied by the disappearance of the phase $(CaO)_3 \cdot Al_2O_3$ and melting of certain amounts of $(CaO)_2 \cdot SiO_2$ and $CaO \cdot Al_2O_3$. At a temperature of 1331.59 ℃, the system contains: $(CaO)_2 \cdot SiO_2$ - 6.7 %; $CaO \cdot Al_2O_3$ - 71.8 %; liquid slag - 21.5 %. Liquid slag has the following chemical composition (Table 6): CaO - 51.9 %; Al_2O_3 - 45.0 %; SiO_2 - 3.1 %. Calculations show that the $(CaO)_2 \cdot SiO_2$ contains 10.6 % CaO and 77.7 % SiO_2; phase $CaO \cdot Al_2O_3$ - 62.1 % and 82.7 %, respectively CaO and Al_2O_3; liquid slag - 27.2 % CaO, 17.3 % Al_2O_3, 22.2 % SiO_2. Thus, at the eutectic point, 22.3 % $(CaO)_2 \cdot SiO_2$ passed into the liquid phase, 10.6 % $CaO \cdot Al_2O_3$ and all $(CaO)_3 \cdot Al_2O_3$. As can be seen, the melting at the first stage of phases with a high content of CaO in them, primarily $(CaO)_3 \cdot Al_2O_3$, contributed to the formation of slag with a high content of this oxide. As the temperature is increased, the melting process proceeds along the boundary curve between the phases $(CaO)_2 \cdot SiO_2$ and $CaO \cdot Al_2O_3$. At 1350 °C, the system contains: $(CaO)_2 \cdot SiO_2$ - 6.4 %; $CaO \cdot Al_2O_3$ - 70.9 %; liquid slag - 22.7 %. Liquid slag has the following chemical composition (Table 6): CaO - 51.5 %; Al_2O_3 - 45.1 %; SiO_2 - 3.4 %. Calculations show that the $(CaO)_2 \cdot SiO_2$ contains 10.1 % CaO and 73.9 % SiO_2; phase $CaO \cdot Al_2O_3$ - 61.4 % and 81.7 %, respectively CaO and Al_2O_3; liquid slag - 28.5 % CaO, 18.3 % Al_2O_3, 26.1 % SiO2. Thus, at a temperature of 1350 °C, additional 3.8 % $(CaO)_2 \cdot SiO_2$ passed into the liquid phase and 1.1 % $CaO \cdot Al_2O_3$.

Table 6 : Chemical composition and sulphide capacity of liquid slag

Temp, °C	CaO	Al_2O_3	SiO_2	log(1/Cs)
1331.59	51.9	45.0	3.1	3.9
1350	51.5	45.1	3.4	3.8
1400	50.0	45.2	4.8	3.6
1450	48.2	44.9	6.9	3.4
1500	44.5	50.6	4.9	3.2
1550	41.0	56.0	3.0	3.0

As can be seen, an increase in temperature is accompanied by an increase in the content of SiO_2 in liquid slag due to the accelerated dissolution of the phase $(CaO)_2 \cdot SiO_2$, which is also fixed by the redistribution of SiO_2 between phases. At the same time, the reduced content of CaO in the $CaO \cdot Al_2O_3$ phase leads to a decrease in the content of this oxide in the liquid phase and the relative stability of the concentration of Al_2O_3.

At 1400 °C, the system contains: $(CaO)_2 \cdot SiO_2$ - 4.7 %; $CaO \cdot Al_2O_3$ - 66.9 %; liquid slag - 28.5 %, thus the amount of the liquid phase increased by 5.7 %. Liquid slag has the following chemical composition: CaO - 50.0 %; Al_2O_3 - 45.2 %; SiO_2 - 4.8 %. Phase $(CaO)_2 \cdot SiO_2$ contains 7.4 % CaO and 54.1 % SiO_2; phase $CaO \cdot Al_2O_3$ - 57.9 % and 77.0 %, respectively CaO and Al_2O_3; liquid slag - 34.7 % CaO, 23.0 % Al_2O_3, 45.9 % SiO_2. When the temperature increased to 1400 °C, an additional 19.8 % $(CaO)2 \cdot SiO_2$ and 5.0 % $CaO \cdot Al_2O_3$ passed into the liquid phase. As can be seen, the processes described earlier are further developed with increasing temperature.

In the process of further increase in temperature during the dissolution of the last volumes $(CaO)_2 \cdot SiO_2$ the system leaves the boundary curve between the phases $(CaO)_2 \cdot SiO_2$ and $CaO \cdot Al_2O_3$ and passes into the region of existence of $CaO.Al_2O_3$ and liquid phase. The latter occurs between 1400 °C and 1450 °C.

At 1450 °C, the system contains: $CaO \cdot Al_2O_3$ - 56.5%; liquid slag - 43.5%. Liquid slag has the following chemical composition: CaO - 48.2 %; Al_2O_3 - 44.9 %; SiO_2 - 6.9 %. $CaO \cdot Al_2O_3$ phase contains 48.9 % CaO and 65.1 % Al_2O_3; liquid slag - 51.1%, 34.9 % and 100 %, respectively CaO, Al_2O_3 and SiO_2. Thus, with an increase in temperature to 1450 °C, an additional 12.9 % $CaO \cdot Al_2O_3$ passed into the liquid phase and all the remaining amount $(CaO)_2 \cdot SiO_2$.

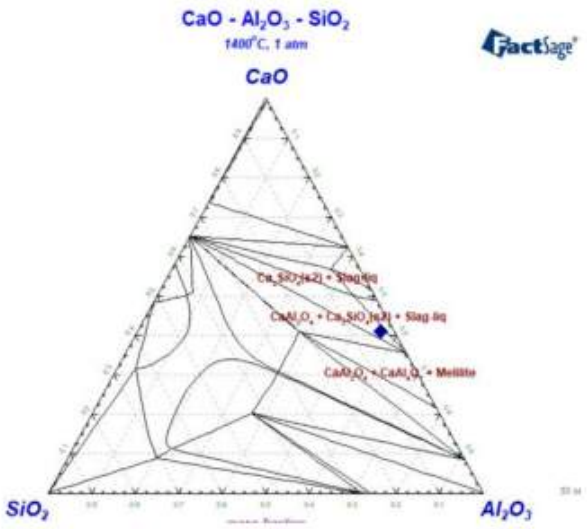
Leaving the system boundary curve between phases $(CaO)_2 \cdot SiO_2$ and $CaO \cdot Al_2O_3$ and transition to the region of existence of $CaO \cdot Al_2O_3$ and liquid phase, which was accompanied by the dissolution of the last volumes $(CaO)_2 \cdot SiO_2$, led to some change in the trends in the evolution of the chemical composition of the liquid phase accompanying the process of melting the synthetic slag. Leaving the system boundary curve is shown by Figure 2.

In the temperature range of 1400 - 1450 °C, more than half of all SiO_2 passed into the liquid phase of the system, which led to an increase in its concentration in the liquid slag Increasing the intensity of $CaO \cdot Al_2O_3$ melting determined a greater decrease in the concentration of CaO compared to Al_2O_3.

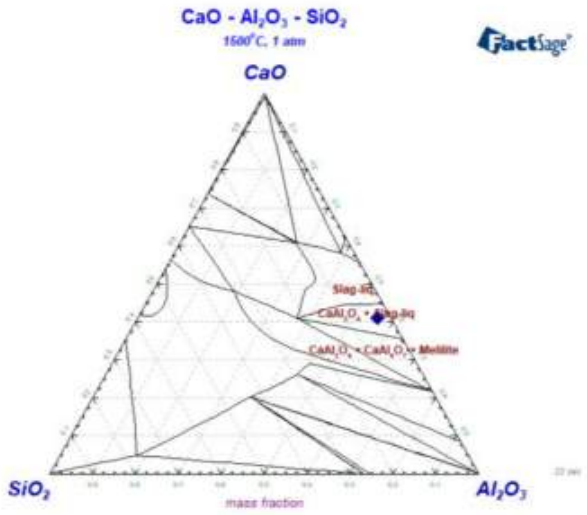
At 1500 °C, the system contains: $CaO \cdot Al_2O_3$ - 38.9 %; liquid slag - 61.1 %. Liquid slag has the following chemical composition: CaO - 44.5 %; Al_2O_3 - 50.6 %; SiO_2 - 4.9 %. $CaO \cdot Al_2O_3$ phase contains 33.7 % CaO and 44.9 % Al_2O_3; liquid slag - 66.3 %, 55.1 % and 100 %, respectively CaO, Al_2O_3 and SiO_2. Thus, with an increase in temperature to 1500 °C, an additional 21.9 % $CaO \cdot Al_2O_3$ passed into the liquid phase.

Entering the liquid phase 20.3 % of the total amount of Al_2O_3 is accompanied by an increase in the concentration of this oxide by 5.6 %, a decrease in the content of CaO by 3.7 %, despite the transition of 15.2 % of its total amount, and SiO_2 by 2.0%. Greater reduction in CaO concentration compared to SiO_2, despite the addition of its additional amount to the slag, is due to its large amount in the slag at a temperature of 1450 °C. If we turn to relative values, then the decrease in CaO concentration was 7.6 %, and SiO_2 - 28.8 %, if the concentration of these oxides at a temperature of 1450 °C is taken as 100%.

At a temperature of 1550 °C, the system is already completely in a liquid state. Additional calculations showed that the final melting of the last crystals of the solid phase occurs at a temperature of 1546 °C. By this time, an all the remaining amount $CaO \cdot Al_2O_3$ has melted, which led to an increase in the content of Al_2O_3 by 5.4 %, a decrease in the content of CaO by 3.5% and SiO_2 by 1.9%. A greater change in the chemical composition of the slag is associated with a large volume of melted $CaO \cdot Al_2O_3$.



(a)



(b)

Figure 2: Investigated system at the temperature 1450 °C (a) and 1500 °C (b) (calculated by FactSage software)

To assess the thermodynamics possibility of carrying out the desulphurization process during the melting of the synthetic slag, the sulphide capacity coefficient was calculated taking into account the change in the chemical composition of the liquid slag and the temperature at which the liquid of this composition is formed. As can be seen from the table, despite the CaO content in the slag decreases at the first stage due to the entry of SiO_2 into the slag due to accelerated melting $(CaO)_2 \cdot SiO_2$ during movement along the boundary curve between phases $(CaO)_2 \cdot SiO_2$ and $CaO \cdot Al_2O_3$, and later due to the accelerated supply of Al_2O_3 during the melting of $CaO \cdot Al_2O_3$, there is a gradual increase in the sulphide capacity of the slag due slag temperature increasing. There, due the development of these conditions, the liquid slag formed during the melting of the synthetic slag has a fairly high sulphide capacity. The latter makes it possible to begin the process of removing sulphur from liquid metal into slag immediately after the adding of slagforming materials into the ladle.

Conclusions

According to results, the use of the synthetic slag ensures the early formation of liquid slag on the metal surface in the steel ladle at the stage of tapping the metal from the steelmaking furnace and creates conditions for the effective sulphur removal. The latter makes possible to successfully create a ladle furnace liquid slag with proper properties for secondary steelmaking, which can ensure to carry out the desulfurization operation, prevent the development of reoxidation processes, including reducing the number of non-metallic inclusions and the consumption of ferroalloys for deoxidation and alloying of steel.

References

[1] A. W. Cramb: Impurities in Engineered Materials, Impact, Reliability and Control, C.L. Briant, eds., Marcel Dekker Inc., New York, (1999), 49-89.

[2] Jin Gyu Kang, Jae Hong Shin, Yongsug Chung & Joo Hyun Park: Metallurgical and Materials Transactions B, 2017.

[3] Branislav Buľko, Marek Molnár, Peter Demeter & et all: Transactions of the Indian Institute of Metals, 2022.

[4] B.-H. Yoon, K.-H. Heo, J.-S. Kim & H.-S. Sohn: Ironmaking & Steelmaking Processes, Products and Applications, 2002.

[5] M Song, M Nzotta & D Sichen: Ironmaking & Steelmaking Processes, Products and Applications, 2011.

[6] Zonghui Liu, Guodong Song, Zhiyin Deng & Miaoyong Zhu: Ironmaking & Steelmaking Processes, Products and Applications, 2021

[7] Zhiyin Deng, Lingzhong Kong, Dong Liang, Miaoyong Zhu: Steel Research International, 2019

RESILIENT REFRACTORY PERFORMANCE SOLUTION: HIGH-PERFORMANCE MgO-C BRICKS REIMAGINED

Pallab Karmakar[1], Dr. Debasish Chandra[1], Dr. Thomas Schemmel[2]

[1] Refratechnik India Pvt. Ltd.; [2] Refratechnik Steel GmbH.

Abstract

Raw-material diversification can improve supply continuity, cost stability and resilience in MgO-C refractory production. In 2025, global magnesite production was approximately 24.2 million t, with China contributing about 62%; Australia, Russia and Austria contributed 3–4% each, while Turkey and Brazil contributed about 8% each. During FY 2024–25, Chinese caustic calcined magnesia exports were 0.085–0.095 million t/month, with annual price fluctuations of 25–30%; fused magnesia exports were 0.045–0.048 million t/month, with price variations of 20–22%. Freight, exchange rate and policy volatility further increase supply risk. This study evaluates Queensland magnesite (QMag), a cryptocrystalline Australian source, as an alternative to Chinese magnesia for Indian steelmaking. Its fine, uniform microstructure, high purity and high C/S ratio were assessed through material characterization, slag-corrosion testing and field trials. A cost-effective microzoning approach was used to validate QMag magnesia in Indian steel plants.

Keywords: Cryptocrystalline magnesite, fused magnesia, C/S ratio, magnesia-carbon bricks, steelmaking.

1. Introduction

MgO-C refractory performance depends strongly on raw Magnesia and carbon quality followed by additives, binders and processing. Raw magnesia selection is governed by chemical purity, $CaO/SiO_2/B_2O_3$ levels, grain size, crystal structure, thermal resistance, corrosion resistance and cost[2, 3, 4]. Recent geopolitical and supply-chain disruptions have highlighted the risk of dependence on a single source. The COVID-19 pandemic caused lockdowns, shipping-space shortages, higher freight rates and longer transit times; the 2022 Russia–Ukraine conflict disrupted natural-gas, coal, oil and electricity markets. For refractory users, freight rates have remained about 60–80% above normal levels during periods of elevated fuel and foreign-exchange costs, while vessel delays continue to affect schedule reliability [11]. Natural-gas and electricity prices have also increased the cost base of high-temperature magnesia processing. These conditions reinforce the need for secure raw-material supply rather than reliance on short-term price advantage alone. Additional MgO challenges include critical-raw-material status, mine-waste utilization, flotation/flash-calcination and other lower-grade feed technologies, CO_2 reduction in mining and processing, refractory recycling, value-added MgO products, and lower-carbon fuels. Because magnesia production is energy intensive, reducing its carbon footprint while maintaining refractory quality is an important development objective.

The strategic requirement is therefore not simply sufficient magnesia, but reliable, geopolitically secure, environmentally sustainable and cost-effective high-quality MgO. For India, alternative or nearby sources, recycling of used MgO refractories and lower-carbon MgO processing can reduce import dependence, improve supply continuity and reduce exposure to abrupt changes in freight, energy, policy and foreign-exchange conditions.

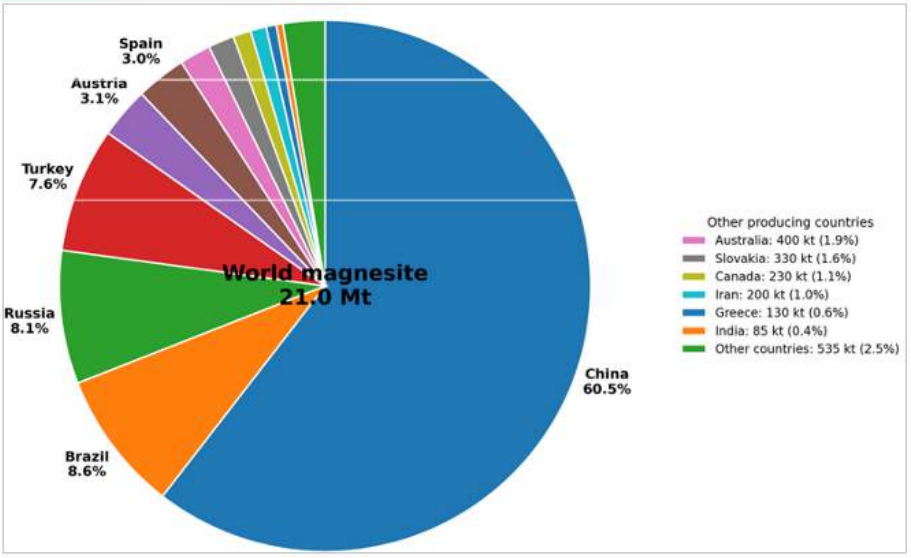


Fig. 1. Global magnesite production by country, 2025[16].

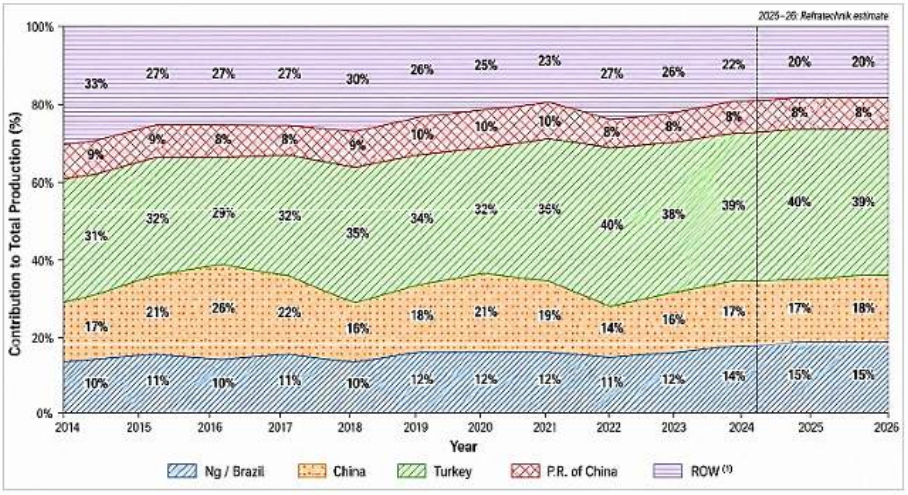


Fig. 2. Indian magnesite consumption by types till 2025

China has dominated refractory magnesia supply for about three decades[1, 6, 10], forcing several non-Chinese producers to exit or reduce refractory-magnesia operations. QMAG has developed caustic calcined magnesia products for hydrometallurgical applications, a growing segment with no Chinese presence, and is a major supplier in that segment. The Indian MgO-C industry has benefited substantially from Chinese magnesia, but the same concentration has created supply, price and geopolitical risk. A diversified raw-material portfolio can therefore provide greater flexibility in recipe design and purchasing.

Indian Magnesia-Carbon industry market requirements

India has limited domestic raw materials suitable for premium MgO-C products, where MgO purity, low impurity levels, crystal structure, thermal resistance and corrosion resistance are critical. Because suitable Indian sources are limited, MgO-C manufacturers have relied heavily on imported magnesia, particularly from China. Fused magnesia has increasingly been used in steelmaking vessels, improving refractory performance and increasing customer expectations on brick performance [12, 15].

Chinese supply has historically offered scale and competitive pricing, but mining, environmental, production and energy restrictions can cause abrupt changes in availability and price. Customers consequently face uncertainty regarding cost planning, customer contracts, inventory management, long-term purchasing, refractory pricing and profit margins[17]. The recurring pattern of low prices followed by supply restrictions and price increases makes long-term MgO cost assumptions difficult. Diversification of MgO sources is therefore increasingly important and strategically relevant.

MgC refractories support steel production and must meet changing requirements for quality, properties, cost and availability. Global steel markets face imported-steel price pressure, decarbonization requirements associated with green steel, continuing consolidation through mergers and acquisitions, and strategic partnerships that can strengthen global supply chains. The refractory industry therefore cannot rely only on conventional steelmaking. MgO and refractory technologies also need to adapt to lower-carbon steelmaking and other applications such as construction, battery raw materials, mining and environmental processing. Such diversification can reduce exposure to lower steel demand, raw-material constraints and increasing environmental regulations.

QMAG and Kunwarara magnesite

QMAG has operated since 1991 and is one of the few non-Chinese producers supplying caustic calcined magnesia (CCM), dead-burned magnesia (DBM) and electro-fused magnesia (EFM). Its product portfolio serves iron and steel, cement, lime, pulp and paper, non-ferrous, ceramics, chemical, environmental and energy applications. The integrated mineral-to-product capability provides an alternative supply base for refractory producers seeking consistent chemistry and controlled grain characteristics.

QMAG Kunwarara Mining Operation

The Kunwarara mine in Queensland is a major cryptocrystalline[2] magnesite deposit located about 65 km north of Rockhampton. The mining area is approximately210 km², with reported reserves/resources of about 600 million ROM metric tons and a mine life exceeding 200



Fig. 3. QMAG operations and product portfolio

Years[12, 13]. Processing includes mobile screening, scrubbing, sizing, media separation, XRT ore sorting and stock blending to maintain consistent quality and grade before calcination. Total production capacity is approximately 300,000 t/y, including about 90,000 t/y DBM and 30,000 t/y EFM[3, 4]. The cryptocrystalline structure provides a fine and relatively uniform grain distribution, which is relevant to producing high-purity magnesia with a high C/S ratio[18, 19, 20].

Fused Magnesia Process Overview

Calcined MgO is size-sorted and blended to meet EFM chemistry requirements, then melted into three 4.5 MW electric-arc furnaces at temperatures above the MgO



Fig. 4. Fused-magnesia furnace operation

melting point (~2800°C). The molten ingot is cooled by water and air to develop the desired crystals, then broken, graded, crushed and sized for bulk or big-bag supply. QMAG sizing provides consistent chemistry across size fractions.

Electro-fused magnesia properties

The EFH series provides distinct purity and microstructural levels. EFH-1 is the premium grade with the highest chemical purity and largest crystal size; EFH-A is intermediate; EFH-2 has lower baseline purity, higher secondary oxides and finer crystal development. The chemical and physical data are retained and comparedwith standard Chinese fused magnesiain Table 1[20, 21, 22, 23]

Microstructural Analysis

Microstructural characterization was performed via scanning electron microscopy (SEM) to evaluate the phase distribution and morphology across the refractory specimens. In the QMAG EFH series (EFH-1, EFH-A, and EFH-2), elevated CaO concentrations promote the formation of highly refractory secondary phases. To achieve this microstructural configuration requires a bulk chemical lime-to-silica (C:S) ratio exceeding 2.5:1[2, 3, 4, 5, 8]. Consequently, the microstructure of the EFH products is dominated by dicalcium silicate (C_2S, Tm- 2130^{0}C) precipitated primarily along the grain boundaries, accompanied by low solute concentrations of lime within the periclase crystal matrix. Conversely, in Chinese fused magnesia (FM) variants characterized by lower C:S ratios, the precipitation of lower-melting-point secondary phases is observed, specifically low levels of merwinite (C_3MS_2, Tm-1580^{0}C) and monticellite (CMS, Tm- 1490^{0}C).

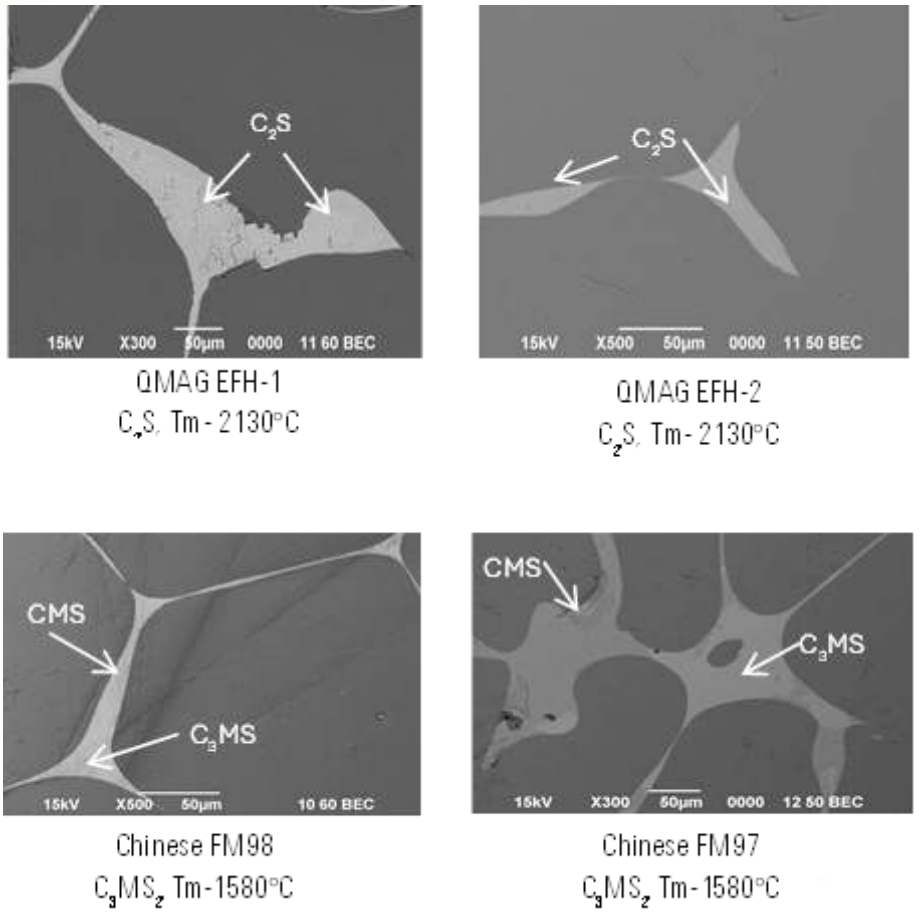


Fig. 5. QMAG EFH microstructuresand phase distribution comparing with Chinese Fused Magnesia

SEM was used to evaluate phase distribution and morphology. In the QMAG EFH series, elevated CaO promotes refractory secondary phases and a bulk C/S ratio above 2.5:1. The microstructure is dominated by dicalcium silicate (C_2S, Tm ≈ 2130°C) along grain boundaries, with low lime solubility in the periclase matrix. By comparison, Chinese fused magnesia with lower C/S ratios shows lower-melting merwinite (C_3MS_2, Tm ≈ 1580°C) and monticellite (CMS, Tm ≈ 1490°C). Thus, phase assemblage and spatial distribution—not MgO purity alone—are key to high-temperature stability.

Slag corrosion test – rotary drum method

Dynamic rotary slag corrosion testing was used to compare high-temperature chemical durability and degradation. Despite slightly lower bulk MgO, QMAG EFH-1 showed superior dynamic slag-corrosion resistance and passivation relative to CFM98[7, 8, 9]. This behavior correlates with improved thermomechanical durability and reduced erosion in industrial steelmaking applications. Although periclase crystallite size can influence macroscopic wear mechanisms, no standardized test methodology is established and empirical correlation between grain-boundary characteristics and volumetric wear is limited. The results therefore indicate that optimizing a refractory against corrosive degradation should prioritize phase assemblage[5], morphology and the spatial distribution of localized secondary phases rather than raw chemical purity alone. Suppressing liquid-phase formation [6]and high-temperature grain-boundary sliding is particularly important for maintaining a stable MgO-C matrix under aggressive slag exposure.

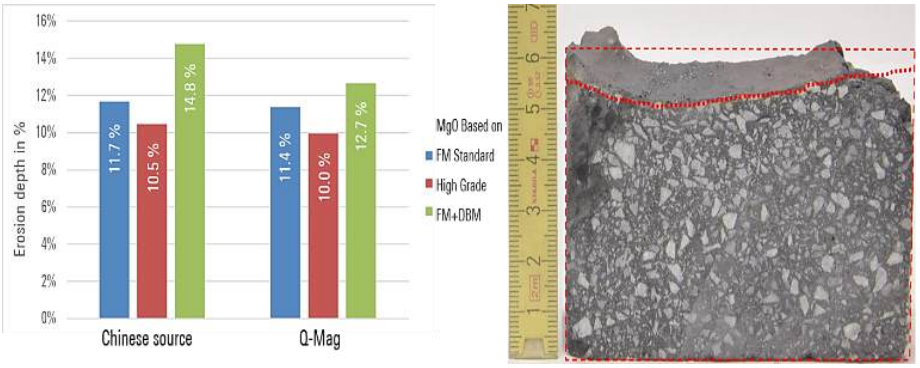


Fig. 6. Rotary slag-corrosion evidence and comparison

Performance reference & case study

In European steel plants - To engineer a tailor-made refractory zoning configuration for integrated steel plants, precise correlation must be established between operational parameters and product properties[15]. The design methodology dictates a comprehensive quantification of specific process parameters, including tapping temperature gradients, holding durations, slag chemistry profiles (basicity ratios and FeO/MnO percentages), secondary operations, oxygen killing etc.

Observations: In the European plants, the standard practice gave a typical ladle final lifetime of about 85–86 heats, with relatively homogeneous wear. The QMAG trials recorded 101 heats for L#01, 94 heats for L#02 and 95 heats for L#03. The impact pad remained the limiting factor for final lifetime, while improved performance was observed in the slag and metal zones (Table 2 & 3).

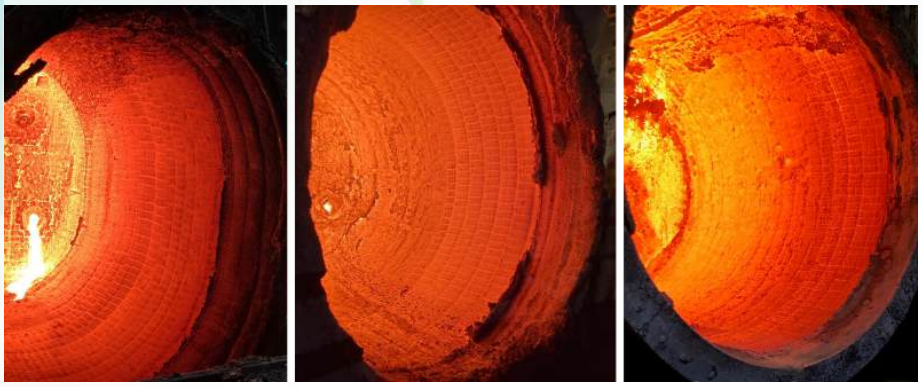


Fig. 7 – European steel plant ladle trials

In Indian Steel Plant - For an integrated steel plant, refractory zoning must correlate operational conditions (Table 4) with product properties. Relevant parameters include tapping-temperature gradients, holding time, slag basicity and FeO/MnO, secondary operations and oxygen killing. The trial used QMAG magnesia in the slag-zone quality with EFH-2, demonstrating the microzoning approach in which the raw-material quality is matched to the local wear mechanism rather than applying one grade uniformly throughout the vessel.



Fig. 8 – Indian steel plant ladle trials

Observation

- Ladle No-1; Actual life -100hts; Calculated Life-117hts, Holding-10,690min
- Ladle No-8; Actual life -101hts; Calculated Life-118hts, Holding-10,330min

These thermochemical and kinetic boundary conditions were evaluated with quantitative leftover-thickness analysis to determine differential erosion rates across critical zones, including purging and non-purging sides of the slag line. Integrating chemical slag corrosion, thermal spalling and mechanical kinetic erosion allows refractory matrix chemistry and thickness gradients to be adjusted dynamically, with the objective of minimizing premature failure and achieving a more uniform, synchronous lining life.

With standard raw materials, the reported erosion rate was about 3.5% higher than with QMAG magnesite in the slag zone, while the average achieved life was about 117.5 heats. The field results support the laboratory microstructural observations: a favorable phase assemblage and high C/S ratio can contribute to improved resistance even when bulk MgO content is not the sole differentiating parameter.

Conclusion

Replacing primary matrix raw materials can strengthen supply-chain resilience by diversifying mineral sources, improving lead-time flexibility and reducing exposure to geopolitical and tariff volatility. The study demonstrates that primary aggregate phases can be substituted on a 1:1 recipe basis without changing the fundamental mineralogical composition or green-body pressing parameters. The alternative matrix showed stable erosion profiles and an improved cost-to-performance balance, with ladle campaign longevity increasing by more than 10%. The modular brick architecture also permits further adjustment to specific metallurgical requirements.

Chemical Analysis (wt %)	QMAG EFH-1	QMAG EFH-A	Chinese FM98	QMAG EFH-2	Chinese FM97
SiO_2	0.48	0.58	0.62	0.75	0.63
CaO	1.81	1.91	1.01	2.40	1.53
Al_2O_3	0.07	0.07	0.16	0.10	0.07
Fe_2O_3	0.10	0.11	0.41	0.12	0.60
Mn_3O_4	0.10	0.11	0.03	0.11	0.05
MgO	97.44	97.24	97.8	96.52	97.5
C:S Ratio	3.7	3.3	1.6	3.2	2.4
Bulk Density ($g.cm^{-3}$)	3.54	3.53	3.55	3.51	3.50
Mean Periclase Crystal Size (µm)	1070	940	730	665	700

Table-1: Physico-chemical properties of fused magnesia

	Standard Practice			Zones	Trial			
Quality	**Recycle Material**	**China DBM**	**FM 98**		**Quality**	**Recycle Material**	**Extra DBM**	**EFH1**
Brand-A	++	++		Interme diate	Brand- X	++	++	
Brand-B		+	+++	Slag Zone	Brand- Y		+	+++
Brand-C	+++	+		Metal zone/Bo ttom	Brand- Z	+++	+	

Table-2: Performance Comparison in European Steel Plants

Standard	Trial
Repair / relining SZ and typical final lifetime of the ladle ~85-86 more or less homogeneous wear in all areas	L#01 Repair / relining SZ and final lifetime 101 heats L#02 Repair / relining SZ and final lifetime 94 heats L#03 Repair / relining SZ and final lifetime 95 heats Main issue is impact pad, limits the final lifetime -> Improved performance in the SZ and MZ

Table-3: Performance Comparison between standard products and trial products in European Steel Plants

Parameters	**Customer**
Ladle Capacity (Mt)	250
Process Route	BOF-LF-VD-Casting
Secondary Operation	LRF & 40-50% VD
Arcing Time (min)	60-80
Tap to Lift Time (min)	120-150
Al/Si- Killing	Both
Slag Basicity	1.6-2
No. of heats/day/ladle	3-4
Target Life	110 heats with 1 repair

Table-4: Operational parameters in Indian Steel Plants

	Standard Practice		Zones	Trial		
Quality	China DBM	FM China		Quality	China DBM	EFH2
Brand-E	++	++	Slag Zone	Brand - P	++	++

Table-5: Performance comparison of products with QMag& Chinese Raw materials

NPP side	PP side	LOT (mm) in PP side
Initial campaign -49hts (Layers no 31-46) rate of erosion mm/ht		
2.80	3.12	45-65
Repair campaign -48hts (Layers no 31-46) rate of erosion mm/ht		
2.77	3.40	40-60

Table-6: Performance comparison of products with QMag& Chinese Raw materials in different zones of a ladle

Reference

1. U.S. Geological Survey (USGS). Mineral Commodity Summaries 2026: Magnesium Compounds. U.S. Geological Survey, Reston, VA, 2026. DOI: 10.3133/mcs2026.

2. Use for: global magnesite production, China/Australia/Russia/Austria/Turkey/Brazil production statistics and supply concentration. The 2026 MCS is the earliest comprehensive USGS source for 2025 world production data.

3. Guo, Z., Ma, Y., and Rigaud, M. "Sinterability of macrocrystalline and cryptocrystalline magnesite to refractory magnesia," International Journal of Ceramic Engineering & Science, 2(6), 303–309, 2020. DOI: 10.1002/ces2.10068.

4. Use for: cryptocrystalline versus macrocrystalline magnesite, sinterability, bulk density, MgO purity, crystal development and CaO/SiO_2 ratio.

5. Nanda, S., Choudhury, A., Katakam, K.S.C., and Sarkar, D. "Raw materials, microstructure, and properties of MgO–C refractories: Directions for refractory recipe development," Journal of the European Ceramic Society, 43(1), 14–36, 2023. DOI: 10.1016/j.jeurceramsoc.2022.09.032.

6. Use for: MgO quality, graphite, resin, antioxidants, microstructure, oxidation resistance and high-temperature performance.

7. Kujur, M.K., Roy, I., Kumar, K., Chintaiah, P., Ghosh, S., and Ghosh, N.K. "Raw materials for manufacturing of superior quality MgO-C bricks," Materials Today: Proceedings, 5, 2359–2366, 2018. DOI: 10.1016/j.matpr.2017.09.242.

8. Use for: purity, bulk density, periclase crystal size, graphite quality and their influence on MgO–C brick performance in BOF/ladle applications.

9. Tsutsui, Y., Katou, K., and Umeda, S. "Magnesia-Carbon Refractories for Converters," Nippon Steel Technical Report, No. 125, 2020.

10. Use for: converter application, MgO clinker, graphite, antioxidants, resin, corrosion resistance, spalling resistance and slag penetration.

11. Guo, Z., Zamboni, S., Gao, J., and Gan, F. “Indispensability and Vulnerability of Magnesia-carbon Bricks for Steelmaking Process,” China’s Refractories, 30(1), 7–16, 2021. DOI: 10.19691/j.cnki.1004-4493.2021.01.002.

12. Use for: vulnerability of MgO–C production to raw-material quality, large-periclase-crystal fused magnesia and steelmaking refractory performance.

13. Sadrnezhaad, S.K., Mahshid, S., Hashemi, B., and Nemati, Z.A. “Oxidation Mechanism of C in MgO–C Refractory Bricks,” Journal of the American Ceramic Society, 89(4), 1308–1316, 2006. DOI: 10.1111/j.1551-2916.2005.00863. x.

14. Use for: graphite oxidation, oxidation kinetics and degradation mechanisms in MgO–C bricks.
15. Use for: modern MgO–C design, oxidation resistance, hot strength and microstructural reinforcement.

16. Use for: comparison of 2024 and 2025 magnesia/magnesite production and establishing the recent trend.

17. Use for: freight-rate volatility, Red Sea disruption, rerouting, increased voyage distance, vessel availability and supply-chain risk.

18. QMAG. “Where We Operate – Kunwarara and Yaamba Magnesite Deposits,” Queensland Magnesia, Australia.

19. Use for: QMAG’s Queensland cryptocrystalline magnesite deposit, beneficiation, processing and international logistics. QMAG describes Kunwarara and Yaamba as one of the world’s largest cryptocrystalline magnesite deposits.

20. QMAG. “Dead burned Magnesia Production,” Queensland Magnesia, Australia.

21. QMAG. “Refractory – DBM and EFM for Refractory Bricks,” Queensland Magnesia, Australia.

22. Use for: application of QMAG magnesia in refractory bricks for iron and steelmaking.

23. QMAG. “Logistics and Sales,” Queensland Magnesia, Australia.

ADVANTAGES OF NON-CEMENT HYBRID BONDED CASTABLE FOR EAF ROOF DELTA OVER REGULAR CASTABLE TECHNOLOGY

Jagadish Chandra Behura[1], Sarada Prasanna Das[1], Dr. Debasish Chandra[1], Dr Thomas Schemmel[2]

[1]Refratechnik India Pvt. Ltd, [2]Refratechnik Steel GmbH.

Abstract

Since last decade, cement free Gel Bonded castable has strengthens its position by increased use in Indian market as unshaped refractory products. The silica sol solutions are aqueous colloidal dispersions of amorphous nano scale SiO2 particles. Sol bonded castable is often considered as good alkali & acid resistant than conventional high alumina cement bonded concretes. It doesn't form any calcium aluminate hydrate phases during setting process; it leads concrete to be heated much faster than cement bonded castable. The incorporation of gel bond in place of conventional binders (High Alumina Refractory Cement) has made it possible to improve the high temperature properties of castable refractories considerably mainly because of the absence of low-melting phases (CA, CA_2, $C_{12}A_7$, C_2AS, C_4AF) and impurities. Several advantages of the gel-bond compositions compared to Cement Bonded castable are less mixing time since gel bond formulations do not require other minor additives or deflocculants like the cement containing castable. Shorter drying time and so reduced drying flaws. This is because water is not added or required for mixing. Better refractoriness because of the absence of melting phases like- anorthite or gehlenite. Colloidal silica being more viscous than the water, help to maintain more separation of refractory particles which, in turn, provide better thermal shock resistance. Better chemical resistance because of the various superior properties of gel bond castable / pumpable. It yields longer campaign life, less downtime and so reduces cost of furnace operation. Longer shelf life since there is no hydratable phase as in LCC, ULCC. The study evaluates the castable's Cold Modulus of Rupture (CMOR), Cold Crushing Strength (CCS), Bulk Density (BD), and Apparent Porosity (AP) after curing at 25°C and firing at 110°C, 1100°C, and 1400°C. Additionally, the study assesses the thermal shock resistance. Furthermore, an example of application will be given proving the efficiency of the technique for practical use.

Introduction

Electric Arc Furnace (EAF) roofs, specifically the central delta section, operate under some of the most punishing conditions in modern steelmaking. This zone faces extreme thermal shock from rapid cycling, mechanical stress due to electrode movement, and severe chemical attack from corrosive slag and volatile gases. For decades, traditional cement-bonded castables (conventional, low-cement, and ultra-low-cement) have been the industry standard. However, the inherent limitations of calcium aluminate cement (CAC) binders often trigger premature lining failure, forcing unscheduled maintenance shutdowns.

Regular cement-bonded castables (including low-cement variants) rely on the hydration of calcium aluminate cement to develop green strength. This chemical mechanism introduces several operational and structural liabilities:

The introduction of calcium oxide (CaO) from the cement binder reacts with silica (SiO_2) and alumina (Al_2O_3) within the castable matrix. At elevated EAF operating temperatures (>1600°C), this reaction forms low-melting liquid phases such as anorthite (CAS_2) and gehlenite (C_2AS). These soft phases compromise hot modulus of rupture (HMOR) and accelerate slag corrosion. During the initial heating cycle, chemically bound water inside the cement hydrates evaporates between 250°C and 500°C. This dehydration destroys the hydraulic bond

before ceramic sintering takes place (occurs >1000°C), leaving a critical temperature window where the refractory risks low mechanical strength. Cement hydrates form a dense, tightly interlocking crystalline microstructure. This low-permeability matrix traps vaporized moisture during rapid heating, generating high internal steam pressures that frequently cause explosive spalling.

To overcome these structural vulnerabilities, non-cement hybrid bonded castable technology represents a paradigm shift. By replacing hydraulic cement binders with an engineered chemical-colloidal matrix, this advanced refractory system eliminates the traditional weaknesses of cement hydration. This paper evaluates the technical advantages of non-cement hybrid bonded castable over regular cement-based technologies, demonstrating how they optimize thermo-mechanical stability, accelerate dry-out schedules, and ultimately extend EAF roof service life in high-productivity steel plants. [6]

Non-cement hybrid bonded castable bypasses these issues by utilizing a dual chemical-colloidal binding mechanism, typically combining hybrid bond with specific chemical setting agents.

[Hybrid Bond] + [Chemical Hardener]

▼

[3D Nanostructured Gel Network]

▼

(Heating)

[Direct Nano-Ceramic Sintering (Zero Lime / CaO)]

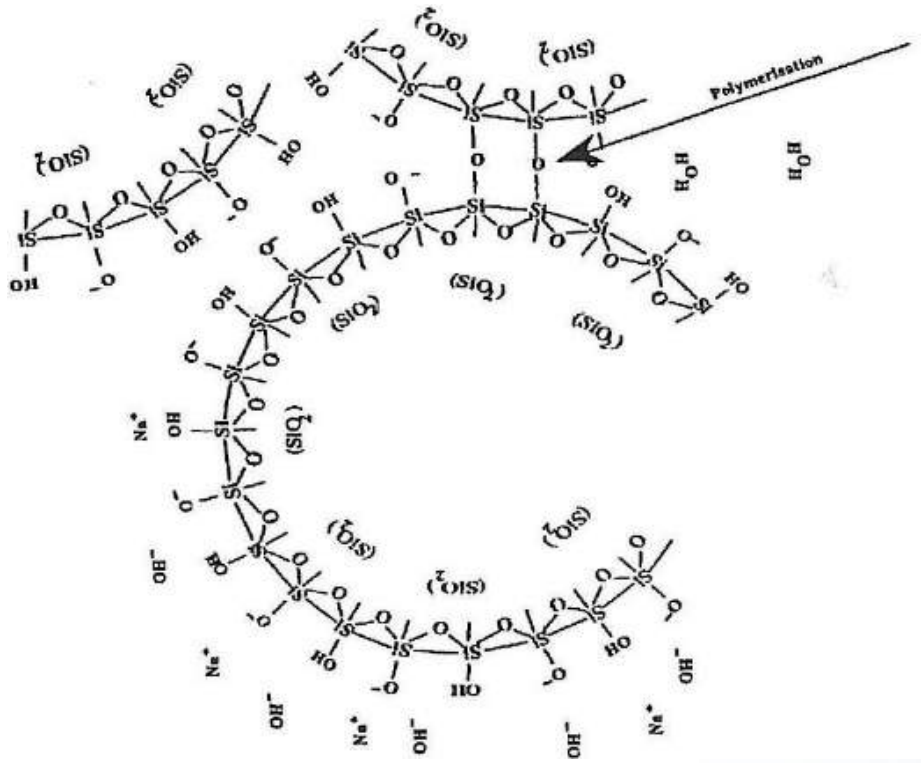


Fig.1. Upon activation, the nano-sized particles (10-50 nm) polymerize into a continuous, three-dimensional gel network.

This gel structure holds the refractory aggregate together without requiring any calcium oxide.

Distinct Technical Advantages for EAF Roof Deltas: as hybrid castable are completely

lime-free, they eliminate the formation of low-melting liquid phases. The nano-silica matrix reacts with the alumina aggregate at high temperatures to form secondary mullite ($3Al_2O_3 \cdot 2SiO_2$), a highly refractory phase characterized by interlocking needle-like crystals. This yields a significantly higher Hot Modulus of Rupture (HMOR) at 1500°C+ and a rigid structural framework that resists chemical erosion from acidic and basic EAF metallurgy slags. The nano-gel network features inherent micro-porosity and structural flexibility. Unlike the rigid, brittle crystal structures found in cement bonds, this nanostructured matrix accommodates localized thermal expansion and contraction. When subjected to the severe thermal cycling of an EAF roof—such as when the roof swings open for scrap charging—the hybrid castable arrests micro-crack propagation, preventing catastrophic structural spalling. Hybrid castable do not suffer from an intermediate temperature weakness zone. As colloidal moisture departs, the siloxane bonds (Si-O-Si) strengthen through a continuous polymerization process. The mechanical strength curve remains stable and linear from ambient drying temperatures straight through to high-temperature ceramic sintering. The dehydration of a nano-silica gel matrix releases physically bound water rather than chemically locked hydrate water. This moisture escapes through a highly permeable network of open micro-channels at relatively low temperatures (100°C - 200°C). Consequently, the steam pressure remains well below the material's tensile strength limit. EAF deltas lined with hybrid castable can be dried and heated at aggressive rates (exceeding 50°C/hr) with zero risk of explosive spalling, drastically cutting furnace commissioning.

Experimental:

To determine the best operational practices for Electric Arc Furnace (EAF) roof deltas across different plants, various castable formulations were studied. The main constituents of these castable included high-alumina silicate aggregates of different fractions, technical and reactive alumina fines, and micro silica (fume silica). High-alumina calcium aluminate cement (HAC) and a hybrid binder were used as the binding systems. The detailed properties of these raw materials are presented in Table 1. Castable formulation was prepared using the PSD formula:

$$CPFT = (D^q - D^qs) / (D^qI - D^qs) \times 100 \quad (i)$$

where, CPFT = cumulative percent finer than (the size D), D = particle size, Ds = minimum particle size, Dl = maximum/largest particle size, q = distribution coefficient/ modulus. In the present work, q values of 0.21 and 0.29 are used and the plot for PSD, used in the study, is shown in Fig-2.

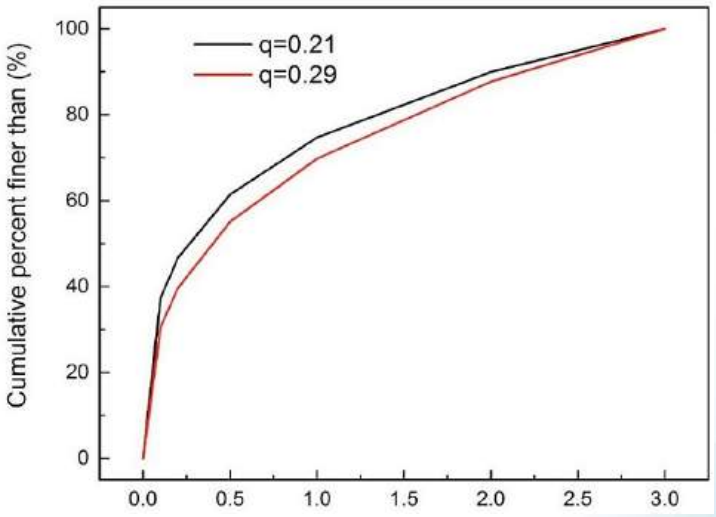


Fig. 2. PSD formulation graph

To rigorously assess performance, comparative lab validations were performed [11, 12, 14] against standard industrial formulations. Raw trial configurations were categorized into standard high-alumina cement (HAC) layouts and Hybrid Bond

layouts. The formulation matrix was designed using Andreasen packing factors of q = 0.21 and q = 0.29. This allowed for a direct structural comparison between the traditional HAC based and the proposed hybrid bond system. The specific experimental combinations and dosing ratios are systematically outlined in Table 2 &3. These configurations were selected to optimize particle packing density and evaluate the subsequent physical properties.

All raw materials were first dry mixed according to the batch composition in a planetary mixer and water or a hybrid bond was added as per requirement, to the dry-mixed batches during continuous mixing until the proper flow consistency was attained. Water was added to the hydraulic bonded high alumina cement (HAC) base composition, while the hybrid bond was added to the hybrid castable to achieve the desired flow consistency on a vibrator to study the flow percentage and setting behaviors. The mixed batches were then casted into 40 mm × 40 mm × 160 mm bar-shaped lubricated moulds on a vibratory table operating at 3200–3600 vibrations/min with an amplitude of ±0.5 mm.

The cast specimens were cured under humid conditions within the mould for 1 day, de-moulded, air-dried for another 1 day, and subsequently oven-dried at 110°C for 1 day. The dried products were then fired at 1000°C and 1500°C with 4-hour soaking time. All firings were conducted in a 1700°C programmable electric resistance furnace.The bulk density (BD) and cold crushing strength (CCS), Modulus of rapture (MOR) & Permanent linear change (PLC) of the dried, 1000°C, and 1550°C heat-treated samples were measured in accordance with the Bureau of Indian Standards IS 10570 (2011) specification. The CCS was measured using a compressive testing machine. Furthermore, the 1500°C fired samples were evaluated for hot modulus of rupture (HMOR) at 1400°C in an HMOR furnace utilizing alumina supporting and mullite loading rods. Phase analysis of the matrix phase (excluding coarse grains to minimize corundum interference and identify trace phases) of the castable fired at 1500°C was carried out using the powder X-ray diffraction (XRD) technique.

Result and Discussion:

Physio-chemical properties of the raw materials (Table 1) indicate that they are pure, containing minimal impurities in the matrix, with high-alumina silicate materials utilized as aggregates. The cement used is a mixture of both calcium aluminate CA and calcium di-aluminate CA2 phases. The hybrid bond is also pure, featuring approximately 30% solid content.

Fig - 2 illustrates the particle size distribution (PSD) of the castable with distribution coefficients of q=0.21 and 0.29. Increasing the “q” value fine content will decrease and course content will increase in the granular compositions. Table – 2& 3 outline the batch compositions of the studied castable. Cement and silica fume are considered the fine components; for compositions containing both, the overall fine content was adjusted by reducing the fine alumina content.

The amount of binder was kept constant across all batches. Water was added to the cement-based composition to achieve the proper flow consistency required for vibration casting. Conversely, no additional water was added to the hybrid-bonded castable; only the hybrid bond itself was introduced to ensure proper casting flow. Furthermore, a marginal decrease in liquid requirement was observed for batches with higher q values even at identical binder contents due to the lower fine content reducing the total surface area requiring wetting. Notably, the total liquid required to achieve a similar consistency was lowest for the compositions containing only the hybrid bond. This reduction is attributed to the high concentration of nanometric, spherical hybrid-bond particles, which significantly enhance fluid mobility.

Flow behaviors study:

The flow behavior of both cement-bonded and hybrid-bonded castable was evaluated at different q factors. The difference between the initial and final flow for all batches was approximately 20%, indicating acceptable workability for practical applications. Furthermore, the formulation with q=0.21 exhibited superior flow behavior compared to q=0.29, demonstrating that a higher content of fine particles enhances flowability. As shown in Fig-3, the hybrid-bonded castable displayed slightly better flow than the cement-bonded variant, suggesting that hybrid-bonded castable offer easier on-site installation during casting.

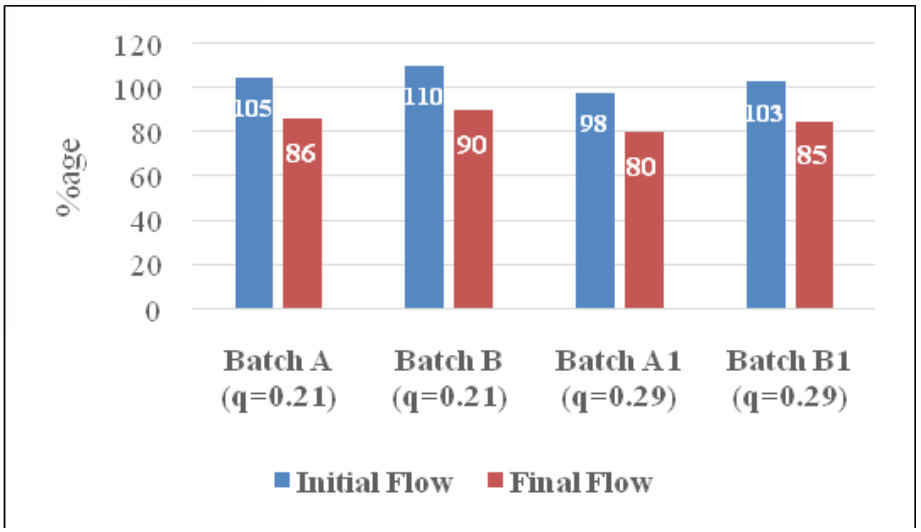


Fig-3. Initial & Final flow%

Setting time study:

As shown in Fig- 4, the setting times for the q = 0.21 composition are slightly longer than those for q = 0.29, which is attributed to minor differences in the water & hybrid bond demands. Furthermore, the hybrid-bonded castable exhibits a longer setting time compared to the cement-bonded castable. For Electric Arc Furnace (EAF) roof delta castable, a prolonged setting time is generally preferred due to the large scale of the precast shapes. Industrial site casting typically requires 3.0-5.0 Mt of material, leading to an extended installation window of 1 to 2 hours. Consequently, a delayed setting mechanism is crucial to maintain workability and ensure a smooth, high-quality surface finish.

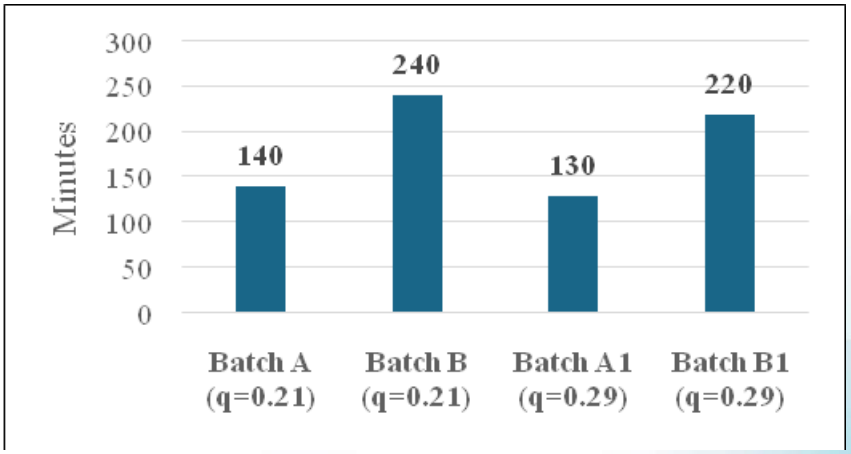


Fig-4. Setting time in Minutes

Phase analysis study:

Phase analysis study of the matrix phase of 1500°C sintered samples are shown in Fig 5A & 5B Hybrid bond containing composition (batch B & B1) showed the presence of mullite ($3Al_2O_3{\cdot}2SiO_2$) phase other than corundum in the matrix[3, 11, 12], confirming the reaction between silica of hybrid bond particles and alumina of the matrix phase at1500°C No other phases were found in the composition Whereas the only cement containing one (batch A & a1) showed the presence of minor amount of mullite, grossite ($CaO{\cdot}2Al_2O_3$), hibonite ($CaO{\cdot}6Al_2O_3$) and anorthite ($CaO{\cdot}Al_2O_3{\cdot}2SiO_2$) along with corundum phase confirm that CA & CA_2 reacts with fume silica and alumina at 1500°C creates some low melting phases which ultimately leads to high corrosion as well as less thermal shook resistance

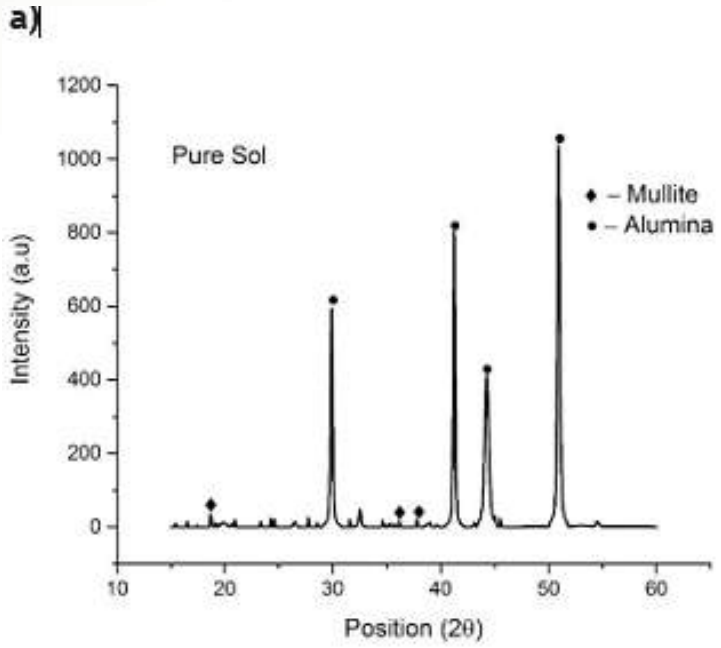


Fig. 5A. Phase Analysis of Hybrid bonded Castable

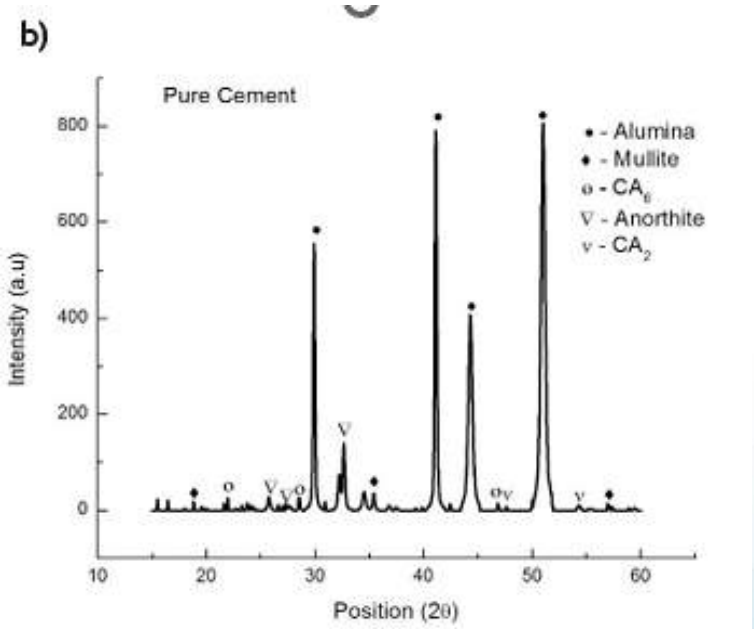


Fig. 5B. Phase Analysis of Cement bonded Castable

Density & Porosity Study:

The bulk density and apparent porosity values of the castable treated at 1000°C are shown in Fig 6. A general trend of higher density values is observed for castable with a higher q value, which may be attributed to a greater proportion of coarser particles in the batch. Furthermore, because the base raw material is identical for both the hybrid and cement-bonded castable, no significant changes were observed in their apparent porosity and bulk density values.

Strength Study:

The cold crushing strength (CCS) and modulus of rupture (MOR) values of the castable treated at different temperatures are shown in Fig. 7 and 8. A general trend of higher strength values with an increasing distribution coefficient was observed across all compositions and heat treatment temperatures.At the drying stage, the cement-bonded castable exhibited higher strength compared to the hybrid-bonded compositions. This is attributed to the formation of stronger hydraulic bonds in the cement-containing samples, whereas the hybrid-bonded samples rely on weaker coagulation bonding. A similar trend was observed at the intermediate temperature of 1000°C, where hybrid-bonded compositions showed lower CCS and MOR values. At high temperatures, the CCS and MOR values surpassed those of both the dried and intermediate-temperature samples due to sintering. Notably, at these elevated temperatures, the hybrid-bonded compositions exhibited superior strength.[4, 8] This improvement

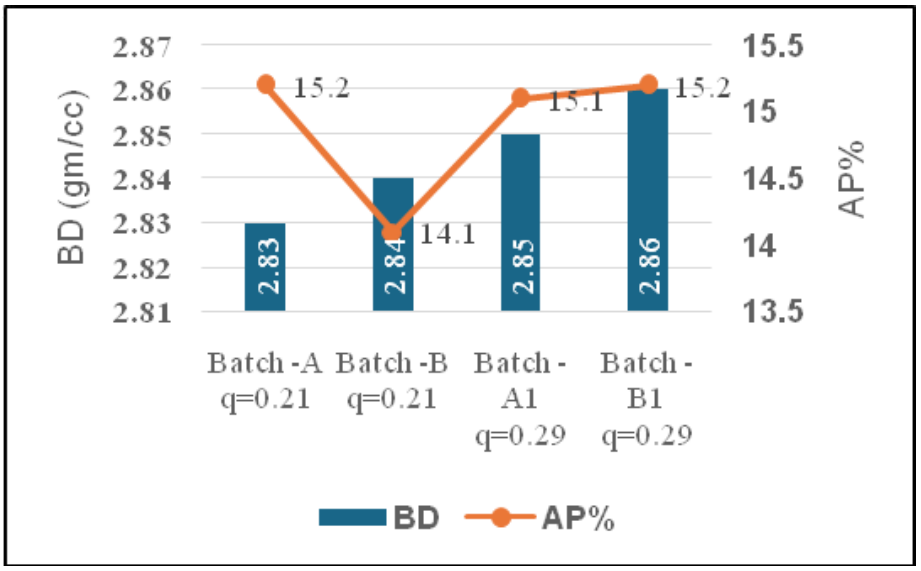


Fig-6.Apparent porosity & Bulk Density(gm/cc) 1000^{0}C

is likely due to enhanced sintering kinetics facilitated by the finer particles, alongside the formation of a mullite phase, as confirmed by the phase analysis. Mullite network formation provides additional structural reinforcement, thereby enhancing mechanical strength. Consequently, for applications exceeding 1500 °C, the hybrid-bonded castable delivers better performance than the conventional hydraulic-bonded castable.

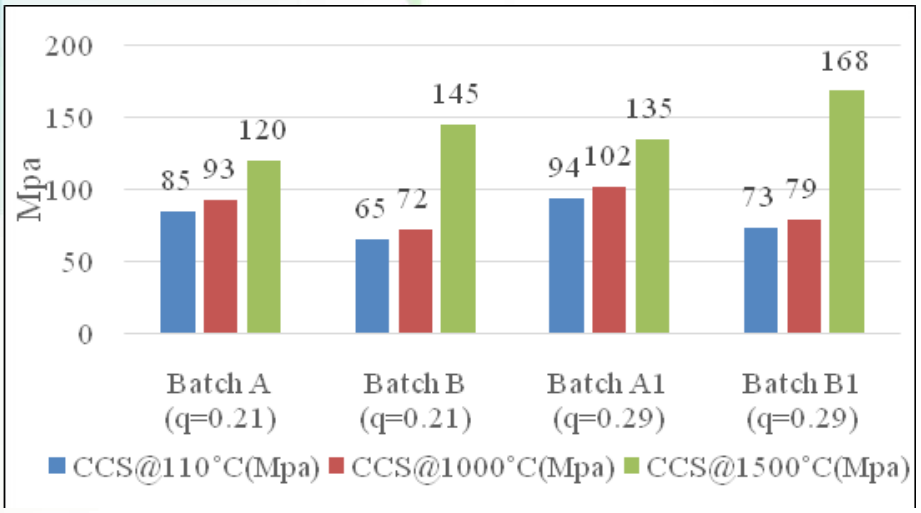


Fig-7. Cold Crushing Strength@1000^{0}C

Hot strength study:

Hot modulus of rupture (HMOR) measurements of the castable samples sintered at 1500 °C were conducted at 1400 °C, with the resulting values illustrated in Fig-9. The HMOR values decreased as the cement binder content increased. Higher hot strength was observed in the hybrid-bonded composition due to a greater extent of mullite formation compared to the cement-containing compositions. Mullite, a high-melting compound, provides structural reinforcement and maintains the strength of the composition at elevated temperatures. Conversely, the introduction of cement reduced the hot strength owing to the formation of low-melting compounds—specifically anorthite—as confirmed by phase analysis. An increasing concentration of cement accelerates anorthite phase formation, leading to a progressive decline in hot strength. Consequently, the minimum hot strength was observed in the purely cement-bonded composition.

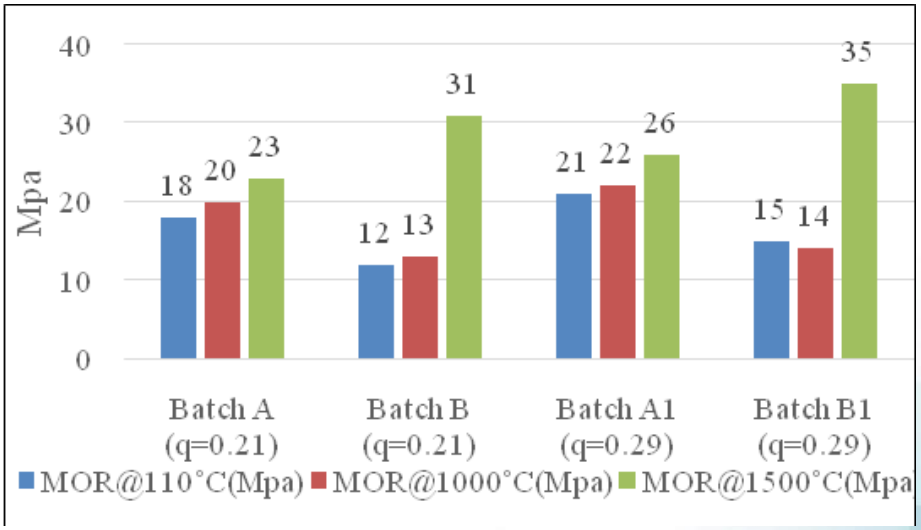


Fig-8. Modulus of Rupture Result

Hybrid Bond ⟶ High Mullite Formation ⟶ High-Melting Network ⟶ Maximum HMOR

Cement Bond ⟶ High Anorthite Formation ⟶ Low-Melting Liquid Phase ⟶ Minimum HMOR

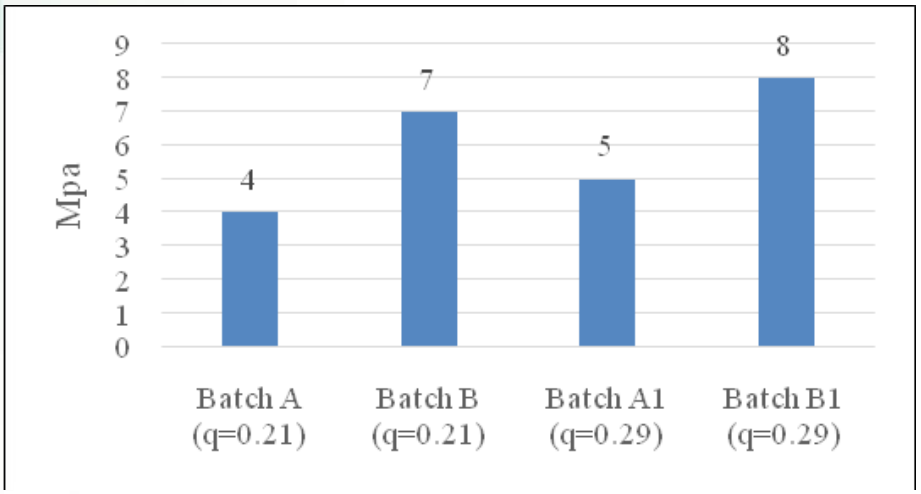


Fig-9. Hot Modulus of Rupture (MPa)1400^{0}C

Industrial Application Case Study:

We migrated this technology to an industrial service trial on an active EAF roof delta to evaluate real performance. The refractory material in the delta region must withstand extreme conditions during the steelmaking cycle such as-

ThermalShock: Rapid temperature fluctuations ranging from ambient air exposure during tapping/charging to operating temperatures exceeding 1650°C during power-on phases.

Chemical Attack: High-temperature corrosion from corrosive slags, volatile vapor phases, and iron oxide (FeO) rich dust.

Mechanical Stress: Vibrations from high-power electrode arcs, electromagnetic forces, mechanical lifting of the roof, and physical abrasion from high-velocity exhaust gases.

Our team studied the operational parameters of different plants (Table-4) and selected Plant A because regular ultra-low-cement castable deltas suffered from frequent premature cracking, spalling, and ring failures, which restricted the number of heats per campaign. Installing the hybrid castable required precise site control to optimize its unique hybrid binding mechanisms. To avoid cold joints, concrete placement must be continuous, utilizing high-frequency immersion vibrators for consolidation while avoiding over-vibration that induces segregation. Because hybrid bonded systems rely on a chemical sol-gel transition rather than hydraulic cement hydration, moisture preservation during curing is critical. Consequently, the cast structure must be immediately covered with plastic sheeting to prevent premature surface drying. Mold stripping is typically performed after 24 hours, depending on ambient temperatures. Subsequently, a controlled green-state curing period of 24 hours at ambient temperature is required prior to the initial heat-up.



Fig. 10 - After casting at site

Throughout the process, strict field precautions are required, including maintaining ambient and material temperatures between 35°C and 40°C. To prevent degradation of the refractory's mechanical properties and density, the prescribed binder-to-powder ratio must not be altered by adding external water. The subsequent dry-out schedule follows a dedicated thermal curve tailored for hybrid bonds. Although hybrid-bonded castable offers higher permeability and lower explosive spalling risks than cement-bonded alternatives, a controlled heating rate of 50°C/hr is necessary to safely liberate chemically bound water.

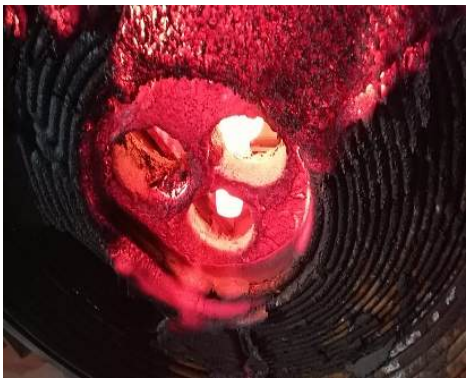




Fig. 11 - Erosion profile after 450 Heats & at final lifetimes

Evaluation of the hybrid-bonded castable roof delta post-campaign confirmed optimal performance with zero structural abnormalities. Quantitative profiling indicated that the refractory successfully mitigated typical wear mechanisms, thermal spalling, and aggressive erosion-corrosion dynamics, validating the architecture shown in Figure11.

To evaluate material efficacy, the team supplied three distinct sets of hybrid-bonded, roof-delta castable. The comprehensive performance characteristics and experimental metrics for each set are systematically detailed in Fig-10.

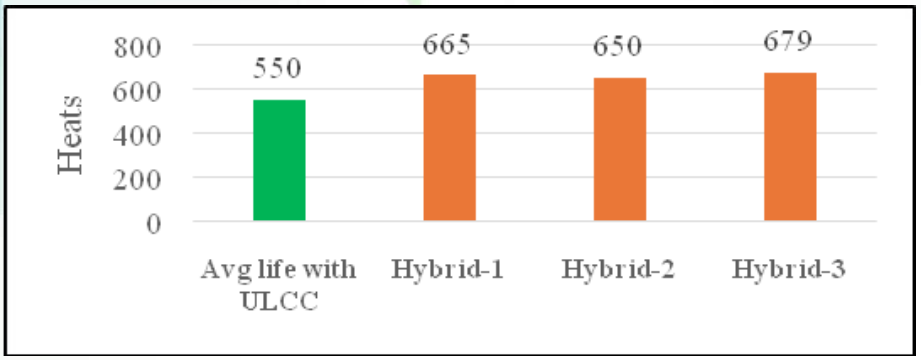


Fig-10. Performance of roof delta in heats

Conclusion:

This study demonstrates that non-cement hybrid bonded castable technology represents a significant paradigm shift over conventional cement-bonded refractories for Electric Arc Furnace (EAF) roof delta applications. By eliminating calcium aluminate cement, this advanced hybrid bonding system successfully bypasses the critical intermediate-temperature strength degradation zone and prevents the formation of low-melting eutectics. The resulting material exhibits superior hot modulus of rupture (HMOR), exceptional thermal shock resistance, and enhanced chemical immunity against corrosive slag and iron oxide vapors.

Industrial trials corroborate these laboratory findings, showing a substantial increase in lining service life, reduced structural spalling, and minimized maintenance downtime. Ultimately, transitioning to non-cement hybrid bonded castable offers steelmakers a highly reliable, high-performance solution that directly optimizes EAF operational efficiency, reduces specific refractory consumption, and lowers overall production costs.

Oxide [mass-%]	Alumina -Silicate	Corundum	FS	HAC	Hybrid Binder
SiO_2	7.2	0.03	96.2	0.21	29.8
Al_2O_3	85.6	99.2	0.4	71.64	
Fe_2O_3	1.85	0.03	0.1	0.11	
CaO		0.02	0.2	26.91	
MgO		0.01	0.1	0.32	
Na_2O+K_2O	0.5	0.01	0.4	0.27	
LOI [%]			0.8		70.1
Average size(mm)	0 - 5	100 % <45	100 % <45		0.2
Bulk density [g/cm^3]	3.2				
App. porosity [%]	6.9				
Spec. surface area [m^2/g]		2.5	~20	0.4	
Phase analysis	corundum	corundum	amorphous	CA_2, CA	

Table-1 Physico-chemical properties of input RM

Material [mass-%]	Batch A1	Batch B1
Alumina - Silicate (0 - 5 mm)	69.7	69.7
Corundum (-325)	23.3	25.3
HAC	3	0
Fume silica	4	5
Deflocculants	0.2	0
Hybrid Binder	0	6
Water	4.9	0

Table - 2 Batch composition of castable with q=0.21

Parameters	Plant-A	Plant-B	Plant-C
Furnace capacity (Mt)	100	50	40
Tap temp. (deg C)	1620 - 1670	1620 - 1650	1620 to 1650
Process time (Min)	50- 60	100-120	50-55
Arcing time (Min)	30-40	80-90	45-47
Tap to tap time (Min)	60-65	100-105	55-65
Stee grades produced	LC/MC = 90/10	Alloy steel	Alloy steel

Table - 3 Batch composition of castable with q=0.29

Material [mass-%]	Batch A	Batch B
Alumina - Silicate (0 - 5 mm)	62.7	62.7
Corundum (-325)	30.3	32.3
HAC	3	0
Fume silica	4	5
Deflocculants	0.2	0
Hybrid Binder	0	6.5
Water	5.5	0

Table - 4 Plant wise operational parameter

References:

1. Banerjee, S.: Recent developments in monolithic refractories.
2. Amer. Ceram. Soc. Bull. 77 (1998) [10] 59–63
3. Masaryk, J.S.: Development and use of low cement self-flow castable. Proc. UNITECR, São Paulo, Brazil (1993) 527–538
4. Sarkar, R.: Refractory technology: Fundamentals and applications. Boca Raton, Fl., USA, (2016) 258
5. Bhattacharyya, A.K.; et al.: Ultra-low cement castable – a new generation of trough bodies for increased cast house life. Interceramic 47 (1998) [4] 249–251
6. Studart, A.R.; et al.: Processing of zero cement self-flowhigh alumina refractory castable by matrix rheological control. Amer. Ceram. Soc.
7. Banerjee, S.: Monolithic refractories – a comprehensive handbook. Singapore 1998, 311
8. Iler, R.K.: The Chemistry of silica: Solubility, polymerization, colloid and surface properties, and biochemistry. New York 1979, 866
9. Nouri-Khezrabad, M., et al., 'Colloidal silica applications in refractory castable: A review', Ceramics International, Vol. 39, No. 4, 2013, pp. 3439-3457.
10. Braulio, M. A. L., et al., 'Cement-free alumina-magnesia castable', Ceramics International, Vol. 37, No. 6, 2011, pp. 1899-1905.
11. Das, S.K.; et al.: No cement high alumina self-flow castable. Amer. Ceram. Soc. Bull. 82 (2003) [2] 55–59
12. Hu, S., et al. (2026). "Synergistic effects of hybrid silica sol–calcium aluminate cement bonding in high-alumina castables." Ceramics International.

PARTIAL REPLACEMENT OF MICROSILICA BY REACTIVE ALUMINA IN CASTABLE APPLICATION

P. Saravanan[1] and Ravi Mohare[2]

Hindalco Innovation Centre-Alumina
Hindalco Industries Limited, Belagavi, Karnataka, India

(1. Lead, Calcination and Product ; 2 Sr TM Calcination and Product)

Email : saravanan.p@adityabirla.com : ravi.mohare@adityabirla.com

Abstract

Low cement castables (LCCs) extensively utilize microsilica to achieve dense particle packing, improved flowability and enhanced mechanical properties. However, microsilica can promote glassy phase formation at elevated temperatures, limiting high-temperature performance. This study investigates the partial replacement of microsilica with reactive alumina in alumina-based LCC formulations and evaluates alternative dispersants to optimize rheological, physical and thermo-mechanical properties. Dispersants were assessed based on casting water demand, flowability, green and fired density, modulus of rupture, cold crushing strength, apparent porosity and hot modulus of rupture. Following dispersant selection, repeatability studies were conducted and castables with varying levels of microsilica substitution were developed while maintaining comparable particle size distribution. Results showed that partial replacement of microsilica with reactive alumina maintained workability and improved refractoriness and high-temperature strength at 1400°C through enhanced ceramic bonding. Excessive replacement reduced flowability and increased porosity, indicating the need for optimized microsilica-alumina balance for superior performance.

Keywords: Low Cement Castable (LCC), Microsilica Replacement, Reactive Alumina,High-Temperature Performance.

1. Introduction

In recent years, the development of highly efficient installation techniques such as pumping or wet gunning of modern castables continues to gain popularity worldwide. The rheological properties are important for Low Cement Castable (LCC) during installation. Microsilica consisting of ultrafine spherical particles, is added in the formulation to improve the rheology, packing density, strength and durability.of the castable. It has been a key component in the development of low and ultra-low cement castable with low water demand.

Even though microsilica improves the flow of the castable, it reduces castable's strength when temperature rises significantly above 1500°C. Castables containing microsilica are not suitable for high temperature application, which may affect the high temperature property by forming glassy phases. Fine Alumina is an alternate material to replace the microsilica in castable formulation. In this study, microsilica has been replaced by alumina with different percentages and thermo-mechanical properties were studied.

2. Conceptual Approach

In Low Cement Castable, microsilica is used to fill up the fine void spaces between the aggregate particles of castable and to improve the flow of the castable with less water demand. Microsilica also improves the mechanical properties at 1000oC because of higher reactivity between microsilica and other components of refractory mix.

Chemically, microsilica consists of amorphous SiO_2 with variable purity.

The ultrafine silica particles form low-melting phases and hot strength falls drastically at 1500oC. While replacing microsilica by any other fine filler the flow of the castable would get affected. The microsilica content should be generally minimum 3 wt% in the castable composition. If the percentage of microsilica goes down, the flow of castable would be affected because of higher water demand. Change in dispersant or changing various aggregate fractions of castable would help to improve the flow of the castable.

3. Experimental Details

3.1 Material Used

In this study, white fused alumina (WFA) aggregates, Non plastic clay (NPC), Sillimanite sand, high alumina cement, microsilica and milled reactive alumina were used for the castable composition. Milled reactive alumina was selected for this study because wide particle size distributed alumina would give the better flow.Although in the existing formulation this type of milled reactive alumina is already present, efforts were made to increase the percentage of alumina proportionally while reducing microsilica in the formulation.

Two types of dispersing additives were evaluated, first is the existing Dispersant-A (Sodium and Citric acid based) & another new Dispersant-B (Polymeric dispersant).The physical and chemical properties of different raw materials used for the preparation of castables have been presented in Table-1 & Table-2

Sample		NPC	WFA	Silimanite Sand	Cement	Microsilica
Specific gravity		2.61	3.81	3.13	-	2.22
PSD, $d_{50,}$	µm	-	-	-	-	4.5
BD - Loose,	g/cc	-	-	2.04	-	0.56
BD - Packed,	g/cc	-	-	2.14	-	0.66
Elemental Analysis by XRF						
SiO_2	%	52	0.046	37.4	-	99
TiO_2	%	1.78	0.007	0.22	0.06	0.2
Fe_2O_3	%	0.63	0.028	0.58	0.1	0.1
Al_2O_3	%	44.6	99.4	59.4	80	0.2
Na_2O	%	Trace	0.48	-	0.4	-
CaO	%	0.44	0.051	0.35	18	0.2

Table-1: Characterisation of Raw Materials

Sample		Milled Reactive Alumina
SSA,	m^2/g	1.29
Water Absorption,	g/100g	23.9
PSD, $d_{50,}$	µm	2.8
BD - Loose,	g/cc	0.81
BD - Packed,	g/cc	1.25
Elemental Analysis by XRF		
SiO_2	%	0.017
TiO_2	%	0.081
Fe_2O_3	%	0.013
Na_2O	%	0.3

Table-2: Characterisation of Alumina

3.2 Castable Batch Preparation

The castable batches were prepared by mixing all graded and fine particles in Hobart mixer by using castable composition as mentioned in Table-4. Initially, different percentages (0 to 50%) of microsilica were replaced by reactive alumina in the castable composition.Primarily,one set of castable batches were prepared with Dispersant-Aand anotherwith Dispersant-B.The dosage of dispersant was optimized as 0.2% to get maximum flow.The water content of 4.0% was added for this study to target a typical flow in the range of 50- 60%.

After mixing, consistency of the castable was checked by flow test. Later, mixed batches were then cast into rectangular steel mould with 9 bars of dimension as 160 x 40 x 40 mm and 4 bars of dimension as 150 x 25 x 25 mm using vibrating table. The castable samples were left in the moulds for 24 h in 100% relative humidity by covering with wet cloth. The cast samples were then demoulded and air-dried for 24 h. Air-dried samples were loaded in oven for drying at 110oC for 24 h.Aset of 3 each of the dried samples were fired at 1000oC and 1400oC for 5 hrs. Subsequently all 3 sets consisting of 3 bars each (Fired at 110oC , 1000oC& 1400oC) were tested for cold crushing strength (CCS), MOR, bulk density and apparent porosity. A set of 4 bars were tested for hot modulus of rupture (HMOR).

3.3 Results

The flow of the castable containing different percentage of microsilica with two different dispersants has been presented in .

Replacement of Microsilica	Flow of castable	
	Dispersant-A	Dispersant-B
%	%	%
0	48	46
10	42	49
20	36	50
30	0	50
40	0	48
50	0	50

Table-3 : Flow of Castable with Different Percentages of Microsilica

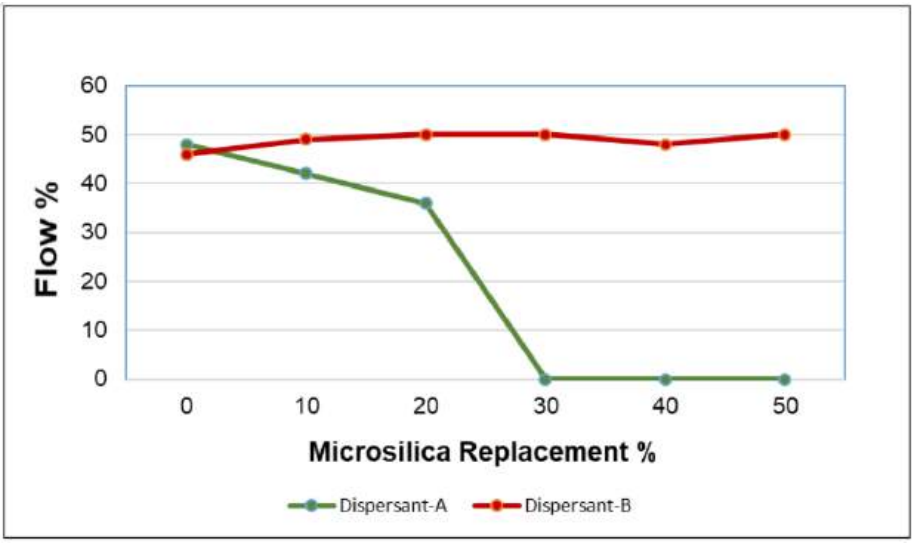


Figure-1 : Flow vs. Microsilica Replacement

It was observed from the Table-3that more than 20% of microsilica could not be replaced by alumina while using existing Dispersant-A. The composition consisting of Dispersant-B showed improved & consistent flow even after reducing the microsilica upto 50% with alumina.This may be because of polymeric structure of Dispersant-B. Based on the results, Dispersant-B was chosen as the right dispersant for further studies.

The microstructure of Microsilica & Milled Alumina observed usingScanning Electron Microscopy (SEM) is shown in Figure-2 & Figure-3 respectively.

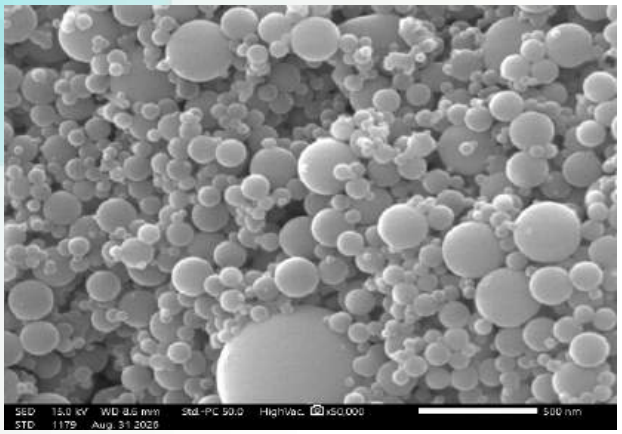


Figure-2: SEM Image of Microsilica

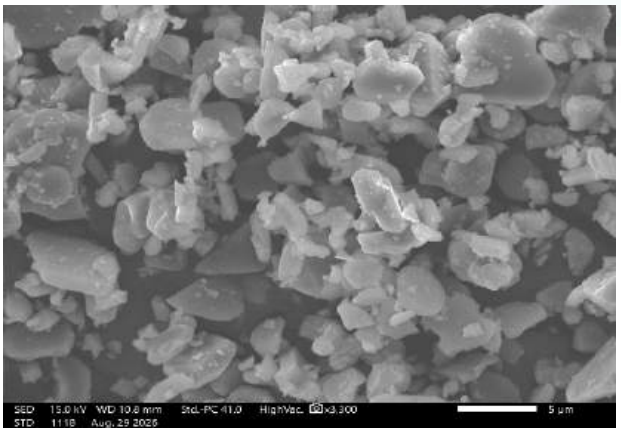


Figure-3: SEM Image of Alumina

It is observed from Figure-2 & 3 that Microsilica is spherical, whereas the reactive alumina is platy or irregular in shape.Although microsilica has of ultrafine spherical particles that improve flowability through a "ball-bearing" effect, controlled replacement with fine reactive alumina can still maintain the desired castable flow. This is because flowability in refractory castables is governed not only by particle shape but also by overall particle size distribution, packing density, dispersion efficiency and water demand. Fine reactive alumina particles occupy the interstitial voids between larger aggregates and matrix particles, contributing to a dense particle packing system. When combined with an effective dispersant the alumina particles remain well dispersed, minimizing agglomeration and maintaining the flow.

The castable batches prepared with all the raw materials & dispersing agents has been present in Table-4

Castable Batch Details								
Formulation %	**Test-1**	**Test-2**	**Test-3**	**Test-4**	**Test-5**	**Test-6**	**Test-7**	**Test-8**
	Dispersant-A		**Dispersant-B**					
NPC	18.9	18.9	18.9	18.9	18.9	18.9	18.9	18.9
WFA	58.1	58.1	58.1	58.1	58.1	58.1	58.1	58.1
Silimanite sand	5	5	5	5	5	5	5	5
Microsilica	3	2.7	3	2.7	2.4	2.1	1.8	1.5
Cement	5	5	5	5	5	5	5	5
Reactive Alumina	10	10.3	10	10.3	10.6	10.9	11.2	11.5
Total	100	100	100	100	100	100	100	100
Dispersant-A	0.2	0.2	-	-	-	-	-	-
Dispersant-B	-	-	0.2	0.2	0.2	0.2	0.2	0.2
Water addition %	4.0	4.0	4.0	4.0	4.0	4.0	4.0	4.0
MicroSilica Replacement %	**0**	**10**	**0**	**10**	**20**	**30**	**40**	**50**

Table-4 : Castable Batch Details

Accordingly the samples were tested for physical and thermo-mechanical properties. The complete analyses of castable with different percentages of microsilica with two different dispersants has been presented in Table-5.

Castable Batch Analysis Results																								
Tests		Test-1			Test-2			Test-3			Test-4			Test-5			Test-6			Test-7			Test-8		
		Dispersant-A						Dispersant-B																
Microsilica Replacement	%	0			10			0			10			20			30			40			50		
Temp. / Time,	°C/h	110/24	1000/5	1400/5	110/24	1000/5	1400/5	110/24	1000/5	1400/5	110/24	1000/5	1400/5	110/24	1000/5	1400/5	110/24	1000/5	1400/5	110/24	1000/5	1400/5	110/24	1000/5	1400/5
BD,	g/cc	2.97	2.95	2.97	2.98	2.94	2.96	2.97	2.91	2.92	2.96	2.92	2.93	2.98	2.92	2.94	2.99	2.93	2.94	2.99	2.93	2.95	2.98	2.94	2.95
AP,	%	9.5	12.4	12.4	9.4	13.3	13.1	8.9	12.8	13.2	8.1	12.7	13.9	8.9	13.3	14.1	8.1	12.8	13.4	7.8	12.9	13.2	8.6	13.2	13.5
MOR,	kg/cm^2	54	169	155	54	138	110	116	153	180	119	142	187	113	160	195	119	164	180	124	141	174	113	138	172
CCS,	kg/cm^2	229	1176	1018	293	1116	921	542	1178	1139	507	1015	1232	502	1135	1247	477	996	1248	490	931	1220	449	827	1107
HMOR	kg/cm^2	-	-	-	-	-	-	-	-	51	-	-	56	-	-	54	-	-	58	-	-	68	-	-	70

Table-5 : Castable batch Analysis Results

The Bulk density, modulus of rupture (MOR), cold crushing strength (CCS) &hot modulus of rupture (HMOR) of castable fired at different temperatures with different percentages of microsilica has been presented in Figures-4, 5, 6 & 7 respectively.

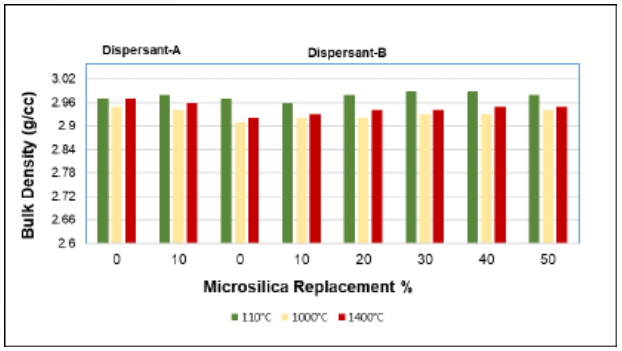


Figure-4 : Bulk Density vs. Microsilica Replacement

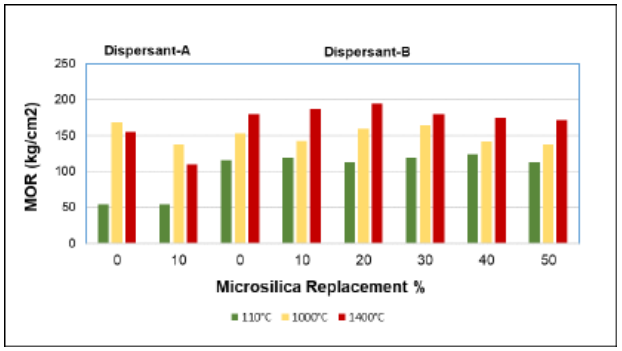


Figure-5 : MOR vs. Microsilica Replacement

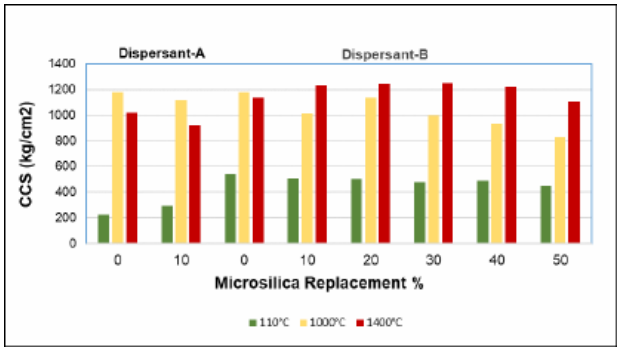


Figure-6 : CCS vs. Microsilica Replacement

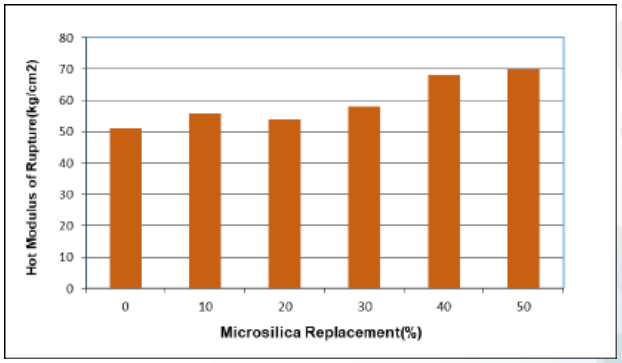


Figure-7 : HMOR vs. Microsilica Replacement

The obtained results indicate that castables formulated using the polymeric Dispersant-B showed better Density, MOR and CCS values than those prepared with Dispersant-A. The superior dispersing performance of Dispersant-B improved matrix densification and particle distribution, leading to enhanced mechanical properties and greater structural stability after firing.

The results of castables prepared with Dispersant-B indicate that, Bulk density of fired castable (at 1000oC and 1400oC) increases with increase in alumina content. This is because of replacement of low

density material (microsilica) by high density material (alumina).The mullite phase improves the mechanical properties like MOR.

The mullite phase formation was less at 1000oC while reducing the microsilica content. While replacing the microsilica by alumina (up to 50%), the HMOR value increased up to 37% without affecting the flow of the castable. Dispersant-B improved the setting property of cement which was reflected on cold crushing strength (CCS) of dried castable.

The castable samples fired at 1400°C, containing different percentages of microsilica replacement with reactive alumina, were subjected to X-Ray Diffraction (XRD)analysis for phase identification and quantification.The findings and quantification results are presented in Figure-6 & Table-6 respectively.

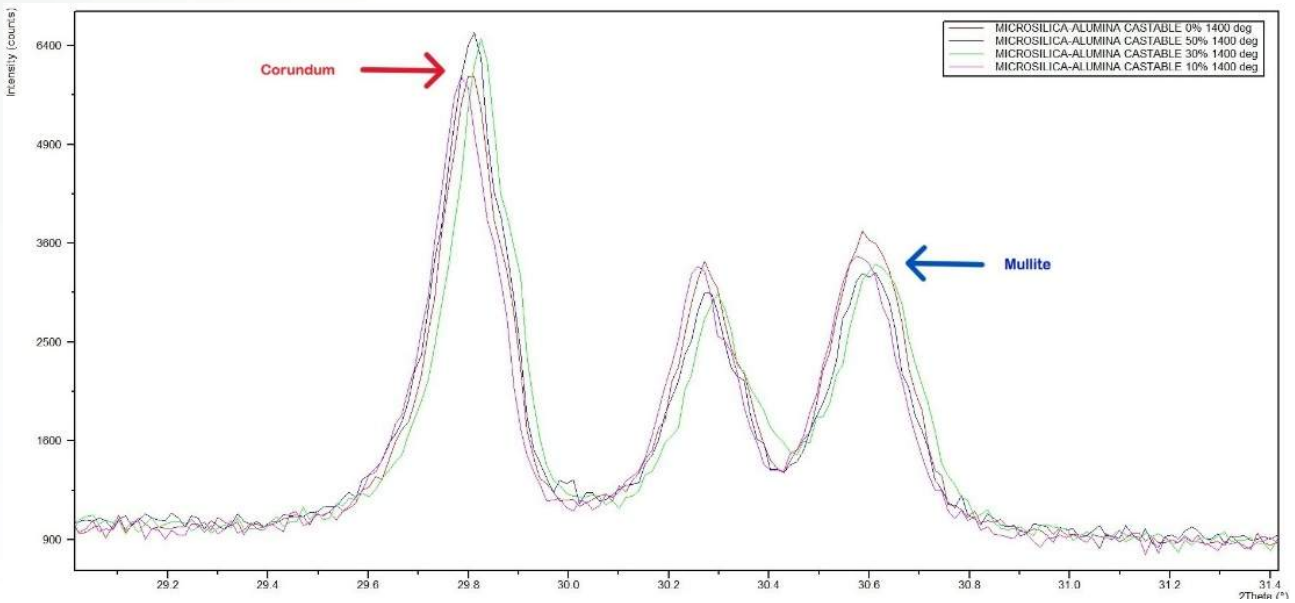


Figure-6 : XRD Phase identification results of castables

Microsilica Replacement	0%	10%	30%	50%
Temp. / Time.	1400 °C /5h			
Corundum	52	56	58	62
Mullite	48	44	42	38

Table-6 : XRD Quantification results of castables

The XRD scan image as observed in Figure-6 & quantification results as per Table-6 of castables fired at 1400°C showed a gradual increase in the corundum (α-Al_2O_3) phase accompanied by a decrease in the mullite phase with increasing alumina substitution. This trend indicates that reducing microsilica content limits the availability of silica for mullite formation, resulting in a higher proportion of corundum in the fired material. Controlled mullite formation is generally beneficial because mullite contributes to ceramic bonding, hot strength, and thermal shock resistance, while increased corundum content enhances refractoriness and high-temperature stability. Therefore, achieving an optimum balance between corundum and mullite is critical for obtaining the desired combination of mechanical strength, refractory performance and operating temperature.

To study the particle morphology and dense packing behaviour, the samples were analysed using Scanning Electron Microscopy (SEM). The micrograph of the castable fired at 1400oCdifferent percentages of microsilica replacement is shown in Figures-7, 8 & 9.

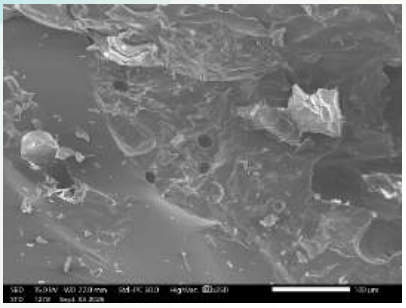


Figure-7 : 0% Micorsilica Replacement

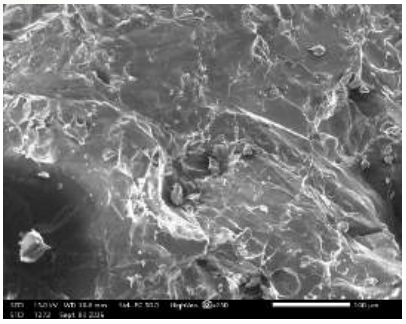


Figure-8 : 30% Micorsilica Replacement

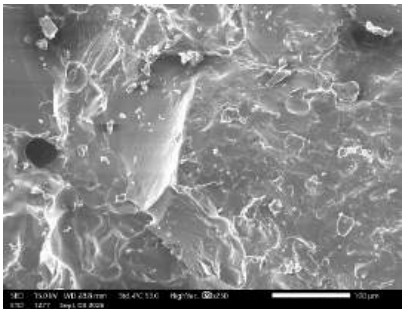


Figure-9 : 50% Micorsilica Replacement

The SEM micrograph of the castable fired at 1400°C showed no significant change in the packing characteristics of the matrix, indicating that the replacement of microsilica with milled reactive alumina did not adversely affect the microstructural densification. This observation suggests that partial replacement of microsilica with alumina is achievable while maintaining dense particle packing, thereby preserving the mechanical properties and overall refractory performance of the castable.

4. Discussions

The polymeric based Dispersant-B accelerate the setting and hydration of calcium aluminate cement. This may be one of the reasons for improved green strength in the castable compared to existing Dispersant-A. These dispersants are specially designed polymers which create gel formation by reacting with microsilica &show different retardation in setting property and change in rheology. Also, the flow of the castable is maintained without affecting setting time of castable. With no microsilica replacement at 1000oC, the microsilica creates the mullite phase by reacting with fine alumina. Hence the mechanical properties are high at this temperature. While increasing the temperature further, microsilica produce glassy phases and reduces high temperature strength. The thermo mechanical properties are reverse while replacing microsilica with alumina. At 1000oC, ceramics bonding starts which leads to low mechanical strength. No glassy phases are produced at higher temperature because of high melting point of alumina which leads to high mechanical strength. HMOR value of the castable containing less microsilica proves this. This type of castables can be used where high temperature properties are required.

5. Conclusions:

1. Replacement of up to 50% of microsilica with reactive alumina was found to be feasible while maintaining the desired level of flowability. However, higher levels of microsilica replacement resulted in a reduction in flowability, which could be effectively restored by changing the dispersant system from Dispersant-A to Dispersant-B.

2. While replacing microsilica with reactive alumina, the physical and mechanical properties of the castables fired at 1000°C were found to be inferior. However, the castables sintered at 1400°C exhibited improved

high-temperature properties, indicating enhanced refractory performance at elevated temperatures.

3. The Hot Modulus of Rupture value of the castable increased by up to 37% when 50% of the microsilica was replaced with reactive alumina. This improvement indicates enhanced high-temperature strength and load-bearing capability, which can be related to the increased alumina content, improved microstructural stability and reduced formation of low-melting glassy phases at higher temperatures.

4. Considering the overall thermo-mechanical properties, an ideal microsilica replacement level of 20-30% with reactive alumina appears to be the most suitable. However the optimum replacement ratio should be determined based on the specific castable formulation and service conditions, as phase development and refractory performance are strongly influenced by composition and operating temperature.

References

1. Hindalco Internal Report: Saravanan, P., Hindalco Industries Limited, 'Evaluation of Aluminas for Castable Applications-Partial Replacement of Microsilica by Alumina.

2. Hindalco Internal Report: Saravanan, P., Hindalco Industries Limited, 'Evaluation of Aluminas for Castable Applications - Fine-tuning of LCC Composition.

3. Rigaud, F.Ye.M., Jia.Q., Zhong.X., 'Rheological Behaviour of Ultra Low Cement Alumina Based Castables', Interceram Vol.53 (2004) 8-12.

TAILORED ALUMINA PARTICLE SIZE DISTRIBUTION IN ENHANCING PACKING DENSITY AND REFRACTORY CASTABLE PROPERTIES

Indu Bajpai* Vikas. S. Patil, Karthikeyan K, Ganesh Basak & Hirak Mitra

*Corresponding author email address: indu.bajpai@adityabirla.com
Contact no: 9016060182

Hindalco Industries Limited, Belagavi, Karnataka

Abstract

Alumina powder characteristics play a critical role in determining the performance of alumina-based low cement refractory castable. Particle size distribution (PSD) engineering and packing density optimization are critical for refractories, as green density and pore architecture govern shrinkage, final densification, and thermo-mechanical reliability. Refractory properties depend strongly on the fine alumina matrix. In this study, alumina powders with engineered particle size distribution like narrow, wide, and bimodal were developed and evaluated to understand their influence on rheology, packing efficiency, and thermo-mechanical properties of low cement refractory castables. Three alumina grades from Hindalo's product basket with specific surface areas ranging between 0.79-3.64 m^2g^{-1} and water absorption ~14-22.8 g/100g were chosen for the study. The castable were dried at 110 °C for 24 h and fired at 1500 °C for 5 h. Bulk density, apparent porosity, and cold crushing strength and modulus of rupture were measured for both dried and fired samples. High-temperature performance was further evaluated through hot modulus of rupture.

Key Words: Bimodal; Thermo-mechanical properties; Particle size distribution; Specific surface area

1. Introduction

The densification of alumina-based refractory castable is governed by solid-state diffusion mechanisms. During firing, bonding develops through neck formation between adjacent particles followed by pore shrinkage, pore elimination, and grain growth. The decreasing particle size significantly increases the sintering driving force due to the corresponding increase in surface curvature and free energy [i]. Additionally, the extent of densification is strongly dependent on initial particle packing because compact particle arrangements provide shorter diffusion paths and greater particle contact area for mass transport [ii].

Particle packing theory has therefore become a fundamental tool for refractory design. According to the modified Andreasen and Dinger-Funk particle packing models, an optimized particle size distribution (PSD) minimizes interparticle voids by allowing smaller particles to occupy the spaces between larger particles. Among various PSD architectures, bimodal distributions have attracted considerable attention because they combine coarse and ultrafine particles within a single system. The coarse fraction contributes to structural packing, while the fine fraction occupies interparticle voids and accelerates sintering [iii]. Therefor castable microstructures engineered through optimized PSD exhibited lower residual porosity and significantly improved mechanical properties compared with poorly packed systems. Moreover, optimization of fine particle distribution improved flowability, reduced water demand, and enhanced densification in advanced refractory castable [iv].

Refractory castable are combinations of refractory aggregates, matrix components, bonding agents, and admixtures. The proportions of each component used vary in each castable composition to achieve the desired properties essentially required for the intended application. Reactive alumina are

widely incorporated into low-cement castable because of their fine particle size and high specific surface area. The incorporation of reactive alumina typically reduces water requirement, improves particle packing, and accelerates densification through enhanced solid-state sintering [v].

In a study conducted on 2-13% bimodal reactive alumina with d50 values of 1.6–3.1 µm and specific surface areas of 2.6–4.0 m^2/g in free flowing castable was found outperform unimodal calcined alumina in water reduction from 5.2% to 3.8% while increasing apparent density from 3.15 to 3.31 g/cm^3 [vi]. An another study showed that substituting conventional 80% calcium aluminate cement with 70% CA-270 cement and bimodal reactive alumina with D50 = 1.8 µm, specific surface area = 3.8 m^2/g lowered water demand from 7.0% to 4.8% and tripled HMOR at 1500°C from 5.8 MPa to 17.4 MPa in vibrational castable [vii].

In the present study, the influence of tailored alumina particle size distributions on the performance of low-cement alumina castable was investigated. A commercially available bimodal reactive alumina was compared with two monomodal calcined alumina exhibiting different particle size characteristics and surface properties. The study was designed to establish the relationship between particle size distribution architecture, packing efficiency, porosity evolution, sintering behaviour, and the resulting thermo-mechanical performance of the castable.

2. Materials and Methods

Alumina powder monomodal and bimodal (AM-1, AM-2, AB) were obtained from Hindalco Industries Limited. The castable formulations were prepared using commercially available white tabular alumina (WTA) aggregates of different size fractions, calcium aluminate cement, dispersing additives, calcined alumina, and bimodal reactive alumina. The coarse aggregate grading was kept constant for all formulations, while the fine alumina component was varied to evaluate the influence of bimodal particle size distribution on castable performance.

The castable batches were prepared by mixing all graded grains and fine particles in Hobart mixer with the use of castable composition given in Table 1. 4.8% water was added with castable batch and mixed for 5 to 6 minutes. After mixing the castable flow was measured as per IS 10570:2011. After measuring the flow, mixed batches were then cast into a rectangular steel mould with dimensions 160x40x40 mm and 150x25x25 mm using vibrating table. The castable samples were left in the mould for 24 hours in humid condition. The cast samples were then demolded, and air dried for 24 h. Air dried sample were loaded in the oven for drying at 110OC for 24 h. The modulus of rupture (MOR) of the cast as well as fired bars were determined using a hydraulic press and cold crushing strength (CCS) values were determined using the broken bars generated after MOR testing. The IS 10570-1983 test method was followed for both type of testing. The apparent porosities of the castables were measured from the broken pieces, after CCS testing. The dried samples were tested for CCS MOR, hot modulus of rupture (HMOR), Bulk density (BD) before and after firing for 5 h at 1100OC and 1500OC. The test method IS 10570-2011 was followed for both CCS and MOR testing.

Table 1: The Batch composition of LC95 castable

Batches No.	Unit	B-1	B-2	B-3
Raw Materials		**Wt.%**	**Wt.%**	**Wt.%**
WTA 3 - 6 mm	%	19	19	19
WTA 1 - 3 mm		16.6	16.6	16.6
WTA 0,5 - 1 mm		8.9	8.9	8.9
WTA 0.2-0.6 mm		13.6	13.6	13.6
WTA 0 - 0,2 mm		16.9	16.9	16.9
WTA – 325#		5	5	5
CA		5	5	5
AM-1		10	-	-
AM-2		-	10	-
AB		-	-	10
Cement		5	5	5
Total		100	100	100
Dispersant		0.1	0.1	0.1

3. Characterizations

The surface morphology of the samples was examined using a scanning electron microscope (SEM, Hitachi, Japan) operated at an accelerating voltage of 20 kV and a beam current of 40 mA. Phase identification was carried out using an X-ray diffractometer (PANalytical, Xpert Pro,Netherlands), with data collected over a 2θ range of 10–100° at a scan rate of 0.01° min^{-1}. Elemental composition was determined using an X-ray fluorescence (XRF) spectrometer (ZSX Primus-II, Rigaku, Japan). Particle size distribution (PSD) was determined using a Sedigraph (Micromeritics III Plus), and the specific surface area (SSA)was measured using the Brunauer – Emmett – Teller method (BET, Nova 4000eSeries).

4. Results and Discussion

The XRD patterns of the alumina powders AB-1, AB-2 anD AB are presented in Figure 1. The diffraction peaks were consistent with those of α-alumina, confirming the phase purity of the material. The characteristic peaks of alpha alumina were detected at 2Θ values 41.08° (1 0 4), 67.92° (1 1 6), 50.83° (1 1 3) 92.91° (1 1 9), 61.87° (0 2 4), 79.11°(2 1 4), 81.25° (0 3 0), 72.38° (1 2 2), 44.16° (1 1 0), 29.73° (0 1 2) and matched with ICSD (Inorganic Crystal Structure Database) card no.63648 and analysed with X'pert high score. All alumina grades exhibited diffraction peaks corresponding to α-Al_2O_3, confirming phase purity and crystallographic stability. No secondary phases were detected within the detection limits of the instrument. The major diffraction peaks corresponded to the characteristic reflections of corundum,

indicating that all aluminas possessed similar crystalline structures.

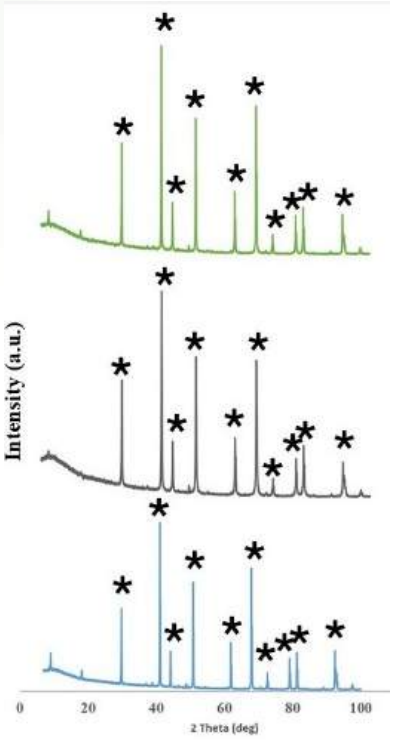


Figure 1. XRD patterns of AM-1, AM-2 and AB alumina.

The chemical compositions of the alumina powders were evaluated by XRF analysis and presented in Table-2. The results confirmed the high purity of the alumina grades used in this study containing alumina content more than 99.5%. The concentrations of SiO_2, Fe_2O_3, and CaO remained below 0.4 wt.% for all fine powders, indicating minimal impurity levels.

Table 2: elemental composition of alumina grades

Parameters	Unit	AM-1	AM-2	AB
Al_2O_3	%	99.56	99.577	99.763
SiO_2		0.01	0.011	0.045
Fe_2O_3		0.019	0.02	0.032
TiO_2		0.006	0.005	0.009
Na_2O		0.403	0.382	0.182
CaO		0.006	0.005	0.009
MgO		0.002	0.002	0.002
LOI		0.23	0.46	0.72
Moisture		0.11	0.23	0.32

Although alkali impurities can influence sintering behaviour by enhancing diffusion kinetics, the impurity levels observed in the present study are relatively low. Therefore, the differences in castable performance are expected to originate primarily from particle engineering parameters such as PSD, SSA, and packing efficiency rather than chemical composition. The high alumina purity also minimizes the possibility of liquid phase formation during firing and provides a suitable basis for evaluating the effect of particle size architecture.

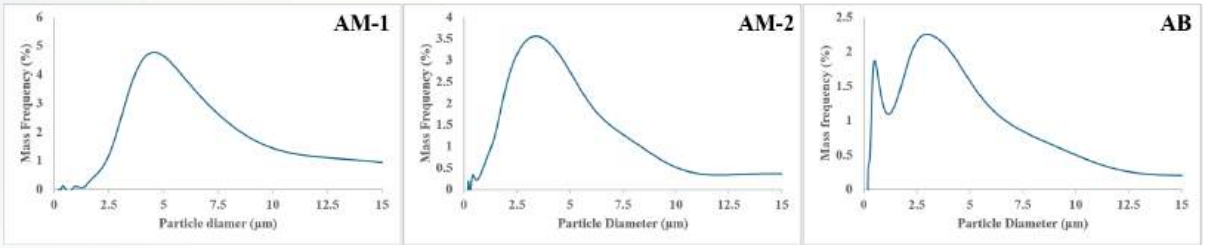


Figure 2. Particle size distribution curves of AM-1, AM-2 and AB.

The AB grade exhibited a bimodal particle-size distribution, with two distinct particle populations: ultrafine particles below 1 µm and a coarser fraction centred around 3–4 µm, whereas AM-1 and AM-2 showed monomodal distributions as presented in Figure 2. The d50 values of AM-1, AM-2 and AB were 5.03 µm, 3.21 µm, and 1.93 µm, respectively and presented in Table-2. Alumina AM-1 exhibited the coarsest and narrowest particle-size distribution, whereas AM-2 showed a finer and moderately broader distribution. AB had the lowest d10, d50, and d90 values and the highest d90/d10 ratio, indicating the finest and broadest particle-size distribution.

Table-3: The particle size distribution by Sedigraph and d90/d10 ratio of fine alumina.

Parameters	Units	AM-1	AM-2	AB
d10	µm	2.69	1.11	0.39
d50		5.03	3.21	1.93
d90		12.37	7.81	6.66
d90/d10	-	4.60	7.04	17.076
SSA	m²/g	0.79	2.31	3.64
Water Absorption	%	22.8	18	14

The specific surface area and water absorption of AM-1, AM-2 and AM alumina are presented in Table 3. The AM-1 possess the lowest SSA 0.79 m²/g and highest water absorption whereas AM-2 has 2.31 m²/g AB has 3.64 m²/g with similar water absorption. The lower SSA of AM-1 is associated with its coarse platelet-like particles, whereas the higher SSA values of AM-2 and AB arise from particle refinement and the presence of finer particle fractions. The highest SSA observed for AB confirms the existence of a substantial ultrafine component, as also evidenced by the PSD and SEM analyses. In a study, the castable with bimodal along with high surface area (~4.7m2/g) were found to generate the lower temperatures between 17.4 and 23.2 °C, whereas those with a low specific surface area (1.0 m2/g) reached higher values between 24.0 and 32.7 °C which indicates the requirement of less energy for mixing [1].

The physical properties including SSA and water absorption are presented in Table-3.

AM-1 exhibited the lowest specific surface area (SSA) of 0.79 m²/g and the highest water absorption of 22.8%. AM-2 showed a higher SSA of 2.31 m²/g and lower water absorption of 18%. AB recorded the highest SSA of 3.64 m²/g and the lowest water absorption of 14%. Overall, the results indicate distinct differences among the three alumina grades in terms of surface area and water absorption characteristics.

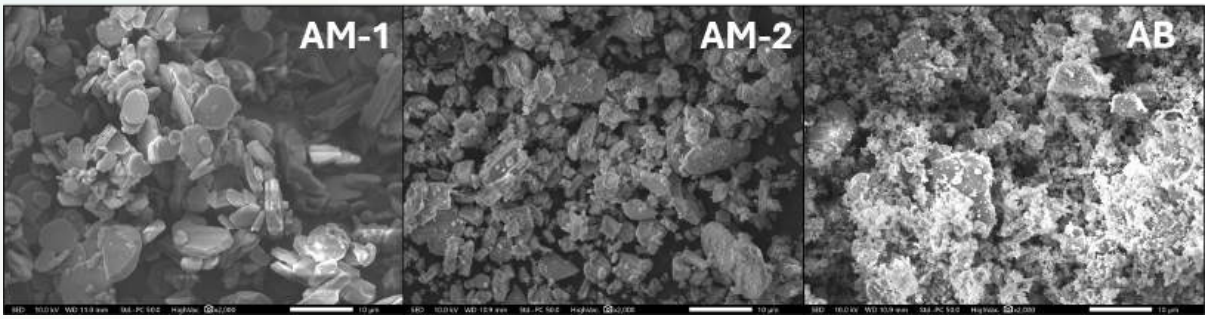


Figure 3: SEM micrographs of AM-1, AM-2 and AB alumina samples.

SEM micrographs presented in Figure 3 reveal significant differences in the morphology of the investigated alumina powders. Sample AM-1 consists predominantly of coarse, well-developed platelet-like particles with smooth surfaces and limited agglomeration, consistent with its low specific surface area (0.79 m²/g) and coarse particle size distribution. Alumina AM-2 exhibits finer angular particles with increased fragmentation and higher particle number density, resulting in a higher specific surface area (2.31 m²/g). In contrast, Alumina AB displays a highly agglomerated microstructure composed of ultrafine particles associated with larger particles, confirming the bimodal particle size distribution observed from PSD analysis.

Table 5. Physical properties of castable

Property	AM-1	AM-2	AB
Vibrational flow (%)	45	52	60
BD at 110 °C (g/cm³)	2.94	3	3.02
BD at 1500 °C (g/cm³)	3.05	3.08	3.11
AP at 1500 °C (%)	17	14.2	11.7

The rheological properties of the castables were strongly influenced by the particle size distribution and morphology of the alumina matrix powders. AM-1 exhibited the lowest vibrational flow (45%) due to its coarse platelet-like particle morphology and water demand. In contrast, AM-2 and AB achieved significantly higher flow values of 52% and 60%, respectively. The bulk density and apparent porosity values are presented in Table 5. AM-1 exhibited the lowest bulk density at both 110 °C (2.94 g/cm³) and 1500 °C (3.05 g/cm³), along with the highest apparent porosity of 17%. AM-2 showed intermediate bulk density values of 3.00 and 3.08 g/cm³ at 110 °C and 1500 °C, respectively, with an apparent porosity of 14.2%. AB achieved the highest bulk density at both temperatures, reaching 3.02 g/cm³ at 110 °C and 3.11 g/cm³ at 1500 °C, while exhibiting the lowest apparent porosity of 11.7%. These results indicate that AB developed a denser and more compact microstructure after firing compared with AM-1 and AM-2.

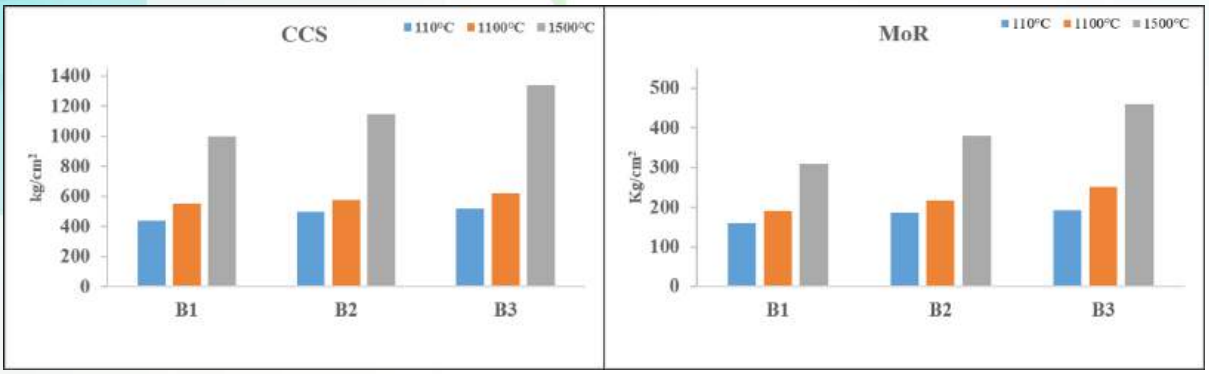


Figure 3: CCS and MOR of castable prepared with AM-1, AM-2, and AB alumina.

The cold crushing strength values of castable batches with all three-alumina AB-1, AB-2 and AB are presented in Figure 3. The strength increased progressively from B1 to B3 at all testing temperatures. At 110°C, CCS increased from 440.2 kg/cm² for B1 to 500.1 kg/cm² for B2 and 516.7 kg/cm² for B3. At 1100°C, the corresponding values increased to 550.4, 575.2, and 618.4 kg/cm², respectively. A substantial improvement was observed after firing at 1500°C, with CCS reaching 1000.7 kg/cm² for B1, 1150.4 kg/cm² for B2, and 1342.7 kg/cm² for B3. Overall, B3 exhibited the highest CCS at all temperatures, indicating superior strength development, particularly after firing at 1500°C.

As presented in Figure 3, the modulus of rupture (MOR) increased progressively from B1 to B3 at all temperatures. At 110°C, the MOR increased from 160.2 kg/cm² for B1 to 187.1 kg/cm² for B2 and 192.4 kg/cm² for B3. At 1100°C, the corresponding values increased to 190.1, 215.8, and 250.0 kg/cm², respectively. After firing at 1500°C, a substantial improvement was observed, with MOR values reaching 310.0 kg/cm² for B1, 380.9 kg/cm² for B2, and 460.2 kg/cm² for B3. Overall, B3 exhibited the highest MOR at all temperatures, indicating superior flexural-strength development, particularly after firing at 1500°C.

The hot modulus of rupture (HMOR) increased progressively from AM-1 to AB. AM-1 exhibited the lowest HMOR of 23.15 kg/cm², followed by AM-2 at 28.02 kg/cm², while AB achieved the highest value of 31.68 kg/cm². Compared with AM-1, the HMOR improved by approximately 21% for AM-2 and 37% for AB. The higher HMOR of AB indicates superior flexural strength and load-bearing capability at the testing temperature. The highest HMOR was obtained for AB, which possessed a bimodal particle size distribution and the highest specific surface area. The presence of ultrafine particles improved packing efficiency and promoted the formation of a dense ceramic bond network during firing. The resulting reduction in porosity and increase in particle contact area enhanced load transfer capability and resistance to crack propagation under high-temperature conditions. These results indicate that the bimodal alumina system provides superior hot mechanical properties through improved densification and microstructural optimization.

5. Conclusions

The bimodal AB alumina exhibited the most favourable particle-size architecture and resulted in superior rheological, physical, and thermo-mechanical properties in the low-cement alumina castable. The AB-containing formulation achieved a vibrational flow of 60%, compared with 47% and 52% for the monomodal formulations. It also exhibited the highest bulk density, increasing from 3.02 g/cm³ at 110°C to 3.11 g/cm³ after firing at 1500°C, whereas the corresponding fired bulk density of the monomodal formulation was 3.05 g/cm³. This improved densification was accompanied by an increase in cold crushing strength from 1000.7 to 1342.7 kg/cm² and

modulus of rupture from approximately 550 to 618 kg/cm². The hot modulus of rupture reached 31.68 kg/cm² for the AB-containing castable, compared with 28.02 kg/cm² for the better-performing monomodal formulation. The greatest strength enhancement was observed after firing at 1500°C. These results suggest that the combined effects of optimized bimodal particle packing, void filling by ultrafine particles, and enhanced sintering activity promoted the formation of a denser and mechanically stronger castable matrix.

6. References

[1]Dangqiang Wang, Xinzhi Wang, Chongjun Xu, Zhengyi Fu, and Jinyong Zhang, Densification mechanism of the ultra-fast sintering dense alumina, AIP Advances 10, 025223 (2020); doi: 10.1063/1.5119030.

[2]Azar, M., Palmero, P., Lombardi, M., Garnier, V., Montanaro, L., Fantozzi, G., Chevalier, J, Effect of initial particle packing on the sintering of nanostructured transition alumina, Journal of the European Ceramic Society, 28 (2008) 1121-1128. DOI: 10.1016/j.jeurceramsoc.2007.10.003.

[3]Abílio P. Silva, Ana M. Segadães, Deesy G. Pinto, Luiz A. Oliveira, Tessaleno C. Devezas, Effect of particle size distribution and calcium aluminate cement on the rheological behaviour of all-alumina refractory castables, Powder Technology 226 (2012) 107–113.

[4]M. Schnabel, A. Buhr, J. Dutton, Rheology of High-Performance Alumina and Spinel Castables, refractories WORLDFORUM 4 (2012) [2].

[5]M. A. Trubitsyn, N. A. Volovicheva,L. B. Furda,1 V. I. Kuzin, and R. V. Zubashchenko, research in the area of preparing activated alumina. Part 1. Methods for preparing reactive alumina, Refractories and Industrial Ceramics, Vol. 63, No. 2, July, 2022. DOI 10.1007/s11148-022-00694-w.

[6]Christian Dünzen, China's Refractories, doi:10.19691/j.cnki.1004-4493.2021.03.002.

[7]Florian Holleyn, Tim Waldstädt, Johannes Kasper, Christian Dannert and Olaf Krause, Effects of Changing the Specific Surface Area in the Ceramic Matrix of CAC-Containing Refractory Castables on the Rheology and Processing, High-Temperature Materials 2025, 2, 10022. doi.org/10.70322/htm.2025.10022.

REDUCING FIRING FUEL COSTS AND IMPROVING QUALITY OF CONTINUOUS CASTING NOZZLES BY UTILIZING RESIN REACTIONS

Keisuke Kachi, SigeruMorimoto, Noriaki Yamauchi

TYK Corporation

1. Introduction

Continuous casting nozzles, such as long nozzles, immersion nozzles, and long stoppers, used in continuous casting processes, are basically formed by CIP (Cold Isostatic Pressing).
Due to their high bulk density and compactness, CIP molded bodies require a much more careful debinding process than friction molded bodies, which are sometimes used without firing.If this debinding process is not done properly, it can lead to internal defects after firing. The higher the bulk density of the material, the higher the risk of this occurring, but if the bulk density is reduced, the strength of the nozzle itself will decrease, which is likely to cause operational problems at the steel mill.These factors make high-speed debinding of nozzles difficult. The longer the debinding process, the higher the firing time and fuel cost per nozzle, leading to increased costs.
This study investigates a binder technology that enables rapid debinding of high bulk density nozzles while suppressing internal defects.

2. Experimental methods

Table 1 shows the chemical composition of the materials used in this verification test. Based on this chemical composition, samples using binder S were assigned to (A), (B), and (C), while samples using binder T were assigned to (D), (E), and (F).
Each sample was then subjected to CIP molding and adjusted to change physical properties such as bulk density.The samples were cylindrical, with a diameter of 50 mm and a height of 100 mm. These samples were placed in a container, filled with powder, and then heated in a reducing atmosphere (Figure 1). The weight loss at each temperature was calculated from the measured sample mass.
Table 2 shows the bulk density, modulus of rupture of samples (A), (B), and (C) after complete debinding.
Table 3 shows the bulk density, modulus of rupture of samples (D), (E), and (F) after complete debinding.Positive correlations were observed between bulk density, modulus of rupture for each sample.

		(A)	(B)	(C)	(D)	(E)	(F)
Chemical composition (%)	C	15					
	ZrO2	85					
Binder		S			T		

Table1 Composition of each sample

Sample name	Bulk density (-)	Modulus of rupture (MPa)
(A)	α	β
(B)	α−0.05	β−1.4
(C)	α−0.11	β−2.8

Table 2 Physical properties of each sample using Binder S

Sample name	Bulk density(-)	Modulus of rupture(MPa)
(D)	δ	ε
(E)	δ−0.04	ε−1.2
(F)	δ−0.10	ε−3.1

Table 3 Physical properties of each sample using Binder T

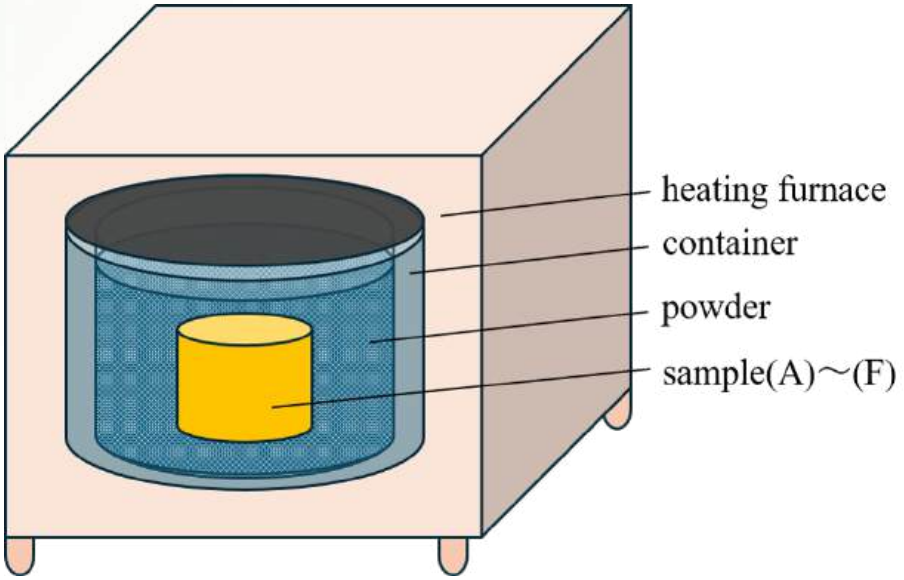


Figure 1 Schematic illustration of the heating test.

3 Test results

3.1 Temperature and Weight Loss Rate

Figure 2 shows a graph illustrating the relationship between weight percentage and the results at various temperatures.
Sample (A), which had the highest bulk density, showed the slowest weight loss up to X°C compared to the other two samples. However, a rapid weight change was observed in the temperature range of X to Y°C. This weight change is thought to be due to the thermal decomposition of the binder resin contained in the sample, which generated and released gas.

Since the rapid release of this gas from the sample is thought to increase the likelihood of intrinsic defects, it can be estimated that samples with high bulk density have a higher risk of internal defect formation during debinding (especially in the temperature range of X to Y°C).
Regarding the reason why sample (A), with its high bulk density, showed a small weight change up to X°C, it is possible that the decrease in porosity amount in the sample with increasing bulk density also plays a role. Samples before the binder resin decomposes have low porosity especially.

3.2 Changes Due to Binder Type Change

Next, the same tests as in 3.1 were performed on samples (D), (E), and (F) prepared using binder T.

Similar to the cases of (A), (B), and (C) above, a positive correlation was observed between the bulk density, modulus of rupture of each

sample.
However, Figure 3, which shows the relationship between temperature and weight loss rate for each of (D), (E), and (F), exhibited significantly different behavior compared to Figure 2.Sample (D), which had the highest density among those using binder T, showed the most rapid weight loss up to X°C. This is the opposite result to that obtained with binder S.

Furthermore, between X and Y°C, while the weight change of sample (D) was the most rapid compared to (E) and (F), the difference was not as significant as that observed with (A), (B), and (C) which used binder S.
This is thought to be due to the release of a large amount of binder components from sample (D) in the temperature range up to X°C.

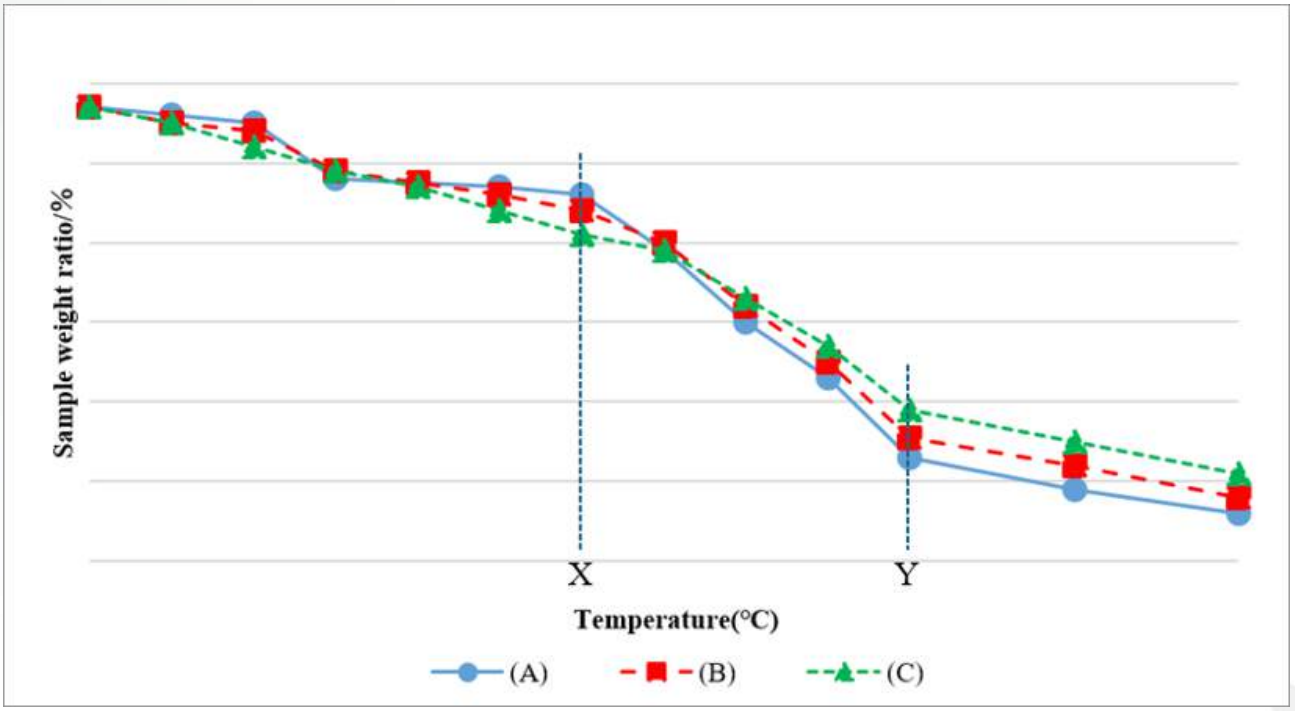


Figure 2. Weight loss rate of each sample (A), (B), and (C) with respect to heating temperature.

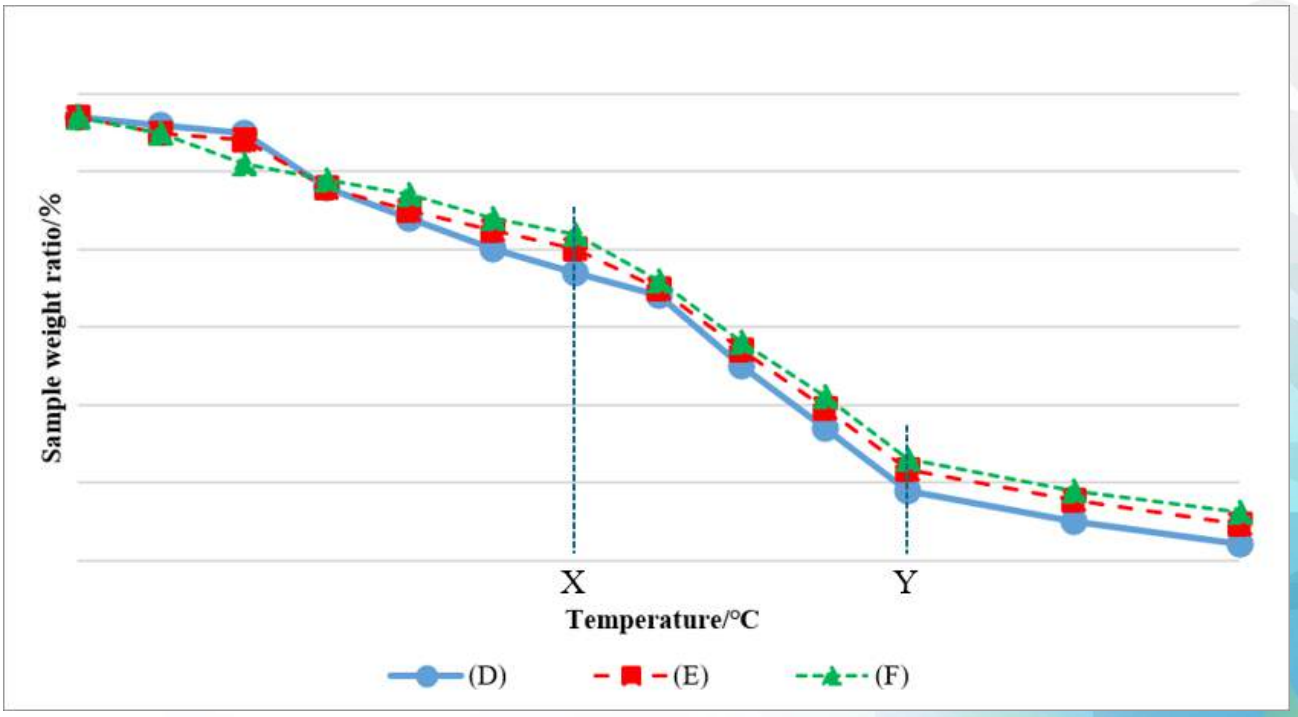


Figure 3. Weight loss rate of each sample (D), (E), and (F) with respect to heating temperature.

3.3 Weight Loss Behavior Depending on Binder Type

It was found that changing the binder type significantly altered the weight loss (gas release) behavior of the sample when changing from low bulk density to high bulk density. To consider this mechanism, we measured the pore size distribution of each sample.As the bulk density increased, the pore volume decreased over the entire pore size range.

In binder T, although the overall pore size decreased, it was confirmed that the pore size actually increased slightly in the range with the smallest pore diameter.

Regarding the reason for the high pore size despite the high bulk density of sample (D), verification in 3-2 confirmed that a large amount of binder components in (D) were released before reaching X°C.

Therefore, it is thought that these pores were generated by the volatilization of low-molecular-weight components in the binder.

As a result, samples with high bulk density have a higher risk of internal defects due to rapid gas release in the thermal decomposition temperature range of the binder resin (X to Y°C). However, in the case of samples with binder T applied, pores increased at a temperature lower than the thermal decomposition initiation temperature due to the volatilization of some binder components. This is thought to allow for efficient gas release and suppression of rapid gas release.

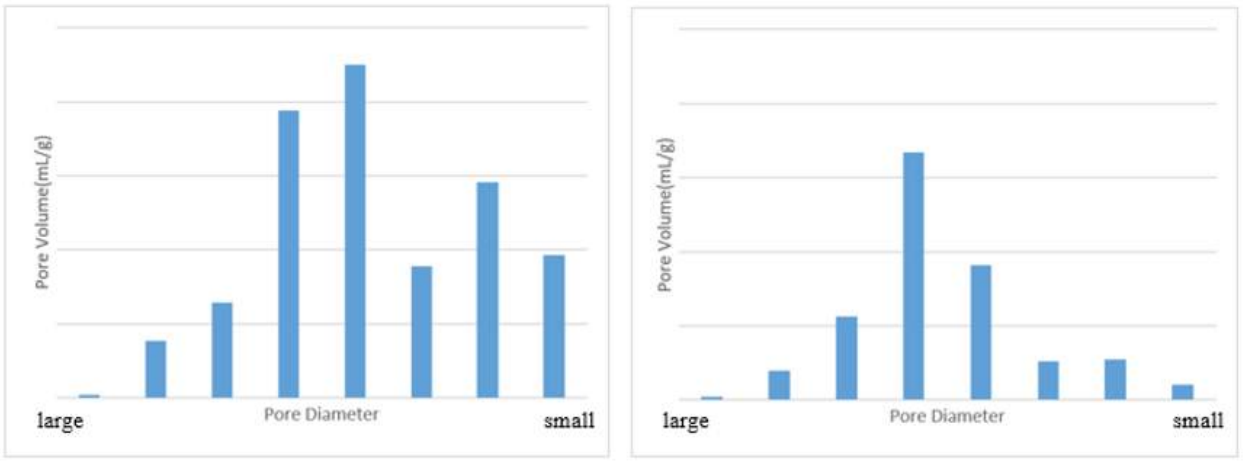


Figure 4. Pore size distribution of samples (A) and (C) after X°C treatment.

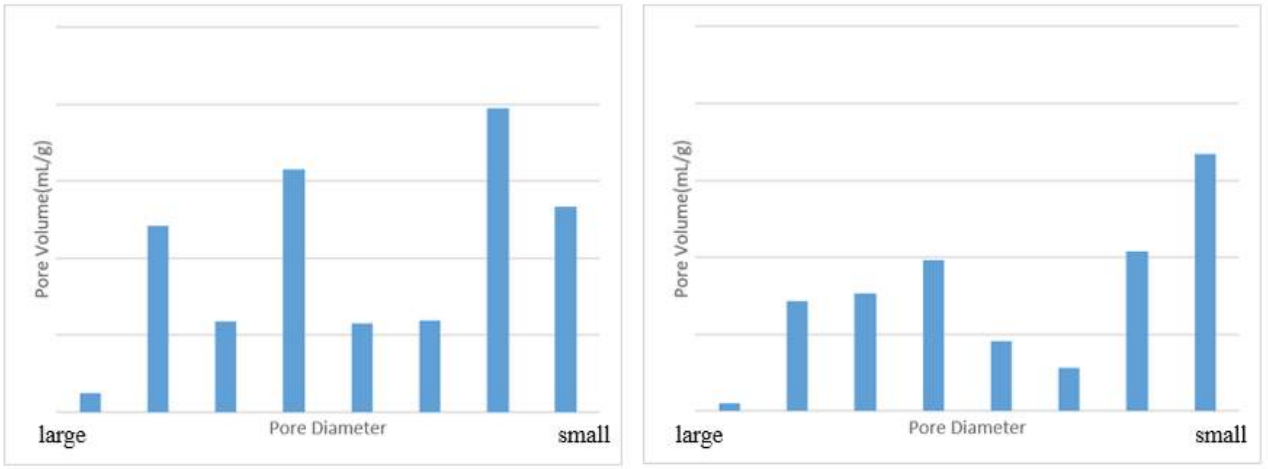


Figure 5. Pore size distribution of samples (D) and (F) after X°C treatment.

4. Conclusions

In this study, we prepared samples under different conditions using the same formulation but varying the binder and density, and measured the weight change during debinding. The following findings were obtained:

- In the heating test of samples based on binder S, while the weight loss up to X°C decreased as the bulk density increased, a rapid weight loss was observed in the X–Y°C temperature range where thermal decomposition of the resin begins. This suggests that increasing the bulk density of the sample increases the risk of internal defects during debinding.
- However, in the heating test of samples based on binder T, samples with higher bulk density also showed a greater weight loss up to X°C. In this case, it is thought that the generation of many small pores in the sample allows for efficient gas release from the binder even in the thermal decomposition temperature range of the resin, thereby reducing the risk of internal defects.

The developed binder technology enables rapid firing of high-density nozzles while minimizing the risk of internal defects, thereby reducing firing time, fuel consumption, and production costs.

DEVELOPMENT OF ECO-FRIENDLY TAP HOLE CLAY FOR BLAST FURNACE

Tuhin Patranabish, Saumen Sinha

Calderys India Refractories Limited

Abstract

The development of eco-friendly tap hole clay is driven by the environment health & safety (EHS) aspect without compromising operational performance. Conventional coal-based binders contain very high levels of polycyclic aromatic hydrocarbons (PAHs), with concentrations reaching ~36,000 ppm. Long-term use of 10–15% of these binders in tap hole clay poses potential human health risks, as highlighted by studies. As per REACH regulation, PAH concentration in tap hole clay must be below 50 ppm. To meet this requirement, unique EHS compliant binder was developed as an alternative to coal-based binder. The total PAH contribution from the binder system in the formulation is less than 50 ppm. The EHS binder was tested and validated in a renowned European laboratory for PAH content and toxicity compliance. The physical properties of EHS binder-based tap hole clay were evaluated and found to be comparable to conventional tar–pitch–resin bonded clay, with no adverse impact on plasticity, extrusion behavior, strength, or oxidation resistance. The developed product was subsequently tested in an Indian blast furnace with a hot metal production capacity of 8500 Ton Per Day (TPD). Field performance indicated satisfactory tap hole length, drill ability, and corrosion resistance, comparable to conventional grades, while ensuring compliance with environmental and safety norms. The study demonstrates that eco-friendly tap hole clay with PAH <50 ppm is a technically viable and sustainable alternative for blast furnace operations, addressing both regulatory and occupational health concerns without sacrificing performance.

Keywords: Tap hole clay, Blast furnace, Eco-friendly binder, PAH reduction, REACH compliance

Introduction

The blast furnace is a counter-current gas-solid reactor in which solid raw materials are charged from the top, while hot air enriched with oxygen is injected from the bottom through the tuyeres. To enhance reactions in the lower zone, steam and pulverized coal are injected, creating a high-temperature raceway zone. The hearth serves as a collection point for molten metal and slag, which are periodically tapped. Among blast furnace operations, cast house activities are the most labor-intensive, requiring efficient practices to maintain optimal drainage rates and ensure the hearth remains dry.

Current Blast Furnaces, featuring bell-less top charging systems, are more productive. Frequent tapping operation requires significant manpower for frequent plugging, quick cast house preparation, drilling operation etc. While drilling machine assists in opening taphole, further optimizing the process is essential. The remaining time is allocated for cast house preparation, ladle placement, and mud gun filling before the tap hole opens. For high slag rates and increased furnace productivity, efficient drainage is crucial[1]. Challenges such as plugging with optimum pressure, achieving required Tap Hole Length (THL), good drill ability means with minimized red balls and minimized spitting after opening to ensure smooth casting for better Cast Duration (CD). Conventional coal-based binder system has been working for decades in Tap Hole Clay (THC) technology. This binder system meets all the required performance parameters. But the EHS aspect is the main shortcoming of conventional coal-based binders. The objective of EHS binder-based THC is to overcome this challenge without sacrificing the performance parameters. Here we plan to develop the EHS binder as an alternative to

coal based binder. The existing resin is already meeting the EHS value and performing well in combination with the coal-based binder in a certain ratio. In this paper, the development of EHS binder will be discussed. And the properties of Eco-Friendly THC will also be discussed in comparison with conventional THC. A comparison of field performance is also presented in the second part of the paper.

Experimental Results and Discussion

A literature study[2] shows that PAH values of coal tar are more than 36000 ppm. Coal Tar Pitch is the residue of coal tar. Hence, coal tar pitch contains a PAH similar to coal tar. Coal Tar and Coal Tar Pitch along with resin, when used in certain ratio, provide good plasticity to the THC. This system is widely used in THC. As an alternative binder system, the EHS binder along with the resin in same ratio did not give the same plasticity to the THC. The ratio of EHS binder and resin was adjusted by taking several laboratory trials to achieve similar plasticity. This technical aspect is essential for maintaining safe performance at the site, while the environmental and health aspects were assessed through evaluation of the PAH concentration in the EHS binder. The concentration of 16 PAH compounds in the EHS binder was evaluated with a European laboratory. The distillation and viscosity of EHS binder was evaluated in comparison with the coal-based binder. PAH concentrations of several samples were evaluated during the development of the EHS binder. The most promising candidates are presented in Table 1.

Table 1: Total PAH concentration of the most promising EHS binder reported by European lab

Type	EHS binder
PAH (Sum of 16 ingredients as selected by EPA)	37.23

Using this binder at 10–15% of the formulation would maintain the PAH content below 20 ppm, thereby meeting the 50 ppm limit for the final product.

Laboratory evaluation of the physical properties showed that the EHS binder can provide similar properties to the THC mixture those obtained with the coal-based binder to the THC. Coal based binder is considered conventional THC.

The empirical formulations using EHS binder, in comparison with conventional THC are presented in Table 2.

Table 2: Empirical formulation of Conventional THC and Eco Friendly THC

Formulation	Conventional THC	Eco Friendly THC
THC mix	85	85
Coal based binder	b	-
EHS binder	-	a
Resin	c	e

The product mixes were initially prepared in the laboratory and after lab evaluation the product mixes were prepared in the plant mixer for production trial. The main advantage during production of Eco-Friendly THC was that there was no emission of odour like Conventional THC. Concentration of the EHS binder system (a+e) was less than that of the Coal-based binder system (b+c). Figure 1 shows the extrusion pressure with respect to the various temperatures of Conventional THC and Eco-Friendly THC.

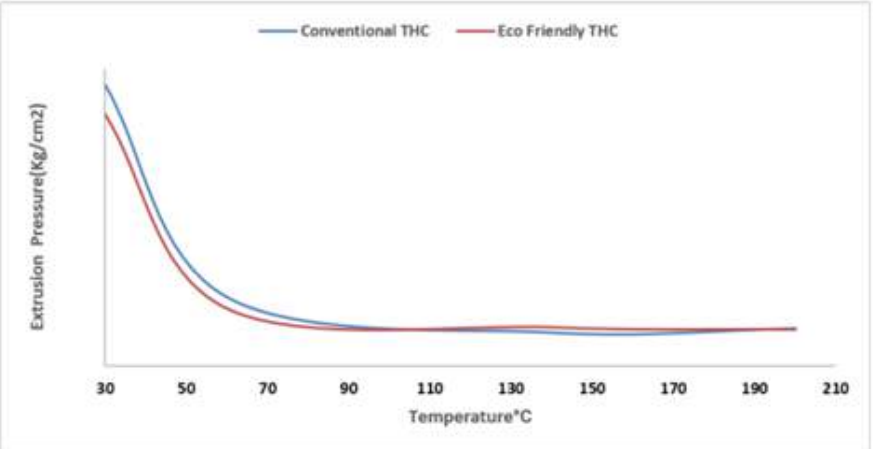


Figure 1: Extrusion Pressure with respect to the temperature

This indicates that the plugging behavior of the two THC mixes was comparable. The physical properties and mechanical strength were also evaluated for both mixes.

Figure 2 illustrates the comparison among the green bulk density (GBD), coked bulk density (CBD) after coking at 1300°C for 3 hours and apparent porosity (AP)% after coking at 1300°C for 3 hours of both the mixes. The bulk density and apparent porosity values are comparable.

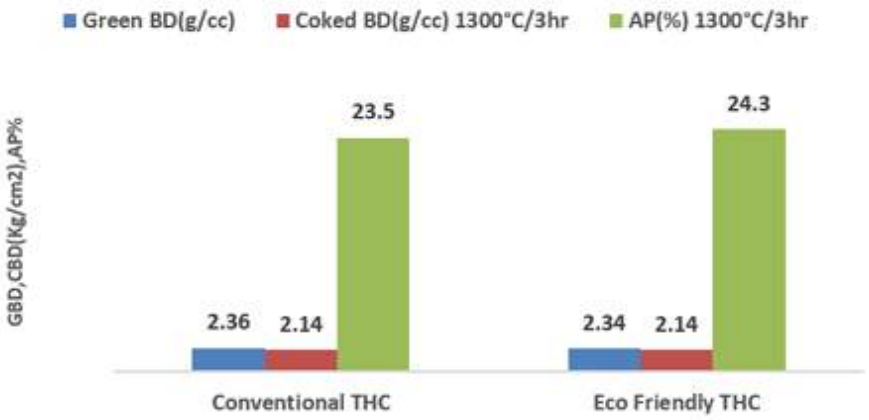


Figure 2: GBD (g/cc), CBD (g/cc) and AP% of THC-coal based binder-Resin vs THC-EHS (Liquid +Pitch)-Resin mixes

Figure 3 illustrates the mechanical strength after coking at 1300°C for 3 hours for both mixes, and the values were found to be in a similar range. The EHS tar-to-resin ratio was adjusted so that the cold crushing strength after coking of the THC-EHS (tar+pitch)-resin mix was comparable to that of the THC-coal based binder-resin mix.

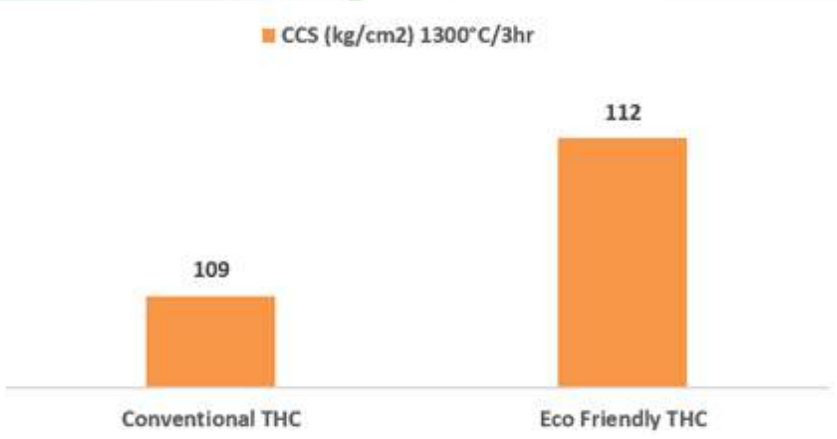


Figure 3 Cold Crushing Strength after coking at 1300°C for 3 hrs

Figure 4 illustrates comparative microscopic photographs under polarized light. The matrix distribution was similar in both cases, and the grain–matrix integrity was comparable. Cracks were not prominent in either formulation.

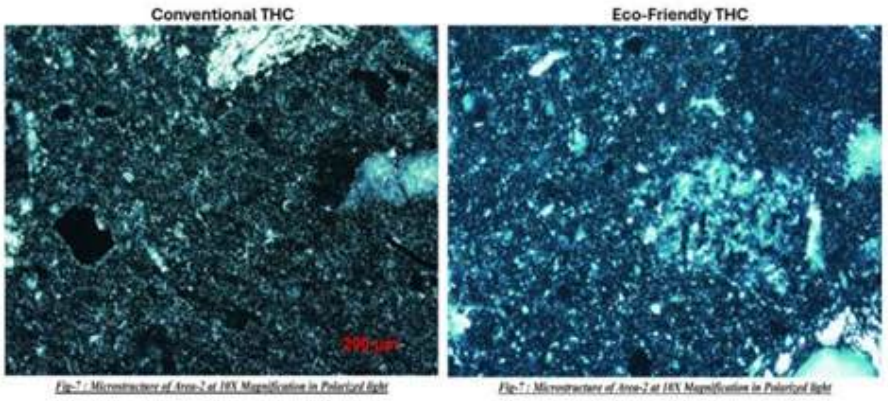


Figure 4: Microscopic photograph

Figure 5 shows the results of a crack-formation test conducted at a faster heating rate up to 800°C for both formulations. Similar surface crack formation was observed for both formulations.



Figure 5: Crack formation test of Conventional THC vs Eco Friendly THC

Figure 6 shows the finger test corrosion of Conventional THC vs Eco-Friendly THC. This test was done in an induction furnace with cast iron and blast furnace slag in 70:30 ratio. The temperature rose to 1550°C during the test.



Figure 6: Finger Test Corrosion of Conventional THC vs Eco Friendly THC

The percentage of corrosion was measured after the test for both the formulations in terms of the reduction of the radius. The corrosion % of Conventional THC and Eco-Friendly THC were 15.5% and 15.8% respectively. This indicates that the corrosion of Eco-Friendly THC should behave in a similar way to Conventional THC.

Field Trial

The site performance results from the 8500 TPD blast furnace are presented in Table 3

Table 3

Performance	Conventional THC	Eco Friendly THC
Plugging Pressure (bar)	190-230	190-230
Tap hole length (m)	4.3-4.5	4.2-4.6
Cast duration (min)	125–150	123–155
Drill bit requirement (nos)	1-2	1-2
Red Balls	Less Intensity	Less Intensity
Spitting Time(min)	3-5	3-5

Plugging pressure was maintained using an appropriate cooling arrangement based on the temperature of the clay inside the barrel and nozzle immediately before plugging for both binder systems.

THL was slightly higher with the Eco Friendly THC, than that of Conventional THC.

The CD was also marginally higher with the Eco Friendly THC than that of Conventional THC. The higher the THL, the higher the CD is.

Drillability was evaluated based on the number of drill bits used to open the tap hole. This was similar to both types of clay.

The intensity of red balls during the opening was very low. Initially rotation of drill bar was used to reach 4.0 m inside the tap hole, and hammering was started afterwards to open the tap hole.

Conclusion

The development of an Eco-Friendly tap hole clay using EHS binder as an alternative to the Conventional coal-based binder system was successfully demonstrated. The developed binder system reduced the PAH content of the tap hole clay to below 50 ppm, thereby addressing the environmental, health, and safety concerns associated with conventional coal based binders. Laboratory evaluation showed that Eco Friendly THC exhibited comparable plasticity, extrusion behavior, bulk density, apparent porosity, cold crushing strength, and crack formation characteristics to the Conventional THC formulation. Microscopic examination further indicated similar matrix distribution and grain–matrix integrity, with no prominent difference in crack formation between the two formulations. The finger-test corrosion results showed comparable corrosion resistance, with corrosion values of 15.5% for the Conventional THC and 15.8% for the Eco Friendly THC. Field trials conducted in an 8500 TPD blast furnace demonstrated comparable plugging pressure, tap-hole length, drillability, spitting behavior, and red ball intensity, and cast duration. Overall, the results demonstrate that the developed Eco-Friendly THC is a technically viable and environmentally safer alternative to Conventional THC providing comparable operational performance while significantly reducing PAH-related environmental and occupational health concerns.

REFERENCE

1) Tuhin Patranabish, Saumen Sinha, Subrata Jana, Prabhakar, Souvik Palui, “Development of Tap Hole Clay for Mini Blast Furnace roducing Foundry Grade Iron” Calderys India Refractories Limited

2) Barbara Mahler, Michael D. Woodside, Peter C. Van Metre “Coal-tar-based pavement sealcoat— Potential concerns for human health and aquatic life” USGS number series, publication year 2016

IMPACT OF MINOR MATRIX CONSTITUENTS ON THE LONG-TERM STABILITY OF SILICA BRICKS IN GLASS TANK FURNACE

Raghunath Sharma[*1], Dileep Kumar C J[1], Ragubans Chaturvedi[1], Srilekha Hanumanthu[1], Divyalakshmi C[2], Shivani S[2]

[1]Saint-Gobain Innovation Hub India, IIT Madras Research Park, Chennai, India

[2]Saint-Gobain Glass India Private Limited, World Glass Complex, Sriperumbudur, India

*Corresponding author: raghunathsharma.mvss@saint-gobain.com

Abstract

Silica bricks are essential structural components of glass tank furnaces because of their excellent high-temperature creep resistance and corrosion products that closely match glass chemistry. Although silica bricks from different suppliers often satisfy standard requirements including chemical composition, crystalline phase content, refractoriness under load, creep resistance and corrosion resistance, notable differences in service performance are observed. This study compares two silica brick grades from geographically separated suppliers. Both met qualification criteria yet exhibited premature degradation during operation likely related to creep and corrosion. Bricks exposed to furnace atmospheres showed reduced refractoriness underload relative to virgin material, suggesting low-temperature matrix liquefaction. Chemical analysis identified minor oxides, particularly BaO and TiO_2. Microstructural examination after alkali vapor exposure revealed enrichment of fluxing species within the matrix. FactSage thermodynamic calculations were performed to evaluate phase evolution and fluxing effects. Results indicated significant liquid formation near 1000°C, complete matrix vitrification above 1400°C and softening.

Keywords: Silica Refractories, Thermodynamic Modelling, Slag Viscosity, Flux Factor

1. Introduction

Silica refractories have been extensively used in the crowns and superstructures of glass tank furnaces because of their exceptional refractoriness under load, high-temperature creep resistance, and chemical compatibility with molten glass environments[1]. The long-term performance of silica refractories is typically evaluated through standardized properties such as chemical composition, bulk density, apparent porosity, phase analysis, refractoriness under load (RUL), creep resistance, and corrosion resistance. However, industrial experience has shown that silica bricks meeting the desired specification often exhibit markedly different campaign lives in service. Silica refractories are manufactured from naturally occurring quartzite deposits whose impurity profiles depend strongly on local geology. Consequently, minor oxides present in the raw materials may vary significantly between suppliers[2]. Although these constituents are generally present in small amounts, they can have a disproportionate influence on phase evolution, liquid formation, and high-temperature deformation behavior. The effect becomes particularly important in glass furnaces where refractories are continuously exposed to alkali-bearing vapors originating from volatilization of batch materials and molten glass constituents. Alkali penetration into silica refractories promotes reactions within the matrix, resulting in the formation of low-melting silicate phases and an increase in the glassy phase fraction[3]. Flux factor (defined as $2 \times (Na_2O + K_2O)$, wt.% : Al_2O_3) is a key compositional parameter governing alkali corrosion, creep deformation, and consequently the campaign life of silica

crown refractories. While previous studies have qualitatively explained these effects using binary phase diagrams and experimental correlations, the influence of minor oxides and their combined effect on phase evolution in the actual multicomponent refractory matrix remains insufficiently understood[4].

In the present work, two commercially available silica brick grades obtained from geographically distinct sources were investigated. Although both products satisfied conventional quality requirements, premature degradation was observed during furnace service. Post-mortem characterization revealed enrichment of alkali species within the matrix together with the presence of minor constituents including BaO and TiO_2. To understand the role of these oxides in refractory performance, thermodynamic calculations were performed using FactSage to evaluate phase evolution, liquid formation, and melt viscosity as a function of temperature. The study demonstrates that seemingly insignificant variations in impurity chemistry can substantially influence matrix vitrification behavior and, ultimately, the service life of silica refractories in glass tank furnaces.

2. Materials and Methods

Silica bricks procured from two geographically distinct regions were investigated in the present study and designated as Brick A and Brick B. The chemical compositions of the as-received bricks were determined by X-ray fluorescence (XRF) using the fusion bead method with Omnian calibration. Phase characterization was carried out using a PANalyticalX'Pert Pro X-ray diffractometer, calibrated using a silicon standard, with the as-received bricks crushed and ground into fine powders before mounting onto sample holders to ensure a flat surface for X-ray incidence. Diffraction patterns were collected over a 2θ range of 5-90° with a step size of 0.013° using Cu Kα radiation ($K\alpha_1$ = 1.54060 Å, $K\alpha_2$ = 1.54443 Å) at an operating condition of 45 kV and 40 mA. Phase identification was performed using HighScore Plus software in conjunction with the ICSD and ICDD PDF-5+ databases. Apparent porosity and bulk density were measured in accordance with ASTM C20, while cold crushing strength (CCS) was determined following IS 1528 (Part 4). The refractoriness under load (RUL) was evaluated using an RUL 421 apparatus in accordance with ISO 1893. Cylindrical specimens measuring 50 mm in diameter and height with a 12.5 mm coaxial bore were subjected to constant compressive stress (0.2 MPa) during heating up to 1680°C, and the RUL value was reported based on the T0.5 criterion (0.5% deformation). In addition to the two as-received bricks, a service-exposed silica brick was also tested to assess the degradation in high-temperature load-bearing performance after industrial exposure. Vapor corrosion experiments were carried out using glass placed in a platinum crucible, over which the refractory specimen was positioned in an inverted configuration and sealed using refractory cement to ensure a gas-tight assembly and promote interaction between the generated vapors and the refractory surface. The entire setup was subsequently heated at 1500°C and maintained for 96 h, after which the samples were cooled and prepared for microstructural analysis. The corroded specimens were sectioned, mounted, polished, and gold-coated for examination using a Quanta FEG scanning electron microscope. Field-emission SEM imaging and energy-dispersive spectroscopy (EDS) were performed at an accelerating voltage of 20 kV, and compositional analyses were acquired from both grain and matrix regions. The EDS-derived compositions were subsequently used as inputs for thermodynamic simulations in FactSage 8.4 version, where equilibrium phase calculations were performed using the Equilib module as a function of temperature to evaluate phase stability, slag formation, phase evolution, and liquid fraction development. FACTPS and FTOxide database were used for the same. Furthermore, the FactSage viscosity module was employed to calculate the temperature-dependent viscosity of the generated liquid phases, thereby assessing the influence of minor oxide constituents on melt fluidity and the corrosion behaviour of the silica refractories.

3. Results and Discussion:

Table 1 summarizes the chemical and physical properties of the investigated silica bricks. Sample B contained 96.55 wt.% SiO_2, while Sample A contained 95.76 wt.% SiO_2. Sample A exhibited slightly higher contents of CaO (2.84 wt.% vs. 2.52 wt.%), Na_2O (0.119 wt.% vs. 0.080 wt.%), K_2O (0.128 wt.% vs. 0.087 wt.%), Al_2O_3 (0.464 wt.% vs. 0.375 wt.%), and Fe_2O_3 (0.384 wt.% vs. 0.220 wt.%). A notable difference was the presence of BaO (0.03 wt.%) in Sample B and TiO_2 (0.031 wt.%) and SO_3 (0.153 wt.%) in Sample A. The apparent porosity was 20.41% and 21.34%, bulk density was 1.83 and 1.80 g/cm³, and CCS was 30.66 and 33 MPa for Samples B and A, respectively. All measured properties were within the typical specification range for silica refractories used in high-temperature glass-tank applications

Sample Name		B	A
Chemical Composition/mass %	SiO_2	96.55	95.758
	CaO	2.52	2.84
	Na_2O	0.08	0.119
	MgO	0.084	0.106
	Al_2O_3	0.375	0.464
	P_2O_5	0.036	0.013
	K_2O	0.087	0.128
	Fe_2O_3	0.220	0.384
	ZrO_2	-	-
	BaO	0.030	-
	SO_3	-	0.153
	TiO_2	-	0.031
Physical properties	Apparent Porosity (%)	20.41	21.34
	Bulk Density (g/cc)	1.83	1.80
	CCS (MPa)	30. 66	33

Table 1: Physical and Chemical Properties of Silica bricks obtained from two geographically different regions

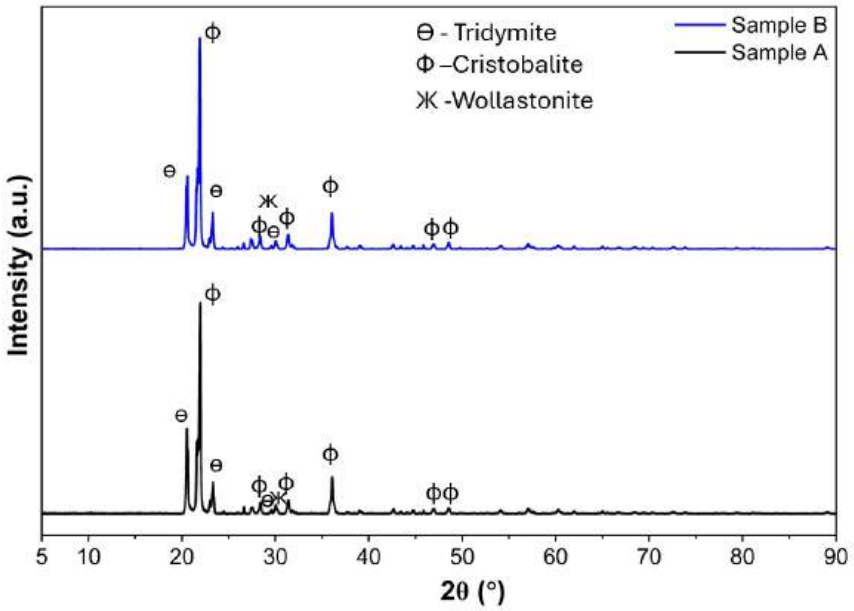


Fig 1: XRD of silica bicks

Figure 2 shows the XRD patterns of silica bricks A and B. Both samples are predominantly composed of cristobalite and tridymite. The diffraction profiles are largely similar. Also, minor wollastonite phase was also detected in both bricks. Figure 3 compares the refractoriness under load of Samples A, B, and the service-exposed silica brick. Both virgin bricks exhibited similar deformation behaviour, with the T0.5 values exceeding the test limit of 1680°C, indicating excellent high-temperature load-bearing capability. In contrast, the corroded sample exhibited a T0.5 below 1650°C, demonstrating a significant reduction in refractoriness after service exposure. The deterioration in RUL performance is attributed to corrosion-induced enrichment of fluxing oxides within the matrix, leading to an increased flux factor, enhanced liquid-phase formation, and consequent softening of the silica framework under load at elevated temperatures.

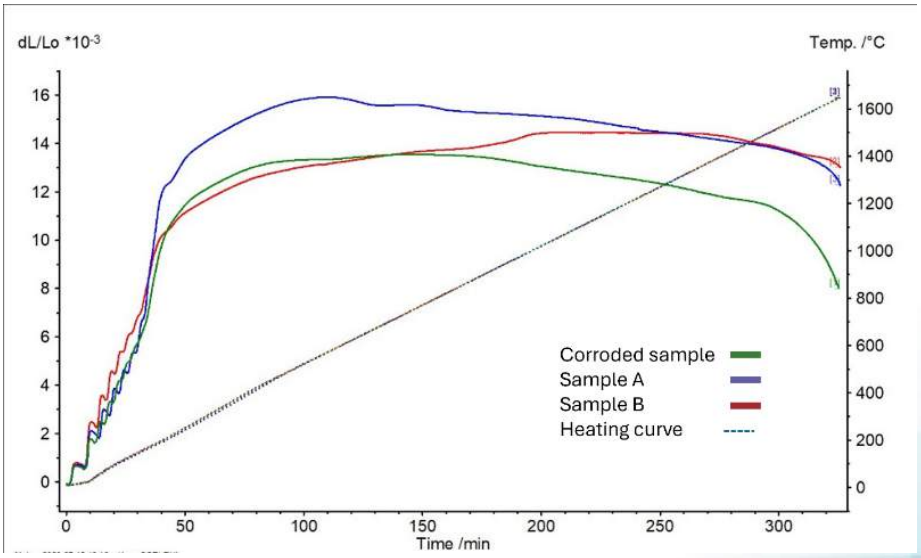
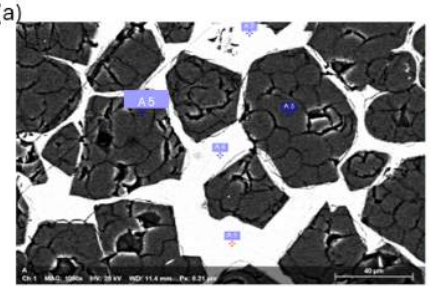


Fig 3 : RUL of the silica bricks including the corroded sample (shown in green)

SEM micrographs (Fig. 4) revealed that both the silica bricks consisted of coarse silica grains embedded within an intergranular matrix. EDS analysis confirmed that the grains were predominantly composed of SiO_2 (>97 wt.%), while the matrix regions were

enriched in CaO, Al_2O_3, MgO, Fe_2O_3, and alkali oxides. Sample A exhibited matrix compositions containing approximately 30 wt.% CaO and 4 wt.% Al_2O_3, whereas Sample B showed slightly higher concentrations of CaO (32-37 wt.%) and Na_2O (4-6 wt.%). Although bulk XRF analysis indicated relatively low alkali contents in both refractories, localized EDS measurements after vapor corrosion revealed significant alkali enrichment within the matrix phase. This preferential accumulation of alkalis in the intergranular regions increases the flux factor and promotes the formation of low-melting liquid phases, while the silica grains largely retained their high purity. Such variations in matrix chemistry are expected to strongly influence liquid-phase generation, high-temperature stability, and corrosion resistance.

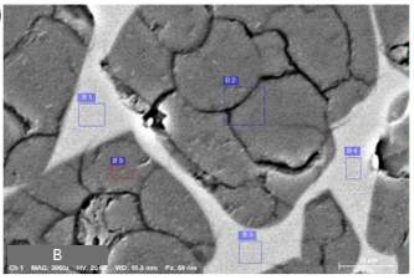
(a)



(b)

Region	P	Na2O	MgO	Al2O3	SiO2	K2O	CaO	TiO2	Fe2O3	SO3
A 1	0.02	3.51	1.36	4.1	57.79	0.96	30.1	0.53	1.58	0.04
A 2	0.01	3.5	1.25	4.29	58.07	0.97	29.67	0.62	1.59	0.02
A 3	0.02	0.01	0.04	0.5	99.23	0.01	0.04	0.05	0.01	0.09
A 4	0	3.8	1.33	4.21	57.13	1.1	30.38	0.45	1.6	0
A 5	0.02	0.09	0	0.53	99.1	0.04	0.08	0.03	0.03	0.09

(c)



(d)

Region	P	SiO2	BaO	Na2O	MgO	K2O	CaO	Al2O3	Fe2O3	SO3
B 1	0.61	51.89	0.38	5.63	0.54	1.23	35.87	1.12	2.27	0.47
B 2	0.43	99.18	0	0.12	0	0	0.1	0.09	0.07	0
B 3	0.58	51.05	0.27	5.42	0.53	1.24	36.93	1.07	2.46	0.44
B 4	0.61	57.7	0.22	4.41	0.41	0.86	31.95	0.99	2.31	0.55
B 5	0.86	97.7	0.04	0.11	0.01	0	0.09	0.41	0	0.78

Fig.4 : SEM and EDS of samples subjected to vapor corrosion

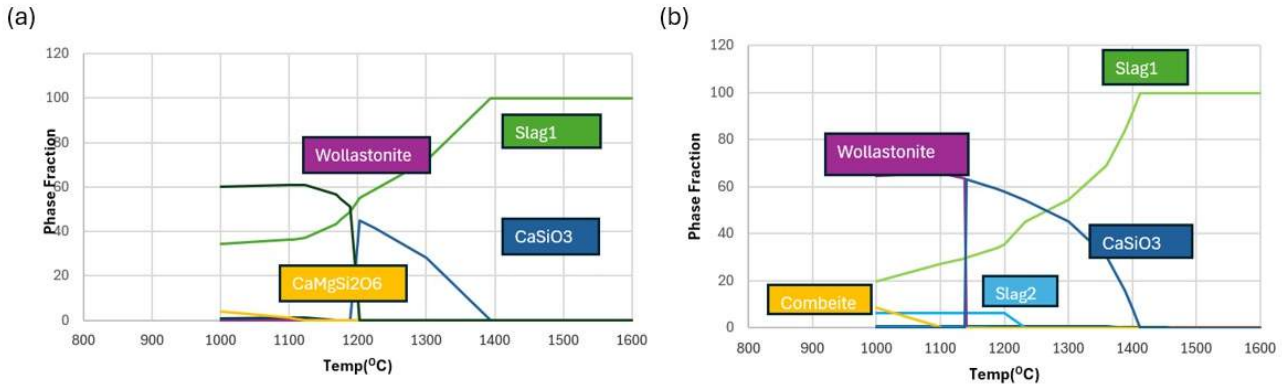


Fig. 5: Factsage simulations showing the phase evolution and associated viscosity

Matrix – Sample A		Matrix – Sample B	
Temperature (in C)	Viscosity (in Poise)	Temperature (in C)	Viscosity (in Poise)
1200	2266.12	1200	97.418
1400	36.95	1400	10.81
1600	9.25	1600	3.075

Table 2:Viscosity as a function of temperature in the matrix region

FactSage simulations indicated distinct liquid-phase evolution behavior for the two matrix compositions. The TiO_2-containing matrix (Sample A) initiated liquid formation at relatively lower temperatures and achieved nearly 100% slag fraction by approximately 1380°C, whereas the BaO-containing matrix (Sample B) required temperatures exceeding

1400°C for complete liquid formation. Despite the earlier and more extensive liquid generation in Sample A, the calculated slag viscosity remained substantially higher, decreasing from 2266 Poise at 1200°C to 9.25 Poise at 1600°C. In contrast, Sample B produced lower-viscosity melts, with viscosities decreasing from 97.4 Poise to 3.1 Poise over the same temperature range. These results suggest that while the TiO_2-containing composition promotes earlier liquid formation, the resulting slag is comparatively more viscous, whereas the BaO-containing composition generates a more fluid melt once formed, potentially enhancing penetration and transport through the refractory matrix.

4. Conclusions

Both silica bricks exhibited chemical, physical, and thermo-mechanical properties within the typical specification range for silica refractories used in high-temperature applications. While the virgin bricks maintained T0.5 values beyond 1680°C, the service-exposed brick showed a marked reduction in RUL (T0.5 < 1650°C), indicating degradation during service. SEM-EDS analysis revealed localized enrichment of alkali species within the matrix following exposure. FactSage simulations showed progressive liquid-phase formation with increasing temperature. The TiO_2-containing composition achieved nearly 100 % slag formation at a lower temperature (~1380°C), whereas the BaO-containing composition required temperatures above 1400°C. However, the former generated significantly more viscous slags, while the latter produced lower-viscosity melts that may facilitate easier liquid transport through the refractory matrix. Overall, the results highlight the critical role of matrix chemistry, especially the minor oxide constituents in governing liquid-phase evolution, viscosity, and the long-term performance of silica refractories under corrosive environments.

References

[1] K. E. S. Mark D. Allendorf, "Thermodynamic Analysis of Slica Refractory Corrosion in Glass- Melting Furnaces," *Journal Of The Electochemical Society*, p. 148 B59, 2001.

[2] P. Sengupta, "Manufacturing and Poperties of Refractories. In: Refractories for the Chemical Industries. Springer, Cham.," *Springer*, pp. 43-84, 2020.

[3] D. Sarkar, Ceramic Processing : Industrial Practices, CRC Press, 2019.

[4] T. K. T. T. Atsuhisa Segawa, "Evaluation of Alkali- Induced Corrosion and Creep Properties of Silica Bricks for Melter Crown in Glass Furnace at Elevated Temperature," *Journal of The Technial Association Of Refractories*, *Japan*, vol. 44, no. 4, pp. 206-211, 2024.

GREEN TAP HOLE CLAY: SUSTAINABLE STEPS TOWARDS CLEANER SOLUTIONS AND CHALLENGES

Paladugu Srinivasa Rao[1], Thierry Joly[2], Rupesh Choudhury[3]

[1] Vesuvius Refractory India Private Limited, Vishakhapatnam, Andhra Pradesh, India.
[2] Vesuvius Europe, avenue de l'Europe, 69150 Décines, France
[3] Vesuvius India Limited, Vishakhapatnam, Andhra Pradesh, India

*Mail: Paladugu.Srinivasarao@vesuvius.com

Abstract

The blast furnace route remains the dominant technology for primary ironmaking; however, it is associated with significant greenhouse gas and hazardous pollutant emissions. Taphole clay (THC), a critical refractory material exposed to severe thermal and chemical conditions, traditionally relies on pitch and resin-based binders that release phenol, formaldehyde, and polycyclic aromatic hydrocarbons (PAHs) during injection, curing, and carbonization. This study presents the development of a next-generation PAH free binder system that replaces conventional binders while maintaining rheological performance, curing behavior, carbon yield, and high-temperature structural integrity. The novel technology eliminates phenolic and PAH-generating constituents while preserving plasticity, extrusion stability, and adhesion to the taphole channel. Thermogravimetric analysis coupled with evolved gas analysis confirmed the absence of hazardous volatile organic emissions during thermal decomposition. Industrial trials in European and North American blast furnaces demonstrated stable extrusion, reliable taphole control, reduced smoke generation, and comparable campaign life, validating a sustainable and immediately deployable solution for cleaner ironmaking operations.

Keywords: Iron making, blast furnace, taphole clay, eco-friendly binder, sustainability

1. Introduction

India is the world's second-largest steel producer and continues to expand its ironmaking capacity though the route of blast furnace to meet growing infrastructure, automotive, and manufacturing demands. The blast furnace remains an important industrial route to produce primary iron. The process operates under highly reducing and chemically aggressive conditions, with temperatures exceeding 1,500°C in the hearth area. Refractory materials used in critical regions must therefore withstand simultaneous exposure to high temperature, molten iron, slag, process gases, mechanical stresses, and chemical attack.

Taphole clay (THC) is a crucial consumable in blast furnace operations. It is injected after each cast to seal the taphole and must withstand at extreme temperatures, molten iron and slag attack, thermal shock, mechanical stresses. The design of taphole clay consists of high-quality refractory aggregates, additives, and liquid binder. However, the development of THC is precisely tailored for each blast furnace with respect to the operational parameters. The performance of taphole clay is one of the critical factors in the smooth running of the blast furnace. Therefore, the taphole clay designed for a particular blast furnace must provide good injectability, efficient taphole sealing, virtuous drillability with no cracks and high corrosion resistance. Traditionally, THC formulations utilize coal tar pitch, phenolic resins, and hydrocarbon-based binders to provide adequate plasticity, green strength, and carbon bonding. However, these conventional binder systems release hazardous emissions such as Phenol, Formaldehyde, Benzene derivatives, Polycyclic aromatic hydrocarbons (PAHs), and volatile organic compounds (VOCs) during high-temperature operation.

The increasing focus on occupational health, environmental compliance, stringent environmental norms, and sustainability necessitates the development of greener alternatives. While significant efforts have been directed towards reducing carbon emissions through energyFigure 1 PAH components in coal tar. efficient operations, raw material optimization, and alternative reducing agents, comparatively less attention has been paid to emissions originating from consumable refractory materials.

The new generation binder technology was developed with the following targets to eliminate phenolic compounds, PAH generating constituents by maintaining similar extrusion characteristics, carbon yield and similar high-temperature properties. It should ensure the same compatibility with existing Mud-guns to enable immediate industrial implementation. The binder is not only a simply liquid to mix or coat the aggregates, but it also plays an important role starting from mixing and storage for proper injection & curing after ageing and high temperature performance. The main poly aromatic hydrocarbons (PAH) are listed in Figure-1 below. As per the EHS regulations few PAH are very harmful and cause severe illness.

Sr No	16 PAH	Number of Rings	Category	Specific limit (mg/kg)	Coal Tar based
1	Naphthalene	2	C	10,000	1502
2	Acenaphthylene	3			32
3	Acenaphthene	3			1550
4	Fluorene	3			1072
5	Phenanthrene	3	C	10,000	3487
6	Anthracene	3	C	10,000	1037
7	Fluoranthene	4			2990
8	Pyrene	4			1868
9	Benz(a)anthracene	4	C	1,000	1032
10	Chrysene	4	CM	1,000	1022
11	Benzo(b)fluoranthene	5	C	1,000	1522
12	Benzo(k)fluoranthene	5	C	1,000	
13	Benzo(a)pyrene	5	CMR	100	856
14	Indeno(123cd)pyrene	6	C	10,000	522
15	Dibenzo(ah)anthracene	5	C	100	171
16	Benzo(ghi)perylene	6			459

Figure 1 PAH components in coal tar.

2. Binder Selection

Vesuvius has been working on the environmentally friendly taphole clays from last few years all over the globe to deliver cleaner and greener solutions to meet the sustainable goals of the customer as well as improve the taphole clay usage environment so that it provides better environment to cast house crew (Ref# Table-1, shown the list of customers using green Taphole clay in America as well European region). The green binder system was designed according to the below four principals. The binder selection was done at Vesuvius Europe Research center by considering all the key parameters.

Table-1: Customer reference using green binder in America & Europe.

Customer	Plant	BF no:	Working volume (m3):
SSAB Tunnplåt AB	Luleå	3	2540
ArcelorMittal	HamiltonDofasco	4	1609
ArcelorMittal	HamiltonDofasco	2	1062
Cleveland Cliffs Burns Harbor	Burns harbour (In)	C	2645
Cleveland Cliffs Burns Harbor	Burns harbour (In)	D	2600
LEW Stelco	Lake Erie Steel -Nanticoke	1	2418

2.1 Hazard reduction

The formulation excludes conventional binder coal tar and PAHrich pitch and avoids binder components capable of generating significant phenol or formaldehyde emissions during curing. Claims such as "PAH-free" must be linked to specified compounds, test conditions, analytical methods, and detection limits

.

2.2 Rheological stability

THC is a Visco-plastic material, its behavior may be described using the Herschel–Bulkley relationship:

$$\tau = \tau 0 + K\dot{\gamma}^{n}$$

where $\tau$is shear stress, $\tau 0$is yield stress, $K$is the consistency coefficient, $\dot{\gamma}$is shear rate, and n is the flow index. The binder must provide sufficient lubrication to reduce particle & wall friction while maintaining stability after extrusion. Stable pressure development is preferable to either excessively high peak pressure or abrupt pressure fluctuations, which can indicate non-uniform binder distribution then further creates internal cracking, or pocket formation in the taphole pipe. For that greener binder system was developed and commercially implemented in Americas and European regions.

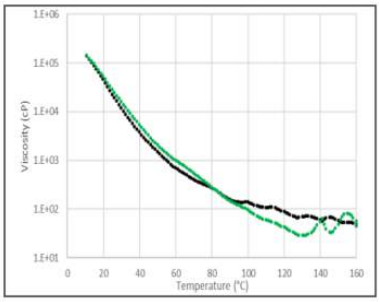


Figure 2a: Comparison in Viscosity of Tar (reference) &

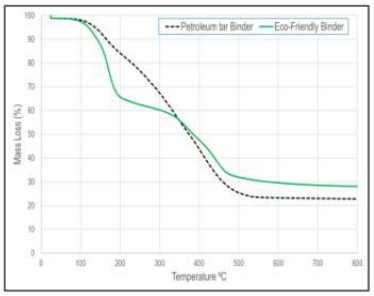


Figure 2b: TGA comparison of Tar & Green Binder.

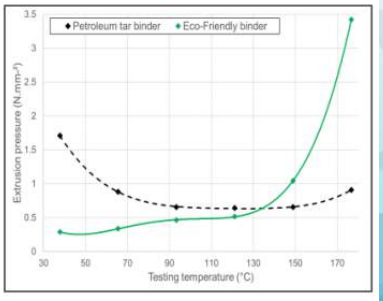


Figure 2c: Comparison of Extrusion properties of Tar &

The viscosity measurements were conducted using Anton Paar rheometer with temperature range of 10 to 160˚C by using rheoplus/32 software.

2.3 Controlled curing property

The binder must remain stable during storage to inject mud-guns easily, however at the same time it should be cured rapidly after entering the hot taphole. During further heating, it must form a continuous carbonaceous bond and followed by ceramic-carbon bond.

2.4 High-temperature functional equivalence

The green taphole clay formulation must achieve performance equivalent to the conventional tar-based THC mixes with the properties of carbonized strength, apparent porosity, corrosion & erosion resistance, thermal shock behavior and taphole adhesion. With these properties the clay behaves very similarly like regular mix while plugging, drilling and during the casting process with very good mushroom integrity.

3. Experimental Procedure

In the present investigation, two experimental taphole clay formulations, designated as Blue and Green, were developed with different binder systems and evaluated against a conventional tar binder system. All compositions were prepared using a Hobart mixer under controlled mixing conditions. The formulations contained a common refractory matrix consisting primarily of bauxite-based aggregates, silicon carbide, clay, and other functional additives, while the binder composition & constituents were varied to assess its influence on processing and high-temperature performance. The extrusion characteristics of the prepared taphole clay formulations were evaluated using a Marshall extrusion tester. Test specimens were prepared with a diameter and height of 50 mm were prepared using a sand rammer. The temperature-dependent behavior of the specimens was subsequently investigated over the temperature range of 200 -1450 °C. Following thermal treatment, the cold crushing strength (CCS) of the specimens was determined using a universal testing machine (UTM). In addition, the corrosion resistance of the different taphole clay formulations was evaluated using an induction furnace corrosion test to assess their resistance under simulated high-temperature service conditions.

Results & Discussions

3.2 Curing Properties of THC mixes:

The development of strength during curing at 200 °C, as presented in Figure 3, indicates that all mixes show progressive strength development with increasing heat-treatment duration. Although the initial curing behavior was broadly comparable among the formulations, distinct differences in CCS became evident with extended thermal treatment of 80 minutes. At 90 -120 min of heat treatment, the blue formulations exhibited CCS values in the range of approximately 8 - 14 MPa, whereas the green formulations developed higher strength, with values ranging from approximately 10-20 MPa. In comparison, the conventional tarbased formulation exhibited considerably lower CCS values of approximately 2-4 MPa under the corresponding curing conditions.

The higher early-stage strength observed for the blue and green formulations indicates more effective development of the binder

refractory network during the curing stage. This behavior is particularly relevant to taphole clay applications because adequate cured strength is required to maintain the integrity of the injected material during the transition from ambient conditions to the high-temperature environment of the blast furnace.

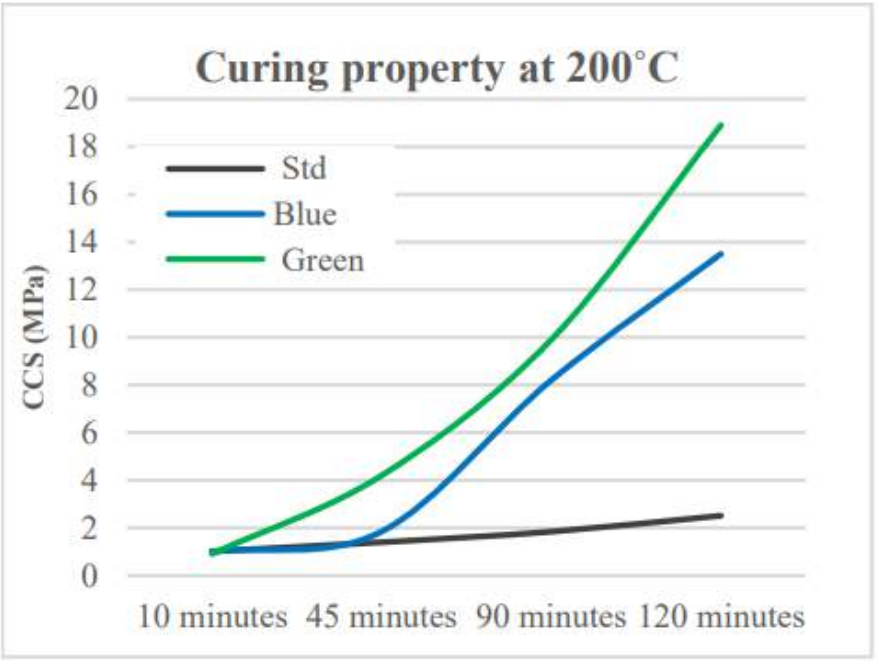
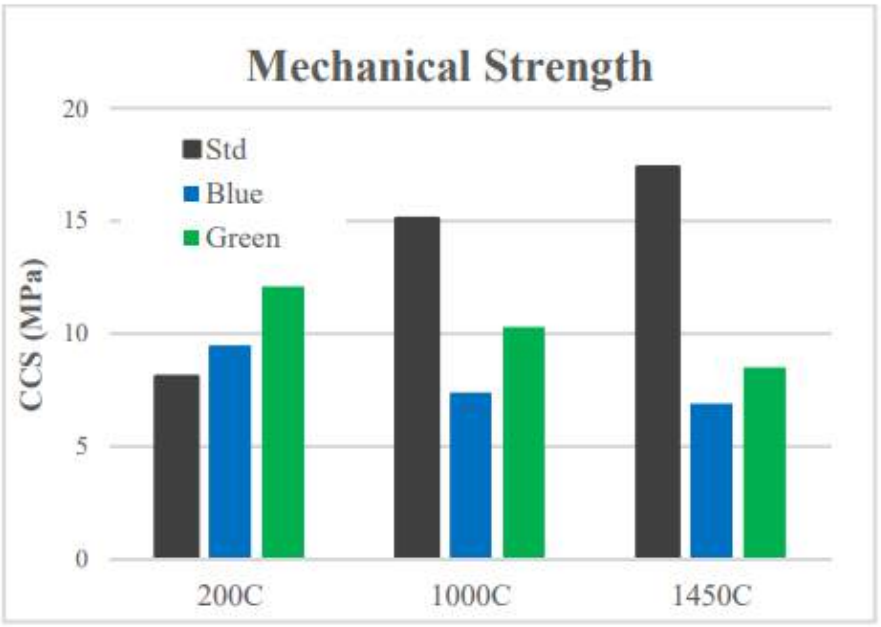


Figure 3: Comparison of strength development of different blue, green THC mixes.

3.3 Mechanical behaviour of the samples:

The variation in CCS as a function of heat-treatment temperature is presented in Figure 3a. at different temperatures like 200, 1000, and 1450 °C. The CCS values remained within relatively narrow ranges of approximately 8 -12 MPa for high temperatures like 1000C & 1450C. A pronounced increase in strength was observed after treatment at 200°C relative to the conventional THC formulation, which exhibited a CCS of approximately 14 -16 MPa for the formulations of blue and green. This is peculiar property of green binder systems which will improve the degassing effect of taphole clay during the applications.



3.4 Corrosion properties of newly developed THC mixes

The corrosion resistance of the taphole clay formulations containing the different binder systems was evaluated using an induction-furnace test, as illustrated in Figure 4(a). Prior to the corrosion experiment, the specimens were heat-treated at 1000 °C for 3 h to establish a representative preconditioned microstructure.

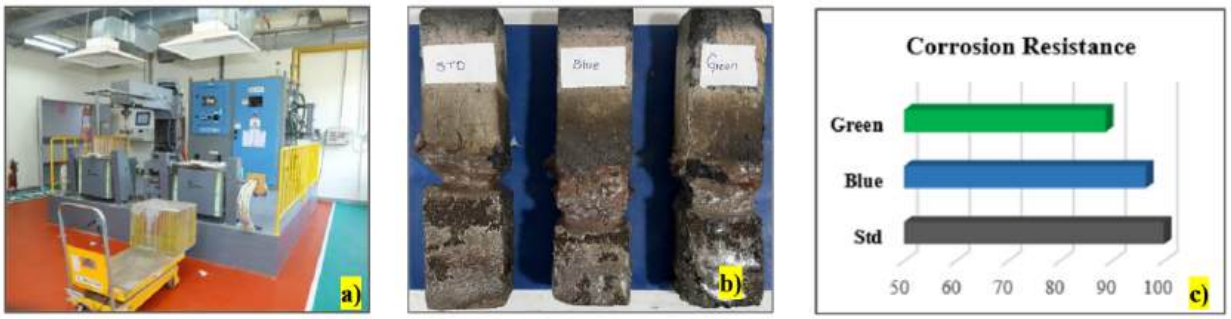


Figure 4: a) Photograph of the Induction furnace, b) Physical appearance of the tested samples, c) Corrosion index profile.

The physical appearance of the specimens following the induction-furnace test is shown in Figure 4(b). The extent of material degradation and the corresponding corrosion depth were evaluated from the post-test specimens. A corrosion index was subsequently calculated for each THC mix based on the measured depth of corrosion, with the conventional mix as a baseline for comparison. As shown in Figure 4(c), the formulations incorporating the newly developed binder systems exhibited lower corrosion indices than the conventional mix, indicating improved resistance to corrosion under the test conditions. Enhanced corrosion resistance is expected to contribute to improved taphole integrity and potentially support longer and more stable casting durations during blast-furnace operation. To perform the slag-corrosion test, slag was collected from one of large blast furnace and the slag chemistry as per table-2 and maintained the very similar conditions like the molten iron temperature of range from 1480 – 1520˚C and samples were on continuous rotation for 45 minutes. The improved performance may be related to differences in binder-derived matrix formation and the resulting high-temperature microstructure; these aspects to be further examined through the phase and microstructural characterization.

Table-2: Slag chemistry

Chemistry	%
SiO_2	36.49
CaO	32.45
Al_2O_3	19.60
MgO	7.18
FeO	0.53
MnO	0.60
TiO_2	0.87
K_2O	0.56
SO_3	1.37
Na_2O	0.33

4. Conclusions

The development of a PAH free binder system for blast furnace taphole clay represents a significant advancement in sustainable ironmaking technology. The green binder reduces Phenol, Formaldehyde, and PAH-generating constituents while maintaining the rheological, thermal, and operational performance required for modern blast furnace operations. Laboratory characterization and industrial-scale trials have demonstrated functional equivalence to conventional THC systems with substantially reduced smoke and hazardous emissions. For Indian blast furnaces, where environmental compliance, worker safety, and sustainable manufacturing are becoming strategic priorities, green taphole clay offers an immediately deployable solution requiring no major process modifications. Its adoption can help steel producers improve environmental performance, enhance occupational health conditions, and support India's transition toward cleaner and more sustainable steelmaking. A green THC will not independently convert conventional blast-furnace steel into green-rated steel because the mass of clay consumed is small relative to iron production. Nevertheless, its adoption is strategically important because it can reduce hazardous emissions (phenol, aldehydes, aromatic vapors, and PAHs) improve cast-house air quality, lower smoke and odor near Mudgun operations. Green THC is primarily a low emission, occupational-health, and sustainable consumables intervention, rather than a major direct blast-furnace CO_2 abatement technology.

References

1. Thierry Joly, Roger Isenbarger, Stephen Draper: Proceedings, UNITECR 2023, End of petroleum tar binder, new generation of taphole clay. Formaldehyde and PAH free technology.
2. Joly, T and all, “Next generation of taphole clay, formaldehyde and PAH free technology”. ICR 2022.

A NEXT-GENERATION SPINEL AGGREGATE FOR SUPERIOR REFRACTORY PERFORMANCE

Ramkrishna Halder, Dr. Aniruddha Samanta, Kanhaiya Lal Bajaj

Indiano Chrome Pvt Ltd, Pune, Maharashtra, 411013, India

Corresponding author's e-mail: hlo2ram@gmail.com

Abstract

Genzee spinel aggregate represents a significant advancement in refractory materials, developed to overcome the limitations of conventional systems through an optimized relatively less alkali composition and engineered microstructure. The elimination of alkali impurities, combined with negligible silica content (ideally ~0.5%), enhances chemical stability and long-term durability. A dense microstructure is achieved via a modified fusion process, producing a refractory-grade spinel–corundum composite in which chromium oxide (Cr_2O_3), free from hexavalent chromium, is incorporated in solid solution within the matrix. This structural design improves corrosion resistance, maintains chemical neutrality, and significantly enhances spalling resistance compared to conventional bauxite- and fused alumina-based aggregates.

To evaluate its functional performance, spinel aggregates were incorporated into low-cement castables (LCC) and compared with spinel-free compositions. Samples were prepared by vibro-casting, cured for 24 h, dried at 110 °C, and fired at 1200 °C, and 1500 °C. Characterization included bulk density, permanent linear change, cold crushing strength, modulus of rupture, thermal shock resistance, and phase evolution.

The results demonstrate that spinel-containing castables exhibit superior high-temperature strength, enhanced thermal shock resistance, and improved structural stability, confirming their suitability for advanced refractory applications.

Keywords: Spinel aggregate, Castables, Thermal shock resistance, High-temperature strength.

1. Introduction

Refractory materials are indispensable in high-temperature industrial operations including the steel, cement, non-ferrous metallurgy, and glass industries. In recent years, the demand for advanced refractory systems with enhanced thermal shock resistance, corrosion resistance, and structural stability has increased substantially due to increasingly aggressive operating environments and longer campaign requirements [1].

Conventional refractory aggregates based on fused alumina and calcined bauxite may exhibit limitations under severe service conditions, including thermal spalling, chemical degradation, and progressive structural deterioration. In particular, alkali impurities and silica-rich secondary phases commonly associated with bauxite-based raw materials can adversely influence refractoriness, slag resistance, and long-term performance [2]. These limitations have encouraged the development of high-purity engineered refractory aggregates with controlled phase composition and reduced levels of deleterious impurities.

Among advanced refractory materials, magnesium aluminate spinel ($MgAl_2O_4$) has attracted considerable attention because of its excellent thermo-mechanical and chemical stability at elevated temperatures [3,4]. Spinel-based refractory aggregates exhibit high refractoriness, good resistance to slag penetration and corrosion, favorable thermal expansion characteristics, and enhanced thermal shock resistance [3,5,6].

Consequently, spinel-containing refractory systems have found increasing application in demanding high-temperature environments, particularly where resistance to thermal cycling and aggressive slags is required [7].

The present work introduces Genzee spinel aggregate, a next-generation refractory aggregate developed through a modified fusion process designed to achieve ultra-low alkali content and an engineered microstructure [4]. The optimized chemistry and phase composition are intended to minimize deleterious secondary phases while improving structural integrity under thermal cycling and corrosive environments.

The objective of this study is to investigate the influence of Genzee spinel aggregate on the performance of low-cement castables and to compare its behavior with that of conventional spinel-free castable systems. Particular emphasis is placed on evaluating physical, thermo-mechanical, and corrosion-resistant properties to determine the suitability of the developed aggregate for advanced refractory applications.

2. Experimental Procedure

2.1 Raw Materials

The Genzee spinel aggregate (Spincor) used in the present study was manufactured through a controlled fusion process to obtain a dense spinel–corundum composite. The aggregate consisted predominantly of Al_2O_3–MgO phases, with Cr_2O_3 incorporated into the spinel structure as a solid solution. The chromium oxide was present without the formation of hexavalent chromium (Cr^{6+}). The relatively high bulk density and low apparent porosity of Spincor indicate its dense structure, making it suitable for use as a refractory aggregate in low-cement castables.

White fused alumina (WFA), calcined alumina, microsilica, and high-alumina cement (HAC) were used as the other principal raw materials for castable preparation. WFA provided the high-alumina aggregate fraction, while calcined alumina was incorporated as a fine alumina component to improve particle packing and matrix densification. Microsilica was used as a reactive fine additive to enhance matrix bonding and promote the formation of a dense microstructure. HAC served as the hydraulic bonding component of the low-cement castable system. The chemical compositions and selected physical properties of the raw materials are presented in Table 1

Parameters	Spincor	WFA	Cal. Alumina	Microsilica	HAC
Al_2O_3 %	76.2	99.3	99.4	0.2	70.1
SiO_2 %	0.4	0.02	0.02	97	1.45
MgO %	16.1	-	-	0.2	0.02
CaO %	0.3	-	-	0.3	26.0
Fe_2O_3 %	0.5	0.02	0.02	0.1	0.12
Cr_2O_3 %	3.9	-	-	-	-
Na_2O %	0.1	0.3	0.3	0.25	0.24
K_2O %	0.02	-	-	0.22	-
LOI %	0.1	0.07	0.1	0.54	0.2
AP %	4.0	4.2	-	-	-
BD (g/cc)	3.5	3.6	-	-	-

Table 1: Physico-chemical analysis of the raw materials used in the castables

2.1.1 XPS Studies: Demonstrating the proof of Spincor; free-form hexavalent chromium (Cr^{6+}) state

The XPS analysis confirms that soluble chromium (Cr) is predominantly present in the trivalent Cr^{3+} oxidation state, with no detectable hexavalent chromium [Cr (VI)] in the analyzed surface [Figure 1]. The material contains Al, Mg, and their corresponding oxides, with chromium incorporated as a solid solution within the magnesia–alumina spinel and corundum phases. This indicates that the chromium is structurally integrated into the oxide matrix rather than being present as a separate, readily soluble chromium compound.

In particular, the core-level XPS spectra the Cr 2p spectrum exhibits the characteristic Cr $2p_1/_2$ and Cr $2p_3/_2$ components at 586.455 and 577.255 eV, respectively, with a spin–orbit splitting of 9.2 eV. These binding energies are consistent with Cr^{3+}–O bonding in chromium oxide/oxide-solid-solution environments. The Cr 2p spin–orbit components, designated as $2p_1/_2$ and $2p_3/_2$, reflect the electronic structure of Cr and its interaction with the surrounding oxygen framework. Notably, no additional Cr (VI) component at higher binding energy (~579–580 eV) is observed, indicating that hexavalent chromium is not detectable in the analyzed surface. Thus, the XPS results confirm that chromium is predominantly present in the trivalent (Cr^{3+}) oxide state. The structural incorporation of Cr^{3+} within the spinel/corundum oxide matrix provides effective chromium immobilization and supports the development of a high-performance, safer and more sustainable product.

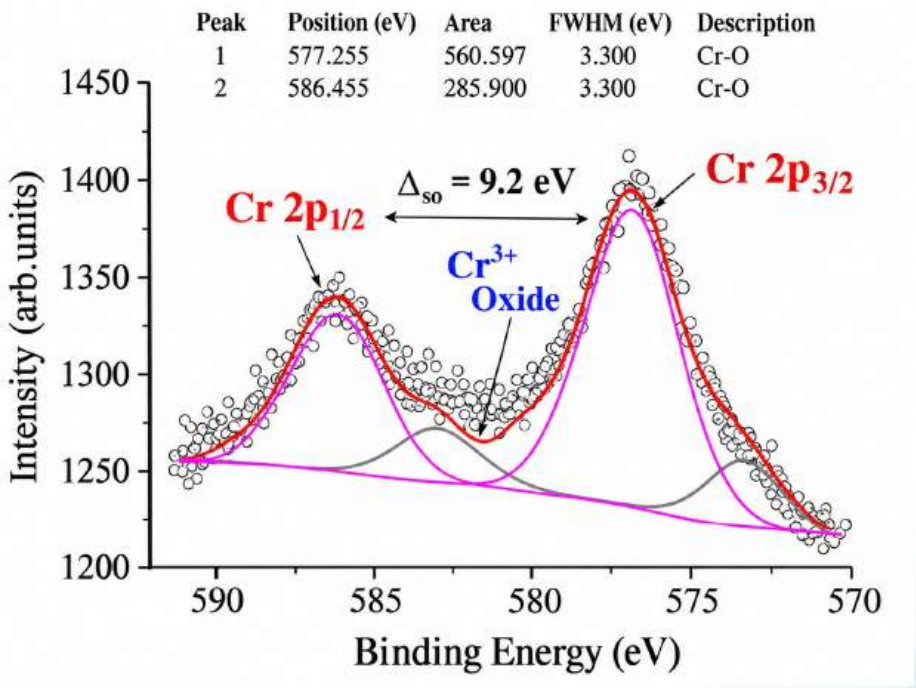


Figure 1: The Core level XPS Spectrum Cr 2p for Spincor

2.2 Castable Preparation

Two low-cement castable compositions were prepared to evaluate the effect of spinel aggregate incorporation on the physical, mechanical, and high-temperature properties of the castables. The formulations consisted of refractory aggregate, calcined alumina, microsilica, high-alumina cement (HAC), and a suitable dispersant. The control composition (C1) was prepared using white fused alumina (WFA) as the principal aggregate, whereas the spinel-containing composition (C2) was prepared by partially replacing WFA with Spincor spinel–corundum aggregate. The detailed formulations are presented in Table 2.

Raw materials used	C1	C2
WFA	79.8	10
Spincor	-	69.8
Cal. Alumina	10	10
Microsilica	5	5
HAC	5	5
Dispersants	0.2	0.2
Water %	5	5

The raw materials were first dry-mixed to obtain a homogeneous distribution of the coarse and fine fractions. Mixing was performed using a Hobart mixer, followed by the gradual addition of **5 wt.% water** to both compositions. Mixing was continued until a homogeneous and workable castable was obtained. The flowability of the fresh castables was evaluated using a vibrating table. The same water addition was maintained for both compositions to facilitate a direct comparison of the effect of Spincor incorporation on the castable properties.

2.3 Sample Preparation

The prepared castables were vibro-cast into standard molds measuring 160 × 40 × 40 mm for the determination of modulus of rupture (MOR) and cold crushing strength (CCS). Cylindrical specimens measuring 50 × 50 mm were prepared for thermal shock resistance (TSR) evaluation.

After casting, the specimens were kept at room temperature for 24 h to allow initial setting and curing. The cured specimens were subsequently dried at 110 °C and then fired at 1000 °C and 1500 °C under controlled heating conditions. The properties of the spinel-containing castable (C2) were compared with those of the spinel-free WFA-based castable (C1) to assess the influence of the Spincor aggregate.

The bulk density (BD) and apparent porosity (AP) of the dried and fired specimens were determined by the water-displacement method based on Archimedes' principle. The MOR and CCS were measured using a compression testing machine in accordance with IS 10570:2011.

3. Results and Discussion

3.1 Physical Properties

The incorporation of Genzee spinel aggregates significantly influenced the physical properties and densification behaviour of the developed castables. An increase in bulk density accompanied by a corresponding reduction in apparent porosity

was observed following high-temperature firing, indicating progressive microstructural densification. Both WFA- and Spincor-based castables exhibited an increase in bulk density after firing at 1600 °C, together with a decrease in apparent porosity [Figure 2]. These changes can be attributed to enhanced particle rearrangement, solid-state diffusion, sintering, and closure of open pores during high-temperature treatment. The resulting densification is expected to promote improved mechanical integrity and structural stability under severe service conditions.

Compared with the WFA-based composition, the Spincor-based castable exhibited a slightly lower bulk density. This behaviour may be associated with differences in the chemical and phase compositions of the aggregates, particularly the comparatively lower Al_2O_3 content and intrinsic density of the Spincor-containing system. Further, the simultaneous increase in bulk density and decrease in apparent porosity after firing at 1600 °C confirm the occurrence of substantial sintering and densification in both compositions. These microstructural changes are favourable for improving the load-bearing capability and dimensional stability of the castables at elevated temperatures.

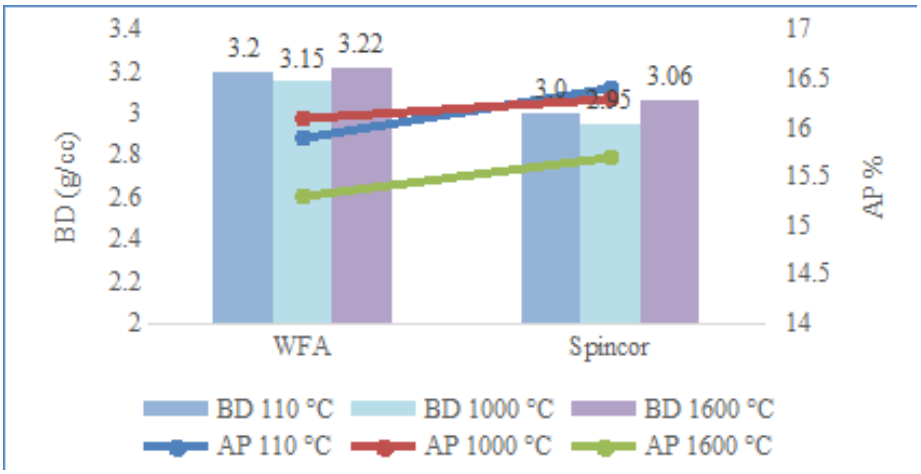


Figure 2: Bulk Density and Apparent Porosity of WFA- and Spincor-based castables at different firing temperatures

3.2 Mechanical Strength

The cold crushing strength (CCS) and modulus of rupture (MOR) increased considerably with increasing firing temperature [Figure 3]. This improvement can be attributed to enhanced ceramic bonding, progressive matrix densification, and the development of stable spinel-containing phases during high-temperature treatment.

During firing, the formation of stronger interparticle and aggregate–matrix bonds reduce interfacial defects and weak bonding regions, thereby increasing the effective load-bearing capacity of the castable. In addition, the development and stabilization of spinel-containing phases contribute to improved structural integrity by strengthening the matrix and aggregate–matrix interfaces. The Spincor-containing castable exhibited comparable mechanical performance to the WFA-based composition, demonstrating effective bonding and densification during high-temperature treatment. The competitive CCS and MOR values of the Spincor-based castable indicate its potential for application in high-temperature refractory systems where

mechanical stability and structural integrity are critical.

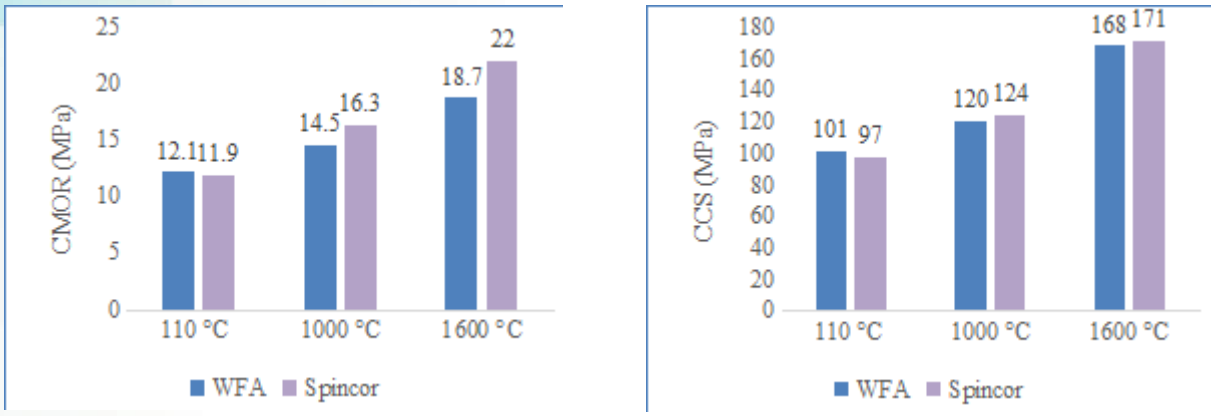


Figure 3: CMOR and CCS of WFA- and Spincor-based castables at different firing temperatures

3.3 Thermal Shock Resistance

Thermal shock resistance was evaluated by repeated water-quenching cycles (up to 30 cycles) using cylindrical specimens pre-fired at 1000 °C. The thermal shock behaviour of the Spincor-based castable was compared with that of the WFA-based castable, as shown in Figure [4].



Figure 4: Thermal Shock Resistance of WFA- and Spincor-based castables at 1000 °C (up to 30 Cycle)

The Spincor-containing castable exhibited superior resistance to repeated thermal cycling compared with the WFA-based composition. The improved thermal shock resistance can be associated with the optimized aggregate–matrix microstructure, controlled thermal expansion, and improved crack-arresting characteristics of the spinel-containing system. The presence of spinel phases and the resulting heterogeneous microstructure can effectively hinder crack initiation and propagation, thereby reducing surface spalling and structural degradation during rapid heating and cooling cycles.

3.4 Corrosion Resistance

Cup corrosion tests were conducted at 1600 °C with a 10 h holding period using basic steel-plant slag in the presence of metallic steel to evaluate the corrosion behaviour of the developed castables, as shown in Figure 5.

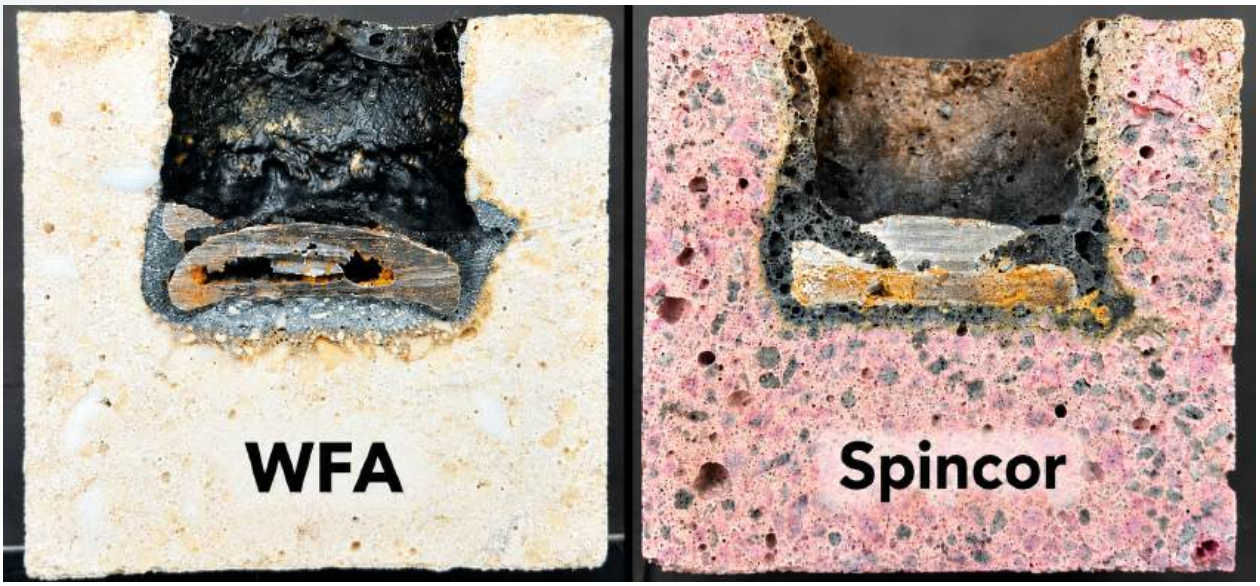


Figure 5: Corrosion resistance of WFA- and Spincor-based castables at 1600 °C with 10 h soaking

The Spincor-containing castable exhibited better resistance to slag penetration and chemical attack than the WFA-based composition. The improved corrosion resistance can be attributed to the low-silica, spinel-rich nature of the aggregate and its enhanced chemical compatibility with the basic slag environment. Furthermore, the presence of chromium oxide in solid solution within the spinel structure may contribute to improved chemical stability and resistance to dissolution and penetration by aggressive slag constituents. The reduced slag infiltration also indicates improved microstructural integrity and lower permeability of the Spincor-based castable.

Overall, the corrosion results demonstrate that the incorporation of Genzee/Spincor spinel aggregate can significantly enhance the resistance of refractory castables to aggressive steel-plant slags and thereby improve their potential service life under severe operating conditions

3.5 Microstructural Analysis

SEM analysis revealed a relatively dense and homogeneous microstructure in the developed castables, with good interfacial bonding between the refractory aggregates and the surrounding matrix. The reduced pore population and improved aggregate–matrix contact observed after high-temperature firing were consistent with the increase in bulk density and mechanical strength.

The microstructure exhibited no pronounced formation of continuous glassy phases,

indicating the development of a comparatively stable ceramic bonding network at elevated temperatures. In addition, the low level of alkali impurities is expected to suppress the formation of low-melting phases, thereby contributing to improved high-temperature stability. The combined effects of microstructural densification, strong aggregate–matrix bonding, and the formation of stable spinel-containing phases contributed to the enhanced mechanical integrity and thermal and corrosion resistance of the Spincor-based castable.

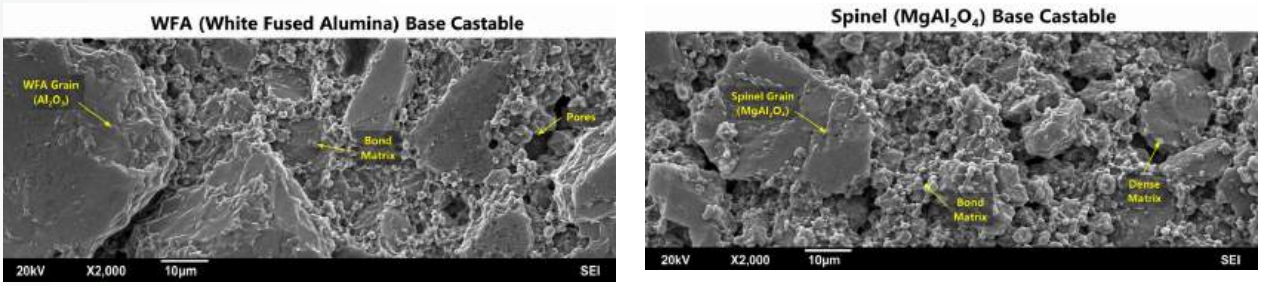


Figure 6: Microstructure of WFA- and Spincor-based sastables after firing at 1600 °C

4. Conclusion

The present study demonstrates that Genzee spinel aggregate significantly enhances the overall performance of low-cement refractory castables. The optimized chemical composition, negligible silica content, and engineered dense microstructure collectively contribute to improved mechanical strength, thermal shock resistance, chemical stability, and high-temperature performance.

The modified fusion process enables the development of a high-quality refractory-grade spinel–corundum composite with superior corrosion resistance and structural durability. Furthermore, the incorporation of chromium oxide in solid solution enhances refractory performance without the formation of hexavalent chromium. Overall, the results confirm that Genzee spinel aggregate is a promising raw material for advanced refractory applications requiring excellent high-temperature reliability, enhanced resistance to thermal and chemical degradation, and extended service life.

5. Future Scope

Further investigations may include:

- Study the thermo-mechanical behaviour of spinel base bricks and castables
- Evaluation in steel ladles, troughs, and cement kiln applications

6. References:

1. Rigaud, M., “Spinel-containing refractories for high-temperature applications,” Refractories Handbook.

2. Routschka, G., and Wuthnow, H., “Pocket Manual Refractory Materials.”

3. Lee, W. E., & Zhang, S. “Melt corrosion of refractories.” *International Materials Reviews*, 44 (1999), 283–301/306.

4. Braun, M., et al. “Spinel-containing alumina-based refractory castables.” *Ceramics International*, 37 (2011).

5. Braun, M., et al. “The corrosion and microstructure relationship for cement-bonded spinel refractory castables.” *Ceramics International*, 37 (2011).

6. Salomão, R., Pandolfelli, V. C., & others. “The corrosion resistance of microsilica-containing Al_2O_3–MgO and Al_2O_3–spinel castables.” *Ceramics International*, 38 (2012), 4783–4789.

7. Sondergeld, C., et al. “Corrosion of magnesium aluminate spinel-rich refractories by sulphur-containing slag.” *Journal of the European Ceramic Society*, 35 (2015), 1613–1620.

8. Effect of Cr_2O_3 additive on alumina-spinel and alumina-magnesia castable. *Ceramics International*, 50 (2024), 42217–42228.

SHINAGAWA & SAINT-GOBAIN PARTNERSHIP: FROM TAPHOLE CLAY TO ADVANCED TROUGH AND RUNNER REFRACTORY SOLUTIONS FOR THE INDIAN STEEL INDUSTRY

Fabiano Rodrigues[1], Eric Sako[2], Deivison Hespanhol[2], Bruno Rangel[1], Priyanshu Kumar[1], Ashis Das[1], Abhishek Paul[1]

[1]Saint-Gobain Performance Ceramics & Refractories
[2]Shinagawa Refra Brazil

Corresponding author e-mail: fabiano.rodrigues@saint-gobain.com

Abstract

The Indian steel industry requires refractory solutions that support high blast furnace productivity, operational reliability, safety and contribute to sustainability improvements. This paper describes the partnership between Shinagawa Refra Group and Saint-Gobain Performance Ceramics & Refractories through its Indian venture Grindwell Norton (SG GNO), which combines proven ironmaking technology with local manufacturing, application engineering and customer support in India. The collaboration first established confidence through licensed taphole clay (THC) manufacture and is now being extended to trough and runner castables. The paper reviews operational challenges in linings durability and maintenance, and presents industrial experience and achievements obtained in South America. Advanced oxidation-resistant castables, shotcrete maintenance, rapid repair materials, hot gunning and wear monitoring have delivered longer campaigns, fewer general repairs, higher availability and reduced personnel exposure. The proposed deployment model enables Indian steelmakers to access globally proven technology with local quality assurance, supply reliability and lifecycle support.

Keywords: blast furnace refractories, taphole clay, trough and runner, technology transfer

1. Introduction

The steel industry faces increasing challenges related to productivity, operational reliability, safety and sustainability. As steelmakers in India pursue higher production rates, cost optimization and lower environmental impact, refractory solutions play a critical role in supporting stable and efficient blast furnace operation.

Shinagawa Refractories is recognized as a leading supplier of refractory materials for iron and steel making applications. Through decades of blast furnace experience, the company has developed solutions covering hearth protection systems, taphole clays, trough and runner lining concepts, repair technologies and wear monitoring methodologies. These solutions have been implemented at major steel producers worldwide, contributing to operational stability and longer campaign life.

Saint-Gobain Performance Ceramics & Refractories combines global materials science expertise with industrial capabilities and a broad manufacturing footprint. In India, these capabilities are supported by Grindwell Norton through local production, technical service, application engineering and customer support, enabling rapid commercialization and technology deployment.

The strategic partnership between Shinagawa and Saint-Gobain combines the

strengths of both organizations. Proven refractory technologies developed by Shinagawa can be manufactured locally and supported by Saint-Gobain's engineering and service infrastructure, creating sustainable value for steelmakers while supporting consistent quality and supply reliability.

2. Building Confidence Through a Successful Taphole Clay Partnership

Cooperation between the two companies in India began in 2020 through a licensing and manufacturing agreement focused on blast furnace THC solutions.

Under this framework, Shinagawa contributes proprietary ironmaking refractory technologies and product development expertise, while Saint-Gobain provides local manufacturing, quality control, logistics management and onsite technical support. This partnership model has enabled the Indian market to benefit from advanced THC solutions adapted to local operating conditions.

After 6 years of collaboration, SG GNO has become a key supplier of Shinagawa's THC technologies to major Indian steel producers. The recognized performance and technical support have established confidence for further technology transfer initiatives. Anchored on a solid foundation, the partnership is now being extended into another critical ironmaking application: trough and runner systems.

3. Advanced Trough and Runner Refractory Solutions

3.1 Challenges in Modern Trough and Runner Operations

Trough and runner (T&R) systems are commonly lined with Al_2O_3-SiC-C castables and operate under severe conditions characterized by molten iron and slag attack, thermal cycling, oxidation of carbon-bearing components, mechanical erosion and maintenance constraints. The main refractory degradation mechanisms and typical wear profile of the main trough are illustrated in Fig. 1.

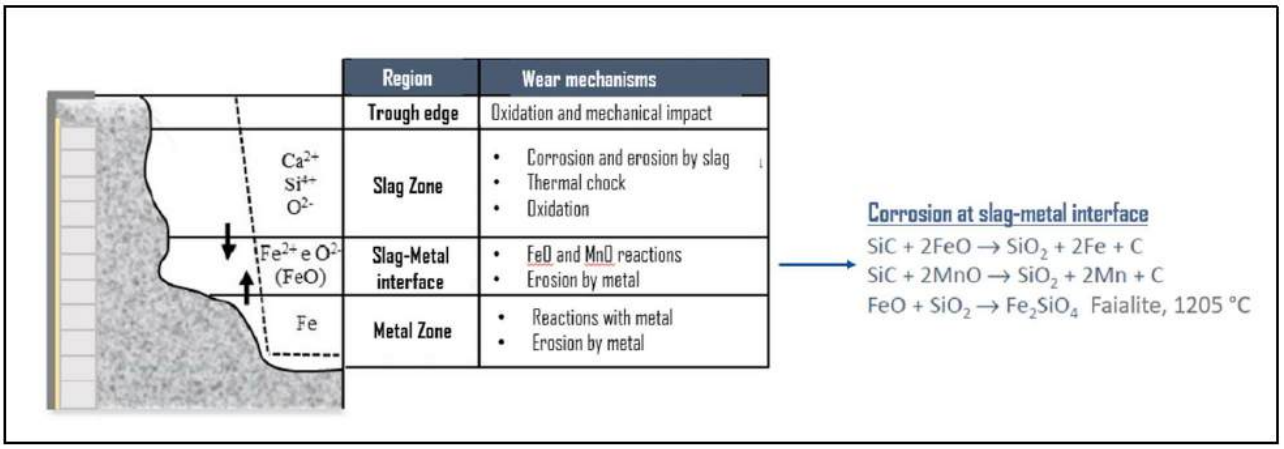


Figure 1 Schematic representation of the main wear rate mechanisms by main trough region

One of the most significant degradation mechanisms in Al2O3-SiC-C castables is oxidation. Oxidation of carbon and silicon carbide increases refractory porosity, facilitates slag and metal penetration and accelerates wear. If not properly controlled, this mechanism can reduce campaign life, increase repair frequency and create operational instability.

Modern blast furnaces also require longer T&R campaigns and greater equipment availability, while maintaining high standards of operational safety and contributing to sustainability improvements. These requirements demand continuous development of refractory materials, lining designs, maintenance methodologies and monitoring techniques, in collaboration with end customers.

3.2 Shinagawa Brazil as an Industrial Reference

Shinagawa Brazil has accumulated extensive experience supporting blast furnace operations throughout South America, with more than 20 references currently in operation. Numerous refractory concepts have been developed to address specific customer needs in terms of T&R maintenance, campaign stability and operational safety. This practical experience has resulted in advanced lining systems, repair technologies and maintenance practices capable of extending campaign life while reducing overall operating costs.

The industrial results obtained in South America, where the refractories technological landscape is very similar to the Indian one, provide a technical foundation for international technology transfer.

3.3 Technology Overview

The T&R technologies developed and deployed by Shinagawa Refractories Brazil combines advanced alumina-carbon-SiC (ACS) working lining materials with low cement or colloidal silica bonding, backup lining systems, innovative repair products and digital monitoring solutions.

Special emphasis has been placed on oxidation-resistant ACS castables, rapid and effective repair practices based on shotcrete technologies. More recently, disruptive drying-free castables have been introduced in the market, with very positive performance so far. Together, these solutions show a significant potential to address the specific challenges of the Indian I&S industry.

4. Demonstrated Benefits and Industrial Value

4.1 Advanced Material Technologies

A significant milestone in Shinagawa's trough technology development was the creation of an anti-oxidation concept for ACS castables.By combining optimized particle-size distribution, reduced water addition, a special deflocculant system and oxidation inhibitors, the developed castable exhibited substantially improved oxidation resistance.

As shown in Fig. 2, laboratory results showed a relative oxidation index of 46% after six hours and 39% after eleven hours compared with the previous-generation material, together with a 14% improvement in corrosion resistance [1].

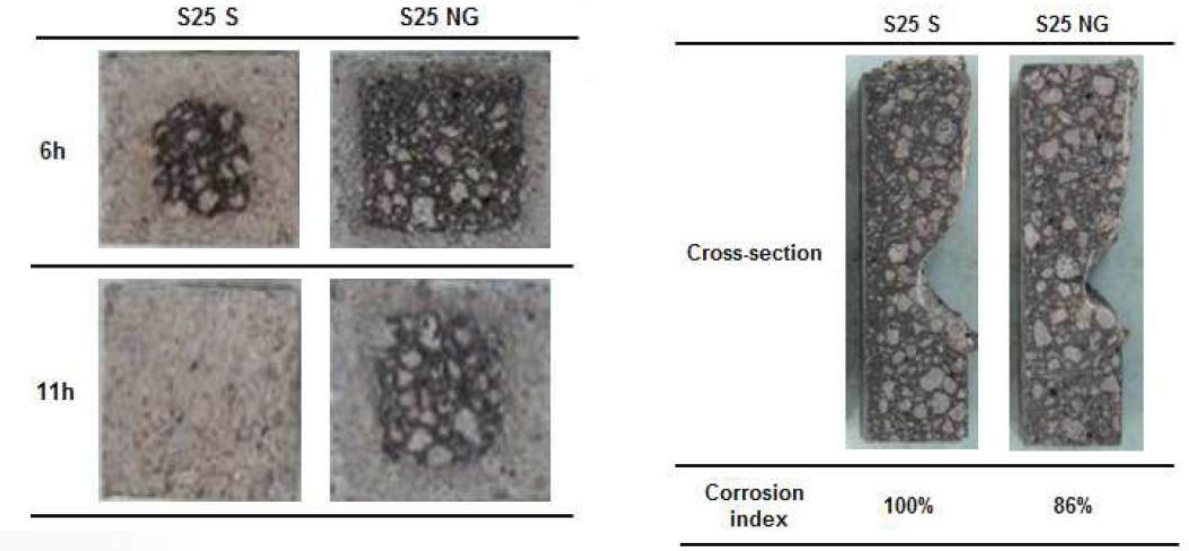


Figure 2 Oxidation tests at 1000°C under air and pig iron and slag corrosion test at 1550°C for 2 hours on traditional (S25 S) and improved (S25 NG) resistance castables

Field applications at a 2-tap hole furnace in Brazil with 3,500 THM/day capacity confirmed the effectiveness of this approach. Combined with shotcrete repair technologies, it allowed main trough operation for approximately 250 days and production of around 300,000 tons of hot metal without unplanned shutdowns, while keeping a substantial safety margin with regards to remaining working lining thickness.

4.2 Improved Availability and Productivity

Implementation of advanced T&R repair technologies and procedures also generated significant operational improvements. In several 2-tap hole furnaces in South America, where repair durations are particularly critical, shotcrete-based maintenance (see Fig. 3) reduced the number of general repairs by 2 or 3. Operational availability exceeded 98%. Campaign throughput increased to more than 300,000 tons in some of these furnaces.



Figure 3 Shotcrete application at a 2-tap hole furnace in South America

These results demonstrate the ability of advanced refractory concepts to increase blast furnace productivity while reducing maintenance requirements.

4.3 Enhanced EHS Performance and Sustainability

In addition to productivity benefits, significant safety improvements were achieved.Reduced repair frequency, hot gunning systems, smoke-free repair materials, laser wear inspection (see Fig. 4) and shotcrete maintenance reduced the need for and duration of operator intervention in high-risk areas. As a result, annual personnel exposure to hazardous conditions was reduced by several thousand man-hours [2].

Sustainability benefits arise from extended refractory campaigns and improved asset utilization.Longer campaigns reduce refractory consumption, waste generation and maintenance interventions. Shorter and less frequent maintenance have a positive impact in fuel consumption, e.g. for castables drying and heat up, and logistics activities, also contributing to improved environmental performance.Advanced T&R technologies therefore support steelmakers in improving sustainability and greenhouse-gas reduction objectives.

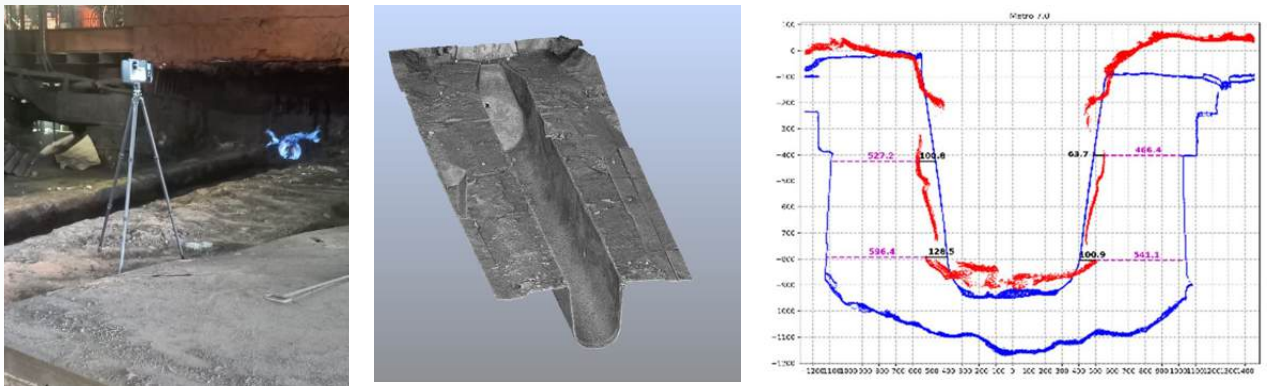


Figure 4 Main trough wear inspection by 3D laser scanning and corresponding wear profile obtained

5. Bringing Proven Technology to India

5.1 Industrial Deployment Model and Customer Support Strategy

The technology transfer model established in India's THC business can now be applied to T&R solutions.Under this approach, Shinagawa provides proven technology, design methodologies and application know-how, while Saint-Gobain delivers local manufacturing, quality assurance and customer support from its plant in Halol.

Indeed, it is well known that successful implementation of T&R solutions relies more than on product supply alone. Application engineering, installation supervision, wear monitoring, performance analysis and continuous improvement are essential components of the supporting services model. These activities are paramount to obtain maximum value from the refractory system throughout its life cycle.Shinagawa Brazil and SG GNO are working in close proximity to deploy in India the most efficient service practices developed in the South American market.

5.2 Opportunities for Indian Steelmakers

By combining advanced product technology, field experience, reliable quality and service excellence, Shinagawa and SG GNO aim at bringing to Indian I&S makers high-performance T&R solutions to support their operational and EHS targets. This is not expected to be a one-shot process. Optimization and further improvement of current performance metrics will require strong collaboration with blast furnace and cast house crews, deep expertise capabilities and continued innovation.

The outstanding R&D capabilities of Saint-Gobain Research India in Chennai will be at the service of our increasingly ambitious goals in T&R performance.

6. Conclusions

The partnership between Shinagawa and Saint-Gobain has demonstrated its value through the transfer, local manufacture and supply of advanced taphole clay solutions in India. This experience validated a business model that combines global refractory expertise with local engineering and manufacturing capabilities.

The industrial experience accumulated by Shinagawa in South America provides a strong technical foundation for expanding the collaboration into advanced trough and runner applications. Developments focused on oxidation resistance, fast repair castables, campaign extension, safety improvement and sustainability have demonstrated measurable benefits in blast furnace operations.

The combination of proven technology, local manufacturing capability, application engineering expertise and customer support creates a compelling value proposition for Indian steelmakers. As the Indian steel industry continues to grow, the Shinagawa-Saint-Gobain partnership represents the next step in the technology transfer journey for advanced ironmaking refractory solutions, supporting higher productivity, safer working conditions and more sustainable blast furnace operations.

References

1. E.Sako et al.:ProceedingsUnitCR 2017.

2. G.Ferreira et al.:ProceedingsABM weekseminar 2025.

IMPROVEMENT OF TAP HOLE CLAY DRILLING BEHAVIOUR FOR HIGH SEVERITY BLAST FURNACE OPERATION

Souvik Palui[1], Dhiraj Raisane[2], Tuhin Patranabish[3], Sushavon Sarkar[4], Sachin Rodi[5]
Calderys India Refractories Limited, Nagpur, India

1. Manager QPC, Calderys, 2. General Manager, I&S Service, Calderys, 3. General Manager, NPD, Calderys 4. General Manager, CCR, Calderys 5. Manager, I&S Service, Calderys

Corresponding Author's e-mail: souvik.palui@calderys.com

ABSTRACT

Tap hole clay (THC) drilling in blast furnaces can be affected by premature puncture, hard drilling and incomplete tap-hole opening before the required tap-hole length is reached. Slag-metal infiltration through cracks in the tap-hole region was considered as a possible mechanism contributing to this problem. Crack Filling Mass (CFM) can be used to seal refractory cracks, but its soft, fine-grained nature can delay sintering during the short Gun-Up-to-Knock-Out (GUTKO) period and can result in increased spitting during casting. In this study, the grain size distribution (GSD) and composition of tap hole clay were modified to improve packing, drillability and resistance to premature puncture. Four compositions were evaluated through laboratory testing and field trials in two high-productivity mini blast furnaces. Increasing the finer fraction and optimizing the alumina-containing aggregate system improved drilling behaviour and reduced the tendency for not-through drilling and premature puncture. The optimized composition also maintained suitable physical properties and hot strength, while providing the required resistance to limit the risk of self-opening and back flashing. After laboratory evaluation, the optimized composition was validated through 3 MT feasibility, 5 MT confirmation, and 16 MT full-scale site trials. The formulation was subsequently adopted as a standard product.

Keywords: Tap hole clay; Blast furnace; Grain size distribution; Drilling behaviour; Premature puncture; Slag metal infiltration; Packing density

1. INTRODUCTION

Blast furnace operation is influenced by several factors, including raw material quality, slag generation rate, pulverized coal injection (PCI), oxygen enrichment, tuyere diameter and gas velocity through it, and the concentrations of SiO2 and MnO2 in the Slag. These factors affect campaign life, productivity, and overall furnace stability. The operating conditions are more demanding in mini blast furnaces (MBFs), particularly in furnaces with a single tap hole, where effective drainage becomes increasingly important as the campaign progresses.

As the campaign progresses, deterioration of the tap hole area is increased, particularly when cast-house practices are not robust or when the tap hole clay is not suitable for the operating conditions. The challenge can be aggravated when the furnace is equipped with low-capacity or inefficient tap-hole maintenance equipment, such as drilling machines and mud guns. These conditions can lead to poor metal and slag drainage, increased tap-hole wear, higher tap-hole temperatures and, in severe cases, tap hole breakthrough. Such problems directly affect furnace stability and production.

A possible explanation for the observed drilling difficulties is slag-metal infiltration through the tap hole region. Such infiltration may occur through cracks developed in the mushroom or along the interface between the refractory wall and the mushroom. During drilling, the early appearance of a "red ball" may indicate the presence of hot gases or hot blast entering through pre-existing cracks or connected pathways. It is hypothesized that continued drilling in such a region could

open or extend these pathways into the refractory wall or along the interface, potentially increasing the risk of tap-hole puncture. If significant infiltration and subsequent solidification occur within the drilling path, the material may become harder, which could explain the requirement for repeated lancing or poking observed during some casting operations.

Complete casting may then become difficult, casting time increases and drainage slows down. This can cause pressure build up in the furnace and may require a reduction in raw-material charging, resulting in production losses.

Rebuilding or extending the tap hole after such a failure is also difficult. Temporary measures may include reducing blast pressure during plugging and stopping the coal burden for one or more days. These measures can further increase production losses.

CFM has been used to seal cracks in the tap-hole region. It can be applied by blending with conventional tap hole clay in certain ratios. CFM can be effective in blind holes, but its application is limited when the plug-to-tap time is short. Because CFM has a soft and fine-grained structure, sintering may not be sufficient within the available GUTKO time of 25–35 minutes, which can lead to excessive spitting during casting. The spitting can block the cast-house runner and floor and make preparation for the next cast more difficult. For this reason, a modification of the standard tap hole clay composition was investigated. The work focused on optimizing GSD and additives to improve packing and promote faster sintering within the available GUTKO time. The objective was to seal cracks, reduce slag-metal infiltration and lower the risk of tap-hole puncture.

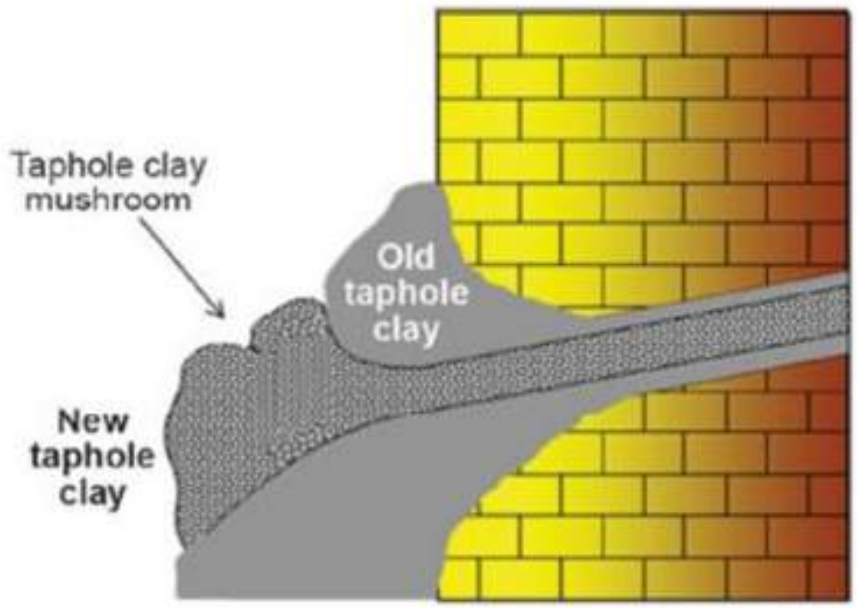


Fig. 1. The “mushroom” formation inside the blast furnace during THC pushing

2. BACKGROUND

A customer was experiencing premature puncture at two high-productivity mini blast furnaces (BF1 and BF2), incomplete drilling, hard drilling and reduced cast length. Similar problems were reported with tap hole clays from different suppliers. Frequent oxygen lancing and poking were required to overcome these problems, which resulted in additional tap-hole damage and inconsistent casting performance.

Table 1 Typical Production Parameters of BF1

SL No.	Description	Value
1	Hot Blast Volume	69320-79928 Nm^3/hr
2	Hot Blast Temperature	1194°C
3	Uptake Temperature	173°-201° C
4	Hot Blast Pressure	2.28 Bar
5	Top Pressure	1.15 Bar
6	PCI Rate	146 Kg/THM
7	Production Rate	1717 MT/Day

Table 2 Typical Production Parameters of BF2

SL No.	Description	Value
1	Hot Blast Volume	112269 Nm^3/hr
2	Hot Blast Temperature	1185° C
3	Uptake Temperature	180°-184° C
4	Hot Blast Pressure	2.70 Bar
5	Top Pressure	1.28 Bar
6	PCI Rate	145 Kg/THM
7	Production Rate	2100 MT/Day

Table 3 Technical Indexes of BF1

SL No.	Description	Value
1	BF Effective Volume	450 m^3
2	Utilization Coefficient	3.5 t/m^3 d
3	Coke Ratio	445 kg/THM
4	Coal Ratio	120 (Max 140) Kg/THM
5	Slag-Hot metal ratio	350 Kg/THM
6	Hot blast Temperature	≥1100° C
7	Oxygen Enrichment Rate	2.40%
8	Furnace Top Pressure	0.3-1.8 Kg/C m^2

9	Pig Iron Output	551000 t/a
10	No of working Tuyeres	11 EA
11	No of Tapholes	1 EA

Table 4 Technical Indexes of BF2

SL No.	Description	Value
1	BF Useful Volume	630 m^3
2	Utilization Coefficient	3.18 t/m^3 d
3	Fuel Ratio	560 Kg/tHM
4	Coal Ratio	120 (Max 180) Kg/tHM
5	Slag Volume	530 kg/tHM
6	Hot blast Temperature	1250° C
7	Oxygen Enrichment Rate	3-6 %
8	Furnace Top Pressure	0.3-1.8 Kg/C m^2
9	Pig Iron Output	700000 t/a
10	No of working Tuyeres	13 EA
11	No of Tapholes	1 EA

Operating data of blast furnaces 1 (BF1) and 2 (BF2) revealed that in the both the furnaces the production rate relative to furnace volume was high. The slag ratio and oxygen enrichment were also high. These operating parameters indicated severe furnace conditions and therefore imposed demanding requirements on tap-hole clay performance.

3. EXPERIMENTAL STUDY

Composition 1 was initially supplied to the site based on the operating conditions. Hard drilling and premature puncture were observed, and in many cases the tap holes were not fully opened during drilling. Better performance was observed when the material was blended with CFM. Since CFM contains a higher proportion of finer particles, this indicated a need to improve the packing and drilling behavior of the tap hole clay. In Composition 2, carbon content was modified to improve drill ability. The GSD was changed only slightly: the fine fraction was increased by 1% by reducing the middle fraction by 1%. Composition 2 performed better than Composition 1 in terms of drill ability and premature-puncture tendency, but the improvement was still below the customer's requirement. The cost of Compositions 1 and 2 was also relatively high. Therefore, the aggregate source was changed in Composition 3 while the other raw materials were kept unchanged. This reduced the Al2O3 content, increased the finer fraction by 3% compared to Composition 1. Composition 3 did not give satisfactory results, and the reduction in Al2O3 content was considered a contributing factor. The formulation was then modified further by reducing the coarser fraction and increasing the finer fraction, while keeping the middle fraction essentially unchanged. This approach was based on the

better behavior observed with the finer CFM blend. In Composition 4, the coarser fraction was reduced by 5% and the finer fraction increased by 5% compared with Composition 3. The alumina content was also optimized.

Table 5 Grain size Distributions of different compositions

Compositions	Coarser Fraction	Medium Fraction	Fine Fraction
Composition 1	X%	Y%	Z%
Composition 2	X%	(Y-1) %	(Z+1) %
Composition 3	(X-1) %	(Y-2) %	(Z+3) %
Composition 4	(X-6) %	(Y-2) %	(Z+8) %
CFM	(X-25) %	(Y+6) %	(Z+19) %

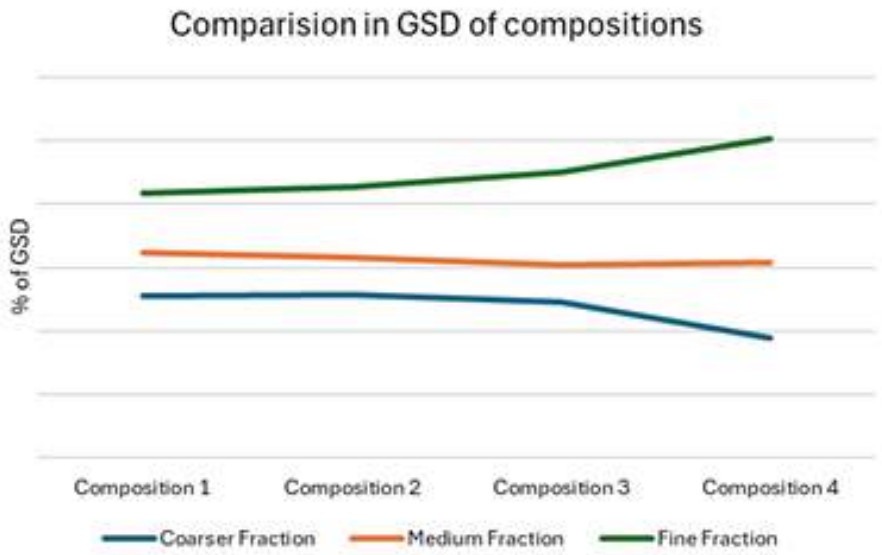


Fig. 2. Comparison of GSD of the compositions

4. RESULTS AND DISCUSSION

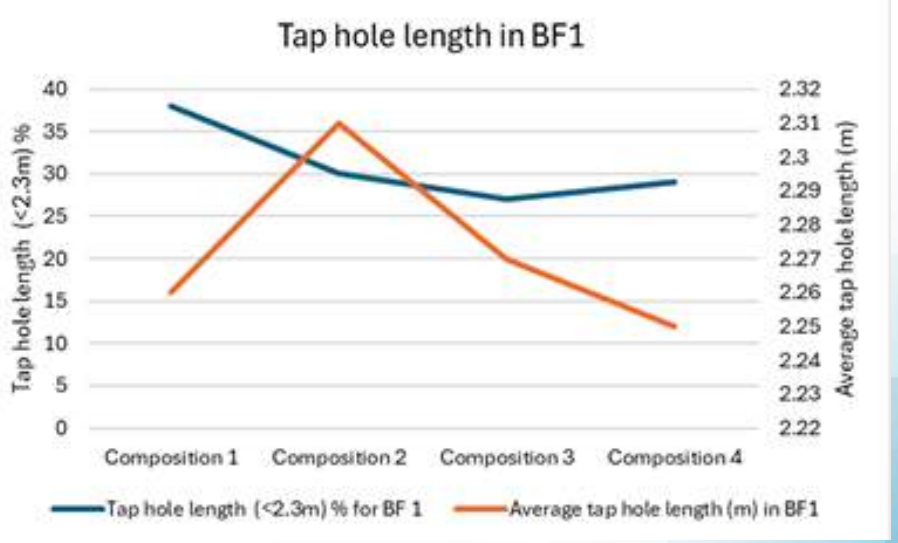


Fig. 3. Tap-hole length in BF1

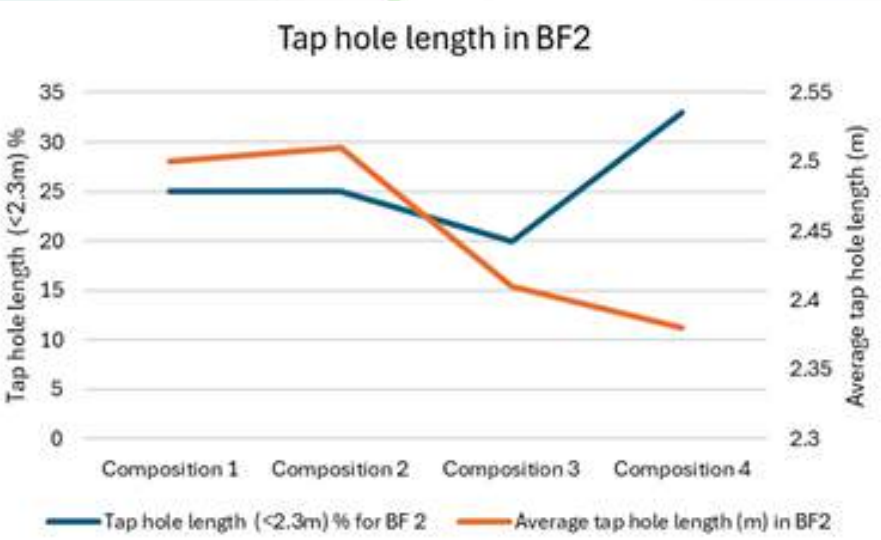


Fig. 4. Tap-hole length in BF2

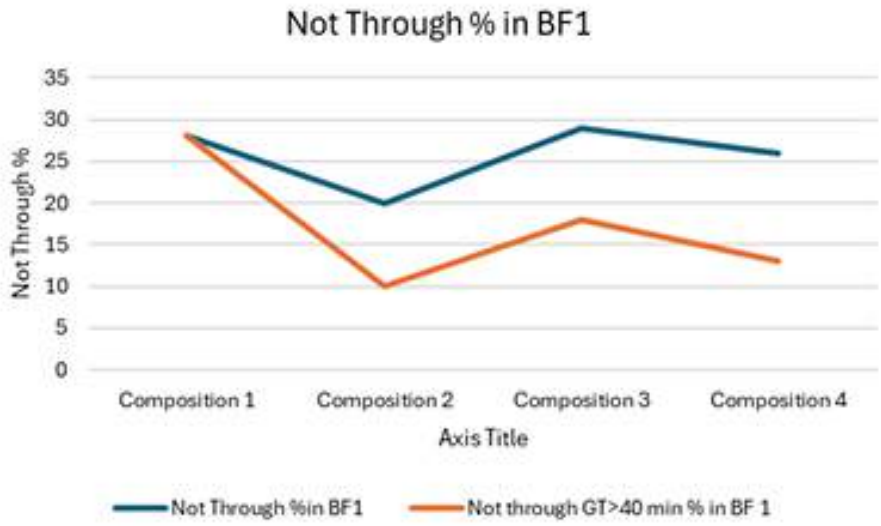


Fig. 5. Not-through drilling (%) in BF1

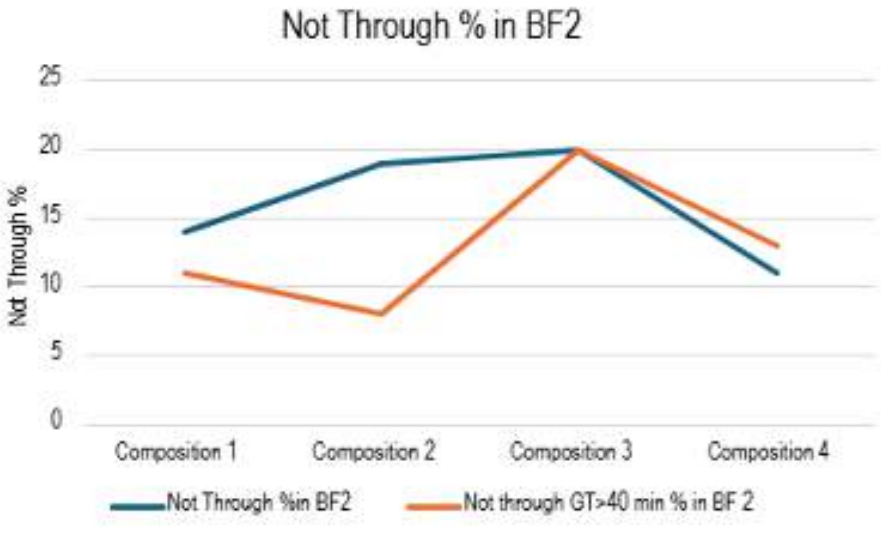


Fig. 6. Not-through drilling (%) in BF2

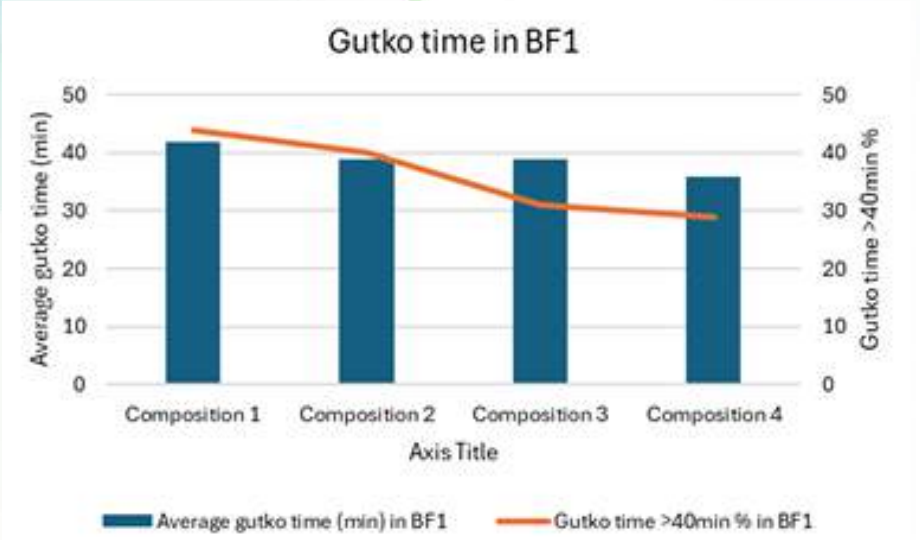


Fig. 7. GUTKO time in BF1

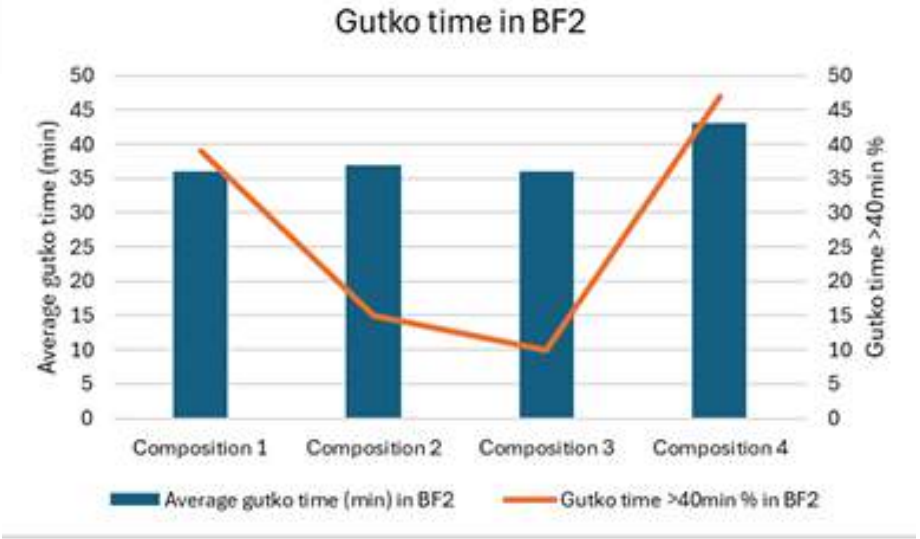


Fig. 8. GUTKO time in BF2

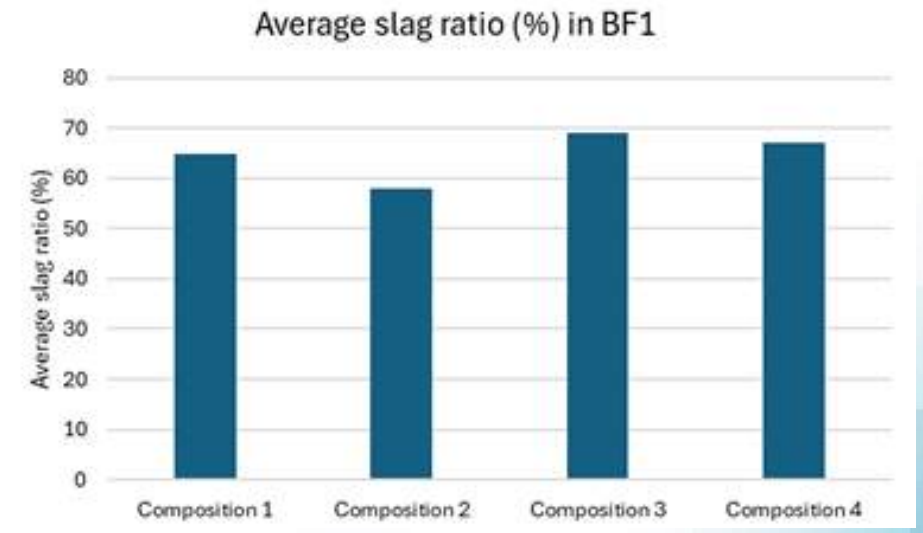


Fig. 9. Slag ratio in BF1

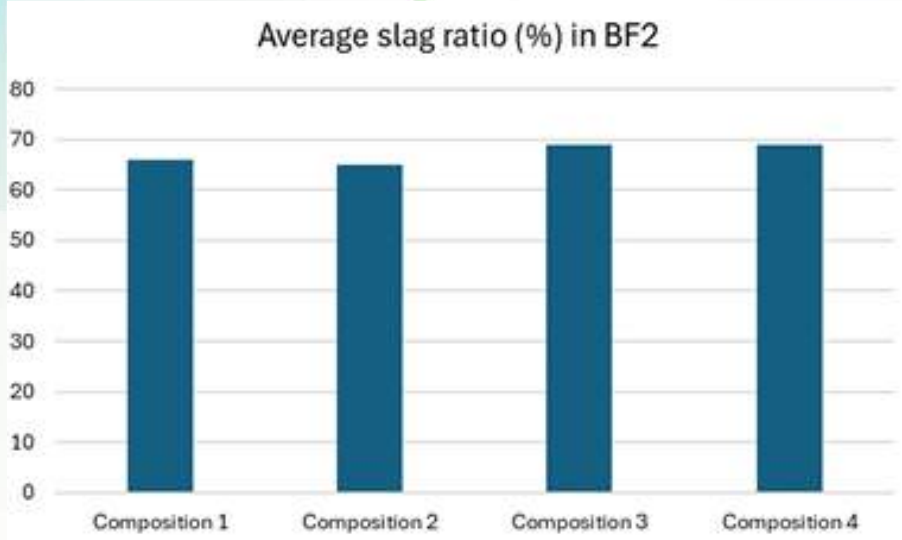


Fig. 10. Slag ratio in BF2

The trial data from the customer's site showed that Composition 2 performed better than Composition 1. However, further optimization was needed to optimize cost without deteriorating performance. Composition 3 showed inferior performance than Composition 2, while Composition 4 gave better results. With the further increase in the finer fraction in Composition 4, the tendency for 'not-through' drilling was reduced significantly.

During the trials, an increase in clay fineness was also accompanied by an increase in plasticity. The higher plasticity was accompanied by less crack formation.

Crack tendency was evaluated by observing surface crack formation on test specimens. The specimens were heated rapidly to 700 °C and then cooled rapidly. The crack patterns obtained with the four formulations are compared in the figure below.

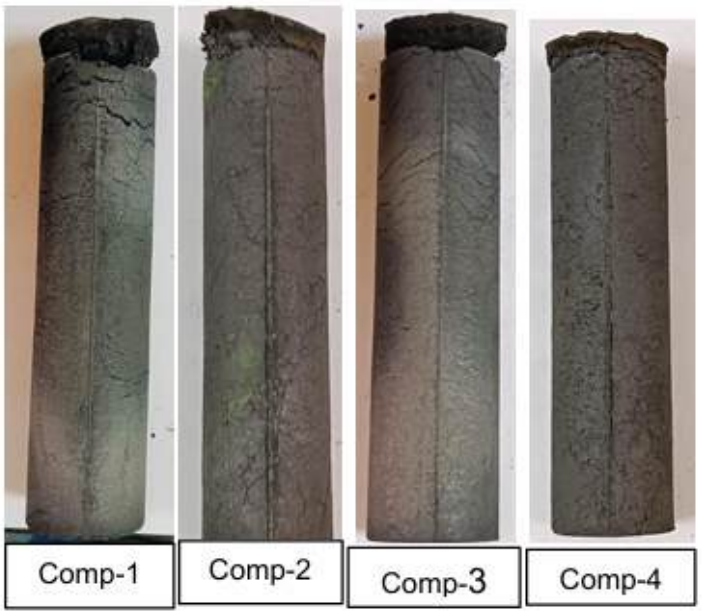


Fig. 11. Comparative appearance of cracks in the four formulations

Increasing the liquid content can improve the plasticity of tap hole clay and can therefore reduce crack formation. However, a higher liquid-binder concentration also increases the volatile content. This can increase mud-gun holding time requirement and may also increase the possibility of back flashing and self-opening.

Table 6 CCS after fired at 1300° C as per EN ISO 1927 – 6

Composition	CCS (kg/cm^2) after coking 1300° C
Composition 1	A
Composition 2	A-25%
Composition 3	A-28%
Composition 4	A-26%

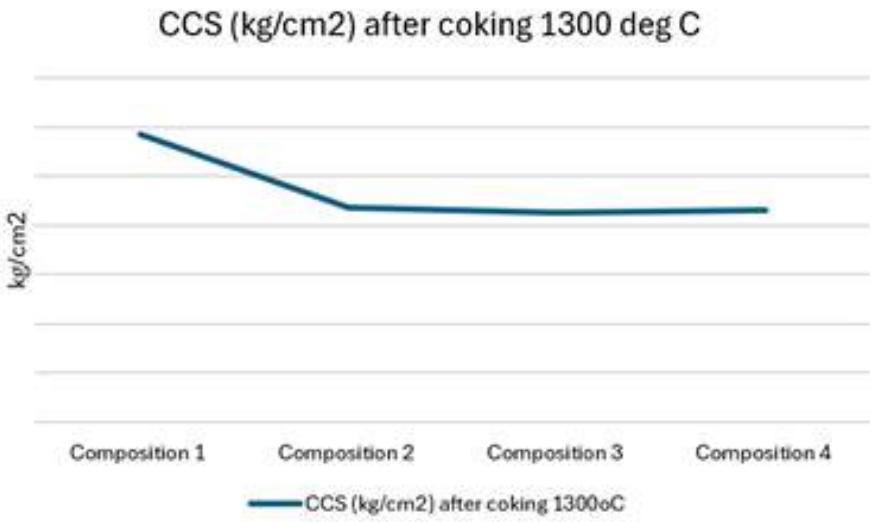


Fig. 12. Comparison of CCS of the compositions

The results show that Composition 1 had the highest CCS at 1300 °C. Composition 2 had reduced CCS with improved drillability. There was no significant difference in CCS between Compositions 3 and 4. The strength obtained with these compositions was considered sufficient to limit the risk of self-opening and back flashing

.

Table 7 AP & BD after fired at 1300° C as per EN ISO 1927 – 6

Composition	Apparent Porosity (%) after 1300°C	FIRED BD(g/cc) after 1300°C
Composition 1	B	C
Composition 2	B-1.4%	C-0.5%
Composition 3	B-6.2%	C-4.1%
Composition 4	B-4.1%	C- 2.3%

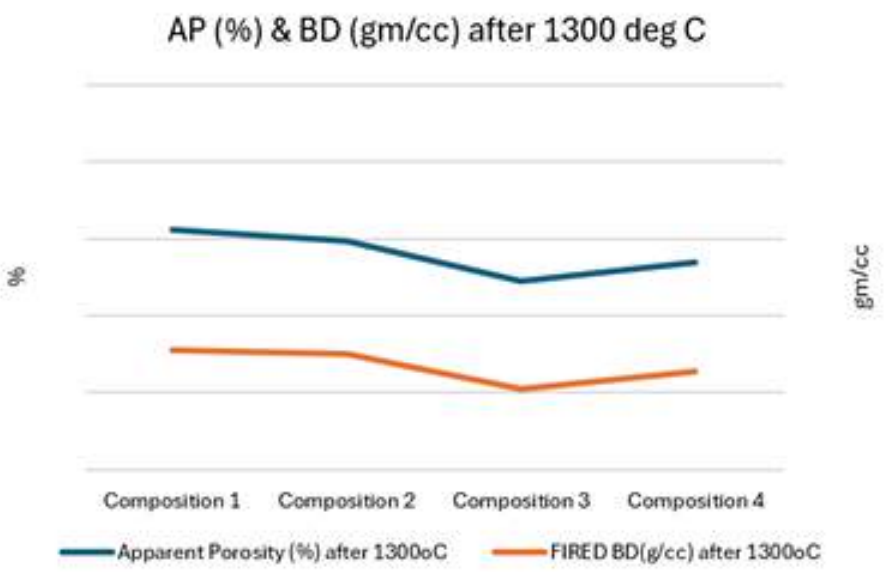


Fig. 13. Comparison of AP & BD of the compositions

The results of apparent porosity (AP) and fired bulk density (BD) after firing at 1300 °C show a reduction in both properties with the change from Composition 1 toward Compositions 3 and 4. Compared with Composition 1, Composition 2 showed only a small reduction in AP and BD. A more pronounced reduction was observed for Composition 3, with decreases of 6.2% in AP and 4.1% in BD. Composition 4 showed an intermediate reduction, with AP and BD decreasing by 4.1% and 2.3%, respectively, relative to Composition 1. These changes are associated with the modification of the aggregate system and grain size distribution, together with the optimized Al_2O_3 content. Composition 4 achieved the required balance between the physical properties and the drilling performance observed during the trials.

5. FIELD VALIDATION

Composition 4 was validated through a staged site trial comprising a 3 MT feasibility trial, a 5 MT confirmation trial and a 16 MT full-scale implementation. All three stages met the operational expectations reported in the study. Following the field validation, Composition 4 was adopted as a standard product.

6. CONCLUSIONS

The trials showed that modifying the grain size distribution and tap hole clay formulation improved drilling behaviour and reduced premature puncture under the high-severity operating conditions of the mini blast furnaces. Increasing the finer fraction, together with optimization of the aggregate and carbon system, provided a better balance between drillability, crack resistance and hot strength. Composition 4 gave better field performance than the preceding formulations.

7. REFERENCES

1. L.R. Nelson and R.J. Hundermark, The tap-hole key to furnace performance, Journal of the Southern African Institute of Mining and Metallurgy, 2016, vol. 116, pp. 465-490.

2. Y. Tang, B. Ma and Z. Gao, Latest research progress of taphole clay for blast furnaces, Refractories, 2020, vol. 54, pp. 452-456.

3. Y. Xu, Research progress of ferro-silicon nitride and its application in refractories, Refractories, 2015, vol. 49, pp. 306-312.

4. H. Wang and G S. Fischman, In situ synthesis of silicon carbide whiskers from silicon nitride powders, Journal of the American Ceramic Society, 1991, vol. 74, pp. 1519-1522.

HYDROJETTING TECHNOLOGY FOR REFRACTORY DISMANTLING IN CFBC BOILER MAINTENANCE

Rishi Mukherjee, Dilip Kosarkar, Surajit Sarkar, M. Omprakash

Calderys India Refractories Ltd., India

ABSTRACT

Scheduled Maintenance of Circulating Fluidized Bed Combustion (CFBC) boilers require periodic removal of existing refractory linings before relining of new refractory can happen. Conventional dismantling methods using jackhammers and pneumatic breakers are labor intensive, generate excessive dust and vibration, and frequently cause damage to boiler tubes and metallic anchors and good adjacent refractory. Hydrojetting technology employs ultra-high pressure water jets operating at 2500-3000 bar to selectively remove refractory while preserving water tubes and anchors. The process utilizes hydraulic penetration into pores and micro-cracks within the refractory structure, causing controlled and precise disintegration. Industrial applications have demonstrated significant improvements in dismantling productivity, worker safety, substrate quality and outage duration. This paper discusses the operating principle, performance benefits and field experience of hydrojetting technology in CFBC boiler maintenance.

Keywords: Hydrojetting, CFBC Boiler, Refractory Dismantling, Maintenance Outage

1. INTRODUCTION

Refractory linings which are installed in side wall, of CFBC boilers protect the water tubes from abrasion, erosion and high temperatures. Periodic replacement of these linings is essential for maintaining boiler reliability and efficiency. Traditionally, the vibro-impact technology is used for removing the refractory lining from surface which is generated by the reciprocating or the rotating action of the equipment and transferring the energy to the sharp pointed tools known as chisel.

1) Pneumatic breakers or Jackhammers
2) Electrical Chippers
3) Pneumatic chippers



Problems with traditional refractory removal method:

- Tube dents and punctures
- Damage to anchors and fins.
- Excessive dust and noise
- High manpower requirements
- Extended shutdown durations
- Unsafe for workers
- Extra time needed for debris removal.

2. HYDROJETTING PRINCIPLE

Hydrojetting utilizes ultra-high-pressure water jets operating between 2500 and 3000 bar to dismantle refractory linings. The water penetrates pores and micro-cracks naturally present within the refractory structure, generating internal hydraulic stresses that propagate cracks and cause fragmentation The removal mechanism can be expressed as:

$$P_w > \sigma_t$$

where:

P_w= Water jet pressure

σ_t= Refractory tensile strength

Unlike mechanical demolition, hydrojetting induces minimal vibration and therefore avoids damage to water tubes and anchors. The technology provides clean surface needed for new refractory installation.

Clean tube surface after Hydrojetting:





3. COMPARISON WITH CONVENTIONAL METHODS

Table I. Performance Comparison

Parameter	Conventional Breaking	Hydrojetting
Removal Mechanism	Mechanical Impact	Hydraulic Fracture
Tube Damage	Frequent	None
Anchor Damage	High	Negligible
Dust Generation	High	Very Low
Vibration	High	Minimal
Surface Quality	Moderate	Excellent
Manpower Requirement	High	Lower
Safety Performance	Moderate	High

Productivity

Industrial demonstrations reported:

• Manual chipping: 0.003 m^3/hr

• Hydrojetting: 0.27 m^3/hr

representing nearly **100 times higher removal efficiency** for dense refractory applications.

4. SAFETY AND ECONOMIC BENEFITS

During Hydrojetting specialized PPEs are worn by the person and only one person with his helper is allowed inside the boiler.





Hydrojetting significantly improves workplace safety by eliminating most dust-related and vibration-related hazards. Since refractory debris is converted into slurry rather than airborne particles, worker exposure to silica dust is substantially reduced.

From an economic standpoint, hydrojetting offers:

- Reduced outage duration
- Elimination of tube repair costs
- Preservation of anchors and fins
- Lower manpower deployment
- Faster relining and startup activities

Although equipment costs are higher than conventional demolition methods, overall maintenance costs are significantly lower due to reduced repair time and outage expenses.

5. INDUSTRIAL CASE STUDY

A CFBC boiler maintenance project was used to compare conventional demolition with hydrojetting.

Table II. Case Study Results

Parameter	Conventional Breaking	Hydrojetting
Area of dismantling	600 sqm	230 sqm
Dismantling Duration	45 Days	10 Days
Tube Dents	800	0
Tube Punctures	200	0
Additional Repair Time	60 Days	0 Days
Equipment Required	23 Breakers/Chippers	1 Hydrojet Unit

Hydrojetting completed the dismantling operation approximately 78% faster while completely eliminating tube damage and subsequent repair activities. The project demonstrated substantial improvements in productivity, safety and outage management.

6. CONCLUSIONS

Hydrojetting technology offers a significant advancement over conventional refractory dismantling methods used in CFBC boiler maintenance.

Key benefits include:

1. Damage-free refractory removal.
2. Complete protection of tubes and anchors.
3. Significant reduction in outage duration.
4. Improved substrate quality for relining.
5. Enhanced worker safety and environmental performance.
6. Lower overall maintenance costs.

Industrial experience confirms that hydrojetting is a reliable, safe and economically attractive solution for refractory dismantling and should be considered the preferred approach for modern CFBC boiler maintenance outages.

ADVANTAGES OF SINGLE-COMPONENT PLASTIC REFRACTORY IN SKID AND POST AREAS OF WALKING BEAM FURNACES

Rishi Mukherjee, Surajit Sarkar, M. Omprakash

CALDERYS INDIA REFRACTORIES LTD

Email: rishi.mukherjee@calderys.com

ABSTRACT

60% Alumina Single component plastic refractory "PLASTIC PRODUCT A" used in the skid and post areas of a walking beam furnace represents a significant advancement over conventional castable and PCPF (precast pre-fired) refractory solution. These zones are subjected to severe mechanical and thermal stresses, including continuous billet/slab movement, impact loading, and rapid temperature fluctuations. In such demanding conditions, plastic refractories provide enhanced durability primarily due to their inherent flexibility. Unlike rigid castable and precast blocks, plastic refractories can absorb mechanical shocks without cracking or spalling, thereby maintaining lining integrity over longer operational cycles. One of the most critical advantages of plastic refractory is the substantial reduction in repair and maintenance time. The material's excellent adhesion properties also ensure strong bonding with existing refractory surfaces, making it particularly effective for patch repairs and localized maintenance. Plastic refractories can also easily conform to complex geometries in skid and post configurations.

Keywords: Plastic Refractory, Walking Beam Furnace, Skid & post, PCPF Block, Furnace Maintenance

1. INTRODUCTION

Walking beam furnaces are widely used in steel plants for reheating billets and slabs prior to rolling. The skid and post areas experience one of the highest level of mechanical load due to continuous movement of hot billet/slab over it. These demanding operating conditions make refractory performance a critical factor in furnace reliability and productivity.

Traditionally, these zones are lined using 70 80% Low cement castable refractories or precast pre-fired blocks. While these materials provide adequate thermal resistance, their rigid structure makes them susceptible to cracking, spalling, and localized damage under impact loading. Maintenance activities are often time consuming, resulting in increased furnace downtime and higher operating costs.

2. Limitations of Conventional Refractory Systems

Castable Refractories

Installation of castable involves several stages, including shuttering, mixing, casting, curing, and controlled dry-out. These activities require significant manpower , precision follow of SOP, dryout cycle and extend maintenance shutdown duration. Castable are extremely rigid and are prone to crack formation under repeated mechanical stresses.

PCPF Blocks

Precast pre-fired blocks provide dimensional accuracy but introduce multiple joints within the lining. These joints often become weak points where flue gas may penetrate and cut the anchors from inside resulting in structural instability. In addition, handling, positioning, anchoring, and alignment of blocks increase maintenance complexity and installation time.

3. Single-Component Plastic Refractory Solution

Usage of “PLASTIC PRODUCT A” ready-to-use softer variety plastic refractory designed for rapid installation and enhanced mechanical durability. Anchors to be welded directly on skid and post. Ceramic blanket is wrapped around the skid posts. “Plastic product A” to be hand rammed by wooden rammers.. Shrinkage cuts are provided for any expansion cushioning. Unlike castable, it does not require water addition, formwork, curing, or extended dry-out schedules. The material can be directly applied by ramming, allowing quick restoration of damaged areas.



Technical Data Sheet:

CHEMICAL ANALYSIS, %

	Range	Typical Value	Test Procedure
Fe2O3	0.8 - 1.4	1.00	IS 12107 Part 6
Al2O3	57 - 61	58.3	IS 12107 Part 3

PHYSICAL PROPERTIES

	Range	Typical Value	Test Procedure
Dry density, g / cc			
after drying at 260°C / 3 hrs	2.10 - 2.40	2.2	IS 10570
CCS, kg/cm2			
after drying at 260°C / 3 hrs	100 - 350	150	IS 10570
after heating at 800°C / 3 hrs	100 - 350	200	IS 10570
after heating at 1550°C / 3 hrs	300 - 650	450	IS 10570
% Retained on 6.3 mm sieve	0 – 5	0.5	IS 1528 Part 14

THERMAL PROPERTIES

	Range	Typical Value	Test Procedure
PLC, %			
After heating at 800°C / 3 hrs	(+0.30) - (-0.30)	- 0.12	IS 10570
After heating at 1550°C / 3 hrs	(+0.50) - (+2.50)	+ 1.80	IS 10570

The plastic nature of the material enables it to absorb impact stresses more effectively than rigid refractory systems. This flexibility helps maintain lining integrity and reduces the likelihood of crack initiation and spalling during service.



Plastic Refractory on Fixed post

4. Technical Advantages

Improved Resistance to Mechanical Shock

Continuous billet movement subjects skid and post linings to repeated impact loading. Plastic refractories absorb these stresses more effectively than castable or precast blocks, resulting in longer service life and reduced maintenance frequency.

Joint-Free Monolithic Structure

Unlike PCPF installations, plastic refractory forms a continuous lining without joints. This eliminates common failure points and reduces thermal leakage, localized wear, and structural instability.

Excellent Adhesion

The material exhibits strong bonding with existing refractory surfaces, making it particularly suitable for localized repairs and patching applications. This property improves repair reliability and reduces the likelihood of premature failure.

Adaptability to Complex Shapes

Skid and post geometries are often difficult to line using rigid precast components. Plastic refractory can be easily shaped to conform to irregular surfaces, ensuring uniform coverage and consistent lining quality.

5. Maintenance and Economic Benefits

The greatest benefit of single-component plastic refractory is the reduction in maintenance time.

Compared with conventional systems single component plastic refractory “PLASTIC PRODUCT A” offers:

- No mixing requirements.
- No shuttering or formwork.
- No curing period.

- Reduced dry-out time.
- Faster application and repair.
- No special skilled personnels needed for application.

These advantages shorten shutdown schedules ,eliminates possibility of human error, and allow furnaces to return to production more quickly. Reduced downtime directly improves plant productivity and lowers overall maintenance costs. Furthermore, the improved durability of the lining reduces repair frequency and extends campaign life.

6. Conclusions

The skid and post areas of walking beam furnaces demand refractory materials capable of withstanding severe mechanical and thermal stresses. Conventional castable and PCPF solutions often face challenges related to cracking, joint failure, and lengthy maintenance procedures. “PLASTIC PRODUCT A” offers the perfect mixture of reliability , structural stability, easy to repair and reduces human error possibilities.

EFFECT OF TAPING TIME ON TAP HOLE CLAY PROPERTIES AND BLAST FURNACE OPERATION

Kuntal M*[1a], Akash G[1b],Morimoto Y[2c], Maruyama K[2d], Bismit G[1e],Sandip S[1f], Ishita D[1g]

[1]Saint-Gobain Performance Ceramics & Refractories,Halol, India
[2]Shinagawa Refra Co. Ltd., Japan

*Corresponding emails: [1a]kuntal.maiti@saint-gobain.com

Abstract

The blast furnace is the most established and efficient route for ironmaking. The tap hole which is located in the lower hearth region of the blast furnace, plays a critical role in the controlled tapping of molten hot metal and slag. Tap hole clay is a vital consumable refractory material that ensures safe, reliable, and stable furnace operation by enabling effective opening and closing of the tap hole. Physical, mechanical properties of tap hole clay and blast furnace's operational condition both can affect the behavior and performance of tap hole clay. Performance Ceramics and Refractories (PCR India), Saint Gobain, India works in a close collaboration with Shinagawa Refra Co. Ltd., Japan on the Tap Hole Clay Technology. PCR India offers tap hole clay with better corrosion resistance of the clay which ensure better taping time and optimized specific consumption of the clay. Reduction in specific consumption not only enhances furnace productivity and operational reliability but also contributes to environmental sustainability by lowering CO_2 emissions and overall carbon footprint associated with ironmaking operations.
This paper focuses mainly on the correlation of tapping time with tap hole clay properties and blast furnace operations. Detailed explanation on the effect of special additive components and the main matrix of Tap Hole clay on slag corrosion resistance with blast furnace operating conditions i.e.rate of production, slag rate, casting practices, raw material characteristics etc. and sustainability by reduction of specific consumptions will be discussed in this paper.

Keywords: Iron making, Tap hole clay, sustainability, additive, blast furnace operation.

1. Introduction

The global steel market size is expected to reach USD 1.92 trillion by 2030[1]. Iron is the major constituent in the Steel production and major manufacturing process of pig iron is through blast furnace. Tap hole plays particularly significant role to maintain blast furnace internal performance and it helps to drain molten metal and slag from blast furnace. Tap hole clay (THC) product needed to close the tap hole after drainage of molten metal and slag. Tap hole clay is a combination of agglomerate and liquid binder. Saint Gobain, India started tap hole clay manufacturing since 2020 along with Shinagawa Refra Co. Ltd. Japan[2]. Saint Gobain - Shinagawa India manufacture customized tap hole clay after detailed analysis of blast furnace cast house practice, cast parameters and furnace operation.
Tapping of blast furnace is essential for safety of blast furnace and safety of coworker at cast house[3]. Blast Furnace operation may run for twenty years with no repairing of the hearth walls and tap hole block as well.Tap hole clay plays role in maintaining the blast furnace operation

which is key to manufacturing molten iron. Tap hole clay should consistently perform for running blast furnace operation safely by ensuring smooth flow when pushed clay to the tap hole by using mudgun to plug the tap hole, cure during pushing into tap hole without shrinkage to ensure tight seal, drilling as per the desired time to open the tap hole, resistance to corrosion and erosion of molten metal and slag and finally maintain a stable and required tap hole length. Tap hole clay properties are important to maintain all those above-mentioned requirements which further depends on blast furnace operation parameters like- liquid level, slag level, hot metal temperature, Gun up to knock out time (GUTKO), casting process, permeability of BF, oxygen enriched blowing[3,4]etc.

Taphole clay consists of oxide refractory materials (corundum or bauxite), ferro-silicon nitride, silicon carbide materials, carbonaceous materials and binders.Taphole clay should have proper workability (plasticity and drillability) and good corrosion/wear resistances to achieve a smooth tapping process. As per blast furnace working environment it is required for taphole clay to withstand prolonged heat exposure and iron/slag attacks.Among all the constituents present in THC, the Nitrides helps to control the porosity and strength which directly effects on changes in tapping time [5].Takashi et.al. has reported that densification of tap hole clay following by (a) reduction of low temperature volatile material in binder and (b) reduction of binder by using ultrafine material[6].Kitamura has reported that carbonaceous materials help to densify tap hole clay and results on improved corrosion resistance by reducing binder content[7].

As per the prior art search, it has been tried to correlate effects of Silicon carbide, Silicon nitride and special additive components to improve cast duration. Apart from composition of tap hole clay in this study it has also been considered effects of furnace operation parameters on tapping duration. Finally it has been related to sustainability with reduction of tap hole clay consumption without affecting the cast iron production quantity. So to produce same quantity of cast iron requirement of tap hole clay is decreasing which reduces the requirement of several raw materials. The decrease of raw material requirement for production of tap hole clay is related to sustainability.

2. Experimental work

Raw materials used are the grains & powders of Al_2O_3, SiO_2, SiC, Fe-Si_3N_4 and different carbonaceous material. For Cast duration improvement different recipe has been designed as mentioned in Table-1. The different grains &powders of required quantities were weighed as per recipe and dry mixed in mixing machine to get homogeneous dry mixture. This homogeneous dry mix kneading was done with binder at 55 - 65^{0}C for several minutes to make various recipes of tap hole clay. The tap hole clay was compacted in the form of rectangular bar having dimensions of 25 mm X 25 mm X 160 mm were prepared by using uniaxial hydraulic press at desired load. After drying for 1 days those rectangular bars were sintered at 1450^{0}C for soaking time of 3 hrs. under a reducing atmosphere. Green density of the sample measured through dimensional changes.

Raw Material (%)	SGS-1	SGS-2
Oxide based Raw Materials	X	X-4
SiC + Si_3N_4	Y	Y+4
C	Z	Z-2
Fines special additive	0	2

Table 1 Composition design of product for cast duration

Linear shrinkages of the samples were measured by using a digital vernier caliper. The density of all the samples was measured following Archimedes principle following standard method of density measurement[8].

Modulus of rupture was measured by following ASTM standard. Corrosion resistance of those sample was measured using dynamic corrosion facility by using inhouse induction furnace at saint gobain, India.

3. Result and discussion

Physical properties

Physical properties	SGS-1	SGS-2
Green Dneisity (gm/cc)	2.29	2.34
AP (%)	26.05	21.89
BD (gm/cc)	1.99	2.08
PLC (%)	+0.92	+1.5
Binder (%)	17.96	15.97

Table -2 Physical properties of different material

Physical properties vary between SGS-1 and SGS-2 sample as mentioned in Table-2. It has been found that porosity decreases in SGS-2 sample compared to SGS-1 sample.

Assuming that decrease in porosity might be due to a reduction in the binder content.Changes on positive permanent linearchange (PLC) were also found in sample SGS-2 than SGS-1.

Mechanical properties:

Properties	SGS-1	SGS-2
CMOR (MPa)	2.7	3.6

Table -3 Mechanical properties of different material

Table 3 shows the mechanical properties of different materials. SGS-2 shows a higherCold Modulus of rupture than of the sample SGS-1 which might be due to lower porosity in the SGS-2 sample [6,7]. During the reducing atmosphere sintering, the inherent phases of different raw materials break and form elevated temperature phases Si_2N_2O and in-situ carbides[5].

Dynamic Corrosion resistance test

Fig.1 is showing the dynamic corrosion facility available at premises of Saint Gobain in India. This dynamic corrosion test facility helps to decide the best product to design for customers. Dynamic corrosion test was conducted using sample bar of SGS-1 and SGS-2 by dipping in molten pig iron and molten slag.

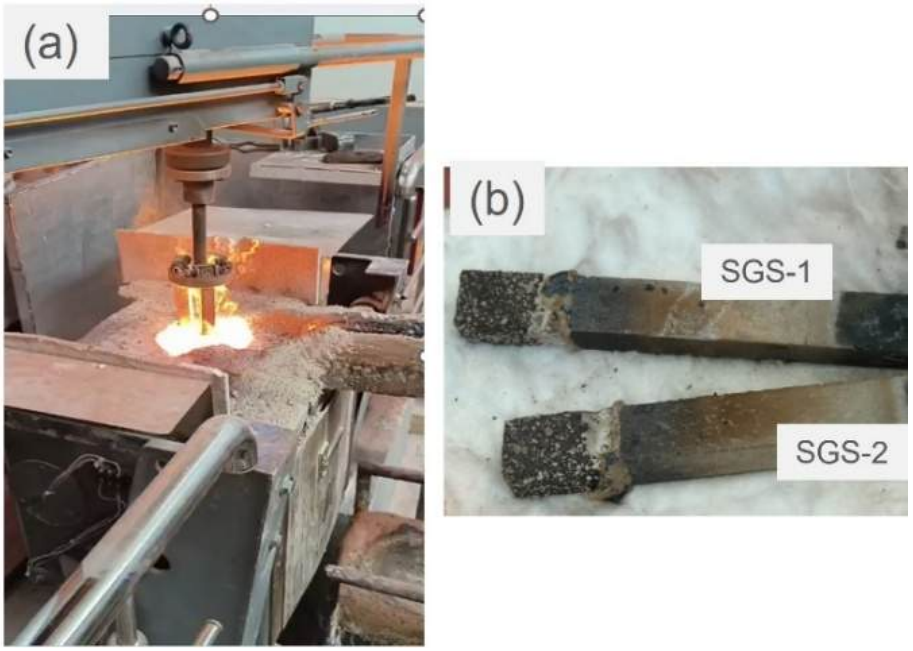


Fig.1 Photograph of (a)Dynamic corrosion test facility @saint Gobain, India and (b) sample after test

SLAG Chemistry (wt%)						
CaO	SiO_2	Al_2O_3	MgO	MnO	FeO	S
38.00	30.74	17.32	10.71	0.14	0.68	0.86

Table -4 Slag chemistry for dynamic corrosion test

Table-4 is showing the slag chemistry which has been used while dynamic corrosion test and pig iron was used with regular chemistry of Pig iron. Quantification of corrosion test has been done by measurement of reduction on thickness of sample. As per dynamic corrosion test, SGS-2 has shown better corrosion resistance than SGS-1.

Product performance @ two tap hole furnace:

	SGS-1	SGS-2
Avg Taphole Length(mtr)	3.80	4.10
Avg tapping time (min)	137	167

Table- 5 Performance details of SGS-1 and SGS-2.

Table 5 shows the performance of SGS-1 and SGS-2 at customer place. SGS-2 product has shown better tapping time than the SGS-1 sample. It is assumed that formation of in-situ carbides increases the corrosion resistance and mechanical strength of tap hole clay.

Furnace operation parameters and cast duration of tap hole clay

Blast furnace operation includes chemical reduction and physical conversion of iron oxides into liquid iron or hot metal. Smooth tapping of molten metal from blast furnace is dependent on tap hole clay properties and several furnace operation parameters. Blast furnace operating conditions i.e., liquid level, production and slag rate, casting practices, raw material characteristics etc. are affecting on cast duration. Productivity of blast furnace is dependent on smooth drainage of the molten material which ensure periodic taping of hot metal and slag from hearth[9].

Liquid level

In blast furnace iron ore, coke and limestone are dumped into the top, and preheated air is blown into the bottom. The raw materials require 6 to 8 hours to descend to the bottom of the furnace where they become the final product of liquid slag and liquid iron[10]. The said tapping interval allows for some accumulation of liquids in the hearth, resulting in a good length of tap when the taphole is opened. If the taphole is opened too quickly, the tap will be too short and result in increased cleaning work on the tap-floor as well as heat losses in the trough. This can then result in an unwanted increase in tap-to-tap time.

With changes in liquid level in blast furnace,taping time of casting changes with parameters like drill bit, tap hole length, casting process, slag rate etc. as described in below,

Drill Bit Dia

Drill bit Dia is related to tapping time. If drill bit diameter is less then tapping time increases (irrespective of tap hole clay properties). Drill bit used to open the taphole, and the choice of drill bit size is highly dependent on the iron production rate in the furnace [3]. When furnace operates with high production rate then it is required that the hearth to be drained of its accumulated liquid iron and slag content as quick to avoid any instabilities. The bigger the drill bit size used to open the tap hole, the faster the hearth will be drained[3].

Tap Hole Length

Tap hole length depends on clay's physical/mechanical properties and cast house practice of blast furnace. The length depends on mud gun capabilities, clay green strength, the amount of clay pushed into tap hole during closing of earlier cast. If tap hole length is short, then hearth carbon brick wall will erode in faster rate. In other hand too long tap hole is also not desirable which may take more time to open the tap hole and oxygen lancing, poking etc. may be needed. The long-optimized tap hole changes the height between tap hole and metal/slag interface which related to tapping time[3]. The hearth liquids exert an upward force to the deadman coke, and this force causes

disturbance in internal pressure and erratic burden descent and stability of deadman changes the Tap hole length.

Casting Practice

Casting practice in blast furnace is known as the process of opening the tap hole then drainage the hot metal/slag and closing the tap hole. Control casting practice is related to maintaining the metal level in the hearth of blast furnace. Non dry and dry closing is related to tapping time. Non dry closing indicates while blow is not found during casting and the tap is closed which results lower tapping time. While furnace is dry (the hearth is empty) and tap hole is still open it allows the high pressurized tuyere's gas to come out through the tap hole which results in erosion of tap hole clay. The cast tracking chart shown in Fig.2 has taken from the reference journal [11]

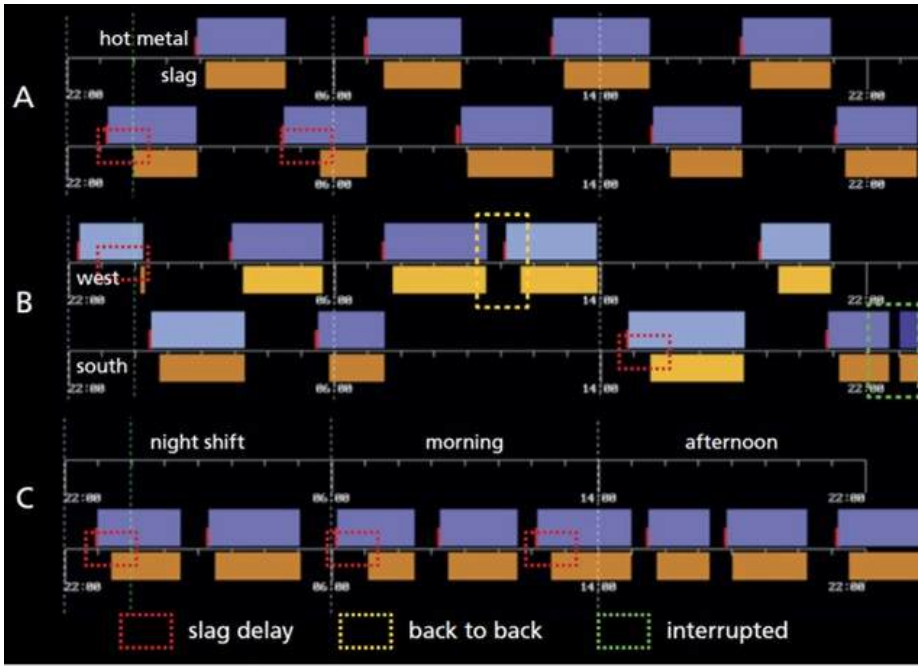


Fig.2 Photograph of Cast tracking charts[11]

Fig.2 shows the cast practice of a two-tap hole furnace with 24-hour overview. In Fig.2 A, B and C is shown as below,
A- represent a day of good casting,
B. represent a day with some problems,
C. shows a day of single taphole operation with slag delays on nearly every cast.

Slag rate and raw material

Formation of slag during iron making depends on raw material being used in blast furnace. Raw material for iron making in blast furnace are iron ore (iron oxide), coke, flux. Iron oxides can come to the blast furnace plant in the form of raw ore, pellets or sinter. This ore is either Hematite (Fe_2O_3) or Magnetite (Fe_3O_4) and the iron content ranges from 50% to 70%. So, it is expecting if iron content is less, then gangue material will be more which quantify as slag formation will be more. Coke is manufactured from coal and flux is from earth crust so purity of coke and flux also responsible for slag formation.

If slag formation is more then there will be more chance of slag corrosion with tap hole clay which results changes in tapping time. Adverse slag composition directly corrodes tap hole clay and reduces the tapping time.

Sustainability on reduction of tap hole clay consumption

As per performance of SGS-2 product mentioned in Table-5, the casting duration has increased by 20% which reduces the number of castingswhich resultsreduction of the consumption of tap hole clay to close the tap.

Metal production target per day (mt)	10000
Cast rate (t/min)	5
Time required to achieve material production/day(min)	2000
Average cast duration with regular clay (min)	137
Average cast duration with modified clay (min)	167
Number of cast requiredto achieve 10000 mt/day, by using regular tap hole clay material	14.6
Number of cast required to achieve 10000 mt/dayby using modified tap hole clay material	12

Table 6: Typical clay consumption calculation to achieve target of per day material production

Tap hole clay constituents several raw materialsto maintain the required properties while closing and opening of tap hole. As per table-1, improvement of tapping time decreases the number of cast to achieve per day material production per day. Reduction of tap hole clay consumption reduces the raw material uses. Raw material synthesis is lengthy process which required energy and earth crust. Raw material extraction from mines requires heavy machinery and vast amounts of energy, which releasesenormous amounts of greenhouse gases[12].

4. Conclusions

This worksshowed that a combination of SiC, Silicon nitride andfine special additives particle material shows desired properties to get better tapping time. The tap hole clay material consumption contributeson sustainability. The followings are the conclusions of this study,

1. Compositional changes in SGS-2 shows better densification properties than SGS-1 sample.
2. Reduction of binder in SGS-2 reduces the volatile material and reduces the porosity in the product, which resultsin better tapping time.
3. Drill bit is related to tapping time
4. Non dry and dry closing is related to tapping time
5. Tapping timereduces the tap hole clay material consumption which is related to sustainability.

5. References

1. https://www.grandviewresearch.com/press-release/global-steel-market.
2. https://www.shinagawa.co.jp/en/pdf/20210415SGSRE.pdf
3. P.G. Geyer and Z. Halifa, “Blast furnace tapping practice at ArcelorMittal South Africa, Vanderbilt park Works”, The Southern African Institute of

Mining and Metallurgy. Furnace Tapping Conference 2014.
4. S. Chew, P. Zulli, P. Austin, J. Mathieson and A. Yu: ISS Ironmaking Conf. Proc., 60, 242–252,2001.
5. Chih-ying liu, Ching-heng shao and Chen-yi chiu, “Effect of Ferro-Silicon Nitride Addition on Taphole Clay” China Steel Technical Report, No. 34, pp 40 to 45, 2021.
6. Takashi Matsunaga, Minoru Kataoka and Ichiro Takita “Densification of Taphole Clay for Blast Furnace”, Taikabutsu /Volume 55, Issue 8,Article overview,2003.
7. Kitamura, Masatsugu, “Study of the high-density taphole mat materials for blast furnace”, Taikabutsu, 53(2), 94-95,2001.
8. Kuntal Maiti, Anjan Sil, “Microstructural relationship with fracture toughness of undoped and rare earths (Y, La) doped Al2O3–ZrO2 ceramic composites”, Ceramics International 37, 2411–2421,2011.
9. Smruti Rekha Dash, “Development of improved tap hole clay for blast furnace tap hole”, Master thesis, 2009.
10. Baidya Nath Roy and Uddeshya Kumar, “Studies on influence of liquid level on blast furnace performance and monitoring of hearth drainage”, International Journal of Latest Trends in Engineering and Technology, Vol.(8) Issue(1), pp.051-057.
11. Rénard Chaigneau, Oscar Lingiardi, Maarten Geerdes, Ivan Kurunov, John Ricketts, “Modern Blast Furnace Ironmaking: An Introduction”, IOS Press, 2015.
12. https://www.eea.europa.eu/en/topics/in-depth/resource-use-and-materials

NON-WETTING CASTABLES FOR ALUMINIUM FURNACES: CORROSION RESISTANCE AND CRYOLITE STABILITY

M. Sathiyakumar*, M. Rajasekhar Reddy, R. Sugumar, S. Sumitha and G. Manari

Totale Global Private Limited, Sriperumbudur – 602 105, Tamil Nadu, INDIA

sathiyakumar@pincgroup.com

Abstract

Refractory linings in aluminium melting and holding furnaces are subject to severe degradation from molten alloy penetration, cryolite attack, and interfacial reactions. These mechanisms shorten furnace campaign life, compromise alloy purity, and increase operational costs. To address these challenges, Totale Global Private Limited (TGPL) has developed advanced non-wetting castables engineered for aluminium industry applications. The flagship products, Tricast NW-AL and its series, were evaluated under static cup testing with Al7075 alloy at 1000°C for 100 hours. The results demonstrated complete resistance to penetration and erosion, confirming their effectiveness in suppressing interfacial reactions between molten aluminium and refractory phases. Complementary cryolite resistance testing, conducted with a Na_3AlF_6–NaF mixture at 950°C for 24 hours, further validated the structural integrity of TGPL's formulations. No signs of melting, deformation, or mechanical strength loss were observed, underscoring their suitability for aggressive electrolytic and pot room environments. The incorporation of non-wetting additives enhances corrosion resistance by promoting the formation of stable interfacial phases such as corundum, celsian, and spinel. These phases act as dense, chemically inert barriers that block molten aluminium and cryolite penetration. Specifically, Phosphate-based additives facilitate in situ corundum generation at the refractory–metal interface, a phase noted for its high thermodynamic stability against Al alloys. In contrast, Ba-based systems react with aluminosilicate matrices to form celsian, which reduces porosity and suppresses diffusion pathways for Mg and Si, thereby limiting alloy–refractory reactions. Spinel formation at interfaces further stabilizes the microstructure under aggressive Mg-containing alloys. TGPL's experimental results confirm that these mechanisms are active in its non-wetting castables. The synergy of corundum, celsian, and spinel formation ensures dense, stable interfacial layers that resist molten aluminium and cryolite attack while minimizing contamination of the alloy by dissolved refractory elements. In addition, TGPL has introduced hot-patch repair materials for sill areas of reverberatory furnaces, which bond effectively with existing linings at 600–800°C, enabling rapid in-situ restoration without extensive downtime. Together, TGPL's non-wetting castables and hot-patch solutions provide a practical pathway for extending furnace campaign life, reducing downtime, and safeguarding alloy quality. By integrating proven non-wetting mechanisms with industrially validated formulations, TGPL advances refractory technology for non-ferrous industries, contributing to more sustainable and cost-efficient aluminium production.

Keywords: Non-wetting castables; Aluminium furnaces; Corrosion resistance; Cryolite stability; non-wetting additives; Celsian phases; Spinel formation

1. Introduction

Refractory linings in primary and secondary aluminium melting and holding furnaces are subjected to some of the harshest operating conditions in the non-ferrous industry. Molten aluminium alloys are highly reducing and readily attack conventional refractory oxides, particularly silica (SiO_2), resulting in the formation of corundum (α-Al_2O_3) layers that expand, crack, and ultimately destroy the lining [1]. In addition, exposure to fluxing agents and aggressive electrolytic species such as cryolite mixtures destabilizes the refractory structure, leading to rapid penetration, chemical erosion, and premature failure [2]. These degradation mechanisms significantly shorten furnace campaign life, compromise alloy purity, and increase operational downtime.

To mitigate molten metal infiltration, non-wetting technology relies on altering the contact angle between the liquid alloy and the refractory substrate. Over the years, several non-wetting additives have been investigated.

Phosphate-based additives promote in-situ corundum formation at the refractory–metal interface, providing a stable barrier against liquid metal reduction [3]. Barium-based systems react with aluminosilicate matrices to synthesize celsian phases ($BaAl_2Si_2O_8$), which reduce open porosity and suppress diffusion pathways for magnesium (Mg) and silicon (Si) [4]. Spinel formation at interfaces further stabilizes the microstructure under aggressive Mg-containing alloys [5].

Despite these technical advances, widespread industrial adoption has been limited by inconsistent field performance and concerns regarding mechanical strength degradation. To overcome these limitations, Totale Global Private Limited (TGPL) has engineered the TRICAST NW-AL series. This study presents the design philosophy, experimental evaluation, and performance results of these castables alongside in-situ hot-patch repair formulations tailored for reverberatory furnace maintenance.

2. Castable and matrix design

The design of high-performance non-wetting castables requires a careful structural balance between high alumina content for refractoriness and the precise integration of active non-wetting additives. The TRICAST NW-AL series utilizes Calcined Bauxite and Fused Corundum aggregates to establish a rigid skeletal backbone capable of enduring high thermal stress. A low to ultra-low cement hydraulic bonding system was selected to minimize lime (CaO) content, thereby avoiding the development of low-melting glassy phases at operating temperatures [6].

The fine reactive matrix was engineered using reactive alumina and micro-silica powders to maximize particle packing density and achieve low open porosity [7]. Non-wetting agents such as phosphate-based additives, bi-phase systems, and barium-containing compounds were incorporated directly into the matrix mix. Upon exposure to service temperatures, these precursors react with the matrix to synthesize in-situ corundum and celsian barrier phases. Additionally, the fine matrix chemistry was tailored so that localized $MgAl_2O_4$ spinel formation occurs automatically when contacting Mg-bearing alloys [3-5]. By combining these complementary phase-formation mechanisms, the refractory develops a self-sealing interfacial barrier that resists both molten alloy infiltration and fluoride salt attack while retaining high mechanical strength

.

3. Experimental details

3.1 Material Formulations and Interfacial Phase Engineering:

Two primary Low to Ultra Low Cement Castable (LCC/ULCC) formulations were produced via vibro-casting using a water demand of 4.50–6.00%:

• **TRICAST NW-AL:** 78% Al_2O_3 nominal content, featuring a Calcined Bauxite aggregate base with targeted non-wetting matrix additives.

• **TRICAST NW-85AL:** 86% Al_2O_3 nominal content, utilizing a Corundum-rich aggregate matrix designed for higher thermal loads.

The core mechanism preventing molten metal penetration in both grades relies on thermally induced phase transformations. "Phosphate-based additives promote in-situ corundum (Al_2O_3) synthesis directly at the refractory–metal contact zone, creating a thermodynamically stable layer against liquid aluminium reduction. Simultaneously, bi-phasic and barium-based additives react with fine matrix silicates at operating temperatures to synthesize celsian ($BaAl_2Si_2O_8$). The formation of celsian densifies the matrix, closes micro-pores, and restricts the inward diffusion of reactive Mg and Si atoms. Spinel-forming additives further encourage localized $MgAl_2O_4$ formation during contact with Al7000-series alloys, preventing localized cratering.

2.2 Corrosion and Cryolite Stability Testing Methods

Castable specimens were vibro-cast into test moulds, cured, dried at 110°C, and pre-fired between 800°C and 1200°C prior to characterization. Performance was evaluated using three distinct corrosion and physical testing protocols:

2.2.1 Static Cup Corrosion Test (Al7075 Alloy)

Castable cup specimens were filled with high-strength Al7075 alloy and held in a furnace at 1000°C for 100 hours to evaluate molten metal penetration and chemical wall erosion.

2.2.2 Cryolite Corrosion Resistance Test

Refractory crucibles were loaded with a synthetic fluoride salt mixture consisting of Na_3AlF_6–NaF (60:40 ratio) and heated to 950°C for 24 hours to simulate electrolytic pot room conditions.

2.2.3 Pure Aluminium Immersion Test

Samples were immersed in liquid pure aluminium at 800°C for 72 hours to confirm baseline metal-contact stability.

2.2.4 Hot-Patch Repair Evaluation

Specialized sill repair formulations were applied directly onto pre-heated refractory substrates at 600–800°C to assess thermal bonding, curing behaviour, and jointless adherence [8].

4. Results and discussion

4.1 Physical Properties and Mechanical Strengths

The physical and mechanical characteristics of the pre-fired castables are summarized below:

Table 1. Physical and Mechanical Properties of TRICAST NW-AL, TRICAST NW-85AL, and Topcrete Alpatch Castables

Properties	Tricast NW-AL	Tricast NW-85AL	Topcrete Alpatch (Hot repair)
Al_2O_3 (%)	76.83	86.15	50.89
Fe_2O_3 (%)	1.25	0.41	0.89
Physical Properties			
BD (g/cc) @110°C/24 hrs	2.95	3.05	
CCS (N/mm2)			
110°C/24 hrs	75.32	83.24	
800°C/3 hrs		95.19	75.2
1000°C/3 hrs	100.21		
1200°C/3 hrs	123.81	106.24	
Thermal Properties			
PLC (%)			
800°C/3 hrs		-0.12	-0.22
1000°C/3 hrs	-0.20		
1200°C/3 hrs	-0.25	-0.22	
Al7075 Corrosion Test 1000°C/100 hrs	Complete resistance (Zero penetration)		-
Cryolite Resistance Test 950°C/24 h	No melting, deformation, or strength loss		-

These products exhibited low permanent linear change (PLC) values, indicating exceptional dimensional stability under severe thermal cycling.

3.1 Resistance to Molten Al7075 Alloy Penetration

In standard aluminosilicate linings, molten metal contact drives silica reduction reactions ($3SiO_2 + 4Al \rightarrow 2Al_2O_3 + 3Si$), causing destructive volumetric expansion.

During static cup testing with aggressive Al7075 alloy at 1000°C for 100 hours, both TRICAST NW-AL and TRICAST NW-85AL exhibited zero metal penetration and complete protection against wall erosion [9]. Post test cross-sectioning confirmed clean alloy release without metal adherence or chemical degradation of the underlying refractory matrix. Chemical analysis of the post-test alloy confirmed stable composition without contamination from dissolved refractory elements [10].

Table 2. Chemical Composition of Al7075 Alloy Before and After Static Cup Corrosion Testing

Alloy	Mg	Si	Fe	Cu	Mn	Cr	Zn	Ti	Al
Before	2.900	0.410	0.500	1.860	0.301	0.279	5.610	0.201	87.010
After	2.896	0.410	0.499	1.857	0.301	0.277	5.610	0.200	87.009

Under cryolite salt testing (Na_3AlF_6–NaF) at 950 °C for 24 hours, the castables retained complete structural integrity. In contrast to conventional CaF_2 or AlF_3 non-wetting systems, which often suffer strength degradation or emit toxic fluorine gas, TGPL's celsian–spinel matrix effectively blocked fluoride salt infiltration into internal pores [2]. The test crucibles exhibited no melting, softening, or loss of mechanical strength. Subsequent immersion in pure aluminium at 800 °C for 72 hours further confirmed long-term interfacial stability.



Figure 1 (a-b). Cross Section of TRICAST NW-AL Specimen After 100 Hours at 1000 °C

Table 3. Refractory–Metal Interface Reaction Pathways for Non-Wetting Additives

$AlPO_4$ Addition	In-situ Corundum Generation	High Thermodynamic Stability
Barium System	Celsian Phase Formation	Porosity Reduction & Diffusion Barrier
Spinel Precursors	$MgAl_2O_4$ Spinel Formation	Resistance to Mg/Si Infiltration



Figure 2. Cryolite Corrosion Resistance Test Crucibles After 24 Hours at 950 °C

4.3 Industrial Hot-Patch Repair Solutions

Mechanical wear and thermal impact at furnace sills, ramps, and door jambs often lead to frequent operational shutdowns. TGPL's hot-patch repair materials provide rapid, high-strength bonding directly to hot existing linings between 600°C and 800 °C, enabling effective in-situ maintenance without requiring full furnace shutdown or cool-down cycles. Topcrete Alpatch products are specifically engineered for rapid firing under hot conditions, delivering high strength and exceptional resistance to thermal shock. Their unique binder system ensures precise mixing, controlled setting, quick drying and heating, and reliable thermal shock resistance, making them ideally suited for patching applications in demanding high-temperature environments.



Figure 4. In-Situ Application of Hot-Patch Repair Material on Operating Aluminium Furnace Sill at 700 °C

6. Conclusion

The experimental evaluation confirms that Totale Global Private Limited's TRICAST NW-AL non-wetting castable series provides an exceptional defense mechanism against the principal degradation vectors in aluminium processing. Under static cup corrosion testing with aggressive Al7075 alloy at 1000°C for 100 hours, the material demonstrated complete resistance to alloy penetration and interfacial erosion,

successfully preventing metal adherence and destructive corundum buildup. Furthermore, exposure to synthetic cryolite salt mixtures (Na_3AlF_6–NaF) at 950°C for 24 hours produced no evidence of melting, volumetric deformation, or mechanical strength loss, proving its durability in aggressive pot room and electrolytic environments.

This high level of corrosion and cryolite resistance is directly driven by targeted interfacial phase engineering within the castable's fine matrix. The synergistic incorporation of phosphate-based additives, barium-containing compounds, and spinel precursors facilitates the in-situ formation of dense corundum, celsian, and spinel phases during thermal operation. These microstructural phases act as inert, highly stable barriers that seal open porosity and block diffusion pathways for reactive alloying elements such as magnesium and silicon. Complemented by hot-patch repair materials that bond effectively onto hot substrates at 600–800°C, this non-wetting castable technology offers an industrially validated solution for rapid in-situ maintenance, extending furnace campaign life while safeguarding melt purity.

References

1. Afshar, S., Allaire, C., "Corrosion Resistance of Aluminosilicate Refractories to Molten Aluminium," Journal of Materials Science, Vol. 36, 2001, pp. 91–99.

2. Siljan, O. J., et al., "Refractories for Aluminium Electrolysis Cells and Melting Furnaces," Light Metals, TMS, 2002.

3. Adabi-Firoozjaei, E., Koshy, P., Sorrell, C. C., "Effects of AlPO4 addition on corrosion resistance of andalusite LCC refractories," Journal of the European Ceramic Society, Vol. 33, 2013, pp. 1067–1075.

4. Shukla, D. P., "Antiwetting additives for aluminosilicate refractories in molten aluminium contact applications," PhD Thesis, Missouri University of Science and Technology, 2009.

5. Adabi-Firoozjaei, E., Koshy, P., Sorrell, C. C., "Assessment of nonwetting materials for aluminium melting furnaces," Journal of the Australian Ceramic Society, Vol. 51, 2015, pp. 139–145.

6. Engel, R., "Refractory considerations for aluminium melting and holding furnaces," The Refractories Engineer, January 2015.

7. Wynn, A., Coppack, J., Steele, T., "Methods of assessing monolithic refractories for aluminium melt-hold furnaces," Aluminium International Today, May/June 2014.

8. WO2013184230A1, "High-temperature nonwetting refractory additive system," World Intellectual Property Organization, 2013.

9. Afshar, S., Allaire, C., "Corrosion Resistance of Aluminosilicate Refractories to Molten Aluminium," Journal of Materials Science, Vol. 36, 2001, pp. 91–99.

10. Allaire, C., "Refractory Linings for Aluminium Holding and Melting Furnaces," Refractories World Forum, Vol. 4, 2012, pp. 65–72.

HYBRID BOND CASTABLES FOR LADLE LININGS: ENHANCED SLAG RESISTANCE AND SERVICE LIFE

M. Sathiyakumar*, M. Rajasekhar Reddy, R. Sugumar, S. Sumitha and G. Manari

Totale Global Private Limited, Sriperumbudur – 602 105, Tamil Nadu, INDIA

sathiyakumar@pincgroup.com

Abstract

Foundry ladles are exposed to severe thermal cycling, slag attack, and mechanical abrasion, which accelerate lining wear and compromise molten metal quality. Conventional low-cement castables (LCCs), though widely used, suffer from residual CaO content that promotes slag adhesion, microcracking, and reduced hot strength. To overcome these limitations, Totale Global Private Limited (TGPL) has developed a Hybrid Bond Castable system (Tricast Hybrid M-Sol and its series), integrating nano bond gel technology with cement-free formulations to deliver superior durability and reliability in foundry ladle applications.

In comparative case studies, the hybrid-bond series was installed as a replacement for LCC-based ladle castables. The new system exhibited a denser microstructure with lower porosity, resulting in significantly improved slag resistance. Operational observations recorded approximately 30–35% less slag sticking than conventional LCC linings. This reduction minimized peeling and abrasion, while the smoother ladle surface enhanced molten metal flow during pouring, reducing turbulence and slag carryover [8].

At the microstructural level, the hybrid bond system utilizes colloidal silica gel networks (Si–O–Si bonding) to eliminate free CaO phases, while nano bonding improves particle packing and interfacial cohesion. The absence of excess CaO reduces vulnerability to alkali and slag attack, and the gel-bonded matrix provides superior thermal shock resistance and abrasion toughness. Laboratory evaluations demonstrated higher green strength, safer dry-out behaviour with minimal explosive spalling, and improved hot modulus of rupture (HMOR) retention under thermal cycling compared to LCCs.

The improved lining performance extended ladle campaign life, reduced downtime, and lowered lifecycle costs by minimizing repair frequency. These outcomes align with global advancements in hybrid refractory technologies, where combining gel bonding with optimized aggregates enhances slag resistance, thermal stability, and mechanical reliability.

In conclusion, TGPL's hybrid-bond castable technology represents a next-generation refractory solution for foundry ladles. By integrating nano bond gel chemistry with a cement-free design, it delivers enhanced slag resistance, smoother metal flow, and extended service life, contributing to more sustainable and cost-efficient non-ferrous foundry operations.

This manuscript presents the design, properties, and industrial validation of three colloidal silica bonded castables developed by Totale Global Private Limited: Tricast Hybrid M-Sol for treatment ladles, Tricast Hybrid RDC for EAF roof delta in-situ castables, and Tricast Hybrid T-Sol for tundish and launder systems. Laboratory evaluation and industrial trials confirm superior drying behaviour, high hot strength, and extended campaign life compared to conventional CAC-bonded systems.

Keywords: Hybrid bond castables; Foundry ladles; Nano-gel bonding technology; Colloidal silica; Slag resistance; Thermal shock resistance; Abrasion resistance; Extended service life

1. Introduction

Calcium aluminate cement (CAC) has long been the binder of choice for monolithic refractories [1]. However, its drawbacks are well documented: the formation of low-melting calcium silicate/aluminate phases (e.g., Gehlenite C_2AS, melting point ~1590°C; Anorthite CAS_2, melting point ~1553°C), poor resistance to thermal shock, and risks of explosive spalling during [2] initial drying due to rapid dehydration of bound hydrate phases (CAH_{10}, C_2AH_8, and C_3AH_6). These limitations are particularly severe in high-temperature steelmaking and foundry environments where microsilica and magnesia are present [3].

Colloidal silica binders offer a fundamentally different approach. They consist of nanosized SiO_2 particles (typically 10–30 nm) suspended in water, typically 40% solids [4]. Upon drying, chemical gelling via hydroxyl condensation (Si–OH + HO–Si➔Si–O–Si + H_2O) forms a rigid 3D silica gel network that provides continuous nano-porosity and safe, rapid drying. At elevated temperatures, the active silica reacts solid-state with fine alumina matrices to form in-situ mullite ($3Al_2O_3.2SiO_2$) and corundum (α-Al_2O_3), phases that impart high mechanical strength and exceptional slag corrosion resistance [5]:

The total absence of CaO eliminates liquid phase formation at operational temperatures (1400–1600°C) and completely avoids CaO-induced contamination risks in clean steel production.

This paper presents the design philosophy, laboratory evaluation, and industrial validation of three colloidal silica bonded castables tailored for specific steel industry applications: Tricast Hybrid M-Sol for treatment ladles, Tricast Hybrid RDC for EAF roof delta sections, and Tricast Hybrid T-Sol for tundish and launder systems.

2. Castable and Matrix Design with Interfacial Phase Engineering

The performance of colloidal silica bonded castables depends not only on the binder chemistry but also on the aggregate skeleton, fine matrix design, and the phases formed at the aggregate–matrix interface. Particle size distribution (PSD) was optimized according to the modified Andreasen packing model (q = 0.21–0.25) to maximize green density and minimize water demand [6]. Each formulation was tailored to balance density, hot strength, and thermal shock resistance for its specific application:

M-Sol (Treatment Ladle):

Sintered high purity -Al_2O_3 aggregates and aluminosilicate refractory aggregates provide thermal shock resistance and mechanical strength. The fine matrix of reactive alumina and microsilica, bonded with colloidal silica sol, ensures high permeability and safe drying. Negative Permanent Linear Change (PLC) values confirm controlled densification and dimensional stability under repeated heating and cooling cycles.

RDC (EAF Roof Delta):

High-alumina aggregates with controlled particle size distribution resist electrode radiation, arc thermal spikes, and slag washing. The matrix promotes corundum phase formation, improving hot strength and slag resistance. A slight positive PLC at 1400–1500°C indicates controlled expansion, accommodating complex thermomechanical stresses in roof delta service.

T-Sol (Tundish/Launder):

A dense sintered high purity -Al_2O_3 aggregates system with ~90% alumina content provides a high-rigidity skeleton that resists liquid steel/slag penetration. The fine matrix densifies around sintered high purity -Al_2O_3 aggregate grains, ensuring dimensional

stability and corrosion resistance at the steel/slag interface.

Binder System & Microstructural Kinetics:

Colloidal silica sol acts as the chemical binder across all three products. During low-temperature drying (110°C), silanol groups (Si-OH) condense into a permeable siloxane (Si-O-Si) gel network that allows steam vapor passage without build-up of explosive internal vapor pressure. At service temperatures, this reactive silica network undergoes solid-state sintering with fine Al_2O_3 particles, forming an interlocking micro-mullite network that locks the coarse aggregate grains.

Interfacial Phase Engineering:

Interfaces between aggregate and matrix are chemically engineered through in-situ mullite and corundum crystallization. This eliminates weak grain boundary zones, enhances stress transfer, and provides exceptional resistance to thermal fatigue and slag corrosion. Each product achieves a tailored balance:

- M-Sol: Mullite-rich interfaces for high thermal shock resistance and crack deflection.
- RDC: Corundum-rich interfaces for maximum hot strength under intense heat flux and electrode radiation.
- T-Sol: Dense -alumina interfaces for high corrosion and erosion resistance at the steel/slag boundary [8].

4. Results and discussion

4.1 Physical Properties and Mechanical Strengths

The physical and mechanical properties of the three colloidal silica bonded castables — Tricast Hybrid M-Sol, Tricast Hybrid T-Sol, and Tricast Hybrid RDC — are summarized in Table 1. Laboratory evaluations confirmed distinct performance characteristics for each system.

Table 1. Physical and Mechanical Properties of TRICAST HYBRID M-SOL, TRICAST HYBRID T-SOL, and TRICAST HYBRID RDC

Properties	TRICAST HYBRID M SOL	TRICAST HYBRID T-SOL	TRICAST HYBRID RDC
Al_2O_3 (%)	64.01	90.65	88.29
Fe_2O_3 (%)	0.71	0.32	0.36
Physical Properties			
BD (g/cc) @110°C/24 hrs	2.51	3.03	2.93
CCS (N/mm2)			
110°C/24 hrs	45.06	56.78	46.50

800°C/3 hrs		61.31	
1000°C/3 hrs	67.37	94.18	91.56
1100°C/3 hrs		120.00	
1200°C/3 hrs	91.68		78.12
1400°C/3 hrs	99.00	130.56	97.56
1500°C/3 hrs	99.81	117.00	85.00
1600°C/3 hrs		125.00	
Thermal Properties			
PLC (%)			
800°C/3 hrs	-0.20	+0.12	0.00
1000°C/3 hrs	-0.12	-0.12	0.00
1100°C/3 hrs		-0.18	
1200°C/3 hrs	-0.18		-0.12
1400°C/3 hrs		-0.37	+0.12
1500°C/3 hrs	-0.12	-0.12	+0.06
1600°C/3 hrs		-0.18	

The results highlight the distinct performance characteristics of each colloidal silica bonded system, reflecting their tailored design for specific applications.

3.1 Tricast Hybrid M-Sol (Treatment/Foundry Ladle)

M-Sol demonstrates balanced alumina content (~64%) with a bulk density of 2.51 g/cc. CCS values rise progressively from 45.06 N/mm^2 at 110°C to nearly 100 N/mm^2 at 1400–1500°C, showing steady strength development as mullite phases form in the matrix. Negative PLC values (-0.20% to -0.12%) confirm controlled shrinkage and matrix densification, which are critical for dimensional stability under repeated thermal cycling. This behaviour ensures that ladle linings resist spalling and maintain joint integrity during successive heats [9].

Trial orders for M-Sol have been secured with a performance guarantee of extending ladle campaign life by 1.52 times compared to conventional CAC-bonded systems, along with reduced patching frequency [8]. The safe drying behaviour, attributed to the highly permeable 3D silica gel network, is expected to minimize explosive spalling [4, 7] during rapid heat-up installation. The combination of mullite-rich interfaces and controlled shrinkage positions M-Sol as a particularly effective solution for foundry ladles where thermal shock and slag attack [5] are severe.

3.2 Tricast Hybrid T-Sol (Tundish/Launder)

T-Sol, with very high alumina content (~90.65%), exhibits superior mechanical strength. Bulk density of 3.03 g/cc indicates a dense, highly packed microstructure, while CCS increases from 56.78 N/mm^2 at 110°C to 130.56 N/mm^2 at 1400°C, reflecting excellent

hot strength. PLC values remain low (-0.12% to -0.37%), confirming dimensional stability even under prolonged thermal exposure.

The Sintered High-Purity -Al_2O_3 skeleton bonded with colloidal silica provides exceptional resistance at the steel/slag interface. Industrial validation showed that tundish and launder linings made with T-Sol maintained smooth metal flow, reduced turbulence, and minimized slag carryover. The dense alumina interfaces resist slag penetration, while the mullite-corundum matrix ensures high corrosion resistance. This makes T-Sol particularly suited for continuous casting operations where interface stability and slag control are critical.

3.3 Tricast Hybrid RDC (EAF Roof Delta)

RDC, formulated with ~88% alumina, shows CCS values of 46.50 N/mm^2 at 110°C, increasing to 97.56 N/mm^2 at 1400°C. Bulk density of 2.93 g/cc supports adequate structural integrity. PLC values are close to zero, with slight controlled expansion (+0.12% at 1400°C and +0.06% at 1500°C), which is optimal for in-situ roof delta castables exposed to extreme thermal gradients.

The colloidal silica binder ensures safe drying and open permeability, reducing the risk of explosive spalling during quick installation shutdowns. Industrial trials confirmed RDC's ability to withstand electrode radiation and slag washing, maintaining roof delta stability over extended campaigns [8]. The slight positive PLC at high temperature provides tight sealing and accommodates thermomechanical stress without structural spalling.

3.4 Comparative Insights and Technical Interpretation

The comparative evaluation of Tricast Hybrid M-Sol, T-Sol, and RDC highlights both their individual strengths and the common advantages of colloidal silica bonded systems. Each formulation demonstrates a distinct balance of mechanical strength, dimensional stability, and industrial suitability, reflecting the deliberate design of aggregate skeletons, fine matrix chemistry, and binder integration.

In terms of strength development, T-Sol exhibits the highest hot strength due to its high alumina content and Sintered High-Purity -Al_2O_3 aggregate system, achieving CCS values above 120 N/mm^2 at elevated temperatures. This makes it particularly effective in tundish and launder applications where interface stability and slag resistance are critical. M-Sol shows balanced strength development, combining progressive CCS increase with thermal shock resistance, which is essential for ladle linings exposed to repeated heating and cooling cycles. RDC provides adequate hot strength tailored for roof delta service, maintaining structural integrity under severe thermal gradients and mechanical stresses.

Dimensional stability is another key differentiator. Negative PLC values in M-Sol and T-Sol confirm shrinkage and matrix densification, which are beneficial for tight linings and help maintain dimensional control during service. In contrast, RDC shows slight expansion at 1400–1500°C, a controlled behaviour that helps accommodate thermal stresses in roof delta applications without compromising structural integrity. This subtle difference in thermal response reflects the tailored design of each product for its specific operating environment. From an industrial relevance perspective, each product aligns closely with its intended application. M-Sol is designed for ladle durability, offering reduced patching frequency and extended campaign life. T-Sol provides tundish and launder interface stability, ensuring smooth metal flow and minimizing slag contamination. RDC delivers resilience in EAF roof delta sections, withstanding electrode radiation and slag washing while maintaining roof delta stability over extended campaigns.

The superior performance of these systems is directly linked to colloidal silica binder

chemistry. During drying, the silica gel network provides permeability, eliminating explosive spalling and ensuring safe installation. At elevated temperatures, silica transforms into mullite and corundum phases, which impart mechanical strength, dimensional stability, and slag corrosion resistance. The absence of CaO avoids low-melting eutectics, ensuring long-term reliability and reducing vulnerability to alkali and slag attack [1, 5].

6. Conclusion

The study of Tricast Hybrid M-Sol, RDC, and T-Sol confirms that colloidal silica bonded castables provide a reliable and technically superior alternative to conventional CAC systems. Their performance is rooted in the unique binder chemistry: nanosized silica particles form a gel network during drying, which ensures permeability and eliminates explosive spalling. At service temperatures, this network transforms into mullite and corundum phases, imparting mechanical strength, dimensional stability, and resistance to slag corrosion.

Each product demonstrates application-specific advantages. M-Sol, with balanced alumina content and stable shrinkage behaviour, is ideally suited for treatment ladles, where repeated thermal cycling demands both strength and resilience. T-Sol, with its high alumina and dense Sintered High-Purity -Al_2O_3 structure, achieves exceptional hot strength and dimensional stability, making it highly effective in tundish and launder systems where steel/slag interface control is critical. RDC, designed for EAF roof delta sections, withstands extreme thermal gradients and mechanical stresses, maintaining integrity under electrode radiation and slag washing.

Collectively, these results validate colloidal silica bonded castables as a new benchmark in monolithic refractory technology. Their proven industrial performance translates into extended campaign life, reduced maintenance interventions, and lower operational costs. By eliminating CaO and leveraging sol-gel chemistry, these systems contribute to more sustainable and efficient steelmaking operations, aligning refractory design with the evolving demands of modern foundry and steel industries.

References

1. Lee, W. E. and Zhang, S., "Refractories for steelmaking," Refractories Handbook, CRC Press, 2004.

2. Ismael, M. R. and Pandolfelli, V. C., "Colloidal silica as a binder for refractory castables," Ceramics International, Vol. 33, No. 6, 2007, pp. 987–993.

3. Salomão, R., et al., "Advances in sol-bonded alumina castables," Journal of the European Ceramic Society, Vol. 43, No. 3, 2023, pp. 1125–1138.

4. Banerjee, S., "Colloidal silica bonded alumina castables: drying and performance," Refractories World Forum, Vol. 6, 2015, pp. 45–52.

5. Foseco Technical Note, "Sol-bonded castables for cupola and ladle applications," Internal Publication, 2019.

6. Andreassen, A. H. M. and Andersen, J., "Über die Beziehung zwischen Kornabstufung und Zwischenraum in Produkten aus losen Körnern (mit einigen Experimenten)," Kolloid-Zeitschrift, Vol. 50, 1930, pp. 217–228.

7. Braulio, M. A. L., et al., "Colloidal silica vs. calcium aluminate cement-bonded alumina castables," Interceram: International Ceramic Review, Vol. 58, 2009, pp. 388–392.

8. Totale Global Private Limited (TGPL), "Industrial validation of Tricast Hybrid MSol, RDC, and TSol," Internal Report, 2026.

9. Nouri-Khozani, M., et al., "Microstructural evolution and mechanical behaviour of nano-gel bonded alumina refractories," Ceramics International, Vol. 46, 2020, pp. 10450–10458.

DEVELOPMENT OF A NOVEL TROWELABLE REFRACTORY FOR ABRASION RESISTANT DUCT LININGS IN PELLETIZING PLANTS

M. Sathiyakumar*, M. Rajasekhar Reddy, R. Sugumar, S. Sumitha and G. Manari

Totale Global Private Limited, Sriperumbudur – 602 105, Tamil Nadu, INDIA

sathiyakumar@pincgroup.com

Abstract

Pelletizing plant induration furnaces subject ductwork to severe thermal and tribological stresses through high-velocity (20–40 m/s), high-temperature (400–1200°C) abrasive particle flows. Conventional castables provide high wear resistance but demand extensive formwork and curing times, limiting their utility for rapid in-situ repairs. This paper presents TRI-WEARCRETE 200F, a fibre-reinforced, high-alumina trowelable refractory engineered for wear-critical duct applications. Formulated with synthetic and natural aggregates, matrix-densifying additives, a proprietary flexible binder, and a dual-fibre reinforcement system, the material delivers a low-porosity, non-slump matrix that bonds monolithically to hex-metal anchors. It achieves a bulk density ≥2.85 g/cc, cold crushing strength ≥160 N/mm2, modulus of rupture ≥10 N/mm^2, and abrasion loss ≤4.50 cc, with service capability from 400°C to 1200°C. A rapid set time of 25–35 minutes enables formwork-free application during short outages, cutting maintenance downtime while extending campaign life across industrial duct systems.

Keywords: Trowelable refractory, abrasion resistance, fibre reinforcement, complex geometry, pelletizing plant.

1. Introduction

Research studies on refractory materials have heavily emphasized the development of monolithic solutions, which provide operational reliability comparable to conventional pre-fired shapes while offering superior installation flexibility [1, 2]. In modern iron ore pelletizing plants, induration furnaces and auxiliary ductwork operate under intense thermo-mechanical and tribological stresses. Gas streams moving at velocities of 20 to 40 m/s carry high concentrations of abrasive iron ore fines and unbaked green pellets through duct systems at temperatures ranging from 400 to 1200°C.

Ductwork components, such as cyclone inlets, mill discharge ducts, dynamic separator return lines, and transition elbows, suffer accelerated erosive wear due to continuous particle impacts. The primary degradation mechanics encountered in these duct environments are detailed in Table 1.

Table 1: Operational degradation mechanisms in pelletizing plant ductwork

Stress Component	Operational Cause	Industrial Consequence / Failure Mode
Mechanical Erosion	High-velocity dust & pellet impacts (20–40 m/s)	Surface grooving, wall thinning, and structural localized breakthrough
Thermal Cycling	Rapid temperature swings during startup & shutdown	Spalling, micro-cracking, and structural delamination
Vibrational Strain	Dynamic process fan load &	Debonding from anchors and

	turbulent gas flows	mechanical fatigue failure
Geometric Complexity	Tight elbows, transition ducting, and internal baffles	Incomplete vibration filling & void formation when using castables

Standard refractory lining methods involve clear performance compromises and engineering considerations: Conventional dense castables deliver excellent cold crushing strength and abrasion resistance, but require complex formwork, extensive anchor systems, and prolonged curing schedules. Conversely, standard trowelables and mortars offer rapid, formwork-free hand application, but lack structural integrity, exhibiting high porosity, poor thermal shock resistance, and rapid wear rates, often resulting in an 8–20 cm^3 loss under ASTM testing [3].

To solve these installation and operational challenges, Totale Global Pvt. Ltd. Developed TRI WEARCRETE 200F to combine the structural durability of high-density castables with the fast-setting, formwork-free application of trowelable refractory materials. This manuscript presents the design, testing, and field validation of TRI-WEARCRETE 200F for pelletizing plant ductwork.

2. Castable and matrix design

Designing monolithic refractories for high-abrasion duct applications requires targeted microstructural engineering. The development of TRI-WEARCRETE 200F was guided by three core design principles:

Aggregates and Particle Packing: Optimised particle packing based on a modified Andreassen model achieves a dense aggregate distribution [4]. Synthetic and natural aggregates, along with silicon carbide, form the wear resistant skeleton to provide extreme abrasion resistance. This matrix is further supported by micronized reactive nano-fillers that penetrate micropores, minimize interstitial void spaces, and enhance overall matrix density to yield a dense, jointless lining.

Hybrid Reinforcement System: A hybrid reinforcement system, incorporating specialized fibres, reinforces structural integrity under thermal and mechanical stress. During initial heat-up, the system creates micro-pore network channels for vapor release to prevent explosive spalling and control settlement cracks. Additionally, the hybrid fibre reinforcement provides post-crack bridging capability, structural toughness, and superior spall resistance under dynamic vibration.

Hydraulic Binder System: A proprietary hydraulic binder enables monolithic bonding to hex-metal anchor mesh, operating with low water demand (8.0–10.0 wt%) to achieve trowelable, non-slump rheology while chemical admixtures minimize overall porosity.

3. Experimental details

3.1 Test Sample Preparation

Refractory batches were prepared by wet-mixing dry ingredients with 8.0–10.0 wt% water in an hobart mixer. Test specimens were hand-trowelled into standard moulds to evaluate non-slump placement behaviour. The samples were cured at room temperature (25°C) for 24 hours. Following demoulding, specimens were dried at 110°C for 24 hours and subsequently fired at target service temperatures for 3 hours prior to characterization.

3.2 Physical and Mechanical Testing

Apparent Porosity (AP), Bulk Density (BD), Cold Crushing Strength (CCS), and Cold Modulus of Rupture (CMOR) were measured according to standard refractory testing methods, with reported values representing the average of three parallel test specimens.

3.3 Abrasion Resistance

Cold abrasion loss testing was conducted in accordance with ASTM C704. Test specimens measuring 100 mm ×100 mm × 25 mm were dried at 110 °C and pre-fired at 816 °C. Silicon carbide grit was blasted against the specimen surfaces, and total volume loss was calculated.

4. Results and discussion

4.1 Physico-Mechanical Properties

The physical and performance characteristics of the TRI-WEARCRETE series across low and high-temperature grades are detailed in Table 2.

The key physical properties of TRI-WEARCRETE 200F highlight its suitability for severe pelletizing plant duct environments. A BD of ≥2.85 g/cc at 110°C ensures the formation of a dense matrix that resists both abrasion and chemical attack. The AP remains controlled at ≤12%, eliminating subsurface voids that typically promote preferential erosion. CCS values of ≥160 N/mm^2 at 110°C confirm that the material maintains mechanical integrity across a wide range of service temperatures, while castable formulations exceed 160 N/mm^2.

Abrasion resistance testing confirmed superior performance compared to conventional trowel products, which typically show volume losses in the range of 8–20 cc. The TRI-WEARCRETE series limits abrasion loss to <1.50 cc in standard formulations and ≤4.50 cc under field specification limits. In standard trowelables, abrasion occurs rapidly via matrix erosion followed by aggregate pull-out. For TRI-WEARCRETE 200F pre-fired at 816°C, the nano-silica modified hydraulic matrix exhibits bonding strength equivalent to the synthetic aggregates. Post-test surface evaluations reveal uniform surface wear without aggregate dislodgement or hole formation, confirming that matrix erosion rates match aggregate wear rates.

Table 2 Physico-mechanical properties and application parameters of the TRI-WEARCRETE series

Properties	TRI-WEARCRETE SERIES				
	Low Temperature			High Temperature	
	200C (Cast)	200F (Flex)	200S (Spray)	200 HTC (Cast)	200 HTF (Flex)
Product Descriptions	Castable product for piping, elbows, and precast shapes where in-situ lining is impractical	Trowel product for versatile applications, ideal for complex geometries with fast,	Sprayable product for large surfaces and complex geometries, enabling very fast installation.	Castable product for high-temperature applications, 200 HTF (Flex) Trowel product for	Trowel product for high-temperature applications, providing excellent wear and heat

	or causes extended downtime.	easy installation.		high-temperature offering excellent wear and heat protection for piping, elbows, and precast shapes where in-situ lining is impractical or causes extended downtime.	protection across diverse uses. Ideal for complex geometries with fast, easy installation.
Temperature Limit (°C)	Up to 400			Up to 1200	
Key Strengths	Abrasion resistance in moderate heat			Abrasion, thermal shock resistance & high strength	
Application Areas	Ducts / elbows, chutes / hoppers, cyclones, slurry pipes and precast shapes			Kiln inlets, burner pipes and high heat zones, cyclone & riser lining	
BD (g/cc)	2.94	2.89	2.62	3.01	2.89
CCS (N/mm2)	171	162	108	175	130
Abrasion Resistance (CC)	<1.50	<1.50	<1.50	<1.00	<1.00
Thermal Conductivity (W/mK)	1.52	1.51	1.51	1.50	1.51
Installation Method	Vibrocasting	Trowelling	Spraying	Vibrocasting	Trowelling

A modulus of rupture of ≥10 MPa at 200°C provides low-temperature flexibility across the 200–600°C range, which is essential for vibration-prone ductwork under dynamic loads. The hybrid fibre reinforcement system bridges microcracks, enhances cyclic fatigue resistance, and prevents spall dislodgement, ensuring long-term durability under demanding operating conditions.

5. Field Applications, Installations, and Performance

5.1 Applications

TRI-WEARCRETE 200F is applicable across a wide range of pelletizing plant components including mill discharge ducts, cyclone inlets, risers, dynamic separator fines return lines, downstream elbows, chutes, fan casings, and impact zones. Its versatility extends to cement, steel, power generation, pelletizing, and mineral processing industries where rapid installation and extended service life are critical to minimizing downtime.

5.2 Field Performance and Execution

Field trials were conducted in iron ore pelletizing plants, applying TRI-WEARCRETE 200F to high-wear duct components including elbow transitions and cyclone inlets. The material demonstrated thixotropic, non-slump characteristics, allowing manual application directly over expanded hex-metal mesh on vertical and overhead duct surfaces without slumping. The initial set time of 25–35 minutes enabled rapid deployment, with final set achieved within 6–8 hours to support large-scale duct projects.

Eliminating formwork reduced total installation shutdown windows by over 50% [6]. Following application, a curing compound was applied over the trowelled lining to form a seamless protective film [7]. This film retained moisture within the refractory surface, allowing full hydration of the hybrid cement system, supporting strength development, and minimizing the risk of premature drying or shrinkage.

Inspections after extended operational campaigns confirmed strong adhesion and dense, void-free coverage with no signs of surface spalling, joint cracking, or anchor debonding under cyclic thermal operating conditions.



Fig.1 Industrial staging area with large duct sections and pre-installed hex-metal mesh anchors ready for trowel application.



Fig.2 Precast, trowel-lined large-diameter ducts demonstrating project scale.

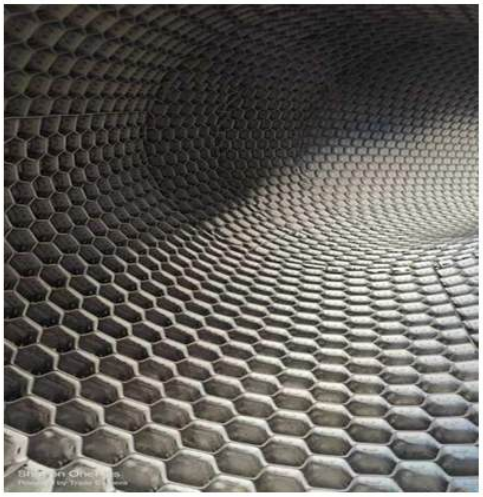


Fig.3 Close-up of hexagonal expanded metal anchor mesh prior to application.

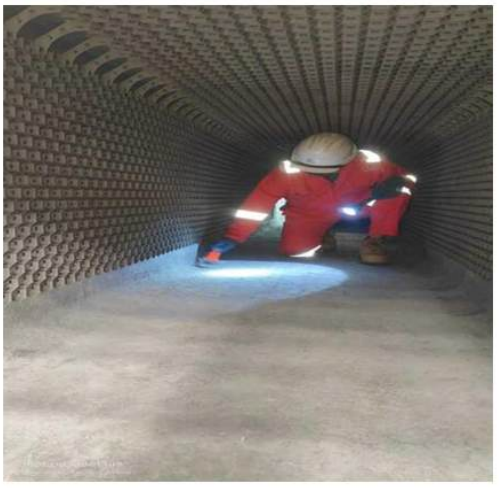


Fig.4 Completed duct bend interior showing trowel lining conforming to complex geometry.

6. Conclusion

TRI-WEARCRETE 200F provides dense, castable-grade wear resistance in a trowelable, formwork-free product. Key conclusions from its development and testing demonstrate that combining fused corundum aggregates, silicon carbide, and nano-silica fillers produces a dense microstructure achieving a bulk density ≥2.85 g/cc, cold crushing strength exceeding 160 MPa in castable formulations, and abrasion loss under 1.50 cc. Additionally, the hybrid fibre mechanism, utilizing a combination of polypropylene and high-tensile steel fibres, effectively controls settlement micro-cracks, prevents explosive spalling during initial heat-up, and improves flexural toughness under dynamic duct vibration. Furthermore, the material offers exceptional installation efficiency through fast initial setting times (25 to 35 minutes) and a non-slump trowelable consistency that allows formwork-free execution in complex duct geometries, cutting shutdown maintenance downtime by over 50% while extending campaign life.

The developed products demonstrate reliable service capability between 400°C and 1200°C (with thermal limits up to 1350°C), offering an effective solution for safeguarding critical ductwork in modern pelletizing operations.

References

1. Sadik, C., El Amrani, I. E., & Albizane, A. (2014). Recent advances in silica-alumina refractory materials: A review. Journal of Asian Ceramic Societies, 2(2), 83–96.

2. Luz, A. P., Braulio, M. A. L., & Pandolfelli, V. C. (2015). Refractory Castable Engineering. Göller Verlag, Baden Baden.

3. Lee, W. E., & Moore, R. E. (1998). Evolution of in situ refractories. Journal of the American Ceramic Society, 81(6), 1385–1410.

4. Parmentier, J., & Tremblay, S. (2009). Fiber-reinforced monolithic refractories for high-stress applications. Refractories World Forum, 1(2), 77–84.

5. Banerjee, S. (1998). Monolithic Refractories: A Comprehensive Handbook. World Scientific / American Ceramic Society.

6. Kraushaar, M., & Wulf, R. (2017). Optimizing installation time and drying profiles for monolithic duct linings in minerals processing. Interceram - International Ceramic Review, 66(4), 32–38.

7. Routschka, G., & Wuthnow, H. (Eds.). (2012). Pocket Manual Refractory Materials: Design, Properties, Testing (4th ed.). Vulkan-Verlag GmbH.

ENHANCING OXIDATION RESISTANCE OF Si_3N_4–BONDED SiC REFRACTORIES FOR COPPER SHAFT FURNACE PERFORMANCE

Ranjan Dey, S. Panneerselvam, R. Krishnakumar, Prabhakar Jha, Subhasis Gangopadhyay, V. T. Eswaran, B. Raghavendra Pai

Carborundum Universal Limited, India

Abstract

Silicon Nitride–bonded Silicon Carbide (Si_3N_4–SiC) refractories consist of SiC grains and Si_3N_4 bond phase. SiC provides high thermal conductivity, strength, and abrasion resistance. Si_3N_4 bond phase provides structural integrity and oxidation resistance. This combination makes them ideal for non-ferrous metallurgical furnaces, especially copper shaft furnaces. Operating environment in a copper shaft furnace is combination of aggressive oxidizing and corrosive environment. Inadequate oxidation resistance results in Formation of SiO_2 layer, Volume changes/internal stress, Loss of mechanical strength, Increased porosity and accelerated slag penetration. All these leads to spalling, structural weakening and premature lining failure. This paper describes improvement carried out in Si_3N_4–SiC refractory for application in Continuous Copper Rod (CCR) Production.

Keywords: Continuous Copper Rod (CCR) furnace, Oxidation, improvement in NBSiC refractory

1. Background

Factors influencing global coper rod market are demand for electricity and infrastructure, shift to Electric Vehicles, transmission and distribution infrastructure for renewable energy and production of more electric powered machinery and appliances.

Production Volume of Refined Copper: According to a report released by the World Bureau of Metal Statistics (WBMS), global refined copper production in 2023 was 27.6261 million tons, consumption was 27.6919 million tons, and there was a supply shortage of 65,800 tons.

Growth Forecast of Refined Copper: Global refined copper demand is projected to reach around 33 million MT in 2035 and 37 million MT by 2050 under the stated policy scenario (International Energy Agency, 2025). Forecast from S&P Global and the International Copper Association (ICAI), that copper demand will reach about 50 million MT by 2050 against current production of 26.5 million MT annually, the demand–supply gap is expected to become acute unless there is a considerable increase in production capacity or technological advancements.

India's copper market is projected to grow at 6.65% CAGR, expanding from $15.09 billion in 2024 to $25.06 billion by 2032. By 2035, 4 million to 5 million MT of copper demand will make India the second largest copper-consuming region behind China, according to industry sources

Consumption vs. Capacity of Copper Rod: While consumption was around 9.7 million MT, the production capacity of copper rods with copper cathode and scrap was around 20 million metric tons annually. The global copper rod market is projected to grow at 4.5% CAGR until 2034.

Market Size of Copper Rod: The global copper rod market was estimated to be around 2.1 million MT in 2023 and expected to grow at a CAGR of 4.5% till 2034.

Furnaces for Copper Rod Production: Shaft Furnace was developed by American Smelting and Refining Company (ASARCO) and used in Continuous Copper Rod (CCR) production. Other furnace types are:

- Reverberatory Furnace: Used for copper scrap smelting and is widely used in copper CCR plants.
- Rotary Furnace: Designed for refining copper scrap. Tilting Refining Furnaces (TRF) and Elliptical
- Tilting Reefing Furnaces (ETRF): These are designed for melting, refining, and casting copper scrap in one flexible unit.
- Induction Furnaces: Suitable for melting and alloying metals with minimal melt losses.

Shaft Furnaces are used for melting copper cathodes (also for anode residues, and high-grade copper scrap). Feedstock electrolytic cathodes are charged into the shaft with a skip hoist. Burners are mounted radially around the lower shaft section. The electrolytic cathode copper sheets are melted in the lower zone of the shaft furnace.

Globally, majority of shaft furnaces or other melting method as part of wire/rod making process are governed by following OEM based design and processes:

- SMS-Contirod [Contirod (Krupp-Hazelett) developed by of Aurubis, Belgium]
- Southwire
- General Electric Dip Forming
- Outokumpu Upcast
- Continuus Properzi
- Lamitref process

Amongst these, globally and also in India, many CCR manufacturers have adopted Shaft furnace by Southwire and SMS Contirod technology. The fundamental difference in the refractory configuration of the CCR shaft furnaces designed by Southwire (SCR System) and SMS Contirod comes down to internal geometry (cylindrical vs. patented conical design) and how the refractory engineering addresses material hang-ups, structural mechanical wear, and friction. Both systems traditionally use high-grade silicon carbide (SiC) or premium alumina-silica bricks backed by heavy insulation to withstand temperatures upward of 1,100°C and copper slag erosion.

In CCR shaft furnaces whether operating on Southwire or SMS Contirod systems, the hot-face refractory lining is primarily composed of Silicon Nitride-bonded Silicon Carbide (Si3N4-SiC). While these non oxide ceramics are chosen for their extreme hardness and thermal shock resistance, they are vulnerable to high-temperature chemical oxidation.

Oxidation of refractories occurs through following chemical and mechanical mechanisms:

I. Gas-Phase Burner Atmosphere Oxidation (Passive vs. Active)

The burner system (using natural gas or propane) controls the internal atmosphere of the furnace. If the air-to-fuel ratio shifts toward an excess of oxygen, the gas phase directly oxidises the SiC matrix at temperatures between 900°C and 1,200°C.

Passive Oxidation (The Protective Glass Phase):

Under normal conditions, excess oxygen reacts with the silicon carbide to form a thin, glassy layer of silica (SiO_2) on the brick surface:

$$SiC+2O_2 \rightarrow SiO_2+CO_2$$

Initially, this glassy SiO_2 fills the surface pores and acts as a barrier that slows down further oxygen diffusion.

Active Oxidation (The Destructive Phase):

If the furnace suffers from micro-atmospheres with very low oxygen partial pressure or extreme localized hot spots (exceeding 1,300°C), the reaction switches to active oxidation. Instead of solid glass, it forms volatile Silicon Monoxide (SiO) gas:

$$SiC+O_2 \rightarrow SiO(g)+CO(g)$$

As SiO escapes as a gas, the refractory loses mass, develops high porosity, and disintegration commences.

II. Liquid Metal Chemical Reduction (The Cu_2O Attack

Solid copper cathodes fed into the top of the furnace carry surface scales, moisture, and atmospheric oxides. As these melt, Cuprous Oxide (Cu_2O) forms inside the molten pool. Thermodynamically, copper oxide acts as a fierce oxidising agent when it touches the non-oxide refractory lining. At the slag line and melting zone, the liquid Cu_2O directly attacks both the Si3N4 bond and SiC grains:

$$SiC+4Cu_2O \rightarrow SiO_2+8Cu+CO_2 \ [\Delta G<0 \text{ at } 1200^\circ C]$$
$$Si3N_4+6Cu_2O \rightarrow 3SiO_2+12Cu+2N_2 \ [\Delta G<0 \text{ at } 1200^\circ C]$$

The Result: The refractory is forcibly oxidised into silica (SiO_2) by the copper melt. The liquid copper oxide is simultaneously reduced to metallic copper, which infiltrates brick matrix and causes severe structural washing.

III. Slag Corrosive Washing & Silica Dissolution

The protective silica (SiO_2) layer formed from passive oxidation should theoretically protect the brick. However, the impurities from copper melting (such as iron, nickel, or alkaline fluxes) form a highly corrosive, fluid slag.

The iron oxides (FeO) and other basic components in the slag chemically react with the newly formed SiO_2 glass, creating low-melting-point compounds like fayalite (Fe_2SiO_4). The slag washes this liquid glass away, continuously exposing a fresh, unreacted layer of SiC to the oxidising atmosphere. This cyclical process, Oxidation → Slag Reaction → Corrosive Washing progressively thins the furnace walls.

System-Specific Oxidation Amplifiers

- **In Southwire (SCR) Systems:** Because the furnace is a straight cylinder, cathode bundles can jam, causing operators to crank up the burner intensity underneath the jam. This localized thermal spiking drastically accelerates the active gas oxidation (SiO gas generation) around the burners.
- **In SMS Contirod Systems:** The conical design prevents physical jams, but if the continuous line changes speeds frequently, fluctuations in the burner's air-to-fuel ratio can alter the furnace atmosphere, inducing alternating redox reactions that weaken the refractory bond structure.

Present work carried out to study effect of selected raw materials in enhancing oxidation resistance which seemed to be very critical properties for the application.

2. Experimental study

Samples prepared in 10 different recipes introducing alumino-Silicate (AS1 &AS2), alkaline earth salt (AES), silica (S1 & S2), reactive alumina (RA), rare earth oxides (REO) in a standard Silicon Nitride Bonded Silicon Carbide formulation (mix of Silicon Carbide grains, Silicon metal powder and binders etc.). Batch details are shown below Table 1:

Table 1: Experimental trial batches

Trial #	1	2	3	4	5	6	7	8	9	10
AS1		3					2	3	3	
AS2		1	1	1	1			1	1	1
AES		1	1	1	2		2			2
S1			3							
S2				3	2					
RA	2					2				
REO	3					5	3	0.3	0.6	3

Sample bricks were pressed, dried and fired at temperatures around 1450 deg. C in nitrogen atmosphere.

Physical tests carried out i.e. Bulk Density, Apparent porosity, strength properties

Oxidation Resistance carried out as per ASTM C 863 (2010) at 1100 deg. C for 100 Hours

Scanning electron microscopy carried out to understand correlation of microstructure with optimum oxidation resistant and growth due to oxidation



Photo 1: Samples prepared from standard bricks for Oxidation Test

3. Result

Oxidation Resistance tested as per ASTM C863 (2010), Test temperature: 1100°C, Duration: 100 hrs., Dimension for all samples is 65X35X35mm. Result shown below in Table 2 and Chart 1.

Table 2: Volume expansion and weight change in Oxidation Test as per ASTM C863 (2010)

Trial #	Volume Expansion (%)				Weight Change (%)			
	Sample #1	Sample #2	Sample #3	Avg. Vol. Expansion	Sample #1	Sample #2	Sample #3	Avg. Weight Change
1	25.14	25.05	24.53	24.91	6.41	6.31	6.24	6.32
2	0.51	0.54	0.67	0.57	2.26	2.25	2.48	2.33
3	0.39	0.51	0.44	0.45	1.57	1.68	1.7	1.65
4	0.31	0.3	0.35	0.32	1.88	1.96	1.86	1.90
5	2.04	1.86	1.75	1.88	1.92	1.83	1.67	1.81
6	35.62	36.17	27.81	33.20	6.01	6.06	5.94	6.00
7	24.82	24.78	23.58	24.39	6.13	5.91	5.68	5.91
8	0.38	0.37	0.46	0.40	2.24	2.28	2.3	2.27
9	0.33	0.41	0.41	0.38	1.86	1.97	2.02	1.95
10	0.49	0.42	0.44	0.45	1.93	1.91	2.02	1.95

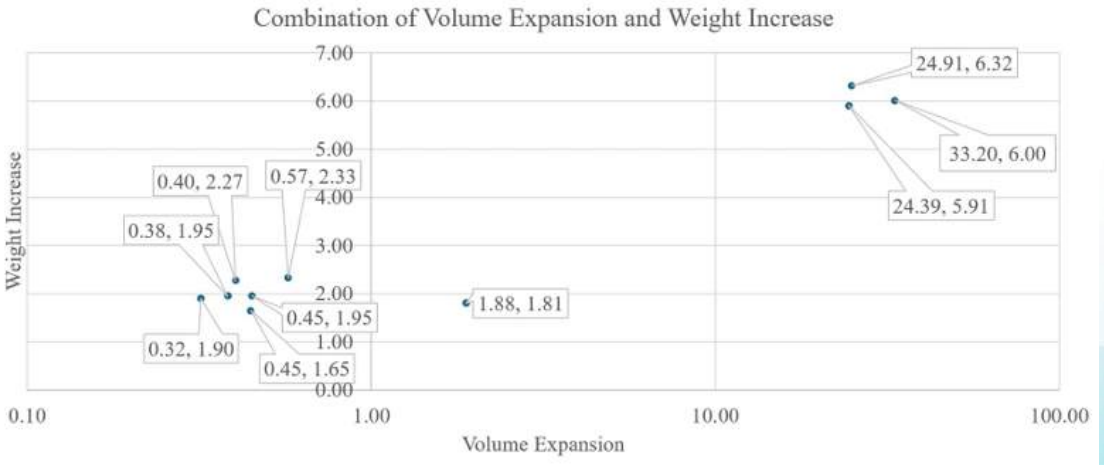


Chart 1: Combination of two critical parameters: Volume Expansion & Weight Change of all trial samples

Bulk Density & Apparent porosity carried out before Oxidation Resistance Test and shown in Table 4.

Trial #	Bulk Density (g/cc)			Apparent Porosity (%)		
	Sample #1	Sample #2	Sample #3	Sample #1	Sample #2	Sample #3
1	2.51	2.56	2.53	22.1	20.6	21.4
2	2.59	2.57	2.55	17.3	17.9	18.5
3	2.65	2.65	2.64	15.4	15.7	15.7
4	2.66	2.66	2.65	15.9	15.9	16.2
5	2.60	2.62	2.63	17.8	17.3	16.7
6	2.60	2.63	2.61	19.9	18.8	19.8
7	2.68	2.67	2.66	17.3	17.3	17.5
8	2.64	2.62	2.63	16.5	16.9	16.9
9	2.65	2.63	2.63	16.3	17.1	17.2
10	2.63	2.62	2.58	17.3	17.8	18.9

Corelation between Apparent porosity (before test), change in Apparent porosity (during oxidation) reviewed against average volume expansion and weight increase

Table 5: Apparent Porosity with outcome of Oxidation Resistance Test

Trial #	Avg. Apparent Porosity before test	Avg. Change in Apparent Porosity	Avg. Vol. Expansion	Avg. Weight Increase
1	21.37	4.50	24.91	6.32
2	17.90	-6.70	0.57	2.33
3	15.60	-4.50	0.45	1.65
4	16.00	-7.20	0.32	1.90
5	17.27	-4.23	1.88	1.81
6	19.50	8.83	33.20	6.00
7	17.37	3.23	24.39	5.91
8	16.77	-7.77	0.40	2.27
9	16.87	-7.80	0.38	1.95
10	18.00	-7.23	0.45	1.95

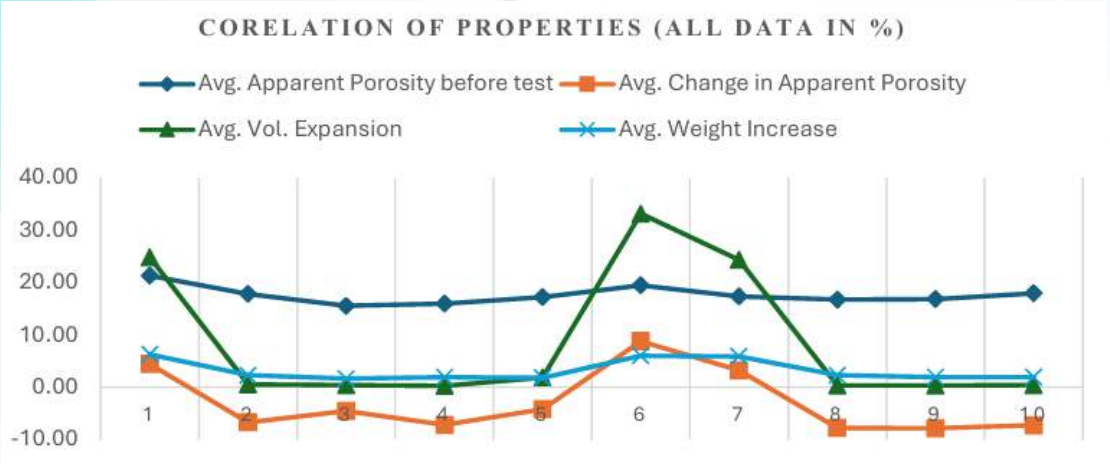
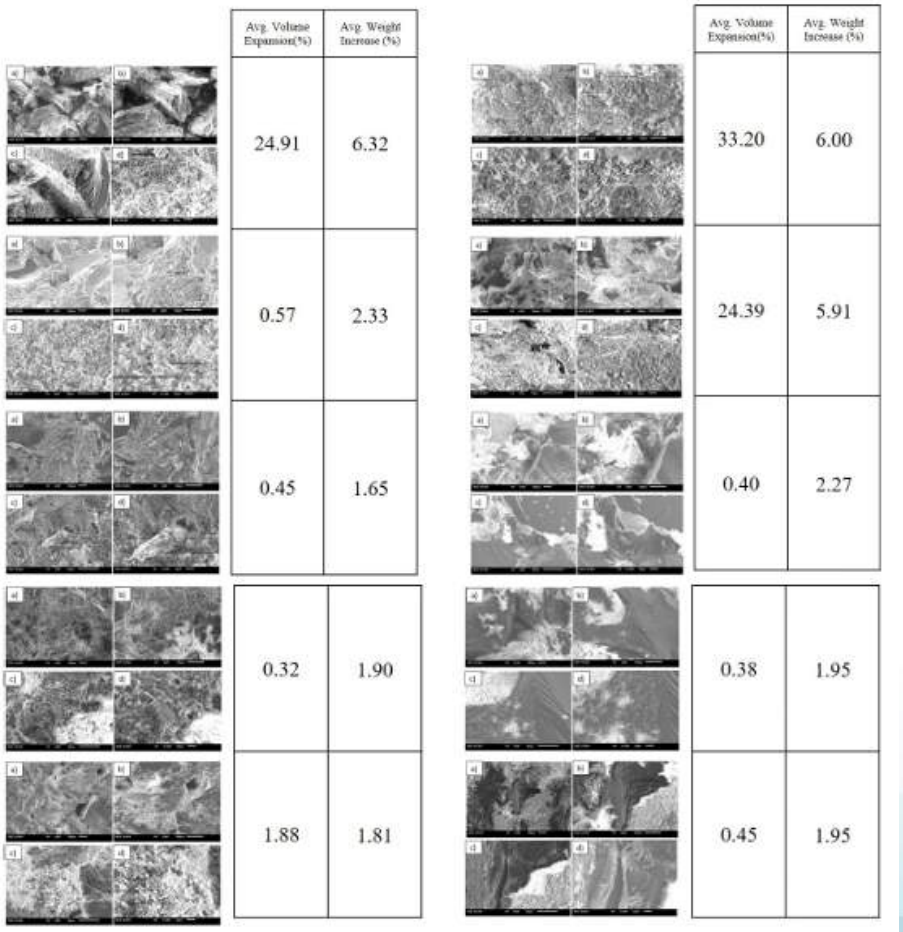


Chart 2: Corelation of Apparent Porosity and changes in Apparent Porosity with Volume Expansion & Weight Increase

Scanning Electron Microscopy (SEM) done on all the samples and shown below, Sample #1 to #5, left side, top to bottom and Samples # 6 to #10, right side, top to bottom [a)100X, b)200X, c)500X, d)1000X]

Photo 2: SEM and corresponding Oxidation Outcome



4. Conclusion

- Out of 10 Trials, six are found to be within 1% Volume expansion and amongst them, trial #3,4,9 and 10 also exhibited weight increase less than 2% which are positive outcome.

- Volume expansion and weight increase due to oxidation follows and therefore related to change in Apparent porosity (in Oxidation) and Apparent Porosity (before Oxidation) respectively.

- Higher volume expansion in trial #1, 6 & 7 to be studied further and best possible NBSiC will be optimized from trial #3,4,9 & 10 for CCR applications.

References

1. Conference proceedings: Global Continuous Casting Forum 2025, Atlanta, GA, USA

2. https://www.databridgemarketresearch.com/nucleus/india-copper-market

3. https://mines.gov.in/webportal/copper

4. ScienceDirect.com

NEW GENERATION SPECIAL CASTABLE FOR FOUNDRY INDUSTRY

Sudip Kumar Paul*, Sandeep Bachhar, Pradeep Kumar, Debalina Mitra, Nishant Kesharwani & Ravikumar Periyasamy

RHI Magnesita India Ltd., Katni, INDIA

Corresponding author's e-mail: sudip.paul@rhimagnesita.com

Abstract

The foundry sector manufactures metal castings through the processes of melting, pouring, and solidifying materials such as iron, steel, and aluminium into moulds, thereby producing accurate components for industries including automotive, aerospace, and construction. Essential processes include patternmaking, mould fabrication melting, pouring, cooling, and finishing, with more than 90% of worldwide production consisting of ferrous metals. Refractories play a crucial role in high-temperature applications within the foundry industry. Refractory materials are utilized for lining ladles, primarily belonging to the hydraulic bonded low cement castable or conventional castable. The new generation Nano Bonded castable has demonstrated superior mechanical properties, exceptional thermal shock resistance & volume stability, better abrasion resistance and slag corrosion resistance at service temperatures, thereby extending the lifespan of the ladle. It ensures desired flowability, workability, and optimization of setting behaviors during application. X-ray diffraction (XRD) was conducted to analyze the phases, while scanning electron microscopy (SEM) was performed to examine the surface topology of the materials. New generation Nano bonded castable provides intangible advantages such as reduced downtime, decreased manpower requirements for repair, and energy savings, with cumulatively has positive financial implication (saving). The refractory's lower thermal conductivity, despite its higher alumina content, contributes to reduced heat dissipation through the ladle walls. Furthermore, the reduced impurity level in base raw materials minimizes the inclusion of impurities in the final product. Final users' references are cited to prove superior product development using appropriate formulation and improved bond system. The average lifespan of a ladle with a capacity of 3 to 5 MT has increased nearly 2.5 to 3 times compared to regularly used conventional & low cement castables with similar chemical compositions materials.

Keywords: Foundry, Abrasion Resistance, Thermal shock resistance, Flowability, Thermal conductivity, Workability, Setting behaviors, Castable, Mechanical properties, Volume stability.

1. Introduction

The foundry industry is one of the key areas supporting manufacturing industries worldwide. Various Cast components produced through foundry operations are extensively used in automotive sectors, railway, aerospace, agricultural equipment, infrastructure, mining, and engineering applications. Refractories constitute a critical part of foundry operations because molten metals at temperatures exceeding 1400°C continuously interact with refractory linings during transportation, treatment, and pouring operations.

Traditionally, silica ramming mass, high alumina based conventional castables (CC) and low cement castables (LCC) have been employed for foundry ladles due to their ease of installation and relatively lower initial costs. However, increasing expectations regarding ladle campaign life, energy efficiency, productivity, and maintenance reduction have highlighted the limitations of conventional hydraulic bonding systems.

Recent advancements in refractory technology have led to the development of

nano-bonded castables. By incorporating nano-scale bonding mechanisms and optimized particle packing concepts, these castables achieve superior pore size distribution, enhanced mechanical strength, excellent volume stability, and improved thermal shock resistance and mechanical stresses.

The present study evaluates the performance of a newly developed Nano Bonded Castable design specifically for foundry ladles used in Iron Foundry. The investigation includes laboratory characterization, microstructural analysis, and industrial validation under actual operating conditions.

2. Challenges Faced by Conventional material used in Foundry Ladle

Foundry ladle operating under cyclic service conditions encounter several degradation mechanisms which are described.

2.1 Thermal Shock Damage

Cycling heating and cooling cycles generate thermal stress in refractory lining resulting in crack formation and propagation in refractory lining resulting in lower life of Refractory castable.

2.2 Slag Corrosion

The vigorous reactions occurring between iron and steelmaking slags and refractory linings result in diminished lining thickness and shortened service life of the Ladle.

2.3 Mechanical Abrasion

Metal turbulence during charging, transportation, and pouring causes abrasion and erosion of the refractory surface

2.4 Structural Deterioration

Hydraulic bonded systems often develop microcracks during dehydration reactions and phase transformations during thermal cycling, and it increases during operation.

2.5 Heat Loss

Higher thermal conductivity results in increased heat dissipation through ladle walls, causing metal temperature losses and energy inefficiency.

To overcome these limitations, a new generation Nano Bonded Castable was developed.

3. Developmental concept of Nano-Bonded Castable Material

The engineered castable incorporates the following constituent elements:

- High-purity alumina-based aggregate materials
- Refined particle size distribution to optimize packing efficiency
- Nano-scale bonding methodology
- Minimal impurity content within the matrix composition.

The underlying design strategy emphasized:

a) Enhancing microstructural density and homogeneity.

b) Enhancing resistance to crack propagation.

c) Better abrasion resistance with optimum strength characteristics.

d) Reducing thermal conductivity properties & better dimensional stability at elevated temperature.

4. Experimental Procedure

The Nano Bonded Castable (NBC) was formulated as

• High purity alumina aggregates

• Superior Matrix concept

Tab.1: Formulation concept of Nano bonded, Conventional & Low Cement Castable

Type	Materials\ Recipe	A (SOL)	B (CC)	C (LC)
Aggregate	Mullite	XXX	XX	XXX
	Calcined Clay	X	X	X
Matrix	CAC70%, S70		XX	X
	Calcined Alumina	X	X	X
	Silica Fume	X		X
	Additive	X		X

Tab. 2: Key features of aggregate & matrix

Material	Type	Purity	Addnl. feature
Mullite	Aggregate	62%	AP 6%, BD 2.6 g/cc
Calcined Clay	Aggregate	42%	AP 5%, BD 2.4 g/cc
CAC70%	Matrix	70%	F2O3 – 0.15%
Calcined Alumina	Matrix	99.40%	d50: 4.7 µm
Silica Fume	Matrix	96%	C-0.5% max.

These castable were mixed with the required amount of liquid/ water addition and checked for vibration flow and setting properties in a climate cabinet. Standard bars were cast, cured for 24 hrs., dried at 110°C for 24 hrs., and then fired at 1200°C/5 hrs. 1400°C/5 hrs. as per EN ISO 1927 standard. Then the bars were checked for bulk density (BD), apparent porosity (AP), cold compressive strength (CCS), cold modulus of rupture or flexural strength (MOR), and permanent linear change (PLC). Hightemperature flexural strength (HMOR) was checked at 1200°C with 30 minutes of soaking time using the pre-fired

bars at 1200°C/5 hrs. Thermal shock was evaluated for checking spalling resistance in a specific spalling cycle (950°C water quenching cycle) as per IS 1528 (Part 3):2010. Castable bars were preferred at 1200°C/5 hrs. and tested abrasion resistance at room temperature.

5. Results and Discussion

5.1 Flowability and Workability

The Nano Bonded Castable demonstrated excellent rheological behavior during lab test and during installation at site.

Optimized particle packing and nano-scale dispersive effects contributed to superior flowability while maintaining structural integrity after setting.

Tab. 3: Casting rheology in castable

Parameters	A (SOL)	B (CC)	C (LC)
Liquid/ Water demand, %	11.0	11.5	5.8
wet out time [sec]	55	70	65
nitial Setting time, mint.	95	65	110
Final Setting time, mint	160	105	180
VIB-Flow [cm]			
F10	190.0	130.0	188.0
F30	168.0	120.0	174.0
F60	148.0	112.0	150.0

5.2 Apparent Porosity (AP)

Apparent porosities were found lower at 1400°C/5 hrs. for Nano bonded material which reduce the slag and metal penetration and improved corrosion resistance during application.

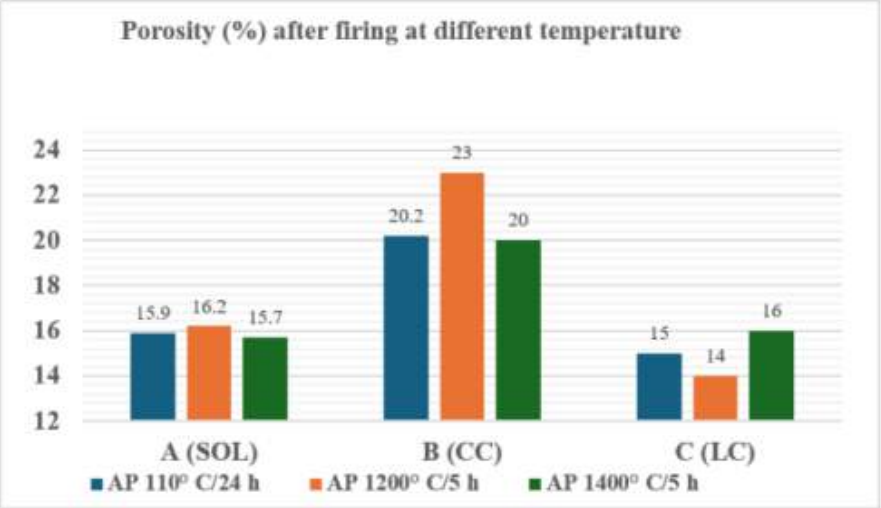


Figure 1: AP at different temperature

5.3 Bulk Density (BD)

Improved Bulk density were found for nano bonded material at elevated temperature this improve the abrasion and mechanical strength.

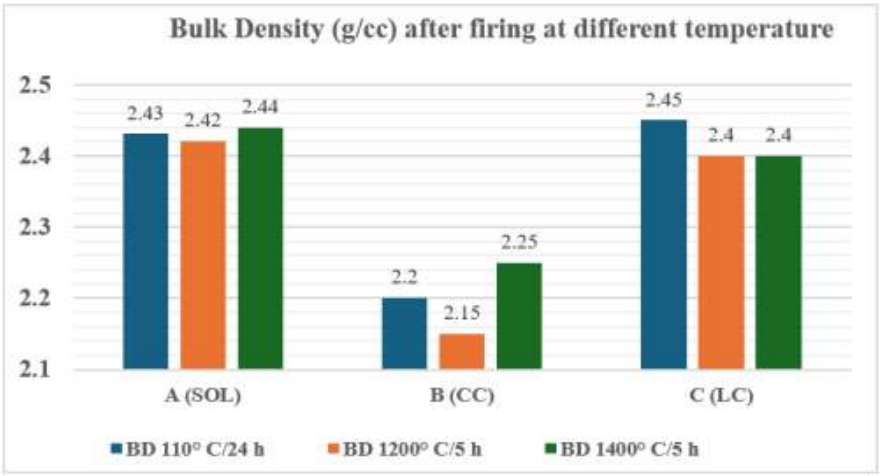


Figure 2 : BD of mixes at different temperature

5.4 Cold Crushing Strength (CCS)

Optimum CCS was observed for Nano bonded material at elevated temperature.

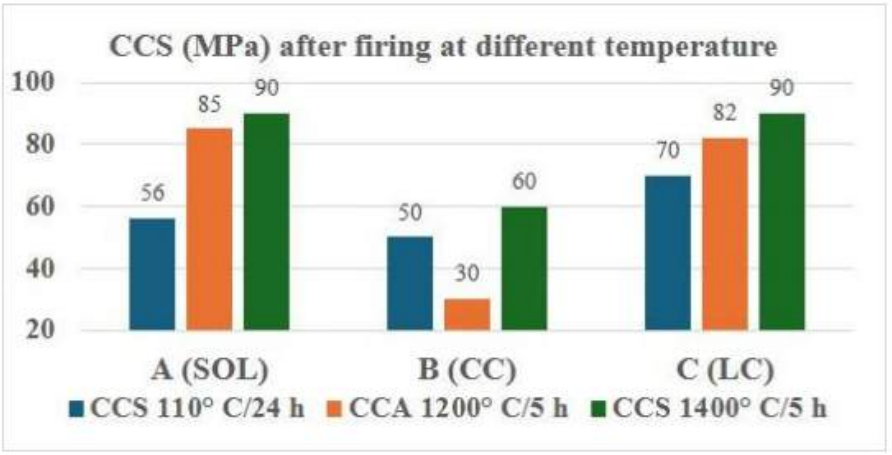


Figure 3: CCS of mixes at different temperature

5.5 Modulus of rupture (MOR)

Optimum MOR was observed for Nano bonded material at elevated temperature.

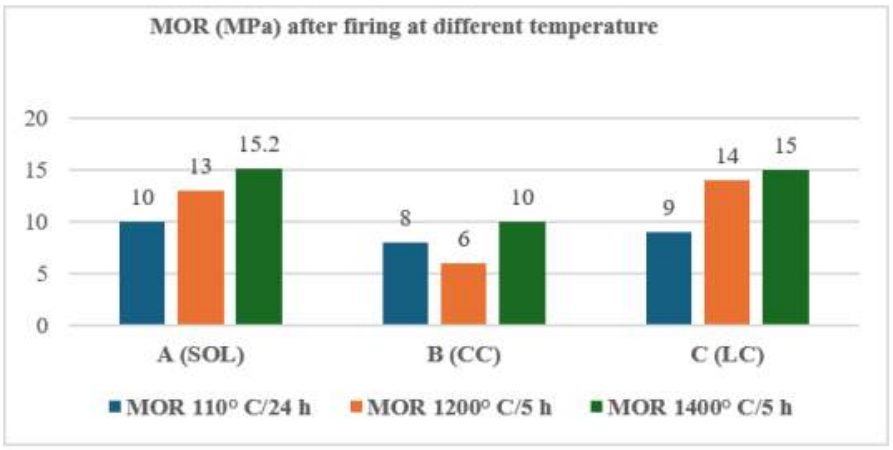


Figure 4: MOR of mixes at different temperature

5.6 Abrasion Resistance

The dense matrix and stronger bond system significantly enhanced abrasion resistance of Nano bonded material.

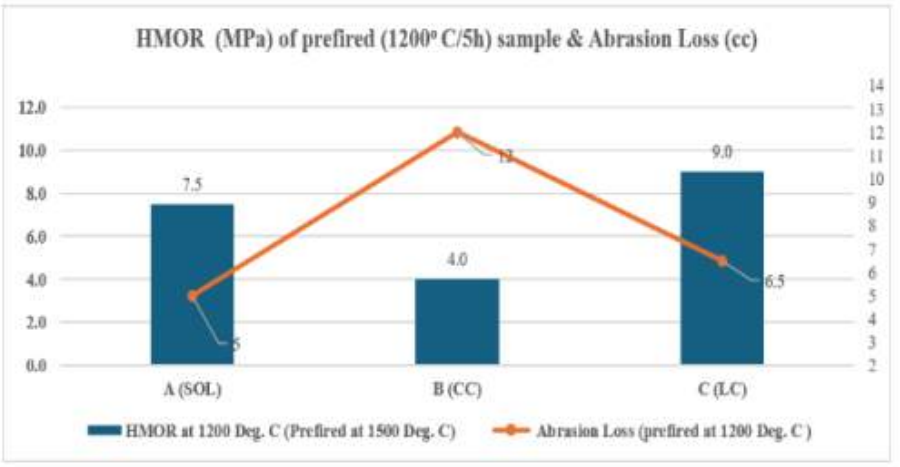


Figure 5: HMOR of mixes after firing at 1200 °C/ 5 hrs & Abrasion Loss

Better abrasion Resistance found in Nano bonded material compared to existing material

• Extended Lifespan: Parts and surfaces last much longer because the material wears down slowly or not at all.

• Lower Maintenance Costs: You do not need to replace or repair items as often.

5.7 Permanent Linear Change (PLC)

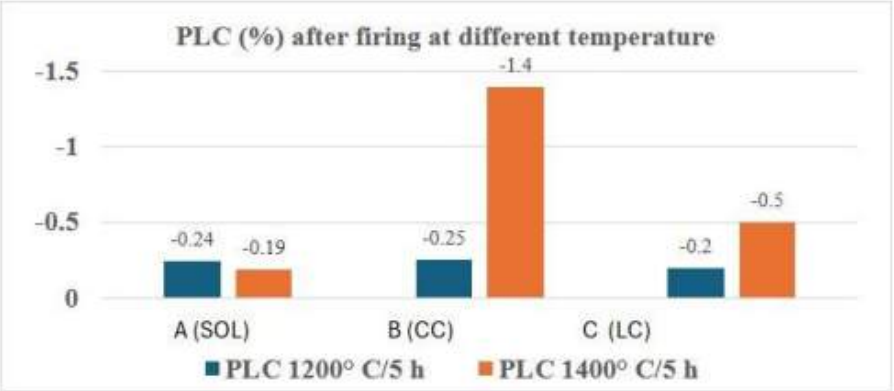


Figure 6: PLC of mixes at different temperature

Permanent linear change measurements showed excellent dimensional stability for Nano bonded materials compared to Low cement and Conventional Castable. Due to excellent volume stability, it reduces the chance for crack formation, improving thermal shock resistance, improving lining integrity and higher campaign life.

Controlled phase formation and uniform sintering behavior were responsible for these improvements.

5.8 Thermal Shock Resistance

Foundry ladles undergo severe temperature fluctuations. The Nano Bonded Castable exhibited Reduced crack propagation

• Improved strain accommodation

• High residual strength after thermal cycling

Tab. 4: Thermal Shock resistance with water quenching method

Parameters	A (SOL)	B (CC)	C (LC)
No. of Cycle (cy.)	No Cracks till 40 Cycle	Cracks after 25 cy.	Cracks after 38 cy.

5.9 Thermal Conductivity

The developed castable exhibited lower effective thermal conductivity which helps lowering shell temperature, reduced heat loss, improved metal temperature retention & lower fuel consumption.

The energy-saving potential contributes directly to overall operational efficiency.

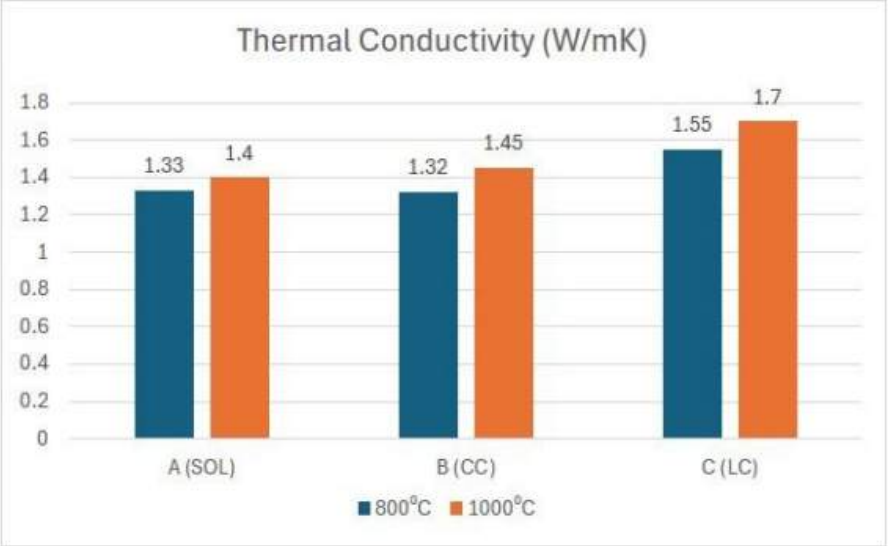


Figure 5: Thermal Conductivity of mixes at different temperature

5.10 XRD Analysis

X-ray diffraction was conducted to identify crystalline phases and bonding mechanisms.

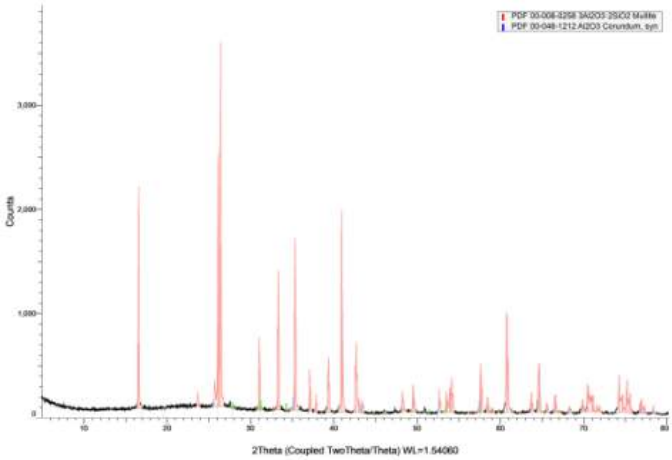


Figure 6: XRD of Nano bonded mix
Mullite – 92.6% and Corundum – 7.4%

The XRD analysis identifies Mullite and Corundum as the main compounds based on their diffraction patterns. Mullite and corundum phases enhance volume stability at elevated temperature of the material. It improves hot strength and abrasion and corrosion resistance.

5.11 SEM Observations

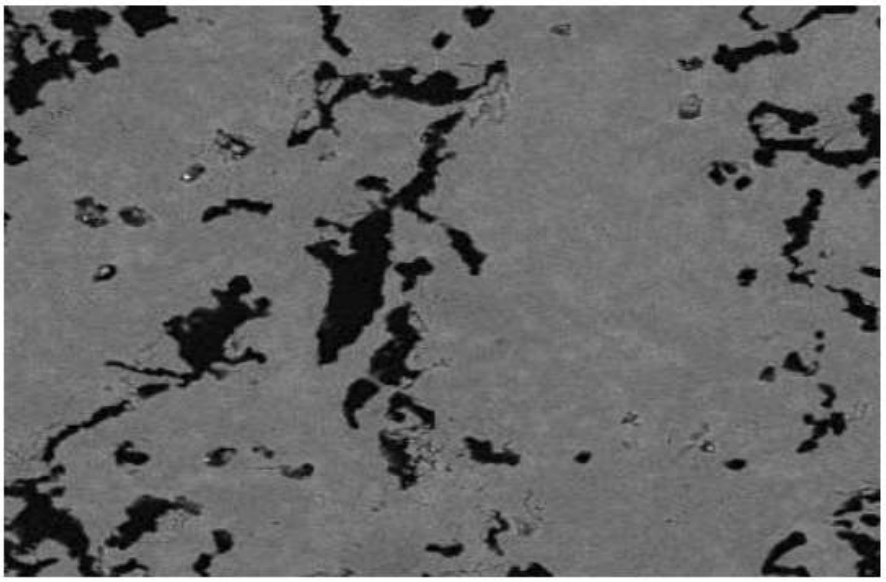


Figure 7: SEM of Nano bonded mix

SEM image shows dense microstructure with uniform matrix and strong particle-to particle bonding. Uniform nano micropore improves thermal shock resistance and corrosion resistance and chemical stability. SEM observations revealed controlled microcrack networks that helped dissipate thermal stresses without catastrophic failure.

6. Performance of the new material

Industrial trials were carried out in foundries processing grey iron and SG iron with ladles ranging from 3 MT to 5 MT capacity and average results were presented in the table below.



Figure 8: Industrial application at site

Tab. 5: Industrial performance of various types of materials used in Iron Foundry

Parameter	B (CC)	C (LC)	A (SOL)
Ladle Life (heats)	700	900	2000
Maintenance Frequency	High	High	Significantly Reduced
Repair Requirement	after 60 heats	after 90 heats	after 200 heats
Energy Efficiency	Moderate	Standard	Good

7. Conclusion

Lower service life of Ladle is vital productivity and energy loss for any Foundry producer. A significant saving on repair time and cost can be done by using suitable refractory material. Selection of the right ingredients helps to develop suitable refractory materials for Ladle of Foundry Industry. A new generation nano-bonded special castable has been developed for foundry ladle applications. The developed Nano bonded castable provides an advanced alternative to conventional and low cement castables used in foundry ladles. The optimized nano-bonding system provides improved matrix integrity and contributes to enhanced mechanical and high-temperature properties. Improved abrasion resistance, slag penetration & corrosion resistance contributes to lower mechanical wear during molten-metal handling and improving lining durability and stability.

The process of appropriate application is essential to achieve the final target using such a developed castable.

Industrial trials in 3–5 MT foundry ladles demonstrated an approximately 2.5–3 times increase in average service life compared with regularly used conventional and low-cement castables having comparable chemical compositions.

References

1. Sudip Paul & Sankha Chatterjee, Development of suitable shotcrete material to achieve better techno-commercial performance of torpedo ladle, IREFCON, 2024, P 19-24

2. Lee, W. E., & Vieira, W. D. Refractory Castables: Developments and Future Perspectives. Journal of the American Ceramic Society.

3. Sudip Paul1 ; Priti Ranjan Mishra2 ; Sanat Ganguli3 , Development of special castable for higher capacity rotary kiln in manufacturing of sponge iron through direct reduction of Iron, UNITECR, 2025

4. Schacht, C. A. Refractories Handbook. CRC Press.

5. Rigaud, M., et al. Castable Refractories for Iron and Steel Industry Applications.

ANALYSIS OF REFRACTORY WEAR IN THE MIDDLE ZONE OF DRI KILNS DUE TO PELLET AND IMPORTED COAL USAGE

Authors: Pradeep Passary & Jaidhish Passary

Abstract

This study investigates accelerated refractory wear in the middle zone of Direct Reduced Iron (DRI) rotary kilns associated with the increased use of iron ore pellets and imported coal, which significantly modify mechanical stresses, thermal profiles, and accretion behaviour. These altered operating conditions intensify higher abrasion, and coating instability, leading to premature degradation of conventional refractory linings and reduced kiln campaign life. A systematic analysis was conducted through field observations, material characterization, and evaluation of key process parameters to identify the underlying wear mechanisms. Based on these insights, optimized refractory compositions were developed with enhanced resistance to thermal stress, and mechanical wear under pellet-based and low-ash coal environments. The implementation of these engineered solutions resulted in improved coating stability and reduced refractory wear in the middle zone. Consequently, significant improvements were achieved in terms of extended campaign life, lower maintenance frequency, enhanced kiln stability, and increased overall operational efficiency, demonstrating a reliable and cost-effective approach for sustaining performance in modern DRI kiln operations.

Synopsis

The DRI industry has undergone significant changes in recent years, driven by the pursuit of higher production and improved operational economics. Increased production levels, the use of RB1 and RB2 coal, the shift from iron ore to pellets, and the occasional use of imported pellets have altered kiln operating conditions considerably. These changes directly affect the thermal, chemical, and operational environment to which refractories are exposed and can contribute significantly to accelerated wear and premature failure, particularly in the middle zone.

This paper seeks to establish a critical distinction: premature refractory failure is not necessarily a refractory failure. While refractory quality and application must certainly be evaluated, premature wear can also arise from changes in process conditions, raw materials, production intensity, operating parameters, or a combination of these factors. Therefore, when operating conditions change substantially, refractory failure should not automatically be attributed to the refractory material or its manufacturer without first examining the complete process.

Through root-cause analysis supported by operational data, years of field experience, and on-ground observations, this paper examines how evolving DRI practices influence refractory behaviour in the middle zone. It identifies key process-related factors contributing to premature wear and highlights the importance of evaluating refractory performance in the context of actual operating conditions rather than in isolation.

As a refractory fraternity, there is a need to collectively move towards a more collaborative and technically rigorous approach to failure analysis. Instead of responding to every premature failure simply through a free-of-cost (FOC) replacement,

the focus should first be on jointly identifying why the failure occurred. Replacing the refractory without addressing the underlying cause may only provide a temporary solution, leaving the same conditions to cause repeated failures, increased downtime and recurring losses.

Moreover, whenever an FOC replacement is provided for a failure that was not caused by the refractory manufacturer, the resulting loss extends beyond the individual manufacturer. It weakens the value of the entire refractory community and contributes to a loss that is ultimately borne by all of us. Such practices can also create an incorrect perception that refractory replacement alone is the appropriate solution, while the actual process-related cause remains unaddressed. Protecting the long-term interests of the refractory industry therefore requires that FOC replacements be considered only after a fair, technically sound and evidence-based assessment of the failure.

This paper therefore calls upon refractory manufacturers, DRI plant operators and industry experts to work together to identify the root causes of premature refractory wear and develop solutions suited to today's evolving operating conditions. A shared, data-driven understanding of failure mechanisms can help distinguish refractory-related failures from process-induced failures, reduce avoidable FOC replacements, protect the collective interests of the refractory community, improve refractory life and plant reliability, and ultimately create a more sustainable and mutually beneficial ecosystem for the DRI and refractory industry.

Introduction

The introduction of iron ore pellets and imported coal into DRI operations has significantly affected refractory performance, particularly in the middle zone of rotary kilns. This zone has become a major concern for both refractory manufacturers and DRI plant operators because refractory wear is accelerated and shell temperatures are higher.

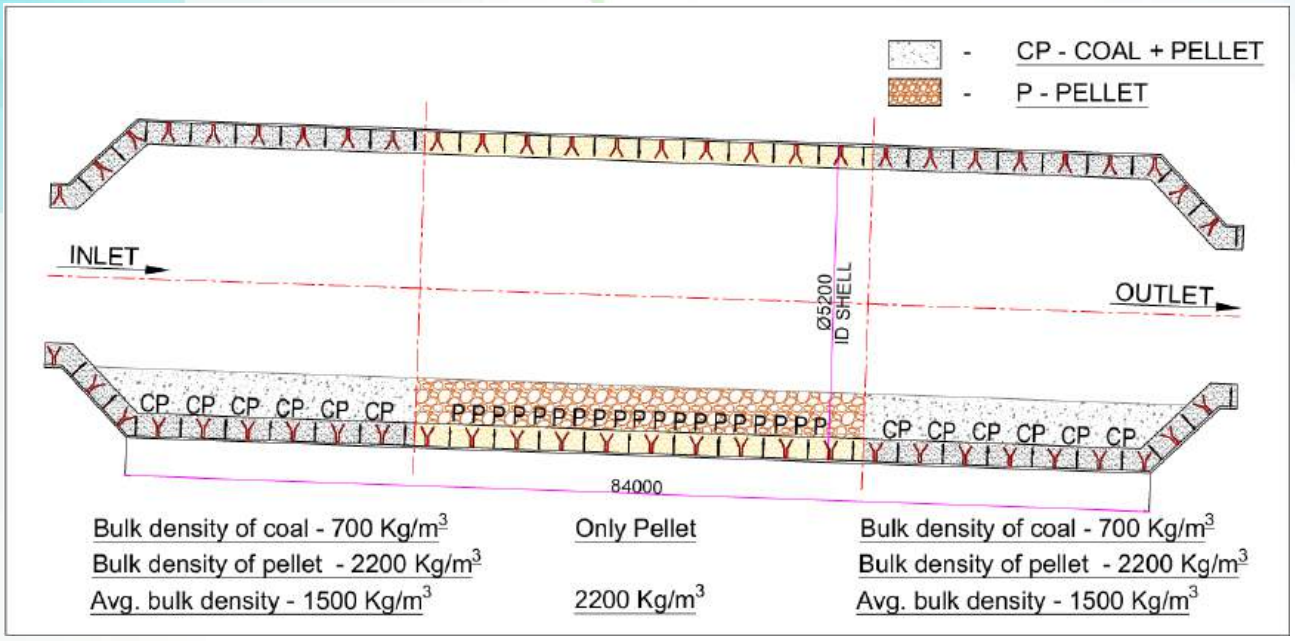
Our R&D team has been continuously investigating the root causes of this issue to develop an effective and sustainable refractory solution. This paper presents our analysis, experimental testing and final recommendations aimed at optimizing both refractory life and kiln performance.

Root Cause Analysis

1. Increased Abrasion Due to Pellets

Iron ore pellets have a higher tumbler index than conventional iron ore. As a result, they generate greater abrasion inside the kiln, particularly against the refractory lining.

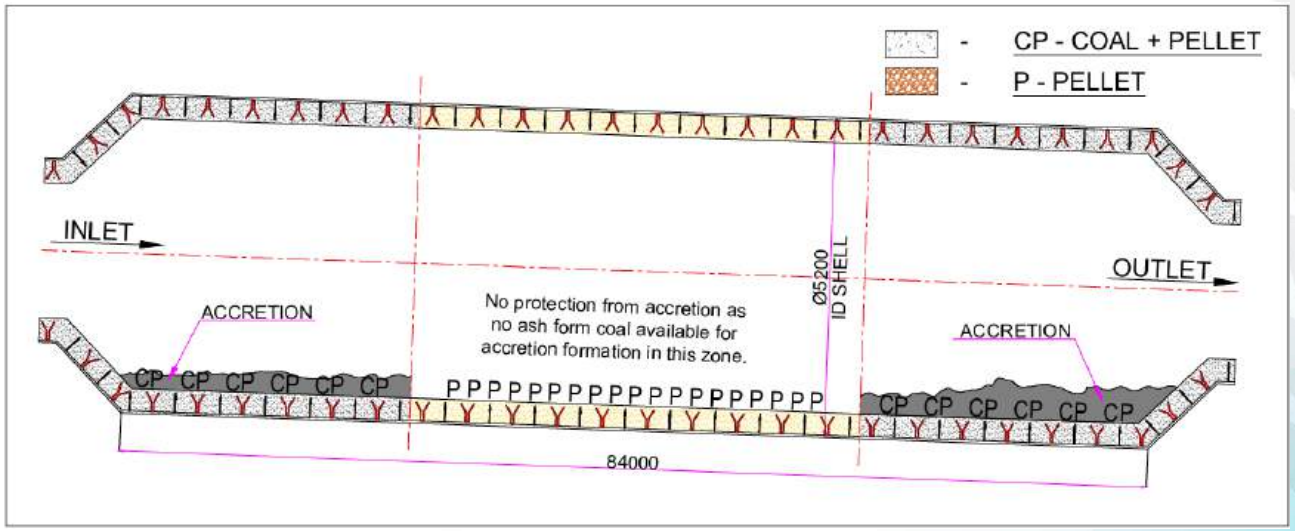
Kilns using pellets therefore experience a substantially higher wear rate than kilns using lump iron ore.



2. Reduced Accretion Layer from Imported Coal

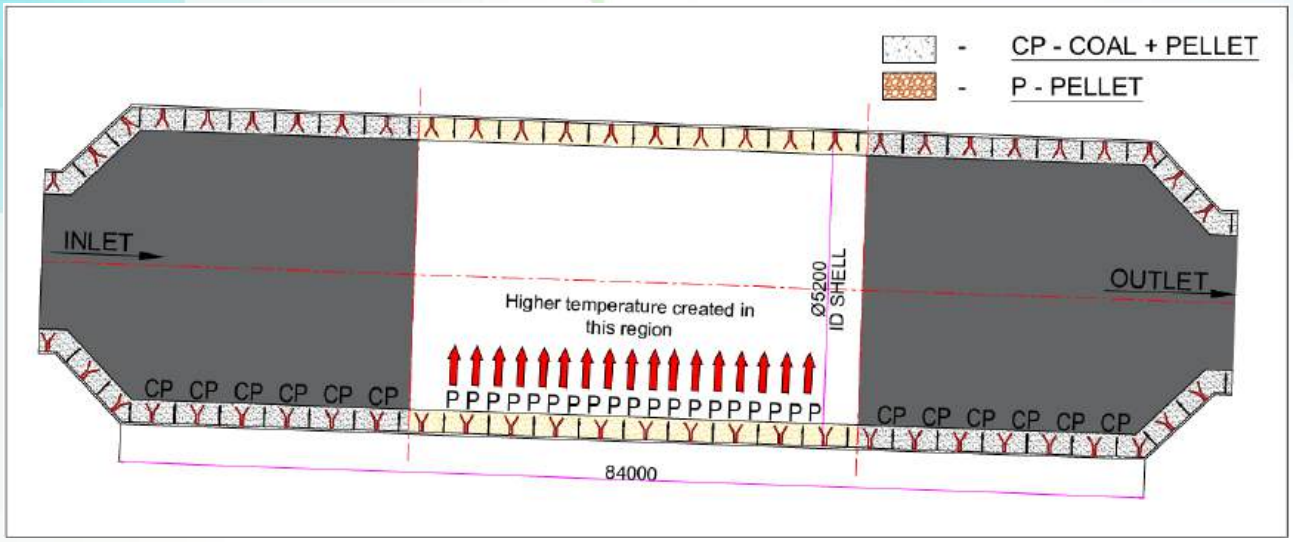
Indian coal generally contains more ash and has a lower ash fusion temperature. This promotes the formation of a natural accretion coating on the refractory surface. The protective accretion layer reduces the direct impact of raw materials and helps maintain a lower shell temperature.

Imported coal, however, contains less ash and therefore produces minimal accretion. The refractory surface is consequently exposed directly to abrasion and thermal loading, resulting in faster wear and higher shell temperatures.



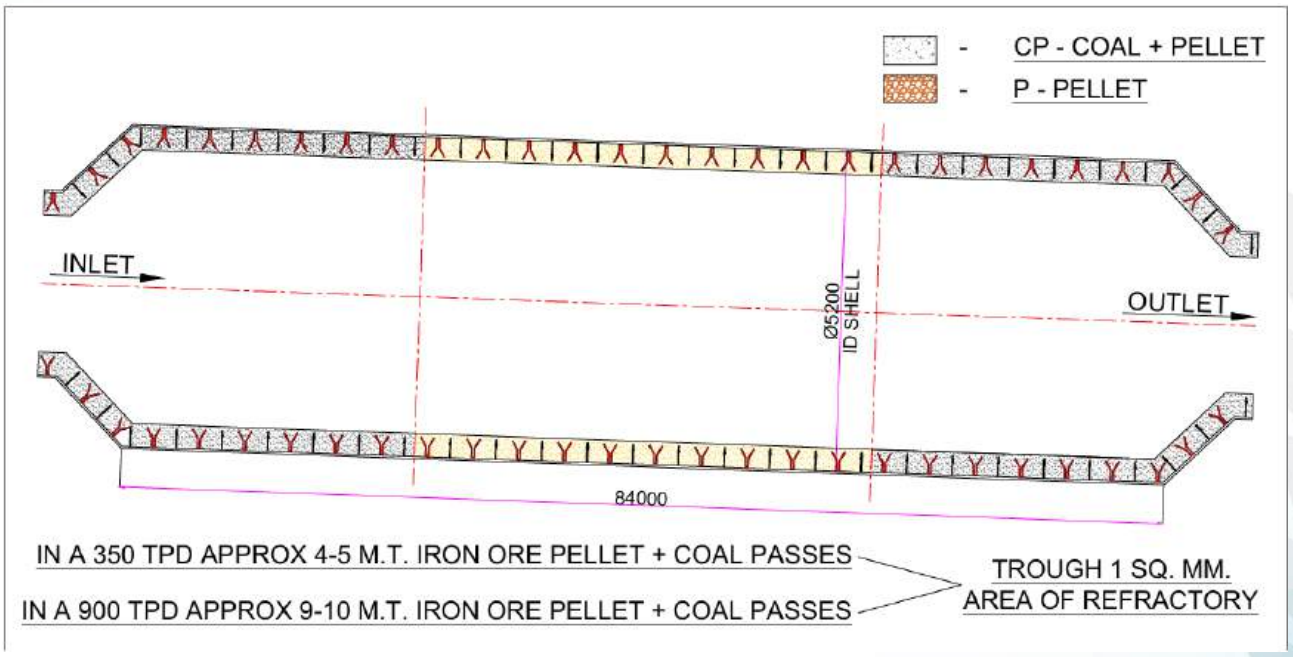
3. Elevated Operating Temperatures

Imported coal and iron ore pellets require higher combustion temperatures to sustain the reduction reactions. Kilns operating with these materials therefore tend to run at higher internal temperatures, which further increases shell temperature and imposes additional thermal stress on the refractory lining.



4. Increased Throughput and Thermodynamic Load

The use of pellets and imported coal has increased DRI productivity, thereby increasing the thermodynamic load within the kiln's fixed cross-sectional area. This higher load accelerates refractory deterioration, particularly in zones where a protective accretion layer is absent.



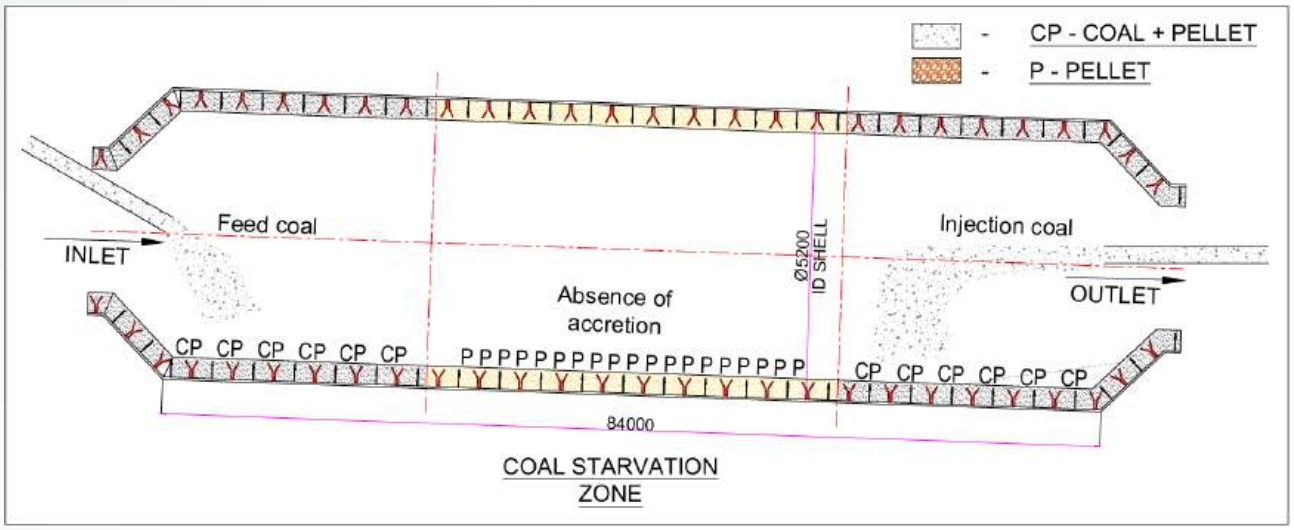
5. Coal Starvation in the Middle Zone

Because imported coal has high fixed carbon (FC) and low ash content, overall coal consumption in DRI operations has decreased considerably. As a result, the middle zone of large kilns often experiences coal starvation and is commonly referred to as the 'no-accretion zone'. This area receives minimal fuel from both the inlet and outlet injection points, resulting in:

- Absence of a protective accretion layer

- Direct contact between the refractory lining and moving red-hot pellets
- Higher shell temperatures even when other operating conditions are comparable to adjacent zones

Consequently, refractory wear in the middle zone is significantly greater than at the inlet or outlet.

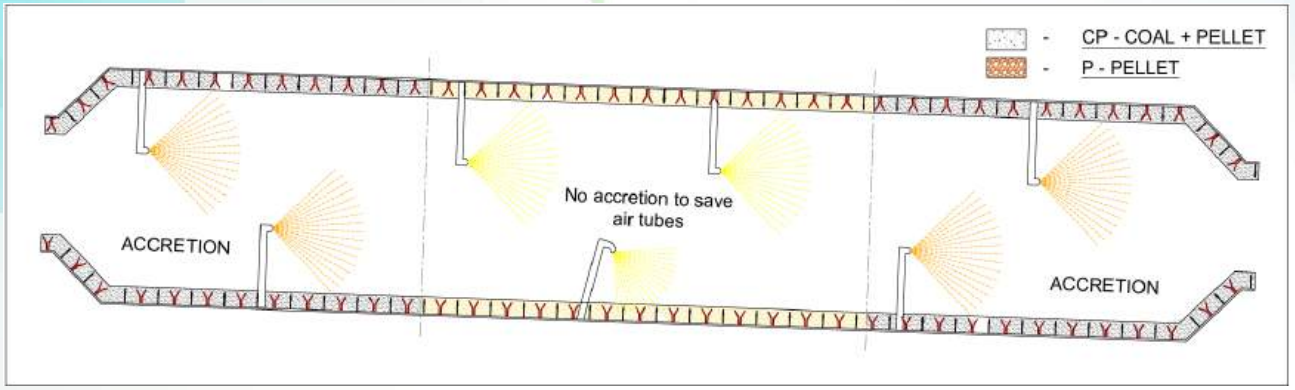


6. Disproportionate Refractory Wear in the Middle Zone Due to Air Tube Malfunction

Air tubes play a critical role in DRI kilns by supplying the air required for combustion. This air is necessary to maintain the high temperatures and reduction reactions required to convert iron ore into metallic iron. Equipped with air swirlers or similar flow-control elements, these tubes are designed to distribute airflow uniformly over the raw-material bed.

It has been observed that large kilns operating with imported coal and pellets experience air-tube failures relatively frequently. When the tubes are damaged by cracking, deformation or breakage, airflow becomes uneven or misdirected and can impinge directly on the kiln lining, adversely affecting kiln performance.

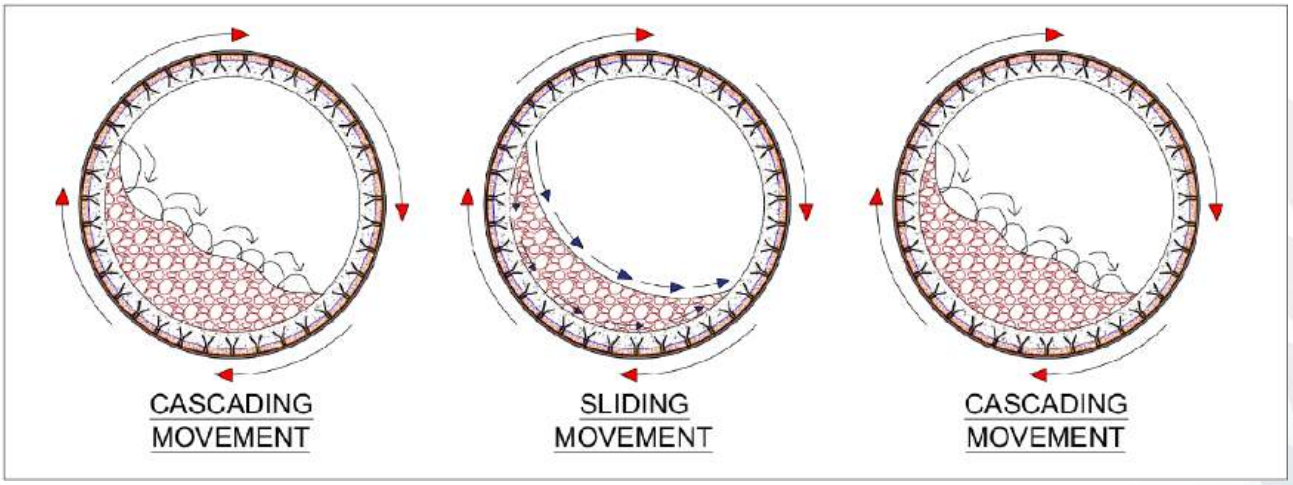
A major consequence is direct flame impingement on the refractory lining, particularly in the middle zone. Such uncontrolled exposure rapidly accelerates localized wear and erosion and can eventually cause this section of the kiln to develop an oval profile.



7. Pellet Movement: Cascading vs. Sliding in the Middle Zone

Because pellets are smooth and spherical, they tend to slide during kiln rotation rather than cascade in the manner of irregular iron ore lumps. At the inlet and outlet, the presence of coal and fines promotes cascading movement. In the middle zone, however, where coal and fines are largely absent, red-hot pellets predominantly slide over the refractory surface.

This sliding motion generates greater frictional force and increases wear of the refractory lining. Pellets also have a higher Tumbler Index, indicating greater mechanical strength and therefore a stronger mechanical impact during movement. Since the middle zone lacks the protective accretion layer, refractory erosion becomes even more severe in this critical region.

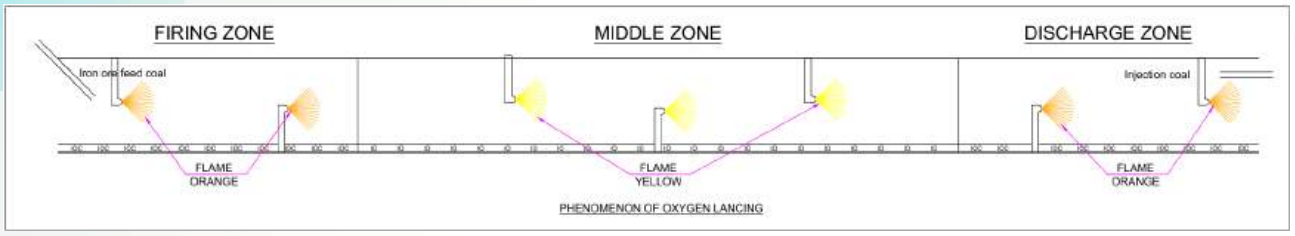


8. Frictional and Lancing Heat Generation

In the middle zone of the kiln, an increase in rotational speed (RPM), combined with reduced coal feed, leads to more frequent collisions between red-hot pellets. These collisions generate localized frictional heat and create concentrated thermal stress on the refractory lining.

At the same time, the lower coal feed and reduced carbon content can result in excess oxygen availability, creating a condition comparable to oxygen lancing. When insufficient carbon is available for reaction, the excess oxygen can raise local temperatures uncontrollably. This produces intense spot heating and further damages

the refractory surface. The combined effect of frictional heat and excess oxygen accelerates refractory wear and reduces refractory service life in the middle zone.



Conclusion

The use of pellets and imported coal has improved DRI throughput, but it has also adversely affected refractory performance, particularly in the middle zone. In the absence of an accretion layer, shell temperature rises and the refractory is subjected to greater mechanical and thermal loading, accelerating wear.

Comparative observations indicate that the same refractory quality generally achieves a longer service life in kilns using Indian coal and lump iron ore than in kilns operating with pellets and imported coal.

REAL KILN FEED TEST - A PRACTICAL EVALUATION FOR DRI KILNS

A PRACTICAL, ZERO-COST AND UNBIASED EVALUATION OF REFRACTORY PERFORMANCE UNDER ACTUAL KILN CONDITIONS

By Research & Development, Passary Refractories

Abstract

This study addresses the critical challenge of selecting suitable refractory materials for the middle (reduction) zone of Direct Reduced Iron (DRI) rotary kilns, where conventional laboratory tests fail to replicate the actual kiln environment characterized by carbon monoxide (CO)-rich reducing atmosphere, temperature cycling, and high accretion and abrasion loads. As a result, inappropriate refractory selection leads to accelerated wear, strong accretion bonding, high radiation, increased coal consumption, and reduced campaign life. To overcome this limitation, a plant-scale, real-condition evaluation method termed the Real Kiln Feed Test (RKFT) was developed, enabling direct comparison of refractory performance within the operating kiln using cube samples subjected to real feed and process conditions. The study evaluates Passary Refractories' mullite-based castable (MC-90) against a conventional calcined bauxite-based castable (CMP-89). Results demonstrate a significant performance difference, with CMP-89 exhibiting ~30.33% weight loss and structural failure within six cycles, while MC-90 showed only ~5.22% weight loss and retained structural integrity. The improved performance of MC-90 is attributed to its homogeneous engineered phase, stability in reducing conditions. The findings validate RKFT as a reliable, zero-cost, zero-bias method and establish mullite-based refractories as a superior solution for enhancing kiln stability, reducing accretion bonding, lowering coal consumption, and extending campaign life in DRI operations.

The Real Challenge in a DRI Kiln

In a DRI kiln, the objective is straightforward: improve kiln performance, reduce coal consumption, control accretion and extend campaign life. However, incorrect refractory selection, excessive wear, high radiation losses, rapid accretion and strong bonding between the refractory lining and accretion can significantly increase operating costs. Conventional laboratory tests are useful, but they do not fully reproduce the actual atmosphere inside an operating DRI kiln. Carbon monoxide exposure, a reducing atmosphere, temperature cycling, sponge iron dust and accretion loads interact in ways that are difficult to replicate in a laboratory furnace. For this reason, Passary Refractories uses a practical plant-scale CO exposure degradation evaluation referred to here as the **Real Kiln Feed Test (RKFT)**. It evaluates refractory performance inside the actual kiln environment rather than relying only on simulated or laboratory conditions.

The Test: Simple, Practical and Transparent

Step 1: Cast a 70 x 70 x 70 mm cube from the castable currently used in the kiln's most critical, middle or reduction zone. Emboss the cube with the letter 'A'.

Step 2: Passary Refractories prepares a cube of the same dimensions using its castable and embosses it with the letter 'B'.

Step 3: Fire both cubes in a laboratory furnace at the plant's operating temperature and record their initial weights.

Step 4: Feed both cubes into the kiln through the feed tube. The cubes travel through the kiln and are discharged along with the sponge iron.

Step 5: After every cycle, measure the cube weights, photograph them, inspect their physical condition and repeat the cycle until failure occurs.

The comparison makes deterioration visible cycle by cycle. One material may lose mass rapidly and eventually fail, while the other may lose weight gradually yet remain structurally stable.

Passary Refractories now uses this method regularly because it provides a clearer understanding of how its products behave under real plant conditions, without depending solely on laboratory test results.

Comparative Evaluation: Passary MC-90 (CASTABLE A) vs Chinese CMP-89 (CASTABLE B)

Two low-cement castables (LCCs) of almost identical chemical specifications were prepared for comparison: one based on Passary Refractories' in-house Synthetic Mullite MC-90 (CASTABLE A) and the other on Chinese CMP-89 (CASTABLE B). The bond, cement, additions, water, curing and firing conditions were kept the same. The principal difference was the raw material base.

Parameter	CASTABLE A	CASTABLE B
Raw material	Passary Synthetic Mullite MC-90	Chinese calcined bauxite CMP-89
Initial cube weight	1150 g	1220 g
Dimensions	70 x 70 x 70 mm	70 x 70 x 70 mm

Note: Both cubes had the same dimensions. The difference in initial weight resulted from the different densities of the raw materials used.

Cycle-by-Cycle Result





After four kiln cycles, CASTABLE B decreased from 1220 g to 850 g, corresponding to approximately 30.33% mass loss. CASTABLE A decreased from 1150 g to 1090 g, corresponding to approximately 5.22% mass loss.

During these cycles, the CASTABLE B cube showed progressive weakening, cracking of the bond, chipping of corners and substantial mass loss. By the sixth cycle, CASTABLE B had broken completely, while CASTABLE A remained in good condition. Real kiln. Real feed. Real CO atmosphere. Real difference.

Additional Test Data

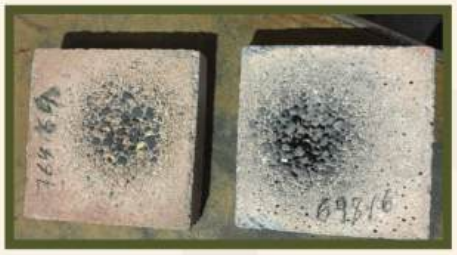
CASTABLE A	CASTABLE B
MC-90	CMP-89
Microsilica	Microsilica
CAC Cement 70%	CAC Cement 70%
Dispersant	Dispersant
PPF	PPF

Hot Modulus of Rupture (HMOR)

HMOR AT 1250 °C	
MC 90	114.31 kg/cm
CMP 89	78.84 kg/cm

ABRASION RESISTANCE AFTER FIRING AT 1200 °C	
MC 90	1.97
CMP 89	7.87

Abrasion Resistance Test



Refrasynth



Why Does CASTABLE A Behave Differently?

1. Chemically and mineralogically homogeneous engineered phase

CASTABLE A behaves as a chemically and mineralogically homogeneous engineered phase. This reduces variability in the raw material base and supports more consistent refractory behaviour.

2. Behaviour in a reducing atmosphere

The DRI reduction zone is an aggressive reducing environment. Under these conditions, the inherent nature of the refractory raw material becomes particularly important.

3. Behaviour of natural calcined bauxite

In a reducing atmosphere, impurity phases present in natural calcined bauxite can become chemically active. This can weaken the grains, promote inter-granular attack and accelerate abrasion.

4. More uniform thermal expansion

CASTABLE A is described as exhibiting more uniform thermal expansion, which helps limit microcracking, thermal-shock-related damage and sudden deterioration. Heterogeneous grains can expand less uniformly and may deteriorate faster.

5. Impurities in combined phases

The document attributes CASTABLE A's stability to impurities such as Fe2O3, CaO, MgO and TiO2 being present in combined phases rather than as free impurities. This is

associated with improved stability, weaker accretion bonding and easier accretion removal.

6. Homogeneity can matter more than a single chemical percentage

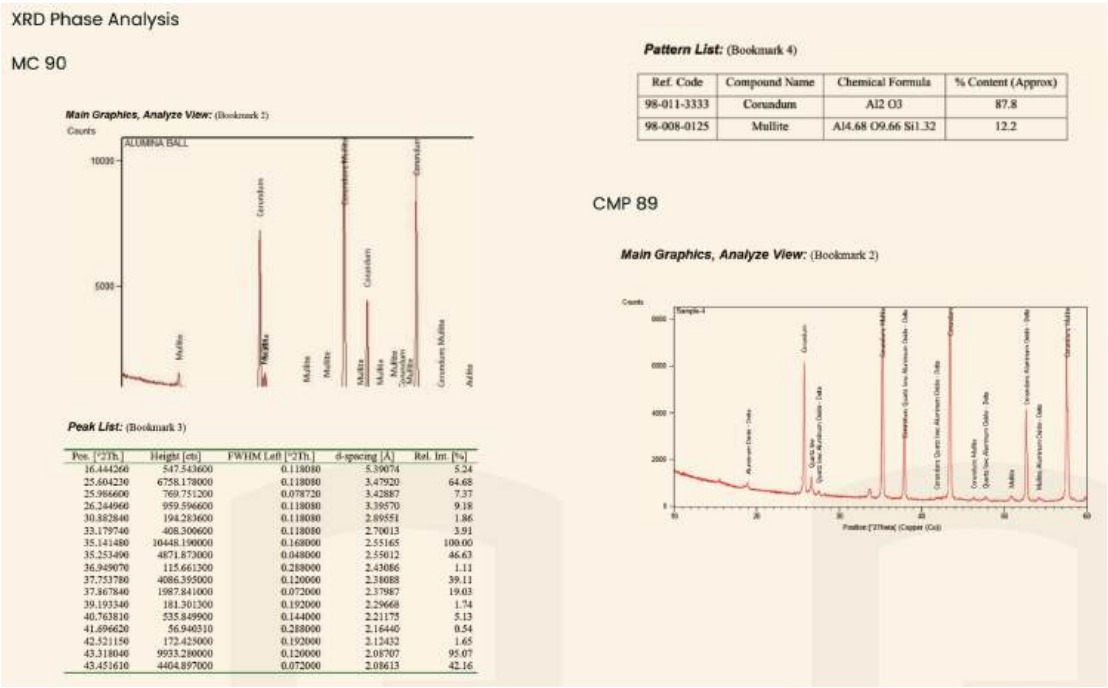
The comparison indicates that stable performance cannot be judged from one chemical value alone. The mineralogical structure and homogeneity of the raw material also influence behaviour under kiln conditions.

7. Potential operational benefits

The document associates the observed behaviour with lower radiation, reduced coal consumption, weaker accretion bonding, longer campaign life, easier shutdown cleaning, lower refractory load and improved kiln stability.

8. Low apparent porosity and anti-wetting behaviour

Low apparent porosity means fewer and more closed pores, reducing the opportunity for slag penetration. The presence of mullite is also described as contributing to anti-wetting behaviour, reducing slag adhesion and limiting degradation from slag attack.


XRD Phase Analysis

MC 90

Main Graphics, Analyze View: (Bookmark 2)

Counts

ALUMINA BALL

Peak List: (Bookmark 3)

Pos. [°2Th.]	Height [cts]	FWHM Left [°2Th.]	d-spacing [Å]	Rel. Int. [%]
16.444260	547.543600	0.118080	5.39074	5.24
25.604230	6758.178000	0.118080	3.47920	64.68
25.966600	769.751200	0.078720	3.42887	7.37
26.244960	959.596600	0.118080	3.39570	9.18
30.382840	194.283600	0.118080	2.89551	1.86
33.179740	408.300600	0.118080	2.70013	3.91
35.141480	10448.190000	0.168000	2.55165	100.00
35.253490	4871.873000	0.048000	2.55012	46.63
36.949070	115.661300	0.288000	2.43086	1.11
37.753780	4086.395000	0.120000	2.38088	39.11
37.867840	1987.841000	0.072000	2.37987	19.03
39.193340	181.301300	0.192000	2.29668	1.74
40.763810	535.849900	0.144000	2.21175	5.13
41.696620	56.940310	0.288000	2.16440	0.54
42.521150	172.425000	0.192000	2.12432	1.65
43.318040	9933.280000	0.120000	2.08707	95.07
43.451610	4404.897000	0.072000	2.08613	42.16

Pattern List: (Bookmark 4)

Ref. Code	Compound Name	Chemical Formula	% Content (Approx)
98-011-3333	Corundum	Al2 O3	87.8
98-008-0125	Mullite	Al4.68 O9.66 Si1.32	12.2

CMP 89

Main Graphics, Analyze View: (Bookmark 2)

Peak List: (Bookmark 3)

Pos. [°2Th.]	Height [cts]	FWHM Left [°2Th.]	d-spacing [Å]	Rel. Int. [%]
15.450880	101.994700	0.236160	5.73502	1.27
18.925980	241.285000	0.137760	4.68910	3.00
25.705600	5619.459000	0.137760	3.46571	69.79
26.633520	730.935000	0.157440	3.34703	9.08
27.485710	133.710200	0.157440	3.24517	1.66
33.752930	354.093000	0.196800	2.65557	4.40
35.231060	7869.173000	0.177120	2.54747	97.73
37.855330	3441.040000	0.118080	2.37669	42.73
41.766090	46.386260	0.314880	2.16275	0.58
43.407210	8052.145000	0.157440	2.08471	100.00
46.231640	108.254300	0.157440	1.96371	1.34
47.693310	136.412900	0.236160	1.90689	1.69
50.823090	174.995400	0.196800	1.79657	2.17
52.600340	3864.841000	0.144000	1.73853	48.00
52.762990	1792.302000	0.072000	1.73786	22.26
54.096570	91.167590	0.336000	1.69393	1.13
57.538320	7464.092000	0.144000	1.60052	92.70
57.709450	3608.571000	0.096000	1.60014	44.82

Pattern List: (Bookmark 4)

Ref. Code	Compound Name	Chemical Formula	% Content (Approx)
98-000-5217	Corundum	Al2 O3	91.2
98-004-6001	Quartz low	O2 Si1	5.3
98-008-0122	Mullite	Al4.44 O9.78 Si1.56	2.5
98-002-3773	Aluminum Oxide - Delta	Al2.67 O4	1

44.612030	40.470430	0.576000	2.02949	0.39
46.130510	131.811700	0.144000	1.96616	1.26
49.268280	43.967070	0.576000	1.84803	0.42
52.495310	4369.310000	0.120000	1.74177	41.82
52.647380	2224.436000	0.072000	1.74141	21.29
53.807130	89.948760	0.384000	1.70236	0.86
57.432270	8683.854000	0.120000	1.60322	83.11
57.602690	4277.368000	0.096000	1.60285	40.94
59.675040	220.880500	0.120000	1.54821	2.11

CHEMICAL ANALYSIS		
Property	MC-90	CMP-89
Al2O3 (%)	89 - 91	87.5 – 88.2
Fe2O3 (%)	1.6 - 1.8	1.6 – 1.8
TiO2 (%)	1.6 – 1.8	3.5 – 3.8
SiO2 (%)	5.0 – 5.5	4.8 – 5.7
CaO (%)	0.4 – 0.55	0.25 – 0.30
MgO (%)	0.2 – 0.4	0.20 – 0.30
Bulk Density (g/cc)	3.25 – 3.30	3.33 – 3.38
Apparent Porosity(%)	3 – 4	4 – 5

Chemical Analysis Reported in the Source

Conclusion

This evaluation is intended as a transparent, practical and plant-based comparison rather than a brochure claim or a conventional sales demonstration. The central principle is simple: allow the actual kiln environment to determine which refractory performs better.

Passary Refractories' proposed evaluation process is:

- Passary first submits an MC-90-based castable cube (CASTABLE A).
- A comparative cube from the plant's existing castable is prepared in the presence of the plant representative.
- Both materials are tested at the plant under the same real kiln conditions.
- The cubes are inspected and weighed cycle by cycle to document the observed difference.

No hidden conditions. No manipulation. No excuses. Let the kiln decide.

For plants seeking to reduce coal consumption, control accretion and improve campaign life, the Real Kiln Feed Test provides a direct way to compare refractory behaviour in the environment that matters most: the operating kiln itself.

Support: If additional assistance is required, Passary Refractories can support the plant team in conducting and demonstrating the test practically at the plant.

REDUCING THERMAL EXPANSION OF MAGNESIA–CARBON REFRACTORIES USED IN CONTINUOUS CASTING OF STEEL MAKING

Shekhar Kumar Shrivastastava[1], Kazi Asif Ahmed[2], Dr Saumen Sinha[3], Satyendra Kumar[4], Chinmay Basu[5], Samit Sengupta[6]

Calderys India Refractories Ltd

1.Director Growth Projects, Calderys, India; 2. Manager, Calderys, India; 3. Director Innovation and Technology APAC-Calderys; 4. Director – Industrial Operations & Projects, SWA-Calderys; 5. Chief Operating Officer, Calderys, India; 6. Business Development Director – Growth Projects, Calderys, India

Corresponding Author's e-mail: shekhar.shrivastava@calderys.com

Abstract

Continuous casting is a widely used technology to produce clean steel around the globe. However, the success of the technology depends on the performance of the continuous casting (CC) Refractories. Precisely, CC Refractories are used to regulate the flow of steel and protect the steel against exposure to the atmosphere during the different processing steps. It is subjected to high thermo-mechanical stress and extreme thermal shock. Hence, it is desirable to improve the reliability of the CC refractory products against high thermal shock and thermo-mechanical stress to achieve safe and efficient operation. Quite often, two or more dissimilar material systems are co-pressed together during manufacturing of CC Refractories to optimize its performance during Steel making. Composite material systems having different thermal expansions in a product, makes them structurally and thermally unstable and reduces its reliability during application. These products have a very high L/D (length/diameter) ratio of 10 to 15, so the reduction in present linear thermal expansion level to improve thermal stability and ensure product performance would be the key objective. As a first step, a standard composition of magnesia-Carbon which has higher thermal expansion compared to Alumina or Zirconia Carbon system generally applied in CC refractory was selected and the work was done to evaluate and modify the present binding system comprising PhenolFormaldehyde (PF) Resin a solid Novolac powder and a solvent. Keeping the same Novolac powder resin and experimenting with solvents and organic additive in the present binding systems have been studied. The study revealed that change in solvent and addition of organic additive resulted in reduction of linear thermal expansion significantly, but the downside of the experiment was its poor mechanical properties (CMOR). The study was extended to compensate for the loss in CMOR by incorporating a small amount of meso-phase carbon as a binding system, which helped in regaining the strength (CMOR) with other comparable properties. Furthermore, oxidation resistance has been evaluated after addition of meso-phase carbon. A quite encouraging result has been observed. Low thermal expansion and high strength are a global requirement for CC Refractories to ensure volume stability and reliability of products.

Keywords: Thermal expansion, Mechanical property, PF Resin, Organic additives.

1. Introduction

Monobloc stopper (MBS) and Sub-entry Nozzle (SEN) are the key components in continuous casting of steel making. The selection of material and geometry of MBS and SEN play a crucial role in achieving precise control of flow of steel against various steel grades. It ensures efficient and troublefree performances of continuous

casters. In pursuit of making cleaner steel, Calcium (Ca) treatment (via Ca-Si or Ca-Fe wire) is done in liquid steel to modify inclusions. Active Ca (more than 25 ppm) in steel aggressively attacks Al2O3 and corrosion rate of Al2O3-C material typically used in MBS nose and SEN seat increases abruptly. Consequently, it reduces durability and reliability of product performance [Refer Table 1 for eutectic temperature of different materials system]. To lower corrosion rate and increase durability the nose of MBS and seat of SEN are changed to MgO-C. So, the ideal MBS for Calcium treated steel would have Al2O3-C body co-pressed with the MgO-C nose [Figure - 1]. MBS with dissimilar material systems having different thermal expansions and chemistry makes it structurally and thermally unstable during application. Differential thermal expansion can lead to spalling, cracking, joint opening and dimensional instability.

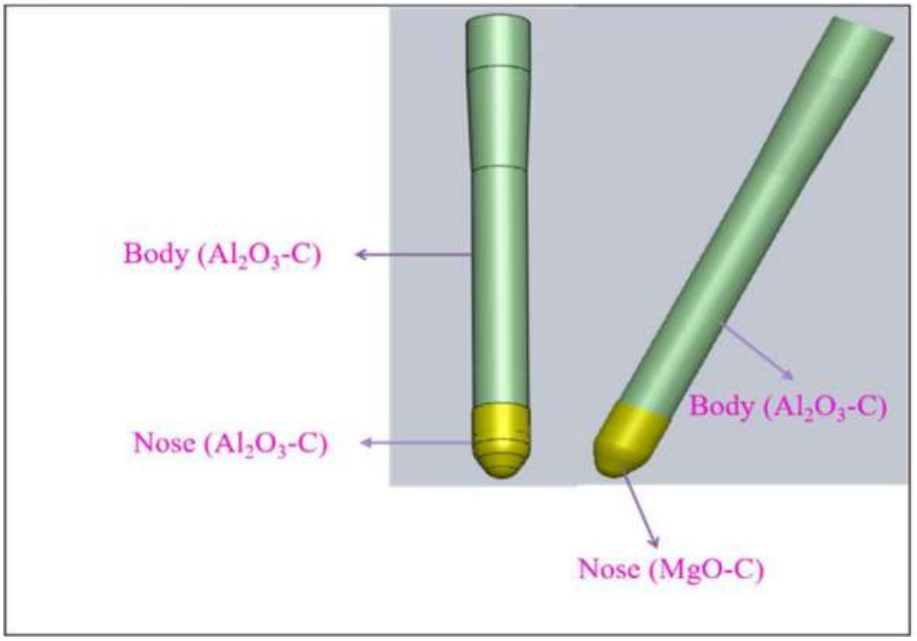


Figure 1 A Schematic diagram of MBS co-pressed with different materials

Reaction with CaO	Al_2O_3	SiO_2	ZrO_2	MgO
Eutectic temperature (°C)	1350	1436	2140	2370

Table 1 Eutectic temperature of different material system

The major field operational failure modes observed in MBS include molten-steel penetration at the nose– body junction, progressive erosion resulting in nose loss or cracking and breakage. Refer equation 1, indicating influence of Linear Thermal Expansion on
Thermal Shock Resistance.

$$R = (T/E\alpha)\, f(v) \quad (1)$$

R = Thermal Shock Resistance
T = Tensile Strength (CMOR)
E = Modulus of Elasticity
α = Coefficient of Thermal Expansion
f(v) = Function of Poisson ratio depending upon the shape of the product

MBS has a very high L/D (length/diameter) ratio approximately 10 to 15 times, so reducing linear thermal expansion gradient of body (Aluminacarbon) and nose (Magnesia-Carbon) and making it to nearly same may improve structural and thermal stability and reduce above stated issues of the field. A standard composition of MgO-C having higher thermal expansion compared to Al2O3-C has been selected and investigated [Refer Table 2 for typical MBS

properties]. Afterwards the work has been extended with an aim to reduce expansion by 1, Modifying the present resin binding system to optimize carbonization, 2, Incorporating expansion compensating organic additives termed as a polymer in the study with the optimized resin system, 3, Addition of meso-phase carbon to optimize carbon bond and 4, Evaluation of oxidation resistance after meso-phase carbon addition.

Properties of MBS	Body	Nose
Al_2O_3%	48.4	4.8
CaO%	0.8	0.9
MgO%	0.65	68.65
SiO_2%	12.5	4.5
Loss on Ignition (%) at 1000°C / 2hrs	32.4	18.54
Linear thermal expansion up to 1200°C (%)	0.56	1.1

Table 2 Typical properties of MBS

Results of the study has been evaluated in terms of measuring binder Viscosity and Carbonization, product's Apparent porosity (AP%), Bulk density (BD), Cold modulus of rupture (CMOR), Linear coefficient of thermal expansion (TE%) up to 1200°C, Oxidation resistance and SEM.

2. MATERIAL AND METHODS

Standard formulation F0 of MgO-C for MBS nose and its properties are shown in Table 3 and Table 4 respectively.

Ingredients	Weight (%)
	F0
C	18.5
MgO	74
Anti-Oxidant (Si, Al)	6
Glass	1.5
Powder Resin (Novolac)	(+) 8.2
Solvent	(+) 5.4

Table 3 Standard formulation of MBS nose (F0)

STD Mix F0	AP (%)	BD (gm/cc)	CMOR (Kg/cm^2)	Thermal Expansion upto 1200°C (%)
Typical	16.5	2.46	102	1.12

Table 4 Properties for formulation F0 of MBS

Standard process flow for MBS manufacturing as shown in Figure 2.

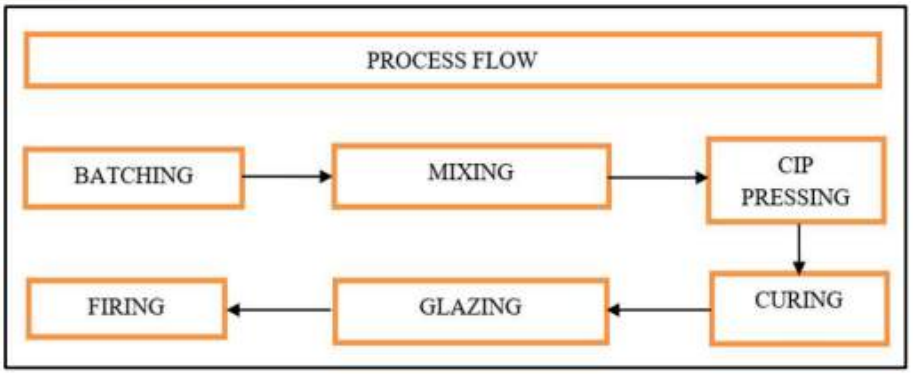


Figure 2 Process Flow for MBS Manufacturing

2.1. OPTIMIZATION OF CARBONIZATION OF THE BINDING SYSTEM

The present binding system comprising PF Resin (Phenol-Formaldehyde) a Novolac powder with 10% Hexa (Hexamethylenetetramine) named 301 and solvent. A standard procedure has been followed to evaluate degree of carbonization. Resin and solvent have been mixed together in the following proportion Powder Resin : Solvent – 60:40. Two solvents, Solvent A and Solvent B have been tested, keeping the same powder resin, results are shown in Table 5.

Powder Resin	Solvent	Mix ratio	Carbon%
301	A	60:40	52.1
301	B	60:40	58.2

Table 5 Degree of carbonization of solvent A and B

Solvent B exhibited a higher degree of carbonization than Solvent A.

2.2 EFFECT OF POLYMER ON VISCOSITY OF RESIN BINDING SYSTEM

To see the effect of polymer on viscosity of Resin with Solvent A and B, polymer addition has been done as per Table 6, and viscosity of Resin melt was measured at various temperatures.

Powder Resin	Solvent	Ratio	Polymer addition (%)
301	A	60:40	0.5
301	B	60:40	0.5

Table 6 Polymer addition in Resin with Solvent A and B

The objective of polymer incorporation is for better coating of binder to aggregate which leads to a homogeneous distribution of carbon components in the mix. Results of viscosity upon polymer addition are shown in Figure 3 and Table 7.

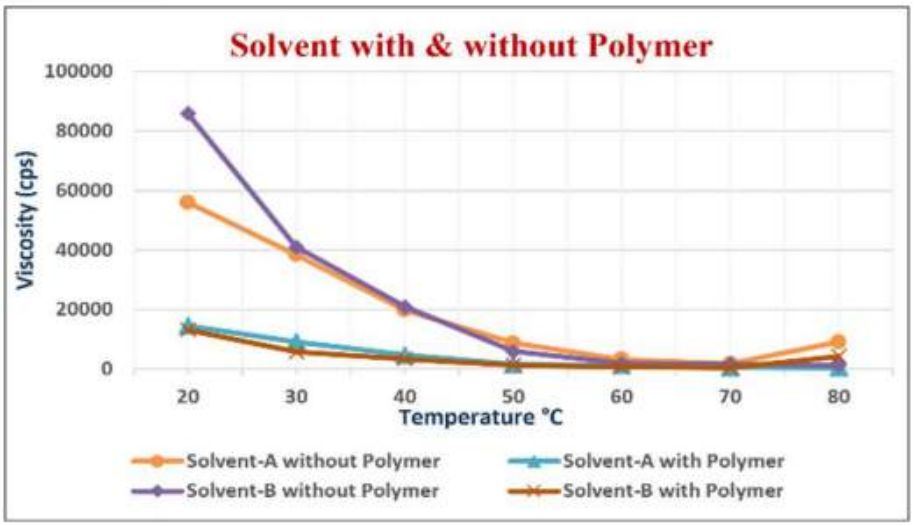


Figure 3 Viscosity of Resin-Polymer at various temp.

Temp (°C)	Solvent-A without Polymer	Solvent-A with Polymer	Solvent-B without Polymer	Solvent-B with Polymer
50	8800	1639	5939	1340
60	3300	1377	2020	742
70	1800	619	1688	379

Table 7 Comparative viscosity of Resin-Polymer system

As shown in Figure 3, polymer addition resulted reduction in viscosity, particularly at the (50 – 70)°C temperature range in both the Solvent A & B. However, with Solvent B has shown a better result. The lower viscosity is expected to improve uniform coating of refractory aggregates, especially graphite flaked due to its non-wettable nature.

Two formulations F1 and F2 have been made as per Table 8 with the combination of Solvents and polymer. Its effect has been thoroughly analyzed.

Ingredients	Weight (%)	Weight (%)
	F1	F2
C	18.5	18.5

MgO	74	74
Anti-Oxidant (Si, Al)	6	6
Glass	1.5	1.5
Powder Resin (Novolac)	(+) 8.2	(+) 8.2
Solvent - A	(+) 5.4	-
Solvent - B	-	(+) 5.4
Polymer	(+) 0.0 ~ 1.0	(+) 0.0 ~ 1.0

Table 8 Polymer addition in mix with Solvent A & B

2.2.1 EFFECT OF POLYMER ADDITION ON SIZE OF GRAPHITE FLAKES (Size 80 µm)

Lower viscosity of Resin system helped to improve coating and uniform distribution. It reduced the need for intensive mixing, resulting in lower graphite flake breakage and assured homogeneous distribution of graphite flakes & carbon bond into the matrix. Homogeneous distribution and larger flakes help to suppress thermal expansion.

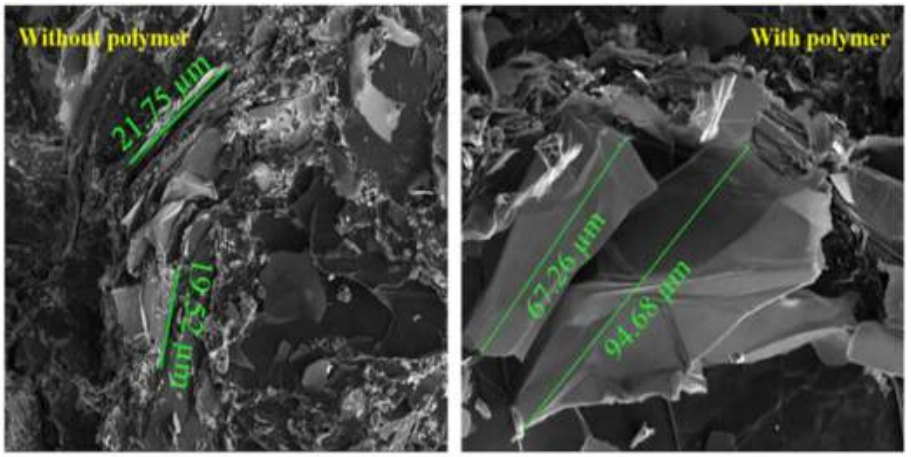


Figure 4 Microstructure of Mix with & without Polymer

In Figure 4 it can be observed that Polymer is helping to reduce breakage of flake graphite during mixing due to less internal friction.

2.2.2 EFFECT OF POLYMER ON LINEAR THERMAL EXPANSION & CMOR

Polymer has been added at different concentrations in formulations F1 & F2 as per Table 8 and their coefficient of linear thermal expansion up to 1200°C and respective CMOR have been evaluated to optimize polymer addition. Results of TE(%) and CMOR of formulations F1 and F2 derivatives are shown in Figure 5 and 6 respectively.

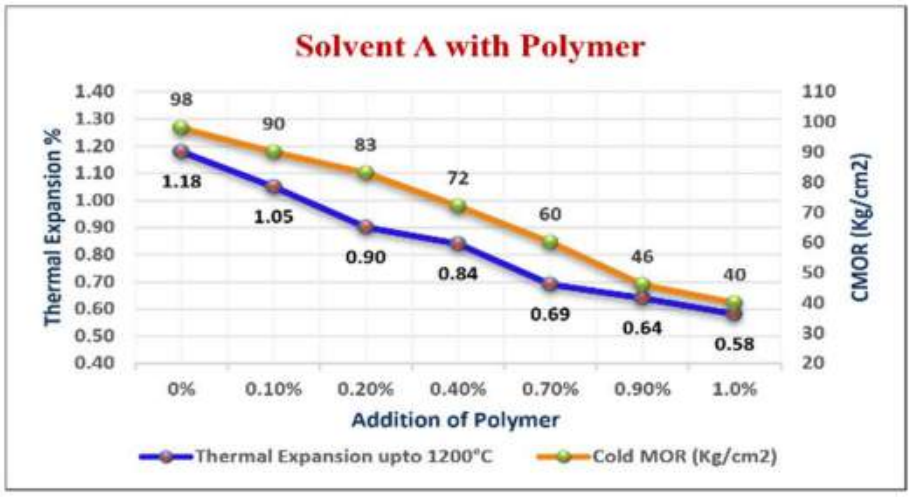


Figure 5 Effect of Polymer on TE(%) and CMOR of F1

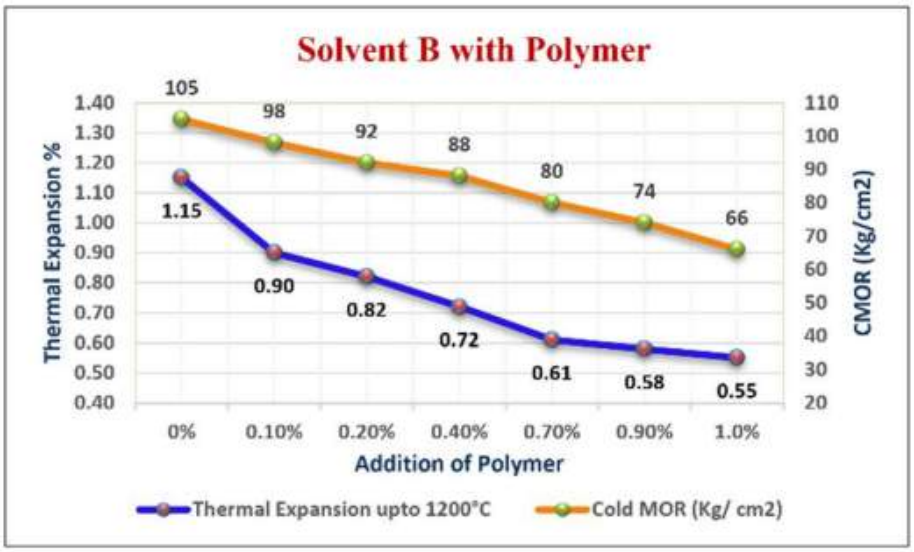


Figure 6 Effect of Polymer on TE(%) and CMOR of F2

From Figure 5 and 6 it shows that in both the formulations F1 and F2, there is a substantial drop of thermal expansion with gradual increase of polymer. However, the drop in CMOR came as a downside of polymer addition. Drop in CMOR and TE(%) are quite linear in nature which requires optimization. Moreover, formulation F2 with solvent B showed comparatively encouraging results in terms of TE(%) and CMOR at 0.7% of polymer addition.

2.3. INCORPORATION OF MESO-PHASE CARBON TO COPENSATE DROP IN CMOR

Mesophase carbon with the varying concentration incorporated in formulation F2 with 0.7% polymer and evaluated.

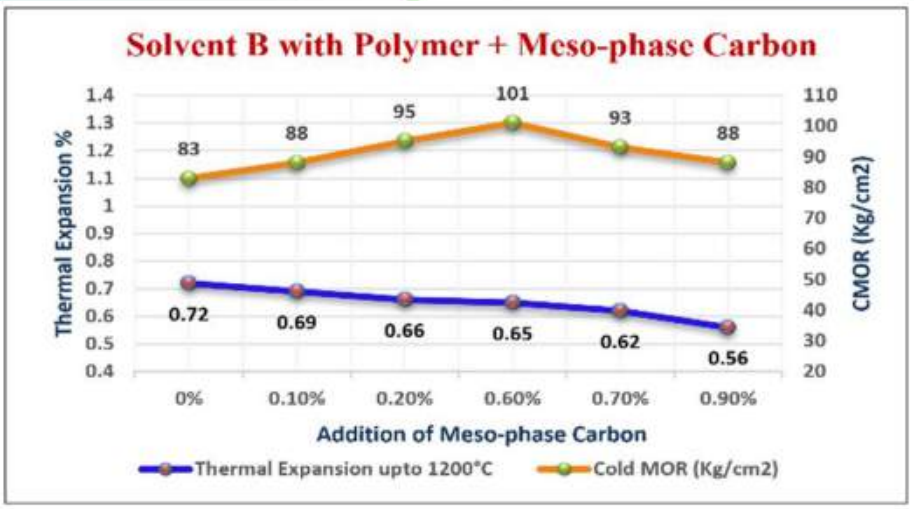


Figure 7 Effect of Mesophase Carbon on TE% & CMOR

From Figure 7, it is observed that with addition of 0.6% of mesophase carbon in formulation F2 with 0.7% polymer, now termed as F3, there is a regain of CMOR without sacrificing TE(%).

2.4 COMPARATIVE STIDY OF OXIDATION RESISTANCE at 1000°C/3hr

After getting encouraging results with meso-phase carbon addition in terms of TE(%) and CMOR, a comparative oxidation resistance of standard formulation (F0), F2 and F3 have been compared. From Figure 8 it is observed that F3 shows better oxidation resistance.

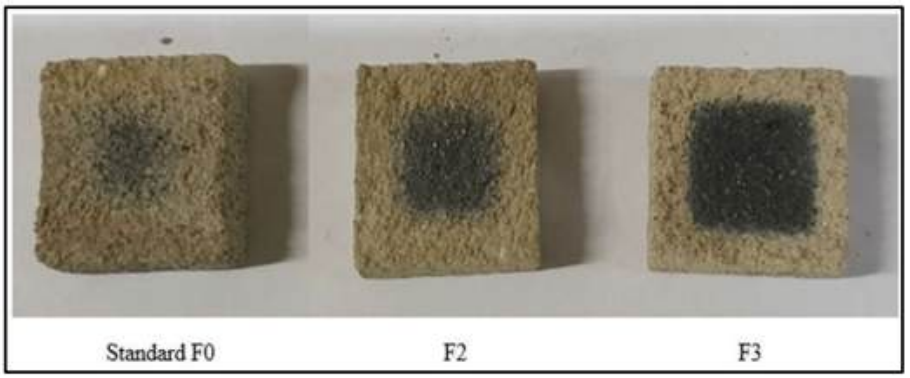


Figure 8 Study of oxidation resistance of F0, F2 & F3

3. CONCLUSION

- MgO–C is preferred for the MBS nose because of its better resistance against Ca-treated steel; however, its differential thermal expansion [Ref Table 2] w.r.t. Al_2O_3–C body make MBS thermally and structurally unstable.
- Carbonization of binder has been optimized by selecting suitable solvents. Solvent B has shown better results [Ref Table 5].
- Incorporation of polymer improved MgO-C mix properties [Ref Table 7, Fig 3 & 4] and suppressed the thermal expansion significantly. At the same time a gradual decrease in CMOR has been noticed [Ref Fig 5, 6].
- Decrease in CMOR has been compensated by addition of meso-phase carbon without

sacrificing TE(%) [Ref Fig 7]. It also improved oxidation resistance [Ref Fig 8].

- MgO-C formulation (F3) developed for MBS nose will have the similar thermal and structural benefits for SEN seat area.
- Lab results of the developed formulations await validation in the field for thermal and structural stability.

4. REFERENCES

1. Michio Inagakia, Keiko Fujitab: Formation of graphite crystals at 1000 - 1200°C from mixtures of vinyl polymers with metal oxides, Pergamon 2001.
2. Kimberly A. Trick and Tony E. Saliba: Mechanisms of the pyrolysis of phenolic resin in a carbon/phenolic composite, Pergamon 1995.
3. Liu Jun, LiHongXia1, Feng Haixia: Influence of carbores binder on the strength of MgO-C Materials, 3rd International Conference on Material, 2015.
4. Zhicheng Liu, Weihua Shen: Low-temperature formation of nanocrystalline b-SiC with high surface area and mesoporosity via reaction of mesoporous carbon and silicon powder, ELSEVIER 2005.
5. A.S. Gokce, C. Gurcan, S. Ozgen, S. Aydin: The effect of antioxidants on the oxidation behavior of magnesia–carbon refractory bricks, Ceramics International 34, 2008.
6. Jigang Wanga, Haiyun Jianga, b, Nan Jiangc: Study on the pyrolysis of phenol-formaldehyde (PF) resin and modified PF resin, Thermochimica Acta 2009.

DEVELOPMENT OF INDIGENOUS BASIC HEARTH MASS FOR THE COLD AND HOT REPAIR OF ELECTRIC ARC FURNACE AND CONARC FURNACE

Pravash Gourav, Raja Sarkar, Bhushan Bobde, Saumen Sinha

Calderys India Refractories Limited, India

Abstract

EAF route is being adopted more in India. This is due to its flexibility in using different raw materials such as scrap, DRI, and hot metal etc. The hearth of Electric Arc Furnaces (EAF) and Conarc furnaces is a very critical zone. It faces high temperature, slag attack, and metal penetration during operation. Due to these harsh conditions, the hearth lining gets damaged over time and needs regular repair to maintain safe and stable furnace operation. As a result, the requirement for reliable and efficient hearth repair materials is increasing.

Suitable dry basic hearth repair mass for EAF and Conarc furnaces are not produced in India. All such products are mostly imported. Also, most available products are designed separately for cold repair and hot repair, which makes operation more complex.

To overcome this gap, we have developed an indigenous product, 'Hearth DVM' under the "Make in India" initiative. The formulation is designed using selected raw materials suitable for Indian conditions
.

The main advantage of this product is that it can be used for both cold and hot repair. It shows quick sinterability, Iron oxide present in the formulation reacts with calcium oxide to form dicalcium ferrite phase ($2CaO.Fe_2O_3$) which serves as the primary ceramic bonding phase during operation. This quick sintering creates a dense, sacrificial protective layer (or "bond") on the bank and bottom of the EAF, minimizing the maintenance downtime of EAF between heats. In the paper grain size distribution, thermomechanical properties at different temperatures were studied for the formulation. Slag corrosion behavior was studied using Factsage 8.2 interaction model at the application temperatures. The product was successfully used in Indian steel plant, helped to maintain hearth profile, improving lining life, and ensuring stable furnace operation. Performance feedback will also be discussed in the paper This development is an important step towards self-reliance, as it is the first indigenous dry hearth repair mass in India with dual application capability.

Keywords: EAF, Hearth DVM, Magnesia, Sintering

1. Introduction

EAF is round bottom with cylindrical side wall shape. The cylindrical side wall is attached to the top of the bottom shape. Electric arc furnace consists of several layers of refractory with steel shell. It has four different zones.

(A) Cylindrical Side wall
(B) Electrode
(C) Roof Electrodes
(D) Bottom hearth

There are two portions of the EAF hearth one is called Working Hearth, and another one is called Sub hearth. Working hearth portion is lined with the DVM monolithic refractory and Sub hearth is lined with the Magnesia Carbon or Magnesite bricks along with high alumina bricks against the steel shell. In working hearth magnesia or dolomite based ramming mass is used which developed strength during the heating of EAF.

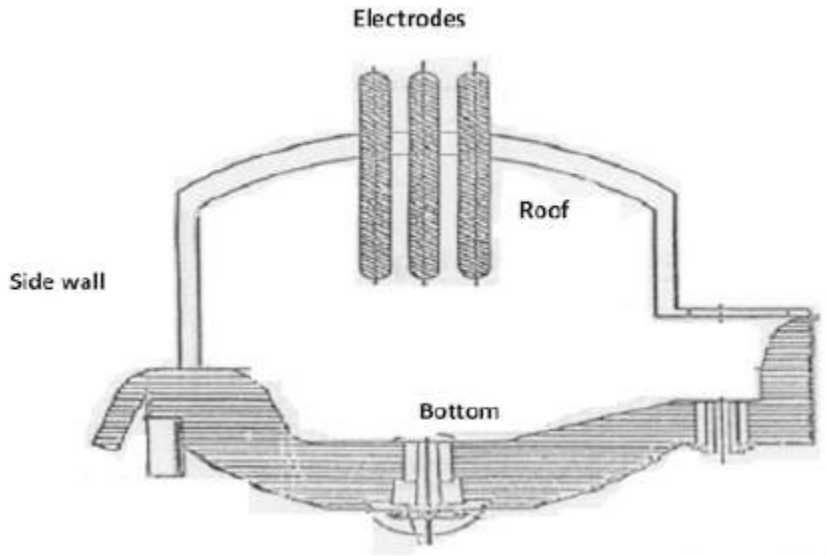


Figure 1 Schematic diagram of EAF

EAF DVM is used for both fettling and ramming in hot and cold conditions respectively. Magnesia based DVM contents 70% to 90% of Periclase and Dolomite based DVM are the double carbonate of Periclase and Lime. Dolomite has 55 % to 60 % lime (CaO) and 40 % to 45 % of MgO. The high melting point of magnesium oxide (2800 °C) in MgO based DVM materials is an advantage as corrosion point of view and dolomite based DVM has Eutectic point of 2300 °C temperature which is more thermodynamically stable to slag and metal [1,2], so Dolomite based DVM has also good corrosion resistance. EAF DVM consists of calcined magnesia and dolomite as the main raw materials with calcium and super fines iron oxide as additives. Fe_2O_3 reacts with CaO to form C2F ($2CaOFe_2O_3$) in the DVM, which acts as the main ceramics bonding phase. Since the melting point of C2F ($2CaOFe_2O_3$) is 1400 °C and it's decreased to DVM consistence of liquid iron so the sintering of EAF DVM starts from 1100 °C. temperature

$$2CaO+Fe_2O_3=2CaO\cdot Fe_2O_3$$

EAF DVM formed different layers during the primary steel making process in electric arc furnace (EAF)[3].

(A) Wear Layers

Wear Layers are directly in contact with hot metal. The thickness of this layer is around 10-20 mm. This layer is in contact with metal pool. When the temperature of the electric arc furnace decreases the color of wear layers becomes graywhite.

(B) Sintering Layers

The sintering layers are dark brown and very dense with no permeability which prevents the penetration of liquid metal inside the EAF DVM. The thickness of these layers is around 40 to 60 mm.

(C) Transiting Layers

This layer is between sintering and unchanged layers. The layers of this zone are half sintered and it is light brown in color. The thickness of these layers is around 50-80 mm.

A CaO/SiO_2 ratio greater than 2 of DBM promotes the formation of ($2CaOFe_2O_3$) in the hearth ramming mass, Calderys EAF DVM contains homogeneous distribution of Fe_2O_3 within the magnesia grains which ensure the uniform formation of $2CaOFe_2O_3$which helps in achieving the quick consistent sintering with higher sintered density uniformly through the grains of ramming mass. This uniform distribution of $2CaOFe_2O_3$ helps in increasing the slag corrosion & erosion resistance[3,4].

Under the reducing condition Fe^{3+} is reduced

to Fe^{2+}& this Fe^{2+} diffused to the magnesia grains,magnesiowustite solid solution is formed,it improved the thermal stability and the corrosion-erosion resistance of hearth ramming mass. For SiO_2 rich slag CaO of ramming mass reacts with SiO_2 and it's formed the dicalcium silicates phase (C2S). Due to diffusion of SiO_2 from slag and formation of dicalcium silicates phase, local viscosity of slag is increased so the penetration of liquid slag inside the hearth ramming mass is minimum hence it prevents the slag penetration inside the ramming mass, so corrosion resistance of EAF hearth mass is high[5].

This paper will discuss the development work of hearth ramming mass based on thermomechanical properties at different temperatures and fact sage analysis.

This paper will also include the field trial feedback of hearth ramming mass and its successful installation of EAF DVM.

2. Experimental

Based on the formulation and additives system, two Cylinders (50mm Dia and Height) were rammed and cured at 250 °C for 4 hours and afterwards fired at 1550 °C for 3 hours.



Figure 2 EAF DVM after Curing at 250 °C

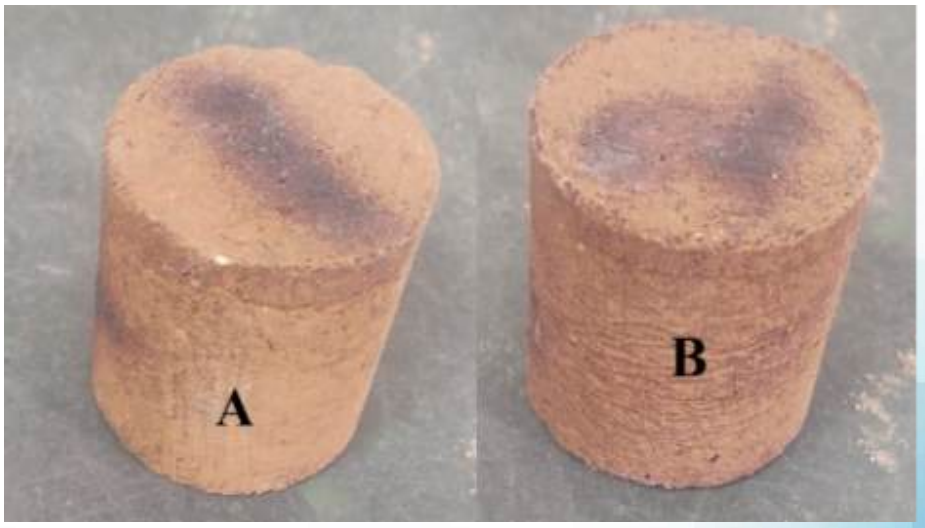


Figure 3 EAF DVM after firing at 1550 °C

3. Results and discussion

(a) Chemical Composition

PRODUCTS	MgO	CaO	Fe_2O_3
EAF DVM	74.80	19.40	02.71

Table 1 Chemical Composition (XRF) of EAF DVM

(b) Grain Size Distribution

EAF DVM has a combination of coarse and fines aggregates. Coarse grains aid in reinforcement of the DVM matrix. The product should have good bond strength to withstand Scrap impact during EAF feeding. Fine particles help in quick sintering of EAF DVM.

(c) Bulk Density&CCS of EAF DVM

High CCS & B.D indicates the dense microstructure and good sintering of hearth ramming mass which has high slag corrosion resistance and mechanical wear resistance.If CCS value of ramming mass exceeds 500 Kg/cm^2 it indicates the deeper sintering of ramming mass happen which is not good for EAF campaign life. Due to higher densification unreacted ramming mass is also sintered behind the working lining of ramming mass so the thermal conductivity is increased through the lining hence the heat loss from the furnace bottom plate will be maximum therefore the shell temperature of EAF will be very high it reduced the campaign life of furnace. Hence CCS value should be between 300& 500 kg/cm^2 to avoid heat loss from shells. Lower CCS value below 300 Kg/cm2 indicates poor sintering and low mechanical strength (low wear resistance) of ramming mass.EAF DVM has CCS value between 300 Kg/cm^2 to 500 Kg/cm^2 which indicates this newly developed product has excellent wear resistance and corrosion resistance.

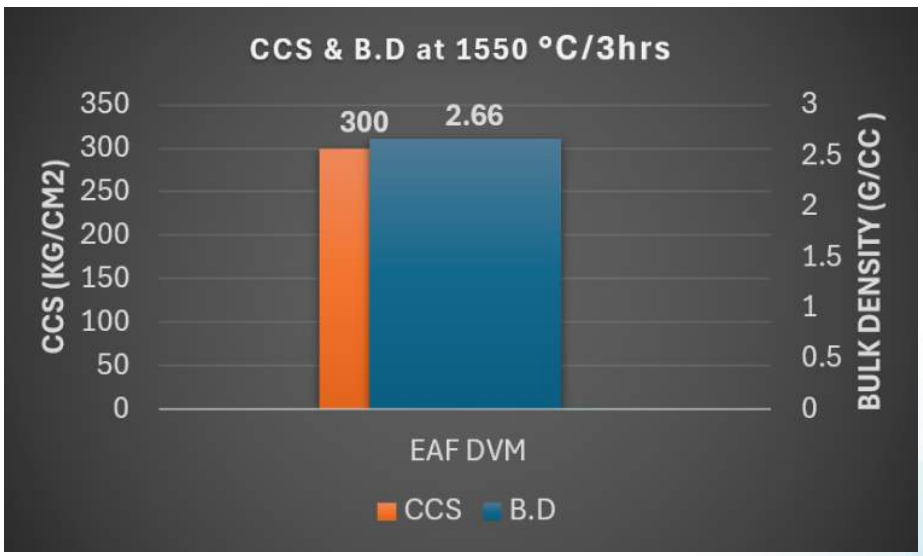


Fig 4 B.D & CCS of EAF DVM After firing at 1550

(d) PLC of EAF DVM

PLC indicates the dimensional & thermal stability of ramming mass; lower PLC value prevents the crack formation under thermal & mechanical stress. PLC value below 4% at 1550 °C/3hrs, indicates the excellent thermal stability. PLC below 4 % also indicates the phase distribution of ramming mass is uniform through the grains of ramming mass. PLC of EAFDVM is -3 to -4 % at 1550 °C/3hrs.

(e) FACT SAGE of EAF DVM

Thermodynamic simulations were performed using FACT SAGE 8.2 at three different temperatures (interaction with following slag at 70:30(slag) ratio). From fact sage analysis it is found that as operation temperature of EAF is increased from 1550 °C to 1650 °C amount of liquid phase formation is increased by 23-24 %.

MgO	Al_2O_3	SiO_2	MnO	Feo	CaO
07	06	15	03	25	40

Table 2 Chemical Analysis (%) of Slag

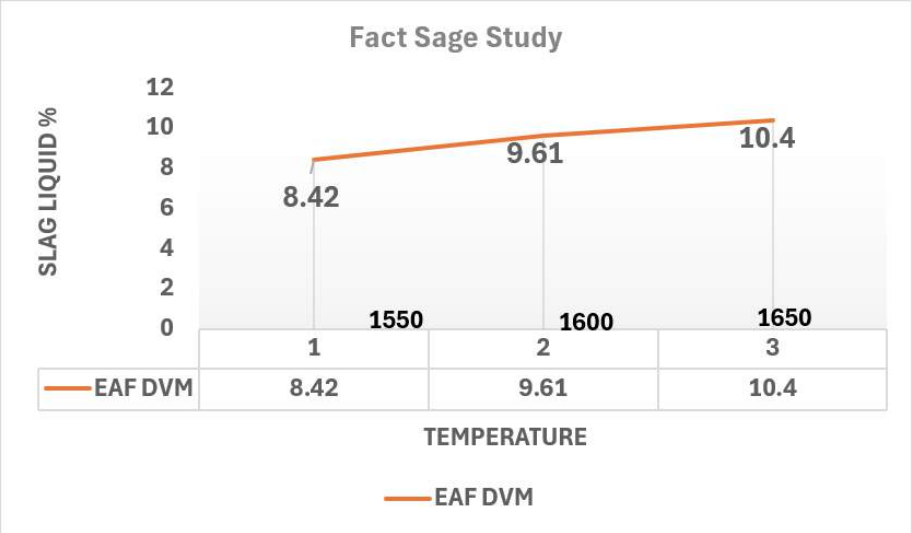


Fig 5 Fact Sage Study at three temperatures

4. Installation & Customer Trial Feedback

EAF DVMramming mass was successfully used in Indian Steel Plant (hearth & bank area). This product achieved 78-85 heats which showed excellent performance characteristics in Hot Condition (Hot fettling) of EAF.

EAF capacity (MT)	200
Operating Mode	Oxygen Blowing +Arcing
Arcing + Blowing Time	72-80 (Mins)
Tapping Temperature	1620-1650 °C

Table 03 Parameters of EAF

Charge Mix (%)	Quantity
Solid Scrap	8-10
DRI	25-35
Liquid Iron	65-75

Table 04 Charge Details

Compound	Slag Chemistry
CaO	40-50
SiO2	15-20
MgO	30-35
P2O5	01-03

Table 05 Indicative Slag Chemistry of EAF

Products	EAF Capacity	Heat Life
EAF DVM	200 MT	78-85

Table 06 Field Trial Feedback

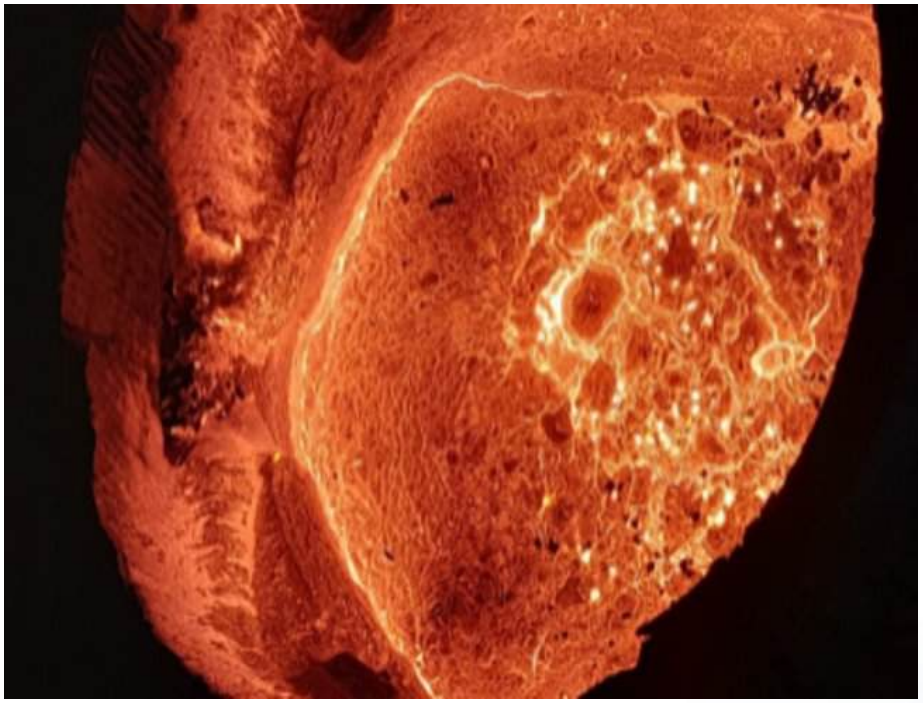


Fig 6 Hearth & Bank Area of EAF DVM

4.Conclusion

EAF DVM has been developed domestically in India. Based on the lab trial analysis (CCS, B.D, PLC) and thermochemical modeling (fact Sage 8.2) EAF DVM products has been successful field trial at Indian Steel Plant in hot condition (fettling), where its gives 78-85 numbers of heats for hot condition. This product has potential to be used in cold conditions also.

References

1. C. Sadik, O. Moudden, A. El Bouari and I.-E. El Amrani, "Review on the elaboration and characterization of ceramics refractories based on magnesite and dolomite," Journal ofAsian Ceramic Societies, pp. 219-233, September 2016.
2. M. C. Wöhrmeyer, J. M. Auvray, B. Li, H. Fryda, M. Szepizydn,D. Pörzgen, N. Li and W. Yan, "Novel Calcium MagnesiumAluminate Bonded Castables for Steel and Foundry Ladles,"in Proceedings of the Unified International Technical Conference on Refractories (UNITECR 2013)., Hoboken, USA, John Wiley & Sons, Inc., 2014.
3. J. LiuXiaodong G. L. Messing, A. R. Selçuker and R. C. Bradt, "Reactive phase casintering of dolomite," in Sinterg and heterogeneous catalysis, Plenum Publishing Corporation, 1984, pp. 329-339.
4. Botnikov, Kh H. A. Yeprem, "Effect of iron oxide addition on the hydration resistance and bulk density of doloma," Journal of the European Ceramic Society, vol. 27, pp. 1651-1655, 2007.
5. 5. M. Umakoshi, K. Mori and Y. Kawai, "Corrosion Kinetics of Refractory Materials in Molten CaO-FeO-SiO2 Slags," in Second International Symposium on Metallurgical Slags and Fluxes, Warrendale, PA, USA, 1984.

DRIVING PRODUCTIVITY EXCELLENCE IN IF GRADE STEEL: A NOBLE INITIATIVE AT TATA STEEL KALINGANAGAR

Nabid Anjum Khan; Sourav Ghosh; Anup Kumar Pandey; Rajnish Anand Jha;
Ashutosh Kumar; Sujat Ali Khan

Abstract

Interstitial Free (IF) steel is a critical product segment at Tata Steel Kalinganagar, primarily catering to automotive and exposed-panel applications due to its superior formability, excellent surface quality, and consistent mechanical properties. However, production of IF grade steel is inherently challenging owing to narrow chemistry control windows, stringent process discipline requirements, high sensitivity to rejections, and extended processing cycles that adversely impact productivity. With increasing customer demand and growing pressure on cost competitiveness, improving IF grade productivity without compromising quality became a strategic imperative. This noble initiative was therefore undertaken with a structured continuous-improvement mindset to enhance IF grade steel production through refractory life enhancement and optimization of critical process parameters, ensuring sustainable gains in productivity and operational excellence. Various initiatives have been undertaken to enhance productivity by optimising operational parameters such as reduction in treatment duration, optimisation of material additions and change in refractory design, and improvement in refractory quality. These measures have significantly improved the availability of RH vessels for IF-grade steel production.

Keywords: Clean Steel, RH Snorkels, Process parameters

1. Introduction

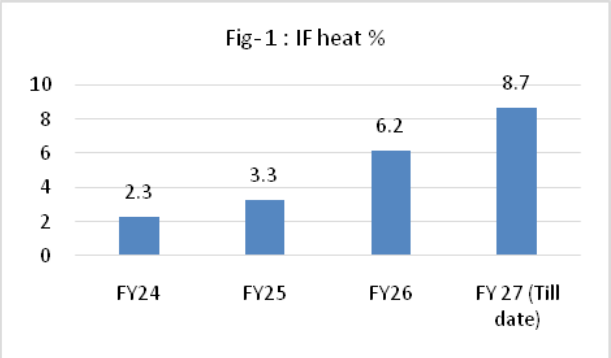
Tata Steel Kalinganagar (TSK) facility in Odisha stands as a landmark achievement in India's steelmaking journey. Conceived and developed as a greenfield project, the plant was designed to overcome the limitations of legacy operations and has rapidly evolved into one of the most advanced and sophisticated integrated steel manufacturing facilities within the Tata Steel group globally.Following the successful commissioning of its 3 MTPA Phase-I expansion and the subsequent Phase-II expansion, the facility has increased its crude steel production capacity to 8 MTPA (Million Tonnes Per Annum). The site is also home to India's largest blast furnace, underscoring its scale and technological excellence. Leveraging cutting-edge metallurgical processes, digital manufacturing technologies, and robust sustainability practices, Kalinganagar is well-positioned to produce next-generation, high-strength steels for critical sectors such as automotive, infrastructure, defence, and energy. Beyond manufacturing excellence, the plant fosters a vibrant ecosystem of collaboration and innovation. It provides opportunities for startups, entrepreneurs, research institutions, and established industries to partner in developing advanced materials, implementing smart manufacturing solutions, and accelerating technological innovation across the steel value chain.

For producing IF (Interstitial Free) steels, which are extensively used in exposed automotive panels, household appliances, and deep-drawing applications, extremely high steel cleanliness is essential. IF steels require ultra-low levels of carbon, nitrogen, oxygen, sulphur, phosphorus, and non-metallic inclusions to achieve superior formability, surface finish, and mechanical performance. At Tata Steel Kalinganagar (TSK), the production of IF-grade steels has

increased significantly over the years, driven by growing demand from the automotive sector. IF-grade production at TSK is shown in Fig. 1.

The RH (Ruhrstahl-Heraeus) degassing process is one of the most efficient secondary steel refining technologies used for producing ultra-clean steels. The process facilitates the removal of dissolved gases such as hydrogen, nitrogen, and oxygen, while also promoting decarburization and inclusion flotation. In this process, the steel ladle is positioned beneath a vacuum chamber equipped with inlet and outlet snorkels immersed in the molten steel. Argon gas is injected through the inlet snorkel, creating a gas-lift effect that continuously circulates molten steel through the vacuum chamber. Under deep vacuum conditions, the molten steel undergoes rapid degassing, enabling the production of demanding steel grades such as IF steels, API steels, and electrical steels. At TSK, the RH unit is a 310-ton SMS Mevac facility with a higher circulation rate and is a critical enabler for advanced steelmaking.

The RH vessel and snorkels are lined with high-performance refractory materials, predominantly magnesia-chrome bricks, to withstand severe thermal shocks, vacuum conditions, steel circulation, and chemical attack during refining operations. Despite their robust design, the refractory lining is subjected to intense wear due to prolonged exposure to high-temperature molten steel and slag. At Tata Steel Kalinganagar, the RH refractory campaign life was initially limited to less than 45 heats, resulting in frequent maintenance shutdowns and reduced RH availability. The problem was further aggravated by extensive metal jamming and skull formation inside the vessel, which increased the relining and refurbishment duration to 12-15 days, adversely affecting steel production and operational flexibility.



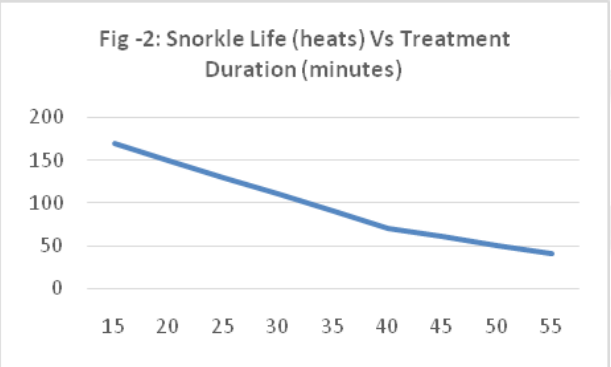


Fig-1 : IF Production trend at TSK
Fig -2 :RH snorkel life vs Treatment duration

Higher Circulation rate increased the erosion of inlet snorkel,resulted in an average refractory wear rate of 2.75-3.25 mm per heat, making the inlet snorkel the critical life-limiting component of the RH system. Consequently, the overall RH refractory campaign life was restricted to 45-50 heats,

Improvement Initiatives

To address the challenges of low refractory life and prolonged relining duration, a series of technical and operational improvement initiatives were undertaken. These included optimization of refractory design and material quality, standardization of gunning and repair practices, improved vessel cleaning methodologies, enhanced process control during RH operation, and reduction of treatment-related thermal and chemical stresses. The objective was to improve refractory wear resistance, minimize metal jamming, reduce maintenance downtime, and enhance RH availability for clean steel production.

1. Optimization of Refractory Design and Material Quality :A comprehensive review of the RH refractory design was carried out based on observed wear and erosion patterns. The conventional uniform lining approach was replaced with a zonal lining concept, wherein refractory quality and thickness were optimized according to area-specific wear profiles. The snorkel brickwork design was modified from straight joints to staggered joints to improve structural integrity and reduce localized erosion. The anchorage system was upgraded by changing the anchor material and design to SS-310 grade anchors, enhancing thermal stability and lining retention. In addition, several design modifications were implemented in the vessel bottom, top ring of the snorkel leg, and critical wear zones to achieve a more uniform erosion pattern throughout the RH vessel and snorkels, thereby maximizing refractory utilization and campaign life.

2. Standardization of Gunning and Repair Practices :Tata Steel Kalinganagar has been equipped with an RH gunning manipulator since 2016, enabling both internal and external snorkel gunning operations. However, due to the large snorkel diameter (iD-750 mm), high surface area, and limited turnaround time available between heats, it was challenging to perform effective repair and gunning in every cycle. To address this issue, a structured daily management system and standardized operating procedures were developed. Repair schedules, inspection criteria, gunning quantity, application sequence, and acceptance standards were clearly defined. This helped ensure timely and consistent execution of refractory maintenance activities within the available maintenance window, leading to improved lining condition and reduced wear progression.

3. Process Control and Thermal Load Reduction :Several process improvements were introduced to reduce refractory wear and thermal stress. Based on the effectiveness of the Top MFL cleaning system, a customized skull cleaning SOP was developed to minimize metal buildup inside the RH vessel resulting 20% decrease in relining duration. Treatment duration was optimized grade-wise to prevent unnecessary refractory exposure, particularly for IF and electrical steel grades. The steel circulation rate was also modified using a gradual ramp-up strategy based on vessel age and lining condition, thereby reducing excessive erosion in the inlet snorkel during the initial stage of campaign life.

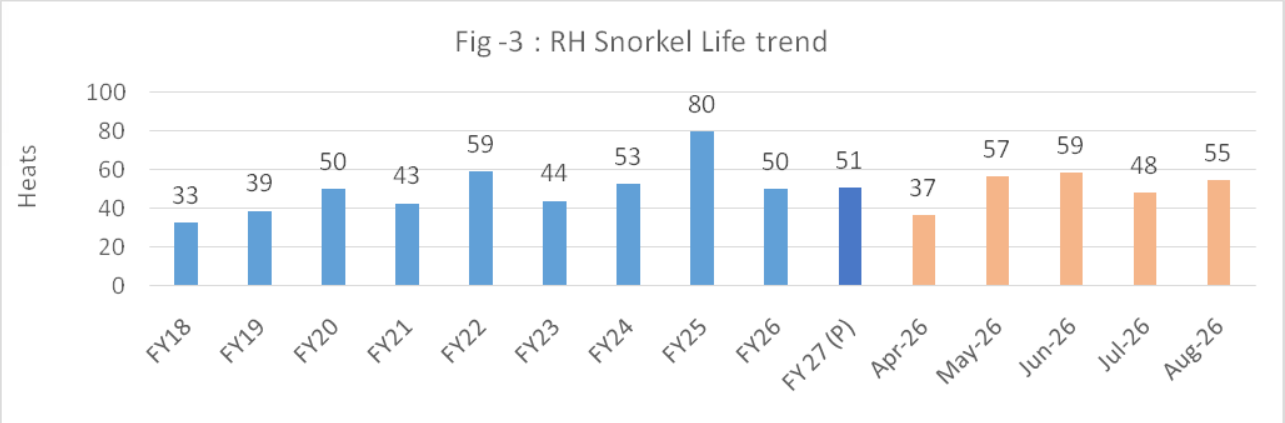
Vacuum system performance was improved through leakage arresting and strengthened maintenance practices, resulting in reduced vacuum cycle duration by 2-3 minutes. To minimize thermal cycling damage, a standardized RH vessel preheating practice of approximately 48 hours was adopted, while the maximum vessel holding time between sequences was restricted to 6 hours. Furthermore, the sequence planning philosophy was modified by reducing long continuous campaigns from 9-10 heats at a stretch to 4+4 heat sequences, thereby lowering refractory thermal shock and extending campaign life. These measures collectively reduced thermal and chemical

attack on the lining and contributed significantly to campaign life enhancement.

Results & Discussion

A significant improvement in RH refractory performance was achieved following the implementation of the above technical and operational initiatives. Despite a substantial increase in the proportion of critical steel grades processed through the RH unit, refractory performance remained stable and sustainable. Prior to FY26, the RH unit processed a mix of approximately 50-70% API grades and 30-50% IF grades. Subsequently, the production mix shifted towards 100% critical grades with complete elimination of API grades, resulting in significantly higher metallurgical demands, longer treatment durations, and increased refractory stress.

Under these more severe operating conditions, the RH snorkel campaign life was successfully stabilized at more than 50 heats (Fig-3), compared with the earlier inconsistent performance and frequent campaign interruptions. Simultaneously, the refractory relining duration was reduced from 12-15 days to 10-12 days through improved skull cleaning practices, reduction in metal jam formation, standardized maintenance procedures, and optimized vessel refurbishment methodologies.



Conclusion

The combined effect of refractory design optimization, systematic gunning practices, improved process control, and thermal cycle management not only enhanced refractory life but also improved RH availability and operational reliability. The stabilized RH performance enabled sustained production of ultra-clean IF-grade steels while reducing maintenance downtime and increasing productivity. The improvement demonstrated that a holistic approach combining refractory engineering, maintenance excellence, and process optimization can effectively mitigate the adverse impact of increased critical-grade production on RH refractory life.

Futurework

To further enhance RH refractory performance and vessel reliability, future efforts will focus on reducing RH treatment duration through improved process optimization and vacuum efficiency, thereby minimizing refractory exposure to thermal and chemical attack. Automation of RH maintenance activities, including gunning, inspection, and repair processes, will be explored to improve consistency and reduce maintenance cycle time. In addition, an online RH vessel health-monitoring system based on thermal imaging cameras will be developed to continuously track refractory condition, identify hot spots, and provide early warning of abnormal wear. Mechanization of RH relining activities is also planned to improve lining quality, reduce relining duration, and enhance safety. These initiatives are expected to further increase RH campaign life, improve vessel availability, and support the growing production of ultra-clean IF-grade steels.

References

1. https://steel.gov.in/
2. Andreas Viertauer et al., RHI Magnesitavoestalpine, AISTch 2019 Paper"Refractory Condition Monitoring and Lifetime Prognosis for RH Degasser".
3. Wang et al., ISIJ International (2020)"A CFD Study on Refractory Wear in RH Degassing Process".
4. World Steel Association, *Steel Statistical Yearbook*.
5. SMS group GmbH, "*RH Vacuum Degassing Technology for Ultra-Clean Steel Production*".
6. H. B. Lüngen and M. Peters, "Vacuum Degassing of Steel in RH Plants," *Steel Research International*, Wiley-VCH.

DESIGN, DISCIPLINE, AND SUSTAINABILITY: A TUNDISH REFRACTORY SUCCESS AT TATA NINL

Sujat Ali Khan, Santanu Saha, Mousam Bag, J Hari Babu, Aayush Shukla, Deepak Kumar

Abstract

Reliable tundish performance is essential for achieving stable continuous casting operations in a single route comprising Basic Oxygen Furnace (BOF), Ladle Furnace (LF) & Continuous Casting Machine (CCM). At Tata NINL, tundish refractory wear and slag-line erosion were causing frequent disruptions in casting sequences and increased refractory consumption. To address these issues, multiple initiatives were undertaken, including tundish lining design modification to balance a 5° inclination, optimization of tundish operating level, improved slag-off practices, and flow modifier design changes. Following implementation, tundish campaign life increased significantly, refractory consumption was reduced, and casting stability improved, with elimination of refractory-related unplanned tundish stoppages. The study demonstrates that sustainable refractory performance can be achieved through an integrated approach combining engineering design improvements with disciplined operational practices.

Introduction

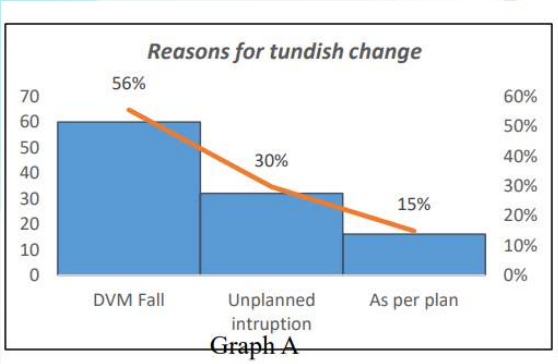
The tundish serves as an intermediate vessel between the ladle & continuous casting mold, playing a critical role in ensuring consistent steel flow, temperature, homogenization & inclusion flotation. The refractory lining of the tundish is continuously exposed to molten steel, slag, thermal cycling & mechanical stress making refractory integrity a key requirement for uninterrupted casting operations.

At TATA NINL, operating through a single BOF-LF- CCM route, tundish reliability directly influences the productivity & casting sequence continuity. During routine operation, excessive wear at turbulence area & slag line were observed. The deterioration often restricts campaign life & increases refractory consumption.

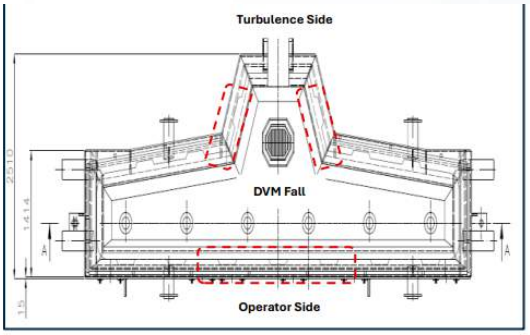
To address these challenges, detailed study was done on design limitations & operational practices contributing to refractory degradation. Based on the findings several corrective measures were implemented, resulting in significant & sustainable improvements.

Problem Statement

Average tundish refractory life is 15 heats against a target of 25 heats, causing increased refractory cost, frequent tundish changes & production losses. Major reasons for reduction of the tundish refractory are DVM fall cases & unplanned sequence break due to interruption as shown in graph A.



Graph A

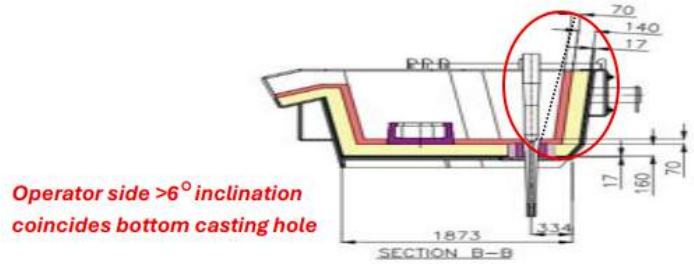


DVM fall is the leading reason, accounting for 60 cases with 56% of all tundish change. More than half of all tundish changes are caused by DVM fall, making it the prime concern. Unplanned interruption is the second most common reason with approx. 32 cases & 30% of the total.

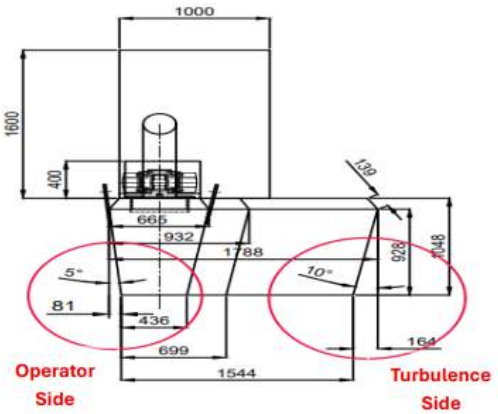
The data indicates that DVM fall cases have greater impact in tundish change & need to be addressed.

Tundish design at NINL

At NINL the inclination of tundish wall at operator side is 5° & at the turbulence side its 10° making the alignment more vertical towards operator side as compared to turbulence side. Increasing the angle of inclination greater than 6° were coinciding the bottom casting holes.



Operator side >6° inclination coincides bottom casting hole



Operator side 5° inclination

Hence the inclination of the freeboard is made at 6° by modifying the dumag with 6° inclination in 300 mm of freeboard zone. With a 6° inward inclination part of DVM weight is supported by the geometry itself. The refractory layer becomes more "self-supporting" reducing the tendency of fall of DVM.

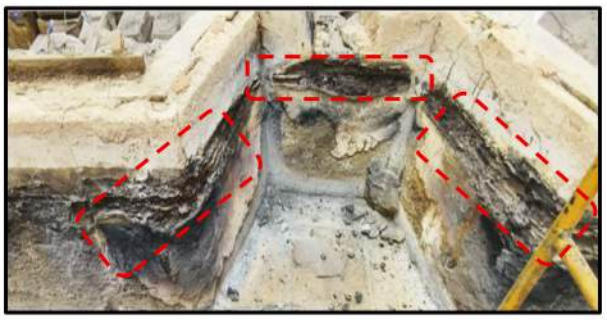




With inclination of 6° at 300 mm freeboard, the performance of tundish refractory life is improved by 4 heats i.e. 19 heats.

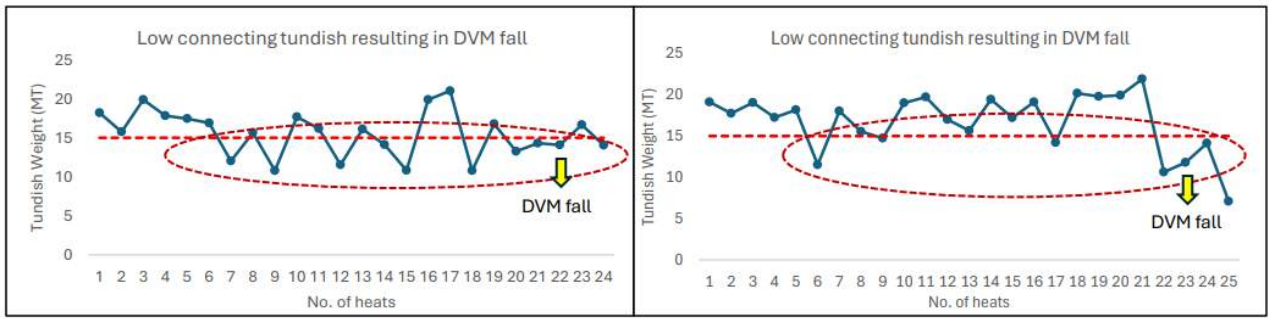
Higher localized erosion in turbulence area:

During further physical observation it was observed that there was abnormal local erosion in the turbulence area (as shown in fig. 1.1). This type of localized erosion indicates irregularities in steel flow inside the tundish due to various factors such as tundish level fluctuation, slag chemistry & volume, ladle shroud inclination & turbostop design.





Tundish level fluctuation



DVM fall incidents were found to be strongly associated with low tundish operating levels. As the metal level decreases, a significant portion of the upper sidewall becomes exposed, making it susceptible to thermal spalling and slag attack, which lead to detachment and fall of DVM. This localized wear and erosion of the upper sidewall become more severe when slag volume fluctuates during casting operations.

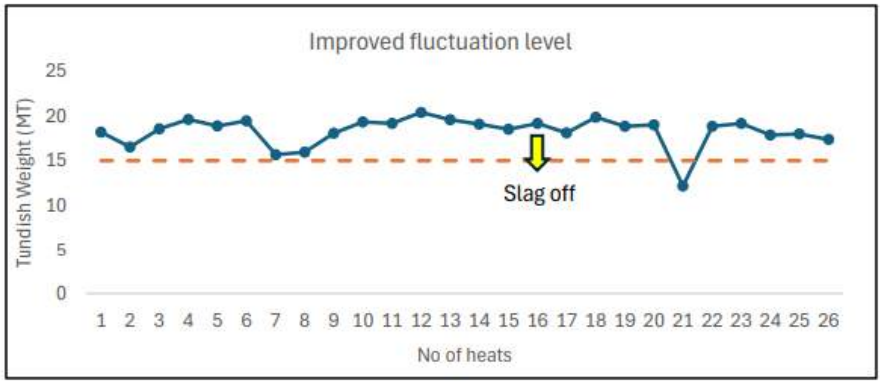
Slag volume fluctuation increase wear of the tundish side wall & DVM through various mechanism:

• Changing slag line position: When slag volume increases, the slag layer rises & contacts a larger area of upper side wall leading to uneven erosion.

• Thermal spalling: The temperature fluctuations generate thermal stress within the lining, repeated fluctuations cause cracking, spalling & weakening of the DVM.

• Localized erosion at low operating tundish: At low tundish levels, the upper side wall is exposed. The combined effect of thermal shock, slag erosion creates a localized thinning, eventually causing DVM to detach & fall.

To mitigate this issue, a slag-off practice was introduced to improve slag management and minimize sidewall exposure. Jointly an SOP was formulated to measure the slag depth after 15 & 21st heat of the sequence & slag off must be done if the slag volume is greater than 20 mm.

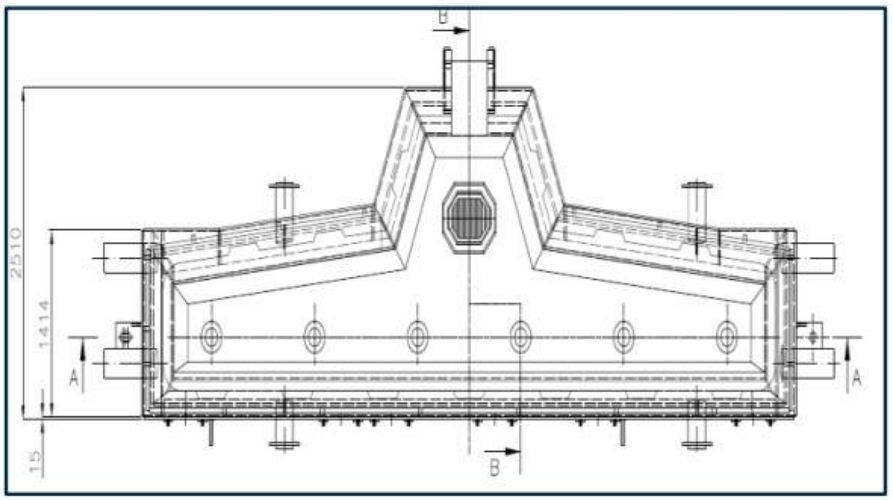


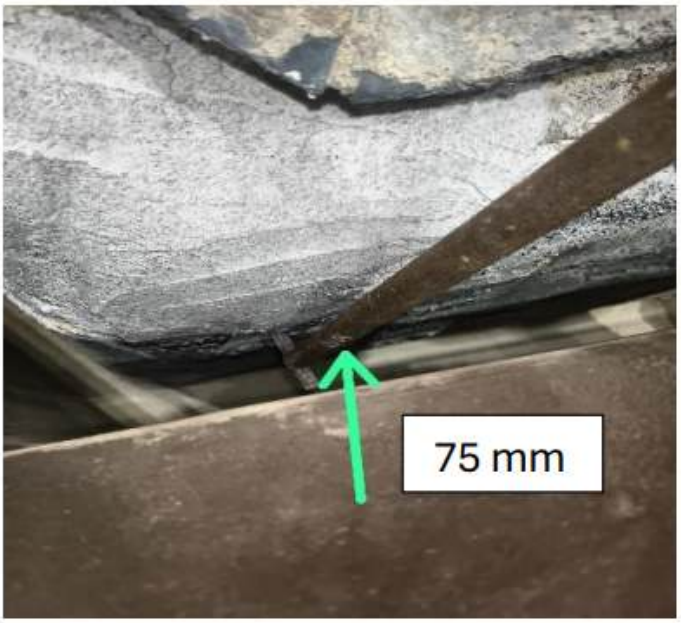
All heats were connected above 15 MT & slag off was done at 16 heats.

Repair practice of tundish backup

After deskulling, it was observed that slag sticking was present on both sides of the turbulence area resulting in damage to the tundish backup lining. The damage tundish backup is subsequently repaired/ patched, which increased the backup lining thickness & consequently reduced the DVM thickness as tabulated in below table:

S. No.	Area	Dimension (mm)
1	Operator Middle	80
2	Operator right	110
3	Operator left	110
4	Narrow right	80
5	Narrow left	72
6	Turbulence right	70
7	Turbulence left	75
8	Opposite operator right	86
9	Opposite operator left	80





A specially designed measuring tool with different dimensional reference is developed to measure the DVM thickness at various locations of the tundish, ensuring accurate & reliable assessment of actual DVM thickness as shown in fig.

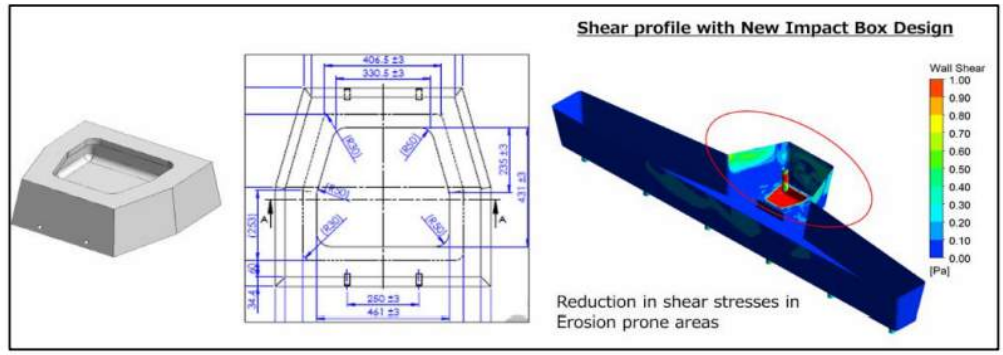
This practice helps to ensure the DVM thickness remains within the specified limit throughout the tundish campaign & to prevent premature refractory failure.

Introduction of newly designed impact box

The objective of the trial is to evaluate a newly designed impact box capable of:

- Reducing shear stress & turbulence in critical erosion prone zone.
- Improving DVM & tundish working lining life.
- Preventing DVM fall incidents.
- Maintaining casting performance without compromising.

Design Development: A modified impact box designed was developed based on CFD analysis. The design retained the present opening geometry while altering the flow pattern to reduce the wall shear stress near the turbulence & operator side. CFD predictions indicate lower erosion potential in critical areas as shown below.



Trial was taken with new designed impact box & following observations were observed:

- Average heat cast 25.33 heats/tundish with casting duration of 18 hrs 08 mins / tundish.
- No slag sticking observed.
- Impact box remained intact.
- No Slag sticking on walls.

Conclusions

The results of this study demonstrate that by systematic approach involving tundish design modification, slag control practices, DVM thickness monitoring & CFD based impact box optimization successfully addressed the major causes.

Key achievements

Parameters	Before improvement	After improvement
Average Tundish life	Average Tundish life	25 Heats
DVM fall incidents	Frequent	Frequent
Slag Sticking	High	Low
Sequence stability	Low	Improved
Refractory Consumption	High	Reduced

The project achieved 67% improvement in tundish campaign life & establishing the sustainable solution for Refractory tundish life enhancement at TATA NINL.

ENHANCING REHEATING FURNACE (ROLLING MILL) CAMPAIGN LIFE: THE IMPACT OF ENGINEERED REACTIVE ALUMINA ON PRECAST BLOCK PERFORMANCE

[1]Dr. S. Adak, [1]Arnab Kr. Das, [1]Mayank Gugalia, [2]Sourojit Pal, [2]Shankha Chatterjee
[1]Mahakoshal Refractories Pvt. Ltd., Katni, [2]Almatis Alumina Pvt Ltd, Kolkata

*Corresponding author e-mail: sukumar.adak@mahakoshal.in

Abstract

Steel reheating furnaces operate under some of the most demanding thermal and mechanical conditions in the metallurgical industry. These furnaces are traditionally lined with dense alumina refractory like Bricks, Precast Blocks, Castables and Gunning materials. Continuous exposure to temperatures above 1200°C, frequent thermal cycling, oxidizing atmospheres, and mechanical abrasion from steel billets put extreme stress on refractory linings. Selecting the right refractory solution is, therefore, not only a matter of material cost but a decisive factor influencing furnace campaign life, energy efficiency, production continuity, and overall operating cost. In case of precast blocks, high densification, hot and cold strength, abrasion resistance and thermal shock resistance determines the service life and performance. Consequently, achieving better matrix properties with high purity raw materials is crucial.

The present case study discusses the influence of reactive alumina in ULC95 based precast blocks made by vibro-casting for the working lining of a reheating furnace. High-purity reactive alumina with engineered particle size distribution translates into lower porosity and better porosity distribution, reduced water demand, better matrix properties, higher densification and improved strength. Consequently, the product has achieved higher thermal cycling ability and improved wear resistance during the application. The joint success story of the precast blocks between Mahakoshal Refractories and Almatis is described in the present case study.

Keywords: Matrix Enhancement, Pre-cast Refractory Block, Reheating Furnace, Reactive Alumina

Introduction

Steel reheating furnace is used to reheat and soften the semi-finished steels (Billets, Blooms, Slabs, etc.) typically to temperatures between 1100 ºC and 1300 ºC, until plastic enough to be rolled to the desired section, size or shape in the Hot Rolling Mill. The reheating furnace must satisfy stringent requirements regarding heating rates to ensure both metallurgical quality and high productivity. In pusher-type furnaces, the severity of operating conditions progressively increases along the direction of steel movement, reaching its maximum in the soaking zone. In side-discharge units, the removal of the heated steel charge imposes additional abrasive forces on the hearth paving. The heating and soaking zones are exposed to several operational challenges, including impact caused by the accidental fall of stacked charges, thermal stresses resulting from frequent cooling during maintenance, and severe abrasion. Mechanical wear is further intensified by the presence of high-temperature scales generated on the steel surface. During maintenance, reheating furnaces are cooled down to ordinary temperature and thus encounter very large temperature fluctuations. Consequently, both the quantity and characteristics of the scale formed play a critical role in determining the service life of hearth refractories in the heating and soaking zones. Traditionally, steel reheating furnaces are lined with dense alumina refractories such as bricks or precast blocks or castables. In particular, the hearth and burner blocks of the furnace are made of PCPF blocks. These PCPF blocks face high erosion due to the movement of heated steel charge and the scales generated on the heated surface.

Case study

Castable technology is quite old but a complex one with continually upgrading material concepts. The choices of aggregate, matrix and binder, and additives depend on the application requirements of that castable. The reheating furnace lining application, especially the precast blocks used in burner and hearth region should demonstrate good properties in terms of volume stability, high cold and hot strength, abrasion resistance and thermal shock resistance, whereas rheological features wise, good flowability and packing.

The selection of raw materials is vital for achieving high density, low porosity, high cold and hot strength and superior erosion resistance. Synthetic high-purity alumina aggregates are highly dense, crystalline and virtually non-porous. They absorb negligible water, leaving almost the entire water for mixing and lubrication between the other raw materials. This results in lower water demand, resulting in lower porosity and higher densification after sintering. It is inevitable to accept that synthetic alumina aggregates are the material of choice for this application. Apart from aggregate, matrix also plays a very vital role for improving application performance by aiding better thermal shock resistance and abrasion or erosion resistance. Selection of high purity fine matrix composition with engineered particle size distribution is essential for filling all the complex and narrow gaps between the aggregates and provide optimal particle packing, which helps to obtain very high strength due to this dense packing.

ULC based high alumina castable is commonly used in the particular PCPF application of rolling mill, where the customer has raised the target performance, in terms extending campaign life duration of the furnace and it's lining refractory blocks. Considering that the alteration of aggregates is quite limited, and consistent stable quality high alumina cement is used, the focus of this paper is on matrix enhancement by considering the features of matrix aluminas and evaluating matrix alumina contributions in properties as well as modification of Anderson Packing Distribution Coefficient, 'q'.

Experimental

The target to this work was to improve strength, reduce abrasion loss and improve spalling resistance. To achieve that same, in the present work, modifications in both aggregate and matrix combination were considered (revised 'q'). In aggregate, synthetic high alumina aggregate like Tabular alumina and WFA were used in coarse and fines. They have similar chemistry but quite different physical parameters and specially they differ in open and closed porosity distributions. Although the technical target was to improve performance controlling properties and performance of precast shapes, the roles of aggregates and matrix were different. The overall chemical composition remains similar, with aggregates, binder, additives and different options of matrix aluminas. The raw materials used in the formulations are listed in Table-1, with their physical and chemical characteristics.

	WTA + WFA	Calcined Alumina X	Reactive Alumina CL 370	70% CAC	Silica Fume	Dispersants
Al_2O_3, %	99.6	99.5	99.7	70	0.2	96
CaO, %	0.037	0.034	0.017	29	0.2	0.02
Na_2O, %	0.25	0.33	0.07	0.21	0.15	0.5
Fe_2O_3, %	0.0178	0.013	0.0178	0.05	0.01	0.01
SiO_2, %	0.0105	0.014	0.017	0.07	98.5	0.02
BET, m2/g	-	0.8	3.06	3.0	25	
D50, µm	-	5.6	2.517	2.5	0.15	2.5
D90, µm	-	11	7.902	7	-	9

Table-1: Chemical and physical analysis of the raw materials.

The Table-2 shows the mix formulation concept with the required raw materials from Table-1. Here, T1 was the benchmark castable which the customer was using and T2 is the improved formulation finally developed for the increase target performance improvement of the customer. The changes were done in weightage distribution of WTA and WFA in coarse and fine both and selection of matrix alumina. In case of currently used formulation calcined alumina grade X has been replaced with bi-modal reactive alumina CL370 to improve the matrix characteristics.

Composition	T1	T2
Tabular alumina + WFA	Xx +Yy	XX+ yy
Calcined Alumina (X)	Z	-
Reactive Alumina (CL370)	-	Z
70% CAC	V	V
Silica Fume	V	V
Dispersant	V	V
PP Fiber	V	V

Table-2: Formulation concept for ULC castable for Reheating Furnace PCPF

The raw materials were dry mixed in Hobart Mixer. Minimum mixing water was added till the mix attains desired flow using vibration technique. The mixed batches were casted in mould of 40*40*160 mm^3 sizes. The mixes were allowed to cure within the mould for 24 hrs. under temperature and humidity-controlled conditions. After de-moulding, they were allowed to air dry for 24 hrs., followed by oven drying at 110 ºC/ 24 hrs. The dried samples were then fired at 800, 1100 and 1300 ºC with 3 hours soaking in each firing profiles. All the samples were then tested for BD, PLC, CCS, CMOR, and Abrasion Resistance (as per ASTM C704 method using the pre-fired bars). Apparent porosity (as per ASTM C20) and thermal spalling resistance (as per water quenching method DIN 51068-1) were checked with the fired bars at 1300 ºC/ 3 hours.

Results and Discussion

The Table-3 indicates reduction is water demand for the improved castable, keeping almost similar flowability till 30 minutes after casting. This was possible due to replacement of calcined alumina X by CL370 which is having significant amount of sub-micron size particles. This change fills the intergranular gaps better, reduced the water demand and still aids in flowability. The reduction of water demand had significant relationship with porosity and strength as well as with thermal shock resistance and abrasion loss.

	T1	T2
Water Demand, %	4.5	3.9
Flowability, F10	92%	85%
Flowability, F30	83%	80%
Initial setting time, hrs	2.5 hrs	2.0 hrs

Table-3: Rheology of Standard and Test Castables

The fig. 1 - 4 explain the changes in Density, Compressive Strengths and Volume Stability of original T1 and improved T2 formulation concepts.

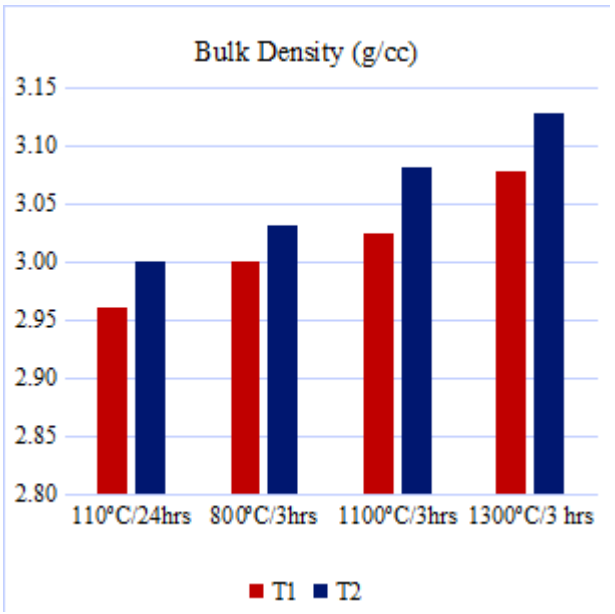


Fig. 1: Changes in bulk density at diff temps.

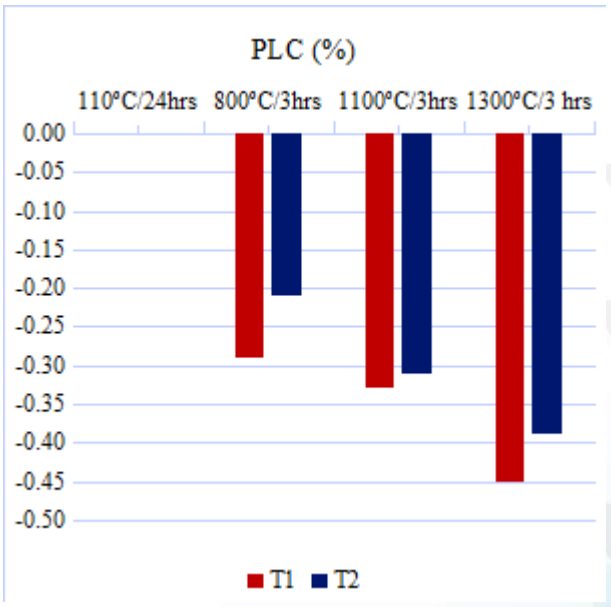


Fig. 2: Changes in PLC at diff temps.

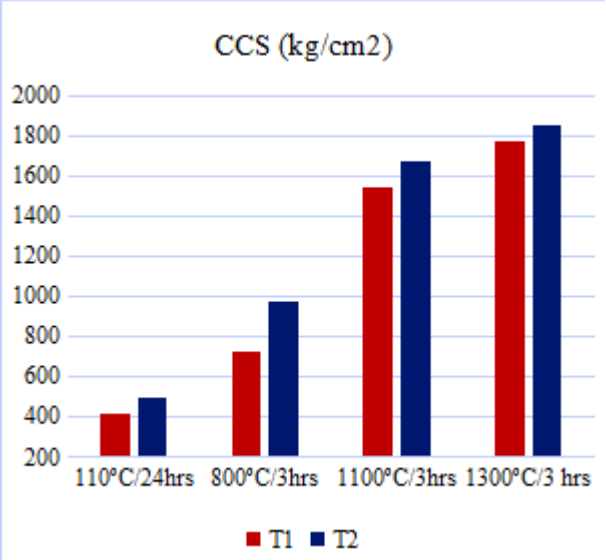


Fig. 3: Changes in CCS at diff temps.

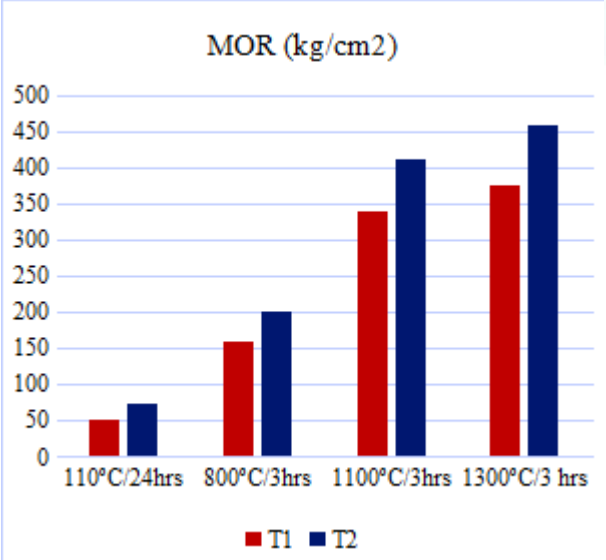


Fig. 4: Changes in Cold MOR at diff temps.

The change from Mono-modal Calcined Alumina X to Bi-modal Reactive Alumina CL370 having significant sub-micron particle content had enhanced particle packing and thus improved the densities. The higher sinterability due to increased proportion of sub-micron particles in bi-modal reactive alumina CL370 in T2 has resulted water demand reduction and improved strengths and finally resulted in reduced abrasion loss. The modifications in weightage distribution among WTA and WFA, both in coarse and fines fractions has resulted in also better thermal shock resistance due to better pore distribution which has also shown changes in Anderson packing distribution coefficient, q from 0.25 in T1 to 0.31 in T2. This change was quite significant due to changes in aggregate distribution ratio among WTA and WFA as well as changes from X to CL370. Finally, the apparent porosity was reduced from 17.5% to 13.2% and still having jump increase in thermal shock resistance from 32 cycles in T1 to 41 cycles in T2.

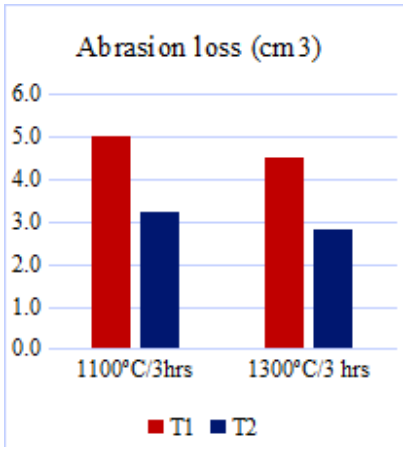


Fig. 5: Changes in abrasion loss

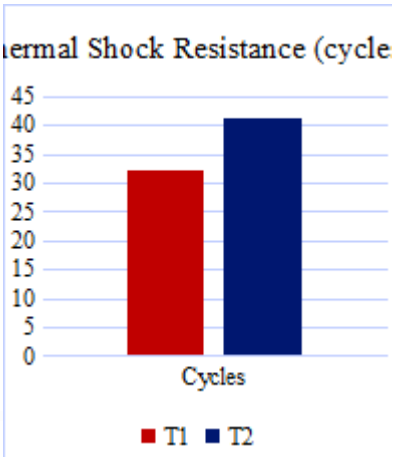


Fig. 6: Changes in thermal spalling

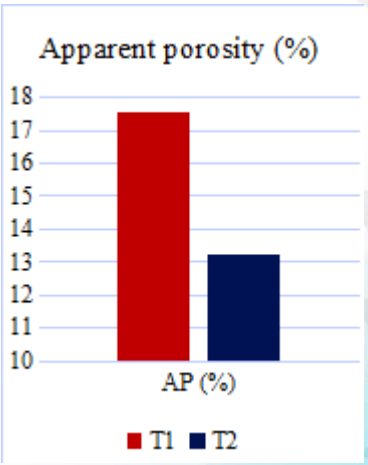


Fig. 7: Changes in AP

As a result of significant improvements in castable properties, T2 was selected for field trial in hearth of reheating furnace where earlier T1 was getting used. The field trial

showed steady improvement in duration of service campaign and reduced partial patching repair consumption.

Conclusion

- Steel Reheating furnaces face extreme harsh thermal and mechanical challenges, and special focus on thermal shock resistance, high mechanical strength and abrasion resistance for used PCPF is necessary.
- Selection of proper raw materials in aggregate and matrix is essential for achieving improvements in apartment porosity, strengths, abrasion resistance and thermal shock resistance.
- Replacement of calcined alumina by reactive alumina improved particle packing, reduced castable water demand, improved porosity and strengths.
- Thermal shock resistance can be improved focusing on WTA more with proper distribution of coarse and fines in WTA and WFA, in spite of significant reduction in apparent porosity.
- Modifications in aggregate and matrix jointly contributed in improvement in abrasion loss.
- With the improved PCPF product of ULC concept, performance of hearth in rolling mill improved, the furnace downturn has reduced significantly, castable patching consumption reduced and the overall productivity has improved.

GREEN RECYCLED REFRACTORIES – MGO-C MAGNESIA CARBON

Mr. Ishan Agarwal

Head Operations and Business Development, Jai Balajee Trading Company (JBTC)

Abstract

The refractory industry is undergoing a significant transformation driven by sustainability objectives, carbon reduction commitments, resource conservation, and circular economy principles. Green refractories, particularly recycled MgO-C (Magnesia Carbon) refractories, are emerging as a strategic solution to address environmental concerns while maintaining operational efficiency in steelmaking and metallurgical industries. The increasing depletion of virgin refractory minerals, rising mining costs, volatile transportation expenses, and stricter environmental regulations have accelerated the adoption of recycled refractory materials worldwide. Green recycled refractories offer valuable alternatives for manufacturing refractory bricks, monolithic products, metallurgical fluxes, and mineral additives. Their utilization reduces dependency on virgin raw materials and lowers carbon emissions associated with extraction, processing, and transportation. India's steel industry, accounting for nearly 70-80% of refractory consumption, is rapidly transitioning toward green steel production through Electric Arc Furnaces (EAF), Hydrogen Direct Reduced Iron (H_2-DRI), and Induction Furnace technologies. This paper examines the development of green recycled MgO-C refractories in India, their technical and environmental benefits, and their role in supporting future green steel initiatives.

Keywords: Green Refractories, MgO-C, Magnesia Carbon, Refractory Recycling, Green Steel, Circular Economy, Sustainability.

Introduction

Refractories are indispensable materials used in high-temperature industrial processes such as steelmaking, cement production, non-ferrous metallurgy, glass manufacturing, and petrochemical operations. Traditional refractory production depends heavily upon virgin raw materials such as magnesite, graphite, dolomite, and alumina. The growing global emphasis on sustainability and carbon neutrality has created increasing demand for environmentally responsible refractory solutions. Green refractory technology seeks to maximize the reuse of valuable minerals through recycling while minimizing environmental impact.

MgO-C refractories represent one of the most widely used refractory systems in steelmaking because of their excellent thermal shock resistance, corrosion resistance, and mechanical strength. Recycling these materials presents enormous potential for reducing waste generation and conserving valuable natural resources.

The Need for Green Refractories

Sustainability Challenges

The refractory industry currently faces:

- Depletion of quality mineral reserves
- Increasing mining and beneficiation costs
- Rising energy consumption
- Carbon emission pressures
- Waste disposal challenges
- Supply chain instability

Green refractory solutions address these challenges by recovering valuable minerals from spent refractories and returning them to the production cycle. The transition toward low-carbon steelmaking is expected to accelerate the adoption of recycled refractory materials and support circular economy objectives within the steel industry.

Input Material	Steelmaking Route	Process Description	Refractory Requirement
Scrap Metal	Electric Arc Furnace (EAF)	Scrap-based steel production using electrical energy	MgO-C bricks for EAF sidewalls, slag lines, and ladles
Scrap Metal / DRI	Hydrogen Direct Reduced Iron (H_2-DRI) + EAF	Low-carbon steelmaking using hydrogen as reducing agent	High-performance MgO-C and alumina-magnesia refractories
Scrap Metal	Induction Furnace (IF)	Metal melting through electromagnetic induction	MgO-based linings and monolithic refractories
Green Steel Production	All Routes	Sustainable and low-carbon steel production	Increased demand for advanced refractory solutions

Table-1: Relationship between scrap-metal-based green steel production routes and the increasing demand for sustainable MgO-C refractory products

Recycling Process

The recycling process generally involves segregation, crushing, magnetic separation, screening, beneficiation, and quality classification.

Input	Processing Step	Intermediate Product	End Use
Virgin MgO-C Refractory	Industrial Service in Steel Plant	Spent Refractory	Collection
Spent Refractory	Segregation	Sorted Material	Crushing
Sorted Material	Crushing & Screening	Refractory Granules	Magnetic Separation
Refractory Granules	Metal Removal	Clean Aggregate	Classification
Clean Aggregate	Beneficiation	Recycled MgO-C Aggregate	Reuse
Recycled Aggregate	Refractory Production	New MgO-C Products	Circular Economy
Recycled Aggregate	Metallurgical Applications	Fluxes & Additives	Green Steel Production

Table 2: Circular economy pathway for recycling spent MgO-C refractories into secondary raw materials



Figure 1. Handling recycled waste now in India

Recycling of MgO-C Refractories

Their unique properties include:

- Excellent thermal shock resistance
- Superior slag resistance
- High temperature stability
- Low wettability to molten steel and slag
- Exceptional mechanical strength

Chemical Composition

Component	Typical Range (%)
MgO	70-90
Graphite	5-20
Carbon Additives	2-10
Antioxidants (Al, Si)	1-5
Binders	1-3

Table 3. Typical Chemical Composition of MgO-C Refractories

Environmental Benefits of Green Refractories

The recycling of spent MgO-C refractories significantly reduces environmental impact compared with manufacturing from virgin raw materials. When virgin refractory manufacturing is normalized to a CO_2 emission index of 100, recycled MgO-C refractory production exhibits an estimated emission index of 60. This corresponds to a potential reduction of approximately 40%. These savings are primarily attributable to reduced extraction of virgin magnesia resources, lower transportation requirements, decreased energy consumption during raw material processing, and diversion of spent refractories from landfill disposal. The results demonstrate the significant role that refractory recycling can play in supporting decarbonization objectives within the steel and refractory industries.

Parameter	Virgin Material Route	Recycled Material Route	Improvement
Mining Requirement	100%	40-60%	Reduced
Transportation Demand	High	Medium	Reduced
Landfill Disposal	High	Very Low	Significant Reduction
Energy Consumption	High	Medium	Reduced
Carbon Footprint	High	Low	Reduced

Table 4. Environmental Benefits of Refractory Recycling

Parameter	Traditional Route	Recycled Route
Raw Material Cost Index	100	75-85
Transport Cost Index	100	70-80
Waste Disposal Cost Index	100	20-30
Resource Utilization	Low	High
Sustainability Rating	Medium	High

Table 5. Indicative economic benefits of recycling

Using a normalized baseline of 100 for virgin refractory manufacturing, recycled MgO-C production demonstrates a potential 40% reduction in lifecycle carbon emissions has been observed. This improvement is primarily attributed to reduced extraction of virgin minerals, lower transportation requirements,

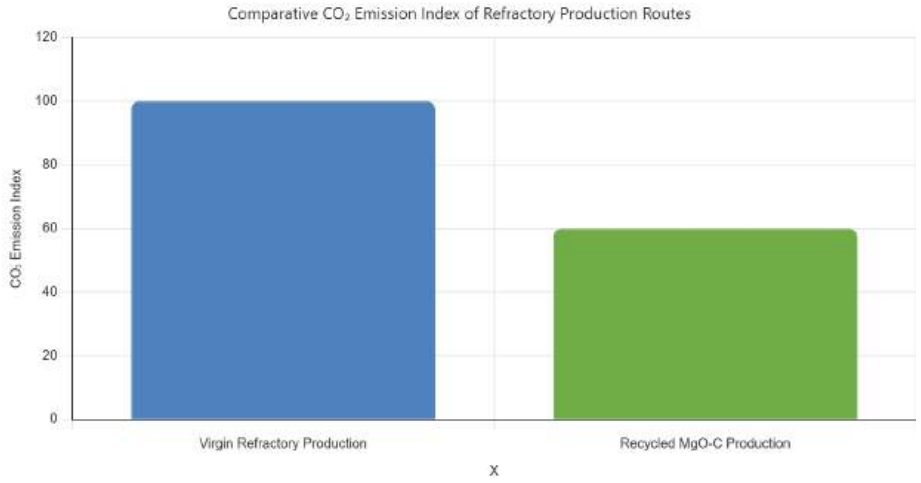


Figure 2. Comparative CO_2 emission index for conventional refractory production and recycled MgO-C refractory production.

decreased energy consumption during beneficiation, and diversion of spent refractory materials from landfill disposal. Such reductions support global decarbonization initiatives and align with sustainability objectives within the steel and refractory industries.

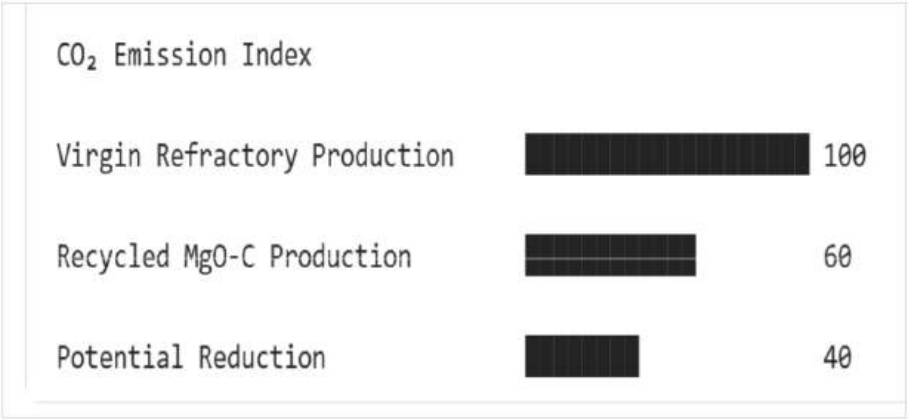


Figure 2: Indicative reduction in carbon footprint through refractory recycling. *Emission Index normalized to virgin refractory production = 100

Parameter	Virgin Raw Materials	Recycled MgO-C Materials
Mining Requirement	High	Low
Energy Consumption	High	Moderate
Transportation Impact	High	Lower
Landfill Generation	High	Minimal
CO_2 Emission Index	100	60
Sustainability Rating	Moderate	High

Table 6. Relative CO_2 emission index comparing conventional refractory production from virgin raw materials with recycled MgO-C refractory production.

Green Steel and Refractory Demand

Steel Industry Dependency:

The steel industry accounts for approximately 70-80% of global refractory consumption. Consequently, future developments in steelmaking directly influence refractory production and consumption patterns. India's National Steel Policy 2017 estimates that ferrous scrap requirements could reach 70-80 million tons annually by 2030, compared with approximately 30 million tons currently consumed. This trend indicates a growing shift toward scrap-based steelmaking routes.

Green Steel Production Routes:

Electric Arc Furnace (EAF) -EAF technology utilizes scrap metal as the primary feedstock and significantly reduces carbon emissions compared with traditional blast furnace operations.

Hydrogen-Based DRI (H_2-DRI) - Hydrogen-based iron reduction offers near-zero carbon steelmaking potential and is expected to become increasingly important in future steel production.

Induction Furnaces - Induction furnaces provide energy-efficient steel production using recycled scrap and increasingly renewable electricity sources.

Input Material	Green Steel Route	Technology Description	Typical Refractory Applications
Scrap Metal	Electric Arc Furnace (EAF)	Steel production using electrical energy and recycled scrap	MgO-C furnace sidewalls, slag line bricks, ladle refractories
Iron Ore + Green Hydrogen	Hydrogen DRI (H_2-DRI) + EAF	Low-carbon ironmaking using hydrogen as reducing agent	MgO-C refractories, tundish linings, ladle refractories
Scrap Metal	Induction Furnace (IF)	Melting of recycled metal through electromagnetic induction	MgO-based dry vibratable linings and monolithic refractories
Green Steel Production	Combined Output	Sustainable steel manufacturing with reduced emissions	Increased demand for high-performance and recycled refractories

Table 7. Green Steel Production Pathways and Associated Refractory Demand

These technologies create substantial opportunities for green refractory products and recycled refractory raw materials.

The transition toward Electric Arc Furnace (EAF), Hydrogen Direct Reduced Iron (H_2-DRI), and Induction Furnace (IF) technologies is expected to accelerate adoption of recycled MgO-C refractories and circular economy practices within the steel industry.

Parameter	Current Estimate	2030 Forecast
Steel Production (MT)	~150	>300
Scrap Requirement (MT)	~30	70-80
Refractory Consumption	High	Very High
Recycled Refractory Usage	Emerging	Rapid Growth

Table 8. Indian Steel Sector and Refractory Recycling Opportunity

Economic Benefits of Recycled MgO-C Refractories

The adoption of green recycled MgO-C refractories provides both environmental and economic advantages. From a sustainability perspective, recycled refractory aggregates reduce the carbon footprint associated with raw material extraction, transportation, and manufacturing. Procurement departments benefit from reduced exposure to volatile global mineral markets and lower dependence on imported refractory raw materials. Operationally, recycling creates a more resilient supply chain by establishing secondary sources of magnesia-bearing materials. Compliance benefits arise from increasing alignment with environmental regulations, carbon reduction initiatives, and ESG reporting requirements. Economically, recycled refractories can lower total lifecycle costs through reduced raw material expenses and minimized landfill disposal costs.

Benefit Area	Impact
Sustainability	Reduced carbon footprint through lower mining, processing, and transportation emissions
Procurement	Reduced dependence on imported and virgin mineral resources
Operations	Improved supply chain reliability and stable raw material availability
Compliance	Better alignment with CBAM, ESG, and corporate sustainability requirements
Economics	Reduced lifecycle operating costs and waste disposal expenses
Circular Economy	Increased recycling rates and improved resource utilization

Table 8. Business Benefits of Adopting Green Recycled Refractories

parameter	Traditional Route	Recycled Route
Raw Material Cost Index	100	75-85
Transport Cost Index	100	70-80
Waste Disposal Cost Index	100	20-30
Resource Utilization	Low	High
Sustainability Rating	Medium	High

Table 9. Potential Savings from Recycled MgO-C Refractories

Furthermore, refractory recycling supports circular economy objectives by converting spent refractories into valuable secondary raw materials for reuse in refractory and metallurgical applications.
Apart from environmental benefits, recycled refractories provide significant economic advantages.

Benefits include:

- Reduced dependence on imported minerals
- Improved supply security
- Lower operational costs
- Reduced disposal expenses
- Improved ESG performance

Future Outlook and Strategic Importance

As Europe moves toward carbon neutrality through policies such as the Carbon Border Adjustment Mechanism (CBAM), Indian steel producers must continue reducing their carbon footprint.
Recycled refractory minerals may become strategically important raw materials in future critical minerals frameworks due to:

- Growing green steel demand
- Rising environmental compliance requirements
- Increasing scarcity of high-quality virgin minerals
- Expansion of circular economy programs

Green recycled MgO-C refractories generate benefits across three key sustainability dimensions: resource conservation, carbon reduction, and waste minimization. By recovering valuable magnesia and carbon-bearing materials from spent refractories, the industry reduces demand for virgin mineral extraction and associated environmental impacts. Recycling processes also lower greenhouse gas emissions by reducing mining, transportation, and raw-material processing requirements. Furthermore, the diversion of spent refractories from landfills supports circular economy objectives by transforming

industrial waste into valuable secondary resources. Collectively, these benefits contribute to the development of a sustainable steel ecosystem and support the global transition toward green steel production.

Sustainability Pillar	Direct Benefit	Industrial Impact
Resource Conservation	Reduced consumption of virgin magnesite and graphite	Lower mining dependency and resource preservation
Carbon Reduction	Reduced CO_2 emissions from mining, processing, and transportation	Improved environmental performance and ESG metrics
Waste Minimization	Diversion of spent refractories from landfill	Enhanced circular economy implementation
Circular Economy	Recovery and reuse of valuable refractory minerals	Increased material efficiency and sustainability
Green Steel Enablement	Support for low-carbon steelmaking routes (EAF, H_2-DRI, IF)	Long-term sustainable steel production

Table 10. Sustainability Benefits of Green Refractories

Conclusion

Green recycled MgO-C Magnesia Carbon refractories represent a highly effective pathway for achieving sustainable steel production and responsible resource utilization. By converting spent refractories into valuable secondary raw materials, steelmakers and refractory manufacturers can significantly reduce dependence on virgin minerals while supporting carbon reduction targets and circular economy goals.

The future expansion of green steel production through EAF, H_2-DRI, and induction furnace routes will further increase opportunities for recycled refractory materials. India is uniquely positioned to become a global leader in green refractory technology by integrating recycling, sustainability, and innovation into its steel manufacturing ecosystem.

The adoption of green recycled MgO-C refractories is therefore not only an environmental necessity but also a strategic business imperative for the steel industry of the future.

References

1. National Steel Policy (NSP), Ministry of Steel, Government of India, 2017.
2. World Steel Association Sustainability Reports.
3. European Union Carbon Border Adjustment Mechanism (CBAM) Publications.
4. UNEP Circular Economy and Resource Efficiency Reports.
5. Technical Literature on MgO-C Refractories and Steelmaking Applications.
6. International Refractory Recycling Best Practice Guidelines.
7. World Refractories Association, *Advancements in Refractory Recycling Techniques*, 2024.
8. European Commission, *Circular Economy Action Plan and Resource Efficiency Initiatives*, European Union.
9. Ministry of Steel, Government of India, *National Steel Policy (NSP) 2017*. [steel.gov.in], [pmindia.gov.in]
10. Press Information Bureau, Government of India, *Steel Scrap Recycling Policy*, Nov. 2019. [pib.gov.in]
11. Industry Today, *Refractories Reused: A Step Toward Sustainability*, 2025. [industrytoday.com]
12. M. Rigaud, "Magnesia-Carbon Refractories: A Review of Properties and Applications," *Journal of Technical Refractories and Industrial Ceramics*.

13. ReSoURCE Project (EU), *Optimizing Recycling of Spent Refractories for CO_2 Savings*, 2024. [project-resource.eu]
14. European Commission, *Carbon Border Adjustment Mechanism (CBAM)*. [taxation-c....europa.eu], [trade.ec.europa.eu]
15. Council of the European Union (Consilium), *Carbon Border Adjustment Mechanism Overview*, updated 2026. [consilium.europa.eu]
16. World Steel Association, *Sustainability Indicators Report*, latest edition.

THE OPERATIONAL STATUS OF THE FIRST COMMERCIAL REX-ROBO LSG AND THE FUTURE DEVELOPMENTS OF REX-ROBO SERIES

Yudai Onoue, Asaki Nimura, Mamoru Yoshimura, Akira Otsuka
Slide Gate Engineering Group, Slide Gate & The Engineering Department,
Engineering & Manufacturing Division,

KROSAKI HARIMA CORPORATION, JAPAN

Corresponding author's e-mail: onoue.f5s.yudai@krosaki.co.jp

Abstract

Slide gate mechanisms are widely used in steelmaking processes worldwide to control the flow of molten steel. However, the maintenance and replacement of refractories still rely heavily on manual labor and operator skills, and are performed under severe high-temperature conditions, creating challenges in safety, operational stability, and maintenance quality. To address these issues, KROSAKI HARIMA CORPORATION has been developing an automated refractory replacement robot, REX-ROBO, since 2018. Designed for full compatibility with our latest ladle slide gate mechanism, R-Gate, the system aims to improve working conditions while ensuring safe and stable maintenance operations. In 2025, the first commercial REX-ROBO was delivered. This paper reports on the system configuration and operational performance of the commercial unit and introduces ongoing developments of new REX-ROBO series functionalities aimed at improving steelmaking efficiency, operational safety, and productivity.

Keywords: Refractory Maintenance, Slide Gate, Automation, Robot

1. Introduction

We have supplied a large number of ladle and tundish slide gate mechanisms to steel manufacturers worldwide. However, refractory maintenance and replacement operations for these slide gate mechanisms still rely heavily on manual labor and operator skills. In addition, these tasks are performed under severe 3Ds (Dirty, Dangerous, and Demanding) working conditions, creating challenges in terms of safety, operational stability, and maintenance quality. To address these issues, we developed and commercialized a new slide gate system, R-Gate, featuring improved safety and operability. As of 2026, a total of 243 units have been supplied. Nevertheless, challenges such as heavy manual work in high-temperature environments and dependence on operator skills still remain. In anticipation of increasing demand for automation of these maintenance operations, we initiated the development of REX-ROBO in 2018. Following laboratory-scale development and verification testing under the actual field trial, the first commercial REX-ROBO LSG unit was delivered in 2025 and is currently in operation.



Figure 1 REX-ROBO under the actual field trial

This paper presents the system configuration and operational performance of the first commercial REX-ROBO LSG unit. In addition, the paper introduces newly developed functionalities of the REX-ROBO Series, which are currently under development to further improve steelmaking efficiency, operational safety, and productivity.

2. REX-ROBO LSG

In this section, the first commercial REX-ROBO LSG unit, developed to automate refractory replacement operations for ladle slide gates, is presented.

2.1 Operating Procedure

Refractory replacement operations for ladle slide gates consist of various maintenance tasks as shown in Table 1. Among these, the primary operations performed by the robot are the replacement of the upper and lower plates and the lower nozzle, support for the installation of the upper nozzle, and opening and closing of the slide gate frames. REX-ROBO LSG is not designed to automate all maintenance tasks. Instead, physically demanding operations such as refractory replacement are carried out by the robot, while relatively light-duty tasks, including frame cleaning and mortar application, are performed by operators. This human-robot collaborative approach effectively combines the strengths of both the robot and human workers. As a result, heavy manual work in high temperature conditions is reduced, allowing operators to shift their role from physically demanding maintenance activities to light-duty tasks and system operation. Furthermore, since the service life of each refractory component differs, the robot operation sequence can be customized according to which refractory components require replacement.

No.	Procedure	Auto/Manual
1	Preparing ladele, Connecting cylinder hose	Manual
2	Oxygen Cleaning	Manual

3	Detaching Lower Nozzle	Auto
4	Opening Slide Gate Frames	Auto
5	Detaching Lower Plate & Upper Plate	Auto
6	Detaching Upper Nozzle (If necessary)	Manual
7	Attaching Upper Nozzle (If necessary)	Auto&Manual
8	Cleaning Slide Gate, Applying Lubricant, Applying Morta	Manual
9	Attaching Lower Plate & Upper Plate	Auto
10	Closing Slide Gate Frames	Auto
11	Attaching Lower Nozzle	Auto
12	Cleaning nozzle hole, Tightening Lower Nozzle	Manual

Table 1 Operation procedure

2.2 Technical Features of REX-ROBO LSG

The REX-ROBO LSG is based on a six-axis articulated robot and is equipped with three types of sensors.

The first is a vision sensor. Since the ladle placed on the maintenance stand is positioned differently each time, the vision sensor is used to compensate for positional deviations. The system can automatically correct misalignments of up to approximately ± 50 mm, enabling stable operation even when the workpiece position is not fixed.

The second is a force sensor. This sensor is used to determine the end position of refractory replacement operations. Combined with the clearance control of the robot hand, the force sensor provides redundancy and enables accurate and reliable replacement work.

The third is a laser displacement sensor. This sensor is used to verify the plate installation position after replacement and to check the face pressure after loading. As a result, stable and consistent maintenance operations can be achieved.

In addition, the system is equipped with a heat-resistant jacket, thermal protection plates, and an air-cooling system for the robot in order to withstand high-temperature operating conditions. Through the combination of these technologies, stable operation can be achieved even in severe environments with high temperatures and dust, where the workpiece position may vary.

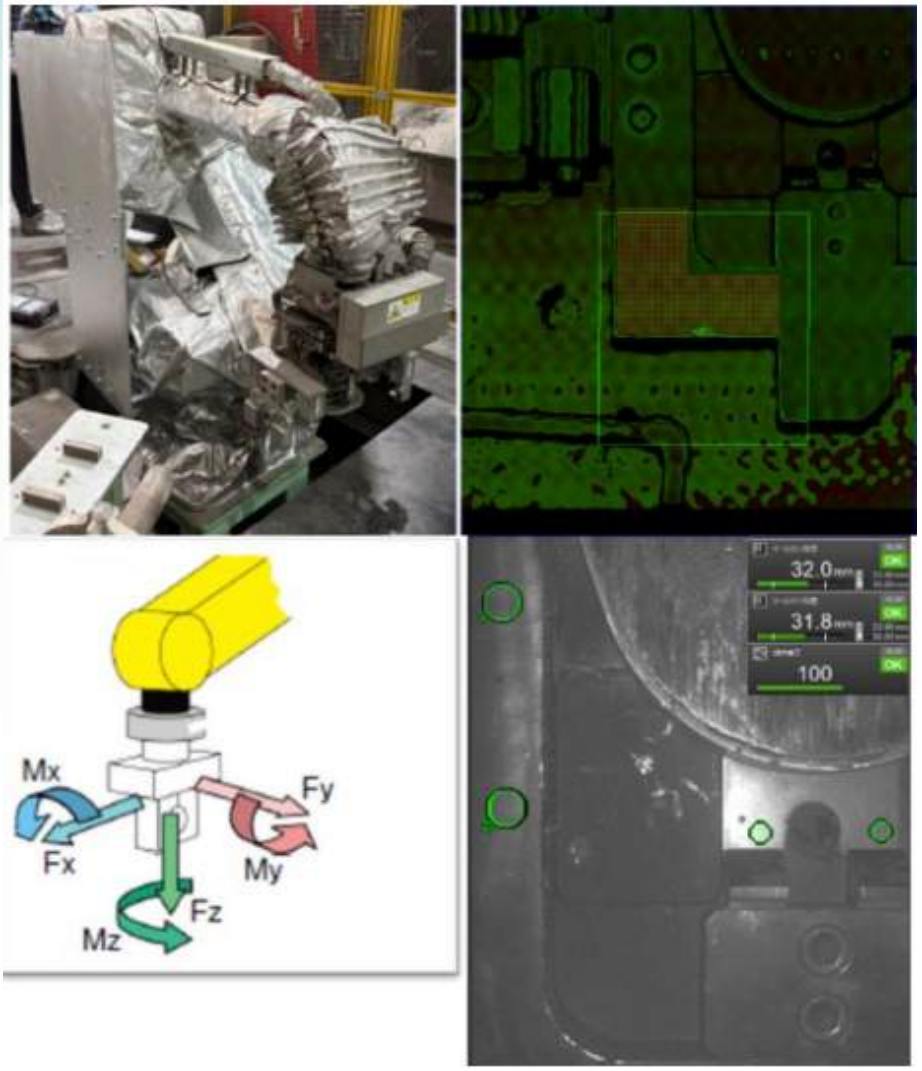


Figure 2 Technical features of REX-ROBO LSG

Furthermore, dedicated plates optimized for robotic handling were initially used during the verification phase. Through redesign of the robot hand the system was successfully adapted to handle standard R-Gate plate refractories, thereby improving compatibility and reducing the need for specialized components. In addition, a recovery function has been implemented that automatically returns the robot to its home position with a single button operation in the event of an abnormal stop during operation.

2.3 R-Gate Modifications for Robotic Operation

To enable robotic operation, several modifications were implemented on the R-Gate system. 1. Addition of position correction markers used as targets for the vision sensor. 2. Addition of handles used by the robot to open the R-Gate frames. 3. Development of a Lower Nozzle Holder suitable for robotic handling. 4. Development of a plate clamping mechanism that can be operated by the robot. By incorporating these features, the R-Gate was successfully adapted for robotic operation, enabling stable and reliable performance of the REX-ROBO system.

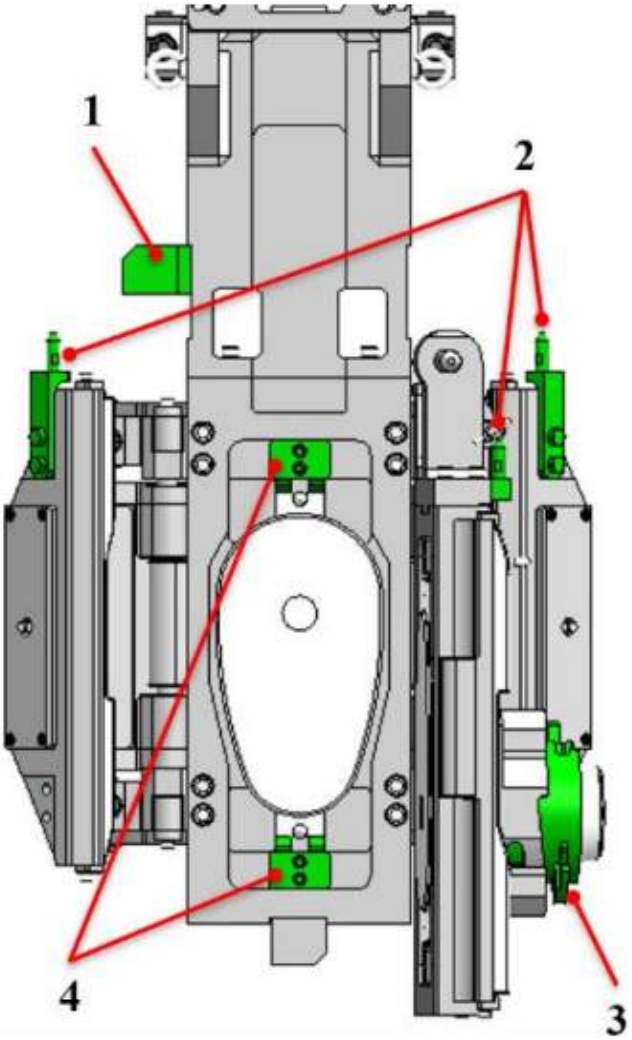


Figure 3 R-Gate modifications for robotic operation

2.4 System Configuration

Figure 4 shows an example of the system configuration of the REX-ROBO LSG. The configuration incorporates all maintenance operations described in Section 2.1. Despite its functionality, the system can be installed within a compact footprint of approximately 6 m × 3.5 m, as illustrated in figure 4.

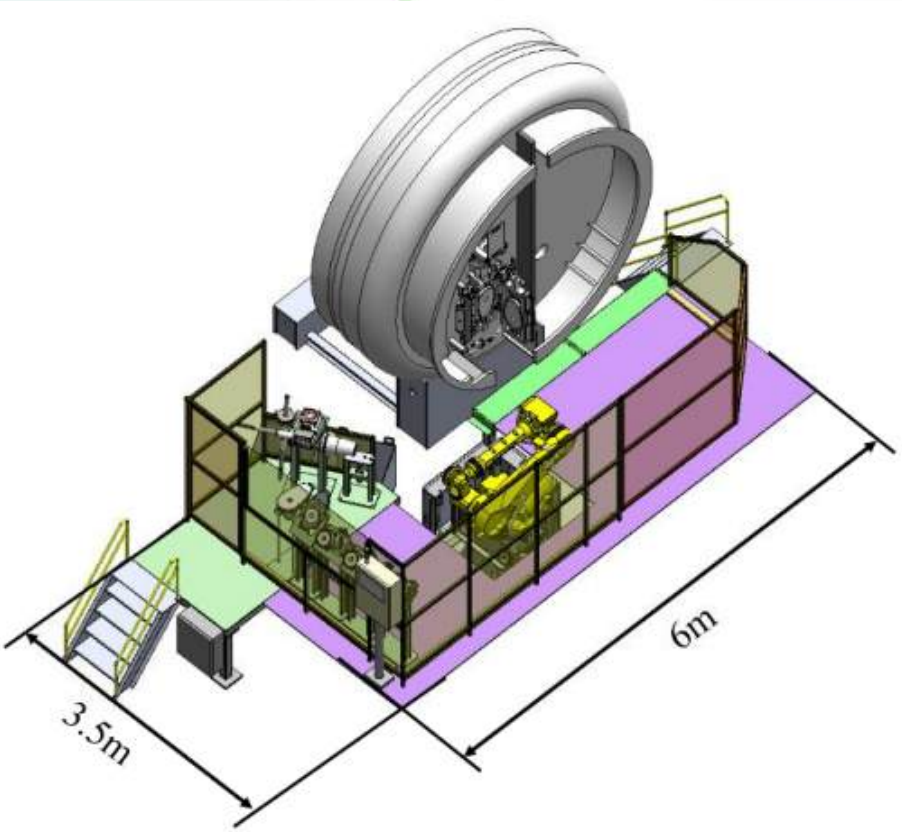


Figure 4 Layout of REX-ROBO in the preparation area

2.5 Operational Performance

The REX-ROBO LSG system was commissioned at a Japanese Mini-mill in 2025. A one-month hot-run trial was conducted after installation, during which 105 refractory replacement cycles were successfully carried out. Continuous improvements based on operational feedback enhanced the reliability of the system, achieving a replacement success rate close to 100%. Operational results are shown in Table 2.

REX-ROBO Operation Procedure	Number of Operations	Success Rate [%]
Adjusting position of R-Gate	105	100
Adjusting position of Lower Nozzle Frame	54	100
Detaching Lower Nozzle	54	96
Openig Spring Boxes	53	100
Openig Slide Frame	53	100
Adjusting position of Lower Plate	52	96
Detaching Lower Plate	50	100
Adjusting position Upper Plate	49	100
Detaching Upper Plate	49	100
Adjusting position of Upper Plate	17	100
Supporting Upper Nozzle handling	17	100
Inserting Upper Nozzle	17	94
Adjusting position of Lower Plate	65	100
Attaching Lower Plate	65	95
Lower Plate Position Verification	65	100
Adjusting position of Upper Plate	64	100
Attaching Upper Plate	64	97
Upper Plate Position Verification	64	100
Adjusting position of Slide Frame	61	100
Closing Slide Frame	61	98
Adjusting position of Spring Boxes	65	100
Closing Spring Boxes	65	100
Checking Face Pressure	65	100
Adjusting position of Lower Nozzle Sleeve	99	100
Attaching Lower Plate	99	97

Table 2 Operational Results of REX-ROBO LSG

In addition, by using REX-ROBO for refractory replacement operations, including upper and lower plates and the lower nozzle, the operator working time in front of the Slide Gate mechanism was reduced from approximately 9 minutes to approximately 7 minutes.

As a result, operator exposure to the hot environment around the Slide Gate mechanism was reduced by approximately 25%.

The introduction of REX-ROBO reduced heavy manual work under high-temperature conditions and improved operational stability by reducing dependence on operator skills and experience.

3. REX-ROBO Series

The REX-ROBO Series is being expanded to support various maintenance applications in addition to the REX-ROBO LSG. Several ongoing developments are introduced below.

3.1 REX-ROBO LANCING



Figure 5 REX-ROBO LANCING

REX-ROBO LANCING is designed to automate oxygen lancing operations for cleaning the inner bore of ladle Slide Gate mechanisms after use in steelmaking operations.
The system specifically targets the initial opening process, which is associated with the highest risk of splash generation during oxygen lancing. The robotic operation was originally developed as an additional function of the REXROBO LSG system.
To enable installation in limited spaces, a dedicated robot system specialized for lancing operations is currently under development.

3.2 REX-ROBO ANALYZER

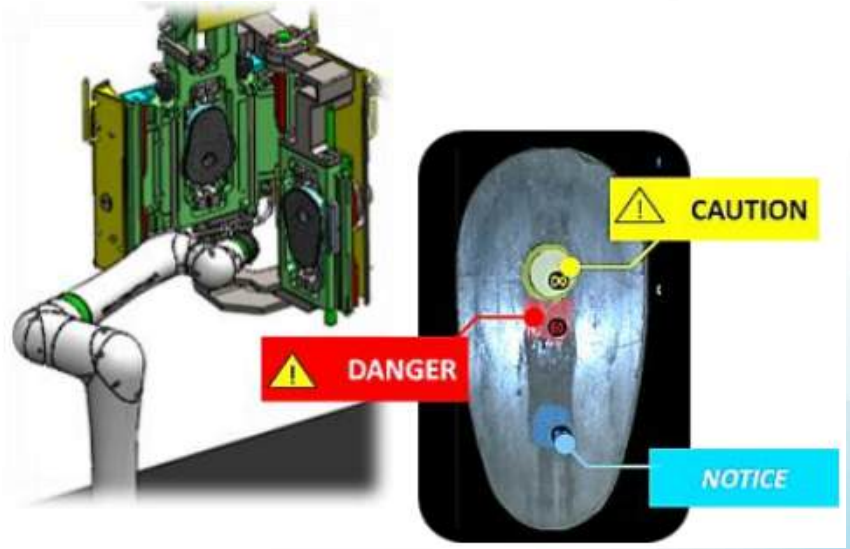


Figure 6 REX-ROBO ANALYZER

REX-ROBO ANALYZER is a robotic inspection system that utilizes artificial intelligence (AI) to detect damage to ladle Slide Gate plates. The system is capable of identifying various types of defects, including bore enlargement, metallic penetration, cracks, and spalling. In addition, the size and location of each defect are quantified and displayed according to its severity level.

By providing objective evaluation criteria and maintaining historical records of plate conditions, the system is expected to contribute to improved maintenance management and the transfer of technical knowledge to future operators.

3.3 REX-ROBO UQC

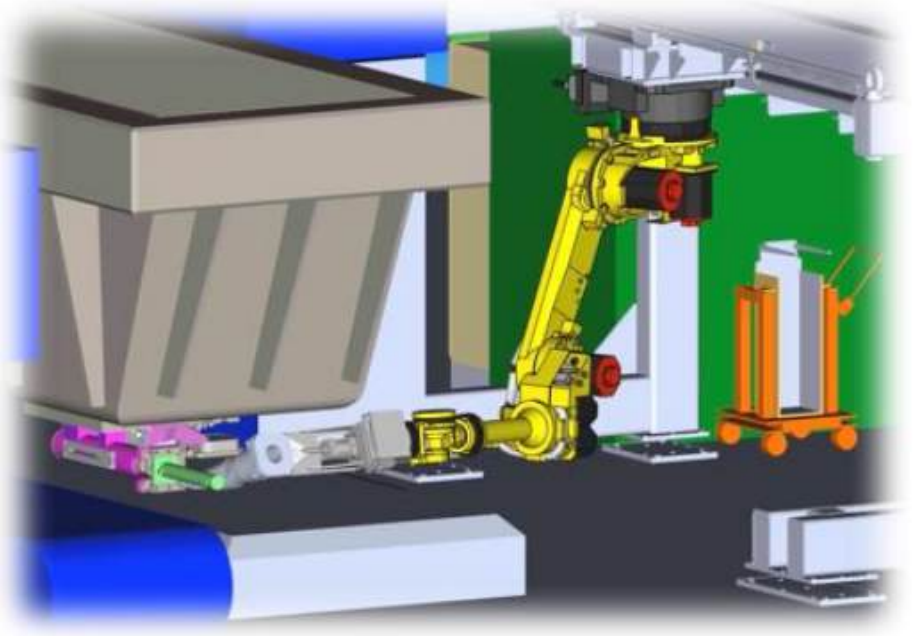


Figure 7 REX-ROBO UQC

REX-ROBO UQC has been developed to automate operations associated with KROSAKI HARIMA's submerged entry nozzle quick-change system.

The robot performs the installation and removal of submerged entry nozzles, as well as the setting of blank plates. By automating these operations, operator workload can be reduced while improving safety and operational consistency.

4. Conclusion

The first commercial REX-ROBO LSG unit was delivered in 2025 and is currently in successful operation.

The system has reduced operator exposure to heavy manual work under high-temperature conditions and has minimized dependence on operator skills, which were the primary objectives.

To further improve safety, productivity, and operational reliability, KROSAKI HARIMA CORPORATION will continue promoting the commercialization of REX-ROBO LSG while accelerating the development and implementation of additional REX-ROBO Series applications.

References

1) Toshihiro Imahase, Akira Otsuka, Junichi Funaro, Nobuyuki Yokoi and Hiroyuki Ohba: AISTech 2016 Conference Proceedings (2016) pp.1661-1671.
2) Mamoru Yoshimura*, Yusuke Yamaguchi, Toshihiro Imahase, Junichi Funaro and Hiroyuki Ohba: UNITECR 2019 Proceedings (2019) pp.153-156.
3) Iori Suetsugu, Shunji Sadano, Akira Otsuka, Mamoru Yoshimura, Toshihiro Imahase: IREFCON 2022 Proceedings (2022) pp.203-205.

ENHANCEMENT OF CORROSION RESISTANCE IN MGO-C FOR CONVERTER

Daisuke TOMITA, Tomoyuki TERASAKA, Naofumi KIDO

Krosaki Harima Corporation

1061, Tenwa, Ako City, Hyogo, 678-0256, Japan
Email* ; tomita.6tz.daisuke@krosaki.co.jp (* : as representative)

Abstract

MgO-C bricks, which have an excellent resistance against slag corrosion and thermal spalling, are widely used as refractory in converter for steelmaking. In converter, side wall of trunnion (Tr) and slag line are one of the most severely worn part by slag corrosion. Therefore, MgO-C qualities which have high corrosion resistance have been developed and applied. In this study, a drastic revision of design based on analysis of wear profile in actual converter vessels was carried out. As a result, it was confirmed that the apparent porosity of MgO-C brick after heat treatment is an important property to improve corrosion resistance. Especially, a new MgO-C quality, which has significantly lower apparent porosity after coking, was developed and the improvement of corrosion resistance was also confirmed. This developed quality showed lower wear rate in an actual converter vessel since it equips enough thermal apallimg resistance as well.

Keywords: Converter , Trunnion and slag line , Apparent porosity , High corrosion resistance

1. Introduction

Converter is a rection furnace to obtain molten steel with controlled chemical compositions such as C, Si, Mn and P by blowing pure oxygen after adding scrap and auxiliary materials such as slaked lime into pig iron tapped from the blast furnace. As a wear lining for converter, MgO-C brick is applied since it has high resistance against corrosion by slag, themal and mechanical spalling. Krosaki Harima has various menu in quality and structure based on experience until now. Especially, Krosaki harima has been making a continuous effort on improvement for some particular "Functional items" such as tap hole sleeve, bottom blowing tuyere, wall bricks at trunnion and charge pad. Bricks for trunnion and slag line, which shall be reported in this document, are the area to show high erosion by slag (Fig.1). In addition, this area is difficult to be repaired during campaign. Therefore, it is sometimes seen that this area limits campaign life of converter vessel. It has been and will be an important work to improve refractory performance which enables production stable at steelmaking plants. Thus a drastic change in quality design has been conducted to develop new MgO-C quality to show better performance at trunnion and slag line in converter. In this report, a series of our consideration is explained.

- Clarification of wear pattern by post-mortem
- Clarification of required properties
- Properties of the developed material
- Performance at actual converter vessel

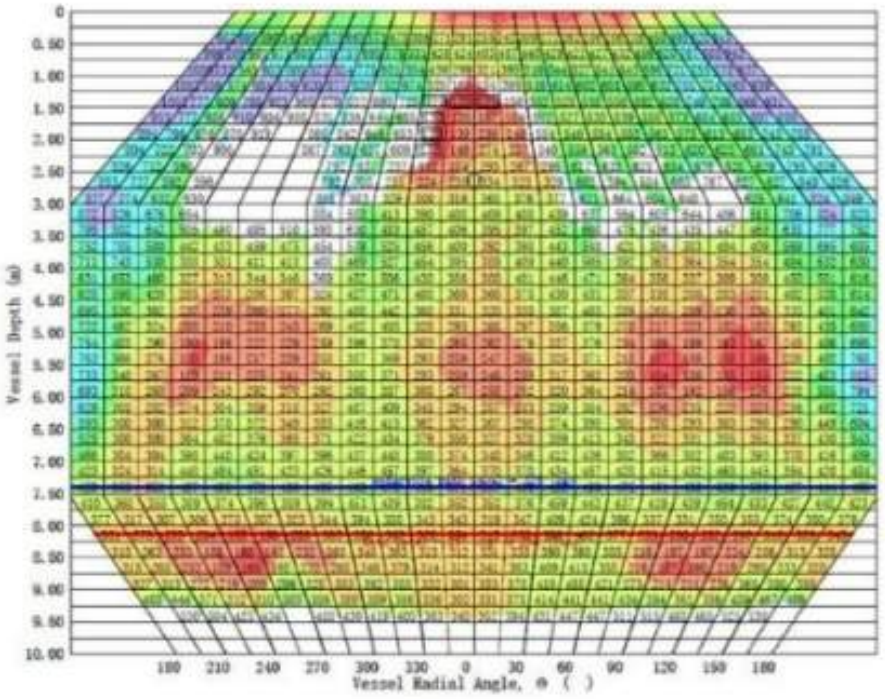


Fig.1 LACAM

2.Discussion

2-1. Fundamental issues of MgO-C bricks after use

Fig. 2 shows wear mechanism of converter bricks at trunnion and slag line. Three main mechanisms are considered; 2 (1) Corrosion by slag during refining, (2) Corrosion by slag during tapping, (3) Thermal spalling by temperature decrease since tapping until next charging of pig iron. At many steel plants, improvement in performance is required for refractory on trunnion and slag line area since these areas have higher wear rate than other areas.

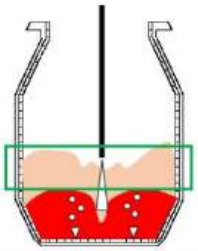
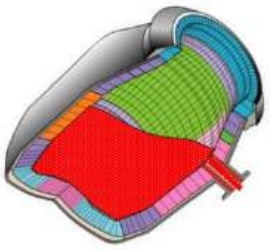
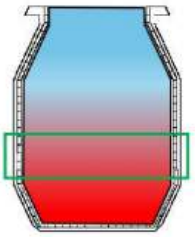
Operation	Blowing	Tapping	Tap to tap
Image			
Wear Mechanism	Corrosion by slag	Corrosion by slag	Thermal spalling
Required Properties	Corrosion resistance	Corrosion resistance	Thermal spalling resistance

Fig.2 Wear mechanism and requirement for MgO-C bricks for converter trunnion and slag line

Post-mortem was carried out to consider improvement in performance. As a reference, values of apparent porosity are shown in Fig.3. The bar graph in black is a value of apparent porosity after coking at 1400 degrees C, measured at laboratory. The bar graph in red is a value of apparent porosity after use in actual converter vessel. Although the black bar graph shows around 8%, the red bar graph shows around 10% (higher than black). Fig.4 shows a microscope photo taken at hot face of used brick. The upper surface in the photo is hot face of the brick. As above mentioned, it is seen that hot surface of the brick is eroded by slag. Details are as follows.

* Thick reacted layer can be seen in which slag penetrates into bricks structure.
* MgO grain is almost dropping off in oxidized layer (pores).

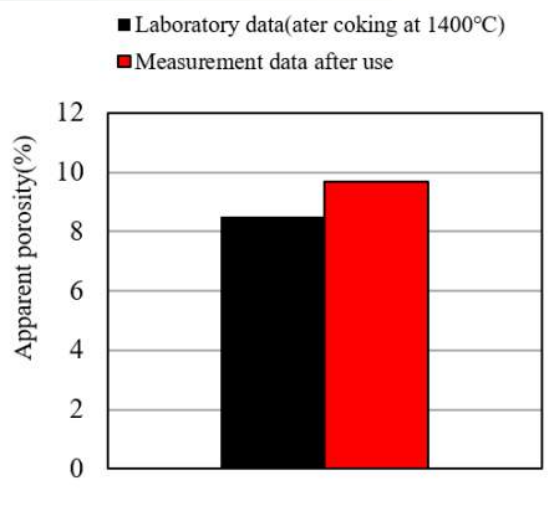
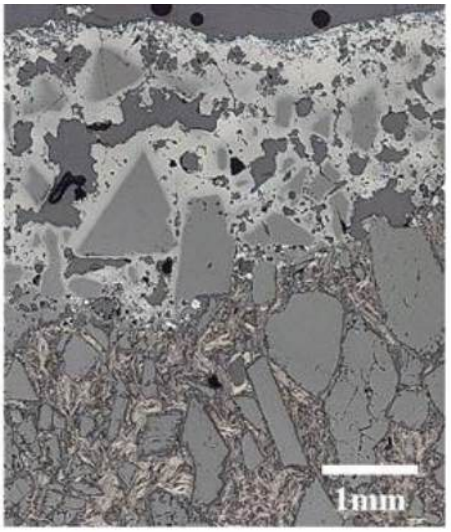


Fig.3 Apparent porosity Fig



4 Microscope of the hot face

Furthermore, Fig.5 and Fig.6 are microscope photos of the same material before / after use in another case. Fig.5 is before use, and Fig.6 is after use.

* In the brick after use, pores are formed surrounding MgO grains. In actual cases, converter runs in 1 campaign for a long time, number of heat can reach some thousands. Therefore, this formation of pores is thought to be caused by the difference of thermal expansion coefficient between MgO grain and graphite. Furthermore, deterioration of structure by repeat of heat load can also affect this phenomenon. Because of these phenomena, the value of apparent porosity after use thought to become higher than lab-based value.

Before use

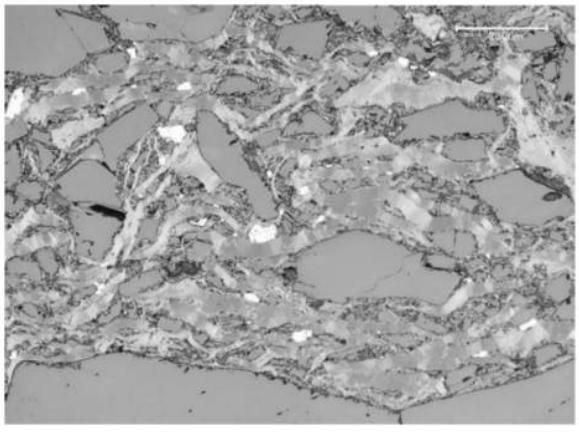


Fig.5

After use

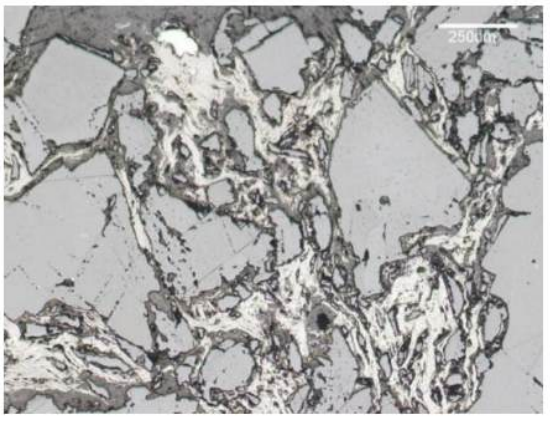


Fig.6

2-2. Other required properties in MgO-C bricks for converter trunnion and slag line area

As described above, it is considered to be the direction of improvement that structure (represented as apparent porosity etc. in quality measurement) of brick should be kept the same as product. It is believed that maintenance of internal structure in brick is expected to improve properties such as corrosion resistance. On the other hand, spalling resistance is also an important property, since a gap in temperature occurs after tapping from converter until next charging of pig iron. In addition, it is seen that converter vessel stops during campaign for some reasons, which makes spalling resistance more important. To describe importance of spalling resistance in MgO-C brick for converter, Fig.7 shows a case of thermal spalling issue of MgO-C brick occurred in an actual converter vessel. Carbon content is one of the most important factors in considering spalling resistance. Fig.8 shows correlation between carbon content and thermal spalling resistance. The higher carbon content, the better thermal spalling resistance, which comes from increase of thermal conductivity according to increase in carbon.

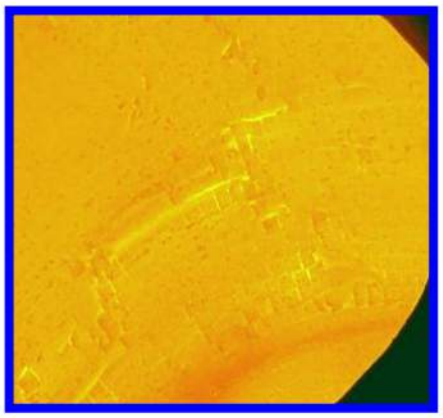


Fig.7 Monitored spalling MgO-C in BOF

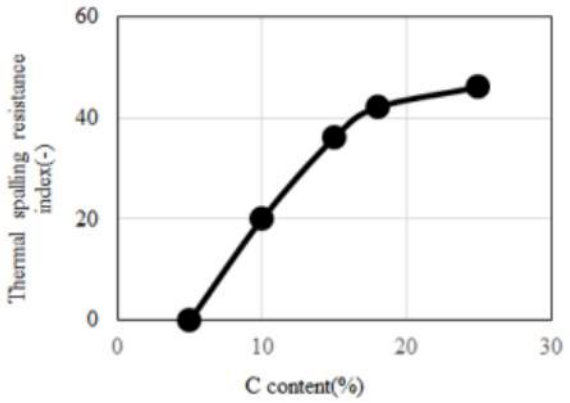


Fig.8 Correlation between carbon content and thermal spalling resistance

2-3. Approach to developed materials

MgO-C qualities with 15% in carbon content are generally selected for converter trunnion and slag line area because of a good balance between corrosion resistance and spalling resistance. This carbon level was also adopted in this report. This time, "Apparent porosity after coking" was focused as an evaluation index of "Maintenance level of internal structure in brick". It means that the lower apparent porosity after coking, the denser structure. Consideration was progressed based on the concept that lowering apparent porosity after coking results in corrosion resistance better.

3. Characteristics of developed materials

Table1 shows overview of developed and conventional materials. Conventional material has 15% of carbon content 4 and is generally used on converter sidewall areas. The developed material is selected 15% of carbon. Fig.9 shows values of apparent porosity after several condition of heat treatment. To minimize the generation of pores by repeat of heat load, all factors such as raw material composition and manufacturing parameters were thoroughly reconsidered. Our "Densification technology" could make apparent porosity after coking remarkably lower. Conventional material shows a tendency of increase in apparent porosity after coking according to repeat of heat. On the other hand, the developed material is able to suppress this tendency.

Materials		Conventional	Developed
Chemical Composition / mass%	MgO	80	80
	C	15	15
Measurement examples（After curing）			
Bulk density	/-	3.01	3.06
Apparent porosity	/%	2.9	2.7
Measurement examples（After coking at 1400℃）			
Bulk density	/-	2.94	3.02
Apparent porosity	/%	8.4	6.9

Table1 Physical properties and characteristics

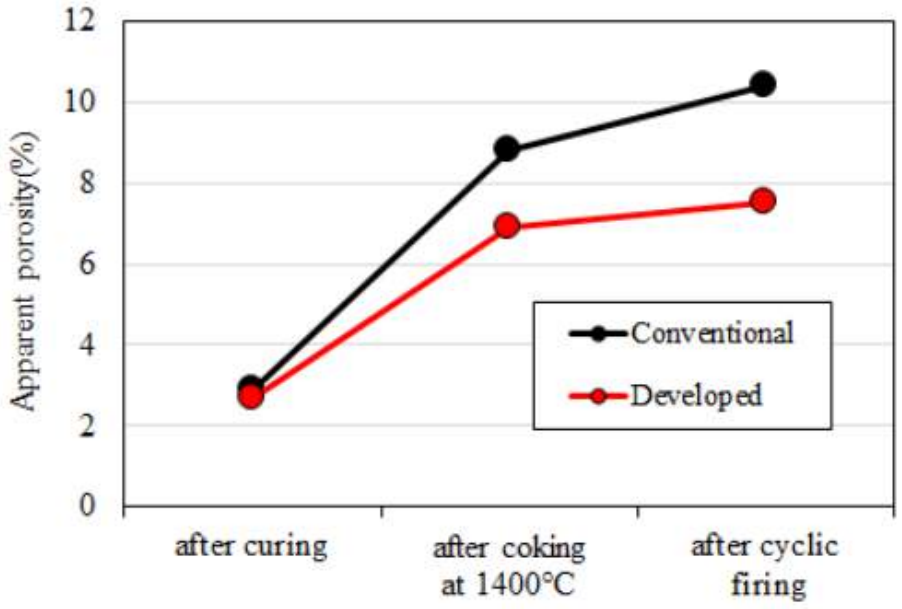


Fig.9 Apparent porosity under heat treatment condition

Fig.10 shows a comparison in corrosion resistance. The developed material could show 20% better corrosion resistance than conventional material. The developed material has lower apparent porosity after coking than conventional material, which is thought to affect this improvement. Fig.11 shows a comparison of spalling resistance. The developed material could achieve spalling resistance in the same level as conventional material even though it has lower apparent porosity after coking. Therefore, the developed material is expected to show remarkable improvement in performance because of better corrosion resistance maintaining spalling resistance similar. The result of the developed material used at an actual converter vessel is being reported in next item.

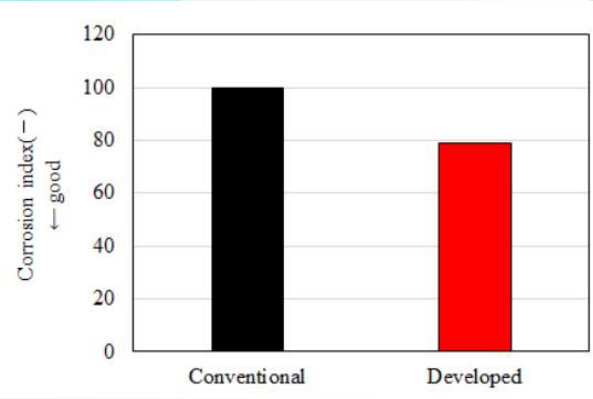


Fig.10 Corrosion index

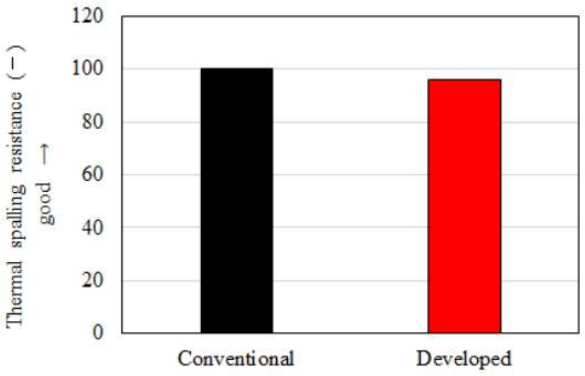


Fig.11 Thermal spalling resistance

4. Example of test result

4-1. Example of test result in use as refractory for converter

A comparable example of test results between conventional and the developed material is explained as follows. Fig.12 shows correlation between wear rate in an actual converter vessel and apparent porosity after repeated coking. A good correlation between these factors can be seen. Furthermore, values of apparent porosity in bricks which were used at converter vessel are shown in Fig.13. It is confirmed that the developed material has lower apparent porosity than conventional material, which implies the developed material could keep internal structure of brick dense. It is confirmed that materials with lower apparent porosity after repeated coking could show lower wear rate in actual converter vessels. Conventional Developed MgO 80 80 C 15 15 Measurement examples（After curing） Bulk density /- 3.01 3.06 Apparent porosity /% 2.9 2.7 Measurement examples（After coking at 1400℃） Bulk density /- 2.94 3.02 Apparent porosity /% 8.4 6.9 Materials Chemical Composition / mass% 5 It is concluded that reduction of apparent porosity after coking is an important property to improve performance of converter campaign life.

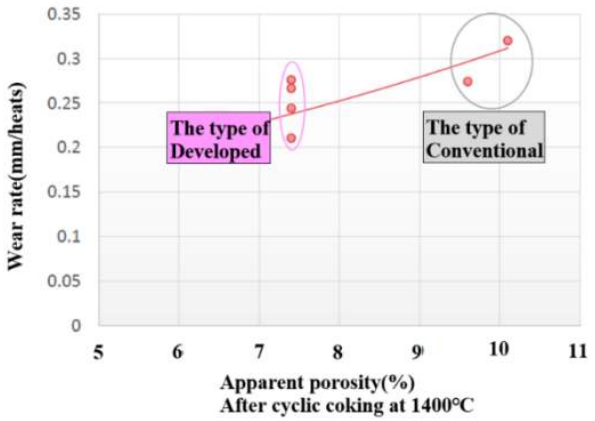


Fig.12 Wear rate in MgO-C bricks for converter trunnion wall（customer A）

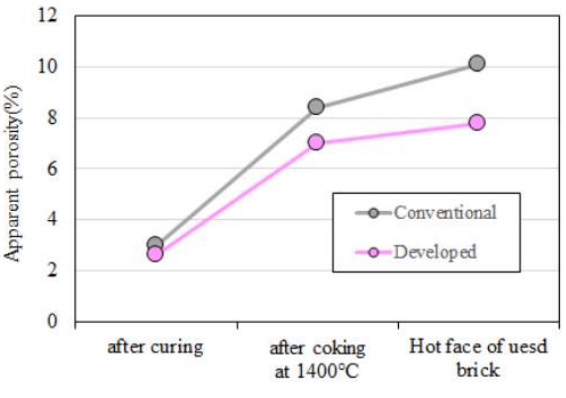


Fig.13 After use apparent porosity

Furthermore, Fig.14 shows index numbers of wear rate at actual converter vessel in customer B. The developed material showed 20% reduction in wear rate. Fig.15 are pictures of cut surfaces for used bricks. The developed material has thicker residual thickness, and no cracks were observed from hot face to cold face which can be said that

the developed material could keep internal structure uniform. From this result, it is confirmed that the developed material has equivalent spalling resistance to conventional material. The developed material has been expanding its application to other steel making plants for their converters with above explained results. Receiving these results, the developed material is widely expanding its application to not only converter, but also to EAF (Electric Arc Furnace).

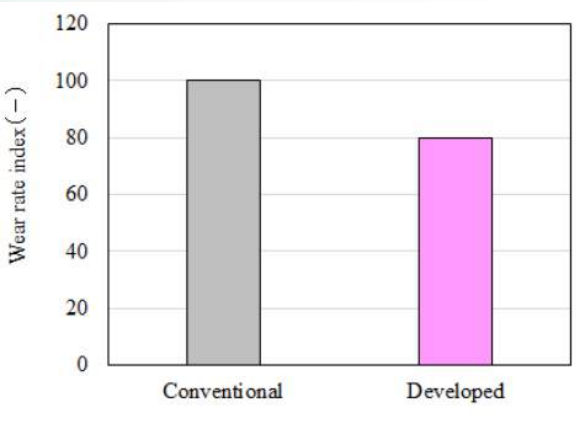


Fig. 14 Wear rate index for converter trunnion wall（customer B）



Fig.15 Cut face of used brick

4-2. Example of test result in use as refractory for EAF

As a refractory for EAF at customer C, the developed material was trialed. The material was applied at "Hot Spot" area, Fig.16 is pictures of appearance and cut surface of used bricks. From the observation of appearance and cut surface, it is confirmed that bricks has not abnormality in structure since no cracks or oxidation are observed. Fig.17 shows apparent porosity of the bricks. It can be said that the brick keeps its structure dense since the values are low. Fig.18 is the heats of vessel (campaign lives), and the developed material could improve the life. From this result, it is confirmed that dense materials like the developed material can also perform better than conventional MgO-C materials at hot spot of EAF where bricks are exposed to high temperature conditions by electrodes, and bricks tend to show high wear.

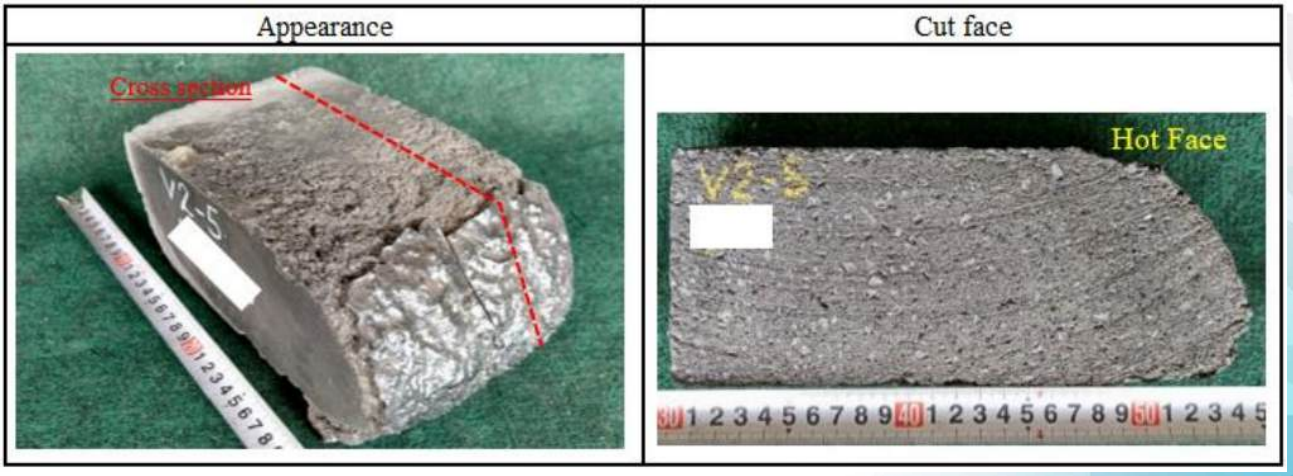
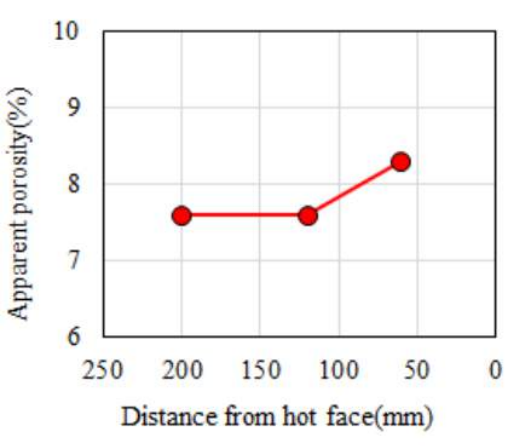


Fig.16 Appearance and cut face of used brick



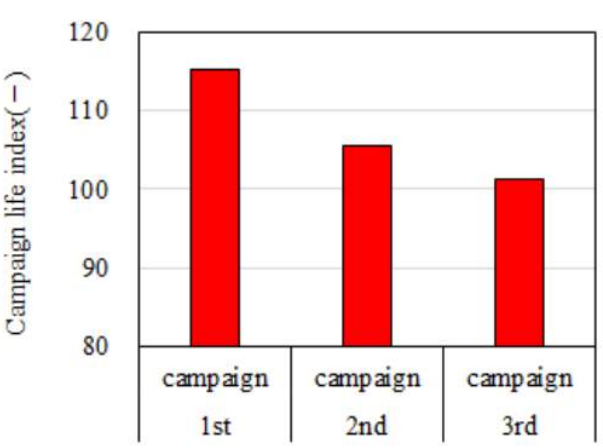


Fig.17 Apparent porosity of used brick

Fig.18 Campaign life index

5. Conclusion

A solution for improvement of corrosion resistance, which has been one of the most important challenges, has been established using our "densification technology" reported in this report. As a result, Krosaki Harima can give proprietary technology for converters in all applications (shown in Table2). Furthermore, it is expected that installation of EAF is expanding worldwide in the viewpoint of carbon neutral, and our densification technology is adoptable to refractory for EAF. It is strongly believed that expansion of our densification technology worldwide is very important for better stability in steel production. Indian crude steel production is expected to expand year by year; therefore, it is quite important to organize condition that Indian supplier can manufacture products with this technology. At this moment, Krosaki Harima is working on establishment of manufacturing technologies by which our Indian group company will be able to manufacture these kinds of materials as soon as possible.

Application			Oxidation	Corrosion	Abrasion	Scrap impact	Spalling	Differentiated technologies
BOF	Upper cone		++++	++			+	High gas phase oxidation
	Barrel	Trunnion	++	+++++			++	Dentification
		Tap side	++	+++			++	
		Impact	++	+++	+++	+++++	+++	TOUGHMAX™
	Lower cone		+	++	++	++	+++	
	Bottom		+		++	++	++	High fracture energy
	Tuyere				++	++	+++++	
	Tap hole sleeve		+++		++++		++	Clean flow

Table2 Wear factor and differentiated technologies at each part of the converter

References

1. Refractory handbook revision 12 , Japan , 2015 , P405-P408

USE OF RECYCLE REFRACTORIES AND ITS IMPACT ON REFRACTORY PRODUCTS

UB Khuntia, Niroj Mandal, Dr. JK Sahu, Ashish Jain

Vishva Vishal Refractory Limited, Bhilai, India

Abstract

The refractory industry is under increasing pressure to reduce production costs, conserve critical mineral resources, and lower greenhouse gas emissions. Ferrous and non-ferrous industries generate large volumes of spent refractories. Effective recycling and reuse show important pathway to achieve long-term environmental and economic sustainability. Published studies demonstrate that the reuse of 1tonne of spent refractory material reduces CO2 emissions by approximately 1.1 tons compared to equivalent virgin refractory aggregates. Because virgin raw materials undergo energy-intensive mining, beneficiation, and high-temperature calcination using fossil fuels.

This study provides a comprehensive evaluation of the beneficiation process to generate high-quality recycled refractory aggregates establishing optimum addition in various products effectively balancing thermo- mechanical and corrosion resistance properties. Authors propose a zonal application concept of recycled- refractories in areas with lower thermo-chemical severity and ensures reliable service performance. Industrial trials conducted to validate laboratory findings. This research offers valuable technical guidance to manufacturers, recyclers and end-users.

Keywords: Recycled, Beneficiation, Zonal application, stopper

1. Introduction

Within the refractory industry, recycling has evolved beyond a mere forward-looking strategy; its tangible contributions to operational efficiency and environmental sustainability are now recognized as essential drivers in reshaping raw material selection and product design. This paper aims to dismantle common recycling myths by presenting a series of evidence-based technical use cases validated at both laboratory and industrial scales.Alternate raw materials against prime raw materials available and its impact on environment is shown in Table-1.

Table.1 Alternatives against prime raw materials

Prime/Natural Material		Limited resources
		High environmental
Synthetic RM	Recycled RM	impact
Require prime RM	Drastically	
High CO2 emission	reduce carbon	
Costly material	foot print	
Energency intensive		

Refractory consumption in various industries & specific consumption of refractories per Mt of finish products are shown in Table-2.

Table-2

	Steel	Cement	Non ferrous	Others
Refractory consumption	70%	12%	7%	4%
Specific consumption kg/Mt steel	~ 10-15	~ 0.9	~ 9	~4

Typical material flow for a steel plant outbreak recycling is shown in Table.3

Table.3 Beneficiation process

Refractory out break	
Sorting/Cheaping /Sieving	
0-100 mm	>100mm
Refining & post treatment	Presorting
Sorting	Land filling~2%
Crushing	Use metallurgical
Magnetic separation	additives
Milling →	Use in refractory
Seiving	application
Drying	
Packing	

Raw Materials used in Refractory Vs CO2 Emission:

The right way to utilised the rejection is of -3R concept i.e. REDUCE—REUSE---RECYCLE

Table.4 Raw materials aggregates represent 70-90% of the refractory's CO2 emission

Raw material	Approx CO2 foot print(t/t)
DBM	1.5-1.9
FM	2.6-5.0
SiC	5.8
Cal.alumina	0.7
Tabular Alumina	2.9
BFA	1.0-1.2
WFA	1.0-1.3
Recycling	<0.1

Table-5 Some of the refractory recycled material available commercially.

Material	SiO2 %	Al2O3 %	Fe2O3 %	CaO %	MgO %
CMC grog	2	2	1	2	92
Washed CMC grog	0.81	1.54	0.84	0.89	95.51
DBM	2	0.2	1	2.5	94.5
FM	0.6	0.3	0.4	1.2	97.5

Material	LOI	BD(gm/cc)
CMC grog	0.5	3.3
Washed CMC grog	0.33	3.43
DBM	0.15	3.38
FM	0.2	3.5

Material	MgO %	Al2O3 %	SiO2%	CaO %	Fe2O3 %
AMC grog-Ty-1	5	90	0.5	0.25	0.3
AMC grog Ty-2	8	83	4.5	0.75	1
WFA		93	5		0.2
HD Bauxite		89			1.8
85% Bauxite	0.4	85	9		2

Material	Na2O	K2O
AMC grog Ty-1	0.10	0.4
AMC grog Ty-2	0.15	0.4
85 Bauxite	0.3	

2. Experimental

Selection of recycle material to blend with prime raw material

- CMC grog can be partially replaced with Prime DBM
- Washed CMC grog can be partially replaced with DBM/FM
- Uncalcined MgO-C can also be used
- AMC Ty-1 grog can be partially replaced with WFA/HD bauxite
- AMC Ty-2 grog can be replaced partially with 85% alumina bauxite
- Uncalcined AMC is also used

Based on recycled material chemistry product mix adjusted as and when required to meet the specification.

2.1 Batch formulation, Results & Discussion

Product mix are designed by blending grog with prime material after completing various lab trials by addition of 10,20,30,40 & 50 % grog to virgin mix. It was found that Optimum addition of 40% recycled material has very low and no impact on performance in the described products (MBS) only.

Mono block stopper as per Table.6 were manufactured. Products were Iso-statically pressed, dried, glaze coated and fired in electric kiln Fig.1

Table-6 Batch Formulation(Body part)

Raw material	MBS(VM)	MBS(RCyM)
Graphite %	12	10
BFA %	48	16
SiO2+SiC+Si %	15	12
Recycled grog %	0	37
Anti-oxidant %	3	3
Bond %	11	11
Resineous binder-liquid %	6	6
Resineous binder-powder %	5	5



Fig: 1 MBS glaze firing virgin material MBS glaze firing with 37% grog

Table-7 Physical Properties:

Sample	AP %	BD (gm/cc)
MBS (VM) body	12.6,14.2,11.9	2.48,2.51,2.50
MBS (RCyM) body	14.8,15.6,16.6	2.42,2.43,2.48

Sample	CCS(kg/cm2)	MOR(kg/cm2)
MBS (VM) body	112,115,110	60,71,66
MBS (RCyM) body	93,87,100	57,67,70

Table-8: Chemical Properties:

	C %	Al2O3 %	SiO2 %	Fe2O3 %	Other %
MBS(VM)	11.3	51.7	16.3	1.3	20.5
MBS(RCyM)	10.7	49.2	20.8	2.6	16.4

2.2 Oxidation Test

Oxidation test was conducted in a lab furnace at 1000 degC/3 hrs.Fig 1. & Table-9 shows the depth of oxidation which is found very less. It indicates that anti-oxidant added in the product mix is optimal.

Table-9: Oxidation test

A	MBS (VM)	Oxidised layer (in mm)	1	0.8	0.9	1
B	MBS (RCyM)	Oxidised layer (in mm)	0.95	0.9	1	0.9

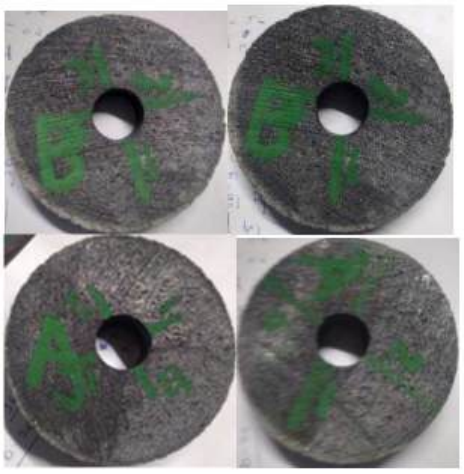


Fig-2 Oxidation test

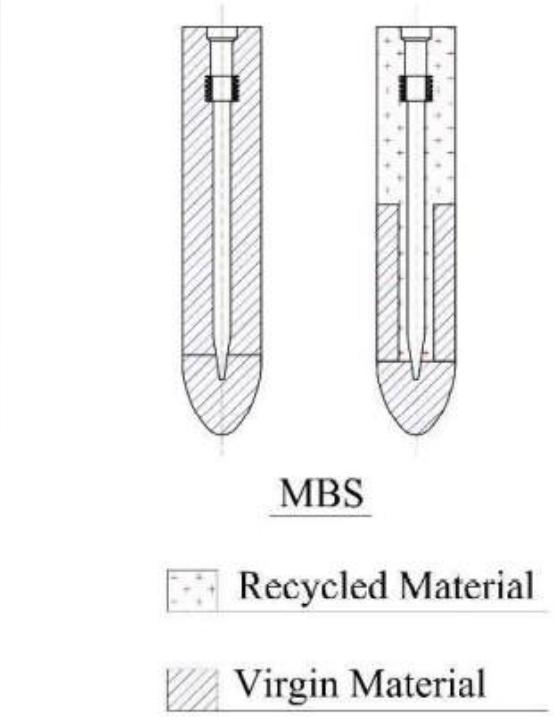
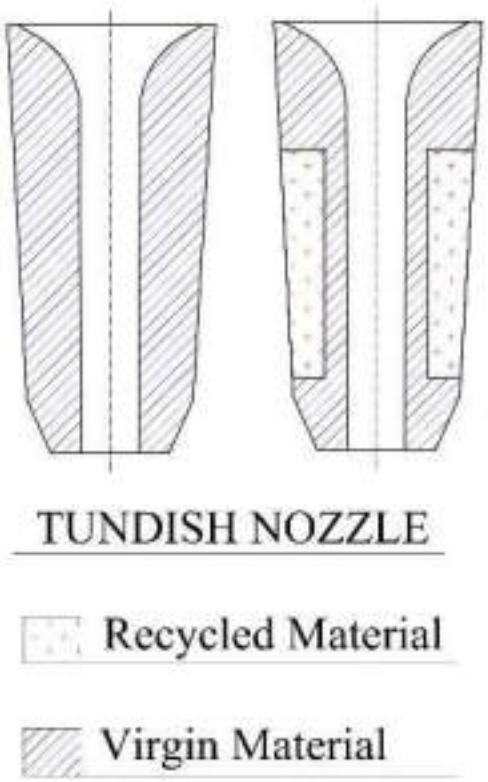


Fig-3 Zonal concept of use of recycle material in MBS



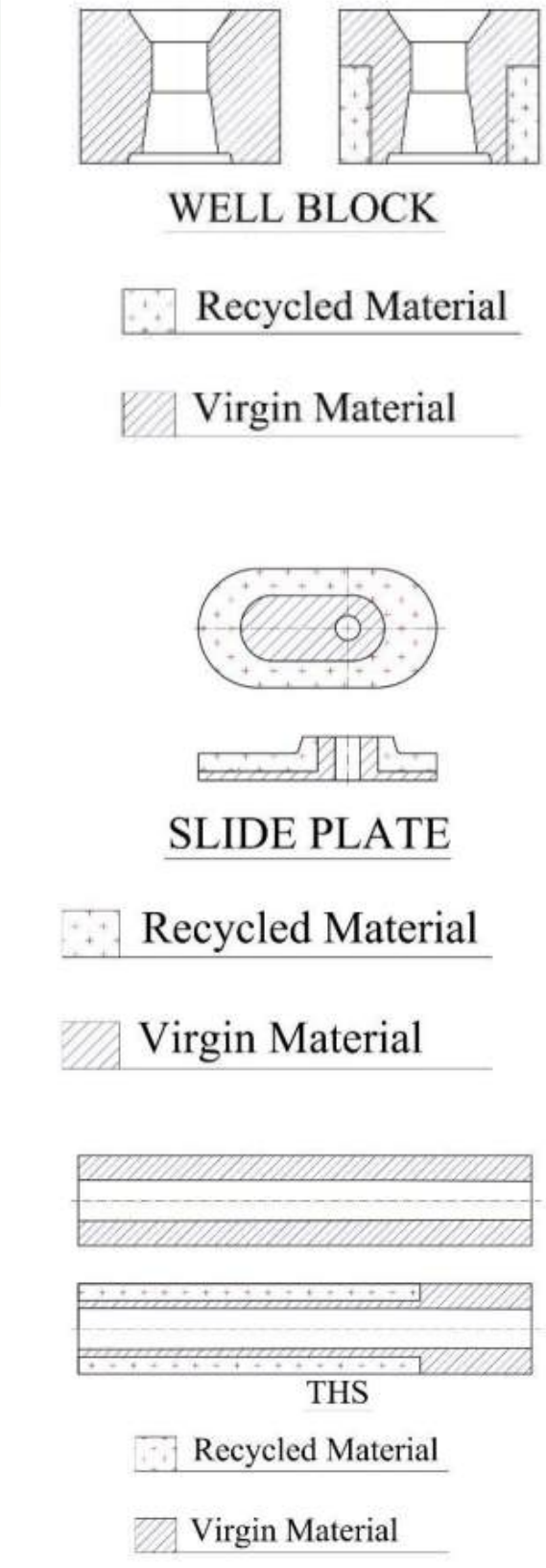


Fig.4 Use of recycle material Zonal concept in TN, Well block, THS,Slide plates

3. Service Performance

About 206 nos of MBS made by blending with recycled material used in one of the integrated steel plants and compared with MBS made with 100% virgin material. The performance of MBS found similar and withstand 10-15 hrs of casting.

4. Conclusion

Besides Monoblock stopper Authors have tried the use of recycled material (zonal concept) in other products like Tap hole sleeves (THS), Tundish nozzle(TN), Slide plates, Well block etc. Precast blocks, Monolithic lances, Alumina carbon tundish nozzles, Slide gate plates etc. Cost economic products were made and the performance found out to be almost similar to products made from virgin material.

Acknowledgment

Authors are thankful to management of Vishva Vishal Refractory Ltd for extending support for publication in the conference proceedings 2-4 Nov. IREFCON-2026.

References

References: 1. Refractory Circulary: Technical Realities behind Recycling myths Jennifer astovezo, Lucas Zimmermannetal - ICR-25 conference, Aachen, Germany 17-18 Sept 2025

2. Horckmans L, Nielsen P, Dierckx P, Ducastel A. Recycling of refractory bricks used in basic steelmaking: A review. Resources, Conservation & Recycling -140) pp.297-304. 2019

3. Efficient and Eco-friendly recycling of refractory materials for a sustainable environment : Suparna Basu ,Sushavon etal ICR 25 Aachen,Germany

4. Yamato, T.Taikabutsu. 63 (9), 426–434 (2011)

DEVELOPMENT OF OPEN-FIRED LADLE SHROUD FOR REUSE APPLICATION

[1]Abhishek King, [1]Manoj Kumar Rout & [1]Ravi Kumar Periyasamy

[1]R&D Flow Control, RHI Magnesita India Limited, Bhiwadi

Presenter Email: abhishek.king@rhimagnesita.com

Co-Author's Email: manojkumar.rout@rhimagnesita.com
Ravikumar.periyasamy@rhimagnesita.com

Abstract

The growing demand for cost-effective refractory solutions continues to drive innovation in the development and optimization of products tailored to evolving customer needs. Among these, ladle shrouds stand out as one of the most critical components due to their extreme exposure to thermal shock—they are deployed without preheating and must withstand rapid temperature escalation up to 1600 °C within seconds. However, in conventional closed-fired route ladle shrouds designed for reuse, cracking during the first heat has been a persistent issue, undermining performance and reliability. Addressing this challenge has been a key focus for our team. To meet customer expectations and eliminate early-life cracking, we have successfully developed a reusable ladle shroud optimized for the open firing process route. The newly developed reusable ladle shroud incorporates tailored in-situ antioxidants to effectively mitigate oxidation during both the manufacturing process and operational use. This strategic addition enhances the product's longevity and structural integrity under extreme thermal conditions. Furthermore, optimized granulometry and refined chemical composition have been employed to significantly improve spalling resistance, ensuring superior performance during rapid thermal cycling and repeated casting operations. This innovation not only improves operational reliability but also contributes to cost savings and sustainability by extending product life.

Keyword: Refractory; Ladle shroud; Open-fired; Reuse

1. Introduction

The refractory materials are designed in such a way that they can withstand a variety of severe service conditions including high temperature conditions. The characteristic feature of all types of refractories is their gradual destruction under operating conditions, and they have been replaced by new ones after the end of their service life. Nowadays, most raw materials that are being used to manufacture refractories are considered essential and extremely important [1] and for that reason there is an increase in prices on market the raw materials [2,3]. The union regulations regarding closed economy are based on the effective usage of natural resources, including secondary raw materials, through recycling technology from spent materials. Given the total global production of refractories, which in 2015 was ca-based steel of 30–35 million tons [4–6], the amount of spent refractories produced annually is significant, because under operating conditions, approximately one third of a refractory materials mass is irreversibly destroyed [7].

The increasing demand for refractory products that combine durability with ease of handling has driven significant innovation in steelmaking consumables. Moreover, the continuous casting process plays a vital role in manufacturing the required steel for the

customers. The major products used in this process are Ladle shrouds, Monoblock stopper, Sub-entry nozzles and Sub-entry shrouds. Moreover, the insertion of other products (such as Nozzle changer, Monotube, Starter tube & Starter ring) for the improvement in existing processes are always appreciated, and it's been a focus for the researchers. Among these, the ladle shroud plays a critical role in ensuring controlled metal flow and minimizing reoxidation during casting operations. Traditionally, ladle shrouds require preheating before use, which not only adds complexity to shop-floor practices but also increases energy consumption and turnaround time. In response to these challenges, the present research investigates the development of an open-fired ladle shroud designed for non-preheating and reusable applications. The study focuses on process optimization to enhance product reliability while eliminating the need for preheating, thereby simplifying handling at the user's end.

This approach provides a dual benefit: operational efficiency and sustainability through reduced energy usage. Ladle shrouds have long been recognized as essential consumables in continuous casting, primarily serving to control steel flow and minimize reoxidation. Prior studies on the role of ladle shrouds emphasize their contribution to steel cleanliness and inclusion reduction, yet most conventional designs rely heavily on preheating to prevent thermal shock. This reliance on preheating has been widely documented in the literature, with researchers noting its effectiveness in extending refractory life but also highlighting significant drawbacks despite incremental improvements in preheating practices, the search for alternatives remains limited.

Parallel to this, the concept of reusable refractory products has gained traction as industries strive for cost efficiency and sustainability. Investigations into tundish linings and ladle refractories demonstrate the potential for multiple-use cycles, reducing both material consumption and waste generation. However, the application of reusability principles to ladle shrouds has received little attention, leaving a gap in consumable innovation. This gap is particularly relevant in the context of energy-efficient casting practices, where eliminating redundant heating steps is a priority. While advances such as optimized burner systems and improved insulation have been explored, specific focus on consumables like ladle shrouds remains scarce. Recent progress in material design and process optimization has opened new possibilities for refractory engineering. Studies on MgO-C composites and alumina-based systems demonstrate enhanced thermal shock resistance and durability, while microstructural tailoring has been shown to improve performance under demanding casting conditions. Yet, few works have integrated these advances into consumables designed explicitly for non-preheating applications. This lack of targeted research underscores the need for innovative approaches that combine material science with practical usability.

However, limited focus on ladle shrouds compared to other refractory products, a scarcity of reusable designs that eliminate preheating requirements, and insufficient quantitative validation under industrial conditions. Addressing these gaps, the present study introduces an open-fired ladle shroud optimized for nonpreheating and reusable application. By leveraging process optimization and advanced material design, the research contributes to the broader agenda of energy-efficient and sustainable steelmaking practices, offering a practical solution that simplifies handling while maintaining performance. The work represents a step forward in refractory product innovation, offering a practical solution that aligns with industry priorities of cost reduction, ease of application, and improved safety. By integrating material design strategies with performance validation, the project demonstrates how refractory engineering can evolve to meet modern steelmaking requirements.

2. Production & Characterization:

Production:

The production was done considering the identified mix quality and the mix was iso-statically pressed with 17500 psi in PVC based mold. Further, the product was fired near 950 deg C and then it was considered for multiple characterization processes.

Characterization:

Physical test: The sample was dried in 110 °C and physical test for apparent porosity, bulk density (tab:1) was performed.

Chemical & Other test: The sample piece received was cleaned. The cleaned sample was dried in 110 °C. The dried sample was grinded in tungsten carbide pulverizer to -200 mesh. The powdered sample was put into 1000 °C for 1 hour in oxidizing atmosphere for loss of ignition determination. Chemical analysis was conducted using Bruker S8 Tiger XRF analyzer on the loss free basis at 1025 °C. The residual carbon content in the sample was estimated from the LECO CS230 Carbon analyzer. Thermal expansion was analyzed by using NETZSCH Dilatometer with considering 1200 °C temperature at 7 °C/min heating rate under argon atmosphere for different composition-based samples. Micromimmitics based mercury porosity instrument was used to analyze the pore size distribution of the matrix. The micrographs of the body were analyzed with the help of Nikon Eclipse LV150N reflected light microscopy at the different magnifications.

3. Result & Discussion:

Physical and chemical property assessments showed that both recipes exhibited comparable baseline characteristics, validating the robustness of the open-fired design. However, the modified granulometry in the Open Fired recipe contributed to improved spalling resistance and enhanced thermal stability. This was further supported by thermal expansion measurements, where similar expansion curves were observed between the two recipes. The improved thermal expansion behavior is indicative of better resistance.

Microstructural analysis indicated the presence of in-situ phase formations in the open-fired ladle shroud, attributed to the incorporation of antioxidants. These phases provided enhanced protection against oxidation both during firing and in service, thereby improving product reliability. The absence of glaze in the inner lining did not compromise performance, confirming that open firing can deliver comparable structural integrity to conventional closed-fired designs.

Closed fired LS **Open fired LS**

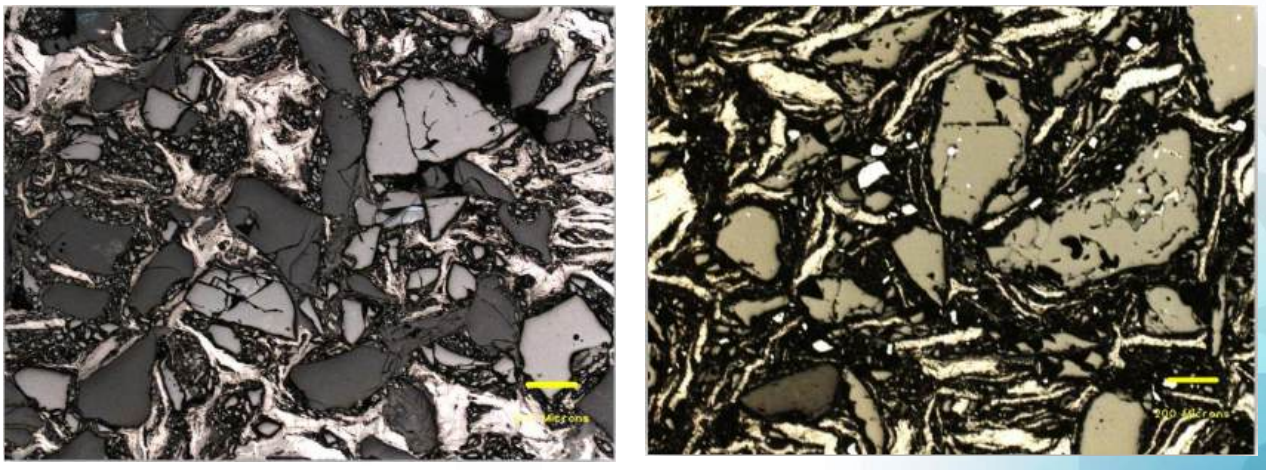


Fig. 1: Optical micrographs of closed fired and open fired matrix



Fig. 2: Product after firing has no glaze inside bore

Performance trials conducted at three customer sites using billet casters demonstrated the practical viability of the open-fired ladle shroud. The product was successfully reused multiple times, including in sequence casting operations, without requiring preheating. This represents a significant operational advantage, as it reduces energy consumption and simplifies handling at the user's end. The elimination of preheating also minimizes turnaround time, aligning with industry demands for efficiency and sustainability to thermal shock, a critical factor in ensuring product longevity under repeated casting cycles.

The findings collectively highlight that process optimization through granulometry modification and antioxidant incorporation can yield a ladle shroud that is both reusable and non-preheating. The open-fired design not only matches the performance of conventional closed-fired shrouds but also introduces operational and environmental benefits. These results underscore the potential of material engineering strategies to transform refractory consumables into more sustainable and user-friendly solutions for modern steelmaking.

Parameter	Closed-fired Ladle Shroud	Open-fired Ladle Shroud
Microstructure	Conventional phase distribution; glaze applied to inner lining	In-situ phase formation due to antioxidants; no glaze required
Preheating Requirement	Mandatory to avoid thermal shock	Not required; product can be used directly
Casting Application	Suitable for standard billet casting	Proven for billet caster and sequence casting
Spalling Resistance	Moderate; granulometry less	Improved due to modified

	optimized	granulometry
Thermal Expansion Behavior	Stable but conventional RTE curve	Similar RTE curve with improved thermal shock resistance
Ease of Handling	Requires preheating and careful lining	Simplified handling; direct use without preheating
Sustainability Impact	Higher energy consumption due to preheating	Energy-efficient; reduced turnaround time and fuel usage

Table 1: Comparative properties of Open fired & Closed fired ladle shroud:

4. Performance Observation:

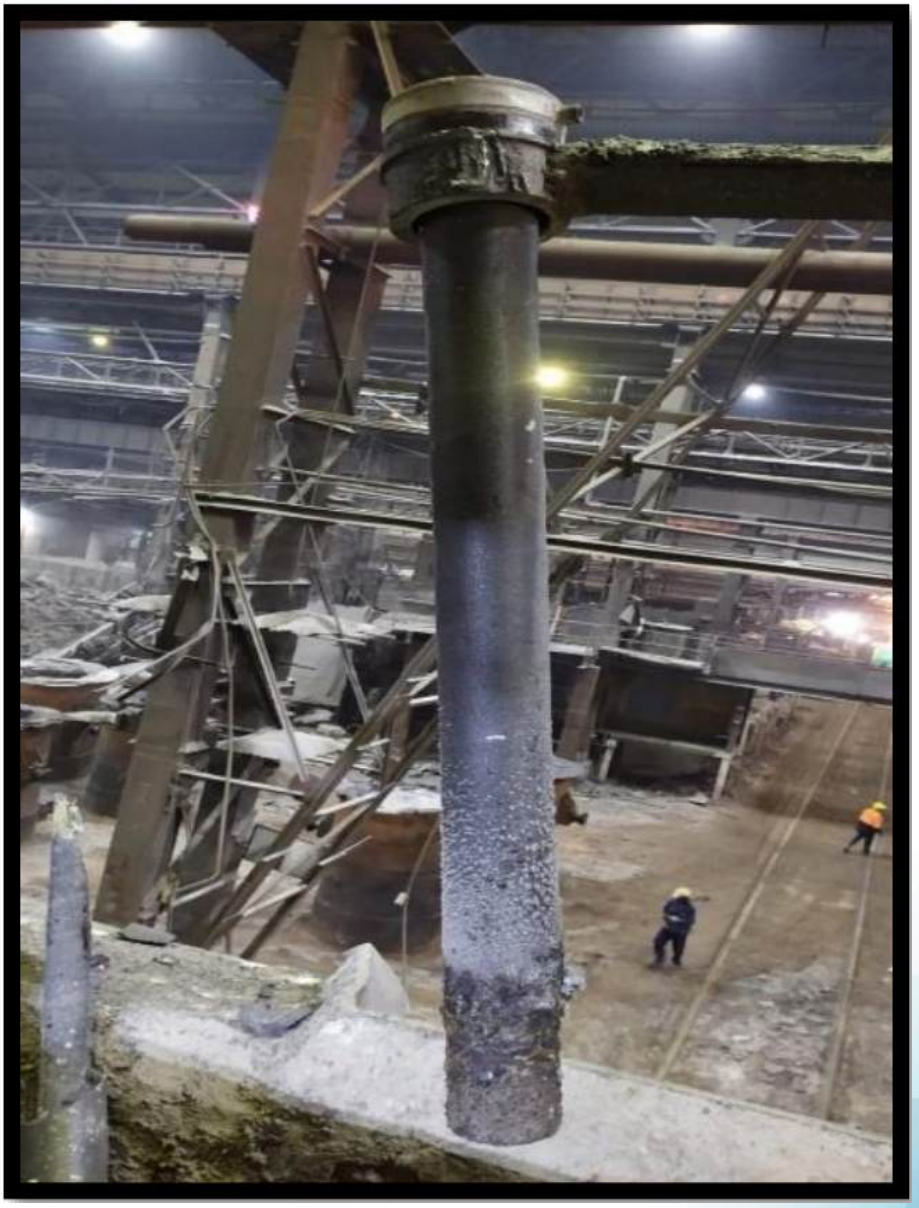


Fig. 3: Photo of ladle shroud after 4 heats at Tata Steel Long Product Ltd. without preheating

Field trials of the open-fired ladle shroud were conducted at customer sites to validate laboratory findings under industrial conditions. The performance was satisfactory at the customer site, with the product Parameter Closed-fired Ladle Shroud Open-fired Ladle Shroud Microstructure Conventional phase distribution; glaze applied to inner lining In-situ phase formation due to antioxidants; no glaze required Preheating Requirement Mandatory to avoid thermal shock Not required; product can be used directly Casting Application Suitable for standard billet casting Proven for billet caster and sequence casting Spalling Resistance Moderate; granulometry less optimized Improved due to modified granulometry Thermal Expansion Behavior Stable but conventional RTE curve Similar RTE curve with improved thermal shock resistance Ease of Handling Requires preheating and careful lining Simplified handling; direct use without preheating Sustainability Impact Higher energy consumption due to preheating Energy-efficient; reduced turnaround time and fuel usage demonstrating stable operation and reliable flow control during casting. Importantly, the ladle shroud was successfully tried for four heats, confirming its reusability and resilience against thermal shock without the need for preheating. This outcome reinforces the laboratory observations of improved spalling resistance and stable thermal expansion behavior. The ability to withstand multiple heats in sequence casting highlights the practical advantage of the open-fired design, offering both operational efficiency and cost savings. By eliminating preheating requirements, the product reduces energy consumption and simplifies handling, aligning with industry priorities for sustainability and productivity.

5. Conclusion

The present study demonstrates the successful development of an open-fired ladle shroud designed for nonpreheating and reusable application. Through process optimization, including antioxidant incorporation and modified granulometry, the product achieved in-situ phase formation that enhanced oxidation resistance and spalling resistance. Comparative evaluation with conventional closed-fired shrouds confirmed that the openfired design delivers equivalent physical and chemical properties while offering distinct operational advantages. Industrial trials at customer sites validated the laboratory findings, with the ladle shroud performing satisfactorily and being reused across four heats without preheating. Overall, the research establishes that open-fired ladle shrouds can serve as a practical and innovative solution in modern steelmaking. By combining material design strategies with industrial validation, the study contributes to advancing refractory consumables toward greater ease of use, cost-effectiveness, and environmental responsibility. Future work may focus on expanding trials across diverse casting environments and quantifying long-term economic benefits to further strengthen the case for widespread adoption.

References

[1] G. Bertrand, D. Cassard, N. Arvanitidis, G. Stanley, Map of critical raw material deposits in Europe, Energy Procedia 97 (2016) 44–50.

[2] Kusiorowski, MgO-ZrO2 refractory ceramics based on recycled magnesia-carbon bricks, Construction and Building Materials 231 (2020) 117084.

[3] S. Shaw, China's increasing environmental focus sends shockwaves through the refractory industry, Refract. Worldforum 11 (2019) 58–62.

[4] J. Czechowski, J. Witek, A. S´ liwa, Przemysł materiałów ogniotrwałych –problematyka badan´ i rozwoju (Refractory industry – research and development), Szkło i Ceramika 2 (2017) 26–27 (in Polish).

[5] C.E. Semler, Review of refractoris markets & research – 2016, Refract. Worldforum 9 (2017) 30–34.

[6] B. Plešinerová, P. Vadász, R. Kamensky, J. Bounziová, J. Derd'ak, D. Medved, Spent magnesia-carbon refractory bricks from steel

production: potentiality of MgO-clinker recovery, Acta Montanistica Slov. 23 (2018) 39–45.

[7] A. Volcaert, Raw materials for refractories: the European perspective, in: D.G. Goski, J.D. Smith (Eds.), Proceedings of the Unified International Technical Conference on Refractories (13th biennial worldwide congress on refractories) UNITECR'13, The American Ceramic Society, 2013, pp. 84–90.

BASIC SLIDE GATE PLATES FOR LADLE FOR HIGH CALCIUM STEEL

S Chatterjee*, A Singh, G Borah, G Ansari, M Rout, R Periyasamy

RHI Magnesita

Abstract

The dominant properties of slide gate (SG) refractories are Thermal shock resistance (TSR) and Corrosion resistance. With the advancement of technology, the demands for higher grade steel is rising. This has led to use of higher amounts of Ca in the steel refining. This poses a big problem for conventional Al_2O_3-C and Al_2O_3-ZrO_2-C slide plates during casting.The Ca vapour from the steel reacts with the amphoteric nature Alumina resulting in quick degradation of the matrix. Zirconia inserts can counter this effect, but these inserts poses a high cost and the same time also has probability of getting ripped off during sliding application if not properly fixed with the slide plate. Magnesia based refractories show promising neutralizing effects against these corrosive vapour, but these Magnesia based refractories have poor TSR. In this paper we have discussed about the development of a magnesia based product which can perform in high calcium steel with field study.

1. Introduction

The initial trend for SG products were oxide bonded one which later converted into carbon bonded along with some additives into it.

A. Damage in Slide gate Plates

The wear in slide gate plates occurs because of the following reasons: i. Abrasion or erosion because of sliding under high temperature and pressure and throttling during casting ii. Stress generation due to expansion in the refractory, which consequences cracks in the refractory body which further facilitates air aspiration and results oxidation in the SG refractories iii.Corrosion takes place in two steps. At first the carbonaceous material gets oxidized by atmospheric oxygen & oxygen ppm present in liquid steel. After then the oxidized film comes contact with different soluble materials in the steel like O, Mn, Ca etc and forms low melting phases and washed away with the flow of the steel and the cycle goes on.

B. Wear Mechanism of SG Refractories in High Calcium Steel

The continuous increasing demand in order to make high specification/low inclusion steel the Ca alloy treatment results heavy erosion in SG refractories. The following image is of a Alumina -ZirconiaCarbon(AZC) SG plate undergoes to casting with Ca around 35 ppm in steel.

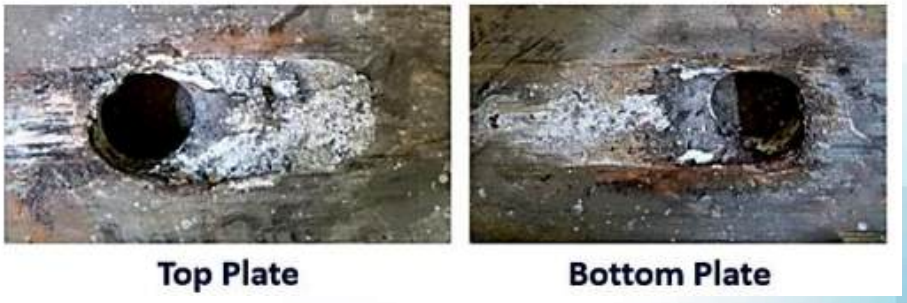


Fig 1 : Damage of AZC plate used for casting high calcium steel

The phenomenon taken place in two stage.

Stage 1 is the depletion of carbon from the refractory because of oxidation and negative pressure generated during casting.
Stage 2 is the reaction between steel & the refractory.

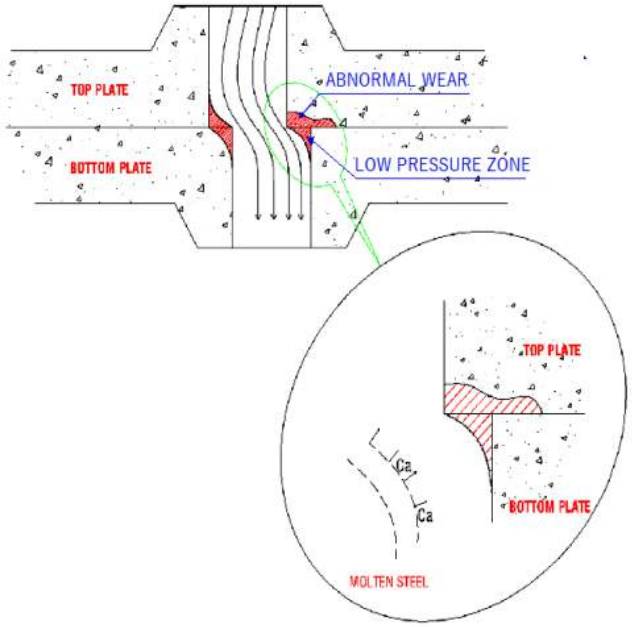


Fig 2 : Wear mechanism in plate by Ca-alloy treated steel

i. REACTION OF STEEL WITH THE BOTTOM PLATE:

The longitudinal side of the bottom plate faces the ferrostatic pressure and flow of the liquid steel. During this casting period the Al_2O_3 & SiO_2 from the refractory reacts with the CaO in the steel to form low melting phase. The rate of reaction is relatively less as compared to the top plate as solid-solid reaction is taken place. The reaction is,

y CaO + x Al2O3 = y CaO.x Al_2O_3
(C_3A,$C_{12}A_7$,CA)
C: CaO, A: Al_2O_3 CaO+ Al_2O_3 + SiO_2 -> Slag Anorthite,Gehelenite

ii. REACTION OF STEEL WITH THE TOP PLATE:

Reaction in the top plate is governed by the low boiling point Ca vapour (1484℃) which hits the top plate. The rate of reaction is very high as solid-gas reaction is taking place.

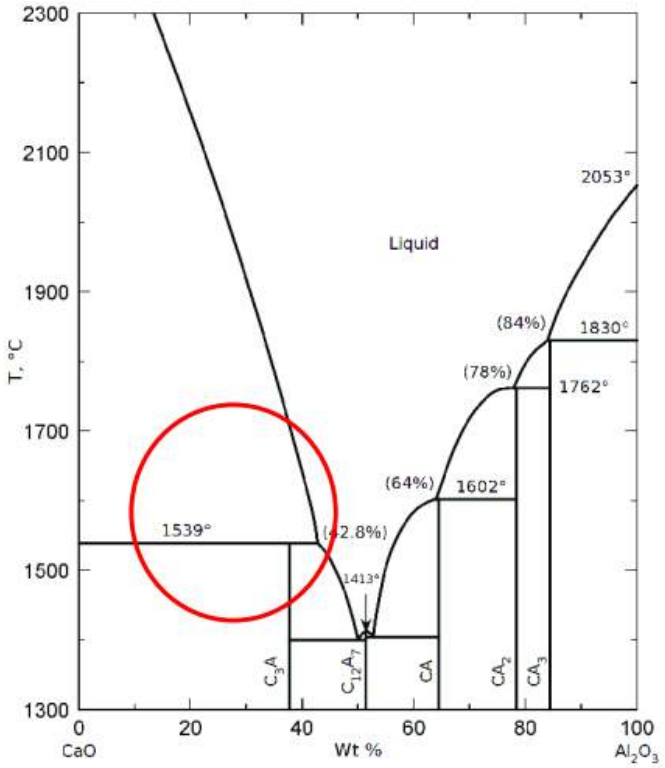


Fig 3 : CaO-Al2O3 Phase diagram

Reactions are,

$[Ca]+(x+1/3)Al_2O_3 = CaO.xAl_2O_3 +2/3\ Al$

$[Ca]+(x+1/3)SiO_2 = CaO.xSiO_2 +1/3\ Al$

Similarly in high Oxygen steel the SiO_2 (from antioxidants) & C from the refractory undergoes reaction with FeO in molten steel resulting sever damage in the SG plate

.

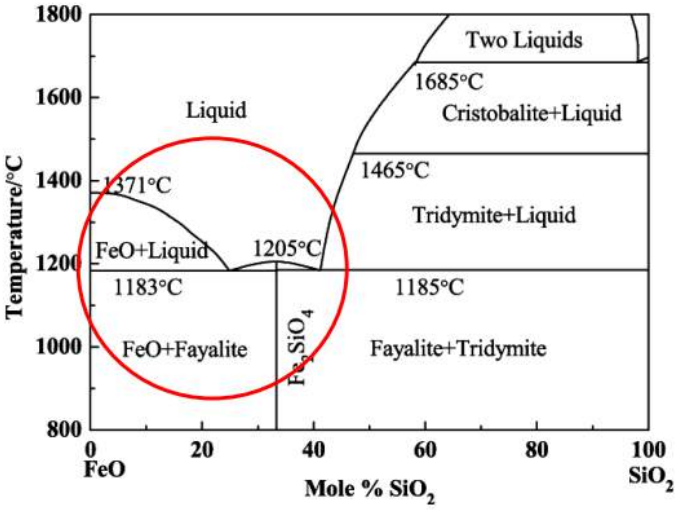


Fig 4 : FeO-SiO2 Phase diagram

Reactions are,

$SiO_2 + 2Fe = FeO + Si$

$FeO + C = Fe + CO\uparrow$

Al_2O_3 from the refractory also forms low temperature phases during the application

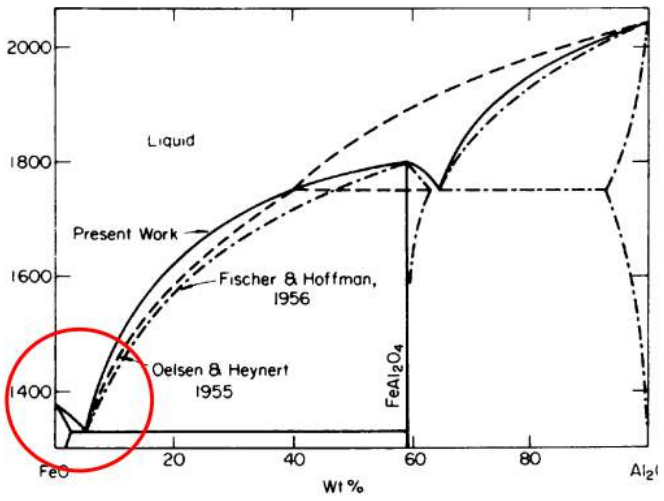


Fig 5 : FeO-Al_2O_3 Phase diagram

C. Basic Slide Gate Plate

It is found that MgO-Al_2O_3-C, MgO-C, ZrO_2 inserted composite plates works the best with high Ca containing steel. Magnesia has the advantage having high corrosion resistance against Ca & CaO and at the same time it is light weight as compared to ZrO_2.

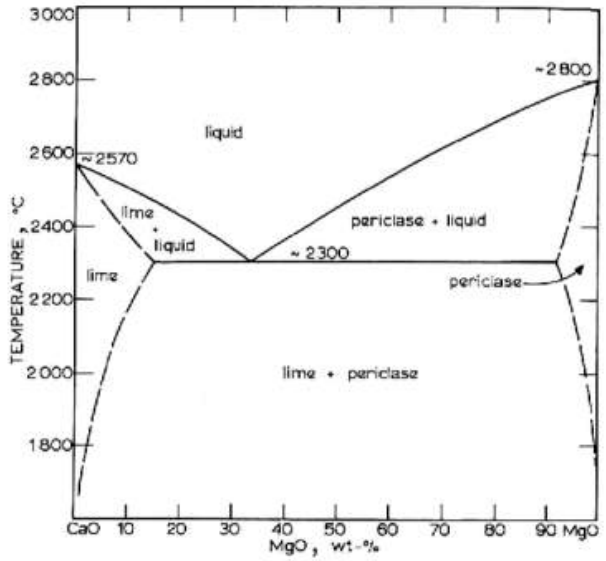


Fig 6 : MgO-CaO Phase diagram

It is also has a good amount of corrosion resistance against FeO

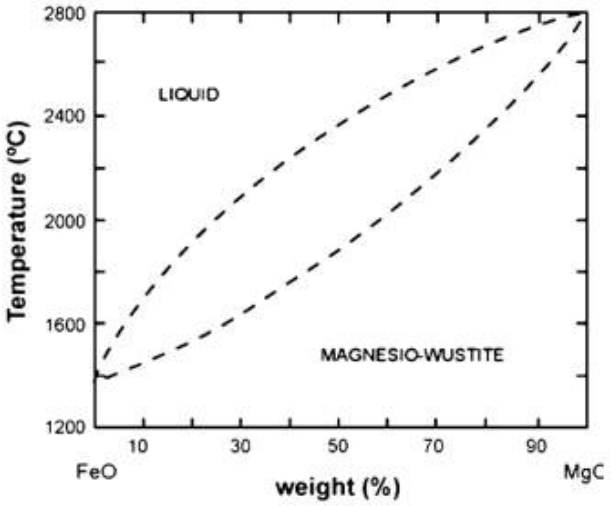


Fig 7 : MgO-FeO Phase diagram

Despite of having high corrosion resistance against Ca,CaO & FeO the thermal shock resistance is poor because of high thermal expansion.

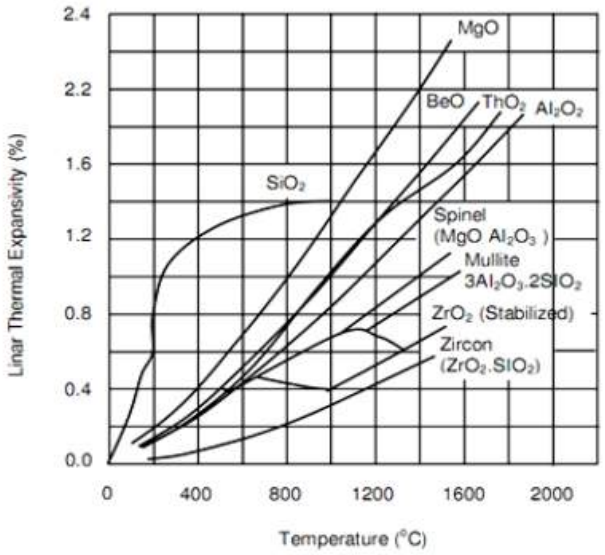


Fig 8 : Thermal expansion curves of various refractory oxides

D. Improvement of thermal shock resistance of Slide Gate Plate

It is general practice to decrease thermal expansion of a oxide system by adding oxides with relatively less thermal expansion.Considering the application environment in mind, Spinel is the most suitable material for this purpose. [The corrosion resistance of the oxides against Ca steel are, MgO>Spinel>Al_2O_3 (ZrO_2 is not considered)]

2. Experimental Procedure:

A. Optimization of Spinel in MgO System

Cylinders were prepared with Magnesia & Spinel fines. These cylinders were dried & fired. Thermal expansion behaviour was measured at 1500 deg C. The corrosion test was done at 1660 Deg C through cup test. The slag contains 60% CaO, 32% Al_2O_3 & 8% Metallic Fe.

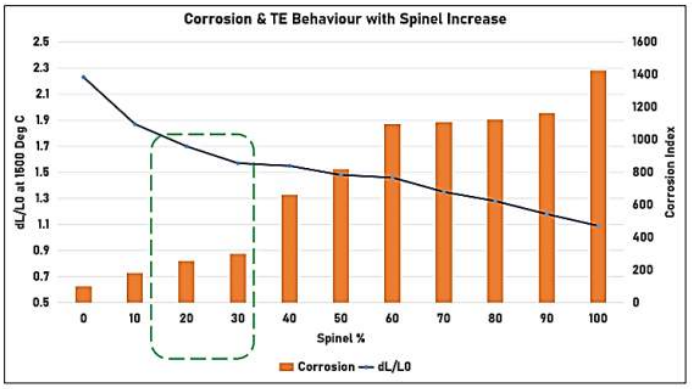


Fig9: Thermal expansion behaviour & corrosion resistance behaviour with increase in spinel

B. Physical & Chemical Properties

Raw materials like Sea water magnesia, Fused Magnesia, Spinel along with carbonaceous compounds & other additives were mixed using resin as binder inside a high intensity mixer and pressed at high specific pressure in the form of slide plate. These slide plates were heat treated & impregnated and the product properties were evaluated.

Chemical Properties:

Parameter	Result
MgO(%)	70.5
Al_2O_3(%)	21.6
C(%)	7.2
Fe_2O_3 (%)	0.46

Physical Properties:

Parameter	Result
AP (%)	5.5
BD (gm/cc)	3.01
CCS (kg/cm^2)	1015
HMOR (kg/cm^2) at 1400, 30 Mins	135

C. Oxidation Resistance

The sample was kept at 1600 deg C for 5 hrs. Sample shows good oxidation resistance. The intermediate between oxide & non oxidized area also shows good strength.The non oxidized area is 68.3%



Fig 10: Oxidation Resistance test

3. Field Performance

The product was tried in Plant A in India.

A. Plant Operational Parameters

Parameters	Plant A
Ladle Capacity	190 Mt
Tapping Temp.	1680 deg C
Caster	Thin Slab Caster
Casting Time	55-65 min
Steel Grade	LC
Treatment	Ca-Alloy
Ca in steel	30-40 ppm
Slide plate bore	Slide plate bore
SG Mechanism & Stroke length	CS-80, 200 mm

B. Plate Performance

The product was trialed under Ca ppm 30 to 40 ppm range in LC Steel grade with a casting time in between 55-65 min per heat.

The plate photographs after application are as follows.



Fig 11: Plate after 4 Heat (Bore erosion 2.5 mm/heat)



Fig12: Plate after 4 Heat (Bore erosion 1.82 mm/heat)

4. Conclusion

The present investigation shows it is possible to use Magnesia-Spinel-Carbon slide plates where Ca ppm > 30 ppm in ladles.

The product performed 4 heats with further potential The magnesia takes part contributing the corrosion resistance whereas the spinel in the composition takes part in the thermal shock resistance

Spinel in between 15-30% range shows the best properties in terms of thermal expansion & corrosion resistance.

5. Way Forward

The quality to be further trialed in other steel plants where Ca is more than 30 ppm for further study.

6. Acknowledgement

The authors are thankful to RHI Magnesita management for providing the opportunity and support for above study and permitting to present this paper in this seminar.

7. Reference

1.T Wakita,K Akamine,T Suruga,J Yoshitomi,K Asano, “THE BASIC SLIDE GATE PLATE FOR CASTING OF Ca-ALLOY TREATED & HIGH OXYGEN STEEL”, UNITECR 2005

2.U. Sengupta,J Tiwari, “DEVELOPMENT OF HIGH PERFORMANCE MAGNESIA-SPINEL CARBON– SLIDE GATE PLATES FOR Ca-Si TREATED STEEL”, UNITECR 2007

3. J Chaudhuri, S Kumar, P Bajoria, G Banerjee,”DESIGN & DEVELOPMENT OF SUITABLE QUALITY SLIDE PLATE FOR CASTING CALCIUM ALLOY TREATED STEEL”, UNITECR 2007

COMPARATIVE STUDY ON SINTERED, FUSED, AND TABULAR ALUMINA AGGREGATES FOR CASTABLES: DENSIFICATION, STRENGTH, CORROSION RESISTANCE, AND SEGREGATION BEHAVIOR

Daimu MUTO and Seiichiro KONO

Ceramics Development Sec., Itochu Ceratech Corporation.

12-8, Shiokusa-cho, Seto-shi, Aichi 489-0895, Japan

Abstract

In India, refractory demand continues to expand in line with the growth of core industries such as steel, cement, aluminium, and glass, and the importance of monolithic refractories is also increasing. Under such circumstances, it is important to clarify how differences in the manufacturing route of alumina aggregates, one of the key factors governing the performance of alumina castables, affect castable properties. In this study, three types of alumina aggregates—sintered alumina, fused alumina, and tabular alumina—were comparatively evaluated, focusing on the role of different particle size ranges and their effects on densification, strength, corrosion resistance, and segregation behavior.

The results showed that, in the particle size range of 5 mm and below used as a main aggregate fraction, the use of lowporosity and high-density sintered alumina tended to contribute to densification of the entire castable body. This is considered advantageous for reducing residual porosity and improving corrosion resistance. In contrast, in the coarse size range of 30– 10 mm, fused alumina, with its irregular shape and rough surface, tended to integrate more readily with the matrix and contributed to improved fired strength. On the other hand, coarse sintered alumina, owing to its dense internal structure, tended to suppress penetration into the aggregate itself and thereby contributed to improved corrosion resistance. Coarse tabular alumina showed a tendency similar to that of sintered alumina, but because of its nearly spherical particle shape, it tended to flow more easily and to exhibit weaker interfacial bonding with the matrix.

Furthermore, coarse aggregates showed different sedimentation and segregation behaviors during vibrationassisted placement depending on their density and particle shape, suggesting a risk of inhomogeneity within the installed body. These results indicate that the optimum aggregate selection for alumina castables should be based not only on the intrinsic properties of the aggregate itself, but also on the role of each particle size range, matrix integration, corrosion resistance, and homogeneity during installation.

Keywords — castables, coarse aggregates, sintered alumina, segregation

1. Introduction

India is one of the major countries in the world with a very large population and has maintained strong economic growth in recent years. According to the World Bank, India is one of the fastest-growing major economies in the world, and since 2000 its real economic scale has nearly quadrupled while per capita income has almost tripled [1]. Against this background of economic growth, capital investment and production expansion in high-temperature industries such as steel, cement, aluminium, and glass are expected to continue over the medium to long term.

Among these industries, the steel sector is particularly important in relation to refractory demand, and statistics from the World Steel Association also show that crude steel production in India has been increasing in recent years [2]. With the growth of such high-temperature industries, refractories are expected to provide not only high

refractoriness, but also ease of installation, labor savings, ease of repair, and improved equipment availability.

To meet these requirements, monolithic refractories, including castables, offer several advantages such as the ability to form a joint-free monolithic structure, high flexibility in installation, and ease of repair. Therefore, although it cannot yet be said that a major shift from brick linings to castable-based linings is clearly underway in India at present, the areas where monolithic linings using castables are required may gradually increase in the future as demands for larger equipment, simplified installation, and shorter maintenance time continue to grow.

At the same time, for the wider application of castables, not only performance but also rational mix design and sufficient densification of the installed body are important. In castable compositions, fine powders constituting the matrix are costly because of the high cost of fine grinding, and they also require a large amount of mixing water because of their high specific surface area. Therefore, reducing the volume fraction of the matrix by adding coarse aggregates is an effective approach for reducing cost and water demand, thereby improving densification after drying and firing [3].

In this context, one of the major factors controlling castable performance is the alumina aggregate. Alumina aggregates such as sintered alumina, fused alumina, and tabular alumina differ in density, pore structure, particle shape, surface condition, and internal microstructure because of differences in their manufacturing routes. As a result, they are expected to affect the densification, strength, corrosion resistance, and segregation behavior of castables in different ways. However, the effects of these aggregate characteristics in each particle size range should be re-examined in a systematic manner.

Accordingly, in this study, three types of alumina aggregates—sintered alumina, fused alumina, and tabular alumina—were comparatively evaluated, with particular attention to the role of each particle size range, in order to clarify their effects on the densification, strength, corrosion resistance, and segregation behavior of alumina castables.

II. EXPERIMENTAL METHOD

A. Properties of raw materials

In this study, sintered alumina, tabular alumina, and fused alumina were comparatively used as dense alumina aggregates. Sintered alumina and tabular alumina are both materials obtained by shaping high-purity alumina raw materials and then firing them at high temperature. In general, tabular alumina is known to have a homogeneous and dense sintered structure [3]. In contrast, fused alumina is produced by melting and solidifying alumina raw materials, and coarse particles may contain relatively large internal pores [3].

All aggregates used had an Al2O3 purity of 99.7 wt% or higher. The aggregate size fractions used were 30–10 mm as coarse aggregates, and 5–3 mm, 3–1 mm, <1 mm, and powder as main aggregate fractions. Figure 1 shows the appearance of the aggregate particles. For the 30–10 mm coarse fraction, sintered alumina and tabular alumina were uncrushed particles, whereas fused alumina consisted of crushed particles. On the other hand, all main aggregate fractions of 5 mm and below were crushed particles.



Fig. 1. Appearance of alumina aggregate particles

Figure 2 shows the bulk specific gravity and apparent porosity of the various alumina aggregate particles as a function of particle size. For the <1 mm fraction, particles smaller than 0.5 mm were removed, and measurements were carried out on the 1–0.5 mm fraction in order to eliminate the influence of very fine particles. Sintered alumina and tabular alumina showed nearly constant values regardless of particle size, and sintered alumina was denser than tabular alumina. In contrast, the density of fused alumina varied markedly with particle size. Coarse fused alumina particles (30–10 mm) showed low density with an apparent porosity exceeding 10%, whereas fine particles (1–0.5 mm) showed an apparent porosity of less than 1%, making them denser than sintered alumina.

This difference is considered to originate from the manufacturing process of each aggregate and the resulting difference in crystal size. Figure 3 shows SEM images of the various alumina aggregate particles. In sintered alumina and tabular alumina, the primary corundum crystal size was approximately 10–100 μm, and the internal pores remained in the range from sub-micrometers to several micrometers. In contrast, the primary corundum crystals in fused alumina were extremely large, ranging from several hundred micrometers to several millimeters, and many coarse pores of several hundred micrometers were also observed. In fused alumina, such coarse pores tend not to remain inside the particles after crushing into finer sizes, resulting in decreased porosity as particle size becomes smaller. A similar tendency may occur in other alumina aggregates as well, but because their original pores are smaller and

more finely dispersed, they do not show such a dramatic density change within the particle size range generally used in refractories. It has been reported that such differences in microstructure originating from raw material type can significantly affect castable properties [4].

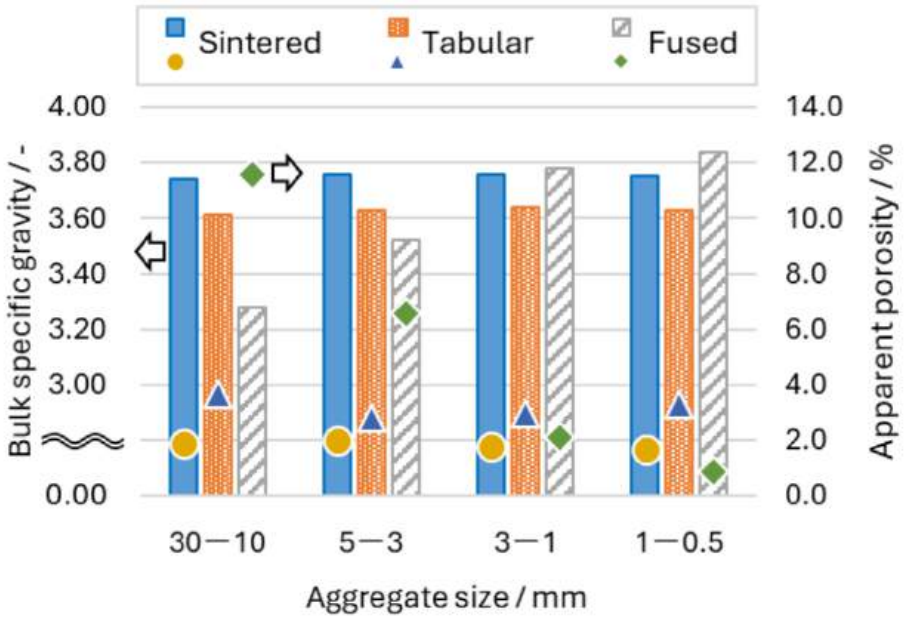


Fig. 2. Bulk specific gravity and apparent porosity of alumina aggregate particles by particle size.

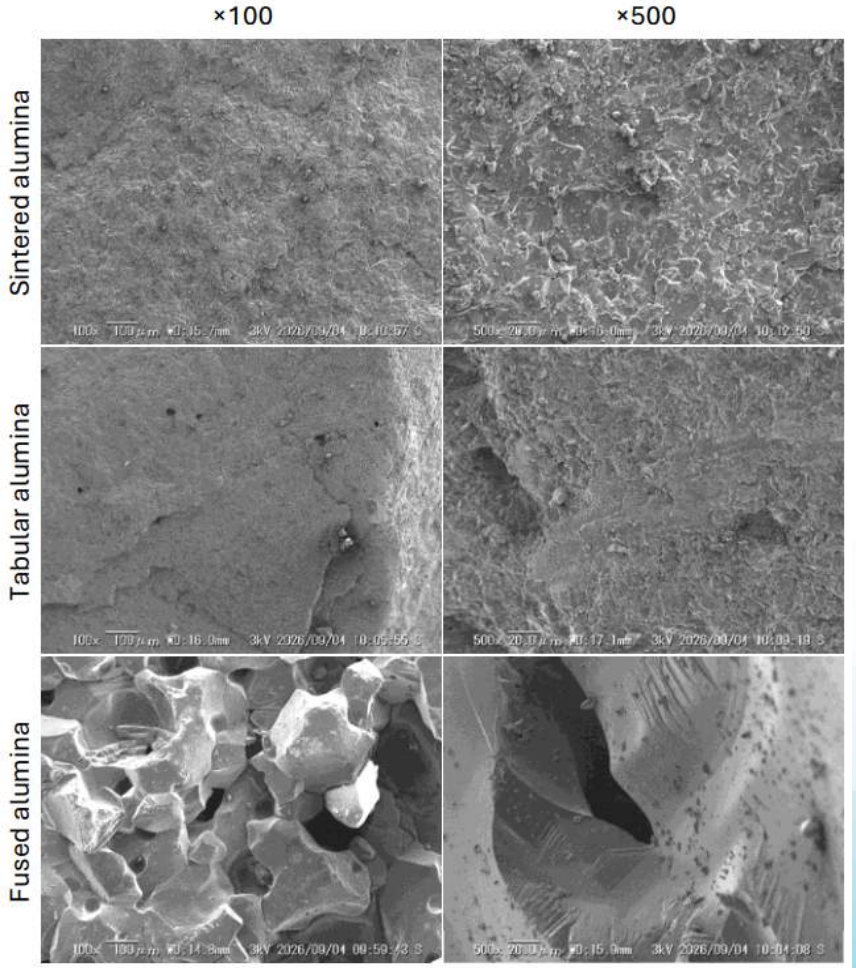


Fig. 3. Microstructures of alumina aggregate particles.

B. Preparation of castable specimens

Table I shows the compositions of the high-alumina castables used in this study. The sample names indicate the combination of alumina aggregate type and particle size range used in each composition. Specifically, the first symbol indicates the coarse aggregate, the second symbol indicates the coarser main aggregate fractions (5–3 mm and 3–1 mm), and the third symbol indicates the finer main aggregate fractions (<1 mm and powder). For example, in NC/S/F, no coarse aggregate was added, sintered alumina was used for the 5–3 mm and 3–1 mm fractions, and fused alumina was used for the <1 mm fraction and powder.

Raw material / Particle size (mm)			Content (wt%)	Sample name / Aggregate combination*1							
				NC/S/S	NC/T/T	NC/F/F	NC/S/F	NC/F/T	S/S/S	T/S/S	F/S/S
Coarse aggregate		30–10*2	(20)*3	-	-	-	-	-	S	T	F
Main aggregate	Large	5–3	10	S	T	F	S	F	S	S	S
	Medium	3–1	20								
	Fine	<1	30	S	T	F	F	T	S	S	S
	Powder		25								
Calcined alumina			5								
Calcium aluminate cement			10								
Dispersant			(0.1)								
Water addition (wt%)				6.3	6.7	6.4	6.0	7.2	6.3	6.3	6.3

TABLE I. COMPOSITIONS OF CASTABLE SPECIMENS

*1 NC indicates that no coarse aggregate was used. S, T, and F denote sintered alumina, tabular alumina, and fused alumina, respectively. In sample NC/S/F, sintered alumina was used for the 5–3 and 3–1 mm fractions, fused alumina was used for the <1 mm fraction and fines.
*2 The 30–10 mm fraction was used only in selected compositions.
*3 Values in parentheses indicate externally added components.

In all compositions, the raw materials other than the alumina aggregates and their mixing ratios were kept constant. Since the fine matrix fraction in castables is costly and requires a large amount of mixing water, the introduction of coarse aggregates has been reported to be effective for reducing matrix volume, lowering cost, and decreasing water demand [3]. In the present study, the effect of coarse aggregates was evaluated also from this viewpoint of mix design.

Mixing was carried out using a mortar mixer. Water was added so that a specified fluidity, i.e., a tap flow value of 190 mm, was obtained, and the batch was mixed for 3 min. The tap flow value was measured in accordance with JIS R 2521. For compositions containing coarse aggregates, the materials other than the coarse aggregates were first mixed for 3 min, after which the coarse aggregates were added and mixing was continued for an additional 1 min.

For the compositions containing coarse aggregates, it was difficult to evaluate fluidity using the mold specified in JIS R 2521. Therefore, the mixed castable was placed in a mold of 200 mm diameter and 60 mm height to measure the free flow, after which a vibration of 3G was applied for 5 s to measure the vibration flow.

C. Evaluation methods

Specimens for density and strength measurements were prepared by casting the mixed castable into steel molds of 40 mm × 40 mm × 160 mm, curing overnight at room temperature, demolding, and then drying at 110°C for 24 h. Part of the dried specimens was then fired in an electric furnace at 1500°C for 3 h. Bulk specific gravity and apparent porosity were measured by the boiling method in accordance with JIS R 2205. The three-point bending strength was measured at room temperature using a Shimadzu Autograph under the conditions of a 100 mm span and a crosshead speed of 1 $mm \cdot min^{-1}$.

The segregation behavior of coarse aggregates was evaluated for the three compositions containing coarse aggregates, namely S/S/S, T/S/S, and F/S/S. The mixed castable was charged into a vertically placed void tube of 100 mm diameter and 1000 mm height over approximately 1 min while applying a vibration of 3G. Vibration was then continued for an additional 1 min. After approximately 2 h, while the castable remained in a cohesive state before sufficient hardening, the tube was cut at positions 300 mm from the top end and 300 mm from the bottom end. The specimens obtained from each section were disintegrated, and the coarse aggregates were separated from the remainder of the castable body. After drying at 110°C for 24 h, the dry weight of the coarse aggregates was defined as W1, and the dry weight of the castable body excluding coarse aggregates was defined as W2. The weight change rate of coarse aggregates, ΔW, was defined by Eq. (1). The designed coarse aggregate addition was 20 wt% on an external addition basis.

$$\Delta W = (W1 / W2) \times 100 - 20 \quad (1)$$

Corrosion resistance was evaluated by a rotary erosion spalling test. The specimens were trapezoidal columns with a height of 115 mm, a thickness of 50 mm, a working-face width of 70 mm, and a back-face width of 130 mm. Two specimens for each composition, six in total, were assembled to form the inner lining of the drum. The test temperature was 1650°C. After the corrosive material was charged, the temperature was held for 30 min, molten slag was discharged, and the system was air-cooled for 20 min. The drum was then reheated to 1650°C in 10 min, and the corrosive material was charged again. This cycle was repeated six times. The corrosive material used was a mixture of steel and slag adjusted to a steel/slag ratio (C/S = 3) of 7:3. In slag attack on alumina refractories, wear is known to progress with the formation of low-melting phases through reactions involving Fe, CaO, and SiO_2. As an index of corrosion resistance, the wear amount was defined as the difference in specimen thickness before and after the test, and the relative value was expressed by taking the wear amount of S/S/S as 100.

III. RESULTS AND DISCUSSION

A. Bulk density and strength of castables

Figure 4 shows the bulk specific gravity of the castable specimens. Among the compositions without coarse aggregates, NC/S/F exhibited the highest density, whereas NC/F/T showed the lowest density. This is considered to be due not only to the difference in density of the aggregates themselves, but also to the strong influence of aggregate porosity on the densification of the whole castable. When fused alumina was used in the coarser main aggregate range, the aggregates retained more water during mixing, resulting in a higher water addition as shown in Table I and, consequently, a lower density of the castable body. On the other hand, NC/S/F consisted of a relatively high-density aggregate combination in each particle size range and required the lowest amount of added water, leading to the highest bulk specific gravity.

A similar tendency was observed in the compositions containing coarse aggregates. Under the condition that the main aggregate was fixed as sintered alumina, the density difference among the coarse aggregates directly appeared as the density difference of the castable body. In addition, all compositions containing coarse aggregates tended to show higher bulk specific gravity than the corresponding compositions without coarse aggregates. This tendency is consistent with the report that the introduction of coarse aggregates reduces the proportion of the fine matrix fraction having a large specific surface area and thereby facilitates lower water demand in the overall composition [3].

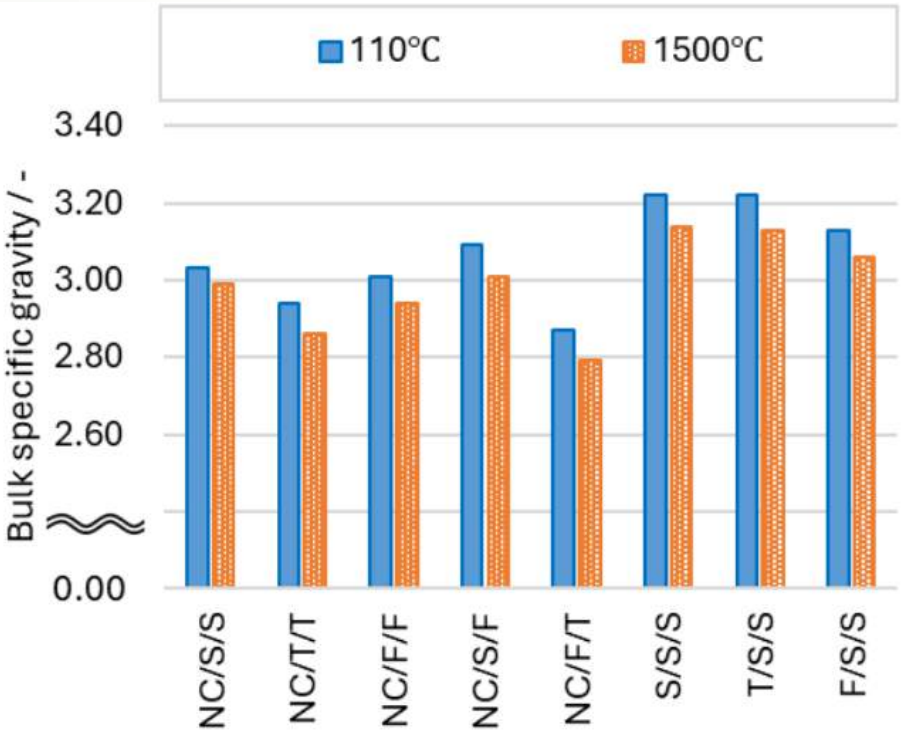


Fig. 4. Bulk specific gravity of castable specimens after drying and firing.

Figure 5 shows the three-point bending strength of the castable specimens. For the compositions without coarse aggregates, strength generally increased with increasing bulk specific gravity. In contrast, for the compositions containing coarse aggregates, strength tended to decrease when sintered alumina or tabular alumina was used as the coarse aggregate.

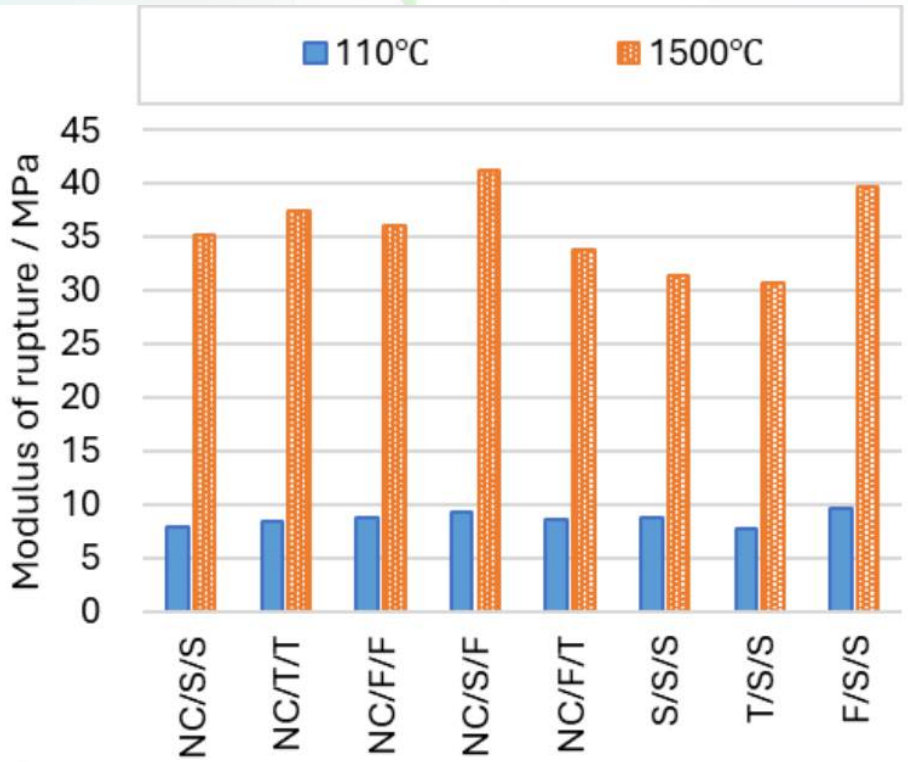


Fig. 5. Modulus of rupture of castable specimens after drying and firing.

Figure 6 shows fracture surfaces after bending for the compositions containing coarse aggregates. In S/S/S and T/S/S, a fracture mode was observed in which the coarse aggregates were pulled out from the matrix. This is considered to be because the coarse aggregates were much stronger than the matrix and because their relatively smooth surfaces resulted in weak bonding at the aggregate/matrix interface. It has also been reported that differences in alumina raw material affect the interfacial condition and fracture behavior of castables, and that interfacial gaps are likely to form along smooth aggregate surfaces [4]. In the present study, such interfacial gaps may also have contributed to the effective reduction of the fracture area.

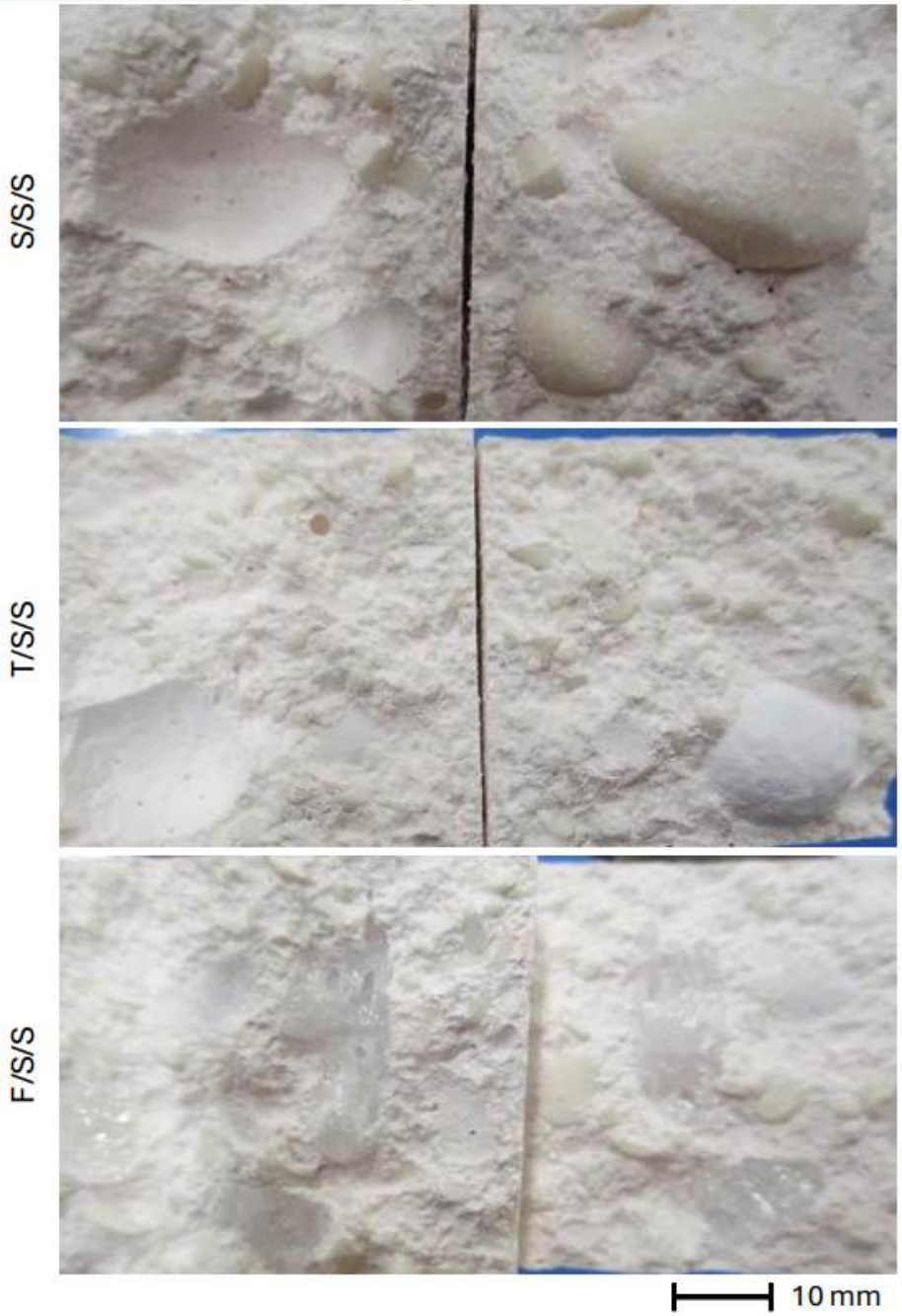


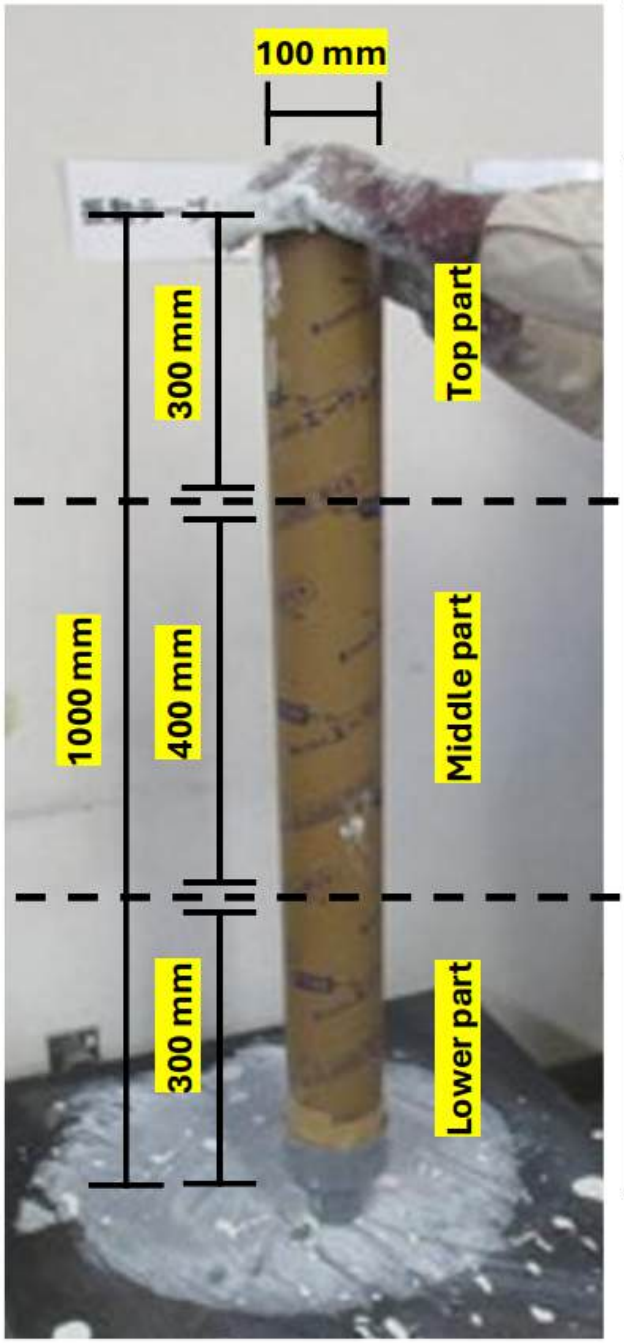
Fig. 6. Fracture surfaces of castable specimens containing coarse aggregates.

In contrast, fused alumina coarse aggregates have irregular shapes and rough surfaces and are therefore more likely to interlock mechanically with the matrix. In addition, fracture of the coarse aggregates themselves was confirmed only in F/S/S. Accordingly, the bonding between the coarse aggregates and the matrix is considered to have been relatively strong in F/S/S, resulting in high bending strength.

The above results indicate that fused alumina coarse aggregates are effective for improving the strength of castables. On the other hand, such differences in interface structure may also affect crack propagation behavior. According to a report on the effect of corundum aggregate shape, non-spherical or angular coarse aggregates can increase fracture energy by causing crack deflection and branching [5]. In the present study as well, crack deflection or branching at the interface may have influenced the fracture behavior in the compositions containing sintered alumina or tabular alumina coarse aggregates.

B. Segregation behavior of coarse aggregates

To evaluate the segregation tendency of coarse aggregates, Figure 7 shows the weight change rate in each section, and Figure 8 shows the free flow and vibration flow values of the compositions containing coarse aggregates.



	S/S/S	T/S/S	F/S/S
ΔW: Weight change rate of coarse aggregates	-8.0%	-8.9%	2.1%
	-0.6%	3.6%	-3.5%
	19.2%	17.2%	11.7%

Fig. 7. Segregation behavior of coarse aggregates.

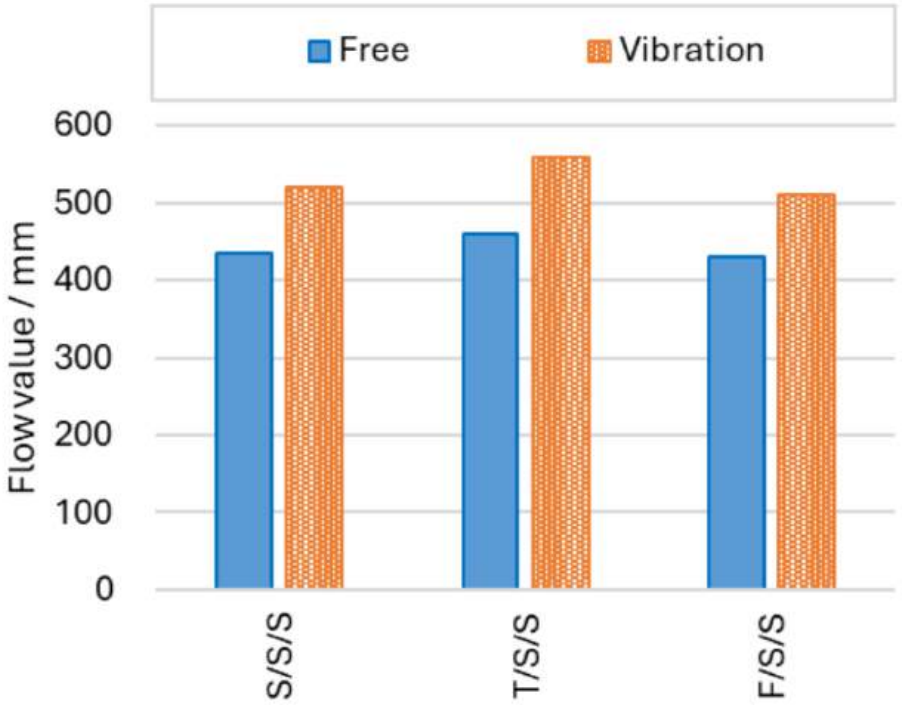


Fig. 8. Flow values of compositions containing coarse aggregates.

Both sintered alumina and tabular alumina coarse aggregates tended to settle during placement, resulting in a larger amount of coarse aggregates in the lower part. In contrast, fused alumina coarse aggregates tended to settle less because their density was lower than that of the other coarse aggregates. However, some particles were also observed to float up toward the top surface of the castable, resulting in the lowest amount of coarse aggregates in the middle section. This is considered to be due to the relatively large variation in density and internal porosity among individual fused alumina coarse particles. Therefore, in fused alumina coarse aggregates, not only quantitative segregation but also qualitative segregation may occur.

Although the settling behavior of coarse aggregates is also considered to be affected by the fluidity of the entire castable, no marked difference in free flow or vibration flow was observed among the three compositions compared in this study.

C. Corrosion resistance

The effect of coarse aggregate type on corrosion resistance was evaluated. Figure 9 shows the results of the rotary erosion spalling test. The wear amount increased in the order of S/S/S < T/S/S < F/S/S.

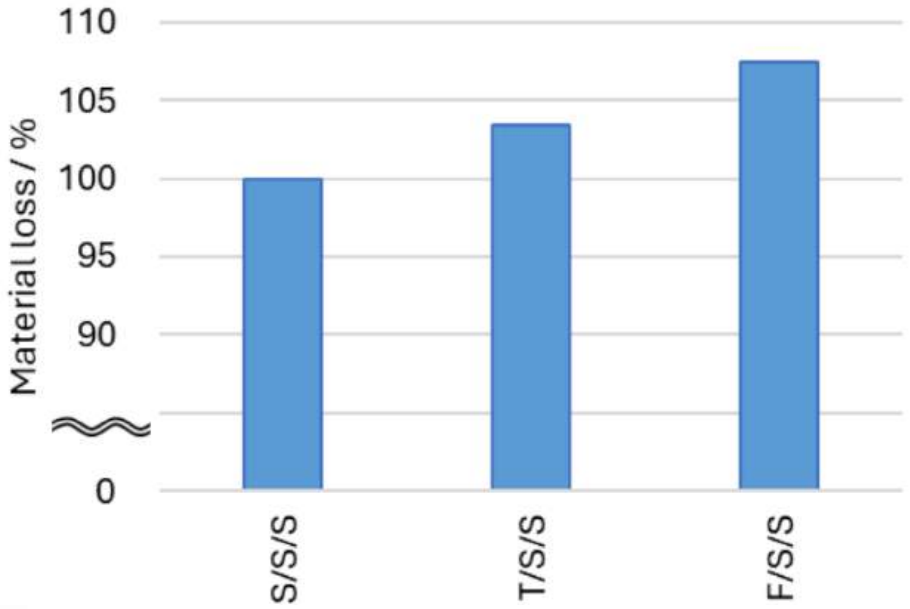


Fig. 9. Relative material loss in the rotary erosion spalling test.

Figure 10 shows photographs of the eroded surfaces after the test, and Figure 11 shows cross sections of the tested specimens. In S/S/S and T/S/S, the coarse aggregates were less eroded than the surrounding matrix and were observed as slightly raised areas on the eroded surface. In contrast, in F/S/S, the positions of the coarse aggregates were less distinct, suggesting that they were eroded at a rate close to that of the matrix. In addition, slag penetration into the coarse aggregates was confirmed in the cross section of F/S/S.

A previous report comparing coarse tabular alumina and fused alumina showed that slag readily penetrates into the macropores present in coarse fused alumina particles, thereby lowering corrosion resistance, whereas tabular alumina, which has a homogeneous and dense sintered structure, exhibits high resistance to slag penetration [3]. In addition, tabular alumina has been generally recognized as a high-performance refractory aggregate because of its homogeneous microstructure, low open porosity, and high resistance to slag penetration [6]. Recent studies have further shown that the pore structure of tabular alumina strongly affects corrosion behavior in ladle slag environments with different basicities, indicating that not only total porosity but also pore morphology and connectivity are critical factors governing slag infiltration and subsequent degradation [7].

From a more general viewpoint, refractory corrosion is understood to progress through a sequence of slag infiltration, interfacial reaction, dissolution, and microstructural change, and microstructural observation is essential for interpreting the dominant degradation mechanism in each case [8]. Braulio et al. also reported that, in alumina-spinel refractories exposed to secondary metallurgical slags, the initial penetration of slag into the open pore network plays a key role in the subsequent corrosion process [9]. The present observations are consistent with this mechanism, in that the coarse fused alumina particles containing larger internal pores allowed slag penetration into the aggregate itself, whereas the denser sintered aggregates suppressed such penetration.

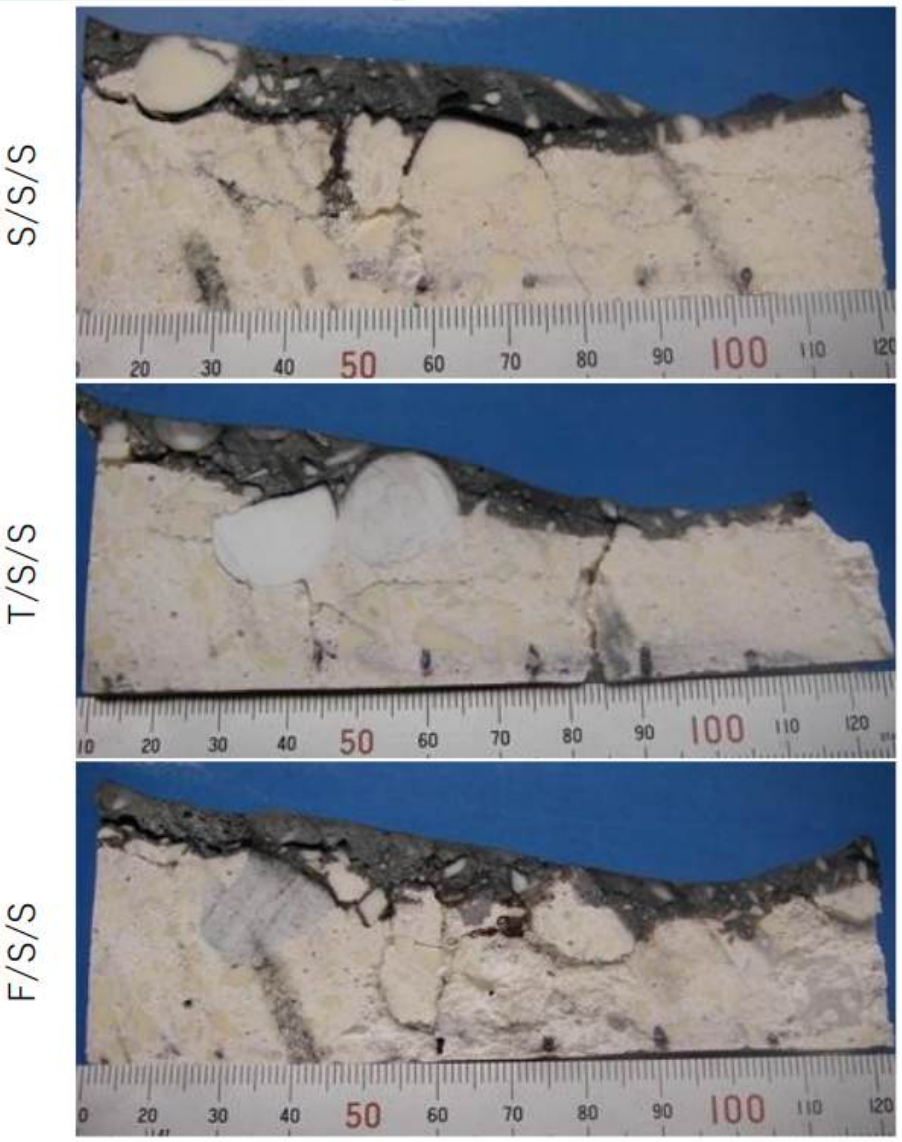


Fig. 10. Eroded surfaces after the rotary erosion spalling test.

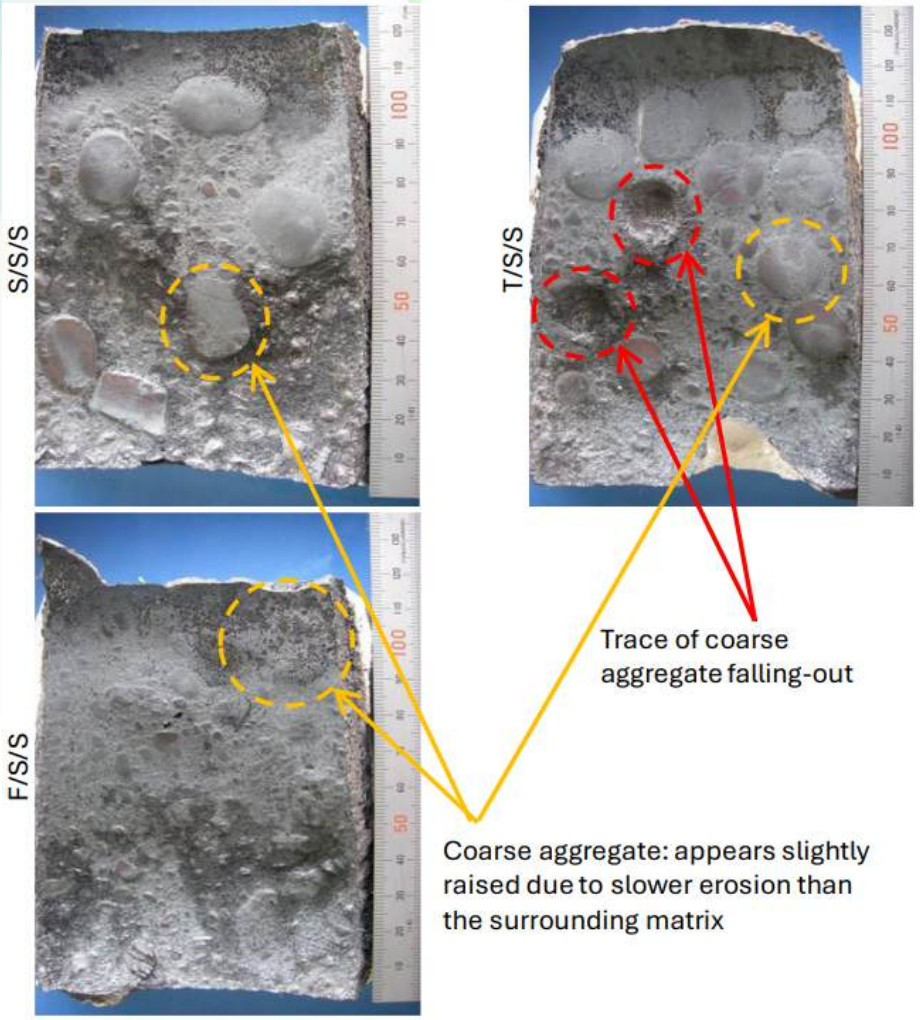


Fig. 11. Cross sections after the rotary erosion spalling test.

Therefore, the corrosion resistance of the present castables is considered to be governed not only by the chemical composition of the aggregate, but also by the density, pore structure, and interfacial integrity between the coarse aggregate and the matrix. Denser aggregates can suppress slag ingress and the formation of low-melting reaction products, thereby improving corrosion resistance.

On the other hand, some problems were also observed for sintered alumina and tabular alumina coarse aggregates. As shown in Figs. 9 and 11, especially in T/S/S, traces were observed where the remaining part of a coarse aggregate had fallen out after more than half of it had been eroded. As mentioned above, this is considered to be because relatively smooth coarse aggregates have weak interfacial bonding with the matrix and may also contain interfacial gaps [4], so that the particle retention force decreases as erosion progresses. Since the tabular alumina coarse aggregates used in this study were nearly spherical, they were particularly prone to falling out. This is considered to be the reason why T/S/S showed greater wear than S/S/S.

IV. CONCLUSIONS

The properties of alumina castables containing various alumina aggregates were comparatively evaluated, and the following findings were obtained:

1) For sintered alumina and tabular alumina,

the physical properties showed relatively small dependence on particle size. In contrast, fused alumina showed a large dependence on particle size: coarse particles had low density and high porosity, whereas finer particles showed higher density and lower porosity.

2) The workability and bulk specific gravity of castables were strongly affected by the porosity of the alumina aggregates. When the same type of aggregate was used over the entire particle size range, the densest installed body was obtained in the order of sintered alumina > fused alumina > tabular alumina. On the other hand, when the aggregate type was optimized by particle size range, the combination of sintered alumina for the coarse side and fused alumina for the fine side was the most effective for densification.

3) Fused alumina was the most effective coarse aggregate for improving strength. This is considered to be because the rough surface of the coarse aggregate enhanced mechanical bonding with the matrix. At the same time, aggregate shape and interfacial condition may also influence crack deflection and branching behavior.

4) Coarse sintered alumina was the most effective for improving slag corrosion resistance. The major causes of deterioration in corrosion resistance were the falling-out of coarse aggregates in tabular alumina and slag penetration into the coarse aggregates in fused alumina.

5) The segregation behavior of coarse aggregates was affected by both density and particle shape. Therefore, when selecting aggregates for alumina castables, it is important to consider not only the material properties of the aggregate itself, but also the role of each particle size range, integration with the matrix, corrosion resistance, and homogeneity during installation.

REFERENCES

[1] World Bank, “India,” World Bank, Country Overview. [Online]. Available: https://www.worldbank.org/en/country/india/overview. [Accessed: Sep. 7, 2026].

[2] World Steel Association, World Steel in Figures 2025. Brussels, Belgium: World Steel Association, 2025.

[3] D. P. Zacherl, M. Schnabel, A. Buhr, D. Schmidtmeier, and X. Liu, “New coarse tabular aggregates for improved castables,” in Proc. 11th Biennial Worldwide Congress on Refractories (UNITECR 2009), Salvador, Brazil, 2009.

[4] T. Ono, D. Muto, and S. Kono, "Influence of Alumina Raw Material on Castable Characteristics," Taikabutsu, vol. 72, no. 1, pp. 7-12, 2020.

[5] W. E. Lee, et al., "Influence of Corundum Aggregate Shape on Thermal Shock Resistance of Alumina Castables," Journal of the European Ceramic Society, vol. 20, no. 5-6, pp. 771-777, 2000.

[6] G. Büchel, X. Liu, A. Buhr, and J. Dutton, “Review of tabular alumina as high performance refractory material,” Interceram Refractories Manual, pp. 6–12, 2007.

[7] J. Ma, H. Zhao, J. Yu, et al., “Action Mechanism of Pore Structure of Tabular Alumina in Corrosion Environment of Ladle Slag with Different Basicities,” Journal of the Chinese Ceramic Society, vol. 50, no. 12, pp. 3284–3292, 2022.

[8] W. E. Lee, “Analysis and interpretation of refractory microstructures in studies of corrosion mechanisms,” Journal of the European Ceramic Society, vol. 27, no. 2–3, pp. 835–842, 2007.

[9] J. G. P. Braulio et al., “Corrosion of Alumina-Spinel Refractory by Secondary Metallurgical Slag Using a Laboratory Induction Furnace,” Materials, vol. 15, no. 10, p. 3425, 2022.

EFFECT OF CaF_2-CONTAINING FLUX ON PHASE STABILITY AND MICROSTRUCTURAL EVOLUTION OF STABILIZED ZIRCONIA GRAINS

N. S. Karthiselva, Sumin, Jishnu, Avishek Ghosh and M. V. Sivakumaran

Electro Minerals Division (EMD), Carborundum Universal Limited
P. B. No. 1, Kalamassery Development Plot PO, Kochi – 683 104, Kerala, INDIA

Corresponding author's e-mail: karthiselvans@cumi.murugappa.com

Abstract

Stabilized zirconia is widely used in steel-contact refractories for its high melting point, chemical stability and resistance to molten metal attack. Contact with CaF_2-bearing steelmaking fluxes can, however, cause stabilizer depletion, chemical dissolution and phase destabilization. This work compares three grades, calcia stabilized zirconia produced by the cast route (CSZ-C), calcia stabilized zirconia produced by the Higgins route (CSZ-H) and magnesia stabilized zirconia (MgSZ), as received, after high-temperature heat treatment, and after exposure at 1550 °C for 3 h to CaO-SiO_2-Al_2O_3 fluxes containing 5, 10 and 15% CaF_2. X-ray diffraction followed the tetragonal-monoclinic phase balance and scanning electron microscopy the grain surface morphology. Thermal phase stability followed CSZ-H ≈ CSZ-C >> MgSZ and resistance to fluoride attack CSZ-H > CSZ-C > MgSZ, showing that both stabilizer chemistry and grain production route govern degradation behaviour.

Keywords: Stabilized zirconia, calcium fluoride, phase stability, refractory degradation.

Introduction

Zirconia (ZrO_2) based refractories occupy a special position among steel-contact materials, combining a melting point near 2680 °C with low thermal conductivity, poor wettability by molten steel and low chemical reactivity towards metal and slag[1]. These are used in continuous casting nozzles, slide gate plates, submerged entry nozzle bands and purging elements, where thermal and chemical loading is severe and localised.

Their usefulness is restricted by polymorphism. Zirconia is monoclinic up to about 1170 °C, tetragonal to 2370 °C, and cubic above that to melting[2]. The tetragonal to monoclinic transformation on cooling is martensitic and carries a volume expansion of some 3 to 5%, generating microcracking and severe loss of strength. Oxides such as CaO, MgO and Y_2O_3 are therefore taken into solid solution, substituting for Zr4+ and generating charge compensating oxygen vacancies that retain the tetragonal or cubic phase to room temperature[3]. Calcia stabilized zirconia (CSZ) and magnesia stabilized zirconia (MgSZ) remain preferred for steelmaking refractories on cost and availability.

Less often examined is the influence of the grain production route. The cast and Higgins fusion routes impose different solidification histories, and so differ in crystal size, in the uniformity of stabilizer distribution and in the monoclinic phase retained at room temperature. Since stabilizer depletion is grain boundary controlled, such differences should translate directly into service behaviour.

Calcium fluoride is a deliberate addition to ladle refining slags, electroslag remelting fluxes, mould powders and welding fluxes. Even in modest amounts it depresses the liquidus and viscosity of CaO-SiO_2-Al_2O_3 melts and raises their capacity to dissolve alumina, which makes it effective for desulphurisation and inclusion absorption[4]. That same fluxing power renders CaF2-bearing melts unusually aggressive towards oxide refractories.

Published work on slag attack of zirconia refractories deals largely with FeO and alumina bearing slags, and the contribution of fluoride is usually inferred rather than isolated. The present work compares three grains, calcia stabilized zirconia from the cast route (CSZ-C) and from the Higgins route (CSZ-H), and magnesia stabilized zirconia (MgSZ), as received, after high-temperature heat treatment, and after exposure to CaF_2-bearing fluxes, using X-ray diffraction (XRD) to follow the tetragonal-monoclinic balance and scanning electron microscopy (SEM) the grain surface morphology. The objective is to establish how stabilizer chemistry and production route jointly govern phase stability and the mode of fluoride induced degradation.

2. Experimental procedure

2.1 Materials

The three grades investigated, CSZ-H, CSZ-C and MgSZ, were all manufactured at the Electro Minerals Division, Carborundum Universal Limited, Kochi, India. Representative grains from each were used for phase and microstructural characterization.

2.2 Heat treatment

Each grade was characterized as received, then subjected to a high-temperature heat treatment in air sufficient to bring the grain to the stability level required in service, followed by furnace cooling, and characterized again. The same schedule was applied to every grade, chosen to bring the two calcia grains to comparable tetragonal and monoclinic levels so that the effect of production route could be separated from that of starting phase composition.

2.3 Interaction with fluoride-bearing flux

Heat treated grains in the 1 to 3 mm size fraction were placed on a bed of synthetic CaO-SiO_2-Al_2O_3-CaF_2 flux and sintered at 1550 °C for 3 h in air. Three flux compositions were used for each grade, containing 5, 10 and 15 % CaF_2. The SiO_2 and Al_2O_3 were held constant at 35 and 10 % and CaO adjusted from 50 to 40 %, so that the fluoride level was the only variable. CaO, SiO_2 and Al_2O_3 were introduced as lime, quartz and calcined alumina respectively.

2.4 Characterization

X-ray diffraction, carried out at room temperature at every stage, identified and quantified the monoclinic and tetragonal phases; scanning electron microscopy assessed grain morphology, grain boundary character and surface degradation.

3. Results and discussion

3.1 Phase analysis

Room temperature phase compositions are summarised in Table 1.

Table 1 Room temperature phase composition (%) of the three stabilized zirconia grades before and after high-temperature heat treatment (T = tetragonal, M = monoclinic)

S. No.	Sample	As-received		After heat treatment	
		T	M	T	M
1	CSZ-C	90.8	9.2	85.4	14.6
2	CSZ-H	22.6	77.4	81.3	18.7
3	MgSZ	27.1	72.9	6.3	93.7

The three grades differ markedly. CSZ-C is thermally stable, its monoclinic content rising only from 9.2 to 14.6 per cent. CSZ-H behaves in the opposite sense, the retained tetragonal content rising from 22.6 to 81.3 per cent, indicating that stabilizer redistribution continues during thermal exposure. MgSZ destabilizes most severely, its monoclinic content reaching 93.7 per cent. Phase stability, governed by both stabilizer chemistry and production route, ranks CSZ-H ≈ CSZ-C >> MgSZ.

3.2 Surface morphology

In the as-received state (Fig. 1) CSZ-C shows fine, uniformly distributed crystals, CSZ-H larger and well developed crystals, and MgSZ a network of elongated needle-like crystals.

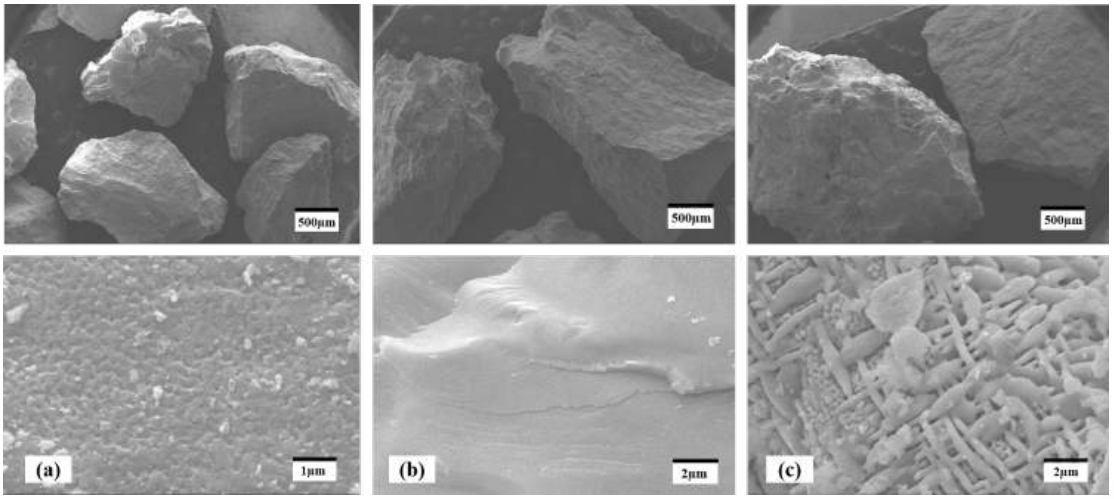


Figure 1 As-received grains: (a) CSZ-C, (b) CSZ-H and (c) MgSZ

After heat treatment (Fig. 2) CSZ-C retains its fine crystalline morphology with only minor surface modification, CSZ-H develops a porous, sponge-like surface consistent with the rearrangement implied by the diffraction data, and MgSZ retains but coarsens its acicular morphology.

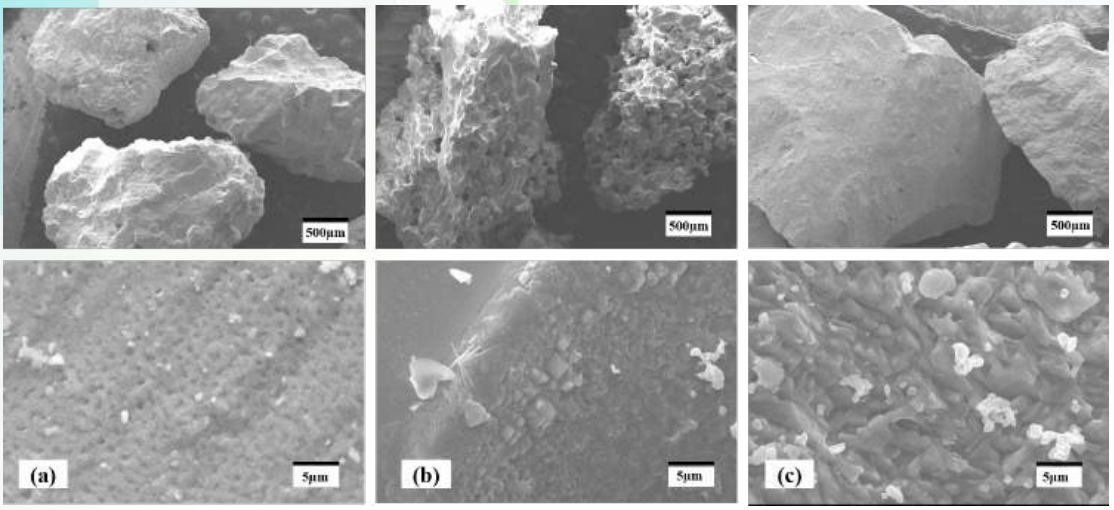


Figure 2 Grains after high-temperature heat treatment: (a) CSZ-C, (b) CSZ-H and (c) MgSZ

The two calcia grains reach comparable tetragonal fractions by different paths: CSZ-C is already near equilibrium as received, whereas CSZ-H gains stability during exposure, its retained tetragonal content rising more than threefold as calcia redistributes uniformly through the grain. The Higgins route grain therefore carries a reserve of stabilizing capacity realised in service rather than consumed before it, an advantage wherever the grain must survive repeated thermal cycles. Its open surface reflects this redistribution rather than loss of integrity, the grain beneath remaining dense and compact (Fig. 3b), and this self-stabilizing behaviour contributes directly to the superior fluoride resistance of CSZ-H.

3.3 Mechanism and phase selectivity of fluoride attack

Degradation is chemical attack on the stabilizer rather than on ZrO_2 itself, and two properties of the flux govern its aggressiveness. First, F- is close in size to O_2- but carries only half its charge, so it replaces bridging oxygen in the silicate network and terminates Si-O-Si chains. Due to this the melt viscosity falls sharply and cation diffusivity rises, so dissolved species are transported away rather than accumulating as a saturated boundary layer, which would otherwise render dissolution self-limiting.

Second, ZrO_2 is only sparingly soluble in such melts whereas CaO and MgO are freely miscible with them, so a grain loses stabilizer long before it loses zirconia. Which stabilizer is lost is decided by the activity gradient. The fluxes used here held 40 to 50 % CaO and no MgO, so the activity of CaO in the liquid is already high and calcia has little reason to leave a CSZ grain, whereas the activity of MgO is effectively zero and magnesia is drawn out of MgSZ continuously. This asymmetry, rather than any intrinsic difference between the two solid solutions, should dominate the comparison; in MgSZ it is aggravated by MgO exsolved at grain boundaries, which the melt attacks preferentially.

Susceptibility therefore scales with stabilizer content, in the order cubic > tetragonal > monoclinic. The cubic phase holds the largest stabilizer inventory and with it the highest concentration of charge compensating oxygen vacancies, which both stabilize the structure and provide the sites through which fluoride enters the anion sublattice. The tetragonal phase, less heavily doped, is correspondingly more durable. Monoclinic zirconia has no stabilizer left to lose and is not itself attacked chemically.

Monoclinic zirconia is nonetheless where the damage becomes manifest. Once a depleted surface layer falls below the stabilizer content needed to retain the tetragonal phase, it reverts to monoclinic on cooling with the attendant 3 to 5 per cent expansion, and the microcracks so formed admit fresh liquid one layer deeper. Attack therefore

advances as a self-sustaining front of leaching, transformation, cracking and renewed penetration rather than by uniform surface recession, which accounts for the low resistance of a grain that is already largely monoclinic.

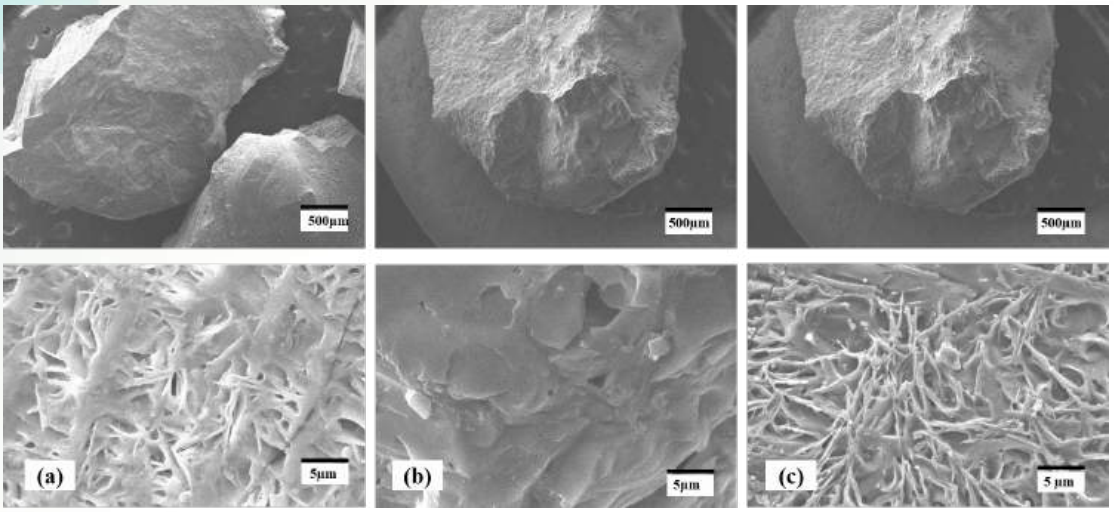


Figure 3 Grains after interaction with CaF2-containing flux: (a) CSZ-C, (b) CSZ-H and (c) MgSZ

Fig. 3 confirms this expectation. CSZ-C (Fig. 3a) develops lath-like reaction products with localised dissolution, CSZ-H (Fig. 3b) remains dense with limited surface attack, and MgSZ (Fig. 3c) shows extensive acicular growth. Degradation follows MgSZ > CSZ-C > CSZ-H.

3.4 Implications for property optimisation

The phase balance that governs chemical resistance also governs mechanical behaviour, and the two impose opposing requirements. At high stabilizer content the grain is fully cubic: dimensionally stable, but coarse grained, weak and, by the argument above, the most readily leached. At low stabilizer content the transformation proceeds unhindered on cooling and the material is unusable.

The optimum lies at an intermediate stabilizer content. A sufficient fraction of metastable tetragonal phase provides transformation toughening[3], the stress field of an advancing crack triggering the transformation and the accompanying dilatation closing the crack tip. A limited monoclinic fraction is likewise beneficial, its microcracks lowering the elastic modulus and conferring the thermal shock tolerance a nozzle requires; beyond that limit strength declines and the microcrack network offers a continuous path for melt penetration.

CSZ-C and CSZ-H, at 85.4 and 81.3% tetragonal, lie within this range, whereas MgSZ at 6.3% retains neither toughening nor shock tolerance. A retained tetragonal fraction near 80% under calcia stabilization is therefore the manufacturing target. The schedule of heat treatment and cooling is correspondingly application specific, since it determines stabilizer uniformity and the resulting microstructure.

4. Conclusions

1. Thermal phase stability follows CSZ-H ≈ CSZ-C >> MgSZ. Heat treatment left CSZ-C almost unchanged, raised the retained tetragonal content of CSZ-H more than threefold, and destabilized MgSZ almost completely.

2. Resistance to the CaF2-bearing fluxes follows CSZ-H > CSZ-C > MgSZ, CSZ-H remaining dense with limited surface attack and MgSZ showing severe acicular growth.

3. Attack proceeds by leaching of the stabilizing oxide rather than dissolution of

ZrO_2. The lime-rich, magnesia-free flux retained calcia but removed magnesia continuously. Stabilizer-rich cubic regions are the most vulnerable, monoclinic zirconia being both the product of attack and the path for further penetration.

4. Optimum performance is not obtained at the highest stabilizer content. A retained tetragonal fraction ~ 80% under calcia stabilization best balances transformation toughening, thermal shock tolerance and resistance to stabilizer leaching, Higgins route grain approaching this condition most closely.

References

1. R.Stevens: Zirconia and Zirconia Ceramics, 2nd Edition, Magnesium Elektron Ltd., Twickenham, UK, 1986, p.1.

2. E.C.Subbarao: Advances in Ceramics, Vol.3, Science and Technology of Zirconia, Am. Ceramic Society, Columbus, USA, 1981, p.1.

3. R.C.Garvie, R.H.Hannink and R.T.Pascoe: Nature, Vol.258, 1975, p.703.

4. Slag Atlas, 2nd Edition, Verlag Stahleisen, Dusseldorf, 1995, p.349.